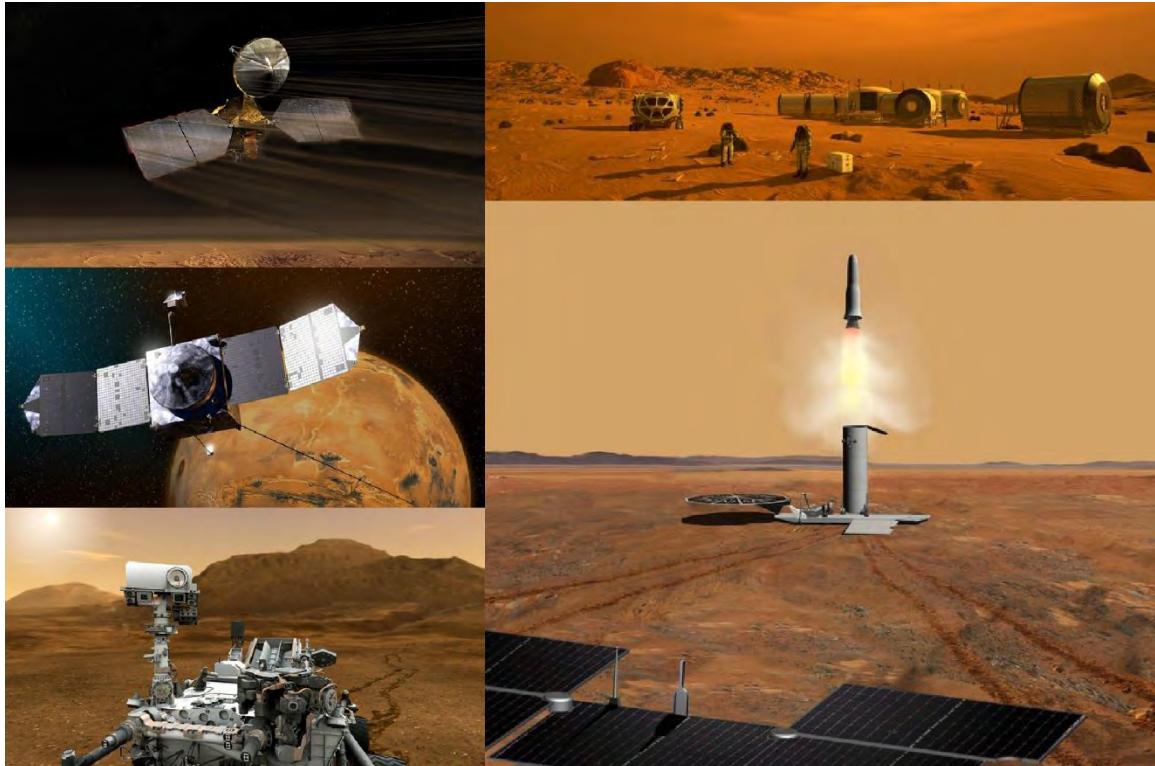


# MARS MISSION DESIGN HANDBOOK (2022-2040)



**JPL D-106417**  
**Release 1.2**  
**November 6, 2023**

Document Custodian: Mark S Wallace

Note: Printed copies of this document may not be relied upon for official purposes. The current version of this document is located in the Product Data Management System of the Pre-Projects and Advanced Studies Office (mep-lib) at JPL. The data contained in this document should only be used for planning purposes.

**JPL**  
Jet Propulsion Laboratory  
California Institute of Technology

National Aeronautics  
and Space Administration



## Signature Page

### Prepared by:

---

Mark S Wallace  
*Inner Planet Mission Analysis Group*

Date

### Contributors:

Ryan Woolley

### Approved by:

---

Try Lam  
*Inner Planet Mission Analysis Group Supervisor*

Date

---

Chad Edwards  
*Mars Exploration Program Advanced Studies Office*

Date

## Change Log

Date	Sections Changed	Reason for Change	Release
10/30/2020	All	New Document	1.0
10/06/2023	3.3 (Table 21) 7.3 (Eq. 15) 8.4.1	Various corrections	1.1
11/06/2023	11.3	Added brief discussion of White Sands Missile Range	1.2

# Table of Contents

<b>1</b>	<b>INTRODUCTION .....</b>	<b>1</b>
1.1	PURPOSE .....	1
1.2	ORGANIZATION .....	1
1.3	TRAJECTORY MODELS.....	1
1.4	LAUNCH PERIOD SELECTION STRATEGY .....	2
<b>2</b>	<b>PLANETARY CONSTANTS AND MODELS .....</b>	<b>4</b>
2.1	OVERVIEW .....	4
2.2	MARS PLANETARY CONSTANTS .....	4
2.2.1	<i>Mars Gravity Field</i> .....	4
2.2.2	<i>Mars Pole and Prime Meridian</i> .....	4
2.2.3	<i>Mars Shape Parameters</i> .....	5
2.2.4	<i>Mars Satellite Data</i> .....	5
2.3	MARS SEASONS .....	6
2.4	MARS TIME SYSTEMS .....	7
2.4.1	<i>Martian Solar Day</i> .....	7
2.5	LOCAL TRUE SOLAR TIME AND LOCAL MEAN SOLAR TIME .....	7
2.5.1	<i>Equation of Time</i> .....	9
2.6	MARS ATMOSPHERE .....	9
2.6.1	<i>Dust Storms</i> .....	11
2.7	EARTH PLANETARY CONSTANTS.....	13
2.7.1	<i>Earth Gravity Field</i> .....	13
2.7.2	<i>Earth Pole and Prime Meridian</i> .....	14
2.7.3	<i>Earth Shape Parameters</i> .....	14
2.7.4	<i>Standard Acceleration of Gravity</i> .....	14
2.7.5	<i>Earth's Moon</i> .....	14
2.7.6	<i>Standard Coordinate Systems</i> .....	15
2.8	SOLAR SYSTEM PLANETARY GRAVITATIONAL PARAMETERS .....	17
2.9	MARS EPHemeris RELATED EVENTS.....	17
<b>3</b>	<b>LAUNCH VEHICLES .....</b>	<b>23</b>
3.1	OVERVIEW .....	23
3.1.1	<i>Rapidly Changing Launch Vehicle Market</i> .....	24
3.1.2	<i>Vehicle Configurations</i> .....	24
3.1.3	<i>Launch Vehicle User's Guides</i> .....	25
3.2	LAUNCH VEHICLE PERFORMANCE.....	27
3.3	LAUNCH AZIMUTH RESTRICTIONS AND DECLINATION PENALTIES .....	29
<b>4</b>	<b>BALLISTIC MISSION DESIGN .....</b>	<b>32</b>
4.1	OVERVIEW .....	32
4.2	LAMBERT SOLUTIONS .....	32
4.3	PORKCHOP PLOTS.....	35
4.4	BROKEN PLANE TRAJECTORIES .....	38
<b>5</b>	<b>SOLAR ELECTRIC PROPULSION MISSION DESIGN .....</b>	<b>40</b>
5.1	OVERVIEW .....	40
5.2	CONSIDERATIONS IN CHOOSING TO USE SEP .....	40
5.3	SPECIFIC IMPULSE VS. THRUST.....	42
5.4	NORMALIZED SEP SYSTEMS .....	44
5.5	DESIGN PROCESS .....	46
5.5.1	<i>Bacon Plots</i> .....	48

5.6	EP CRUISE STAGES FOR LANDERS.....	50
5.7	FURTHER READING .....	51
<b>6</b>	<b>PLANETARY FLYBYS.....</b>	<b>52</b>
6.1	OVERVIEW .....	52
6.2	EARTH-EARTH LOOPS.....	52
6.3	EARTH BACKFLIPS .....	54
6.4	MARS-MARS LOOPS .....	55
6.5	MARS BACKFLIP .....	56
6.6	VENUS FLYBYS .....	57
<b>7</b>	<b>LANDER MISSION DESIGN.....</b>	<b>58</b>
7.1	OVERVIEW .....	58
7.2	ENTRY, DESCENT, AND LANDING (EDL).....	58
7.3	SURFACE ACCESSIBILITY .....	61
7.4	EDL COMMUNICATIONS .....	68
7.4.1	<i>Direct to Earth</i> .....	69
7.4.2	<i>Relay Communications</i> .....	70
<b>8</b>	<b>ORBITER MISSION DESIGN.....</b>	<b>72</b>
8.1	OVERVIEW .....	72
8.2	ORBIT DESIGN .....	72
8.2.1	<i>Introduction</i> .....	72
8.2.2	<i>Non-Spherical Gravity</i> .....	72
8.2.3	<i>Drag Perturbations</i> .....	79
8.3	ORBIT INSERTION .....	82
8.3.1	<i>Introduction</i> .....	82
8.3.2	<i>High-Thrust Orbit Insertion</i> .....	82
8.3.3	<i>Aerocapture</i> .....	85
8.4	AEROBRAKING .....	85
8.4.1	<i>Aerobraking Overview</i> .....	85
8.4.2	<i>Aerobraking Design</i> .....	86
8.4.3	<i>Modeling Assumptions</i> .....	87
8.4.4	<i>Aerobraking Data</i> .....	88
<b>9</b>	<b>ROUNDTRIP MISSION DESIGN .....</b>	<b>101</b>
9.1	OVERVIEW .....	101
9.2	CONJUNCTION-CLASS MISSIONS.....	101
9.3	OPPOSITION-CLASS MISSIONS .....	102
<b>10</b>	<b>EARTH TO MARS BALLISTIC TRANSFER DATA: 2022-2040 .....</b>	<b>104</b>
10.1	OVERVIEW .....	104
10.2	SUMMARY OF OPPORTUNITIES.....	104
10.3	LANDER LAUNCH PERIODS.....	110
10.4	ORBITER LAUNCH PERIODS.....	156
10.5	PORKCHOP PLOTS.....	202
10.5.1	<i>Introduction</i> .....	202
10.5.2	<i>Earth to Mars 2022</i> .....	203
10.5.3	<i>Earth to Mars 2024</i> .....	220
10.5.4	<i>Earth to Mars 2026</i> .....	237
10.5.5	<i>Earth to Mars 2028</i> .....	254
10.5.6	<i>Earth to Mars 2031</i> .....	271
10.5.7	<i>Earth to Mars 2033</i> .....	288
10.5.8	<i>Earth to Mars 2035</i> .....	305

10.5.9	<i>Earth to Mars 2037</i> .....	322
10.5.10	<i>Earth to Mars 2039</i> .....	339
<b>11</b>	<b>MARS TO EARTH BALLISTIC TRANSFER DATA: 2024-2041</b> .....	<b>356</b>
11.1	OVERVIEW .....	356
11.2	SUMMARY OF OPPORTUNITIES .....	356
11.3	LAUNCH PERIODS .....	360
11.4	PORKCHOP PLOTS.....	374
11.4.1	<i>Introduction</i> .....	374
11.4.2	<i>Mars to Earth 2024</i> .....	375
11.4.3	<i>Mars to Earth 2026</i> .....	379
11.4.4	<i>Mars to Earth 2028</i> .....	383
11.4.5	<i>Mars to Earth 2031</i> .....	387
11.4.6	<i>Mars to Earth 2033</i> .....	391
11.4.7	<i>Mars to Earth 2035</i> .....	395
11.4.8	<i>Mars to Earth 2037</i> .....	399
11.4.9	<i>Mars to Earth 2039</i> .....	403
11.4.10	<i>Mars to Earth 2041</i> .....	407
<b>12</b>	<b>ROUNDTrip MISSION TRANSFER DATA: 2022-2041</b> .....	<b>411</b>
12.1	OVERVIEW .....	411
12.2	VENUS-ENABLED TRAJECTORIES .....	412
12.3	CONJUNCTION-CLASS DESIGNS .....	414
12.4	OPPOSITION-CLASS DESIGNS .....	419
<b>13</b>	<b>APPENDICES</b> .....	<b>421</b>
13.1	GRAVITY COEFFICIENTS.....	421
13.1.1	<i>MRO120D</i> .....	421
13.1.2	<i>GGM05C</i> .....	422
13.1.3	<i>Converting Between Normalized and Un-Normalized Gravity Coefficients</i> .....	423
13.2	REFERENCES .....	424

## List of Figures

FIGURE 1: LONGITUDE OF THE SUN FOR DETERMINING THE SEASONS OF MARS .....	6
FIGURE 2: DEFINITION OF LTST AND LMST .....	8
FIGURE 3: EQUATION OF TIME VS THE LONGITUDE OF THE SUN .....	9
FIGURE 4: SIMPLIFIED MEAN MARS ATMOSPHERE MODEL AND UNDERLYING VARIATION .....	10
FIGURE 5: COMPARISON OF SIMPLIFIED MARS ATMOSPHERE MODELS AT DIFFERENT SOLAR ACTIVITY LEVELS .....	11
FIGURE 6: ATMOSPHERIC OPACITY (TAU) VS. LS AS MEASURED BY OPPORTUNITY AND CURIOSITY.....	12
FIGURE 7: MRO RECORDED DRAG PER ORBIT THROUGH FEB 1, 2019 VS. LS .....	13
FIGURE 8: EARTH MEAN EQUATOR AND EQUINOX OF J2000 (EME2000) .....	15
FIGURE 9: IAU MARS POLE AT THE J2000 EPOCH.....	16
FIGURE 10: IAU MARS FIXED AT THE J2000 EPOCH .....	16
FIGURE 11: EARTH-MARS AND SUN-MARS RANGES: 2022-2041 .....	21
FIGURE 12: SUN-EARTH-MARS AND SUN-MARS-EARTH ANGLES: 2022-2041 .....	21
FIGURE 13: EARTH AND SUN LATITUDE AT MARS: 2022-2041 .....	21
FIGURE 14: LONGITUDE OF THE SUN AND DUST STORM SEASONS: 2022-2041.....	22
FIGURE 15 SNAPSHOT OF LSP LAUNCH VEHICLE PERFORMANCE QUERY TOOL. (EXTRACTED FROM <a href="https://elvperf.ksc.nasa.gov/">HTTPS://ELVPERF.KSC.NASA.GOV/</a> ON 1/14/20) .....	23
FIGURE 16: FALCON 9 AND FALCON HEAVY FAIRING DIMENSIONS .....	26
FIGURE 17: ATLAS V 5-METER FAIRING DIMENSIONS .....	27
FIGURE 18: ATLAS V 4-METER FAIRING DIMENSIONS .....	27
FIGURE 19: LAUNCH VEHICLE C3 CURVES .....	28
FIGURE 20: LAUNCH VEHICLE CAPABILITIES TO A REPRESENTATIVE MARS C3=10.....	28
FIGURE 21: PARK ORBIT INCLINATIONS FROM KENNEDY SPACE CENTER / CAPE CANAVERAL .....	30
FIGURE 22: PARK ORBIT INCLINATIONS FROM VANDENBERG.....	30
FIGURE 23: EAST COAST LAUNCH DECLINATION PERFORMANCE PENALTY .....	31
FIGURE 24: EXAMPLES OF EARTH-MARS TRAJECTORIES .....	33
FIGURE 25: TYPE III+ (BLACK) AND TYPE III- (GREEN) TRAJECTORIES FOR THE SAME EARTH DEPARTURE AND MARS ARRIVAL DATES .....	34
FIGURE 26: EXAMPLE EARTH TO MARS PORKCHOP (2026 TYPE I/II) .....	37
FIGURE 27: INSIGHT PORKCHOP PLOT .....	38
FIGURE 28: TOTAL PROPELLANT FRACTIONS FOR CHEMICAL VS. SEP THRUSTERS.....	41
FIGURE 29: TRADABILITY OF MARGINS ALLOWS FOR GREATER FLEXIBILITY IN SEP MISSIONS.....	42
FIGURE 30: EXAMPLE THROTTLE CURVES FOR ION AND HALL THRUSTERS.....	44
FIGURE 31: VARIATIONS IN ACCELERATION, MASS, AND POWER AS SOLAR DISTANCE INCREASES. ISP IS HELD CONSTANT AT 1500 S (SMALL HALL THRUSTER) OR 3500 S (LARGE ION THRUSTER). THE POWER LEVEL IS SIZED SUCH THAT IT PROVIDES 100% OF THE THRUSTER'S MAX POWER AT EARTH, 75% OF MAX POWER AT MARS, OR FULLY POWERED AT MARS. ....	45
FIGURE 32: TYPICAL ΔV REQUIREMENTS FROM EARTH TO MARS.....	47
FIGURE 33: PROCESS ALGORITHM FOR AN SEP MISSION ARCHITECTURE DESIGN TOOL THAT SIMULTANEOUSLY OPTIMIZES BOTH SPACECRAFT AND TRAJECTORY.....	48
FIGURE 34: EXAMPLE BACON PLOT WITH BALLISTIC PORKCHOP PLOT SUPERIMPOSED. THE LAUNCH DATE AT EARTH SPANS ONE SYNODIC PERIOD (780 DAYS). DIAGONAL LINES SHOW TRANSFER TIMES IN YEARS. CONTOUR LINES SHOW THE TOTAL DELIVERED MASS TO MARS FOR A GIVEN LAUNCH VEHICLE – WITH BLUE BEING THE HIGHEST. SEP ALLOWS FOR NEARLY CONTINUOUS LAUNCH PERIODS AND INCREASED DELIVERY MASS FOR LONGER FLIGHT TIMES. THE MAGENTA DOTS REPRESENT THE MAXIMUM MASS DELIVERED FOR A GIVEN TIME-OF-FLIGHT.....	49
FIGURE 35: EXAMPLE OF AN EARTH-EARTH LOOP FOLLOWED BY A TYPE I EARTH-TO-MARS TRAJECTORY .....	52
FIGURE 36: LAUNCH DECLINATION AND PERIHELION FOR A BALLISTIC EARTH-EARTH LOOP.....	54
FIGURE 37: EXAMPLE OF AN EARTH BACKFLIP FOLLOWED BY A TYPE I EARTH-TO-MARS TRAJECTORY .....	54
FIGURE 38: MARS GRAVITY ASSIST GEOMETRY FOR A MARS-MARS LOOP .....	55
FIGURE 39: PERMISSIBLE APPROACH DIRECTIONS TO INITIATE A BALLISTIC MARS-MARS LOOP (200 KM MINIMUM FLYBY ALTITUDE).....	56
FIGURE 40: PERMISSIBLE APPROACH DECLINATIONS TO INITIATE A BALLISTIC NORTH (BLUE) AND SOUTH (RED) MARS BACKFLIP (200 KM MINIMUM FLYBY ALTITUDE).....	57
FIGURE 41: MARS SCIENCE LABORATORY ENTRY, DESCENT, AND LANDING SEQUENCE .....	58
FIGURE 42: INSIGHT ENTRY, DESCENT, AND LANDING SEQUENCE .....	59

FIGURE 43: DESCENT CENTRAL ANGLE ILLUSTRATED .....	60
FIGURE 44: DESCENT CENTRAL ANGLE AND TIME VARIATION WITH ENTRY VELOCITY FOR VARIOUS ENTRY FLIGHT PATH ANGLES ASSUMING AN INSIGHT-LIKE LANDER.....	60
FIGURE 45: ENTRY VELOCITY VARIATIONS .....	61
FIGURE 46: LOCUS OF ENTRY AND LANDING POINTS .....	61
FIGURE 47: LANDING LOCUS CO-LATITUDE VS. APPROACH V-INFINITY FOR VARIOUS ENTRY FLIGHT PATH ANGLES ASSUMING AN INSIGHT-LIKE LANDER.....	62
FIGURE 48: ARBITRARY VIEW OF THE PHOENIX ENTRY AND LANDING LOCI .....	63
FIGURE 49: VIEW FROM THE NORTH POLE OF THE PHOENIX ENTRY AND LANDING LOCI .....	64
FIGURE 50: ARBITRARY VIEW OF THE MSL ENTRY AND LANDING LOCI.....	65
FIGURE 51: VIEW FROM THE NORTH POLE OF THE MSL ENTRY AND LANDING LOCI .....	66
FIGURE 52: ARBITRARY VIEW OF A SEP-ENABLED SOUTH BACKFLIP TRAJECTORY'S ENTRY AND LANDING LOCI .....	67
FIGURE 53: VIEW FROM THE NORTH POLE OF A SEP-ENABLED SOUTH BACKFLIP TRAJECTORY'S ENTRY AND LANDING LOCI.....	68
FIGURE 54: ARTIST CONCEPT OF THE MARCO CUBESATS MONITORING THE INSIGHT EDL .....	71
FIGURE 55: ECLIPSE DURATION DURING A MARS YEAR FOR CIRCULAR SUN-SYNCHRONOUS ORBITS (MORNING).....	76
FIGURE 56: ECLIPSE DURATION DURING A MARS YEAR FOR CIRCULAR SUN-SYNCHRONOUS ORBITS (AFTERNOON) .....	77
FIGURE 57: REQUIRED INCLINATION FOR A CIRCULAR SUN-SYNCHRONOUS ORBIT.....	77
FIGURE 58: EXAMPLE OF A REPEAT GROUND TRACK .....	78
FIGURE 59: FROZEN, SUN-SYNCHRONOUS, GROUND-TRACK REPEAT ORBIT MEAN ALTITUDES AND REPEAT DURATIONS .....	78
FIGURE 60: FROZEN, SUN-SYNCHRONOUS, GROUND-TRACK REPEAT ORBIT MEAN ALTITUDES AND ECCENTRICITIES .....	79
FIGURE 61: DRAG MAKE-UP $\Delta V$ VS. CIRCULAR ORBIT ALTITUDE WITH THE "HIGH" ATMOSPHERE MODEL.....	80
FIGURE 62: DRAG MAKE-UP $\Delta V$ VS. CIRCULAR ORBIT ALTITUDE WITH THE "MEAN" ATMOSPHERE MODEL.....	80
FIGURE 63: DRAG MAKE-UP $\Delta V$ VS. CIRCULAR ORBIT ALTITUDE WITH THE "LOW" ATMOSPHERE MODEL .....	81
FIGURE 64: CIRCULAR ORBIT LIFETIME WITH THE "HIGH" ATMOSPHERE MODEL .....	81
FIGURE 65: CIRCULAR ORBIT LIFETIME WITH THE "MEAN" ATMOSPHERE MODEL.....	81
FIGURE 66: CIRCULAR ORBIT LIFETIME WITH THE "LOW" ATMOSPHERE MODEL .....	82
FIGURE 67: MARS ORBIT INSERTION $\Delta V$ AT 250 KM ALTITUDE .....	83
FIGURE 68: MARS ORBIT INSERTION $\Delta V$ AT 300 KM ALTITUDE .....	83
FIGURE 69: MARS ORBIT INSERTION $\Delta V$ AT 350 KM ALTITUDE .....	83
FIGURE 70: MARS ORBIT INSERTION $\Delta V$ AT 400 KM ALTITUDE .....	84
FIGURE 71: MARS ORBIT INSERTION $\Delta V$ AT 100 KM ALTITUDE .....	85
FIGURE 72: AEROBRAKING DURATION VS. ORBIT PERIOD WITH $10 \text{ kg/m}^2$ BALLISTIC COEFFICIENT.....	90
FIGURE 73: ASCENDING NODE DRIFT VS. AEROBRAKING DURATION WITH $10 \text{ kg/m}^2$ BALLISTIC COEFFICIENT.....	90
FIGURE 74: AEROBRAKING $\Delta V$ VS. AEROBRAKING DURATION WITH $10 \text{ kg/m}^2$ BALLISTIC COEFFICIENT .....	90
FIGURE 75: AEROBRAKING DURATION VS. ORBIT PERIOD WITH $20 \text{ kg/m}^2$ BALLISTIC COEFFICIENT.....	91
FIGURE 76: ASCENDING NODE DRIFT VS. AEROBRAKING DURATION WITH $20 \text{ kg/m}^2$ BALLISTIC COEFFICIENT.....	91
FIGURE 77: AEROBRAKING $\Delta V$ VS. AEROBRAKING DURATION WITH $20 \text{ kg/m}^2$ BALLISTIC COEFFICIENT .....	91
FIGURE 78: AEROBRAKING DURATION VS. ORBIT PERIOD WITH $30 \text{ kg/m}^2$ BALLISTIC COEFFICIENT.....	92
FIGURE 79: ASCENDING NODE DRIFT VS. AEROBRAKING DURATION WITH $30 \text{ kg/m}^2$ BALLISTIC COEFFICIENT.....	92
FIGURE 80: AEROBRAKING $\Delta V$ VS. AEROBRAKING DURATION WITH $30 \text{ kg/m}^2$ BALLISTIC COEFFICIENT .....	92
FIGURE 81: AEROBRAKING DURATION VS. ORBIT PERIOD WITH $40 \text{ kg/m}^2$ BALLISTIC COEFFICIENT.....	93
FIGURE 82: ASCENDING NODE DRIFT VS. AEROBRAKING DURATION WITH $40 \text{ kg/m}^2$ BALLISTIC COEFFICIENT.....	93
FIGURE 83: AEROBRAKING $\Delta V$ VS. AEROBRAKING DURATION WITH $40 \text{ kg/m}^2$ BALLISTIC COEFFICIENT .....	93
FIGURE 84: AEROBRAKING DURATION VS. ORBIT PERIOD WITH $50 \text{ kg/m}^2$ BALLISTIC COEFFICIENT .....	94
FIGURE 85: ASCENDING NODE DRIFT VS. AEROBRAKING DURATION WITH $50 \text{ kg/m}^2$ BALLISTIC COEFFICIENT.....	94
FIGURE 86: AEROBRAKING $\Delta V$ VS. AEROBRAKING DURATION WITH $50 \text{ kg/m}^2$ BALLISTIC COEFFICIENT .....	94
FIGURE 87: AEROBRAKING DURATION VS. ORBIT PERIOD WITH $0.15 \text{ W/cm}^2$ PEAK HEATING .....	95
FIGURE 88: ASCENDING NODE DRIFT VS. AEROBRAKING DURATION WITH $0.15 \text{ W/cm}^2$ PEAK HEATING .....	95
FIGURE 89: AEROBRAKING $\Delta V$ VS. AEROBRAKING DURATION WITH $0.15 \text{ W/cm}^2$ PEAK HEATING .....	95
FIGURE 90: AEROBRAKING DURATION VS. ORBIT PERIOD WITH $0.20 \text{ W/cm}^2$ PEAK HEATING .....	96
FIGURE 91: ASCENDING NODE DRIFT VS. AEROBRAKING DURATION WITH $0.20 \text{ W/cm}^2$ PEAK HEATING .....	96
FIGURE 92: AEROBRAKING $\Delta V$ VS. AEROBRAKING DURATION WITH $0.20 \text{ W/cm}^2$ PEAK HEATING .....	96
FIGURE 93: AEROBRAKING DURATION VS. ORBIT PERIOD WITH $0.25 \text{ W/cm}^2$ PEAK HEATING .....	97

FIGURE 94: ASCENDING NODE DRIFT VS. AEROBRAKING DURATION WITH 0.25 W/CM <sup>2</sup> PEAK HEATING.....	97
FIGURE 95: AEROBRAKING ΔV VS. AEROBRAKING DURATION WITH 0.25 W/CM <sup>2</sup> PEAK HEATING .....	97
FIGURE 96: AEROBRAKING DURATION VS. ORBIT PERIOD WITH 0.30 W/CM <sup>2</sup> PEAK HEATING.....	98
FIGURE 97: ASCENDING NODE DRIFT VS. AEROBRAKING DURATION WITH 0.30 W/CM <sup>2</sup> PEAK HEATING.....	98
FIGURE 98: AEROBRAKING ΔV VS. AEROBRAKING DURATION WITH 0.30 W/CM <sup>2</sup> PEAK HEATING .....	98
FIGURE 99: AEROBRAKING DURATION VS. ORBIT PERIOD WITH 0.40 W/CM <sup>2</sup> PEAK HEATING.....	99
FIGURE 100: ASCENDING NODE DRIFT VS. AEROBRAKING DURATION WITH 0.40 W/CM <sup>2</sup> PEAK HEATING.....	99
FIGURE 101: AEROBRAKING ΔV VS. AEROBRAKING DURATION WITH 0.40 W/CM <sup>2</sup> PEAK HEATING .....	99
FIGURE 102: AEROBRAKING DURATION VS. ORBIT PERIOD WITH 0.50 W/CM <sup>2</sup> PEAK HEATING.....	100
FIGURE 103: ASCENDING NODE DRIFT VS. AEROBRAKING DURATION WITH 0.50 W/CM <sup>2</sup> PEAK HEATING.....	100
FIGURE 104: AEROBRAKING ΔV VS. AEROBRAKING DURATION WITH 0.50 W/CM <sup>2</sup> PEAK HEATING .....	100
FIGURE 105: EXAMPLE CONJUNCTION-CLASS MISSION .....	101
FIGURE 106: MIXING-AND-MATCHING TYPE I/II AND TYPE III/IV OPPORTUNITIES ALLOWS FOR A VARIABLE STAY TIME, FROM LESS THAN 30 DAYS TO MULTIPLE YEARS.....	102
FIGURE 107: EXAMPLE VENUS-ENABLED OPPOSITION-CLASS MISSIONS WITH INBOUND (LEFT) AND OUTBOUND (RIGHT) VENUS GRAVITY ASSISTS.....	102
FIGURE 108: MINIMUM C3 AND ASSOCIATED VHP FOR EARTH-TO-MARS TYPE I AND II TRAJECTORIES, 2022-2039 .....	105
FIGURE 109: MINIMUM C3 AND ASSOCIATED VHP FOR EARTH-TO-MARS TYPE III- AND IV- TRAJECTORIES, 2022-2039 .....	105
FIGURE 110: MINIMUM C3 AND ASSOCIATED VHP FOR EARTH-TO- MARS TYPE III+ AND IV+ TRAJECTORIES, 2022-2039.....	106
FIGURE 111: MINIMUM VHP AND ASSOCIATED C3 FOR EARTH-TO-MARS TYPE I AND II TRAJECTORIES, 2022-2039 .....	106
FIGURE 112: MINIMUM VHP AND ASSOCIATED C3 FOR EARTH-TO-MARS TYPE III- AND IV- TRAJECTORIES, 2022-2039 .....	106
FIGURE 113: MINIMUM VHP AND ASSOCIATED C3 FOR EARTH-TO-MARS TYPE III+ AND IV+ TRAJECTORIES, 2022-2039 .....	107
FIGURE 114: C3/VHP PARETO FRONTS FOR EARTH TO MARS TYPE I AND II TRAJECTORIES .....	107
FIGURE 115: C3/VHP PARETO FRONTS FOR EARTH TO MARS TYPE III- AND IV- TRAJECTORIES .....	107
FIGURE 116: C3/VHP PARETO FRONTS FOR EARTH TO MARS TYPE III+ TRAJECTORIES .....	108
FIGURE 117: MAXIMUM LAUNCH MASS WITH ASSOCIATED CAPTURE MASS AND ARRIVAL LS FOR EARTH-TO-MARS TYPE I AND II "LANDER" LAUNCH PERIODS, 2022-2039 .....	108
FIGURE 118: MAXIMUM LAUNCH MASS WITH ASSOCIATED CAPTURE MASS AND ARRIVAL LS FOR EARTH-TO-MARS TYPE III- AND IV- "LANDER" LAUNCH PERIODS, 2022-2039 .....	108
FIGURE 119: MAXIMUM LAUNCH MASS WITH ASSOCIATED CAPTURE MASS AND ARRIVAL LS FOR EARTH-TO-MARS TYPE III+ AND IV+ "LANDER" LAUNCH PERIODS, 2022-2039 .....	109
FIGURE 120: MAXIMUM CAPTURED MASS WITH ASSOCIATED LAUNCH MASS AND ARRIVAL LS FOR EARTH-TO-MARS TYPE I AND II "ORBITER" LAUNCH PERIODS, 2022-2039 .....	109
FIGURE 121: MAXIMUM CAPTURED MASS WITH ASSOCIATED LAUNCH MASS AND ARRIVAL LS FOR EARTH-TO-MARS TYPE III- AND IV- "ORBITER" LAUNCH PERIODS, 2022-2039 .....	109
FIGURE 122: MAXIMUM CAPTURED MASS WITH ASSOCIATED LAUNCH MASS AND ARRIVAL LS FOR EARTH-TO-MARS TYPE III+ AND IV+ "ORBITER" LAUNCH PERIODS, 2022-2039 .....	110
FIGURE 123: EARTH TO MARS 2022 TYPE I LANDER LAUNCH PERIODS - REACHABLE LATITUDES, EQUIVALENT C3, AND VHP .....	111
FIGURE 124: EARTH TO MARS 2022 TYPE I LANDER LAUNCH PERIODS - LMST OF LANDING AT VARIOUS LATITUDES .....	111
FIGURE 125: EARTH TO MARS 2022 TYPE I LANDER LAUNCH PERIODS - EARTH ELEVATION AT LANDING AT VARIOUS LATITUDES.....	111
FIGURE 126: EARTH TO MARS 2022 TYPE II LANDER LAUNCH PERIODS - REACHABLE LATITUDES, EQUIVALENT C3, AND VHP .....	112
FIGURE 127: EARTH TO MARS 2022 TYPE II LANDER LAUNCH PERIODS - LMST OF LANDING AT VARIOUS LATITUDES .....	112
FIGURE 128: EARTH TO MARS 2022 TYPE II LANDER LAUNCH PERIODS - EARTH ELEVATION AT LANDING AT VARIOUS LATITUDES.....	112
FIGURE 129: EARTH TO MARS 2022 TYPE III- LANDER LAUNCH PERIODS - REACHABLE LATITUDES, EQUIVALENT C3, AND VHP .....	113
FIGURE 130: EARTH TO MARS 2022 TYPE III- LANDER LAUNCH PERIODS - LMST OF LANDING AT VARIOUS LATITUDES .....	113
FIGURE 131: EARTH TO MARS 2022 TYPE III- LANDER LAUNCH PERIODS - EARTH ELEVATION AT LANDING AT VARIOUS LATITUDES .....	113
FIGURE 132: EARTH TO MARS 2022 TYPE IV- LANDER LAUNCH PERIODS - REACHABLE LATITUDES, EQUIVALENT C3, AND VHP .....	114
FIGURE 133: EARTH TO MARS 2022 TYPE IV- LANDER LAUNCH PERIODS - LMST OF LANDING AT VARIOUS LATITUDES.....	114
FIGURE 134: EARTH TO MARS 2022 TYPE IV- LANDER LAUNCH PERIODS - EARTH ELEVATION AT LANDING AT VARIOUS LATITUDES .....	114
FIGURE 135: EARTH TO MARS 2022 TYPE III+ LANDER LAUNCH PERIODS - REACHABLE LATITUDES, EQUIVALENT C3, AND VHP .....	115
FIGURE 136: EARTH TO MARS 2022 TYPE III+ LANDER LAUNCH PERIODS - LMST OF LANDING AT VARIOUS LATITUDES .....	115
FIGURE 137: EARTH TO MARS 2022 TYPE III+ LANDER LAUNCH PERIODS - EARTH ELEVATION AT LANDING AT VARIOUS LATITUDES....	115
FIGURE 138: EARTH TO MARS 2024 TYPE I LANDER LAUNCH PERIODS - REACHABLE LATITUDES, EQUIVALENT C3, AND VHP .....	116
FIGURE 139: EARTH TO MARS 2024 TYPE I LANDER LAUNCH PERIODS - LMST OF LANDING AT VARIOUS LATITUDES .....	116





FIGURE 248: EARTH TO MARS 2039 TYPE II LANDER LAUNCH PERIODS - EARTH ELEVATION AT LANDING AT VARIOUS LATITUDES.....	152
FIGURE 249: EARTH TO MARS 2039 TYPE III- LANDER LAUNCH PERIODS - REACHABLE LATITUDES, EQUIVALENT C3, AND VHP .....	153
FIGURE 250: EARTH TO MARS 2039 TYPE III- LANDER LAUNCH PERIODS - LMST OF LANDING AT VARIOUS LATITUDES .....	153
FIGURE 251: EARTH TO MARS 2039 TYPE III- LANDER LAUNCH PERIODS - EARTH ELEVATION AT LANDING AT VARIOUS LATITUDES ....	153
FIGURE 252: EARTH TO MARS 2039 TYPE IV- LANDER LAUNCH PERIODS - REACHABLE LATITUDES, EQUIVALENT C3, AND VHP .....	154
FIGURE 253: EARTH TO MARS 2039 TYPE IV- LANDER LAUNCH PERIODS - LMST OF LANDING AT VARIOUS LATITUDES.....	154
FIGURE 254: EARTH TO MARS 2039 TYPE IV- LANDER LAUNCH PERIODS - EARTH ELEVATION AT LANDING AT VARIOUS LATITUDES ....	154
FIGURE 255: EARTH TO MARS 2039 TYPE III+ LANDER LAUNCH PERIODS - REACHABLE LATITUDES, EQUIVALENT C3, AND VHP .....	155
FIGURE 256: EARTH TO MARS 2039 TYPE III+ LANDER LAUNCH PERIODS - LMST OF LANDING AT VARIOUS LATITUDES .....	155
FIGURE 257: EARTH TO MARS 2039 TYPE III+ LANDER LAUNCH PERIODS - EARTH ELEVATION AT LANDING AT VARIOUS LATITUDES....	155
FIGURE 258: EARTH TO MARS 2022 TYPE I ORBITER LAUNCH PERIODS - REACHABLE INCLINATION, LAUNCH MASS, AND VHP .....	157
FIGURE 259: EARTH TO MARS 2022 TYPE I ORBITER LAUNCH PERIODS - ASCENDING NODE LMST AND PERIAPSIS LATITUDE (92 DEG INCLINATION) .....	157
FIGURE 260: EARTH TO MARS 2022 TYPE II ORBITER LAUNCH PERIODS - REACHABLE INCLINATION, LAUNCH MASS, AND VHP .....	158
FIGURE 261: EARTH TO MARS 2022 TYPE II ORBITER LAUNCH PERIODS - ASCENDING NODE LMST AND PERIAPSIS LATITUDE (92 DEG INCLINATION) .....	158
FIGURE 262: EARTH TO MARS 2022 TYPE III- ORBITER LAUNCH PERIODS - REACHABLE INCLINATION, LAUNCH MASS, AND VHP .....	159
FIGURE 263: EARTH TO MARS 2022 TYPE III- ORBITER LAUNCH PERIODS - ASCENDING NODE LMST AND PERIAPSIS LATITUDE (92 DEG INCLINATION) .....	159
FIGURE 264: EARTH TO MARS 2022 TYPE IV- ORBITER LAUNCH PERIODS - REACHABLE INCLINATION, LAUNCH MASS, AND VHP.....	160
FIGURE 265: EARTH TO MARS 2022 TYPE IV- ORBITER LAUNCH PERIODS - ASCENDING NODE LMST AND PERIAPSIS LATITUDE (92 DEG INCLINATION) .....	160
FIGURE 266: EARTH TO MARS 2022 TYPE III+ ORBITER LAUNCH PERIODS - REACHABLE INCLINATION, LAUNCH MASS, AND VHP .....	161
FIGURE 267: EARTH TO MARS 2022 TYPE III+ ORBITER LAUNCH PERIODS - ASCENDING NODE LMST AND PERIAPSIS LATITUDE (92 DEG INCLINATION) .....	161
FIGURE 268: EARTH TO MARS 2024 TYPE I ORBITER LAUNCH PERIODS - REACHABLE INCLINATION, LAUNCH MASS, AND VHP .....	162
FIGURE 269: EARTH TO MARS 2024 TYPE I ORBITER LAUNCH PERIODS - ASCENDING NODE LMST AND PERIAPSIS LATITUDE (92 DEG INCLINATION) .....	162
FIGURE 270: EARTH TO MARS 2024 TYPE II ORBITER LAUNCH PERIODS - REACHABLE INCLINATION, LAUNCH MASS, AND VHP .....	163
FIGURE 271: EARTH TO MARS 2024 TYPE II ORBITER LAUNCH PERIODS - ASCENDING NODE LMST AND PERIAPSIS LATITUDE (92 DEG INCLINATION) .....	163
FIGURE 272: EARTH TO MARS 2024 TYPE III- ORBITER LAUNCH PERIODS - REACHABLE INCLINATION, LAUNCH MASS, AND VHP .....	164
FIGURE 273: EARTH TO MARS 2024 TYPE III- ORBITER LAUNCH PERIODS - ASCENDING NODE LMST AND PERIAPSIS LATITUDE (92 DEG INCLINATION) .....	164
FIGURE 274: EARTH TO MARS 2024 TYPE IV- ORBITER LAUNCH PERIODS - REACHABLE INCLINATION, LAUNCH MASS, AND VHP.....	165
FIGURE 275: EARTH TO MARS 2024 TYPE IV- ORBITER LAUNCH PERIODS - ASCENDING NODE LMST AND PERIAPSIS LATITUDE (92 DEG INCLINATION) .....	165
FIGURE 276: EARTH TO MARS 2024 TYPE III+ ORBITER LAUNCH PERIODS - REACHABLE INCLINATION, LAUNCH MASS, AND VHP .....	166
FIGURE 277: EARTH TO MARS 2024 TYPE III+ ORBITER LAUNCH PERIODS - ASCENDING NODE LMST AND PERIAPSIS LATITUDE (92 DEG INCLINATION) .....	166
FIGURE 278: EARTH TO MARS 2026 TYPE I ORBITER LAUNCH PERIODS - REACHABLE INCLINATION, LAUNCH MASS, AND VHP .....	167
FIGURE 279: EARTH TO MARS 2026 TYPE I ORBITER LAUNCH PERIODS - ASCENDING NODE LMST AND PERIAPSIS LATITUDE (92 DEG INCLINATION) .....	167
FIGURE 280: EARTH TO MARS 2026 TYPE II ORBITER LAUNCH PERIODS - REACHABLE INCLINATION, LAUNCH MASS, AND VHP .....	168
FIGURE 281: EARTH TO MARS 2026 TYPE II ORBITER LAUNCH PERIODS - ASCENDING NODE LMST AND PERIAPSIS LATITUDE (92 DEG INCLINATION) .....	168
FIGURE 282: EARTH TO MARS 2026 TYPE III- ORBITER LAUNCH PERIODS - REACHABLE INCLINATION, LAUNCH MASS, AND VHP .....	169
FIGURE 283: EARTH TO MARS 2026 TYPE III- ORBITER LAUNCH PERIODS - ASCENDING NODE LMST AND PERIAPSIS LATITUDE (92 DEG INCLINATION) .....	169
FIGURE 284: EARTH TO MARS 2026 TYPE IV- ORBITER LAUNCH PERIODS - REACHABLE INCLINATION, LAUNCH MASS, AND VHP.....	170
FIGURE 285: EARTH TO MARS 2026 TYPE IV- ORBITER LAUNCH PERIODS - ASCENDING NODE LMST AND PERIAPSIS LATITUDE (92 DEG INCLINATION) .....	170
FIGURE 286: EARTH TO MARS 2026 TYPE III+ ORBITER LAUNCH PERIODS - REACHABLE INCLINATION, LAUNCH MASS, AND VHP .....	171
FIGURE 287: EARTH TO MARS 2026 TYPE III+ ORBITER LAUNCH PERIODS - ASCENDING NODE LMST AND PERIAPSIS LATITUDE (92 DEG INCLINATION) .....	171

INCLINATION) .....	171
FIGURE 288: EARTH TO MARS 2028 TYPE I ORBITER LAUNCH PERIODS - REACHABLE INCLINATION, LAUNCH MASS, AND VHP .....	172
FIGURE 289: EARTH TO MARS 2028 TYPE I ORBITER LAUNCH PERIODS - ASCENDING NODE LMST AND PERIAPSIS LATITUDE (92 DEG INCLINATION) .....	172
FIGURE 290: EARTH TO MARS 2028 TYPE II ORBITER LAUNCH PERIODS - REACHABLE INCLINATION, LAUNCH MASS, AND VHP .....	173
FIGURE 291: EARTH TO MARS 2028 TYPE II ORBITER LAUNCH PERIODS - ASCENDING NODE LMST AND PERIAPSIS LATITUDE (92 DEG INCLINATION) .....	173
FIGURE 292: EARTH TO MARS 2028 TYPE III- ORBITER LAUNCH PERIODS - REACHABLE INCLINATION, LAUNCH MASS, AND VHP .....	174
FIGURE 293: EARTH TO MARS 2028 TYPE III- ORBITER LAUNCH PERIODS - ASCENDING NODE LMST AND PERIAPSIS LATITUDE (92 DEG INCLINATION) .....	174
FIGURE 294: EARTH TO MARS 2028 TYPE IV- ORBITER LAUNCH PERIODS - REACHABLE INCLINATION, LAUNCH MASS, AND VHP .....	175
FIGURE 295: EARTH TO MARS 2028 TYPE IV- ORBITER LAUNCH PERIODS - ASCENDING NODE LMST AND PERIAPSIS LATITUDE (92 DEG INCLINATION) .....	175
FIGURE 296: EARTH TO MARS 2028 TYPE III+ ORBITER LAUNCH PERIODS - REACHABLE INCLINATION, LAUNCH MASS, AND VHP .....	176
FIGURE 297: EARTH TO MARS 2028 TYPE III+ ORBITER LAUNCH PERIODS - ASCENDING NODE LMST AND PERIAPSIS LATITUDE (92 DEG INCLINATION) .....	176
FIGURE 298: EARTH TO MARS 2031 TYPE I ORBITER LAUNCH PERIODS - REACHABLE INCLINATION, LAUNCH MASS, AND VHP .....	177
FIGURE 299: EARTH TO MARS 2031 TYPE I ORBITER LAUNCH PERIODS - ASCENDING NODE LMST AND PERIAPSIS LATITUDE (92 DEG INCLINATION) .....	177
FIGURE 300: EARTH TO MARS 2031 TYPE II ORBITER LAUNCH PERIODS - REACHABLE INCLINATION, LAUNCH MASS, AND VHP .....	178
FIGURE 301: EARTH TO MARS 2031 TYPE II ORBITER LAUNCH PERIODS - ASCENDING NODE LMST AND PERIAPSIS LATITUDE (92 DEG INCLINATION) .....	178
FIGURE 302: EARTH TO MARS 2031 TYPE III- ORBITER LAUNCH PERIODS - REACHABLE INCLINATION, LAUNCH MASS, AND VHP .....	179
FIGURE 303: EARTH TO MARS 2031 TYPE III- ORBITER LAUNCH PERIODS - ASCENDING NODE LMST AND PERIAPSIS LATITUDE (92 DEG INCLINATION) .....	179
FIGURE 304: EARTH TO MARS 2031 TYPE IV- ORBITER LAUNCH PERIODS - REACHABLE INCLINATION, LAUNCH MASS, AND VHP .....	180
FIGURE 305: EARTH TO MARS 2031 TYPE IV- ORBITER LAUNCH PERIODS - ASCENDING NODE LMST AND PERIAPSIS LATITUDE (92 DEG INCLINATION) .....	180
FIGURE 306: EARTH TO MARS 2031 TYPE III+ ORBITER LAUNCH PERIODS - REACHABLE INCLINATION, LAUNCH MASS, AND VHP .....	181
FIGURE 307: EARTH TO MARS 2031 TYPE III+ ORBITER LAUNCH PERIODS - ASCENDING NODE LMST AND PERIAPSIS LATITUDE (92 DEG INCLINATION) .....	181
FIGURE 308: EARTH TO MARS 2033 TYPE I ORBITER LAUNCH PERIODS - REACHABLE INCLINATION, LAUNCH MASS, AND VHP .....	182
FIGURE 309: EARTH TO MARS 2033 TYPE I ORBITER LAUNCH PERIODS - ASCENDING NODE LMST AND PERIAPSIS LATITUDE (92 DEG INCLINATION) .....	182
FIGURE 310: EARTH TO MARS 2033 TYPE II ORBITER LAUNCH PERIODS - REACHABLE INCLINATION, LAUNCH MASS, AND VHP .....	183
FIGURE 311: EARTH TO MARS 2033 TYPE II ORBITER LAUNCH PERIODS - ASCENDING NODE LMST AND PERIAPSIS LATITUDE (92 DEG INCLINATION) .....	183
FIGURE 312: EARTH TO MARS 2033 TYPE III- ORBITER LAUNCH PERIODS - REACHABLE INCLINATION, LAUNCH MASS, AND VHP .....	184
FIGURE 313: EARTH TO MARS 2033 TYPE III- ORBITER LAUNCH PERIODS - ASCENDING NODE LMST AND PERIAPSIS LATITUDE (92 DEG INCLINATION) .....	184
FIGURE 314: EARTH TO MARS 2033 TYPE IV- ORBITER LAUNCH PERIODS - REACHABLE INCLINATION, LAUNCH MASS, AND VHP .....	185
FIGURE 315: EARTH TO MARS 2033 TYPE IV- ORBITER LAUNCH PERIODS - ASCENDING NODE LMST AND PERIAPSIS LATITUDE (92 DEG INCLINATION) .....	185
FIGURE 316: EARTH TO MARS 2033 TYPE III+ ORBITER LAUNCH PERIODS - REACHABLE INCLINATION, LAUNCH MASS, AND VHP .....	186
FIGURE 317: EARTH TO MARS 2033 TYPE III+ ORBITER LAUNCH PERIODS - ASCENDING NODE LMST AND PERIAPSIS LATITUDE (92 DEG INCLINATION) .....	186
FIGURE 318: EARTH TO MARS 2035 TYPE I ORBITER LAUNCH PERIODS - REACHABLE INCLINATION, LAUNCH MASS, AND VHP .....	187
FIGURE 319: EARTH TO MARS 2035 TYPE I ORBITER LAUNCH PERIODS - ASCENDING NODE LMST AND PERIAPSIS LATITUDE (92 DEG INCLINATION) .....	187
FIGURE 320: EARTH TO MARS 2035 TYPE II ORBITER LAUNCH PERIODS - REACHABLE INCLINATION, LAUNCH MASS, AND VHP .....	188
FIGURE 321: EARTH TO MARS 2035 TYPE II ORBITER LAUNCH PERIODS - ASCENDING NODE LMST AND PERIAPSIS LATITUDE (92 DEG INCLINATION) .....	188
FIGURE 322: EARTH TO MARS 2035 TYPE III- ORBITER LAUNCH PERIODS - REACHABLE INCLINATION, LAUNCH MASS, AND VHP .....	189
FIGURE 323: EARTH TO MARS 2035 TYPE III- ORBITER LAUNCH PERIODS - ASCENDING NODE LMST AND PERIAPSIS LATITUDE (92 DEG INCLINATION) .....	189

INCLINATION) .....	189
FIGURE 324: EARTH TO MARS 2035 TYPE IV- ORBITER LAUNCH PERIODS - REACHABLE INCLINATION, LAUNCH MASS, AND VHP .....	190
FIGURE 325: EARTH TO MARS 2035 TYPE IV- ORBITER LAUNCH PERIODS - ASCENDING NODE LMST AND PERIAPSIS LATITUDE (92 DEG INCLINATION) .....	190
FIGURE 326: EARTH TO MARS 2035 TYPE III+ ORBITER LAUNCH PERIODS - REACHABLE INCLINATION, LAUNCH MASS, AND VHP .....	191
FIGURE 327: EARTH TO MARS 2035 TYPE III+ ORBITER LAUNCH PERIODS - ASCENDING NODE LMST AND PERIAPSIS LATITUDE (92 DEG INCLINATION) .....	191
FIGURE 328: EARTH TO MARS 2037 TYPE I ORBITER LAUNCH PERIODS - REACHABLE INCLINATION, LAUNCH MASS, AND VHP .....	192
FIGURE 329: EARTH TO MARS 2037 TYPE I ORBITER LAUNCH PERIODS - ASCENDING NODE LMST AND PERIAPSIS LATITUDE (92 DEG INCLINATION) .....	192
FIGURE 330: EARTH TO MARS 2037 TYPE II ORBITER LAUNCH PERIODS - REACHABLE INCLINATION, LAUNCH MASS, AND VHP .....	193
FIGURE 331: EARTH TO MARS 2037 TYPE II ORBITER LAUNCH PERIODS - ASCENDING NODE LMST AND PERIAPSIS LATITUDE (92 DEG INCLINATION) .....	193
FIGURE 332: EARTH TO MARS 2037 TYPE III- ORBITER LAUNCH PERIODS - REACHABLE INCLINATION, LAUNCH MASS, AND VHP .....	194
FIGURE 333: EARTH TO MARS 2037 TYPE III- ORBITER LAUNCH PERIODS - ASCENDING NODE LMST AND PERIAPSIS LATITUDE (92 DEG INCLINATION) .....	194
FIGURE 334: EARTH TO MARS 2037 TYPE IV- ORBITER LAUNCH PERIODS - REACHABLE INCLINATION, LAUNCH MASS, AND VHP .....	195
FIGURE 335: EARTH TO MARS 2037 TYPE IV- ORBITER LAUNCH PERIODS - ASCENDING NODE LMST AND PERIAPSIS LATITUDE (92 DEG INCLINATION) .....	195
FIGURE 336: EARTH TO MARS 2037 TYPE III+ ORBITER LAUNCH PERIODS - REACHABLE INCLINATION, LAUNCH MASS, AND VHP .....	196
FIGURE 337: EARTH TO MARS 2037 TYPE III+ ORBITER LAUNCH PERIODS - ASCENDING NODE LMST AND PERIAPSIS LATITUDE (92 DEG INCLINATION) .....	196
FIGURE 338: EARTH TO MARS 2039 TYPE I ORBITER LAUNCH PERIODS - REACHABLE INCLINATION, LAUNCH MASS, AND VHP .....	197
FIGURE 339: EARTH TO MARS 2039 TYPE I ORBITER LAUNCH PERIODS - ASCENDING NODE LMST AND PERIAPSIS LATITUDE (92 DEG INCLINATION) .....	197
FIGURE 340: EARTH TO MARS 2039 TYPE II ORBITER LAUNCH PERIODS - REACHABLE INCLINATION, LAUNCH MASS, AND VHP .....	198
FIGURE 341: EARTH TO MARS 2039 TYPE II ORBITER LAUNCH PERIODS - ASCENDING NODE LMST AND PERIAPSIS LATITUDE (92 DEG INCLINATION) .....	198
FIGURE 342: EARTH TO MARS 2039 TYPE III- ORBITER LAUNCH PERIODS - REACHABLE INCLINATION, LAUNCH MASS, AND VHP .....	199
FIGURE 343: EARTH TO MARS 2039 TYPE III- ORBITER LAUNCH PERIODS - ASCENDING NODE LMST AND PERIAPSIS LATITUDE (92 DEG INCLINATION) .....	199
FIGURE 344: EARTH TO MARS 2039 TYPE IV- ORBITER LAUNCH PERIODS - REACHABLE INCLINATION, LAUNCH MASS, AND VHP .....	200
FIGURE 345: EARTH TO MARS 2039 TYPE IV- ORBITER LAUNCH PERIODS - ASCENDING NODE LMST AND PERIAPSIS LATITUDE (92 DEG INCLINATION) .....	200
FIGURE 346: EARTH TO MARS 2039 TYPE III+ ORBITER LAUNCH PERIODS - REACHABLE INCLINATION, LAUNCH MASS, AND VHP .....	201
FIGURE 347: EARTH TO MARS 2039 TYPE III+ ORBITER LAUNCH PERIODS - ASCENDING NODE LMST AND PERIAPSIS LATITUDE (92 DEG INCLINATION) .....	201
FIGURE 348: EARTH TO MARS 2022 TYPE I/II - LAUNCH AND ARRIVAL ENERGY .....	205
FIGURE 349: EARTH TO MARS 2022 TYPE I/II – MAXIMUM REACHABLE NORTH AND SOUTH LATITUDE.....	206
FIGURE 350: EARTH TO MARS 2022 TYPE I/II – LANDING LMST FOR PROGRADE ENTRIES.....	207
FIGURE 351: EARTH TO MARS 2022 TYPE I/II – LANDING LMST FOR RETROGRADE ENTRIES.....	208
FIGURE 352: EARTH TO MARS 2022 TYPE I/II – LMST OF THE ASCENDING NODE FOR NORTH AND SOUTH APPROACHES.....	209
FIGURE 353: EARTH TO MARS 2024 TYPE III/IV– LAUNCH AND ARRIVAL ENERGY .....	210
FIGURE 354: EARTH TO MARS 2022 TYPE III/IV– MAXIMUM REACHABLE NORTH AND SOUTH LATITUDE .....	211
FIGURE 355: EARTH TO MARS 2022 TYPE III/IV– LANDING LMST FOR PROGRADE ENTRIES .....	212
FIGURE 356: EARTH TO MARS 2022 TYPE III/IV– LANDING LMST FOR RETROGRADE ENTRIES .....	213
FIGURE 357: EARTH TO MARS 2022 TYPE III/IV– LMST OF THE ASCENDING NODE FOR NORTH AND SOUTH APPROACHES .....	214
FIGURE 358: EARTH TO MARS 2024 TYPE III/IV+ – LAUNCH AND ARRIVAL ENERGY .....	215
FIGURE 359: EARTH TO MARS 2022 TYPE III/IV+ – MAXIMUM REACHABLE NORTH AND SOUTH LATITUDE .....	216
FIGURE 360: EARTH TO MARS 2022 TYPE III/IV+ – LANDING LMST FOR PROGRADE ENTRIES.....	217
FIGURE 361: EARTH TO MARS 2022 TYPE III/IV+ – LANDING LMST FOR RETROGRADE ENTRIES .....	218
FIGURE 362: EARTH TO MARS 2022 TYPE III/IV+ – LMST OF THE ASCENDING NODE FOR NORTH AND SOUTH APPROACHES.....	219
FIGURE 363: EARTH TO MARS 2024 TYPE I/II - LAUNCH AND ARRIVAL ENERGY .....	222
FIGURE 364: EARTH TO MARS 2024 TYPE I/II – MAXIMUM REACHABLE NORTH AND SOUTH LATITUDE.....	223

FIGURE 365: EARTH TO MARS 2024 TYPE I/II – LANDING LMST FOR PROGRADE ENTRIES.....	224
FIGURE 366: EARTH TO MARS 2024 TYPE I/II – LANDING LMST FOR RETROGRADE ENTRIES.....	225
FIGURE 367: EARTH TO MARS 2024 TYPE I/II – LMST OF THE ASCENDING NODE FOR NORTH AND SOUTH APPROACHES.....	226
FIGURE 368: EARTH TO MARS 2024 TYPE III/IV- – LAUNCH AND ARRIVAL ENERGY .....	227
FIGURE 369: EARTH TO MARS 20242 TYPE III/IV- – MAXIMUM REACHABLE NORTH AND SOUTH LATITUDE .....	228
FIGURE 370: EARTH TO MARS 2024 TYPE III/IV- – LANDING LMST FOR PROGRADE ENTRIES .....	229
FIGURE 371: EARTH TO MARS 2024 TYPE III/IV- – LANDING LMST FOR RETROGRADE ENTRIES .....	230
FIGURE 372: EARTH TO MARS 2024 TYPE III/IV- – LMST OF THE ASCENDING NODE FOR NORTH AND SOUTH APPROACHES .....	231
FIGURE 373: EARTH TO MARS 2024 TYPE III/IV+ – LAUNCH AND ARRIVAL ENERGY .....	232
FIGURE 374: EARTH TO MARS 2024 TYPE III/IV+ – MAXIMUM REACHABLE NORTH AND SOUTH LATITUDE .....	233
FIGURE 375: EARTH TO MARS 2024 TYPE III/IV+ – LANDING LMST FOR PROGRADE ENTRIES.....	234
FIGURE 376: EARTH TO MARS 2024 TYPE III/IV+ – LANDING LMST FOR RETROGRADE ENTRIES .....	235
FIGURE 377: EARTH TO MARS 2024 TYPE III/IV+ – LMST OF THE ASCENDING NODE FOR NORTH AND SOUTH APPROACHES.....	236
FIGURE 378: EARTH TO MARS 2026 TYPE I/II - LAUNCH AND ARRIVAL ENERGY .....	239
FIGURE 379: EARTH TO MARS 2026 TYPE I/II – MAXIMUM REACHABLE NORTH AND SOUTH LATITUDE.....	240
FIGURE 380: EARTH TO MARS 2026 TYPE I/II – LANDING LMST FOR PROGRADE ENTRIES.....	241
FIGURE 381: EARTH TO MARS 2026 TYPE I/II – LANDING LMST FOR RETROGRADE ENTRIES.....	242
FIGURE 382: EARTH TO MARS 2026 TYPE I/II – LMST OF THE ASCENDING NODE FOR NORTH AND SOUTH APPROACHES.....	243
FIGURE 383: EARTH TO MARS 2026 TYPE III/IV- – LAUNCH AND ARRIVAL ENERGY .....	244
FIGURE 384: EARTH TO MARS 20262 TYPE III/IV- – MAXIMUM REACHABLE NORTH AND SOUTH LATITUDE .....	245
FIGURE 385: EARTH TO MARS 2026 TYPE III/IV- – LANDING LMST FOR PROGRADE ENTRIES .....	246
FIGURE 386: EARTH TO MARS 2026 TYPE III/IV- – LANDING LMST FOR RETROGRADE ENTRIES .....	247
FIGURE 387: EARTH TO MARS 2026 TYPE III/IV- – LMST OF THE ASCENDING NODE FOR NORTH AND SOUTH APPROACHES .....	248
FIGURE 388: EARTH TO MARS 2026 TYPE III/IV+ – LAUNCH AND ARRIVAL ENERGY .....	249
FIGURE 389: EARTH TO MARS 2026 TYPE III/IV+ – MAXIMUM REACHABLE NORTH AND SOUTH LATITUDE .....	250
FIGURE 390: EARTH TO MARS 2026 TYPE III/IV+ – LANDING LMST FOR PROGRADE ENTRIES.....	251
FIGURE 391: EARTH TO MARS 2026 TYPE III/IV+ – LANDING LMST FOR RETROGRADE ENTRIES .....	252
FIGURE 392: EARTH TO MARS 2026 TYPE III/IV+ – LMST OF THE ASCENDING NODE FOR NORTH AND SOUTH APPROACHES.....	253
FIGURE 393: EARTH TO MARS 2028 TYPE I/II - LAUNCH AND ARRIVAL ENERGY .....	256
FIGURE 394: EARTH TO MARS 2028 TYPE I/II – MAXIMUM REACHABLE NORTH AND SOUTH LATITUDE.....	257
FIGURE 395: EARTH TO MARS 2028 TYPE I/II – LANDING LMST FOR PROGRADE ENTRIES.....	258
FIGURE 396: EARTH TO MARS 2028 TYPE I/II – LANDING LMST FOR RETROGRADE ENTRIES.....	259
FIGURE 397: EARTH TO MARS 2028 TYPE I/II – LMST OF THE ASCENDING NODE FOR NORTH AND SOUTH APPROACHES.....	260
FIGURE 398: EARTH TO MARS 2028 TYPE III/IV- – LAUNCH AND ARRIVAL ENERGY .....	261
FIGURE 399: EARTH TO MARS 20282 TYPE III/IV- – MAXIMUM REACHABLE NORTH AND SOUTH LATITUDE .....	262
FIGURE 400: EARTH TO MARS 2028 TYPE III/IV- – LANDING LMST FOR PROGRADE ENTRIES .....	263
FIGURE 401: EARTH TO MARS 2028 TYPE III/IV- – LANDING LMST FOR RETROGRADE ENTRIES .....	264
FIGURE 402: EARTH TO MARS 2028 TYPE III/IV- – LMST OF THE ASCENDING NODE FOR NORTH AND SOUTH APPROACHES .....	265
FIGURE 403: EARTH TO MARS 2028 TYPE III/IV+ – LAUNCH AND ARRIVAL ENERGY .....	266
FIGURE 404: EARTH TO MARS 2028 TYPE III/IV+ – MAXIMUM REACHABLE NORTH AND SOUTH LATITUDE .....	267
FIGURE 405: EARTH TO MARS 2028 TYPE III/IV+ – LANDING LMST FOR PROGRADE ENTRIES.....	268
FIGURE 406: EARTH TO MARS 2028 TYPE III/IV+ – LANDING LMST FOR RETROGRADE ENTRIES .....	269
FIGURE 407: EARTH TO MARS 2028 TYPE III/IV+ – LMST OF THE ASCENDING NODE FOR NORTH AND SOUTH APPROACHES.....	270
FIGURE 408: EARTH TO MARS 2031 TYPE I/II - LAUNCH AND ARRIVAL ENERGY .....	273
FIGURE 409: EARTH TO MARS 2031 TYPE I/II – MAXIMUM REACHABLE NORTH AND SOUTH LATITUDE.....	274
FIGURE 410: EARTH TO MARS 2031 TYPE I/II – LANDING LMST FOR PROGRADE ENTRIES.....	275
FIGURE 411: EARTH TO MARS 2031 TYPE I/II – LANDING LMST FOR RETROGRADE ENTRIES.....	276
FIGURE 412: EARTH TO MARS 2031 TYPE I/II – LMST OF THE ASCENDING NODE FOR NORTH AND SOUTH APPROACHES.....	277
FIGURE 413: EARTH TO MARS 2031 TYPE III/IV- – LAUNCH AND ARRIVAL ENERGY .....	278
FIGURE 414: EARTH TO MARS 20312 TYPE III/IV- – MAXIMUM REACHABLE NORTH AND SOUTH LATITUDE .....	279
FIGURE 415: EARTH TO MARS 2031 TYPE III/IV- – LANDING LMST FOR PROGRADE ENTRIES .....	280
FIGURE 416: EARTH TO MARS 2031 TYPE III/IV- – LANDING LMST FOR RETROGRADE ENTRIES .....	281
FIGURE 417: EARTH TO MARS 2031 TYPE III/IV- – LMST OF THE ASCENDING NODE FOR NORTH AND SOUTH APPROACHES .....	282
FIGURE 418: EARTH TO MARS 2031 TYPE III/IV+ – LAUNCH AND ARRIVAL ENERGY .....	283

FIGURE 419: EARTH TO MARS 2031 TYPE III/IV+ – MAXIMUM REACHABLE NORTH AND SOUTH LATITUDE .....	284
FIGURE 420: EARTH TO MARS 2031 TYPE III/IV+ – LANDING LMST FOR PROGRADE ENTRIES.....	285
FIGURE 421: EARTH TO MARS 2031 TYPE III/IV+ – LANDING LMST FOR RETROGRADE ENTRIES .....	286
FIGURE 422: EARTH TO MARS 2031 TYPE III/IV+ – LMST OF THE ASCENDING NODE FOR NORTH AND SOUTH APPROACHES.....	287
FIGURE 423: EARTH TO MARS 2033 TYPE I/II - LAUNCH AND ARRIVAL ENERGY .....	290
FIGURE 424: EARTH TO MARS 2033 TYPE I/II – MAXIMUM REACHABLE NORTH AND SOUTH LATITUDE.....	291
FIGURE 425: EARTH TO MARS 2033 TYPE I/II – LANDING LMST FOR PROGRADE ENTRIES.....	292
FIGURE 426: EARTH TO MARS 2033 TYPE I/II – LANDING LMST FOR RETROGRADE ENTRIES.....	293
FIGURE 427: EARTH TO MARS 2033 TYPE I/II – LMST OF THE ASCENDING NODE FOR NORTH AND SOUTH APPROACHES.....	294
FIGURE 428: EARTH TO MARS 2033 TYPE III/IV– – LAUNCH AND ARRIVAL ENERGY .....	295
FIGURE 429: EARTH TO MARS 20332 TYPE III/IV– – MAXIMUM REACHABLE NORTH AND SOUTH LATITUDE .....	296
FIGURE 430: EARTH TO MARS 2033 TYPE III/IV– – LANDING LMST FOR PROGRADE ENTRIES .....	297
FIGURE 431: EARTH TO MARS 2033 TYPE III/IV– – LANDING LMST FOR RETROGRADE ENTRIES .....	298
FIGURE 432: EARTH TO MARS 2033 TYPE III/IV– – LMST OF THE ASCENDING NODE FOR NORTH AND SOUTH APPROACHES .....	299
FIGURE 433: EARTH TO MARS 2033 TYPE III/IV+ – LAUNCH AND ARRIVAL ENERGY .....	300
FIGURE 434: EARTH TO MARS 2033 TYPE III/IV+ – MAXIMUM REACHABLE NORTH AND SOUTH LATITUDE .....	301
FIGURE 435: EARTH TO MARS 2033 TYPE III/IV+ – LANDING LMST FOR PROGRADE ENTRIES.....	302
FIGURE 436: EARTH TO MARS 2033 TYPE III/IV+ – LANDING LMST FOR RETROGRADE ENTRIES .....	303
FIGURE 437: EARTH TO MARS 2033 TYPE III/IV+ – LMST OF THE ASCENDING NODE FOR NORTH AND SOUTH APPROACHES.....	304
FIGURE 438: EARTH TO MARS 2035 TYPE I/II - LAUNCH AND ARRIVAL ENERGY .....	307
FIGURE 439: EARTH TO MARS 2035 TYPE I/II – MAXIMUM REACHABLE NORTH AND SOUTH LATITUDE.....	308
FIGURE 440: EARTH TO MARS 2035 TYPE I/II – LANDING LMST FOR PROGRADE ENTRIES.....	309
FIGURE 441: EARTH TO MARS 2035 TYPE I/II – LANDING LMST FOR RETROGRADE ENTRIES.....	310
FIGURE 442: EARTH TO MARS 2035 TYPE I/II – LMST OF THE ASCENDING NODE FOR NORTH AND SOUTH APPROACHES.....	311
FIGURE 443: EARTH TO MARS 2035 TYPE III/IV– – LAUNCH AND ARRIVAL ENERGY .....	312
FIGURE 444: EARTH TO MARS 20352 TYPE III/IV– – MAXIMUM REACHABLE NORTH AND SOUTH LATITUDE .....	313
FIGURE 445: EARTH TO MARS 2035 TYPE III/IV– – LANDING LMST FOR PROGRADE ENTRIES .....	314
FIGURE 446: EARTH TO MARS 2035 TYPE III/IV– – LANDING LMST FOR RETROGRADE ENTRIES .....	315
FIGURE 447: EARTH TO MARS 2035 TYPE III/IV– – LMST OF THE ASCENDING NODE FOR NORTH AND SOUTH APPROACHES .....	316
FIGURE 448: EARTH TO MARS 2035 TYPE III/IV+ – LAUNCH AND ARRIVAL ENERGY .....	317
FIGURE 449: EARTH TO MARS 2035 TYPE III/IV+ – MAXIMUM REACHABLE NORTH AND SOUTH LATITUDE .....	318
FIGURE 450: EARTH TO MARS 2035 TYPE III/IV+ – LANDING LMST FOR PROGRADE ENTRIES.....	319
FIGURE 451: EARTH TO MARS 2035 TYPE III/IV+ – LANDING LMST FOR RETROGRADE ENTRIES .....	320
FIGURE 452: EARTH TO MARS 2035 TYPE III/IV+ – LMST OF THE ASCENDING NODE FOR NORTH AND SOUTH APPROACHES.....	321
FIGURE 453: EARTH TO MARS 2037 TYPE I/II - LAUNCH AND ARRIVAL ENERGY .....	324
FIGURE 454: EARTH TO MARS 2037 TYPE I/II – MAXIMUM REACHABLE NORTH AND SOUTH LATITUDE.....	325
FIGURE 455: EARTH TO MARS 2037 TYPE I/II – LANDING LMST FOR PROGRADE ENTRIES .....	326
FIGURE 456: EARTH TO MARS 2037 TYPE I/II – LANDING LMST FOR RETROGRADE ENTRIES.....	327
FIGURE 457: EARTH TO MARS 2037 TYPE I/II – LMST OF THE ASCENDING NODE FOR NORTH AND SOUTH APPROACHES.....	328
FIGURE 458: EARTH TO MARS 2037 TYPE III/IV– – LAUNCH AND ARRIVAL ENERGY .....	329
FIGURE 459: EARTH TO MARS 20372 TYPE III/IV– – MAXIMUM REACHABLE NORTH AND SOUTH LATITUDE .....	330
FIGURE 460: EARTH TO MARS 2037 TYPE III/IV– – LANDING LMST FOR PROGRADE ENTRIES .....	331
FIGURE 461: EARTH TO MARS 2037 TYPE III/IV– – LANDING LMST FOR RETROGRADE ENTRIES .....	332
FIGURE 462: EARTH TO MARS 2037 TYPE III/IV– – LMST OF THE ASCENDING NODE FOR NORTH AND SOUTH APPROACHES .....	333
FIGURE 463: EARTH TO MARS 2037 TYPE III/IV+ – LAUNCH AND ARRIVAL ENERGY .....	334
FIGURE 464: EARTH TO MARS 2037 TYPE III/IV+ – MAXIMUM REACHABLE NORTH AND SOUTH LATITUDE .....	335
FIGURE 465: EARTH TO MARS 2037 TYPE III/IV+ – LANDING LMST FOR PROGRADE ENTRIES.....	336
FIGURE 466: EARTH TO MARS 2037 TYPE III/IV+ – LANDING LMST FOR RETROGRADE ENTRIES .....	337
FIGURE 467: EARTH TO MARS 2037 TYPE III/IV+ – LMST OF THE ASCENDING NODE FOR NORTH AND SOUTH APPROACHES.....	338
FIGURE 468: EARTH TO MARS 2039 TYPE I/II - LAUNCH AND ARRIVAL ENERGY .....	341
FIGURE 469: EARTH TO MARS 2039 TYPE I/II – MAXIMUM REACHABLE NORTH AND SOUTH LATITUDE.....	342
FIGURE 470: EARTH TO MARS 2039 TYPE I/II – LANDING LMST FOR PROGRADE ENTRIES .....	343
FIGURE 471: EARTH TO MARS 2039 TYPE I/II – LANDING LMST FOR RETROGRADE ENTRIES .....	344
FIGURE 472: EARTH TO MARS 2039 TYPE I/II – LMST OF THE ASCENDING NODE FOR NORTH AND SOUTH APPROACHES .....	345

FIGURE 473: EARTH TO MARS 2039 TYPE III/IV- – LAUNCH AND ARRIVAL ENERGY .....	346
FIGURE 474: EARTH TO MARS 20392 TYPE III/IV- – MAXIMUM REACHABLE NORTH AND SOUTH LATITUDE .....	347
FIGURE 475: EARTH TO MARS 2039 TYPE III/IV- – LANDING LMST FOR PROGRADE ENTRIES .....	348
FIGURE 476: EARTH TO MARS 2039 TYPE III/IV- – LANDING LMST FOR RETROGRADE ENTRIES .....	349
FIGURE 477: EARTH TO MARS 2039 TYPE III/IV- – LMST OF THE ASCENDING NODE FOR NORTH AND SOUTH APPROACHES .....	350
FIGURE 478: EARTH TO MARS 2039 TYPE III/IV+ – LAUNCH AND ARRIVAL ENERGY .....	351
FIGURE 479: EARTH TO MARS 2039 TYPE III/IV+ – MAXIMUM REACHABLE NORTH AND SOUTH LATITUDE .....	352
FIGURE 480: EARTH TO MARS 2039 TYPE III/IV+ – LANDING LMST FOR PROGRADE ENTRIES .....	353
FIGURE 481: EARTH TO MARS 2039 TYPE III/IV+ – LANDING LMST FOR RETROGRADE ENTRIES .....	354
FIGURE 482: EARTH TO MARS 2039 TYPE III/IV+ – LMST OF THE ASCENDING NODE FOR NORTH AND SOUTH APPROACHES.....	355
FIGURE 483: MINIMUM C3 AND ASSOCIATED VHP FOR MARS TO EARTH TYPE I AND II TRAJECTORIES, 2022-2041 .....	357
FIGURE 484: MINIMUM C3 AND ASSOCIATED VHP FOR MARS TO EARTH TYPE III- AND IV- TRAJECTORIES, 2022-2041.....	357
FIGURE 485: MINIMUM C3 AND ASSOCIATED VHP FOR MARS TO EARTH TYPE III+ AND IV+ TRAJECTORIES, 2022-2041 .....	357
FIGURE 486: MINIMUM VHP AND ASSOCIATED C3 FOR MARS TO EARTH TYPE I AND II TRAJECTORIES, 2022-2041 .....	358
FIGURE 487: MINIMUM VHP AND ASSOCIATED C3 FOR MARS TO EARTH TYPE III- AND IV- TRAJECTORIES, 2022-2041.....	358
FIGURE 488: MINIMUM VHP AND ASSOCIATED C3 FOR MARS TO EARTH TYPE III+ AND IV+ TRAJECTORIES, 2022-2041 .....	358
FIGURE 489: C3/VHP PARETO FRONTS FOR MARS TO EARTH TYPE I AND II TRAJECTORIES .....	359
FIGURE 490: C3/VHP PARETO FRONTS FOR MARS TO EARTH TYPE III- AND IV- TRAJECTORIES .....	359
FIGURE 491: C3/VHP PARETO FRONTS FOR MARS TO EARTH TYPE III+ AND IV+ TRAJECTORIES.....	359
FIGURE 492: MARS TO EARTH 2024 TYPE I LAUNCH PERIODS.....	360
FIGURE 493: MARS TO EARTH 2024 TYPE II LAUNCH PERIODS.....	361
FIGURE 494: MARS TO EARTH 2024 TYPE III- LAUNCH PERIODS.....	361
FIGURE 495: MARS TO EARTH 2024 TYPE IV- LAUNCH PERIODS .....	361
FIGURE 496: MARS TO EARTH 2024 TYPE III+ LAUNCH PERIODS.....	362
FIGURE 497: MARS TO EARTH 2026 TYPE I LAUNCH PERIODS.....	362
FIGURE 498: MARS TO EARTH 2026 TYPE II LAUNCH PERIODS.....	362
FIGURE 499: MARS TO EARTH 2026 TYPE III- LAUNCH PERIODS.....	363
FIGURE 500: MARS TO EARTH 2026 TYPE IV- LAUNCH PERIODS .....	363
FIGURE 501: MARS TO EARTH 2026 TYPE III+ LAUNCH PERIODS.....	363
FIGURE 502: MARS TO EARTH 2026 TYPE IV+ LAUNCH PERIODS.....	364
FIGURE 503: MARS TO EARTH 2028 TYPE I LAUNCH PERIODS.....	364
FIGURE 504: MARS TO EARTH 2028 TYPE II LAUNCH PERIODS.....	364
FIGURE 505: MARS TO EARTH 2028 TYPE III- LAUNCH PERIODS.....	365
FIGURE 506: MARS TO EARTH 2028 TYPE IV- LAUNCH PERIODS .....	365
FIGURE 507: MARS TO EARTH 2028 TYPE III+ LAUNCH PERIODS.....	365
FIGURE 508: MARS TO EARTH 2028 TYPE IV+ LAUNCH PERIODS.....	366
FIGURE 509: MARS TO EARTH 2031 TYPE I LAUNCH PERIODS.....	366
FIGURE 510: MARS TO EARTH 2031 TYPE II LAUNCH PERIODS.....	366
FIGURE 511: MARS TO EARTH 2031 TYPE IV- LAUNCH PERIODS .....	367
FIGURE 512: MARS TO EARTH 2033 TYPE I LAUNCH PERIODS.....	367
FIGURE 513: MARS TO EARTH 2033 TYPE II LAUNCH PERIODS.....	367
FIGURE 514: MARS TO EARTH 2033 TYPE III- LAUNCH PERIODS.....	368
FIGURE 515: MARS TO EARTH 2033 TYPE IV- LAUNCH PERIODS .....	368
FIGURE 516: MARS TO EARTH 2035 TYPE I LAUNCH PERIODS.....	368
FIGURE 517: MARS TO EARTH 2035 TYPE II LAUNCH PERIODS.....	369
FIGURE 518: MARS TO EARTH 2035 TYPE III- LAUNCH PERIODS.....	369
FIGURE 519: MARS TO EARTH 2035 TYPE IV- LAUNCH PERIODS .....	369
FIGURE 520: MARS TO EARTH 2037 TYPE I LAUNCH PERIODS.....	370
FIGURE 521: MARS TO EARTH 2037 TYPE II LAUNCH PERIODS.....	370
FIGURE 522: MARS TO EARTH 2037 TYPE III- LAUNCH PERIODS.....	370
FIGURE 523: MARS TO EARTH 2037 TYPE IV- LAUNCH PERIODS .....	371
FIGURE 524: MARS TO EARTH 2039 TYPE I LAUNCH PERIODS.....	371
FIGURE 525: MARS TO EARTH 2039 TYPE II LAUNCH PERIODS.....	371
FIGURE 526: MARS TO EARTH 2039 TYPE III- LAUNCH PERIODS.....	372

FIGURE 527: MARS TO EARTH 2039 TYPE IV- LAUNCH PERIODS .....	372
FIGURE 528: MARS TO EARTH 2041 TYPE I LAUNCH PERIODS.....	372
FIGURE 529: MARS TO EARTH 2041 TYPE II LAUNCH PERIODS.....	373
FIGURE 530: MARS TO EARTH 2041 TYPE III- LAUNCH PERIODS .....	373
FIGURE 531: MARS TO EARTH 2041 TYPE IV- LAUNCH PERIODS .....	373
FIGURE 532: MARS TO EARTH 2041 TYPE III+ LAUNCH PERIODS.....	374
FIGURE 533: MARS TO EARTH 2024 TYPE I//II – LAUNCH/ARRIVAL ENERGY AND UTTR LANDING TIMES .....	376
FIGURE 534: MARS TO EARTH 2024 TYPE III//IV- – LAUNCH/ARRIVAL ENERGY AND UTTR LANDING TIMES.....	377
FIGURE 535: MARS TO EARTH 2024 TYPE III//IV+ – LAUNCH/ARRIVAL ENERGY AND UTTR LANDING TIMES .....	378
FIGURE 536: MARS TO EARTH 2026 TYPE I//II – LAUNCH/ARRIVAL ENERGY AND UTTR LANDING TIMES .....	380
FIGURE 537: MARS TO EARTH 2026 TYPE III//IV- – LAUNCH/ARRIVAL ENERGY AND UTTR LANDING TIMES.....	381
FIGURE 538: MARS TO EARTH 2026 TYPE III//IV+ – LAUNCH/ARRIVAL ENERGY AND UTTR LANDING TIMES .....	382
FIGURE 539: MARS TO EARTH 2028 TYPE I//II – LAUNCH/ARRIVAL ENERGY AND UTTR LANDING TIMES .....	384
FIGURE 540: MARS TO EARTH 2028 TYPE III//IV- – LAUNCH/ARRIVAL ENERGY AND UTTR LANDING TIMES.....	385
FIGURE 541: MARS TO EARTH 2028 TYPE III//IV+ – LAUNCH/ARRIVAL ENERGY AND UTTR LANDING TIMES .....	386
FIGURE 542: MARS TO EARTH 2031 TYPE I//II – LAUNCH/ARRIVAL ENERGY AND UTTR LANDING TIMES .....	388
FIGURE 543: MARS TO EARTH 2031 TYPE III//IV- – LAUNCH/ARRIVAL ENERGY AND UTTR LANDING TIMES.....	389
FIGURE 544: MARS TO EARTH 2024 TYPE III//IV+ – LAUNCH/ARRIVAL ENERGY AND UTTR LANDING TIMES .....	390
FIGURE 545: MARS TO EARTH 2033 TYPE I//II – LAUNCH/ARRIVAL ENERGY AND UTTR LANDING TIMES .....	392
FIGURE 546: MARS TO EARTH 2033 TYPE III//IV- – LAUNCH/ARRIVAL ENERGY AND UTTR LANDING TIMES.....	393
FIGURE 547: MARS TO EARTH 2033 TYPE III//IV+ – LAUNCH/ARRIVAL ENERGY AND UTTR LANDING TIMES .....	394
FIGURE 548: MARS TO EARTH 2035 TYPE I//II – LAUNCH/ARRIVAL ENERGY AND UTTR LANDING TIMES .....	396
FIGURE 549: MARS TO EARTH 2035 TYPE III//IV- – LAUNCH/ARRIVAL ENERGY AND UTTR LANDING TIMES.....	397
FIGURE 550: MARS TO EARTH 2035 TYPE III//IV+ – LAUNCH/ARRIVAL ENERGY AND UTTR LANDING TIMES .....	398
FIGURE 551: MARS TO EARTH 2037 TYPE I//II – LAUNCH/ARRIVAL ENERGY AND UTTR LANDING TIMES .....	400
FIGURE 552: MARS TO EARTH 2037 TYPE III//IV- – LAUNCH/ARRIVAL ENERGY AND UTTR LANDING TIMES.....	401
FIGURE 553: MARS TO EARTH 2037 TYPE III//IV+ – LAUNCH/ARRIVAL ENERGY AND UTTR LANDING TIMES .....	402
FIGURE 554: MARS TO EARTH 2039 TYPE I//II – LAUNCH/ARRIVAL ENERGY AND UTTR LANDING TIMES .....	404
FIGURE 555: MARS TO EARTH 2039 TYPE III//IV- – LAUNCH/ARRIVAL ENERGY AND UTTR LANDING TIMES.....	405
FIGURE 556: MARS TO EARTH 2039 TYPE III//IV+ – LAUNCH/ARRIVAL ENERGY AND UTTR LANDING TIMES .....	406
FIGURE 557: MARS TO EARTH 2041 TYPE I//II – LAUNCH/ARRIVAL ENERGY AND UTTR LANDING TIMES .....	408
FIGURE 558: MARS TO EARTH 2041 TYPE III//IV- – LAUNCH/ARRIVAL ENERGY AND UTTR LANDING TIMES.....	409
FIGURE 559: MARS TO EARTH 2041 TYPE III//IV+ – LAUNCH/ARRIVAL ENERGY AND UTTR LANDING TIMES .....	410

## List of Tables

TABLE 1: MARS GRAVITY FIELD PARAMETERS .....	4
TABLE 2: MARS POLE AND PRIME MERIDIAN PARAMETERS .....	5
TABLE 3: MARS SHAPE PARAMETERS .....	5
TABLE 4: PHOBOS GRAVITATIONAL AND SHAPE PARAMETERS .....	5
TABLE 5: DEIMOS GRAVITATIONAL AND SHAPE PARAMETERS.....	5
TABLE 6: MARS SEASONS.....	6
TABLE 7: OFFSET BETWEEN MARS IAU VECTOR AND MARS VERNAL EQUINOX DIRECTIONS .....	8
TABLE 8: SIMPLIFIED MARS ATMOSPHERE MODEL PARAMETERS .....	11
TABLE 9: EARTH GRAVITY PARAMETERS.....	13
TABLE 10: EARTH POLE AND PRIME MERIDIAN PARAMETERS.....	14
TABLE 11: EARTH SHAPE PARAMETERS.....	14
TABLE 12: LUNAR GRAVITY AND SHAPE PARAMETERS .....	14
TABLE 13: COORDINATE FRAME DEFINITIONS .....	15
TABLE 14: GRAVITATION PARAMETERS OF DE438 .....	17
TABLE 15: GRAVITATION PARAMETERS FROM MAR097 .....	17
TABLE 16: ASTRONOMICAL CONSTANTS.....	17
TABLE 17: SEASONS, APSES, AND SEASON STARTS: 2022-2041.....	18
TABLE 18: ATLAS V BASE CONFIGURATIONS .....	24
TABLE 19: FALCON BASE CONFIGURATIONS.....	25
TABLE 20: LAUNCH VEHICLE CURVE FIT COEFFICIENTS.....	28
TABLE 21: EAST COAST LAUNCH DECLINATION PERFORMANCE PENALTY COEFFICIENTS.....	31
TABLE 22: V-INFINITY VECTOR PARAMETERS .....	35
TABLE 23: SELECTION OF SEP THRUSTERS AND ASSOCIATED PARAMETERS.....	43
TABLE 24: RULES-OF-THUMB FOR MARS SEP MISSIONS .....	46
TABLE 25: OPTIMAL DATE RANGES FOR SEP TRANSFERS .....	50
TABLE 26: ASCENDING NODE AND ARGUMENT OF PERIAPSIS RATES FOR VARIOUS ORBIT SIZES AND INCLINATIONS.....	73
TABLE 27: HISTORICAL MARS AEROBRAKING MISSIONS.....	88
TABLE 28: EARTH TO MARS 2022 OPTIMAL LAUNCH/ARRIVAL DATA .....	203
TABLE 29: EARTH TO MARS 2024 OPTIMAL LAUNCH/ARRIVAL DATA .....	220
TABLE 30: EARTH TO MARS 2026 OPTIMAL LAUNCH/ARRIVAL DATA .....	237
TABLE 31: EARTH TO MARS 2028 OPTIMAL LAUNCH/ARRIVAL DATA .....	254
TABLE 32: EARTH TO MARS 2031 OPTIMAL LAUNCH/ARRIVAL DATA .....	271
TABLE 33: EARTH TO MARS 2033 OPTIMAL LAUNCH/ARRIVAL DATA .....	288
TABLE 34: EARTH TO MARS 2035 OPTIMAL LAUNCH/ARRIVAL DATA .....	305
TABLE 35: EARTH TO MARS 2037 OPTIMAL LAUNCH/ARRIVAL DATA .....	322
TABLE 36: EARTH TO MARS 2039 OPTIMAL LAUNCH/ARRIVAL DATA .....	339
TABLE 37: MARS TO EARTH 2024 OPTIMAL LAUNCH/ARRIVAL DATA .....	375
TABLE 38: MARS TO EARTH 2026 OPTIMAL LAUNCH/ARRIVAL DATA .....	379
TABLE 39: MARS TO EARTH 2028 OPTIMAL LAUNCH/ARRIVAL DATA .....	383
TABLE 40: MARS TO EARTH 2031 OPTIMAL LAUNCH/ARRIVAL DATA .....	387
TABLE 41: MARS TO EARTH 2033 OPTIMAL LAUNCH/ARRIVAL DATA .....	391
TABLE 42: MARS TO EARTH 2035 OPTIMAL LAUNCH/ARRIVAL DATA .....	395
TABLE 43: MARS TO EARTH 2037 OPTIMAL LAUNCH/ARRIVAL DATA .....	399
TABLE 44: MARS TO EARTH 2039 OPTIMAL LAUNCH/ARRIVAL DATA .....	403
TABLE 45: MARS TO EARTH 2041 OPTIMAL LAUNCH/ARRIVAL DATA .....	407
TABLE 46: EARTH-VENUS-MARS TRAJECTORIES DEPARTING EARTH 2020-2040.....	412
TABLE 47: MARS-VENUS-EARTH TRAJECTORIES DEPARTING MARS 2022-2041.....	413
TABLE 48: CLASSICAL CONJUNCTION-CLASS MISSIONS .....	415
TABLE 49: SLOW-OUTBOUND CONJUNCTION-CLASS MISSIONS.....	416
TABLE 50: SLOW-INBOUND CONJUNCTION-CLASS MISSIONS .....	417
TABLE 51: LONG CONJUNCTION-CLASS MISSIONS .....	418
TABLE 52: EARTH-VENUS-MARS OPPOSITION-CLASS MISSIONS.....	419

TABLE 53: MARS-VENUS-EARTH OPPOSITION-CLASS MISSIONS.....	420
TABLE 54: MARS GRAVITY PARAMETERS (NORMALIZED) .....	421
TABLE 55: EARTH GRAVITY PARAMETERS (NORMALIZED).....	422

## Acknowledgements

The authors would like to thank Fernando Abilleira for the use of the Mars Mission Opportunity Design Data Handbook (2010-2020) as a starting point for this document. Specific contributions for new content are due to Ryan Park & Alex Konopliv (gravity field information), Eric Haddox (declination penalty data), Evgeniy Skylanskiy (entry trajectory data), Sean Wager (seasonal effects of drag), and Mark Lemmon (seasonal effects on surface lighting).

The authors would also like to thank Chad Edwards, Roby Wilson, Ralph Roncoli, Austin Nicholas, and Fernando Abilleria for their review & comments..

This work was performed at the Jet Propulsion Laboratory, California Institute of Technology, Pasadena, California, under contract to the National Aeronautics and Space Administration.

Any questions or comments regarding this document may be directed to:

Mark S. Wallace  
Jet Propulsion Laboratory

M/S 301-121  
4800 Oak Grove Drive  
Pasadena, CA 91109

Phone: (818) 354-4236  
Email: [Mark.S.Wallace@jpl.nasa.gov](mailto:Mark.S.Wallace@jpl.nasa.gov)

# 1 Introduction

## 1.1 Purpose

The purpose of this handbook is to provide a high-level understanding of the major considerations of Mars mission design and the variation in the parameters of those designs from one launch opportunity to another during the 2022-2040 timeframe. Rather than provide the answers for every possible mission design, it is intended to guide the reader in asking the right questions and to aid in the discussion of major trades that go into a mission design. When do we go? Is the mission ballistic, or does it use a low-thrust (e.g. solar-electric propulsion) system? How heavy can our spacecraft be? How is orbit achieved? Where and when can we land?

## 1.2 Organization

This handbook is generally organized into two main sections. Chapters 2 through 9 discuss Mars Mission Design in a general sense. Chapter 2 discusses models and ephemerides upon which the designs are based and Chapter 3 discusses launch vehicles. Chapters 4 through 6 cover the interplanetary phases, while Chapters 7 and 8 discuss the “at Mars” parts of the mission design. The interplanetary phase and the “at Mars” phases are, of course, interrelated. Chapter 9 discusses the special topic of designing a round-trip mission, such as for sample return or one with a human crew.

Chapters 10 through 12 contain detailed data for the various interplanetary mission designs, including “porkchop plots” (see Section 4.3). It is these final chapters that contain most of the data specific to the 2022-2040 interval.

## 1.3 Trajectory Models

The interplanetary trajectory models used throughout this document are patched conics [1]. Patched conics are a classical orbital mechanics technique where the problem is simplified to a single central body and the spacecraft. The spacecraft is considered to move with pure Keplerian motion while within the sphere of influence of the current central body and then jumps from one central body to the next. For example, an Earth-to-Mars trajectory starts as an outbound hyperbola at Earth, becomes a Sun-centered ellipse in heliocentric space, and then is modeled as an inbound hyperbola at Mars. The outbound and inbound asymptotes at Earth and Mars, respectively, are determined by differencing the heliocentric velocity of the spacecraft at the planetary position from the planetary velocity at those positions. Low thrust solutions expand upon the patched conic method by modeling the engine thrust as a series of impulsive maneuvers [2].

Once in orbit, a spacecraft trajectory can be modeled as a Keplerian orbit subject to various perturbations. The largest ones are non-spherical gravity, atmospheric drag, and the effect of 3rd body gravity (e.g. the effect of the Sun’s gravity on a spacecraft in Mars orbit). Most of these are neglected for the purposes of this handbook. A larger, but still much-reduced 8th degree-and-order gravity field is used for the aerobraking analyses (Section 8.4). Atmospheric drag is ignored entirely except for a simplified exponential model used in aerobraking. Third body effects are ignored entirely.

The Entry, Descent, and Landing (EDL) sequence has been simplified to the “descent central time and angle” method. This method allows the mission designer to map an entry state down to the surface by rotating the entry state position in-plane by the “descent central angle” to find

the inertial landing site. The surface-relative site is then found by adding the descent time to the entry time and rotating the inertial landing site into the planet-relative coordinate system at that landing time. This eliminates the need for computationally-costly EDL trajectory propagations. However, the descent central angle and time are both functions of the entry velocity and the entry flight path angle as well as the EDL system design itself. This dependence is discussed in Section 7.2.

## 1.4 Launch Period Selection Strategy

The launch/arrival strategy for a mission is the ultimate expression of a mission design. It is a balancing of many requirements across the mission, from the project schedule to the flight system design to how the spacecraft will ultimately be operated. It is almost never a simple optimization of a single parameter. Since we cannot possibly anticipate every possible mission design that may be pondered in the next twenty years, we have chosen to illustrate only a few mission designs with the intent of illuminating the differences between the various launch opportunities.

For Earth-to-Mars designs, we have selected two 20-day launch periods with a constant arrival date. The 20-day duration is consistent with JPL Design Principles [3], and a constant arrival date is a common constraint applied by many flight projects – particularly landers. The Design Principles state that the launch period be long enough that there is at least a 99% chance of launching and that 20 days should be used if insufficient statistics are available. A constant arrival date means that much of the mission plan can be done before launch including DSN scheduling and the post-arrival activity timeline. This is particularly relevant for landers, not least because then only a single atmosphere profile would have to be considered. A constant arrival date achieves this simplification of planning at the expense of variable arrival geometries. Some missions may wish to keep some aspect of their arrival geometry constant (e.g. the ascending node of the post-capture orbit or the local solar time of landing) instead.

The first Earth-to-Mars launch period is the maximum launch mass launch period. We call this the “Lander” launch period because landers are typically less impacted by higher entry velocities. The launch period was selected to maximize the minimum launch performance across the 20-day launch period, including declination penalties if appropriate. In the absence of a declination penalty, the optimization is insensitive to the shape of the launch capability vs. launch energy (C3) curve. The lowest C3 is optimal. However, if there is a declination penalty, then the shape does matter. If the launch capability drops quickly with increasing C3, then it may be optimal to accept a larger declination penalty over a higher C3. The launch vehicle curve used here is consistent with the “High Performance” vehicle defined by the 2019 Discovery Announcement of Opportunity [4], which is itself consistent with KSC’s curve for a Falcon Heavy (Recovery) vehicle. See Chapter 3.

The second Earth-to-Mars launch period is the maximum captured mass launch period. This is dubbed the “Orbiter” launch period, as it maximizes the mass in Mars orbit after a Mars Orbit Insertion (MOI) maneuver has been performed. It neither maximizes the launch mass, as in the “Lander” launch period, nor minimizes the MOI propellant required. It is, rather, a balancing of both. The optimization will select the launch period with the largest minimum mass after the MOI propellant is expended. This is sensitive to both the launch vehicle curve in the presence of declination penalties, like the “Lander” launch period, but also to the propulsion system assumed. For the purposes of this handbook, a 300-second specific impulse system was

assumed. The monopropellant systems carried by the Mars Reconnaissance Obiter (MRO) and the Mars Atmosphere and Volatile Evolution (MAVEN) missions had a lower specific impulse, but bipropellant systems have larger. 300 seconds was deemed a good “average” value. Finite burn losses (see Section 8.3.2) are neglected.

Finally, for Mars-to-Earth designs, we considered only a single minimum departure velocity launch period. Mars departures have a more complex relationship to the outbound declination than launch vehicles, and the 20-day launch period is an overly conservative assumption. A low-thrust spiral up-and-out can reach a 99% probability of escape threshold on a single targeted departure date with proper missed-thrust margins. A high-thrust departure need consider only the probability of missing the departure date due to an anomaly preventing the burn. We assume that two opportunities to depart separated by a week is sufficient to meet a 99% probability of departure, and so a 7-day “launch period” is presented.

## 2 Planetary Constants and Models

### 2.1 Overview

The shape, orientation, and location of Mars, as well as Earth, are critically important data for the mission designer. As our knowledge improves, this data gets incrementally better. This information is independent of how the spacecraft travels to Mars or back. In addition to the obvious importance for the trajectory design, this information drives other aspects of the mission design, such as thermal analyses, power availability, and communications. A set of standard time systems are also provided.

The following information is generally taken from the InSight Planetary Constants and Models Document (PCMD) [5], with updates as appropriate.

### 2.2 Mars Planetary Constants

#### 2.2.1 Mars Gravity Field

The most current Mars gravity field is MRO120D, which is a 120<sup>th</sup> degree and order model [6]. It was developed using data collected from MGS, Odyssey, and MRO through April 30<sup>th</sup>, 2012. The Mars orientation is constrained by the inclusion of surface tracking data from both Viking Landers, Mars Pathfinder, and the Mars Exploration Rover Opportunity while parked during its 5<sup>th</sup> Martian winter (2012). This orientation model is the same as that used by Pathfinder, with the constants re-estimated in the gravity solution. Appendix 13.1.1 lists the normalized coefficients for an 8 × 8 subset of the MRO120D gravity field. In addition, the appendix indicates where the full MRO120D field can be found. Table 1 contains the most important values. It should be noted that the MRO120D field's GM differs from the value in the MAR097 Satellite Ephemeris [7]. The difference between the two values is 2e-3 km<sup>3</sup>/s<sup>2</sup>. Care should be taken to use the value most appropriate for a given application. The MAR097 value is appropriate for approach navigation, as it was generated using the entire solar system, while MRO120D's value may be best used for orbital consideration, as it is consistent with the harmonic field and was estimated using orbital assets.

**Table 1: Mars Gravity Field Parameters**

Symbol	Value	Description
R <sub>ref</sub>	3396.0 km	Reference Radius
GM <sub>Mars</sub>	42828.37362069909 km <sup>3</sup> /s <sup>2</sup>	Gravitational Parameter from MAR097
GM <sub>Mars</sub>	42828.37581575610 km <sup>3</sup> /s <sup>2</sup>	Gravitational Parameter from MRO120D
D <sub>SOI</sub>	5.8 × 10 <sup>5</sup> km	Mars Sphere of Influence
J <sub>2Mars</sub>	0.8750220924537 × 10 <sup>-3</sup>	Mars 2 <sup>nd</sup> Degree Zonal (Normalized)
J <sub>2Mars</sub>	0.1956608880540579 × 10 <sup>-2</sup>	Mars 2 <sup>nd</sup> Degree Zonal (Un-normalized)
J <sub>3Mars</sub>	0.118970150373 × 10 <sup>-4</sup>	Mars 3 <sup>rd</sup> Degree Zonal (Normalized)
J <sub>3Mars</sub>	0.3147654313269162 × 10 <sup>-4</sup>	Mars 3 <sup>rd</sup> Degree Zonal (Un-normalized)

#### 2.2.2 Mars Pole and Prime Meridian

The Mars pole and prime meridian values in Table 2 are based upon the definitions in the IAU/IAG 2000 report [8]. High precision precession and nutation models are used for navigation

purposes, but these are sufficient for preliminary planning.

**Table 2: Mars Pole and Prime Meridian Parameters**

Symbol	Value	Description
$\alpha_{\text{Mars}}$	$317.68143 - 0.1061*T \text{ deg}$	Right Ascension of Mars Pole in EME2000
$\delta_{\text{Mars}}$	$52.8865 - 0.0609*T \text{ deg}$	Declination of Mars Pole in EME2000
$W_{\text{Mars}}$	$176.630 + \dot{W}_{\text{Mars}} * D \text{ deg}$	Prime Meridian with respect to Mars IAU Vector
$W^Y_{\text{Mars}}$	$350.89198226 \text{ deg/day}$	Rotational Rate of Mars
T	$\frac{D}{36525}$	Centuries past Epoch of J2000
D	2451545.0	Reference Epoch of J2000 in Julian Days
J2000	Jan 1, 2000 12:00:00 ET	Calendar date of J2000 Reference Epoch. See Section 5.1.1 for a description of ET.

### 2.2.3 Mars Shape Parameters

The Mars radii that should be used for determining Earth, Sun, and spacecraft visibility are taken from the IAU/IAG 2000 report [8] and are contained in Table 3. The values for radii were computed using an ellipsoidal surface fit to MOLA data at a uniform angular spacing of 0.5 degrees in latitude and longitude [9].

**Table 3: Mars Shape Parameters**

Symbol	Value	Description
$R_{\text{Mars-Equator}}$	3396.19 km	Equatorial Radius of Mars
$R_{\text{Mars-Pole}}$	3376.20 km	Polar Radius of Mars
f	0.00588600756	Mars Flattening Factor

### 2.2.4 Mars Satellite Data

The gravitational parameters for the Martian satellites Phobos and Deimos (Tables 4 and 5) are taken from the MAR097 ephemeris [7], while the shape models are taken from the IAU/IAG 2000 report [8].

**Table 4: Phobos Gravitational and Shape Parameters**

Symbol	Value	Description
$GM_{\text{Phobos}}$	$7.087546066894452 \times 10^{-4} \text{ km}^3/\text{s}^2$	Gravitational Parameter from MAR097
$R_{\text{Phobos-mean}}$	11.1 km	Mean radius of Phobos
$R_{\text{Phobos-equatx}}$	13.4 km	Sub-planet equatorial radius of Phobos
$R_{\text{Phobos-equaty}}$	11.2 km	Along-orbit equatorial radius of Phobos
$R_{\text{Phobos-polar}}$	9.2 km	Polar radius of Phobos

**Table 5: Deimos Gravitational and Shape Parameters**

Symbol	Value	Description
$GM_{\text{Deimos}}$	$9.615569648120313 \times 10^{-5} \text{ km}^3/\text{s}^2$	Gravitational Parameter from MAR097

Symbol	Value	Description
$R_{\text{Deimos-mean}}$	6.2 km	Mean radius of Deimos
$R_{\text{Deimos-equatx}}$	7.5 km	Sub-planet equatorial radius of Deimos
$R_{\text{Deimos-equaty}}$	6.1 km	Along-orbit equatorial radius of Deimos
$R_{\text{Deimos-polar}}$	5.2 km	Polar radius of Deimos

## 2.3 Mars Seasons

The seasons of Mars are determined by the longitude of the Sun as viewed from Mars relative to the vernal equinox of Mars. The longitude of the Sun, typically referred to as "L<sub>s</sub>" (pronounced as "L sub s"), is effectively a measure of the position of Mars in its orbit. L<sub>s</sub> is measured eastward from the vernal equinox in the orbital plane of Mars as shown in Figure 1 [10]. Table 6 indicates the relationship between L<sub>s</sub> and the seasons on Mars.

Table 6: Mars Seasons

L <sub>s</sub>	Event	Season
0°	Vernal Equinox	Start of northern spring / southern fall
90°	Summer Solstice	Start of northern summer / southern winter
180°	Autumnal Equinox	Start of northern fall / southern spring
270°	Winter Solstice	Start of northern winter / southern summer

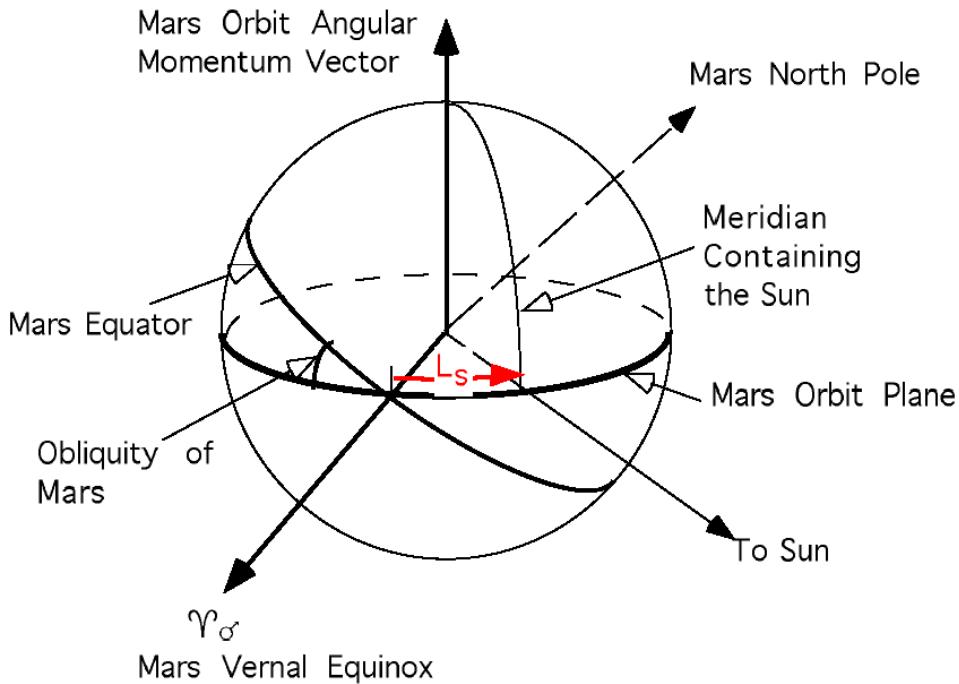


Figure 1: Longitude of the Sun for Determining the Seasons of Mars

## 2.4 Mars Time Systems

### 2.4.1 Martian Solar Day

The Martian solar day is called a Sol, and it is approximately 40 minutes longer than an Earth day. The mean Sol is computed from the rotation rate of Mars and the rate of the fictitious mean sun (FMS), described in the next section. In one mean Sol, Mars rotates through 360 deg plus the amount that the mean sun moved during that time:

$$1 \frac{\text{deg}}{\text{Sol}} = 360 \text{ deg} + \left( \dot{\alpha}_{FMS} \frac{\text{deg}}{\text{day}} \right) \left( \kappa \frac{\text{days}}{\text{Sol}} \right) (1 \text{ Sol}) \quad (1)$$

where  $\kappa$  represents the ratio of days per Sol and the  $\dot{\alpha}_{FMS}$  is the rate of the fictitious mean sun (0.5240384 deg/day). Solving for  $\kappa$  produces the following relationship:

$$\kappa \frac{\text{days}}{\text{Sol}} = \frac{360 \text{ deg}}{(\dot{W}_{Mars} - \dot{\alpha}_{FMS}) \text{deg/day}} \quad (2)$$

where  $\dot{W}_{Mars}$ , the rotation rate of Mars from Reference [11] and has the value 350.89198521 deg/day. This is a different value from that of Table 2 (Section 2.2.2), as that value does not account for the Mars nutation. See Reference [11] for further details. The mean Sol is thus:

$$\begin{aligned} 1 \text{ Sol} &= 1.02749125 \text{ days} \\ &= 88775.244 \text{ seconds} \\ &= 24 \text{ hours, } 39 \text{ minutes, } 35.244 \text{ seconds} \end{aligned}$$

## 2.5 Local True Solar Time and Local Mean Solar Time

Local true solar time (LTST) and local mean solar time (LMST) are given by Reference [12]:

$$\text{LTST} = (\alpha_p - \alpha_{TS} \text{ deg}) \frac{\frac{24 \text{ hr}}{360 \text{ deg}} + 12 \text{ hr}}{} \quad (3)$$

$$\text{LMST} = (\alpha_p - \alpha_{FMS} \text{ deg}) \frac{\frac{24 \text{ hr}}{360 \text{ deg}} + 12 \text{ hr}}{} \quad (4)$$

where  $\alpha_p$  is the Areocentric Right Ascension (ARA) of a point on the surface of Mars,  $\alpha_{TS}$  is the ARA of the true sun, and  $\alpha_{FMS}$  is the ARA of the Fictitious Mean Sun (FMS). The ARA is an angle measured in the Mars mean equator plane eastward from the vernal equinox vector to the intersection of the meridian containing the point and the equator (see Figure 2). In practice, there is no generally accepted definition of the vernal equinox of Mars, so the IAU vector is used instead. The relationships above are still valid for IAU-referenced angles as long as all three right ascension values are referenced to the IAU vector at the same epoch.

These equations convert the difference in angles from degrees to true or mean solar hours, with 12 hours representing the time that the true or mean sun is at zenith (local noon). The conventional method for computing the times above are to compute  $\alpha_{TS}$  from the planetary ephemeris file and  $\alpha_{FMS}$  from a fit of the Mars ephemeris for the period applicable to a given mission. Reference [13] describes a least-squares quadratic fit for the computation of  $\alpha_{FMS}$  over 134 Mars orbits spanning calendar years 1874 to 2126. Below is the expression for  $\alpha_{FMS}$  for the epoch of J2000, adjusted to reflect the Mars IAU vector given for the epoch of J2000.

$$\alpha_{FMS} = (270.3863 - \Psi(t) \text{ deg}) + (0.5240384 \text{ deg/day})(t - t_0) \quad (5)$$

Where  $t_0$  is the reference J2000 epoch,  $t$  is the current Julian date, and  $\Psi(t)$  is the offset between the Mars vernal equinox and IAU vectors (see Table 7).

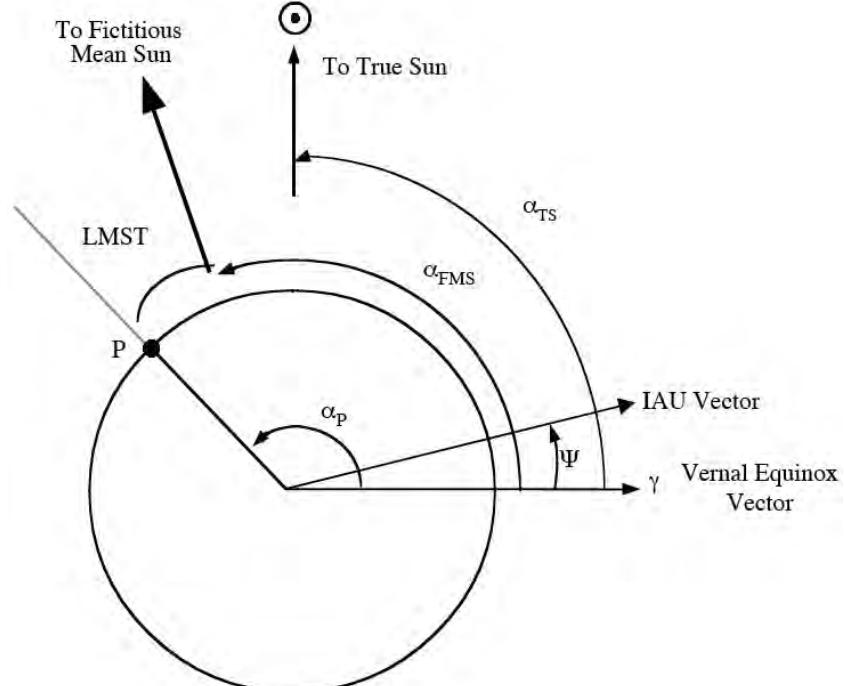


Figure 2: Definition of LTST and LMST

The first term in parentheses in the equation for  $\alpha_{FMS}$  has a constant  $270.3863^\circ$  offset with respect to the Mars vernal equinox [13], and a time-dependent offset  $\Psi(t)$  to transform it into the IAU frame for the current epoch.  $\Psi(t)$  is measured positive eastward along the Mars mean equator from the vernal equinox to the IAU vector. It is computed using the algorithm given in [13], with the results for the 2022-2041 time frame given in Table 7. The table shows that the offset between the Mars IAU frame and the Mars vernal equinox increases at a rate of approximately  $0.001$  deg/year. Therefore, missions that are expected to last more than a year must account for this correction in computing  $\alpha_{FMS}$ . In addition, the equation in [11] includes a quadratic term, which has been ignored here because it contributes less than  $0.0001$  deg over the next 20 years.

Table 7: Offset between Mars IAU vector and Mars vernal equinox directions

Epoch	Julian Date	$\Psi(t)$ (deg)
01-Jan-2022 12:00:00 ET	2459581.0	136.7780
01-Jan-2023 12:00:00 ET	2459946.0	136.7791
01-Jan-2024 12:00:00 ET	2460311.0	136.7801
01-Jan-2025 12:00:00 ET	2460677.0	136.7812
01-Jan-2026 12:00:00 ET	2461042.0	136.7823
01-Jan-2027 12:00:00 ET	2461407.0	136.7833
01-Jan-2028 12:00:00 ET	2461772.0	136.7844
01-Jan-2029 12:00:00 ET	2462138.0	136.7855

Epoch	Julian Date	$\Psi(t)$ (deg)
01-Jan-2030 12:00:00 ET	2462503.0	136.7865
01-Jan-2031 12:00:00 ET	2462868.0	136.7876
01-Jan-2032 12:00:00 ET	2463233.0	136.7886
01-Jan-2033 12:00:00 ET	2463599.0	136.7897
01-Jan-2034 12:00:00 ET	2463964.0	136.7908
01-Jan-2035 12:00:00 ET	2464329.0	136.7918
01-Jan-2036 12:00:00 ET	2464694.0	136.7929
01-Jan-2037 12:00:00 ET	2465060.0	136.7939
01-Jan-2038 12:00:00 ET	2465425.0	136.7950
01-Jan-2039 12:00:00 ET	2465790.0	136.7961
01-Jan-2040 12:00:00 ET	2466155.0	136.7971
01-Jan-2041 12:00:00 ET	2466521.0	136.7982

### 2.5.1 Equation of Time

The equation of time (EOT) is the difference between the right ascension of the fictitious mean sun and the right ascension of the true sun:

$$\begin{aligned} \text{EOT} &= \alpha_{\text{FMS}} - \alpha_{\text{TS}} \text{ deg} && \text{(Equation of Time in degrees)} \\ &= \text{LTST} - \text{LMST} && \text{(Equation of Time in minutes)} \end{aligned} \quad (6)$$

where  $\alpha_{\text{TS}}$  can be computed from planetary ephemeris data. The EOT can be converted to minutes to determine the time difference between the LTST and the LMST. Figure 3 shows the EOT in minutes as a function of Ls. It can be seen from the figure that the LTST can vary from the LMST by as much as 50 minutes over the duration of the Martian year.

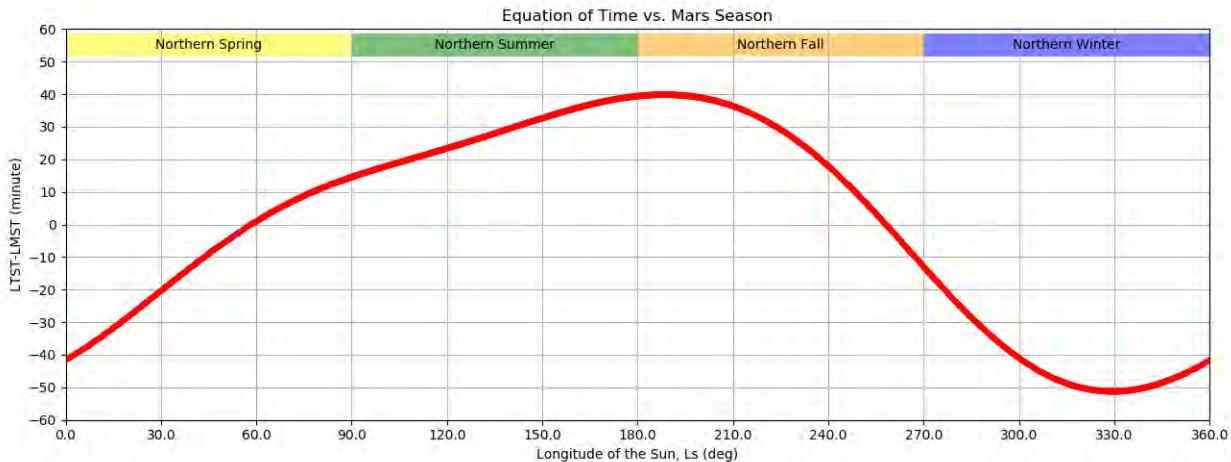


Figure 3: Equation of Time vs the Longitude of the Sun

## 2.6 Mars Atmosphere

The atmosphere of Mars, like all planetary atmospheres, is complex and variable. Complex models exist which consider the latitude and longitude, the position of the sun, the season, the

solar distance, and solar activity, plus global and regional dust storm activity. The MarsGram2010 atmospheric density model, for example, has almost two dozen input parameters. For preliminary analysis, this is far more complex than is warranted. A 12-layer exponential density model has been developed for this document which uses the default settings for the MarsGram2010 model and the 50<sup>th</sup> percentile of the global density variation over a Mars year. This model was run with three different fixed solar activity levels. The “mean” model uses  $150 \times 10^{-22} \text{ W/m}^2/\text{Hz}$  at 1 AU, or 150 “solar flux units (sfu)”. This represents the 50<sup>th</sup> percentile of activity at solar maximum. Solar activity can vary from 70 sfu at solar minimum to 240 sfu at a high-activity solar maximum. These represent the “low” and “high” density models, respectively.

Each layer in the model is defined by the density,  $\rho_0$ , at a reference height,  $h_0$ , an exponential decay with scale height,  $H$ , as in Equation 7. This model is continuous; the top of each layer has the same density as the bottom of the next.

$$\rho(h) = \rho_0 e^{(h_0-h)/H} \quad (7)$$

The 1<sup>st</sup>, 50<sup>th</sup>, and 99<sup>th</sup> percentile of the global variation over a Mars year with 150 sfu solar activity, along with the result of the simplified model, are illustrated in Figure 4. The variations are similar in magnitude for the low and high-density data as well. Figure 5 shows the simplified model at 70, 150, and 240 sfu. The parameters for the three models are tabulated in Table 8.

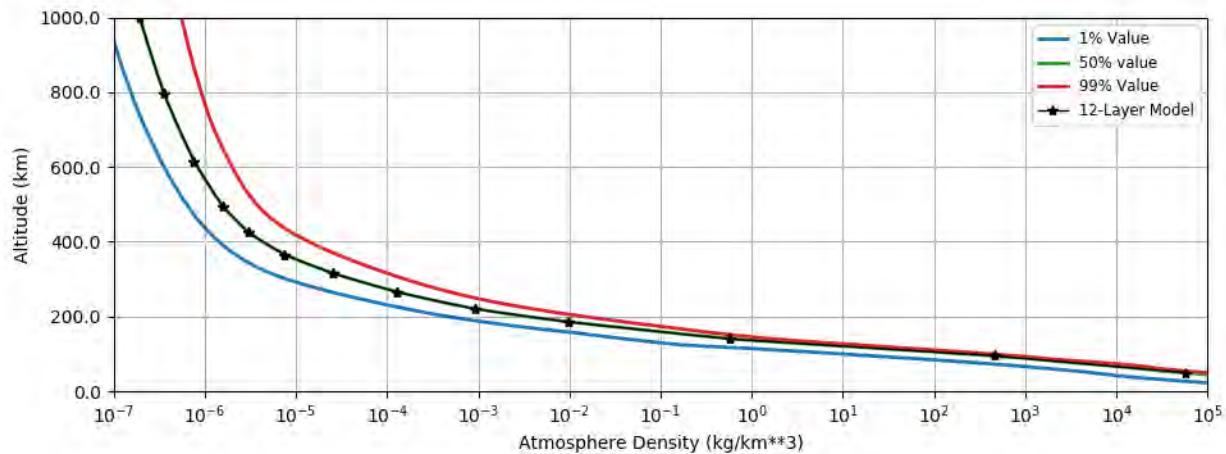


**Figure 4: Simplified Mean Mars Atmosphere Model and Underlying Variation**

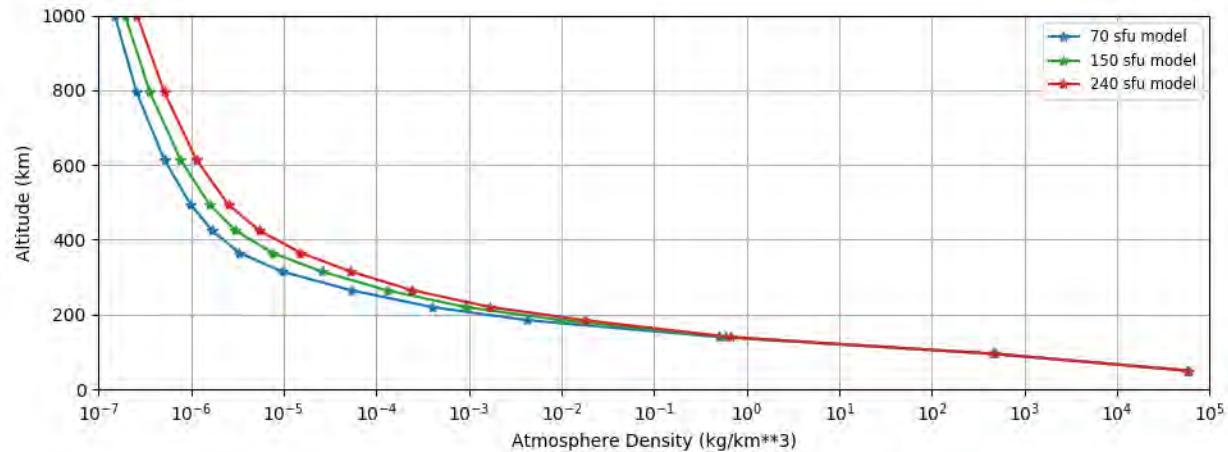


Figure 5: Comparison of Simplified Mars Atmosphere Models at Different Solar Activity Levels

Table 8: Simplified Mars Atmosphere Model Parameters

Altitude Range (km)	Reference Altitude, $h_0$ (km)	"Low" Reference Density, $\rho_0$ (kg/km <sup>3</sup> )	"Low" Scale Height, H (km)	"Mean" Reference Density, $\rho_0$ (kg/km <sup>3</sup> )	"Mean" Scale Height, H (km)	"High" Reference Density, $\rho_0$ (kg/km <sup>3</sup> )	"High" Scale Height, H (km)
< 95	50	5.8627E+04	9.4	5.7330E+04	9.3	5.8022E+04	9.3
95-140	95	4.7987E+02	6.6	4.5976E+02	6.7	4.5985E+02	6.9
140-185	140	5.0294E-01	9.4	5.7819E-01	11.1	6.5863E-01	12.4
185-220	185	4.1811E-03	14.9	9.8922E-03	14.7	1.7590E-02	14.9
220-265	220	4.0021E-04	22.3	9.1724E-04	23.0	1.6877E-03	23.3
265-315	265	5.3165E-05	29.2	1.2946E-04	30.9	2.4378E-04	32.5
315-365	315	9.5829E-06	46.8	2.5604E-05	40.7	5.2465E-05	40.5
365-425	365	3.2928E-06	89.3	7.5043E-06	65.4	1.5279E-05	57.5
425-495	425	1.6822E-06	129.3	2.9975E-06	108.0	5.3864E-06	91.2
495-615	495	9.7890E-07	183.8	1.5673E-06	165.9	2.4998E-06	151.1
615-795	615	5.0959E-07	261.6	7.6043E-07	237.7	1.1298E-06	226.9
> 795	795	2.5610E-07	381.0	3.5660E-07	333.4	5.1104E-07	302.5

## 2.6.1 Dust Storms

Mars is prone to global and regional dust storms. These storms lift significant quantities of fine dust particles into the atmosphere. These dust particles have two effects; first, they limit the light reaching the ground. How much they do so is tracked by an atmospheric opacity term known as "tau." This is an exponential term; the direct light reaching the surface is only  $e^{-\tau}$  the light at the top of the atmosphere. For example, if the tau is 3 ( $e^{-3} = 0.05$ ), only 5% of the light at the top of the atmosphere reaches the surface. The record highest measured tau of 10.4 meant that dust blocked 99.997% of the light. The "global dust storm season" spans roughly Ls 200° to 305° (the equivalent of mid-October to late January), while the regional dust storm season expands that to the Ls 155° to 330° range (late August to late February). However, regional storms can occur at any time, and the worst global dust storm ever recorded, the 2018 storm which ended

the Opportunity rover's mission, began at Ls 186°.

Figure 6 illustrates the measured tau as a function of Ls for Opportunity and Curiosity (provided by Mark Lemmon, from a forthcoming paper). The shaded regions are historical data, while the red and blue points indicate the tau measured by Curiosity and Opportunity, respectively, during the 2018 storm. The regional and global storms experienced by these vehicles (including the 2007 storm that Opportunity survived around Ls 270) can be seen in the large spikes followed by long decay.

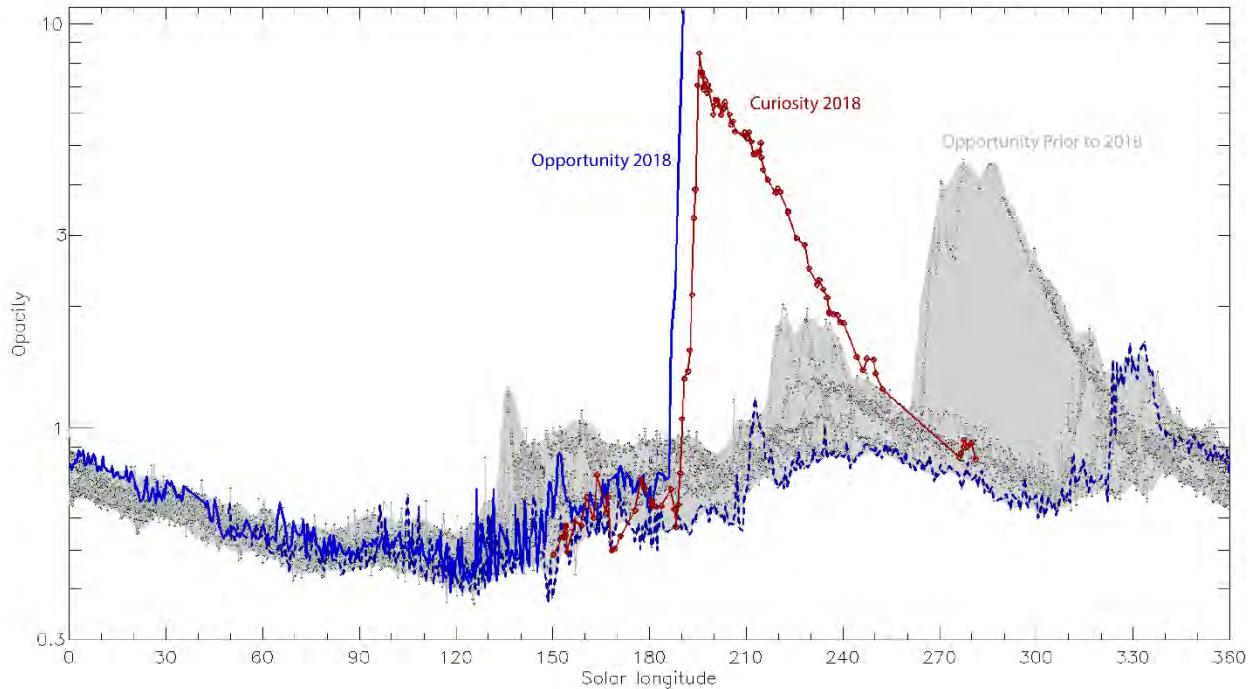


Figure 6: Atmospheric Opacity (tau) vs. Ls as Measured by Opportunity and Curiosity

The second major effect is to change the distribution of density by altitude – generally increasing it at higher altitudes. For a lander, this reduces the peak deceleration and peak heating, but increases the total integrated heating and lowers the parachute deployment altitude, all else being equal [14]. In addition, it increases both the absolute value and the variability of drag at orbital altitudes, as illustrated in Figure 7 (modified from [15]). The dust storms are harder to discern in this plot, but the seasonal effect of increased tau on a global scale is readily apparent in the greater drag  $\Delta V$  in the second half of the Martian year.

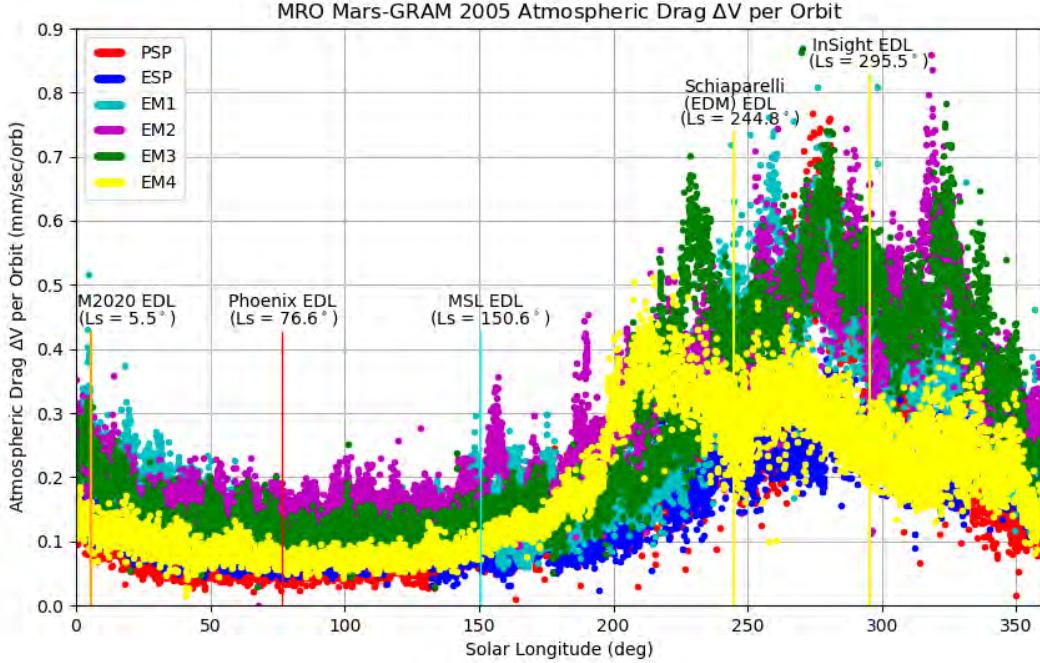


Figure 7: MRO Recorded Drag per Orbit through Feb 1, 2019 vs. Ls

## 2.7 Earth Planetary Constants

### 2.7.1 Earth Gravity Field

The Earth gravity field currently recommended for use is the GRACE (Gravity Recovery and Climate Experiment) gravity model GGM05C [16]. This is a 360<sup>th</sup> spherical harmonic degree and order model that combines GRACE K-band range-rate, attitude, and accelerometer data, GOCE data, and surface gravity and mean sea surface information. Appendix 13.1.2 lists the normalized coefficients for an 8 x 8 subset of the GGM05C gravity field. Table 9 contains the most important values.

Table 9: Earth Gravity Parameters

Symbol	Value	Description
R <sub>Earth-Ref</sub>	6378.1363 km	Reference Radius
GM <sub>Earth</sub>	398600.43539224955 km <sup>3</sup> /s <sup>2</sup>	Gravitational parameter from DE438
J <sub>2 Earth</sub>	0.00048416945732	Earth 2 <sup>nd</sup> degree zonal (Normalized)
J <sub>2 Earth</sub>	0.0010826358191967033	Earth 2 <sup>nd</sup> degree zonal (Un-normalized), Epoch J2000, no permanent tide
D <sub>SOI-Earth</sub>	9.25 x 10 <sup>5</sup> km	Earth Sphere of Influence, calculated at 1 AU

The GM<sub>Earth</sub> value specified in the GGM05C Earth gravity field is 398600.4355974172 km<sup>3</sup>/s<sup>2</sup>. This value differs slightly from the GM<sub>Earth</sub> value in the DE438 ephemeris. The two different values are both “equally correct”, but they represent the Earth GM in two different reference frames. The GGM05C model was developed assuming a geocentric reference frame. The JPL planetary and satellite ephemerides (including the GMs of the other solar system bodies), on the other hand, were developed using a solar-system-barycentric-based time scale. These two time frames differ slightly due to relativistic effects. Since the units of GM involve time (km<sup>3</sup>/s<sup>2</sup>), the

value of  $GM_{\text{Earth}}$  is slightly different in the geocentric reference frame as compared to the solar system barycentric reference frame. Once this conversion is done, the values differ by less than one part in a billion. For more information on the transformation between the geocentric and solar system barycentric reference frames and how the selection of those frames affect the value of  $GM_{\text{Earth}}$ , see References [17] and [18].

### 2.7.2 Earth Pole and Prime Meridian

For mission analysis purposes, the Earth pole and prime meridian values in Table 10 are taken from the IAU/IAG 2000 report [8]. The T and D symbols are defined in Table 2. Higher-precision coordinate frames are used for navigation purposes.

**Table 10: Earth Pole and Prime Meridian Parameters**

Symbol	Value	Description
$\alpha_{\text{Earth}}$	$0.0 - 0.641^*T \text{ deg}$	Right Ascension of Earth Pole in EME2000
$\delta_{\text{Earth}}$	$90 - 0.057^*T \text{ deg}$	Declination of Earth Pole in EME2000
$W_{\text{Earth}}$	$190.147 + \dot{W}_{\text{Earth}}^*D \text{ deg}$	Prime Meridian with respect to Earth IAU Vector
$\dot{W}_{\text{Earth}}$	$360.9856235 \text{ deg/day}$	Rotational Rate of Earth

### 2.7.3 Earth Shape Parameters

The Earth radii that should be used for determining sun and spacecraft visibility during launch and early cruise in Table 11 are taken from the IAU/IAG 2000 report [8]:

**Table 11: Earth Shape Parameters**

Symbol	Value	Description
$R_{\text{Earth-Equator}}$	6378.14 km	Equatorial Radius of Earth
$R_{\text{Earth-Pole}}$	6356.75 km	Polar Radius of Earth
$f$	0.00335364228	Earth Flattening Factor

### 2.7.4 Standard Acceleration of Gravity

The recommended value of the acceleration due to gravity at Earth's surface,  $g_n$ , used in the calculation of specific impulse, "gs" of acceleration, etc., is specified by the Committee on Data for Science and Technology (CODATA) [19] as exactly  $9.80665 \text{ m/s}^2$ .

### 2.7.5 Earth's Moon

The gravitational parameter for the Moon was also taken from the DE438 planetary ephemeris.

**Table 12: Lunar Gravity and Shape Parameters**

Symbol	Value	Description
$GM_{\text{Moon}}$	$4.902800110010225e+03 \text{ km}^3/\text{s}^2$	Gravitational Parameter from DE438
$R_{\text{Moon}}$	1737.4 km	Mean Lunar Radius from IAU/IAG 2000

## 2.7.6 Standard Coordinate Systems

The coordinate systems used to describe the orientation of Earth and Mars are taken from Reference [13]. High-precision models are generally used for navigation purposes, but for initial planning purposes, the models described here are sufficient. See Table 13 and Figures 8 to 10.

**Table 13: Coordinate Frame Definitions**

Coordinate System	Description
<b>Earth Frames</b>	
"EME2000"	Earth Mean Equator and Equinox of J2000. See Section 142.7.2 and Figure 8
"IAU Earth Pole"	Earth Mean Equator and Equinox of Date, See Section 2.7.2
"IAU Earth Fixed"	Earth Mean Equator and Prime Meridian of Date, See Section 2.7.2
<b>Mars Frames</b>	
"IAU Mars Pole"	Mars Mean Equator and IAU-Vector of Date, See Section 2.2.2 and Figure 9
"IAU Mars Fixed"	Mars Mean Equator and Prime Meridian of Date, See Section 2.2.2 and Figure 10.

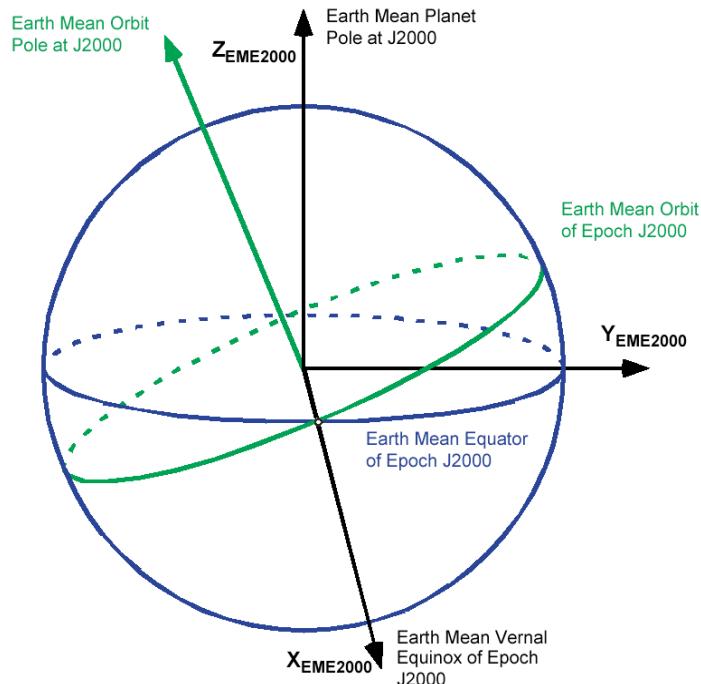


**Figure 8: Earth Mean Equator and Equinox of J2000 (EME2000)**

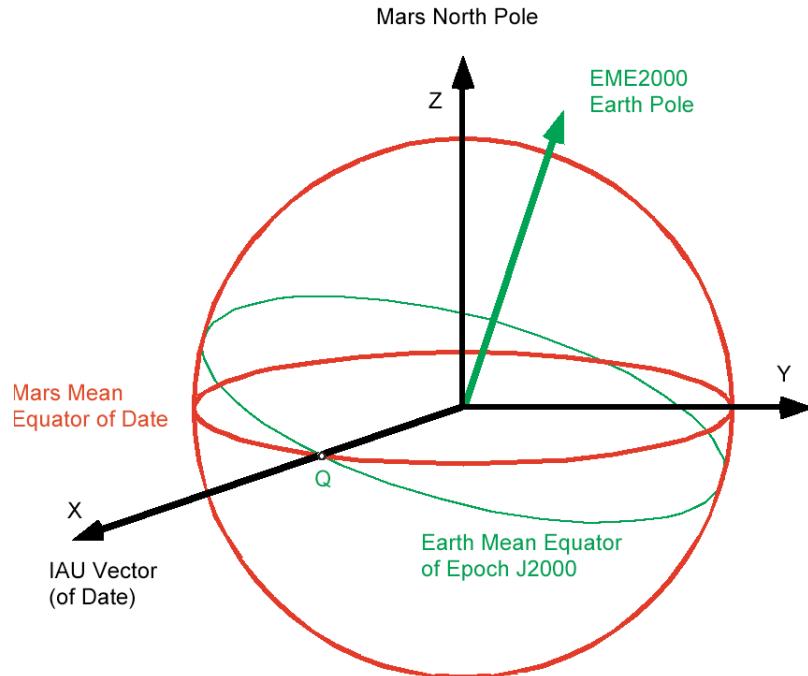


Figure 9: IAU Mars Pole at the J2000 Epoch

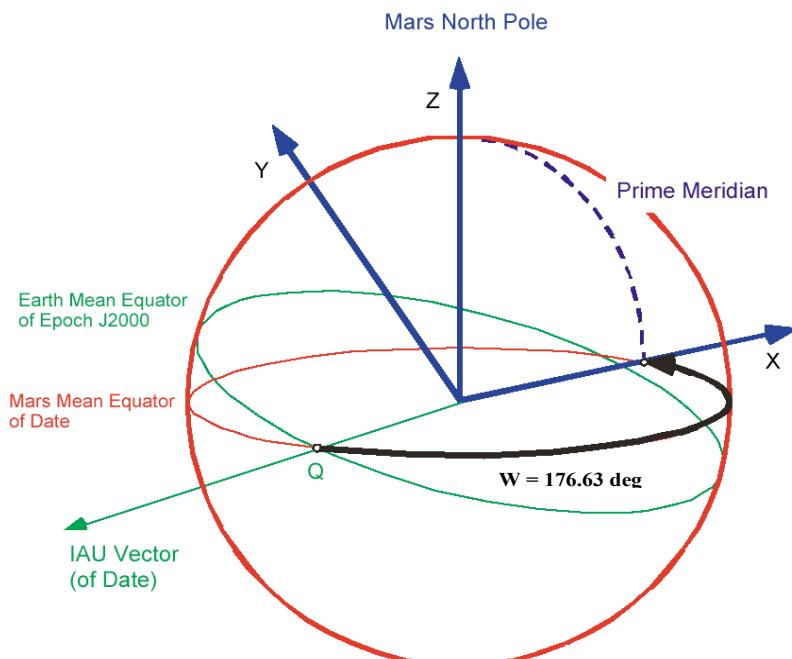


Figure 10: IAU Mars Fixed at the J2000 Epoch

## 2.8 Solar System Planetary Gravitational Parameters

The latest planetary ephemeris is DE438 [20] and the satellite ephemeris is MAR097 [7]. The gravitational parameters within DE438 are given in Tables 14 and 15. The values for the speed of light and astronomical unit (AU) are also taken from DE438 and repeated in Table 16.

**Table 14: Gravitation Parameters of DE438**

Body	GM (km <sup>3</sup> /s <sup>2</sup> )	Comment
Sun	1.327124400419394e+11	
Mercury	2.203178000000002e+04	
Venus	3.248585920000001e+05	
Earth Barycenter	4.035032355022598e+05	Within the Earth SOI, use the values for the Earth and Moon, below.
Earth	3.986004353922496e+05	
Moon	4.902800110010225e+03	
Jupiter Barycenter	1.267127641334462e+08	
Saturn Barycenter	3.794058520000000e+07	
Uranus Barycenter	5.794556465751792e+06	
Neptune Barycenter	6.836527100580024e+06	

**Table 15: Gravitation Parameters from MAR097**

Body	GM (km <sup>3</sup> /s <sup>2</sup> )	Comment
Mars Barycenter	4.282837442560939e+04	Within the Mars SOI, use the values for Mars, Phobos, and Deimos, below.
Mars	4.282837362069909e+04	
Phobos	7.087546066894452e-04	
Deimos	9.615569648120313e-05	

**Table 16: Astronomical Constants**

Symbol	Value	Description
c	299792.458 m/s	Speed of light
AU	149597870.6992925 km	Astronomical unit
F1_AU	1366.1 W/m <sup>2</sup>	Solar constant; total solar irradiance at 1 AU [21]

## 2.9 Mars Ephemeris Related Events

Table 17 provides information about major events, such as the start of Mars seasons, minimum and maximum Earth-Mars and Sun-Mars ranges, as well as the start and end of solar conjunction (defined here as a Sun-Earth-Mars angle less than 5 degrees). Figures 11 through 14 illustrate the evolution of those parameters with time, as well.

**Table 17: Seasons, Apses, and Season Starts: 2022-2041**

Date (ET)	Event	Earth-Mars Range (AU)	Sun-Mars Range (AU)	Sun-Earth-Mars Angle (deg)	Solar Longitude, Ls (deg)
24-Feb-2022	Start of Northern Fall	2.023	1.466	43.137	180.0
21-Jun-2022	Mars Perihelion	1.348	1.381	69.914	251.2
21-Jul-2022	Start of Northern Winter	1.190	1.388	77.504	270.0
1-Dec-2022	Minimum Earth-Mars Range	0.544	1.525	169.824	347.1
26-Dec-2022	Start of Northern Spring	0.608	1.557	155.428	0.0
30-May-2023	Mars Aphelion	1.991	1.666	56.699	71.1
12-Jul-2023	Start of Northern Summer	2.281	1.657	41.175	90.0
18-Oct-2023	Maximum Earth-Mars Range	2.550	1.575	9.484	134.9
1-Nov-2023	Start of Solar Conjunction	2.544	1.558	5.000	142.0
4-Dec-2023	End of Solar Conjunction	2.495	1.516	5.000	159.0
12-Jan-2024	Start of Northern Fall	2.387	1.466	15.887	180.0
8-May-2024	Mars Perihelion	1.949	1.382	42.345	251.2
7-Jun-2024	Start of Northern Winter	1.835	1.388	48.432	270.0
12-Nov-2024	Start of Northern Spring	0.936	1.557	107.940	0.0
12-Jan-2025	Minimum Earth-Mars Range	0.642	1.623	173.439	29.2
16-Apr-2025	Mars Aphelion	1.290	1.666	92.320	71.2
29-May-2025	Start of Northern Summer	1.678	1.657	71.171	90.0
29-Nov-2025	Start of Northern Fall	2.424	1.466	10.688	180.0
30-Nov-2025	Maximum Earth-Mars Range	2.424	1.465	10.431	180.5
21-Dec-2025	Start of Solar Conjunction	2.418	1.441	5.000	192.4
29-Jan-2026	End of Solar Conjunction	2.381	1.403	5.000	216.3
26-Mar-2026	Mars Perihelion	2.304	1.381	17.015	251.1
25-Apr-2026	Start of Northern Winter	2.256	1.388	23.091	270.0
30-Sep-2026	Start of Northern Spring	1.670	1.557	65.890	0.0
20-Feb-2027	Minimum Earth-Mars Range	0.678	1.665	175.511	65.5
4-Mar-2027	Mars Aphelion	0.697	1.666	161.135	71.2
16-Apr-2027	Start of Northern Summer	0.955	1.657	115.563	90.0
17-Oct-2027	Start of Northern Fall	2.130	1.466	37.210	180.0
11-Feb-2028	Mars Perihelion	2.350	1.381	8.430	251.2
27-Feb-2028	Start of Solar Conjunction	2.367	1.383	5.000	261.3
12-Mar-2028	Start of Northern Winter	2.380	1.387	2.114	270.0
13-Apr-2028	End of Solar Conjunction	2.404	1.408	5.000	289.9
11-May-2028	Maximum Earth-Mars Range	2.412	1.435	11.275	307.1
17-Aug-2028	Start of Northern Spring	2.247	1.557	36.679	0.0
19-Jan-2029	Mars Aphelion	1.053	1.666	109.691	71.2

Date (ET)	Event	Earth-Mars Range (AU)	Sun-Mars Range (AU)	Sun-Earth-Mars Angle (deg)	Solar Longitude, Ls (deg)
3-Mar-2029	Start of Northern Summer	0.717	1.657	151.385	90.0
29-Mar-2029	Minimum Earth-Mars Range	0.647	1.643	173.367	101.4
3-Sep-2029	Start of Northern Fall	1.563	1.466	65.439	180.0
29-Dec-2029	Mars Perihelion	2.071	1.381	34.692	251.3
28-Jan-2030	Start of Northern Winter	2.180	1.388	27.837	270.0
5-May-2030	Start of Solar Conjunction	2.481	1.479	5.000	328.0
13-Jun-2030	End of Solar Conjunction	2.539	1.530	5.000	349.0
29-Jun-2030	Maximum Earth-Mars Range	2.545	1.550	9.247	357.0
5-Jul-2030	Start of Northern Spring	2.544	1.557	10.880	0.0
7-Dec-2030	Mars Aphelion	1.794	1.666	66.421	71.2
19-Jan-2031	Start of Northern Summer	1.374	1.657	87.681	90.0
12-May-2031	Minimum Earth-Mars Range	0.553	1.558	169.784	142.2
22-Jul-2031	Start of Northern Fall	0.844	1.466	103.647	180.0
16-Nov-2031	Mars Perihelion	1.510	1.381	63.144	251.2
16-Dec-2031	Start of Northern Winter	1.680	1.388	55.681	270.0
22-May-2032	Start of Northern Spring	2.517	1.557	14.407	0.0
24-Jun-2032	Start of Solar Conjunction	2.606	1.596	5.000	16.2
27-Jul-2032	Maximum Earth-Mars Range	2.637	1.627	4.908	31.4
27-Jul-2032	End of Solar Conjunction	2.637	1.627	5.000	31.5
24-Oct-2032	Mars Aphelion	2.376	1.666	35.260	71.2
6-Dec-2032	Start of Northern Summer	2.073	1.657	51.879	90.0
8-Jun-2033	Start of Northern Fall	0.479	1.466	156.166	180.0
5-Jul-2033	Minimum Earth-Mars Range	0.423	1.435	169.472	195.6
3-Oct-2033	Mars Perihelion	0.783	1.381	100.775	251.2
2-Nov-2033	Start of Northern Winter	0.973	1.388	89.840	270.0
9-Apr-2034	Start of Northern Spring	2.167	1.557	41.039	0.0
4-Aug-2034	Start of Solar Conjunction	2.667	1.659	5.000	54.3
19-Aug-2034	Maximum Earth-Mars Range	2.675	1.663	1.154	61.1
3-Sep-2034	End of Solar Conjunction	2.668	1.666	5.000	67.4
11-Sep-2034	Mars Aphelion	2.658	1.666	7.874	71.2
24-Oct-2034	Start of Northern Summer	2.530	1.657	22.626	90.0
26-Apr-2035	Start of Northern Fall	1.116	1.466	87.253	180.0
21-Aug-2035	Mars Perihelion	0.411	1.381	149.555	251.3
11-Sep-2035	Minimum Earth-Mars Range	0.380	1.385	172.150	264.7
20-Sep-2035	Start of Northern Winter	0.386	1.388	172.408	270.0
25-Feb-2036	Start of Northern Spring	1.545	1.557	72.083	0.0

Date (ET)	Event	Earth-Mars Range (AU)	Sun-Mars Range (AU)	Sun-Earth-Mars Angle (deg)	Solar Longitude, Ls (deg)
29-Jul-2036	Mars Aphelion	2.599	1.666	18.367	71.2
8-Sep-2036	Start of Solar Conjunction	2.659	1.658	5.000	89.2
10-Sep-2036	Start of Northern Summer	2.659	1.657	4.381	90.0
11-Sep-2036	Maximum Earth-Mars Range	2.659	1.657	4.264	90.2
8-Oct-2036	End of Solar Conjunction	2.635	1.642	5.000	102.3
13-Mar-2037	Start of Northern Fall	1.805	1.466	54.245	180.0
8-Jul-2037	Mars Perihelion	1.070	1.381	82.860	251.2
7-Aug-2037	Start of Northern Winter	0.905	1.388	92.450	270.0
11-Nov-2037	Minimum Earth-Mars Range	0.494	1.478	168.944	327.4
12-Jan-2038	Start of Northern Spring	0.808	1.557	120.409	0.0
17-Jun-2038	Mars Aphelion	2.217	1.666	45.223	71.3
29-Jul-2038	Start of Northern Summer	2.448	1.657	30.633	90.0
6-Oct-2038	Maximum Earth-Mars Range	2.590	1.607	8.204	121.2
16-Oct-2038	Start of Solar Conjunction	2.588	1.597	5.000	125.9
17-Nov-2038	End of Solar Conjunction	2.543	1.560	5.000	141.3
29-Jan-2039	Start of Northern Fall	2.281	1.466	26.410	180.0
26-May-2039	Mars Perihelion	1.737	1.381	52.621	251.3
25-Jun-2039	Start of Northern Winter	1.604	1.387	58.954	270.0
30-Nov-2039	Start of Northern Spring	0.688	1.557	136.216	0.0
28-Dec-2039	Minimum Earth-Mars Range	0.611	1.591	172.001	13.9
3-May-2040	Mars Aphelion	1.579	1.666	76.673	71.3
15-Jun-2040	Start of Northern Summer	1.938	1.657	58.761	90.0
9-Nov-2040	Maximum Earth-Mars Range	2.476	1.514	10.764	159.9
29-Nov-2040	Start of Solar Conjunction	2.468	1.488	5.000	170.7
16-Dec-2040	Start of Northern Fall	2.451	1.467	0.727	180.0
5-Jan-2041	End of Solar Conjunction	2.420	1.443	5.000	191.4
12-Apr-2041	Mars Perihelion	2.198	1.381	26.945	251.4
12-May-2041	Start of Northern Winter	2.123	1.388	32.869	270.0
17-Oct-2041	Start of Northern Spring	1.390	1.557	79.553	0.0

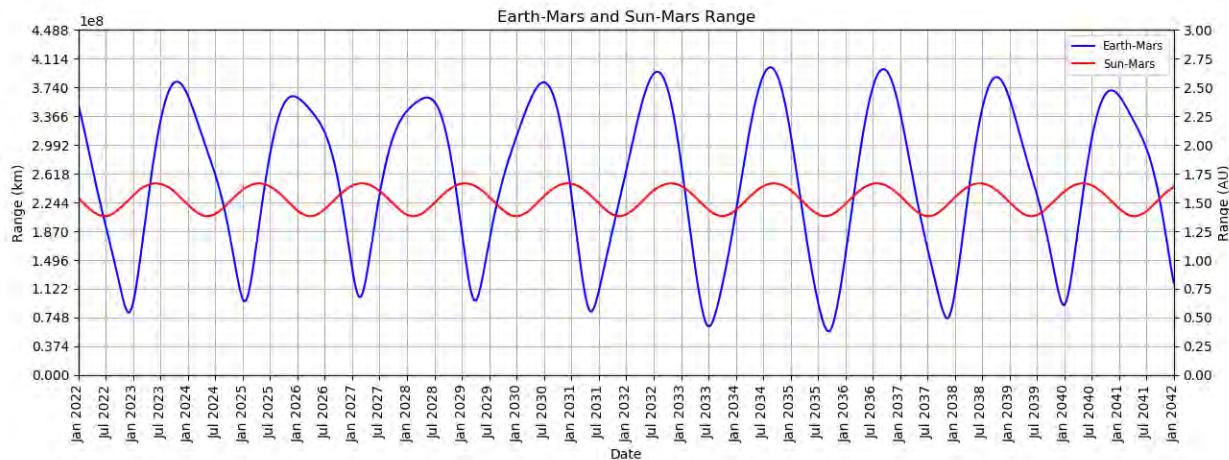


**Figure 11: Earth-Mars and Sun-Mars Ranges: 2022-2041**

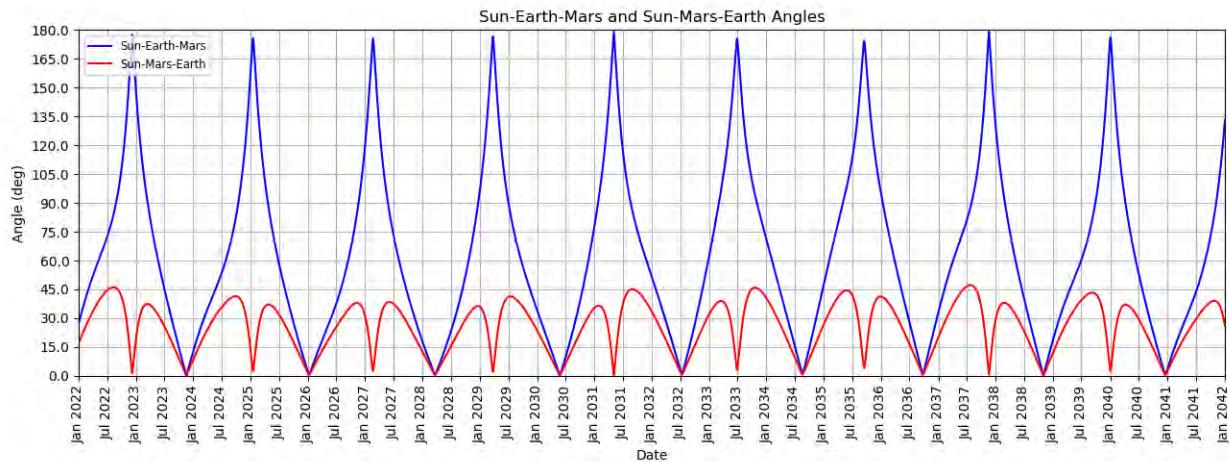


**Figure 12: Sun-Earth-Mars and Sun-Mars-Earth Angles: 2022-2041**

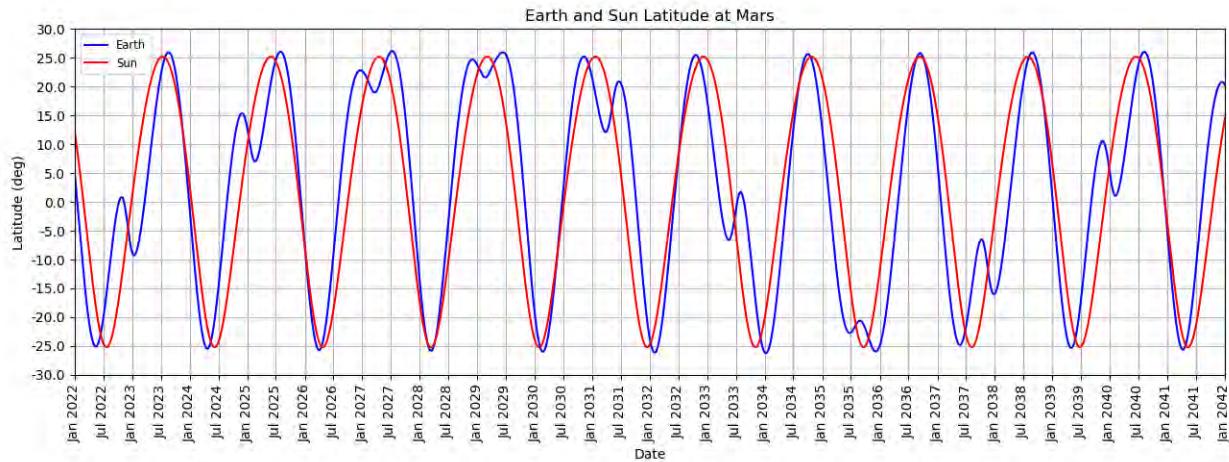


**Figure 13: Earth and Sun Latitude at Mars: 2022-2041**

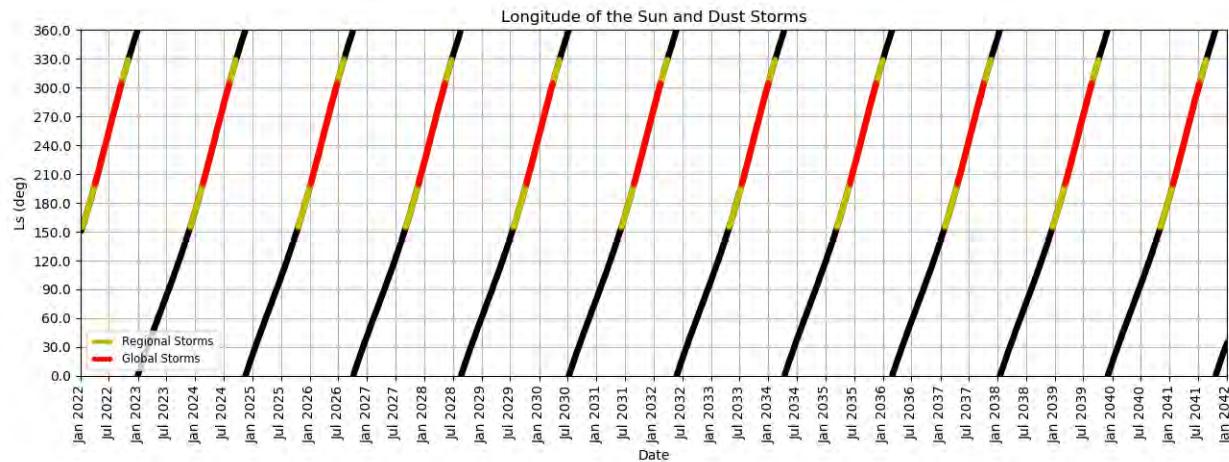


Figure 14: Longitude of the Sun and Dust Storm Seasons: 2022-2041

## 3 Launch Vehicles

### 3.1 Overview

Early mission analysis and planning must consider the performance characteristics of potential launch vehicles. This performance is typically represented in the form of maximum launch mass (or throw mass) vs. the required escape energy (i.e. C3). These are typically called “C3 curves”, and can often be characterized quite well by a quadratic or cubic curve fit (see Section 3.2)

NASA’s Launch Services Program (LSP), based at Kennedy Space Center, manages launch vehicle procurement for all NASA missions. They provide contract management, launch engineering support, and estimates of vehicle performance cost. They also offer mission analysis, trajectory modeling, etc. through their Flight Dynamics Branch. LSP manages contracts with current and future launch providers through the National Launch Services (NLS) contract. The current contract is known as NLS II, which runs from 2010 – 2025. Launch Vehicles can be on-ramped and off-ramped on a rolling basis. Launch vehicles on the NLSII contract and their performances can be queried at <https://elvperf.ksc.nasa.gov/>. Figure 15 shows a screenshot of such a query for C3 = 10 km<sup>2</sup>/s<sup>2</sup>.

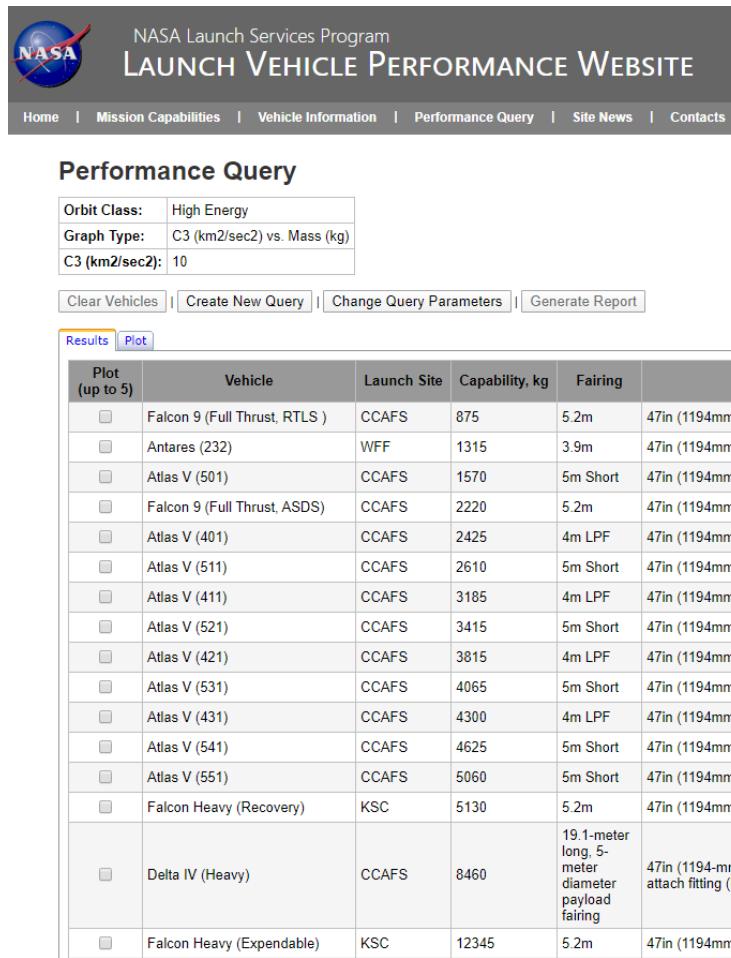


Figure 15 Snapshot of LSP Launch Vehicle Performance Query Tool.  
(Extracted from <https://elvperf.ksc.nasa.gov/> on 1/14/20)

### 3.1.1 *Rapidly Changing Launch Vehicle Market*

As this handbook is being written (late 2020), much of the launch vehicle industry is in flux. ULA has discontinued production on its Delta line and is in the process of phasing out the Atlas V by mid-decade. They are developing the Vulcan line to take its place. In addition, Blue Origin is developing New Glenn. Both of these new heavy lift launch vehicles are targeting initial launches in 2021. The information presented here is limited to what is known about currently flying vehicles.

### 3.1.2 *Vehicle Configurations*

Current launch vehicles included in NLSII are:

- United Launch Alliance (ULA) - Atlas V and Delta IV Heavy
- Northrop Grumman - Antares, Pegasus, and Taurus XL
- Space X – Falcon 9 and Falcon Heavy

Each launch vehicle can be launched in a number of configurations. For example, the Atlas V family has 11 offered configurations which vary the fairing diameter and the number of attached solid rocket boosters (SRB).

**Table 18: Atlas V Base Configurations**

Configuration	Stage 1	Stage 2	Fairing Length	Fairing Diameter	Payload Interface
Atlas V 401	Atlas: RD-180	Centaur: RL10C-1	LPF: 12 m (39.3 ft)	4.2 m (13.8 ft)	1194 mm (47 in) PSR with lightweight C22 adapter
Atlas V 501	Atlas: RD-180	Centaur: RL10C-1	Short: 20.7 m (68 ft)	5.4 m (17.7 ft)	1194 mm (47 in) PSR with lightweight C22 adapter

Table 18 shows the characteristics of the Atlas V 4-m and 5-m variants in their base configuration. SRBs can be added to the 401 and 501 configurations to increase the performance capability. Additionally, the RL10A-4-2 may be available as an enhancement to Centaur performance. The additional configurations are as follows:

- Atlas V 411 adds 1 SRB to the 401 configuration.
- Atlas V 421 adds 2 SRBs to the 401 configuration.
- Atlas V 431 adds 3 SRBs to the 401 configuration.
- Atlas V 511 adds 1 SRB to the 501 configuration.
- Atlas V 521 adds 2 SRBs to the 501 configuration.
- Atlas V 531 adds 3 SRBs to the 501 configuration.
- Atlas V 541 adds 4 SRBs to the 501 configuration.
- Atlas V 551 adds 5 SRBs to the 501 configuration.

Fairings of greater length are available for spacecraft that require a larger fairing volume:

- 4.2 m Extended Payload Fairing (EPF) is 12.9 m (42.3 ft)
- 4.2 m Extra Extended Payload Fairing (XEPF) is 13.8 m (45.3 ft)
- 5.4 m Medium is 23.5 m (77 ft)

SpaceX currently offers two performance levels for the Falcon 9 Full Thrust on NLS-II, which differ in the way that the first stage booster is recovered. The first level includes booster

performance holdbacks to allow for a Return-to-Launch-Site (RTLS) first stage recovery. The second level provides higher performance by allowing the first stage to be recovered via the SpaceX Automated Spaceport Drone Ship (ASDS), positioned downrange from the launch site. The first stage may also be expended to boost performance, but performance of that scenario is not provided publicly at this time.

**Table 19: Falcon Base Configurations**

Configuration	Stage 1	Stage 2	Fairing Diameter	Payload Interface
Falcon 9 Full Thrust	9 Merlin 1D Engines	1 Merlin 1D Vacuum (MVacD) Engine	5.2 m (17.1 ft)	36.9 in (937 mm) or 47 in (1194 mm)
Falcon Heavy	3 cores, each with 9 Merlin 1D Engines	1 Merlin 1D Vacuum (MVacD) Engine	5.2 m (17.1 ft)	36.9 in (937 mm) or 47 in (1194 mm)

The Falcon Heavy is also offered at two performance levels. The first level includes booster performance holdbacks to allow for first stage recovery of all three cores at the launch site. The second level provides higher performance by utilizing the full vehicle capability, foregoing recovery of the first stage cores. These levels provide the bookends of possible performance scenarios. It is possible to recover one or two cores on the drone ship or expend them in order to reach other performance targets.

### 3.1.3 *Launch Vehicle User's Guides*

More details on the specific characteristics of individual launch vehicles can typically be found in published “User’s Guides”. These guides are typically publicly available for download from the provider’s website or by request. They can contain valuable information such as performance, dimensions, payload accommodations, and environments. The fairing dimensions for Falcon and Atlas from their respective user’s guides are shown in Figures 16 through 18.

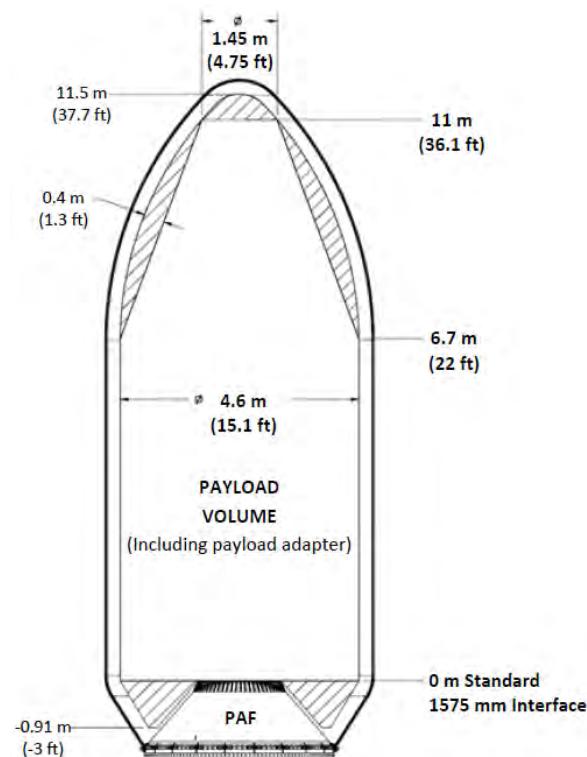
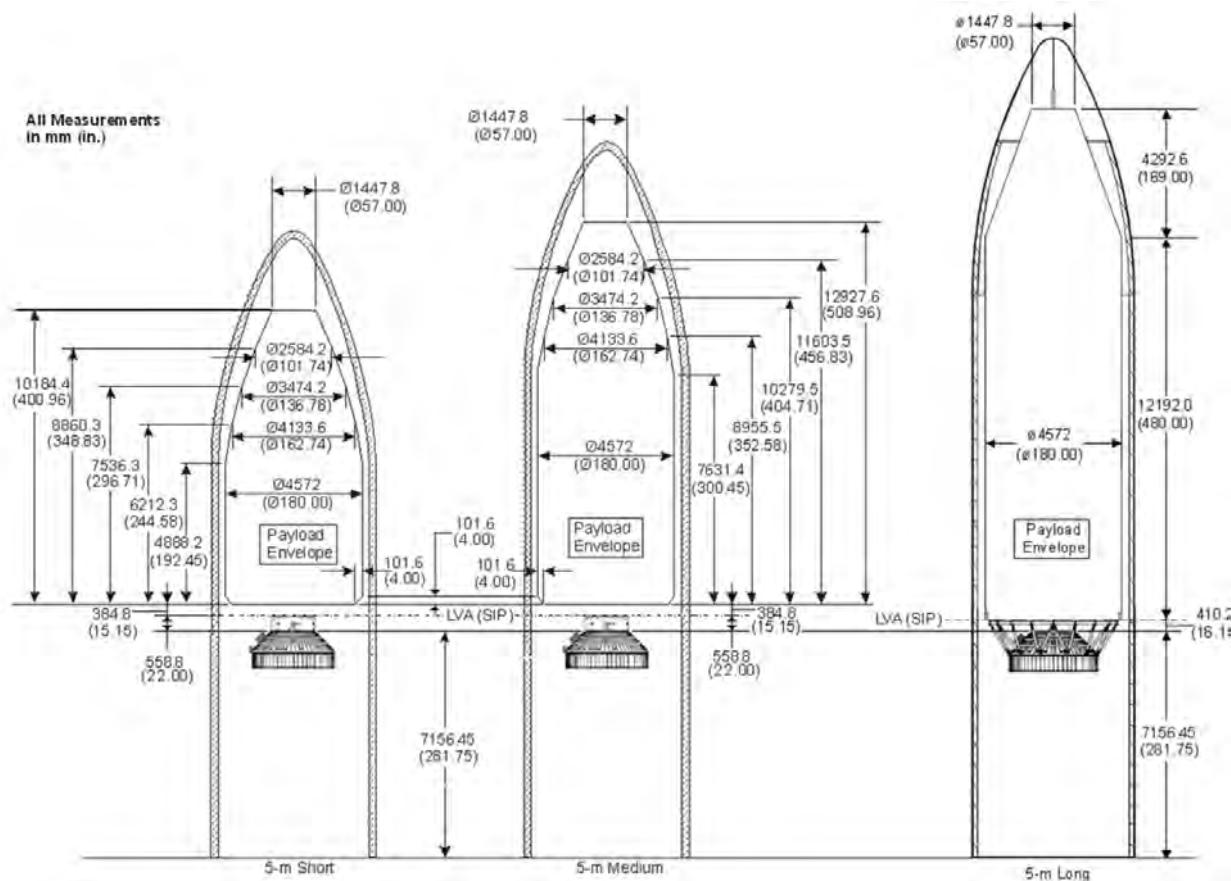
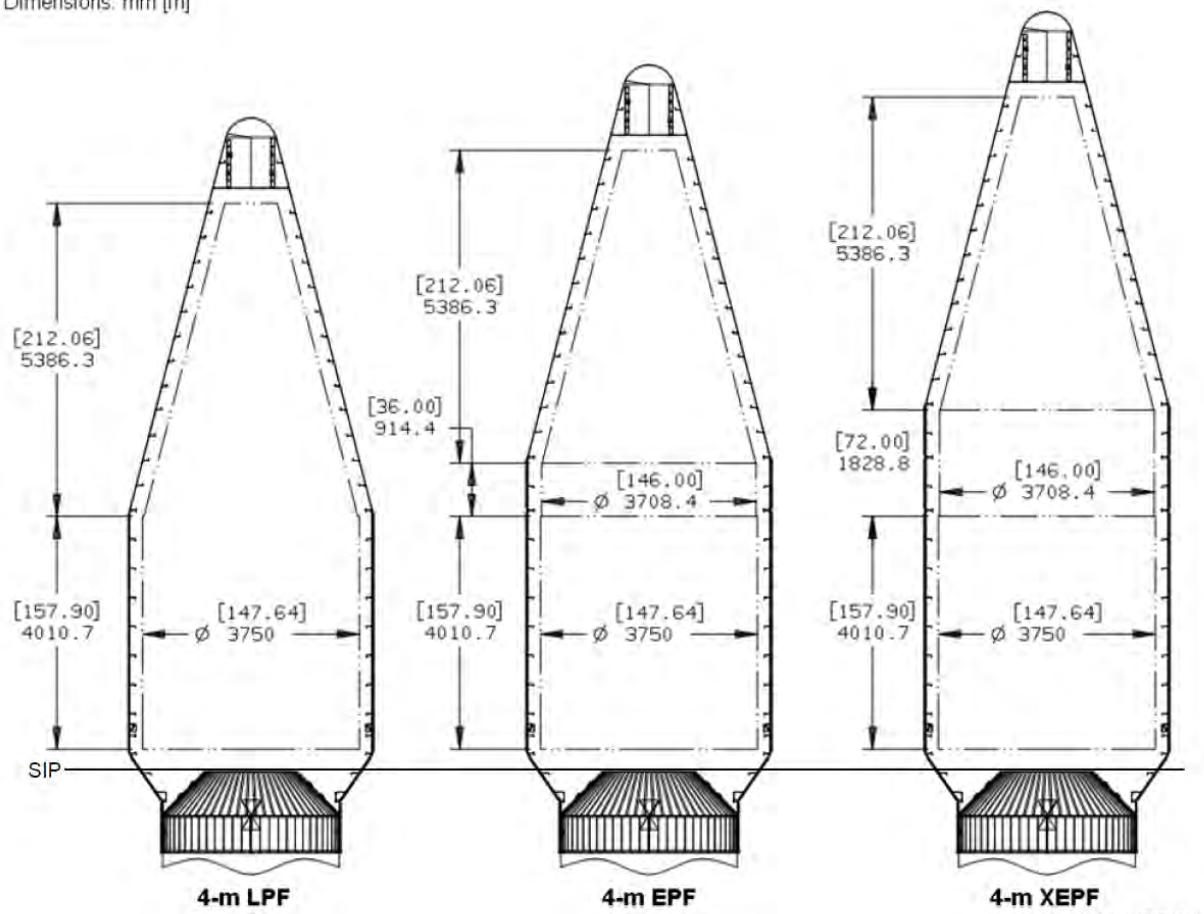


Figure 16: Falcon 9 and Falcon Heavy Fairing Dimensions



**Figure 17: Atlas V 5-meter Fairing Dimensions**

Dimensions: mm [in]



AVUG11\_F06\_03b

**Figure 18: Atlas V 4-meter Fairing Dimensions**

### 3.2 Launch Vehicle Performance

For ballistic missions, the C3 requirement for a given opportunity can be attained directly from the porkchop plots shown in Chapter 10. For missions using solar electric propulsion (SEP), the C3 is co-optimized along with mass and time-of-flight. Therefore, the C3 versus lift-capability relationship for a given launch vehicle is an important input to the optimization process. The launch vehicle performance curves for a few selected launch vehicles are given in Figure 19.

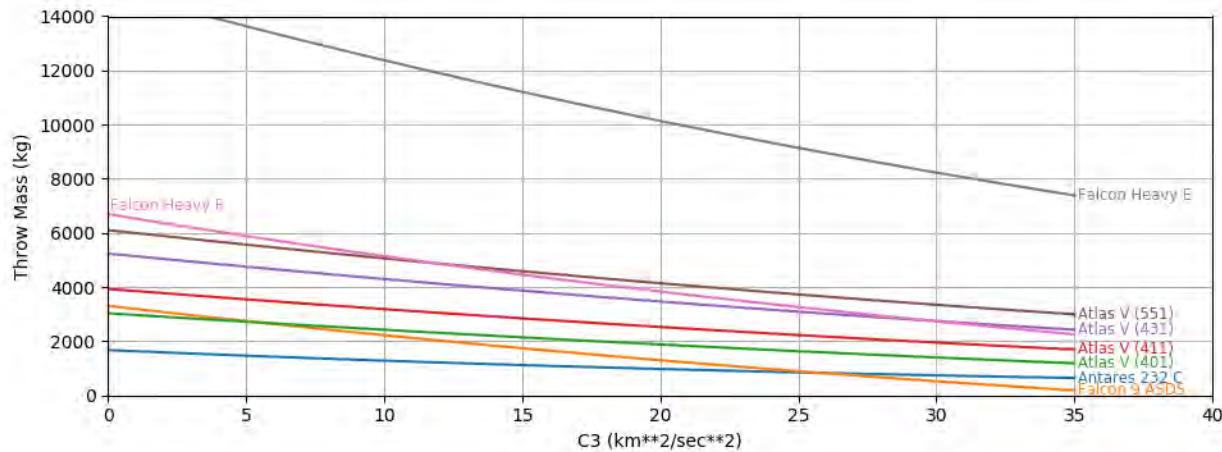


**Figure 19: Launch Vehicle C3 Curves**

Typical C3 requirements for trajectories to Mars can be found in Chapter 10. Figure 20 shows some launch vehicles capabilities to a representative Mars C3 requirement of  $10 \text{ km}^2/\text{s}^2$ .

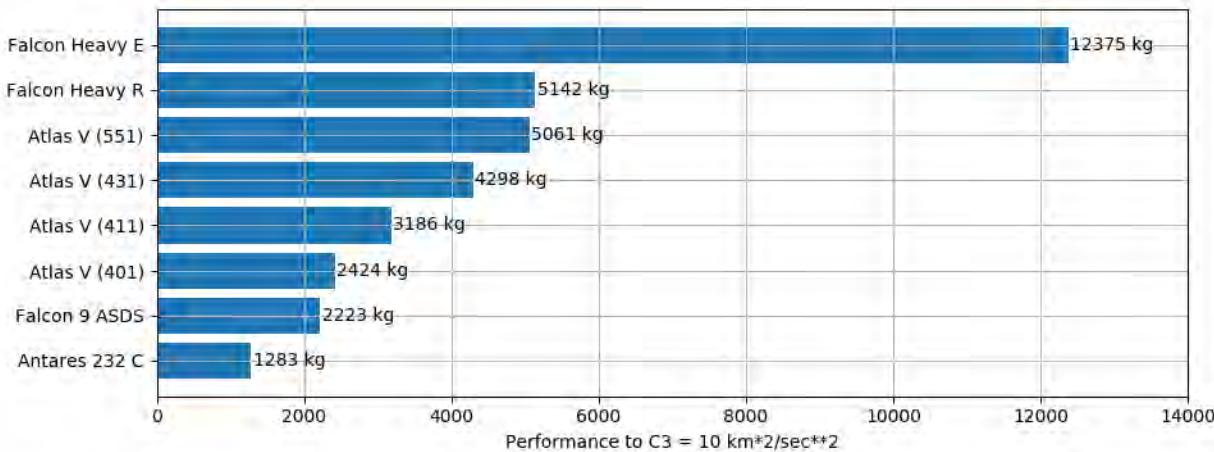


**Figure 20: Launch Vehicle Capabilities to a Representative Mars C3=10.**

In order to estimate launch vehicle performance without repeated queries of the KSC launch website, estimated curve fit coefficients for selected launch vehicles are given in Table 20. The curve used is a 3<sup>rd</sup> order polynomial in C3 such that the performance is as in Equation 8, valid over the range -5 to 40  $\text{km}^2/\text{s}^2$

$$m = \sum_{i=0}^3 a_i C_3^i \quad (8)$$

**Table 20: Launch Vehicle Curve Fit Coefficients.**

Launch Vehicle	a0 (kg)	a1 (kg/(km <sup>2</sup> /s <sup>2</sup> ))	a2 (kg/(km <sup>2</sup> /s <sup>2</sup> ) <sup>2</sup> )	a3 (kg/(km <sup>2</sup> /s <sup>2</sup> ) <sup>3</sup> )
Antares 232 C	1676.8	-44.453	0.53582	-0.003156
Atlas V (501)	2096.2	-55.974	0.33974	0.000132
Atlas V (401)	3033.7	-64.215	0.32704	-0.000054
Atlas V (511)	3265.5	-69.172	0.37028	-0.000218

Launch Vehicle	a0 (kg)	a1 (kg/(km <sup>2</sup> /s <sup>2</sup> ))	a2 (kg/(km <sup>2</sup> /s <sup>2</sup> ) <sup>2</sup> )	a3 (kg/(km <sup>2</sup> /s <sup>2</sup> ) <sup>3</sup> )
Atlas V (411)	3930.8	-78.700	0.42261	0.000023
Atlas V (521)	4193.1	-81.947	0.43788	0.000000
Atlas V (421)	4655.5	-88.675	0.47389	0.000070
Atlas V (531)	4941.0	-92.839	0.49452	0.000389
Atlas V (431)	5237.0	-99.301	0.53555	0.000163
Atlas V (541)	5595.6	-102.823	0.56678	-0.000023
Atlas V (551)	6105.8	-110.700	0.62261	0.000023
Falcon 9 RTLS	1770.0	-86.594	-0.27175	-0.001883
Falcon 9 ASDS	3307.7	-116.881	0.86083	-0.001988
Falcon Heavy R	6696.0	-169.042	1.42723	-0.006384
Falcon Heavy E	14991.9	-281.832	2.08622	-0.006955

### 3.3 Launch Azimuth Restrictions and Declination Penalties

For a launch window to exist, the launch site must pass through the plane of the parking orbit. This places restrictions on the orbital inclinations. The chosen inclination, along with the latitude of the launch site, defines the required launch azimuth. The launch azimuth is typically measured clockwise from North to the velocity vector. A launch due East would take most advantage of the Earth's rotation. A launch due East at the equator would have 464.5 m/s provided by the Earth's rotation. On the other hand, a launch from Kennedy Space Center (Latitude: 28.5 degrees) would have 408.2 m/s provided by the Earth's rotation.

Kennedy Space Center (Cape Canaveral) is located on the eastern coast of Florida, at approximately 28.5 degrees North latitude. Launch azimuth is constrained at the Cape between 35 and 120 degrees due to land mass overflight restrictions. All launches from Cape Canaveral are therefore restricted in inclination between 28.5 and 60 degrees. Cape Canaveral is the launch site for all USA equatorial launches (through orbit changes) and all crewed missions. Vandenberg Air Force Base is located on the southern central coast of California at approximately 34.4 degrees North latitude. Launch azimuths there are constrained to between 147 and 201 degrees, though sub-orbital launches are allowed up to 281 degrees. Satellite inclinations between 63 and 107 degrees are accomplished at Vandenberg. Most USA launches into polar orbits are done from Vandenberg. The allowable launch azimuths and resulting inclinations accessible from Kennedy Space Center are illustrated in Figure 21 and from Vandenberg in Figure 22. These azimuth limits can be exceeded with mission-specific analyses.

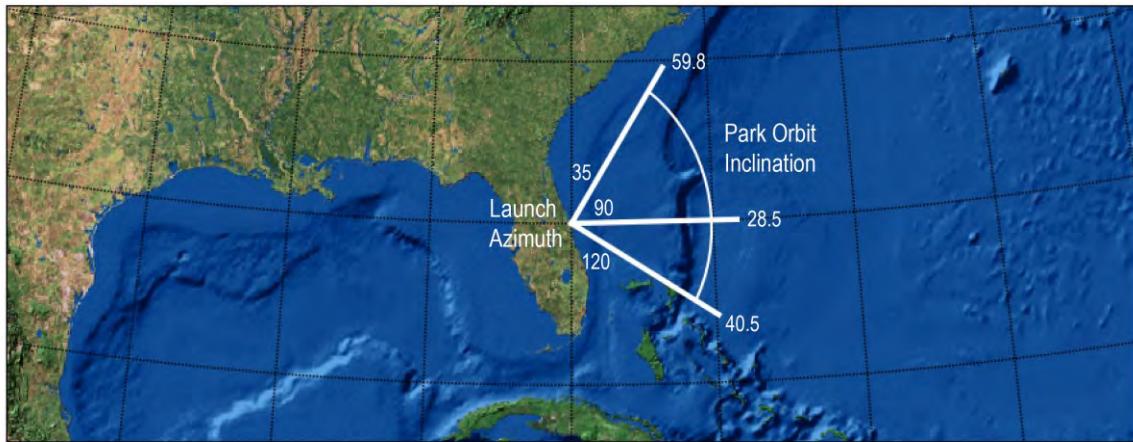


Figure 21: Park Orbit Inclinations from Kennedy Space Center / Cape Canaveral

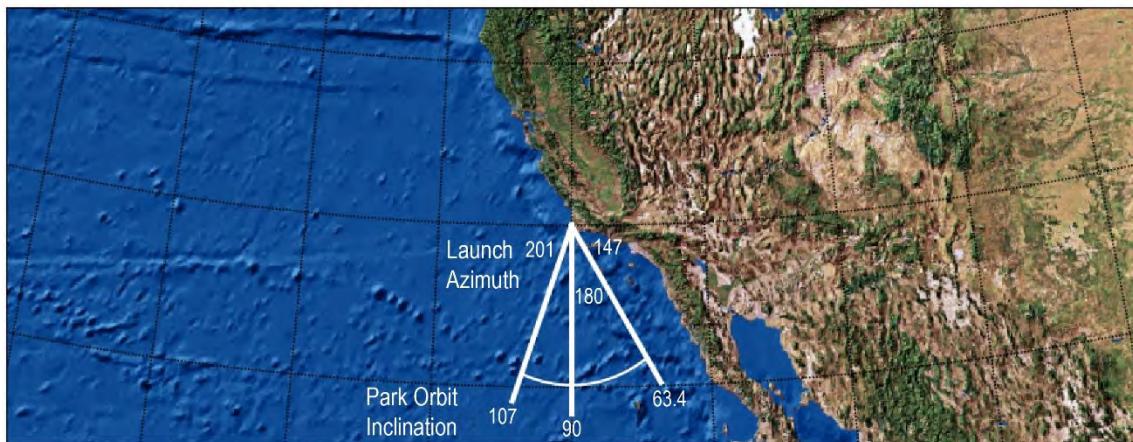


Figure 22: Park Orbit Inclinations from Vandenberg

Launch vehicle performance from the east coast is degraded for park orbit inclinations higher than 28.5 degrees, as illustrated in Figure 23. The piecewise polynomial interpolation was provided by KSC, the parameters of which are tabulated in Table 21. A west coast launch cannot take advantage of the Earth's rotation in the same way as an east coast launch, and so park orbit inclinations up to 70 deg suffer a 20% penalty (a multiplier of 0.8) relative to an easterly launch from the east coast. Higher inclinations suffer penalties in the 40% (multiplier of 0.6) range.

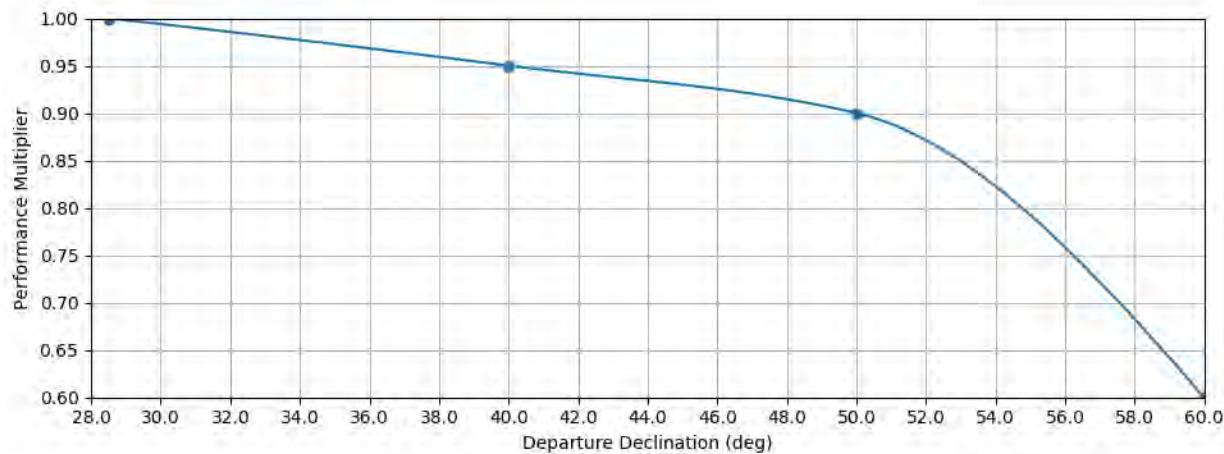


Figure 23: East Coast Launch Declination Performance Penalty

Table 21: East Coast Launch Declination Performance Penalty Coefficients

DLA Range	a0 ( $)$ )	a1 ( $\text{deg}^{-1}$ )	a2 ( $\text{deg}^{-2}$ )	a3 ( $\text{deg}^{-3}$ )
$ \text{DLA}  \leq 28.5$	1	0	0	0
$28.5 <  \text{DLA}  \leq 40$	1	-3.998989e-03	-3.363295e-05	2.868940e-07
$40 <  \text{DLA}  \leq 50$	0.95	-4.658722e-03	2.888872e-04	-3.230150e-05
$50 <  \text{DLA}  \leq 60$	0.9	-8.571429e-03	-3.035714e-03	8.928571e-05

## 4 Ballistic Mission Design

### 4.1 Overview

A ballistic mission design is the most common way to get to Mars. The spacecraft is launched, and, except for a few small maneuvers en route, coasts to Mars. This coasting is dominated by the gravity of sun. The trajectory is thus an ellipse in heliocentric space. Other forces are relatively minor perturbations – essential for the high-fidelity modeling required for a launch vehicle target specification or operations, but ignorable for preliminary design.

Optionally, a large deep space maneuver of several hundred m/s of  $\Delta V$  or more can be included in the design. Such a maneuver results in a trajectory described by two (or more) heliocentric ellipses. This is generally referred to as “broken-plane” trajectory.

### 4.2 Lambert Solutions

A “Lambert Solution” is the general solution to how to fit an ellipse between two points (e.g. Earth’s location at launch and Mars’s location at arrival) with the Sun at one of the foci of the ellipse and a given flight time between those two points. The equation that describes the solution must be solved numerically, but there are many algorithms for doing so. Ref [1] has an excellent discussion. In general, given the starting position, a targeted position, and a desired time of flight, there is a single prograde solution. For interplanetary mission design purposes, these three parameters are (generally) not independent. Mars’s location at arrival is dictated by the launch date (which sets Earth’s position) and the flight time, for example. Thus, launch date and the arrival date uniquely define a ballistic interplanetary trajectory. The exception is when the desired flight time results in at least one complete revolution about the sun. There may be two solutions for a given launch-date/arrival-date pair in that case.

Lambert Solutions are classified by “Type.” A trajectory that traverses less than 180 deg of arc is a “Type I” solution. One that traverses between 180 deg and 360 deg is a “Type II”. See Figure 24. This distinction is important for two reasons. First, since Earth and Mars are not in co-planar orbits, the closer the transfer comes to 180 deg, the further and further out of the ecliptic the trajectory must become, and the more and more energy is required to get onto the required heliocentric ellipse. Second, a Type II trajectory has a navigation challenge; a maneuver close to the point where the trajectory has 180 deg of traverse to go can become exceptionally large. This point is typically not long after launch, and so removing the launch bias and cleaning up the launch vehicle injection errors requires some additional analysis. This is rarely a significant penalty.

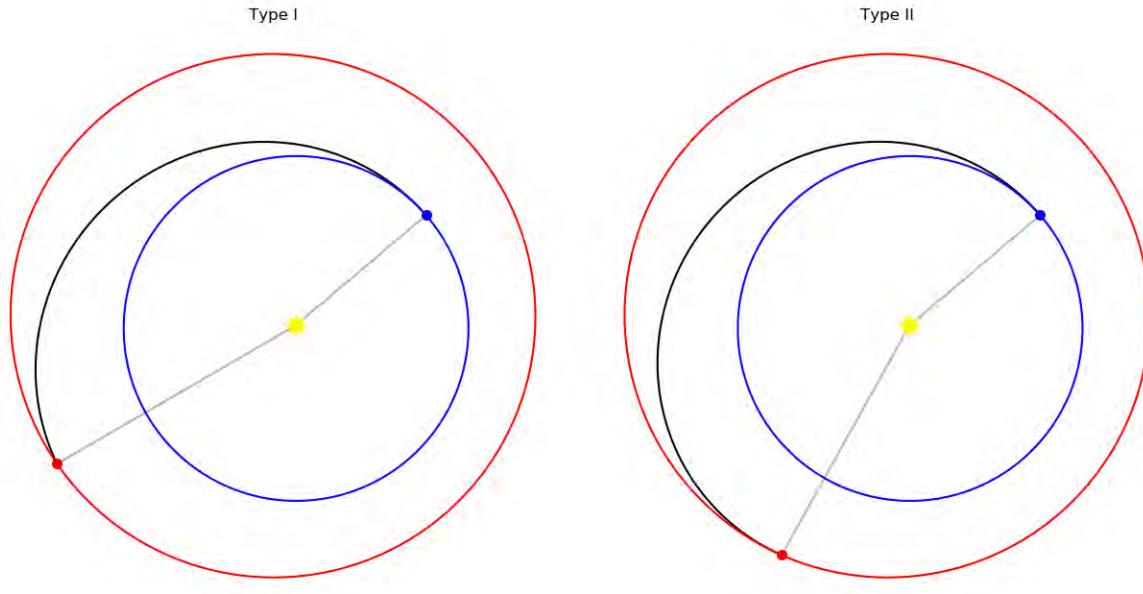


**Figure 24: Examples of Earth-Mars Trajectories**

Trajectories with transfer angles between 360 deg and 540 deg (one to one and a half revolutions about the sun) are “Type III” trajectories. Similarly to the Type I/Type II pairing, a “Type IV” trajectory traverses between 540 deg and 720 deg (one and a half to two revolutions). This schema is extensible to solutions that involve more than two revolutions about the sun (Types V, VI, and beyond), but the transfer times are exceptionally long and aren’t typically considered.

Trajectory types with at least one complete revolution (III and above) can, but do not always, have two solutions to Lambert’s problem. These solutions involve ellipses with larger or smaller semi-major axes. These are referred to as the “long period” and “short period” solutions and are designated with a “+” or “-”, respectively. Thus, a “Type III+” trajectory is a long period solution that traverses between 360 deg and 540 deg of arc. For example, there are two Type III solutions for an Earth departure on June 19, 2026 and a Mars arrival on June 20, 2028. The long-period solution has a heliocentric semi-major axis of 1.31 AU, a launch energy ( $C_3$ ) of  $12.7 \text{ km}^2/\text{s}^2$ , and an arrival  $v_{\infty}$  of 3.1 km/s. The short-period solution has a heliocentric semi-major axis of 1.23 AU, a  $C_3$  of  $25.1 \text{ km}^2/\text{s}^2$ , and an arrival  $v_{\infty}$  of 4.9 km/s. The two transfers are illustrated in Figure 25.

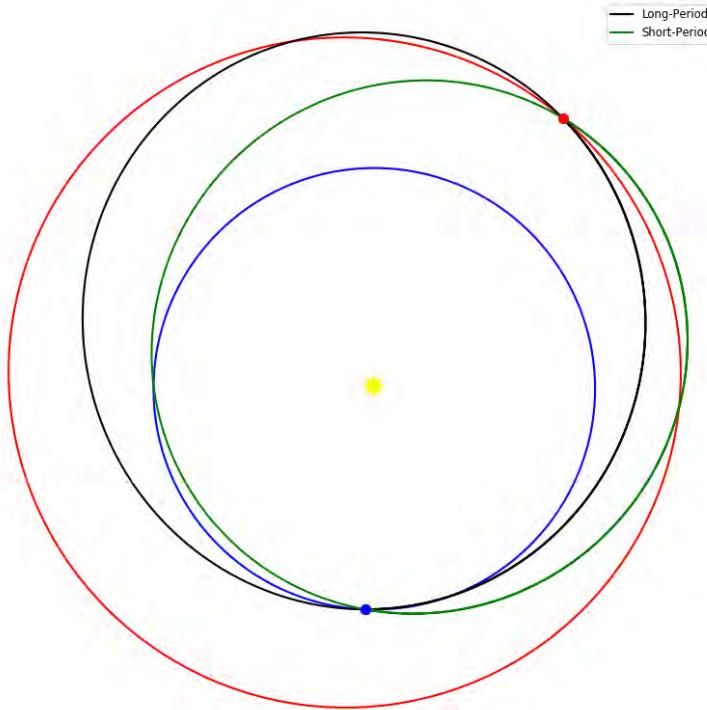


**Figure 25: Type III+ (black) and Type III- (green) trajectories for the same Earth departure and Mars arrival dates**

Once the heliocentric ellipse has been identified, the heliocentric velocity of the spacecraft on that ellipse at departure and arrival can be differenced from the planets' velocities at those points to yield the "v-infinity vector." These vectors are thus the asymptotes of the departure and arrival hyperbolae, respectively, and determine the departure and arrival energies and geometries. They are typically considered in spherical coordinates (magnitude, declination, and right ascension), and the primary effects of each parameter are captured in Table 22.

**Table 22: V-Infinity Vector Parameters**

Symbol	Name	Primary Effect
<b>Launch/Departure</b>		
C3	Launch Energy, the magnitude of the inbound v-infinity vector squared	Launch performance (or departure $\Delta V$ required)
DLA	Declination of the Launch Asymptote	Sets minimum park orbit inclination; if higher than launch site latitude, a launch vehicle penalty is applied.
RLA	Right Ascension of the Launch Asymptote	Sets the launch time of day
<b>Arrival</b>		
VHP	Approach V-Infinity	$\Delta V$ required for orbit insertion (orbiters) Determines entry velocity (landers)
DAP	Declination of the Arrival Asymptote	Defines minimum achievable inclination (orbiters) Contributes to maximum north/south reachable latitude (landers)
RAP	Right Ascension of the Arrival Asymptote	Longitude of the ascending node (orbiter) Landing time of day (landers)

### 4.3 Porkchop Plots

Since a launch-date/arrival-date pair uniquely defines a ballistic interplanetary trajectory and the associated energies and geometries, a classic way to visualize the trade space is to plot contours on a so-called “porkchop plot.” These plots have launch date on the horizontal axis and arrival date on the vertical axis. A simple porkchop plot will show contours of constant v-infinity vector parameters, such as C3, DLA, and VHP. These are mission-independent, being defined solely by the solution to Lambert’s Problem. Mission-specific, “derived” plots translate the v-infinity vector parameters into other geometries, such as the maximum reachable north latitude, the landing time at a target latitude, the longitude of the ascending node of a particular orbit, the launch mass, or the post-capture orbit period. These other parameters depend on other inputs, like launch vehicle performance (see Sections 3.2 and 3.3), the descent central angle (see Section 7.2), and propulsion assumptions (see Section 8.3).

Figure 26 is an example of a basic porkchop plot. The launch date axis (horizontal) spans late 2026 to mid-2027, while the arrival date axis (vertical) spans mid-2027 to mid-2028. The launch energy (C3), in blue, shows the two lobes of a porkchop, separating the Type I (lower-right) and Type II (upper-left) trajectories. The “ridge” separating these lobes is a consequence the difference in heliocentric inclinations of the orbits of Earth and Mars. All of the contours are masked above a C3 of 50 km<sup>2</sup>/s<sup>2</sup> for clarity. A high-performing launch vehicle can certainly launch spacecraft beyond a C3 of 50 km<sup>2</sup>/s<sup>2</sup>, but this is a reasonable limit to highlight the structure. Some features to note for this particular opportunity:

- 1) Most of the Type I region has relatively high declinations; the 30 and 40 deg contours bracket the minimum C3 contour of 15 km<sup>2</sup>/s<sup>2</sup> (which is itself a relatively high C3 for a Mars mission).
- 2) The lowest-VHP section of the Type I does not have this declination problem; the DLA is about 20 deg here.
- 3) The Type II region requires a lower C3 and declinations. The penalty region is only at higher C3s. The VHP is lower throughout.

- 4) The minimum energy transfers (lowest C3 and lowest arrival velocity) occur with an arrival date corresponding to an Ls of 150 deg or so, in late northern summer and the start of the regional dust storm season.
- 5) The Sun-Earth-Mars conjunctions (Sun-Earth-Probe (SEP) angle  $\leq 5$  deg, in grey) are several months after the lowest energy part of the porkchop, as is typical for a Type I/II.

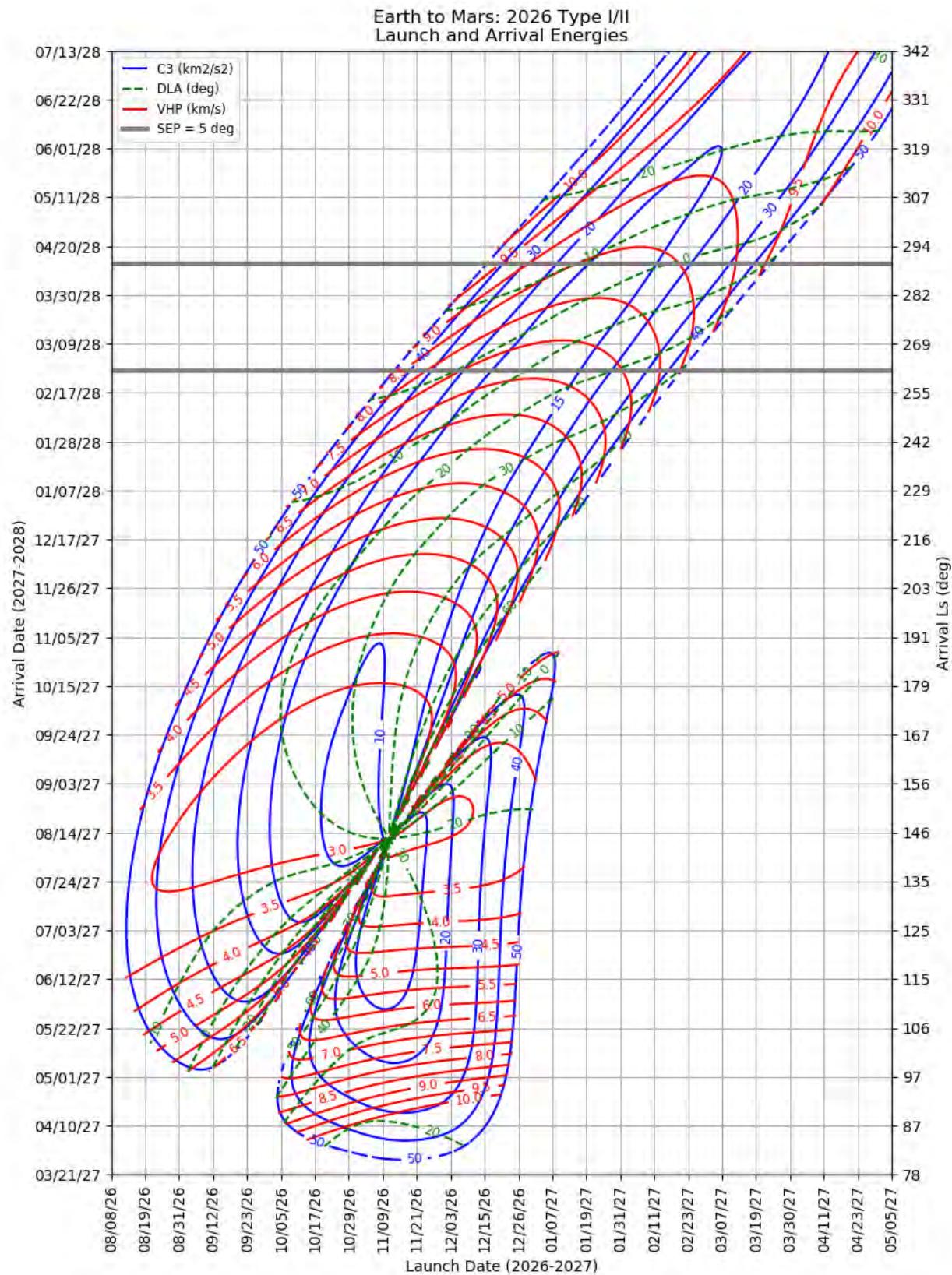


**Figure 26: Example Earth to Mars Porkchop (2026 Type I/II)**

In addition to contours, a porkchop can also include shaded regions that illustrate launch/arrival date pairs that meet some Boolean condition. This is typically done for EDL Communication (see Section 7.4) performance; the shaded regions are those where a particular asset has full (or occasionally partial) visibility to the lander during its EDL sequence, subject to the various necessary assumptions.

Figure 27 is the porkchop plot for the 2018 InSight mission and illustrates how a project may use a specific porkchop. It is a zoomed-in view of the Type I region. The blue contour is the C3, with the  $28 \text{ km}^2/\text{s}^2$  contour in bold. This was the largest C3 that their Atlas V 401 would be able to deliver the spacecraft. The red VHP contour of  $3.94 \text{ km/s}$  yielded the maximum-permissible inertial entry velocity of  $6.31 \text{ km/s}$ . The secondary scale on the right is the longitude of the sun ( $L_s$ ), showing that the launch period (black boxes) was during the global dust storm season. The blue, green, peach, and purple shaded regions illustrate the InSight launch/arrival pair for which the various orbiters (MRO and MAVEN) and Earth (DTE) had line of sight from entry to landing + 60 sec subject to the various assumptions in the title. This porkchop was used to determine the launch/arrival strategy of “a 35-day launch period extending May 5<sup>th</sup> to June 8<sup>th</sup>, 2018 with a constant arrival date on November 26<sup>th</sup>, 2018 to maximize the MRO capability without driving DTE right to edge of its capability.” [22]

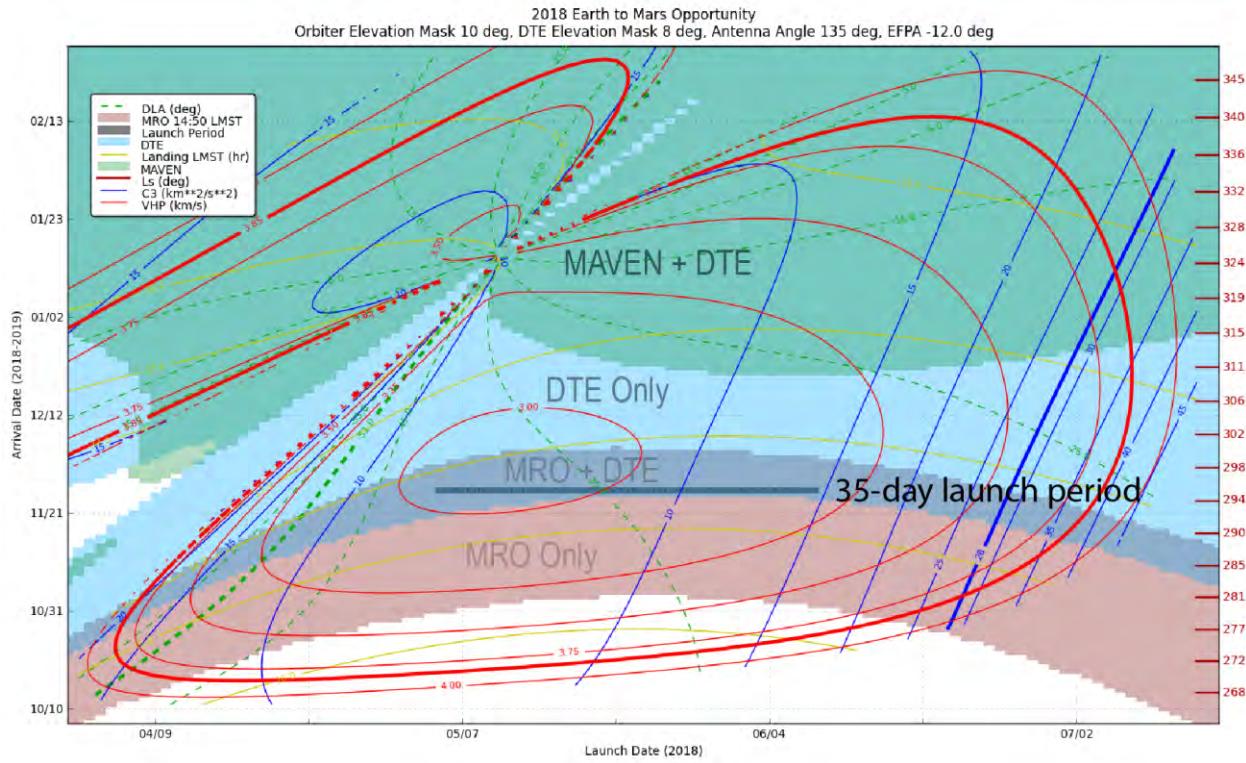


Figure 27: InSight Porkchop Plot

#### 4.4 Broken Plane Trajectories

A second class of ballistic mission designs called “Broken Plane” trajectories seeks to break the one-to-one relationship between the launch/arrival date pair and the trajectory. A broken plane trajectory uses a large deep space maneuver to modify the trajectory. The two main uses are to “tunnel through the ridge” between the Type I and Type II lobes of the porkchop and to launch with a very low declination when the launch/arrival pair would require a larger value. In

both cases, the heliocentric orbit experiences a plane change at the deep space maneuver, hence a “broken plane” maneuver.

The maneuver sizes vary from hundreds of m/s to a few km/s of  $\Delta V$ , and so they are rarely useful for maximizing the mass delivered to Mars outside of the region of the ridge or when the DLA penalty is large. Instead, broken plane maneuvers are best suited to achieving geometries that are enabling for a design. The number of options for what a broken plane trajectory can do in terms of reducing the launch declination and either or both of the launch and arrival energies, changing the landing time of day, or other geometric changes is very large and very project-specific and so we do not present detailed porkchop data for broken plane maneuvers.

## 5 Solar Electric Propulsion Mission Design

### 5.1 Overview

The advancement of solar-electric propulsion (SEP) technologies and larger, light-weight solar arrays offer a tremendous advantage to Mars orbiters in terms of both mass and timeline flexibility. These advantages are multiplied for round-trip orbiters (e.g. potential Mars sample return) where a large total  $\Delta V$  would be required. This is due in large part to the order-of-magnitude increase in specific impulse (Isp) vs. traditional chemical propellants. The trade-off comes in the form of the need for very large power systems and significantly lower thrust with SEP. Even with these trades, SEP can still offer Mars missions 50% or more mass delivered, along with timeline flexibility measured in months to years. The analysis of low-thrust trajectories requires the use of optimization techniques whose results are highly dependent on mission parameters such as thruster type, power level, sun distance, dry mass, etc.

SEP technologies have advanced significantly over the past few decades. While satellites have been using electric propulsion for station keeping since the 1960's, it was not until the past two decades that the commercial market started regularly adopting the technology. Now it is regularly used in commercial spacecraft buses, both for station keeping and orbit raising. By 2017, over 248 spacecraft had employed electric propulsion in Earth orbit. It is now more common for GEO spacecraft to use SEP than chemical propulsion. The vast majority are either gridded ion or Hall-effect thrusters, which are technologies replacing the arcjet systems of previous decades. SEP has also been used to go beyond Earth orbit, reaching destinations such as comets (Deep Space 1), asteroids large and small (Dawn, Hayabusa), and dwarf planets (Dawn).

### 5.2 Considerations in choosing to use SEP

SEP is primarily advantageous for missions that have a high  $\Delta V$  requirement. When the total mission  $\Delta V$  grows beyond the exhaust velocity (i.e. Isp\*g, or around 2 - 3 km/s for chemical propellants) the propellant mass is more than two times the dry mass, and quickly grows from there. For SEP with the same  $\Delta V$  requirement, the propellant load goes from 67% of the wet mass to less than 15%. Figure 28 further illustrates the benefits of higher Isp's for large  $\Delta V$  missions. The upper two lines, representing chemical thrusters, show that propellant mass increasingly dominates total mission mass. The lower two, on the other hand, show that SEP can significantly reduce propellant loads out to 8 km/s and beyond.

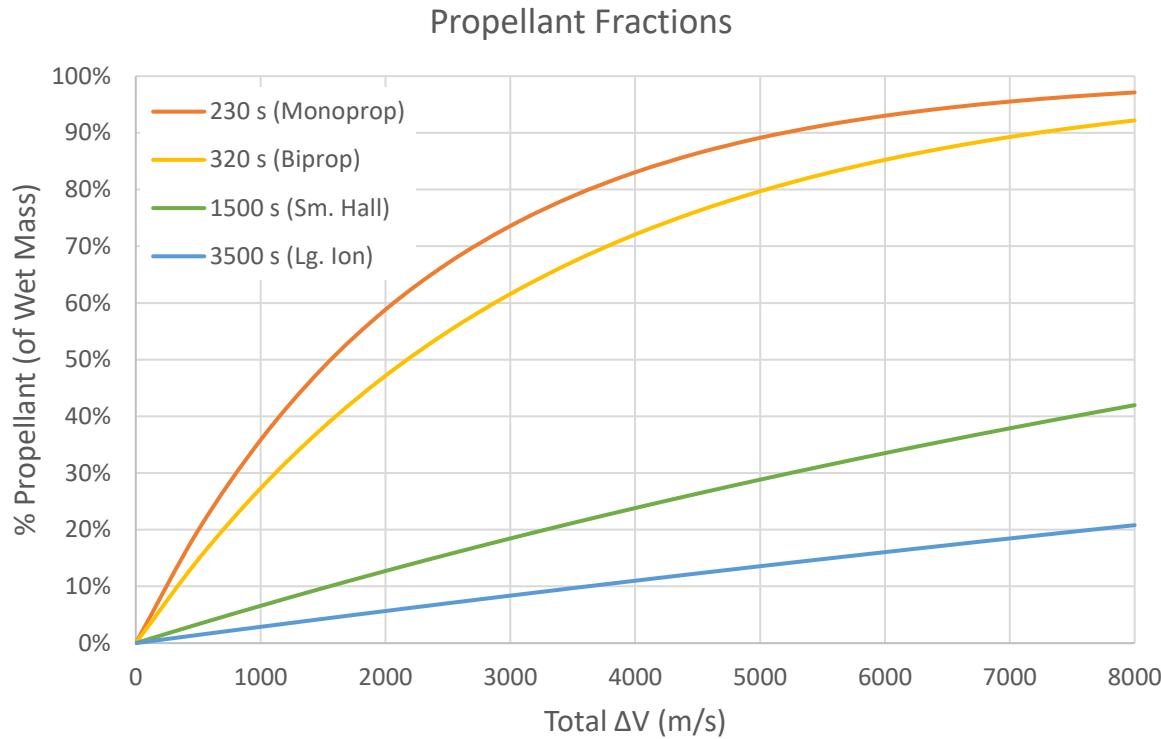


**Figure 28: Total Propellant Fractions for Chemical vs. SEP Thrusters**

This substantial mass savings can be mission enabling. While the decision whether to use SEP technology in a mission concept is primarily influenced by propulsion demands, there are many other considerations to bear in mind:

Benefits:

- **High Isp** - leading to reduced propellant loads. Can be 5-10x more efficient than chemical propellants. Ranges from 800 – 4000 seconds. Can enable missions that would be unaffordable or impossible with chemical propulsion.
- **Smaller launch vehicle** – reduced wet mass or launch energy requirements may allow for smaller, lower-cost launch vehicles or increased competition.
- **Extra power** – larger solar arrays for propulsion also leads to extra power available for other systems once the final orbit is achieved.
- **Reduced g loads** – low-thrust does not produce the large accelerations and vibrations typical of chemical thrust.
- **Safer propellants** – xenon and other SEP propellants are often inert and inherently safer to handle than chemical propellants such as hydrazine. This can save money in integration costs and can be a major factor when being considered as a secondary.
- **No critical events** – low-thrust maneuvers take place over days to months and do not have critical events such as injection burns where an anomaly could result in mission loss.
- **Tradable margins** – low-thrust trajectory optimization allows for much greater

flexibility in trading margins such as mass, power, time, etc. (See Figure 29)

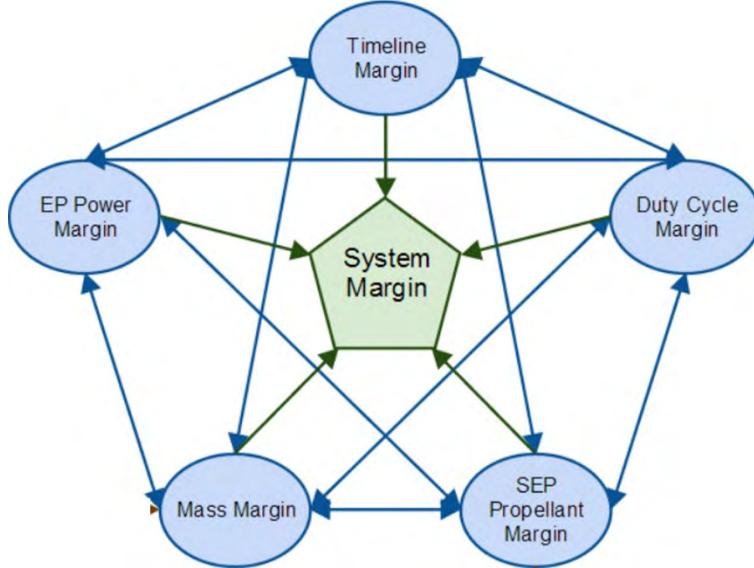


Figure 29: Tradability of margins allows for greater flexibility in SEP missions

- **Flexible timelines including long launch periods** – Low-thrust trajectories are inherently flexible. Changes in launch and arrival dates may only result in very small propellant penalties. Launch periods of 6 months or longer are possible with similar arrival dates.
- **Less demanding launch targets** – the nearly continuous thrust of SEP trajectories can easily correct inaccuracies in launch vehicle injections.

#### Challenges:

- **Large power requirements** – SEP thrusters typically need many kW's of electrical power, requiring large solar arrays.
- **More complex mission design** - difficult to optimize and choose among many solutions. Changes in mass, propulsion, or power during design iterations also necessitate trajectory redesigns.
- **Cost risk** – despite the increasing number of SEP missions being flown, there is still much uncertainty in the cost associated with incorporating SEP systems for Mars. For some Earth missions, SEP has been shown to be cheaper.
- **Technology risk** – although SEP is now very common in Earth orbiters, it is not commonly used in deep space. There are some challenges associated with using SEP for planetary missions, namely the long life, throughput, and illumination variation with solar distance.
- **Complex operations** – the “always-on” nature of most low-thrust trajectories require more navigational support throughout cruise and mission operations.

### 5.3 Specific Impulse vs. Thrust

Solar electric thrusters utilize electrical power from solar arrays to accelerate ions in order to create thrust. While they come in many varieties, the most common can be broken into two types: Hall-effect and gridded ion. In Hall thrusters, the thruster generates and traps electrons in a magnetic field, using them to ionize the onboard propellant -- in most cases the inert gas xenon

-- into an exhaust plume of plasma that accelerates the spacecraft forward. A gridded ion thruster also starts by ionizing a neutral gas, creating a cloud of positive ions. These ions are then accelerated by the Coulomb force along an electric field created between two or more grids. Temporarily stored electrons are reinjected by a neutralizer in the cloud of ions after it has passed through the electrostatic grid, so the gas becomes neutral again and can freely disperse in space. The lifetime of gridded thrusters is often limited by erosion of the exhaust grids. Advanced Hall thrusters can take advantage of magnetic shielding, thus vastly improving total throughput.

The thruster efficiency is defined as the ratio of the kinetic energy of the exhaust particles (or jet energy), to the electrical input power to the propulsion system. Typical efficiency values range from 40 – 65%. Peak efficiency is usually attained near the maximum input power of the thruster, and decreases as power drops. Thrust ( $T$ ) is related to the efficiency ( $\eta$ ) and specific impulse ( $I_{sp}$ ) through the equation:

$$T = 2\eta P / I_{sp} g \quad (9)$$

where  $P$  is the power and  $g = 9.80665 \text{ m/s}^2$ . This equation shows that if  $I_{sp}$  and efficiency are held constant, then thrust is linearly proportional to the input power. Table 23 lists a few large SEP thrusters along with their key parameters such as power, thrust, efficiency, and  $I_{sp}$ . Note that the gridded ion thrusters typically have a higher  $I_{sp}$  and less thrust than Hall thrusters. Larger thrusters also tend to be more efficient than smaller thrusters (not shown on this table).

**Table 23: Selection of SEP Thrusters and Associated Parameters.**

Thruster Name	Type	Mode	Power [kW]	Thrust [mN]	Isp [s]	Efficiency [ $\eta$ ]	Thrust/Power [mN/kW]	Throughput [kg]*	String Mass [kg]*
XR-5 (BPT-4000)	Hall	High Thrust	4.8	281	1865	51%	58	900	34
		High Isp	4.8	252	2010	53%	52	900	34
SPT-140	Hall	-	4.9	262	1720	45%	54	333	28
XIPS	Ion	-	5.0	173	3507	59%	34	250	50
NEXT-C	Ion	High Thrust	6.9	227	3999	65%	33	600	84
		High Isp	6.9	219	4077	64%	32	600	84
HERMeS	Hall	-	13.5	612	2805	62%	45	3400	114

\*Notional values. May be outdated.

SEP thrusters can typically be throttled by adjusting either the current (A) or voltage (V) of their input through a power processing unit (PPU). More current typically equates to more thrust, and likewise, voltage leads to higher specific impulse. Gridded ion engines will often operate at voltages greater than 1 kW, whereas Hall thrusters are more typically in the 300 – 800 W range. Most PPU's provide power at discrete combinations of current and voltage, called throttle points. This forms a grid of possible Isp's and thrust values. In practice, the throttle points that provide either the highest thrust or Isp for a given input power are used to create continuous "thruster curves" that can be fit by a polynomial and fed into trajectory optimizers. Figure 30 shows an example of thrust and Isp curves for ion and Hall thrusters. Note that the thrust curves are fairly

linear, but  $I_{sp}$  decreases rapidly at lower powers due to inefficiencies in these regimes.

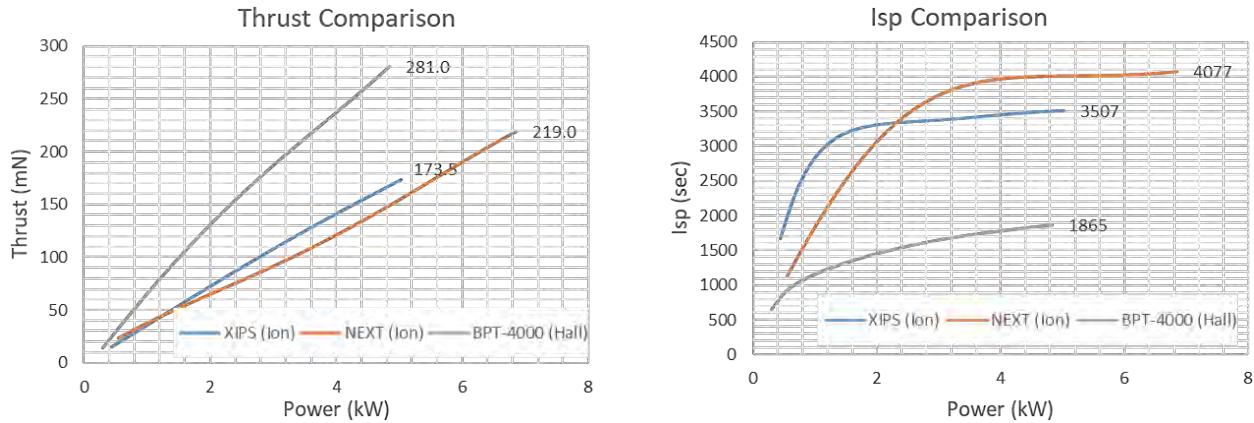
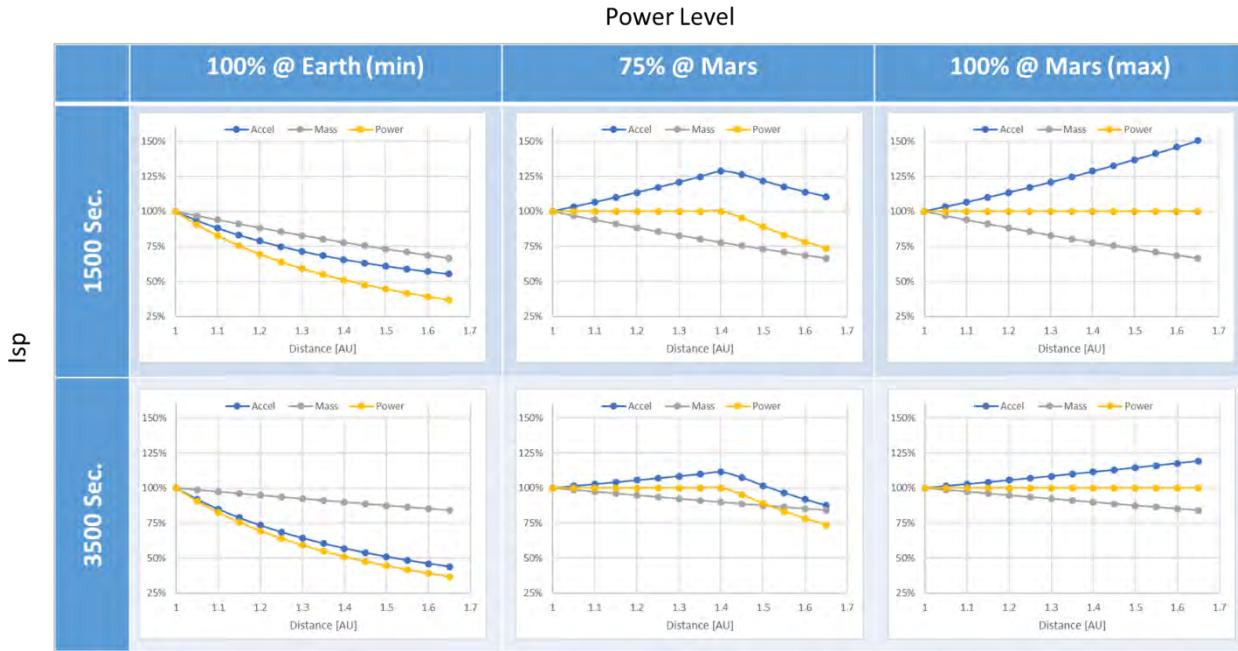


Figure 30: Example Throttle Curves for Ion and Hall Thrusters

## 5.4 Normalized SEP Systems

Estimating the performance of SEP missions, or the proper sizing of the SEP system itself, requires some generalizations. Compared to traditional ballistic trajectories and near-impulsive chemical maneuvers, low-thrust SEP is far less intuitive. To first order, a low-thrust trajectory to Mars is a nearly-continuous maneuver – first accelerating away from Earth, then thrusting to circularize and match the velocity of Mars, and finally spiraling down the Mars gravity well to the desired orbit. Of course, much depends on the mission specifics such as starting and ending points, propulsion systems, and time-of-flight.

The most straightforward simplification of a low-thrust trajectory is to assume starting and stopping at  $C_3 = 0 \text{ km}^2/\text{s}^2$  (i.e. the sphere-of-influence) with respect to Earth and Mars, and by holding both specific impulse and acceleration constant. While this is mathematically satisfying, it is impractical and not achievable in real-world missions. It is difficult to discuss the optimization of low-thrust trajectories without knowing the detailed properties of the engines being used. To first order, it may be sufficient to assume a constant  $I_{sp}$  and efficiency. This is particularly true when the power level remains nearly constant over the trajectory, such as during spirals at Earth or Mars (the Martian eccentricity, however, does cause a fair bit of variation). In this case, the thrust is linearly proportional to input power. However, in reality, most thrusters vary in  $I_{sp}$  and efficiency as power varies. In fact, the power-processing unit (PPU) can often vary both current and voltage to create multiple operating throttle points. Trajectory optimization routines can use these points, or a polynomial fit of thrust vs. power and mass flow rate vs. power, to optimize heliocentric trajectories that have varying solar power.



**Figure 31: Variations in acceleration, mass, and power as solar distance increases. Isp is held constant at 1500 s (small Hall thruster) or 3500 s (large Ion thruster). The power level is sized such that it provides 100% of the thruster's max power at Earth, 75% of max power at Mars, or fully powered at Mars.**

Figure 31 illustrates how various parameters change with solar distance given the assumption that Isp and efficiency are held constant, subject to the maximum output of the engine. The top row of plots is representative of a small Hall thruster (1500 sec) and the bottom row represents a large Ion thruster (3500 sec). As solar distance increases, power available decreases as  $1/r^2$ , leading to changes in engine output. Three power scenarios are shown – 1) just enough power for full thrust at Earth, 2) 75% of maximum power at Mars (with excess power unused near Earth), and 3) 100% of maximum power at Mars (meaning full thrust is always available). In these plots, mass (gray lines) decreases as propellant is expended through constant thrusting. This decrease in mass leads to an increase in acceleration even when thrust remains constant. However, once power starts dropping, thrust and acceleration also begin to drop.

Another thruster parameter crucial to interplanetary SEP missions is the maximum throughput of each engine. This can be expressed in kilograms, hours, or total impulse. It is necessary to have thrusters that can provide the high  $\Delta V$ 's required for the trip from Earth to Mars – as much as 10 km/s or more, where up to half of the wet mass could be propellant.

The key thruster parameters needed are:

- Maximum and minimum input power [kW]
- Thruster string (with PPU, gimbal, etc.) mass [kg]
- Thrust vs. Power curve [N vs. kW]
- Mass flow rate (or Isp) vs. power curve [g/s or sec vs. kW]
- Maximum throughput [kg, hrs, or N/s]

It is important to select thrusters that are sufficiently sized for the mass and  $\Delta V$  of the desired mission. We have found that a good rule-of-thumb is to select engines and power levels to give initial acceleration levels of 0.15 – 0.3 mm/s<sup>2</sup>. This can be achieved via one thruster, or multiple smaller ones. As mentioned, it is also critical to use engines with enough throughput capability.

It is possible to carry extra “spare” engines to cover the requirement, but the mass penalty can be high. Table 24 lists some other rules-of-thumb that can be useful in preliminary SEP mission design.

**Table 24: Rules-of-Thumb for Mars SEP Missions**

Parameter	Suggested Rule	Comment
Initial Acceleration at Earth	0.15 – 0.3 mm/s <sup>2</sup> or 15 – 30 µg (micro g's)	Assumes maximum engines at full thrust with full power at 1 AU. (0.05 – 0.4 mm/s <sup>2</sup> still feasible for longer or shorter TOFs)
Solar Array Power Density	11-15 kg/kW	Assumes flexible substrate (e.g. UltraFlex)
Efficiency of Large SEP Thruster	60%	Typically, slightly higher for ion engines. Small thrusters should use 40-50%
Isp for ion thruster	3500 – 4000 s	Lower for thrusters < 2 kW
Isp for Hall thruster	1500 – 2500 s	Typically scales with size
Initial Power Need Estimate	60-80% of thruster saturation at Mars	Thrusters do not need to be fully powered at Mars, otherwise much power is wasted early in the trajectory
Alternate Initial Power Need Estimate	5-10 W/kg of estimated wet mass	Can be used when a specific thruster is not known

## 5.5 Design Process

A first-order estimate of the total wet mass of a SEP mission can be obtained by making a series of assumptions and using some basic equations to calculate propellant needs.

The basic process is as follows:

1. Estimate the dry mass of the spacecraft
2. Estimate the specific impulse and thrust of the SEP system
  - a. Choose a thruster (such as one from Table 23) so that the thrust gives sufficient acceleration at Earth
  - b. Estimate a power level, possibly using the ROTs in Table 24
3. Estimate the total  $\Delta V$  needed for the mission, bearing in mind that low-thrust  $\Delta V$  requirements depend on thrust levels and time-of-flight, and often vary greatly from impulsive maneuver requirements.
  - a. Figure 32 can be used to estimate  $\Delta V$ , given specified starting and ending points.
  - b. Heliocentric  $\Delta V$  can be reduced with more C3 energy provided by the launch vehicle (Up to around 10-20 km<sup>2</sup>/s<sup>2</sup>, beyond that  $\Delta V$  increases again).
  - c. Estimates for  $\Delta V$  during circular, coplanar spirals can be obtained by simply using the difference in circular velocity at the start and end. By this method, capture from infinity is just the final orbit's circular velocity (e.g. 3 km/s for low Mars orbit). More detailed corrections can be found in [23]. Elliptical and non-coplanar captures are more complex.
4. Use the rocket equation and the Isp to determine the propellant mass needed:

$$M_{\text{prop}} = M_{\text{dry}} [e^{(\Delta V / I_{\text{sp}} g)} - 1] \quad (10)$$

Where  $M_{\text{prop}}$  is the total propellant (usually xenon) needed,  $M_{\text{dry}}$  is the dry mass of the spacecraft plus suitable margins, and  $g = 9.8 \text{ m/s}^2$ .

5. An initial estimate for the total wet mass of the mission is then  $M_{\text{wet}} = M_{\text{dry}} + M_{\text{prop}}$

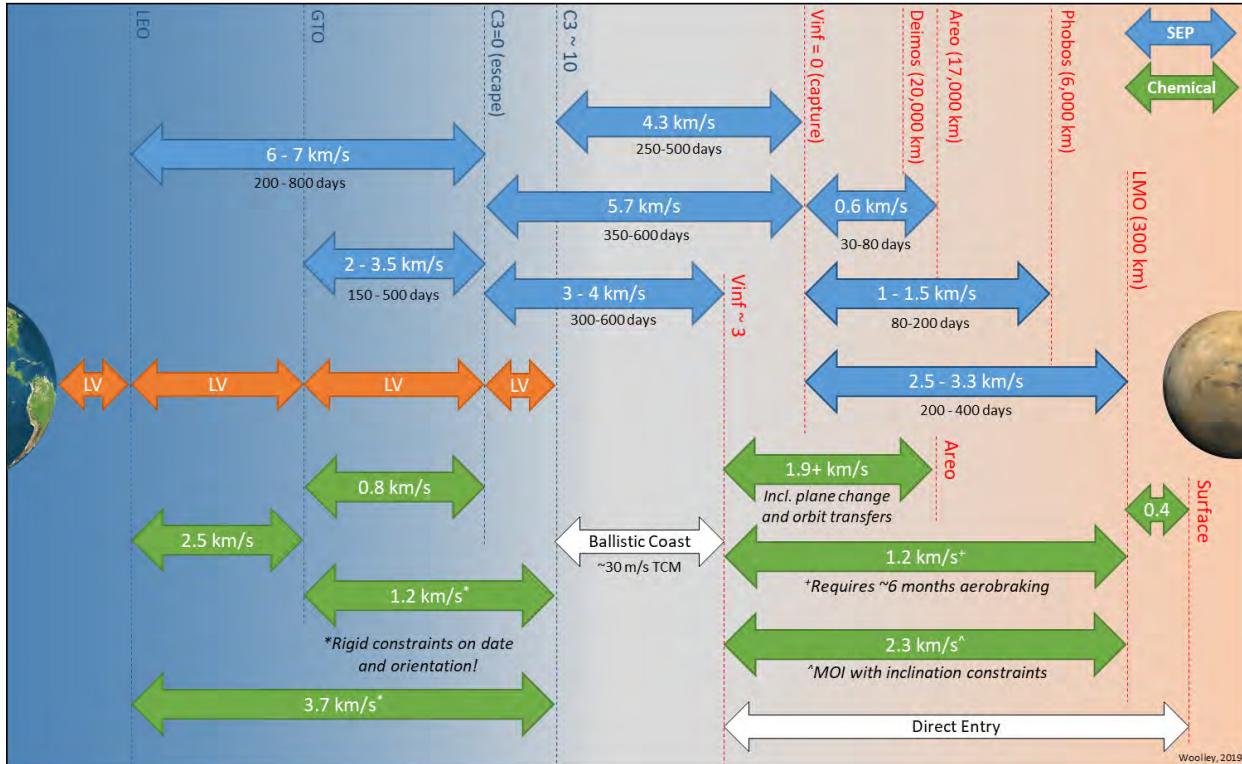
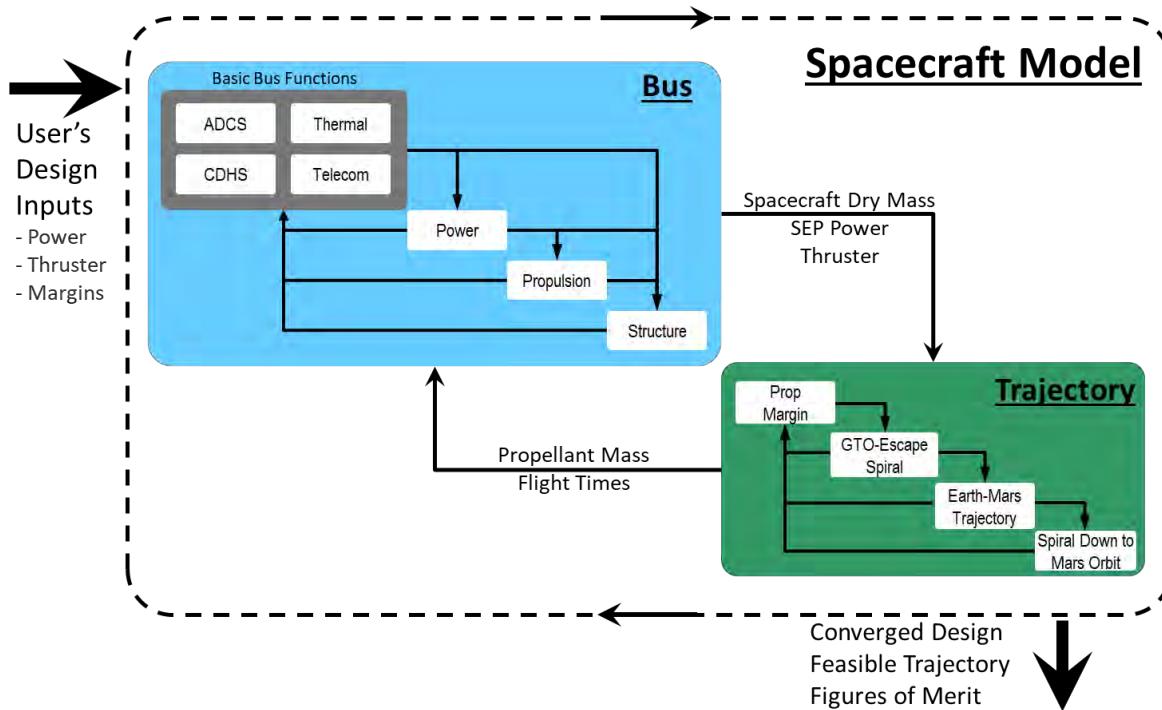


Figure 32: Typical  $\Delta V$  Requirements from Earth to Mars

A major challenge in formulating interplanetary mission concepts utilizing electric propulsion is the large number of trajectory variables that must be considered (thrust profile, flyby options, launch vehicle delivery), all of which are affected by spacecraft design variables (power, mass, thruster, payload, staging). This is significantly more complex than traditional ballistic/chemical mission design and early concepts are often suboptimal as a result, potentially missing valuable options. It is important to simultaneously optimize the spacecraft design alongside the trajectory given mission constraints and objectives.

The mission design process consists of an iteration loop between a spacecraft module and a trajectory module (See Figure 33). These modules can be as simple or complex as desired. A tool created for this process can be an effective method to design a SEP mission to Mars orbit. The trajectory module consists of a combination of parametric curve fits and a large database of optimized low-thrust trajectories. The spacecraft module has basic parametric models of key spacecraft subsystems that vary with wet mass. For more details, see [24].



**Figure 33: Process Algorithm for an SEP Mission Architecture Design Tool that Simultaneously Optimizes both Spacecraft and Trajectory**

### 5.5.1 Bacon Plots

A “bacon plot” is the SEP analog to the ballistic porkchop plot. It is a set of contours that represent key parameters of trajectories plotted over a range of launch and arrival dates. Bacon plots differ from porkchop plots in that they are mission-specific. The launch-date/arrival-date pairs do not uniquely define a trajectory, as in the ballistic case. An appropriate objective function, as well as the characteristics of the propulsion system, power system, and masses, must be considered in order to optimize the trajectory for each launch/arrival date pair. Many bacon plots must be created to assess the impact of the various assumptions, such as power levels or engine choices.

The contours displayed in the launch date/arrival date space can be any number of trajectory parameters from the optimizer output, but typically the most useful is to show maximum delivered mass (when given a starting constraint) or minimum propellant mass (when given an end constraint). Figure 34 shows a typical Earth to Mars bacon plot with maximum mass contours. As the colored contours progress from red to blue, more mass can be delivered to low Mars orbit for a given launch vehicle and low-thrust propulsion system. The contours for a ballistic porkchop plot (with aerobraking) are shown for the same transfers. The porkchop plot uses the same contour lines and shows the relatively small region where ballistic transfers are possible. The magenta dots show the maximum mass delivered for each given time-of-flight.

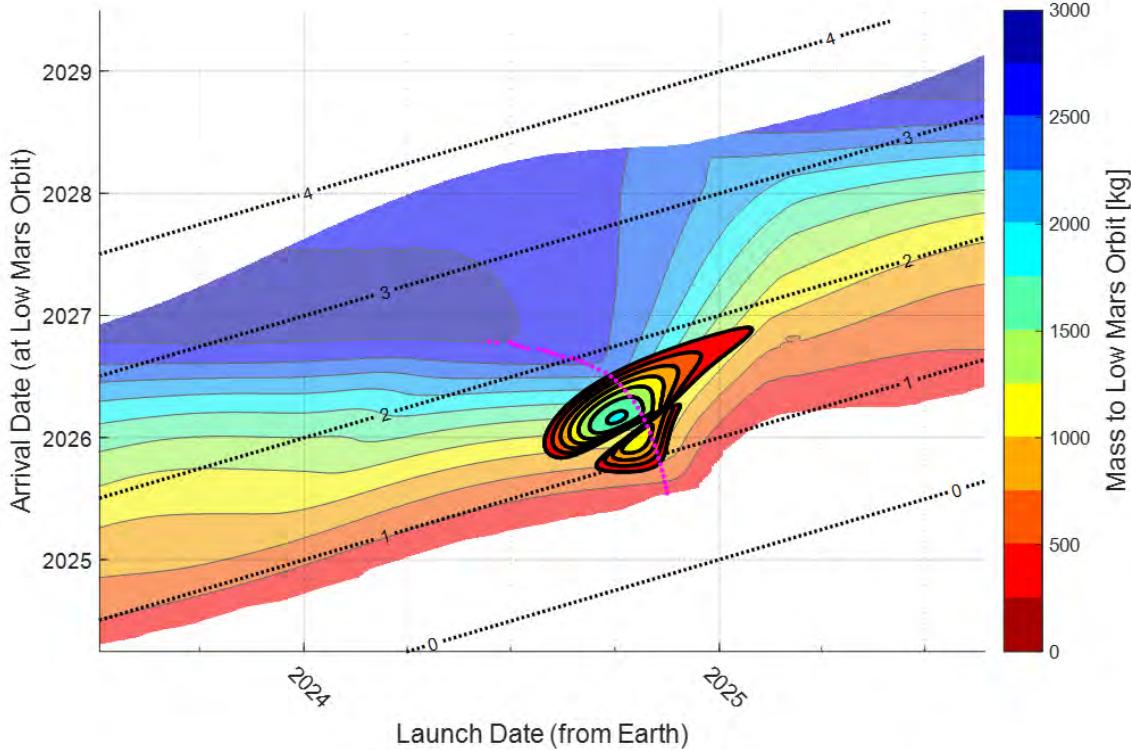


**Figure 34: Example Bacon Plot with Ballistic Porkchop Plot Superimposed.** The launch date at Earth spans one synodic period (780 days). Diagonal lines show transfer times in years. Contour lines show the total delivered mass to Mars for a given launch vehicle – with blue being the highest. SEP allows for nearly continuous launch periods and increased delivery mass for longer flight times. The magenta dots represent the maximum mass delivered for a given time-of-flight.

There are a few items of note when assessing a bacon plot. The first is that the contours are typically open rather than closed, creating continuous bands of launch opportunities with times of flight fluctuating with the synodic cycle. Rarely are discontinuities found, and when they do appear, it is typically due to optimizer convergence issues. Each point on the plot represents an optimal solution for the date pair, but there are suboptimal solutions “below” each point. As previously mentioned, each bacon plot must be defined by a number of assumptions. The transfers are not mission independent as they are with porkchop plots. The following parameters define a unique bacon plot:

- Starting state (Starting mass and location/orbit or LV performance curve)
- Ending state (Mars rendezvous, orbit, entry velocity, etc.)
- Thruster set (includes type, mode, and quantity of active thrusters)
- Power level (power available for SEP, typically defined at 1 AU)

Note that the trajectory between that starting state and the ending state can be comprised of multiple segments or phases. For example, a trajectory from launch vehicle to low Mars orbit is comprised of a heliocentric leg (launch C3 to Mars rendezvous, defined as a v-infinity of 0 km/s in the patched-conic sense) and a spiral leg down to low orbit. The combined masses,  $\Delta V$ 's, durations, etc. are represented in bacon plot contours. Typically, either the starting state or ending state will contain the objective function of the optimizer, while the other contains an end constraint (e.g. specifying a starting mass and maximizing the ending mass). In theory, a bacon plot could be constructed for the combined phases of an Earth-Mars-Earth round-trip, as long

as the parameters for each segment are clearly defined. In complex mission formulation, however, it is usually more efficient to create bacon plots for each leg and survey the possible combinations with a search algorithm.

As mentioned, bacon plots typically consist of open contour lines which span across all launch dates rather than the closed contours of porkchop plots. Bacon plots do, however, still follow the same 26-month synodic period, creating opportunities where more performance is possible with shorter transfer times. These roughly align with ballistic optima, but are much more open and subject to the assumptions behind the bacon plot. Table 25 gives the dates that are roughly the “centers” of each opportunity for mission planning, bearing in mind that each unique mission could find an optimal solution many months before or after the dates given. In fact, launch may occur virtually any time if longer trip times are acceptable.

**Table 25: Optimal Date Ranges for SEP Transfers.**

Opportunity	~Optimum*	Start Date	End Date
2020	6/29/2020	3/21/2020	10/7/2020
2022	8/18/2022	5/10/2022	11/26/2022
2024	10/6/2024	6/28/2024	1/14/2025
2026	11/25/2026	8/17/2026	3/5/2027
2028	1/13/2029	10/5/2028	4/23/2029
2031	3/4/2031	11/24/2030	6/12/2031
2033	4/22/2033	1/12/2033	7/31/2033
2035	6/11/2035	3/3/2035	9/19/2035
2037	7/30/2037	4/21/2037	11/7/2037
2039	9/18/2039	6/10/2039	12/27/2039
2041	11/6/2041	7/29/2041	2/14/2042

\*Approx. optimal launch date. The true “optimum” region can vary by up to ±100 days, depending on specifics. These dates do not apply to Mars-to-Earth, which typically have an optimal arrival date rather than departure.

Low-thrust transfers also don’t vary as significantly from opportunity to opportunity as do ballistic transfers. To first order, it is reasonable to add 780 days (~1 synodic period) to a solution and it will still be valid.

## 5.6 EP Cruise Stages for Landers

Adding solar electric propulsion to a Mars lander cruise stage can open up additional design possibilities beyond what is possible with a nearly-ballistic (i.e., TCMs totaling less than about 50 m/s) transfer. There are similarities with large chemical propulsion deep-space maneuvers (DSMs), such as broken-plane maneuvers, but the much higher specific impulse of a SEP system can enable a much larger  $\Delta V$  to be imparted for a given propellant load.

As with a ballistic cruise stage, it is generally preferable to launch with a positive C3, thus avoiding spiraling up at the Earth, and to arrive at Mars with v-infinity greater than 0 km/s, since the Mars atmosphere provides an efficient means of slowing the landed stage. As a consequence, SEP-augmented transfer families still have a porkchop-like structure, but can have much larger regions of feasibility. When programmatic constraints on the launch date or

when landing season constraints on the arrival date are outside the optimal dates of a ballistic transfer, a SEP cruise stage can deliver more landed mass or allow the use of a smaller launch vehicle. In addition, a SEP cruise stage can allow a longer launch period than what may be possible ballistically. A SEP cruise stage also allows flexibility in the Mars arrival geometry, which would otherwise be fixed for a ballistic transfer with given launch and arrival dates. In particular, this allows the entry velocity to be adjusted and the landing local solar time (LST) to be directly controlled to be within the bounds required for Terrain Relative Navigation (TRN) or EDL communications.

A SEP cruise stage deviates from the ballistic cruise stage heritage used by landed missions since the 1997 Mars Pathfinder mission through Mars 2020. Notably, it requires the integration of an electric propulsion system and needs a larger power system and solar arrays. A SEP system would use a 3-axis stabilized cruise stage, which has been used on previous Mars missions such as Phoenix and InSight, whereas a spinning cruise stage was used for Pathfinder, the Mars Exploration Rovers, Mars Science Laboratory, and Mars 2020. Depending on the thrust available, the benefit of a SEP cruise stage may be more pronounced for longer transfers to Mars (such as Type III or IV, or transfers with a Mars flyby) where more time is available to impart  $\Delta V$ . A SEP design has the benefit of not having critical events (as opposed to DSMs which could be critical events) in cruise, but a robust SEP trajectory requires consideration of missed thrust due to spacecraft safe modes to be included in the design process. Furthermore, the low-thrust trajectory would likely have built-in roughly month-long coasts after launch (for checkout) and before arrival (for EDL preparation). Navigation of a SEP cruise stage is an important consideration as well; analysis has shown that the required accuracies are likely achievable.

## 5.7 Further Reading

For more about SEP systems and Mars Mission Design, the authors recommend [25], [26], [27], [28], and [29]

## 6 Planetary Flybys

### 6.1 Overview

Flying direct from Earth to Mars is not the only path. One may consider adding planetary flybys to the itinerary, trading flight time and some complexity for desired geometries or timeline. Unlike for the outer planets, adding a flyby does not generally reduce propellant requirements. Mars and Earth are simply too close to each other. An exception is  $v$ -infinity leveraging where the mission launches with a low C3 and then performs a maneuver en route to an Earth gravity assist, or uses a Mars gravity assist followed by a maneuver to reduce the propellant required to achieve a lower Mars approach velocity.

Adding a flyby to a Mars-to-Earth trajectory is also possible. However, this chapter considers planetary flybys in the context of Earth-to-Mars transfers.

### 6.2 Earth-Earth Loops

The most straightforward option for adding a planetary flyby is the Earth-Earth Loop. In this trajectory, the spacecraft launches from Earth, flies by the Earth a year later, and then continues to Mars. The Earth-Mars leg is identical to a normal Earth-Mars trajectory, but the Earth-Earth leg in front of it means the spacecraft launches a year earlier. The Earth-Mars porkchop or bacon plot can then be used if the Earth-Earth loop is ballistic for the launch energy and Mars arrival conditions.

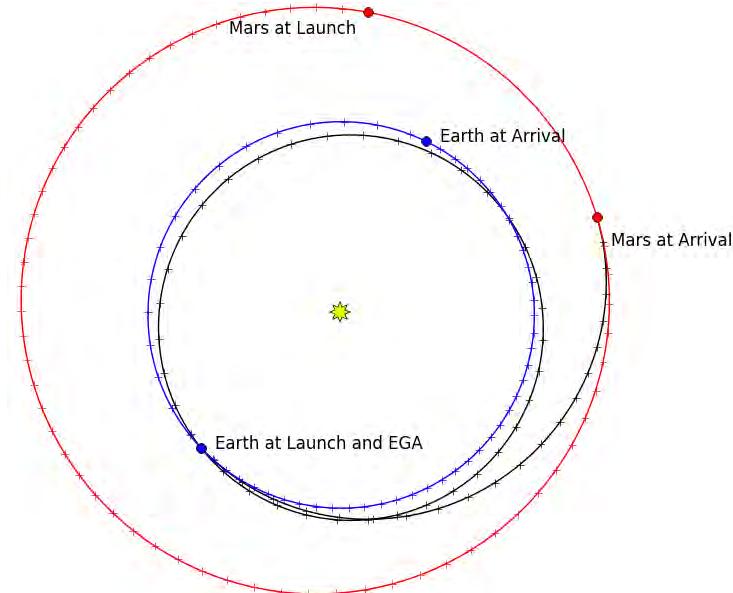


Figure 35: Example of an Earth-Earth Loop followed by a Type I Earth-to-Mars Trajectory

There are a few reasons to consider an Earth-Earth Loop. The first is programmatic. Sometimes when a launch is possible programmatically does not line up nicely with when a launch is possible astrodynamically. For example, the 2014 Discovery AO required that the mission launch no later than December 31<sup>st</sup>, 2021, with selection to occur no earlier than September 2016 [30]. The low-energy portion of the Type I/II 2020 Earth-Mars opportunity in July/August 2020 is only 46 months from the no-earlier-than selection date and a mere 42 months after the announcement that Lucy and Psyche had been selected (January 4<sup>th</sup>, 2017)

[31]. Either is a little short for most missions. Regardless, the Mars 2020 Rover mission was scheduled to launch in this opportunity, precluding the use of an Atlas from Florida. A non-Atlas launch vehicle or a VAFB launch could solve that, but the compressed schedule would remain. If the compressed schedule were impossible, the only option for a direct Earth-Mars mission would have been the Type III/IV- in November/December 2021 (see Chapter 10), arriving in February 2024, for a 26-month flight time. However, by adding an Earth-Earth loop in front of the 2022 Type I/II opportunity, a launch in September 2021 with a September 2022 flyby would arrive at Mars in April (Type I) or October (Type II) 2023, for an 18 or 25 month flight time. Depending on the mission requirements, this may be a more attractive option than the Type III/IV- beyond the reduction in flight time.

The second reason to consider an Earth-Earth Loop is to eliminate large declination penalties. For example, the Type I opportunity in 2022 requires very high launch declinations across the low-C3 region, as does the Type I in 2033. An Earth-Earth loop can launch into a low declination and the Earth flyby could be used to achieve the required outbound declination. This would not be recommended in the case of small performance penalties as the Earth-Earth loop is not “free.” Some propellant would be required for additional trajectory correction maneuvers to target and clean up the flyby. For a Mars-to-Earth trajectory this aspect of an Earth-Earth loop can be used to re-position the inbound v-infinity vector to enable a landing at a specific site when it would otherwise be impossible due to an unfavorable approach declination, or the ballistic opportunities offer an undesirable set of geometries, such as the landing time.

The third reason to consider an Earth-Earth Loop is unique to SEP missions. The specific impulse of a SEP system is significantly larger than a rocket upper stage, and an Earth-Earth loop can be used to launch with a low C3. The spacecraft can then thrust en route to an Earth flyby at a higher C3 (this technique is referred to as “v-infinity leveraging”), at which point it can either coast to Mars or continue thrusting. A classical v-infinity leveraging maneuver is performed at aphelion or perihelion to encounter the Earth at a different point in its orbit and increase the v-infinity more than the deep space  $\Delta V$  itself. In terms of delivered mass, for Earth-Mars transfers, this is generally only useful with the higher specific impulse of a SEP system. This may offer higher delivered mass to Mars than a direct transfer. The more the leveraging, the longer the time between launch and the Earth gravity assist. For Mars-to-Earth trajectories, this leveraging can be used to reduce the propellant required to achieve the desired approach velocity.

In addition to the added flight time, Earth-Earth loops have other downsides. If the spacecraft contains significant radiological material, such as a radioisotope thermoelectric generator (RTG), then the presence of an Earth flyby in the trajectory complicates the launch approval process. The backward contamination planetary protection requirements of performing an Earth gravity assist with Mars samples on board would also need to be considered. More common, however, is the thermal issue. As illustrated in Figure 35, above, perihelion is less than 1 AU (about 0.9 AU, as shown). This is an (almost) unavoidable feature of a ballistic Earth-Earth loop, and SEP-driven trajectories are more efficient with a lower perihelion. A lower perihelion means more thermal loading from the sun, which must be considered in the spacecraft thermal design. In general, the higher the required C3, the lower the perihelion. Higher declination can be accepted for a higher perihelion. There is also a seasonal dependence; launches near the equinoxes have higher perihelions than those near the solstices. See Figure 36.

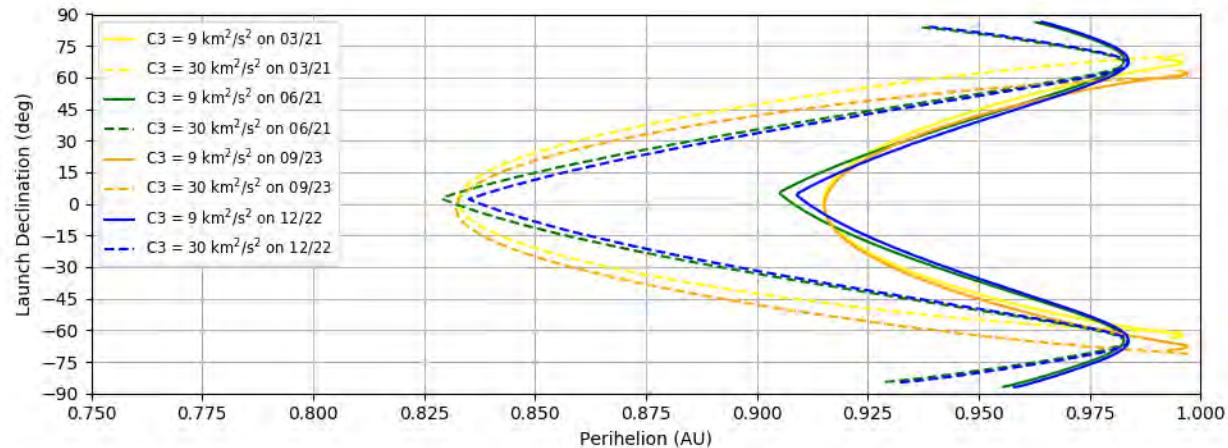


Figure 36: Launch Declination and Perihelion for a Ballistic Earth-Earth Loop

### 6.3 Earth Backflips

A special case of the Earth-Earth loop is the Earth Backflip, also known as a pi transfer or nodal re-encounter. The ballistic Earth-Earth Loop puts the spacecraft into a heliocentric orbit with the same orbit period as the Earth. A backflip trajectory puts the spacecraft in a heliocentric orbit with the same orbit period and eccentricity as the Earth. The excess energy (from a positive C3) goes into the inclination, which gives the trajectory type its name. The spacecraft launches at one node and re-encounters the Earth half a year (hence “pi-transfer”) at the opposite node hence (“nodal re-encounter”). An example of an ascending-to-descending backflip is illustrated in Figure 37. This trajectory is only possible with very high declinations, since the spacecraft must fly toward the ecliptic north or south, and the Earth’s equator is inclined by 23.5 deg from the ecliptic. Thus the declination must be approximately  $\pm 67.5$  deg. Figure 36 illustrates this; the points with perihelion around 1 AU and very high declinations are Earth backflips.

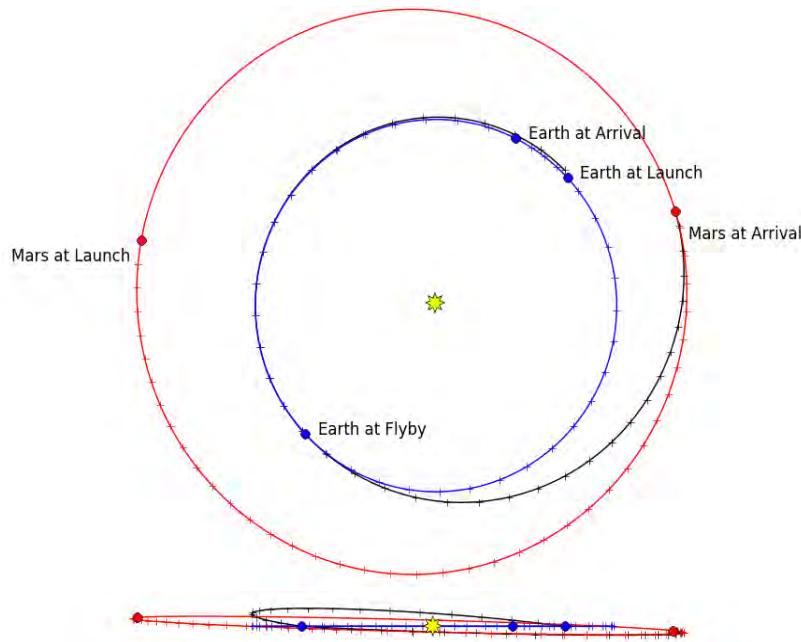


Figure 37: Example of an Earth Backflip followed by a Type I Earth-to-Mars Trajectory

This high declination and the attendant launch mass penalty is a major disadvantage of the Earth backflip. So why consider it? In addition to the programmatic considerations, it is potentially useful in the event of a launch slip. The next Earth-Mars opportunity is 26 months later; using an Earth-Earth loop would reduce the wait to 14 months, which might be too short and a perihelion much below 1 AU might be unacceptable to the flight system. A backflip, if feasible from a launch perspective, would avoid the thermal issue and offer a 20-month timeline for the slip. A backflip is also potentially useful for an Earth return trajectory for all the same reasons that a Mars backflip might be beneficial to a Mars lander, as described in Section 6.5.

## 6.4 Mars-Mars Loops

Just like one could add an Earth flyby to the front of an Earth-Mars transfer, one could add a Mars flyby to the back end. A Mars-Mars loop would fly by Mars and then re-encounter it a Mars year (22.5 months) later and would allow the designer some freedom to choose the inbound v-infinity vector direction (DAP and RAP). There is also the potential for v-infinity leveraging – to reduce the incoming velocity – with a SEP system. These benefits come at the cost of increased flight time. Also, like the Earth-Earth Loop, the post-flyby heliocentric orbit will have a perihelion and aphelion below and above that of Mars. The potentially problematic issue is the aphelion. If it is dramatically beyond Mars's, then the available power (for a solar-powered spacecraft) may be too low, and reduced solar thermal input could present problems for the flight system.

For orbiters, the primary value is in changing the longitude of the ascending node for a given inclination (see Section 8.1). A lander could benefit from landing at a different time of day or at an otherwise unreachable latitude. See Section 7.3 for more about site accessibility. However, since the Mars-Mars Loop returns to Mars a Mars year later, the arrival season cannot be changed in this way, but the timing of conjunction can be altered.

However, getting onto a Mars-Mars Loop is not always possible ballistically. In order to return a Mars year later, the spacecraft must have the same heliocentric velocity magnitude as Mars after the flyby. This, coupled with a minimum flyby altitude constraint, defines how far off the Mars velocity vector the inbound v-infinity vector may be, defined in Equation 11 using the geometry of Figure 38.

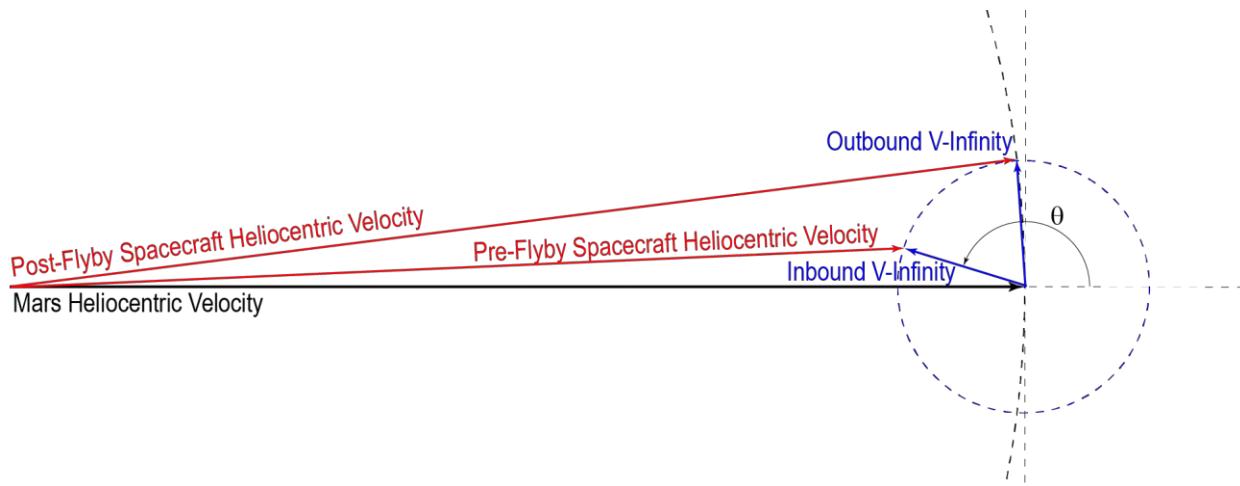


Figure 38: Mars Gravity Assist Geometry for a Mars-Mars Loop

$$\pi - \cos^{-1} \left( \frac{v_\infty}{2v_M} \right) + 2 \sin^{-1} \left( \frac{\mu}{\mu + r_p v_\infty^2} \right) \leq \theta \leq \pi - \cos^{-1} \left( \frac{v_\infty}{2v_M} \right) - 2 \sin^{-1} \left( \frac{\mu}{\mu + r_p v_\infty^2} \right) \quad (11)$$

Here,  $v_\infty$  is the magnitude of the inbound v-infinity vector,  $v_M$  is the magnitude of Mars's velocity about the sun (22.0 km/s to 26.5 km/s),  $\mu$  is the gravitational parameter of Mars (see Section 2.2), and  $r_p$  is the minimum allowable flyby radius.

Figure 39 illustrates this bound for a 200 km minimum altitude and the average Mars velocity. In this plot, the shaded region shows the combinations of spacecraft v-infinity magnitude (VHP, on the horizontal) and approach direction relative to the Mars heliocentric velocity direction (on the vertical) that can be used to set up a Mars-Mars loop, with recent missions noted. If the VHP is less than about 2.1 km/s, a Mars-Mars loop can be entered regardless of the approach direction. The minimum VHP for a ballistic Earth-Mars transfer is approximately 2.3 km/s, so a SEP transfer would be required to achieve that velocity. A Hohmann transfer between circular, co-planar orbits results in an approach direction 180 degrees from the heliocentric velocity vector at the outer planet, which is consistent with the high angles of the historical missions.

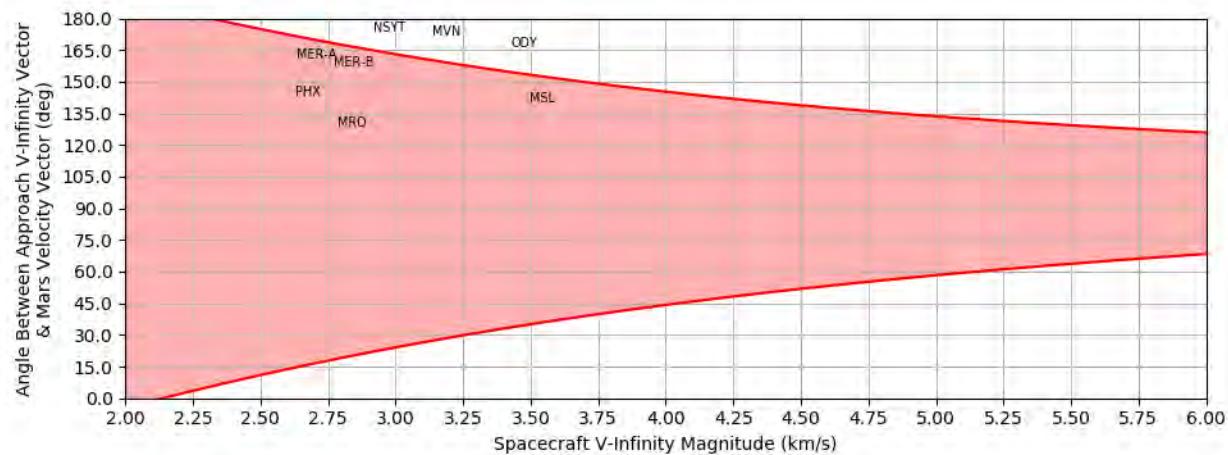


Figure 39: Permissible Approach Directions to Initiate a Ballistic Mars-Mars Loop (200 km minimum flyby altitude)

## 6.5 Mars Backflip

Like the Earth Backflip, a Mars Backflip is a special case of the Mars-Mars Loop where the spacecraft re-encounters Mars half a Mars year later. A mission which must arrive during a particular season but is constrained to launch when that isn't possible may be able to solve that via a backflip. Since the spacecraft arrives at Mars half a Mars year later, there is a 180 deg change in Ls with a backflip. A mid-summer arrival becomes a mid-winter arrival, and vice versa. The other effect is that a backflip sets the approach direction for the return. Regardless of the original incoming trajectory, the outbound leg has a declination of  $\pm 64.8$  deg, and the returning trajectory has a declination of the opposite sign. For our purposes, a "North Backflip" is one with a -64.8 deg outbound declination and a +64.8 deg return – the spacecraft is flying south-to-north on final approach. A "South Backflip" has the opposite sense. This may be useful if the landing approach azimuth must be oriented in this way. The other benefit is that the longitude of the ascending node can be much more freely chosen with this approach. Small changes in the approach targeting lead to relatively larger changes in the ascending node for small changes in the resulting inclination, in contrast to a more-equatorial approach, where these two parameters vary in a more one-to-one fashion.

Like a Mars-Mars Loop, setting up a ballistic Mars Backflip is relatively difficult. Mars is small and does not offer much bending on a flyby, so getting the outbound declination to  $\pm 64.8$  deg

relative to the Mars equator requires either a very low approach velocity or an inbound declination near the desired value as defined by Equation 12.

$$\Delta\delta \leq \pm 2 \sin^{-1} \left( \frac{\mu}{\mu + r_p v_\infty^2} \right) \quad (12)$$

Here,  $\Delta\delta$  is the difference between the inbound declination and the outbound declination to set up the backflip (e.g. -64.8 deg for a North Backflip) and the other parameters are as defined in Section 6.4.

To initiate a North or South Backflip regardless of the approach direction requires a VHP less than 0.5 km/s, as illustrated in Figure 40. A ballistic trajectory with a VHP of 2.5 km/s must have an approach declination greater (more northerly) than -15 deg to set up a North Backflip and less (more southerly) than 15 deg for South Backflip. Historically, the two MER missions could have done a backflip from either direction, while the InSight, Phoenix, and Odyssey missions would have been constrained to a North Backflip. MRO and MAVEN would have been constrained to a South Backflip.

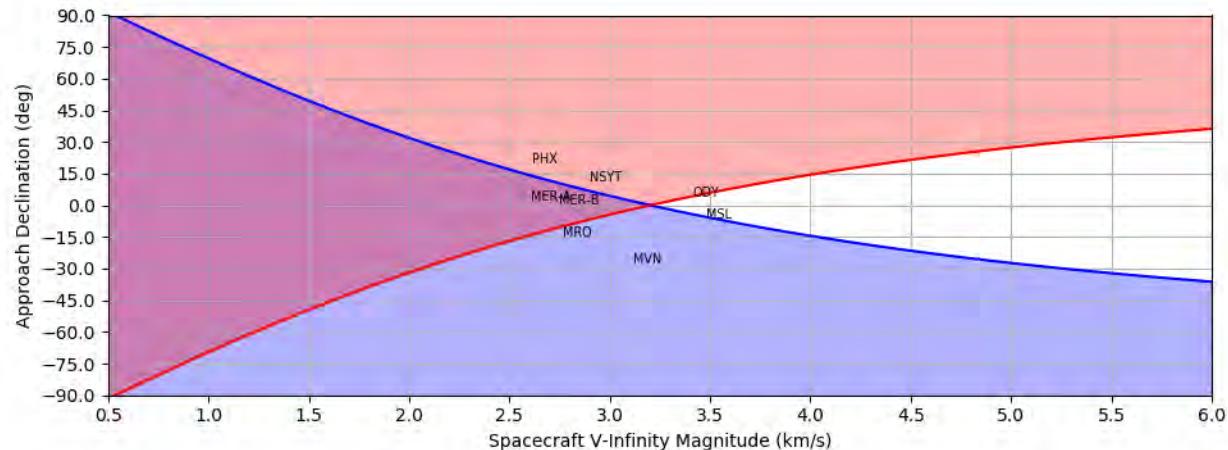


**Figure 40: Permissible Approach Declinations to Initiate a Ballistic North (blue) and South (red) Mars Backflip (200 km minimum flyby altitude)**

## 6.6 Venus Flybys

Finally, adding a Venus flyby to the mission plan is really only useful for the Opposition-Class round-trip mission design to enable a short stay-time at Mars. A Venus flyby presents far greater thermal input from the sun due to the lower perihelion (0.72 AU) and the planetary IR from Venus itself during the flyby. The velocities at Mars are also much greater. Perihelion at 0.72 and aphelion at Mars requires that the spacecraft have much lower heliocentric velocity at aphelion, which results in significantly greater Mars-relative velocities. This incurs a significant mass penalty, either in propellant for orbit capture (or Mars departure) or to handle the additional heat load on entry. As a result, the short timeline of a roundtrip mission must be of paramount importance for a Venus flyby to be considered.

See Section 9.3 for a fuller discussion of Opposition-Class roundtrip missions.

## 7 Lander Mission Design

### 7.1 Overview

For our purposes, a “Lander Mission” is one which enters the Martian atmosphere from a hyperbolic approach, descends to the surface, and operates there for a time. Every surface mission since Mars Pathfinder in 1997 has used this architecture (the Viking landers were deployed from orbit). The mission design for “Landers,” in this context, is dominated by reaching the required landing site within the capability of the landing system design while meeting the critical event coverage requirements. A Viking-style landing from orbit remains a possibility, but is not within the scope of this document.

### 7.2 Entry, Descent, and Landing (EDL)

The problem of how to slow a spacecraft from hyperbolic speeds ( $> 5 \text{ km/s}$ ) to a safe touchdown on the surface at few meters per second is beyond the scope of this document. Every mission to date has used a combination of a heat shield, parachutes, and rockets. Viking, Phoenix, and InSight all used rockets attached to the lander, while Pathfinder and the Mars Exploration Rovers used rockets attached to the backshell (the final touchdown was cushioned by airbags), and the Mars Science Laboratory (MSL) used rockets attached to a descent-stage “sky crane.” In addition to heatshields, parachutes, and rockets, the entry vehicle may have guidance or not. Most missions have not, but MSL used and the upcoming Mars 2020 mission will use entry guidance. M2020 is using terrain-relative navigation in terminal guidance as well. The MSL [32] and InSight [33] EDL sequences are illustrated in Figures 41 and 42, respectively.

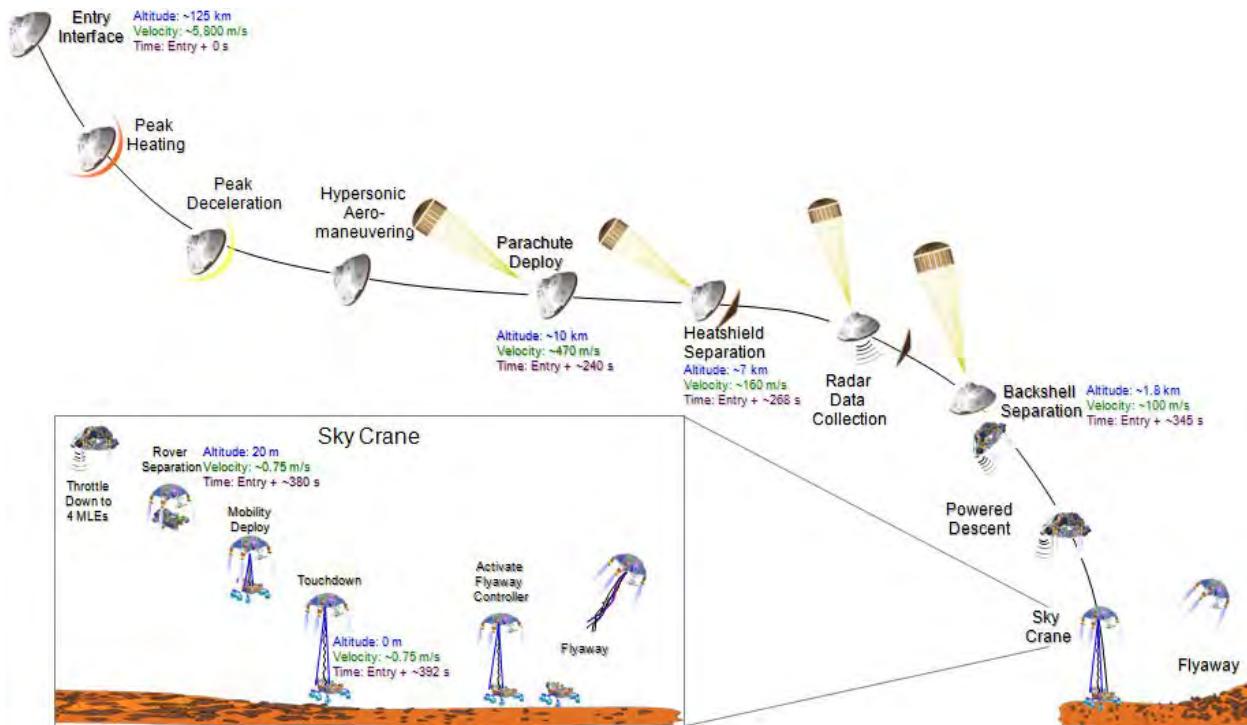


Figure 41: Mars Science Laboratory Entry, Descent, and Landing Sequence

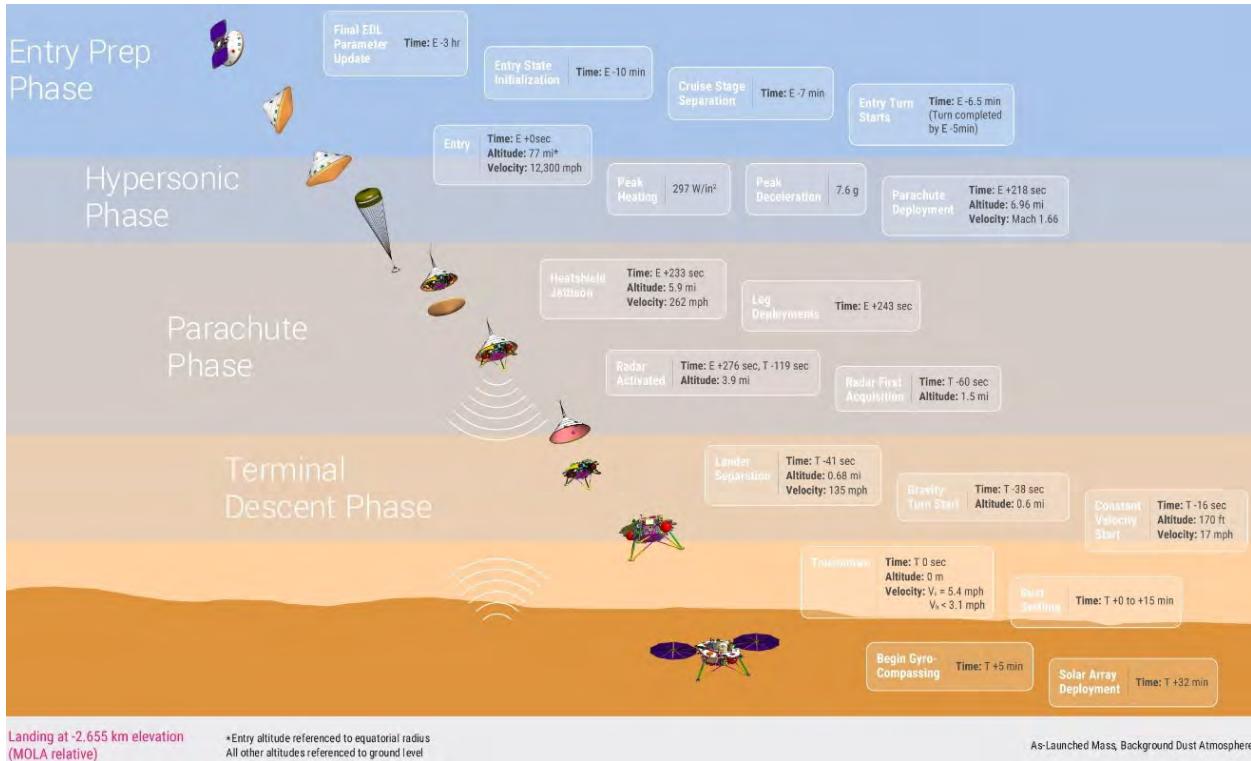


Figure 42: InSight Entry, Descent, and Landing Sequence

An EDL trajectory is obviously a very complex thing. There are a lot of moving parts and the trajectory is highly coupled to assumptions about things like hypersonic drag, when the parachute deploys, how long until the thrusters turn on, and other parameters. Many of these parameters require simulation of flight software to fully capture the trajectory. However, the EDL trajectory can be approximated via the “descent central angle and time” assumption.

The descent central angle and time assumption maps the entry, typically defined at 3522.2 km radius (approximately 125 km altitude), to the landing site by rotating the entry position about the entry trajectory pole through the “descent central angle,” as illustrated in Figure 43. This yields the landing site latitude and longitude in inertial space. The landing epoch (and thus the surface-relative position) is found by adding the “descent time” to the entry epoch. The descent central angle is a measure of how far downrange the landing site is from the entry point, and the descent time indicates how long this takes. InSight’s nominal trajectory flew approximately 781 km downrange from the entry point in 377 seconds. This translates to a descent central angle of 13.2 deg.

Figure 44 shows the variation in descent central angle and descent time for an InSight-like EDL trajectory assuming a 600 kg entry mass with a 2.65-meter heatshield; a vehicle with a smaller area/mass ratio (e.g. heavier with the same heatshield or a smaller heatshield for the same mass) would go further downrange in less time. The maximum feasible velocity would be lower, and the steepest feasible entry flight path angle would be shallower. Further, a mission with a different design, like MSL, which used entry guidance and a sky-crane, may have very different behavior. MSL’s parameters are shown by the black star. Note in particular that MSL went much further downrange than InSight would have at MSL’s steeper entry flight path angle (-15.5 deg vs -12.0 deg).

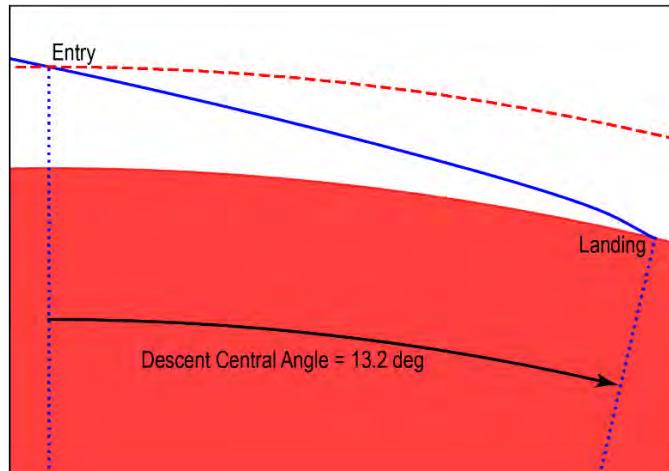


Figure 43: Descent Central Angle Illustrated

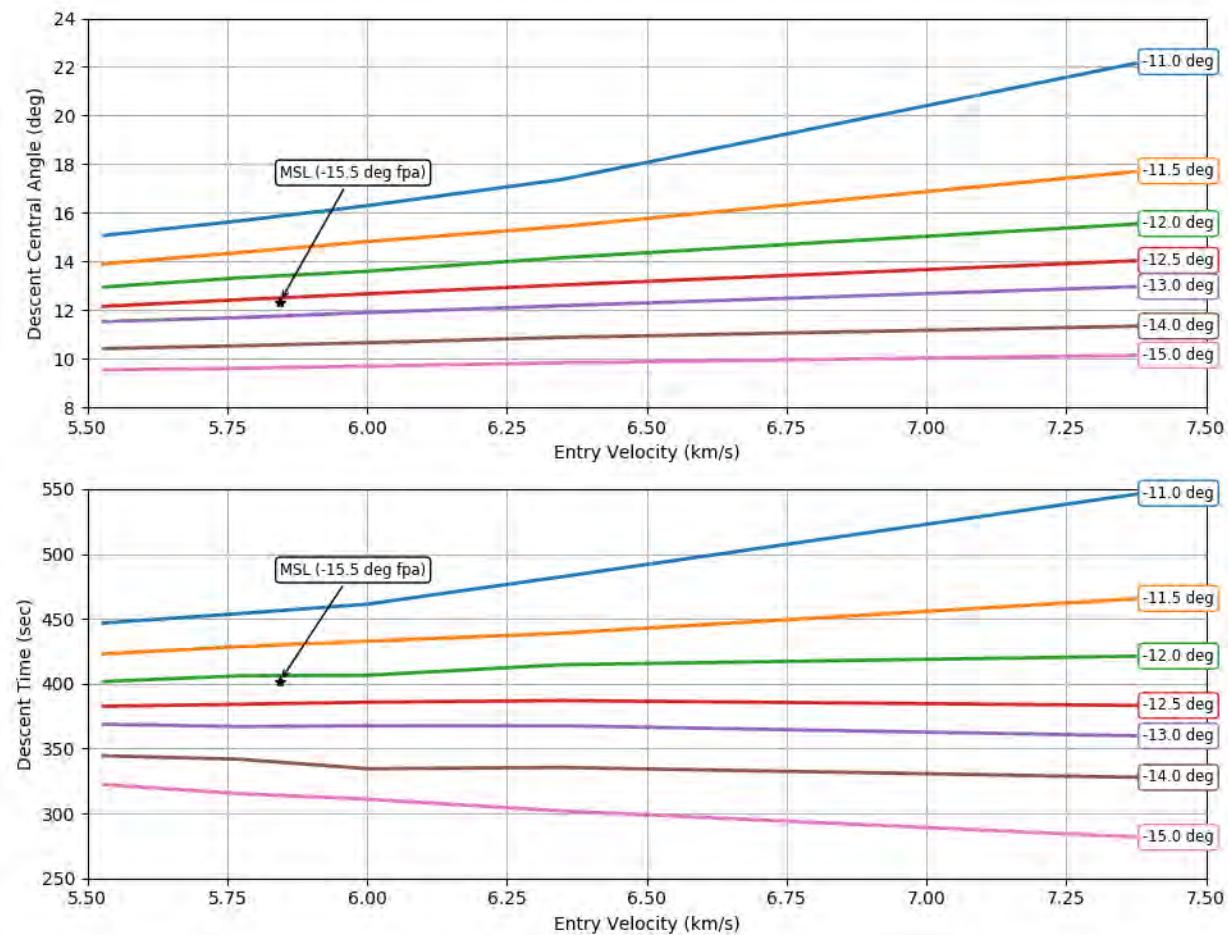


Figure 44: Descent Central Angle and Time Variation with Entry Velocity for various Entry Flight Path Angles assuming an InSight-like lander

The entry velocity quoted in Figure 44 is the atmosphere-relative entry velocity. It varies with the approach  $v$ -infinity, but also with the flight path azimuth and the latitude of entry due to the rotation of Mars. A retrograde entry (azimuth 270 deg) at the equator can have an entry velocity up to 1000 m/s greater than a prograde (azimuth 90 deg) entry at the equator, as illustrated in

Figure 45. This is the difference between flying with a head- or tail-wind. In addition, there is a weak dependence on the entry flight path angle; the  $\pm 488$  m/s variation depicted is for a -12.0 deg entry flight path angle. It is slightly reduced to  $\pm 480$  m/s at -15.5 deg.

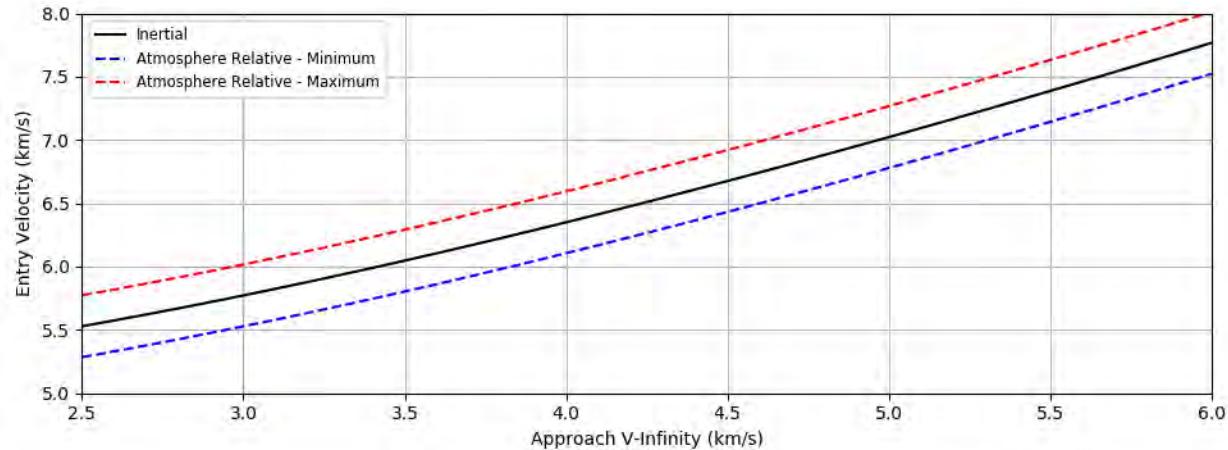


Figure 45: Entry Velocity Variations

### 7.3 Surface Accessibility

What parts of the surface are accessible is a function of the approach state (velocity and approach direction) and the EDL system design (descent central angle and time). It can be assessed by defining the locus of entry points and then mapping that locus down to the surface via the descent central angle and time approximation. The locus of landing points is then a small circle (i.e. a latitude-like circle, excluding the equator) on the surface centered on the v-infinity vector's pierce point, as illustrated in Figure 46 which illustrates the orbit geometry roughly in the plane of the approach hyperbola. This plane is defined, in part, by the B-Plane angle. There are three components of this locus's construction: the periapsis-approach angle,  $\varepsilon$ , the true anomaly at entry,  $f$ , and the descent central angle,  $\theta$ . If the inbound v-infinity vector is the pole of a coordinate system, then the co-latitude,  $\Phi$ , of the landing locus is as in Equations 13 and 14 and the longitude is the B-Plane angle. The loci are defined as the plane of the hyperbola is rotated about the v-infinity vector.

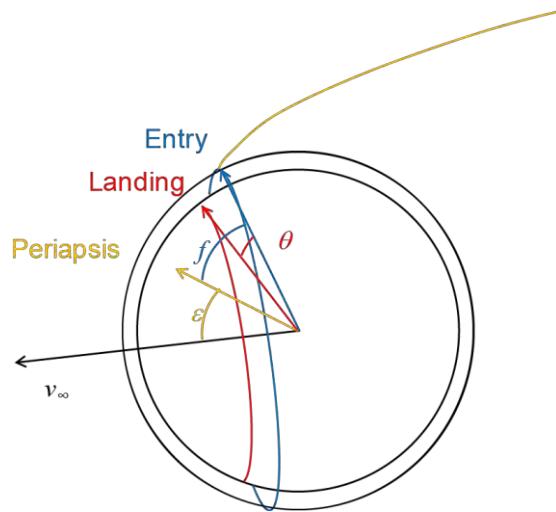


Figure 46: Locus of Entry and Landing Points

$$\Phi = \varepsilon + f - \theta \quad (13)$$

$$\Phi = \cos^{-1} \left( \frac{1}{1+\Psi} \right) + \cos^{-1} \left( \frac{r_p(2+\Psi)-r_e}{r_e(1+\Psi)} \right) - \theta \quad (14)$$

Here,  $r_p$  is the periapsis radius, defined in Equation 15,  $\Psi$  is a hyperbola shape parameter, defined in Equation 16, and  $r_e$  is the entry radius, typically defined as 3522.2 km.

$$r_p = \frac{\mu}{v_\infty^2} \left[ \sqrt{1 + \left( \frac{r_e v_\infty^2}{\mu} \right) \left( 2 + \frac{r_e v_\infty^2}{\mu} \right) \cos^2 \gamma} - 1 \right] \quad (15)$$

$$\Psi = \frac{r_p v_\infty^2}{\mu} \quad (16)$$

Here,  $\mu$  is the gravitational parameter (see Section 2.2),  $v_\infty$  is the approach v-infinity, and  $\gamma$  is the entry flight path angle. One feature to note among these relationships is that, for a fixed approach v-infinity, a steeper entry flight path angle corresponds to an entry further from periapsis (smaller  $f$ ), which partially offsets the larger descent central angle (larger  $\theta$ ). The landing locus co-latitude is dominated by the approach-periapsis angle, however, as illustrated in Figure 47.

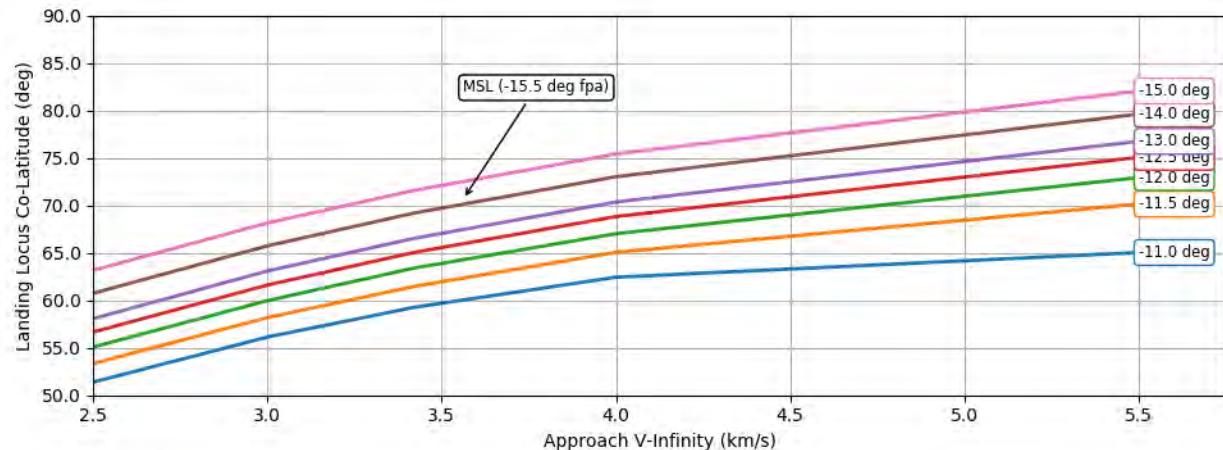


**Figure 47: Landing Locus Co-Latitude vs. Approach V-Infinity for various Entry Flight Path Angles assuming an InSight-like lander.**

The landing locus describes a latitude-like circle on the planet centered on the inbound v-infinity vector rather than the pole. Figures 48 through 53 show this locus (and that of entry) from above the North Pole and from an arbitrary longitude above the equator for three trajectories. Figures 48 and 49 show the loci for the Phoenix mission, which landed near the North Pole in 2008. Figures 50 and 51 illustrate the loci for the MSL mission, which landed near the equator in 2012. Figures 52 and 53 illustrate the loci for a South Backflip trajectory that used SEP to enable the backflip. Finding the points on these loci is a matter of translation from the v-infinity coordinate system to the pole coordinate system. It can also be done directly by determining the entry states directly using a fixed inbound v-infinity vector, periapsis radius, and entry flight path while sweeping the inbound B-Plane angle. These states can then be mapped down to the surface using the descent central angle.

The band of reachable latitudes can be determined by taking the approach declination (DAP) and adding or subtracting the landing locus co-latitude,  $\Phi$ , as defined in Equation 14, noting that a value in excess of 90 deg must be subtracted from 180 deg. Figures 52 and 53 illustrate this

effect. There, the DAP is 66.7 deg and  $\Phi$  is 66.3 deg. DAP +  $\Phi$  is 133 deg, yielding a maximum reachable latitude of 47 deg.

These plots show Mars oriented at some arbitrary epoch, and so the longitude of the sites under the loci is arbitrary. The longitude of the landing site can be selected by advancing or delaying the arrival date by half a sidereal day. Recalculating the inbound v-infinity vector is not generally necessary for preliminary analyses, as it does not change dramatically over that duration; less than half a degree is typical. As a result, the various geometries (time of day, Earth's elevation at landing, the relative position of *in situ* orbiters) do not change with landing longitude.

Arbitrary View on 25-MAY-2008  
VHP = 2.676 km/s  
DAP = 21.59 deg RAP = 63.53 deg  
FPA = -12.50 deg DCA = 12.25 deg  
  
Accessibile Latitudes: 36.9 S to 80.1 N

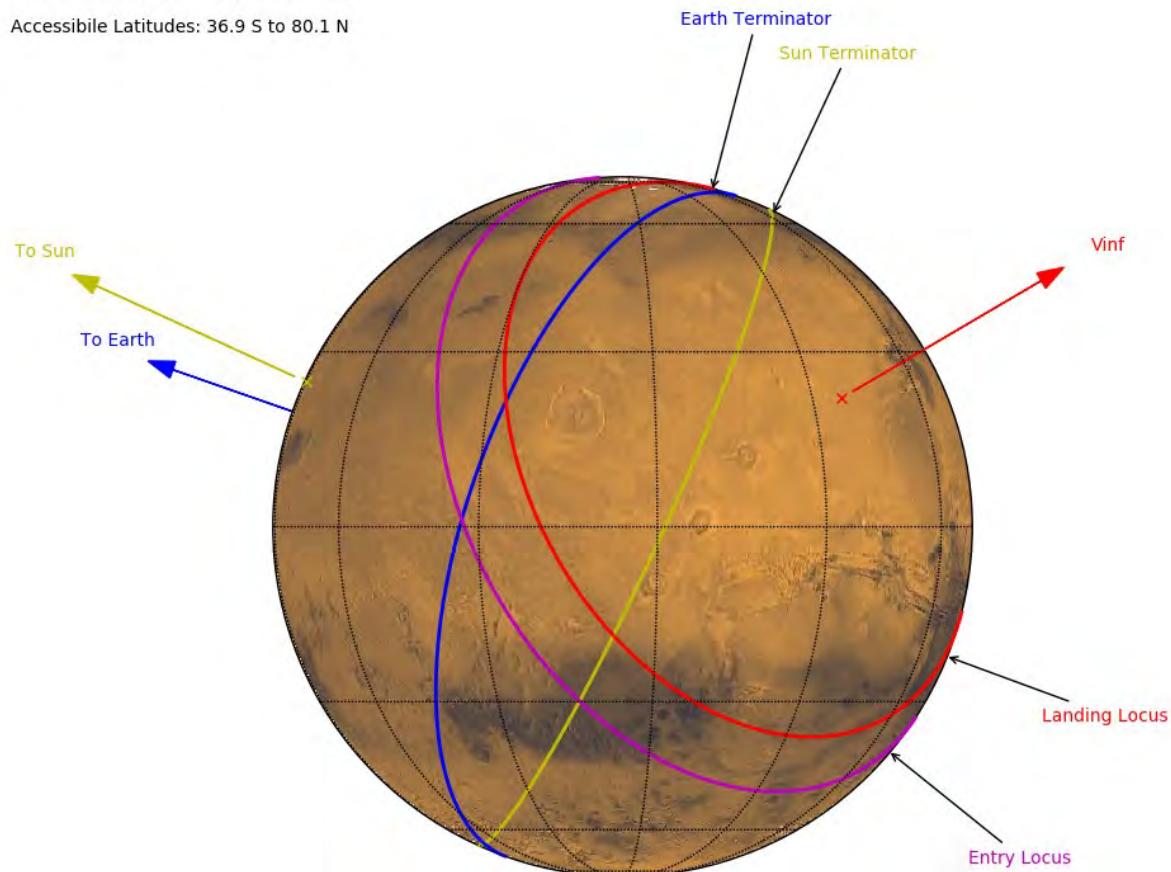


Figure 48: Arbitrary View of the Phoenix Entry and Landing Loci

View from North Pole on 25-MAY-2008

VHP = 2.676 km/s  
DAP = 21.59 deg RAP = 63.53 deg  
FPA = -12.50 deg DCA = 12.25 deg

Accessible Latitudes: 36.9 S to 80.1 N

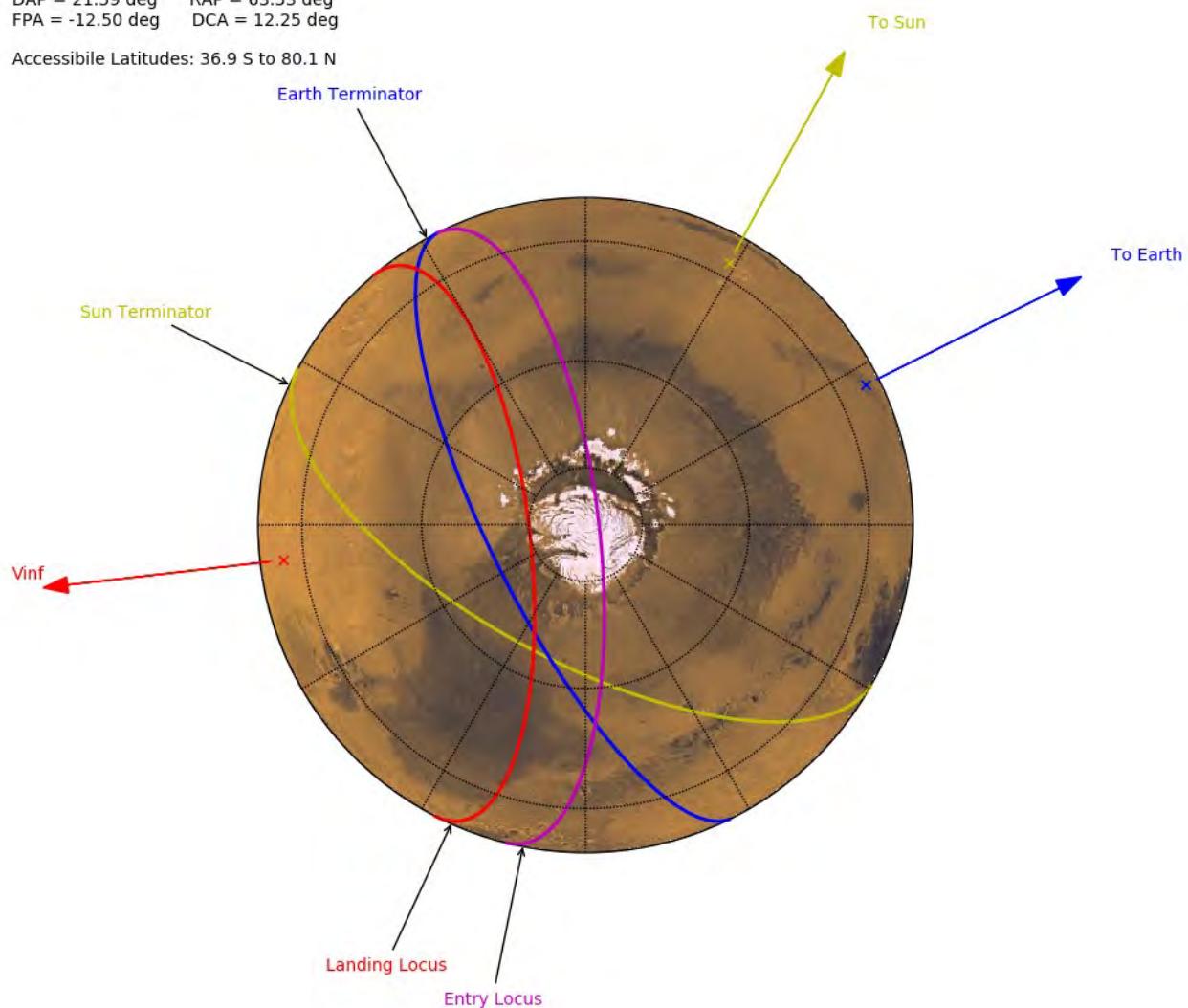


Figure 49: View from the North Pole of the Phoenix Entry and Landing Loci

Arbitrary View on 06-AUG-2012  
VHP = 3.542 km/s  
DAP = -4.60 deg RAP = 141.17 deg  
FPA = -15.50 deg DCA = 12.34 deg

Accessible Latitudes: 75.1 S to 65.9 N

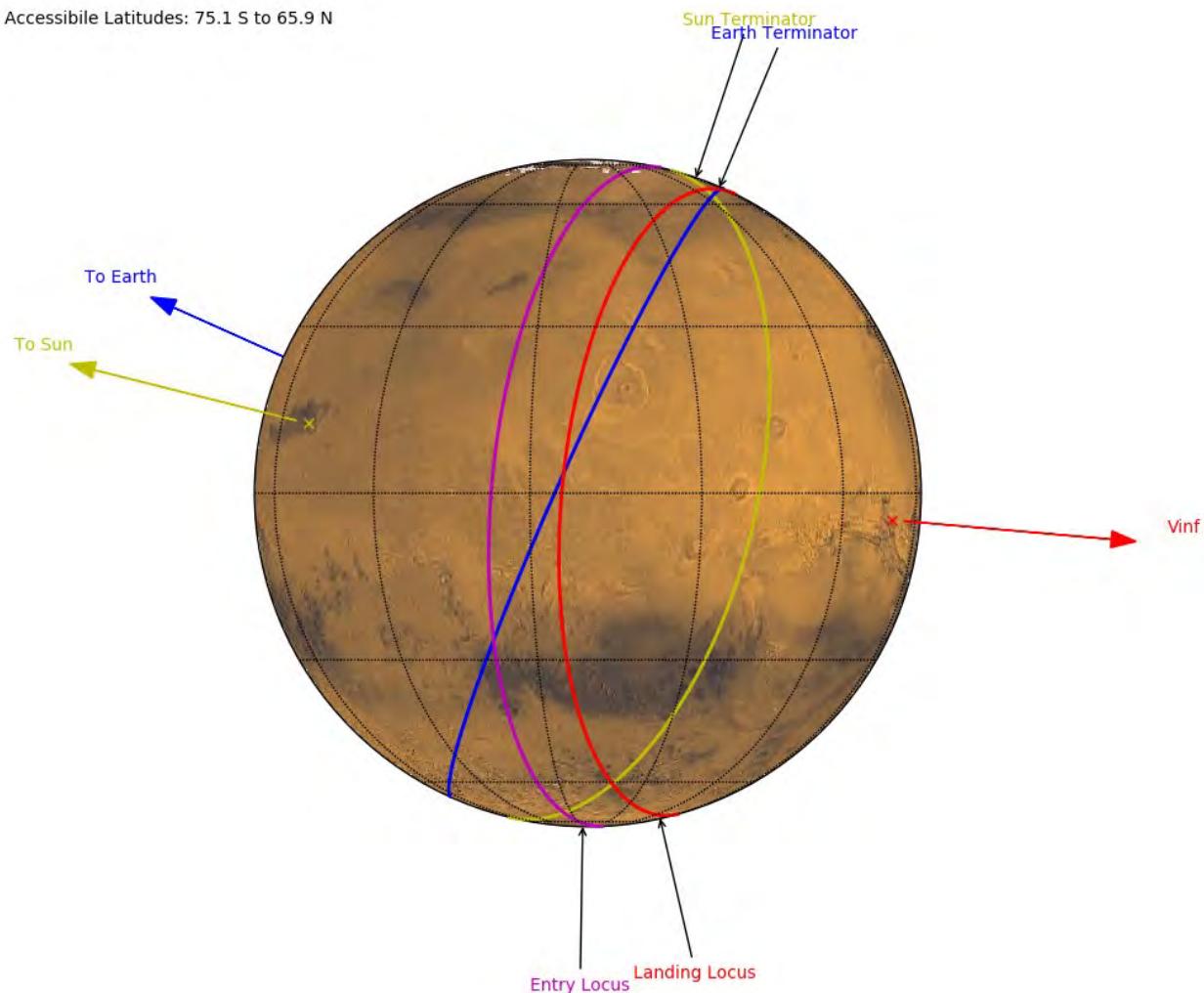


Figure 50: Arbitrary View of the MSL Entry and Landing Loci

View from North Pole on 06-AUG-2012  
VHP = 3.542 km/s  
DAP = -4.60 deg RAP = 141.17 deg  
FPA = -15.50 deg DCA = 12.34 deg

Accessible Latitudes: 75.1 S to 65.9 N

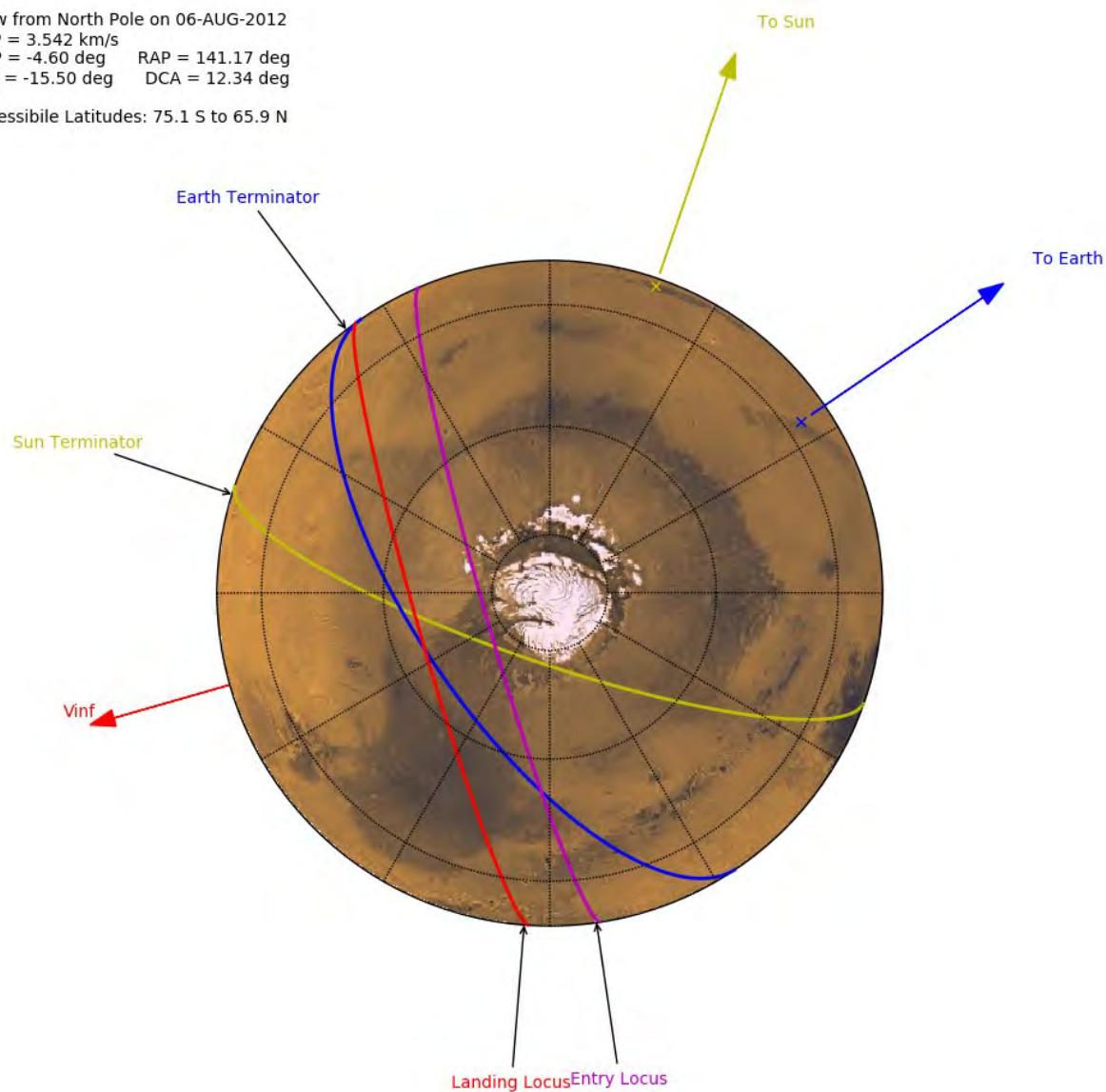


Figure 51: View from the North Pole of the MSL Entry and Landing Loci

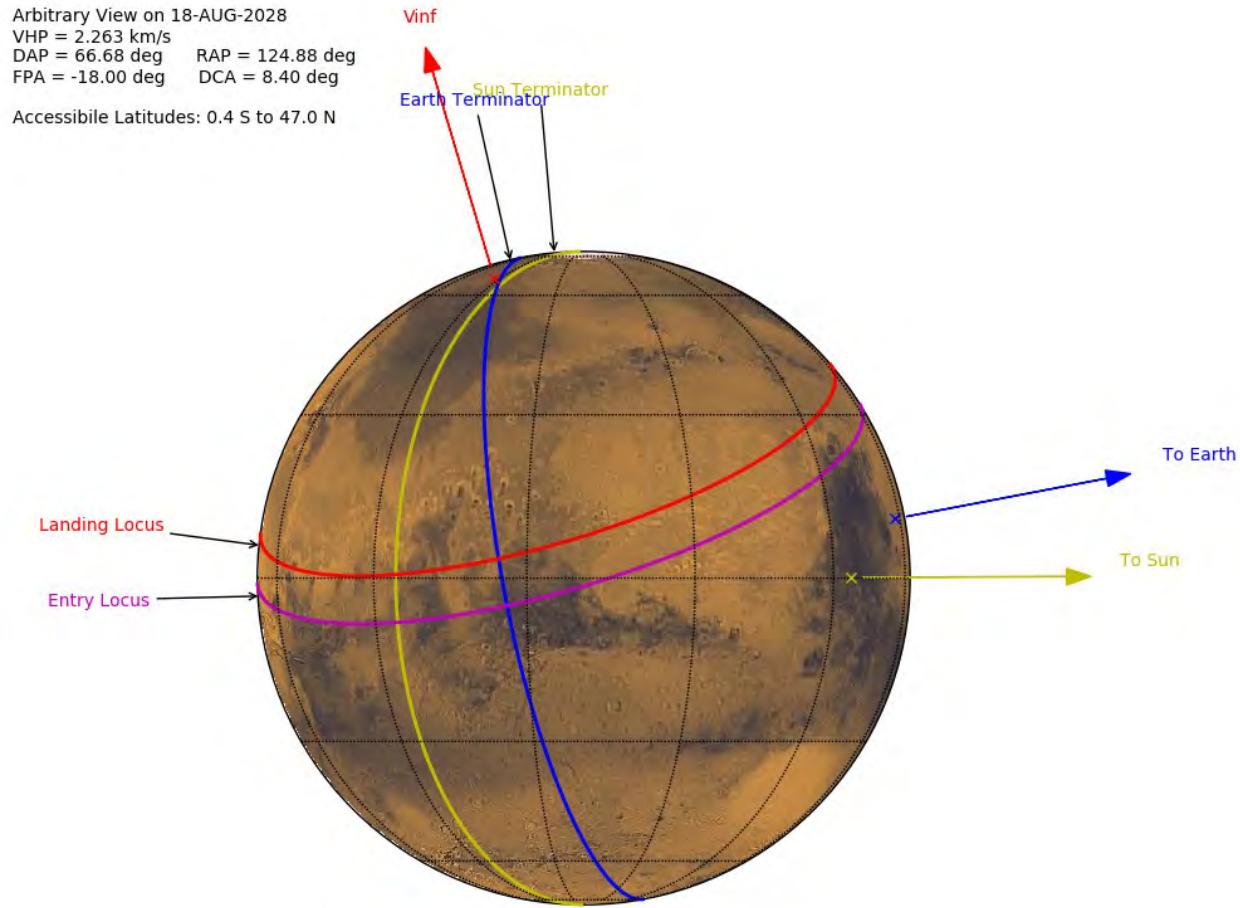


Figure 52: Arbitrary View of a SEP-Enabled South Backflip Trajectory's Entry and Landing Loci

View from North Pole on 18-AUG-2028  
VHP = 2.263 km/s  
DAP = 66.68 deg RAP = 124.88 deg

FPA = -18.00 deg DCA = 8.40 deg

Accessible Latitudes: 0.4 S to 47.0 N

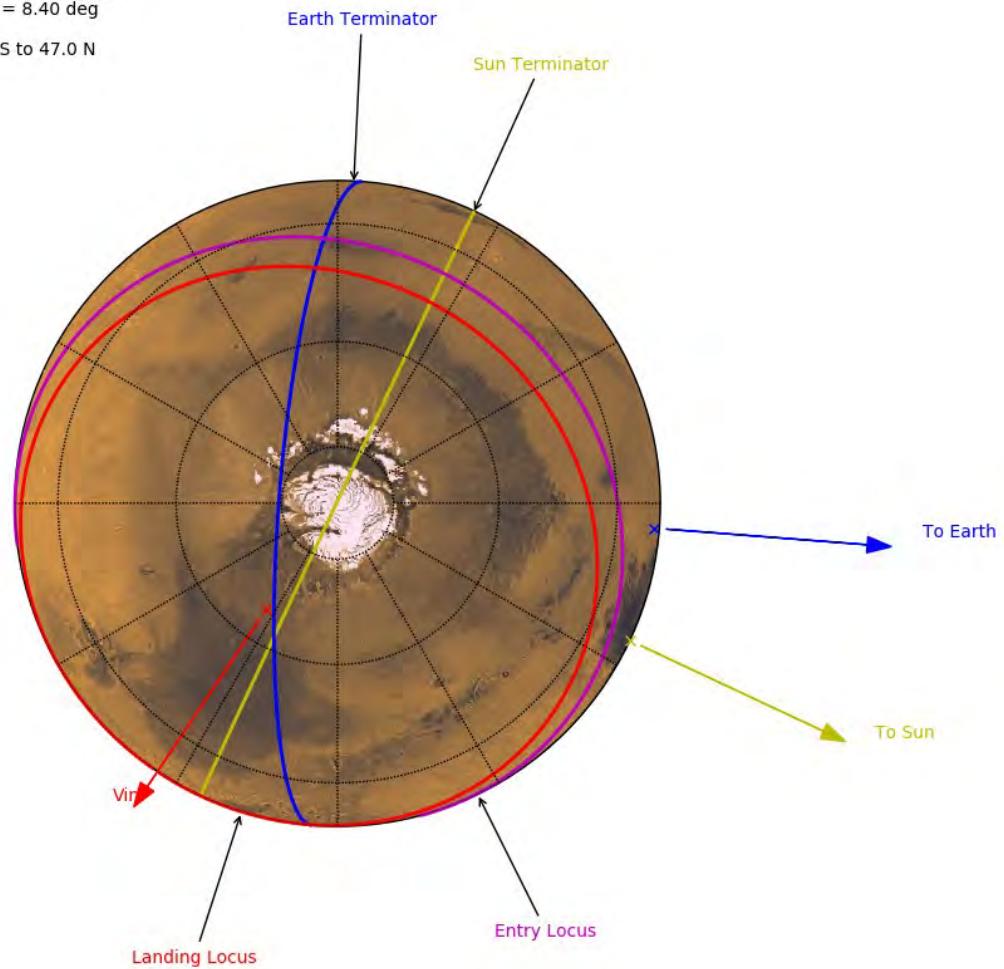


Figure 53: View from the North Pole of a SEP-Enabled South Backflip Trajectory's Entry and Landing Loci

## 7.4 EDL Communications

Every mission since 2000 has had a “critical event coverage” requirement, which often drives the mission design as much as, if not more than, launch vehicle performance or entry velocity. The 2003 Mars Exploration Rovers [34], the 2007 Phoenix lander [35], the 2011 MSL rover [36], and the 2018 InSight lander [22] were all required to have a communication path from the spacecraft back to Earth - either on a direct-to-Earth downlink or via a proximity link to an in-view relay orbiter - during the EDL sequence. The data thus returned are intended to aid in the reconstruction of any anomaly that should befall the spacecraft during EDL. These data would be invaluable to the resulting investigation and would aid future missions in avoiding the same fate. In addition, there is a strong desire for near-real-time assessment of the progress of EDL. Though the round-trip light time is greater than the duration of EDL and thus no intervention would be possible, there is a very human desire to know how our robotic proxy is doing as quickly as possible. Having multiple assets in place, as well, provides redundancy in the event one or more assets are unavailable for any reason.

The data required can be broadly categorized by the available link budget. In descending

order, they are: telemetry, tones, and aliveness. A telemetered link contains data about the state of the spacecraft; accelerations, gyro rates, flight software states, and potentially imagery. A tones link contains far less information - possibly only software states (e.g. “parachute deploy commanded”), but can be closed with far less signal strength. Finally, an “aliveness” link is simply the presence of signal. The state of the spacecraft may not be known beyond “it is still functioning,” but some information is better than none in an anomaly investigation, and so such is generally an acceptable contingency link. InSight used a telemetered link to MRO and the MarCO spacecraft over UHF, but ground stations on Earth “eavesdropped” for a real-time aliveness link as a backup in case those spacecraft were unavailable. That link had a rudimentary tones capability when the UHF signal dropped to carrier only after certain events, which would be detected in the received power back on Earth. Likewise, the Doppler shift associated with parachute deploy could also be detected. MER and MSL also employed a DTE X-band link, with Multiple Frequency Shift Keying modulating to convey low rate (~1 bps) telemetry during EDL, in addition to the high rate (8-32 kbps) on the UHF link.

In general, if the link can be closed at both entry and landing, then the link can be closed for the entire trajectory. A detailed link budget is generally outside the scope of early mission design analysis, and so we generally consider a few geometric proxies. The first proxy is that the asset must be within the antenna field-of-view and not occulted by Mars at entry. MER, Phoenix, MSL, and InSight all had wrap-around antennas on their backshells. This allowed a nearly full-sky ( $4\pi$  steradian) field of view with a cut-out for the heat shield. This translated into a requirement that the asset under consideration be within some angle of the atmosphere relative anti-velocity vector. This vector is itself a proxy for the attitude of spacecraft at entry; the heat shield is pointed in the atmospheric ram direction. InSight’s 45 deg sphere-cone and zero nominal angle-of-attack meant that Earth, MRO, and the MarCOs had to have an “antenna angle” less than 135 deg.

The second proxy is that the asset must be above some horizon mask at landing and at some time after landing. This horizon mask may be to ensure that the asset is above local topography (e.g. a crater rim), to ensure that the link is not complicated by multipath off the surface, or both. A robust mask also acts as margin for an EDL that goes long or short in either time or distance. The “time after landing” portion of this proxy also serves that purpose.

Assets can be considered in two broad categories: Direct-to-Earth (DTE) and relay. Relay paths can be further divided by what kind of asset is providing the relay. An *in situ* orbiter such as MRO can provide relay support but it may have limited ability to change its orbit to suit the lander. An *in situ* orbiter could also be pre-positioned in an orbit specifically designed to support EDL. Finally, an asset could be sent along with the lander and perform a flyby designed to support EDL. This is what the MarCO cubesats did in 2018 in support of the InSight EDL [22].

#### 7.4.1 *Direct to Earth*

A Direct-to-Earth link is the closest-possible real-time link, as it is delayed only by light-time and the ground system’s latency. A relay link will have additional latencies built in – these can vary from a few seconds to several hours. A DTE link has the benefit, as well, of being dependent only on the lander’s trajectory and is thus relatively easy to assess. For a given latitude landing site and entry direction (prograde vs. retrograde), the entry state is either visible from Earth or it is not, and the landing site is visible or it is not. Consider the MSL entry locus depicted in Figure 50. The prograde entries are visible from the illustrated perspective, and any landing site north of the equator would have full DTE visibility if a 0 deg elevation mask is applied. Between the

equator and 30 S, entry is visible but landing is not, and anything south of 30 S would be invisible from Earth. Enforcing an elevation mask would shift these breakpoints slightly north. MSL, which landed at 5.4 S, lost DTE shortly before landing.

All of this is considering only whether Earth is in the sky above the landing site; it does not account for whether or not a suitable ground station back on Earth has Mars in its sky. Such an assessment is only possible when the landing longitude is known in addition to the latitude. The phasing of Earth's rotation is the key; the local solar time (on Mars) of landing may be insensitive to changes of plus or minus half a Martian sidereal day, but the elevation of Mars at a particular ground station on Earth certainly is. Fortunately, there are deep space tracking network stations (the DSN, plus those operated by ESA and JAXA) all over the world and it is reasonable to assume that X- or Ka-Band DTE would be possible from any landing site with Earth in its sky. A UHF link, which is far less capable and cannot generally carry telemetry over interplanetary distances, requires other stations, but these are also widely distributed. They may require special teaming arrangements, however, so identifying the need early is highly desirable.

#### 7.4.2 *Relay Communications*

Relay communications are more complex to analyze than DTE. In this case, the relay asset's trajectory must also be considered. For a given spacecraft orbit, a "phasing window" is defined as the span of mean anomalies at the entry epoch where the lander's entry state is visible at the entry epoch and the asset is sufficiently above the horizon at the landing epoch.

A phasing window may or may not exist, depending the orbit geometry. For a sun-synchronous orbit, a necessary but not sufficient condition is that the local solar time of landing be near the local solar time of either the ascending or descending node of the orbit. The value of "near" depends on the orbiter's altitude, the latitude of landing, and horizon mask applied. A good rule of thumb is that landing is visible within 45-60 minutes of the orbiter's LMST at the equator for a low altitude sun-synchronous orbiter like MRO or Odyssey. In contrast, a lander near the pole, like Phoenix, can land at almost any LMST and any polar orbiter should be able to support EDL.

Determining the size of the phasing window is a matter of stepping through the possible mean anomalies of the orbiter at the entry epoch and then checking whether the geometric proxy requirements are met at the epochs of interest (entry, landing, etc). This must be repeated for every landing latitude and set of arrival conditions (e.g. the Lambert solution launch-date/arrival-date pair). This is a very computationally intense task, but one which lends itself to parallelization. Tools exist to do this assessment [37].

If a phasing window does exist, it must be wide enough to be useful. The ability of the orbiter's navigation team to position the spacecraft in its orbit is constrained by maneuver execution errors and uncertainty in the estimate of future atmospheric density and its effect on the orbit period. The InSight and MSL missions both used a 5 deg phasing window requirement to cover MRO's  $\pm 30$  sec (approximately  $\pm 1.6$  deg) phasing control capability with some margin. Other orbiters may have more or less control, and coordination with those navigation teams is essential.

Finally, if the relay asset is hyperbolic, such as the MarCO cubesats or the oft-studied "Smart Cruise Stage," which diverts to provide communication, then the mission design can be freed from the constraints of EDL communications. In general, such assets can always provide full coverage of EDL.

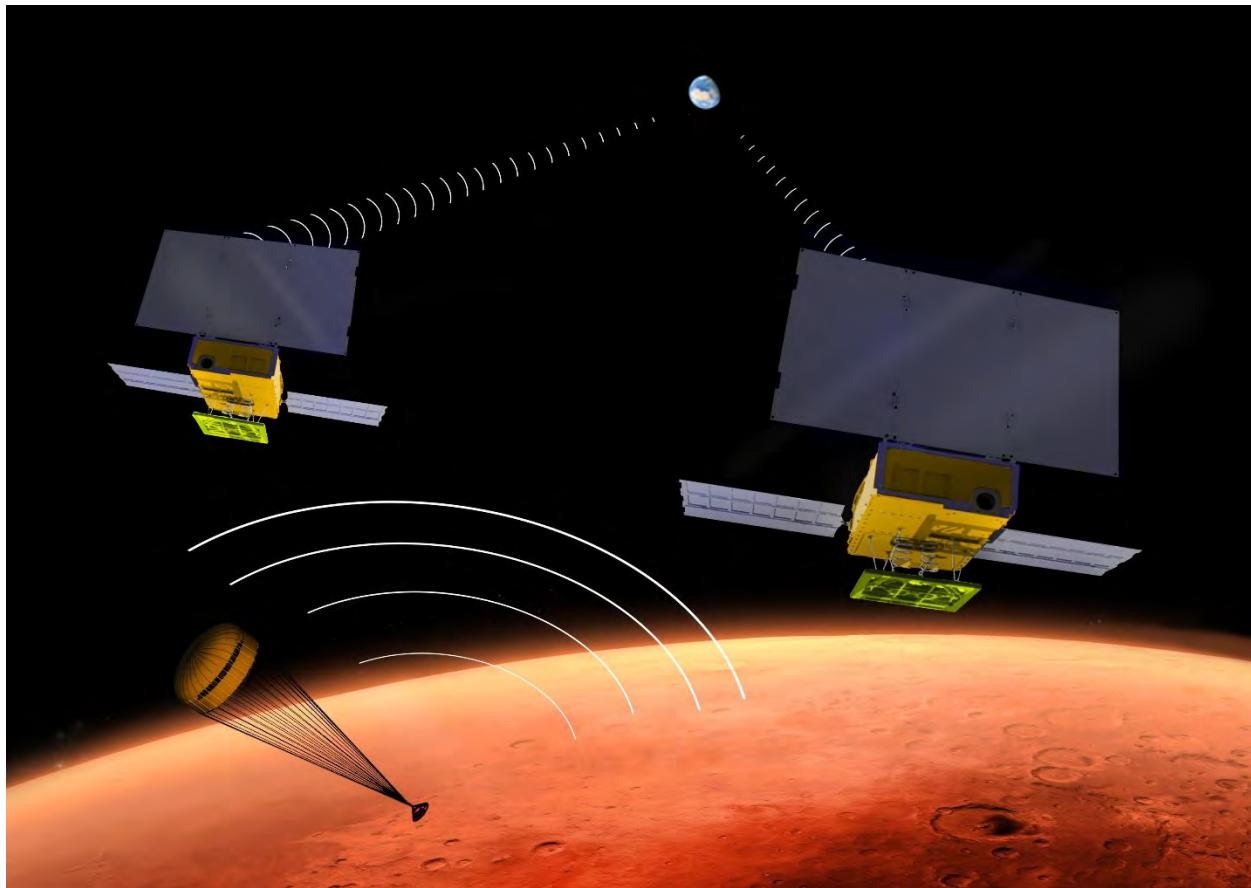


**Figure 54: Artist Concept of the MarCO CubeSats monitoring the InSight EDL**

## 8 Orbiter Mission Design

### 8.1 Overview

In contrast to landers, an orbiter's mission design has many more requirements, constraints, and design objectives. An Orbiter mission design consists of three components. The first is the final orbit. What does the mission hope to achieve at Mars, and what geometries must the mission design provide to support those objectives? What limits are placed on those geometries by the flight system design? And so on. The second is how the spacecraft captures into orbit from its interplanetary trajectory. Finally, the spacecraft must get from the immediate post-orbit-insertion orbit to the designed orbit for the primary mission. This can be done with the propulsion system (either high- or low-thrust), but the aerocapture technique is also potentially available as an option.

### 8.2 Orbit Design

#### 8.2.1 Introduction

Most orbits about Mars are dominated by two perturbations: the non-spherical gravity of Mars and atmospheric drag. Third body perturbations are significant only for very large orbits or those that get exceptionally close to Phobos or Deimos. Solar gravity perturbations are essential for Lagrange-point orbits, such as Halo orbits, but the features that make them appealing in the Sun-Earth system or Earth-Moon system are not particularly useful at Mars. Phobos and Deimos-centered Halo orbits require exceptionally high-frequency/high-accuracy maintenance (see [38]). Mars-Sun halo orbits also exist, but are not widely studied or useful due to the low Mars to Sun mass ratio. As a result, we focus here on classic perturbed Keplerian orbits.

#### 8.2.2 Non-Spherical Gravity

The longitude of the ascending node (Equation 17) and the argument of periapsis (Equation 18) both precess under the influence of the non-spherical gravity of Mars, while the remaining elements see no long-term variation.

$$\dot{\Omega} = -\frac{3}{2}J_2 n \left(\frac{R}{p}\right)^2 \cos i \quad (17)$$

$$\dot{\omega} = \frac{3}{2}J_2 n \left(\frac{R}{p}\right)^2 \left(2 - \frac{5}{2}\sin^2 i\right) \quad (18)$$

The mean motion,  $n$ , and semi-latus rectum (or radius when the true anomaly is 90 deg),  $p$ , are defined as:

$$n = \sqrt{\frac{\mu}{a^3}} \quad (19)$$

$$p = a(1 - e^2) \quad (20)$$

Here,  $a$ ,  $e$ ,  $i$ ,  $\omega$ , and  $\Omega$  are the semi-major axis, eccentricity, inclination, argument of periapsis, and longitude of the ascending node, respectively, while  $\mu$  is the gravitational parameter,  $J_2$  is the 2<sup>nd</sup> degree zonal harmonic (aka the oblateness term), and  $R$  is the equatorial radius of Mars (see Table 1). Table 26 shows the results of these calculations for orbits with periapsis altitudes from 200 to 500 km, periods from 3 to 48 hours, and a range of inclinations.

**Table 26: Ascending Node and Argument of Periapsis Rates for Various Orbit Sizes and Inclinations**

Altitude of Periapsis (km)	Altitude of Apoapsis (km)	Semi-Major Axis (km)	Eccentricity	Inclination (deg)	Period (hours)	Node Rate (deg/day)	Apsidal Rate (deg/day)
200	3048.834	5020.417	0.283725	30	3	-3.961600	6.289884
200	8946.830	7969.415	0.548775	30	6	-1.360842	2.160628
200	13893.776	10442.888	0.655651	30	9	-0.793882	1.260456
200	18309.316	12650.658	0.715746	30	12	-0.554432	0.880279
200	33171.335	20081.668	0.820931	30	24	-0.246115	0.390759
200	56763.321	31877.660	0.887194	30	48	-0.114568	0.181900
200	3048.834	5020.417	0.283725	60	3	-2.287231	0.571808
200	8946.830	7969.415	0.548775	60	6	-0.785683	0.196421
200	13893.776	10442.888	0.655651	60	9	-0.458348	0.114587
200	18309.316	12650.658	0.715746	60	12	-0.320102	0.080025
200	33171.335	20081.668	0.820931	60	24	-0.142094	0.035524
200	56763.321	31877.660	0.887194	60	48	-0.066146	0.016536
200	3048.834	5020.417	0.283725	90	3	0.000000	-2.287231
200	8946.830	7969.415	0.548775	90	6	0.000000	-0.785683
200	13893.776	10442.888	0.655651	90	9	0.000000	-0.458348
200	18309.316	12650.658	0.715746	90	12	0.000000	-0.320102
200	33171.335	20081.668	0.820931	90	24	0.000000	-0.142094
200	56763.321	31877.660	0.887194	90	48	0.000000	-0.066146
200	3048.834	5020.417	0.283725	120	3	2.287231	0.571808
200	8946.830	7969.415	0.548775	120	6	0.785683	0.196421
200	13893.776	10442.888	0.655651	120	9	0.458348	0.114587
200	18309.316	12650.658	0.715746	120	12	0.320102	0.080025
200	33171.335	20081.668	0.820931	120	24	0.142094	0.035524
200	56763.321	31877.660	0.887194	120	48	0.066146	0.016536
200	3048.834	5020.417	0.283725	150	3	3.961600	6.289884
200	8946.830	7969.415	0.548775	150	6	1.360842	2.160628
200	13893.776	10442.888	0.655651	150	9	0.793882	1.260456
200	18309.316	12650.658	0.715746	150	12	0.554432	0.880279
200	33171.335	20081.668	0.820931	150	24	0.246115	0.390759
200	56763.321	31877.660	0.887194	150	48	0.114568	0.181900
300	2948.834	5020.417	0.263806	30	3	-3.869269	6.143290
300	8846.830	7969.415	0.536227	30	6	-1.309330	2.078841
300	13793.776	10442.888	0.646075	30	9	-0.760273	1.207095
300	18209.316	12650.658	0.707841	30	12	-0.529706	0.841021
300	33071.335	20081.668	0.815952	30	24	-0.234256	0.371932
300	56663.321	31877.660	0.884057	30	48	-0.108813	0.172764

Altitude of Periapsis (km)	Altitude of Apoapsis (km)	Semi-Major Axis (km)	Eccentricity	Inclination (deg)	Period (hours)	Node Rate (deg/day)	Apsidal Rate (deg/day)
300	2948.834	5020.417	0.263806	60	3	-2.233924	0.558481
300	8846.830	7969.415	0.536227	60	6	-0.755942	0.188986
300	13793.776	10442.888	0.646075	60	9	-0.438944	0.109736
300	18209.316	12650.658	0.707841	60	12	-0.305826	0.076456
300	33071.335	20081.668	0.815952	60	24	-0.135248	0.033812
300	56663.321	31877.660	0.884057	60	48	-0.062823	0.015706
300	2948.834	5020.417	0.263806	90	3	0.000000	-2.233924
300	8846.830	7969.415	0.536227	90	6	0.000000	-0.755942
300	13793.776	10442.888	0.646075	90	9	0.000000	-0.438944
300	18209.316	12650.658	0.707841	90	12	0.000000	-0.305826
300	33071.335	20081.668	0.815952	90	24	0.000000	-0.135248
300	56663.321	31877.660	0.884057	90	48	0.000000	-0.062823
300	2948.834	5020.417	0.263806	120	3	2.233924	0.558481
300	8846.830	7969.415	0.536227	120	6	0.755942	0.188986
300	13793.776	10442.888	0.646075	120	9	0.438944	0.109736
300	18209.316	12650.658	0.707841	120	12	0.305826	0.076456
300	33071.335	20081.668	0.815952	120	24	0.135248	0.033812
300	56663.321	31877.660	0.884057	120	48	0.062823	0.015706
300	2948.834	5020.417	0.263806	150	3	3.869269	6.143290
300	8846.830	7969.415	0.536227	150	6	1.309330	2.078841
300	13793.776	10442.888	0.646075	150	9	0.760273	1.207095
300	18209.316	12650.658	0.707841	150	12	0.529706	0.841021
300	33071.335	20081.668	0.815952	150	24	0.234256	0.371932
300	56663.321	31877.660	0.884057	150	48	0.108813	0.172764
400	2848.834	5020.417	0.243887	30	3	-3.786511	6.011893
400	8746.830	7969.415	0.523679	30	6	-1.261782	2.003349
400	13693.776	10442.888	0.636499	30	9	-0.729203	1.157766
400	18109.316	12650.658	0.699937	30	12	-0.506846	0.804726
400	32971.335	20081.668	0.810972	30	24	-0.223300	0.354536
400	56563.321	31877.660	0.880920	30	48	-0.103500	0.164329
400	2848.834	5020.417	0.243887	60	3	-2.186143	0.546536
400	8746.830	7969.415	0.523679	60	6	-0.728490	0.182123
400	13693.776	10442.888	0.636499	60	9	-0.421006	0.105251
400	18109.316	12650.658	0.699937	60	12	-0.292628	0.073157
400	32971.335	20081.668	0.810972	60	24	-0.128922	0.032231
400	56563.321	31877.660	0.880920	60	48	-0.059756	0.014939
400	2848.834	5020.417	0.243887	90	3	0.000000	-2.186143

Altitude of Periapsis (km)	Altitude of Apoapsis (km)	Semi-Major Axis (km)	Eccentricity	Inclination (deg)	Period (hours)	Node Rate (deg/day)	Apsidal Rate (deg/day)
400	8746.830	7969.415	0.523679	90	6	0.000000	-0.728490
400	13693.776	10442.888	0.636499	90	9	0.000000	-0.421006
400	18109.316	12650.658	0.699937	90	12	0.000000	-0.292628
400	32971.335	20081.668	0.810972	90	24	0.000000	-0.128922
400	56563.321	31877.660	0.880920	90	48	0.000000	-0.059756
400	2848.834	5020.417	0.243887	120	3	2.186143	0.546536
400	8746.830	7969.415	0.523679	120	6	0.728490	0.182123
400	13693.776	10442.888	0.636499	120	9	0.421006	0.105251
400	18109.316	12650.658	0.699937	120	12	0.292628	0.073157
400	32971.335	20081.668	0.810972	120	24	0.128922	0.032231
400	56563.321	31877.660	0.880920	120	48	0.059756	0.014939
400	2848.834	5020.417	0.243887	150	3	3.786511	6.011893
400	8746.830	7969.415	0.523679	150	6	1.261782	2.003349
400	13693.776	10442.888	0.636499	150	9	0.729203	1.157766
400	18109.316	12650.658	0.699937	150	12	0.506846	0.804726
400	32971.335	20081.668	0.810972	150	24	0.223300	0.354536
400	56563.321	31877.660	0.880920	150	48	0.103500	0.164329
500	2748.834	5020.417	0.223969	30	3	-3.712575	5.894504
500	8646.830	7969.415	0.511131	30	6	-1.217816	1.933543
500	13593.776	10442.888	0.626923	30	9	-0.700423	1.112071
500	18009.316	12650.658	0.692032	30	12	-0.485667	0.771100
500	32871.335	20081.668	0.805992	30	24	-0.213154	0.338428
500	56463.321	31877.660	0.877783	30	48	-0.098584	0.156523
500	2748.834	5020.417	0.223969	60	3	-2.143456	0.535864
500	8646.830	7969.415	0.511131	60	6	-0.703106	0.175777
500	13593.776	10442.888	0.626923	60	9	-0.404390	0.101097
500	18009.316	12650.658	0.692032	60	12	-0.280400	0.070100
500	32871.335	20081.668	0.805992	60	24	-0.123065	0.030766
500	56463.321	31877.660	0.877783	60	48	-0.056917	0.014229
500	2748.834	5020.417	0.223969	90	3	0.000000	-2.143456
500	8646.830	7969.415	0.511131	90	6	0.000000	-0.703106
500	13593.776	10442.888	0.626923	90	9	0.000000	-0.404390
500	18009.316	12650.658	0.692032	90	12	0.000000	-0.280400
500	32871.335	20081.668	0.805992	90	24	0.000000	-0.123065
500	56463.321	31877.660	0.877783	90	48	0.000000	-0.056917
500	2748.834	5020.417	0.223969	120	3	2.143456	0.535864
500	8646.830	7969.415	0.511131	120	6	0.703106	0.175777

Altitude of Periapsis (km)	Altitude of Apoapsis (km)	Semi-Major Axis (km)	Eccentricity	Inclination (deg)	Period (hours)	Node Rate (deg/day)	Apsidal Rate (deg/day)
500	13593.776	10442.888	0.626923	120	9	0.404390	0.101097
500	18009.316	12650.658	0.692032	120	12	0.280400	0.070100
500	32871.335	20081.668	0.805992	120	24	0.123065	0.030766
500	56463.321	31877.660	0.877783	120	48	0.056917	0.014229
500	2748.834	5020.417	0.223969	150	3	3.712575	5.894504
500	8646.830	7969.415	0.511131	150	6	1.217816	1.933543
500	13593.776	10442.888	0.626923	150	9	0.700423	1.112071
500	18009.316	12650.658	0.692032	150	12	0.485667	0.771100
500	32871.335	20081.668	0.805992	150	24	0.213154	0.338428
500	56463.321	31877.660	0.877783	150	48	0.098584	0.156523

These effects can be leveraged to enable various special classes of orbits. The first class of orbits is the “sun-synchronous” orbit, where the node rate (Equation 17) is set equal to the mean motion of the sun (0.524 deg/day). As a result, the ascending node remains at the same local mean solar time over time. This is useful for missions that image the surface, as shadows (optical) and thermal states (infrared) beneath the orbit remain nearly constant, simplifying interpretation of the images. The geometry with respect to the sun remains nearly constant as well, meaning that eclipse durations remain consistent over the course of the mission, subject to seasonal variations as the sub-solar latitude moves from one solstice to the other and back. These variations are most pronounced for the “face on” orbits with an ascending node at 6 am or pm LMST, as shown in Figures 55 and 56, which assume a circular orbit. If the orbit is circular or nearly-so, the “synchronous inclination” is purely a function of the mean altitude, as illustrated in Figure 57. For low mars orbits, this is about 93-94 deg.

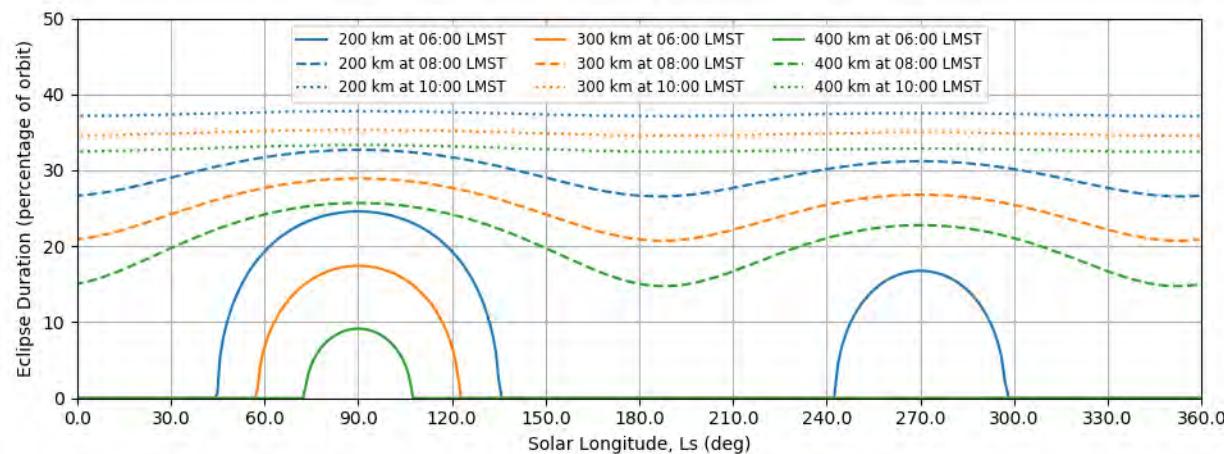


**Figure 55: Eclipse Duration during a Mars Year for Circular Sun-Synchronous Orbit (Morning)**

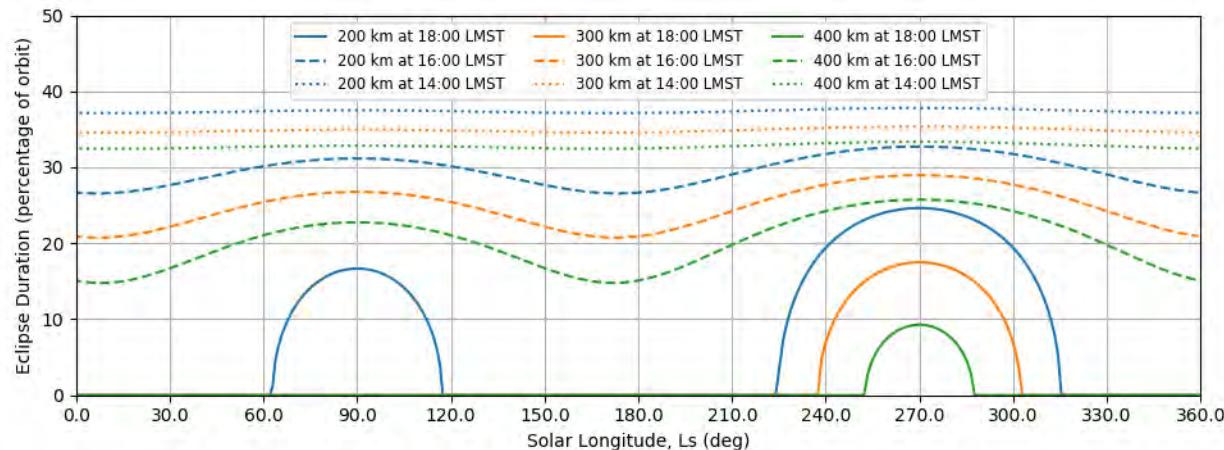


**Figure 56: Eclipse Duration during a Mars Year for Circular Sun-Synchronous Orbits (Afternoon)**

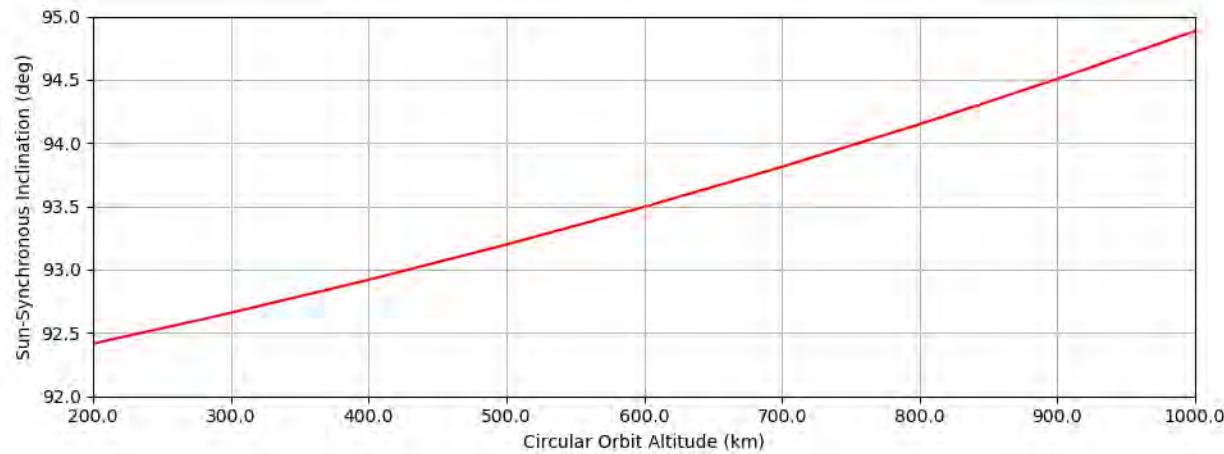


**Figure 57: Required Inclination for a Circular Sun-Synchronous Orbit**

Second, an orbit may be “frozen,” meaning the argument of periapsis remains in the same location. The altitude vs. latitude relationship is thus a constant. Equation 18 can be made to be zero with the “critical inclination” of 63.4 degrees, but a near-polar frozen orbit with periapsis at the South Pole ( $\omega = -90$  deg) can be achieved by using the effect of the 3<sup>rd</sup> zonal harmonic,  $J_3$ , and choosing an inclination, eccentricity, and semi-major axis that satisfy Equation 21.

$$RJ_3 \sin i = 2aeJ_2 \quad (21)$$

Finally, the orbit can be a “ground track repeat” orbit, which flies the same orbit path as a function of latitude and longitude, illustrated in Figure 58. This is useful for missions looking for changes in the surface, as the geometries with respect to the surface are nearly invariant. They are also very convenient for relay orbiters, as the sequence of passes above the surface repeat. A ground track repeat orbit has integer  $K$  orbits in integer  $N$  sols, where  $K$  and  $N$  are mutually prime and meet the condition of Equation 22:

$$K(\omega_p + \dot{\omega}) = N(\dot{\Omega} + \dot{M}) \quad (22)$$

where  $\omega_p$  is the inertial rotation rate of Mars ( $7.088 \times 10^{-5}$  rad/sec),  $\dot{\omega}$  is the apsidal rate, defined in Equation 18,  $\dot{\Omega}$  is the node precession rate, defined in Equation 17, and  $\dot{M}$  is the mean anomaly rate under the influence of J2, defined as:

$$\dot{M} = n \left( 1 + \frac{3R}{2p} J_2 \sqrt{1 - e^2} \left( 1 - \frac{3}{2} \sin^2 i \right) \right) \quad (23)$$

Note that the repeat cycle will not be an integer number of sols unless the orbit is also sun-synchronous. The node drift with respect to the sun line will cause the repeat cycle to be shorter than a sol if the orbit has a sub-synchronous inclination and longer if super-synchronous.

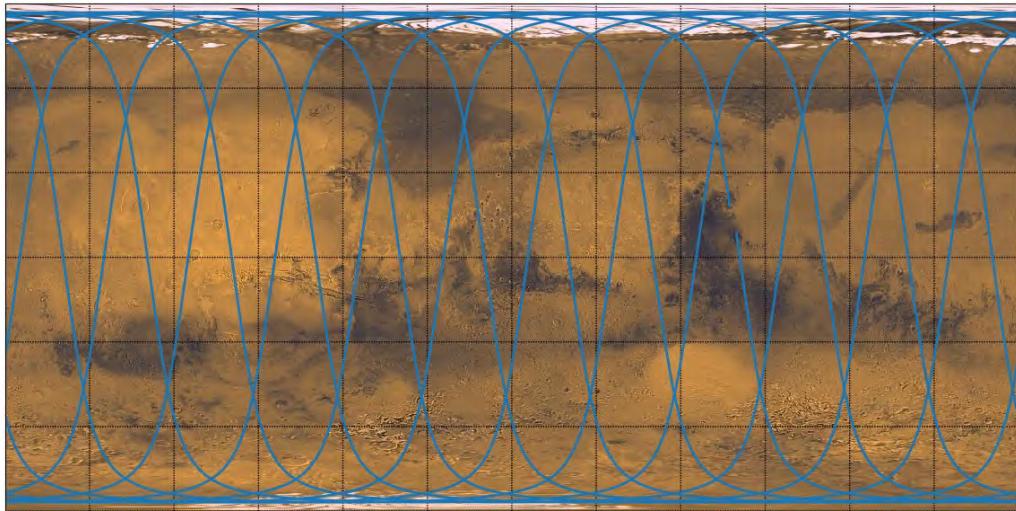


**Figure 58: Example of a Repeat Ground Track**

These three features may be combined. The 2001 Mars Odyssey and 2005 Mars Reconnaissance Orbiter (MRO) spacecraft used frozen, sun-synchronous orbits. MRO's orbit is also a very nearly ground-track repeat orbit. A scatter plot of sun-synchronous, frozen, ground-track repeat orbits is illustrated in Figure 59. The inclinations of these orbits essentially follow the curve of Figure 57, while the eccentricities vary from 0.0061 to 0.0075, as shown in Figure 60.

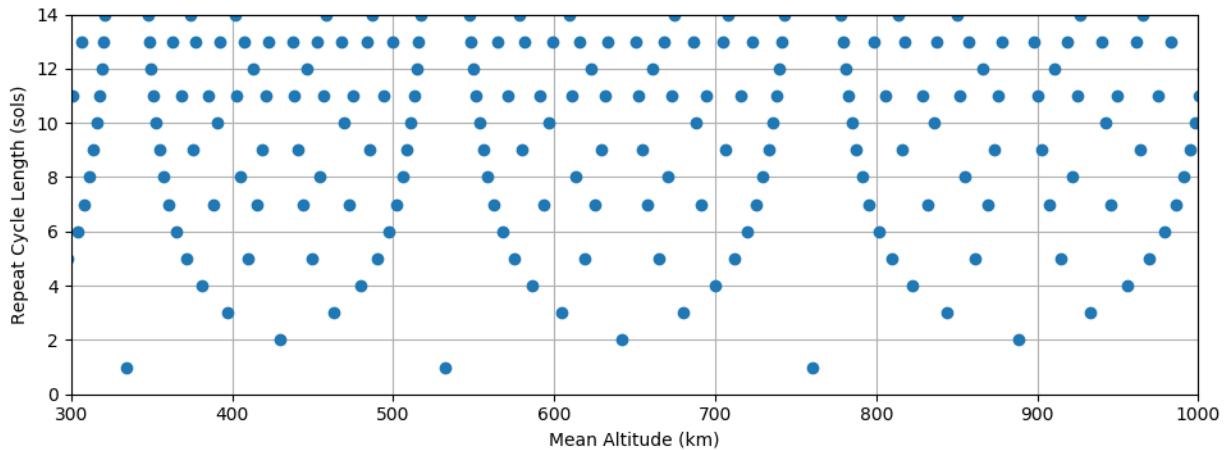


**Figure 59: Frozen, Sun-Synchronous, Ground-Track Repeat Orbit Mean Altitudes and Repeat Durations**

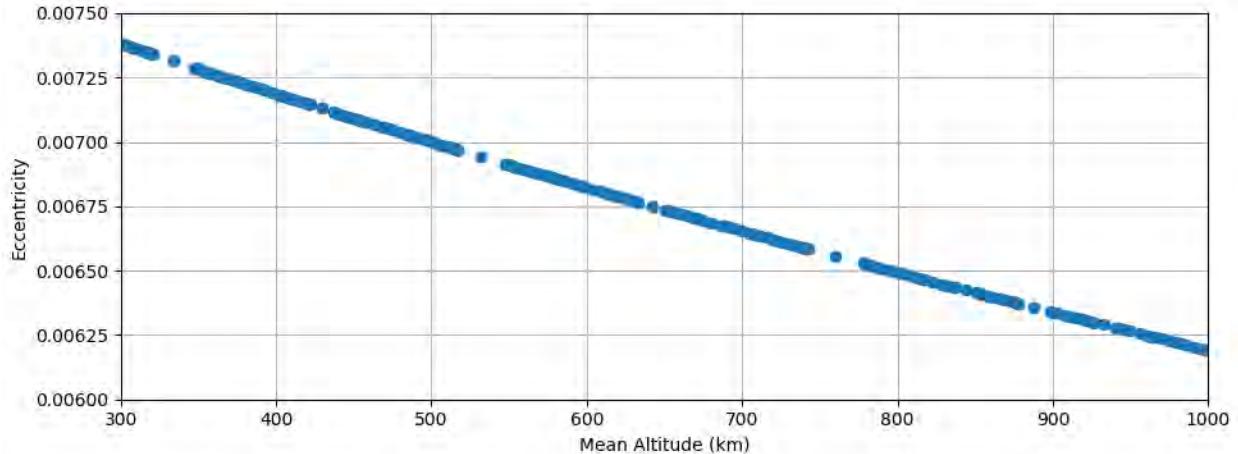


Figure 60: Frozen, Sun-Synchronous, Ground-Track Repeat Orbit Mean Altitudes and Eccentricities

### 8.2.3 Drag Perturbations

The spacecraft's interactions with the atmosphere act to remove energy from its orbit – reducing its semi-major axis. For a highly elliptical orbit, this preferentially takes the form of reducing the apoapsis altitude. Once the orbit is mostly circularized, the orbit remains near-circular until the periapsis altitude is reduced below a critical altitude and the spacecraft deorbits. Uncompensated for, this effect will drive an orbit off a ground-track repeat or sun-synchronous condition. However, an orbit that is frozen will remain so.

The acceleration due to drag acts against the atmosphere-relative velocity vector with magnitude  $a_D$ :

$$a_D = \frac{\rho v^2}{2\beta} \quad (24)$$

where  $\rho$  is the atmospheric density,  $v$  is the spacecraft velocity relative to the atmosphere, and  $\beta$  is the ballistic coefficient, which is dependent on the spacecraft size and shape:

$$\beta = \frac{m}{C_D A} \quad (25)$$

$C_D$  is the coefficient of drag. A value of 2.0 is commonly used for spacecraft at orbital altitudes; a different value is necessary when deeper in the atmosphere, such as for aerocapture.  $A$  is the cross-sectional area of the spacecraft projected along the atmosphere-relative velocity vector, and  $m$  is the spacecraft mass. A spacecraft with large solar arrays can have a large time-dependent variation on this parameter as the arrays go from edge-on to face-on to the flow, depending on the concept of operations. A spacecraft may have fixed arrays sized to accept large cosine losses and have no such variation, while one with gimbaled arrays tracking the sun may have such. The average cross-sectional area of a spacecraft, regardless of orientation, can be estimated as the sum of six orthogonal projections divided by four.

To first order, this acceleration is a function of the orbit altitude and ballistic coefficient. However, it is seasonal, as discussed in Section 2.6. High-drag seasons such as northern winter/perihelion and solar maxima will see larger drag accelerations. This is offset, on average, by low-drag seasons and solar minima. For preliminary analysis, we can neglect this effect and use the simplified, altitude-only atmosphere model. For a circular orbit, we can simply substitute

the circular orbit velocity into Equation 24 and get the  $\Delta V$  per unit time to maintain the orbit, illustrated in Figures 61 through 63 for the three atmosphere models. This assumes that the difference between inertial and atmosphere-relative velocity averages out over the course of an orbit. The drag acceleration can be numerically integrated over an orbit for eccentric orbits.

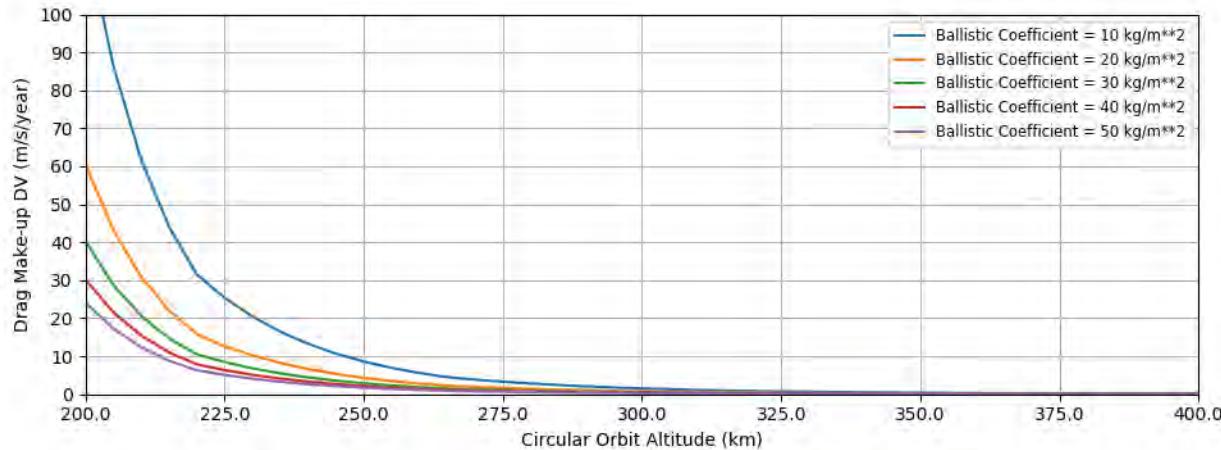


**Figure 61: Drag Make-Up  $\Delta V$  vs. Circular Orbit Altitude with the "High" Atmosphere Model**

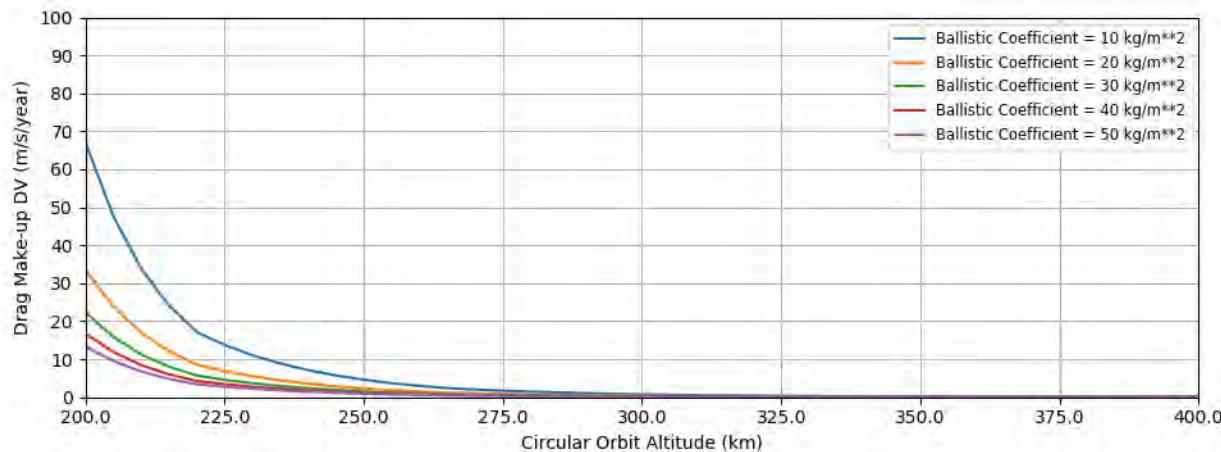


**Figure 62: Drag Make-Up  $\Delta V$  vs. Circular Orbit Altitude with the "Mean" Atmosphere Model**

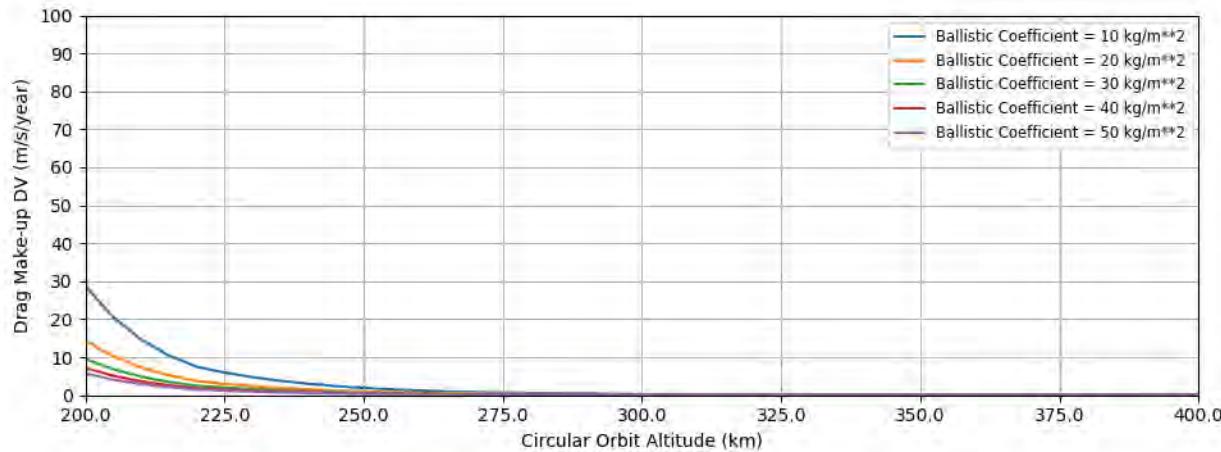


**Figure 63: Drag Make-Up ΔV vs. Circular Orbit Altitude with the "Low" Atmosphere Model**

Once a spacecraft ceases to be controlled, drag will eventually deorbit the spacecraft if it is low enough and/or its ballistic coefficient is low enough (more balloon than bowling ball). Figures 64 to 66 illustrates the orbit lifetime under the simplified models for various orbit altitudes, per Equation 26.

$$\dot{a} = -\frac{\rho}{\beta} \sqrt{\mu a} \quad (26)$$

Here,  $\rho$  varies with altitude (as per Equation 7), so this rate is a function of the semi-major axis,  $a$ , twice over, and is numerically integrated until the altitude is 125 km.

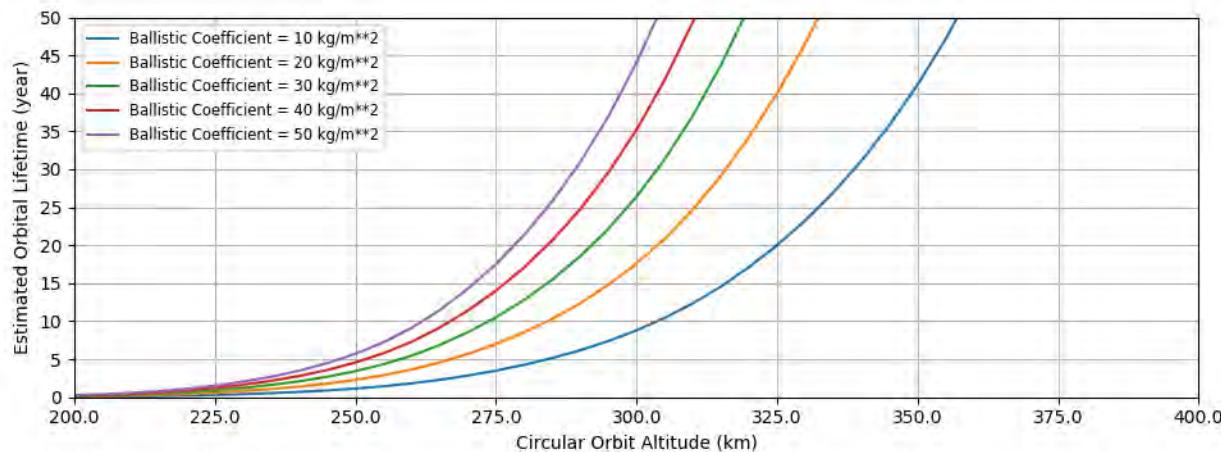


**Figure 64: Circular Orbit Lifetime with the "High" Atmosphere Model**

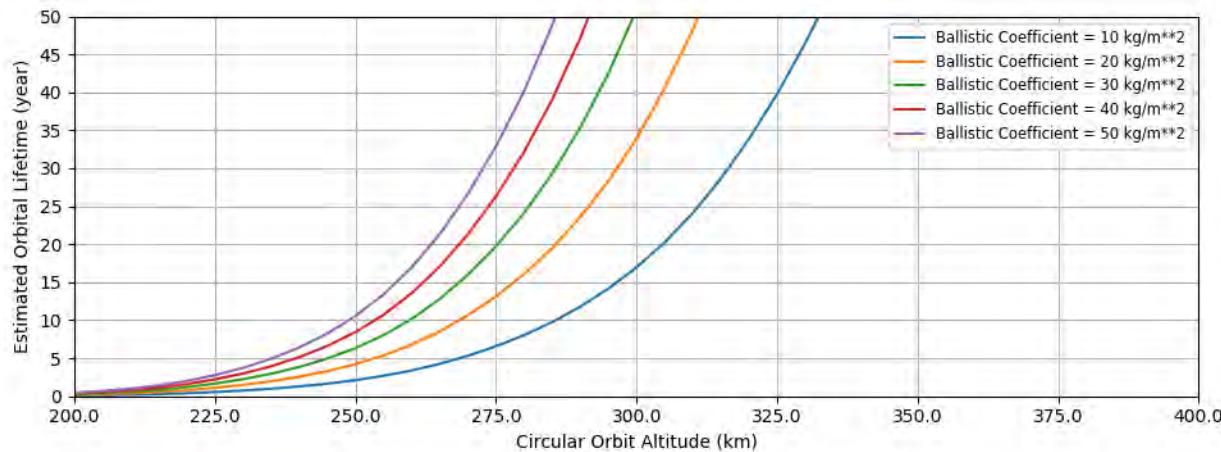


**Figure 65: Circular Orbit Lifetime with the "Mean" Atmosphere Model**

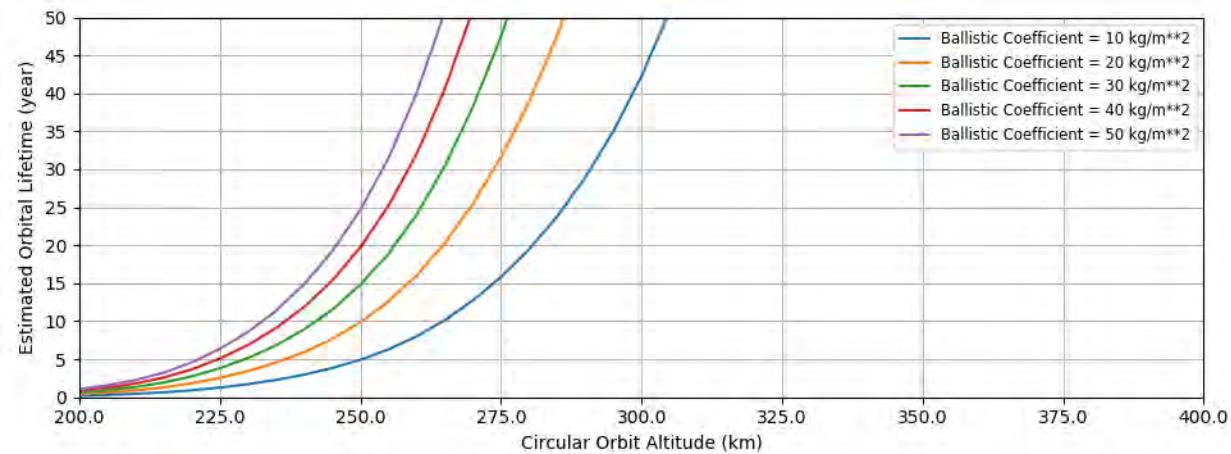


**Figure 66: Circular Orbit Lifetime with the "Low" Atmosphere Model**

The forward planetary protection requirements codified in NPR 8020.12D are stated as a probabilistic requirement [39]. As of this writing, the requirement is for the spacecraft to have a less than 1% chance of deorbiting within 20 years of launch and less than 5% chance of deorbiting between 20 and 50 years of launch. More detailed modeling, including statistical consideration of the solar activity and the variation over a Mars year [40], is typically required, unless the orbit is high enough that even a continuous 240-sfu atmosphere is insufficient to deorbit the spacecraft.

## 8.3 Orbit Insertion

### 8.3.1 *Introduction*

Orbit capture or orbit insertion is typically a critical event where the spacecraft reduces its specific energy below  $0 \text{ km}^2/\text{s}^2$  and changes its trajectory from a flyby to captured in orbit about Mars. Simply having negative energy is not necessarily sufficient to be captured. If the post-insertion orbit is highly eccentric, solar tides may pull the spacecraft back out of orbit and into interplanetary space. More importantly, the orbit must remain captured even in the event of a significant (e.g.  $3\sigma$ ) under-burn. An eccentricity of 0.95 (which is about a 6-sol orbit) is a typical rule of thumb for the largest-desirable post-capture target orbit.

### 8.3.2 *High-Thrust Orbit Insertion*

A spacecraft on a hyperbolic approach ( $v_{\infty} > 0 \text{ km/s}$ ) must supply a sufficiently large  $\Delta V$  to capture. This can be done either with a high-thrust propulsion system (a Mars Orbit Insertion, or MOI, burn) or by using the drag from a sufficiently deep passage through the atmosphere of Mars (aerocapture). Regardless, the  $\Delta V$  as a function of incoming  $v_{\infty}$  (VHP) and capture periapsis altitude required is the same and are plotted in Figures 67 to 70 for altitudes between 250 and 400 km. These are idealized impulsive  $\Delta V$ s and do not include any losses.

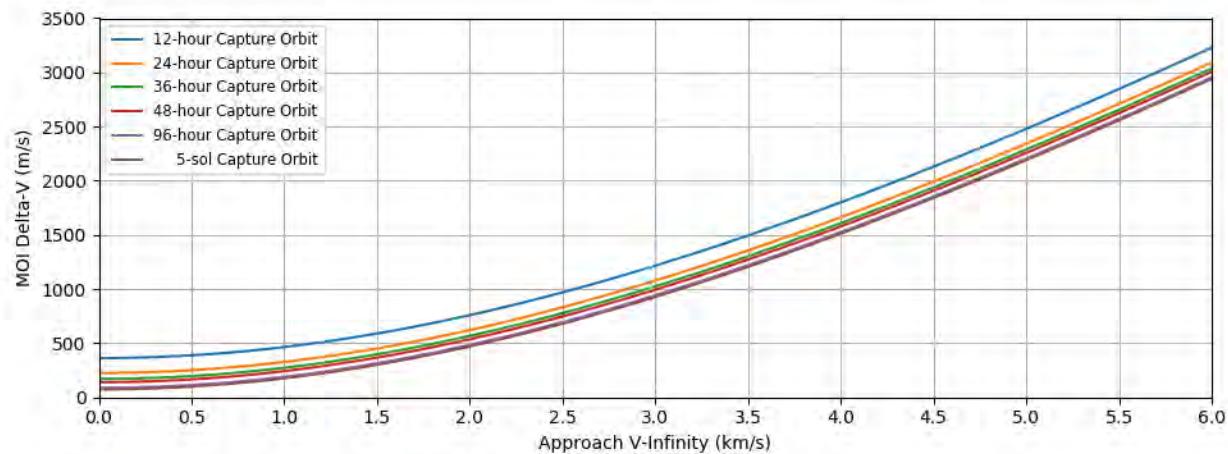


**Figure 67: Mars Orbit Insertion ΔV at 250 km Altitude**

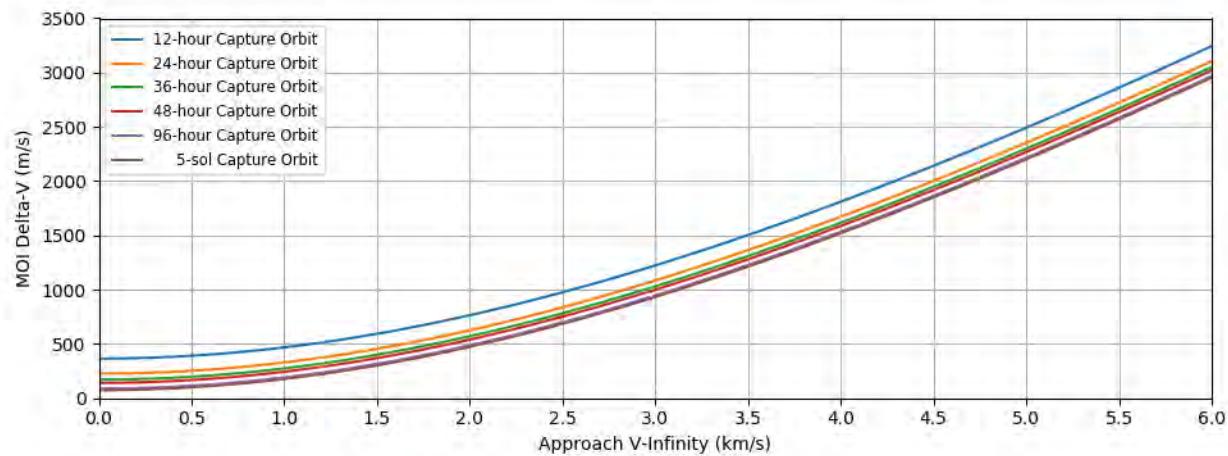


**Figure 68: Mars Orbit Insertion ΔV at 300 km Altitude**

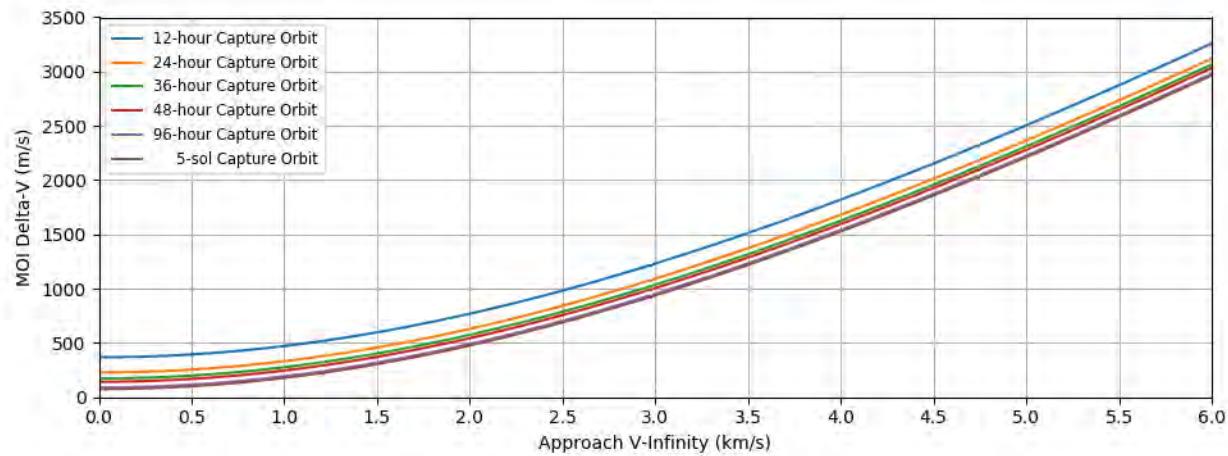


**Figure 69: Mars Orbit Insertion ΔV at 350 km Altitude**

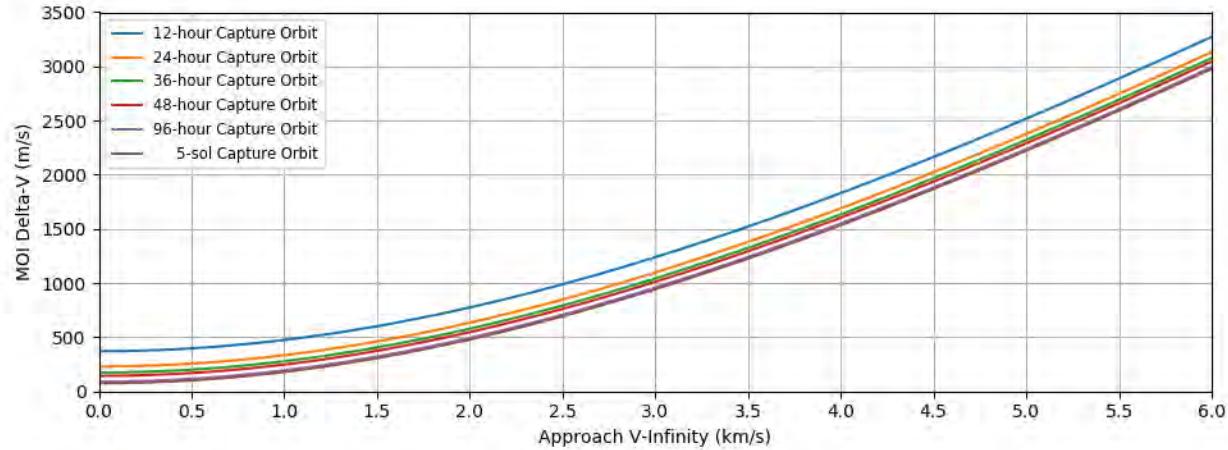


Figure 70: Mars Orbit Insertion  $\Delta V$  at 400 km Altitude

A Mars Orbit Insertion (MOI) burn will suffer “finite burn” or “gravity” losses since the entire  $\Delta V$  cannot be achieved at the optimal periapsis location. For spacecraft with relatively low thrust for their mass, a large required  $\Delta V$ , or both, these losses can be a significant fraction of the total  $\Delta V$  required. The time required to complete the burn is:

$$t_b = \frac{m_0}{T} g_0 I_{sp} \left( 1 - e^{-\Delta V / g_0 I_{sp}} \right) \quad (27)$$

where  $m_0$  is the total spacecraft mass before the burn,  $T$  is the thrust,  $g_0$  is the surface gravity on Earth (9.80665 m/s),  $I_{sp}$  is the propulsion system specific impulse, and  $\Delta V$  is the idealized  $\Delta V$  required of the burn. An empirical model for the finite burn losses,  $\Delta V_L$ , is:

$$\Delta V_L = \frac{\mu t_b^2}{48r^3} \Delta V \quad (28)$$

where  $\mu$  is the gravitational parameter (see Section 2.2.1) and  $r$  is the periapsis radius during the burn. This model gives reasonable agreement with integrated finite-burn solutions for burn arcs less than 135 deg.

The orientation of a post-capture orbit is dependent on the approach v-infinity magnitude (VHP), declination (DAP), and right ascension (RAP), as well as the targeting B-Plane angle and the orbit insertion burn. The discussion which follows assumes an along-track, in-plane burn.

The locus of eccentricity vectors (which point from the center of Mars to periapsis) after orbit insertion is similar to the locus of entry points discussed in Section 7.3, but much simplified. The periapsis radius is directly selected rather than being a complex function of the entry flight path angle as the flight path angle is zero at periapsis. The eccentricity vector specifies the argument of periapsis directly, and the cross product of the inbound v-infinity vector and the eccentricity vector defines the orbit plane. These vary together as the targeting B-Plane angle sweeps across the locus. As a result, the orbit plane (inclination and longitude of ascending node) and orientation (argument of periapsis) are independent of the orbit period but are tied together via the single free parameter of the B-Plane angle.

The reachable inclinations are determined entirely by DAP; a prograde orbit can be no lower than the absolute value of the DAP, and a retrograde orbit can be no more equatorial than 180 deg minus the absolute value of the DAP. For example, a spacecraft with an approach

declination of 15 deg can be inserted into any orbit inclination between 15 and 165 deg. For each reachable inclination, there are two B-Plane angle solutions – a “north approach” with a negative value and a “south approach” with a positive value. Each has a unique argument of periapsis/longitude of node pairing.

### 8.3.3 Aerocapture

An alternative to the large propellant loads required of an MOI is aerocapture. In an aerocapture maneuver, the spacecraft uses the drag acceleration from the atmosphere of Mars to achieve the capture  $\Delta V$ . The  $\Delta V$  itself is slightly lower due to the lower altitude (see Figure 71), and there are no finite burn losses to consider. However, there are three challenges associated with aerocapture.

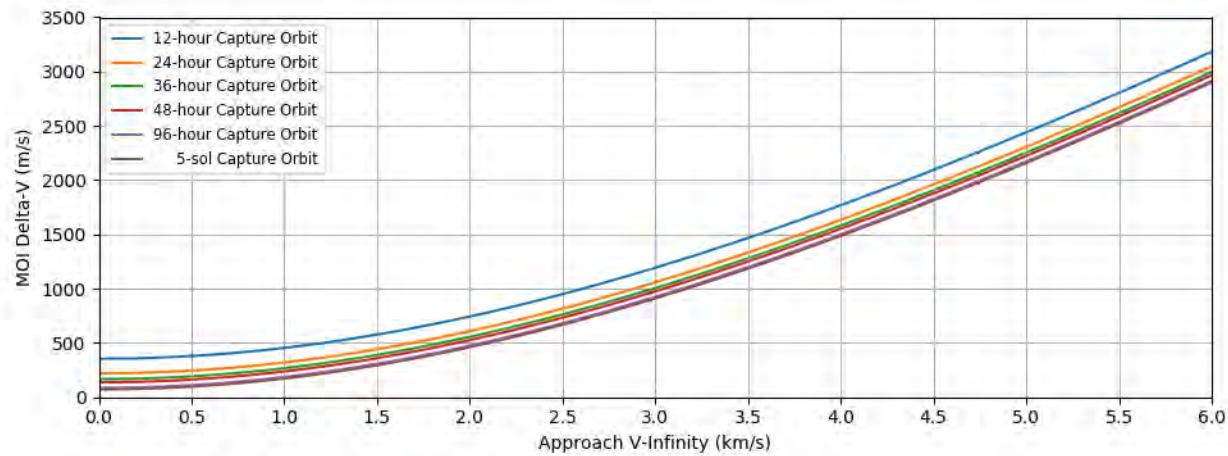


Figure 71: Mars Orbit Insertion  $\Delta V$  at 100 km Altitude

The first challenge is the heating. The spacecraft will experience significant heat loads during the aeropass – less than an EDL mission would, but more than what an unshielded spacecraft can typically tolerate. Thus, the spacecraft must have a heat shield of some sort. Sizing this, like designing an EDL system (see Section 7.2), is beyond the scope of this document. Second, there is a significant targeting challenge. The atmosphere is variable on day-to-day basis and the difference between deorbiting on a high-density day and failing to capture on a low-density day may be too small for an open-loop system. Various techniques have been studied for solving this issue, including roll guidance (*à la* MSL) and accumulated-acceleration triggered reductions in the effective drag area.

The final challenge is the post-aerocapture maneuver. Assuming a successful aerocapture, the periapsis of the post-capture orbit remains deep inside the atmosphere, and a maneuver is required to raise periapsis out of it lest the spacecraft deorbit on the next periapsis passage. If the post-capture orbit has large period uncertainties, then some level of on-board design may be required to determine the timing and sizing of this maneuver. A canned maneuver may be possible if the uncertainties are small enough, which would likely require some form of closed-loop guidance on the aerocapture maneuver itself.

## 8.4 Aerobraking

### 8.4.1 Aerobraking Overview

Aerobraking is a common technique used to reduce the orbit period of a planetary orbiter by

dropping periapsis into the upper atmosphere of a planet and using the resulting drag. The use of this technique can reduce the required delta-v budget by well over a thousand meters per second. It was first demonstrated at Venus during the Magellan extended mission [41], [42] in 1993 and on many Mars orbiters since, from the Mars Global Surveyor (MGS) [43] in 1997 to ESA's Trace Gas Orbiter (TGO) [44] in 2017.

Traditionally, aerobraking operations have been divided into Walk-in, Main, and Walk-out phases. Although there are slight variations in phase divisions or naming convention among missions, the core contents and features of the aerobraking-phase definition are similar.

The walk-in period typically lasts from a few days to several weeks, depending on the spacecraft's capability and the space environment. Magellan completed its walk-in in 3 days while ExoMars Trace Gas Orbiter spent 47 days in its first Walk-in phase. There are no absolute rules to dictate the walk-in duration. The key is to lower the orbit periapsis altitude in a series of gradual steps carried out by executing propulsive maneuvers at apoapsis. The "test-the-water" approach has two major purposes. The first is to find the adequate atmosphere "layer" (i.e. to acquire the desired periapsis altitude) for the aerobraking main phase and to do so safely. Second, prior to committing to the Main-phase operations, a walk-in phase provides an excellent "first-look" opportunity to characterize the atmospheric conditions, gauge the spacecraft design and capability, and verify the aerobraking operation readiness state. Many "first time" events or activities are exercised in this phase, such as operation processes, interfaces, spacecraft and ground systems configurations, aerobraking command sequences, and atmospheric model correlations. This phase offers a chance to evaluate if operations are ready to initiate the Main phase.

A majority of the energy is removed during the Main phase. It typically takes a few months to a year to execute depending on the initial conditions, design approaches, target, environment, and trajectory geometry. Main-phase is characterized by using small propulsive aerobraking maneuvers (ABMs), executed at apoapsis, to fine-tune periapsis altitude to satisfy a defined corridor parameter (e.g. heating rate, dynamic pressure). The periapsis altitude needs to be low enough to produce adequate drag to achieve desired orbit within time constraints imposed by energy balance concerns relative to trajectory requirements. It also needs to be high enough to avoid violating spacecraft heating limits and/or maximum allowable dynamic pressure requirements.

Throughout aerobraking, a minimum orbit lifetime is maintained. During the walk-out phase, periapsis altitude is raised to satisfy orbit lifetime constraints, should problems occur during the final days of aerobraking. This may result in more frequent ABMs to meet this requirement. The walk-out phase lasts approximately a few weeks and is terminated with a periapsis raise maneuver (Aerobraking Exit maneuver, ABX) as part of the transfer to the target orbit.

#### 8.4.2 *Aerobraking Design*

Aerobraking mission design has many drivers. For some missions, such as the Mars Reconnaissance Orbiter [45], there is a need to achieve the science orbit by a certain time so that the sun-synchronous ascending node can be at the right local solar time. For others, there is a desire to complete aerobraking as quickly as possible. Regardless of what drives the timeline, the aerobraking mission profile must send the spacecraft deep enough into the atmosphere to get enough drag to be useful, but not so deep that the resulting aerodynamic environment exceeds a subsystem limit. The aerothermal heating could overheat the spacecraft,

the drag torques could exceed the spacecraft's control authority, or the simple dynamic pressure could exceed a mechanical limit. In addition, particularly in the end game, the spacecraft's orbital lifetime must be sufficiently long as to avoid undue risk.

When designing an aerobraking trajectory, all of these things must be considered. The aerodynamic environment can be parameterized as a limit in three factors: the dynamic pressure (Equation 29), the dynamic heating (Equation 30), and the integrated heating (Equation 31):

$$q = \frac{1}{2} \rho v^2 \quad (29)$$

$$\dot{q} = \frac{1}{2} \rho v^3 \quad (30)$$

$$J = \int_{t_1}^{t_2} \frac{1}{2} \rho v^3 dt \quad (31)$$

where  $\rho$  is the atmospheric density,  $v$  is the atmosphere-relative velocity, and the times  $t_1$  and  $t_2$  are the start and end of a drag pass. The dynamic pressure will yield the acceleration due to drag when multiplied by a ballistic coefficient and a coefficient of drag. The goal then is to tune the drag to meet the timeline requirement without exceeding the limits placed on the other parameters. These limits frequently have significant (100% or more) margin applied to them to accommodate uncertainties in the atmosphere, navigation uncertainties, and maneuver execution errors.

The next key parameter is the operations tempo and orbital lifetime. How often are we permitted to perform a maneuver to tune the trajectory? The more frequently maneuvers are executed, the more active the operations team must be, but the better the trajectory can follow the variations in atmospheric density or, more importantly, counter gravitational perturbations. Solar tides can drive the periapsis altitude up or down and the more frequently a maneuver can be performed, the more this effect can be countered. For example, if solar tides are pulling periapsis out of the atmosphere, a maneuver could target the lowest altitude consistent with meeting the aerodynamic requirements, but the drag on each subsequent pass would be less and less. If the tides are strong enough, or the maneuver frequency is low enough, periapsis could be pulled entirely out of the atmosphere.

The question of orbital lifetime can be thought of as a missed-maneuver constraint. How long must the trajectory meet the dynamic pressure, dynamic heating, and/or integrated heating limits if a maneuver is missed for any reason? The longer this duration, the less risk is incurred by dipping into the atmosphere, but the longer aerobraking might take. For example, if solar tides are pushing periapsis down into the atmosphere, this factor would force each maneuver to target altitude higher than would otherwise be desired so that the aerodynamic limits would not be met until at least the end of the missed-maneuver "buffer."

#### 8.4.3 Modeling Assumptions

The aerobraking design is dependent on the properties of the spacecraft, as well as operational and margin policies. The simulations leading to the data in Section 8.4.4 assumed various ballistic coefficients ( $10\text{-}50 \text{ kg/m}^2$ ) and maximum allowable heat rates ( $0.15 \text{ W/cm}^2$  to  $0.5 \text{ W/cm}^2$ ), a maneuver every two days, and a 48-hour missed-maneuver buffer. A maneuver every other day is about as rapid a tempo as can be reasonably expected. Odyssey had a similar schedule, MAVEN used a Monday-Wednesday-Friday schedule, and MRO performed a maneuver only once per week. More relaxed operational tempos lead to longer campaigns, but

do not materially increase the  $\Delta V$  required. The 48-hour missed maneuver buffer is consistent with historical Mars mission requirements (see Table 27).

**Table 27: Historical Mars Aerobraking Missions**

Mission	Duration (mo.)	Period Reduction (hrs)	Corridor Control Parameter	Orbit Lifetime Requirement (hrs)	Number of ABMs (all types, incl ABX)
Mars Global Surveyor	10.5 (1997-1999)	45. to 2.0	Dynamic Pressure	48	92
Odyssey	2.7 (2001-2002)	18.6 to 2.0	Dynamic Heating	24	33
Mars Reconnaissance Orbiter	5.0 (2006)	35.0 to 2.0	Dynamic Heating	48	27
Trace Gas Orbiter (ESA)	9.0 (2017-2018)	24.0 to 2.0	Dynamic Heating	48	67

In terms of dynamics, an  $8 \times 8$  degree-and-order gravity field was used, along with solar tide perturbations and MarsGram2010 with a constant 150 sfu solar activity level. The atmosphere model described in Section 2.6 lacks the time-and-spatial variations that drive the aerobraking  $\Delta V$  budget. All of the simulations began with a 92-deg inclined, 48-hour orbit with a 250 km periapsis at the equator. A 92 deg inclination was chosen so that the results of these simulations could be used to assess node drift from orbit insertion to the final orbit acquisition for a sun-synchronous orbit. The initial epoch was set to the start of Northern winter ( $L_s = 270$ ) to capture a mean atmosphere. The node was similarly set to maximize the rate at which periapsis is initially pulled out of the atmosphere. This is a weak effect. The periapsis altitude difference between a maximally-raising node to a maximally-reducing node is about 5 km after a single orbit.

#### 8.4.4      *Aerobraking Data*

The plots in this section are intended to permit the reader to do first-order aerobraking design and trades. They are organized in triplets. The first plot in the triplet is the aerobraking duration as a function of initial orbit period. These durations do not include a walk-in phase, since those durations are a matter of risk posture and policy more than the ballistic coefficient or heat rate. However, they do include the walk-out phase, which is a function of these parameters. A spacecraft with a lower permissible heat rate, in particular, will have a much longer walk-out phase.

The second plot in each triplet is the node drift as a function of duration. This drift is a function of orbit period, shape, and inclination. All of the aerobraking trajectories generated for these plots assumed a 92 deg inclination with the intent that these node drift plots would illustrate aerobraking duration trades to target an ascending node time for a low sun-synchronous orbit. For example, if the initial local mean solar time of the ascending node, based on the incoming trajectory and approach direction, were 4 hours ahead of the desired node, then a drift of -4 hours would be required to achieve the desired node. Due to being larger than the sun-synchronous orbit at 92 deg, the ascending node recesses (moves earlier in LTST) during the campaign.

The third plot in each triplet is the aerobraking  $\Delta V$ , excluding aerobraking exit (ABX) and walk-in, but including the walk-out, as a function of duration. The  $\Delta V$  is a function of the time to go (typically 1 m/s/month prior to walk-in) but is dominated by the walk-out phase, which is independent of the time to go but is dependent on the ballistic coefficient and maximum heat rate. The required  $\Delta V$  budget for aerobraking must include ABX (typically  $\approx 20$  m/s) and the walk-in (typically  $\approx 10$  m/s), plus an allocation for the variability in the atmosphere (typically 20-30%), and some additional for long aerobraking campaigns to deal with the potential for safe modes.

This triplet of plots is repeated for fixed ballistic coefficients with various peak heating limits and for fixed peak heating limits with various ballistic coefficients. Note that the scales change for each plot; this was done for readability.

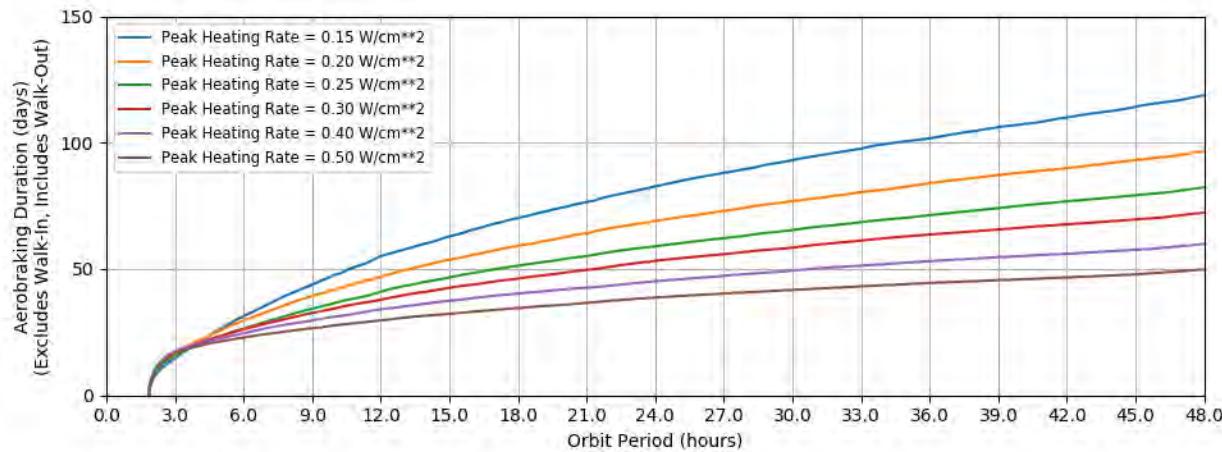


**Figure 72: Aerobraking Duration vs. Orbit Period with  $10 \text{ kg/m}^2$  Ballistic Coefficient**

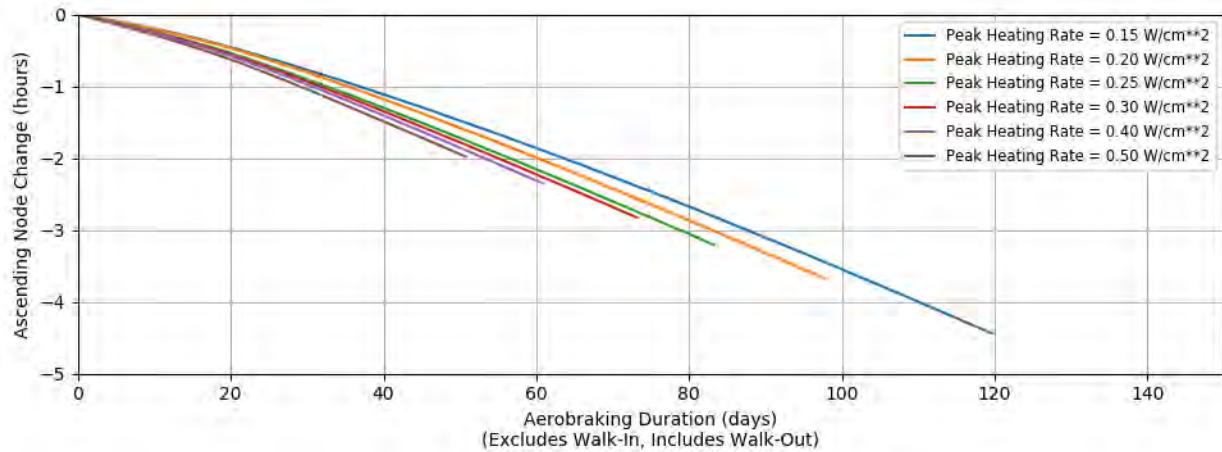


**Figure 73: Ascending Node Drift vs. Aerobraking Duration with  $10 \text{ kg/m}^2$  Ballistic Coefficient**

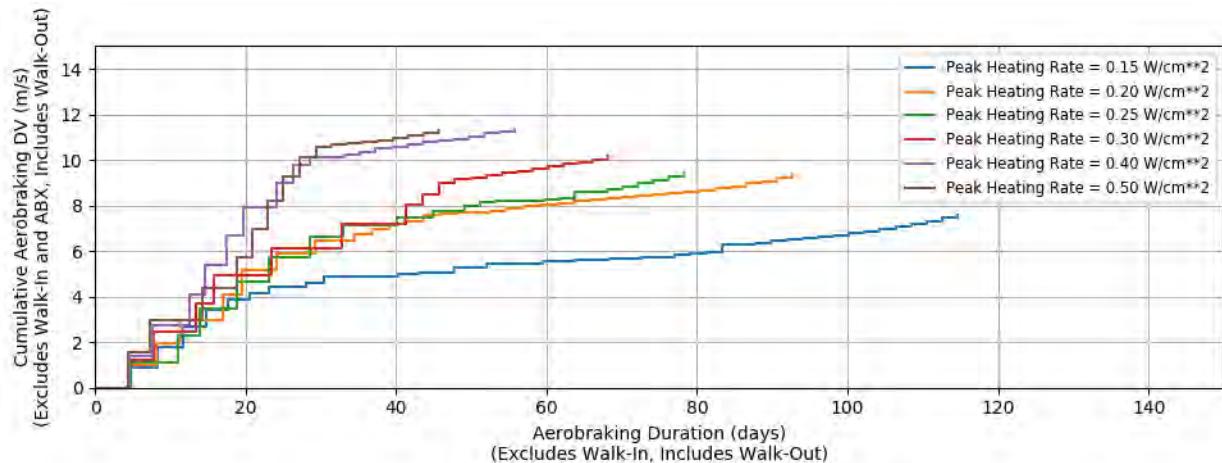


**Figure 74: Aerobraking  $\Delta V$  vs. Aerobraking Duration with  $10 \text{ kg/m}^2$  Ballistic Coefficient**

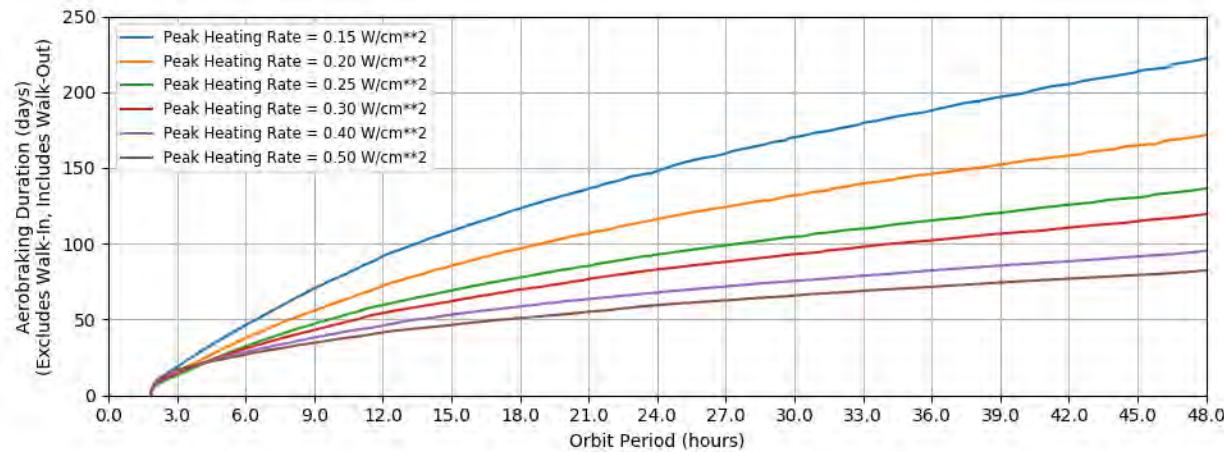


**Figure 75: Aerobraking Duration vs. Orbit Period with  $20 \text{ kg/m}^2$  Ballistic Coefficient**

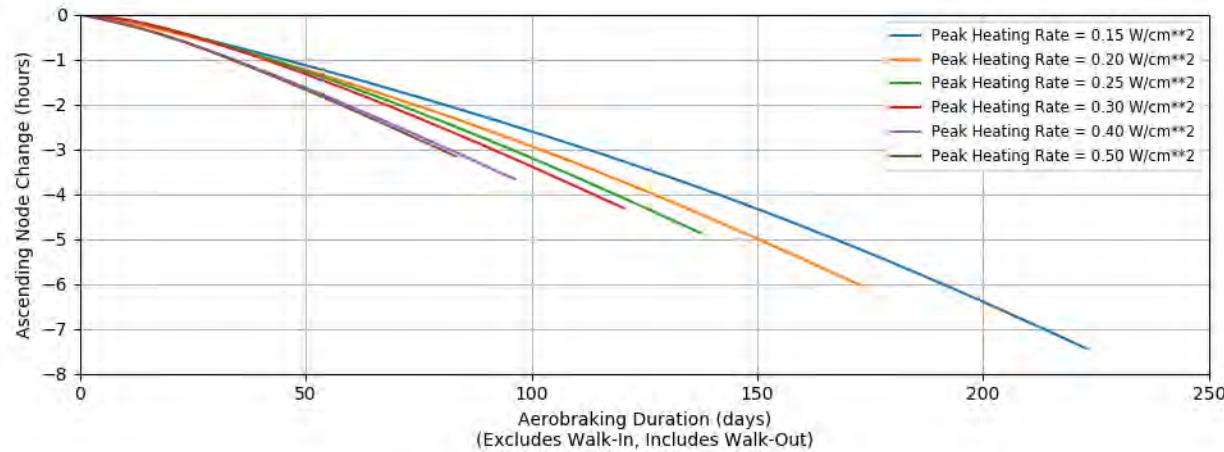


**Figure 76: Ascending Node Drift vs. Aerobraking Duration with  $20 \text{ kg/m}^2$  Ballistic Coefficient**

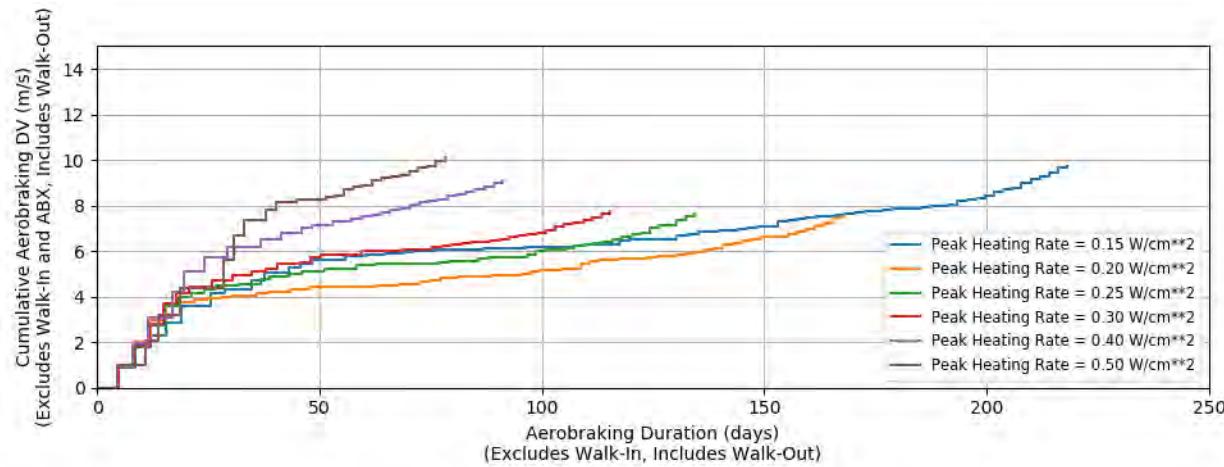


**Figure 77: Aerobraking  $\Delta V$  vs. Aerobraking Duration with  $20 \text{ kg/m}^2$  Ballistic Coefficient**

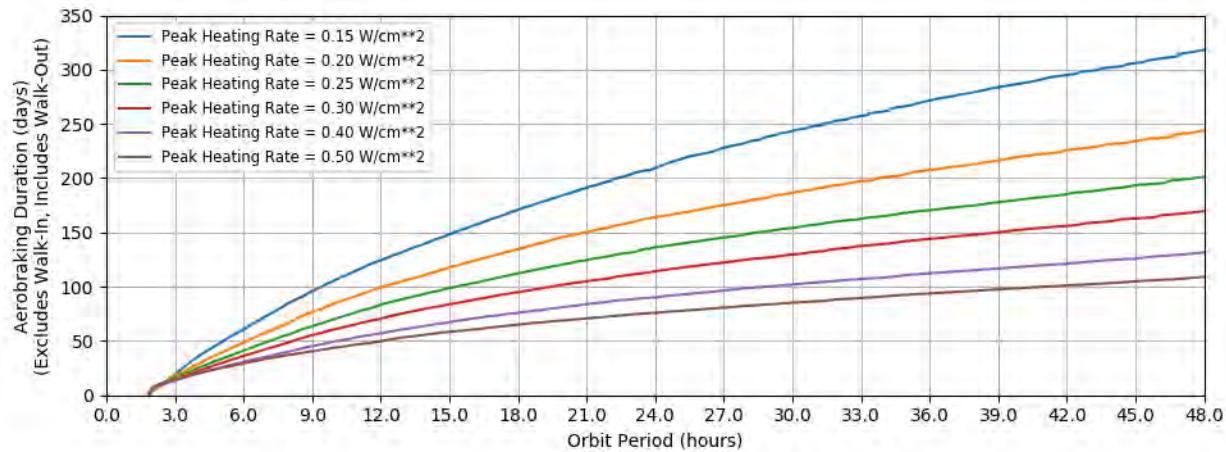


**Figure 78: Aerobraking Duration vs. Orbit Period with 30 kg/m<sup>2</sup> Ballistic Coefficient**

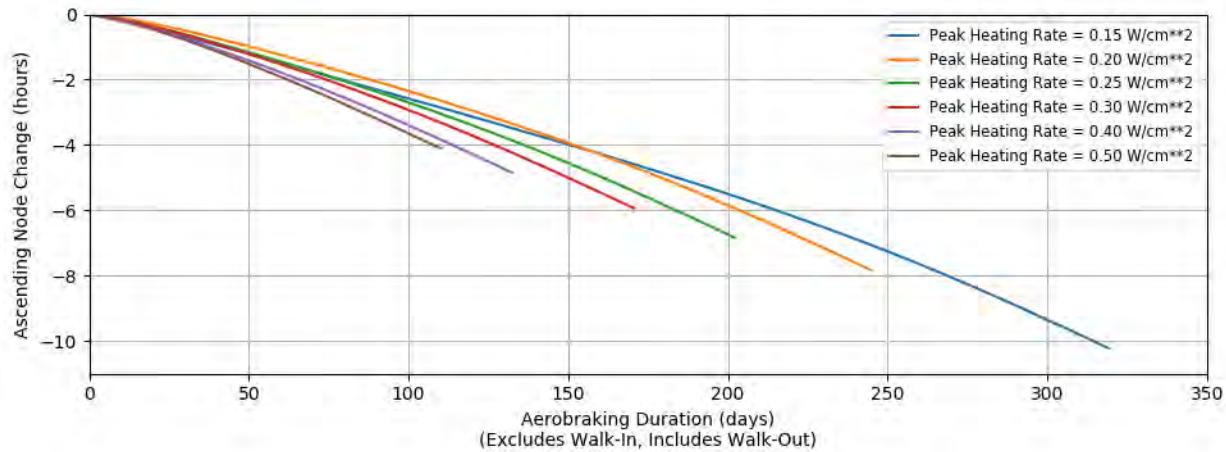


**Figure 79: Ascending Node Drift vs. Aerobraking Duration with 30 kg/m<sup>2</sup> Ballistic Coefficient**

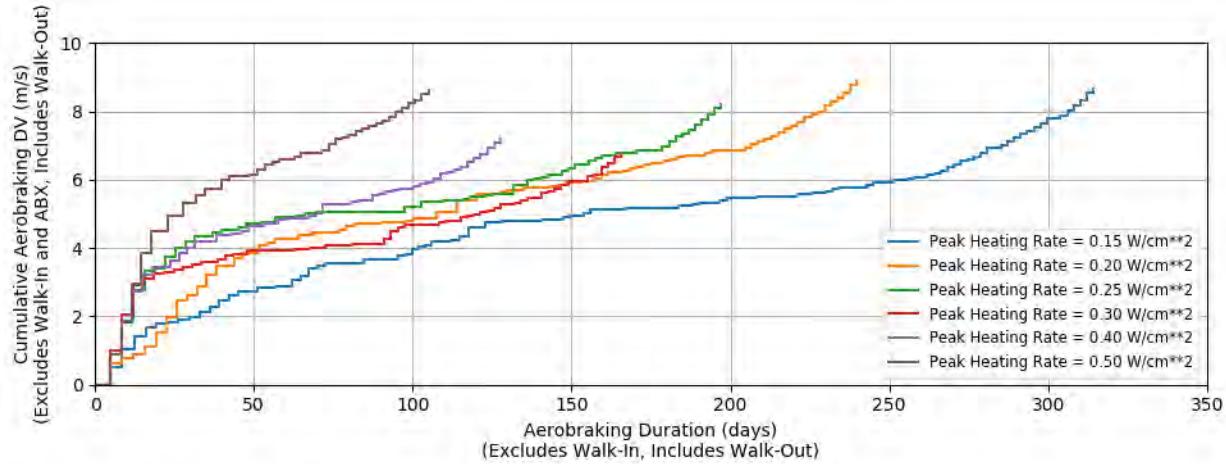


**Figure 80: Aerobraking ΔV vs. Aerobraking Duration with 30 kg/m<sup>2</sup> Ballistic Coefficient**

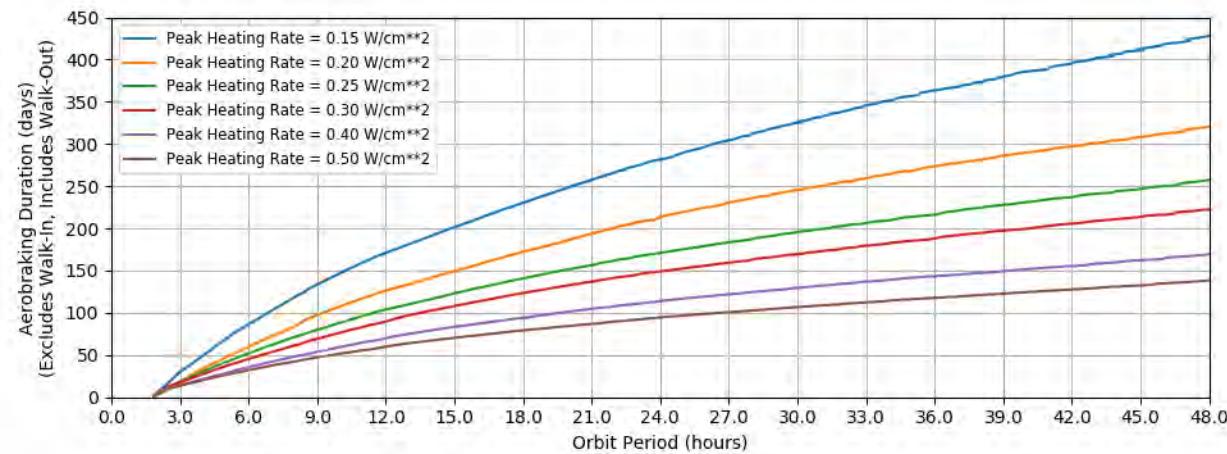


**Figure 81: Aerobraking Duration vs. Orbit Period with 40 kg/m<sup>2</sup> Ballistic Coefficient**

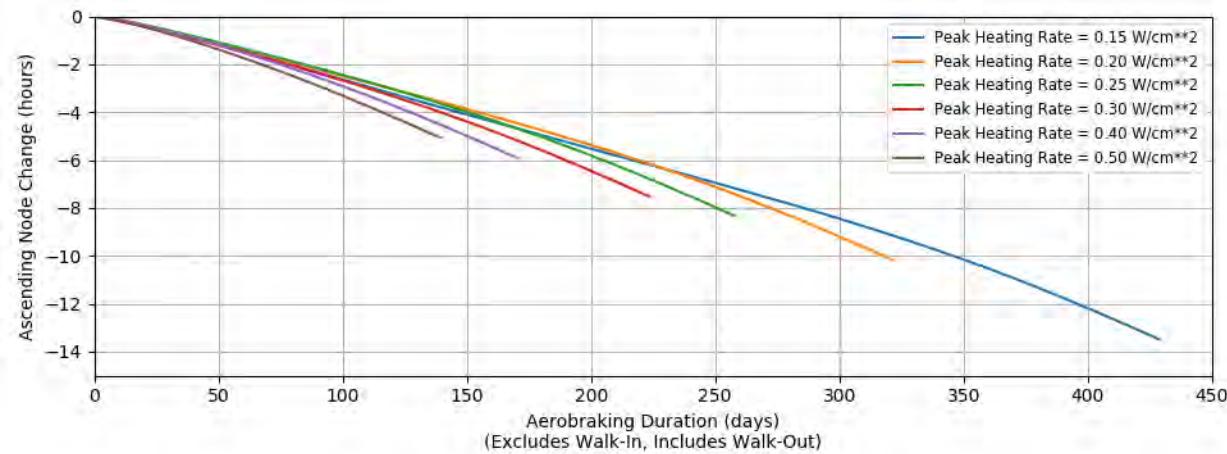


**Figure 82: Ascending Node Drift vs. Aerobraking Duration with 40 kg/m<sup>2</sup> Ballistic Coefficient**

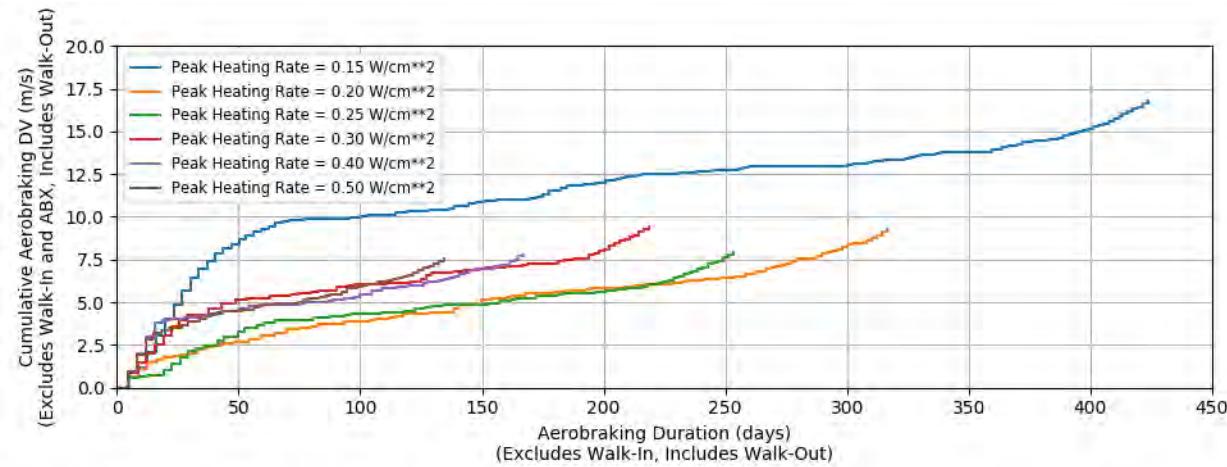


**Figure 83: Aerobraking  $\Delta V$  vs. Aerobraking Duration with 40 kg/m<sup>2</sup> Ballistic Coefficient**

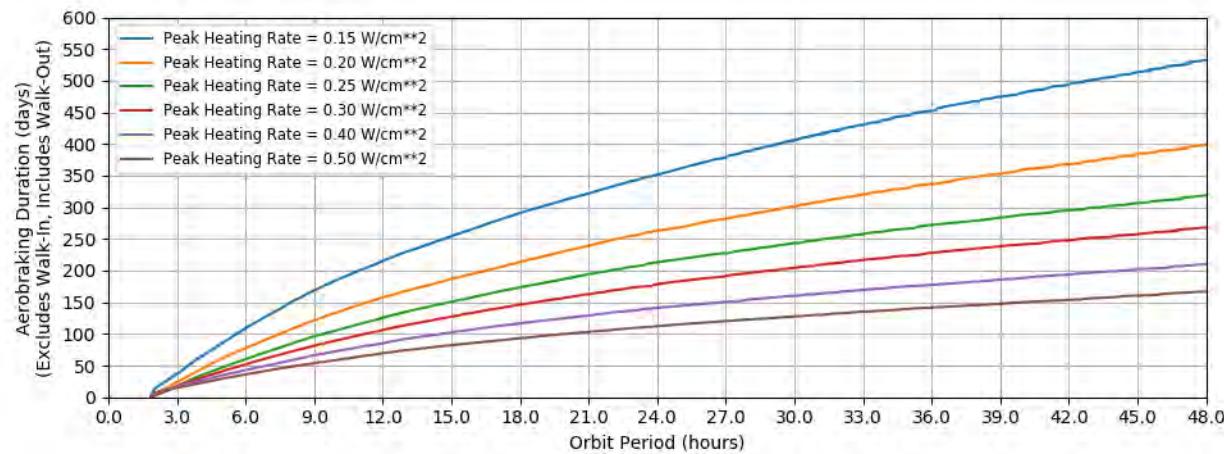


**Figure 84: Aerobraking Duration vs. Orbit Period with 50 kg/m<sup>2</sup> Ballistic Coefficient**

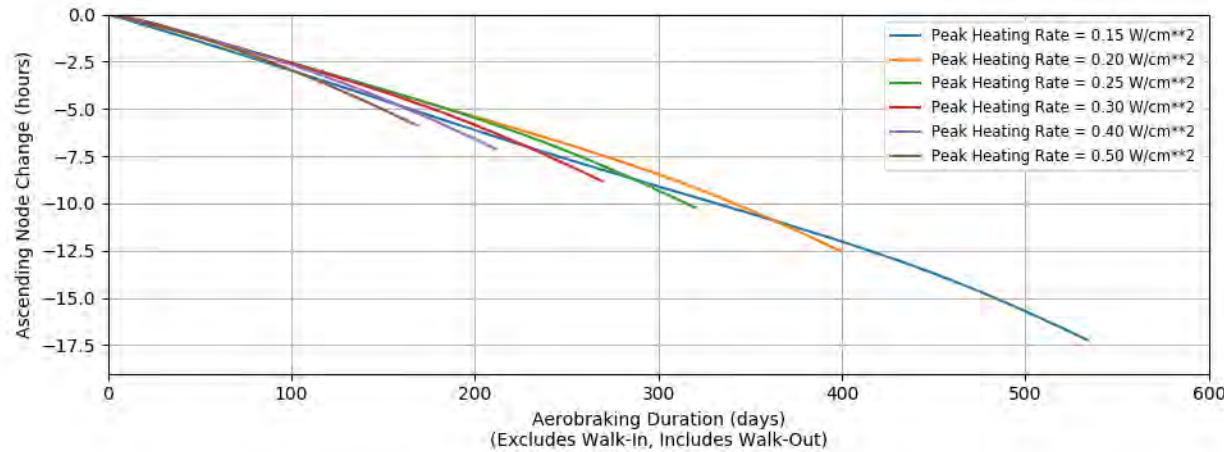


**Figure 85: Ascending Node Drift vs. Aerobraking Duration with 50 kg/m<sup>2</sup> Ballistic Coefficient**

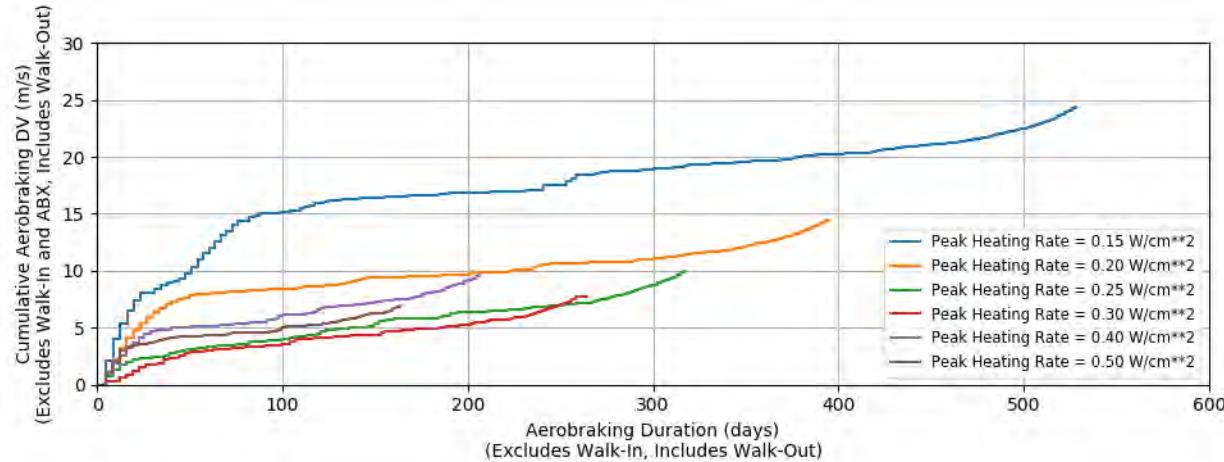


**Figure 86: Aerobraking ΔV vs. Aerobraking Duration with 50 kg/m<sup>2</sup> Ballistic Coefficient**

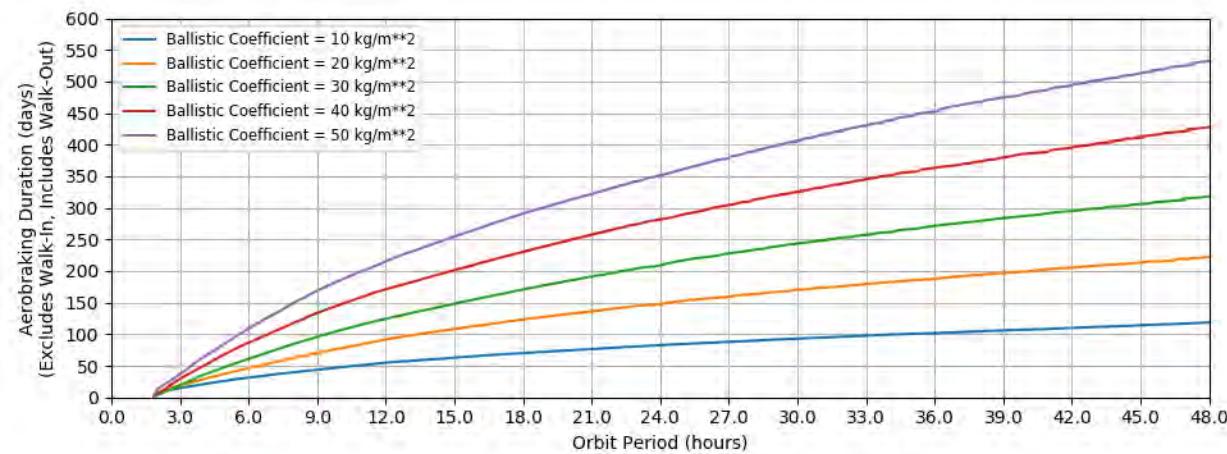


Figure 87: Aerobraking Duration vs. Orbit Period with 0.15 W/cm<sup>2</sup> Peak Heating

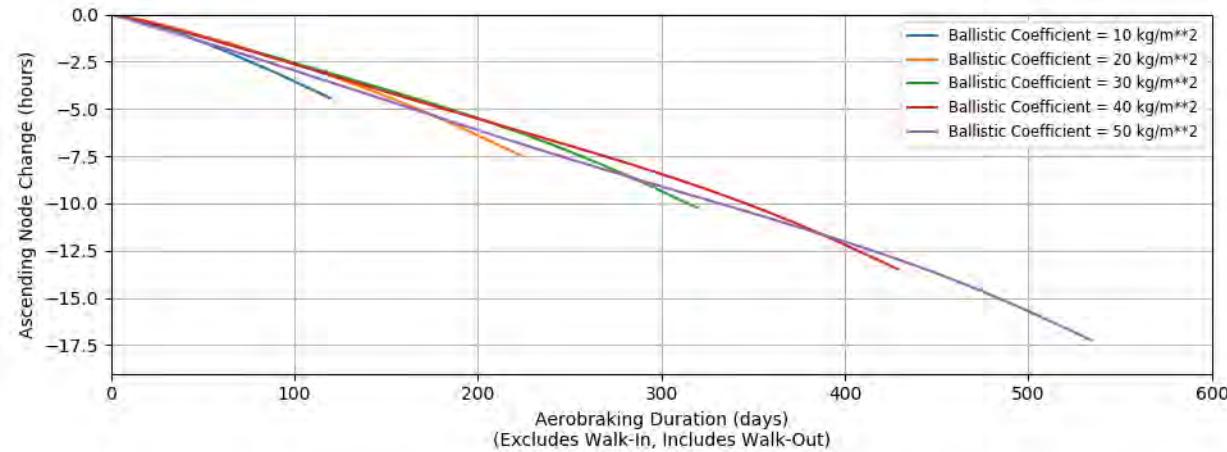


Figure 88: Ascending Node Drift vs. Aerobraking Duration with 0.15 W/cm<sup>2</sup> Peak Heating

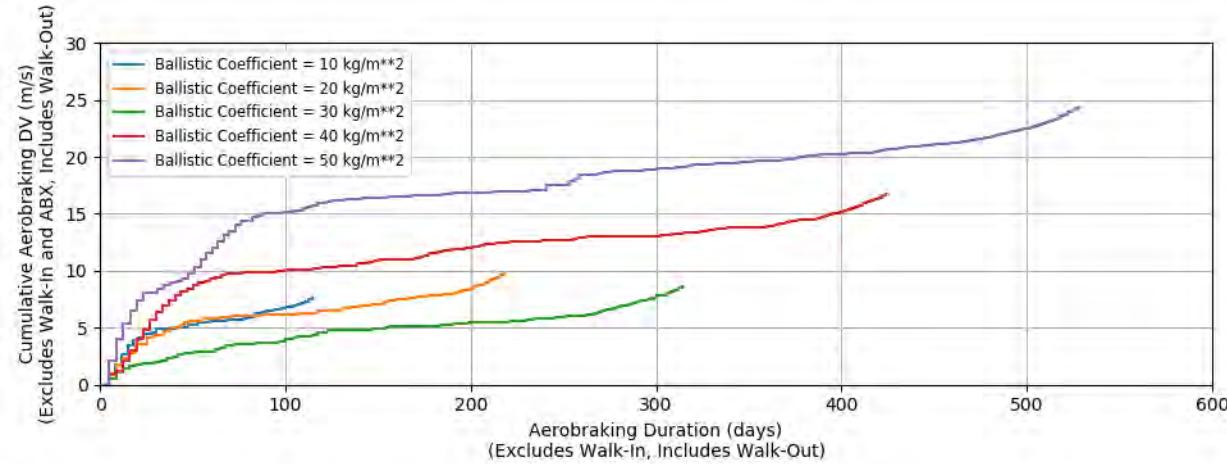


Figure 89: Aerobraking ΔV vs. Aerobraking Duration with 0.15 W/cm<sup>2</sup> Peak Heating

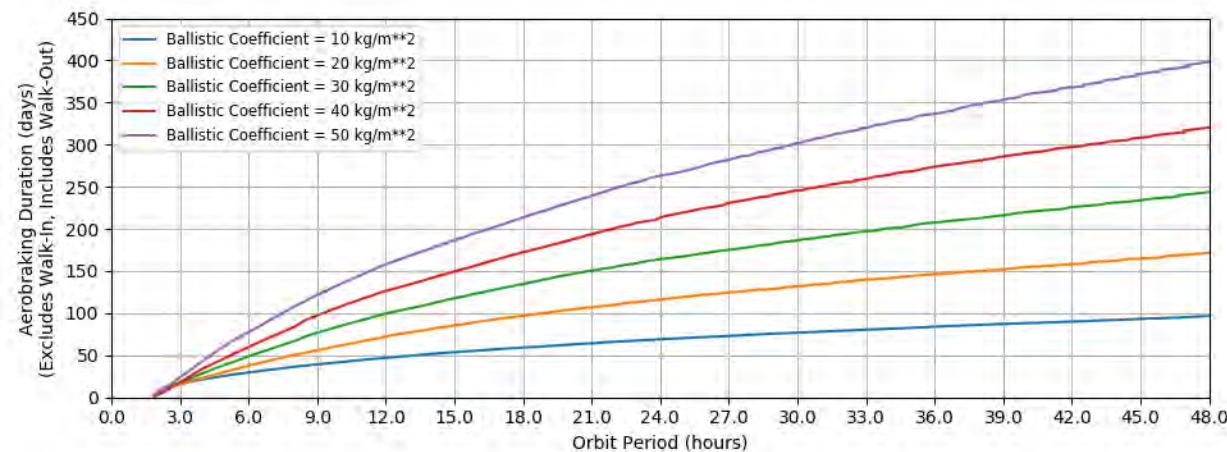


Figure 90: Aerobraking Duration vs. Orbit Period with 0.20 W/cm<sup>2</sup> Peak Heating

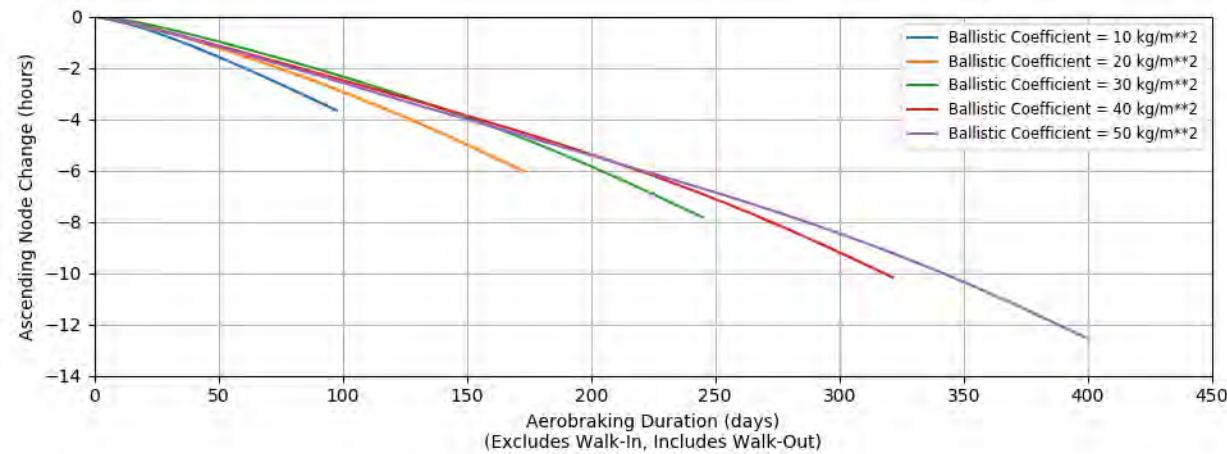


Figure 91: Ascending Node Drift vs. Aerobraking Duration with 0.20 W/cm<sup>2</sup> Peak Heating

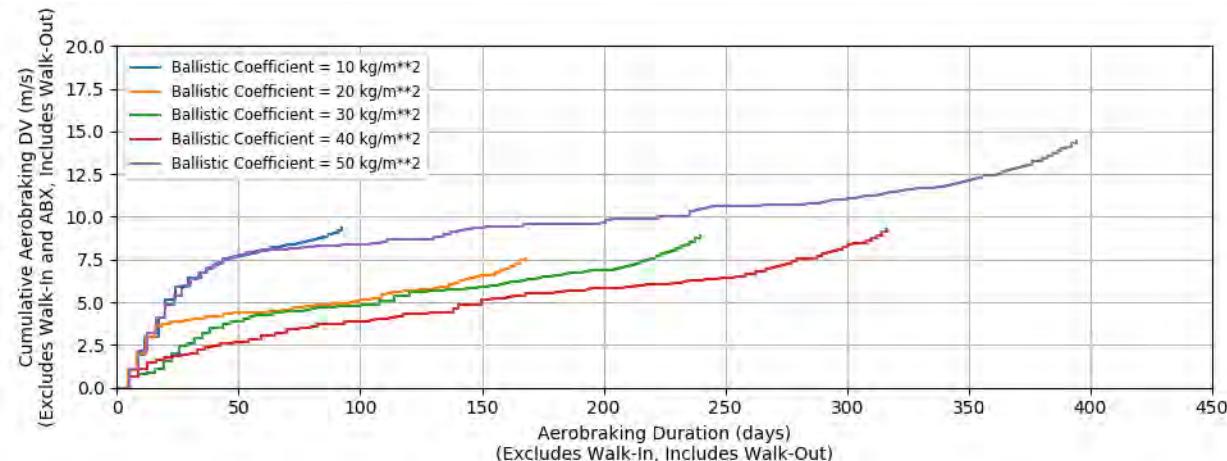


Figure 92: Aerobraking ΔV vs. Aerobraking Duration with 0.20 W/cm<sup>2</sup> Peak Heating

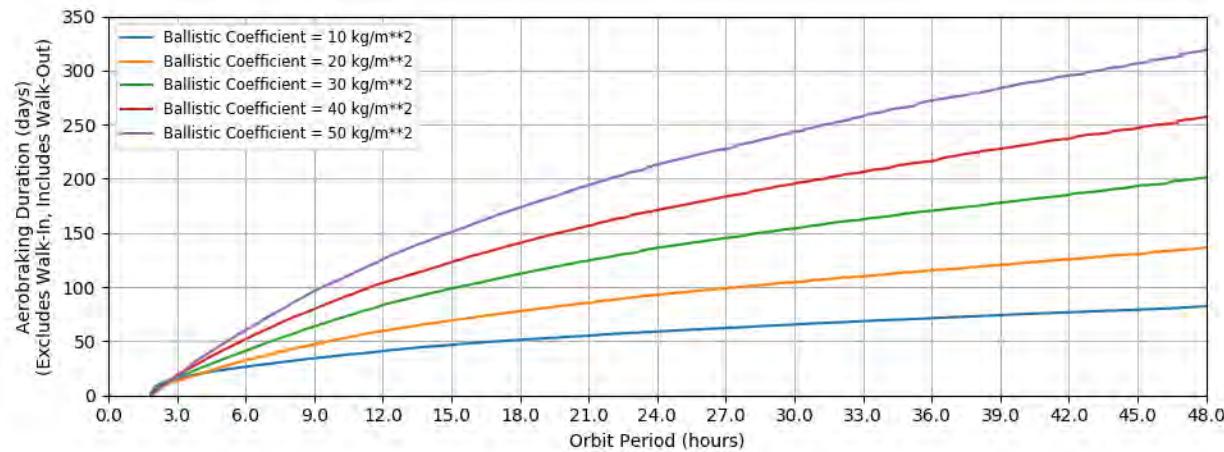


Figure 93: Aerobraking Duration vs. Orbit Period with 0.25 W/cm<sup>2</sup> Peak Heating

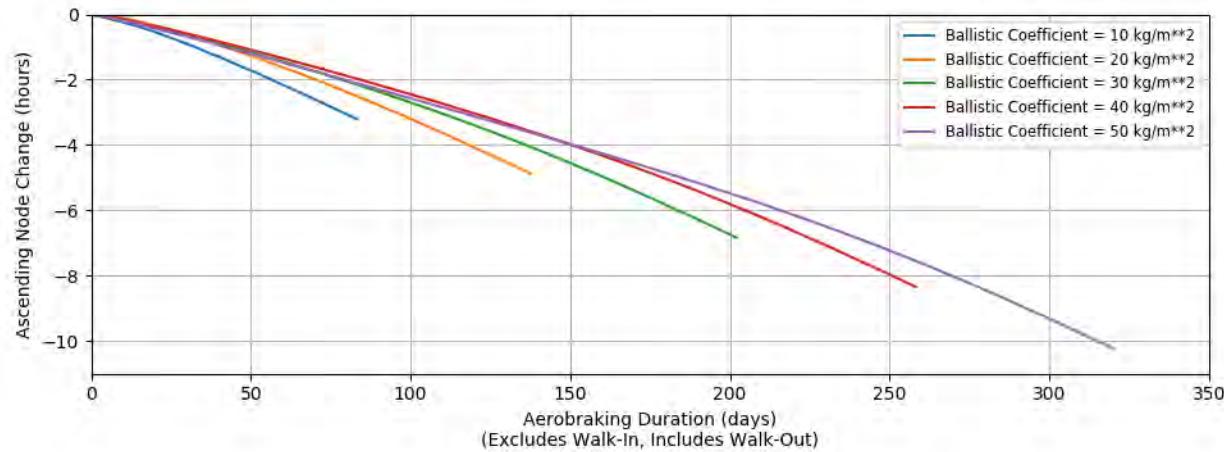


Figure 94: Ascending Node Drift vs. Aerobraking Duration with 0.25 W/cm<sup>2</sup> Peak Heating

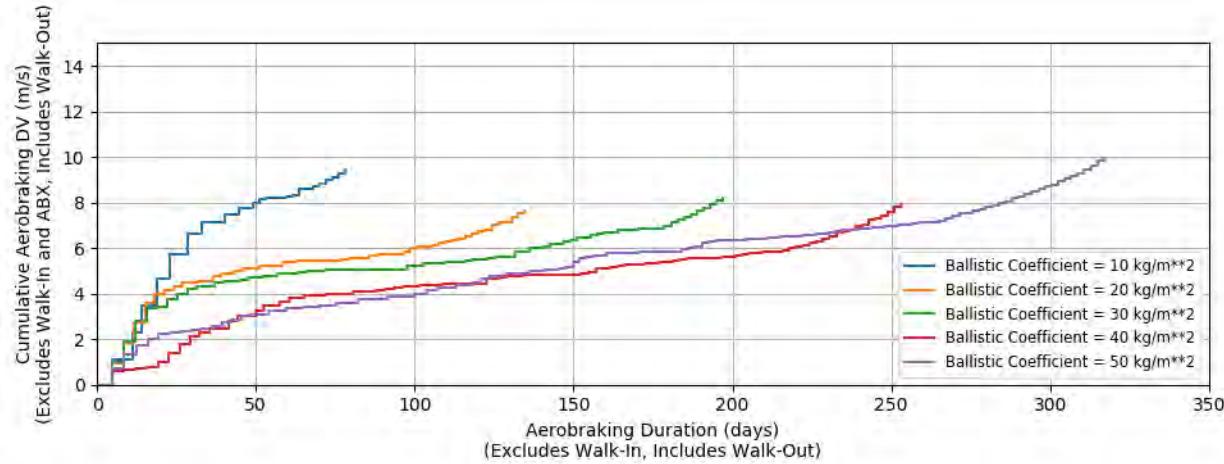
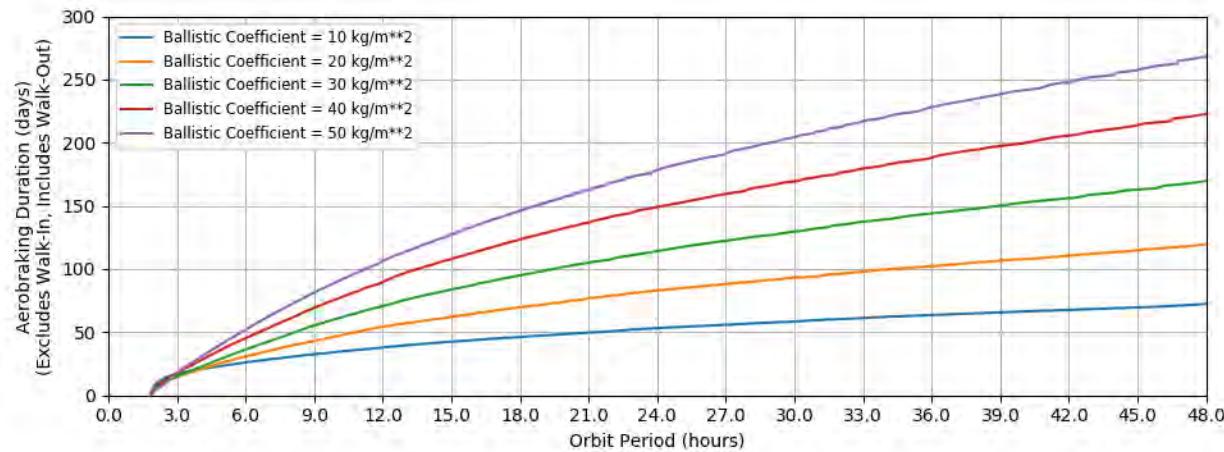
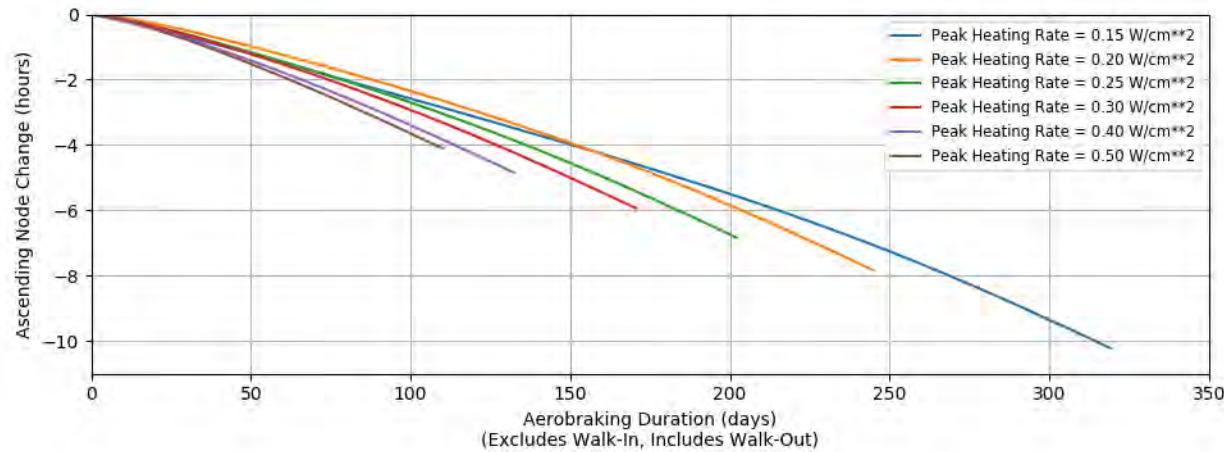


Figure 95: Aerobraking ΔV vs. Aerobraking Duration with 0.25 W/cm<sup>2</sup> Peak Heating



**Figure 96: Aerobraking Duration vs. Orbit Period with 0.30 W/cm<sup>2</sup> Peak Heating**



**Figure 97: Ascending Node Drift vs. Aerobraking Duration with 0.30 W/cm<sup>2</sup> Peak Heating**

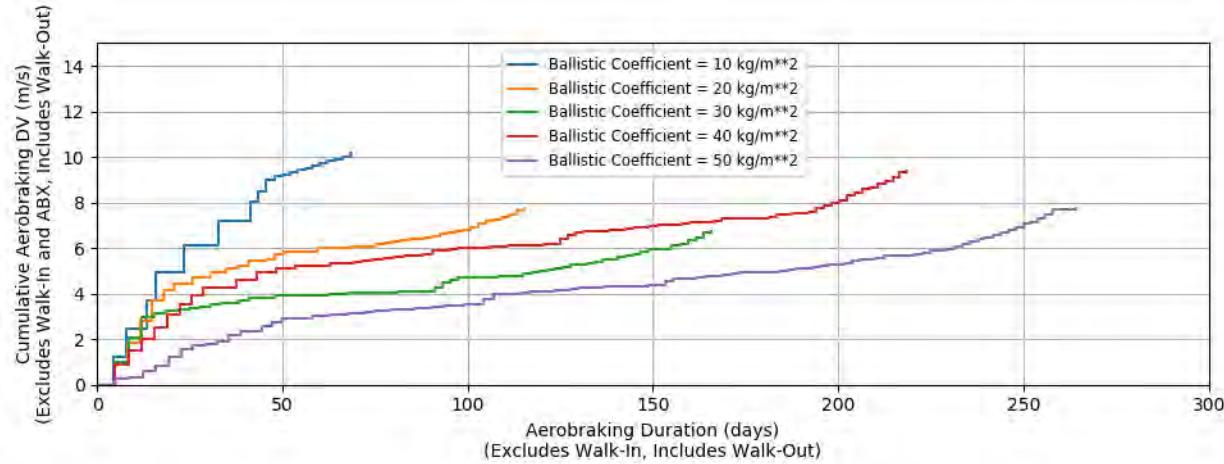


**Figure 98: Aerobraking ΔV vs. Aerobraking Duration with 0.30 W/cm<sup>2</sup> Peak Heating**

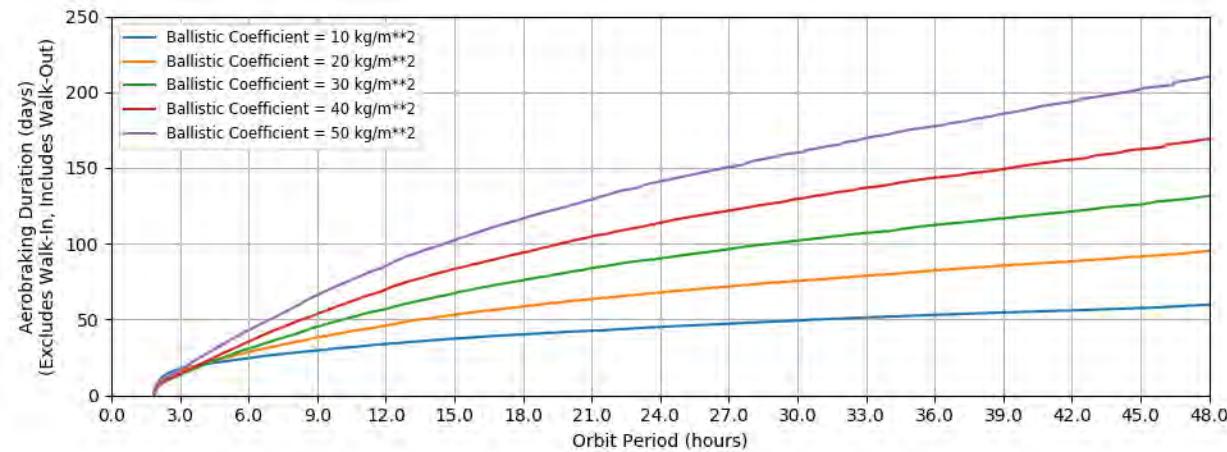


Figure 99: Aerobraking Duration vs. Orbit Period with 0.40 W/cm<sup>2</sup> Peak Heating

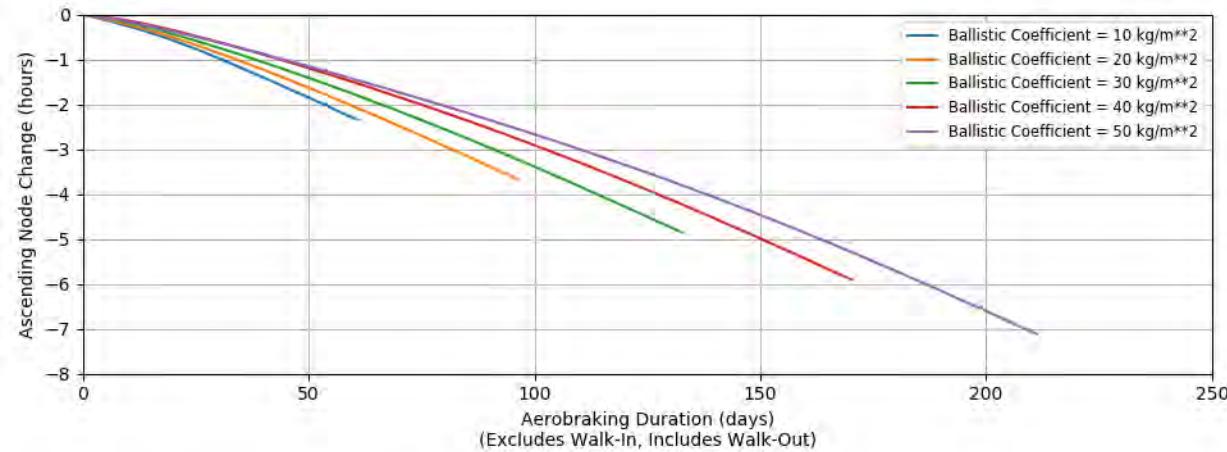


Figure 100: Ascending Node Drift vs. Aerobraking Duration with 0.40 W/cm<sup>2</sup> Peak Heating

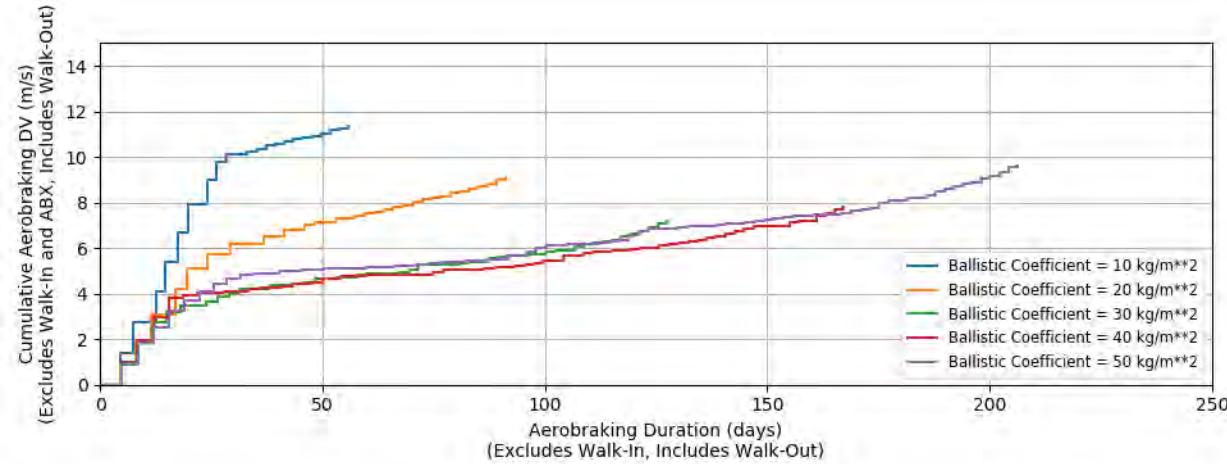


Figure 101: Aerobraking ΔV vs. Aerobraking Duration with 0.40 W/cm<sup>2</sup> Peak Heating

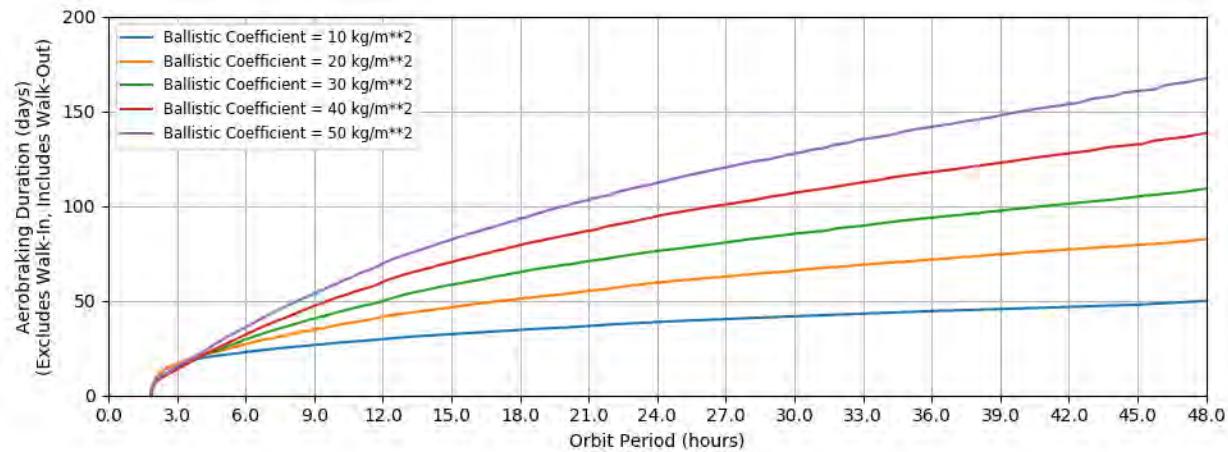


Figure 102: Aerobraking Duration vs. Orbit Period with 0.50 W/cm<sup>2</sup> Peak Heating

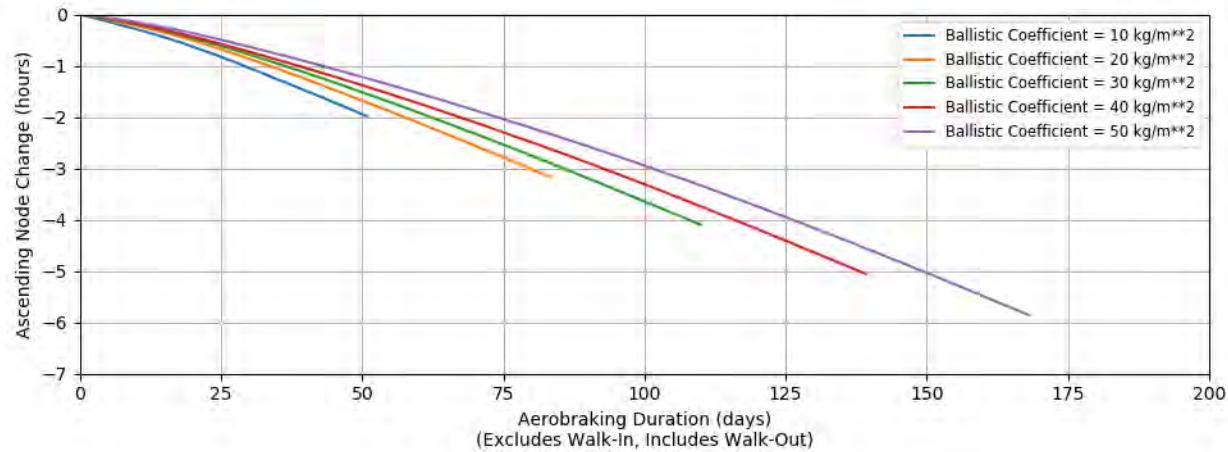


Figure 103: Ascending Node Drift vs. Aerobraking Duration with 0.50 W/cm<sup>2</sup> Peak Heating

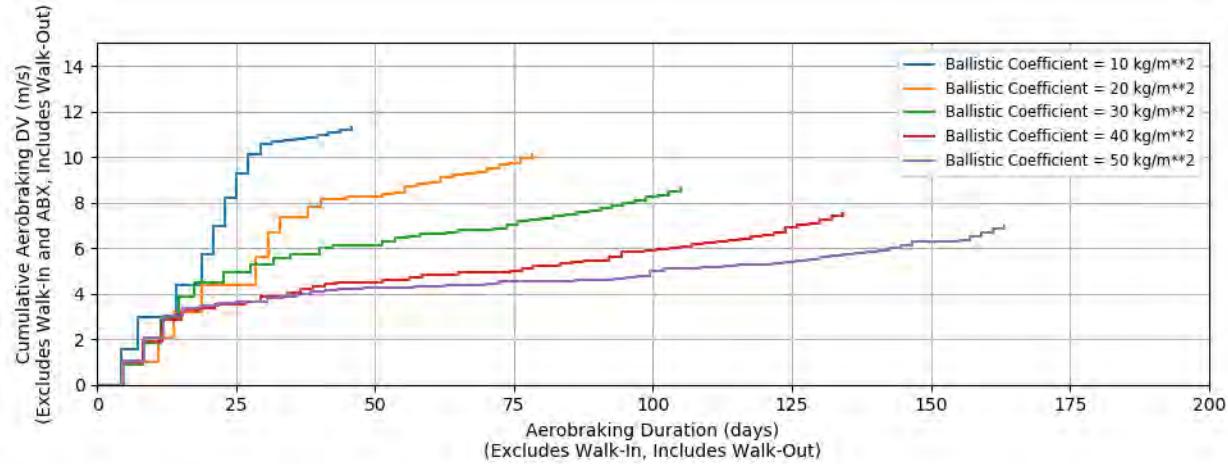


Figure 104: Aerobraking ΔV vs. Aerobraking Duration with 0.50 W/cm<sup>2</sup> Peak Heating

## 9 Roundtrip Mission Design

### 9.1 Overview

There are, broadly, two types of roundtrip missions. The “Conjunction-Class” missions, which feature long stay-times at Mars, require the least energy, as they take advantage of sequential ballistic transfers. However, the long stay times are problematic for a human crew for multiple reasons - consumables mass and radiation exposure being but two. The “Opposition-Class” missions alleviate the timeline by utilizing a Venus flyby on either the outbound or inbound legs but are more energetic. Both are described below.

### 9.2 Conjunction-Class Missions

A “Conjunction-Class” mission, also known as a “long-stay” mission minimizes the  $\Delta V$  necessary by accepting a long stay time at Mars. Just as Earth-to-Mars opportunities repeat every 26 months, so to do Mars-to-Earth opportunities. In general, the departure date for minimum-C3 Type I or II transfer to Earth is about 15 months after the arrival date of a minimum-energy Type I or II transfer to Mars.

For example, the maximum-capture-mass launch period for an Earth to Mars transfer in 2033 is a Type II launching in late April and early May 2033 and arriving in early February 2034. The next minimum-C3 Mars-to-Earth opportunity (a Type I) departs Mars in May 2035, 15 months later. It returns to Earth in late November 2035, for a total flight time of 936 days (30 months), of which 458 days (15 months) is at Mars. This is a traditional Conjunction-Class mission, illustrated in Figure 105.

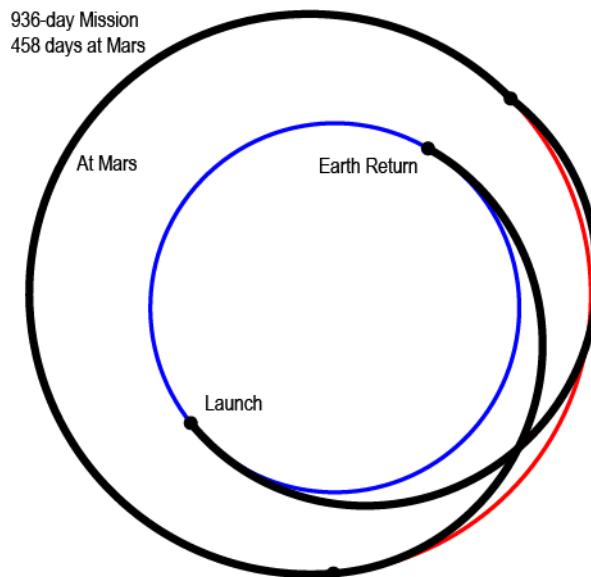
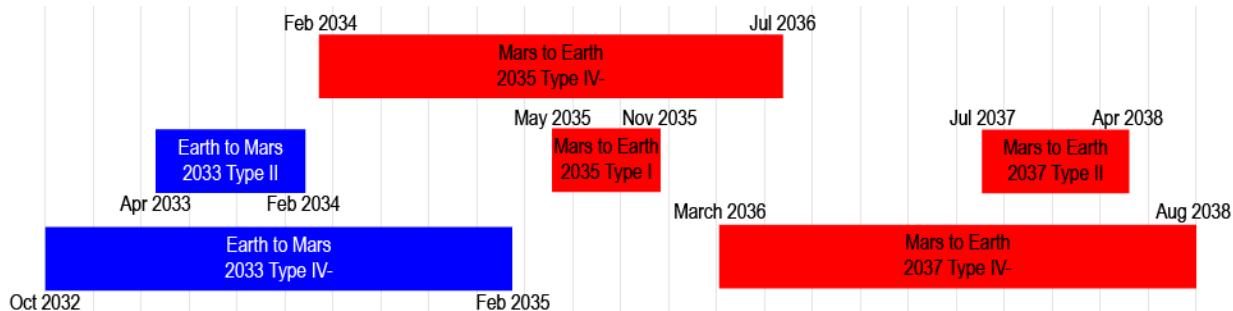


Figure 105: Example Conjunction-Class mission

A less-traditional Conjunction-Class mission would mix-and-match Type III and IV transfers with Type I and II transfers. The Type IIIs and IVs depart Earth about 6 months before the Types I and II, but arrive almost 15 months later. Likewise, Type III and IV transfers from Mars depart 14 months early and arrive 7 months later. A Type I or II return would depart Mars right around the time a Type III or IV outbound arrives, and a Type III or IV return would depart Mars right around the time a Type I or II outbound arrives. The stay times could be very short, but the total

flight time would be 6 or 7 months longer in total. Longer stay times could be had by waiting to the next opportunity. For example, a mission could have a 26-month stay time by using a Type III or IV outbound and a Type I or II return.



**Figure 106: Mixing-and-Matching Type I/II and Type III/IV opportunities allows for a variable stay time, from less than 30 days to multiple years.**

### 9.3 Opposition-Class Missions

In contrast to the Conjunction-Class missions, an “Opposition-Class” mission minimizes the flight time at the expense of increased mission  $\Delta V$ . In extreme cases, this can be done by using the fringes of a ballistic transfer, but it is more commonly achieved by adding a Venus flyby to the itinerary, either on the outbound (Earth to Mars) or inbound (Mars to Earth) leg, as in Figure 107. This requires more  $\Delta V$  on the part of the spacecraft, but less than using non-optimal transfers. If a Venus flyby is added on the inbound leg, the spacecraft must have a larger v-infinity on Mars departure to reduce its heliocentric velocity enough to drop perihelion down to Venus’s orbit. Consider a spacecraft with 0 km/s v-infinity; its perihelion remains at Mars’s – increasing the v-infinity lowers perihelion. If, instead, a Venus flyby is added on the outbound leg, the spacecraft arrives with a larger v-infinity. If the mission is performing a direct entry or an aerocapture, the mass penalty may not be as large, as the energy can be bled off by the atmosphere.

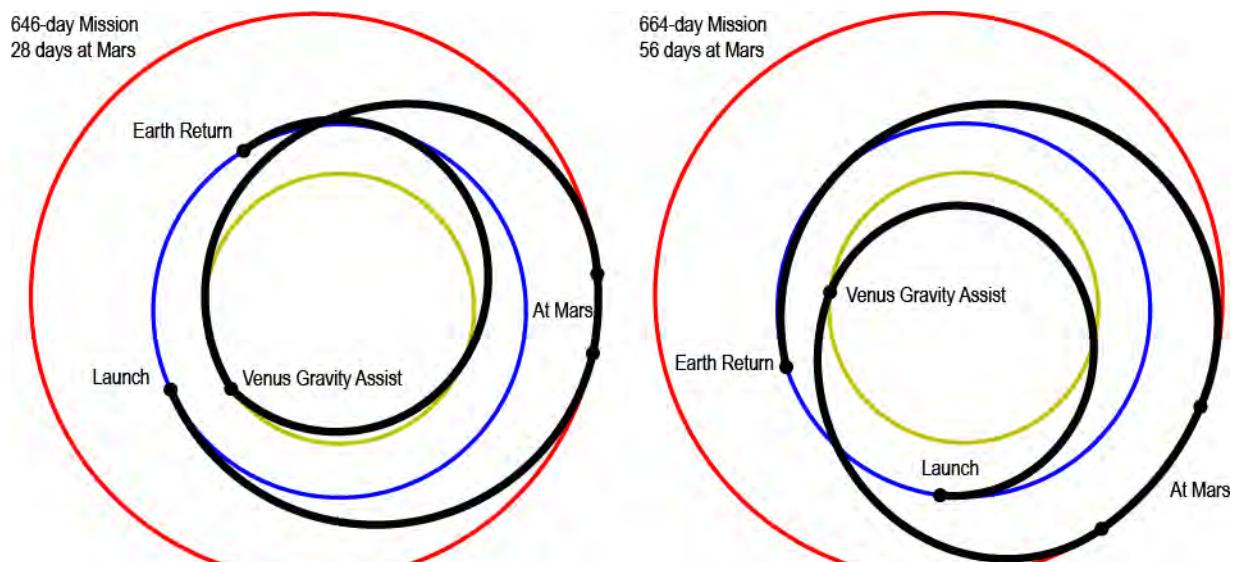


**Figure 107: Example Venus-enabled Opposition-Class missions with inbound (left) and outbound (right) Venus Gravity Assists**

The Earth/Venus synodic period is 19 months (583 days), and the Venus/Mars synodic period

is a mere 11 months (334 days). However, Mars must be in the right place relative to Venus when the flyby occurs for an Earth-Venus-Mars transfer to take place, and likewise, Earth must be in the right place with respect to Venus for a Mars-Venus-Earth transfer to take place. The v-infinity inbound to Venus (from the Earth-Venus leg) must have the same magnitude as the v-infinity outbound from Venus (from the Venus-Mars leg), and the directions of those v-infinity vectors must not be so different that the hyperbola connecting them must go sub-surface. Both constraints must be met for a ballistic transfer<sup>1</sup> to take place, and so not every Mars-Venus or Earth-Venus opportunity can be used to build an Opposition-Class mission. Many can, but not all of them. See Section 12.4 for details.

---

<sup>1</sup> Mismatches in either can be compensated for with a high-thrust burn at periapsis or using SEP on either or both heliocentric legs, but consideration of these are beyond the scope of this work

## 10 Earth to Mars Ballistic Transfer Data: 2022-2040

### 10.1 Overview

Not all Earth-to-Mars ballistic opportunities are created equal. That Mars is in a noticeably elliptical orbit means that more or less energy is required to reach Mars and the spacecraft arrives with more or less energy depending on where Mars is in its orbit. The inclination of Mars with respect to the Earth orbital plane, combined with the obliquity of both Mars and Earth mean that the spacecraft departs from Earth and arrives at Mars from variable directions. These energies and geometries thus vary from one opportunity to the next. Some opportunities require more (or less) energy, have higher (or lower) declinations, etc. The broad character of these opportunities repeats approximately every 15 years (or 7 opportunities) when Earth and Mars are in alignment at nearly the same locations in their orbits. For example, the 2022 and 2037 opportunities are very similar to each other; missions would depart Earth in September of that year and arrive in October of the following year at Ls 130. There is a longer-term periodicity of opportunities every 32 years. The 2037 and 2005 opportunities are even more like each other than either are to 2022, for example, but all three are very similar. The longest-term, and most-similar periodicity is every 56 years.

This chapter contains porkchop plots for the 10 Earth-to-Mars ballistic opportunities in the 2022-2040 timeframe, as well as summary information about the opportunities themselves and “optimal” lander and orbiter launch periods.

### 10.2 Summary of Opportunities

There are many ways of comparing one ballistic opportunity to another. Within each opportunity and type (e.g. 2022 Type II, 2030 Type IV-), there is a single launch/arrival date pair that minimizes the launch energy (C3) and another pair that minimizes the hyperbolic approach velocity (VHP). There may be large gradients about these minima, however, so it is useful to consider the effect of a 20-day launch period on these minima. How C3, the launch declination (DLA) and VHP interact is also important. To that end, “optimal” launch periods have been generated for each opportunity and type. The launch period that maximizes the launch mass is the “Lander” launch period, and the launch period that maximizes the mass captured into orbit is the “Orbiter” launch period. The methods are described in Section 1.4.

Figures 108 through 110 illustrate the C3 and VHP for two trajectory types (I and II, III- and IV-, III+ and IV+, respectively) for each Earth-to-Mars opportunity when the C3 is minimized. Figures 111 through 113 do the same for minimized VHP. All of these plots have the C3 axis capped at  $35 \text{ km}^2/\text{s}^2$  and the VHP axis capped at 7 km/s. The Type III+ and IV+ trajectories frequently exceed one or both of these limits, but they are held constant at those levels to aid in comparison. The Type IV+ trajectories, in particular, are extremely high-energy opportunities. For this reason, they are excluded from the Pareto front plots in Figures 114 through 116. The Pareto front is the set of C3/VHP pairs where one cannot reduce the C3 without increasing VHP and vice versa. The globally minimum C3 is the left most-point on these curves, while the globally minimum VHP is the bottom-most point. A short curve indicates that the C3 and VHP minima are well aligned. That is, the minimizing launch/arrival date pairs are near each other in the porkchop.

Figures 117 through 119 illustrate the launch mass and captured mass for two trajectory types

(I and II, III- and IV-, III+ and IV+, respectively) for each Earth-to-Mars opportunity when the 20-day launch period is optimized to maximize the launch mass, assuming a fixed arrival date. Figures 120 through 122 do the same for maximized capture mass. All of these plots include the longitude of the sun at the optimized arrival date as well. 20-day launch periods could not be found for any of the Type IV+ opportunities.

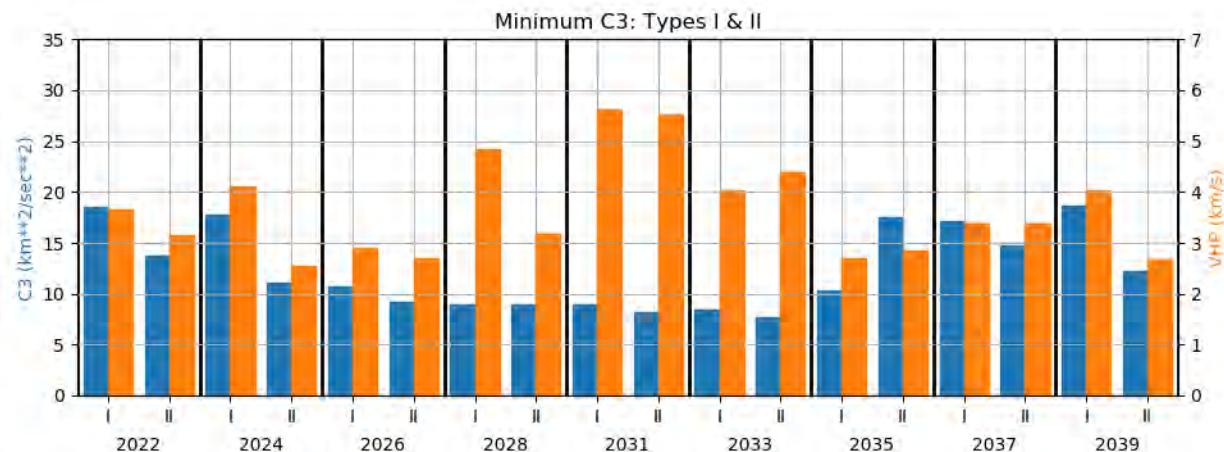


Figure 108: Minimum C3 and Associated VHP for Earth-to-Mars Type I and II Trajectories, 2022-2039

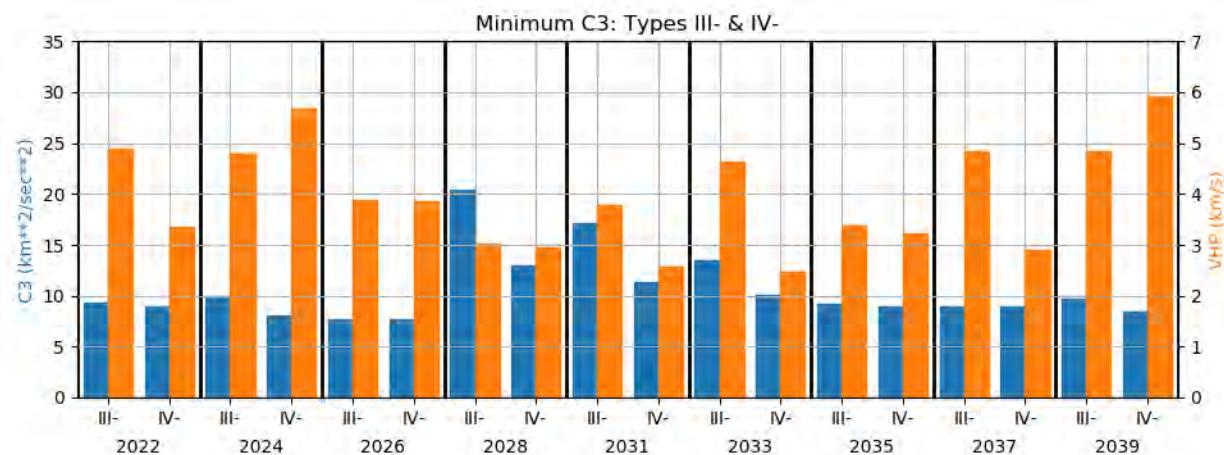


Figure 109: Minimum C3 and Associated VHP for Earth-to-Mars Type III- and IV- Trajectories, 2022-2039

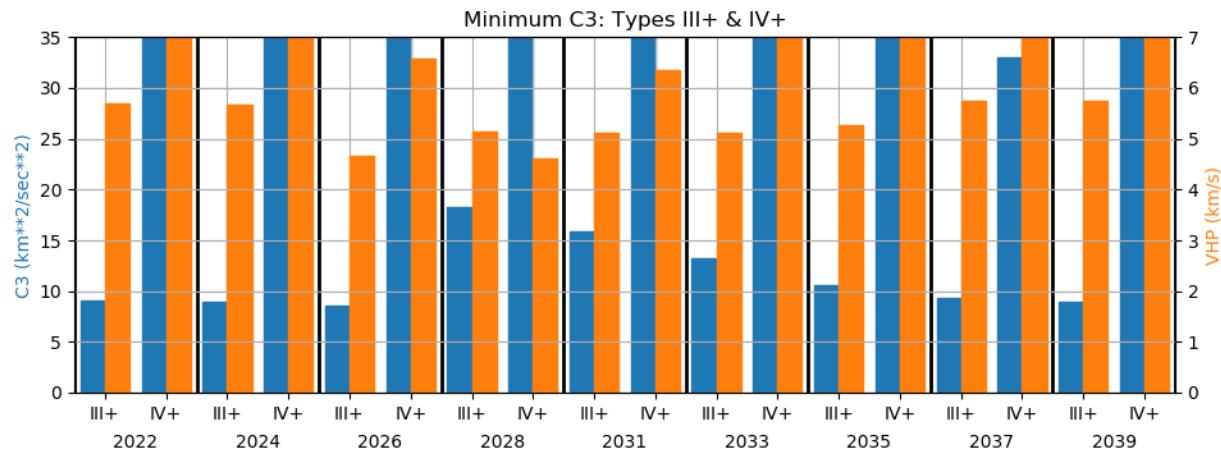


Figure 110: Minimum C3 and Associated VHP for Earth-to- Mars Type III+ and IV+ Trajectories, 2022-2039

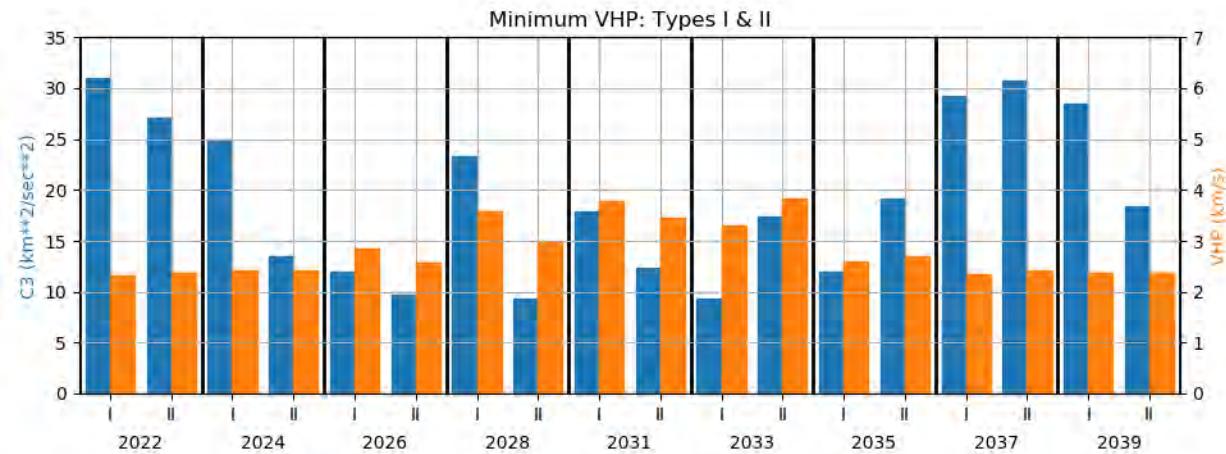


Figure 111: Minimum VHP and Associated C3 for Earth-to- Mars Type I and II Trajectories, 2022-2039

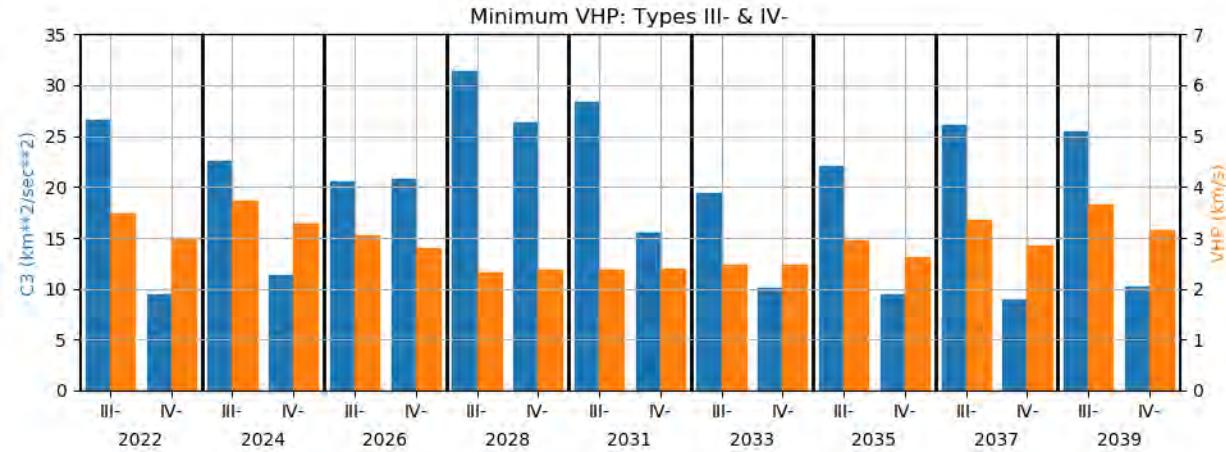


Figure 112: Minimum VHP and Associated C3 for Earth-to- Mars Type III- and IV- Trajectories, 2022-2039

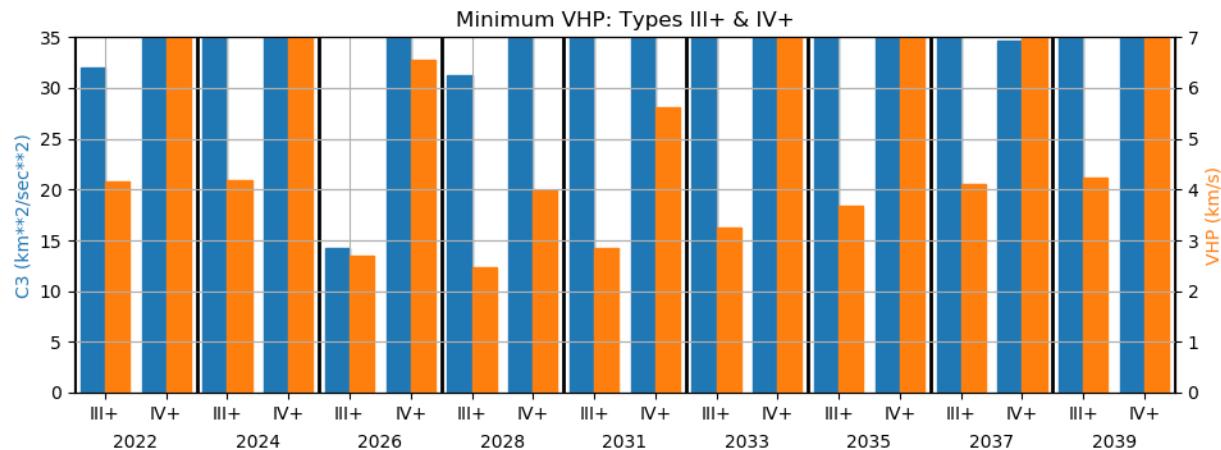


Figure 113: Minimum VHP and Associated  $C_3$  for Earth-to-Mars Type III+ and IV+ Trajectories, 2022-2039

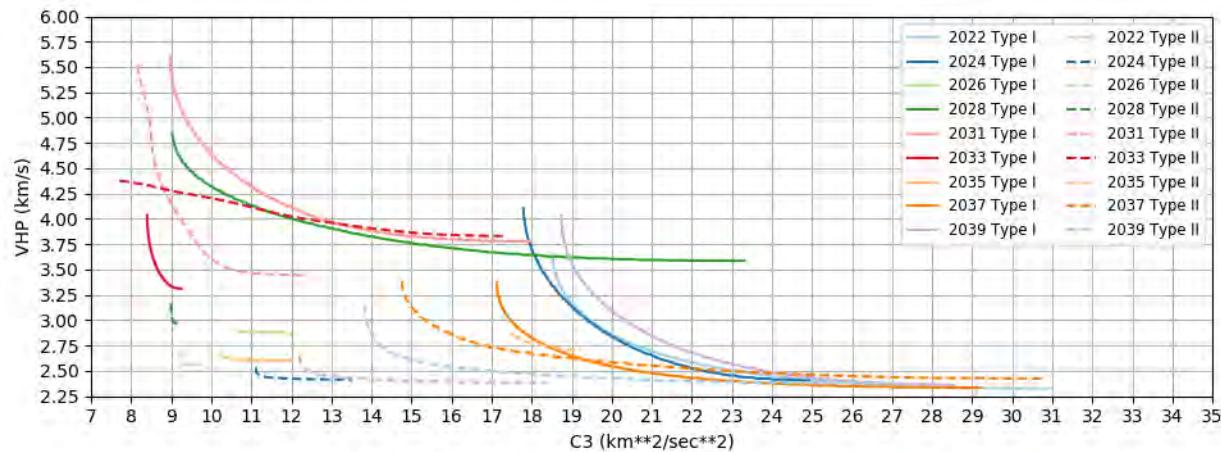


Figure 114:  $C_3$ /VHP Pareto Fronts for Earth to Mars Type I and II Trajectories

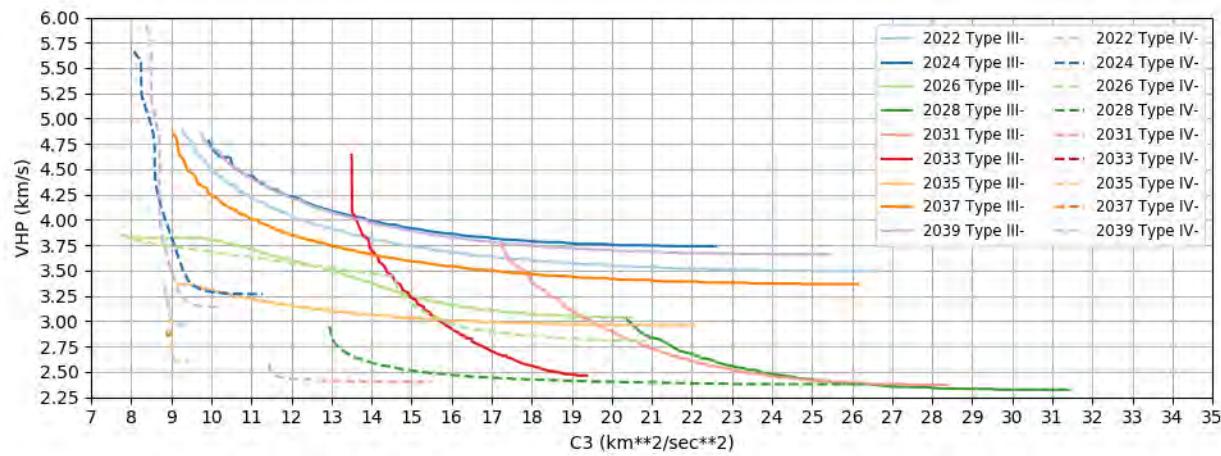


Figure 115:  $C_3$ /VHP Pareto Fronts for Earth to Mars Type III- and IV- Trajectories

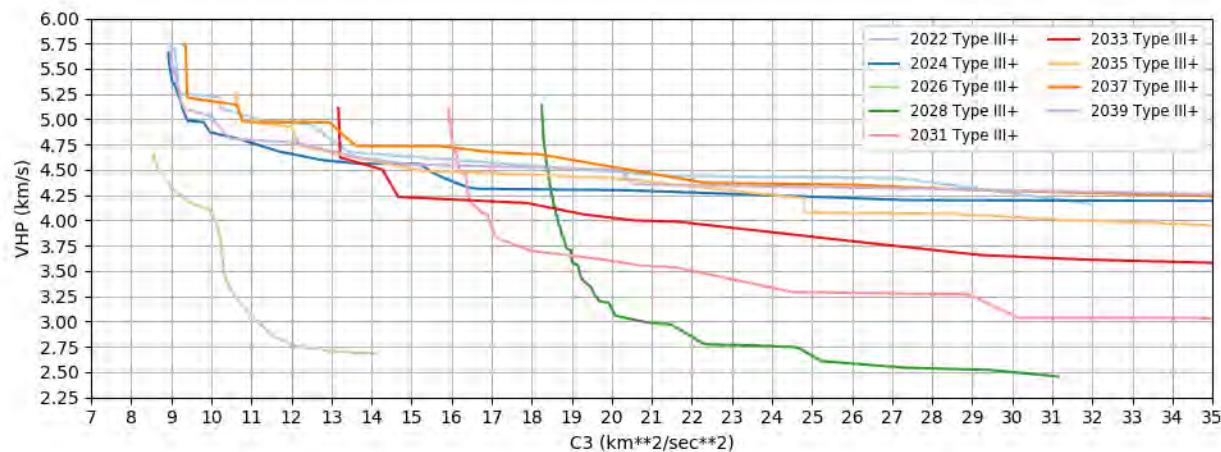


Figure 116: C3/VHP Pareto Fronts for Earth to Mars Type III+ Trajectories

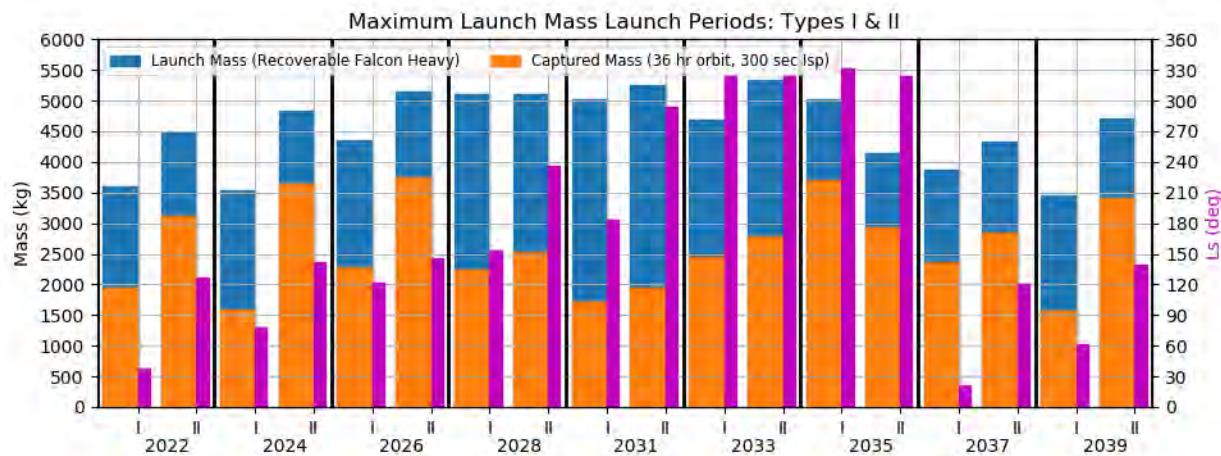


Figure 117: Maximum Launch Mass with Associated Capture Mass and Arrival Ls for Earth-to-Mars Type I and II “Lander” Launch Periods, 2022-2039

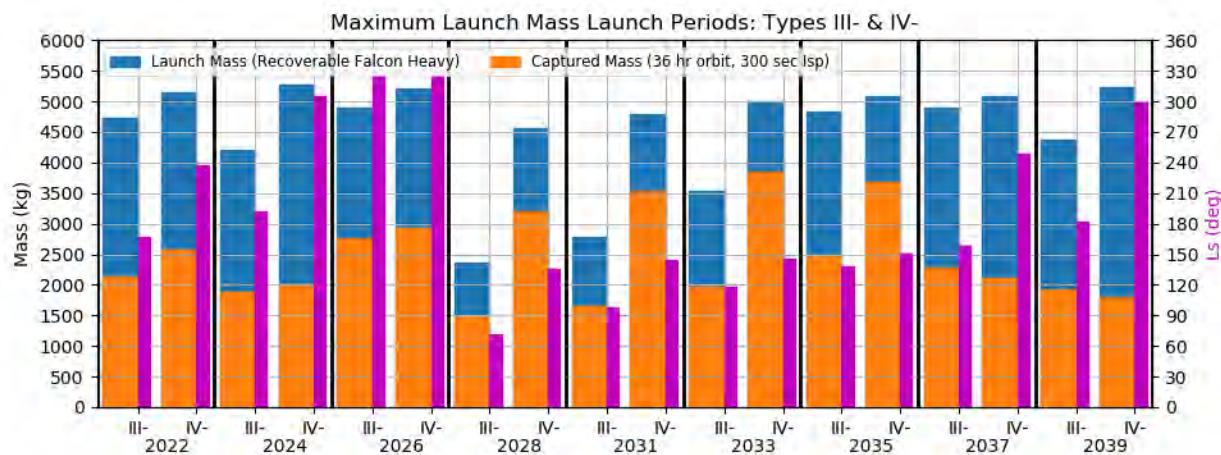
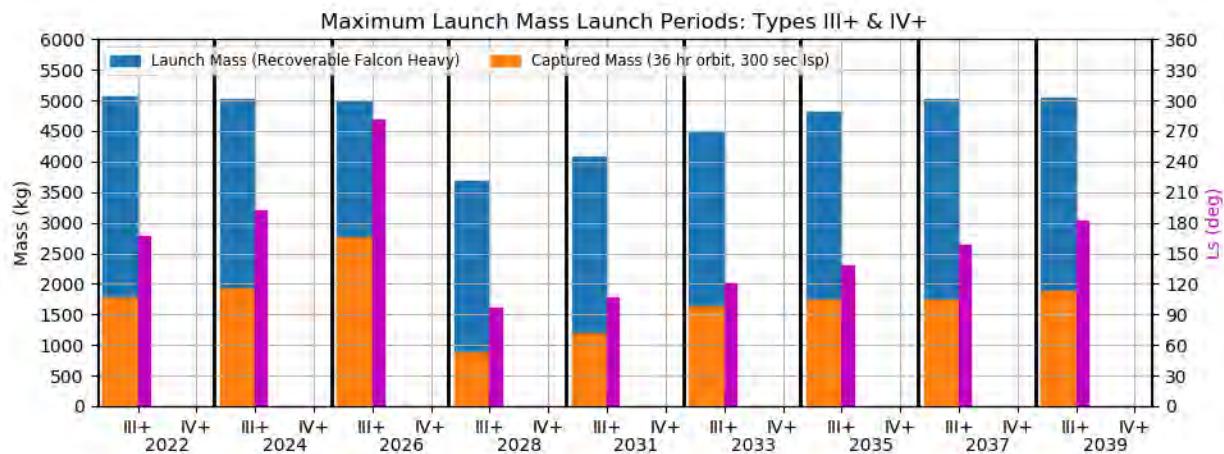
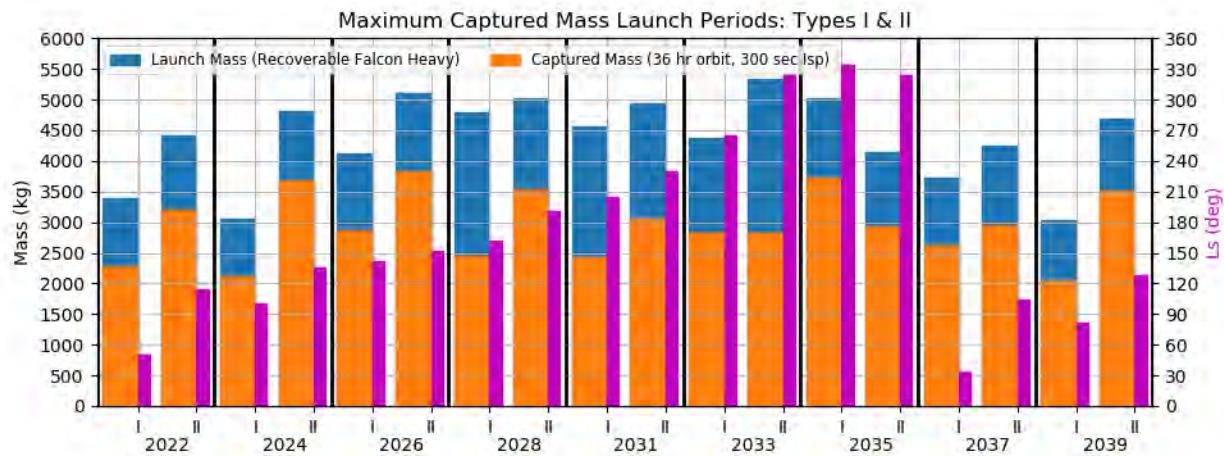


Figure 118: Maximum Launch Mass with Associated Capture Mass and Arrival Ls for Earth-to-Mars Type III- and IV- “Lander” Launch Periods, 2022-2039



**Figure 119: Maximum Launch Mass with Associated Capture Mass and Arrival Ls for Earth-to-Mars Type III+ and IV+ "Lander" Launch Periods, 2022-2039**



**Figure 120: Maximum Captured Mass with Associated Launch Mass and Arrival Ls for Earth-to-Mars Type I and II "Orbiter" Launch Periods, 2022-2039**

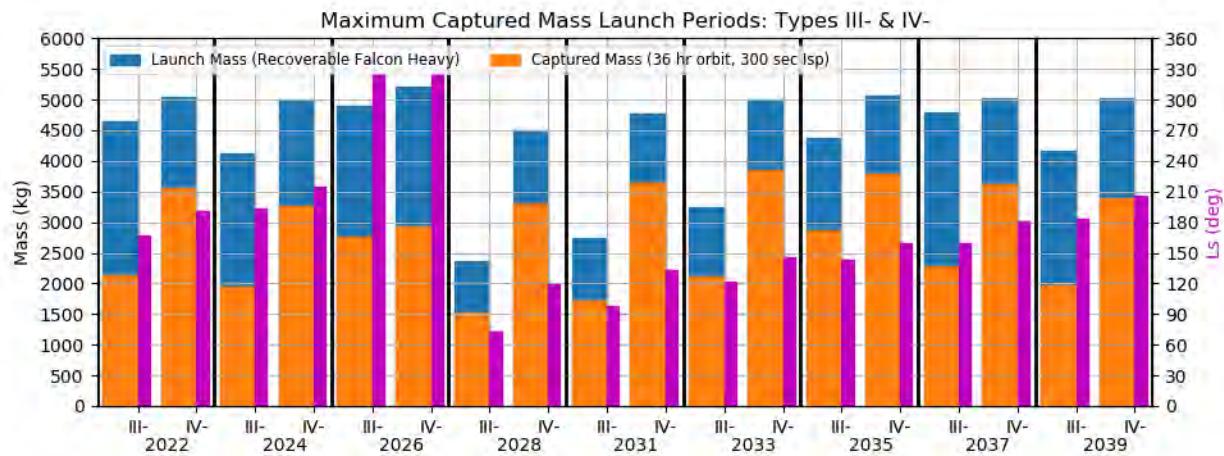


**Figure 121: Maximum Captured Mass with Associated Launch Mass and Arrival Ls for Earth-to-Mars Type III- and IV- "Orbiter" Launch Periods, 2022-2039**

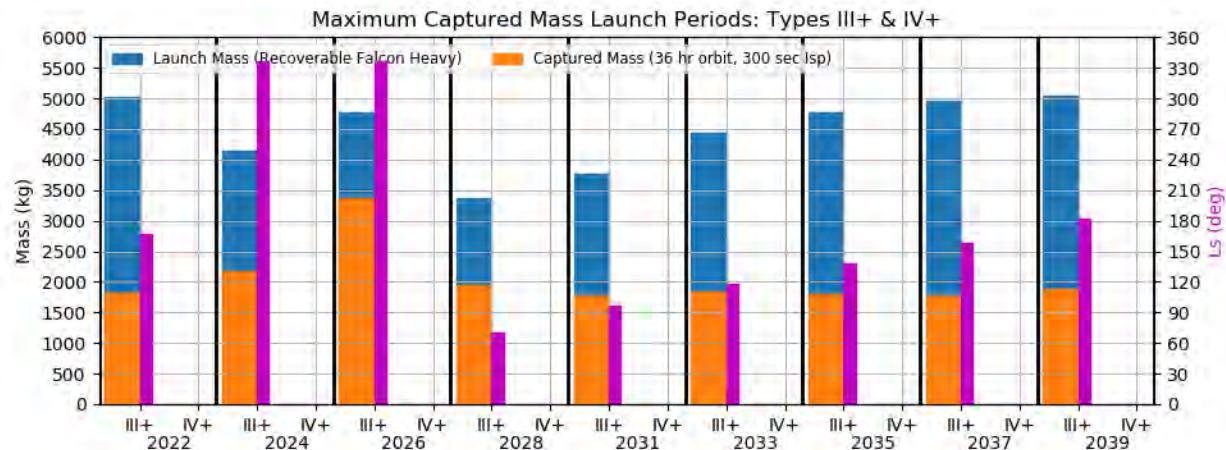


Figure 122: Maximum Captured Mass with Associated Launch Mass and Arrival Ls for Earth-to-Mars Type III+ and IV+ “Orbiter” Launch Periods, 2022-2039

### 10.3 Lander Launch Periods

Besides optimal mass, there are other potential objectives in designing a launch period for a lander. One is to examine the furthest north or south the lander can reach. For example, the Phoenix lander went to high northern latitudes in 2008 while the Mars Polar Lander targeted high southern latitudes in 1999 because those were the accessible poles during their respective opportunities. Another is to consider EDL communication constraints, such as the local mean solar time or Earth elevation at landing for orbiter relay or direct-to-Earth links, respectively. The season (Ls) of landing may also drive the design, such as solar power on the surface or atmospheric density during EDL.

With this in mind, Figures 123 through 257 plot the maximum north and south latitudes, the LMST of landing at the equator and 30 deg latitude, and the elevation of the Earth at landing at those locations plus the latitude extrema for both prograde and retrograde entries as a function of the offset in the mass-optimal arrival date. Each point on these curves is a separate 20-day launch period with the launch date re-optimized for the maximum launch mass. This optimization includes the declination penalties, which are recast back into the C3 as a declination-penalized “equivalent C3.” The arrival dates are shifted earlier and later from the optimal until the equivalent C3 increased above  $60 \text{ km}^2/\text{s}^2$  or the VHP exceeded 7 km/s. As a result, the spread of viable arrival dates varies significantly from opportunity to opportunity. In the LMST and Earth Elevation plots (e.g. Figures 124 and 125), the pair of lines of each color-and-style indicate the minimum and maximum value across the launch period.

The local solar time of landing and the maximum reachable latitude of a lander are dependent on the entry flight path angle and the descent central angle. These plots assume an entry flight path angle of -14.5 deg and a descent central angle of 12.6 deg. These values are consistent with the values of the previous edition of the Mars Handbook and result in landing co-latitudes approximately in the middle of the span illustrated in Figure 47.

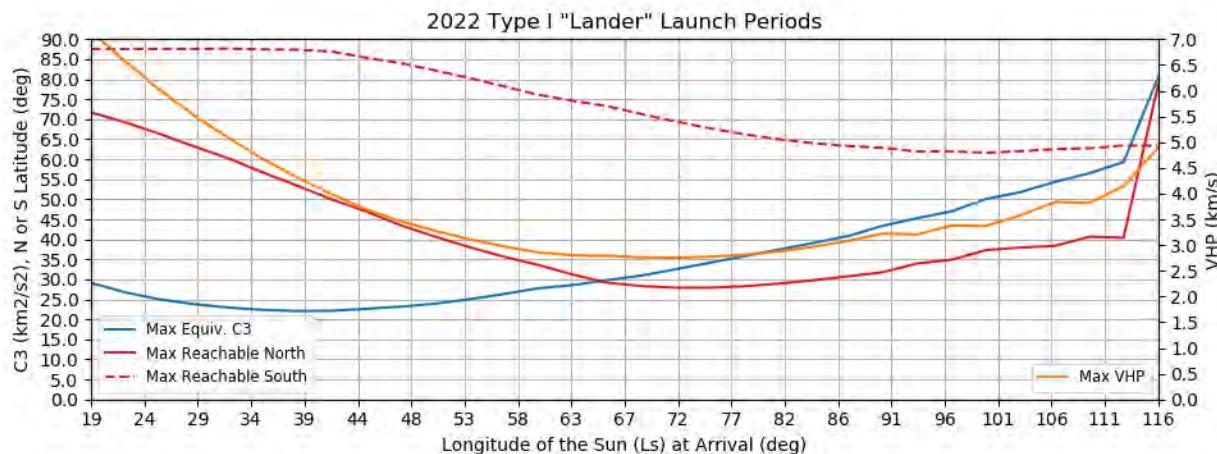


**Figure 123: Earth to Mars 2022 Type I Lander Launch Periods - Reachable Latitudes, Equivalent C3, and VHP**

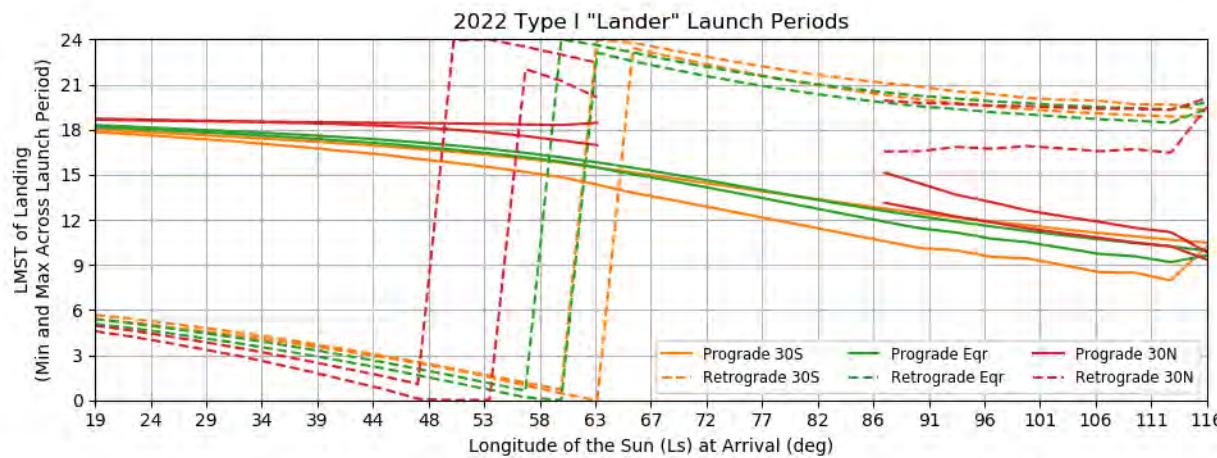


**Figure 124: Earth to Mars 2022 Type I Lander Launch Periods - LMST of Landing at Various Latitudes**

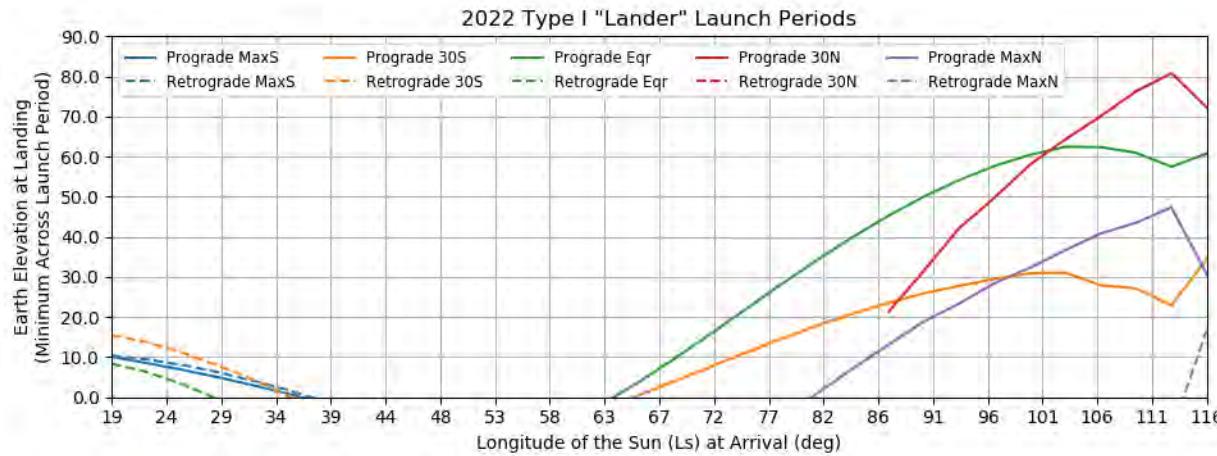


**Figure 125: Earth to Mars 2022 Type I Lander Launch Periods - Earth Elevation at Landing at Various Latitudes**

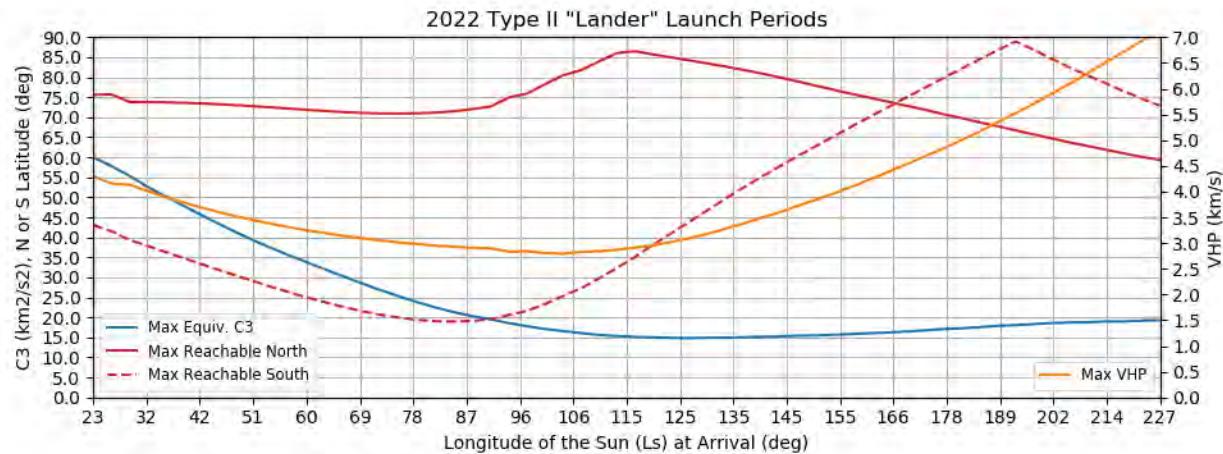


Figure 126: Earth to Mars 2022 Type II Lander Launch Periods - Reachable Latitudes, Equivalent C3, and VHP

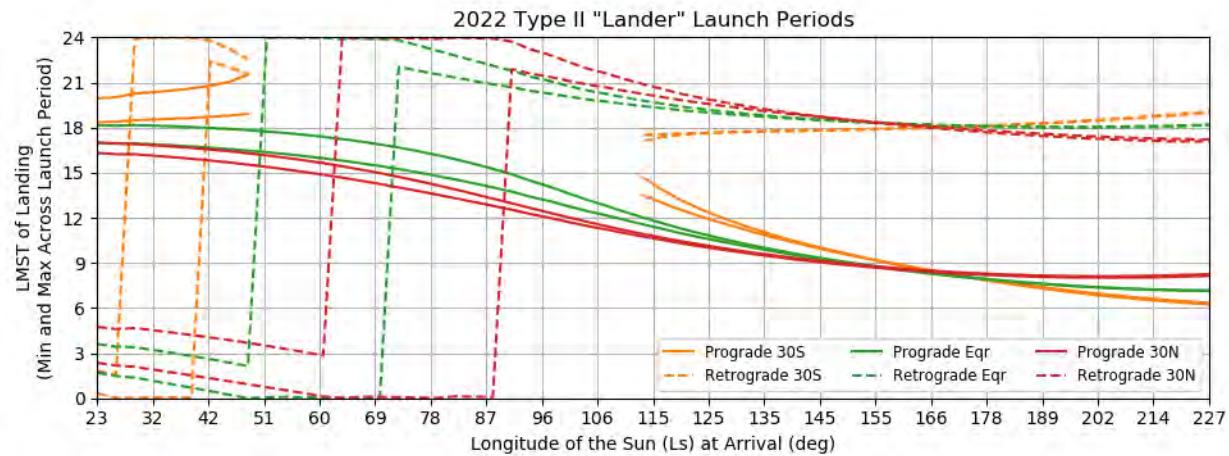


Figure 127: Earth to Mars 2022 Type II Lander Launch Periods - LMST of Landing at Various Latitudes

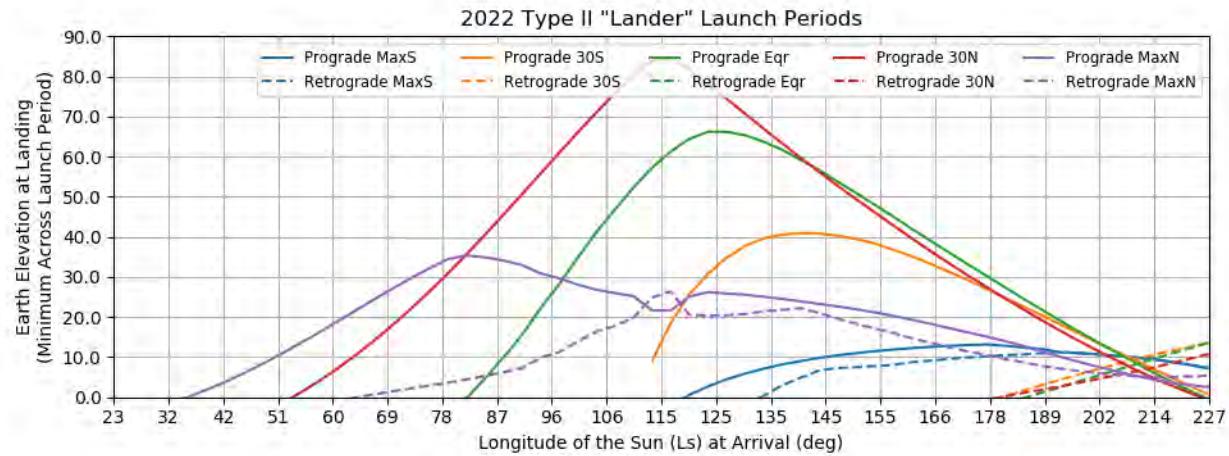


Figure 128: Earth to Mars 2022 Type II Lander Launch Periods - Earth Elevation at Landing at Various Latitudes

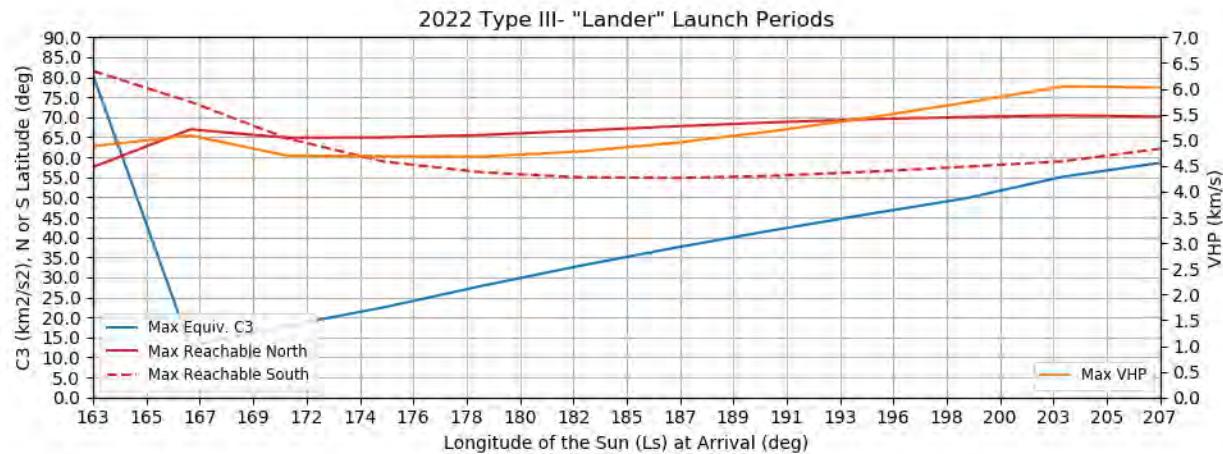


Figure 129: Earth to Mars 2022 Type III- Lander Launch Periods - Reachable Latitudes, Equivalent C3, and VHP

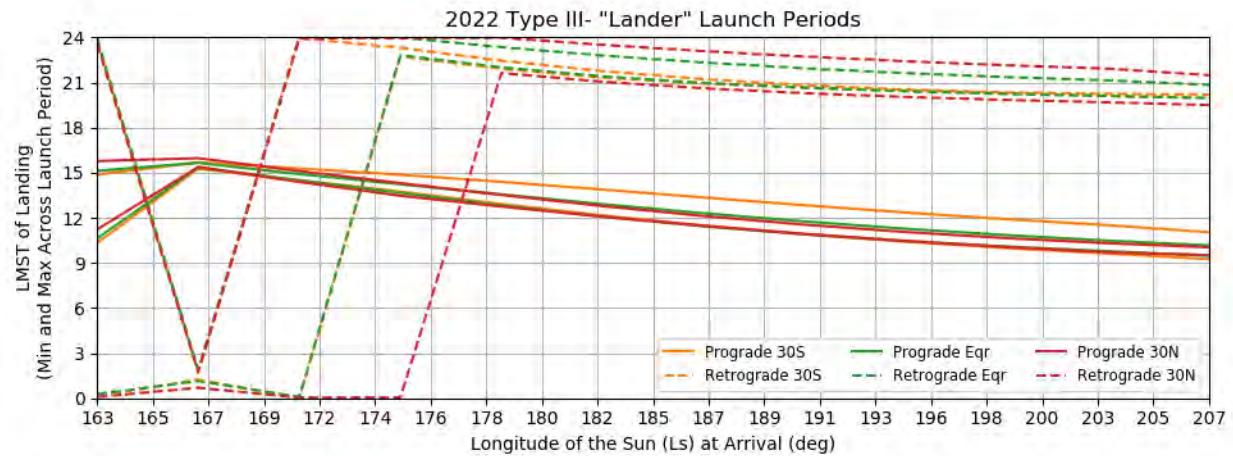


Figure 130: Earth to Mars 2022 Type III- Lander Launch Periods - LMST of Landing at Various Latitudes

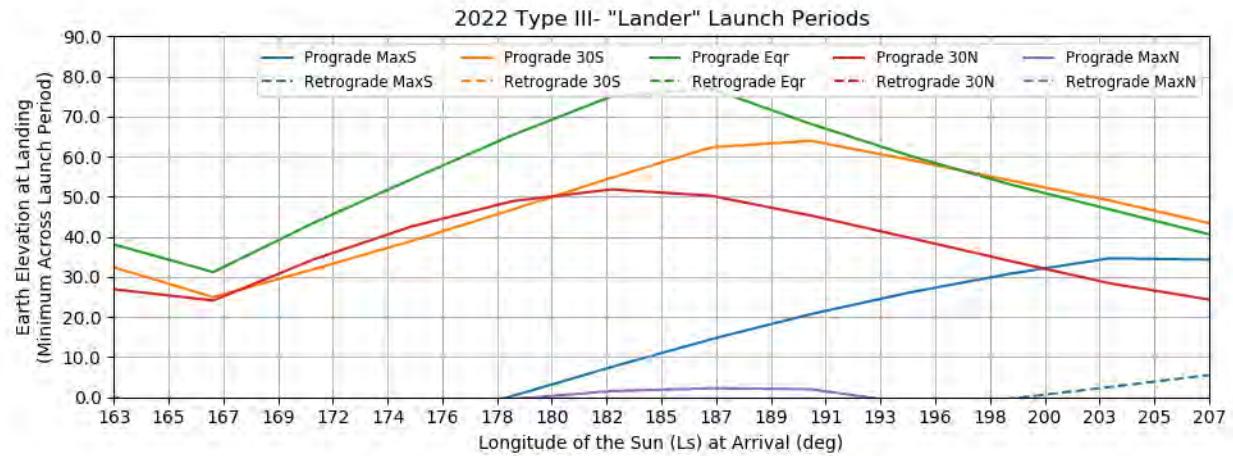
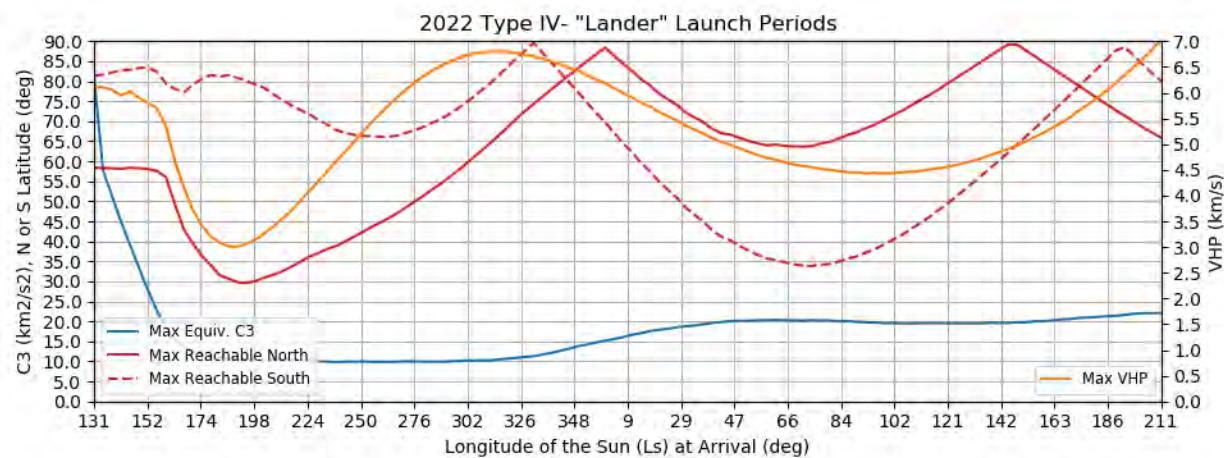
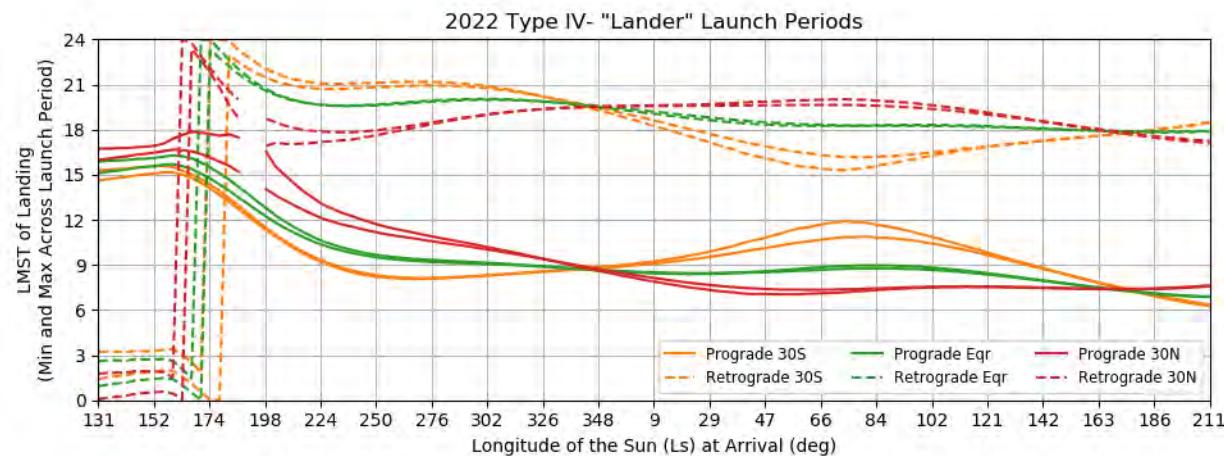


Figure 131: Earth to Mars 2022 Type III- Lander Launch Periods - Earth Elevation at Landing at Various Latitudes



**Figure 132: Earth to Mars 2022 Type IV- Lander Launch Periods - Reachable Latitudes, Equivalent C3, and VHP**



**Figure 133: Earth to Mars 2022 Type IV- Lander Launch Periods - LMST of Landing at Various Latitudes**

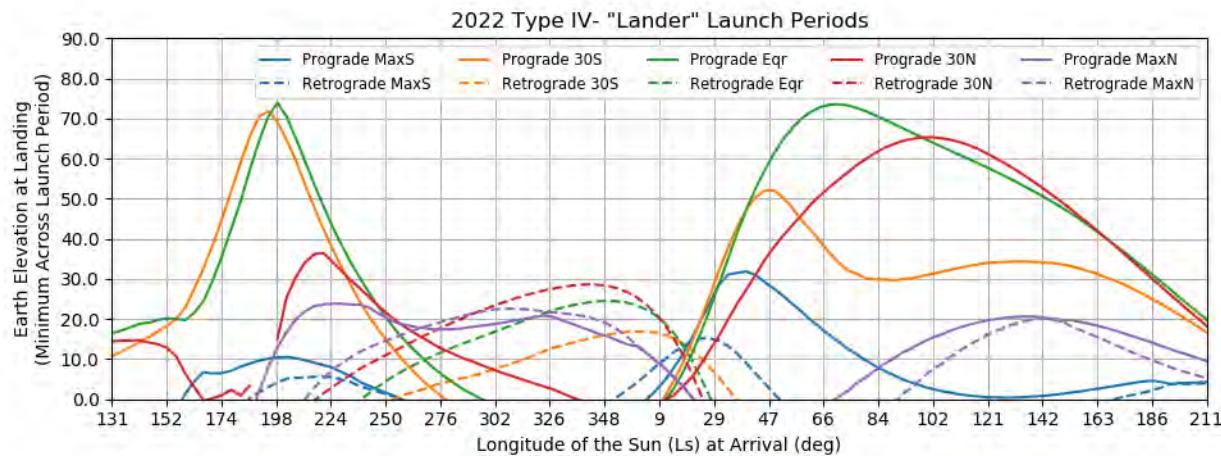


**Figure 134: Earth to Mars 2022 Type IV- Lander Launch Periods - Earth Elevation at Landing at Various Latitudes**

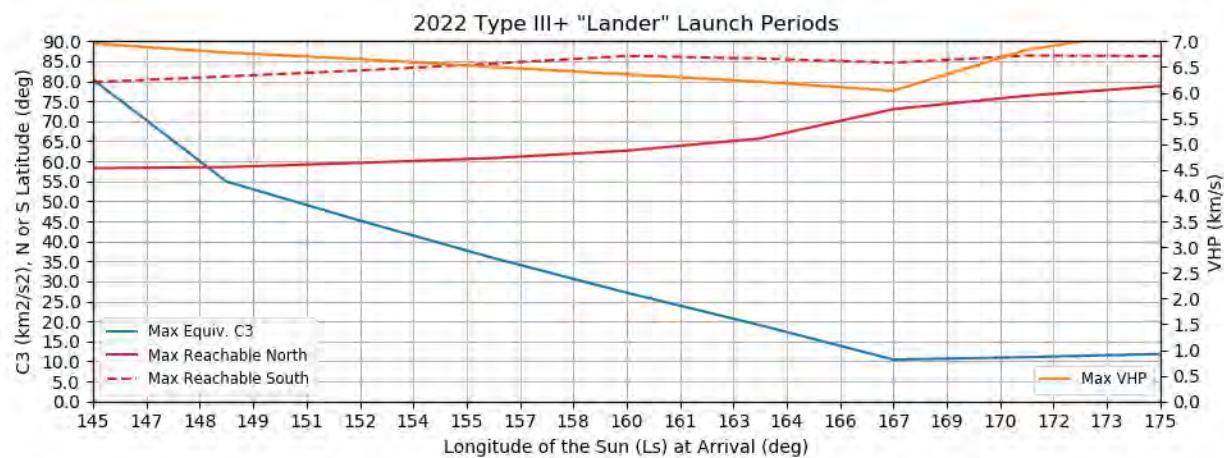


Figure 135: Earth to Mars 2022 Type III+ Lander Launch Periods - Reachable Latitudes, Equivalent C3, and VHP

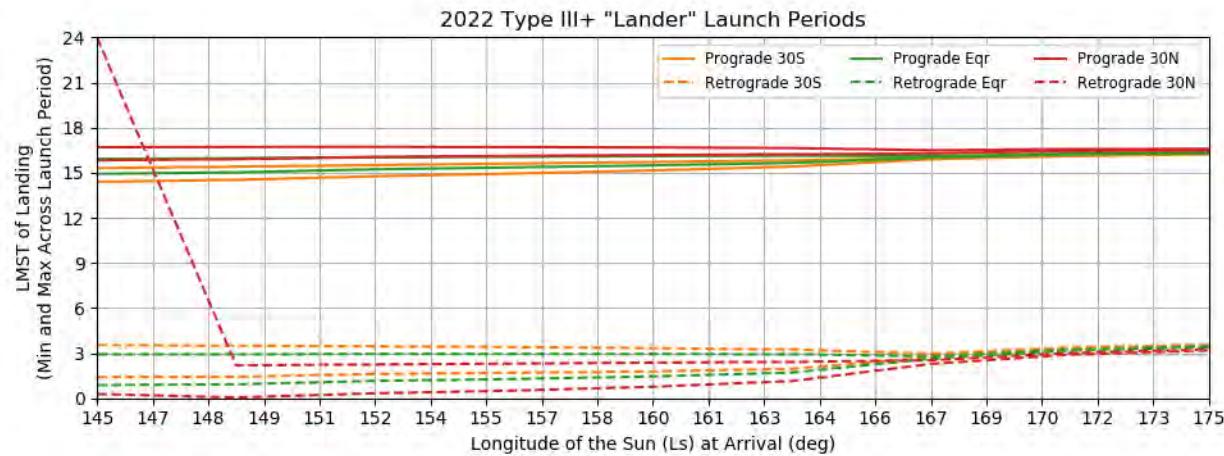


Figure 136: Earth to Mars 2022 Type III+ Lander Launch Periods - LMST of Landing at Various Latitudes

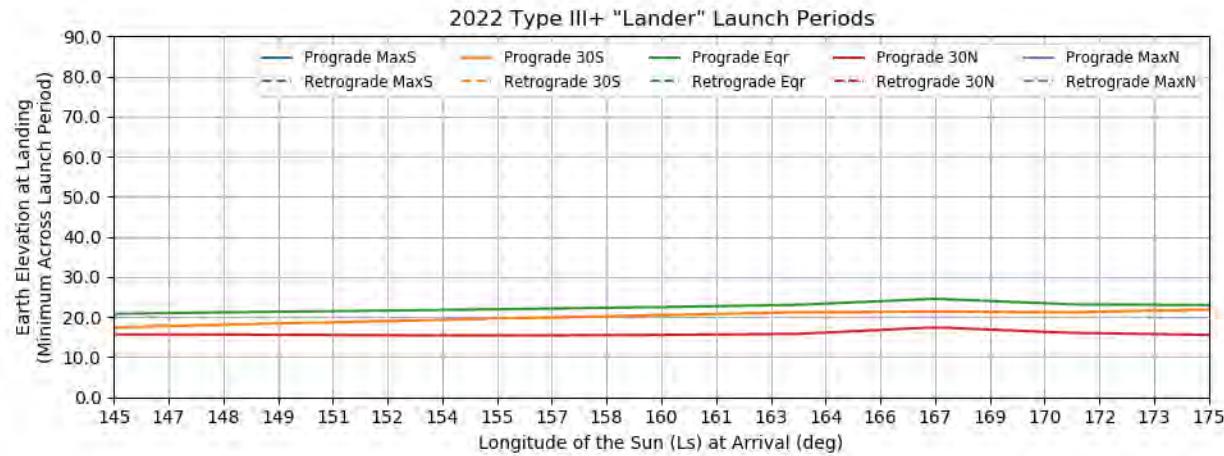
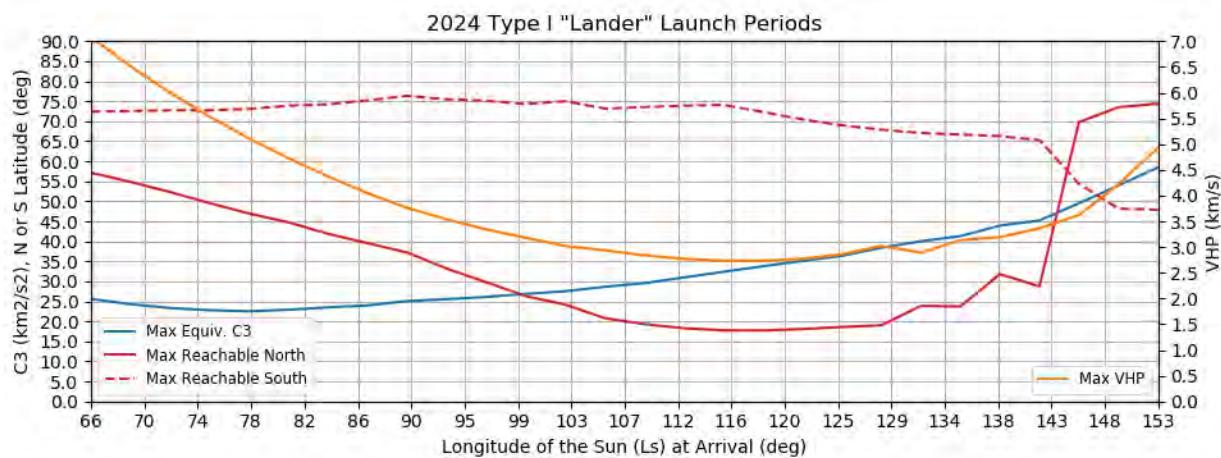
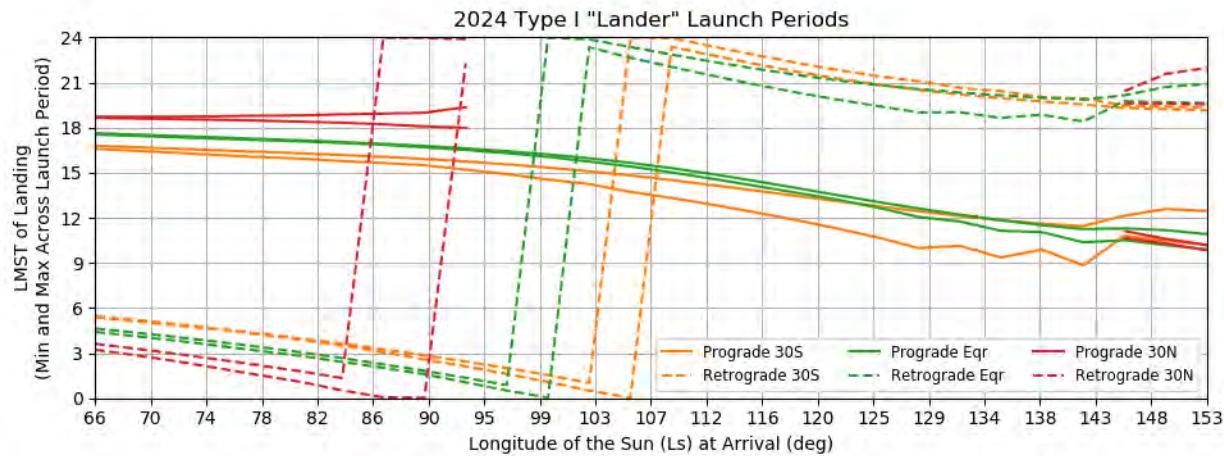


Figure 137: Earth to Mars 2022 Type III+ Lander Launch Periods - Earth Elevation at Landing at Various Latitudes



**Figure 138: Earth to Mars 2024 Type I Lander Launch Periods - Reachable Latitudes, Equivalent C3, and VHP**



**Figure 139: Earth to Mars 2024 Type I Lander Launch Periods - LMST of Landing at Various Latitudes**

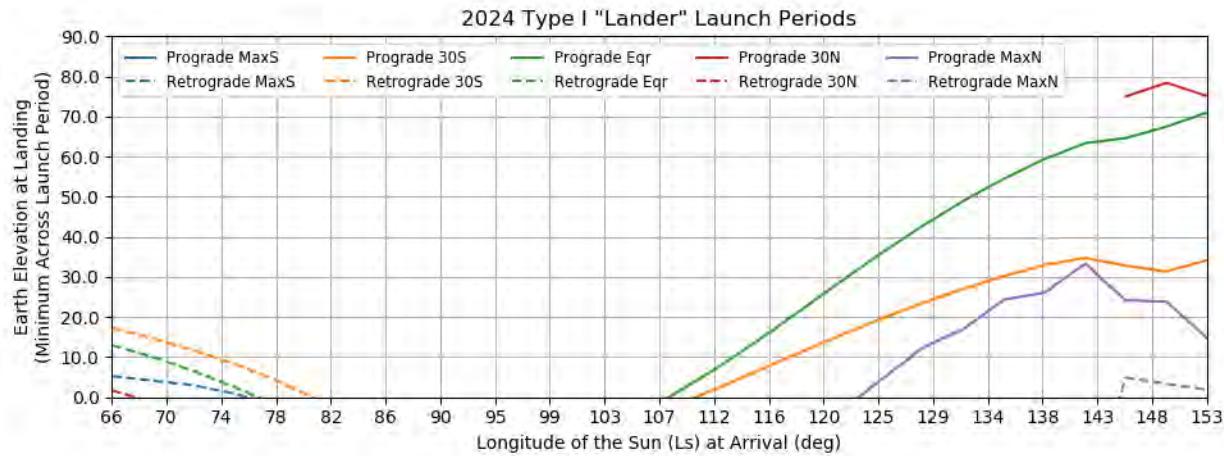


**Figure 140: Earth to Mars 2024 Type I Lander Launch Periods - Earth Elevation at Landing at Various Latitudes**

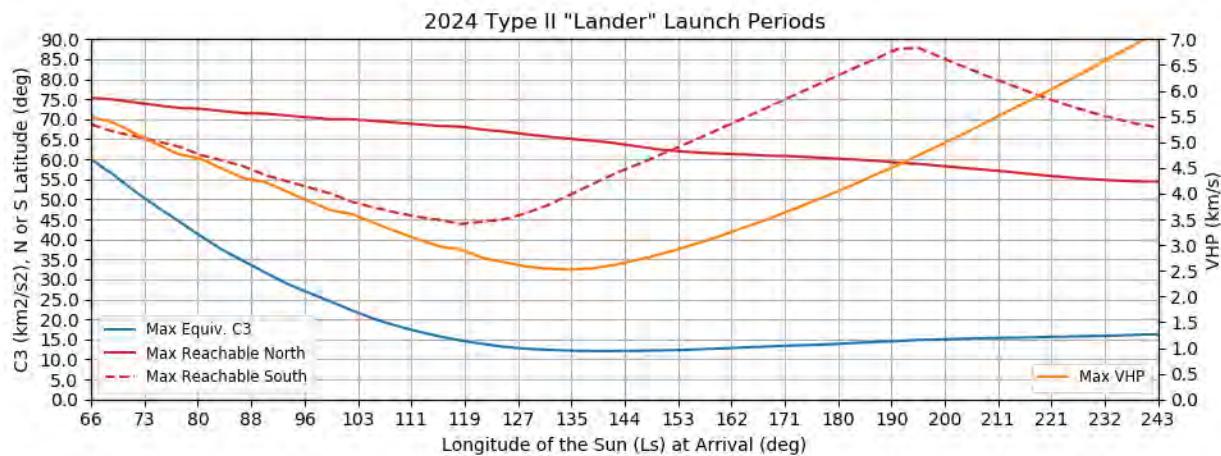


Figure 141: Earth to Mars 2024 Type II Lander Launch Periods - Reachable Latitudes, Equivalent C3, and VHP

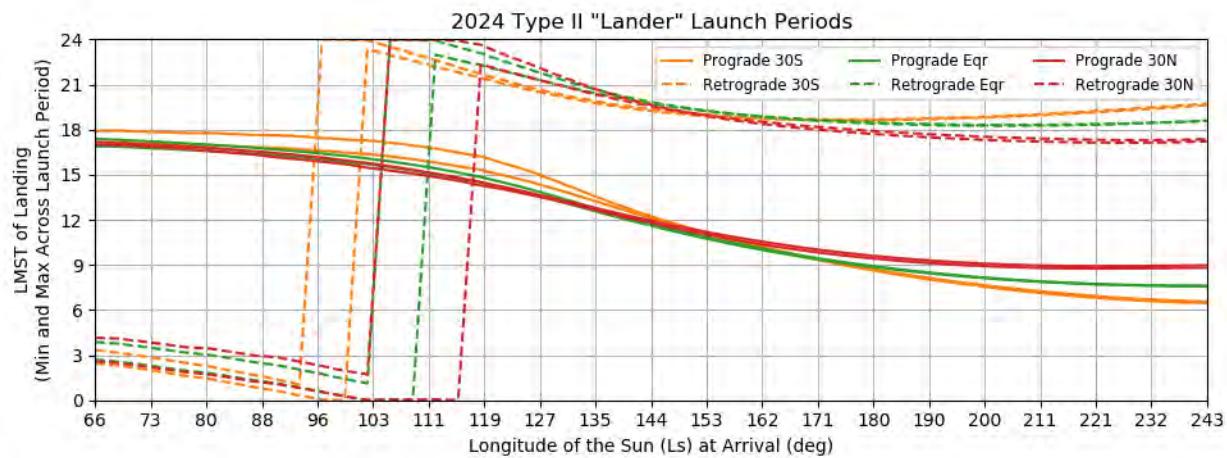


Figure 142: Earth to Mars 2024 Type II Lander Launch Periods - LMST of Landing at Various Latitudes

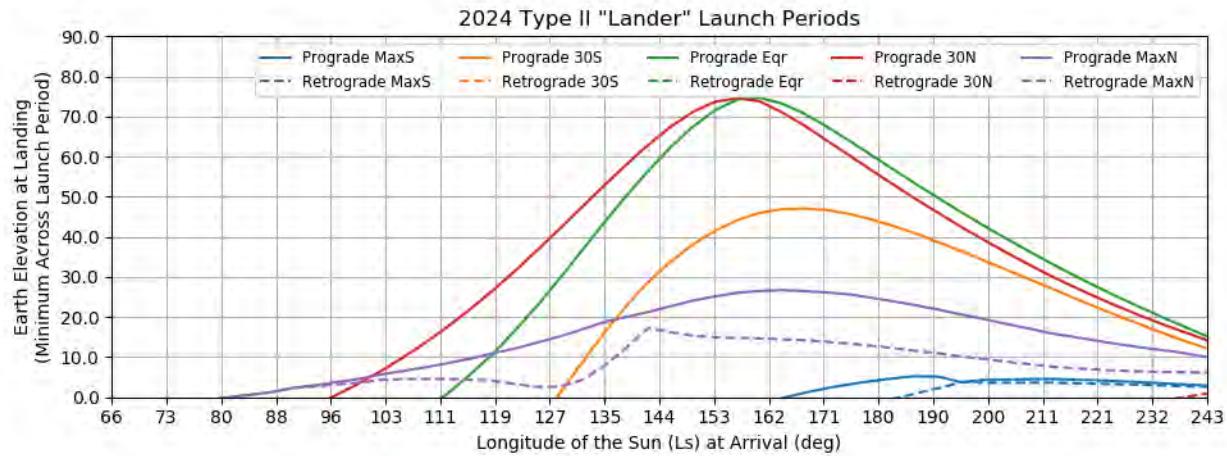


Figure 143: Earth to Mars 2024 Type II Lander Launch Periods - Earth Elevation at Landing at Various Latitudes

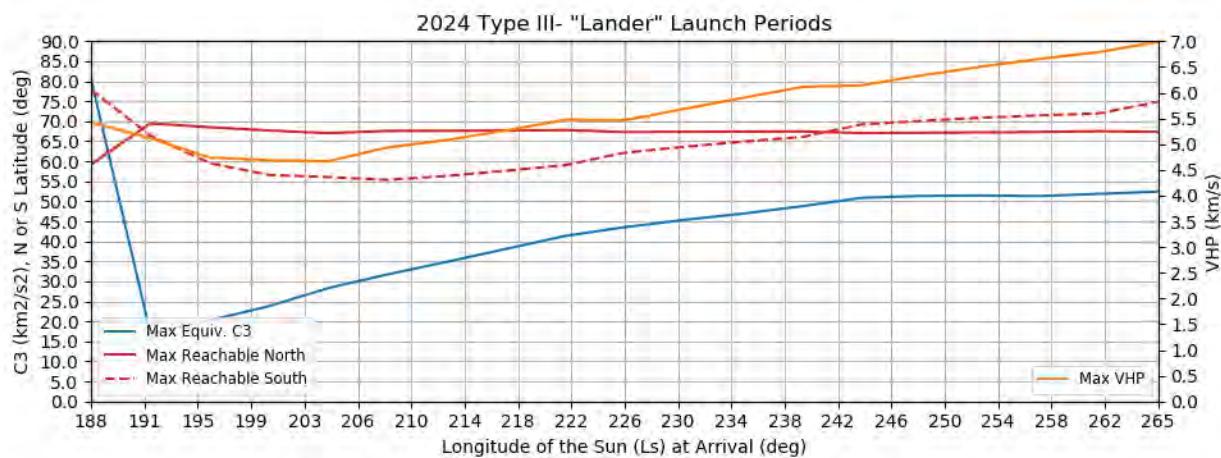


Figure 144: Earth to Mars 2024 Type III- Lander Launch Periods - Reachable Latitudes, Equivalent C3, and VHP

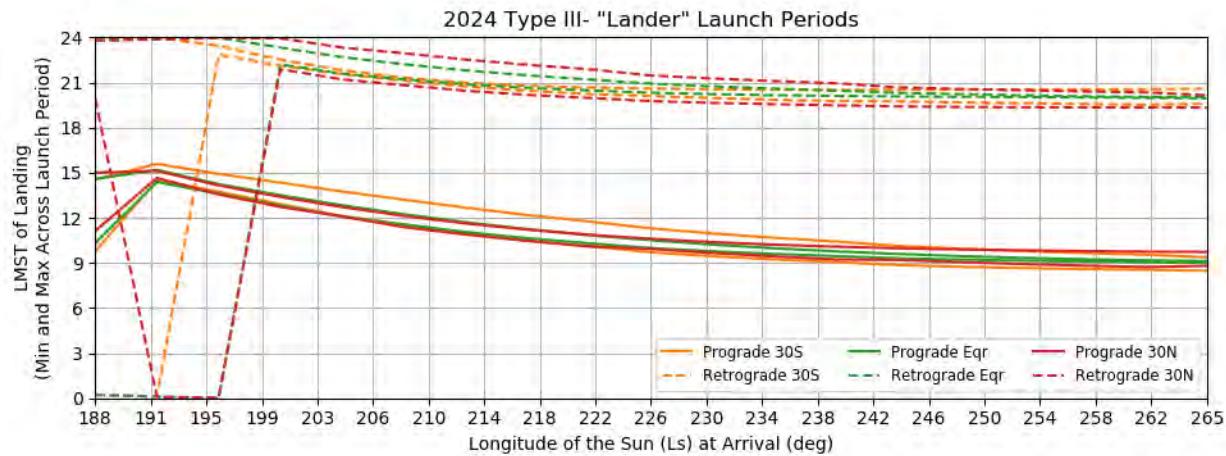


Figure 145: Earth to Mars 2024 Type III- Lander Launch Periods - LMST of Landing at Various Latitudes

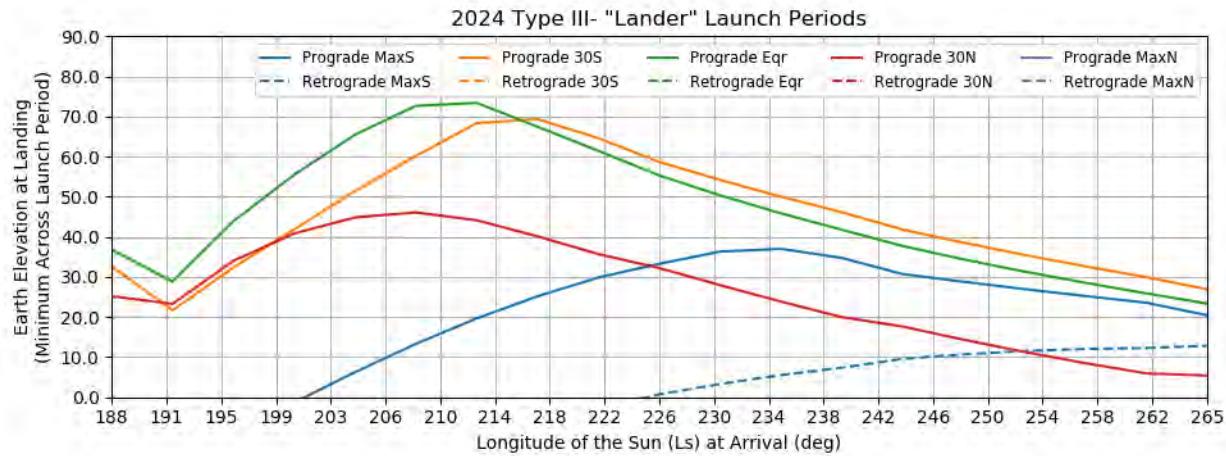


Figure 146: Earth to Mars 2024 Type III- Lander Launch Periods - Earth Elevation at Landing at Various Latitudes

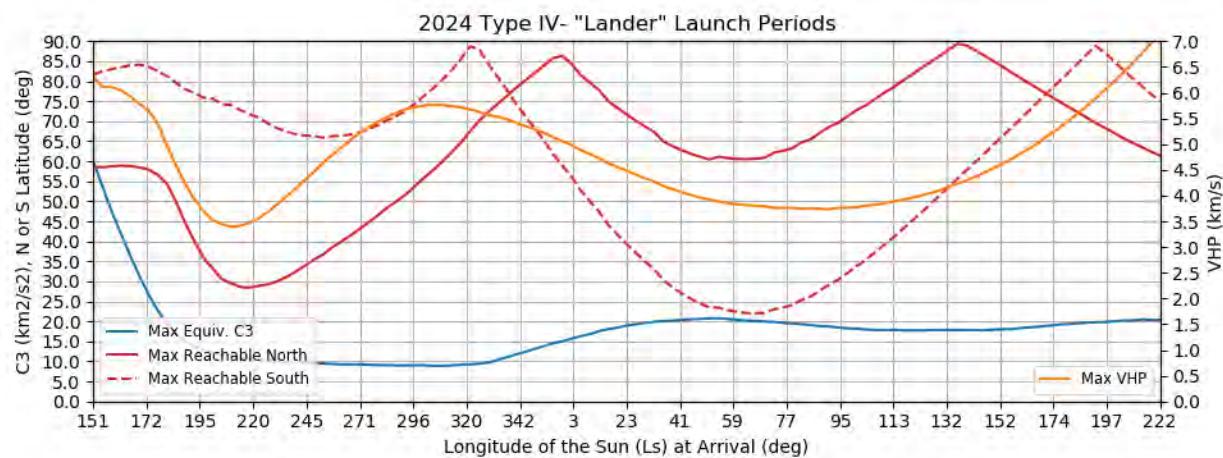


Figure 147: Earth to Mars 2024 Type IV- Lander Launch Periods - Reachable Latitudes, Equivalent C3, and VHP

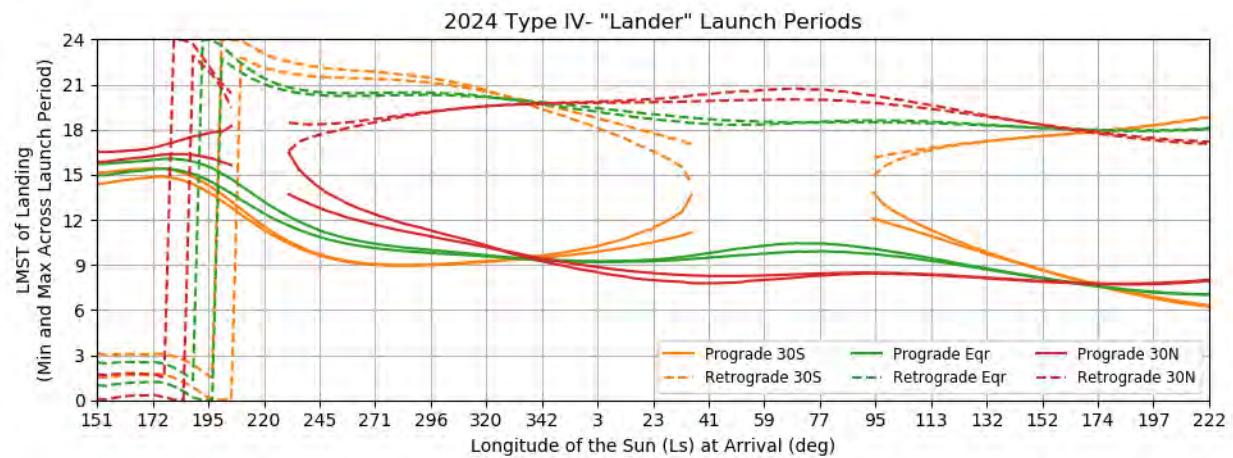


Figure 148: Earth to Mars 2024 Type IV- Lander Launch Periods - LMST of Landing at Various Latitudes

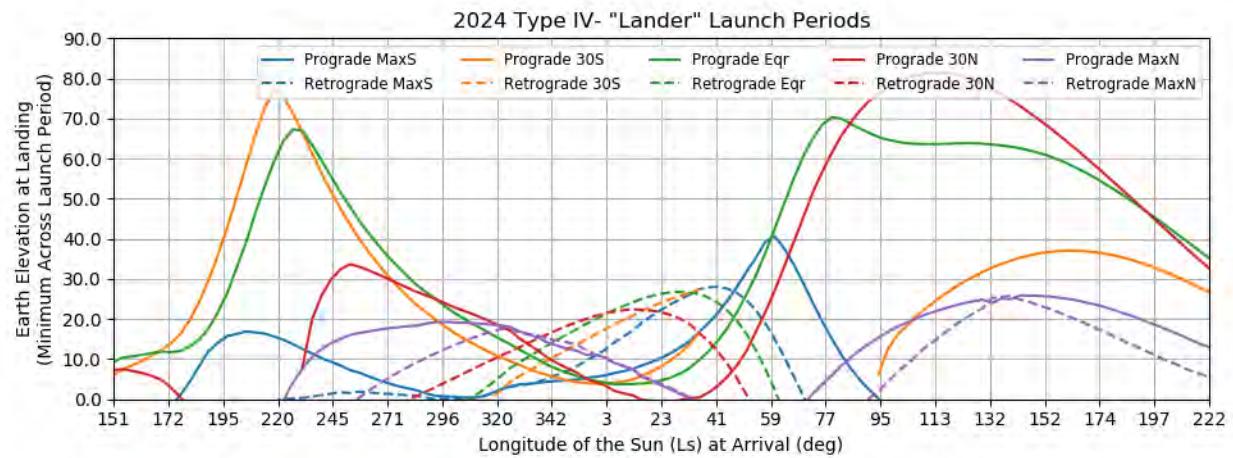
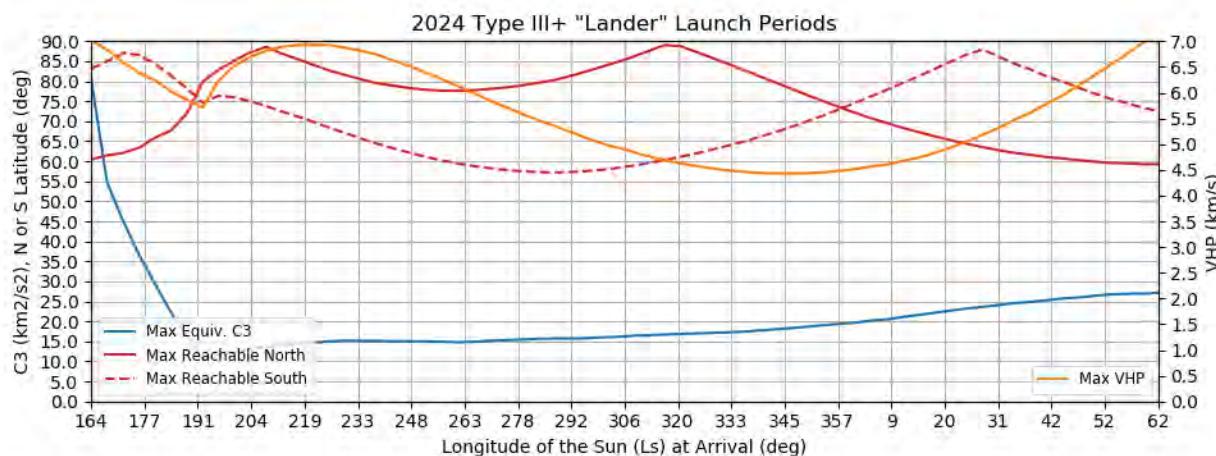
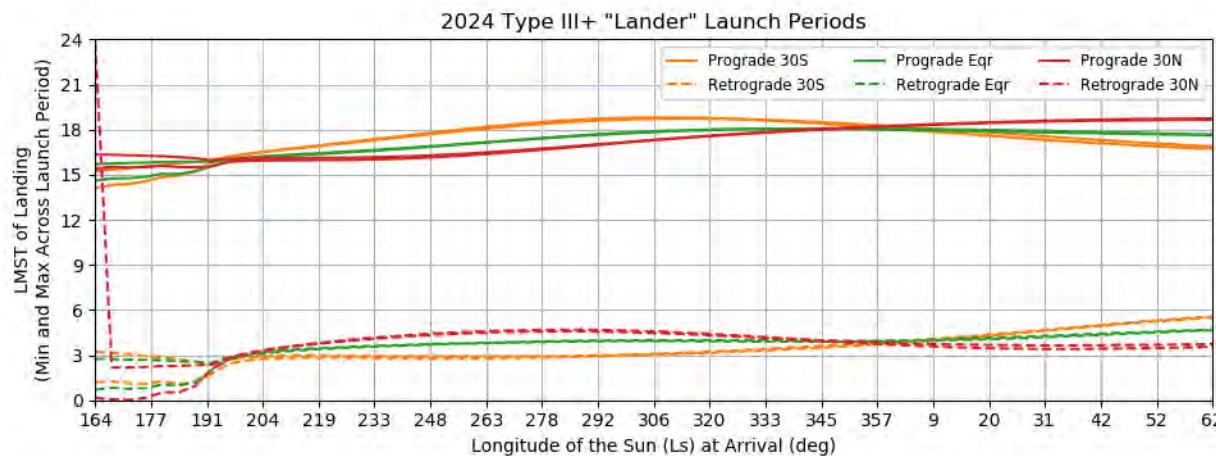


Figure 149: Earth to Mars 2024 Type IV- Lander Launch Periods - Earth Elevation at Landing at Various Latitudes



**Figure 150: Earth to Mars 2024 Type III+ Lander Launch Periods - Reachable Latitudes, Equivalent C3, and VHP**



**Figure 151: Earth to Mars 2024 Type III+ Lander Launch Periods - LMST of Landing at Various Latitudes**

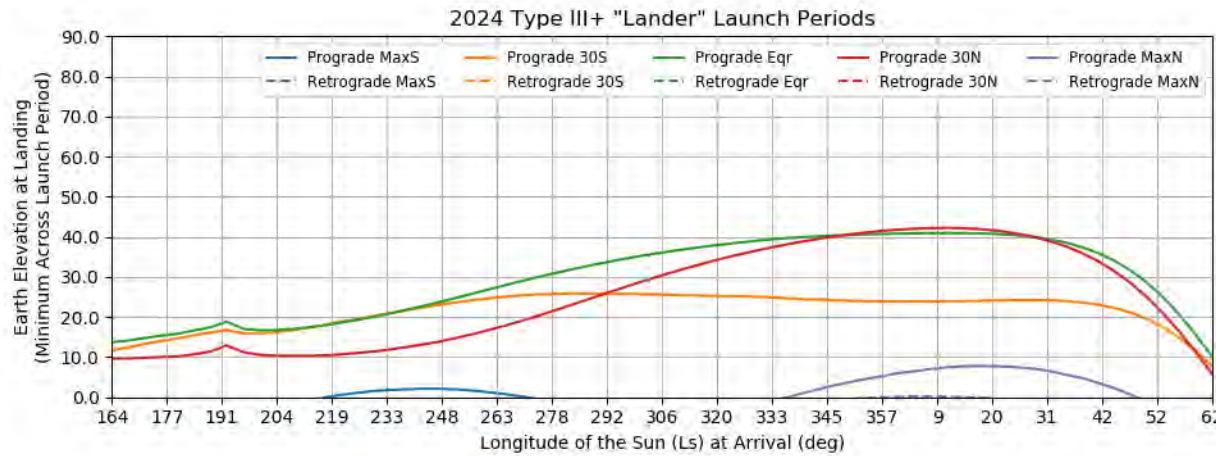


**Figure 152: Earth to Mars 2024 Type III+ Lander Launch Periods - Earth Elevation at Landing at Various Latitudes**

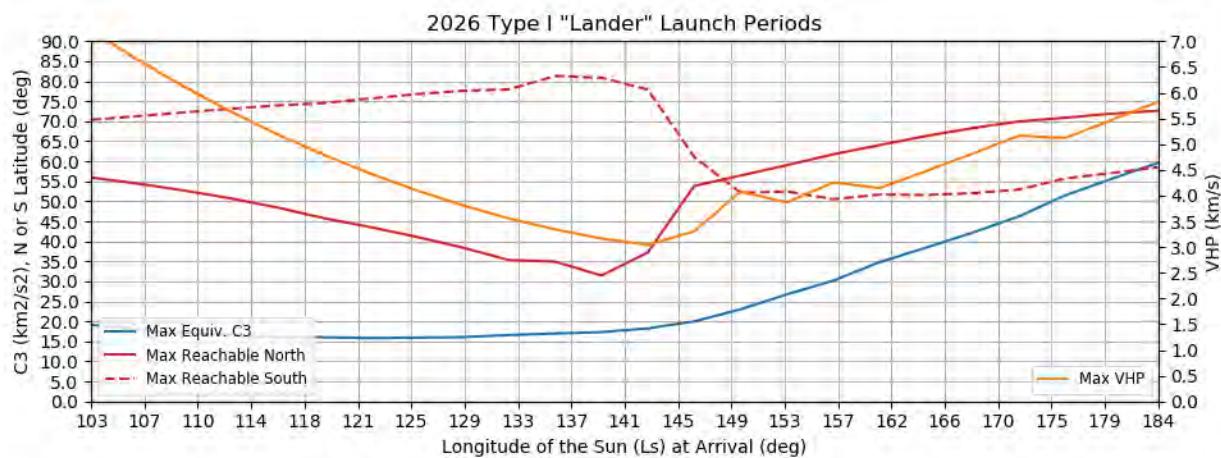


**Figure 153: Earth to Mars 2026 Type I Lander Launch Periods - Reachable Latitudes, Equivalent C3, and VHP**

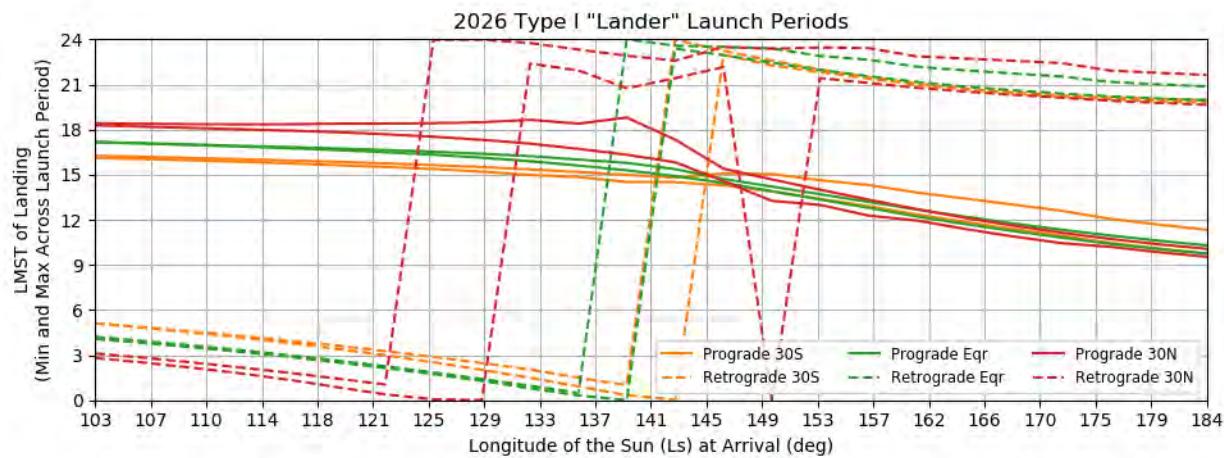


**Figure 154: Earth to Mars 2026 Type I Lander Launch Periods - LMST of Landing at Various Latitudes**

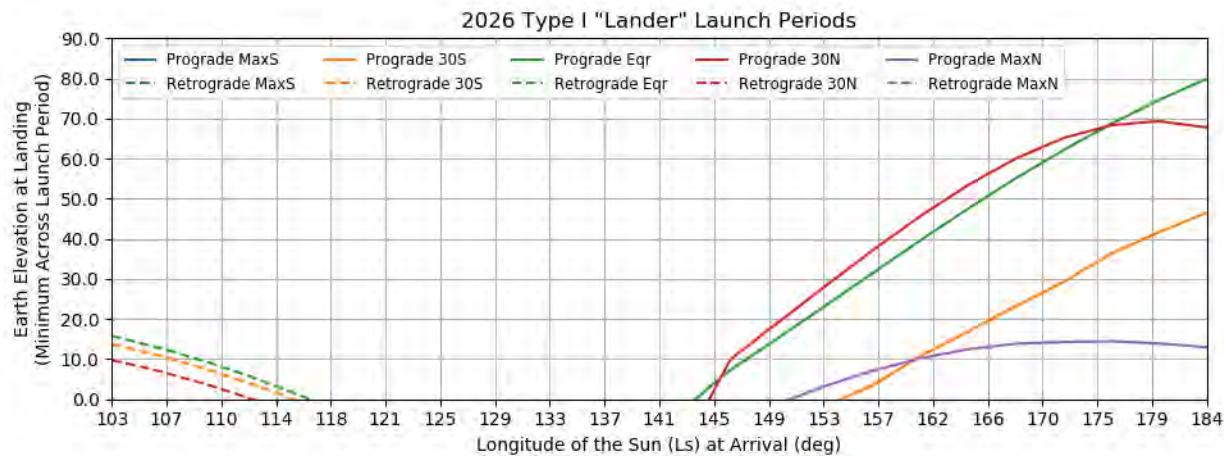


**Figure 155: Earth to Mars 2026 Type I Lander Launch Periods - Earth Elevation at Landing at Various Latitudes**

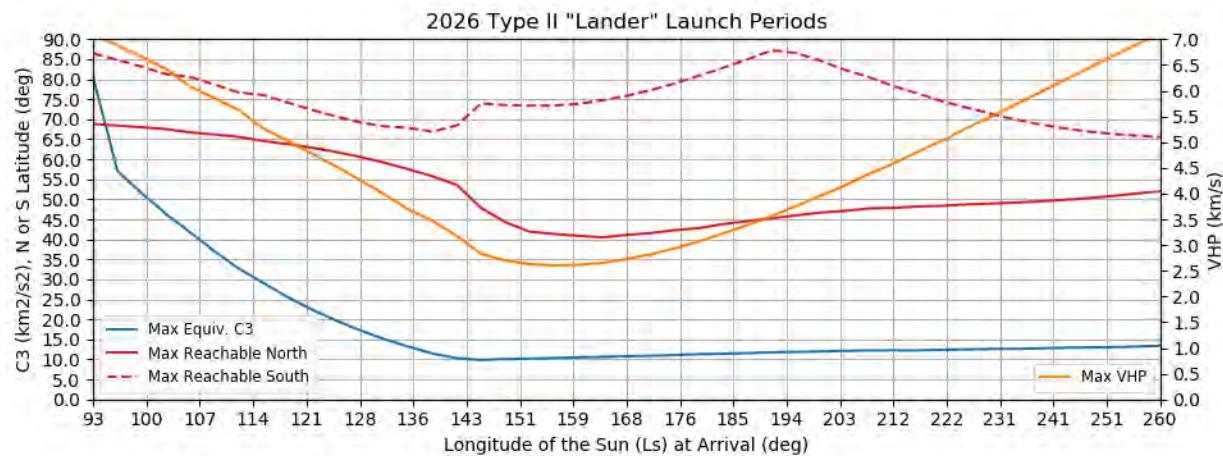


Figure 156: Earth to Mars 2026 Type II Lander Launch Periods - Reachable Latitudes, Equivalent C3, and VHP

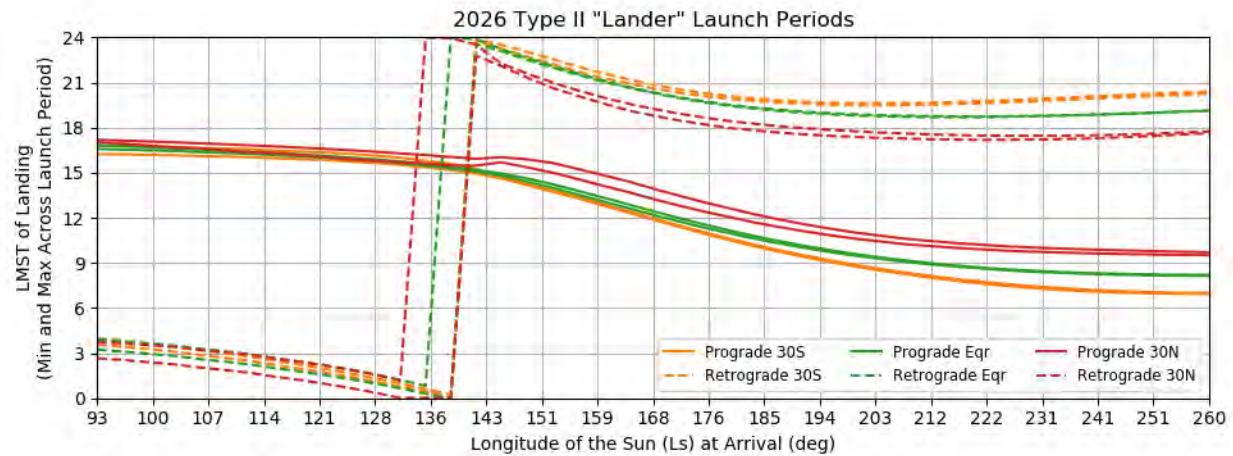


Figure 157: Earth to Mars 2026 Type II Lander Launch Periods - LMST of Landing at Various Latitudes

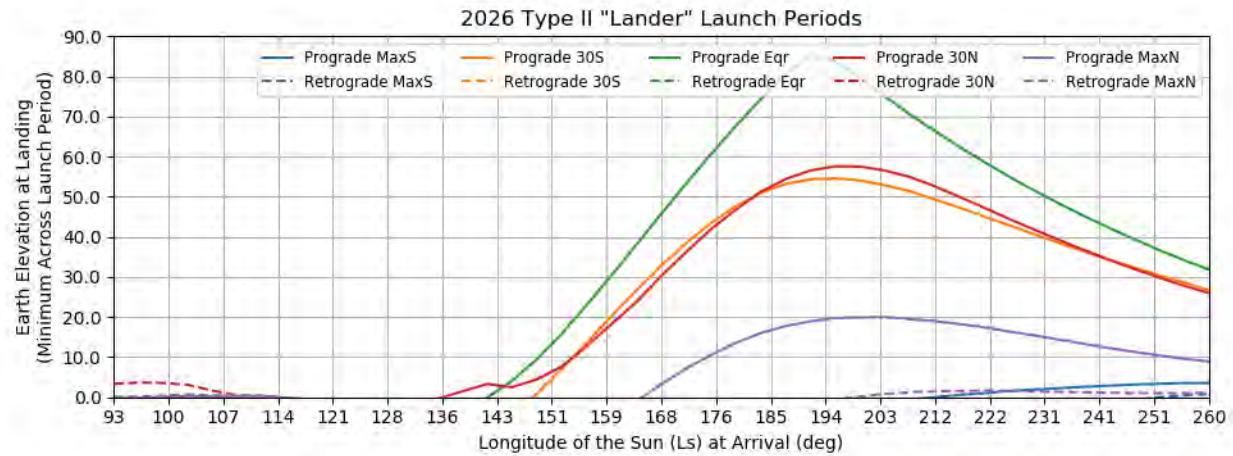
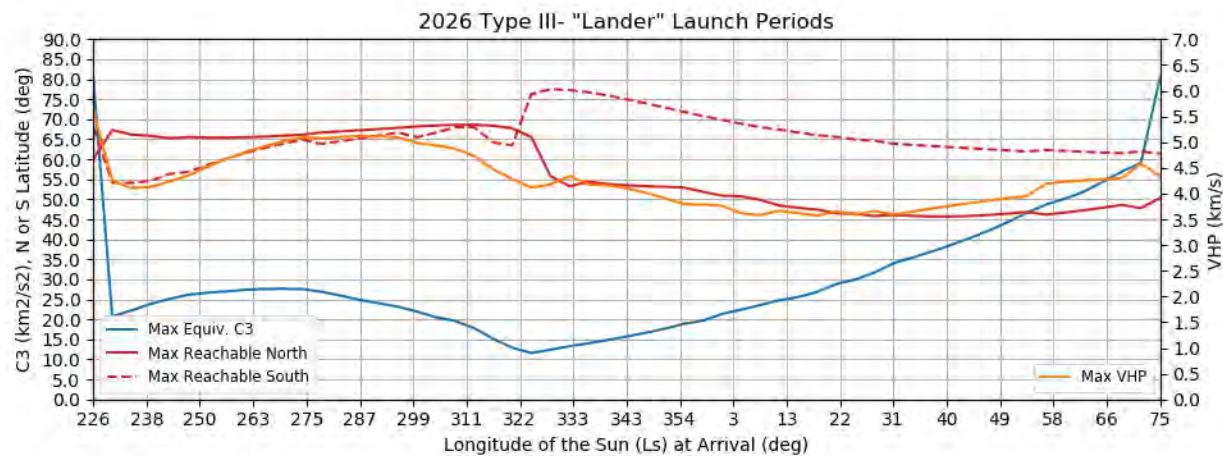
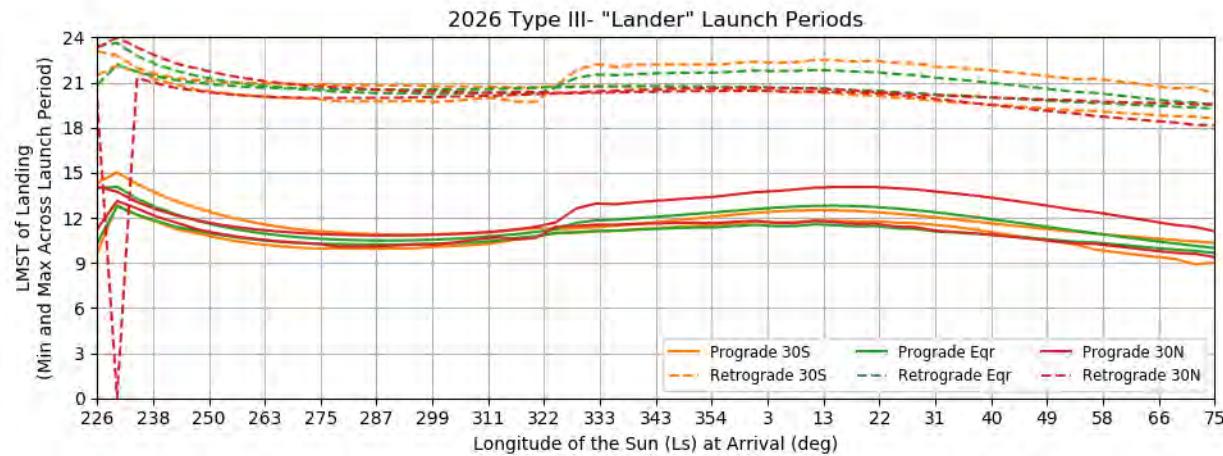


Figure 158: Earth to Mars 2026 Type II Lander Launch Periods - Earth Elevation at Landing at Various Latitudes



**Figure 159: Earth to Mars 2026 Type III- Lander Launch Periods - Reachable Latitudes, Equivalent C3, and VHP**



**Figure 160: Earth to Mars 2026 Type III- Lander Launch Periods - LMST of Landing at Various Latitudes**

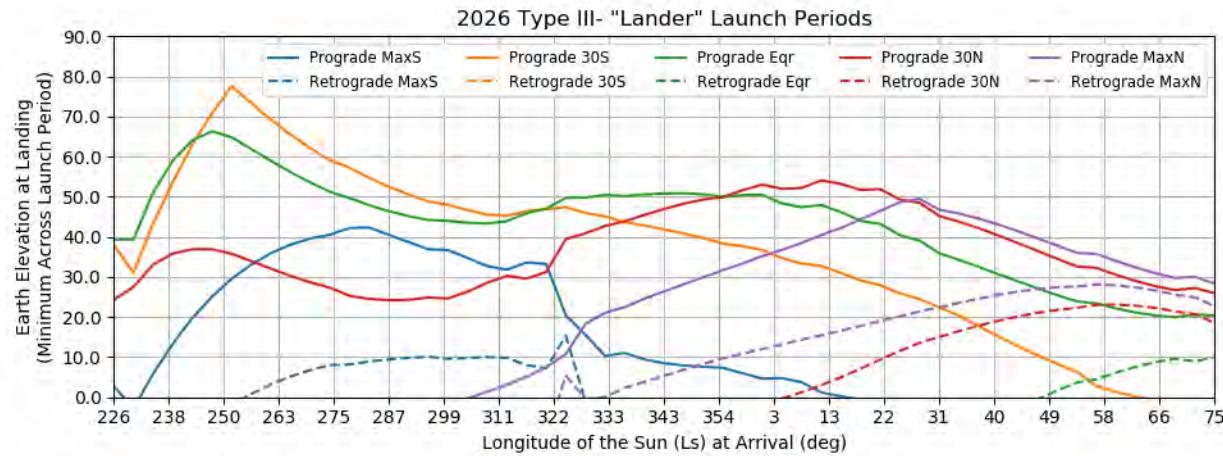


**Figure 161: Earth to Mars 2026 Type III- Lander Launch Periods - Earth Elevation at Landing at Various Latitudes**

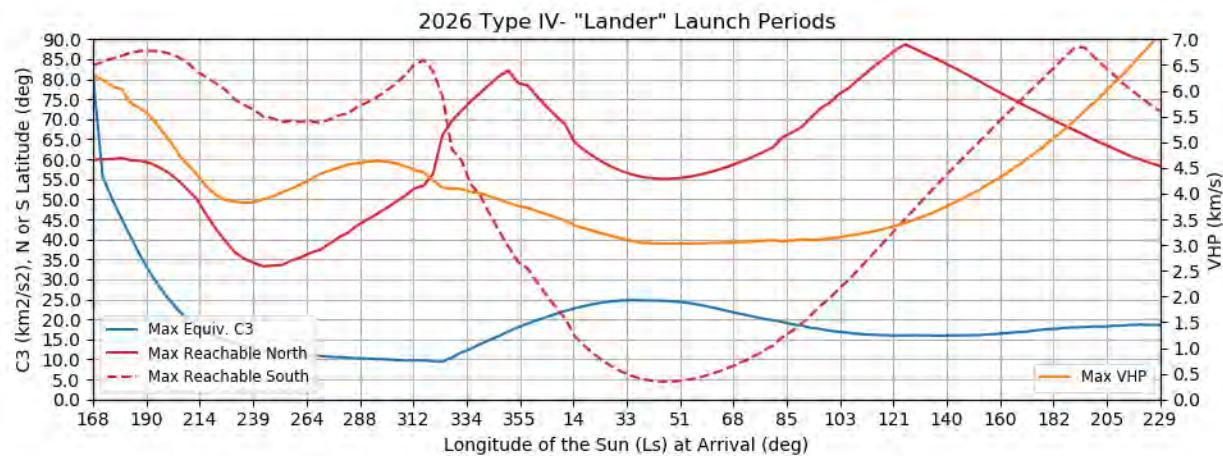


Figure 162: Earth to Mars 2026 Type IV- Lander Launch Periods - Reachable Latitudes, Equivalent C3, and VHP

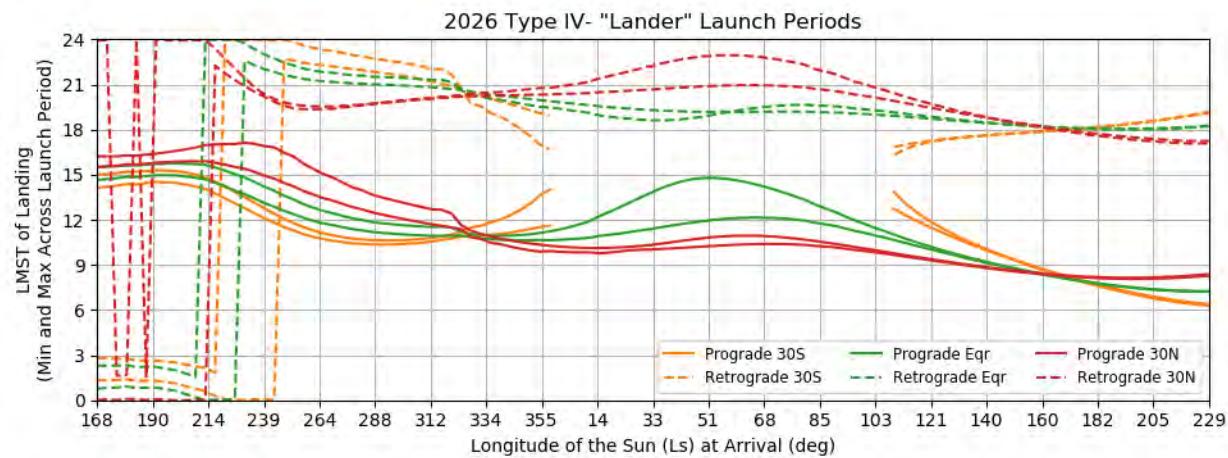


Figure 163: Earth to Mars 2026 Type IV- Lander Launch Periods - LMST of Landing at Various Latitudes

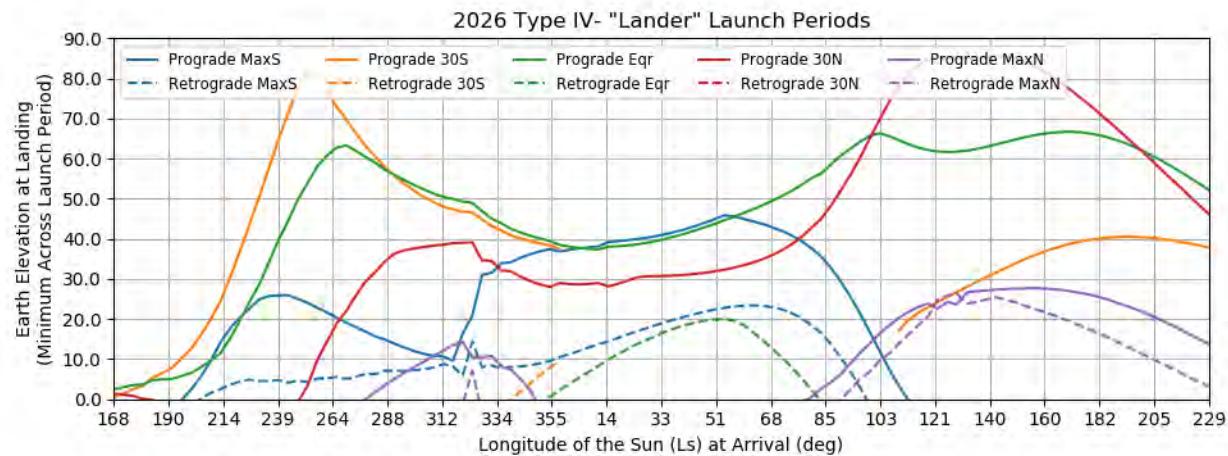


Figure 164: Earth to Mars 2026 Type IV- Lander Launch Periods - Earth Elevation at Landing at Various Latitudes

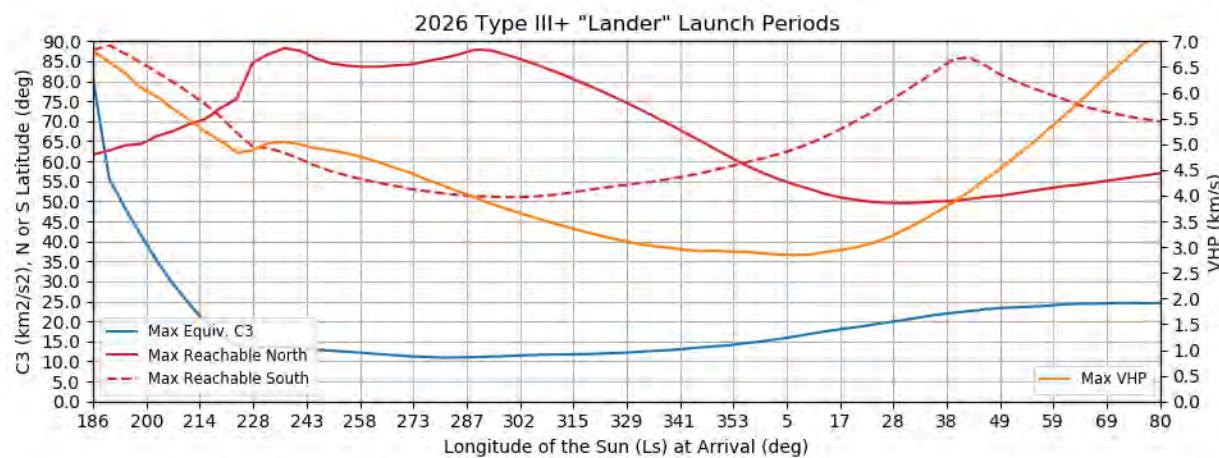


Figure 165: Earth to Mars 2026 Type III+ Lander Launch Periods - Reachable Latitudes, Equivalent C3, and VHP

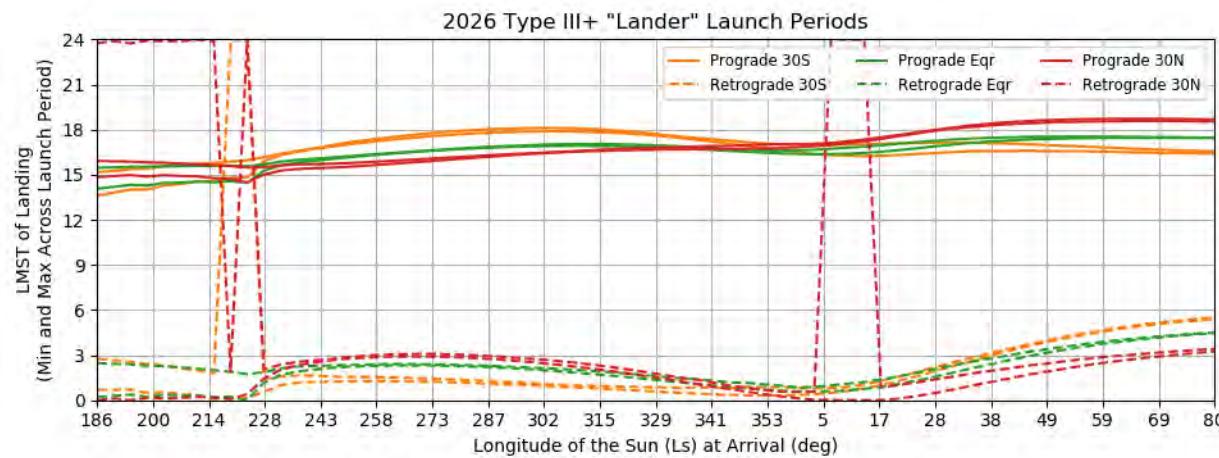


Figure 166: Earth to Mars 2026 Type III+ Lander Launch Periods - LMST of Landing at Various Latitudes

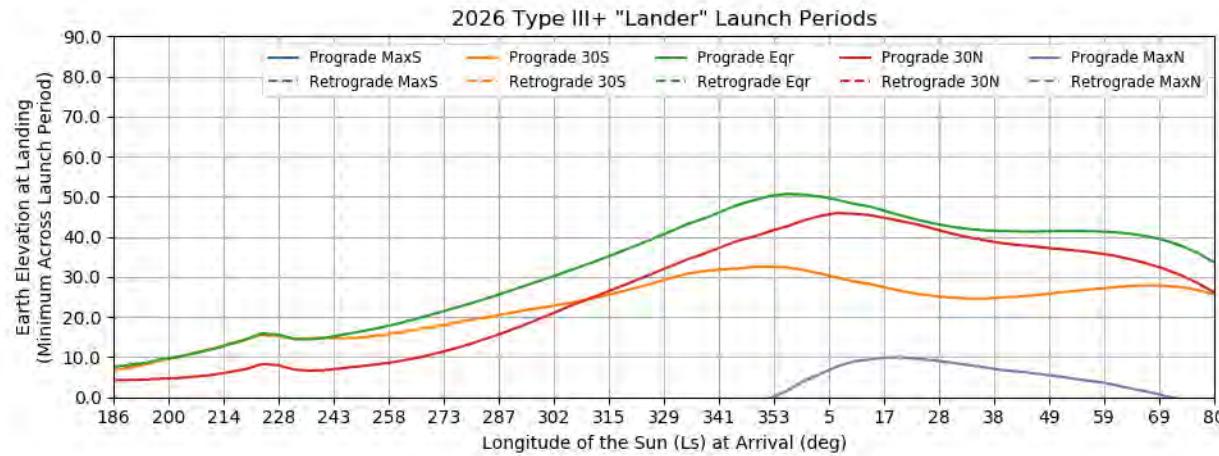
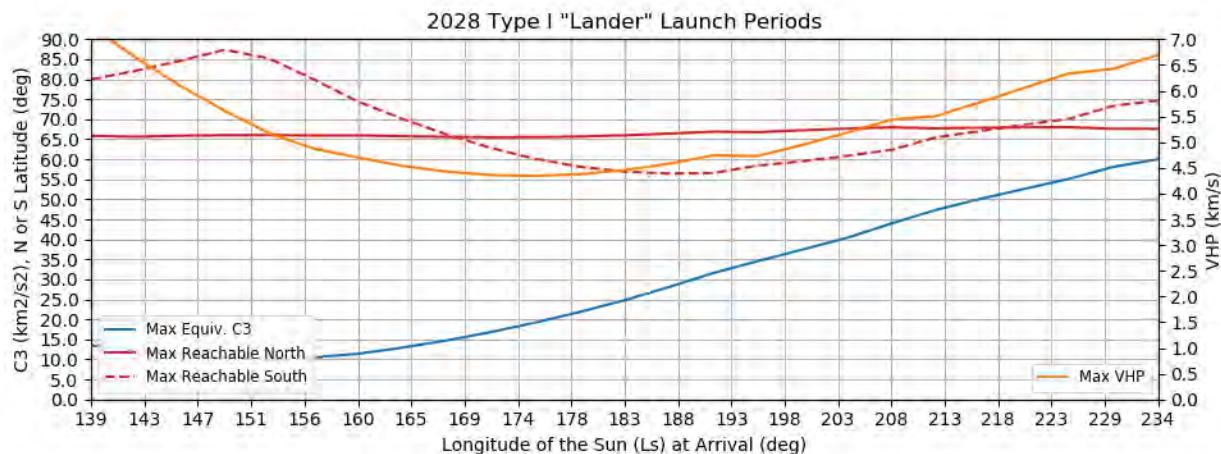
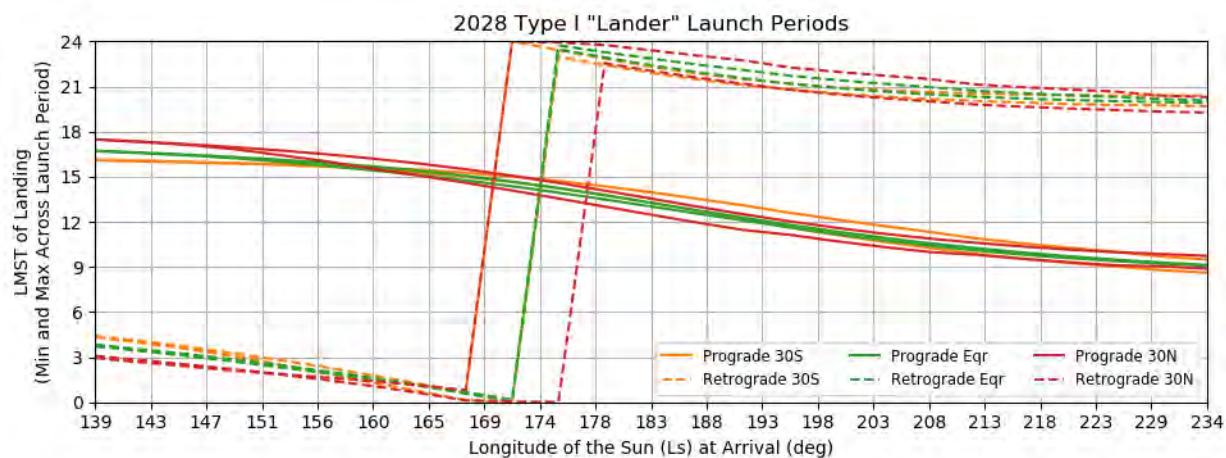


Figure 167: Earth to Mars 2026 Type III+ Lander Launch Periods - Earth Elevation at Landing at Various Latitudes



**Figure 168: Earth to Mars 2028 Type I Lander Launch Periods - Reachable Latitudes, Equivalent C3, and VHP**



**Figure 169: Earth to Mars 2028 Type I Lander Launch Periods - LMST of Landing at Various Latitudes**

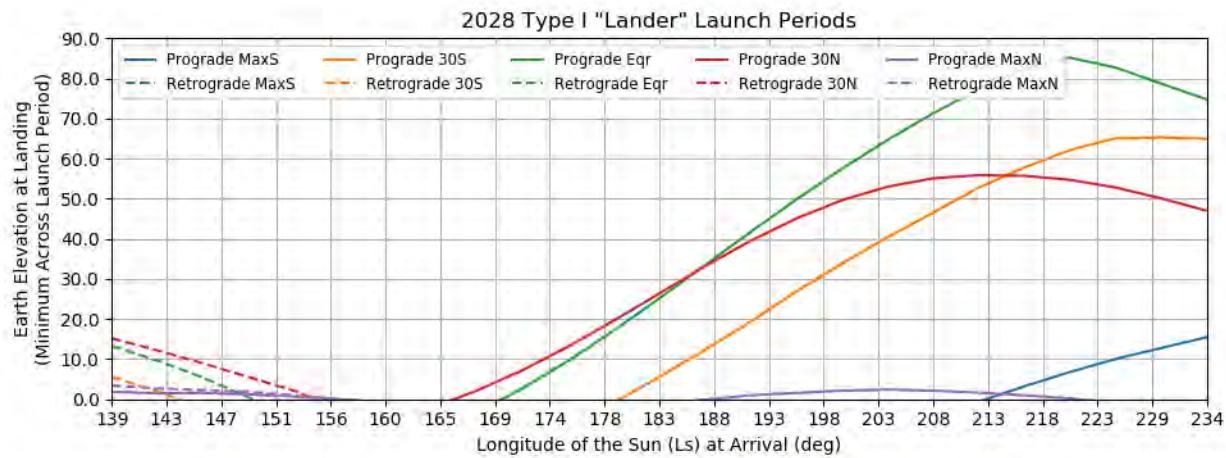


**Figure 170: Earth to Mars 2028 Type I Lander Launch Periods - Earth Elevation at Landing at Various Latitudes**

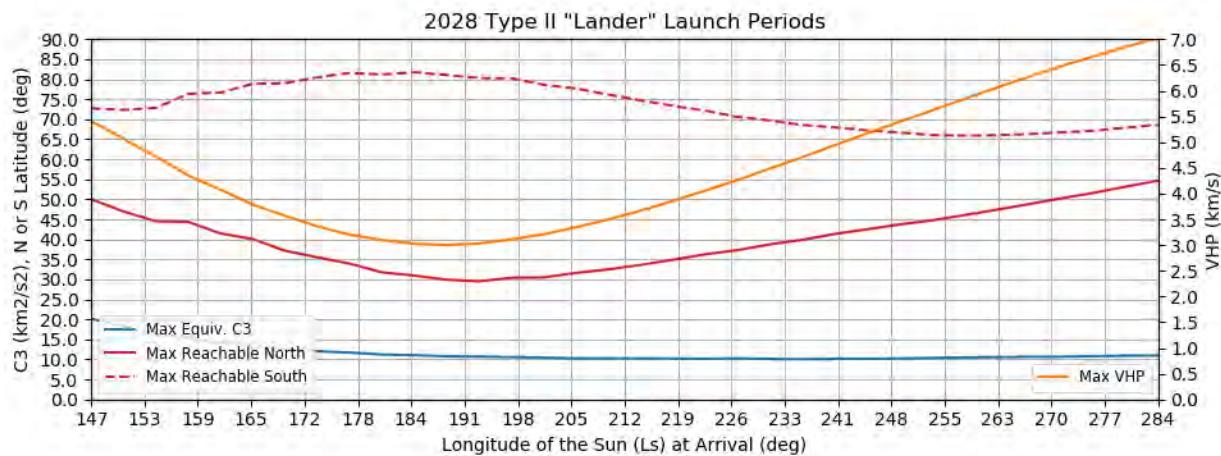


Figure 171: Earth to Mars 2028 Type II Lander Launch Periods - Reachable Latitudes, Equivalent C3, and VHP

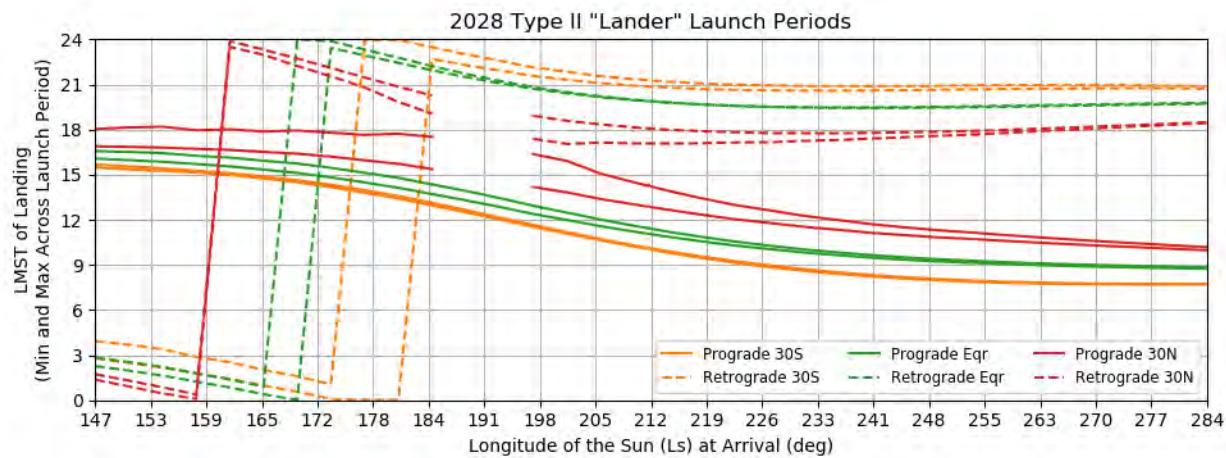


Figure 172: Earth to Mars 2028 Type II Lander Launch Periods - LMST of Landing at Various Latitudes

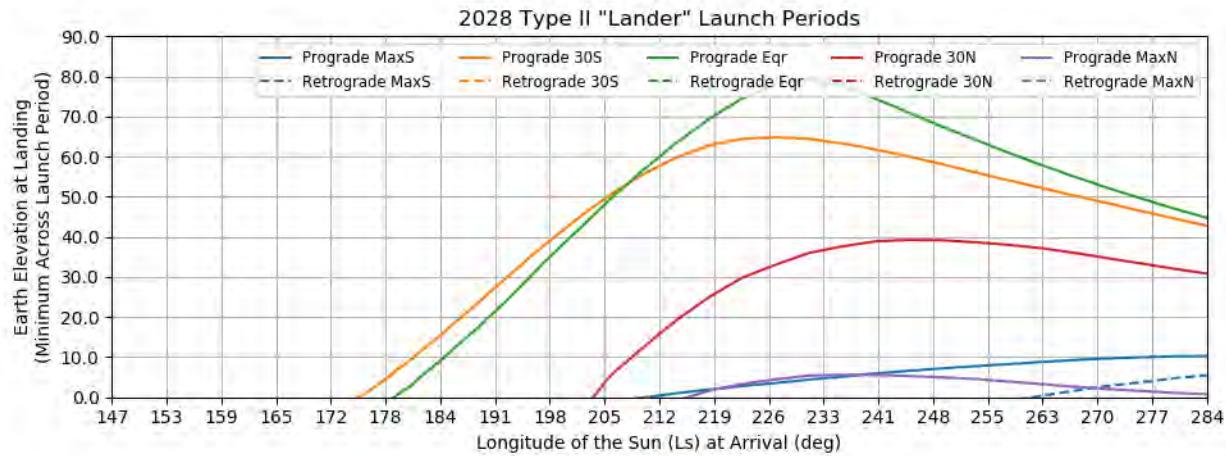


Figure 173: Earth to Mars 2028 Type II Lander Launch Periods - Earth Elevation at Landing at Various Latitudes

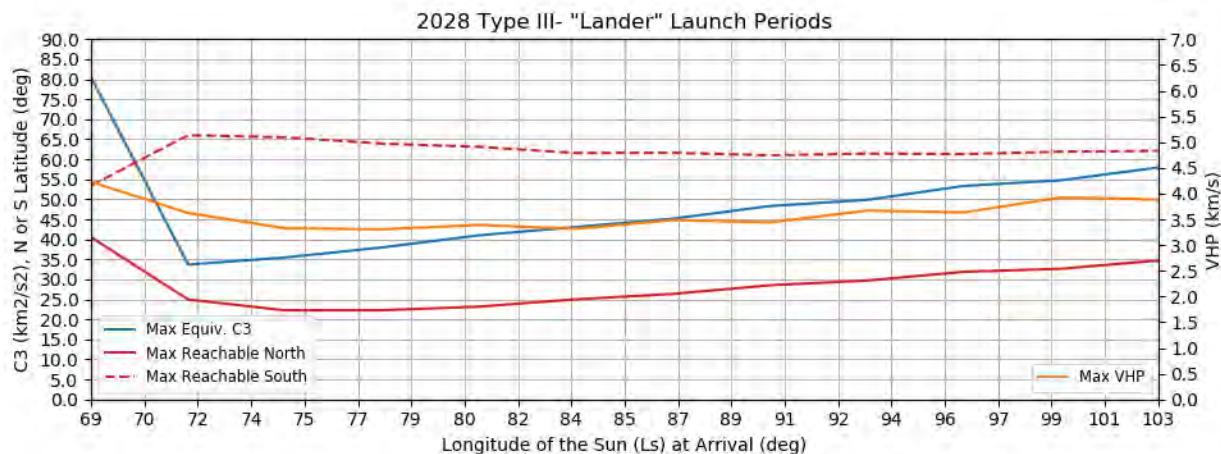


Figure 174: Earth to Mars 2028 Type III- Lander Launch Periods - Reachable Latitudes, Equivalent C3, and VHP

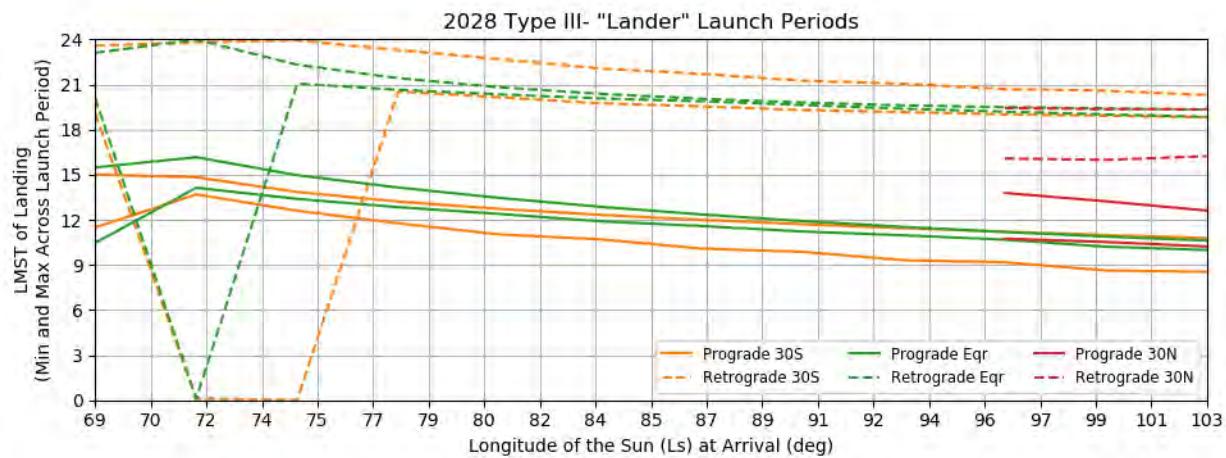


Figure 175: Earth to Mars 2028 Type III- Lander Launch Periods - LMST of Landing at Various Latitudes

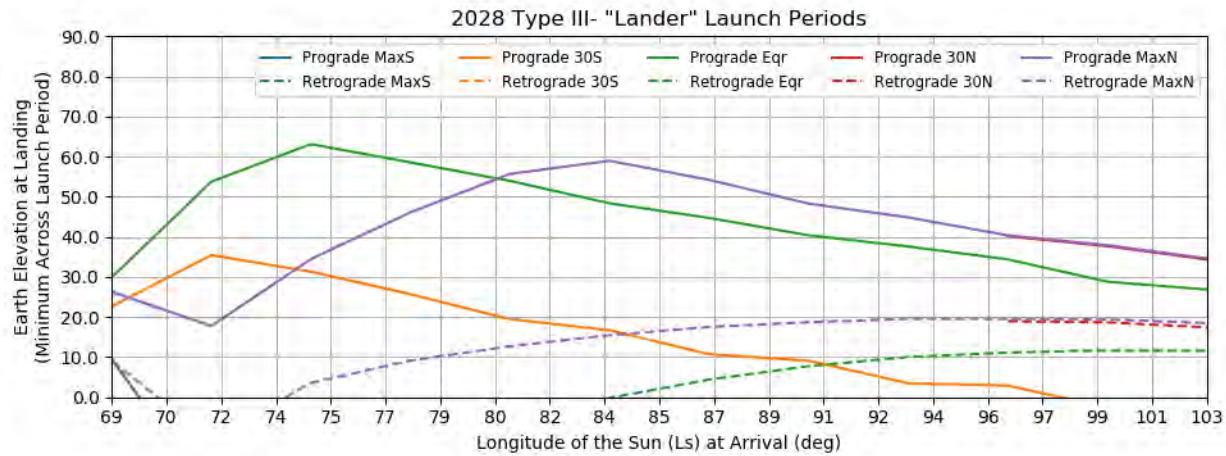
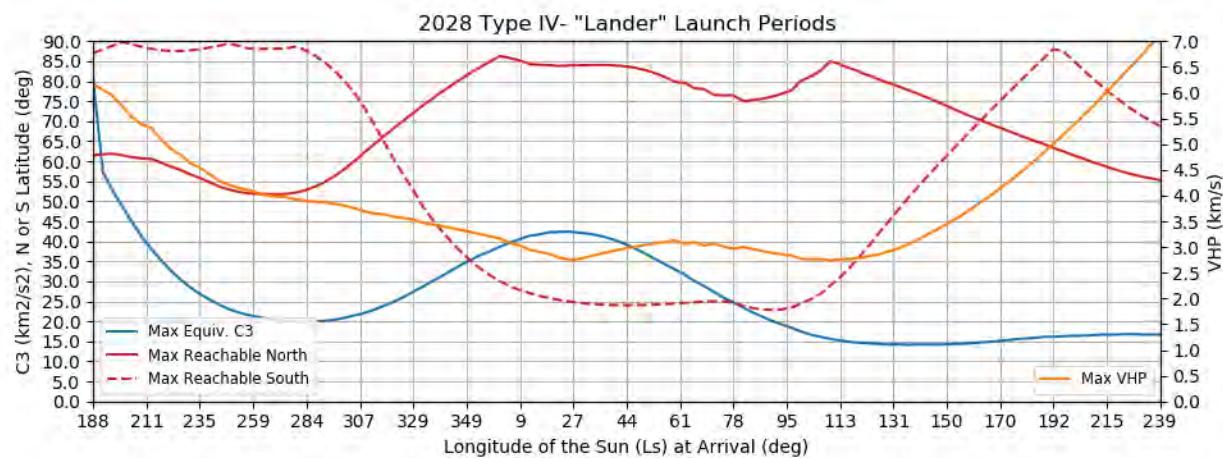
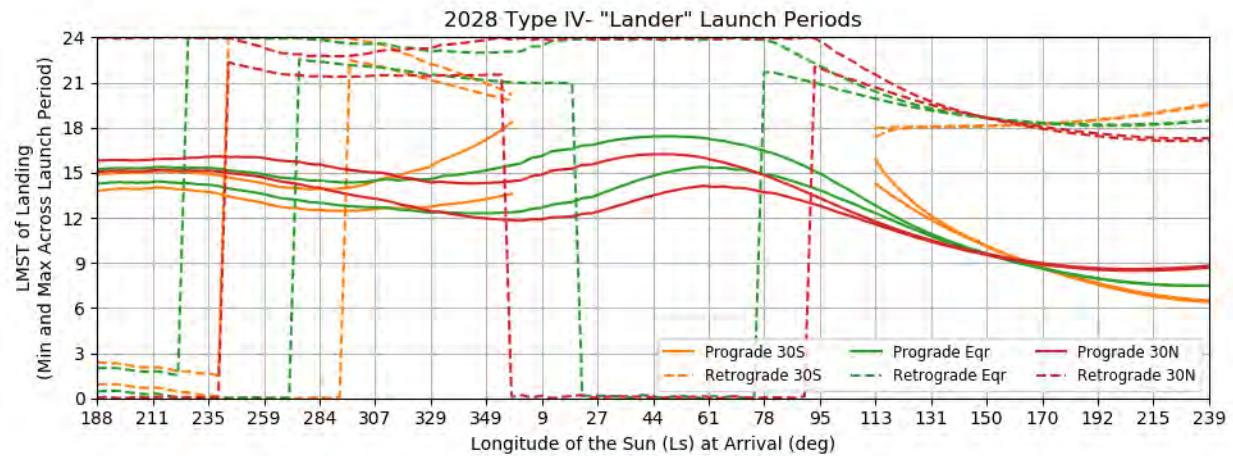


Figure 176: Earth to Mars 2028 Type III- Lander Launch Periods - Earth Elevation at Landing at Various Latitudes



**Figure 177: Earth to Mars 2028 Type IV- Lander Launch Periods - Reachable Latitudes, Equivalent C3, and VHP**



**Figure 178: Earth to Mars 2028 Type IV- Lander Launch Periods - LMST of Landing at Various Latitudes**

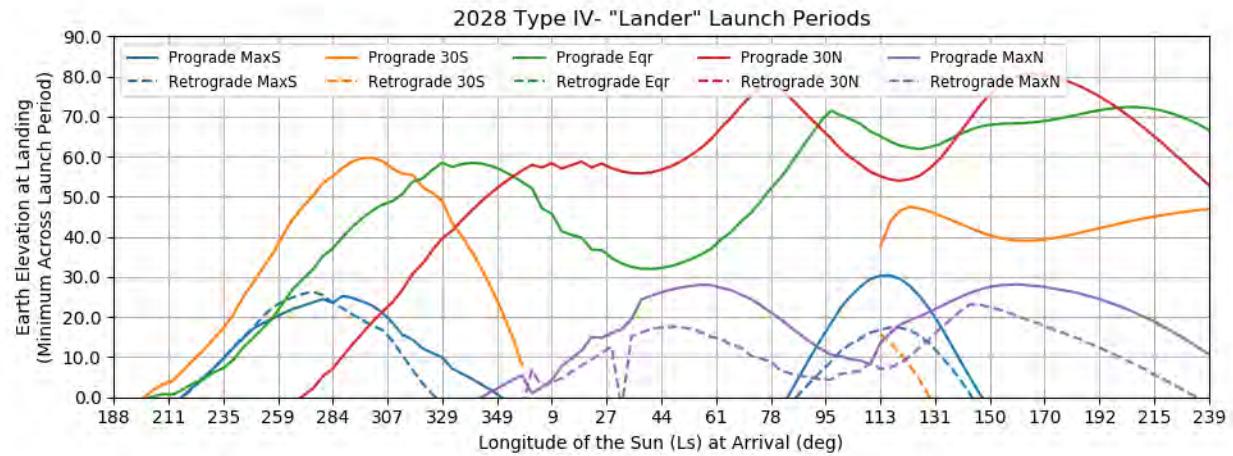


**Figure 179: Earth to Mars 2028 Type IV- Lander Launch Periods - Earth Elevation at Landing at Various Latitudes**

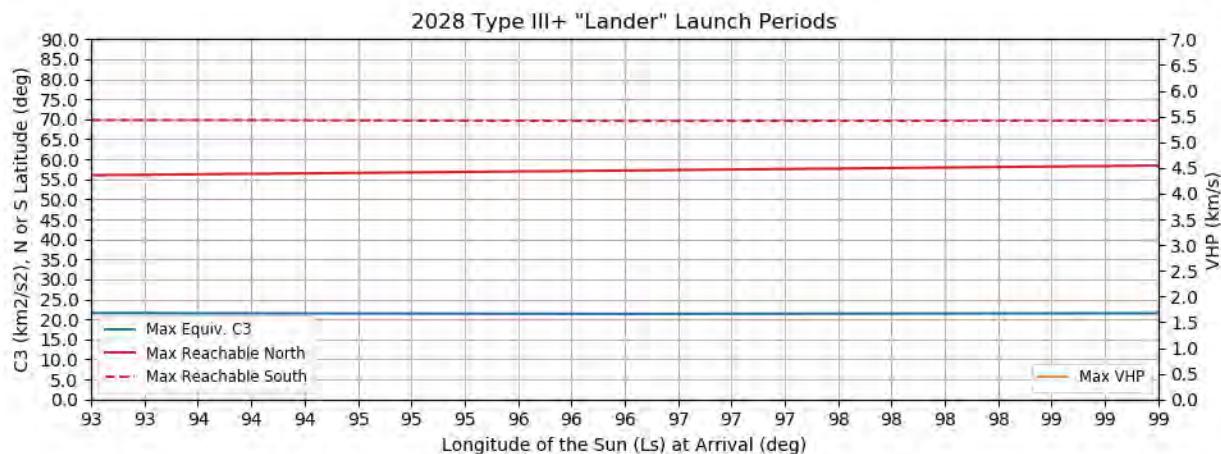


Figure 180: Earth to Mars 2028 Type III+ Lander Launch Periods - Reachable Latitudes, Equivalent C3, and VHP

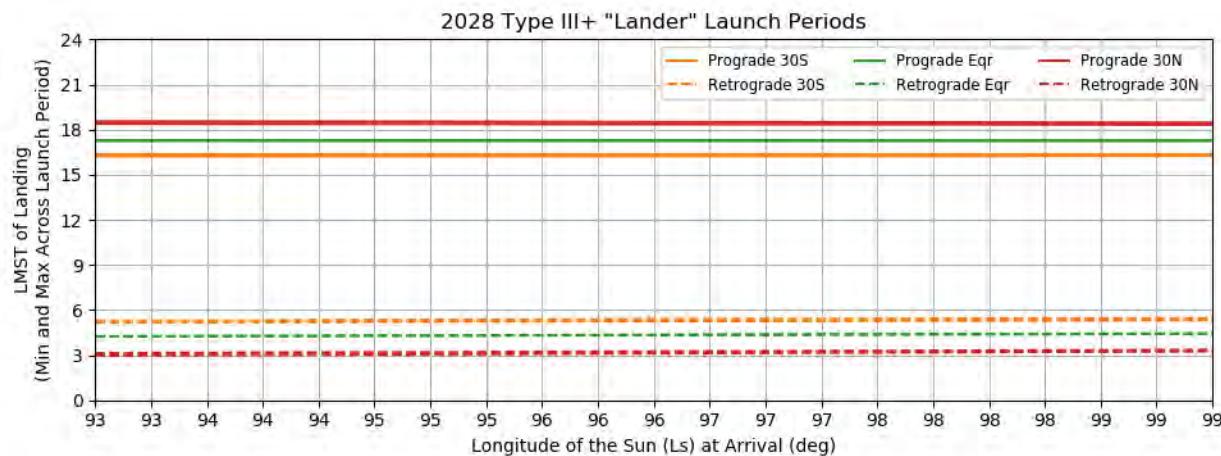


Figure 181: Earth to Mars 2028 Type III+ Lander Launch Periods - LMST of Landing at Various Latitudes

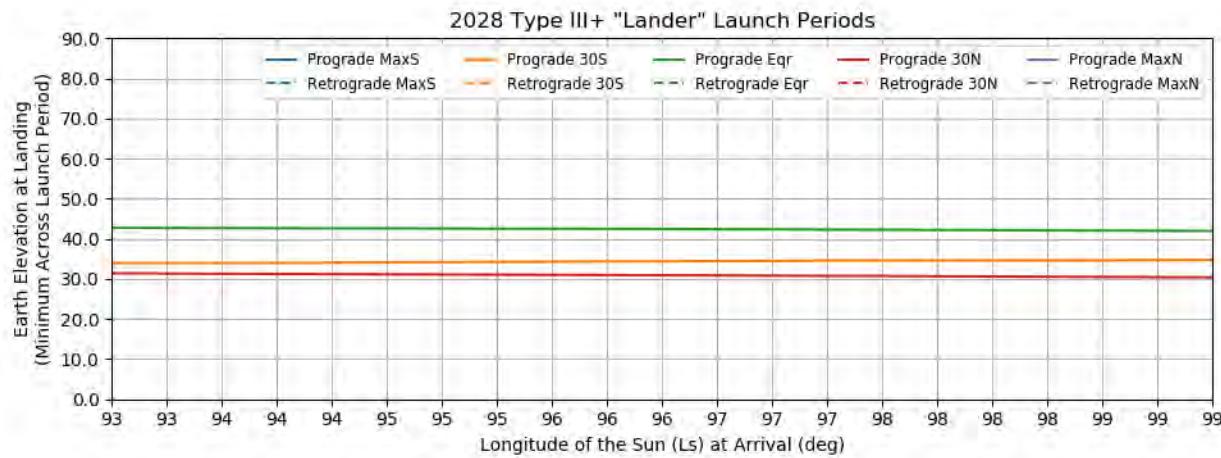


Figure 182: Earth to Mars 2028 Type III+ Lander Launch Periods - Earth Elevation at Landing at Various Latitudes

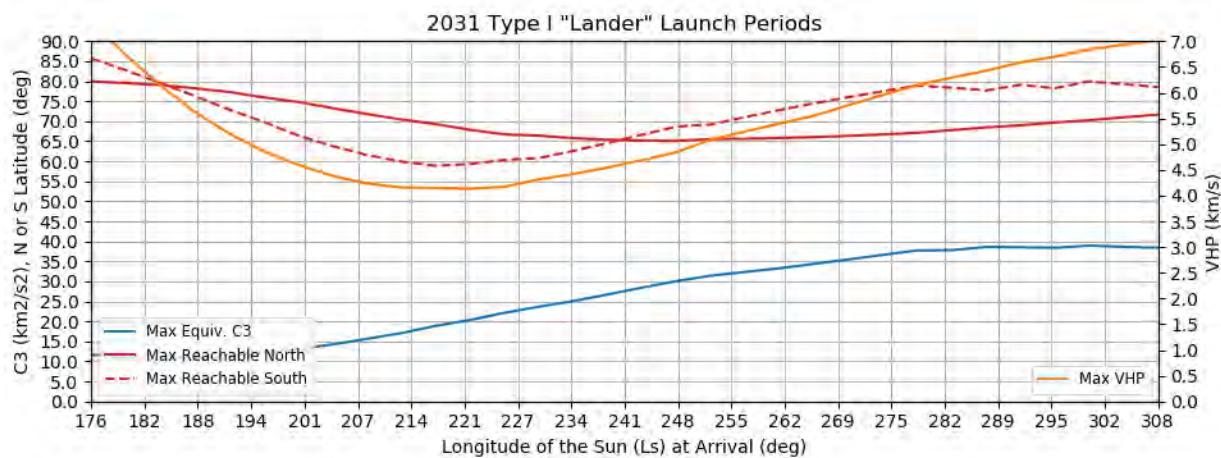


Figure 183: Earth to Mars 2031 Type I Lander Launch Periods - Reachable Latitudes, Equivalent C3, and VHP

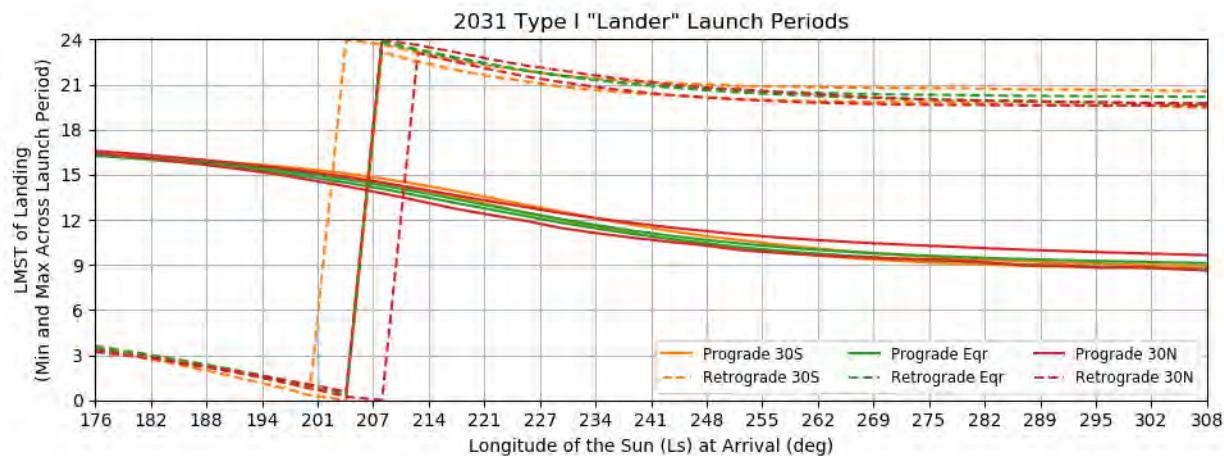


Figure 184: Earth to Mars 2031 Type I Lander Launch Periods - LMST of Landing at Various Latitudes

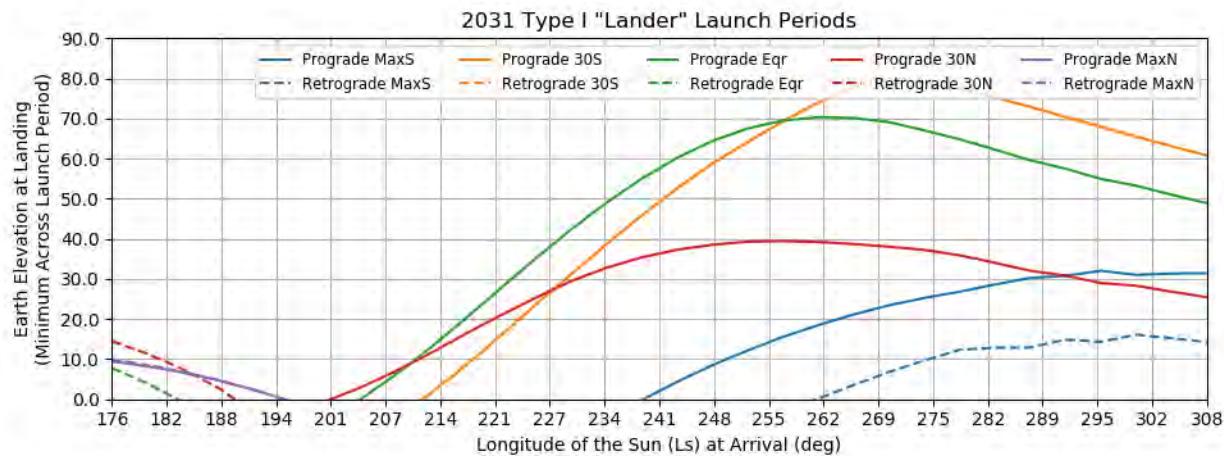


Figure 185: Earth to Mars 2031 Type I Lander Launch Periods - Earth Elevation at Landing at Various Latitudes

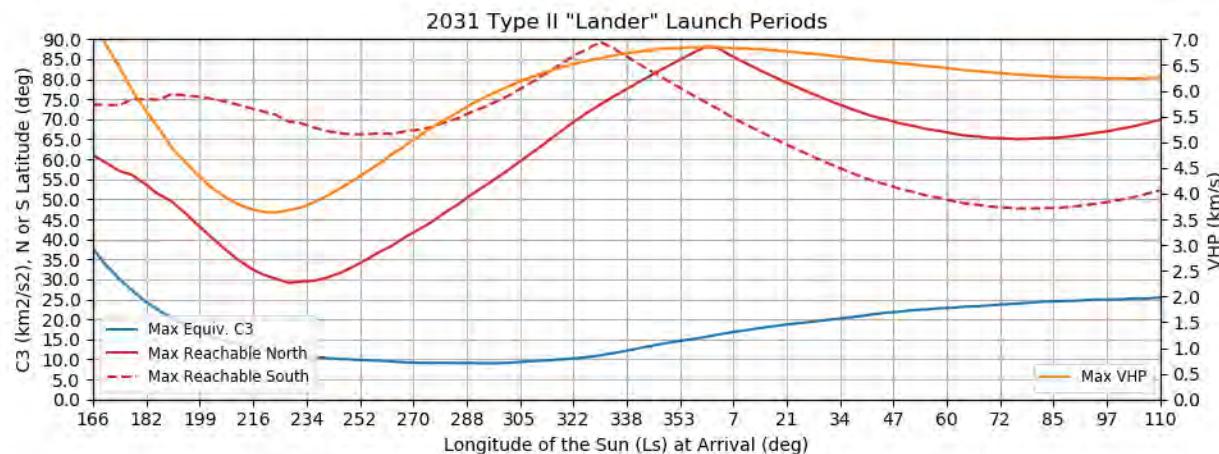


Figure 186: Earth to Mars 2031 Type II Lander Launch Periods - Reachable Latitudes, Equivalent C3, and VHP

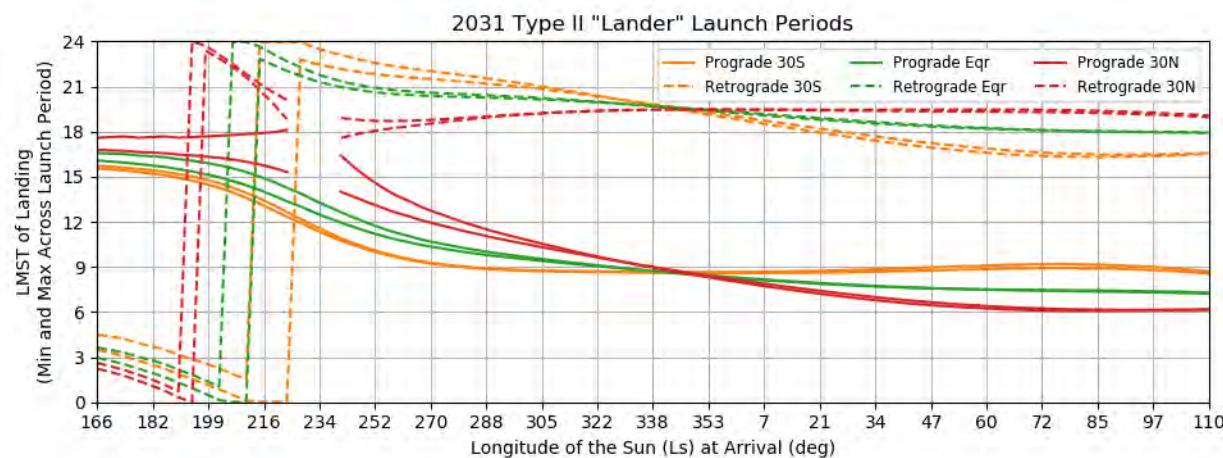


Figure 187: Earth to Mars 2031 Type II Lander Launch Periods - LMST of Landing at Various Latitudes

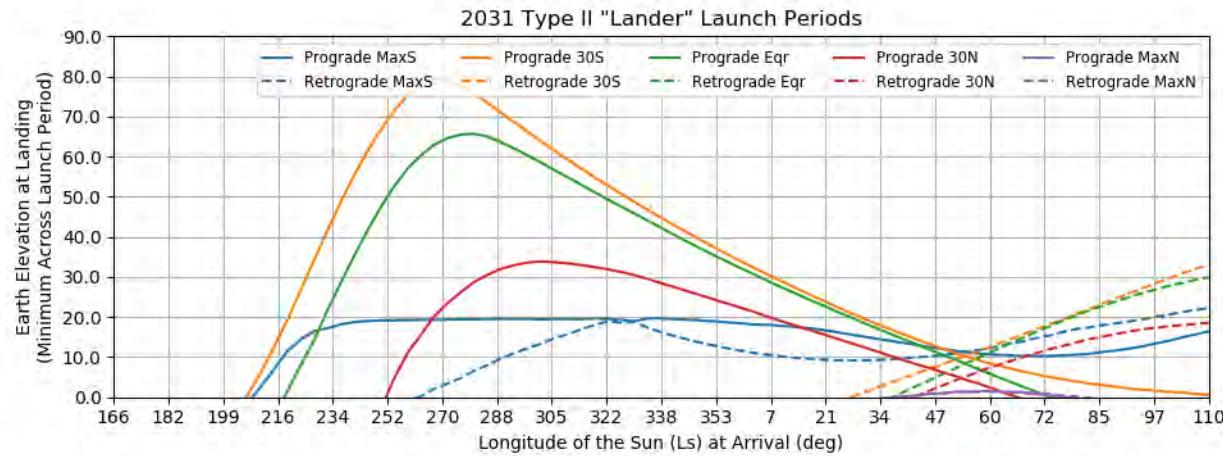


Figure 188: Earth to Mars 2031 Type II Lander Launch Periods - Earth Elevation at Landing at Various Latitudes

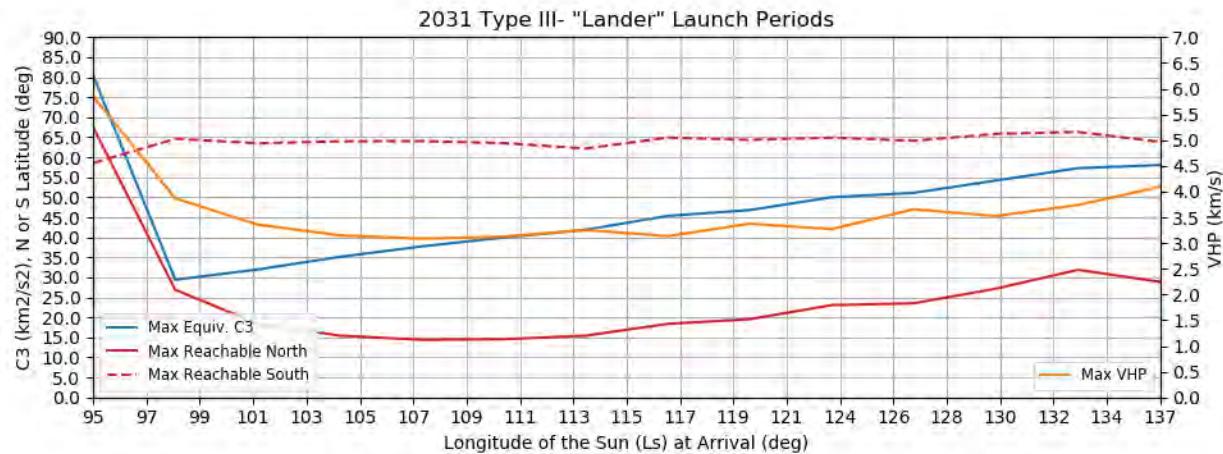


Figure 189: Earth to Mars 2031 Type III- Lander Launch Periods - Reachable Latitudes, Equivalent C3, and VHP

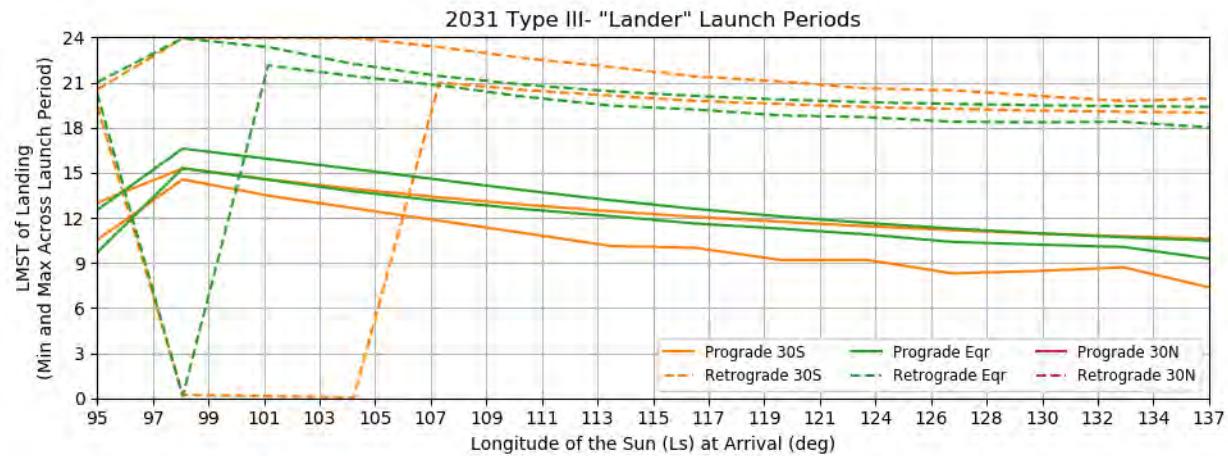


Figure 190: Earth to Mars 2031 Type III- Lander Launch Periods - LMST of Landing at Various Latitudes

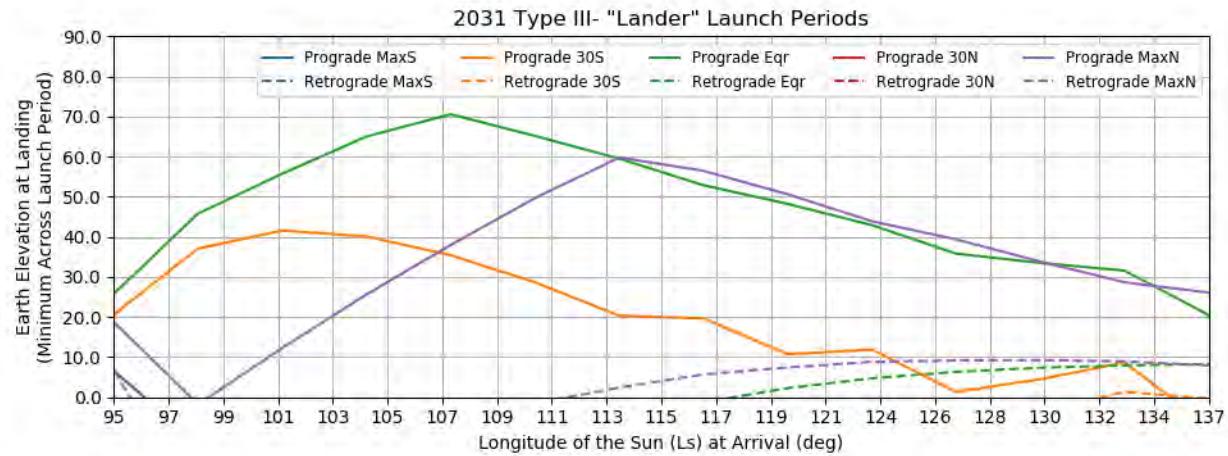
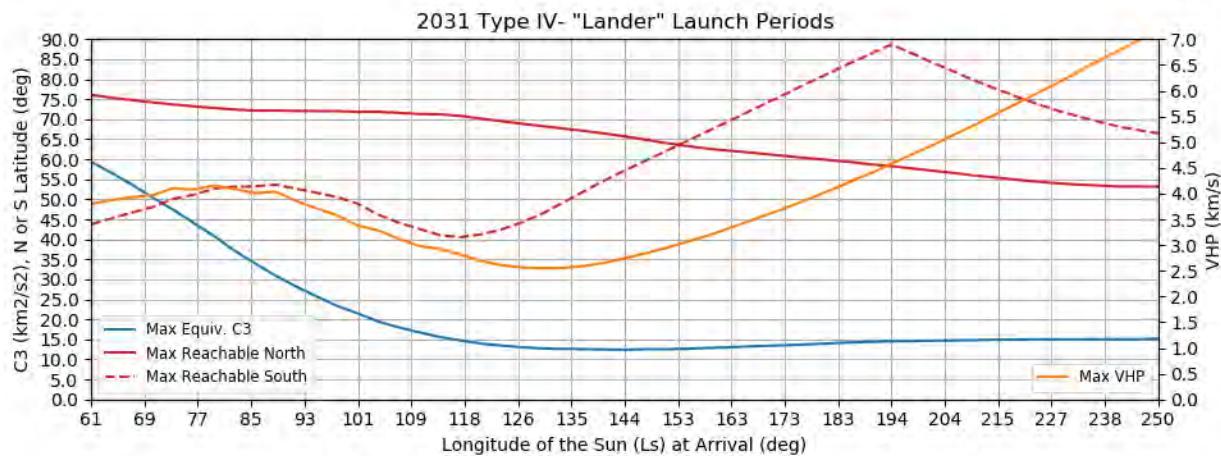
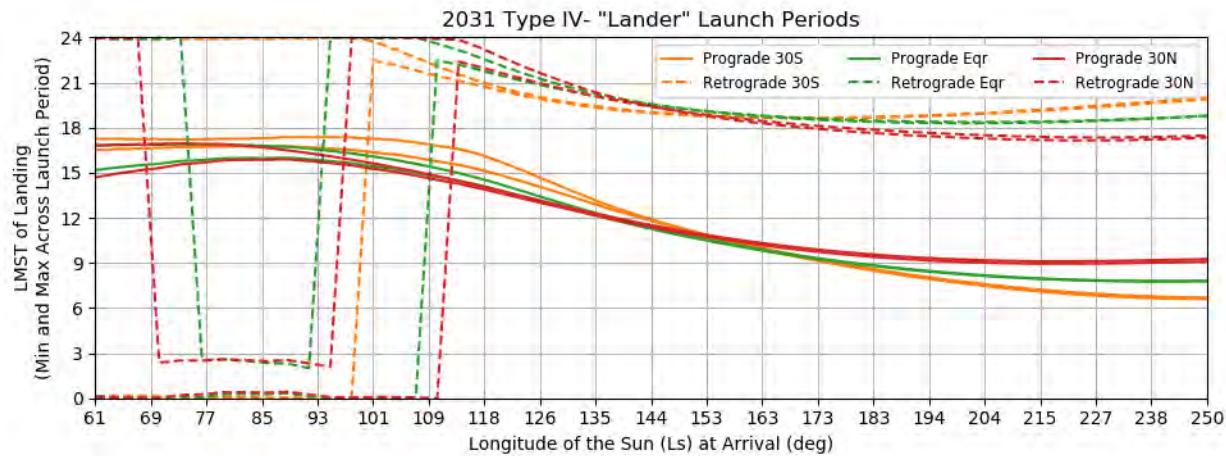


Figure 191: Earth to Mars 2031 Type III- Lander Launch Periods - Earth Elevation at Landing at Various Latitudes



**Figure 192: Earth to Mars 2031 Type IV- Lander Launch Periods - Reachable Latitudes, Equivalent C3, and VHP**



**Figure 193: Earth to Mars 2031 Type IV- Lander Launch Periods - LMST of Landing at Various Latitudes**

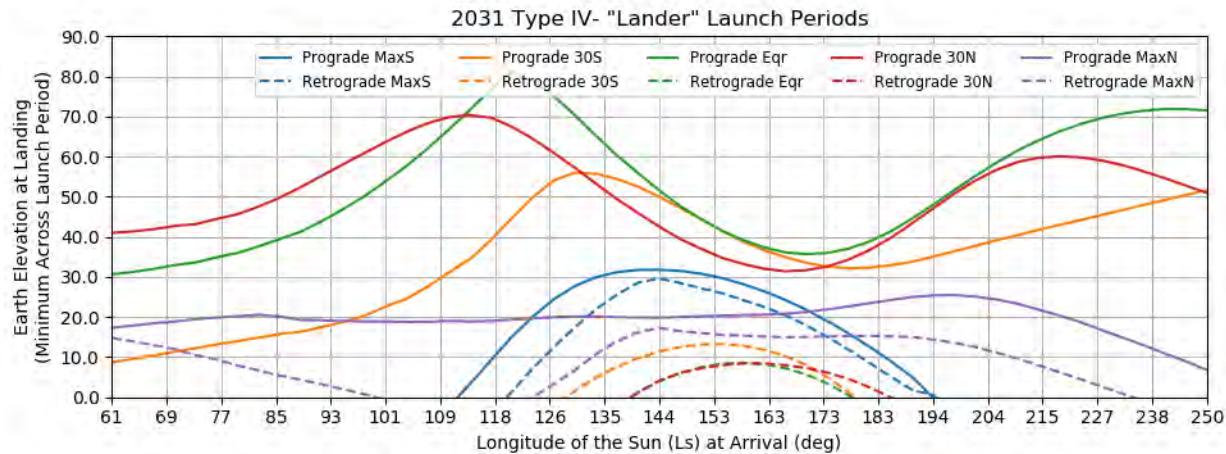


**Figure 194: Earth to Mars 2031 Type IV- Lander Launch Periods - Earth Elevation at Landing at Various Latitudes**

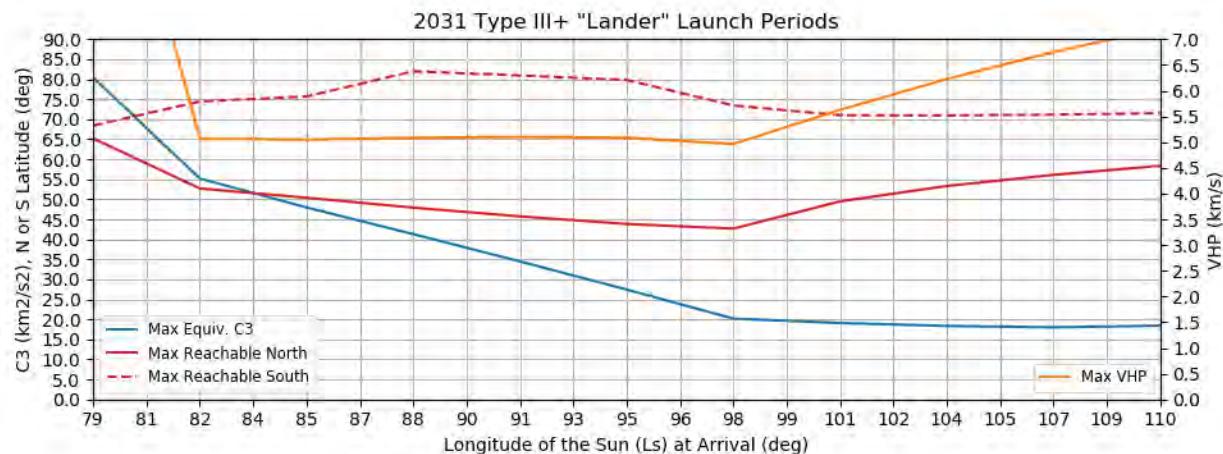


Figure 195: Earth to Mars 2031 Type III+ Lander Launch Periods - Reachable Latitudes, Equivalent C3, and VHP

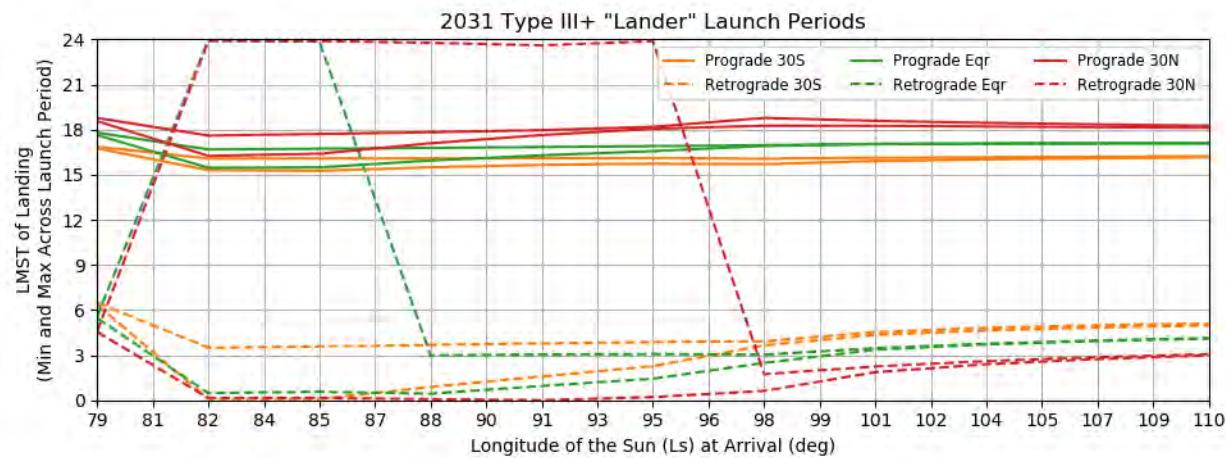


Figure 196: Earth to Mars 2031 Type III+ Lander Launch Periods - LMST of Landing at Various Latitudes

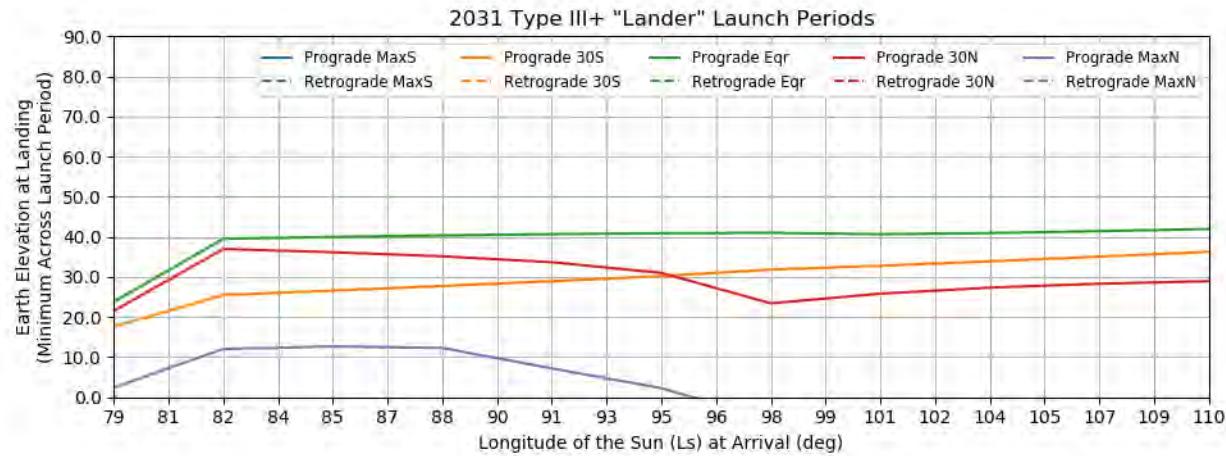
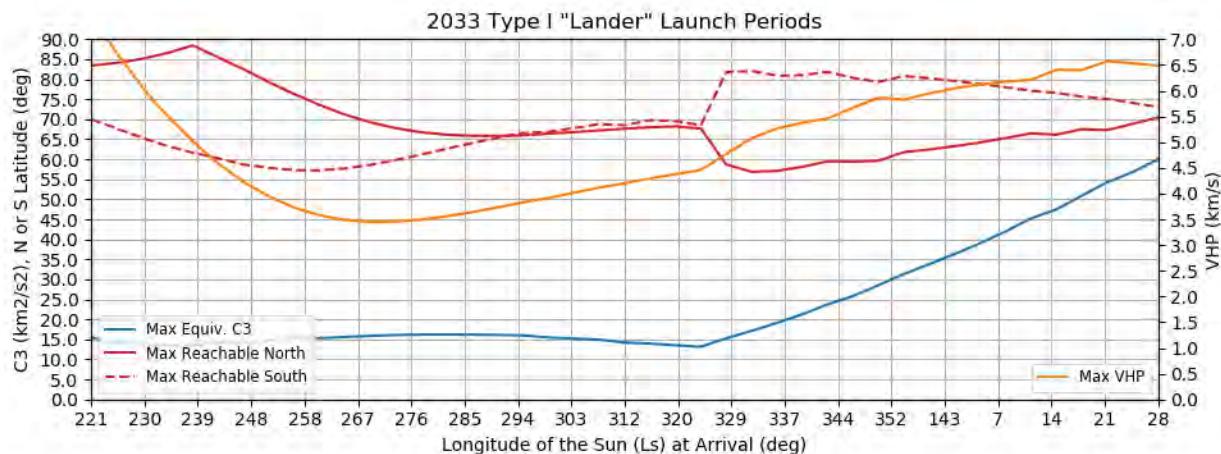
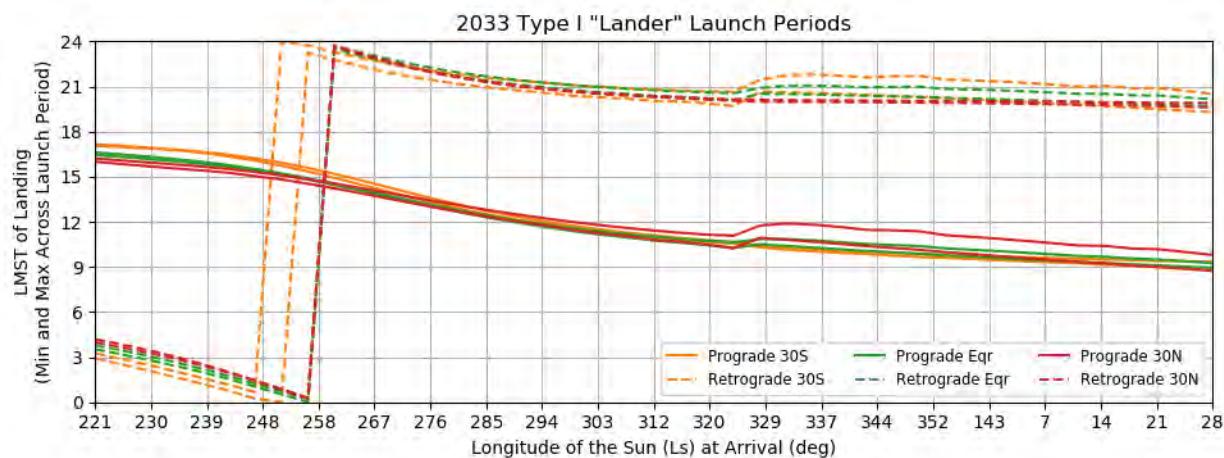


Figure 197: Earth to Mars 2031 Type III+ Lander Launch Periods - Earth Elevation at Landing at Various Latitudes



**Figure 198: Earth to Mars 2033 Type I Lander Launch Periods - Reachable Latitudes, Equivalent C3, and VHP**



**Figure 199: Earth to Mars 2033 Type I Lander Launch Periods - LMST of Landing at Various Latitudes**

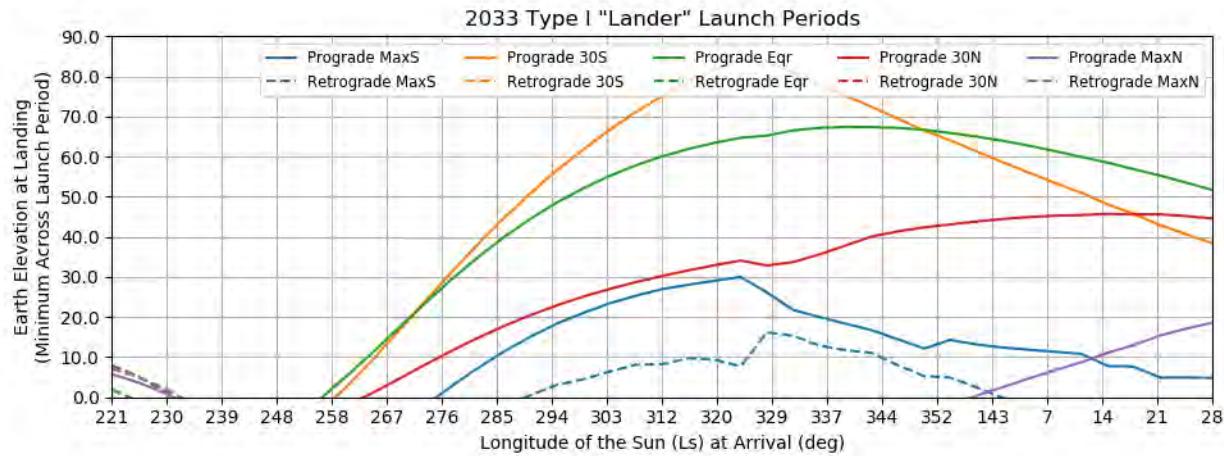


**Figure 200: Earth to Mars 2033 Type I Lander Launch Periods - Earth Elevation at Landing at Various Latitudes**

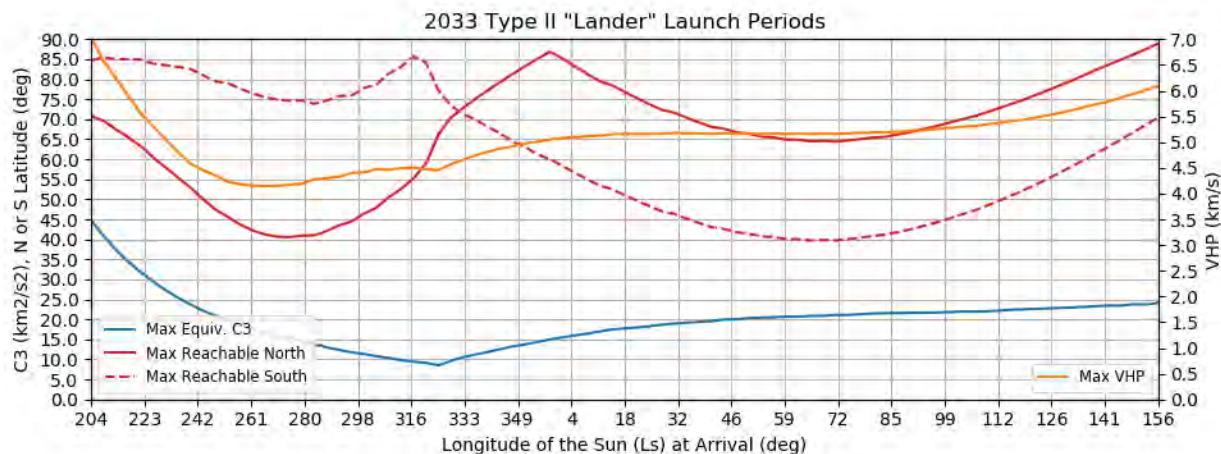


**Figure 201: Earth to Mars 2033 Type II Lander Launch Periods - Reachable Latitudes, Equivalent C3, and VHP**

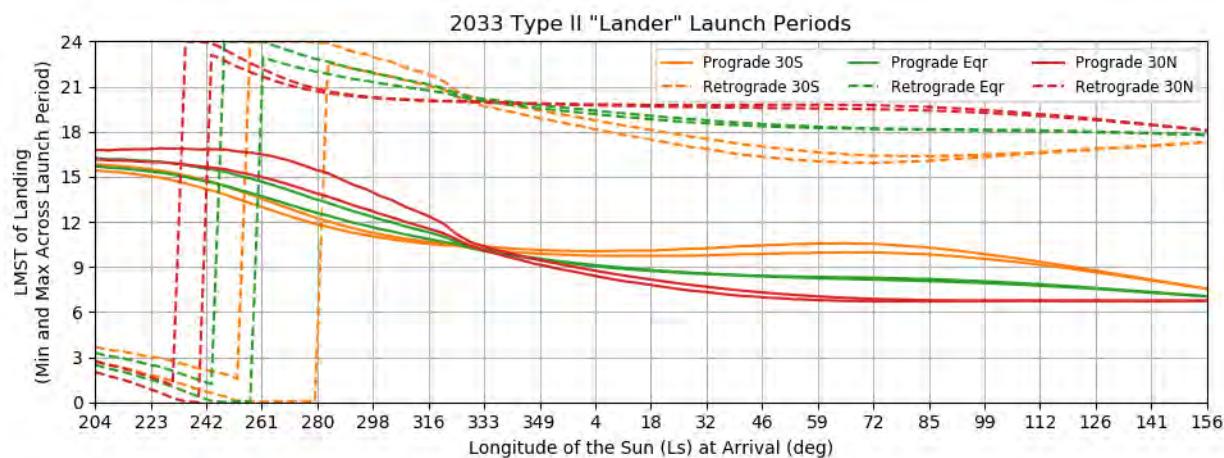


**Figure 202: Earth to Mars 2033 Type II Lander Launch Periods - LMST of Landing at Various Latitudes**

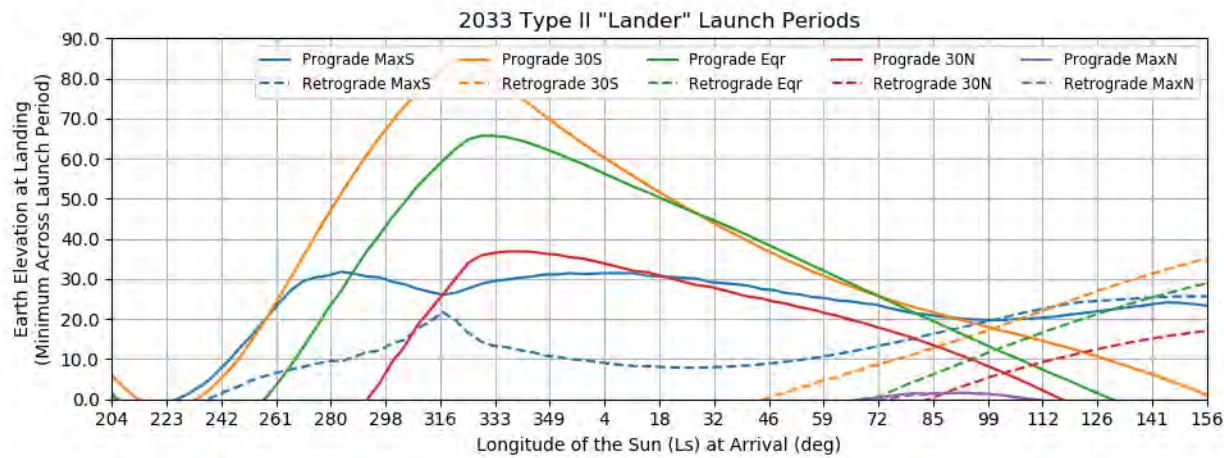


**Figure 203: Earth to Mars 2033 Type II Lander Launch Periods - Earth Elevation at Landing at Various Latitudes**

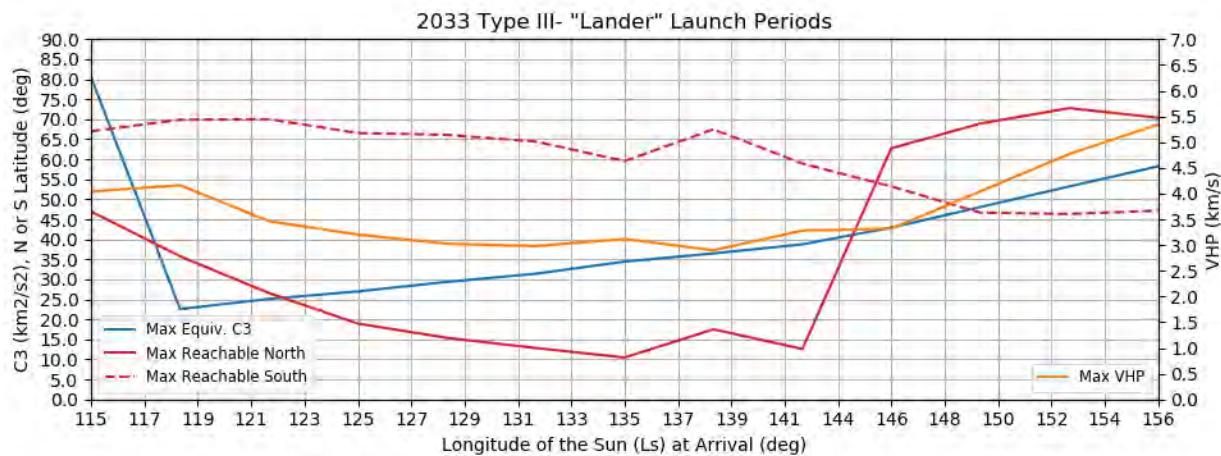


Figure 204: Earth to Mars 2033 Type III- Lander Launch Periods - Reachable Latitudes, Equivalent C3, and VHP

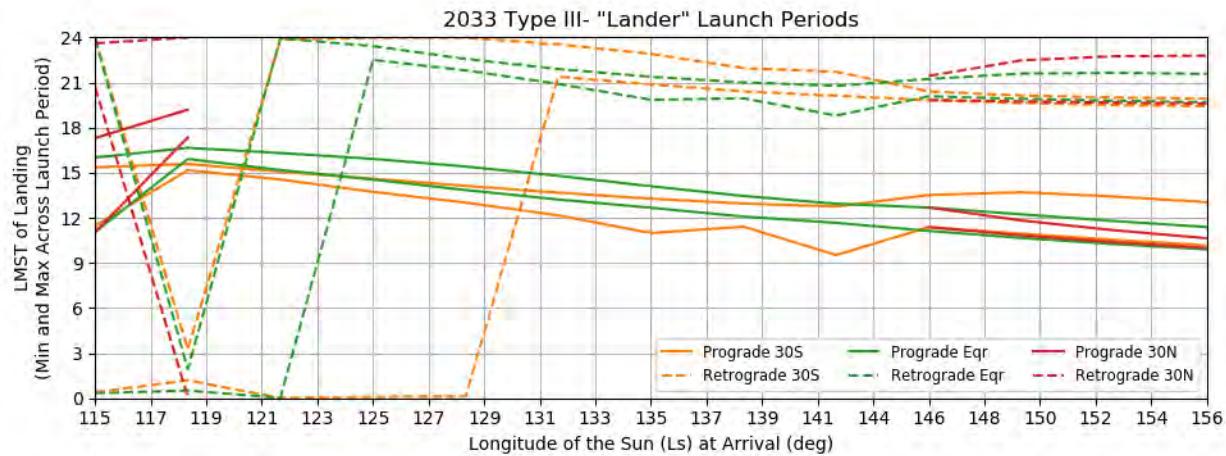


Figure 205: Earth to Mars 2033 Type III- Lander Launch Periods - LMST of Landing at Various Latitudes

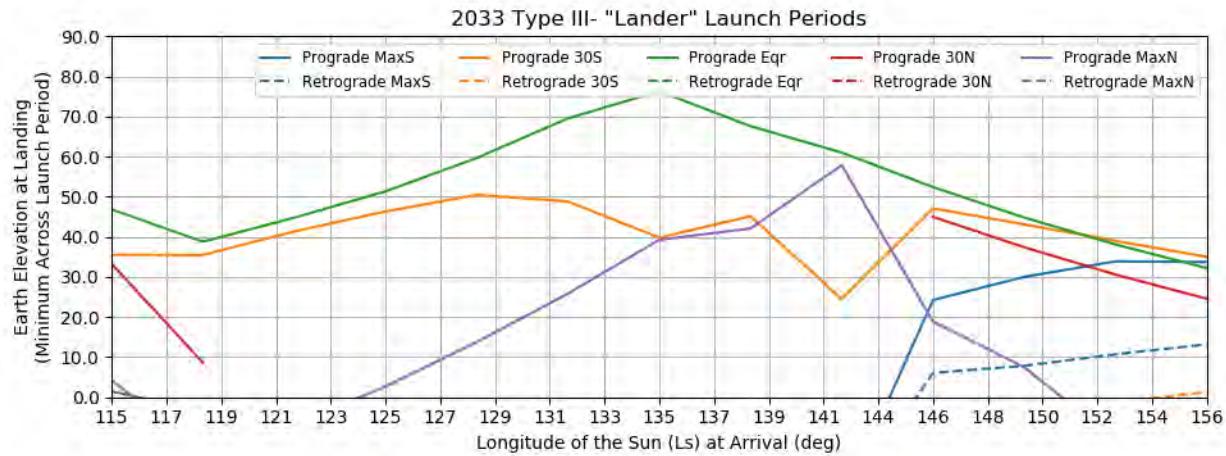
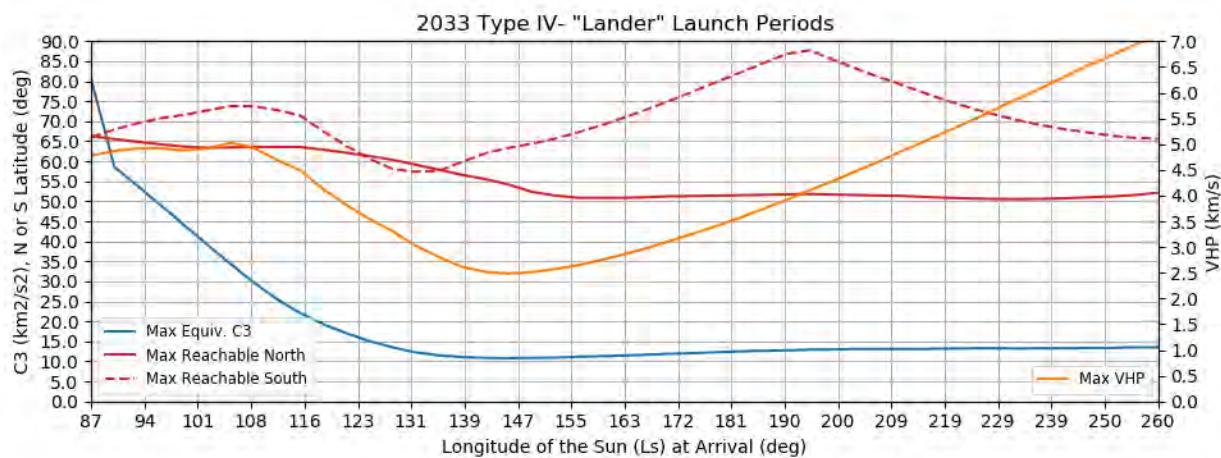
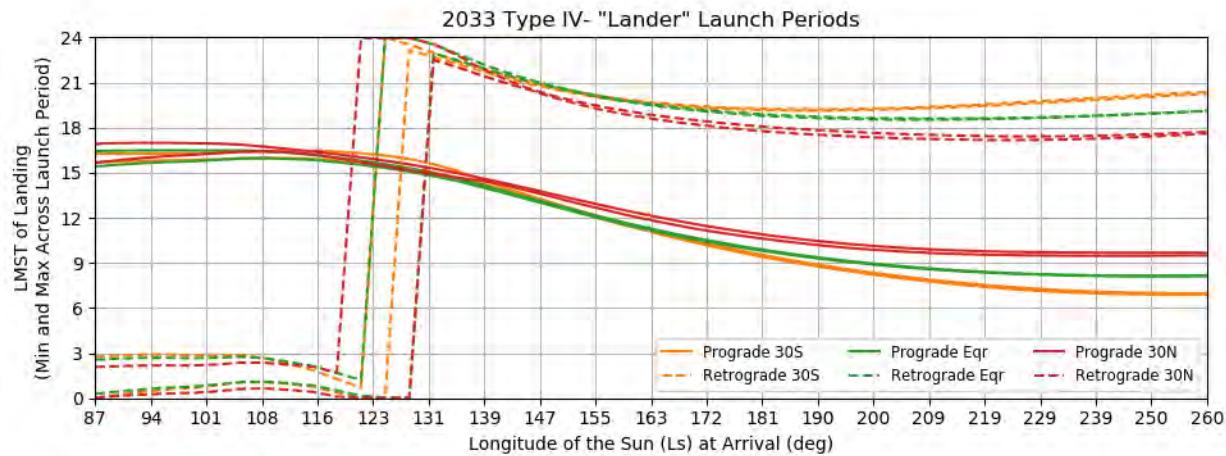


Figure 206: Earth to Mars 2033 Type III- Lander Launch Periods - Earth Elevation at Landing at Various Latitudes



**Figure 207: Earth to Mars 2033 Type IV- Lander Launch Periods - Reachable Latitudes, Equivalent C3, and VHP**



**Figure 208: Earth to Mars 2033 Type IV- Lander Launch Periods - LMST of Landing at Various Latitudes**

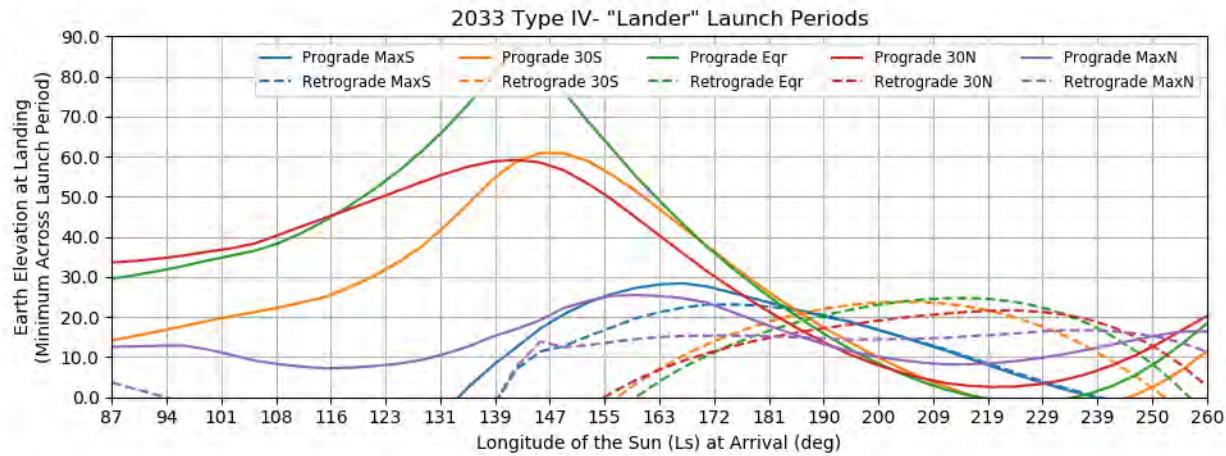


**Figure 209: Earth to Mars 2033 Type IV- Lander Launch Periods - Earth Elevation at Landing at Various Latitudes**

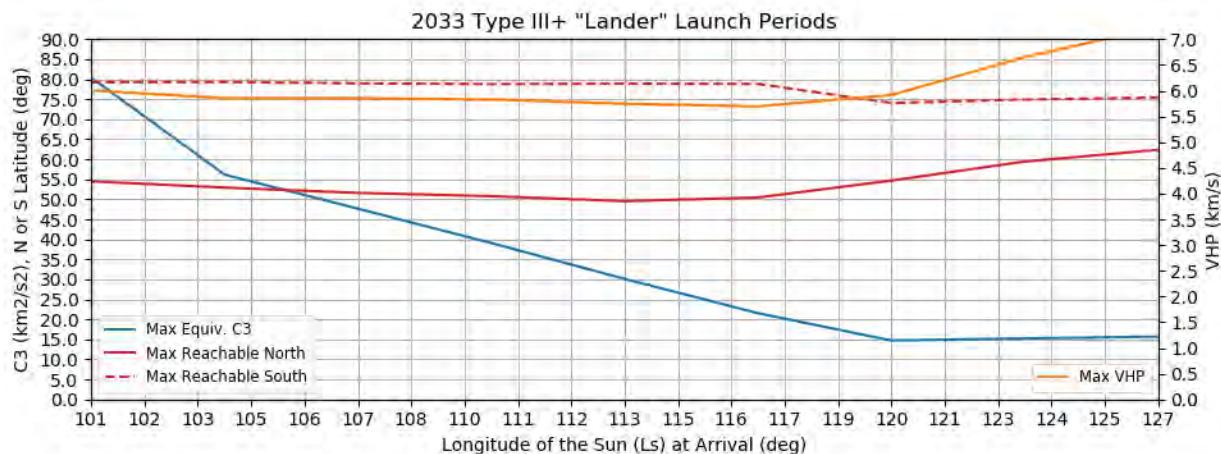


Figure 210: Earth to Mars 2033 Type III+ Lander Launch Periods - Reachable Latitudes, Equivalent C3, and VHP

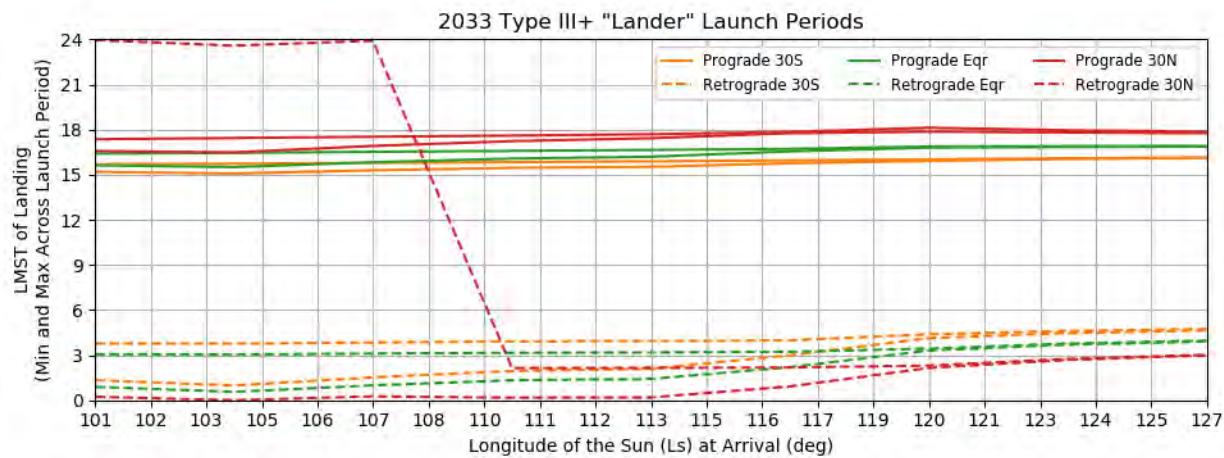


Figure 211: Earth to Mars 2033 Type III+ Lander Launch Periods - LMST of Landing at Various Latitudes

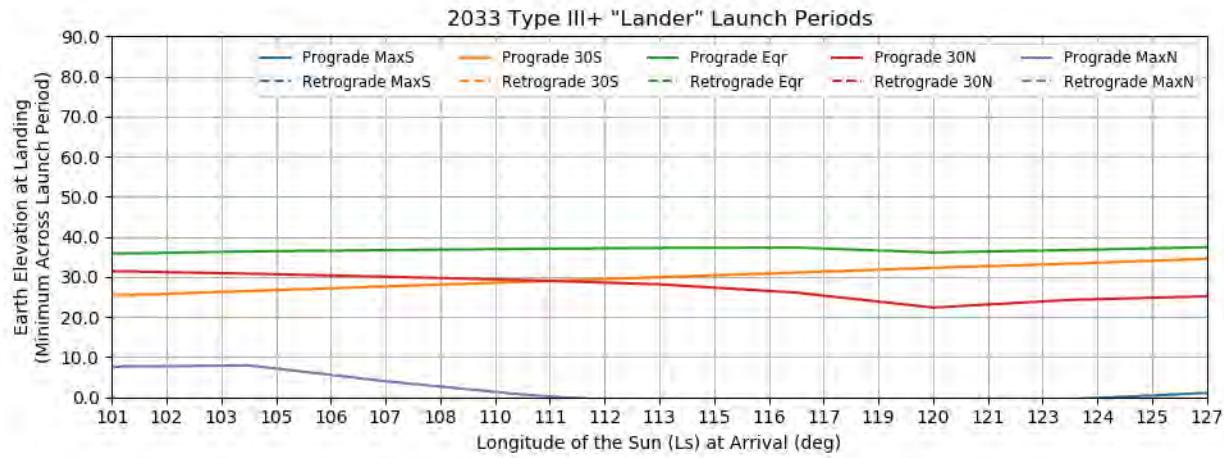


Figure 212: Earth to Mars 2033 Type III+ Lander Launch Periods - Earth Elevation at Landing at Various Latitudes

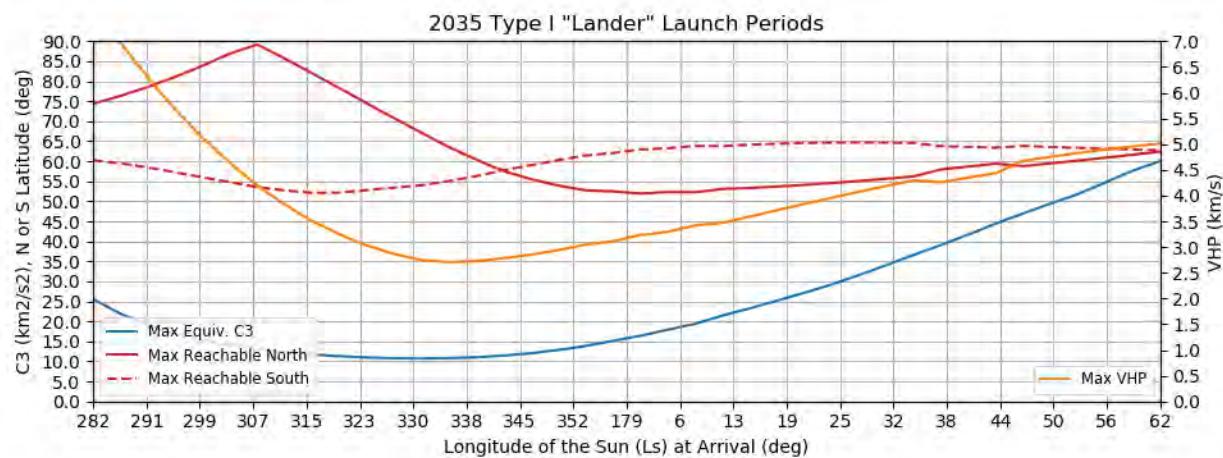


Figure 213: Earth to Mars 2035 Type I Lander Launch Periods - Reachable Latitudes, Equivalent C3, and VHP

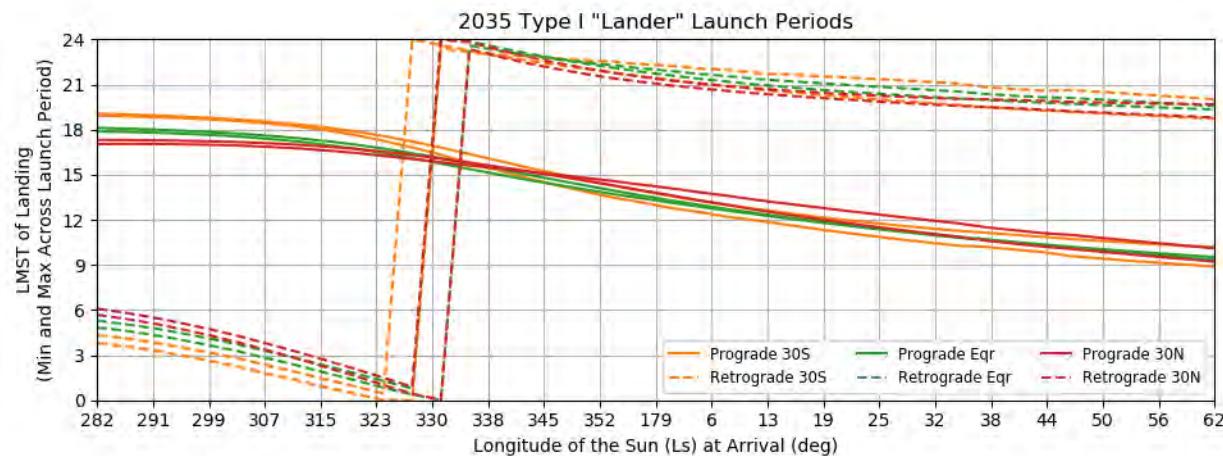


Figure 214: Earth to Mars 2035 Type I Lander Launch Periods - LMST of Landing at Various Latitudes

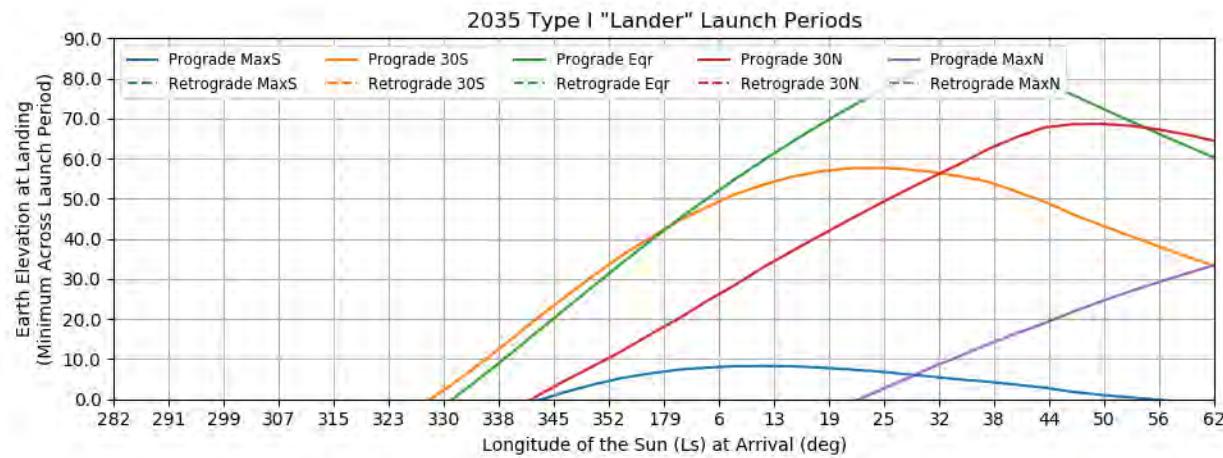


Figure 215: Earth to Mars 2035 Type I Lander Launch Periods - Earth Elevation at Landing at Various Latitudes

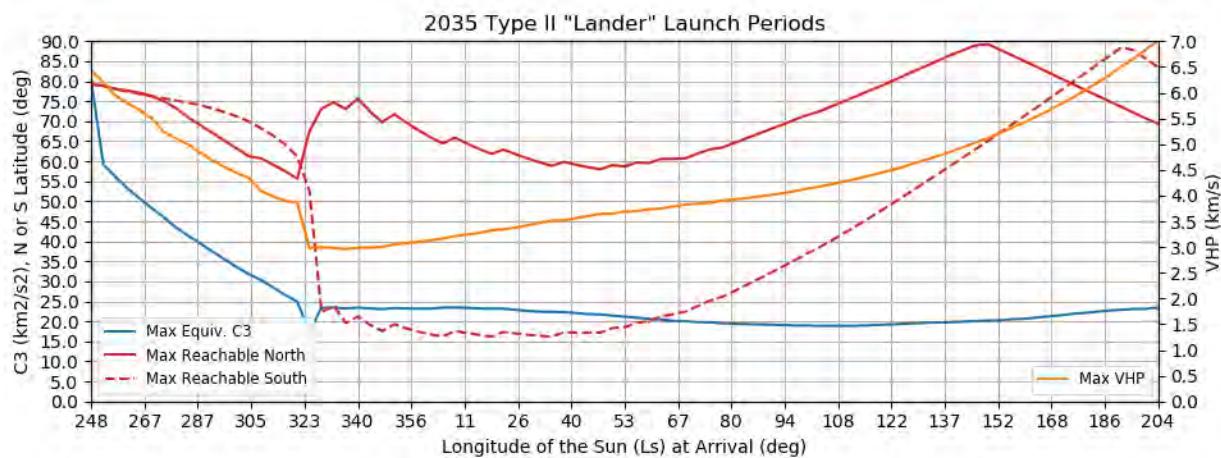


Figure 216: Earth to Mars 2035 Type II Lander Launch Periods - Reachable Latitudes, Equivalent C3, and VHP

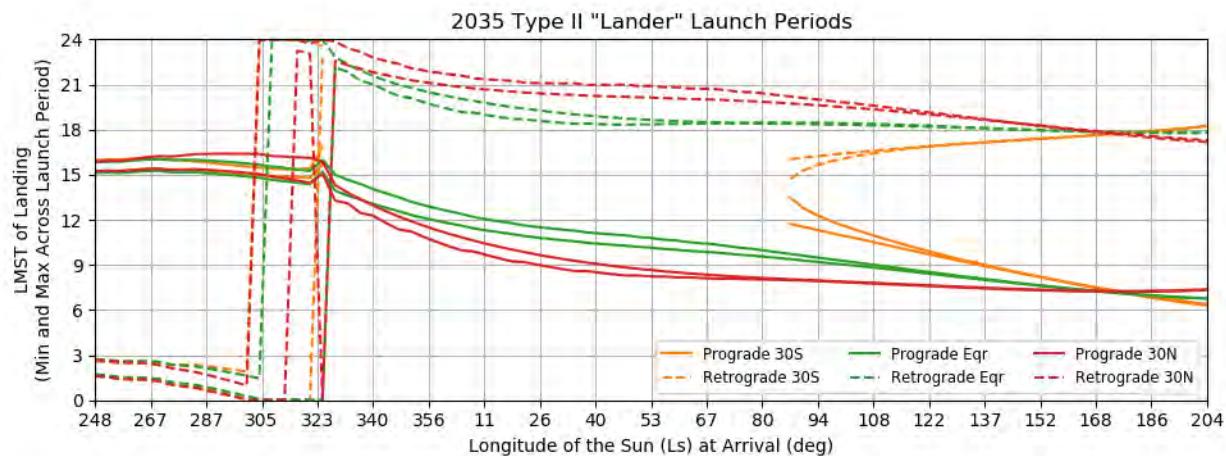


Figure 217: Earth to Mars 2035 Type II Lander Launch Periods - LMST of Landing at Various Latitudes

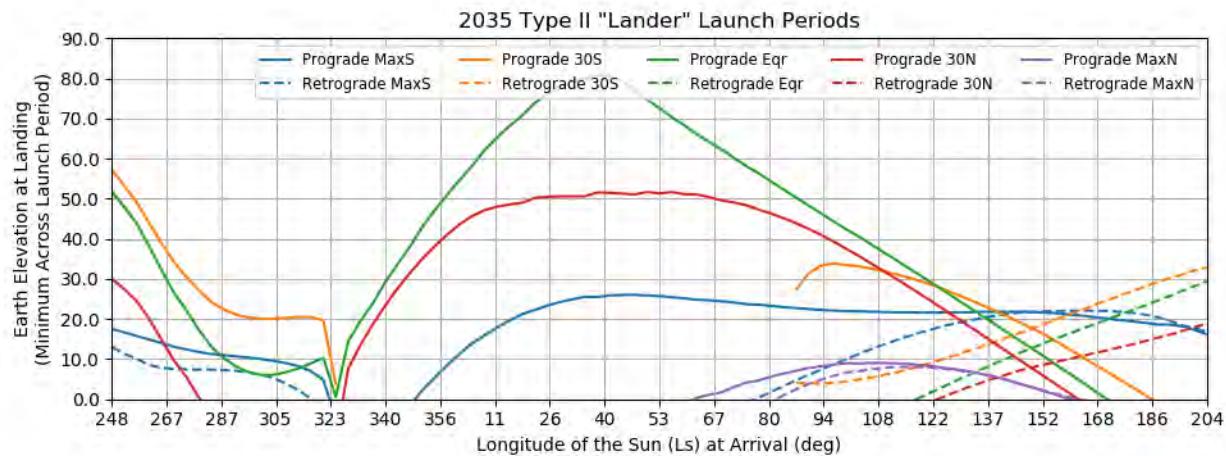


Figure 218: Earth to Mars 2035 Type II Lander Launch Periods - Earth Elevation at Landing at Various Latitudes

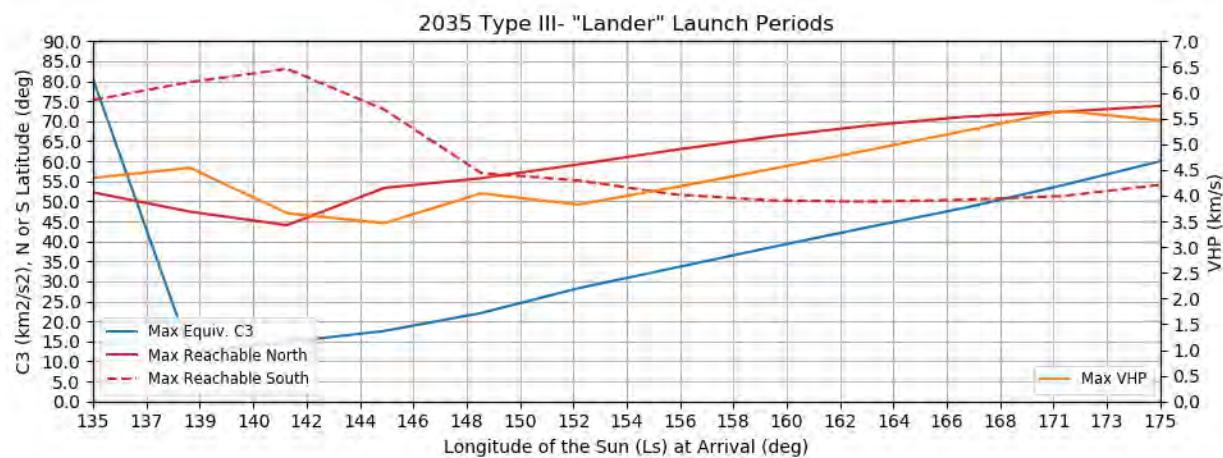


Figure 219: Earth to Mars 2035 Type III- Lander Launch Periods - Reachable Latitudes, Equivalent C3, and VHP

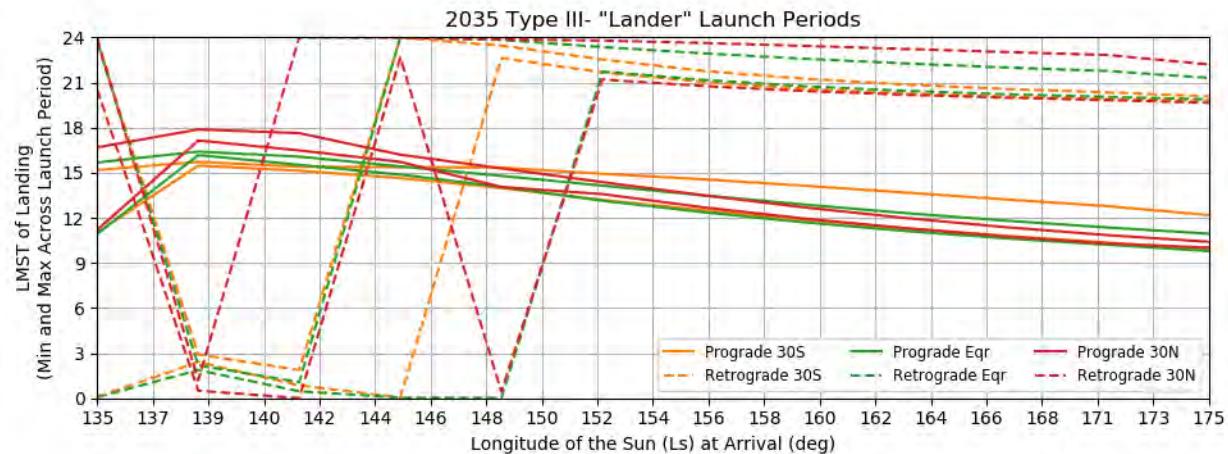


Figure 220: Earth to Mars 2035 Type III- Lander Launch Periods - LMST of Landing at Various Latitudes

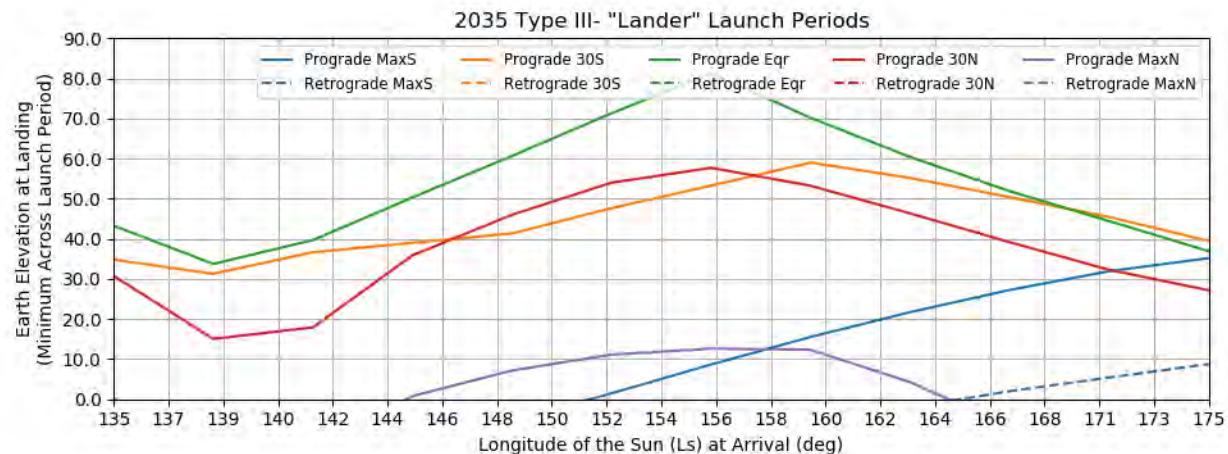


Figure 221: Earth to Mars 2035 Type III- Lander Launch Periods - Earth Elevation at Landing at Various Latitudes

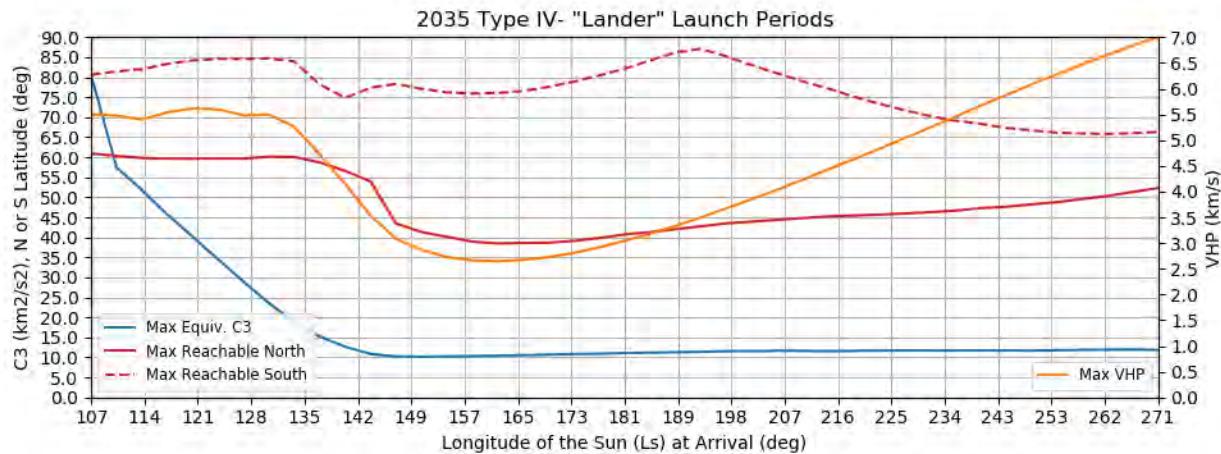


Figure 222: Earth to Mars 2035 Type IV- Lander Launch Periods - Reachable Latitudes, Equivalent C3, and VHP

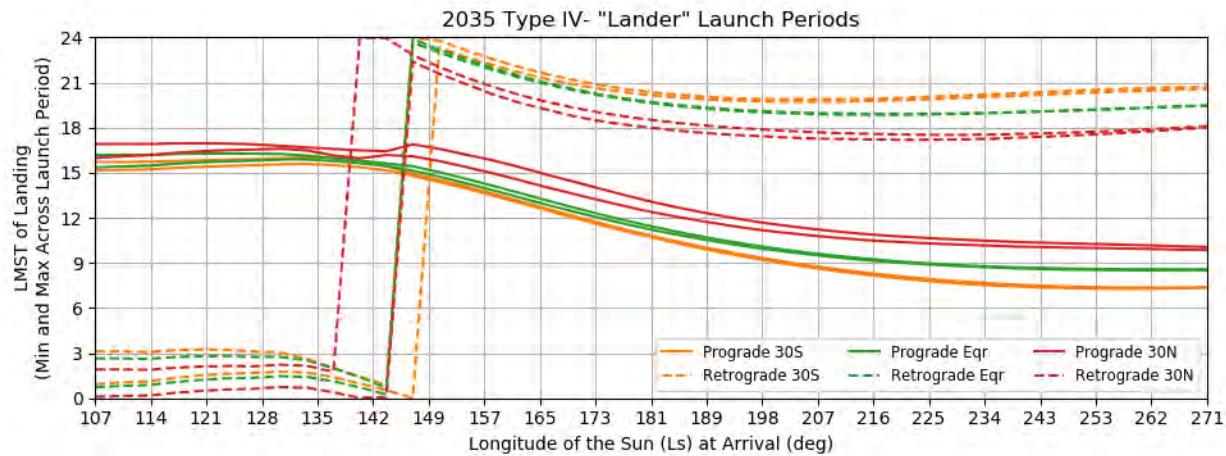


Figure 223: Earth to Mars 2035 Type IV- Lander Launch Periods - LMST of Landing at Various Latitudes

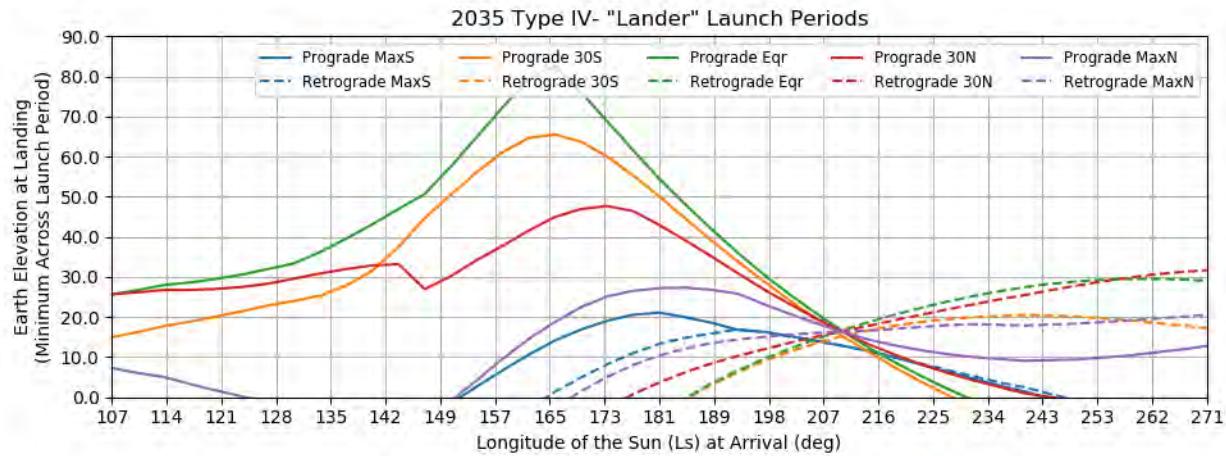


Figure 224: Earth to Mars 2035 Type IV- Lander Launch Periods - Earth Elevation at Landing at Various Latitudes

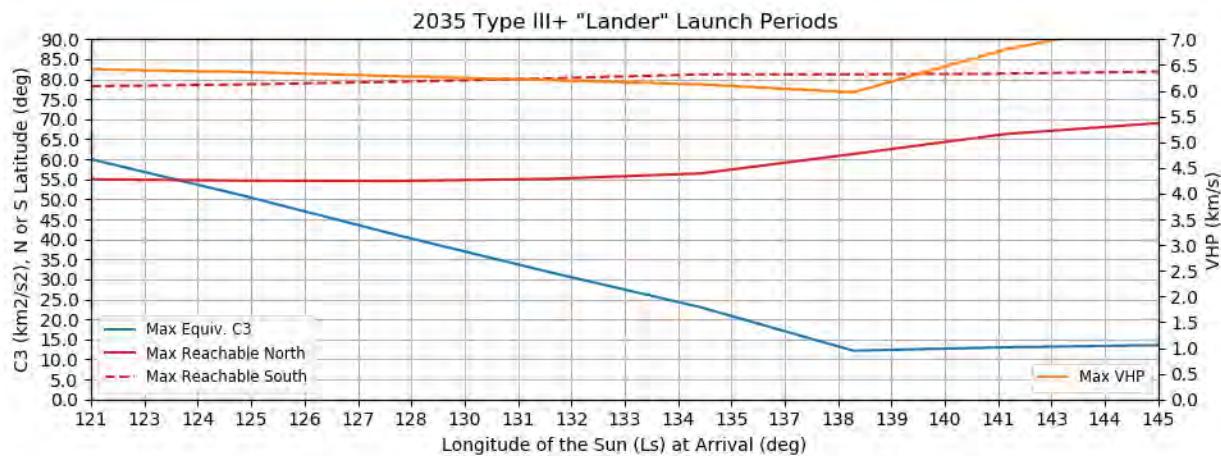


Figure 225: Earth to Mars 2035 Type III+ Lander Launch Periods - Reachable Latitudes, Equivalent C3, and VHP

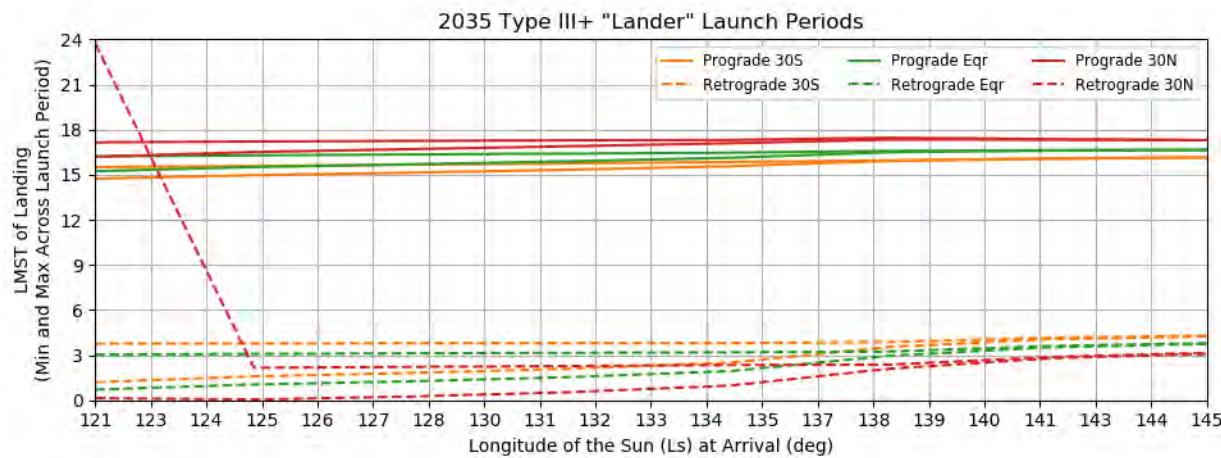


Figure 226: Earth to Mars 2035 Type III+ Lander Launch Periods - LMST of Landing at Various Latitudes

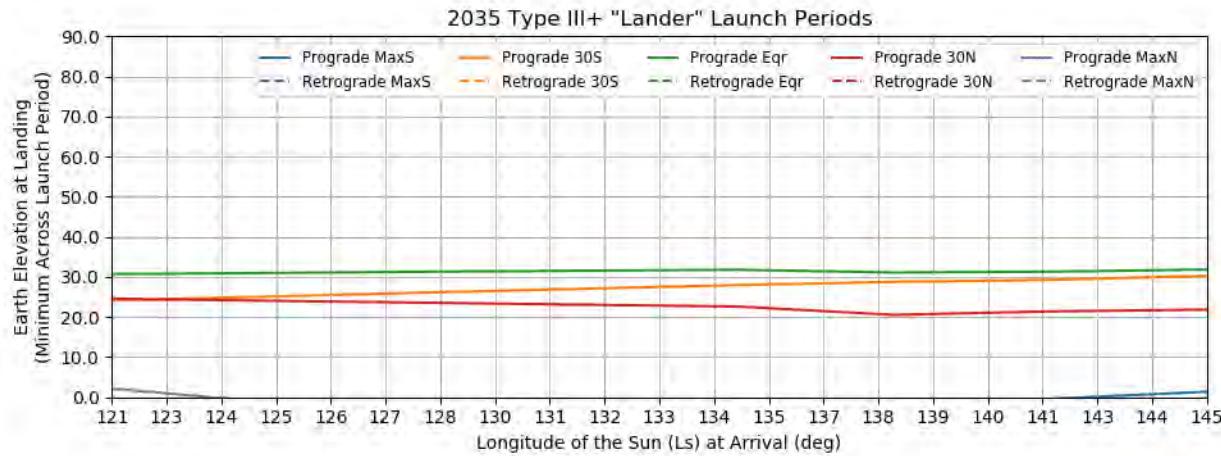
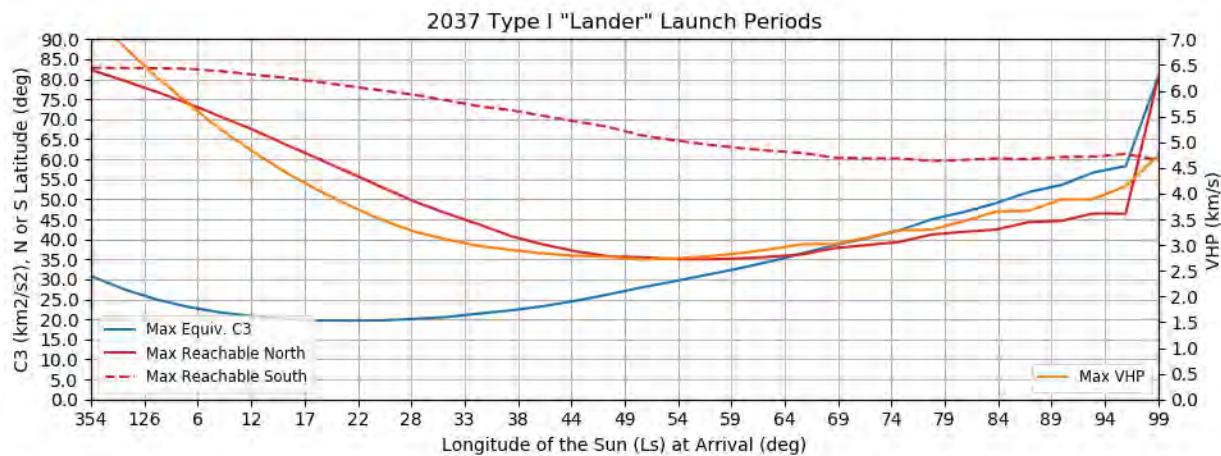
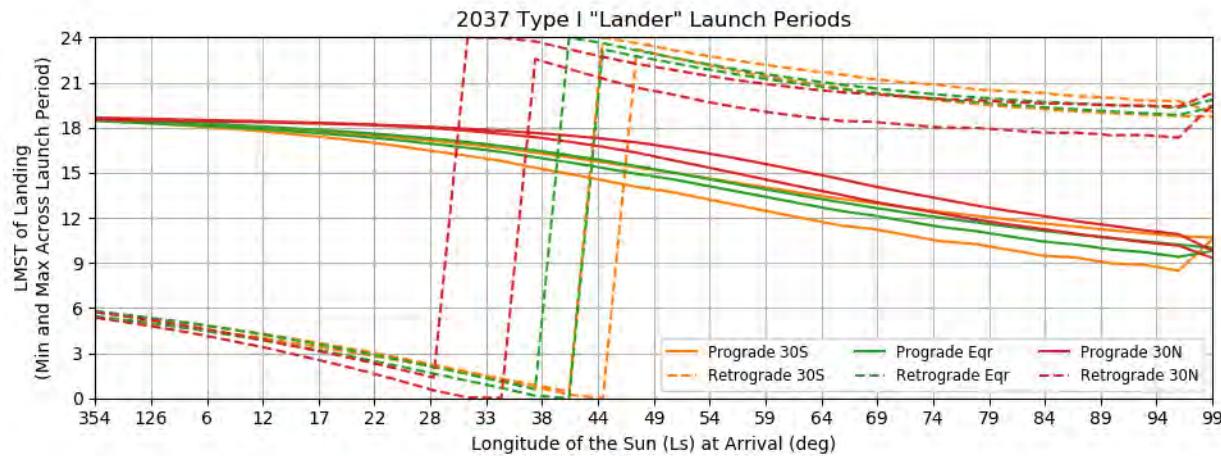


Figure 227: Earth to Mars 2035 Type III+ Lander Launch Periods - Earth Elevation at Landing at Various Latitudes



**Figure 228: Earth to Mars 2037 Type I Lander Launch Periods - Reachable Latitudes, Equivalent C3, and VHP**



**Figure 229: Earth to Mars 2037 Type I Lander Launch Periods - LMST of Landing at Various Latitudes**

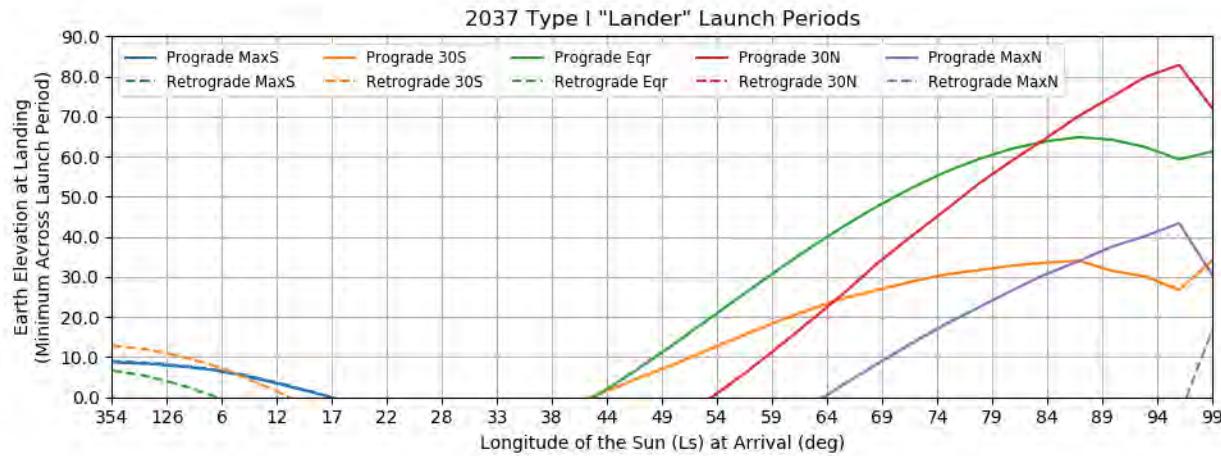


**Figure 230: Earth to Mars 2037 Type I Lander Launch Periods - Earth Elevation at Landing at Various Latitudes**

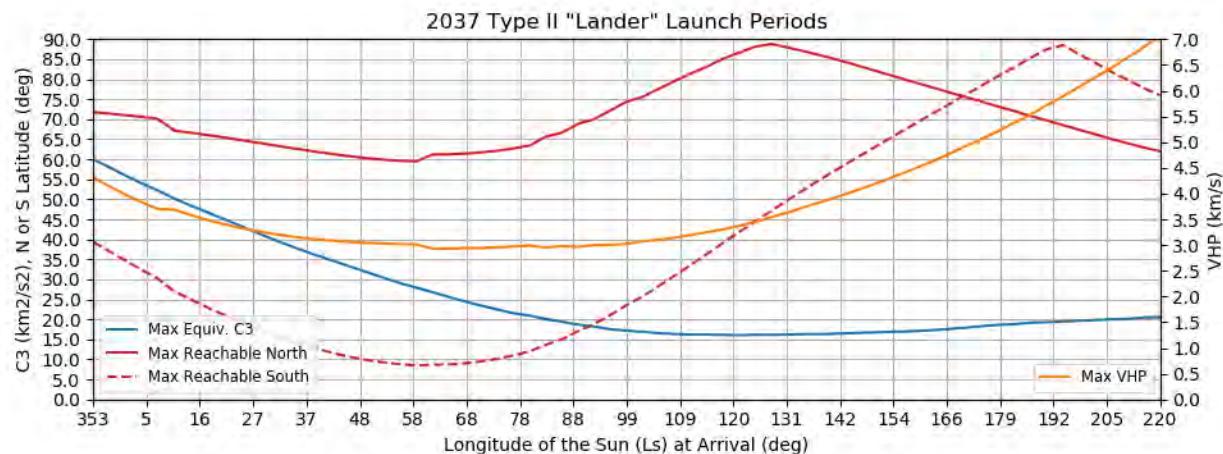


Figure 231: Earth to Mars 2037 Type II Lander Launch Periods - Reachable Latitudes, Equivalent C3, and VHP

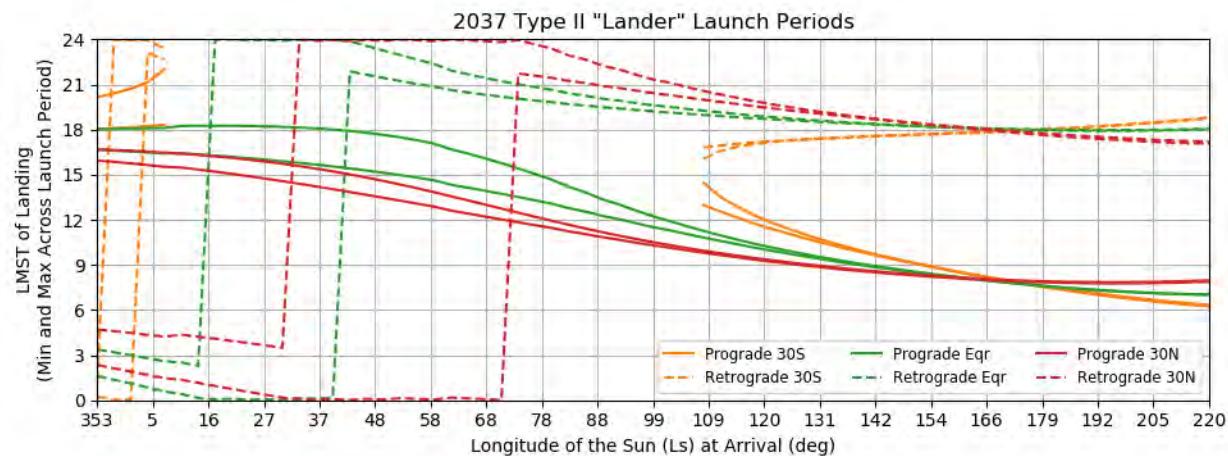


Figure 232: Earth to Mars 2037 Type II Lander Launch Periods - LMST of Landing at Various Latitudes

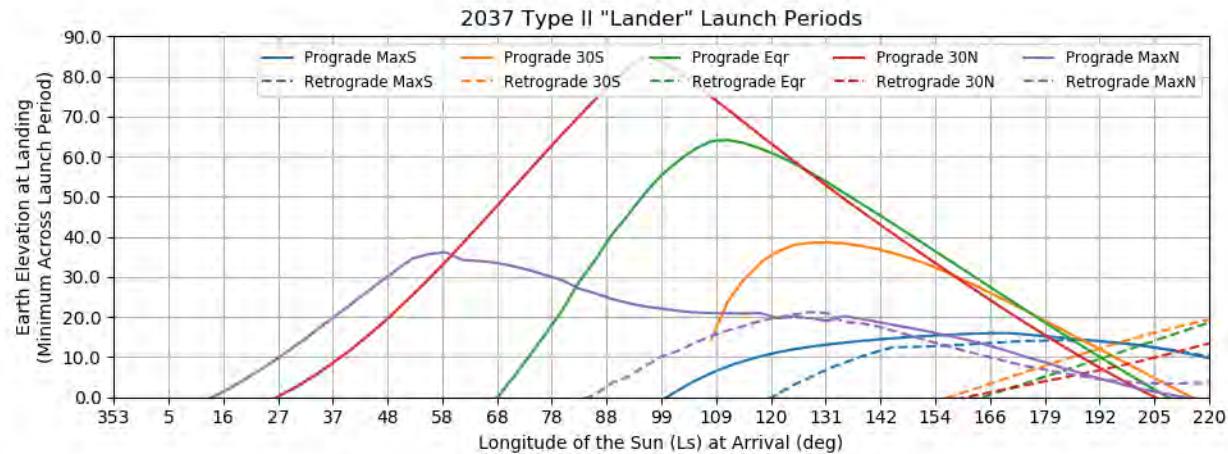


Figure 233: Earth to Mars 2037 Type II Lander Launch Periods - Earth Elevation at Landing at Various Latitudes

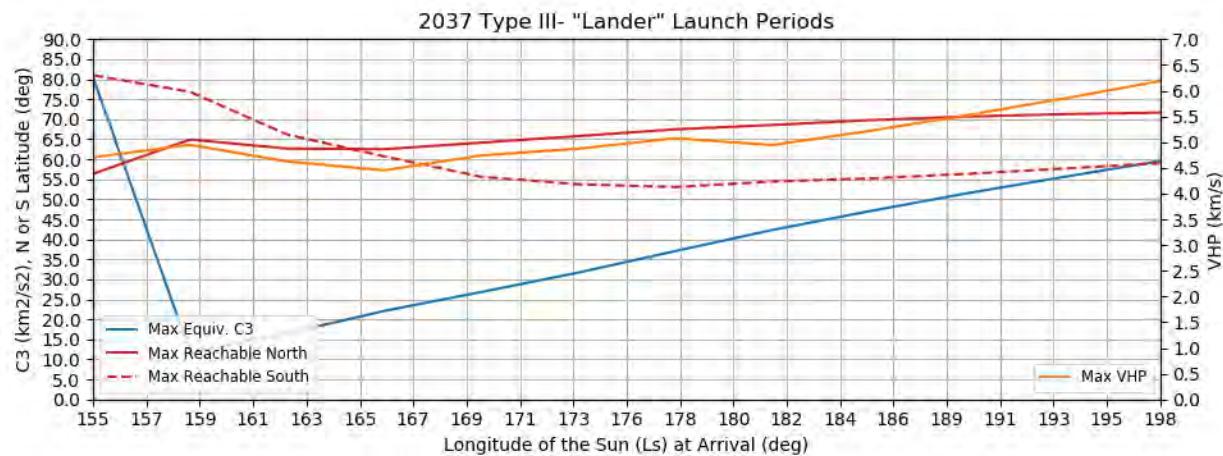


Figure 234: Earth to Mars 2037 Type III- Lander Launch Periods - Reachable Latitudes, Equivalent C3, and VHP

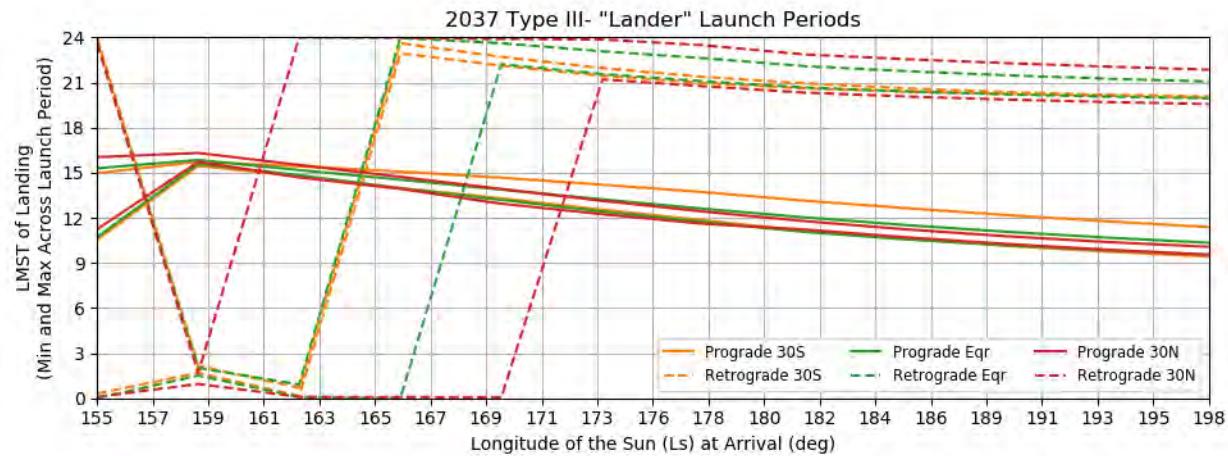


Figure 235: Earth to Mars 2037 Type III- Lander Launch Periods - LMST of Landing at Various Latitudes

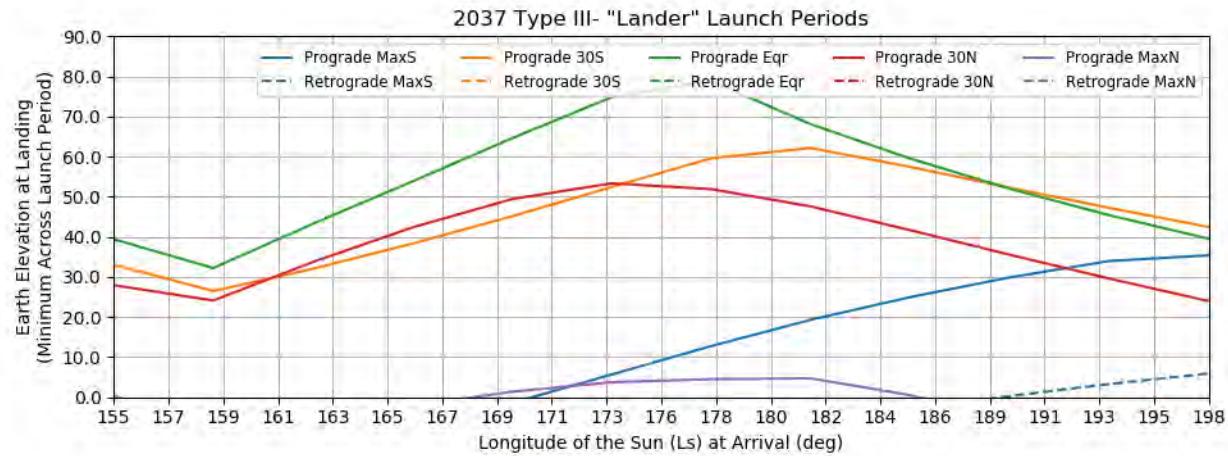
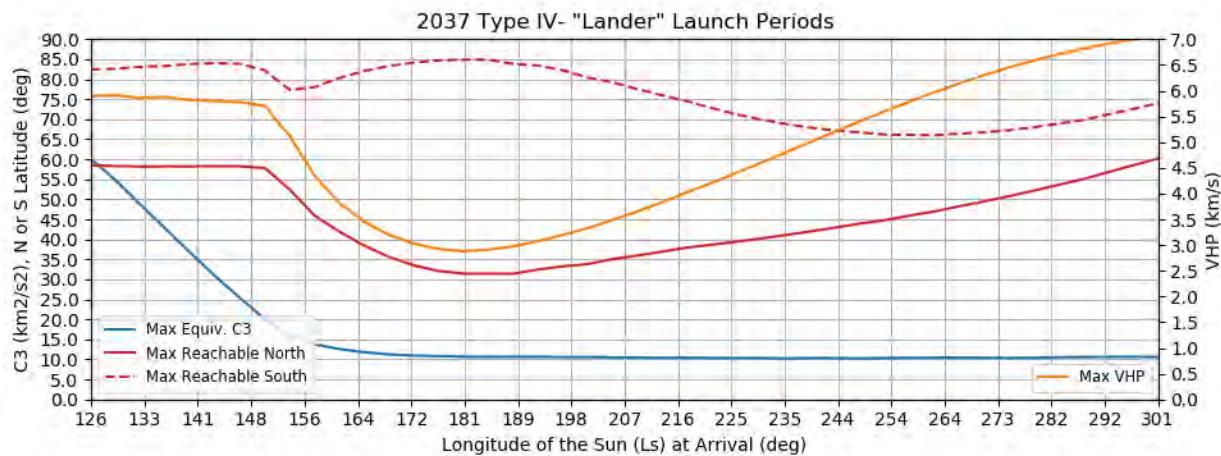
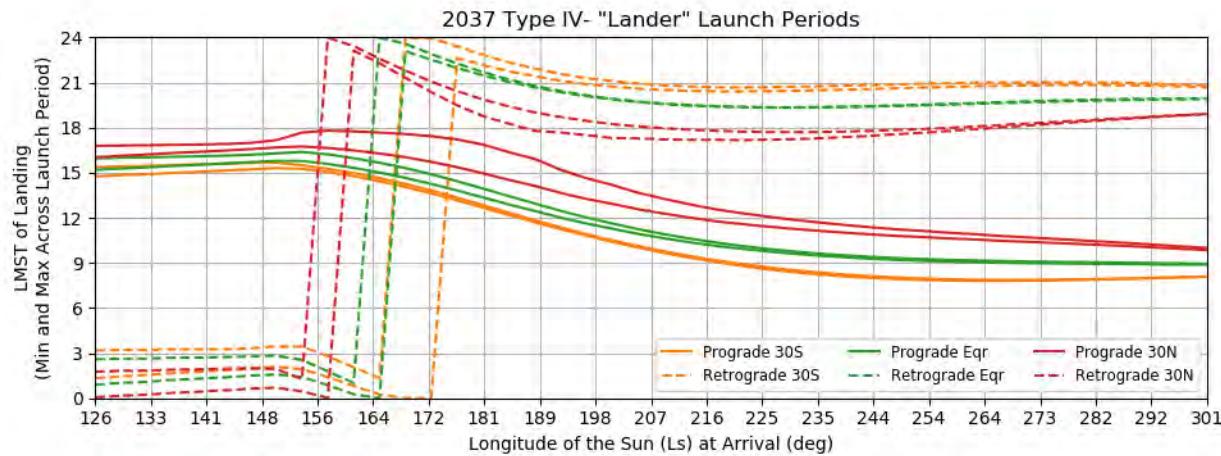


Figure 236: Earth to Mars 2037 Type III- Lander Launch Periods - Earth Elevation at Landing at Various Latitudes



**Figure 237: Earth to Mars 2037 Type IV- Lander Launch Periods - Reachable Latitudes, Equivalent C3, and VHP**



**Figure 238: Earth to Mars 2037 Type IV- Lander Launch Periods - LMST of Landing at Various Latitudes**

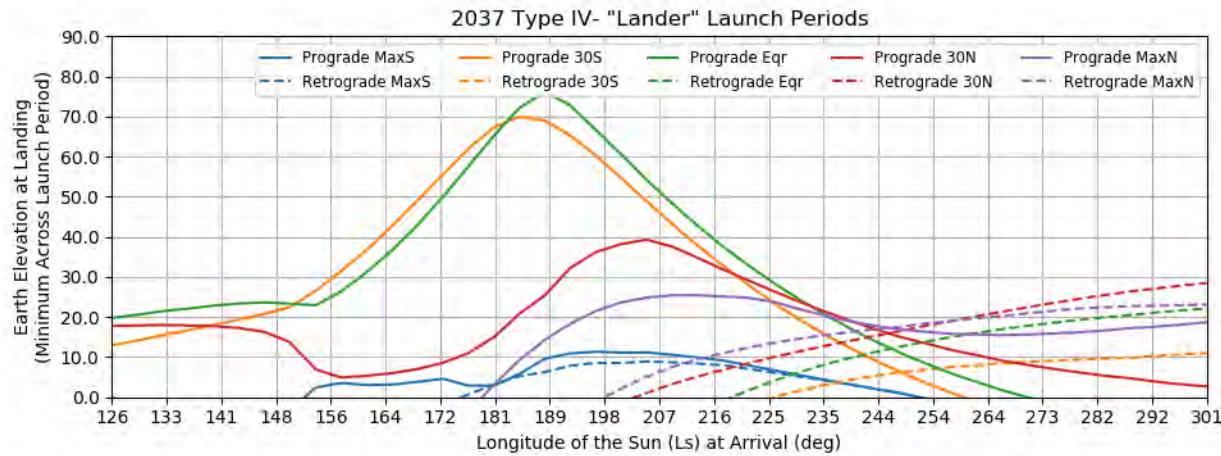


**Figure 239: Earth to Mars 2037 Type IV- Lander Launch Periods - Earth Elevation at Landing at Various Latitudes**

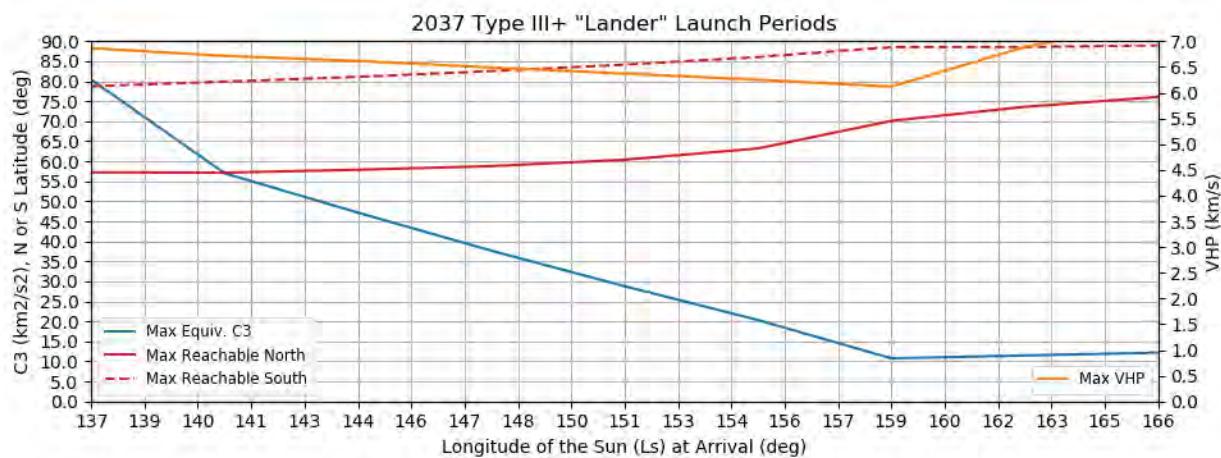


Figure 240: Earth to Mars 2037 Type III+ Lander Launch Periods - Reachable Latitudes, Equivalent C3, and VHP

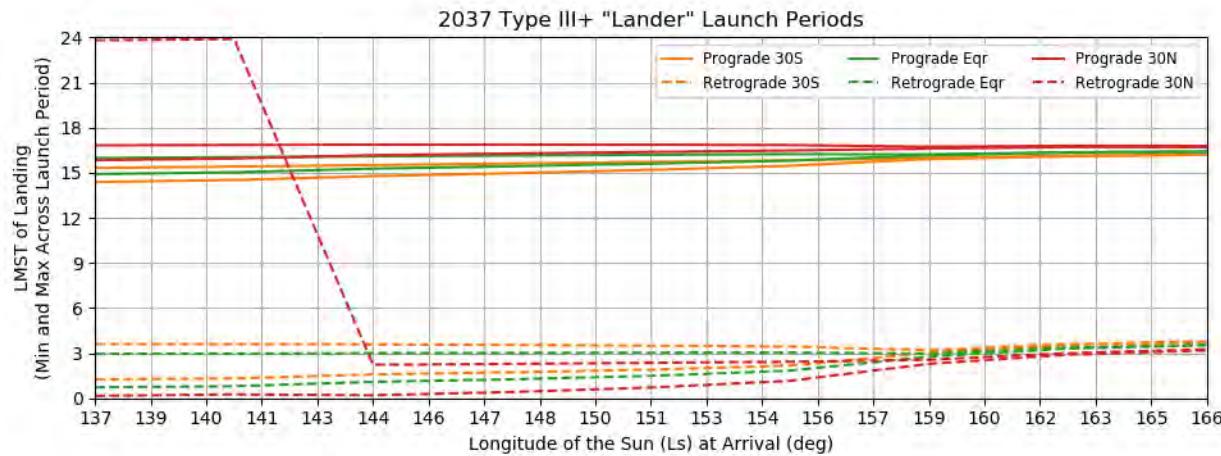


Figure 241: Earth to Mars 2037 Type III+ Lander Launch Periods - LMST of Landing at Various Latitudes

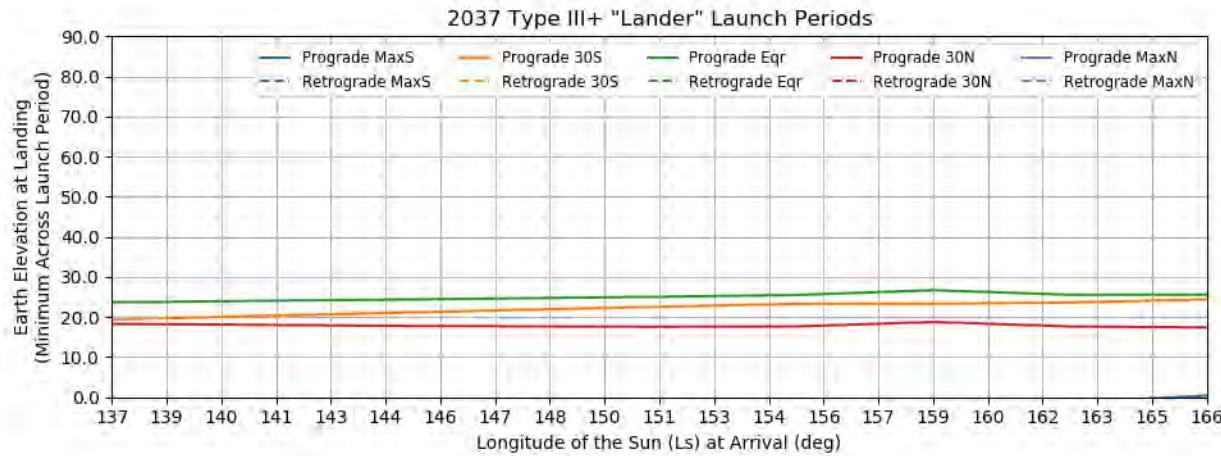


Figure 242: Earth to Mars 2037 Type III+ Lander Launch Periods - Earth Elevation at Landing at Various Latitudes

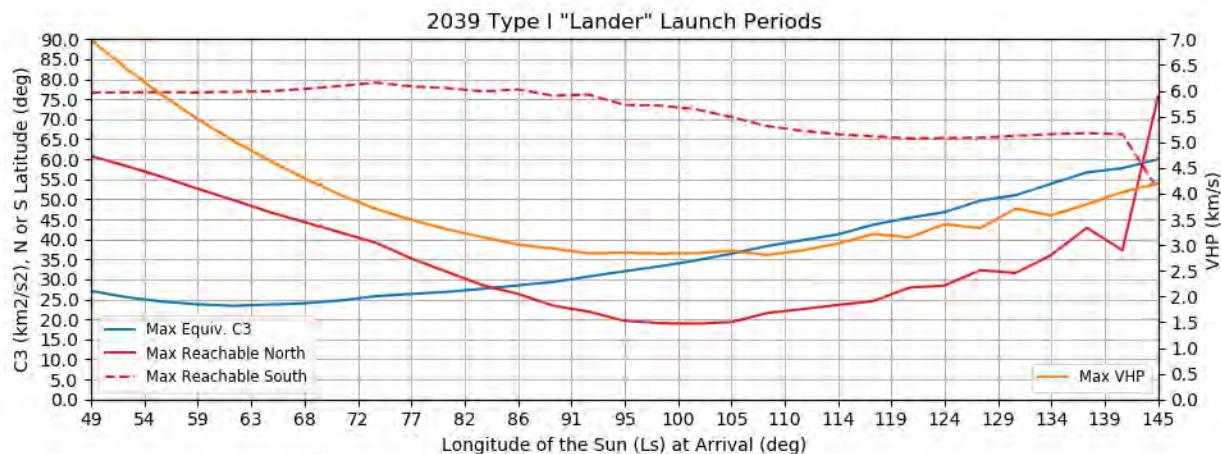


Figure 243: Earth to Mars 2039 Type I Lander Launch Periods - Reachable Latitudes, Equivalent C3, and VHP

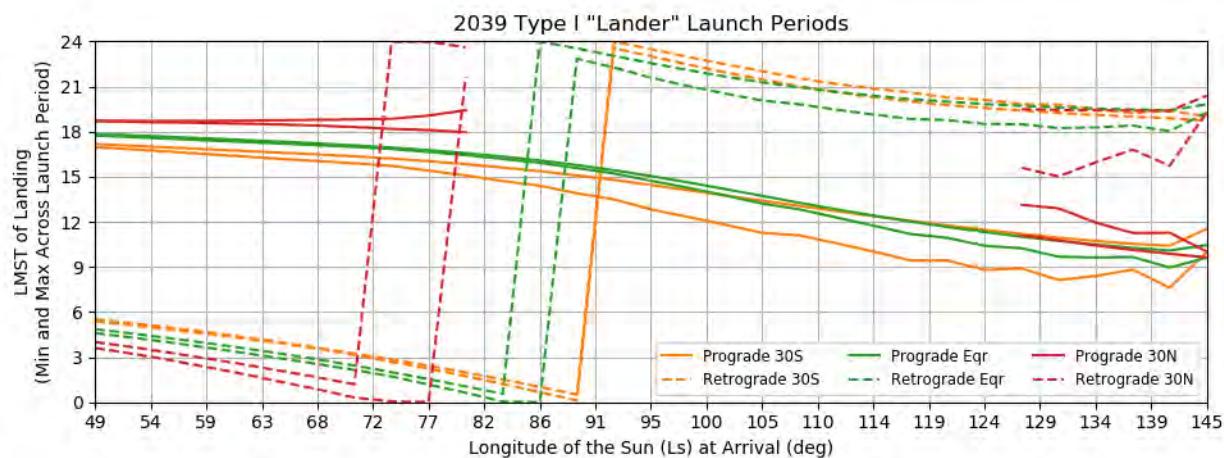


Figure 244: Earth to Mars 2039 Type I Lander Launch Periods - LMST of Landing at Various Latitudes

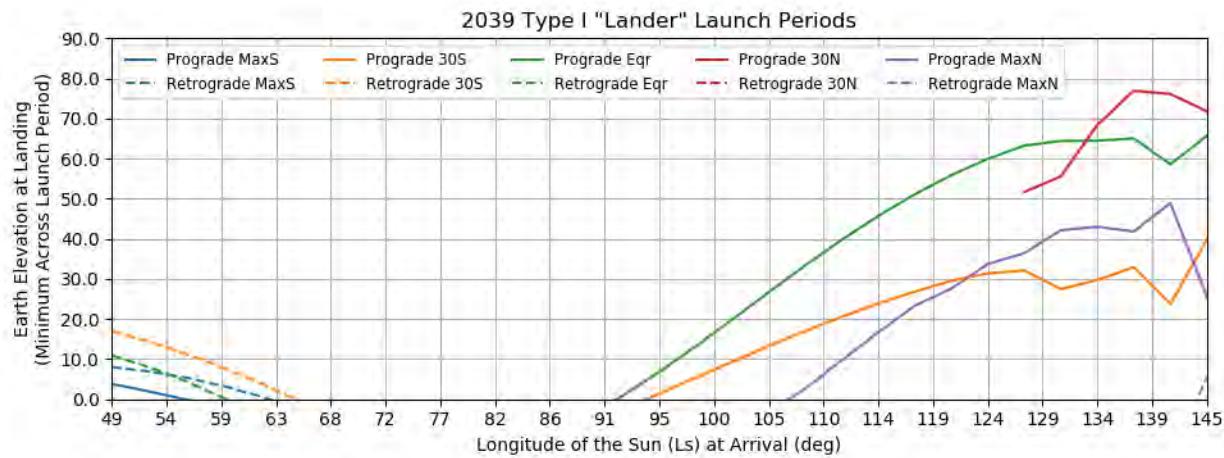


Figure 245: Earth to Mars 2039 Type I Lander Launch Periods - Earth Elevation at Landing at Various Latitudes

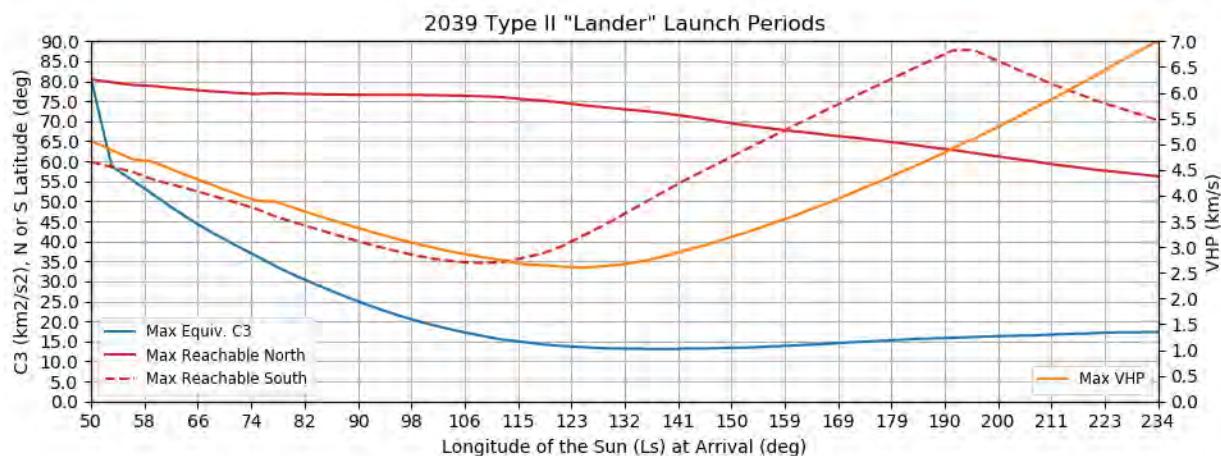


Figure 246: Earth to Mars 2039 Type II Lander Launch Periods - Reachable Latitudes, Equivalent C3, and VHP

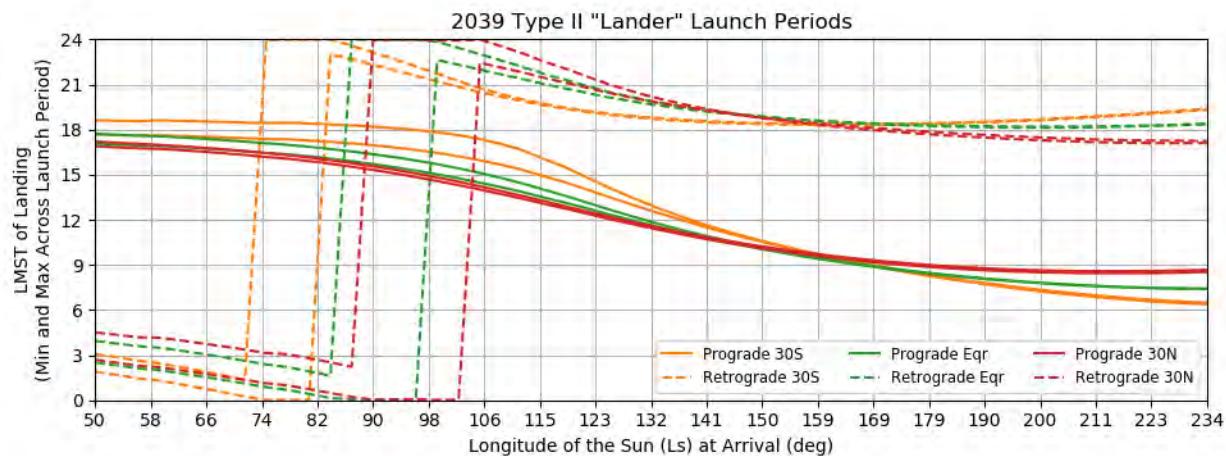


Figure 247: Earth to Mars 2039 Type II Lander Launch Periods - LMST of Landing at Various Latitudes

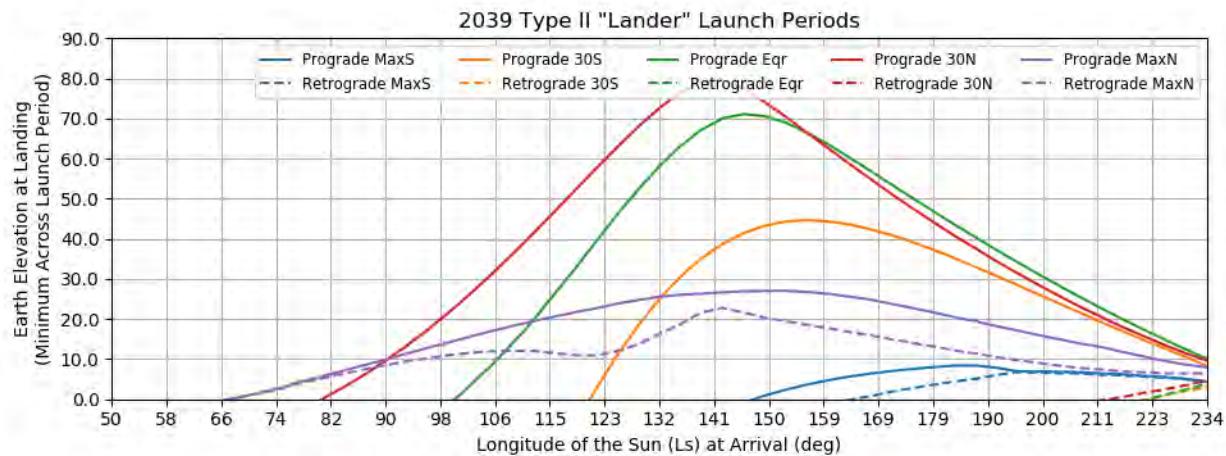


Figure 248: Earth to Mars 2039 Type II Lander Launch Periods - Earth Elevation at Landing at Various Latitudes

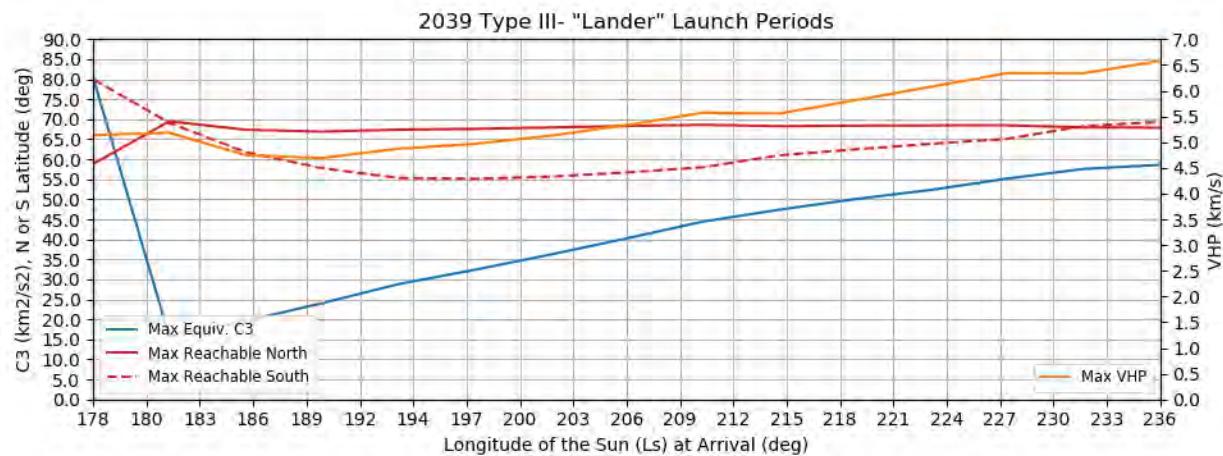


Figure 249: Earth to Mars 2039 Type III- Lander Launch Periods - Reachable Latitudes, Equivalent C3, and VHP

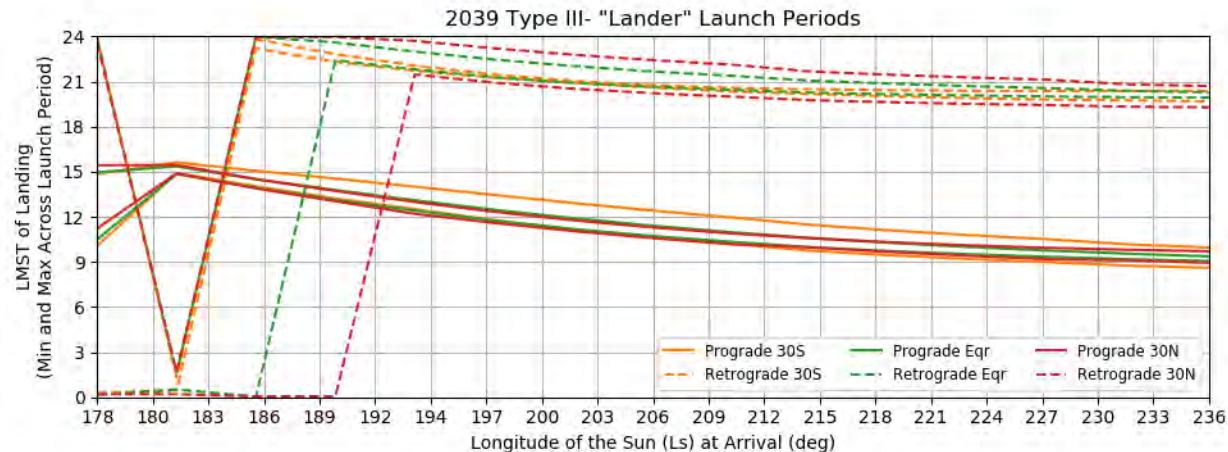


Figure 250: Earth to Mars 2039 Type III- Lander Launch Periods - LMST of Landing at Various Latitudes

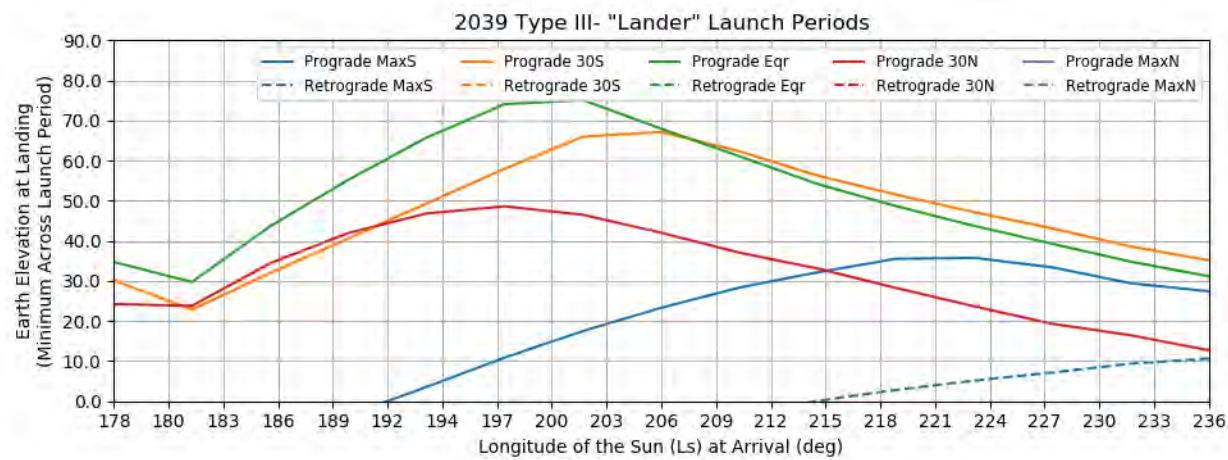
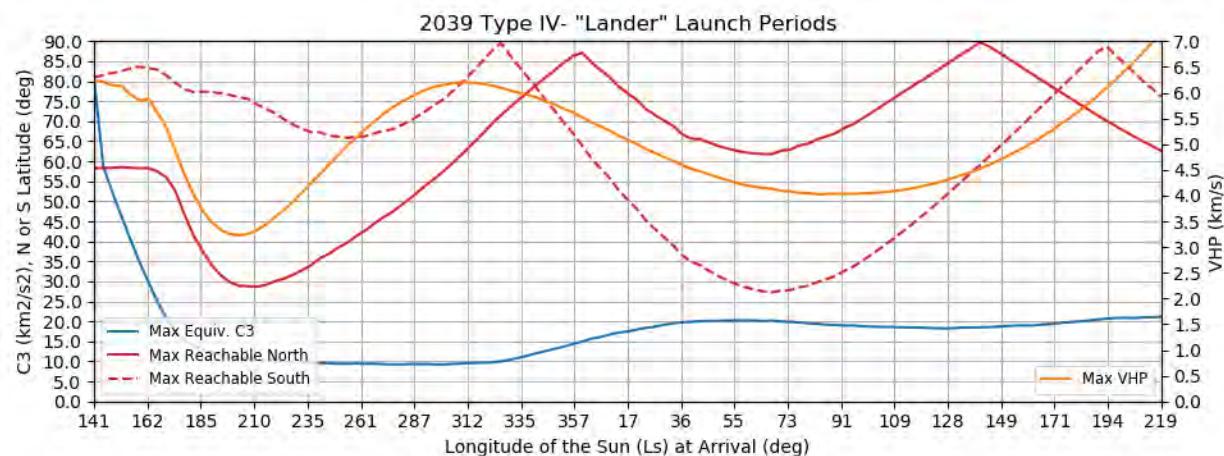
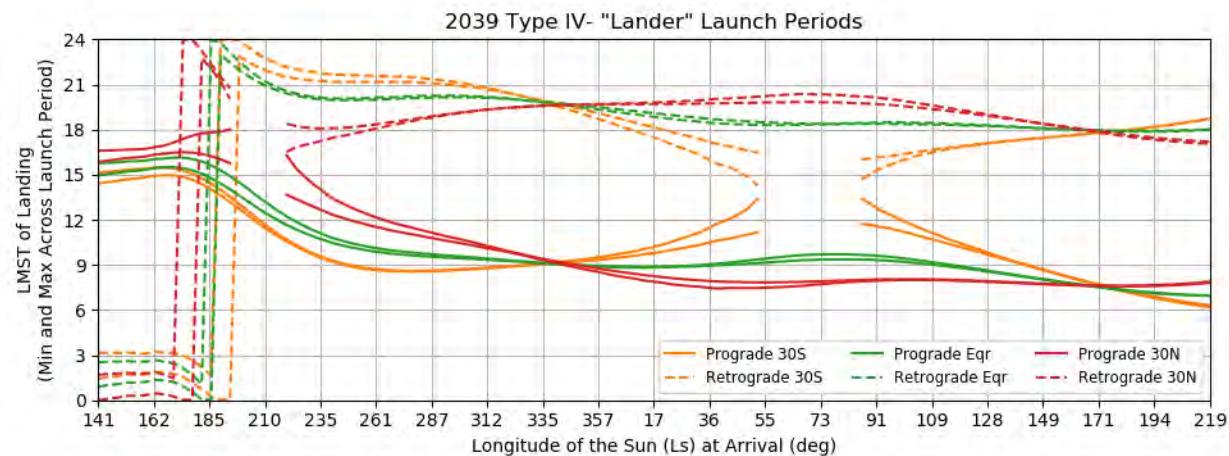


Figure 251: Earth to Mars 2039 Type III- Lander Launch Periods - Earth Elevation at Landing at Various Latitudes



**Figure 252: Earth to Mars 2039 Type IV- Lander Launch Periods - Reachable Latitudes, Equivalent C3, and VHP**



**Figure 253: Earth to Mars 2039 Type IV- Lander Launch Periods - LMST of Landing at Various Latitudes**

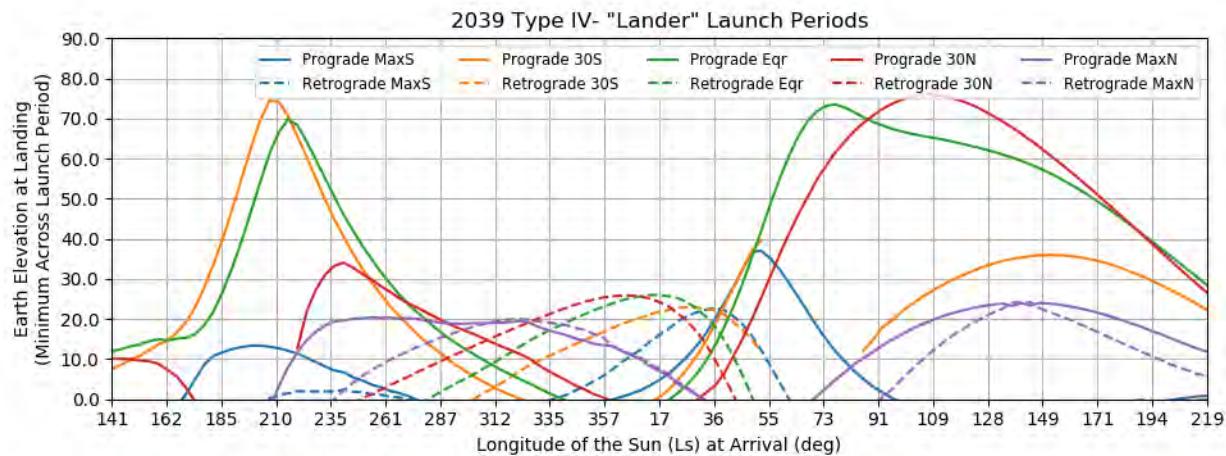


**Figure 254: Earth to Mars 2039 Type IV- Lander Launch Periods - Earth Elevation at Landing at Various Latitudes**

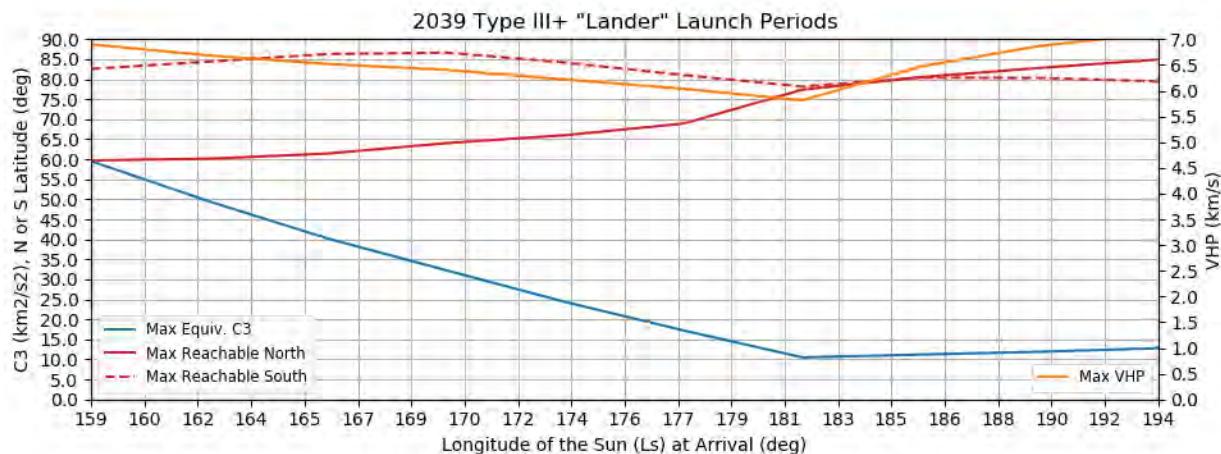


Figure 255: Earth to Mars 2039 Type III+ Lander Launch Periods - Reachable Latitudes, Equivalent C3, and VHP

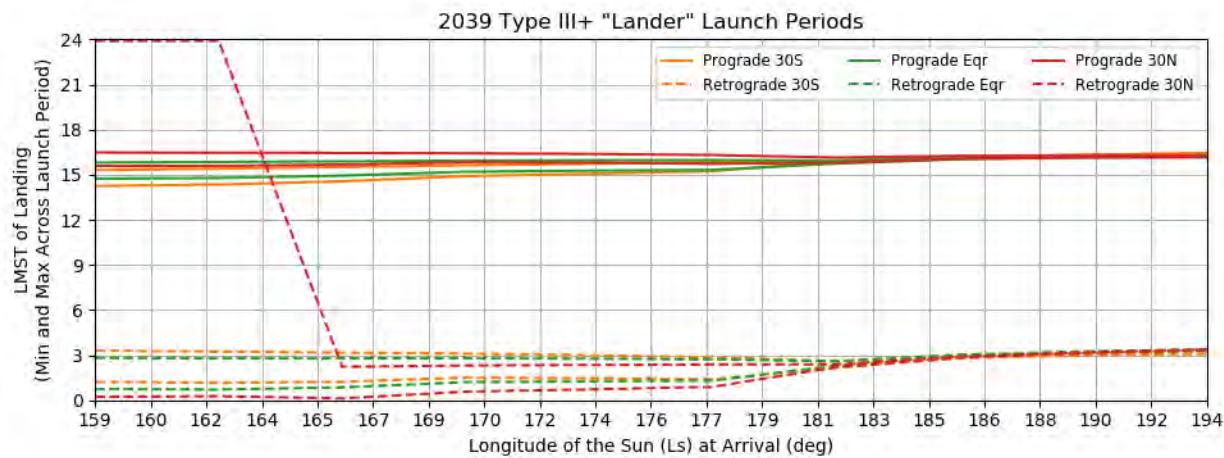


Figure 256: Earth to Mars 2039 Type III+ Lander Launch Periods - LMST of Landing at Various Latitudes

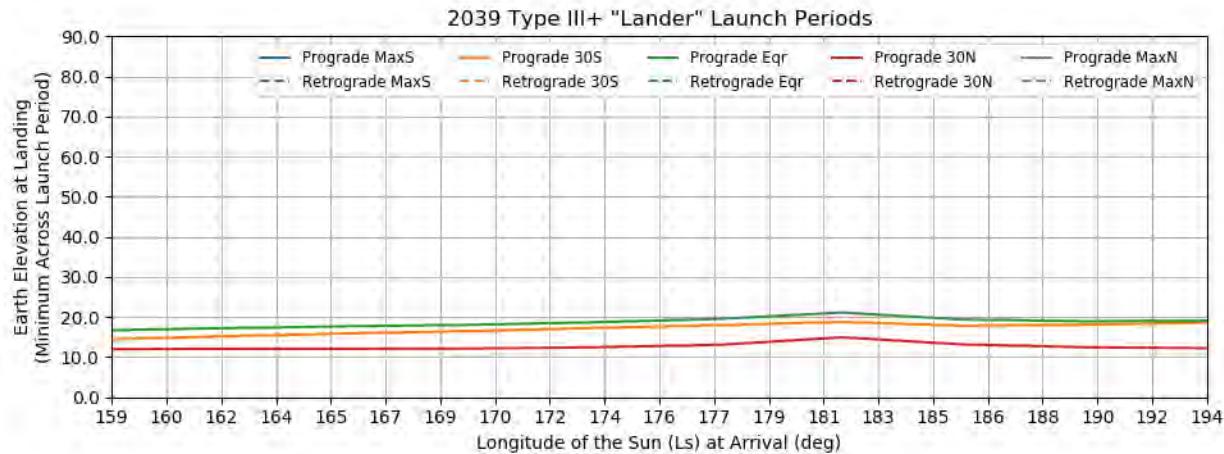


Figure 257: Earth to Mars 2039 Type III+ Lander Launch Periods - Earth Elevation at Landing at Various Latitudes

## 10.4 Orbiter Launch Periods

Besides optimal mass, there are other potential objectives in designing a launch period for an orbiter, and they are all dependent on the orbit inclination chosen. The reachable orbit inclination with a single in-plane burn at periapsis varies with the approach geometry, and the geometry of that orbit (ascending node location, latitude of periapsis, etc) are dependent on the selected orbit. Since this latter parameter is a continuum, we have chosen to focus this variation on 92 deg inclined orbits. This is the inclination of a sun-synchronous orbit, and is almost always reachable. It takes a truly exceptional approach geometry to be unable to reach 92 deg inclination, and sun-synchronicity is a commonly-desired feature.

With this in mind, Figures 123 through 257 plot the minimum reachable inclination, LMST of the ascending node, and periapsis latitude for North and South approaches as a function of the offset in the mass-optimal arrival date. The minimum inclination can be thought of as the minimum distance from the equator. A 40 deg minimum inclination means that 40 to 130 deg is reachable. Each point on these curves is a separate 20 day launch period with the launch date re-optimized for the maximum captured mass. This optimization includes the declination penalties, which are recast back into the C3 as a declination-penalized “equivalent C3.” The arrival dates are shifted earlier and later from the optimal until the equivalent C3 increased above  $60 \text{ km}^2/\text{s}^2$  or the VHP exceeded 7 km/s. As a result, the spread of viable arrival dates varies significantly from opportunity to opportunity. In the LMST and periapsis latitude plots, (e.g. Figure 259), the pair of lines of each color-and-style indicate the minimum and maximum value across the launch period.

The local mean solar time of the ascending node of an orbiter is dependent on the periapsis altitude and the targeted inclination. These plots assume 400 km and 92.9 deg, again to be consistent with the previous edition of the Handbook. 92.9 deg is also near the sun-synchronous inclination for a low Mars orbiter.

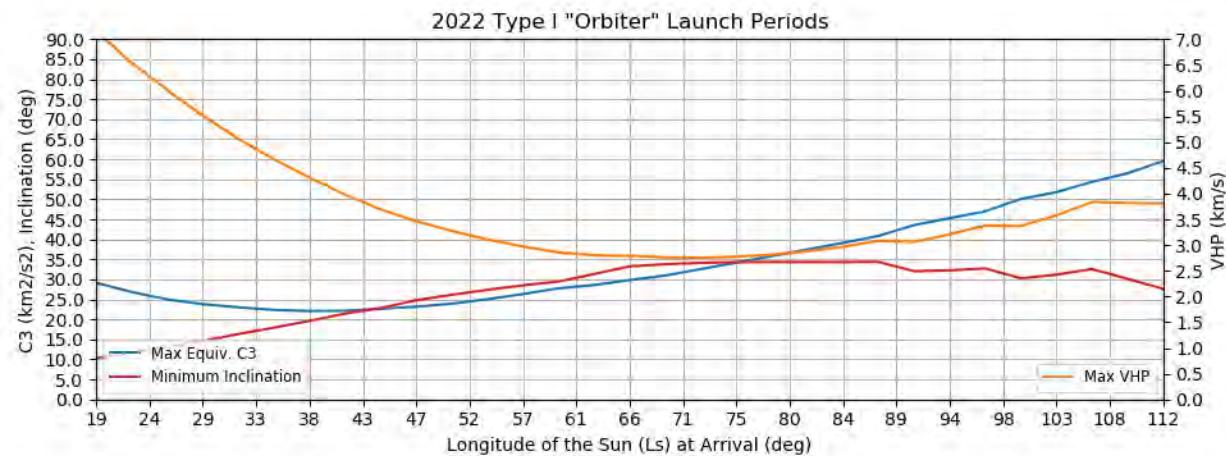


Figure 258: Earth to Mars 2022 Type I Orbiter Launch Periods - Reachable Inclination, Launch Mass, and VHP

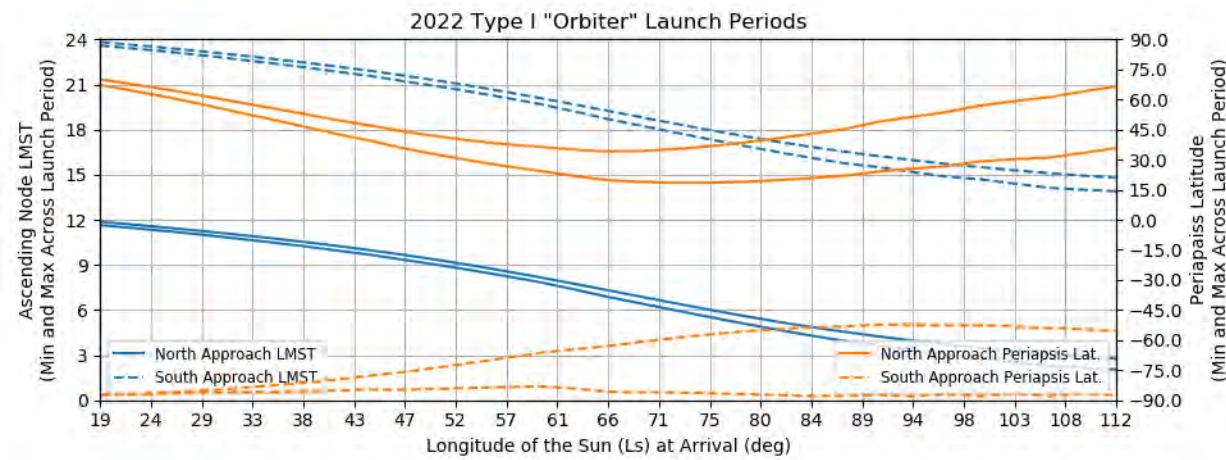


Figure 259: Earth to Mars 2022 Type I Orbiter Launch Periods - Ascending Node LMST and Periapsis Latitude (92 deg inclination)

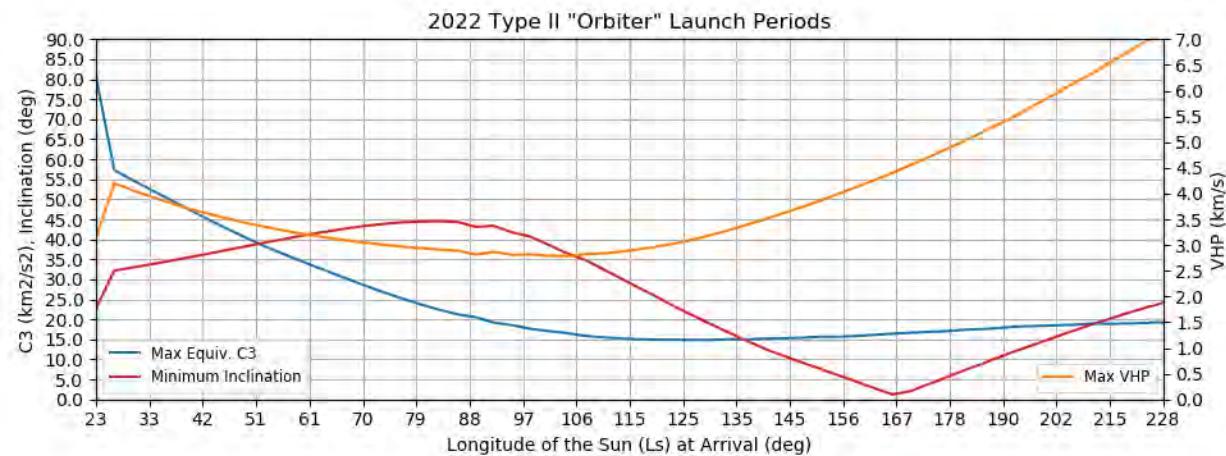


Figure 260: Earth to Mars 2022 Type II Orbiter Launch Periods - Reachable Inclination, Launch Mass, and VHP

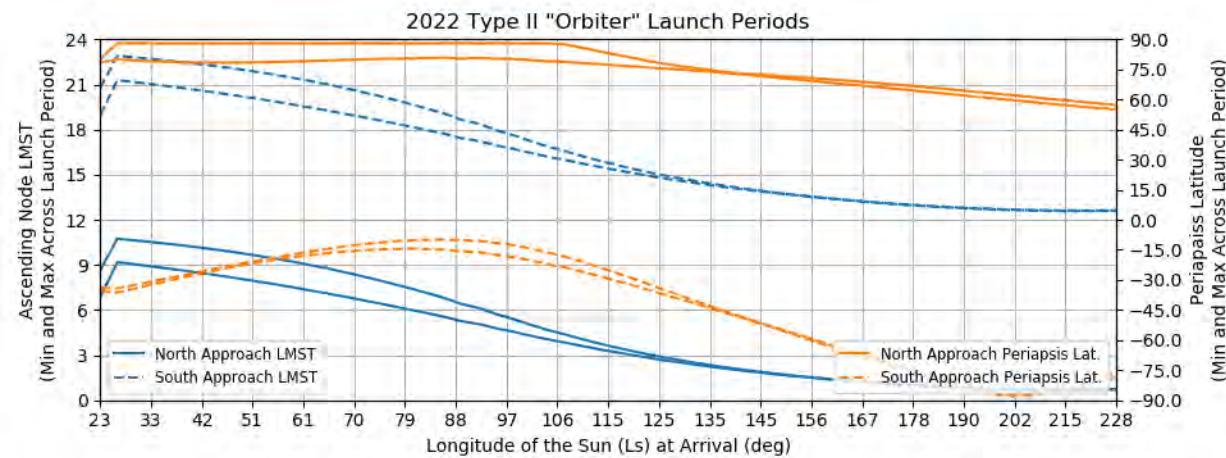


Figure 261: Earth to Mars 2022 Type II Orbiter Launch Periods - Ascending Node LMST and Periapsis Latitude (92 deg inclination)

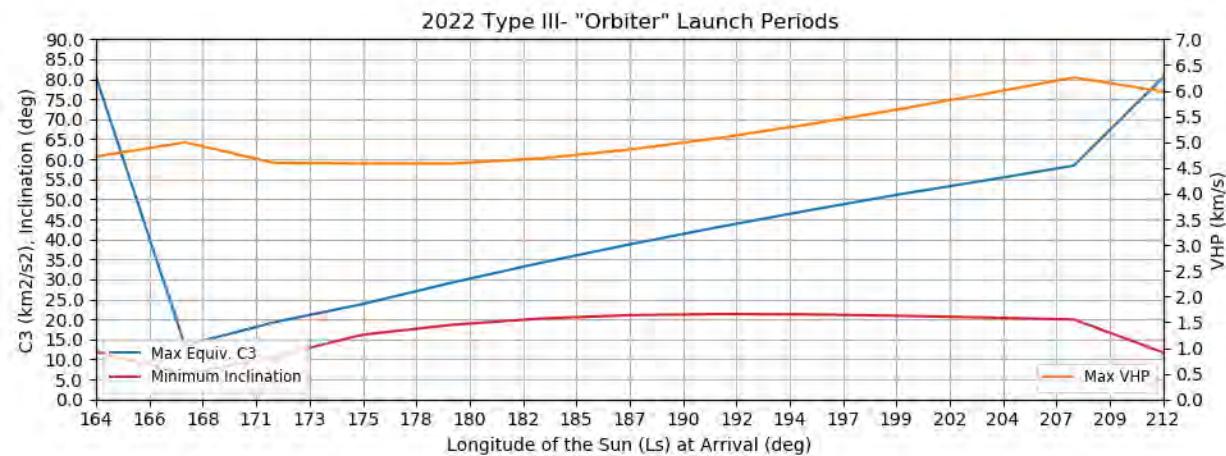


Figure 262: Earth to Mars 2022 Type III- Orbiter Launch Periods - Reachable Inclination, Launch Mass, and VHP

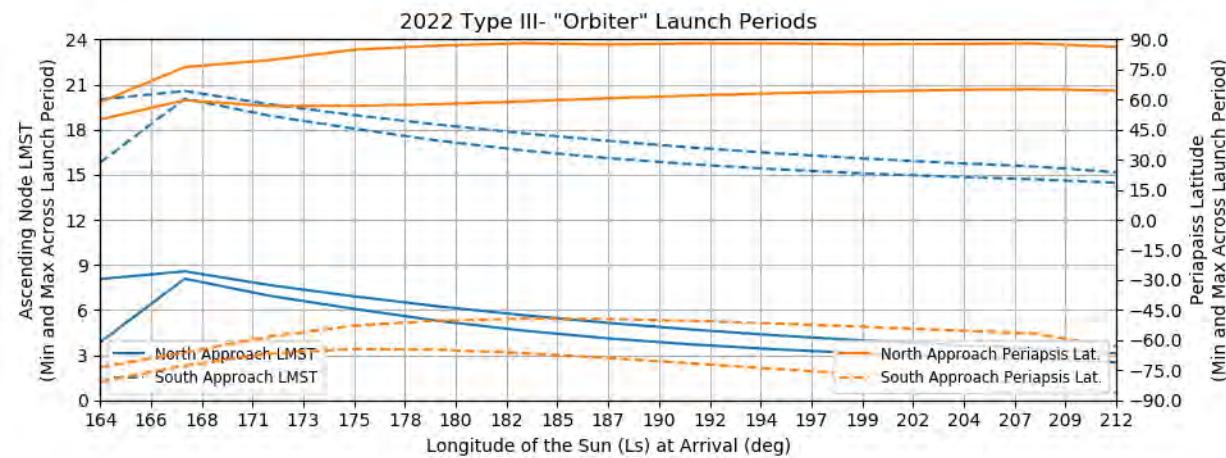


Figure 263: Earth to Mars 2022 Type III- Orbiter Launch Periods - Ascending Node LMST and Periapsis Latitude (92 deg inclination)

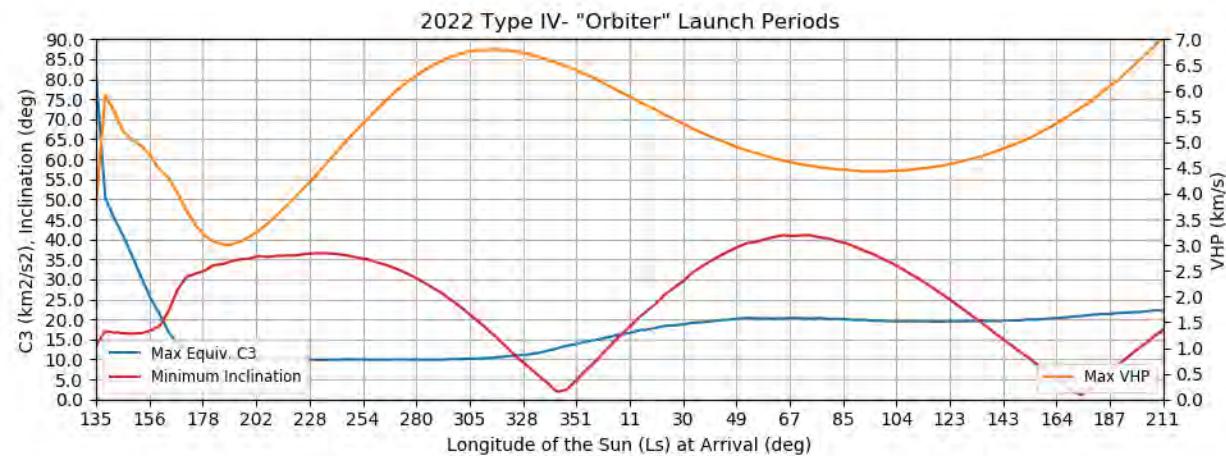


Figure 264: Earth to Mars 2022 Type IV- Orbiter Launch Periods - Reachable Inclination, Launch Mass, and VHP

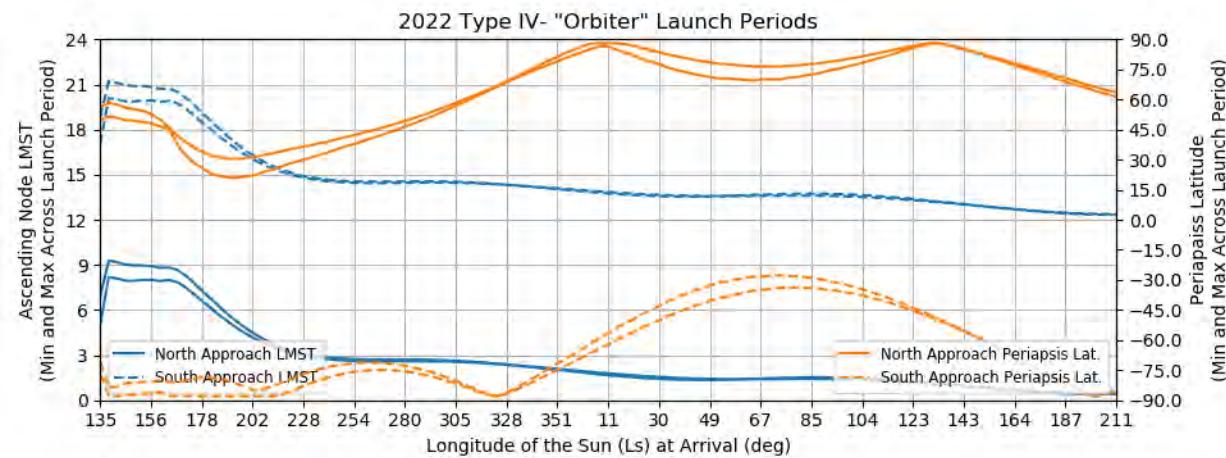


Figure 265: Earth to Mars 2022 Type IV- Orbiter Launch Periods - Ascending Node LMST and Periapsis Latitude (92 deg inclination)

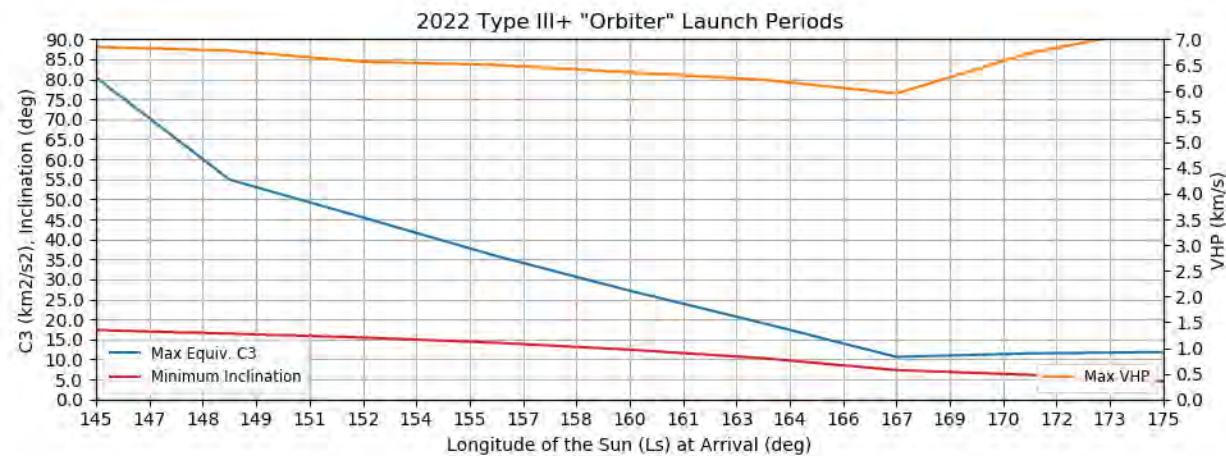


Figure 266: Earth to Mars 2022 Type III+ Orbiter Launch Periods - Reachable Inclination, Launch Mass, and VHP

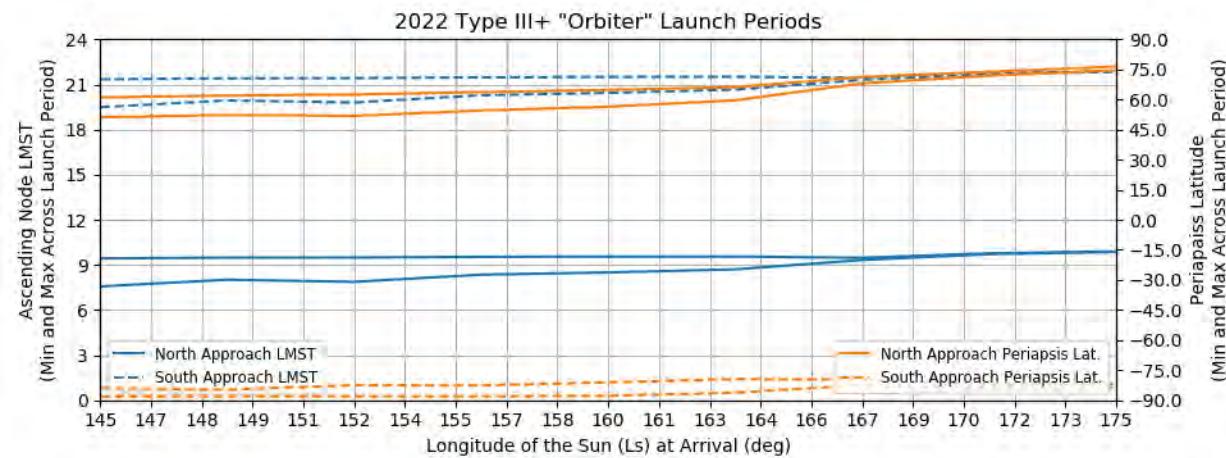


Figure 267: Earth to Mars 2022 Type III+ Orbiter Launch Periods - Ascending Node LMST and Periapsis Latitude (92 deg inclination)

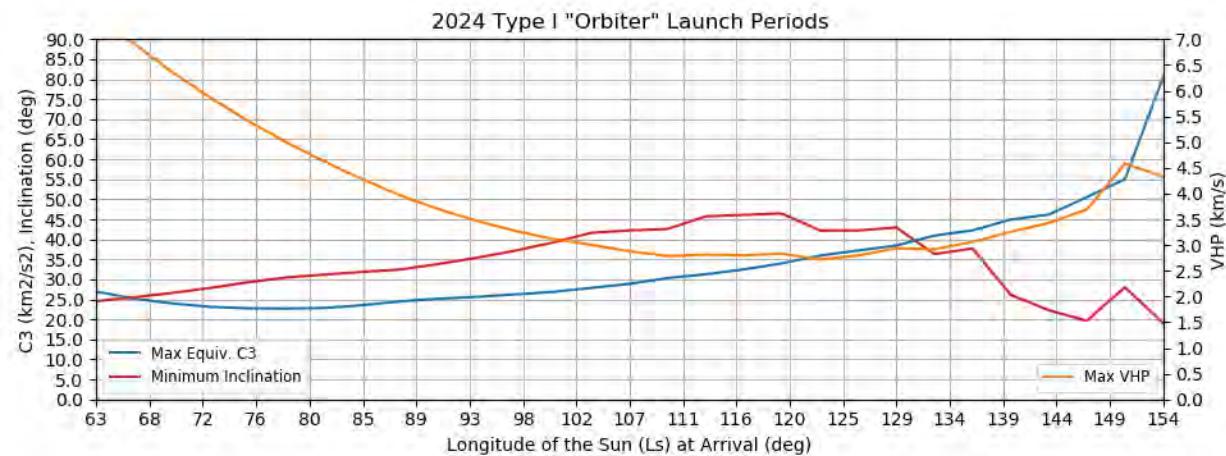


Figure 268: Earth to Mars 2024 Type I Orbiter Launch Periods - Reachable Inclination, Launch Mass, and VHP

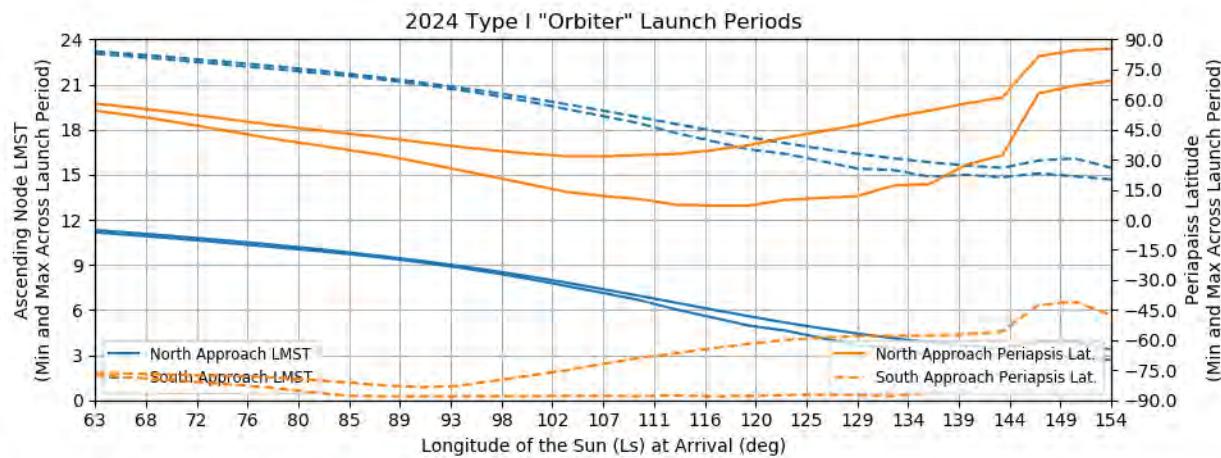


Figure 269: Earth to Mars 2024 Type I Orbiter Launch Periods - Ascending Node LMST and Periapsis Latitude (92 deg inclination)

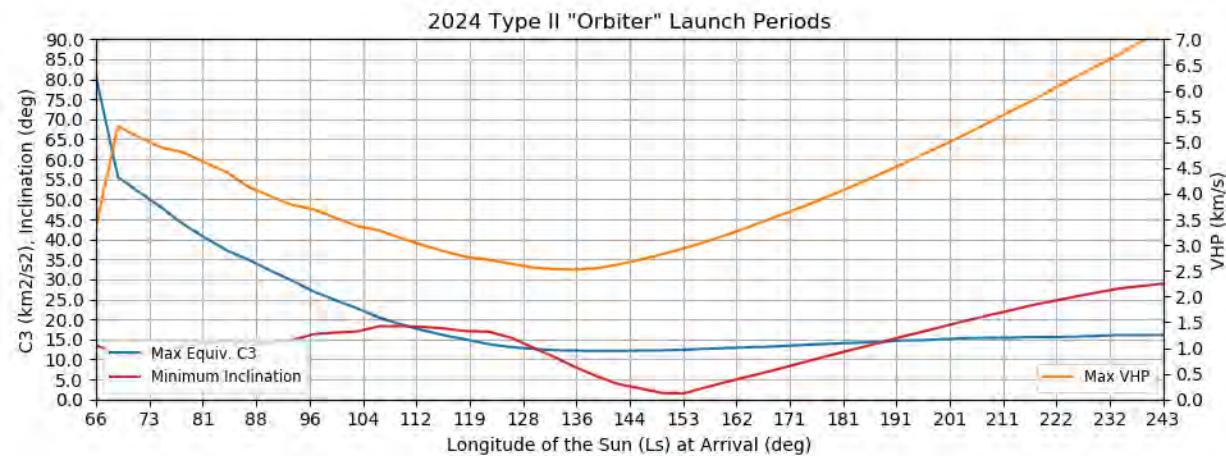


Figure 270: Earth to Mars 2024 Type II Orbiter Launch Periods - Reachable Inclination, Launch Mass, and VHP

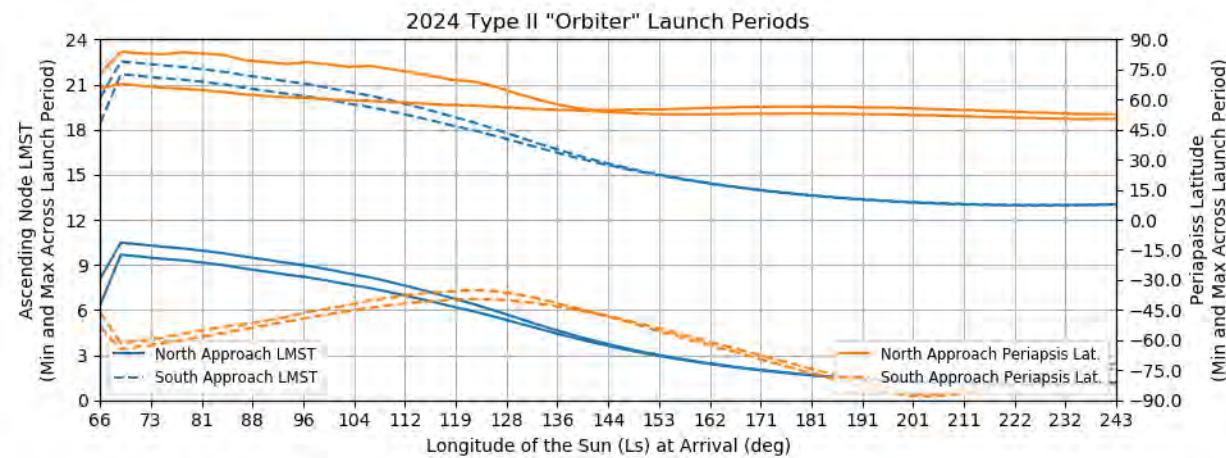


Figure 271: Earth to Mars 2024 Type II Orbiter Launch Periods - Ascending Node LMST and Periapsis Latitude (92 deg inclination)

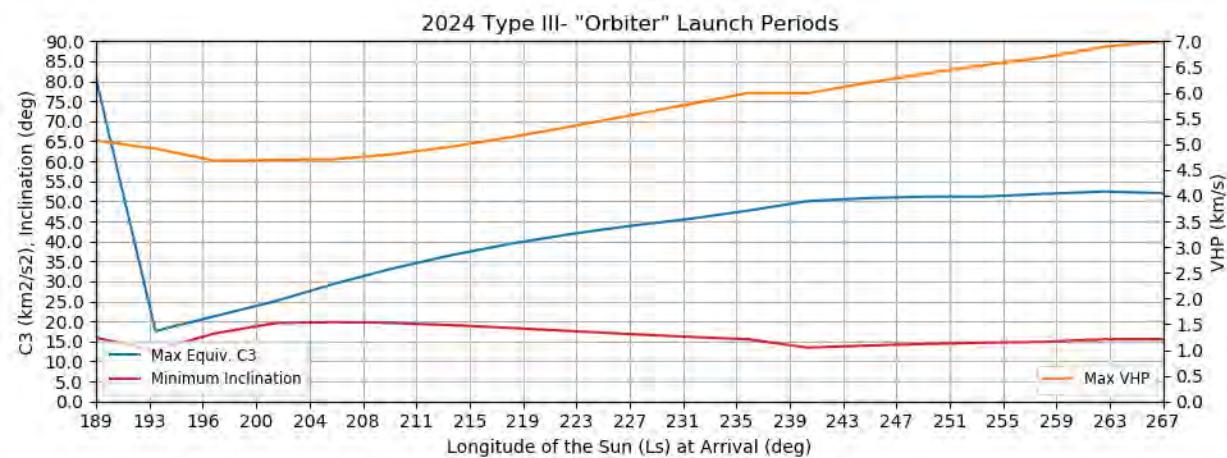


Figure 272: Earth to Mars 2024 Type III- Orbiter Launch Periods - Reachable Inclination, Launch Mass, and VHP

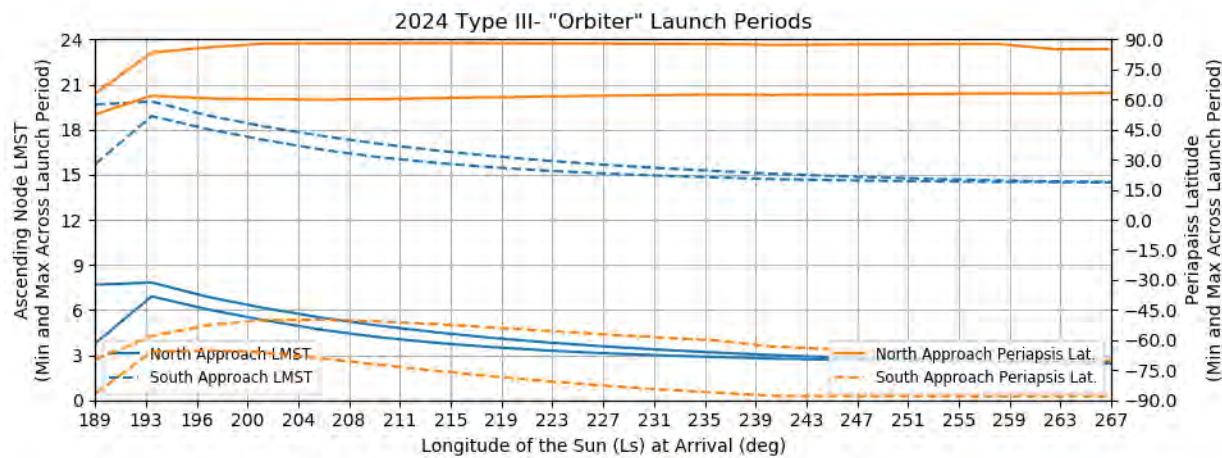


Figure 273: Earth to Mars 2024 Type III- Orbiter Launch Periods - Ascending Node LMST and Periapsis Latitude (92 deg inclination)

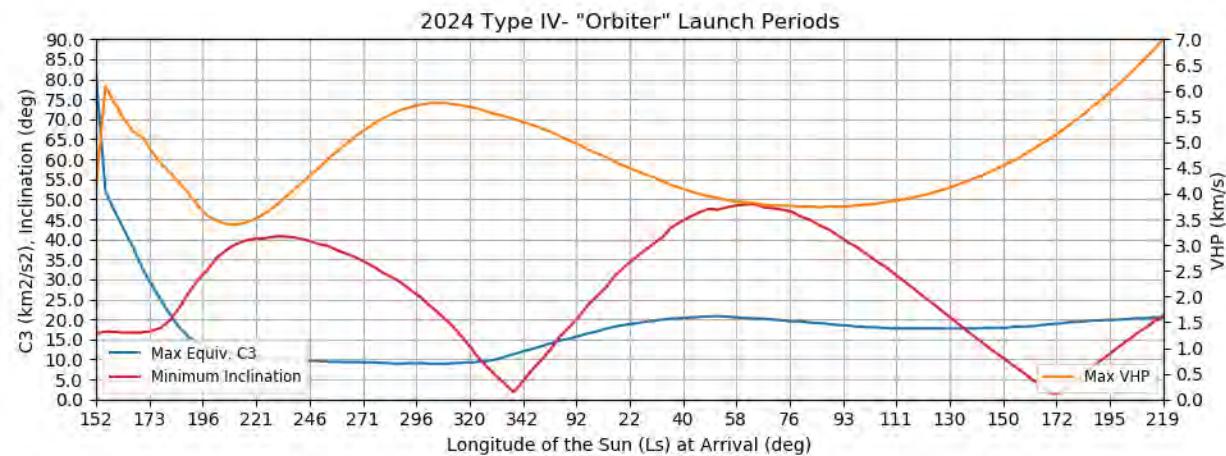


Figure 274: Earth to Mars 2024 Type IV- Orbiter Launch Periods - Reachable Inclination, Launch Mass, and VHP

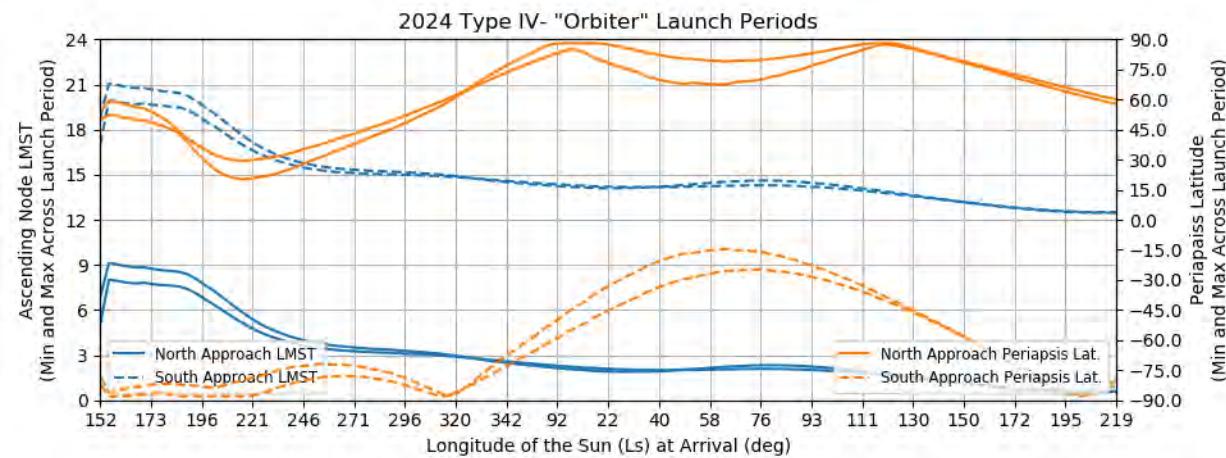


Figure 275: Earth to Mars 2024 Type IV- Orbiter Launch Periods - Ascending Node LMST and Periapsis Latitude (92 deg inclination)

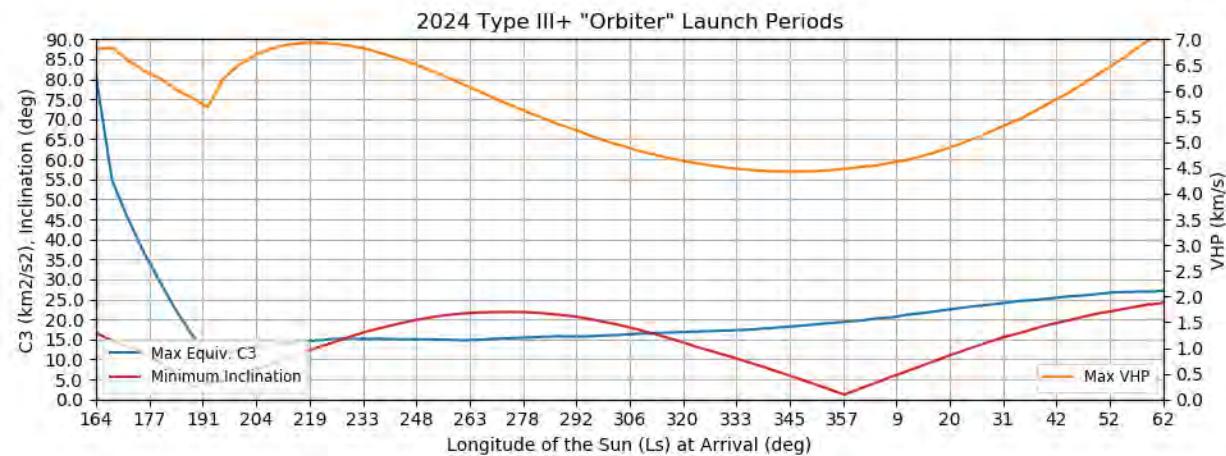


Figure 276: Earth to Mars 2024 Type III+ Orbiter Launch Periods - Reachable Inclination, Launch Mass, and VHP

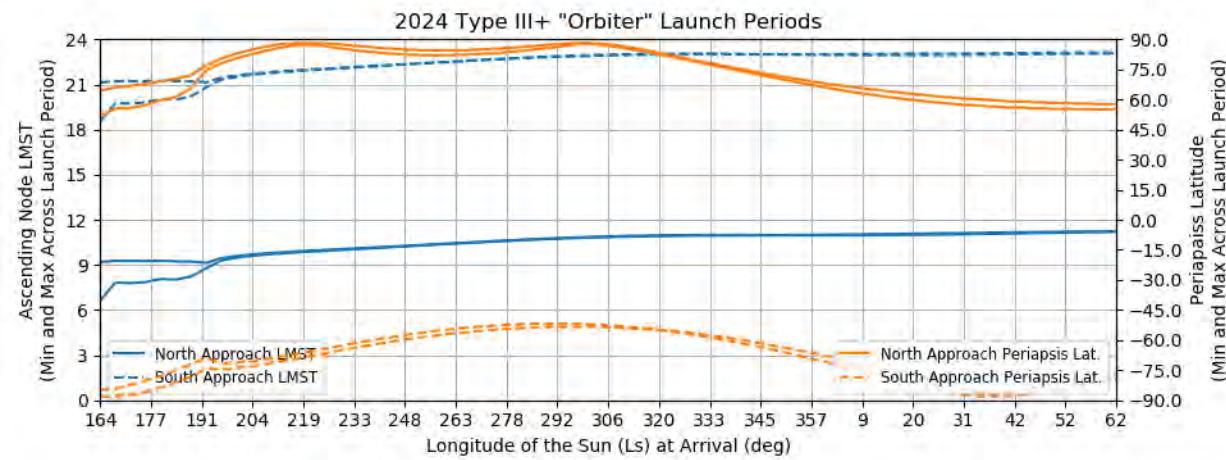


Figure 277: Earth to Mars 2024 Type III+ Orbiter Launch Periods - Ascending Node LMST and Periapsis Latitude (92 deg inclination)

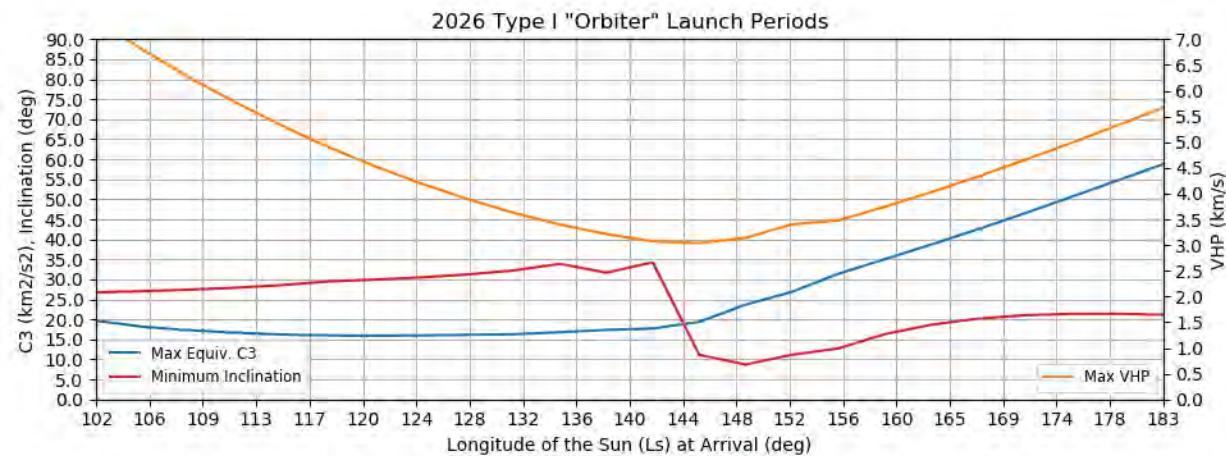


Figure 278: Earth to Mars 2026 Type I Orbiter Launch Periods - Reachable Inclination, Launch Mass, and VHP

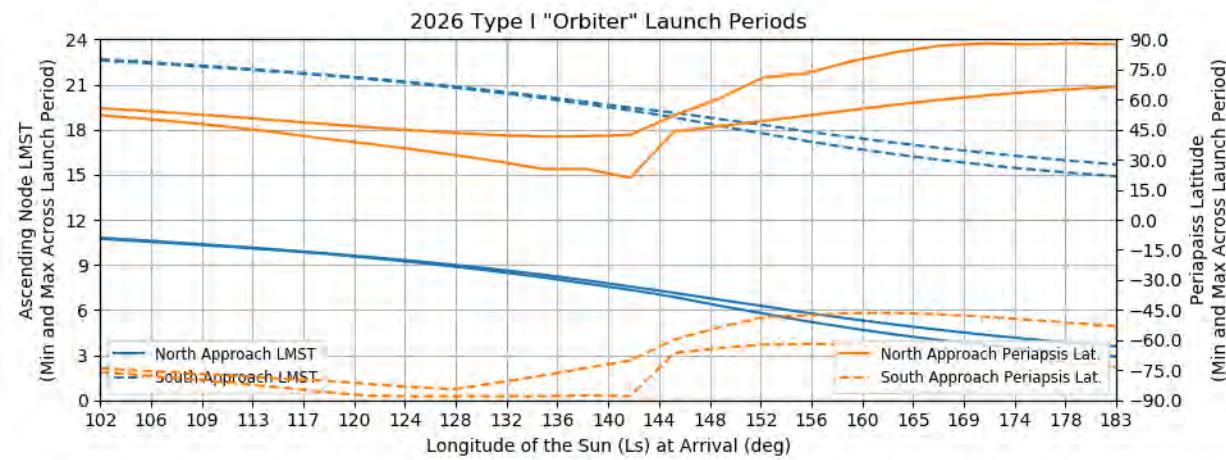


Figure 279: Earth to Mars 2026 Type I Orbiter Launch Periods - Ascending Node LMST and Periapsis Latitude (92 deg inclination)

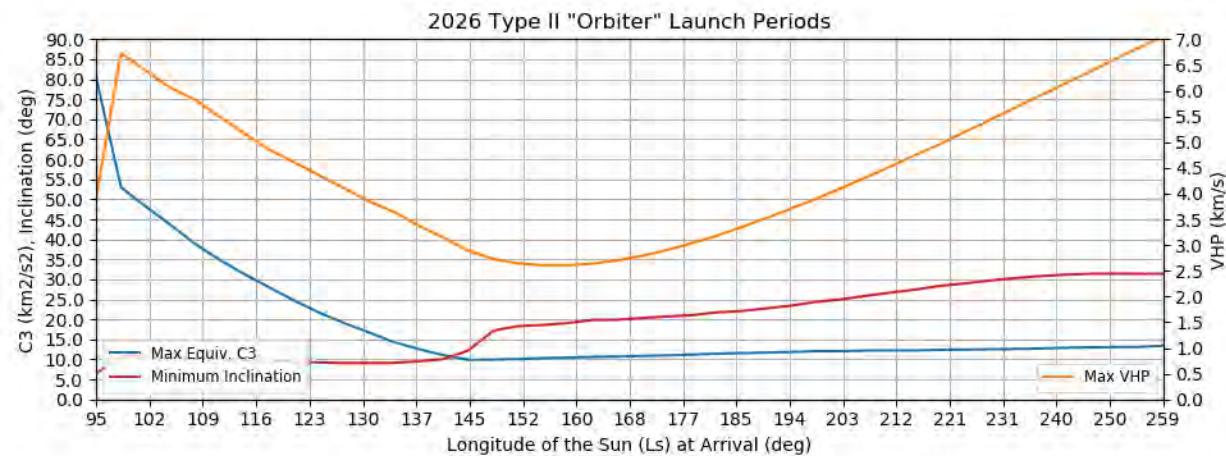


Figure 280: Earth to Mars 2026 Type II Orbiter Launch Periods - Reachable Inclination, Launch Mass, and VHP

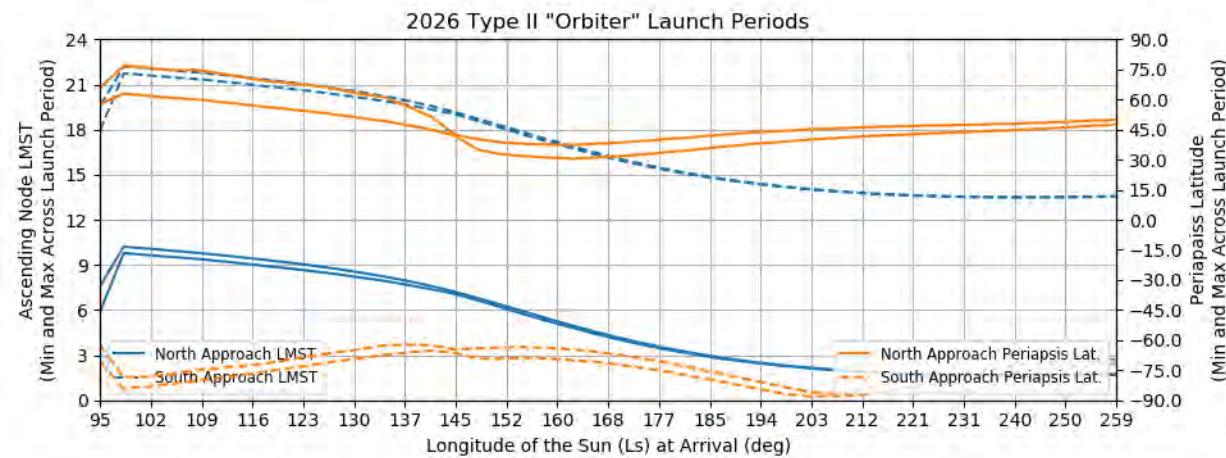


Figure 281: Earth to Mars 2026 Type II Orbiter Launch Periods - Ascending Node LMST and Periapsis Latitude (92 deg inclination)

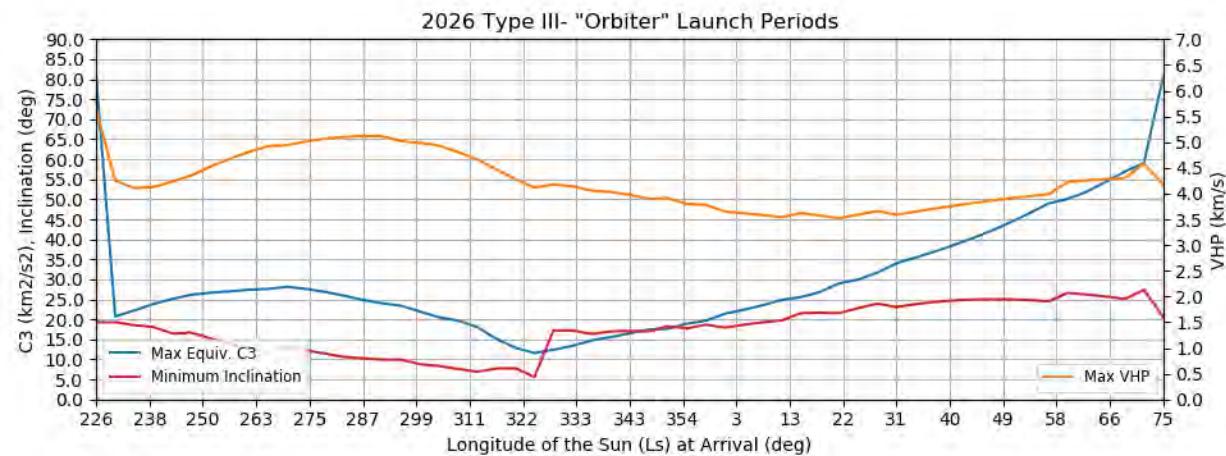


Figure 282: Earth to Mars 2026 Type III- Orbiter Launch Periods - Reachable Inclination, Launch Mass, and VHP

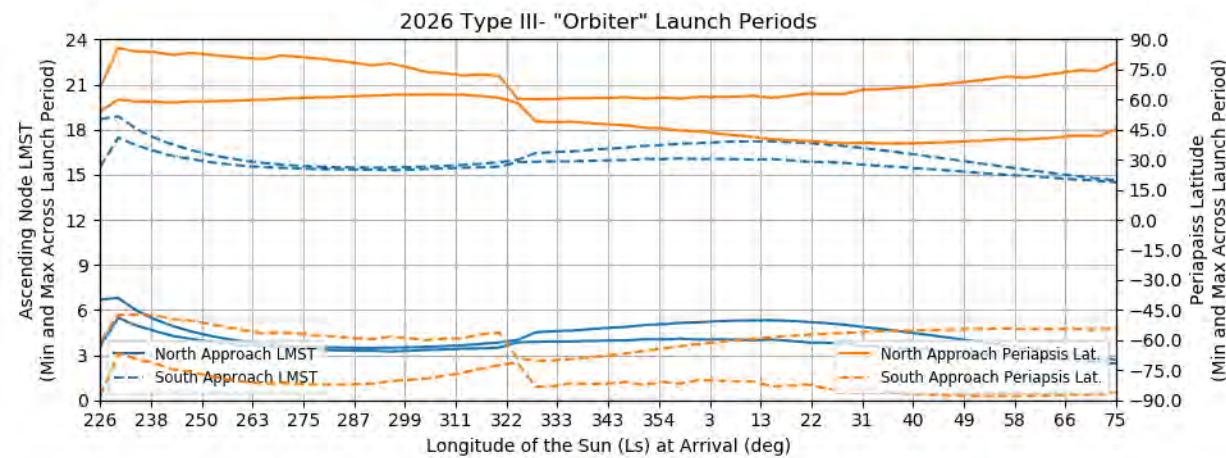


Figure 283: Earth to Mars 2026 Type III- Orbiter Launch Periods - Ascending Node LMST and Periapsis Latitude (92 deg inclination)

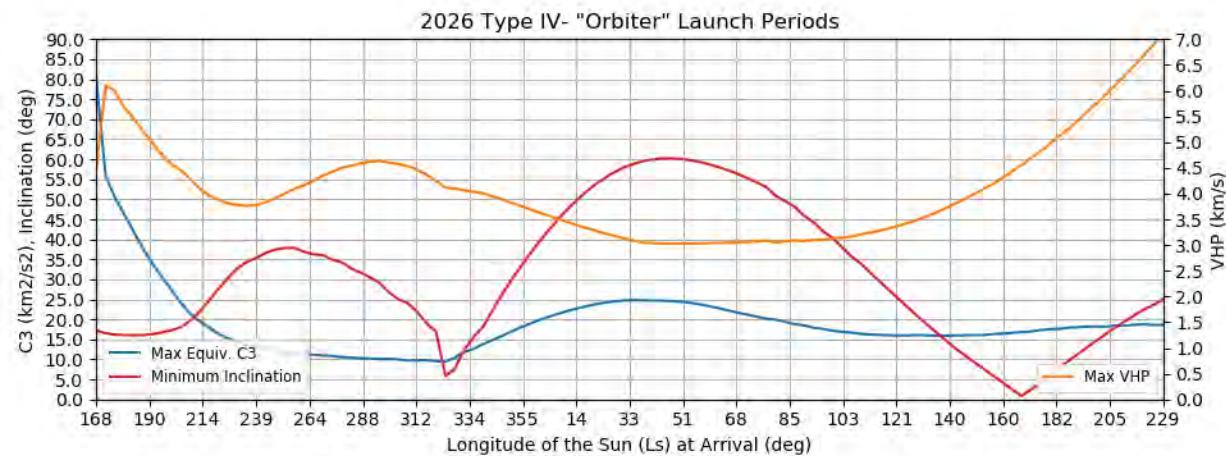


Figure 284: Earth to Mars 2026 Type IV- Orbiter Launch Periods - Reachable Inclination, Launch Mass, and VHP

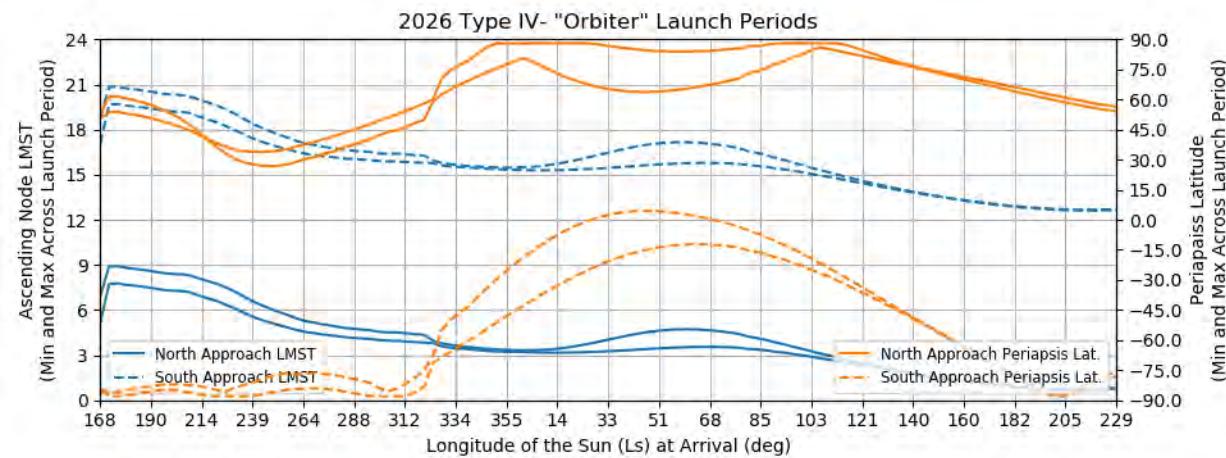
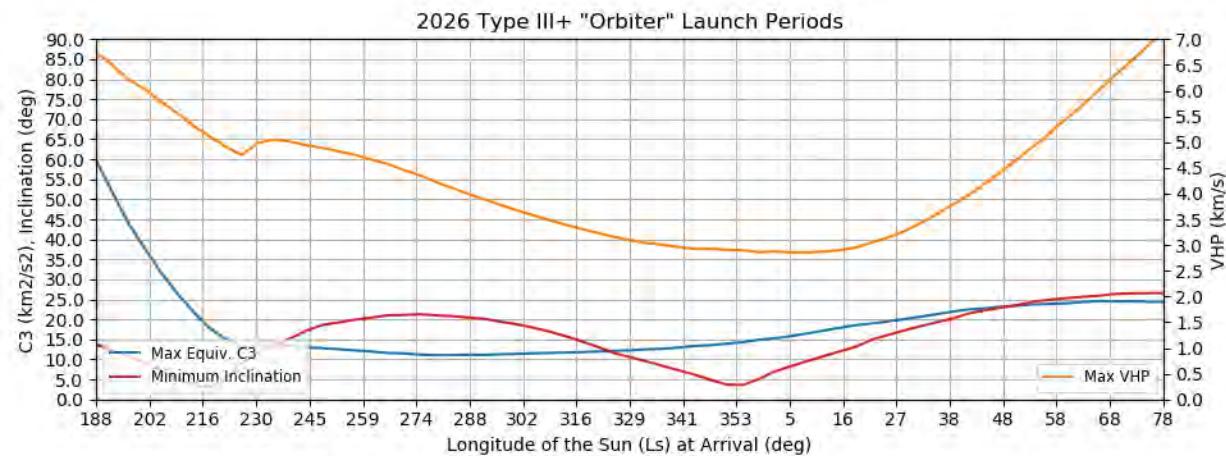
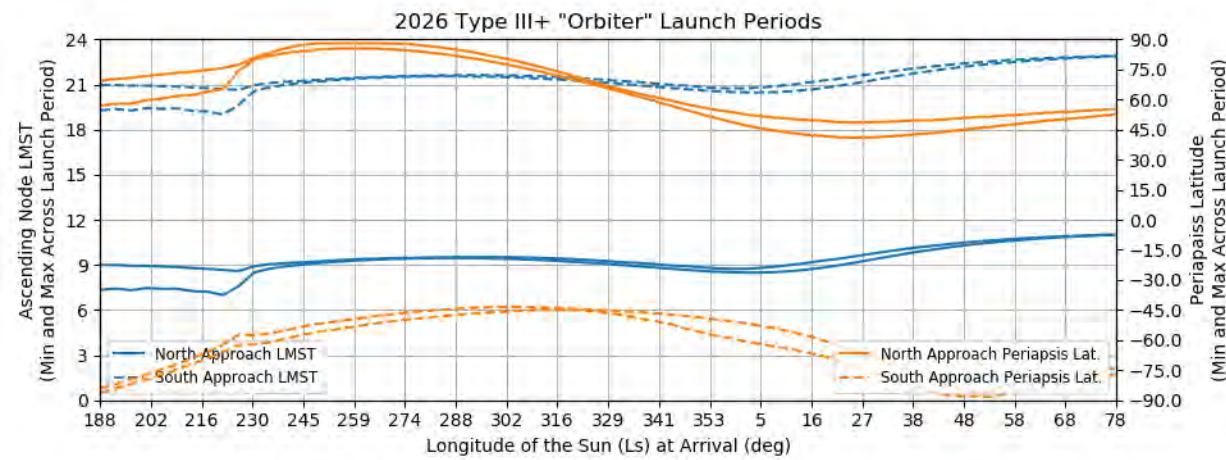


Figure 285: Earth to Mars 2026 Type IV- Orbiter Launch Periods - Ascending Node LMST and Periapsis Latitude (92 deg inclination)



**Figure 286: Earth to Mars 2026 Type III+ Orbiter Launch Periods - Reachable Inclination, Launch Mass, and VHP**



**Figure 287: Earth to Mars 2026 Type III+ Orbiter Launch Periods - Ascending Node LMST and Periapsis Latitude (92 deg inclination)**

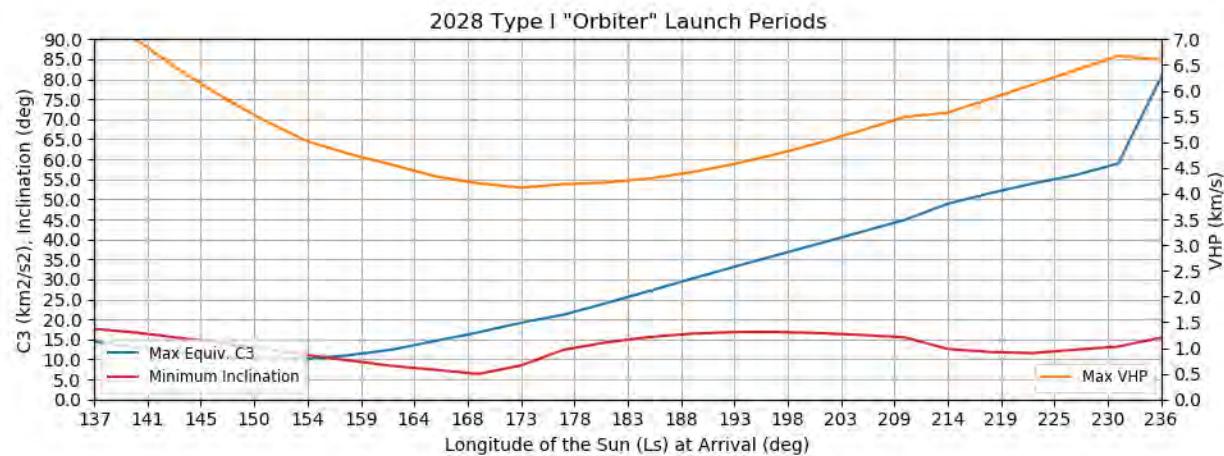


Figure 288: Earth to Mars 2028 Type I Orbiter Launch Periods - Reachable Inclination, Launch Mass, and VHP

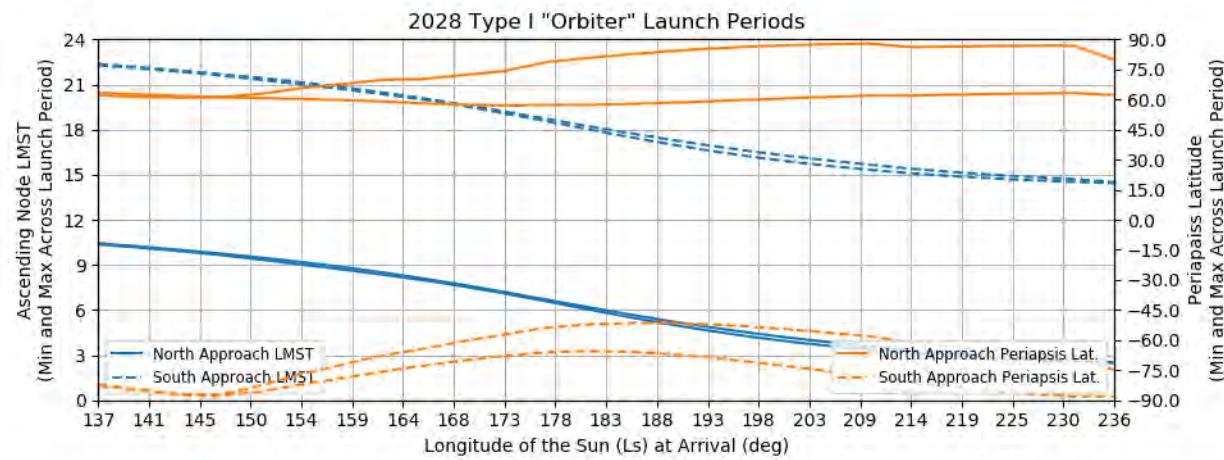


Figure 289: Earth to Mars 2028 Type I Orbiter Launch Periods - Ascending Node LMST and Periapsis Latitude (92 deg inclination)

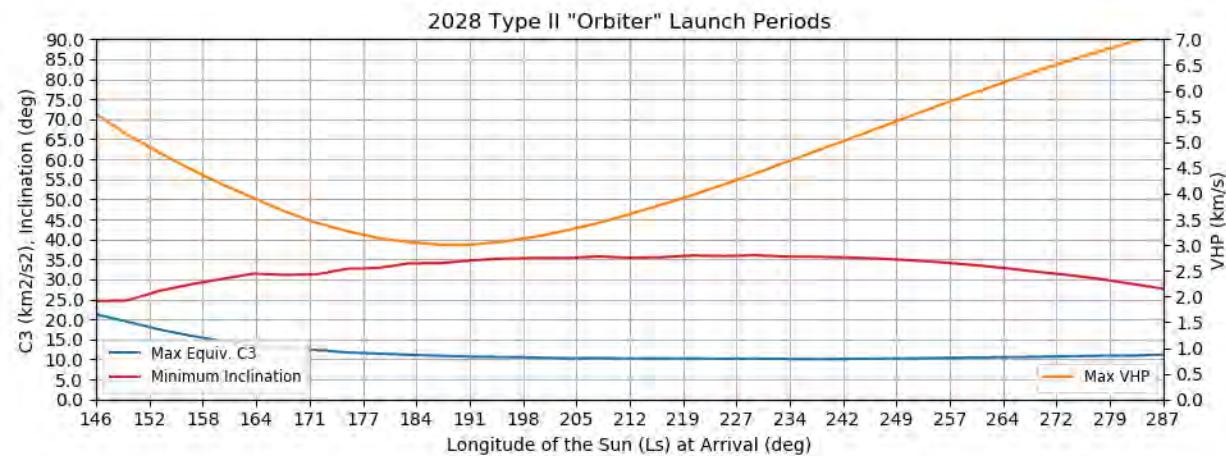


Figure 290: Earth to Mars 2028 Type II Orbiter Launch Periods - Reachable Inclination, Launch Mass, and VHP

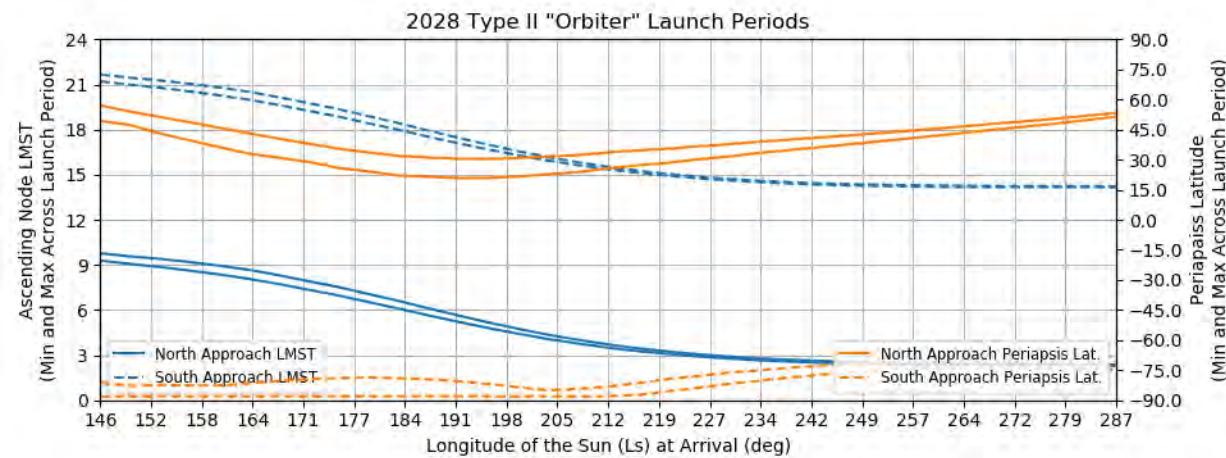


Figure 291: Earth to Mars 2028 Type II Orbiter Launch Periods - Ascending Node LMST and Periapsis Latitude (92 deg inclination)

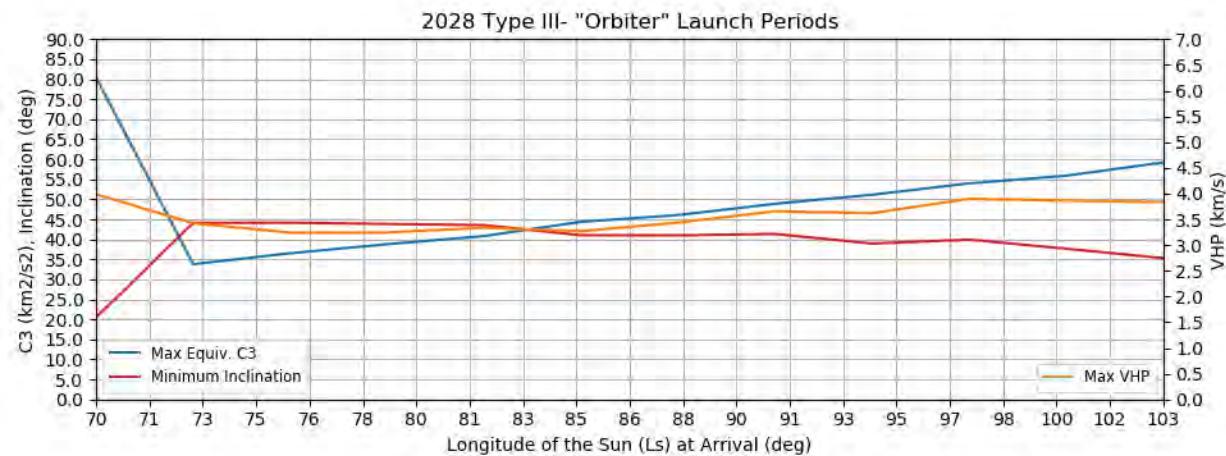


Figure 292: Earth to Mars 2028 Type III- Orbiter Launch Periods - Reachable Inclination, Launch Mass, and VHP

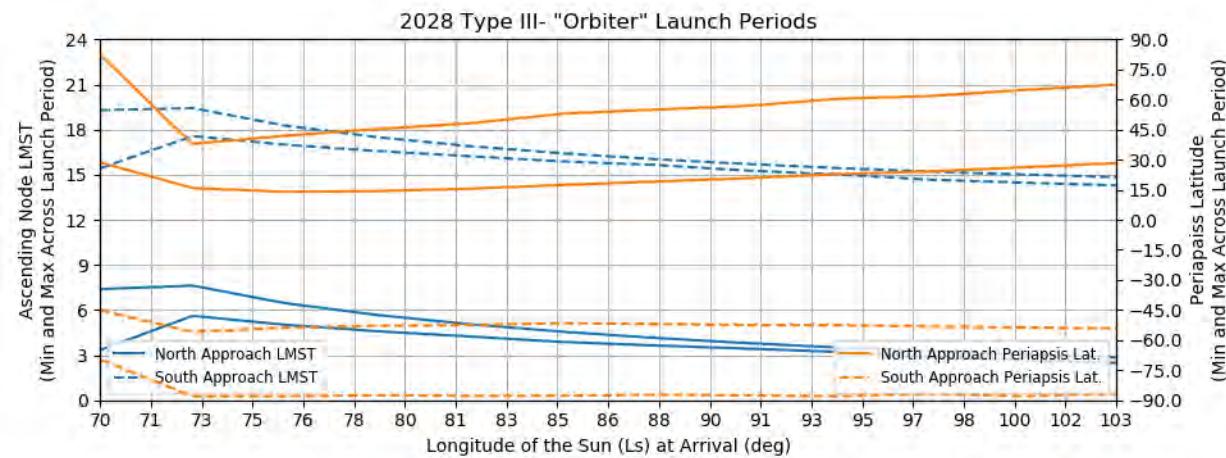


Figure 293: Earth to Mars 2028 Type III- Orbiter Launch Periods - Ascending Node LMST and Periapsis Latitude (92 deg inclination)

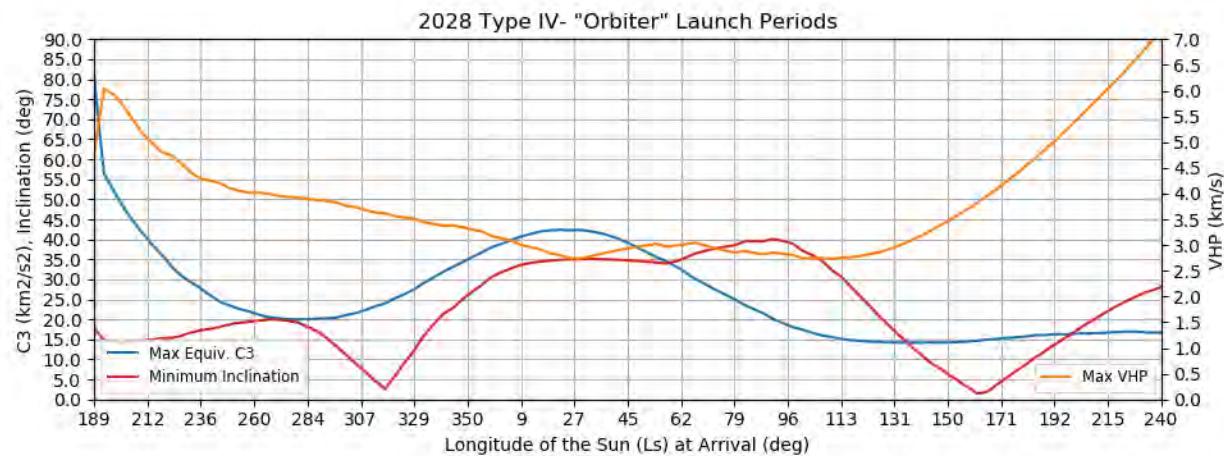


Figure 294: Earth to Mars 2028 Type IV- Orbiter Launch Periods - Reachable Inclination, Launch Mass, and VHP

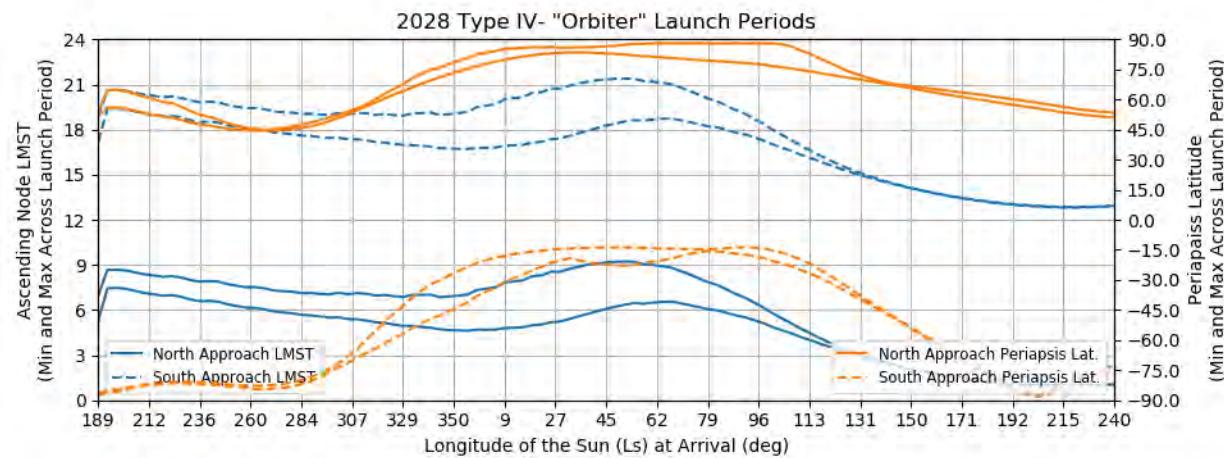


Figure 295: Earth to Mars 2028 Type IV- Orbiter Launch Periods - Ascending Node LMST and Periapsis Latitude (92 deg inclination)

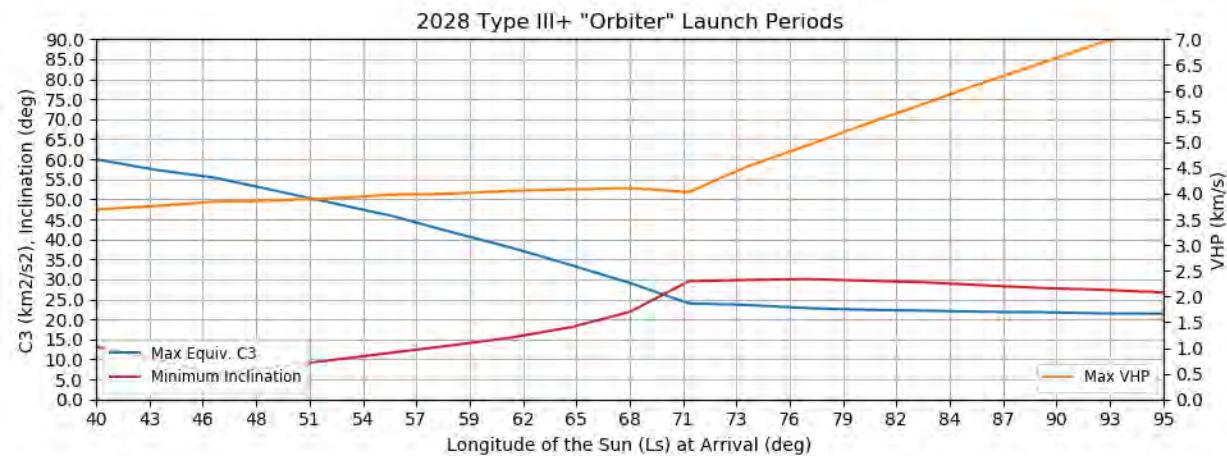


Figure 296: Earth to Mars 2028 Type III+ Orbiter Launch Periods - Reachable Inclination, Launch Mass, and VHP

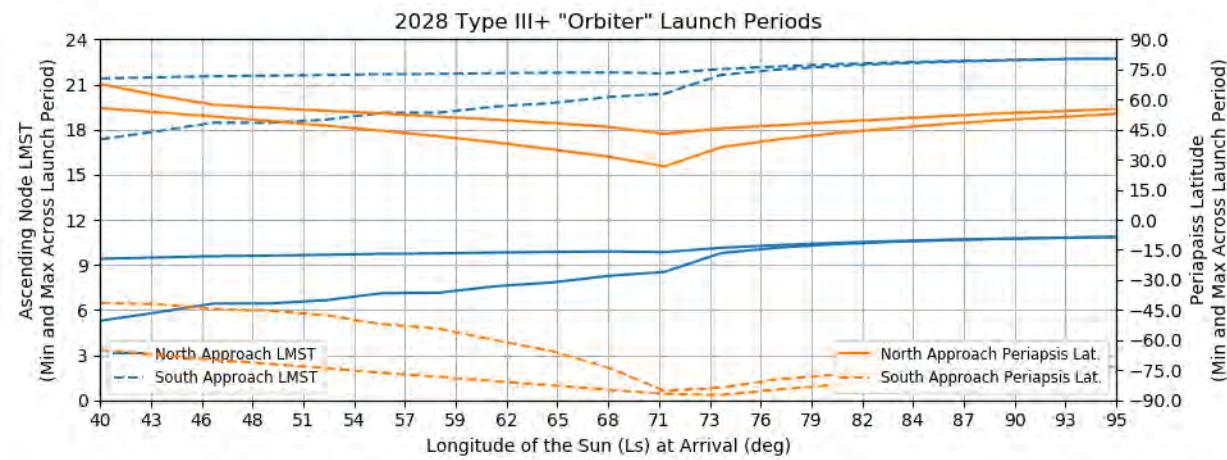


Figure 297: Earth to Mars 2028 Type III+ Orbiter Launch Periods - Ascending Node LMST and Periapsis Latitude (92 deg inclination)

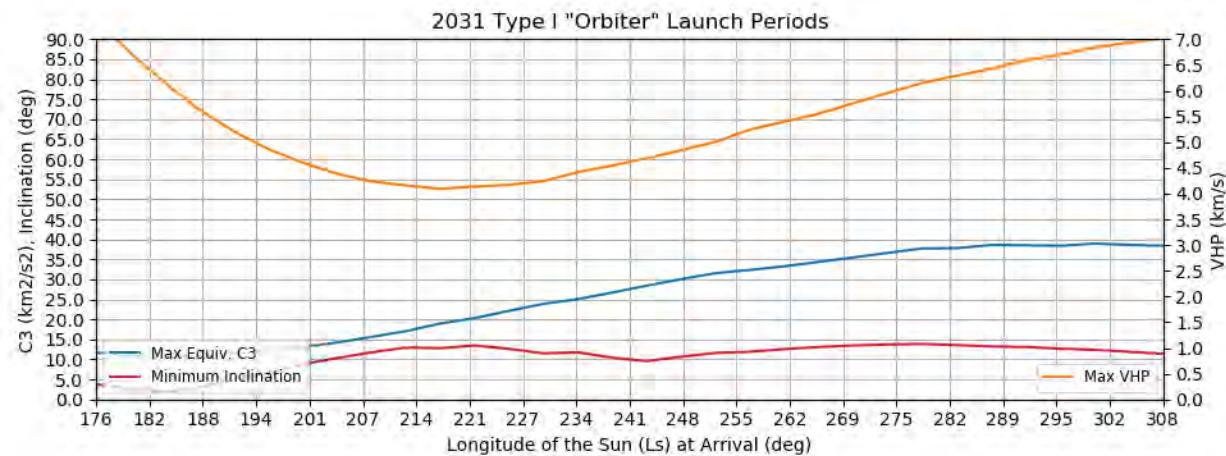


Figure 298: Earth to Mars 2031 Type I Orbiter Launch Periods - Reachable Inclination, Launch Mass, and VHP

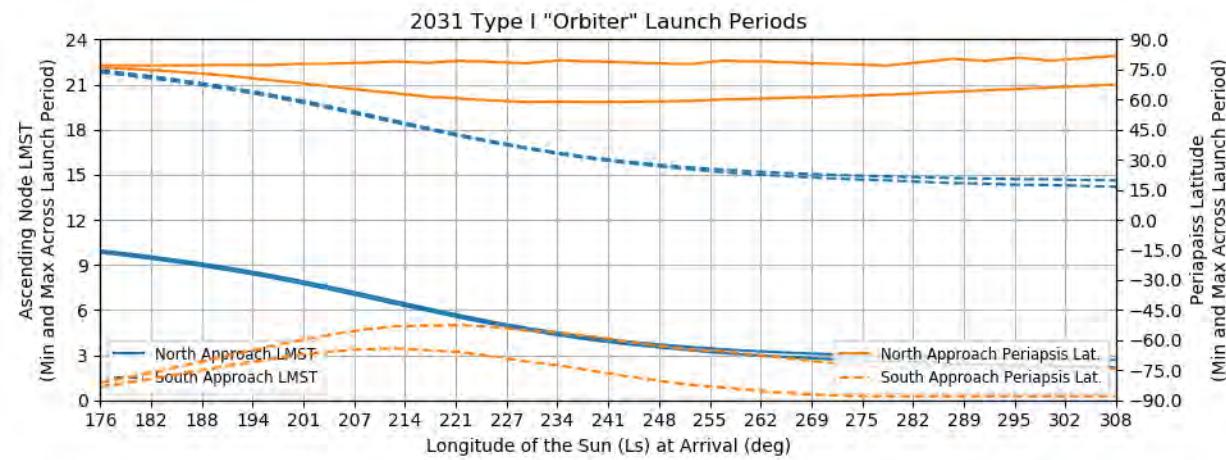
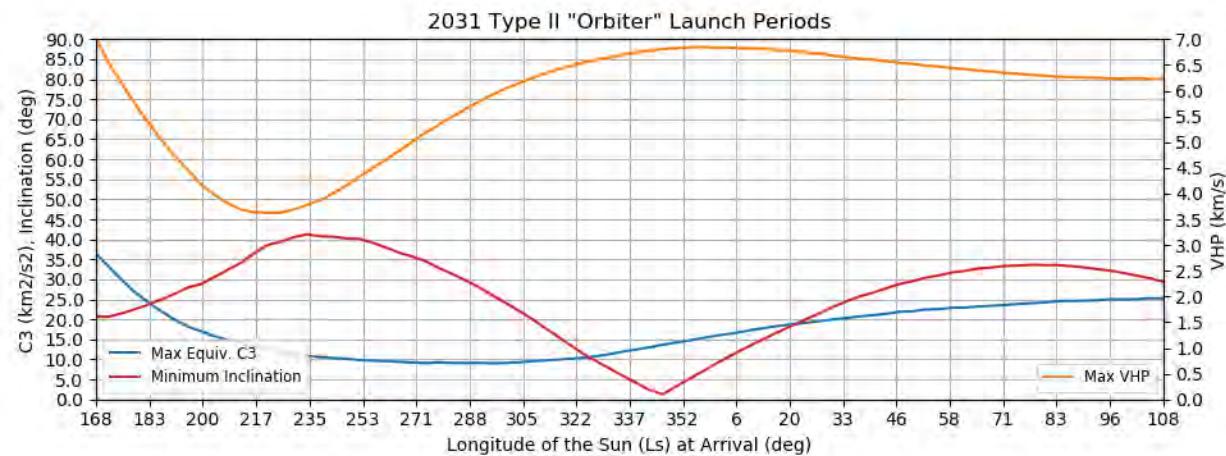
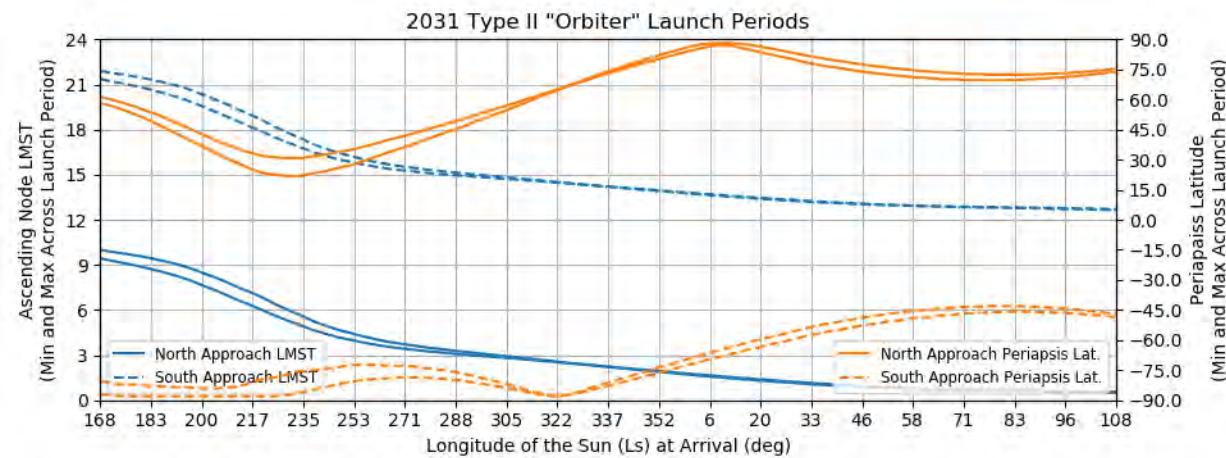


Figure 299: Earth to Mars 2031 Type I Orbiter Launch Periods - Ascending Node LMST and Periapsis Latitude (92 deg inclination)



**Figure 300: Earth to Mars 2031 Type II Orbiter Launch Periods - Reachable Inclination, Launch Mass, and VHP**



**Figure 301: Earth to Mars 2031 Type II Orbiter Launch Periods - Ascending Node LMST and Periapsis Latitude (92 deg inclination)**

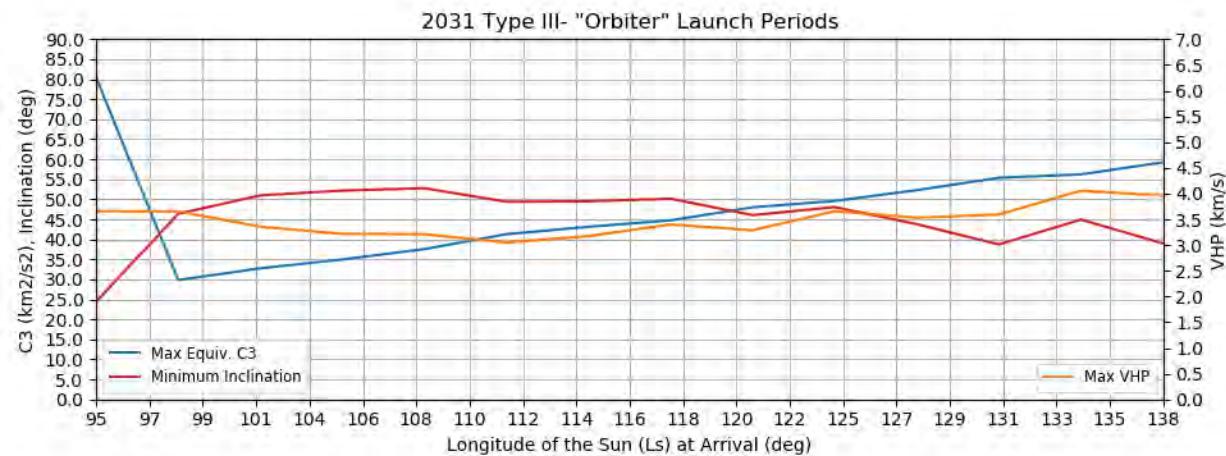


Figure 302: Earth to Mars 2031 Type III- Orbiter Launch Periods - Reachable Inclination, Launch Mass, and VHP

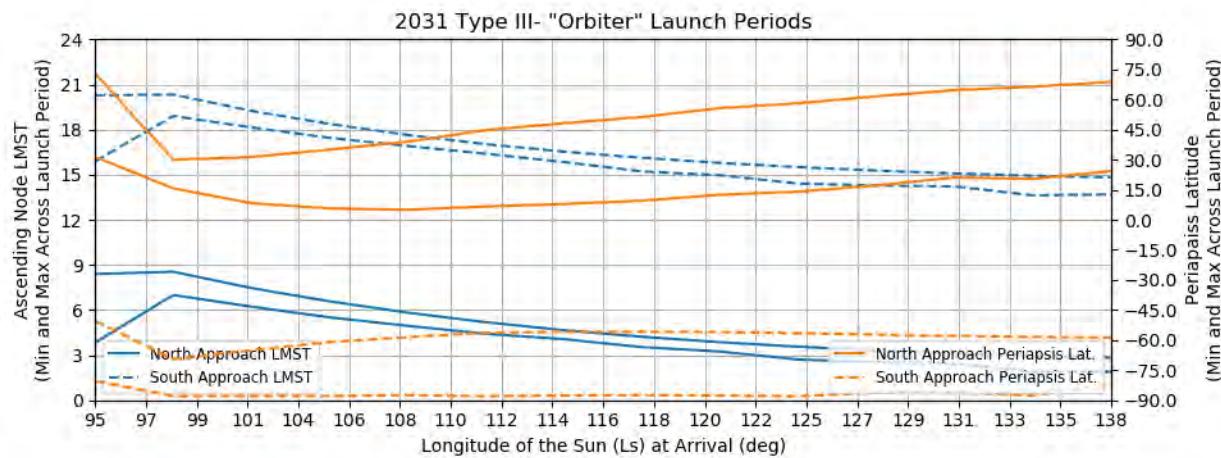


Figure 303: Earth to Mars 2031 Type III- Orbiter Launch Periods - Ascending Node LMST and Periapsis Latitude (92 deg inclination)

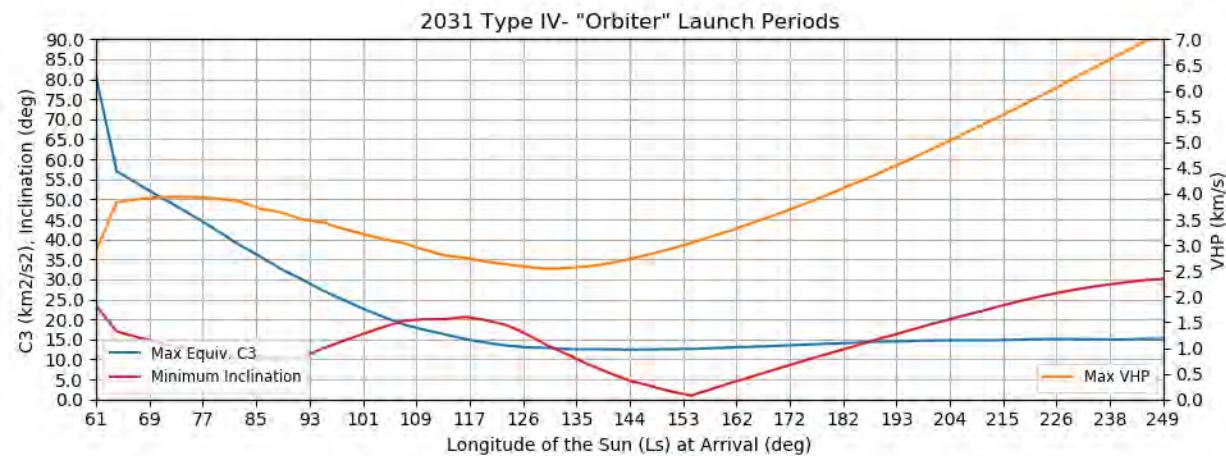


Figure 304: Earth to Mars 2031 Type IV- Orbiter Launch Periods - Reachable Inclination, Launch Mass, and VHP

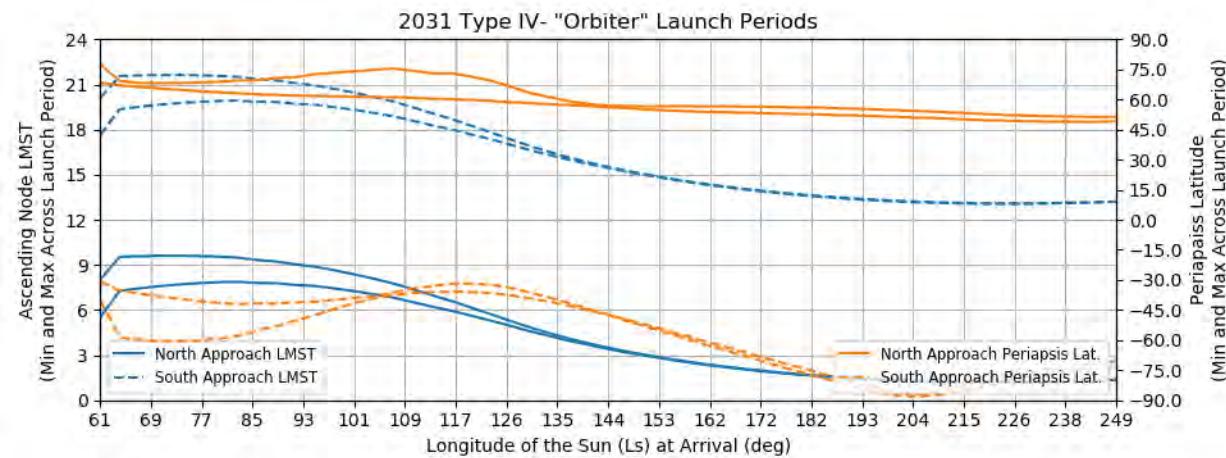


Figure 305: Earth to Mars 2031 Type IV- Orbiter Launch Periods - Ascending Node LMST and Periapsis Latitude (92 deg inclination)

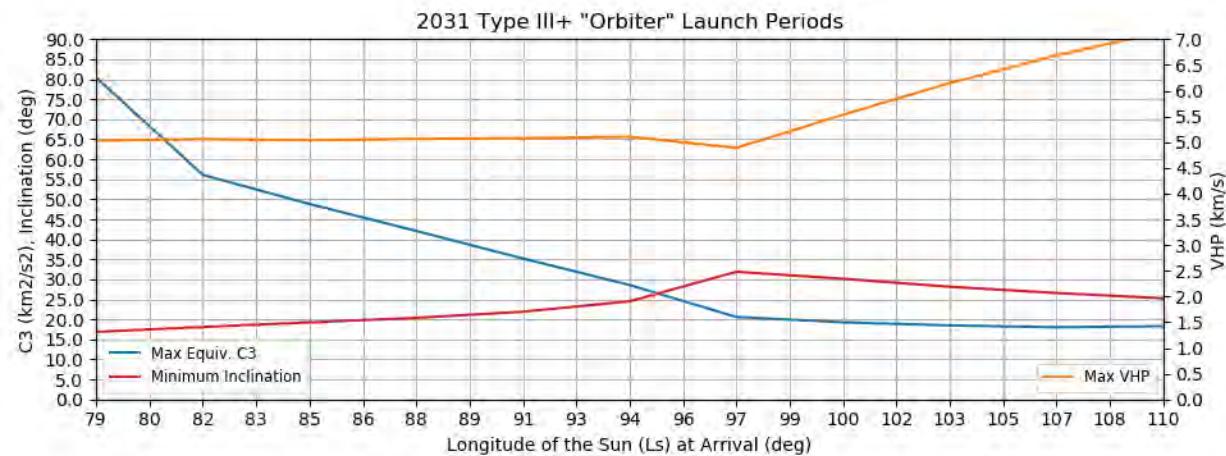


Figure 306: Earth to Mars 2031 Type III+ Orbiter Launch Periods - Reachable Inclination, Launch Mass, and VHP

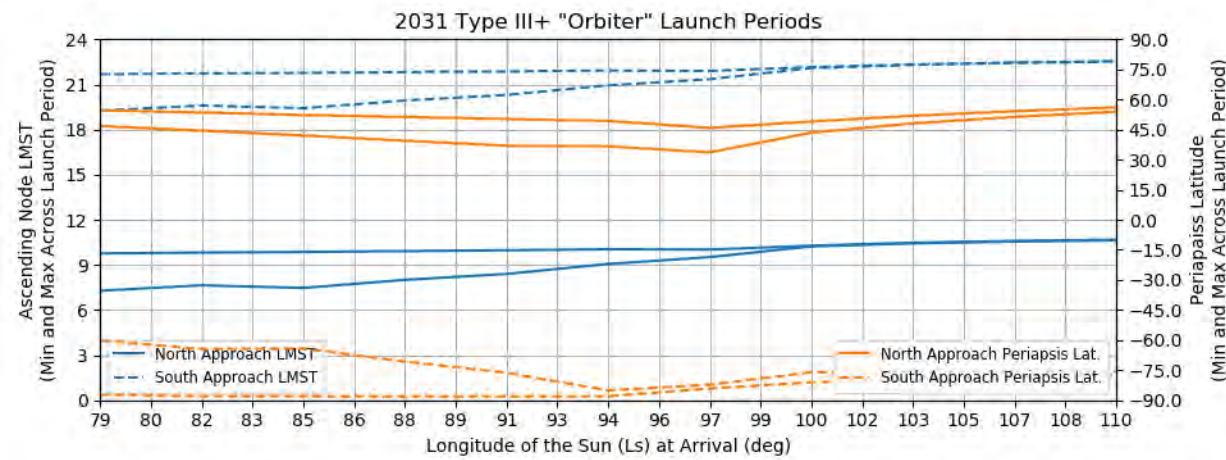


Figure 307: Earth to Mars 2031 Type III+ Orbiter Launch Periods - Ascending Node LMST and Periapsis Latitude (92 deg inclination)

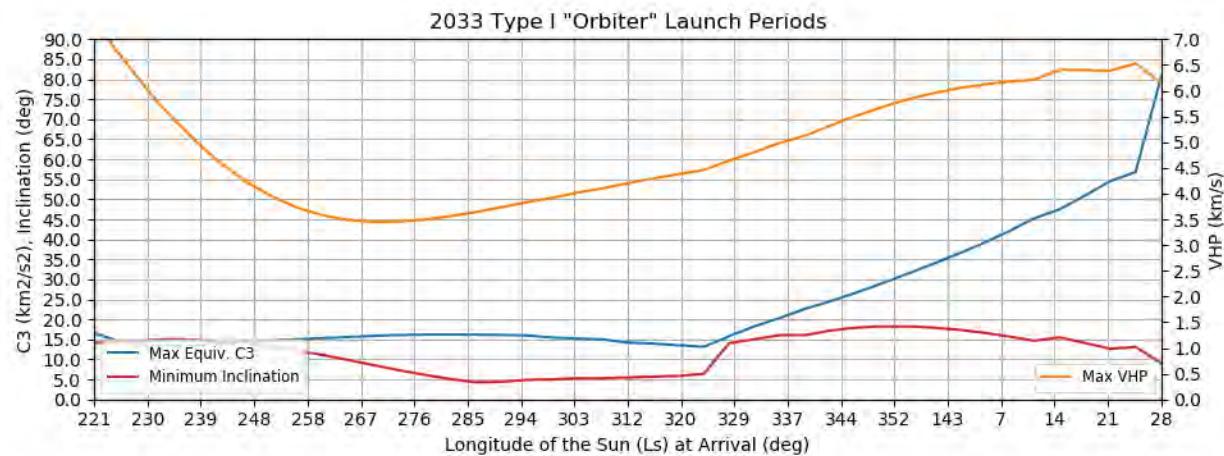


Figure 308: Earth to Mars 2033 Type I Orbiter Launch Periods - Reachable Inclination, Launch Mass, and VHP

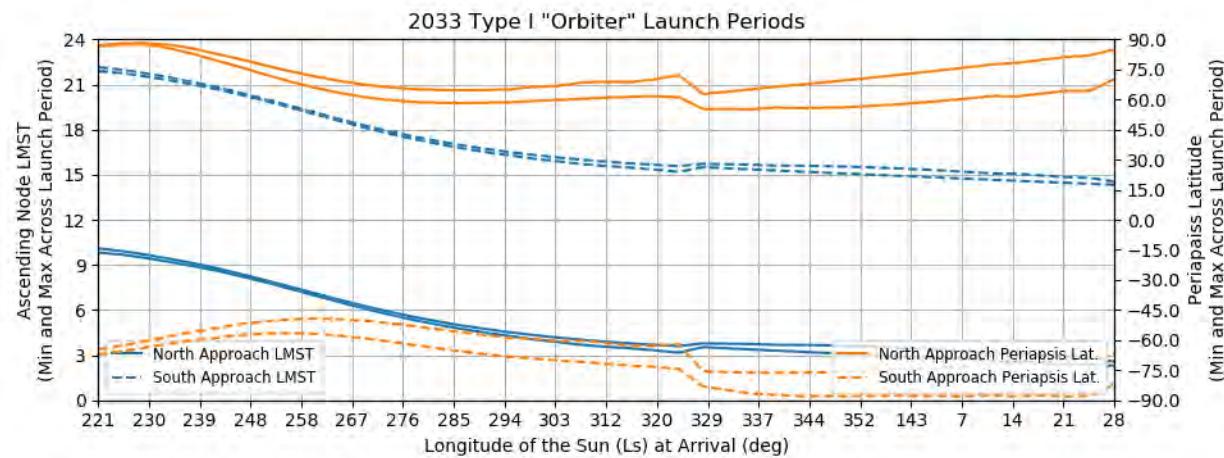


Figure 309: Earth to Mars 2033 Type I Orbiter Launch Periods - Ascending Node LMST and Periapsis Latitude (92 deg inclination)

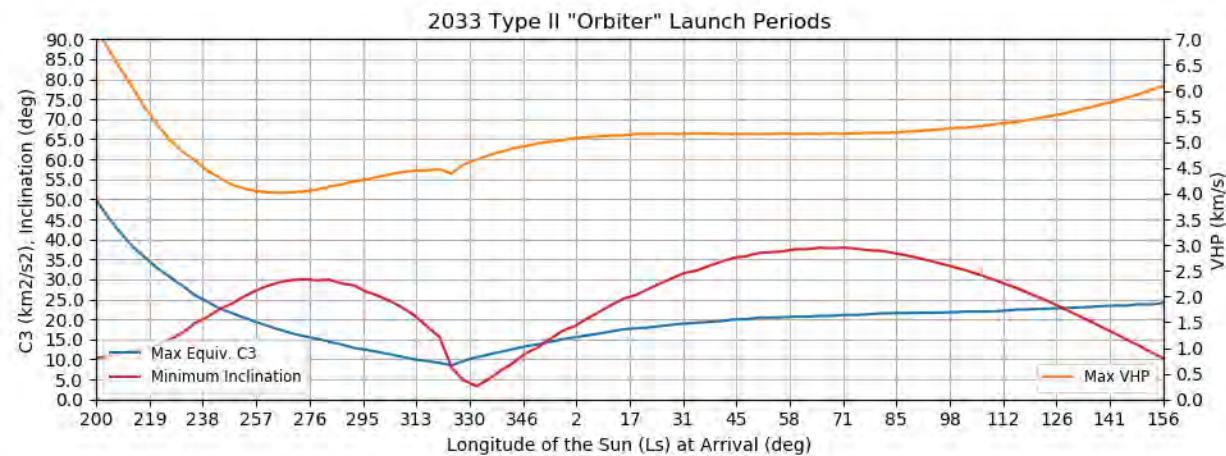


Figure 310: Earth to Mars 2033 Type II Orbiter Launch Periods - Reachable Inclination, Launch Mass, and VHP

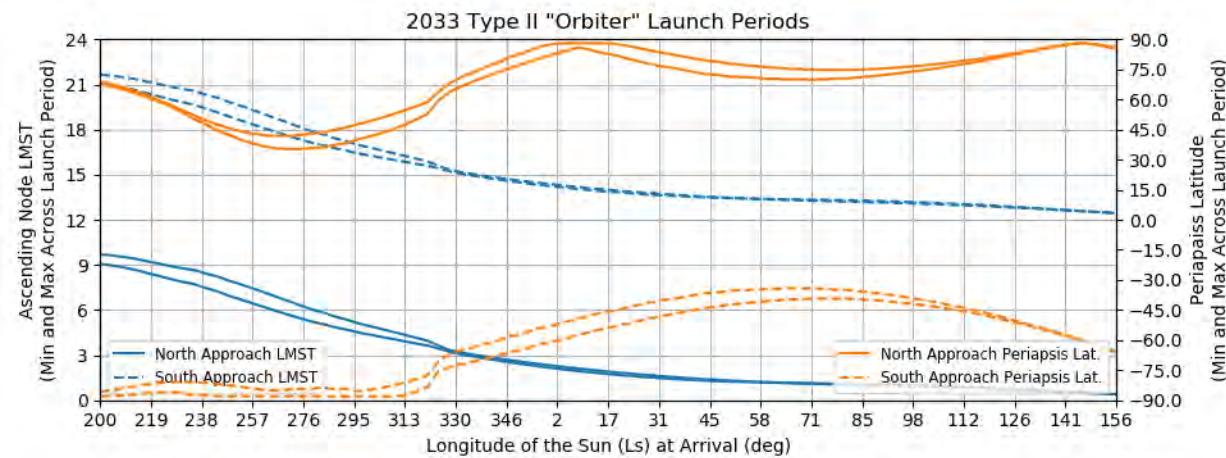


Figure 311: Earth to Mars 2033 Type II Orbiter Launch Periods - Ascending Node LMST and Periapsis Latitude (92 deg inclination)

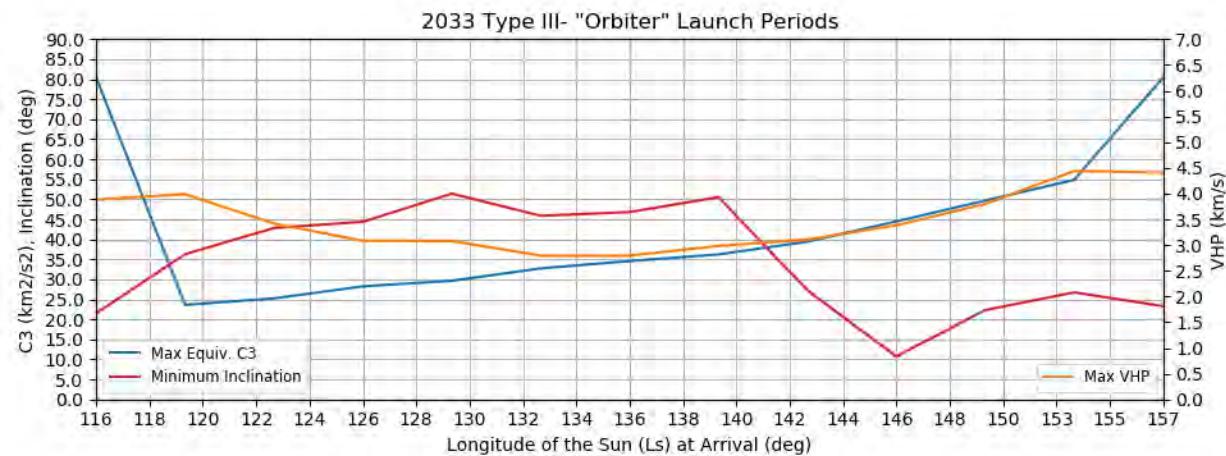


Figure 312: Earth to Mars 2033 Type III- Orbiter Launch Periods - Reachable Inclination, Launch Mass, and VHP

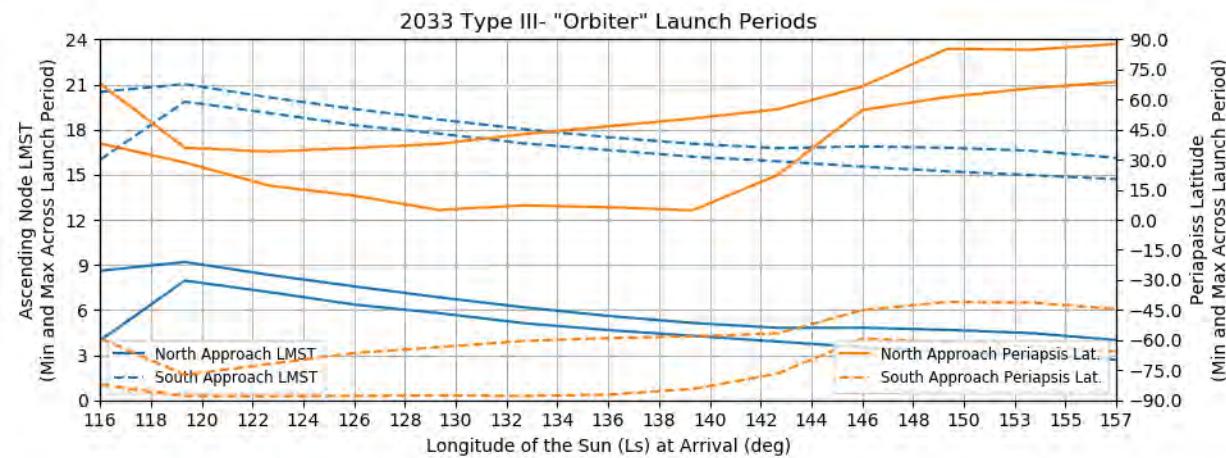


Figure 313: Earth to Mars 2033 Type III- Orbiter Launch Periods - Ascending Node LMST and Periapsis Latitude (92 deg inclination)

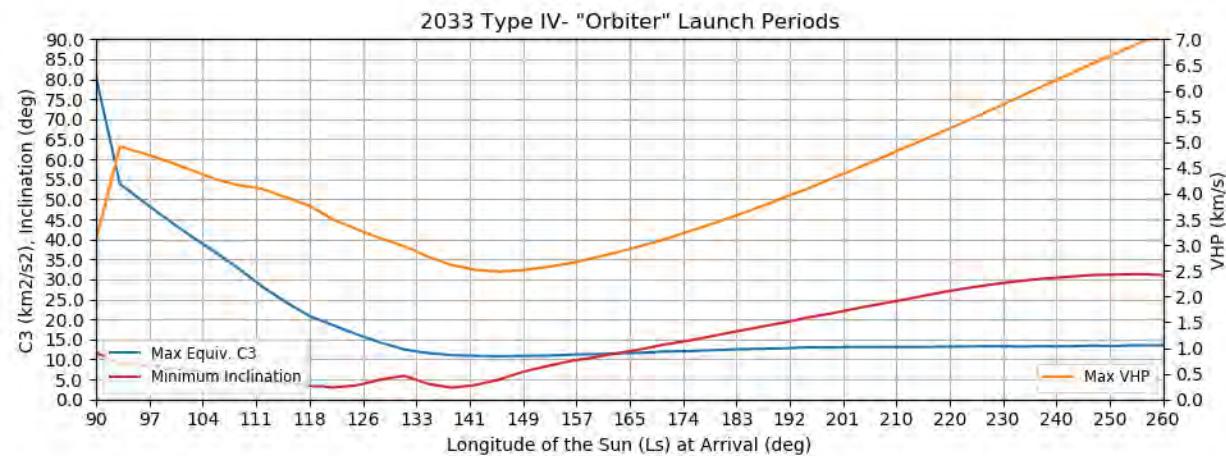


Figure 314: Earth to Mars 2033 Type IV- Orbiter Launch Periods - Reachable Inclination, Launch Mass, and VHP

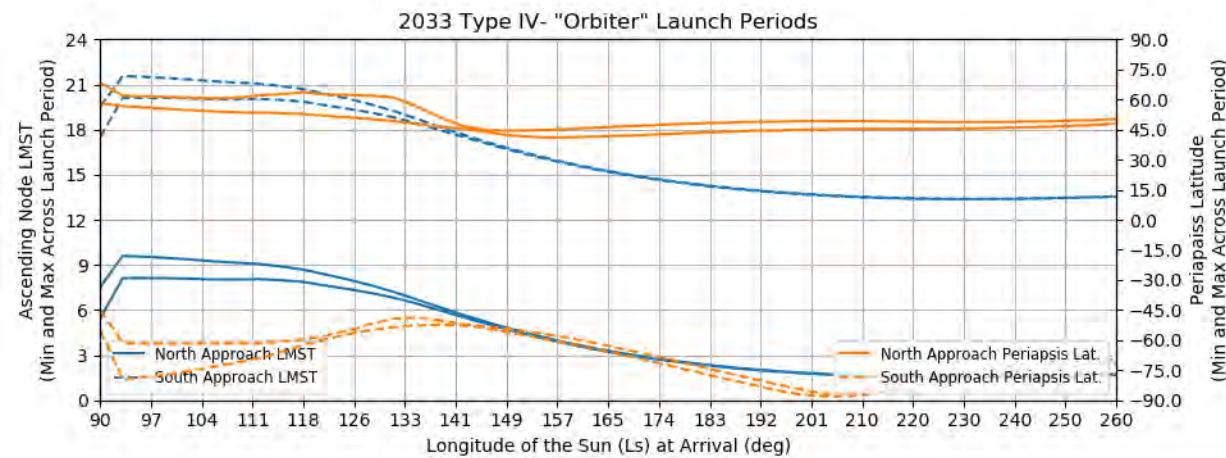


Figure 315: Earth to Mars 2033 Type IV- Orbiter Launch Periods - Ascending Node LMST and Periapsis Latitude (92 deg inclination)

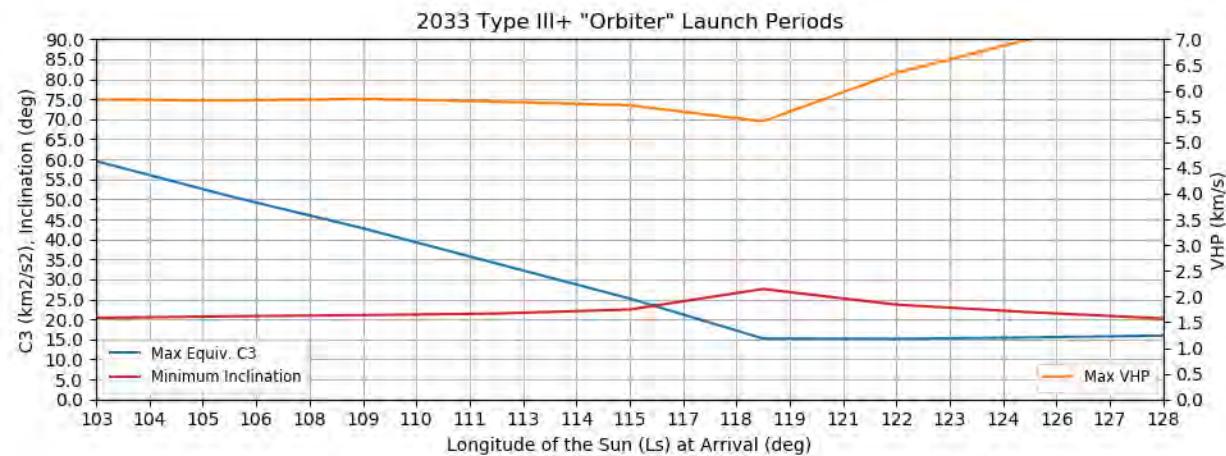


Figure 316: Earth to Mars 2033 Type III+ Orbiter Launch Periods - Reachable Inclination, Launch Mass, and VHP

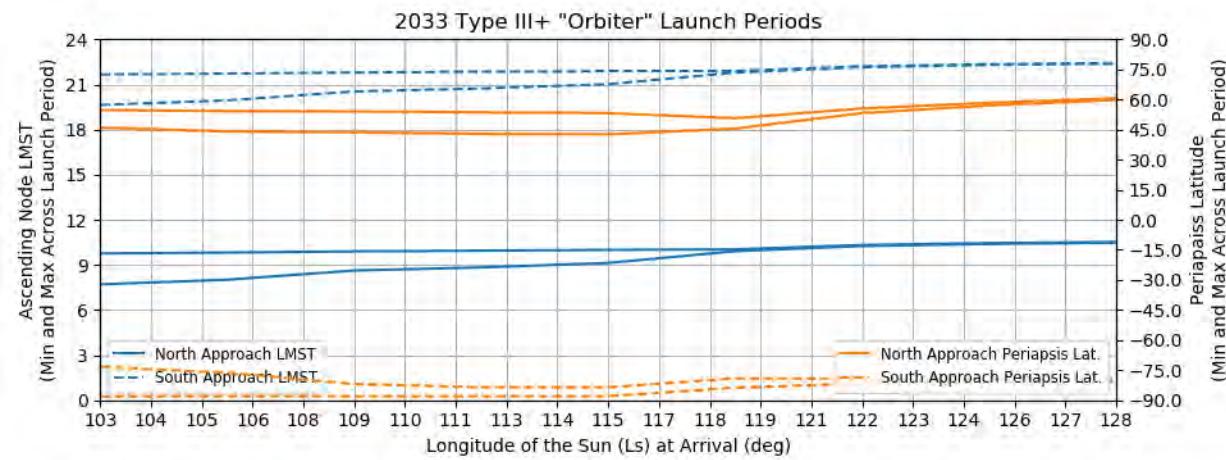


Figure 317: Earth to Mars 2033 Type III+ Orbiter Launch Periods - Ascending Node LMST and Periapsis Latitude (92 deg inclination)

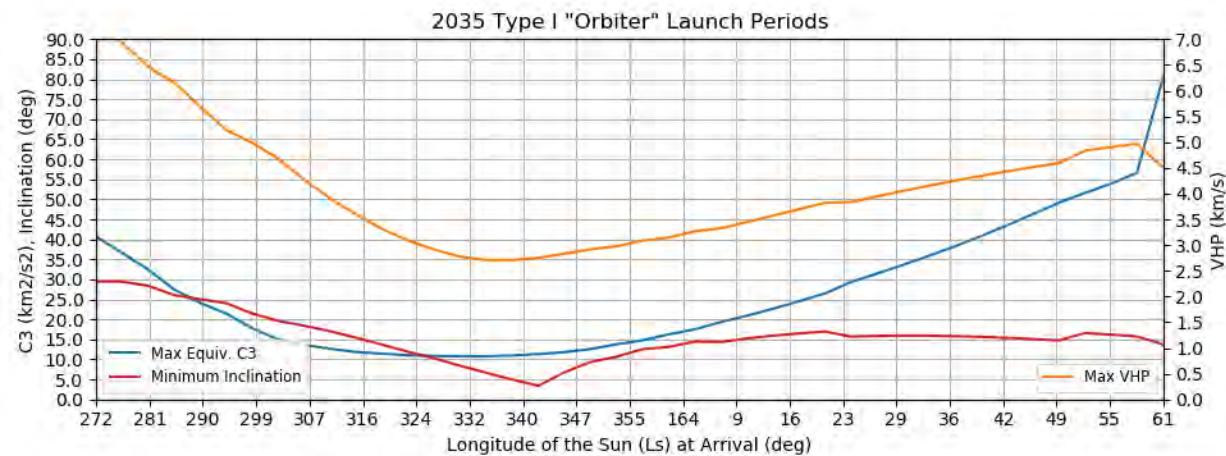


Figure 318: Earth to Mars 2035 Type I Orbiter Launch Periods - Reachable Inclination, Launch Mass, and VHP

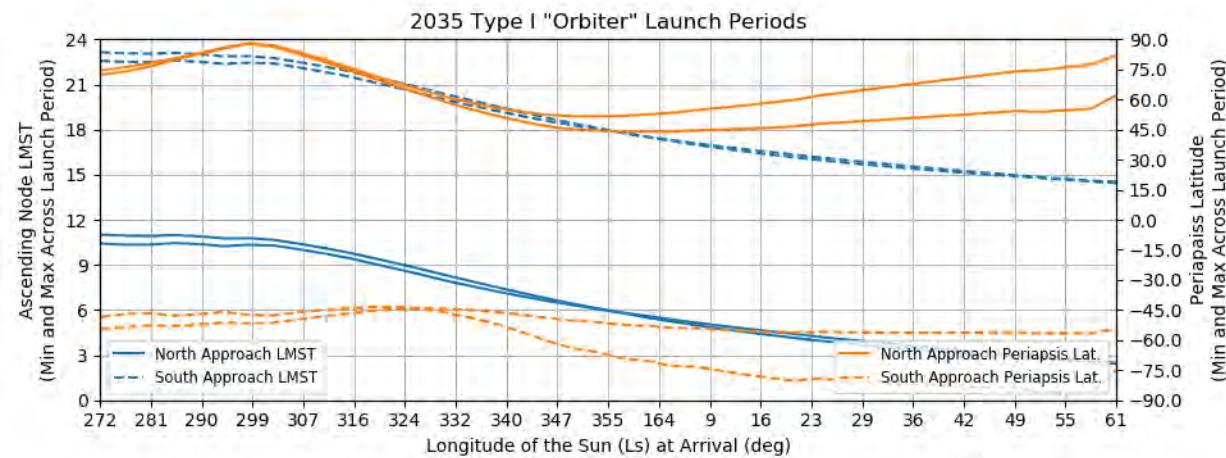


Figure 319: Earth to Mars 2035 Type I Orbiter Launch Periods - Ascending Node LMST and Periapsis Latitude (92 deg inclination)

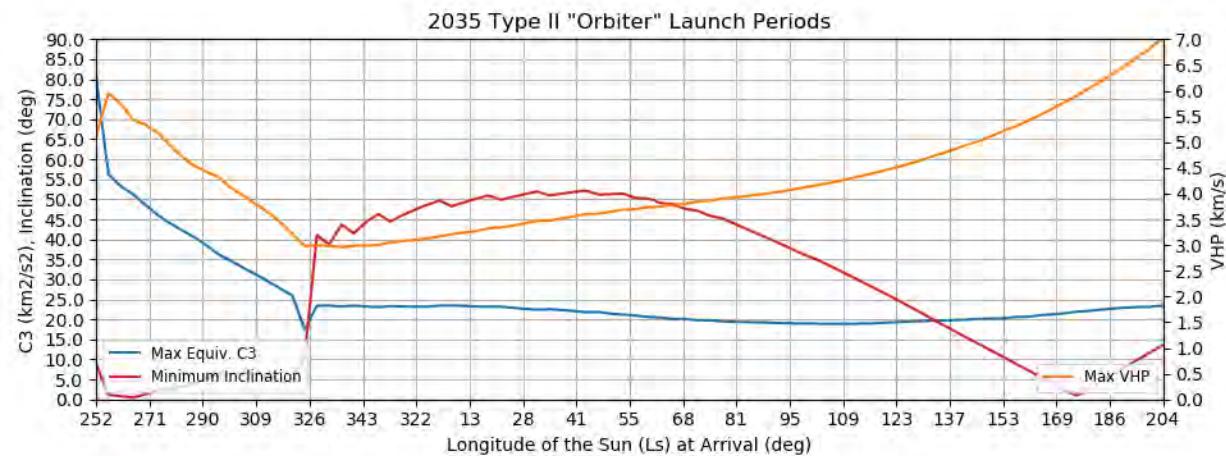


Figure 320: Earth to Mars 2035 Type II Orbiter Launch Periods - Reachable Inclination, Launch Mass, and VHP

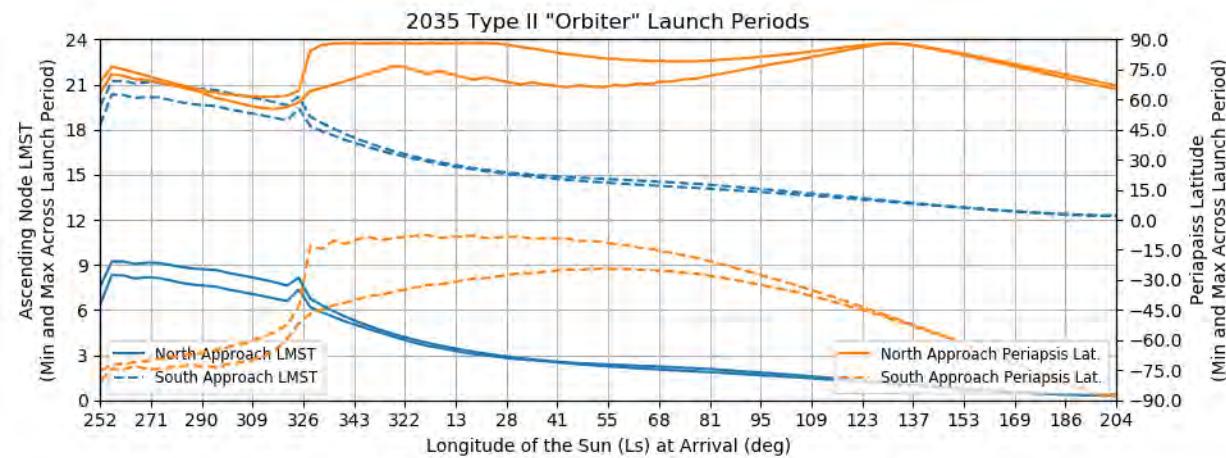


Figure 321: Earth to Mars 2035 Type II Orbiter Launch Periods - Ascending Node LMST and Periapsis Latitude (92 deg inclination)

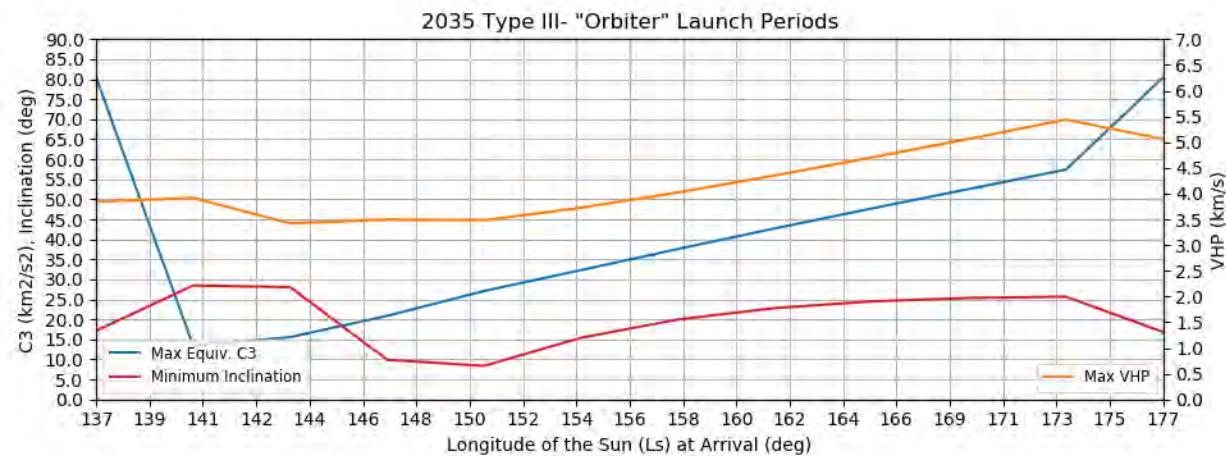


Figure 322: Earth to Mars 2035 Type III- Orbiter Launch Periods - Reachable Inclination, Launch Mass, and VHP

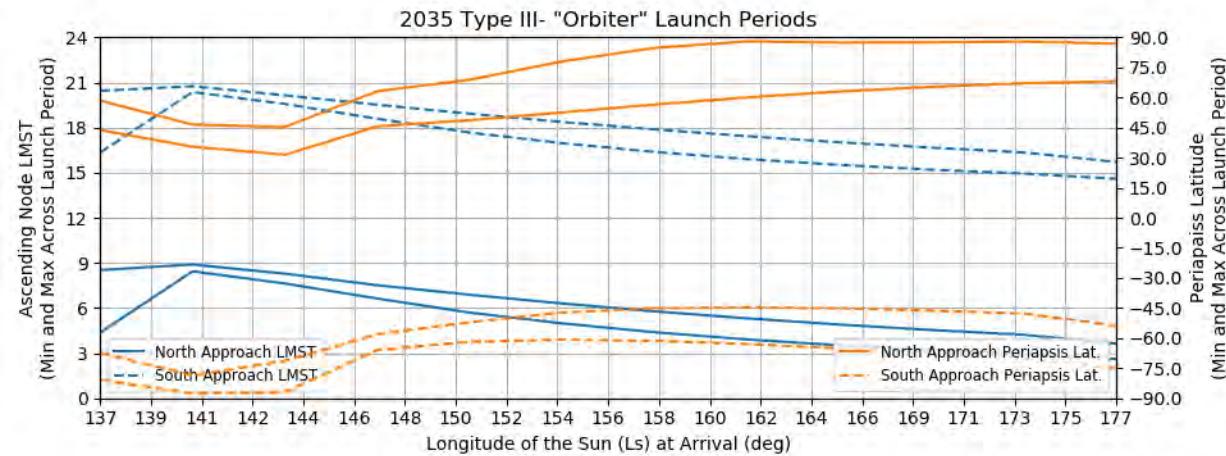


Figure 323: Earth to Mars 2035 Type III- Orbiter Launch Periods - Ascending Node LMST and Periapsis Latitude (92 deg inclination)

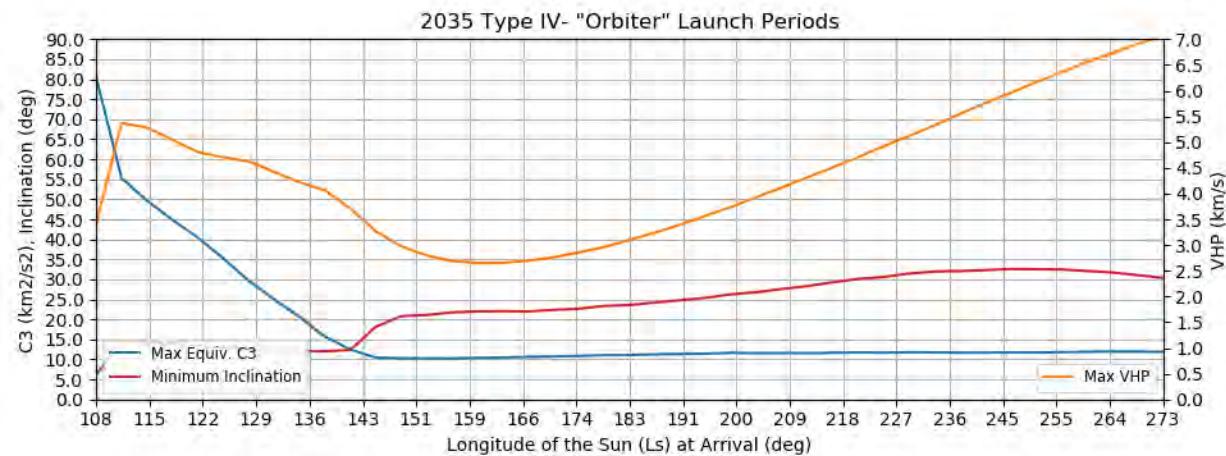


Figure 324: Earth to Mars 2035 Type IV- Orbiter Launch Periods - Reachable Inclination, Launch Mass, and VHP

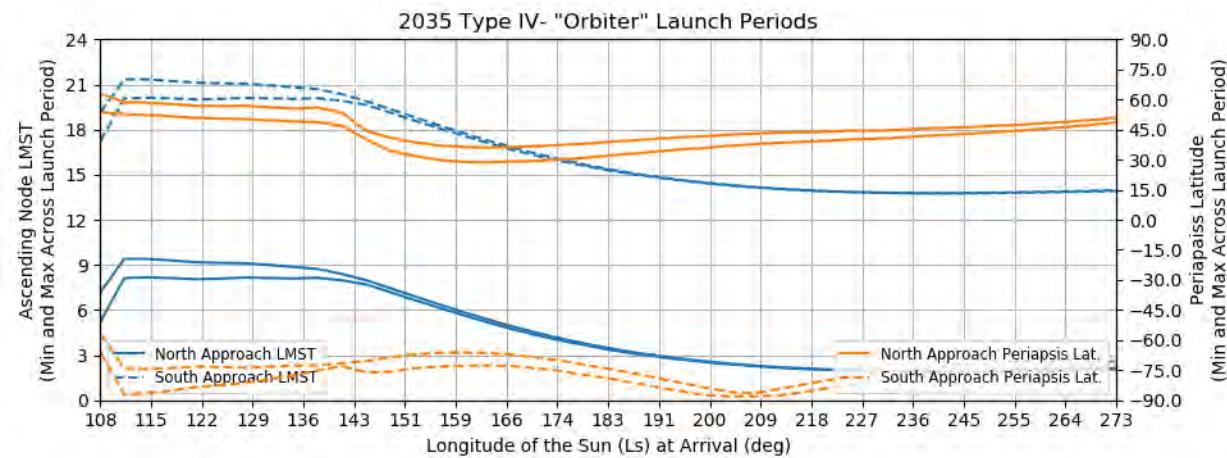


Figure 325: Earth to Mars 2035 Type IV- Orbiter Launch Periods - Ascending Node LMST and Periapsis Latitude (92 deg inclination)

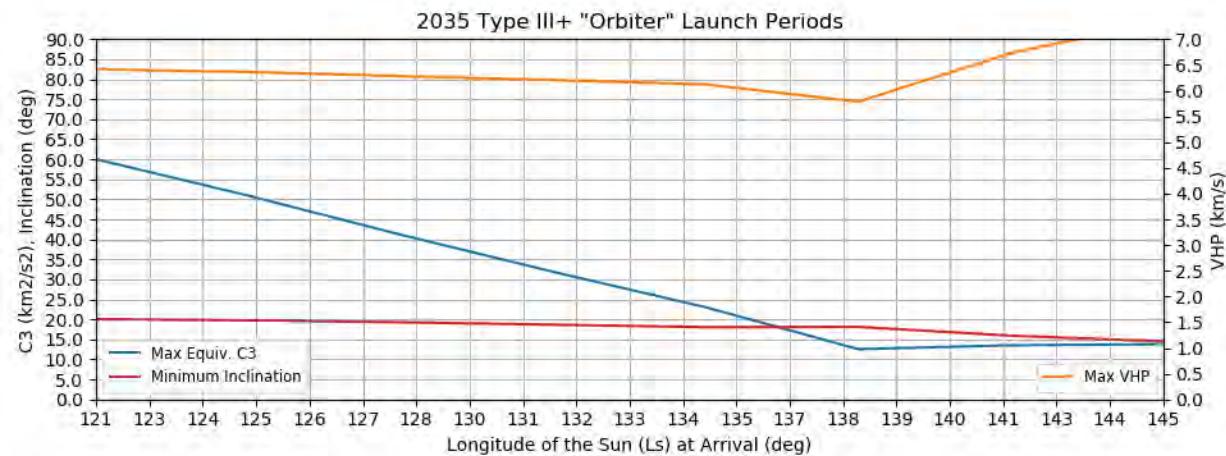


Figure 326: Earth to Mars 2035 Type III+ Orbiter Launch Periods - Reachable Inclination, Launch Mass, and VHP

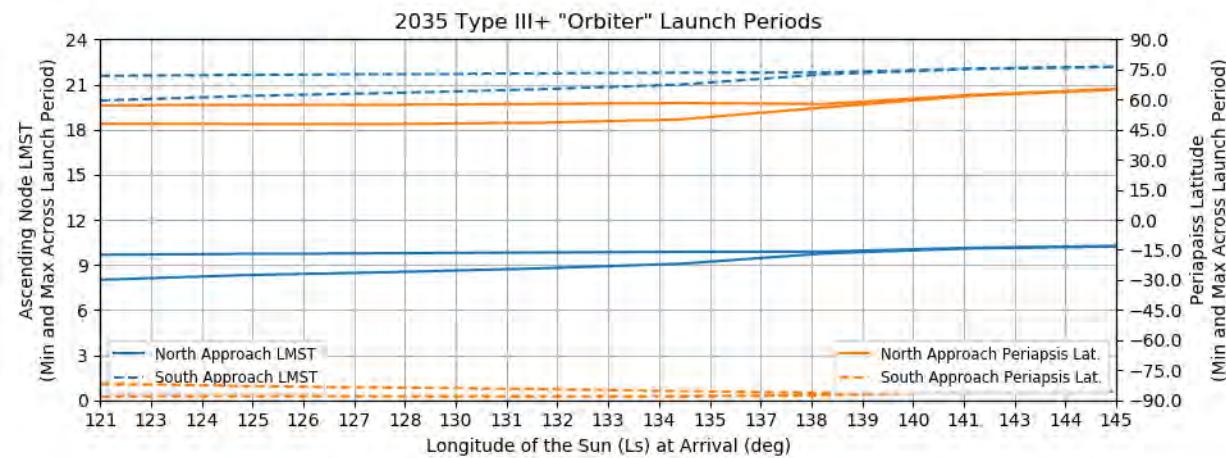


Figure 327: Earth to Mars 2035 Type III+ Orbiter Launch Periods - Ascending Node LMST and Periapsis Latitude (92 deg inclination)

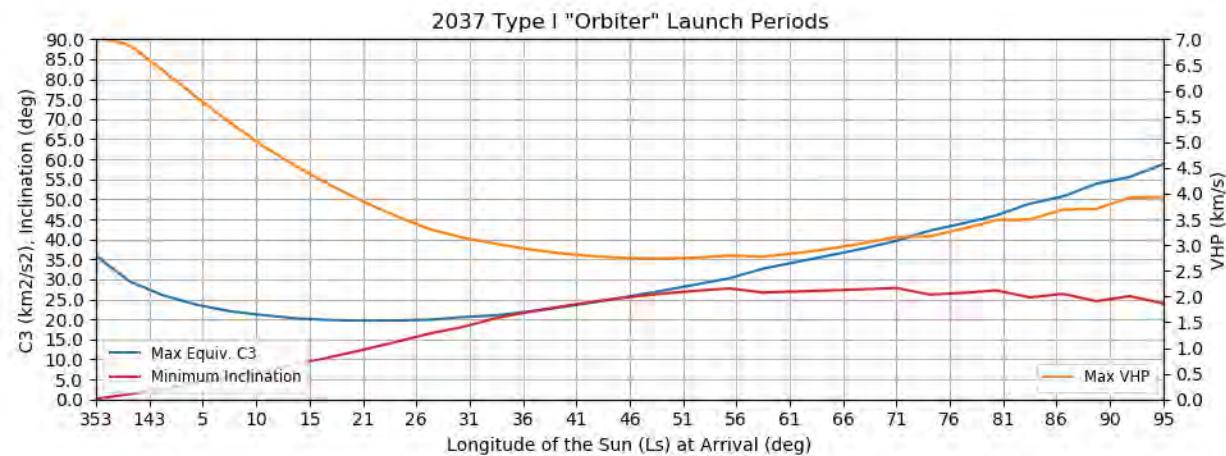


Figure 328: Earth to Mars 2037 Type I Orbiter Launch Periods - Reachable Inclination, Launch Mass, and VHP

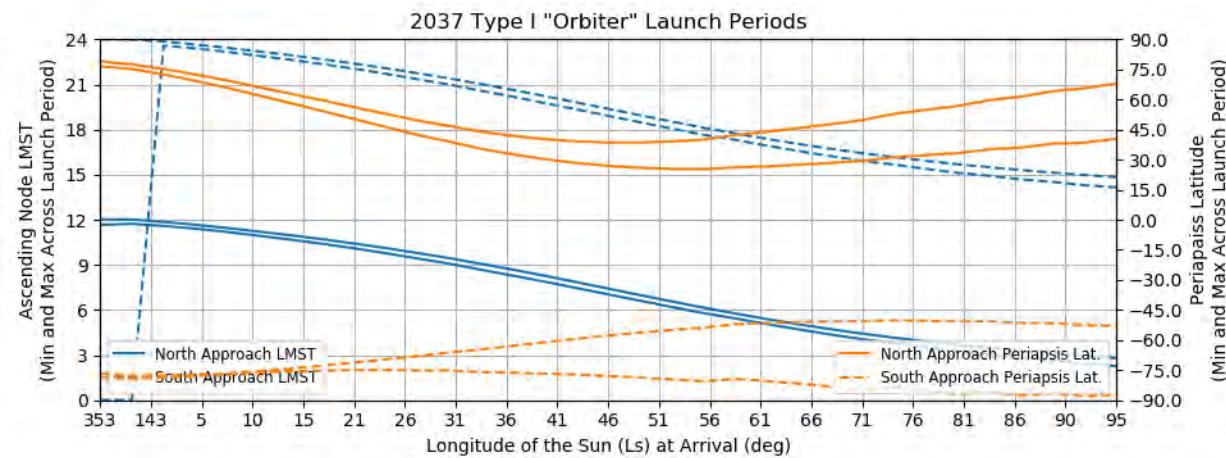


Figure 329: Earth to Mars 2037 Type I Orbiter Launch Periods - Ascending Node LMST and Periapsis Latitude (92 deg inclination)

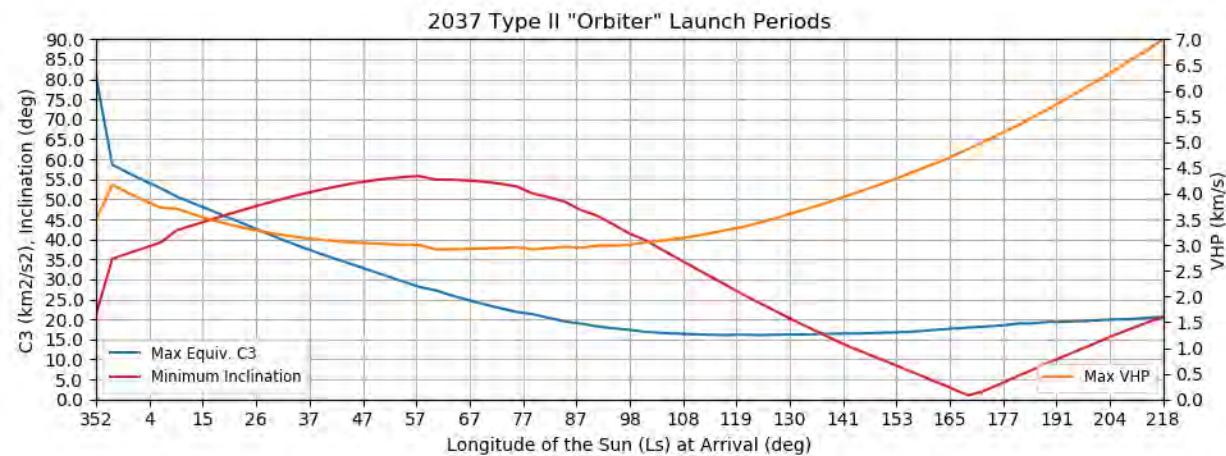


Figure 330: Earth to Mars 2037 Type II Orbiter Launch Periods - Reachable Inclination, Launch Mass, and VHP

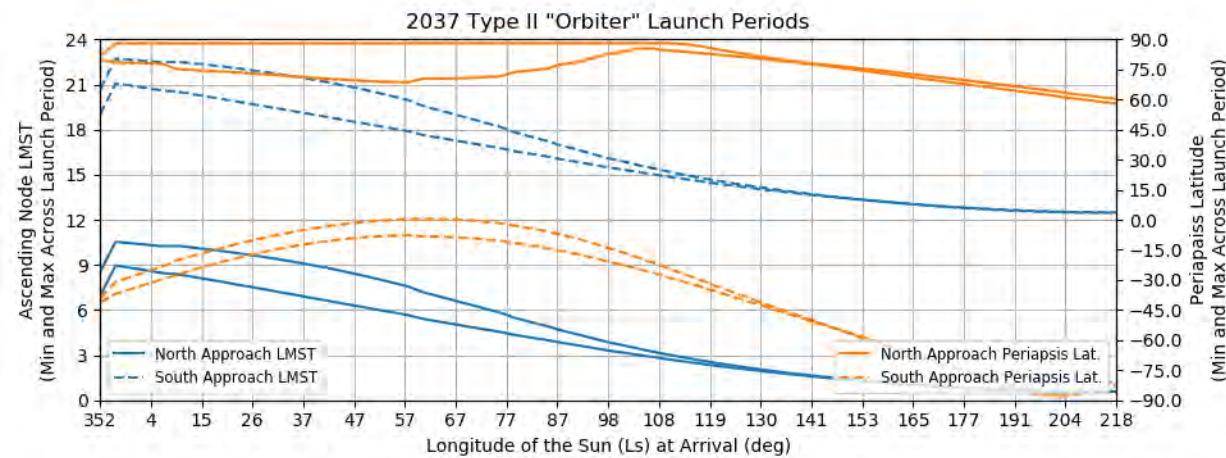


Figure 331: Earth to Mars 2037 Type II Orbiter Launch Periods - Ascending Node LMST and Periapsis Latitude (92 deg inclination)

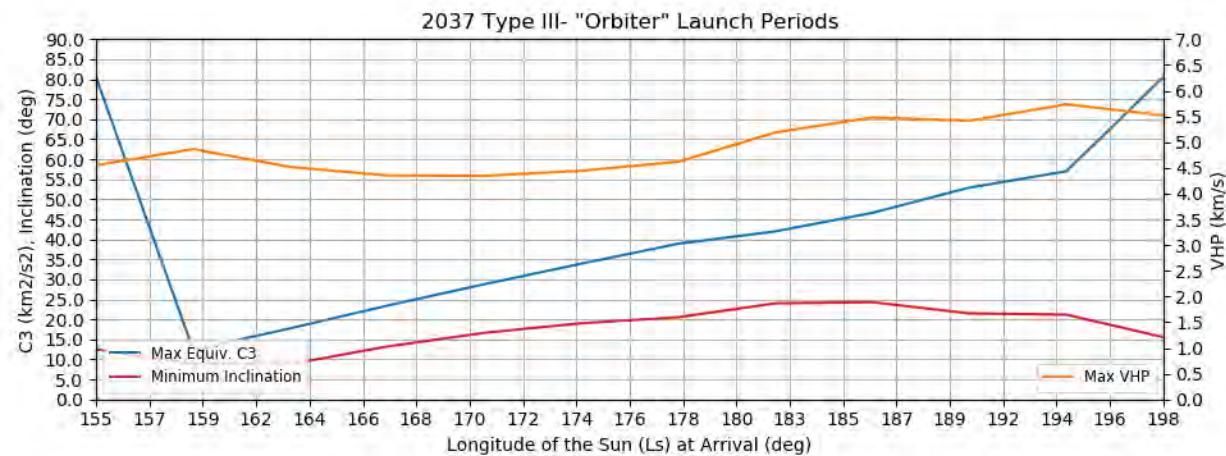


Figure 332: Earth to Mars 2037 Type III- Orbiter Launch Periods - Reachable Inclination, Launch Mass, and VHP

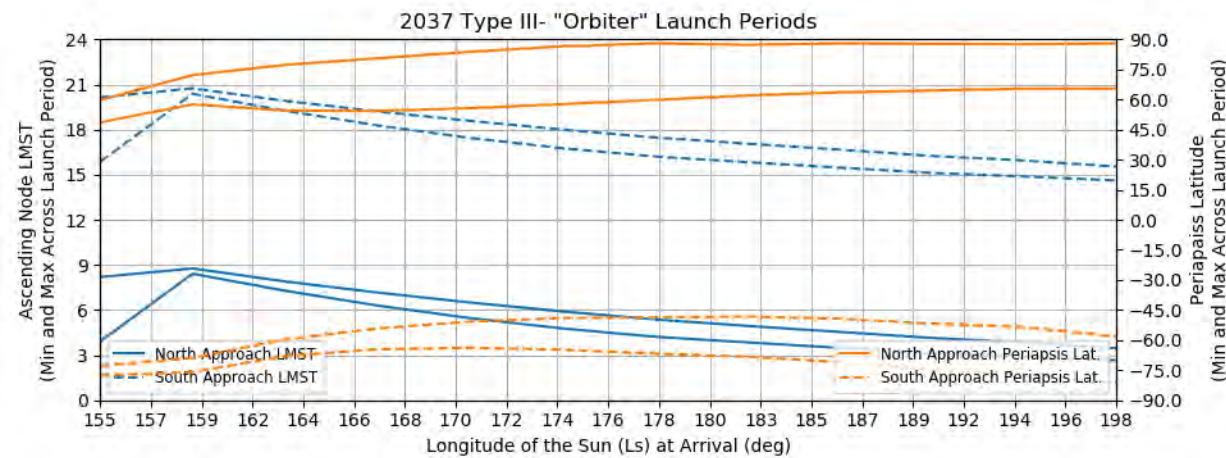


Figure 333: Earth to Mars 2037 Type III- Orbiter Launch Periods - Ascending Node LMST and Periapsis Latitude (92 deg inclination)

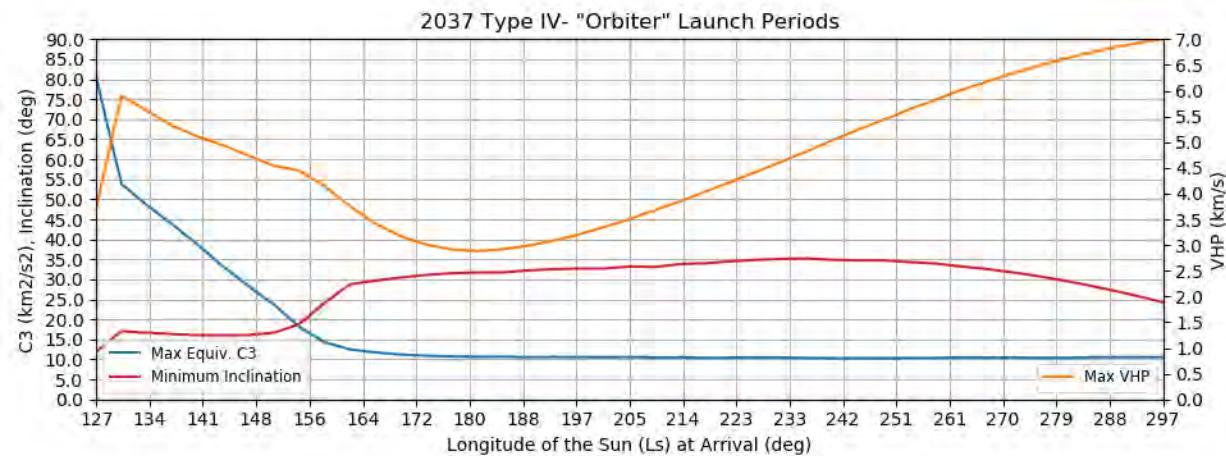


Figure 334: Earth to Mars 2037 Type IV- Orbiter Launch Periods - Reachable Inclination, Launch Mass, and VHP

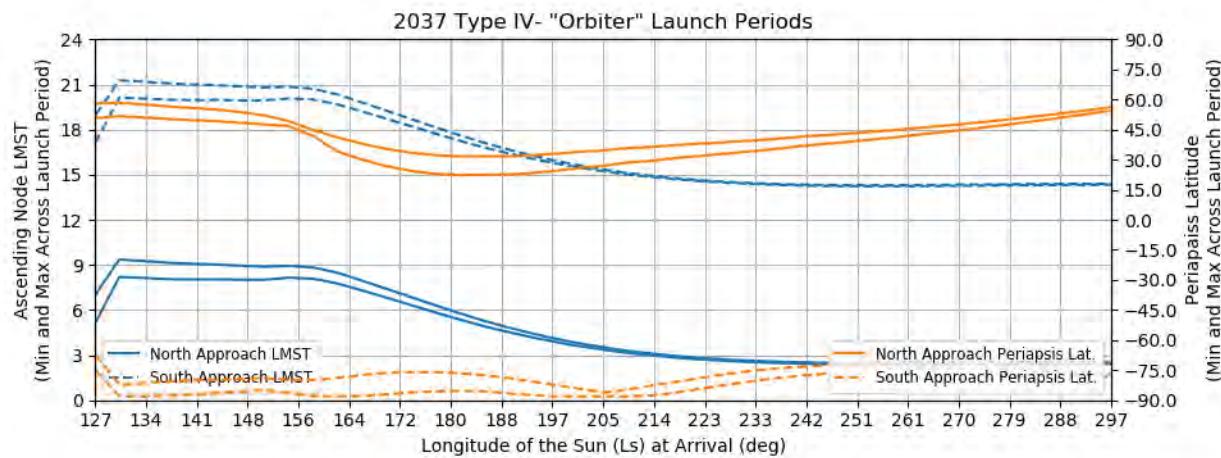


Figure 335: Earth to Mars 2037 Type IV- Orbiter Launch Periods - Ascending Node LMST and Periapsis Latitude (92 deg inclination)

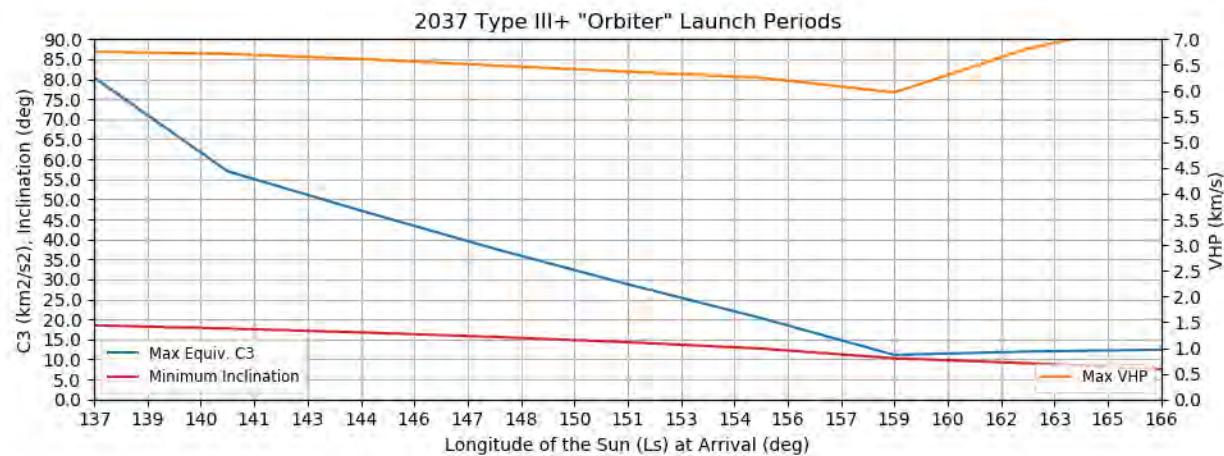


Figure 336: Earth to Mars 2037 Type III+ Orbiter Launch Periods - Reachable Inclination, Launch Mass, and VHP

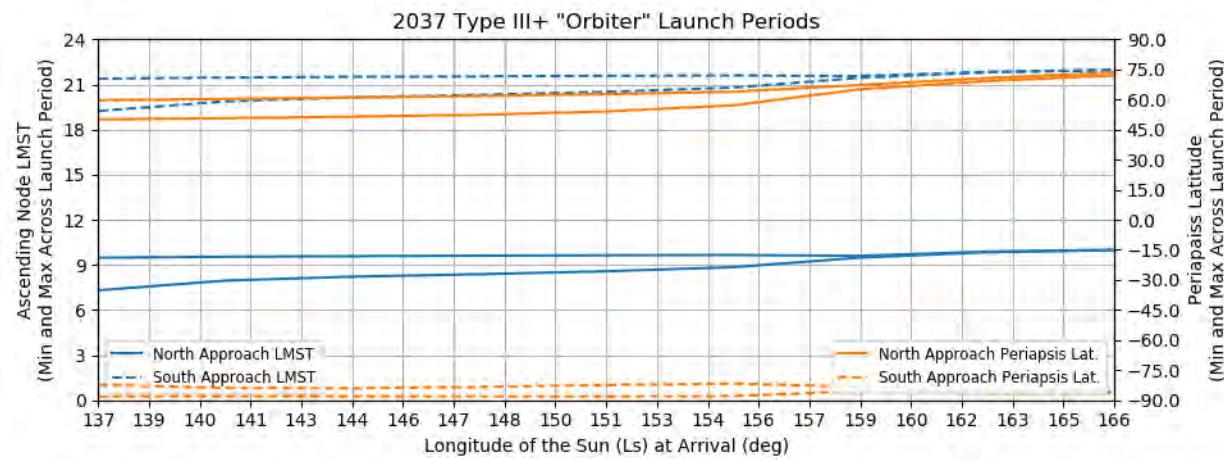


Figure 337: Earth to Mars 2037 Type III+ Orbiter Launch Periods - Ascending Node LMST and Periapsis Latitude (92 deg inclination)

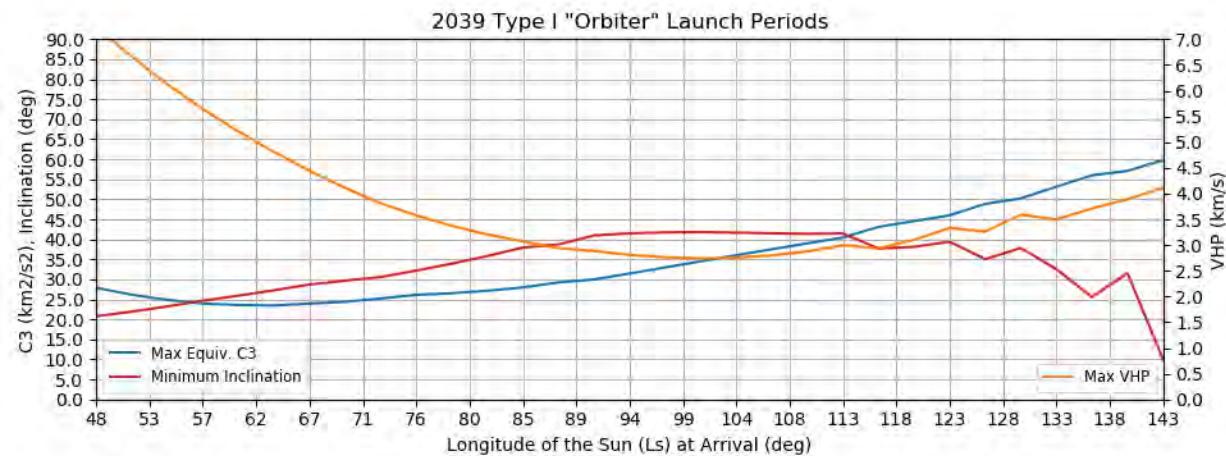


Figure 338: Earth to Mars 2039 Type I Orbiter Launch Periods - Reachable Inclination, Launch Mass, and VHP

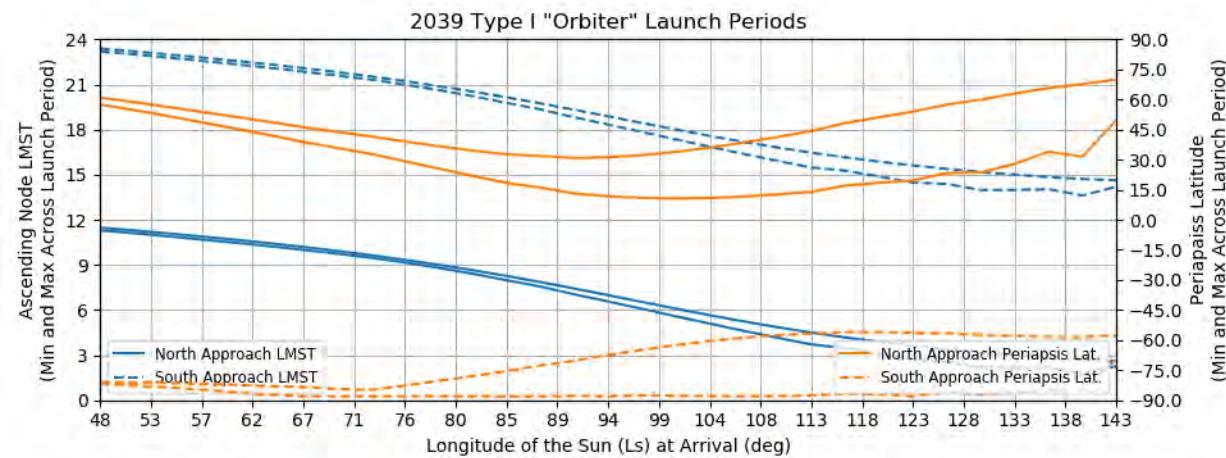


Figure 339: Earth to Mars 2039 Type I Orbiter Launch Periods - Ascending Node LMST and Periapsis Latitude (92 deg inclination)

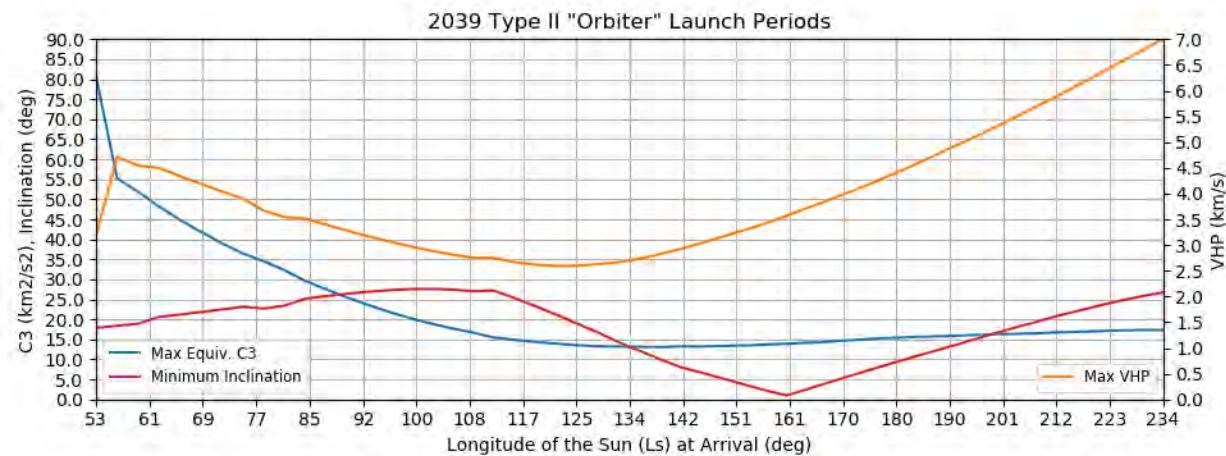


Figure 340: Earth to Mars 2039 Type II Orbiter Launch Periods - Reachable Inclination, Launch Mass, and VHP

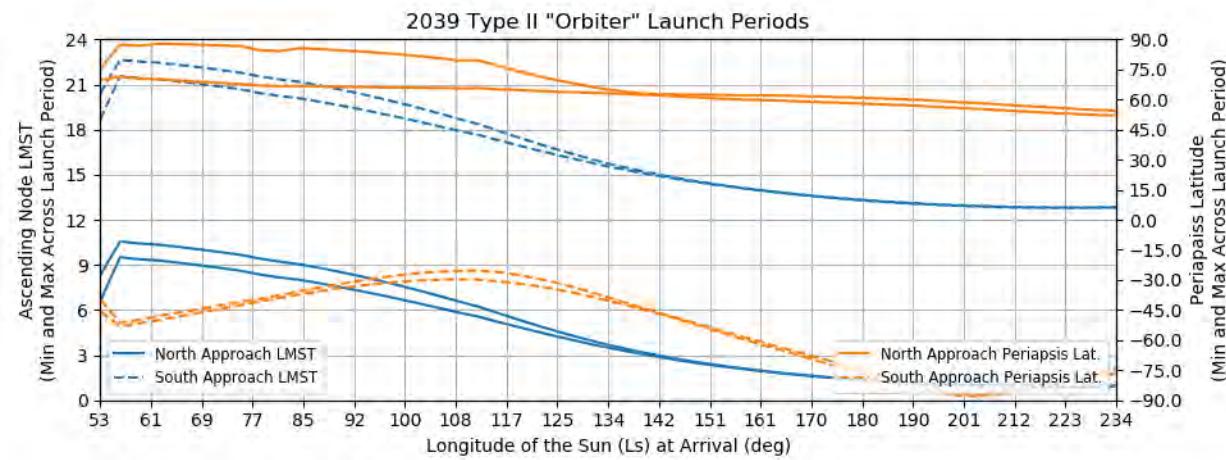


Figure 341: Earth to Mars 2039 Type II Orbiter Launch Periods - Ascending Node LMST and Periapsis Latitude (92 deg inclination)

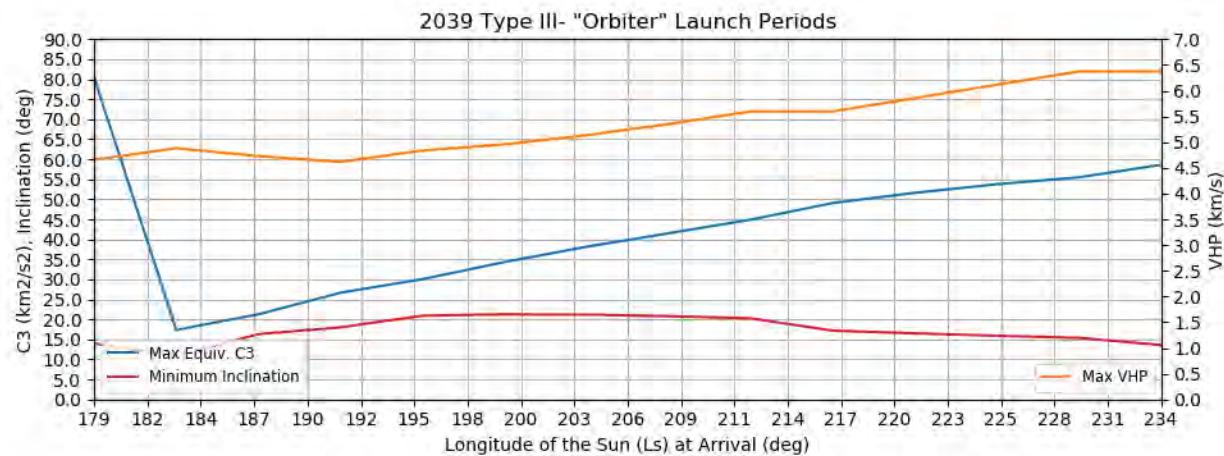


Figure 342: Earth to Mars 2039 Type III- Orbiter Launch Periods - Reachable Inclination, Launch Mass, and VHP

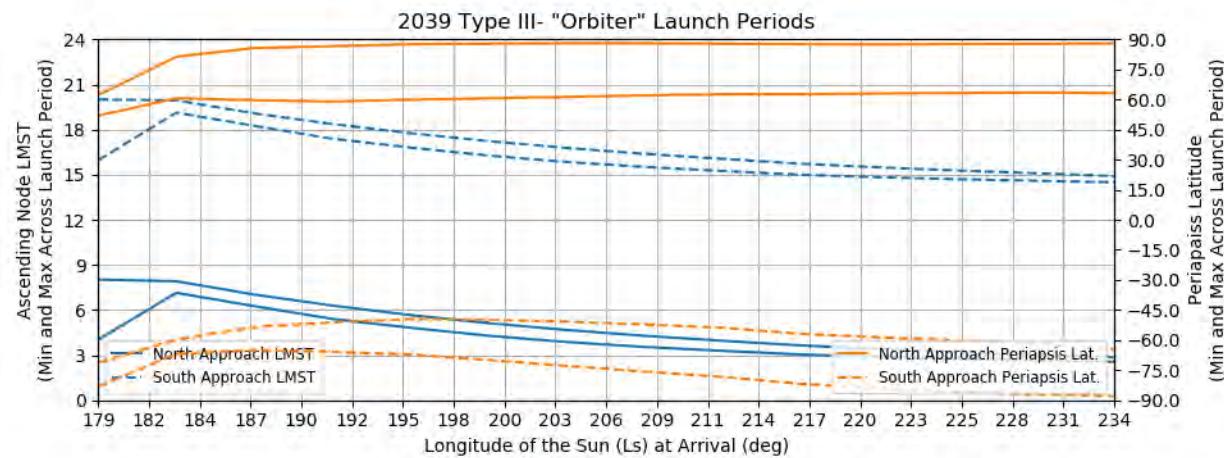


Figure 343: Earth to Mars 2039 Type III- Orbiter Launch Periods - Ascending Node LMST and Periapsis Latitude (92 deg inclination)

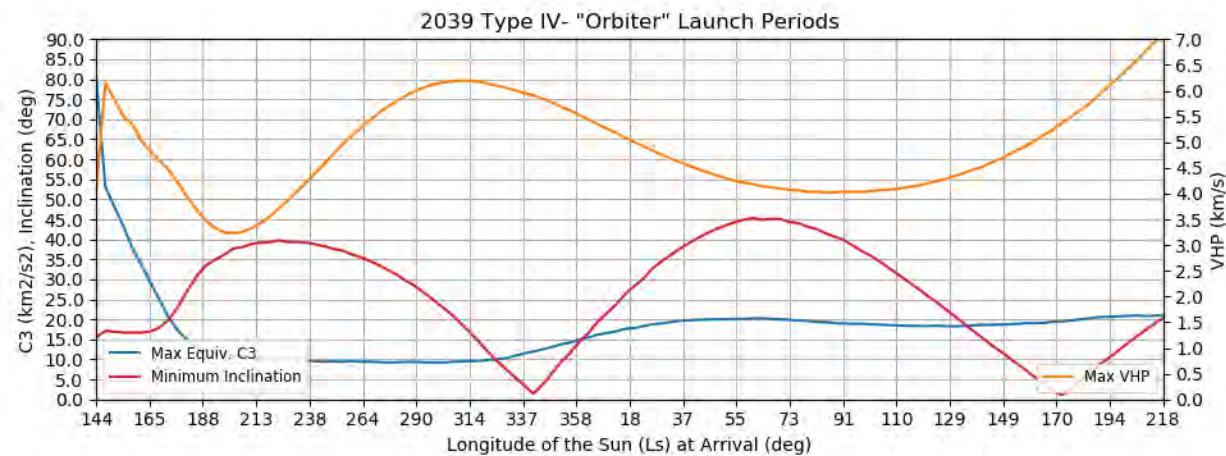


Figure 344: Earth to Mars 2039 Type IV- Orbiter Launch Periods - Reachable Inclination, Launch Mass, and VHP

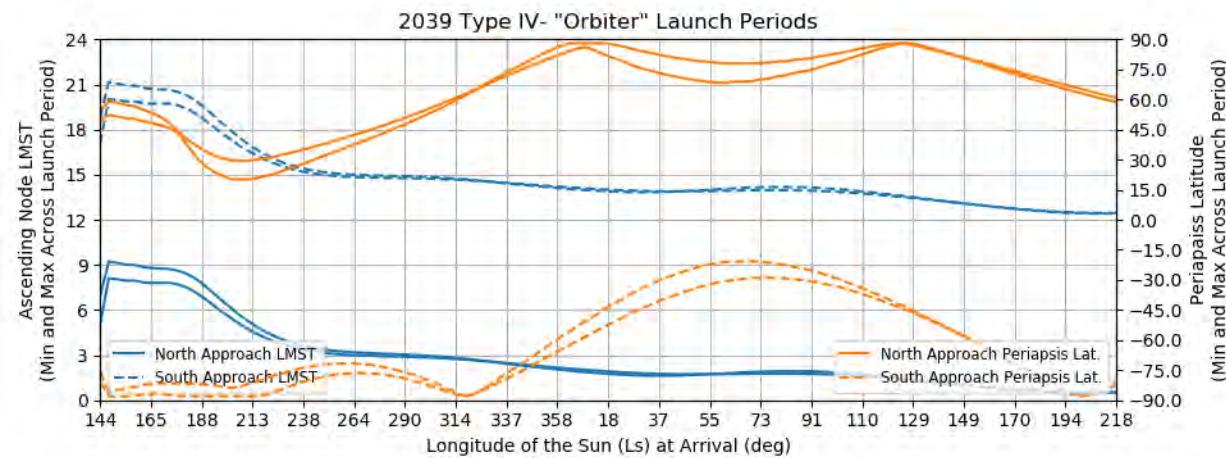


Figure 345: Earth to Mars 2039 Type IV- Orbiter Launch Periods - Ascending Node LMST and Periapsis Latitude (92 deg inclination)

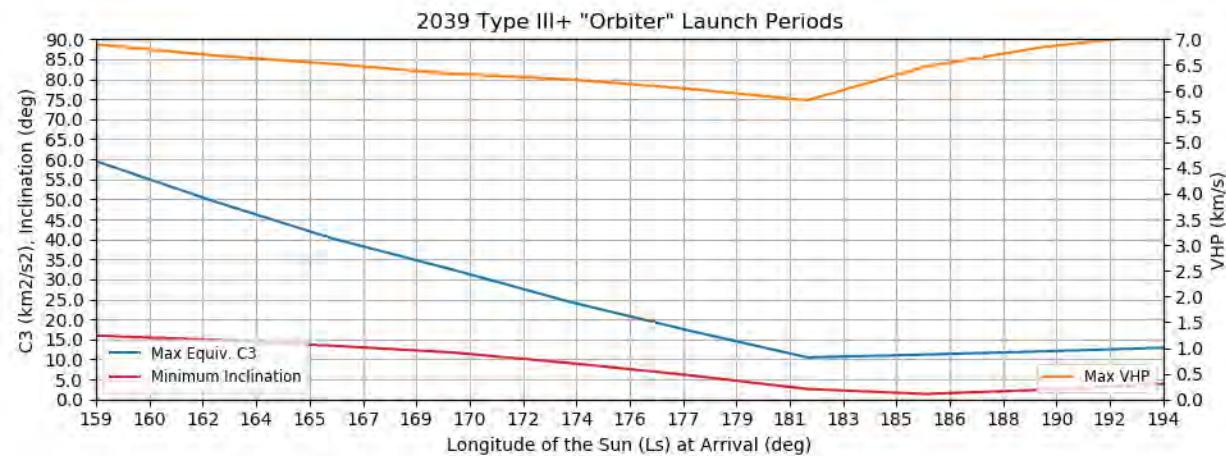


Figure 346: Earth to Mars 2039 Type III+ Orbiter Launch Periods - Reachable Inclination, Launch Mass, and VHP

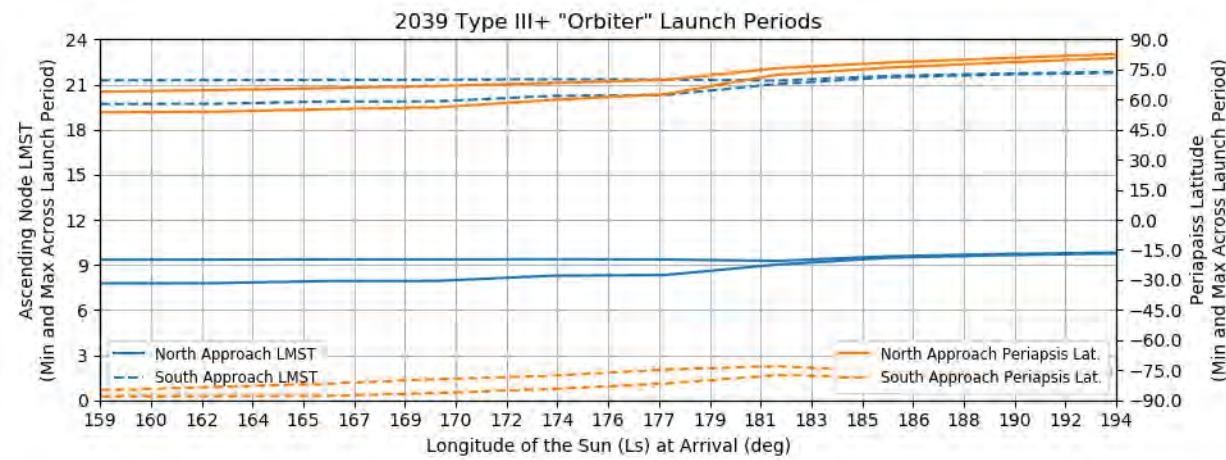


Figure 347: Earth to Mars 2039 Type III+ Orbiter Launch Periods - Ascending Node LMST and Periapsis Latitude (92 deg inclination)

## 10.5 Porkchop Plots

### 10.5.1 *Introduction*

This selection of porkchop plots are a representative set. For readability, each plot only contains a few contours, and for brevity, only a few sets of contours are included. The local solar time of landing and the maximum reachable latitude of a lander are dependent on the entry flight path angle and the descent central angle. These plots assume an entry flight path angle of -14.5 deg and a descent central angle of 12.6 deg. These values are consistent with the values of the previous edition of the Mars Handbook and result in landing co-latitudes approximately in the middle of the span illustrated in Figure 47. The local mean solar time of the ascending node of an orbiter is dependent on the targeted inclination, while the argument of periapsis is additionally dependent on the periapsis altitude. These plots assume 400 km and 92.9 deg, again to be consistent with the previous edition of the Handbook. 92.9 deg is also near the sun-synchronous inclination for a low Mars orbiter.

For porkchops with different parameters, please see the Porkchop Plot Tool at <https://mars-handbook.jpl.nasa.gov>. This interactive webtool allows the user to select specific contours of interest and define parameters which drive those contours (e.g. a different flight path angle). Additional display modes and contour settings make it easy to see quickly survey future launch opportunities and generate a custom plot with the desired data.

### 10.5.2 Earth to Mars 2022

This section contains porkchop plots for the Earth-to-Mars 2022 opportunities. Table 28 contains the optimal single-day transfers for minimum launch energy (C3) and arrival velocity (VHP) as well as the maximum launch-mass and captured-mass launch periods for each trajectory type within the opportunity. These data should only be used for preliminary analysis and planning purposes.

**Table 28: Earth to Mars 2022 Optimal Launch/Arrival Data**

Optimization Criteria	Trajectory Type	Departure Date (dd-mmm-yyyy)	Arrival Date (dd-mmm-yyyy)	Launch Energy, C3 (km <sup>2</sup> /s <sup>2</sup> )	Declination of the Launch Asymptote, DLA (deg)	Approach V-Infinity, VHP (km/s)
<b>Single-Day Optimization</b>						
Minimum C3	I	08-Sep-2022	31-Mar-2023	18.5	45.9	3.66
Minimum C3	II	17-Sep-2022	09-Oct-2023	13.8	17.2	3.16
Minimum C3	III-	25-Dec-2021	20-Dec-2023	9.3	-16.2	4.89
Minimum C3	IV-	04-Dec-2021	29-Feb-2024	8.9	29.0	3.35
Minimum C3	III+	02-Jan-2022	20-Dec-2023	9.1	-16.7	5.70
Minimum C3	IV+	20-Nov-2021	04-Dec-2023	38.6	10.6	7.67
Minimum VHP	I	06-Oct-2022	11-Jun-2023	31.0	36.6	2.32
Minimum VHP	II	25-Jul-2022	09-Jun-2023	27.1	5.5	2.38
Minimum VHP	III-	11-Jan-2022	02-Jan-2024	26.6	5.7	3.49
Minimum VHP	IV-	20-Nov-2021	27-Jan-2024	9.4	25.4	2.97
Minimum VHP	III+	17-Jan-2022	04-Dec-2023	32.0	12.4	4.16
Minimum VHP	IV+	20-Nov-2021	04-Dec-2023	38.6	10.6	7.67
<b>Launch Period Optimization</b>						
Maximum Launch Mass	I	31-Aug-2022	17-Mar-2023	19.4	47.0	4.17
		20-Sep-2022		21.3	36.3	4.32
Maximum Launch Mass	II	05-Sep-2022	01-Oct-2023	14.8	16.9	3.09
		25-Sep-2022		15.1	12.6	3.11
Maximum Launch Mass	III-	15-Dec-2021	20-Dec-2023	12.0	-33.7	5.09
		04-Jan-2022		13.8	1.0	4.17
Maximum Launch Mass	IV-	16-Dec-2021	17-Apr-2024	9.8	14.5	4.66
		05-Jan-2022		10.0	29.1	4.67
Maximum Launch Mass	III+	26-Dec-2021	20-Dec-2023	10.2	-25.4	6.04
		15-Jan-2022		10.6	-9.5	5.92
Maximum Launch Mass	IV+	Not Possible				
Maximum Captured Mass	I	06-Sep-2022	14-Apr-2023	19.3	52.4	3.27
		26-Sep-2022		23.5	35.4	3.19
Maximum Captured Mass	II	29-Aug-2022	04-Sep-2023	15.2	11.7	2.78

Optimization Criteria	Trajectory Type	Departure Date (dd-mmm-yyyy)	Arrival Date (dd-mmm-yyyy)	Launch Energy, C3 (km <sup>2</sup> /s <sup>2</sup> )	Declination of the Launch Asymptote, DLA (deg)	Approach V-Infinity, VHP (km/s)
		18-Sep-2022		15.5	2.4	2.89
Maximum Captured Mass	III-	15-Dec-2021	21-Dec-2023	12.6	-34.6	5.00
		04-Jan-2022		14.5	1.5	4.06
Maximum Captured Mass	IV-	12-Nov-2021	01-Feb-2024	10.6	19.4	3.01
		02-Dec-2021		9.5	37.0	3.02
Maximum Captured Mass	III+	27-Dec-2021	20-Dec-2023	9.8	-23.9	5.95
		16-Jan-2022		10.8	-9.2	5.95
Maximum Captured Mass	IV+			Not Possible		

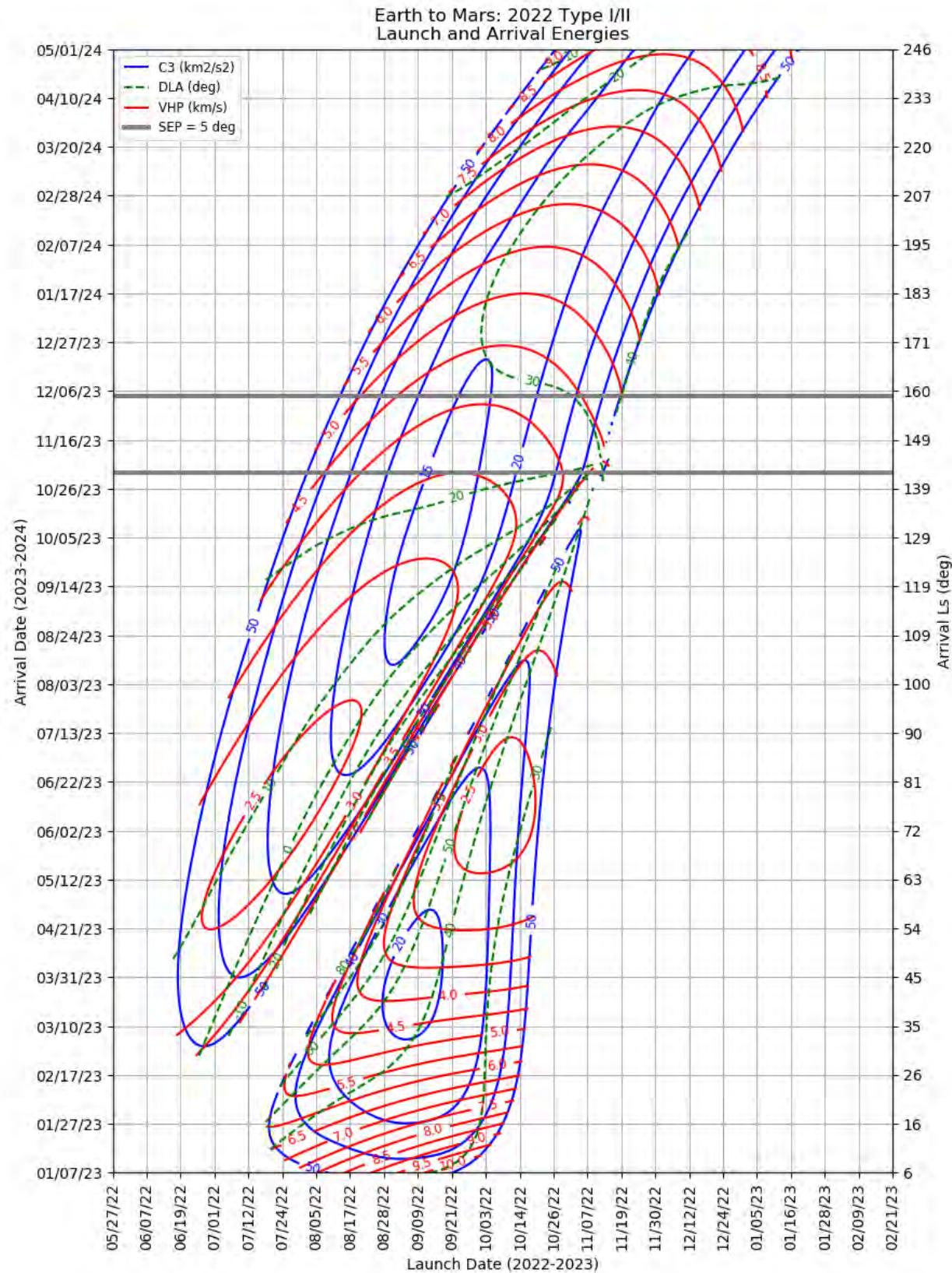


**Figure 348: Earth to Mars 2022 Type I/II - Launch and Arrival Energy**

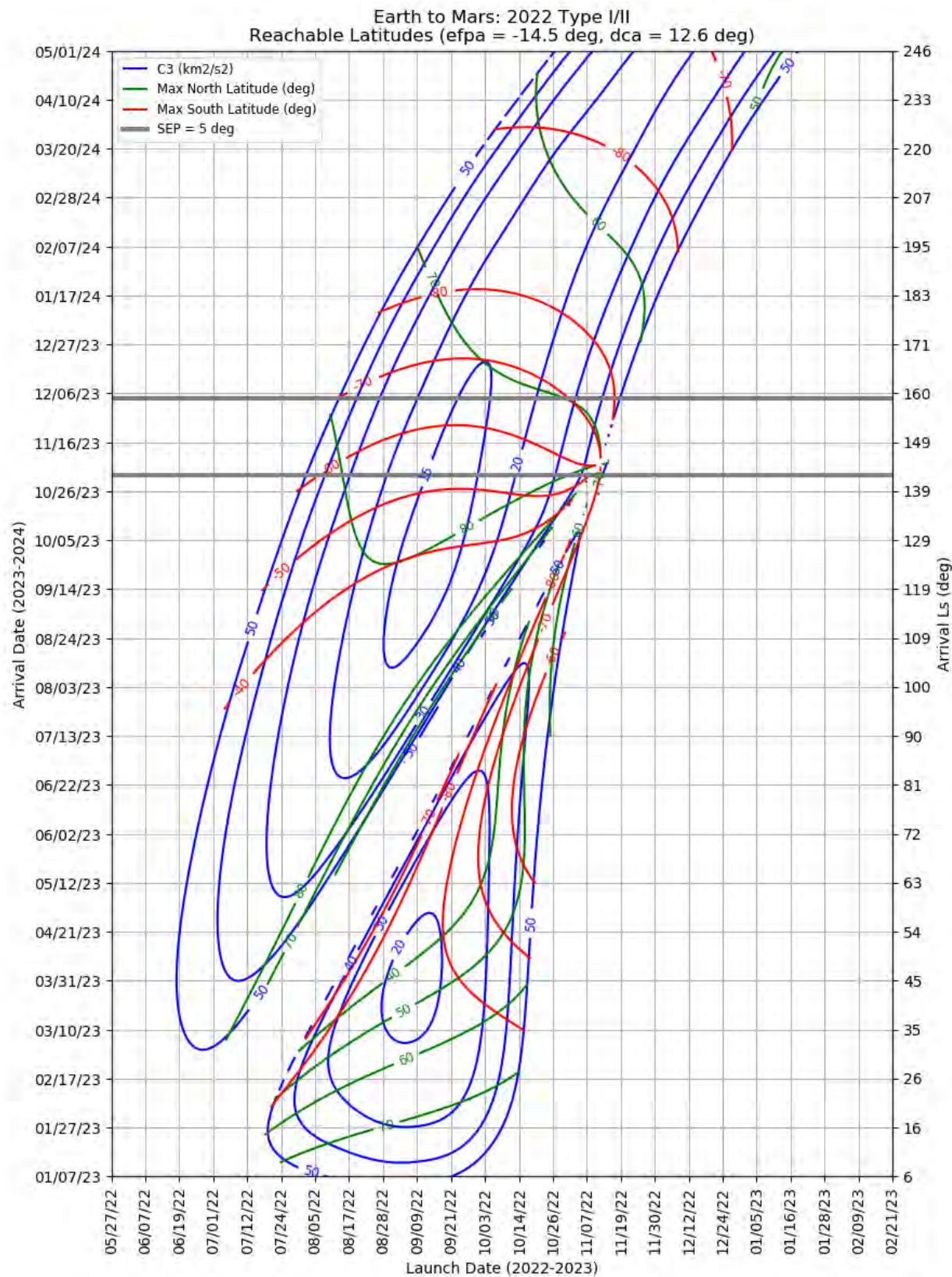


**Figure 349: Earth to Mars 2022 Type I/II – Maximum Reachable North and South Latitude**

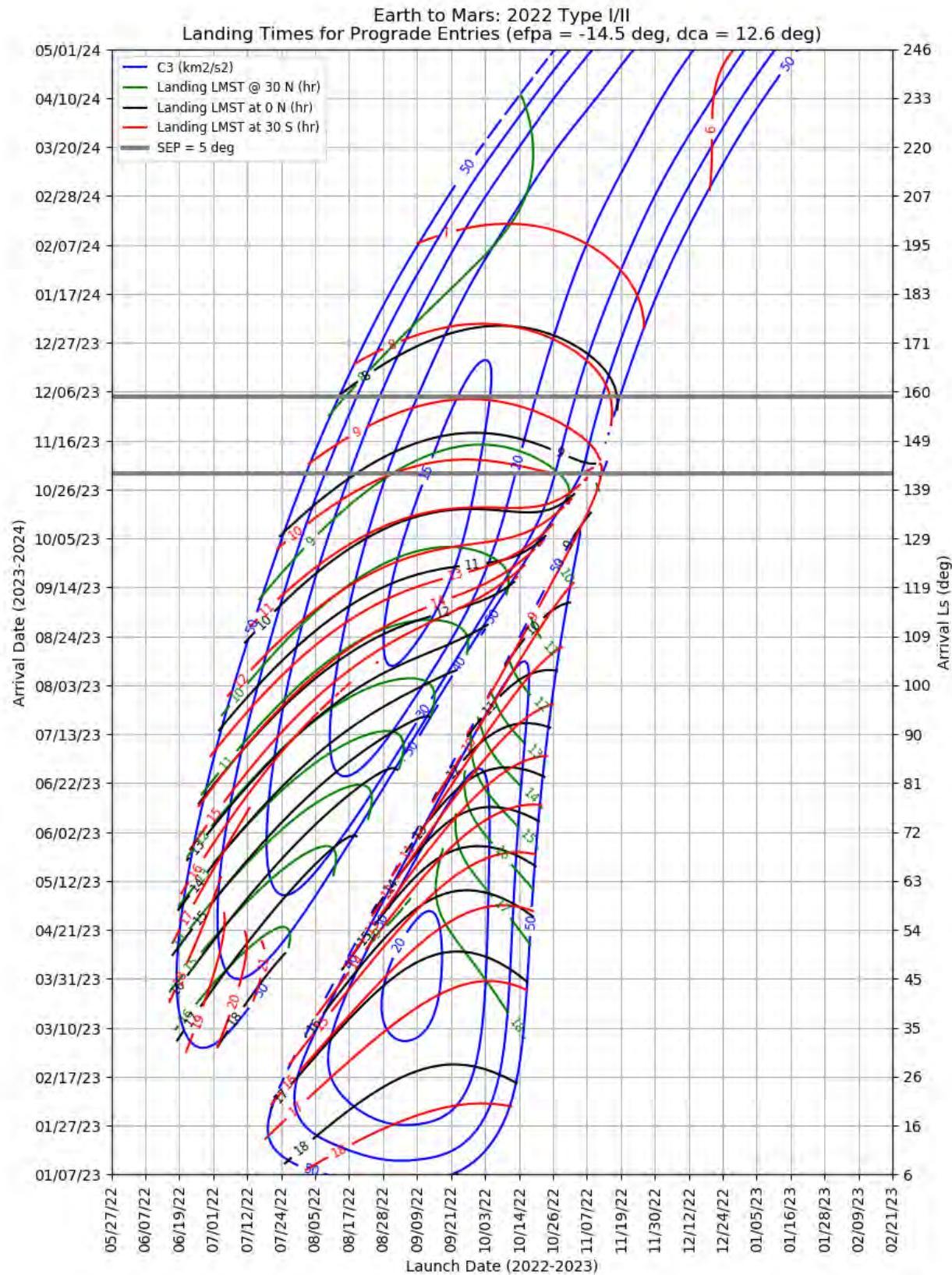
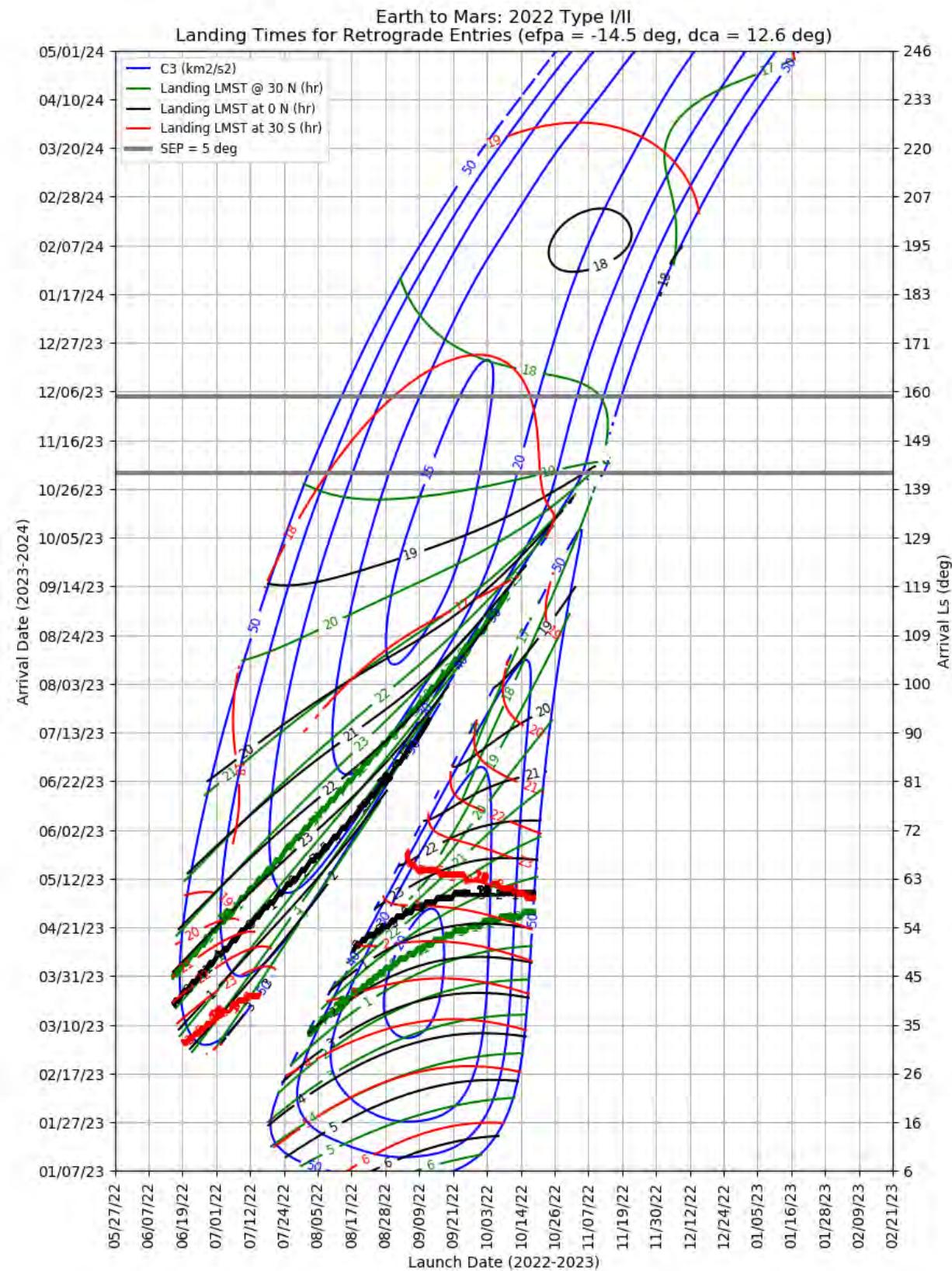
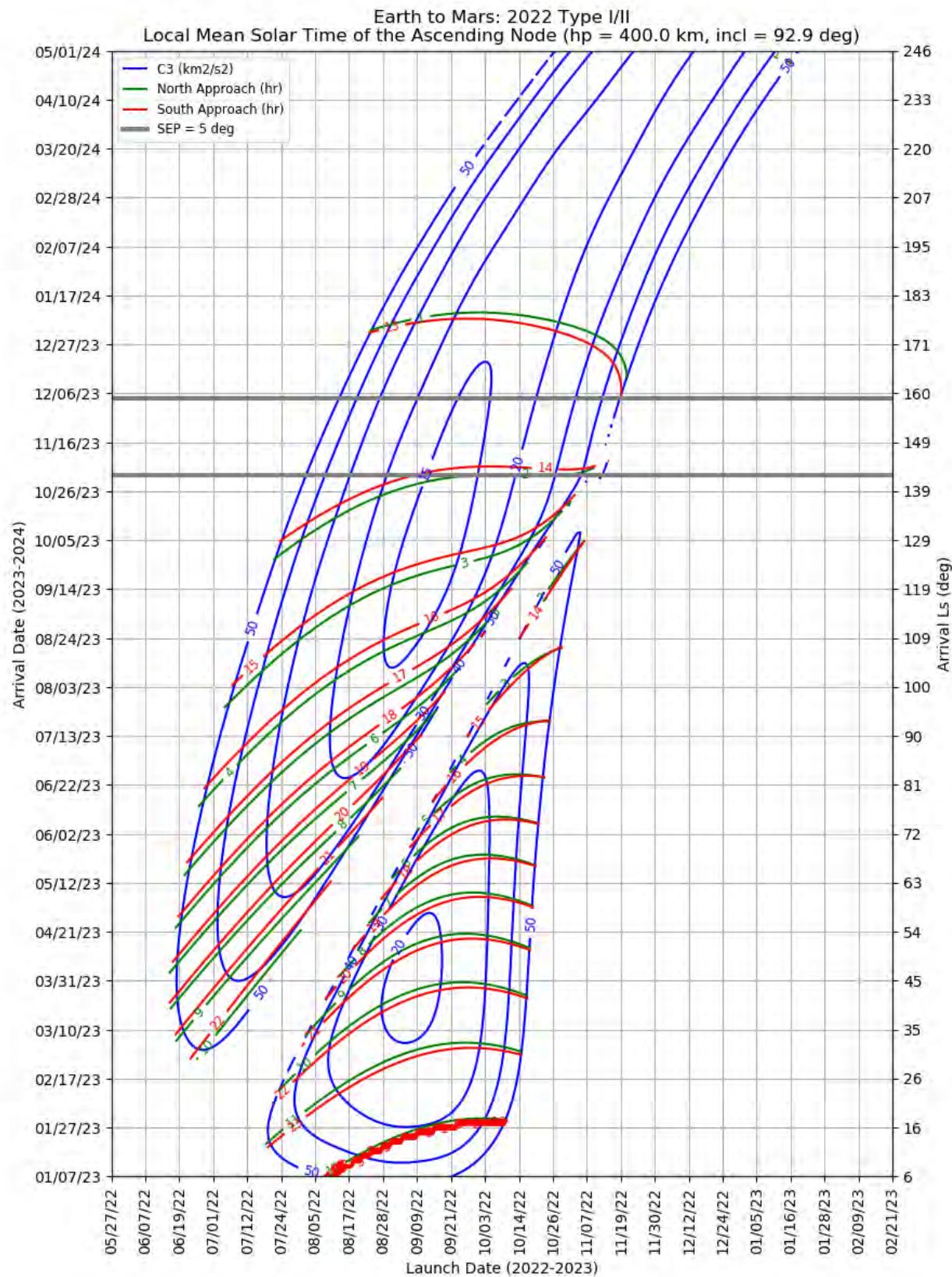


Figure 350: Earth to Mars 2022 Type I/II – Landing LMST for Prograde Entries



**Figure 351: Earth to Mars 2022 Type I/II – Landing LMST for Retrograde Entries**



**Figure 352: Earth to Mars 2022 Type I/II – LMST of the Ascending Node for North and South Approaches**

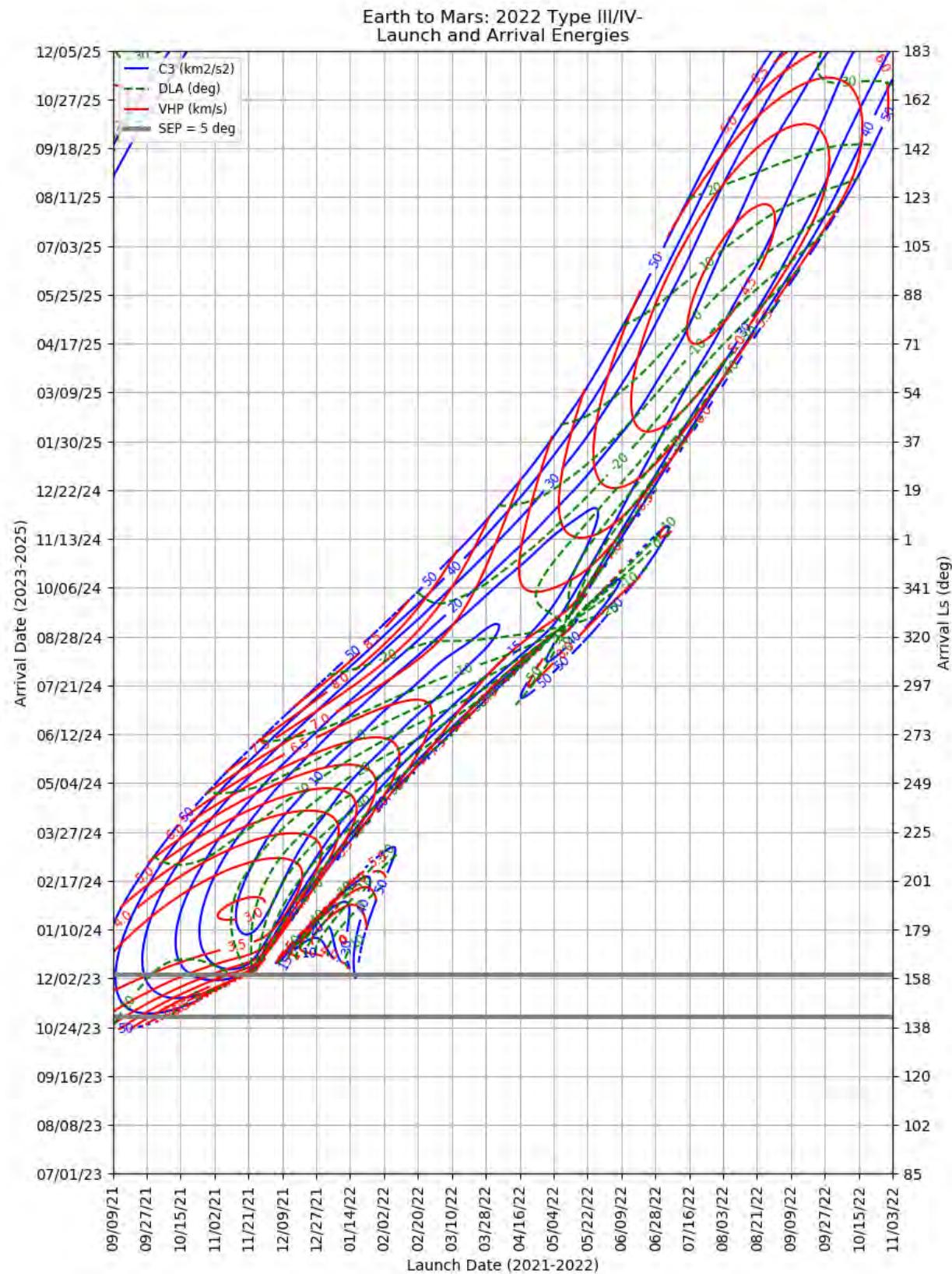


Figure 353: Earth to Mars 2024 Type III/IV- – Launch and Arrival Energy

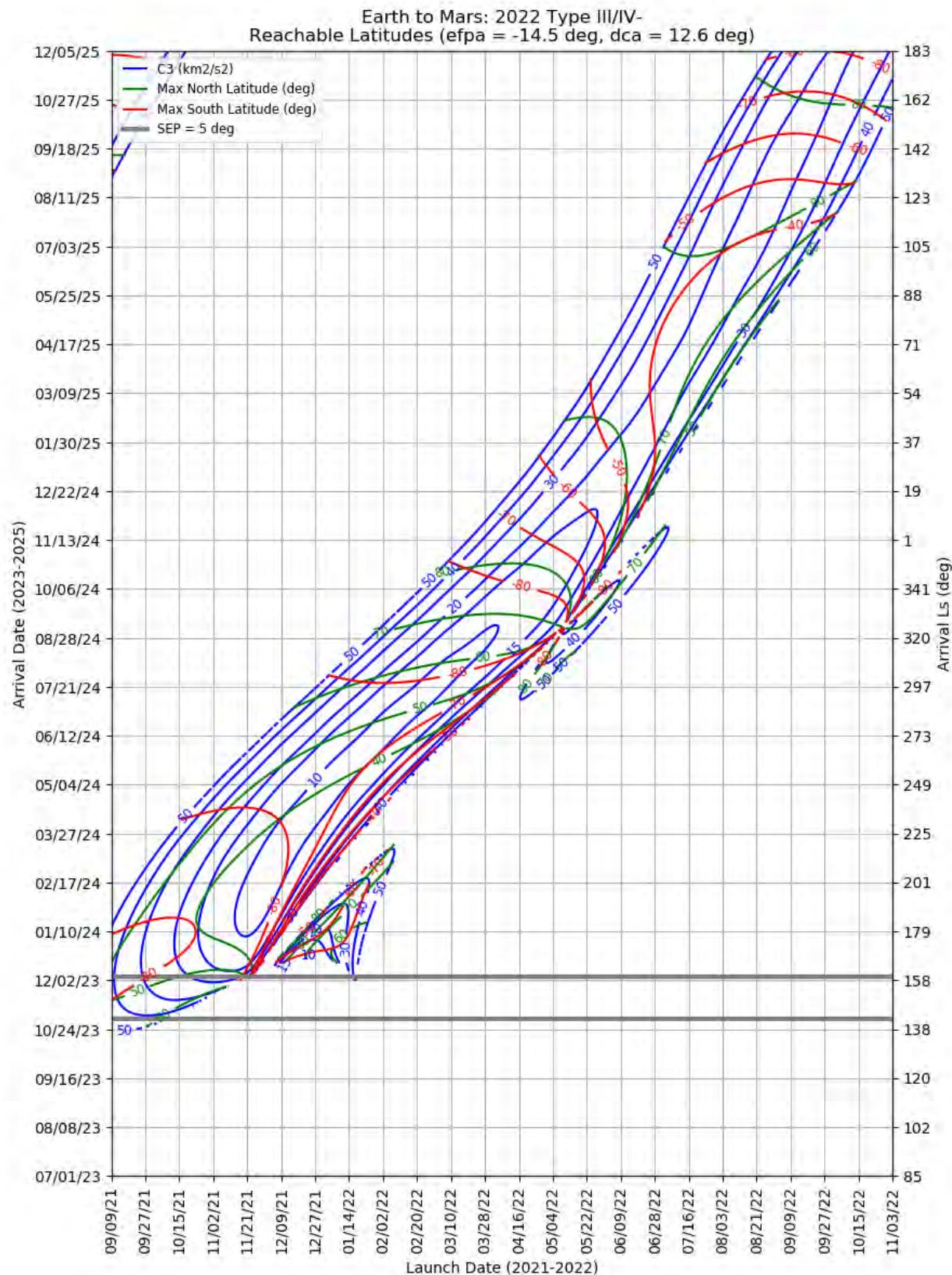
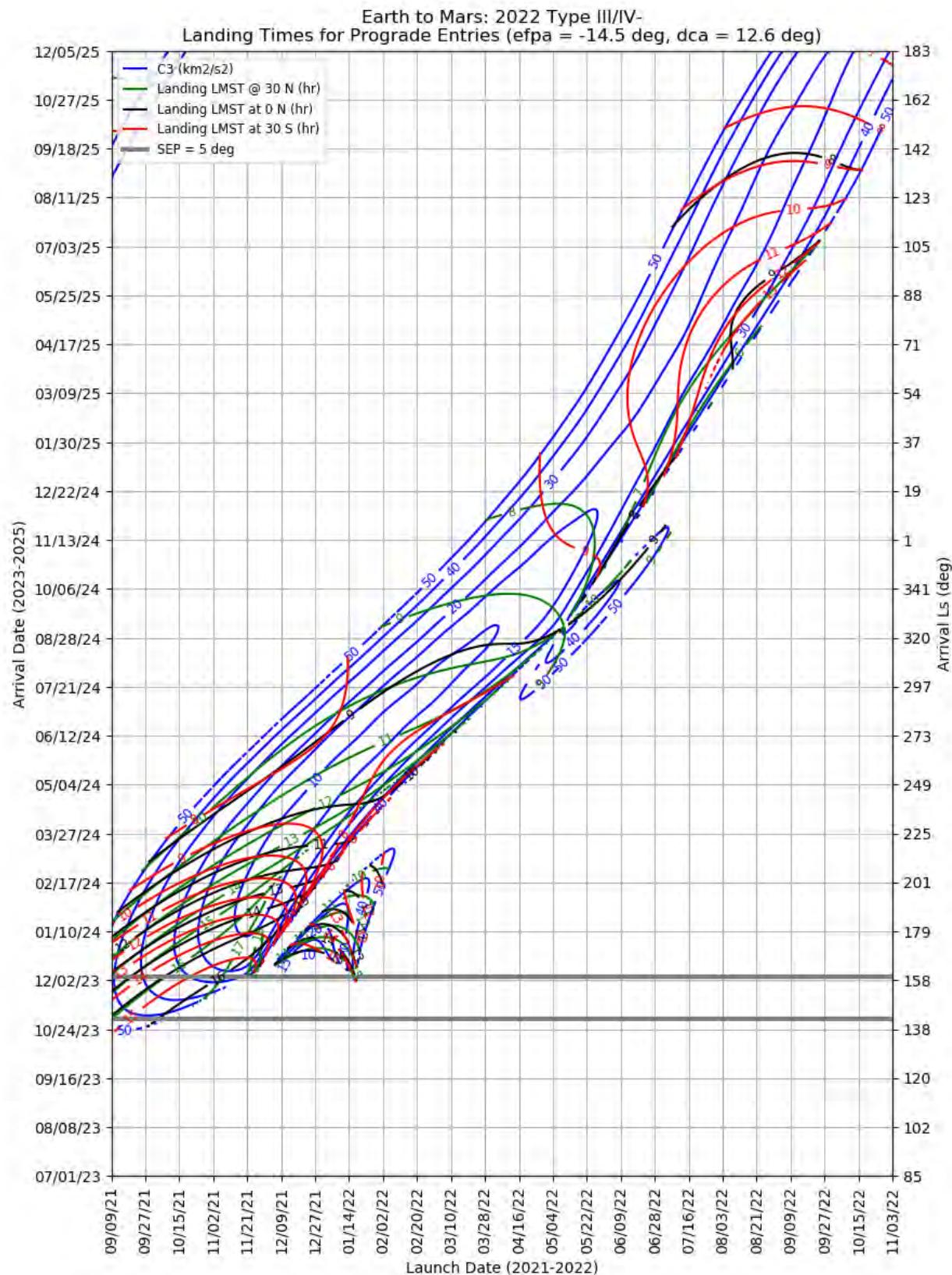


Figure 354: Earth to Mars 2022 Type III/IV- – Maximum Reachable North and South Latitude



**Figure 355: Earth to Mars 2022 Type III/IV- – Landing LMST for Prograde Entries**

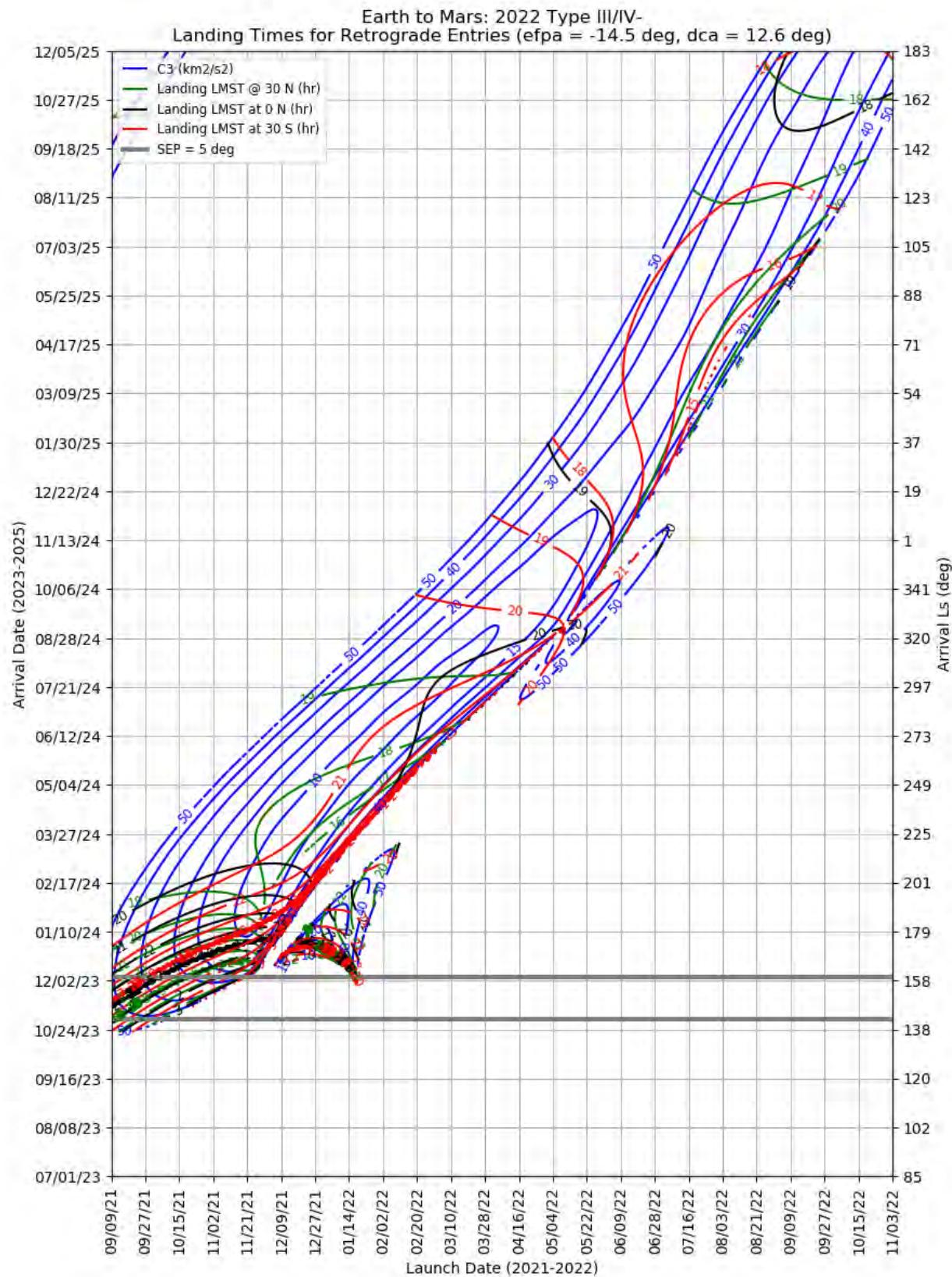
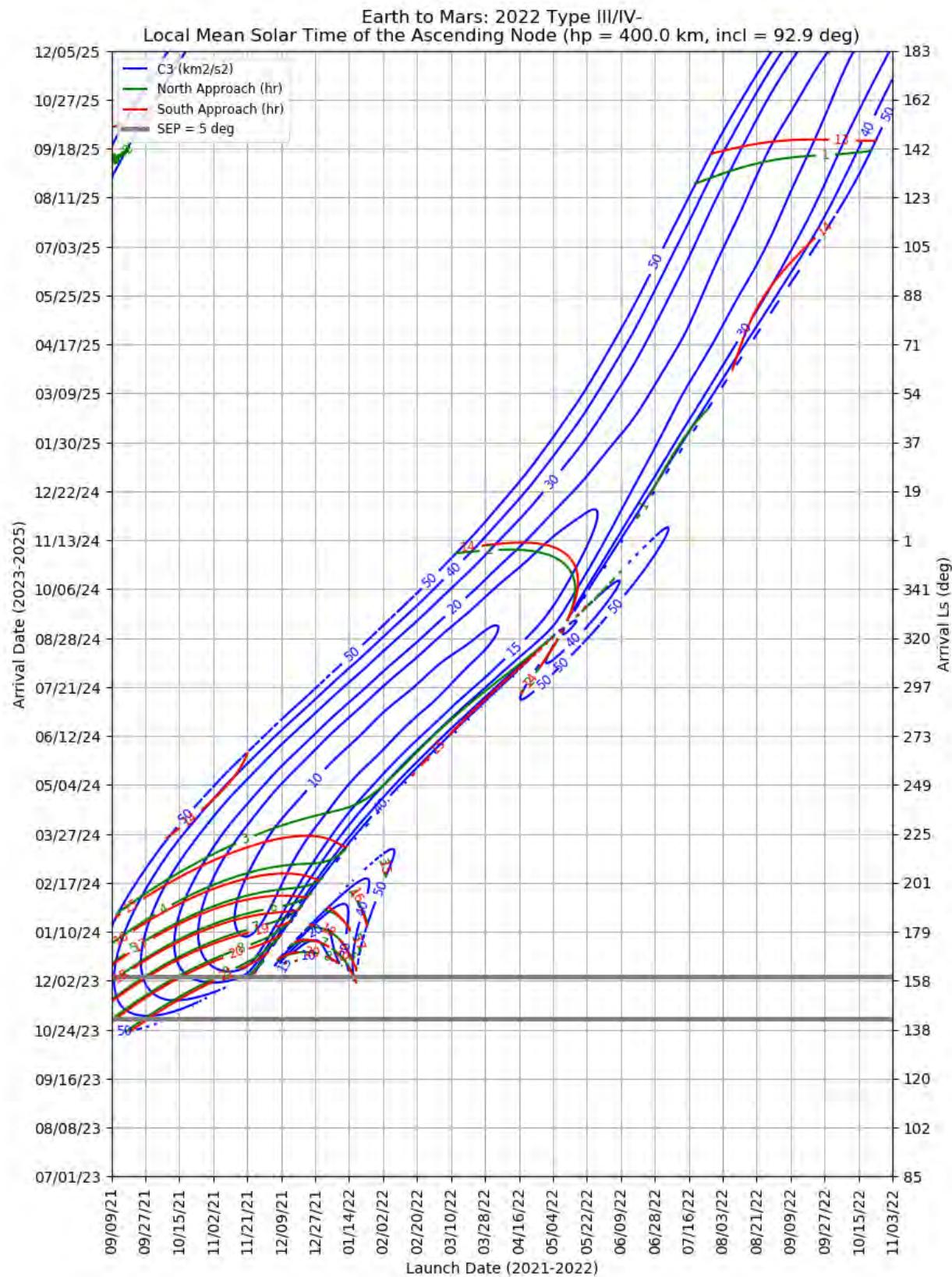
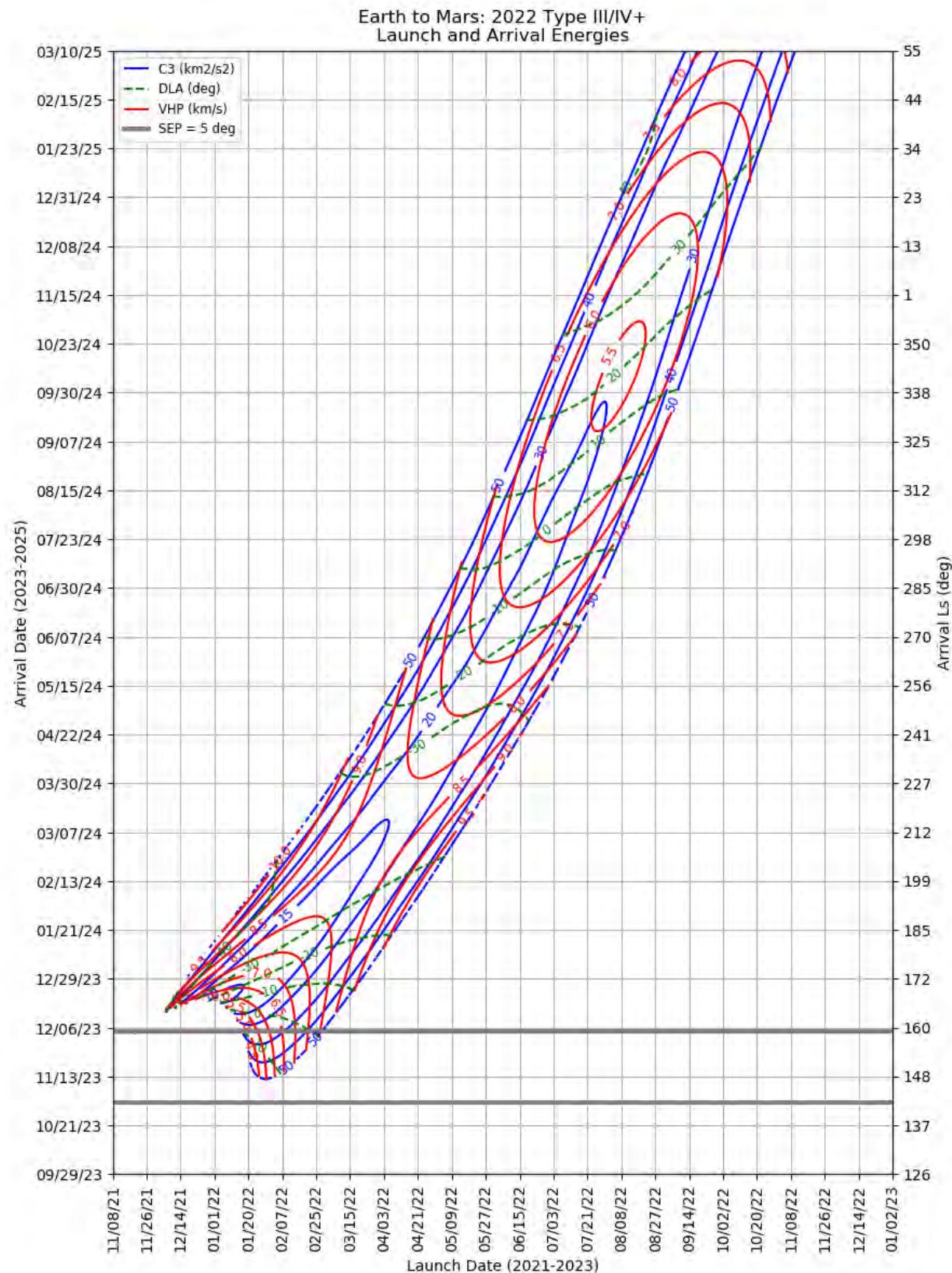


Figure 356: Earth to Mars 2022 Type III/IV- – Landing LMST for Retrograde Entries



**Figure 357: Earth to Mars 2022 Type III/IV- – LMST of the Ascending Node for North and South Approaches**



**Figure 358: Earth to Mars 2024 Type III/IV+ – Launch and Arrival Energy**

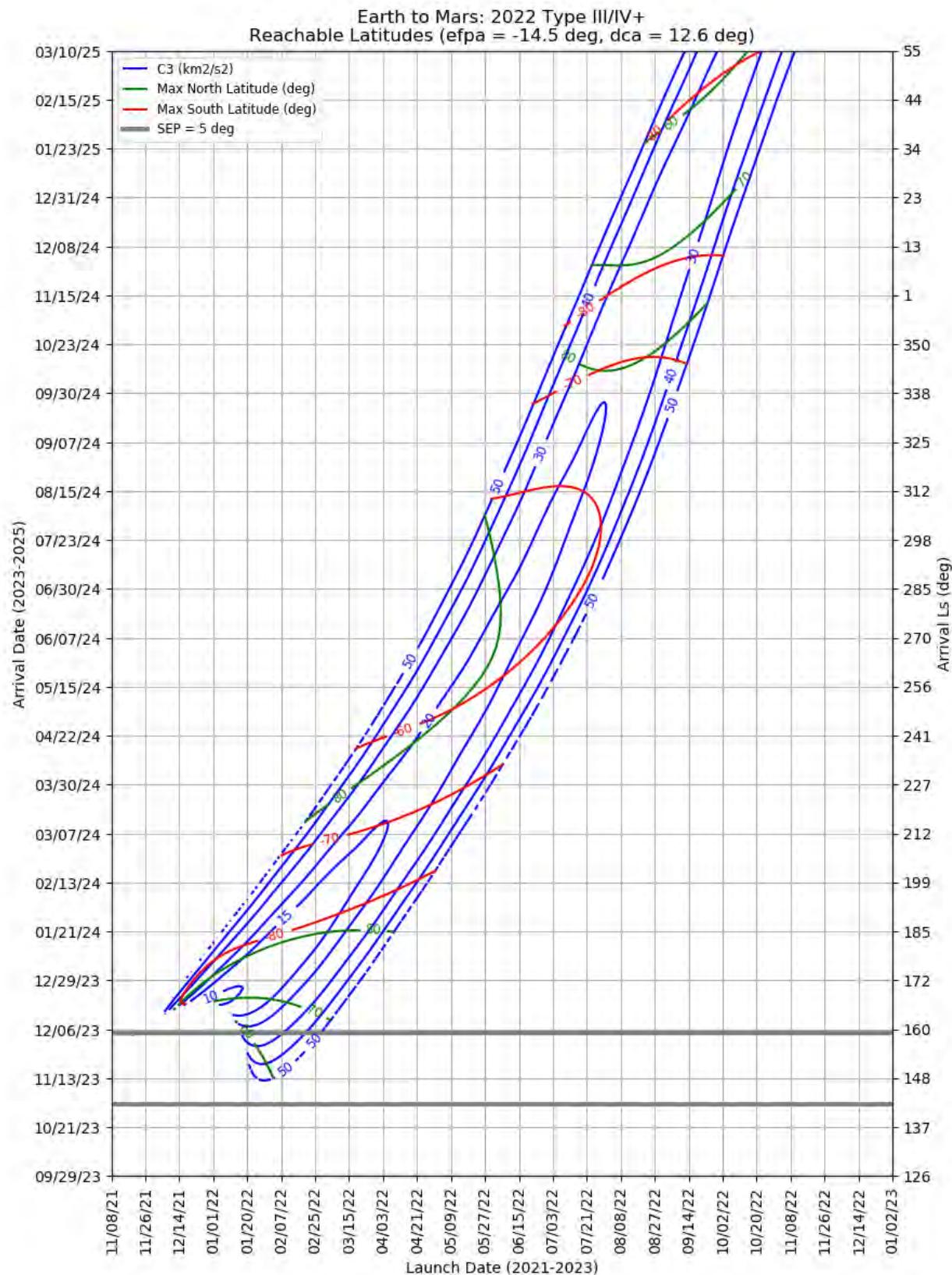


**Figure 359: Earth to Mars 2022 Type III/IV+ – Maximum Reachable North and South Latitude**

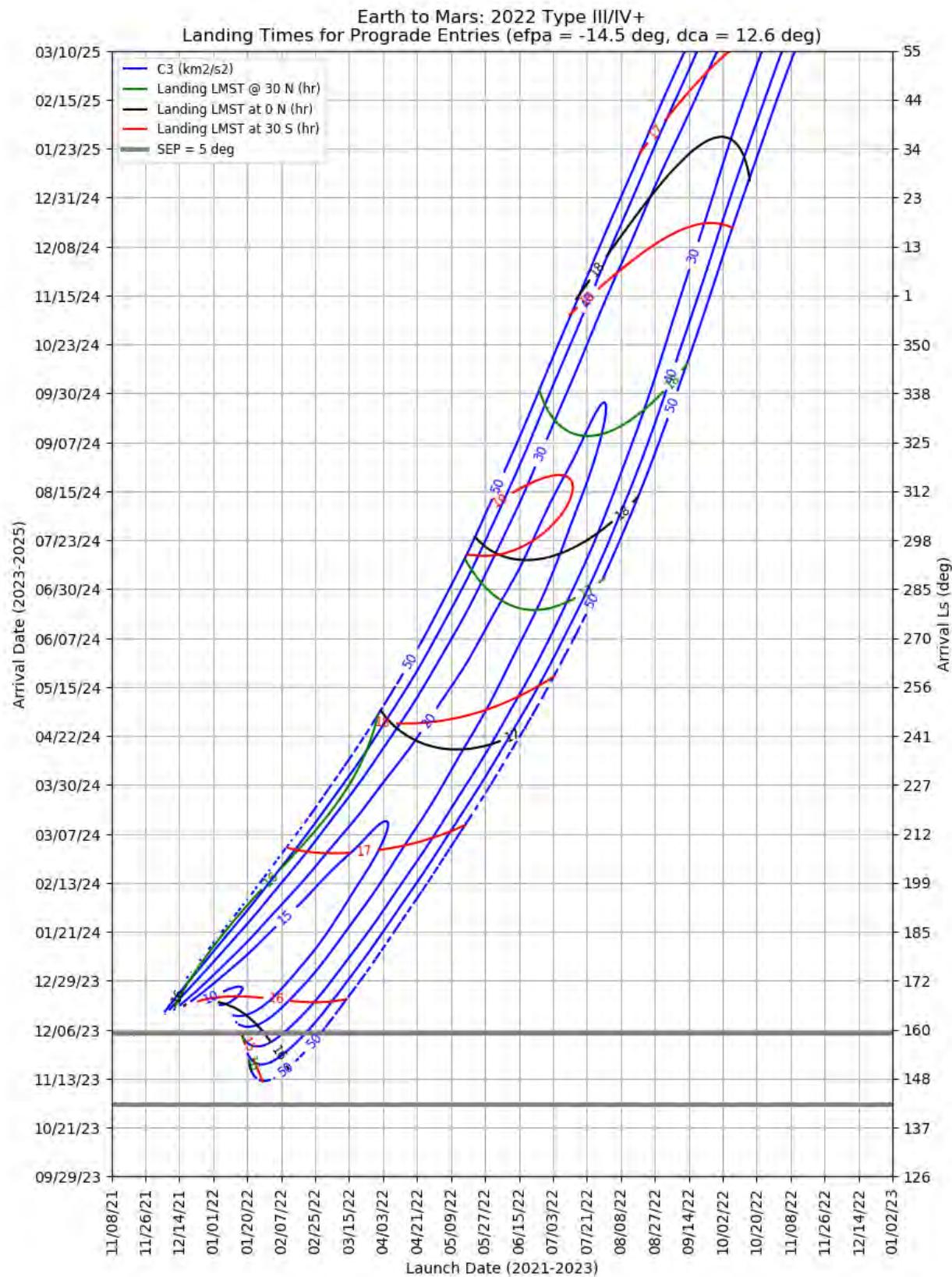
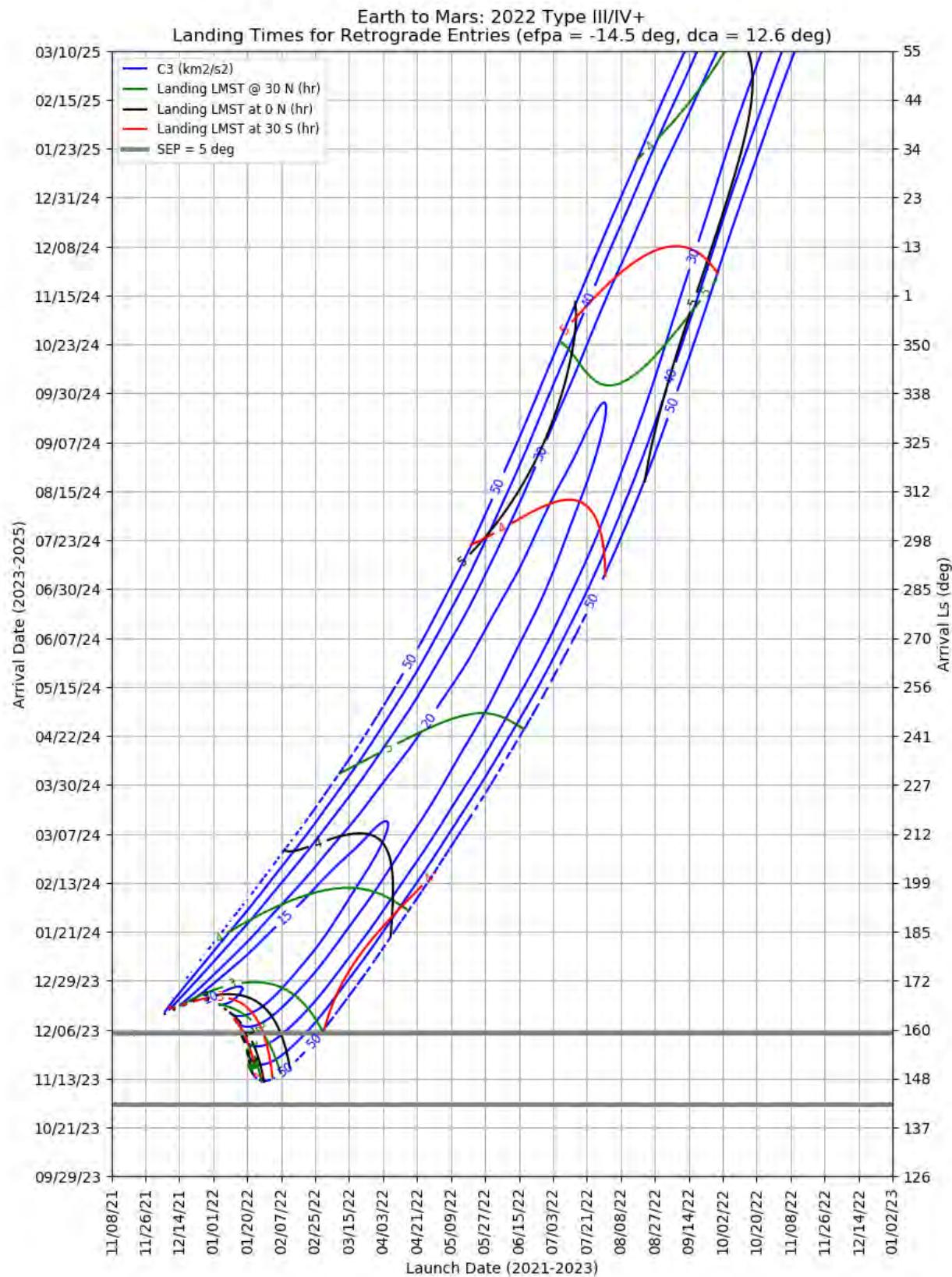


Figure 360: Earth to Mars 2022 Type III/IV+ – Landing LMST for Prograde Entries



**Figure 361: Earth to Mars 2022 Type III/IV+ – Landing LMST for Retrograde Entries**

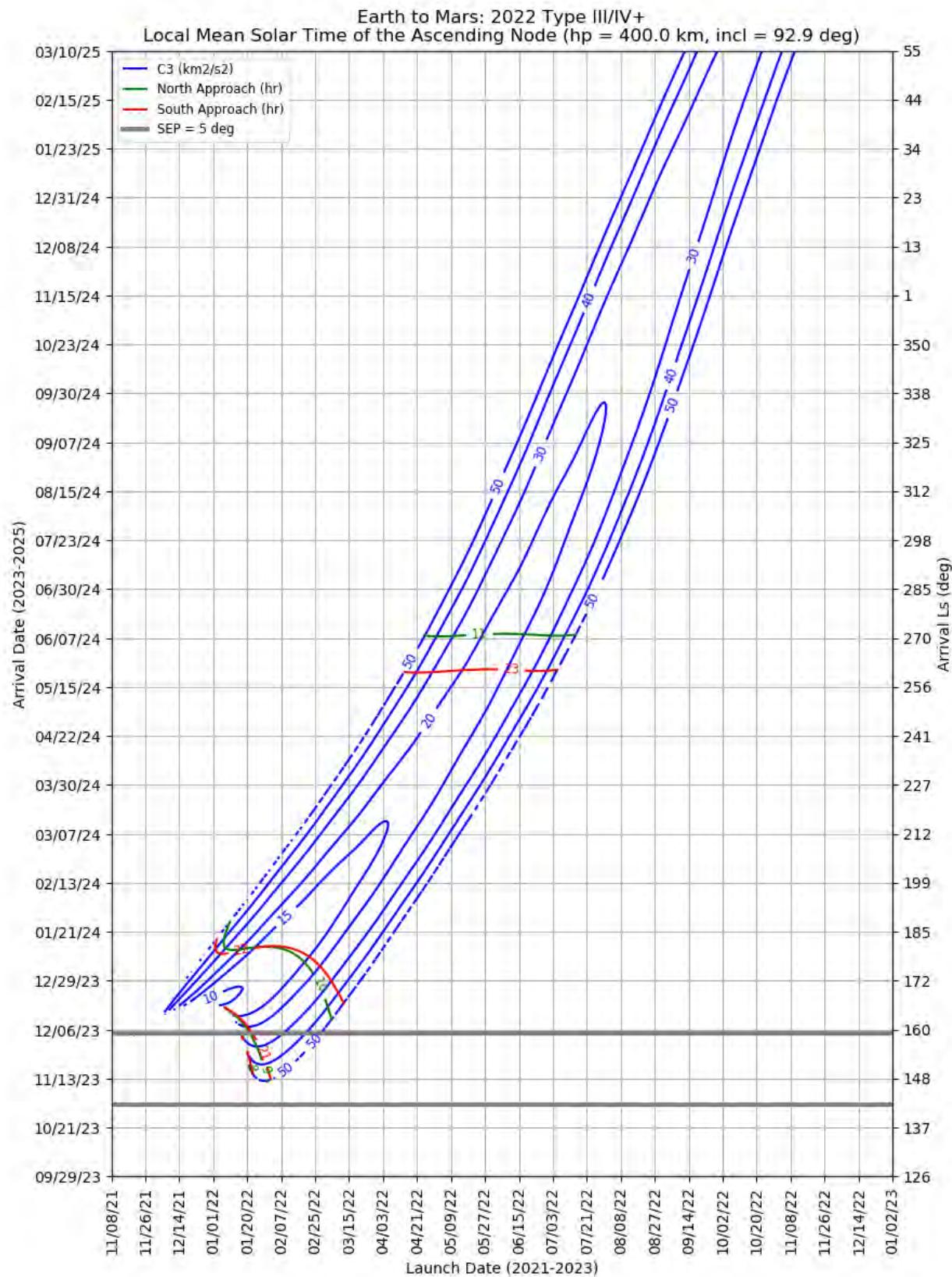


Figure 362: Earth to Mars 2022 Type III/IV+ – LMST of the Ascending Node for North and South Approaches

### 10.5.3 Earth to Mars 2024

This section contains porkchop plots for the Earth-to-Mars 2024 opportunities. Table 29 contains the optimal single-day transfers for minimum launch energy (C3) and arrival velocity (VHP) as well as the maximum launch-mass and captured-mass launch periods for each trajectory type within the opportunity. These data should only be used for preliminary analysis and planning purposes.

**Table 29: Earth to Mars 2024 Optimal Launch/Arrival Data**

Optimization Criteria	Trajectory Type	Departure Date (dd-mmm-yyyy)	Arrival Date (dd-mmm-yyyy)	Launch Energy, C3 (km <sup>2</sup> /s <sup>2</sup> )	Declination of the Launch Asymptote, DLA (deg)	Approach V-Infinity, VHP (km/s)
<b>Single-Day Optimization</b>						
Minimum C3	I	13-Oct-2024	21-May-2025	17.8	50.3	4.10
Minimum C3	II	05-Oct-2024	15-Sep-2025	11.1	20.3	2.54
Minimum C3	III-	24-Jan-2024	20-Dec-2025	9.9	-35.5	4.78
Minimum C3	IV-	11-Mar-2024	09-Jun-2026	8.1	-5.0	5.67
Minimum C3	III+	06-Feb-2024	22-Dec-2025	8.9	-36.5	5.66
Minimum C3	IV+	18-Dec-2023	13-Dec-2025	99.1	11.8	10.67
Minimum VHP	I	03-Nov-2024	05-Aug-2025	24.9	42.2	2.41
Minimum VHP	II	17-Sep-2024	17-Aug-2025	13.5	13.4	2.42
Minimum VHP	III-	06-Feb-2024	29-Dec-2025	22.6	-9.1	3.74
Minimum VHP	IV-	02-Dec-2023	14-Jan-2026	11.3	13.8	3.27
Minimum VHP	III+	13-Feb-2024	26-Nov-2025	38.7	3.3	4.19
Minimum VHP	IV+	10-May-2024	26-Jul-2026	122.5	7.1	8.50
<b>Launch Period Optimization</b>						
Maximum Launch Mass	I	05-Oct-2024	02-May-2025	19.2	50.0	4.97
		25-Oct-2024		21.2	40.2	5.12
Maximum Launch Mass	II	26-Sep-2024	19-Sep-2025	12.1	20.9	2.61
		16-Oct-2024		12.3	21.7	2.60
Maximum Launch Mass	III-	15-Jan-2024	20-Dec-2025	12.7	-51.2	5.11
		04-Feb-2024		18.3	-9.6	3.90
Maximum Launch Mass	IV-	11-Mar-2024	22-Jun-2026	8.9	-12.6	5.76
		31-Mar-2024		9.0	-4.0	5.76
Maximum Launch Mass	III+	29-Jan-2024	20-Dec-2025	9.1	-38.2	5.35
		18-Feb-2024		10.9	-25.5	5.74
Maximum Launch Mass	IV+	Not Possible				
Maximum Captured Mass	I	15-Oct-2024	22-Jun-2025	20.1	59.2	3.12
		04-Nov-2024		26.6	37.0	2.99
Maximum Captured Mass	II	24-Sep-2024	06-Sep-2025	12.2	18.0	2.48

Optimization Criteria	Trajectory Type	Departure Date (dd-mmm-yyyy)	Arrival Date (dd-mmm-yyyy)	Launch Energy, C3 (km <sup>2</sup> /s <sup>2</sup> )	Declination of the Launch Asymptote, DLA (deg)	Approach V-Infinity, VHP (km/s)
		14-Oct-2024		12.4	15.6	2.53
Maximum Captured Mass	III-	15-Jan-2024	22-Dec-2025	13.8	-50.3	4.91
		04-Feb-2024		19.0	-9.7	3.83
Maximum Captured Mass	IV-	06-Dec-2023	28-Jan-2026	10.8	13.1	3.36
		26-Dec-2023		10.6	32.4	3.45
Maximum Captured Mass	III+	13-Jul-2024	15-Aug-2026	17.4	17.5	4.46
		02-Aug-2024		17.7	10.7	4.41
Maximum Captured Mass	IV+			Not Possible		

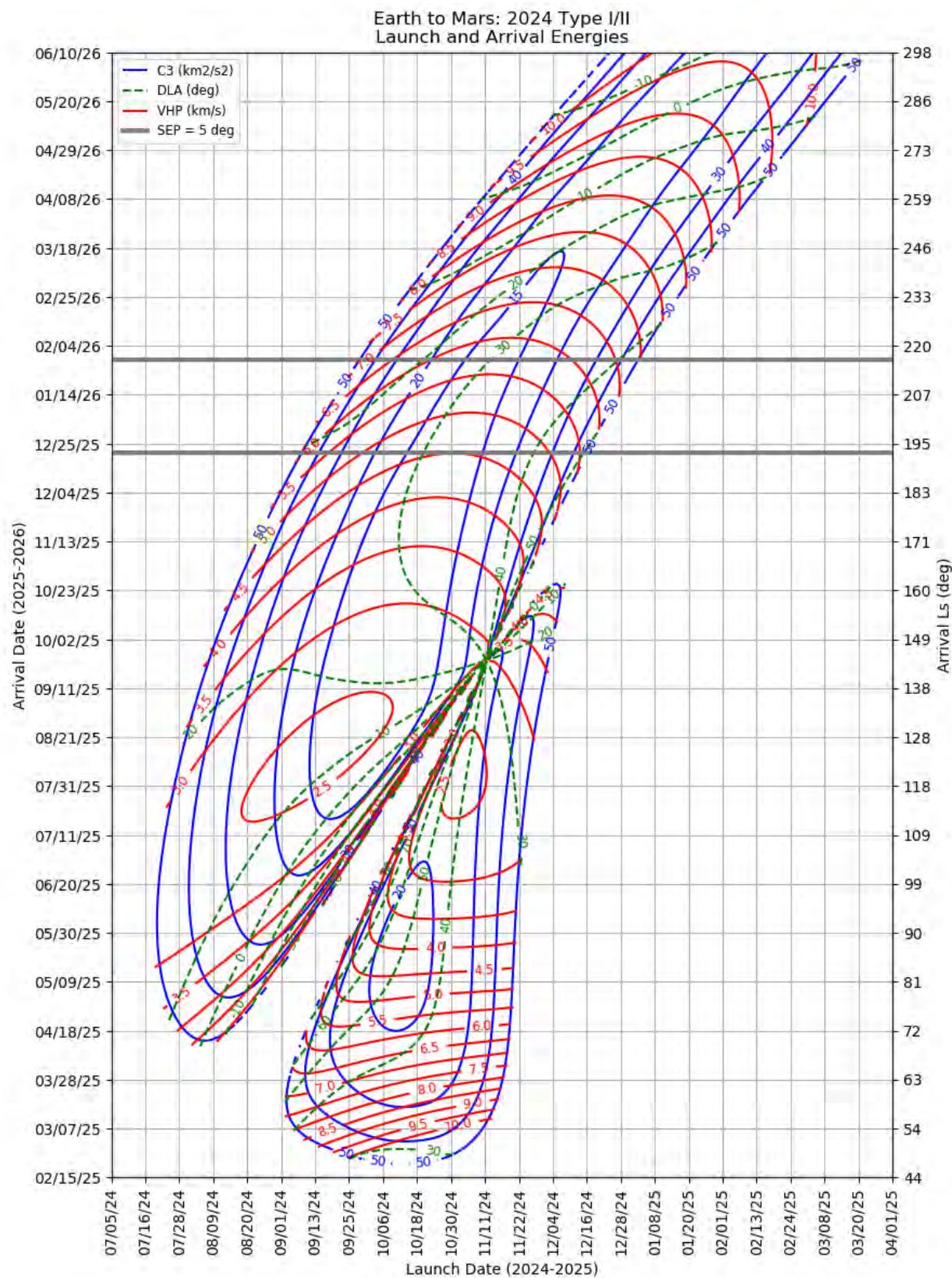


**Figure 363: Earth to Mars 2024 Type I/II - Launch and Arrival Energy**

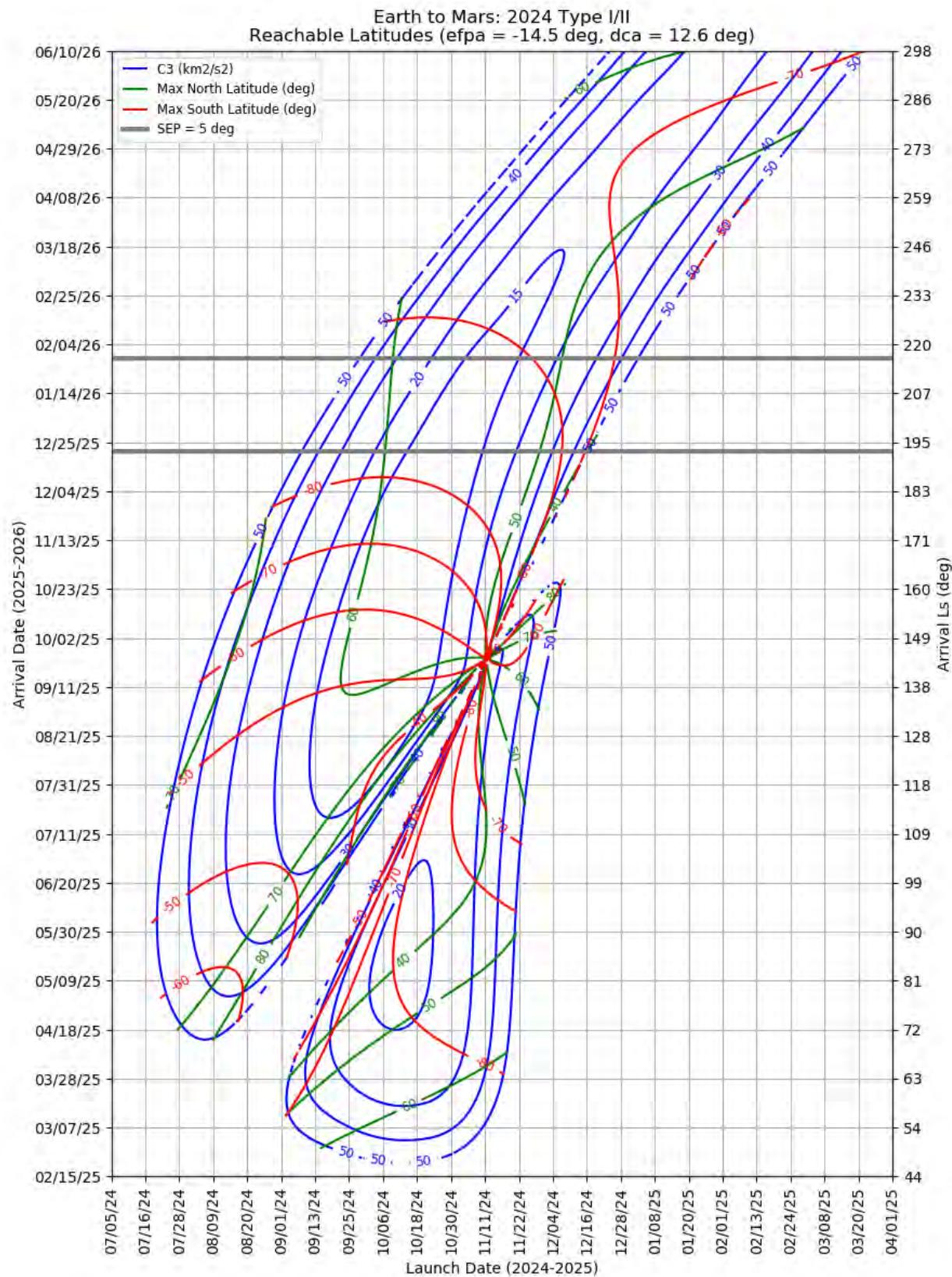


**Figure 364: Earth to Mars 2024 Type I/II – Maximum Reachable North and South Latitude**

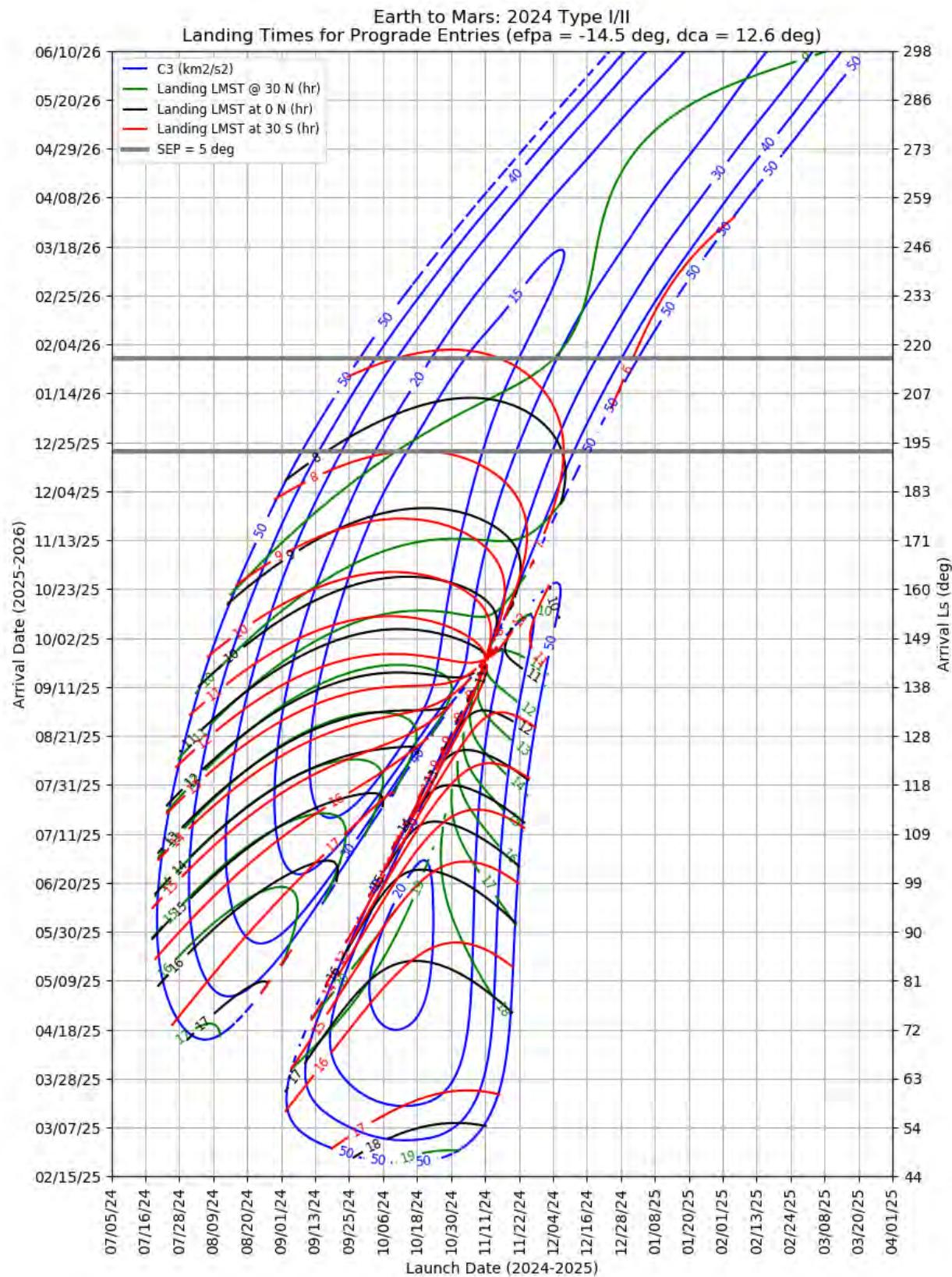


**Figure 365: Earth to Mars 2024 Type I/II – Landing LMST for Prograde Entries**

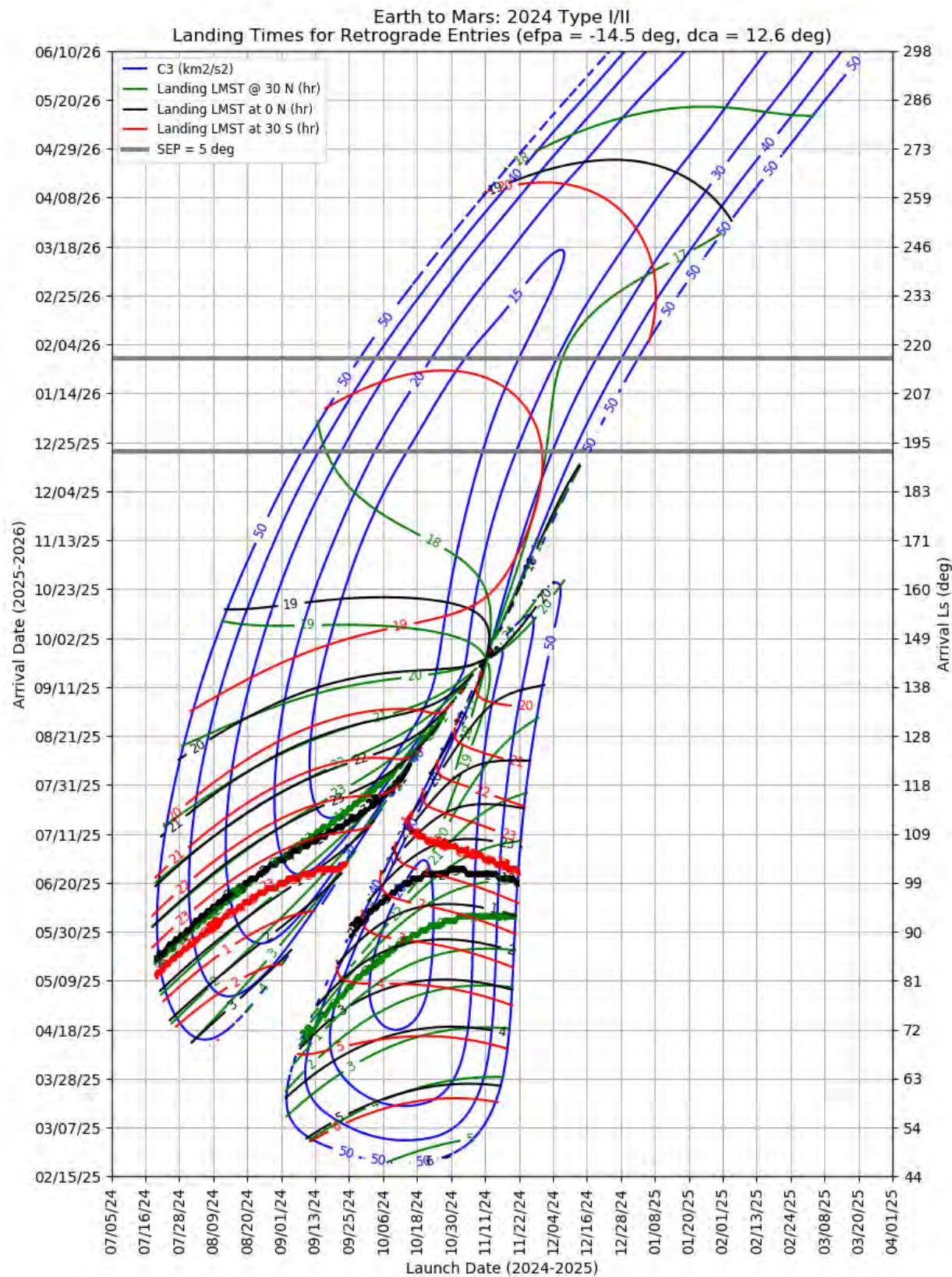


**Figure 366: Earth to Mars 2024 Type I/II – Landing LMST for Retrograde Entries**

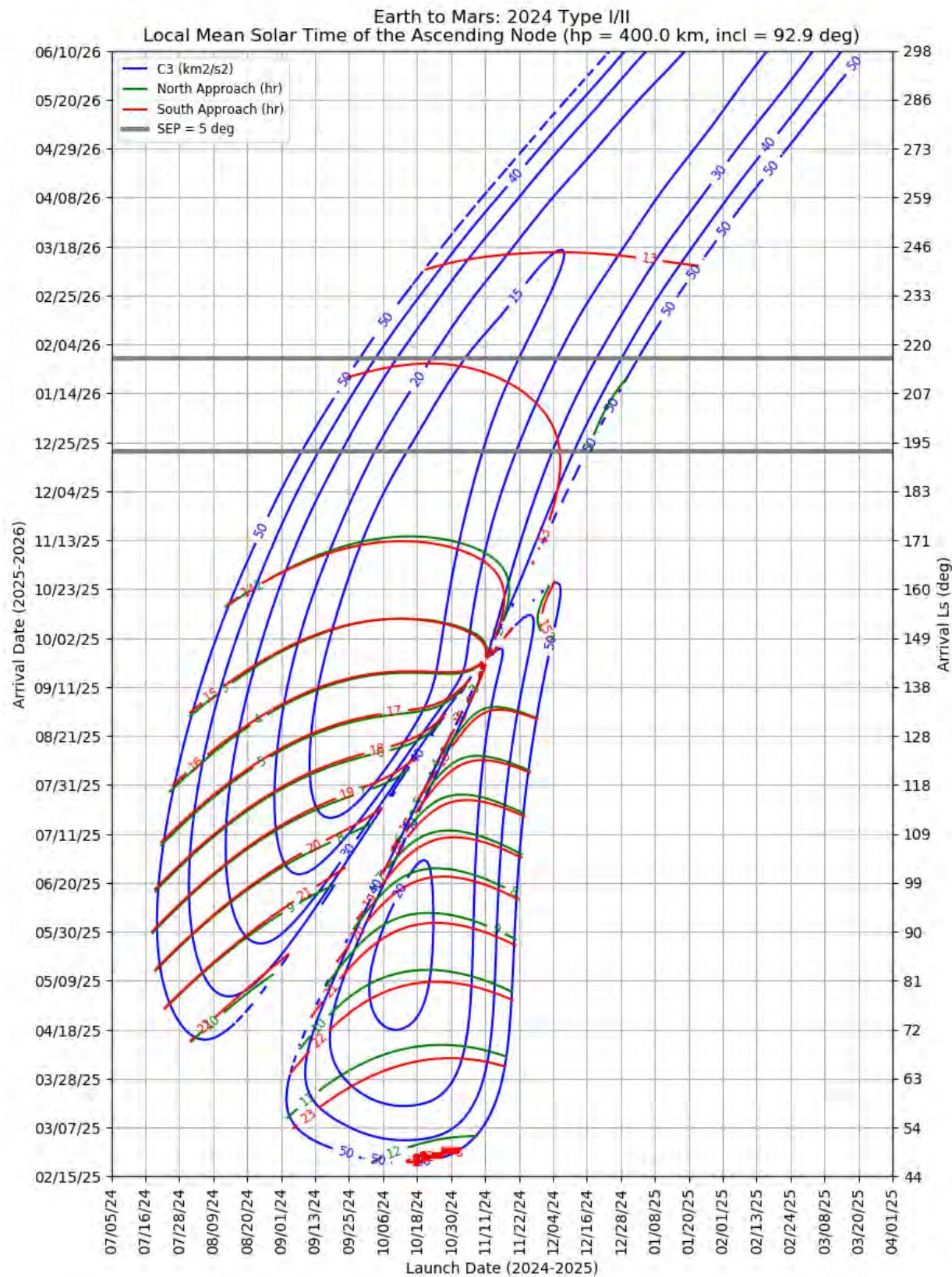


Figure 367: Earth to Mars 2024 Type I/II – LMST of the Ascending Node for North and South Approaches

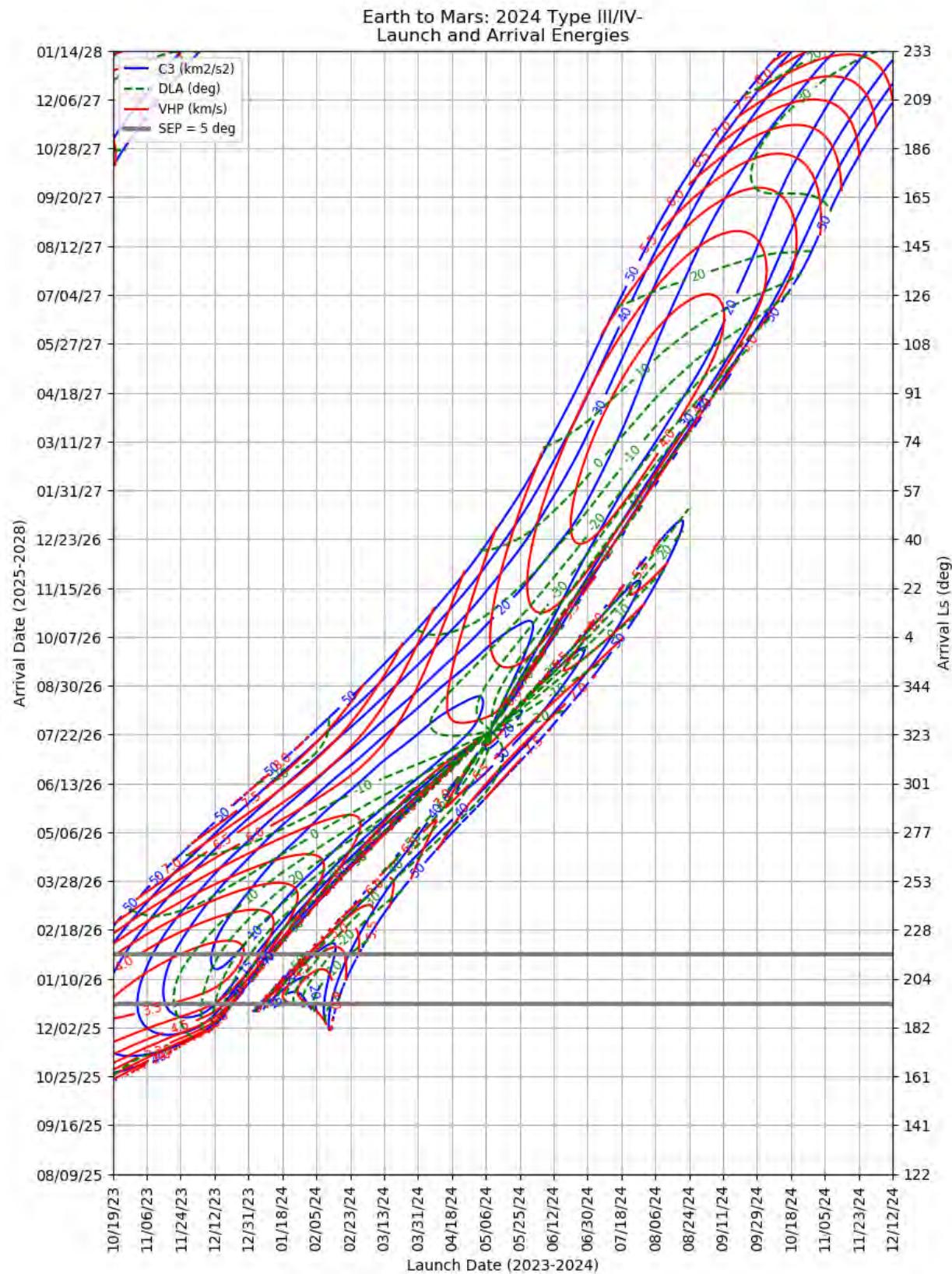
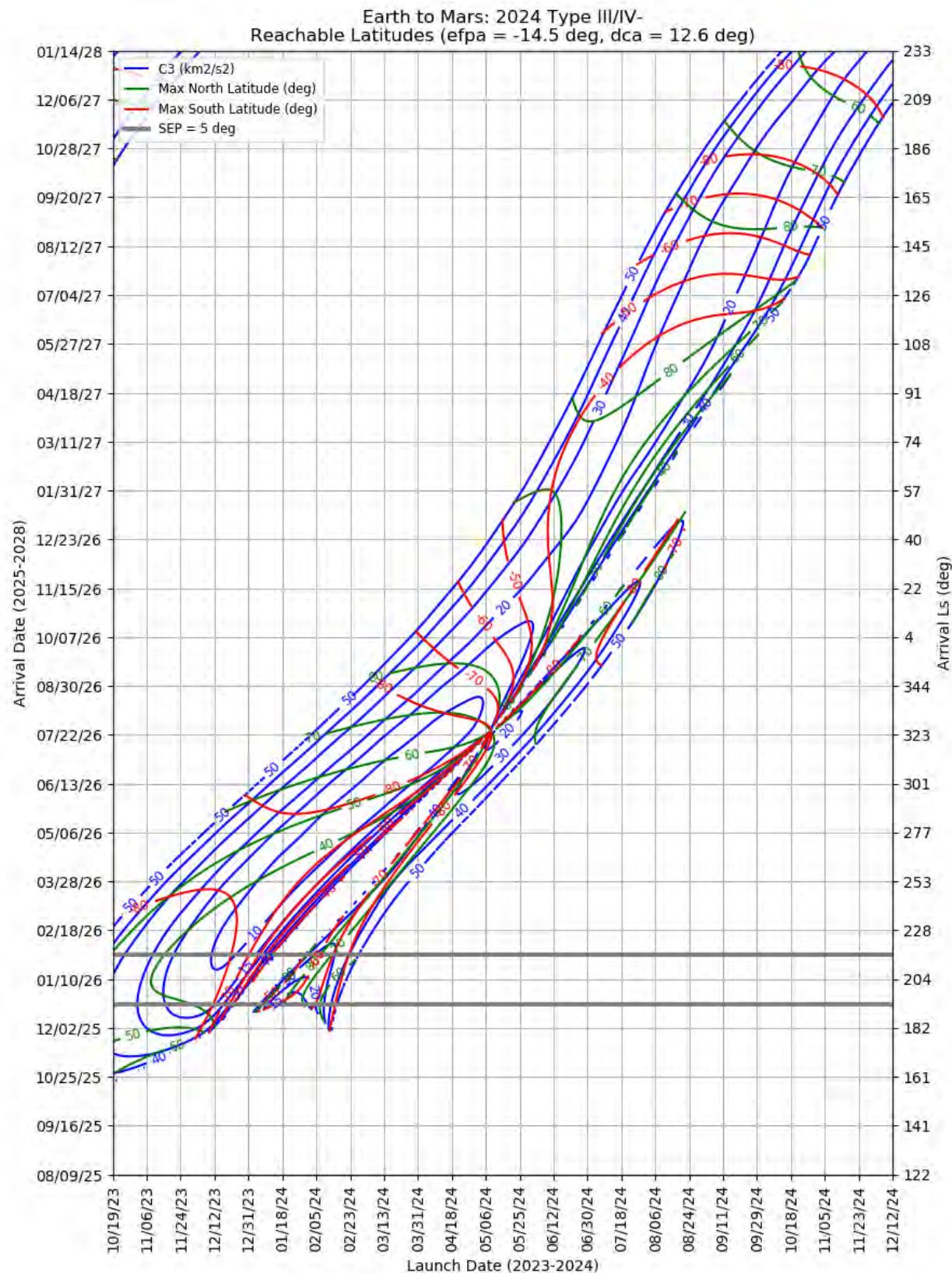
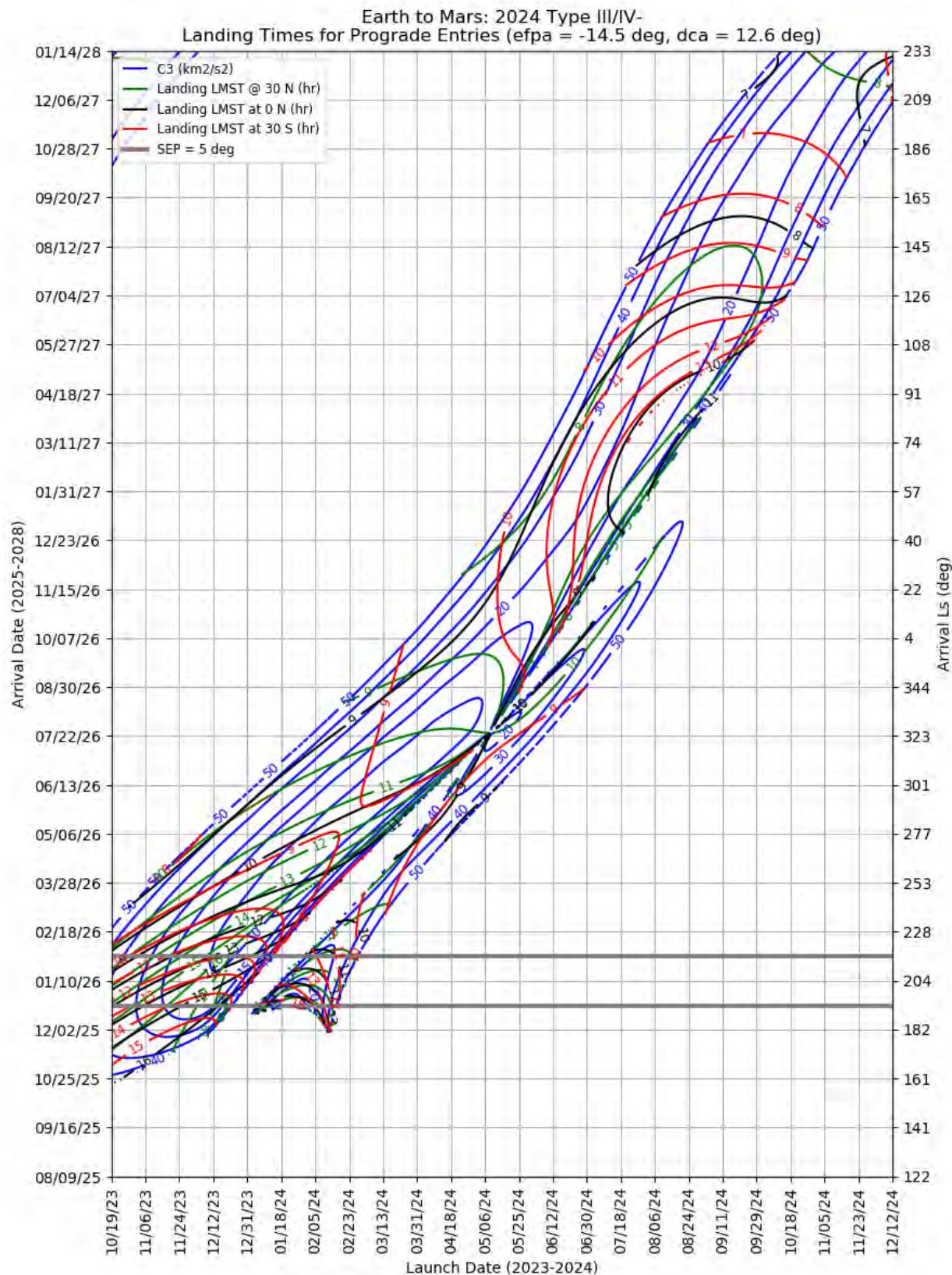


Figure 368: Earth to Mars 2024 Type III/IV- – Launch and Arrival Energy



**Figure 369: Earth to Mars 20242 Type III/IV – Maximum Reachable North and South Latitude**



**Figure 370: Earth to Mars 2024 Type III/IV- – Landing LMST for Prograde Entries**

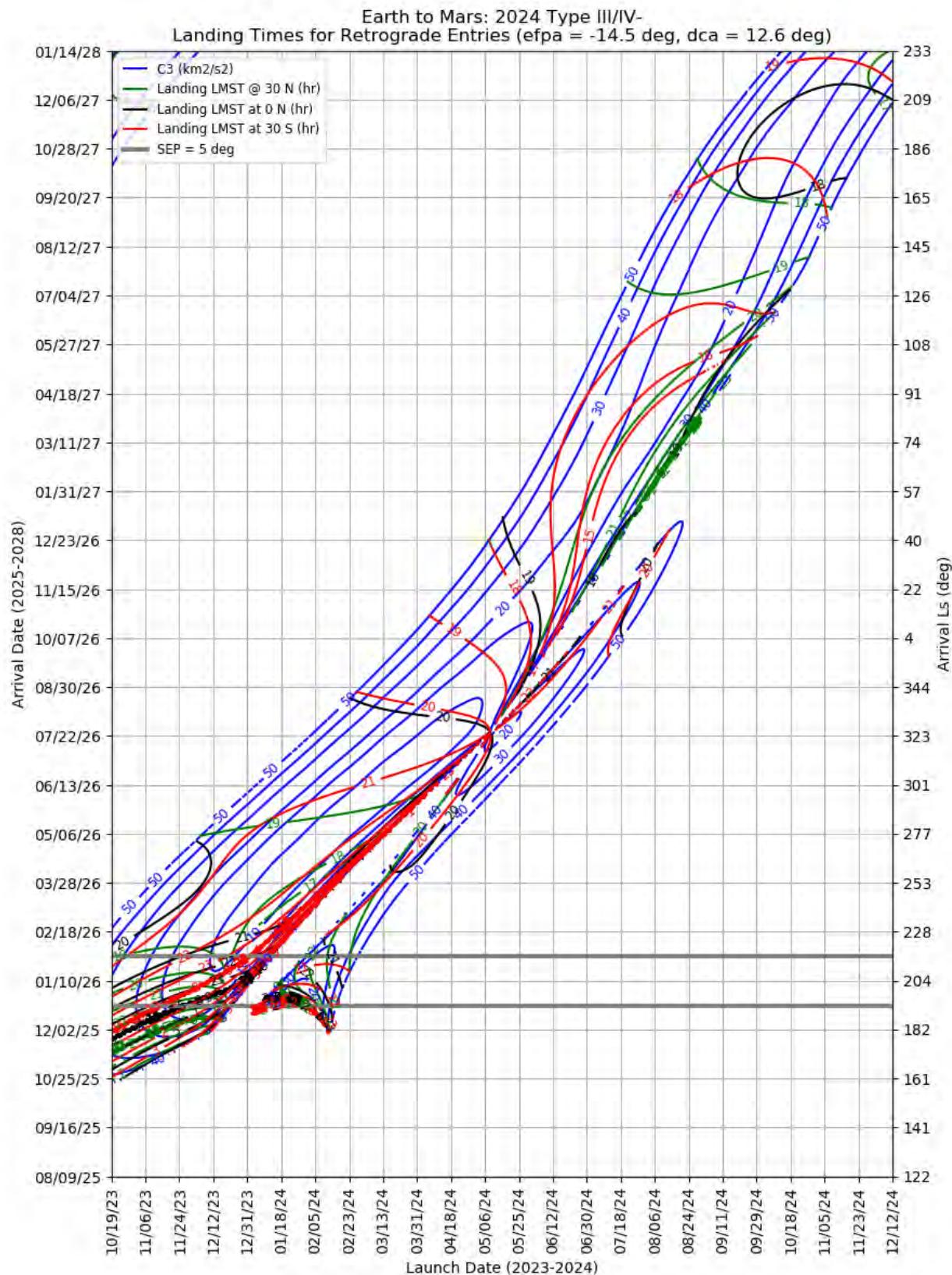


Figure 371: Earth to Mars 2024 Type III/IV- – Landing LMST for Retrograde Entries

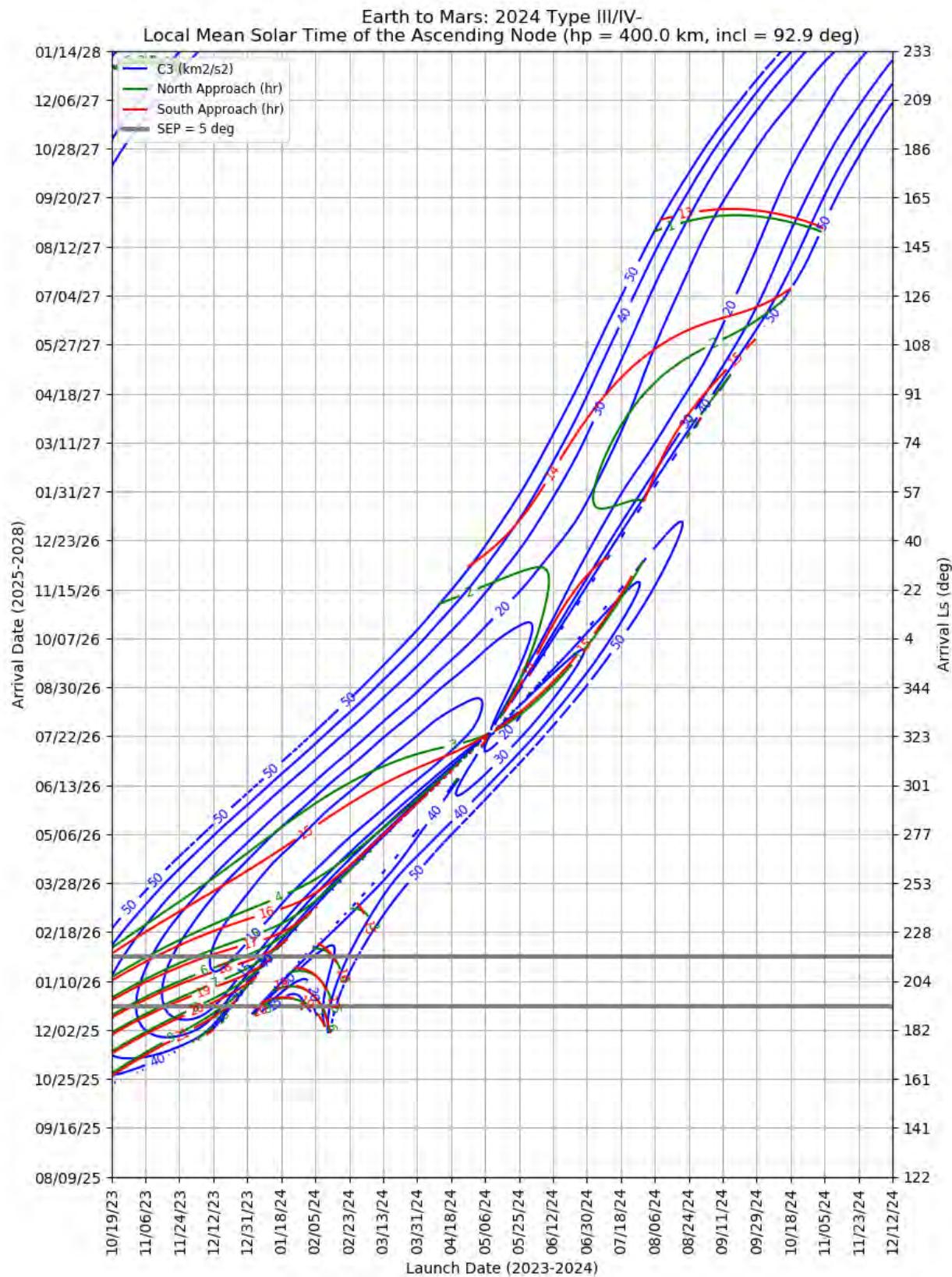
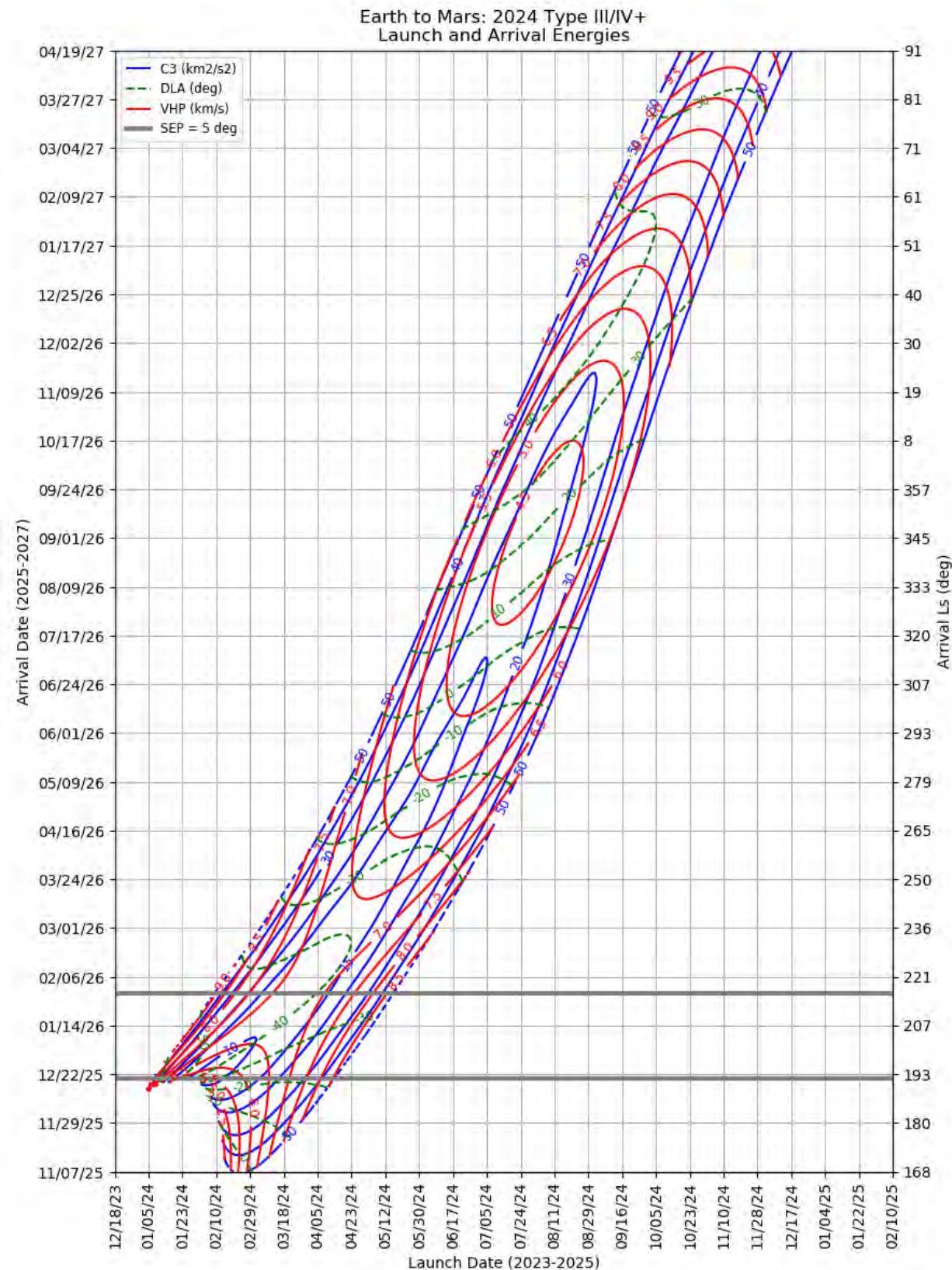
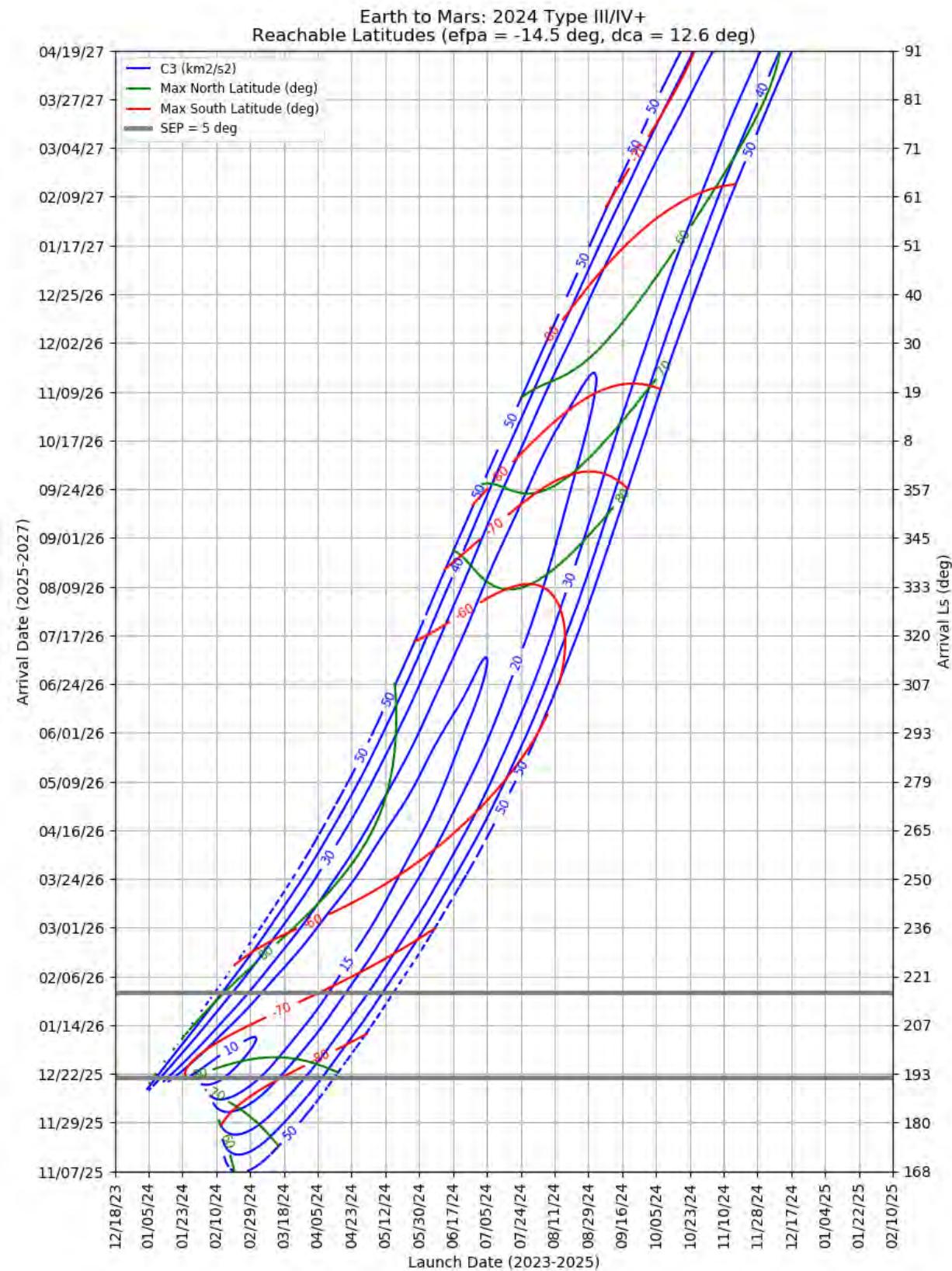


Figure 372: Earth to Mars 2024 Type III/IV- – LMST of the Ascending Node for North and South Approaches



**Figure 373: Earth to Mars 2024 Type III/IV+ – Launch and Arrival Energy**



**Figure 374: Earth to Mars 2024 Type III/IV+ – Maximum Reachable North and South Latitude**

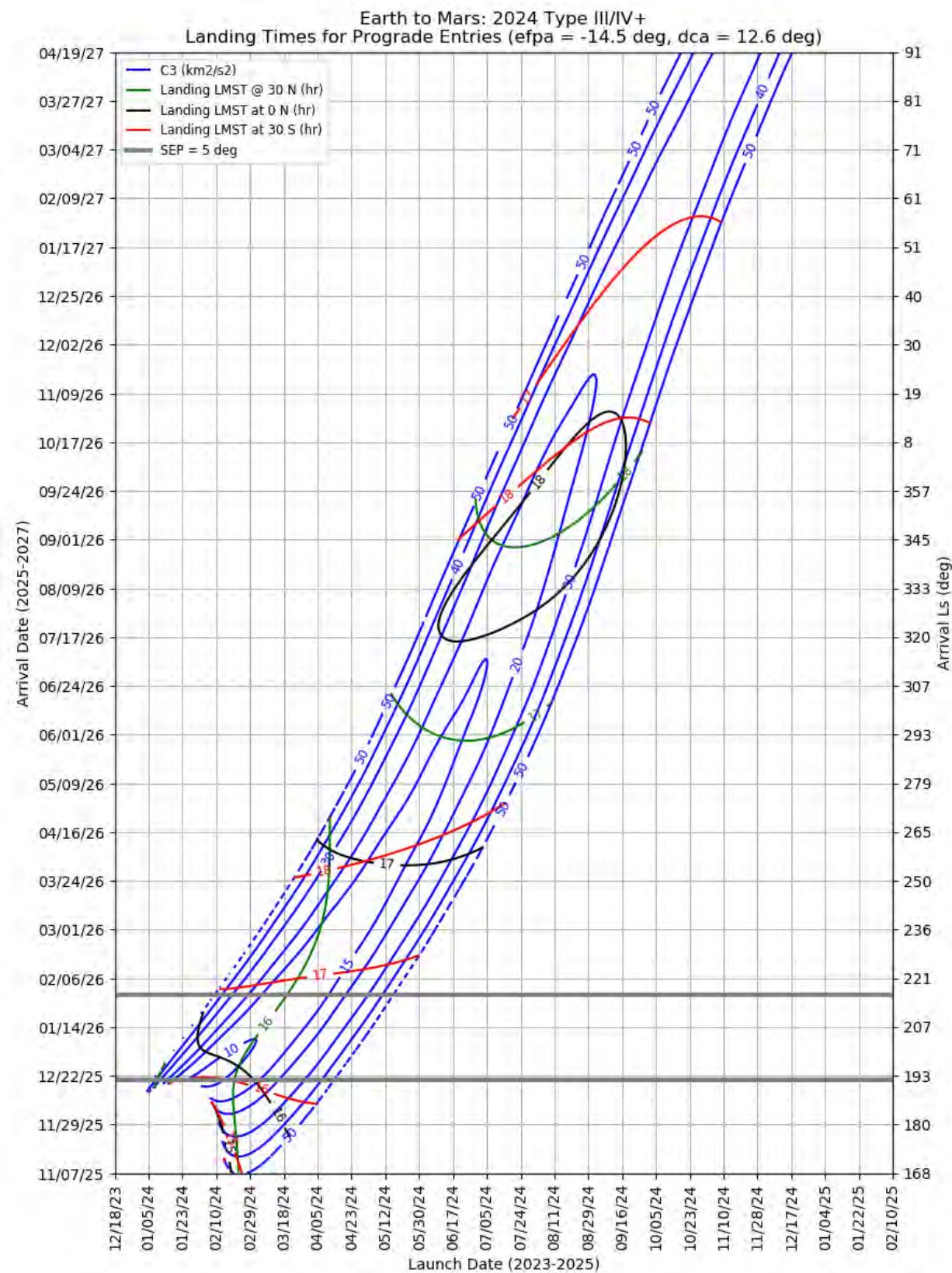
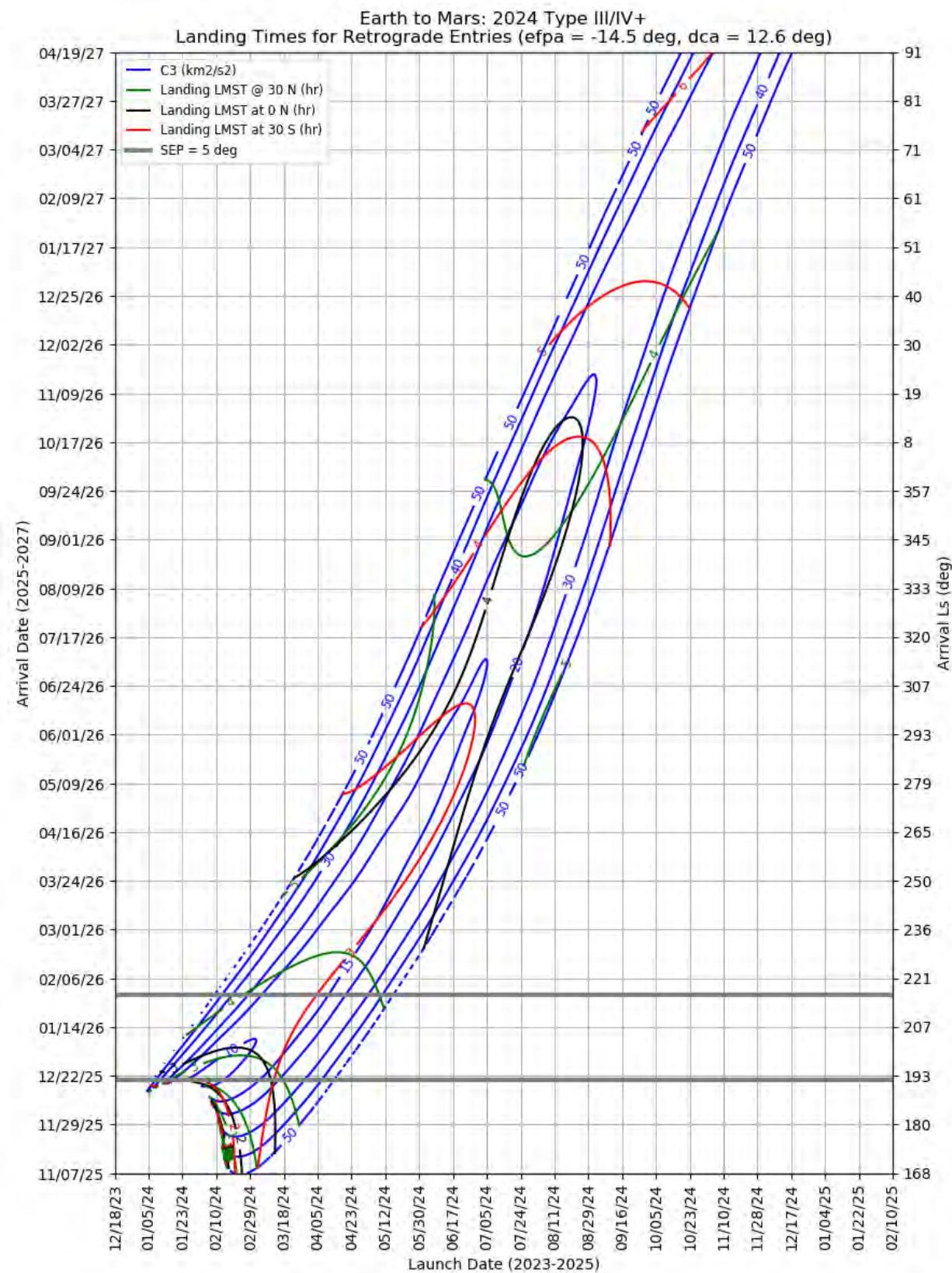


Figure 375: Earth to Mars 2024 Type III/IV+ – Landing LMST for Prograde Entries



**Figure 376: Earth to Mars 2024 Type III/IV+ – Landing LMST for Retrograde Entries**

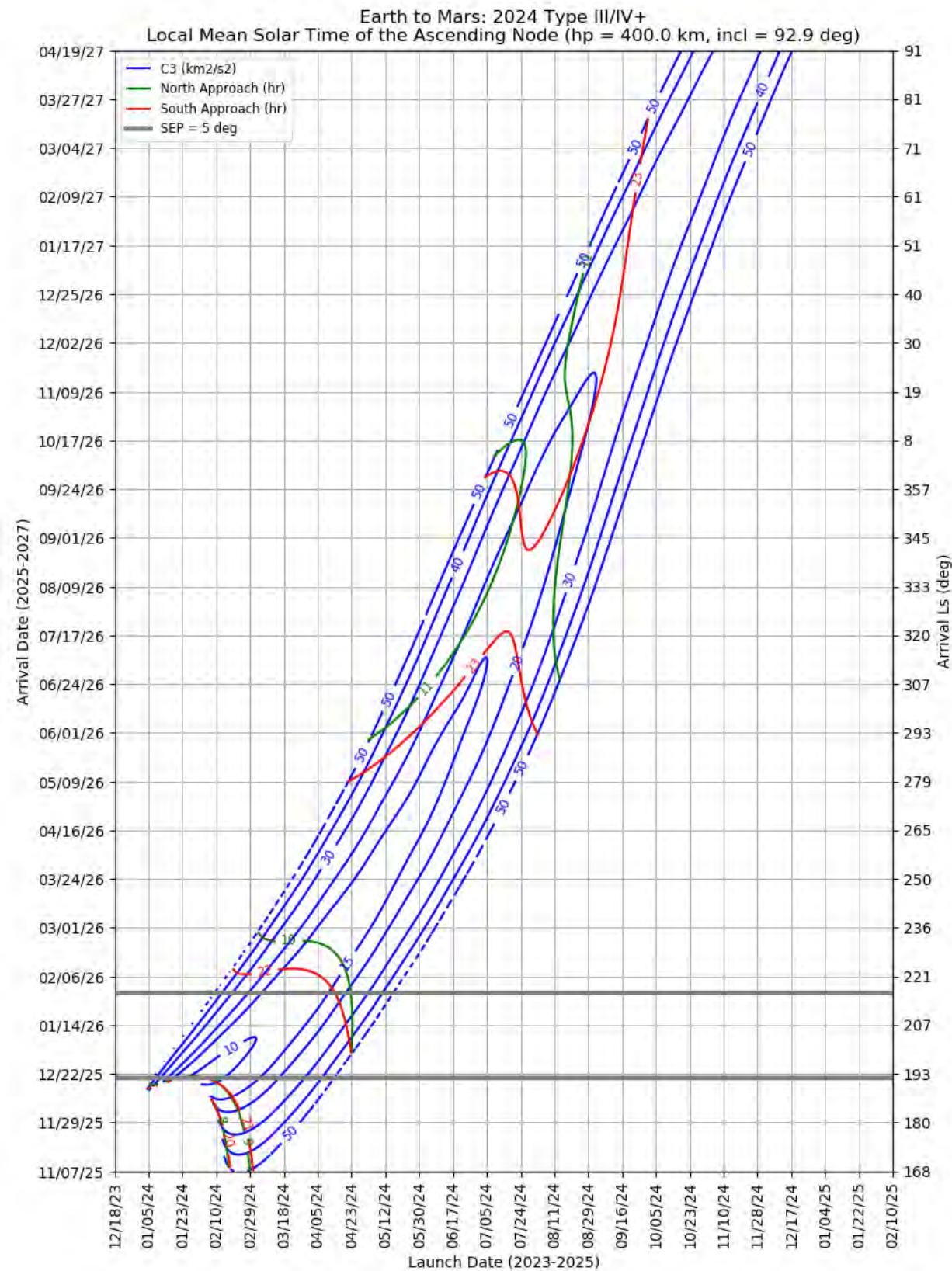


Figure 377: Earth to Mars 2024 Type III/IV+ – LMST of the Ascending Node for North and South Approaches

#### 10.5.4 Earth to Mars 2026

This section contains porkchop plots for the Earth-to-Mars 2026 opportunities. Table 30 contains the optimal single-day transfers for minimum launch energy (C3) and arrival velocity (VHP) as well as the maximum launch-mass and captured-mass launch periods for each trajectory type within the opportunity. These data should only be used for preliminary analysis and planning purposes.

**Table 30: Earth to Mars 2026 Optimal Launch/Arrival Data**

Optimization Criteria	Trajectory Type	Departure Date (dd-mmm-yyyy)	Arrival Date (dd-mmm-yyyy)	Launch Energy, C3 (km <sup>2</sup> /s <sup>2</sup> )	Declination of the Launch Asymptote, DLA (deg)	Approach V-Infinity, VHP (km/s)
<b>Single-Day Optimization</b>						
Minimum C3	I	13-Nov-2026	11-Aug-2027	10.7	25.6	2.89
Minimum C3	II	31-Oct-2026	20-Aug-2027	9.2	23.6	2.71
Minimum C3	III-	11-May-2026	11-Jun-2028	7.7	-14.6	3.87
Minimum C3	IV-	10-May-2026	11-Jun-2028	7.7	-16.4	3.86
Minimum C3	III+	20-Mar-2026	11-Jan-2028	8.6	-54.1	4.66
Minimum C3	IV+	10-May-2026	11-Jun-2028	80.8	11.5	6.57
Minimum VHP	I	12-Nov-2026	10-Aug-2027	12.0	42.5	2.86
Minimum VHP	II	07-Nov-2026	08-Sep-2027	9.7	33.7	2.56
Minimum VHP	III-	03-Aug-2026	02-Oct-2028	20.5	29.4	3.04
Minimum VHP	IV-	19-Jul-2026	29-Dec-2028	20.8	-6.6	2.81
Minimum VHP	III+	30-Jul-2026	22-Aug-2028	14.2	23.2	2.69
Minimum VHP	IV+	11-May-2026	13-Jun-2028	84.9	-0.2	6.56
<b>Launch Period Optimization</b>						
Maximum Launch Mass	I	04-Nov-2026	27-Jun-2027	13.5	43.4	4.35
		24-Nov-2026		15.8	31.1	4.44
Maximum Launch Mass	II	21-Oct-2026	14-Aug-2027	9.9	17.7	2.80
		10-Nov-2026		10.1	27.2	2.81
Maximum Launch Mass	III-	11-May-2026	11-Jun-2028	7.7	-14.6	3.87
		31-May-2026		12.1	-20.3	4.15
Maximum Launch Mass	IV-	21-Apr-2026	11-Jun-2028	9.4	-12.4	4.11
		11-May-2026		7.7	-14.6	3.87
Maximum Launch Mass	III+	14-May-2026	30-Mar-2028	10.9	-24.3	4.19
		03-Jun-2026		11.1	-27.5	4.17
Maximum Launch Mass	IV+	Not Possible				
Maximum Captured Mass	I	11-Nov-2026	06-Aug-2027	13.3	49.7	2.98
		01-Dec-2026		18.3	23.9	3.08

Optimization Criteria	Trajectory Type	Departure Date (dd-mmm-yyyy)	Arrival Date (dd-mmm-yyyy)	Launch Energy, C3 (km <sup>2</sup> /s <sup>2</sup> )	Declination of the Launch Asymptote, DLA (deg)	Approach V-Infinity, VHP (km/s)
Maximum Captured Mass	II	19-Oct-2026	26-Aug-2027	10.1	20.7	2.64
		08-Nov-2026		9.9	32.2	2.63
Maximum Captured Mass	III-	11-May-2026	11-Jun-2028	7.7	-14.6	3.87
		31-May-2026		12.1	-20.3	4.15
Maximum Captured Mass	IV-	21-Apr-2026	11-Jun-2028	9.4	-12.4	4.11
		11-May-2026		7.7	-14.6	3.87
Maximum Captured Mass	III+	26-Jun-2026	03-Jul-2028	12.6	14.0	3.01
		16-Jul-2026		12.8	4.8	2.92
Maximum Captured Mass	IV+	Not Possible				

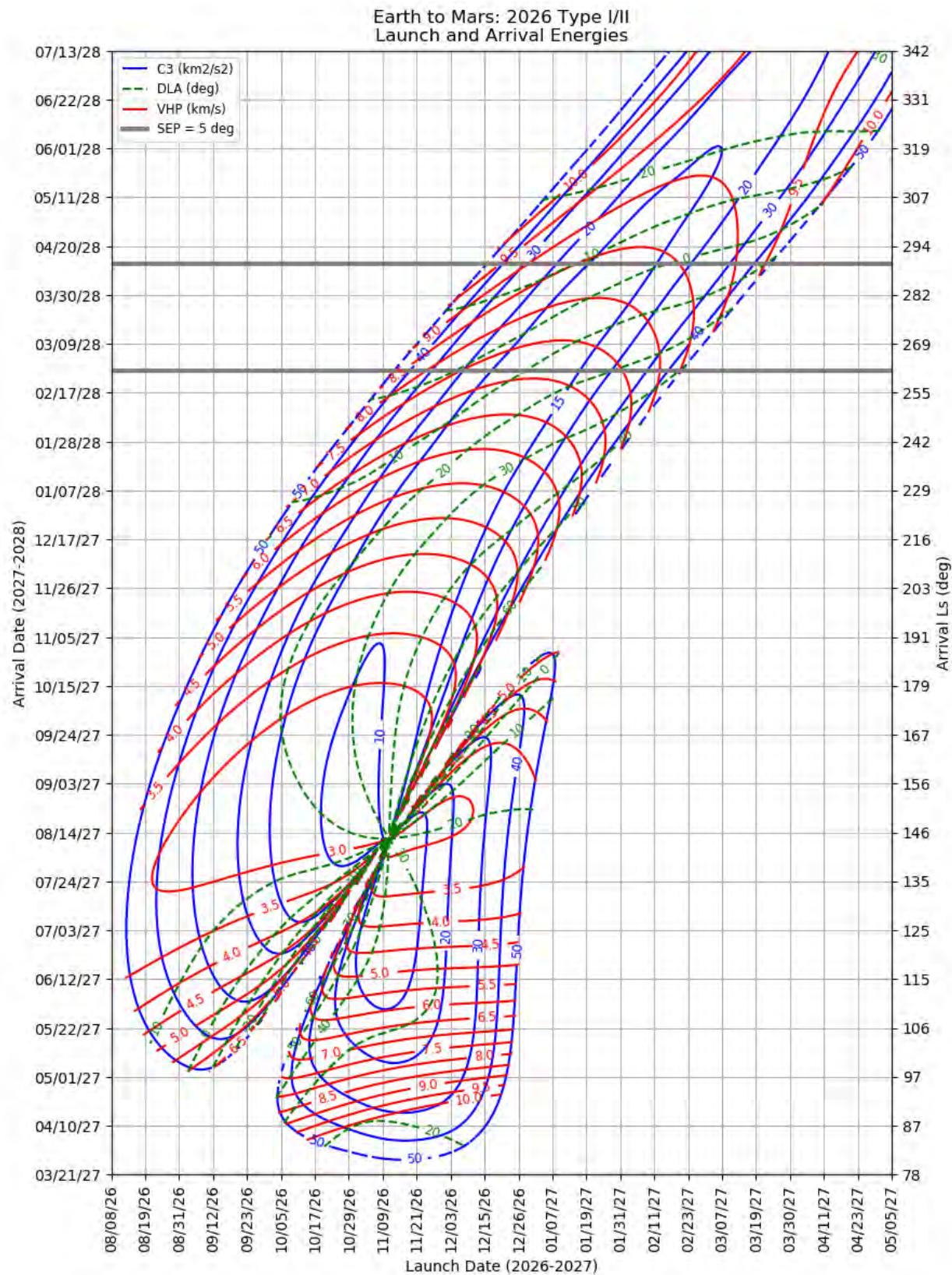
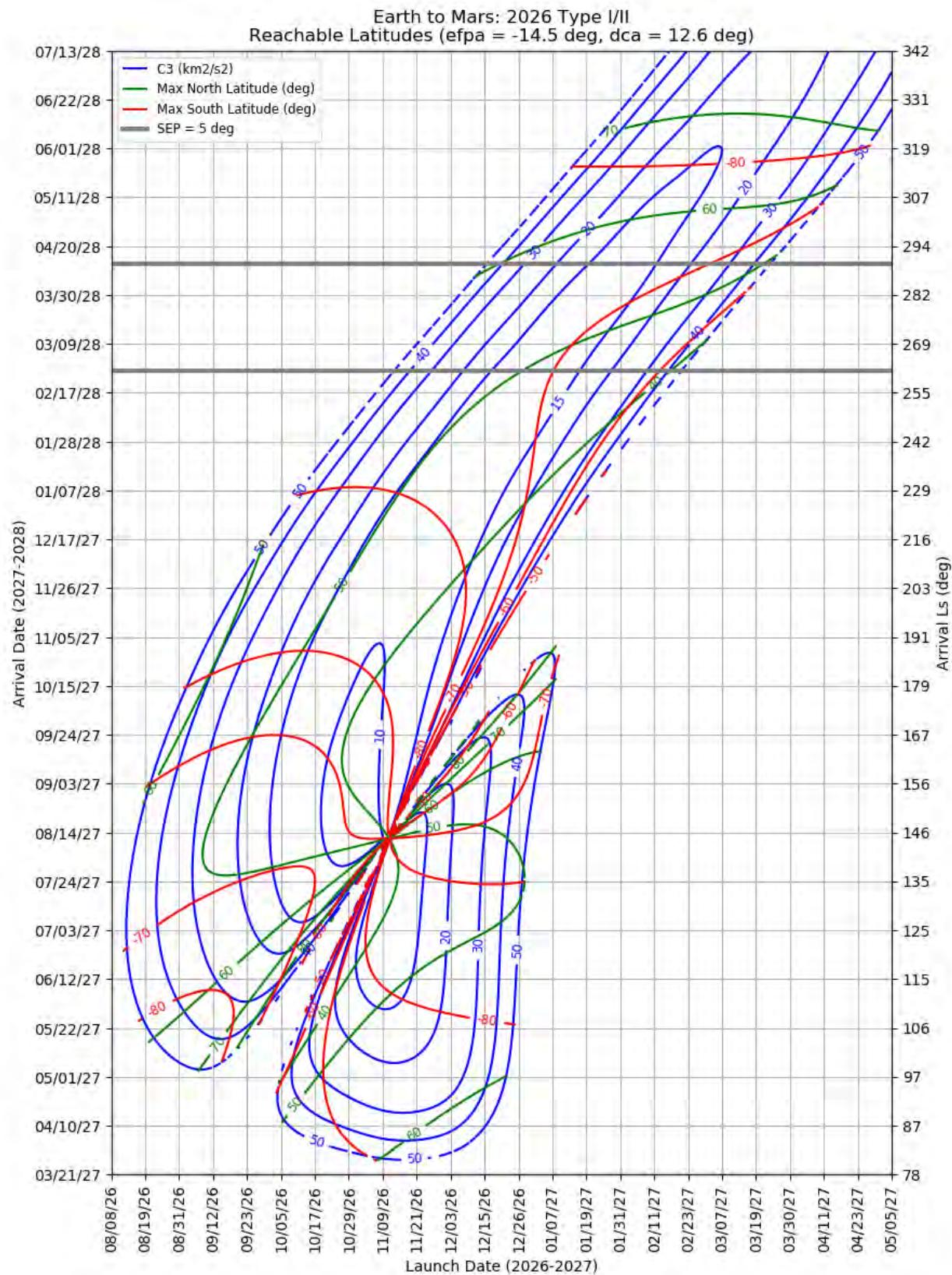
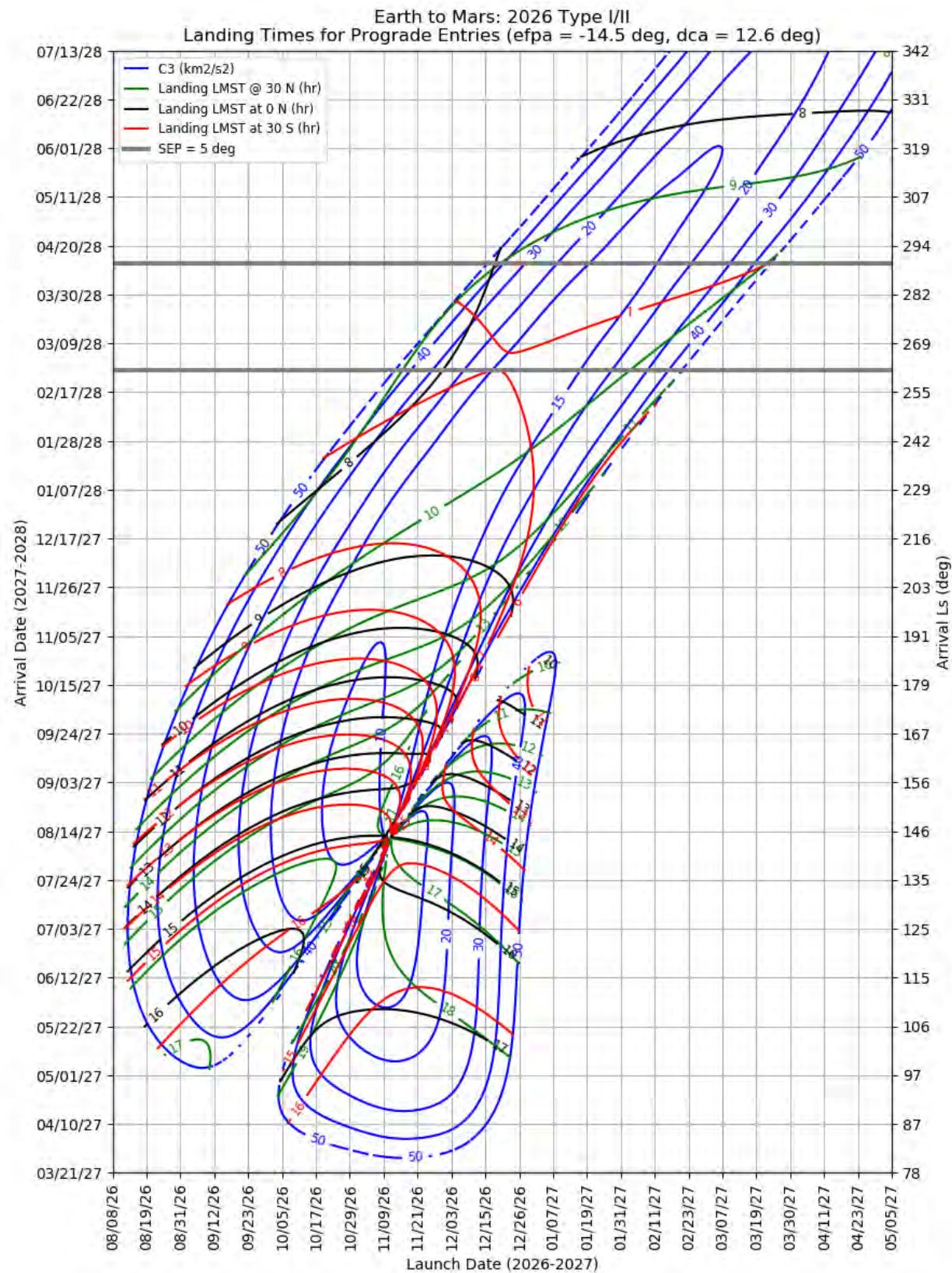


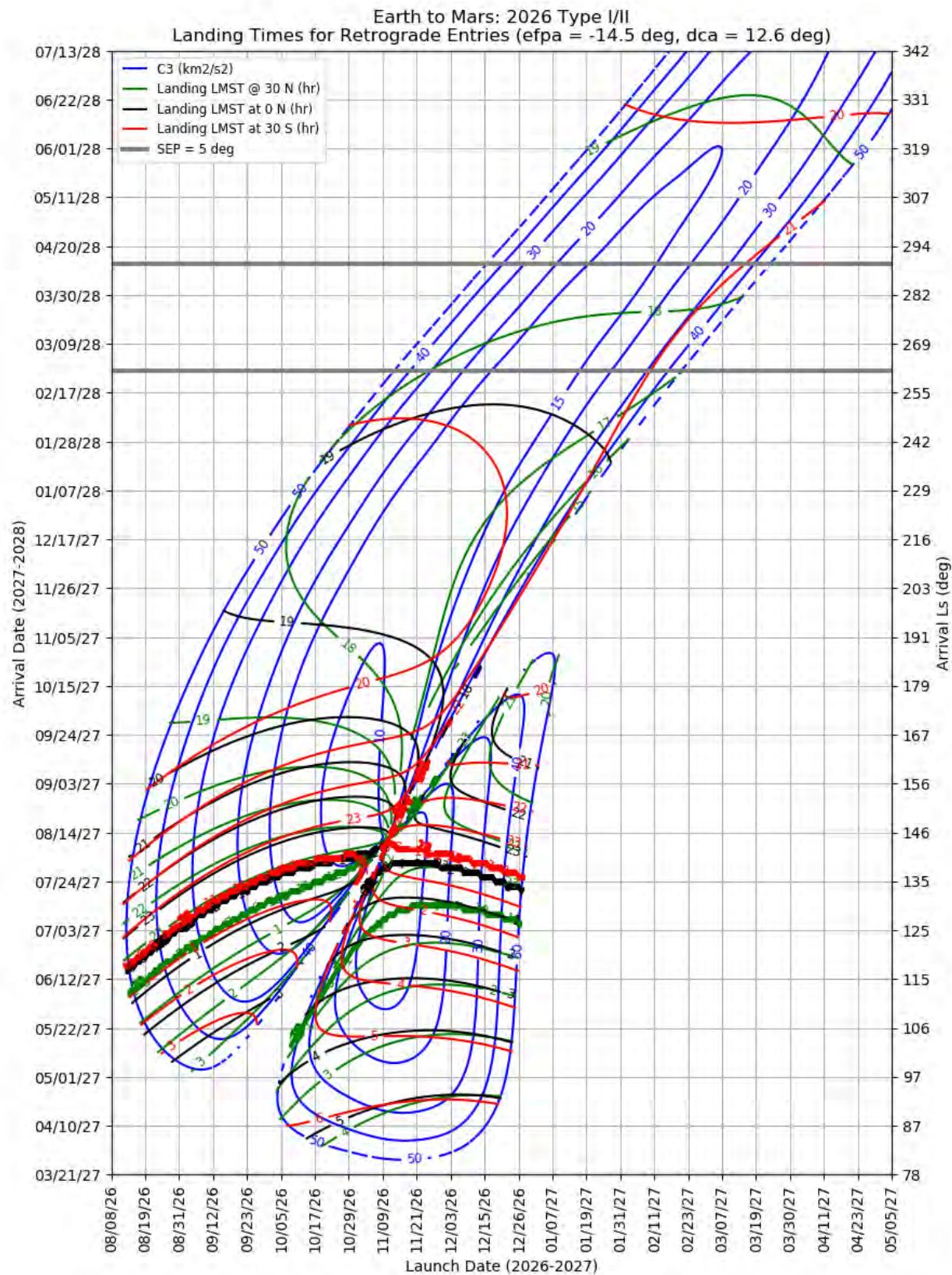
Figure 378: Earth to Mars 2026 Type I/II - Launch and Arrival Energy



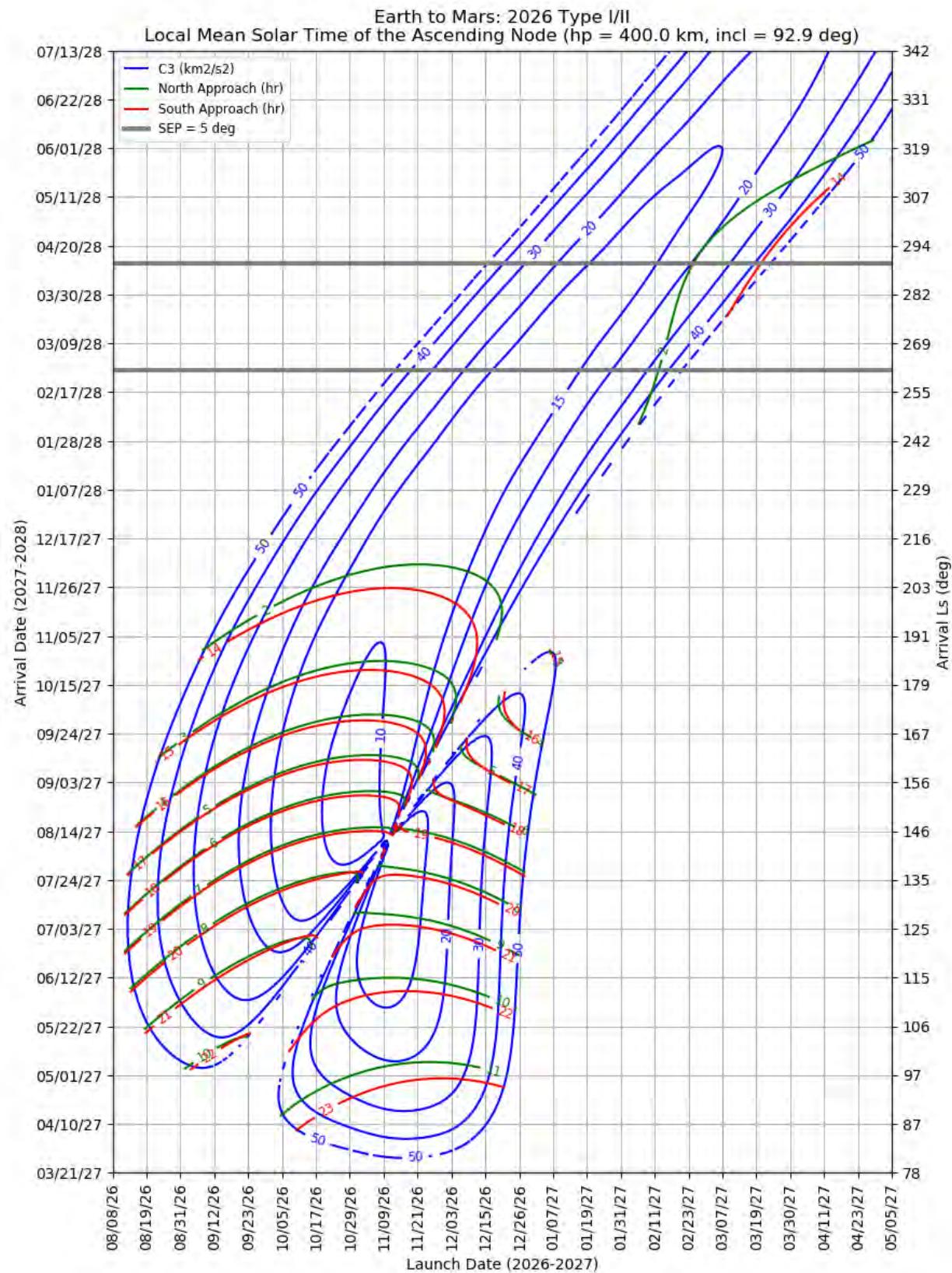
**Figure 379: Earth to Mars 2026 Type I/II – Maximum Reachable North and South Latitude**



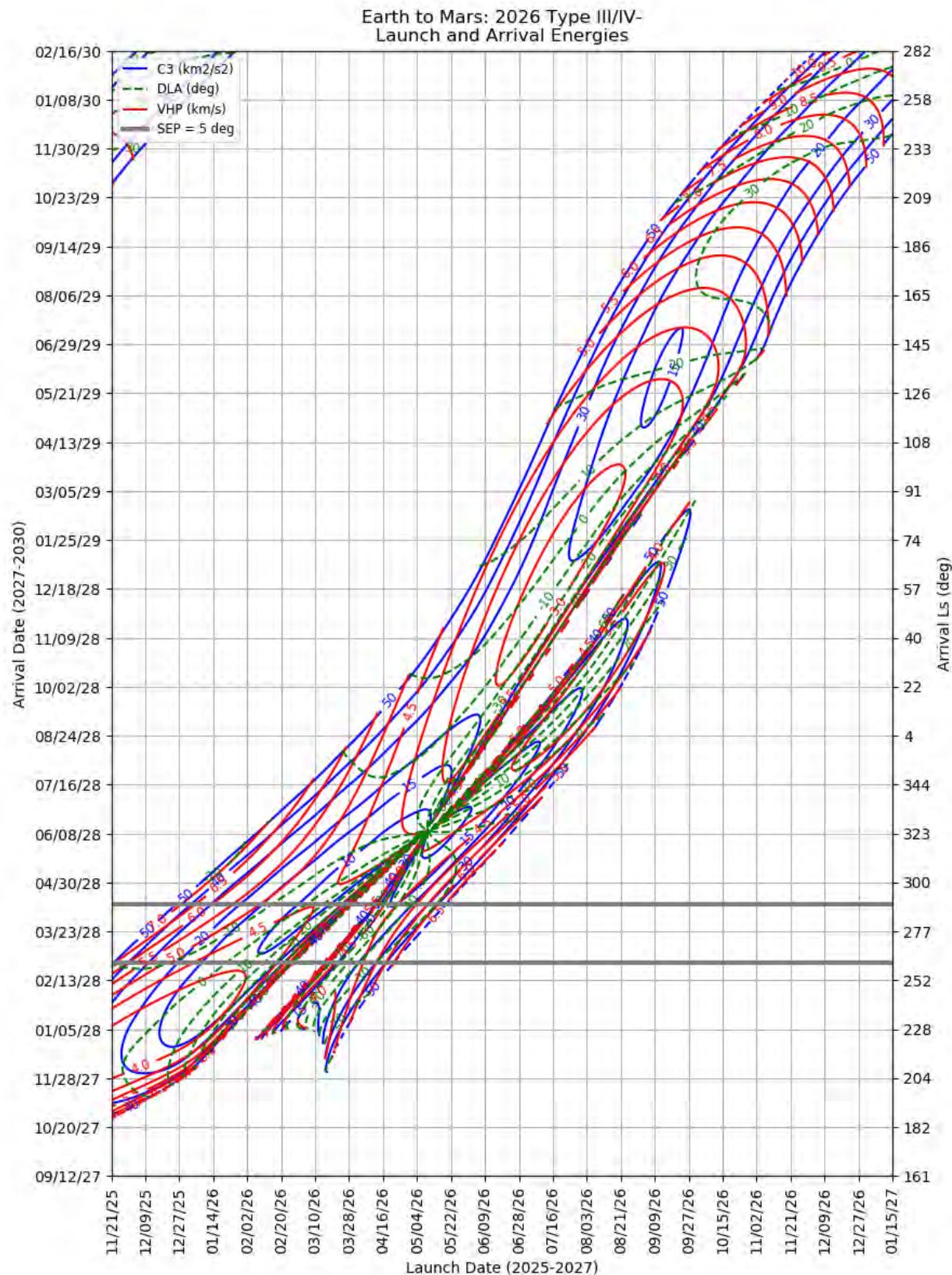
**Figure 380: Earth to Mars 2026 Type I/II – Landing LMST for Prograde Entries**



**Figure 381: Earth to Mars 2026 Type I/II – Landing LMST for Retrograde Entries**



**Figure 382: Earth to Mars 2026 Type I/II – LMST of the Ascending Node for North and South Approaches**



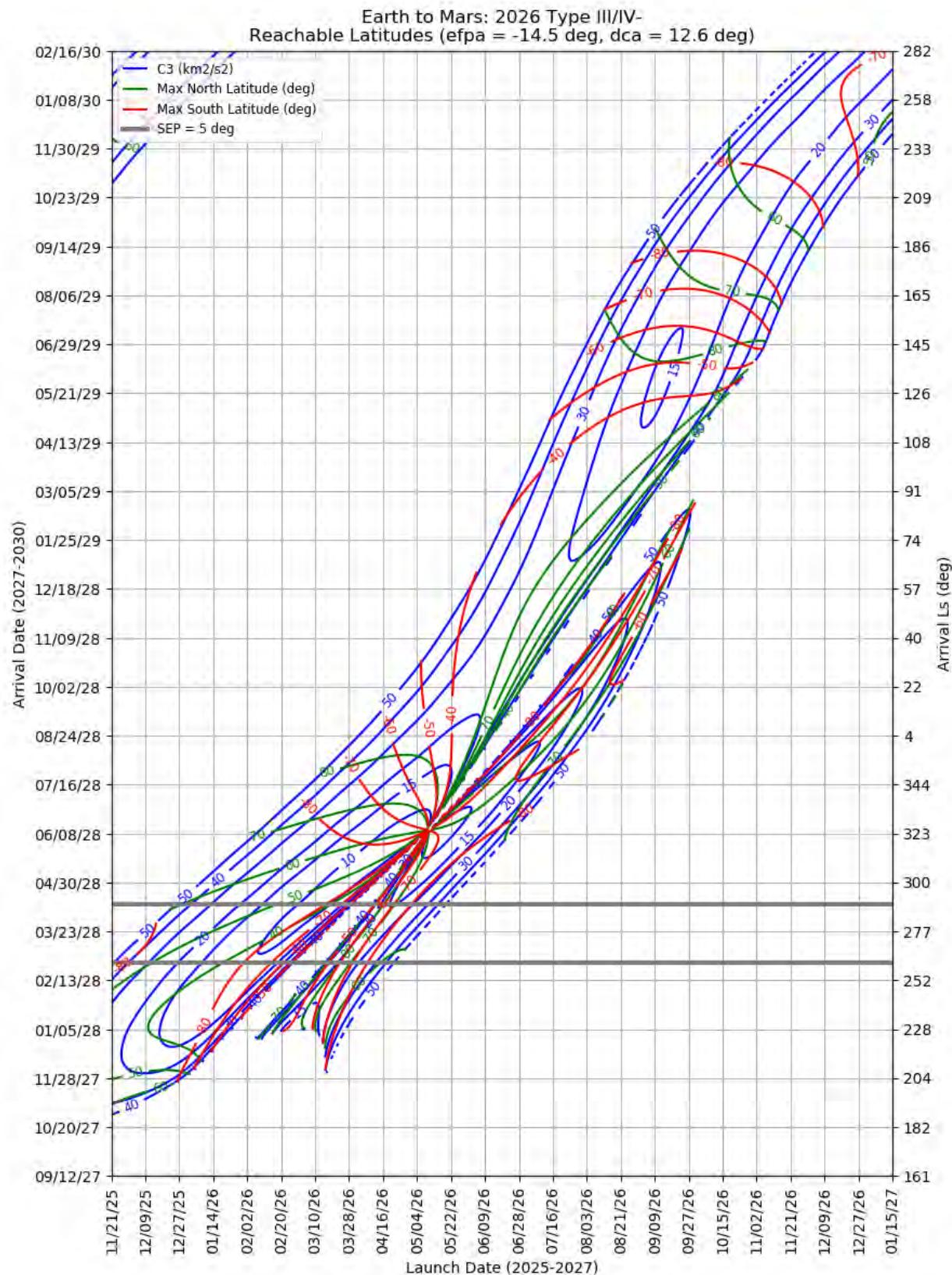
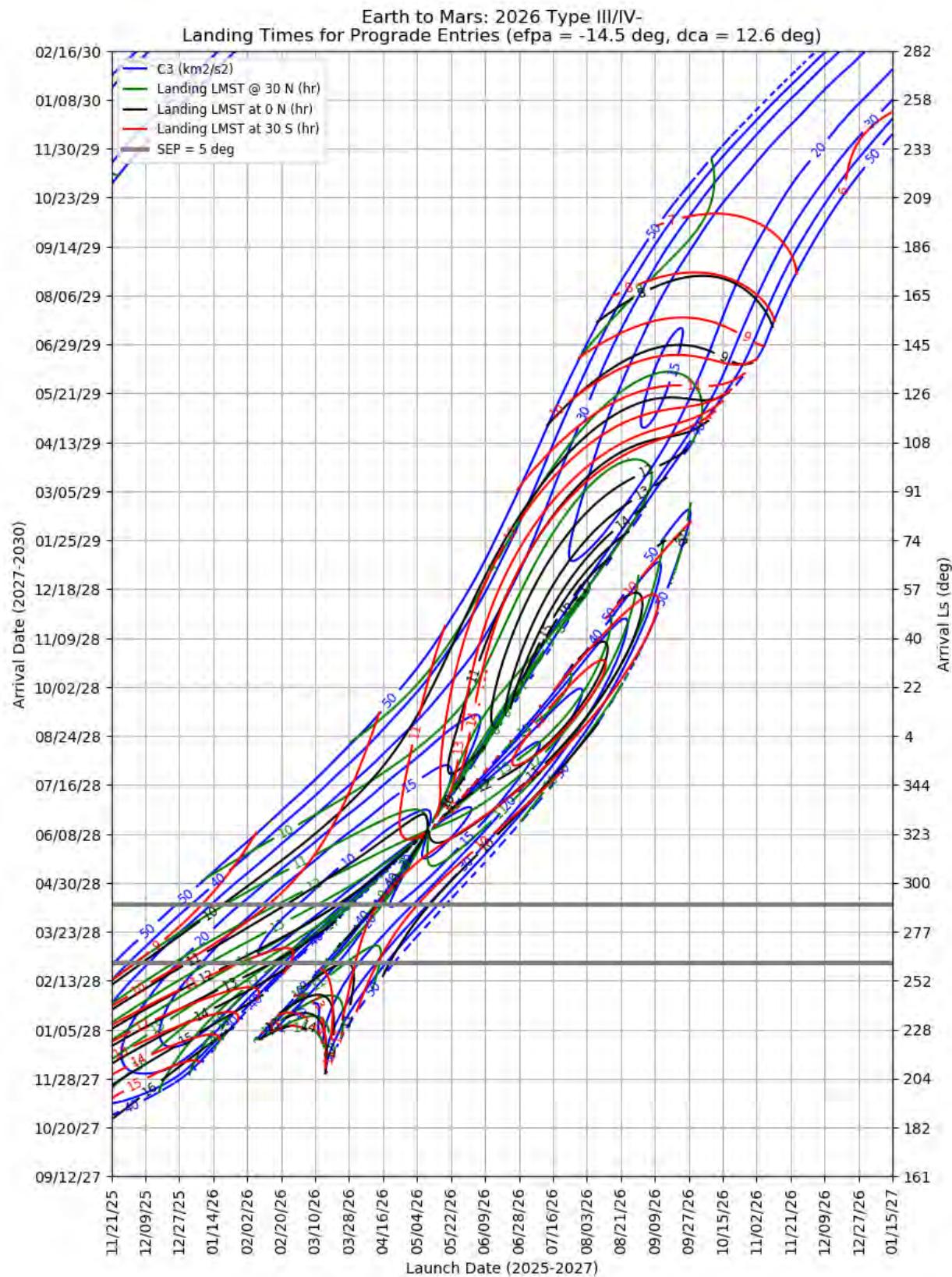


Figure 384: Earth to Mars 2026 Type III/IV – Maximum Reachable North and South Latitude



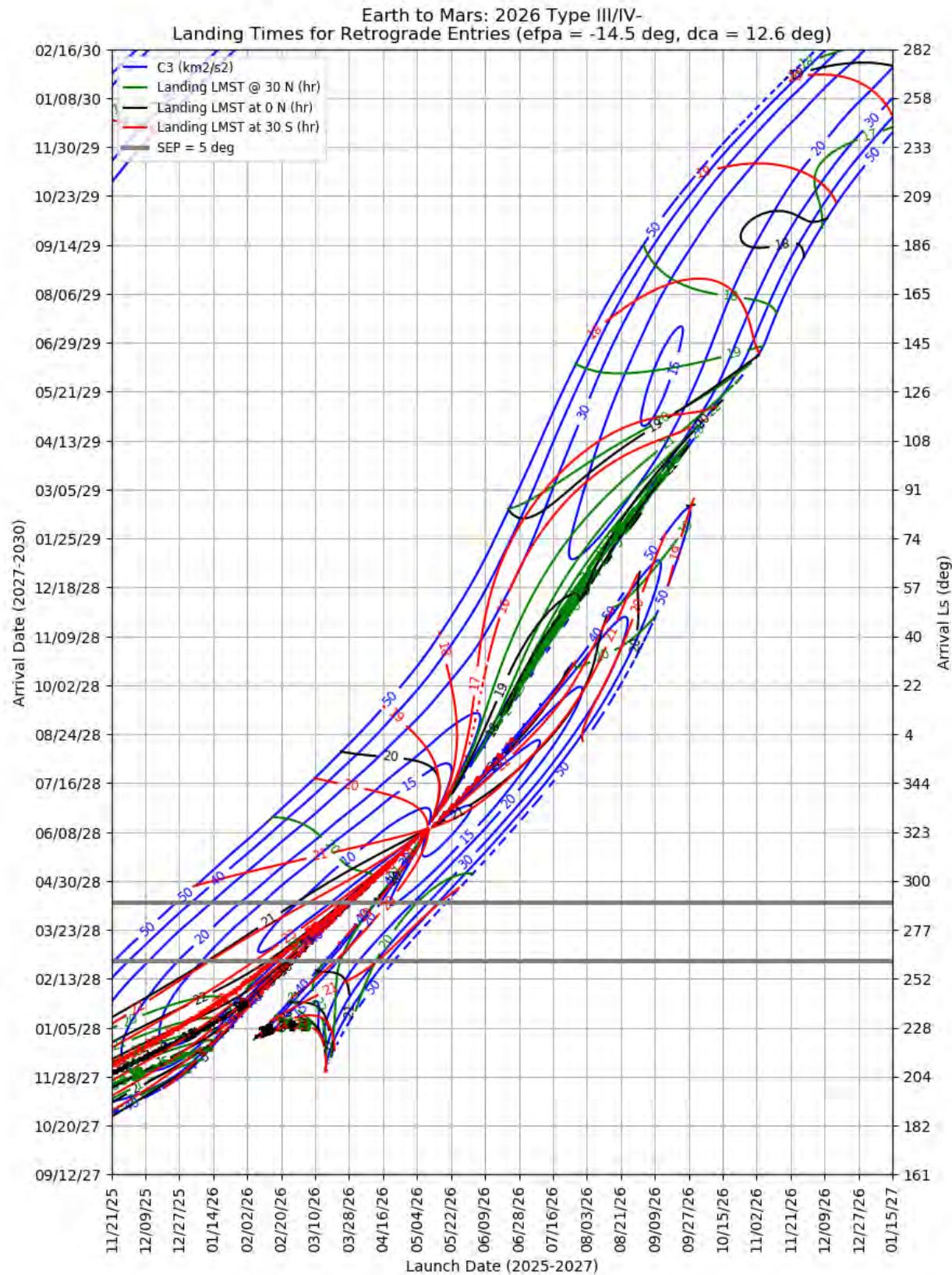
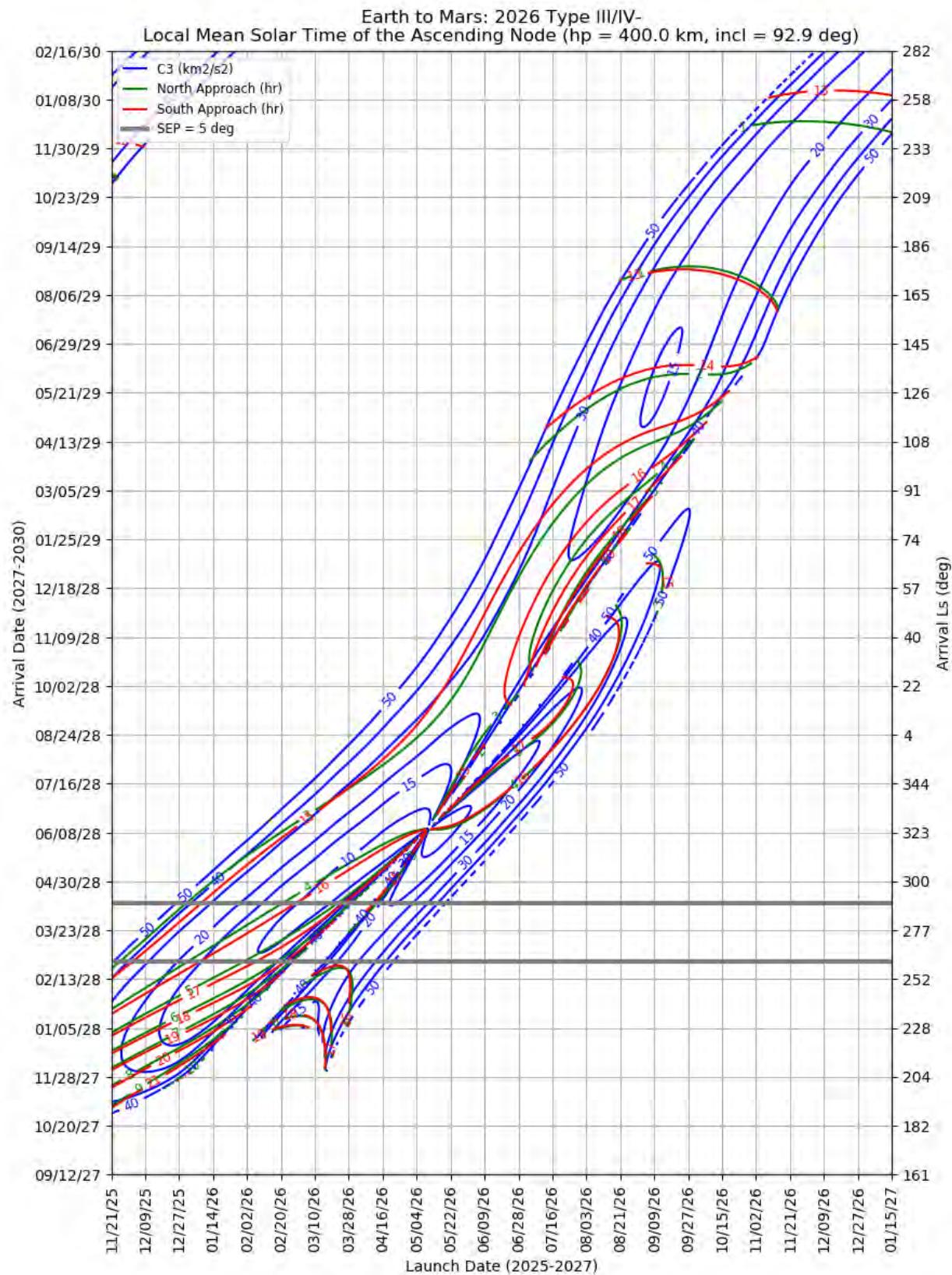
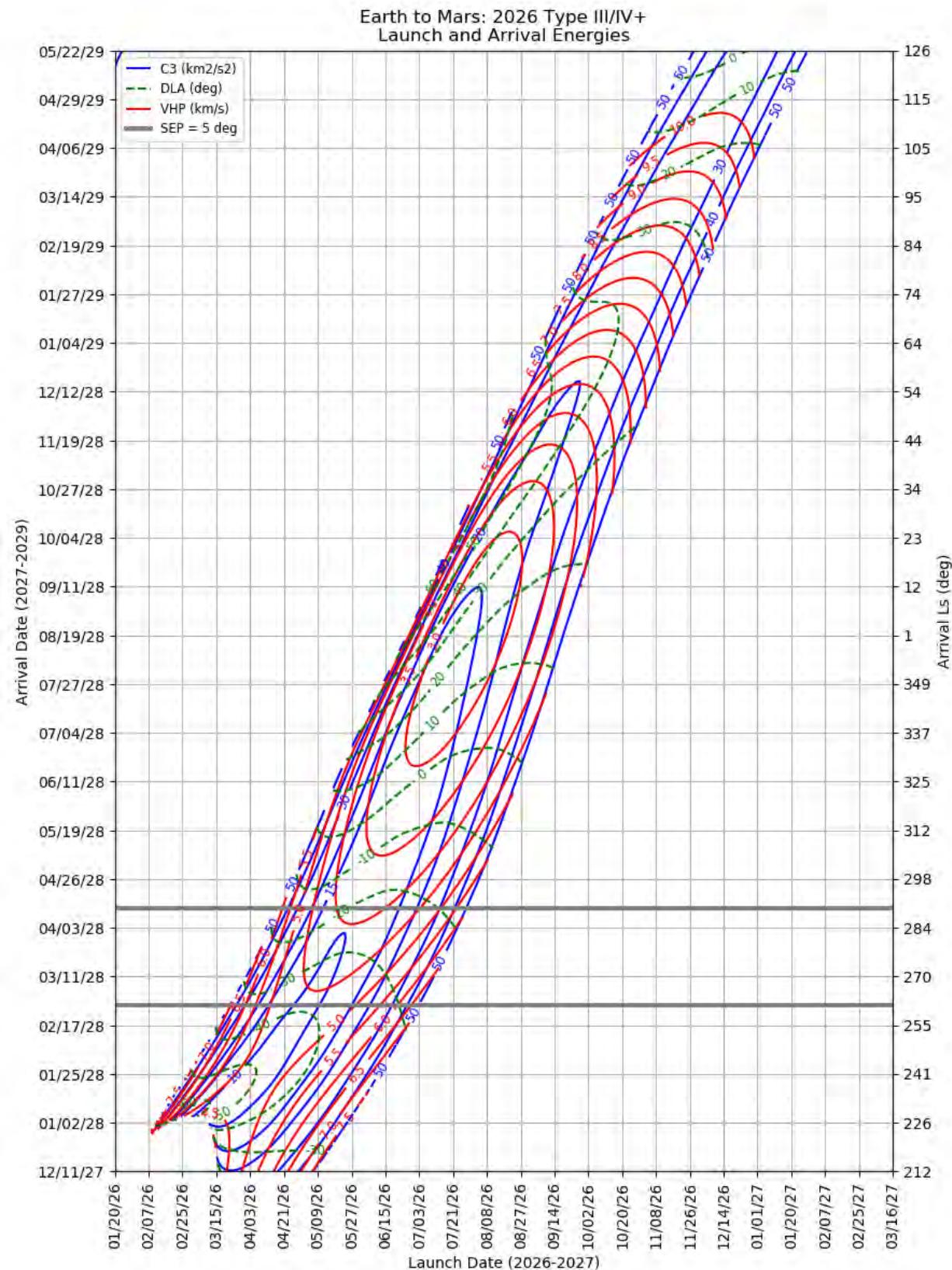


Figure 386: Earth to Mars 2026 Type III/IV- – Landing LMST for Retrograde Entries



**Figure 387: Earth to Mars 2026 Type III/IV- – LMST of the Ascending Node for North and South Approaches**



**Figure 388: Earth to Mars 2026 Type III/IV+ – Launch and Arrival Energy**

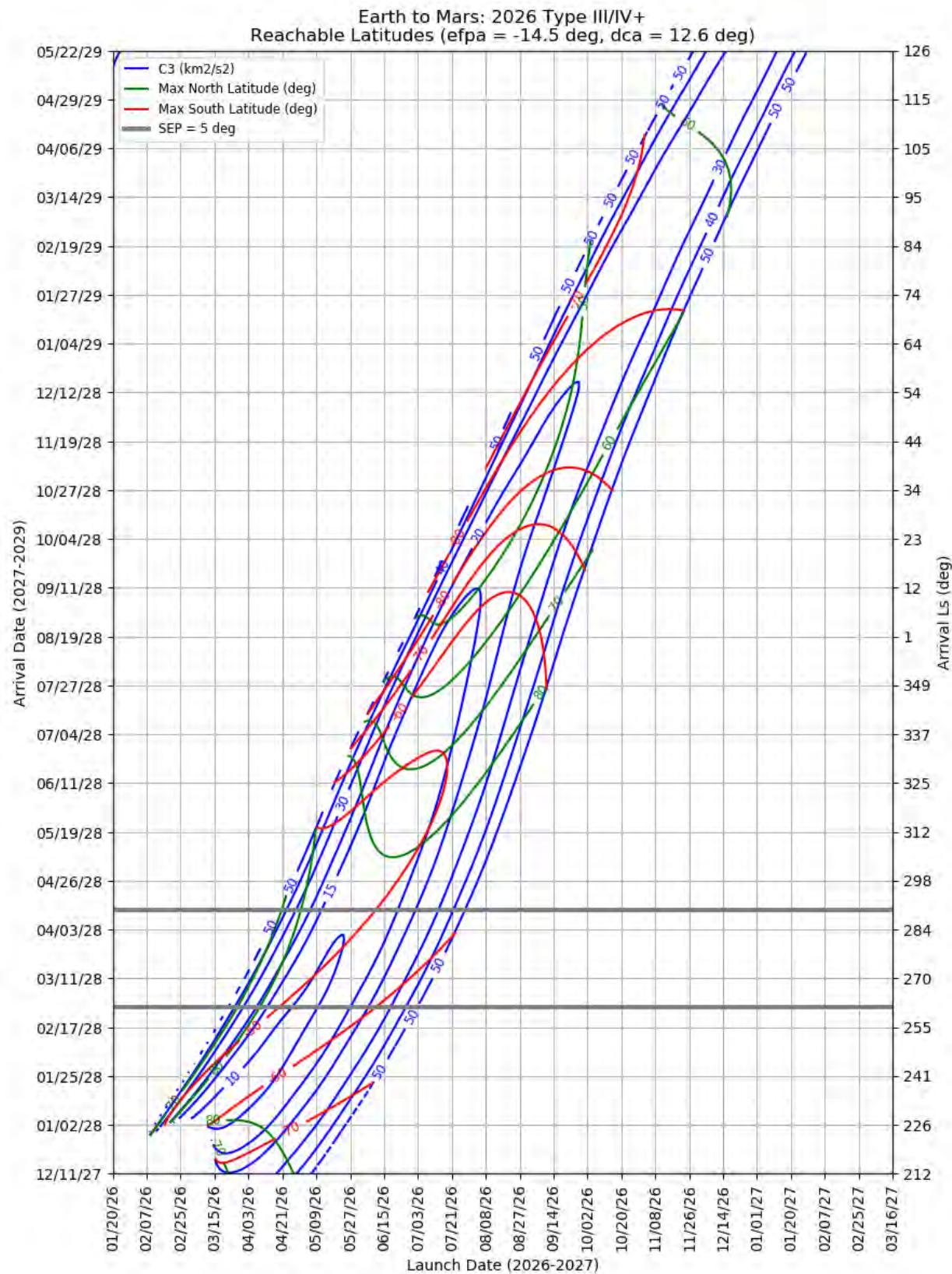


**Figure 389: Earth to Mars 2026 Type III/IV+ – Maximum Reachable North and South Latitude**

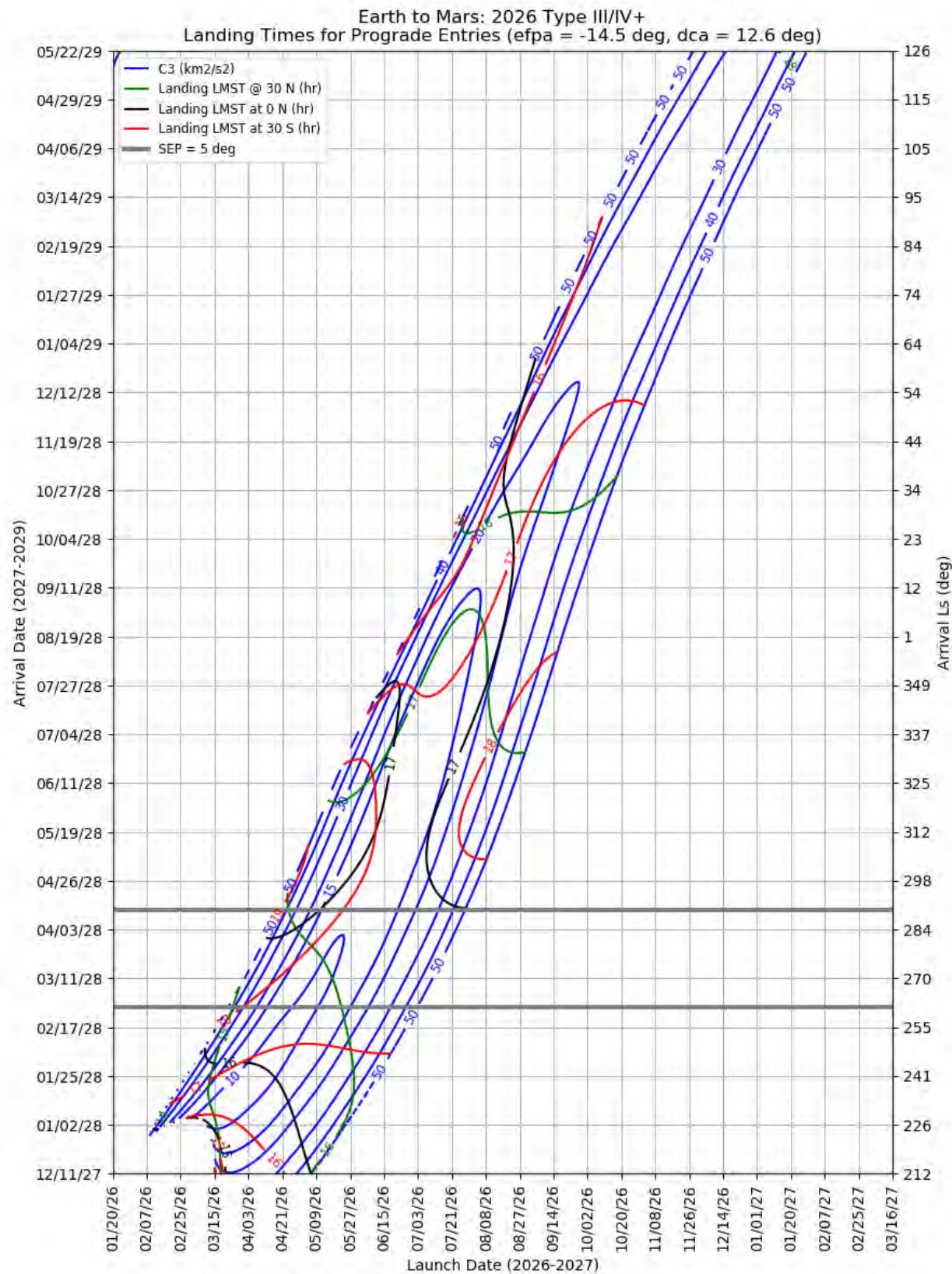


Figure 390: Earth to Mars 2026 Type III/IV+ – Landing LMST for Prograde Entries

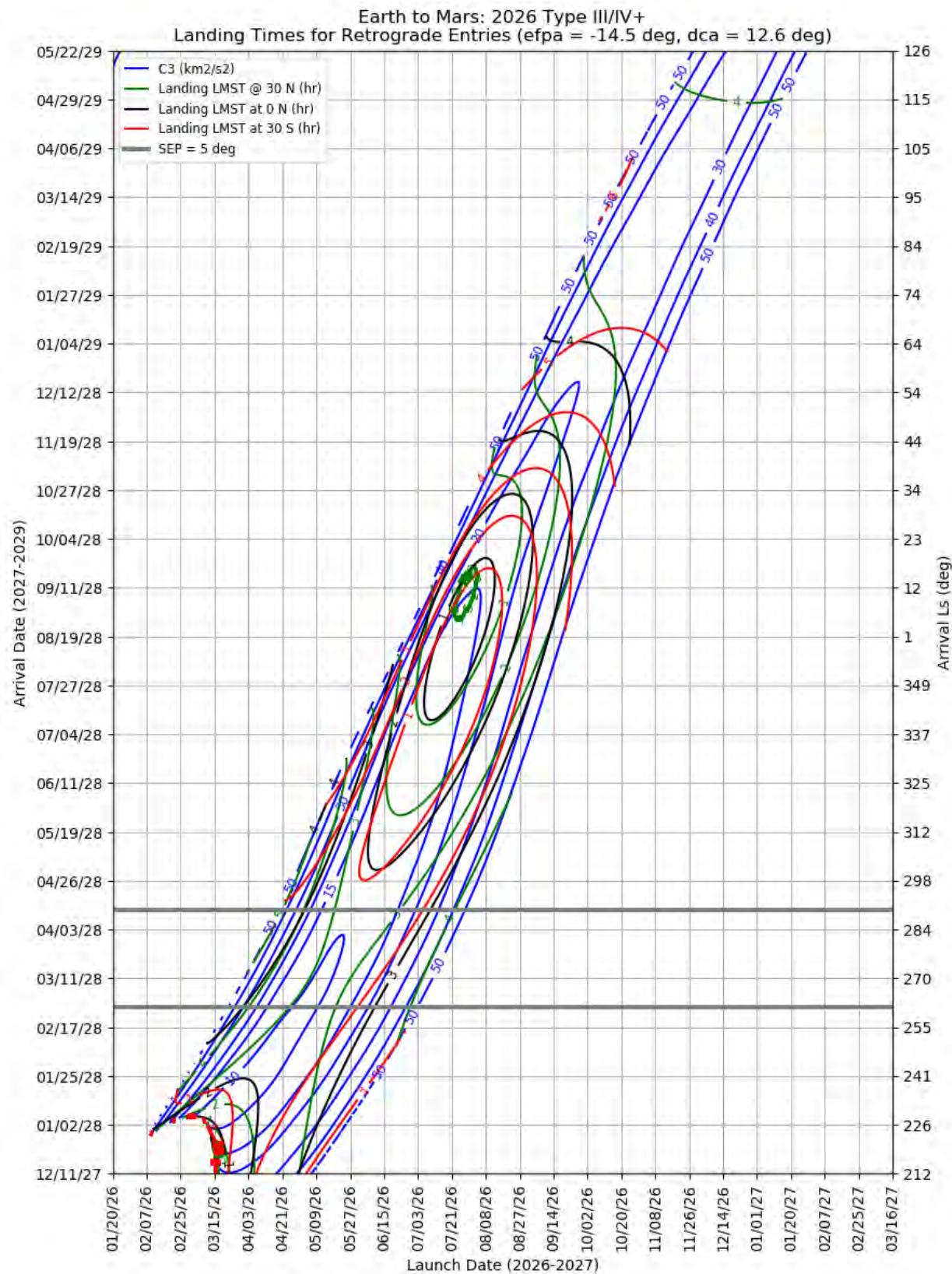


Figure 391: Earth to Mars 2026 Type III/IV+ – Landing LMST for Retrograde Entries

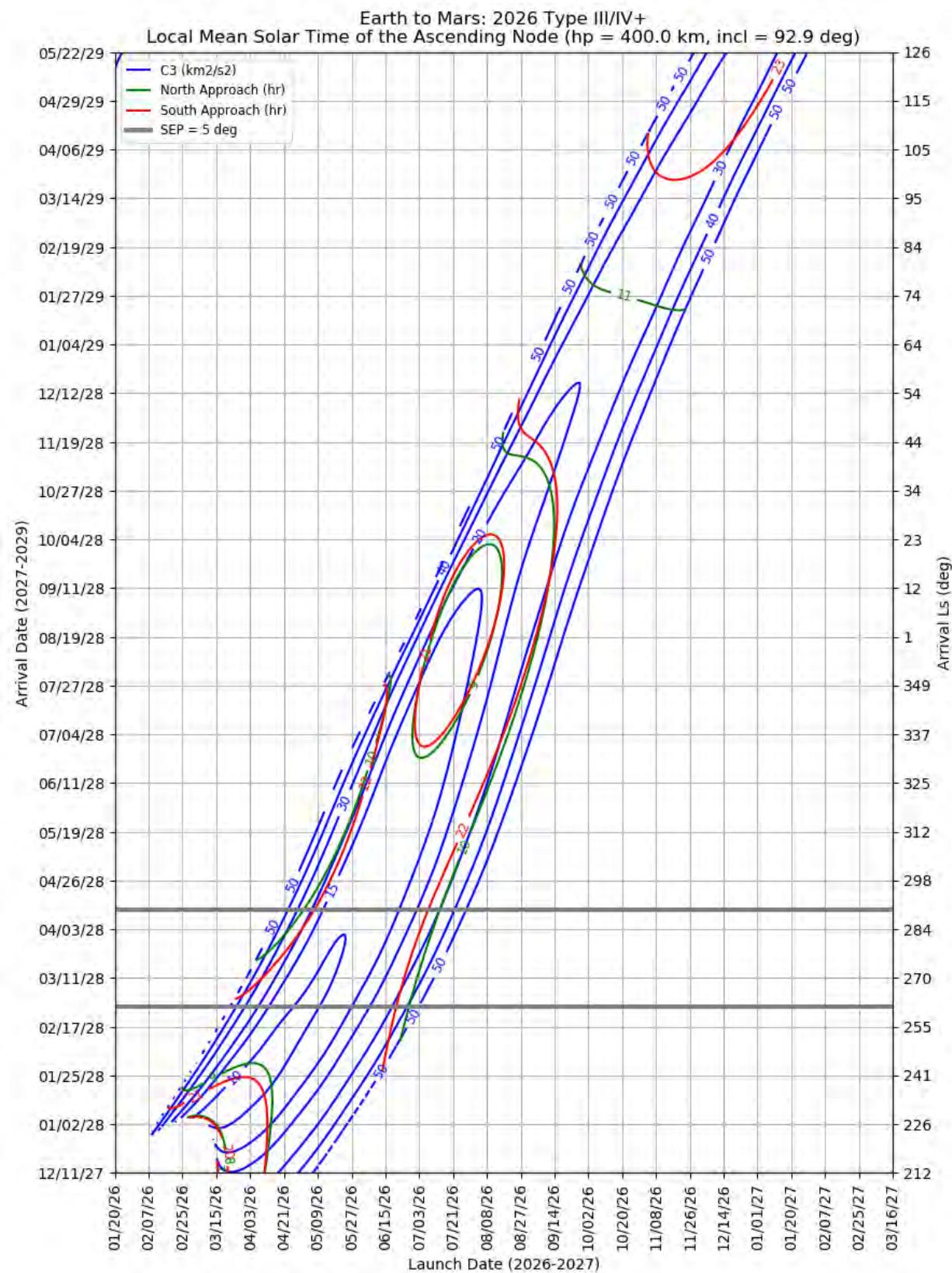


Figure 392: Earth to Mars 2026 Type III/IV+ – LMST of the Ascending Node for North and South Approaches

### 10.5.5 Earth to Mars 2028

This section contains porkchop plots for the Earth-to-Mars 2028 opportunities. Table 31 contains the optimal single-day transfers for minimum launch energy (C3) and arrival velocity (VHP) as well as the maximum launch-mass and captured-mass launch periods for each trajectory type within the opportunity. These data should only be used for preliminary analysis and planning purposes.

**Table 31: Earth to Mars 2028 Optimal Launch/Arrival Data**

Optimization Criteria	Trajectory Type	Departure Date (dd-mmm-yyyy)	Arrival Date (dd-mmm-yyyy)	Launch Energy, C3 (km <sup>2</sup> /s <sup>2</sup> )	Declination of the Launch Asymptote, DLA (deg)	Approach V-Infinity, VHP (km/s)
<b>Single-Day Optimization</b>						
Minimum C3	I	11-Dec-2028	21-Jul-2029	9.0	-4.8	4.85
Minimum C3	II	30-Nov-2028	11-Oct-2029	9.0	29.3	3.17
Minimum C3	III-	24-Sep-2028	08-Dec-2030	20.4	54.0	3.02
Minimum C3	IV-	20-Sep-2028	24-Apr-2031	13.0	18.4	2.95
Minimum C3	III+	15-Oct-2028	27-Dec-2030	18.3	45.1	5.14
Minimum C3	IV+	18-Apr-2028	05-Apr-2030	43.1	17.4	4.62
Minimum VHP	I	16-Jan-2029	04-Sep-2029	23.3	0.4	3.59
Minimum VHP	II	20-Nov-2028	18-Sep-2029	9.3	25.8	2.97
Minimum VHP	III-	03-Oct-2028	09-Dec-2030	31.4	35.1	2.32
Minimum VHP	IV-	26-Jul-2028	19-Dec-2030	26.3	5.1	2.38
Minimum VHP	III+	04-Oct-2028	21-Nov-2030	31.2	32.6	2.46
Minimum VHP	IV+	30-Apr-2028	01-May-2030	44.2	6.1	3.98
<b>Launch Period Optimization</b>						
Maximum Launch Mass	I	30-Nov-2028	15-Jul-2029	10.0	-11.3	5.13
		20-Dec-2028		10.2	4.1	5.18
Maximum Launch Mass	II	12-Dec-2028	05-Dec-2029	10.0	15.2	4.71
		01-Jan-2029		10.2	28.9	4.69
Maximum Launch Mass	III-	14-Sep-2028	09-Dec-2030	27.8	72.5	3.62
		04-Oct-2028		33.4	33.7	2.34
Maximum Launch Mass	IV-	12-Sep-2028	29-Apr-2031	14.2	20.1	3.05
		02-Oct-2028		14.4	18.5	3.06
Maximum Launch Mass	III+	01-Nov-2028	03-Feb-2031	21.3	29.3	7.41
		21-Nov-2028		21.5	30.3	7.38
Maximum Launch Mass	IV+	Not Possible				
Maximum Captured Mass	I	09-Dec-2028	01-Aug-2029	10.8	-21.9	4.56
		29-Dec-2028		12.8	3.4	4.34
Maximum Captured Mass	II	12-Nov-2028	23-Sep-2029	10.6	19.0	3.01

Optimization Criteria	Trajectory Type	Departure Date (dd-mmm-yyyy)	Arrival Date (dd-mmm-yyyy)	Launch Energy, C3 (km <sup>2</sup> /s <sup>2</sup> )	Declination of the Launch Asymptote, DLA (deg)	Approach V-Infinity, VHP (km/s)
		02-Dec-2028		9.6	37.2	3.02
Maximum Captured Mass	III-	15-Sep-2028	11-Dec-2030	27.5	71.2	3.42
		05-Oct-2028		35.2	32.8	2.36
Maximum Captured Mass	IV-	04-Sep-2028	26-Mar-2031	14.6	13.5	2.69
		24-Sep-2028		14.8	5.5	2.81
Maximum Captured Mass	III+	26-Sep-2028	07-Dec-2030	20.1	51.4	3.06
		16-Oct-2028		22.7	39.9	4.08
Maximum Captured Mass	IV+			Not Possible		

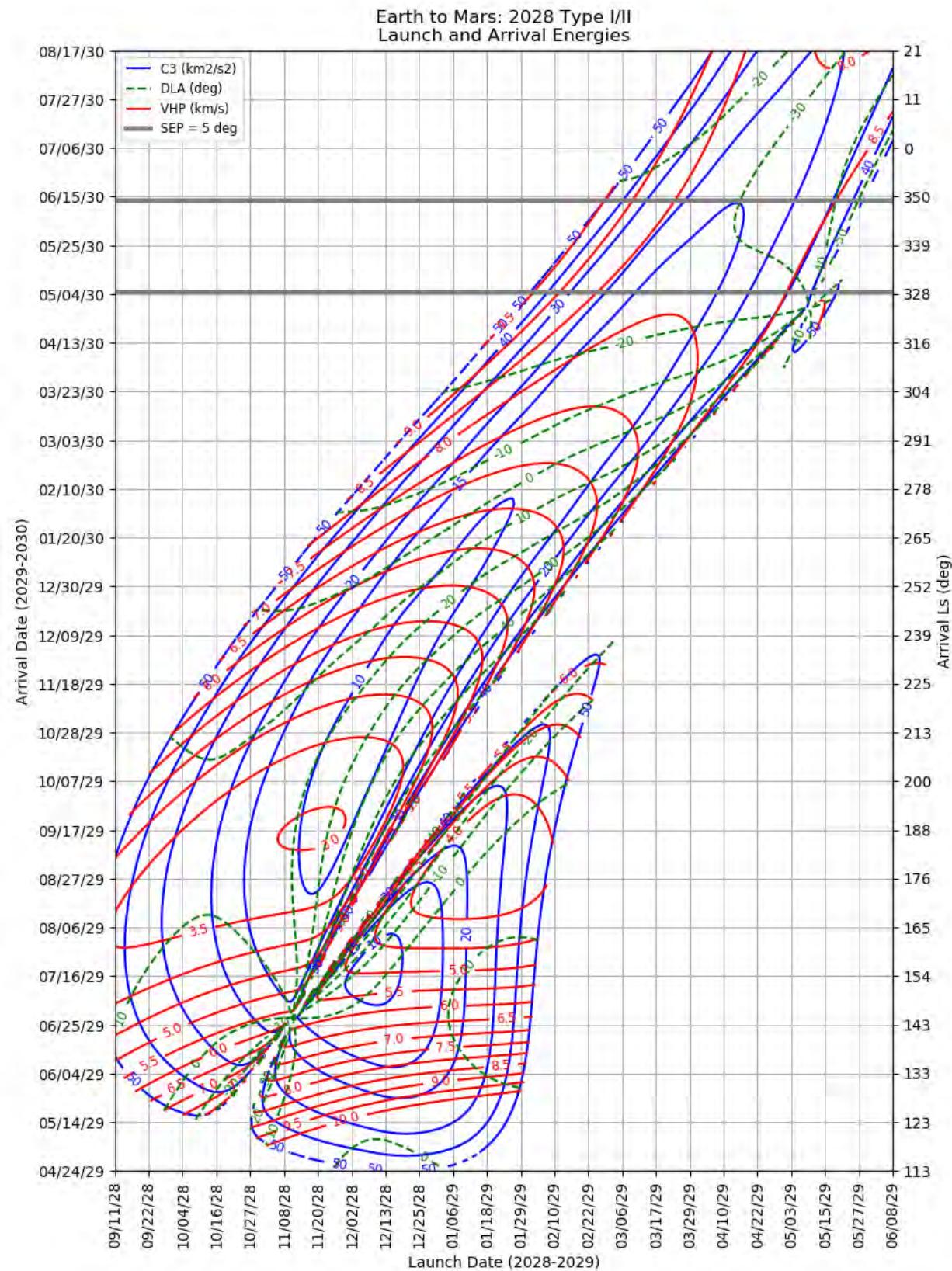


**Figure 393: Earth to Mars 2028 Type I/II - Launch and Arrival Energy**

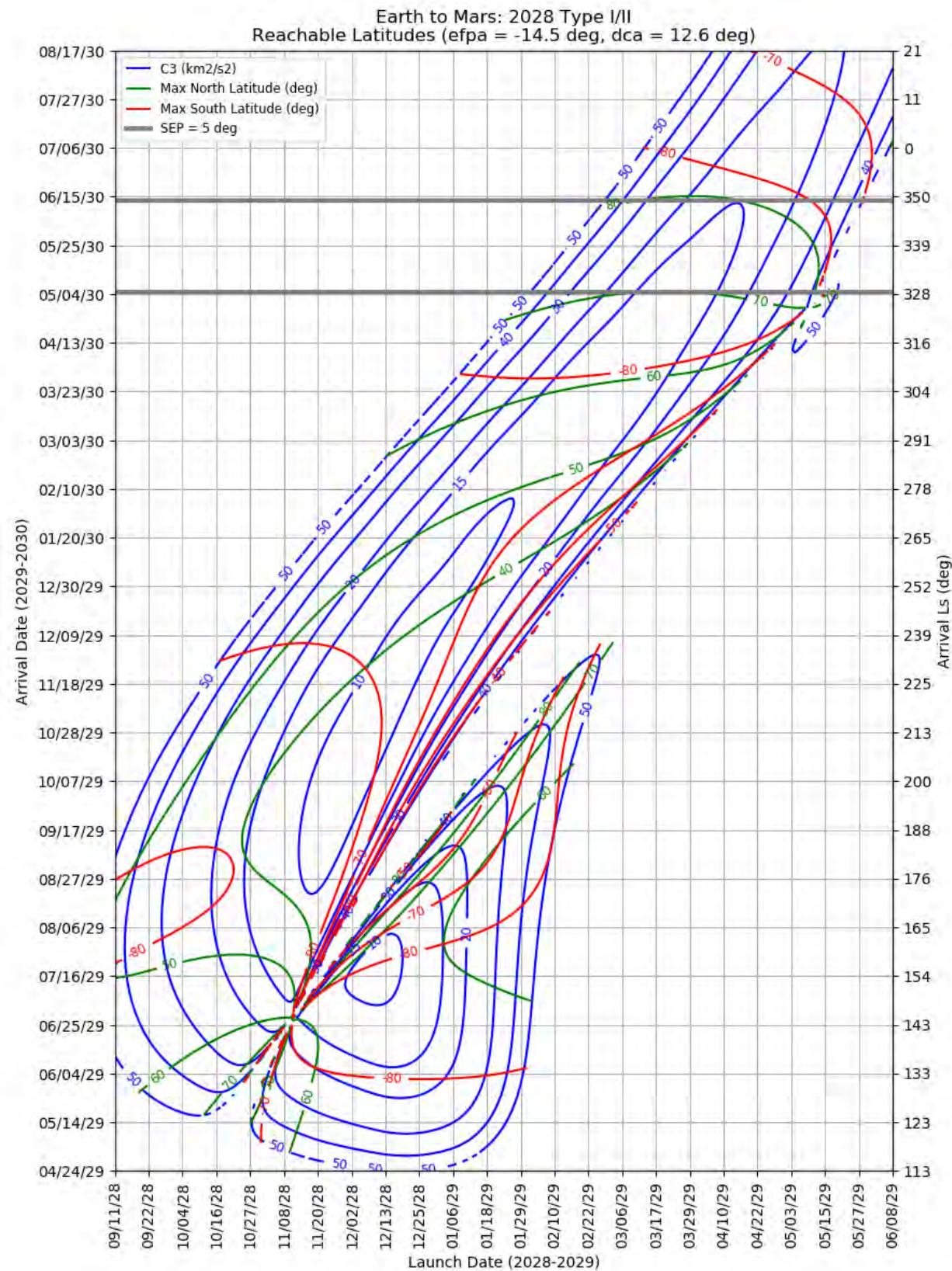


**Figure 394: Earth to Mars 2028 Type I/II – Maximum Reachable North and South Latitude**

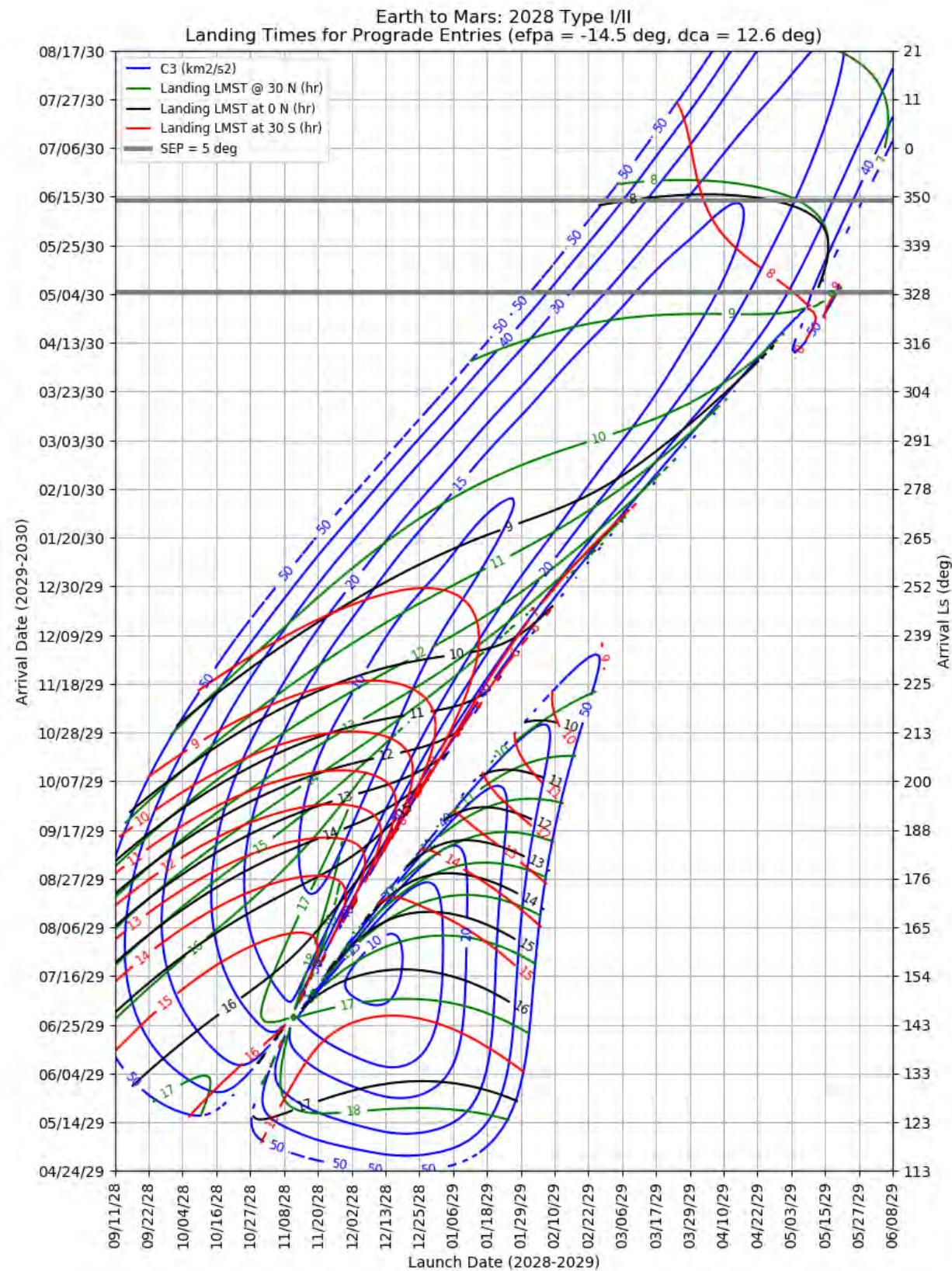
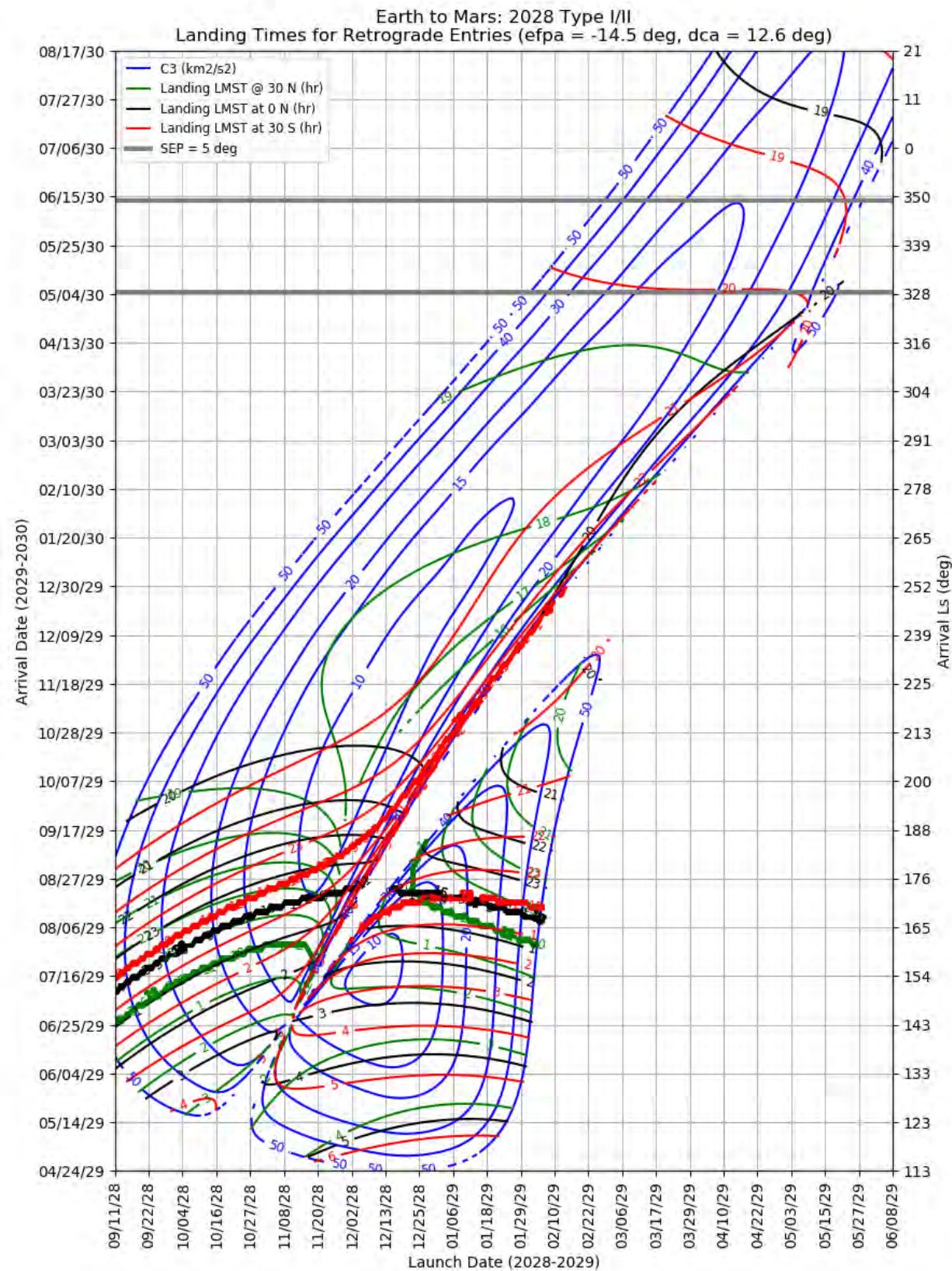


Figure 395: Earth to Mars 2028 Type I/II – Landing LMST for Prograde Entries



**Figure 396: Earth to Mars 2028 Type I/II – Landing LMST for Retrograde Entries**

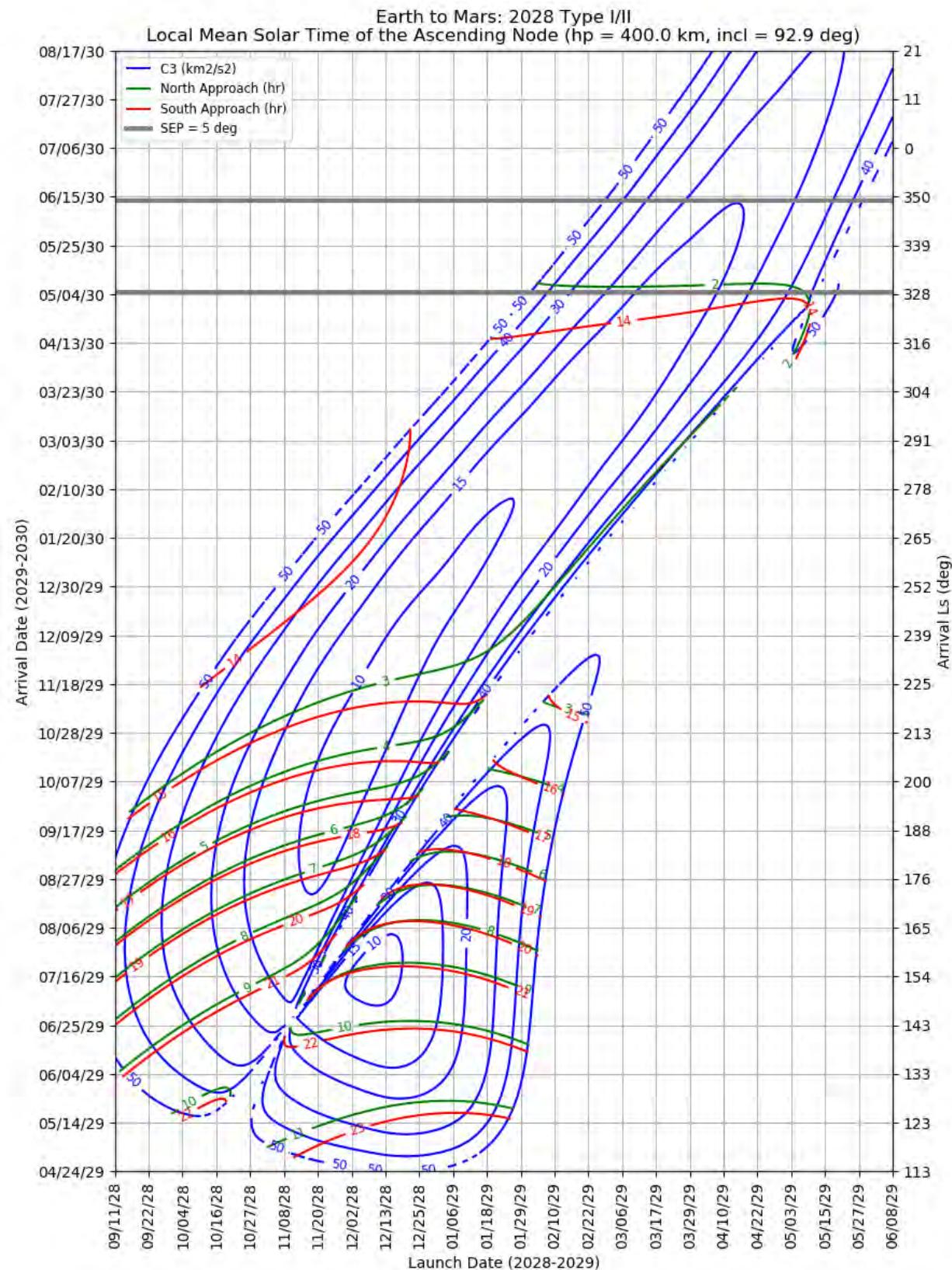


Figure 397: Earth to Mars 2028 Type I/II – LMST of the Ascending Node for North and South Approaches

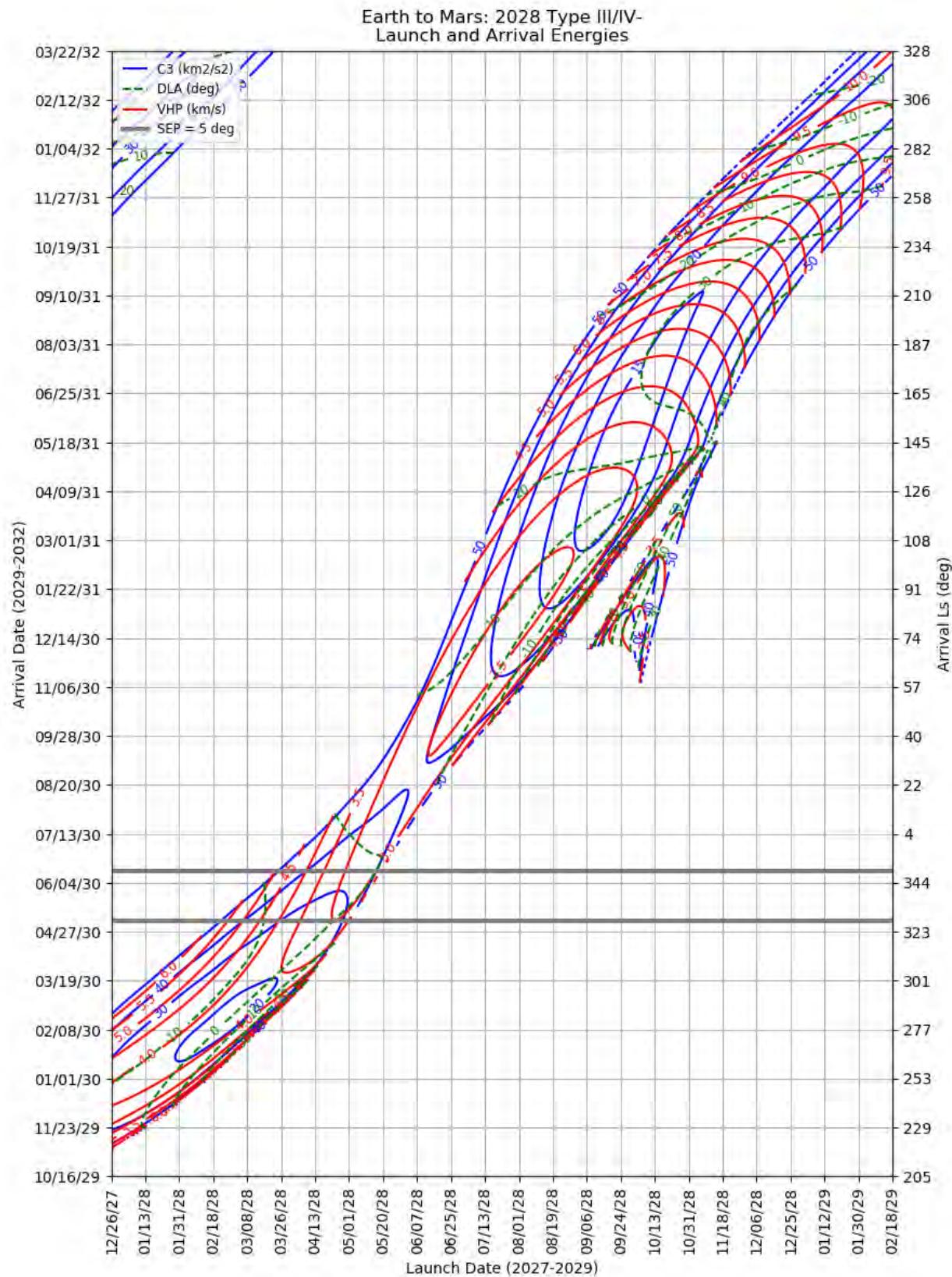
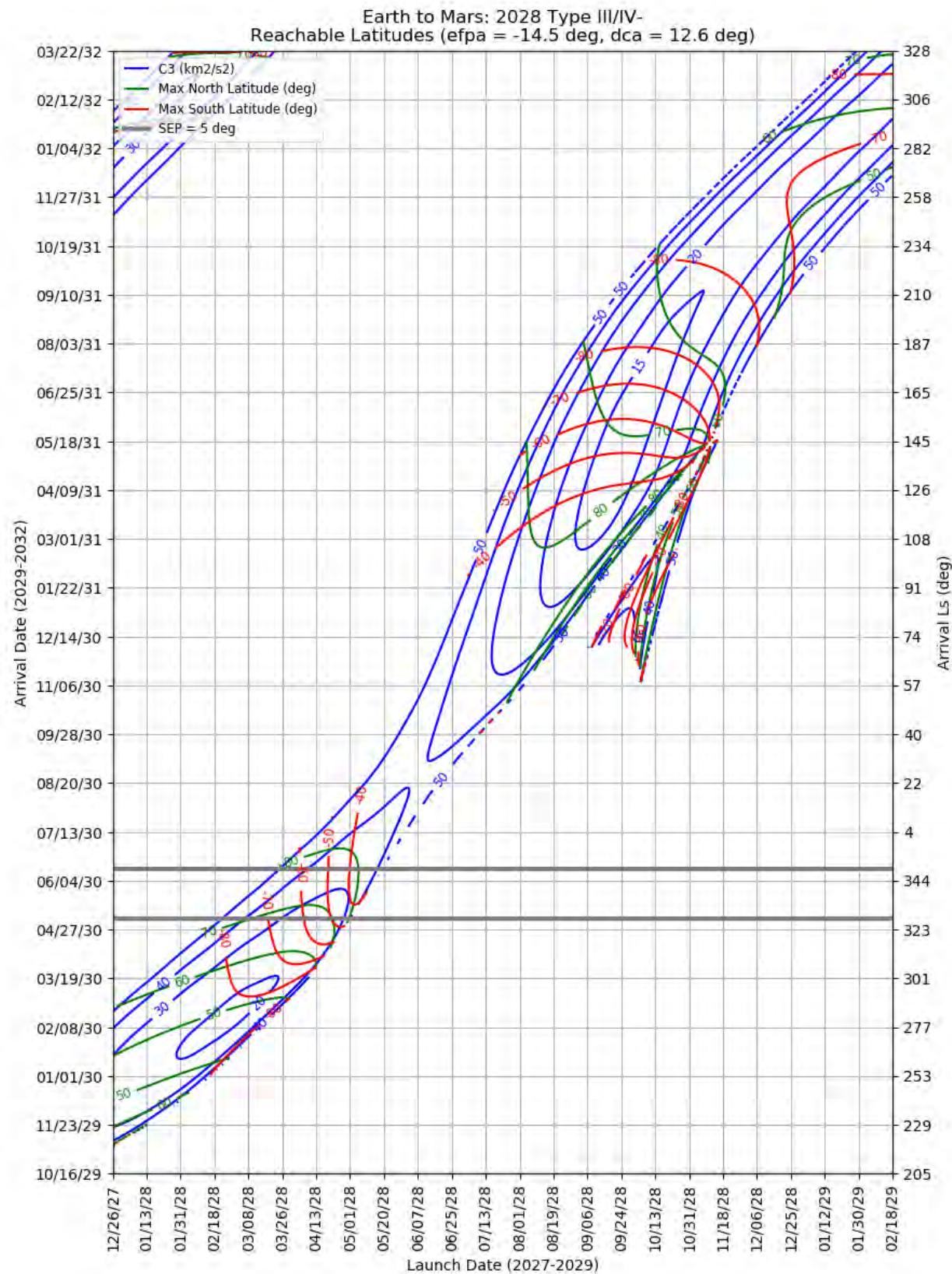


Figure 398: Earth to Mars 2028 Type III/IV- – Launch and Arrival Energy



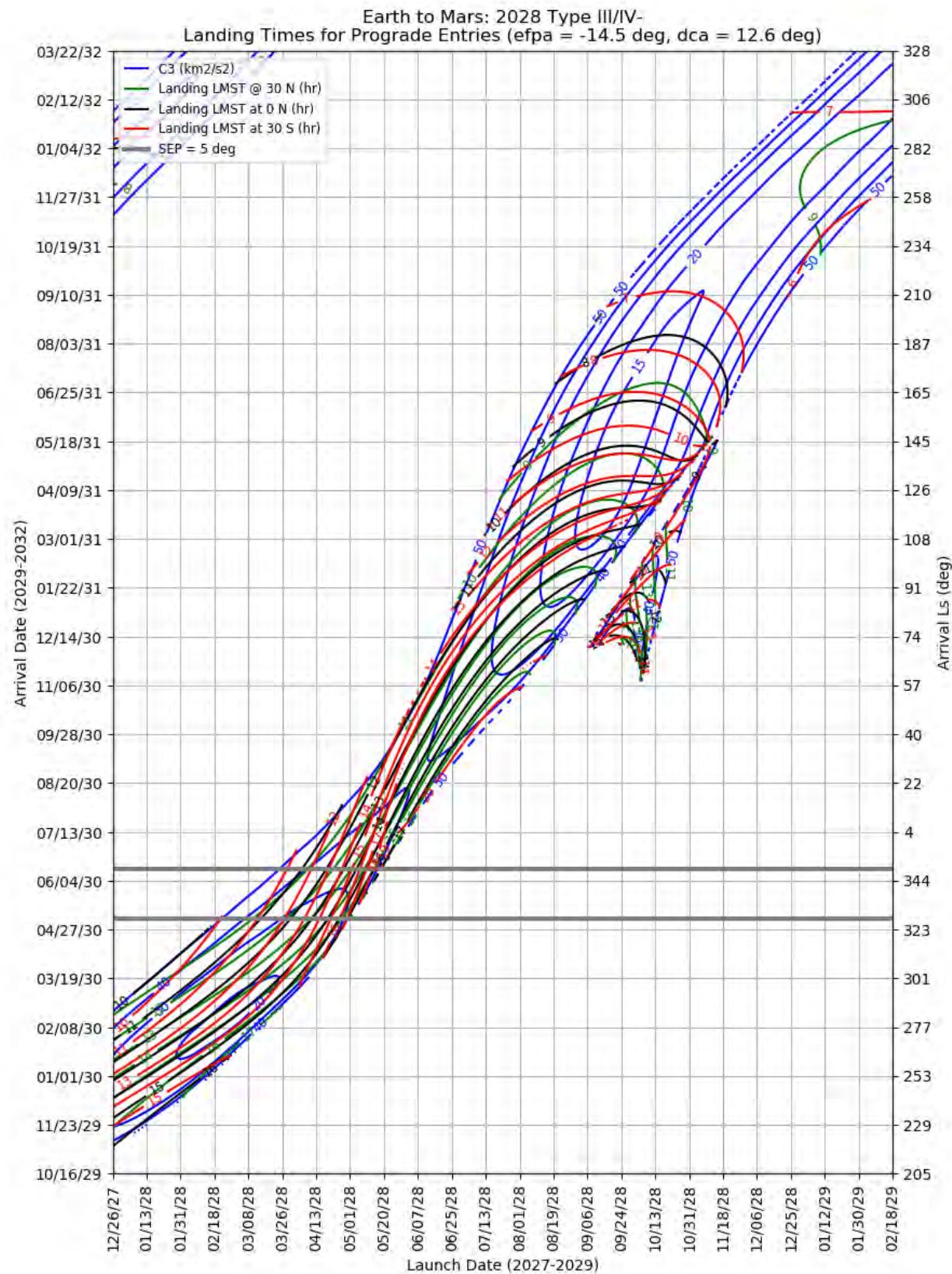
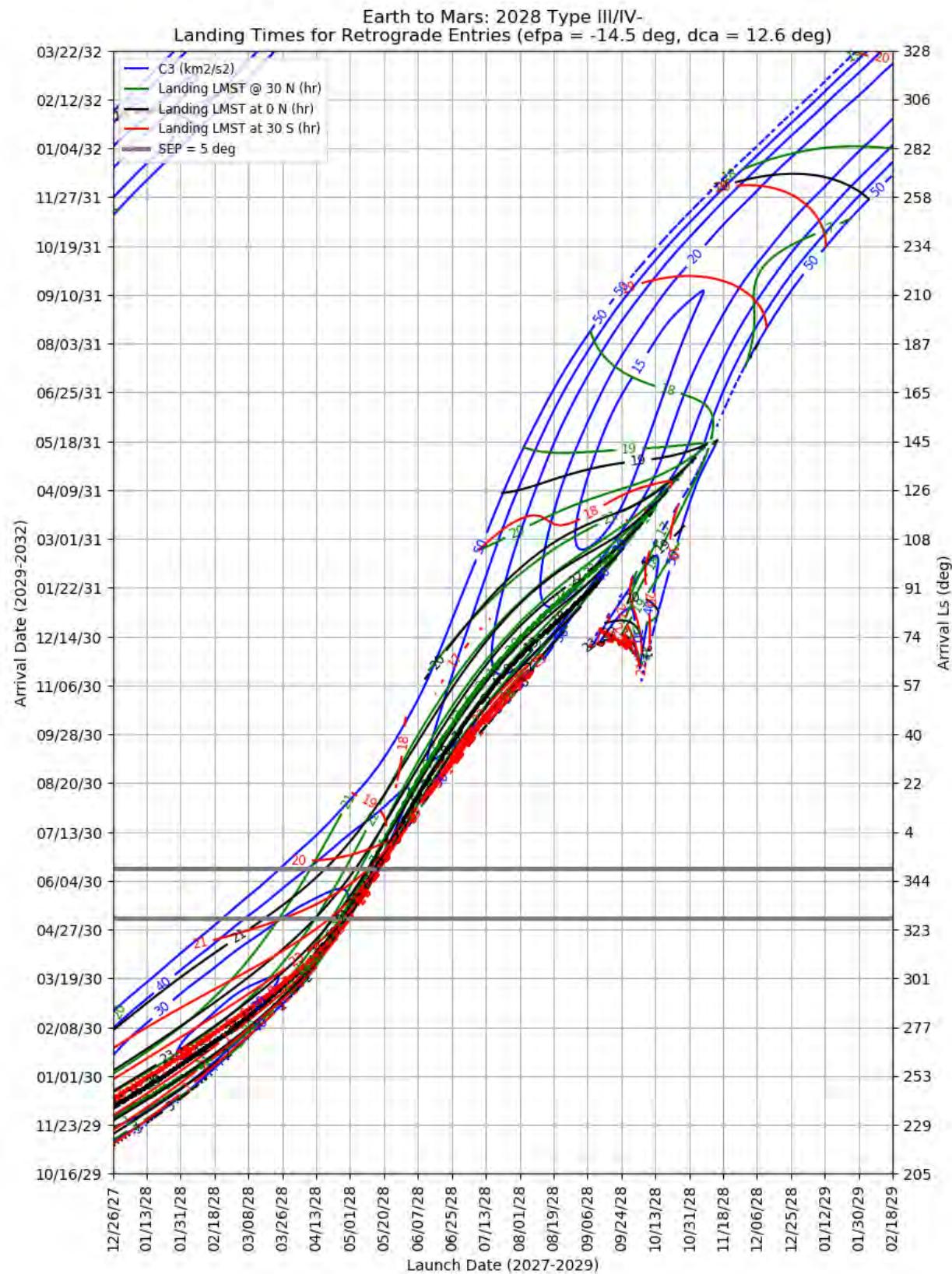


Figure 400: Earth to Mars 2028 Type III/IV- – Landing LMST for Prograde Entries



**Figure 401: Earth to Mars 2028 Type III/IV- – Landing LMST for Retrograde Entries**

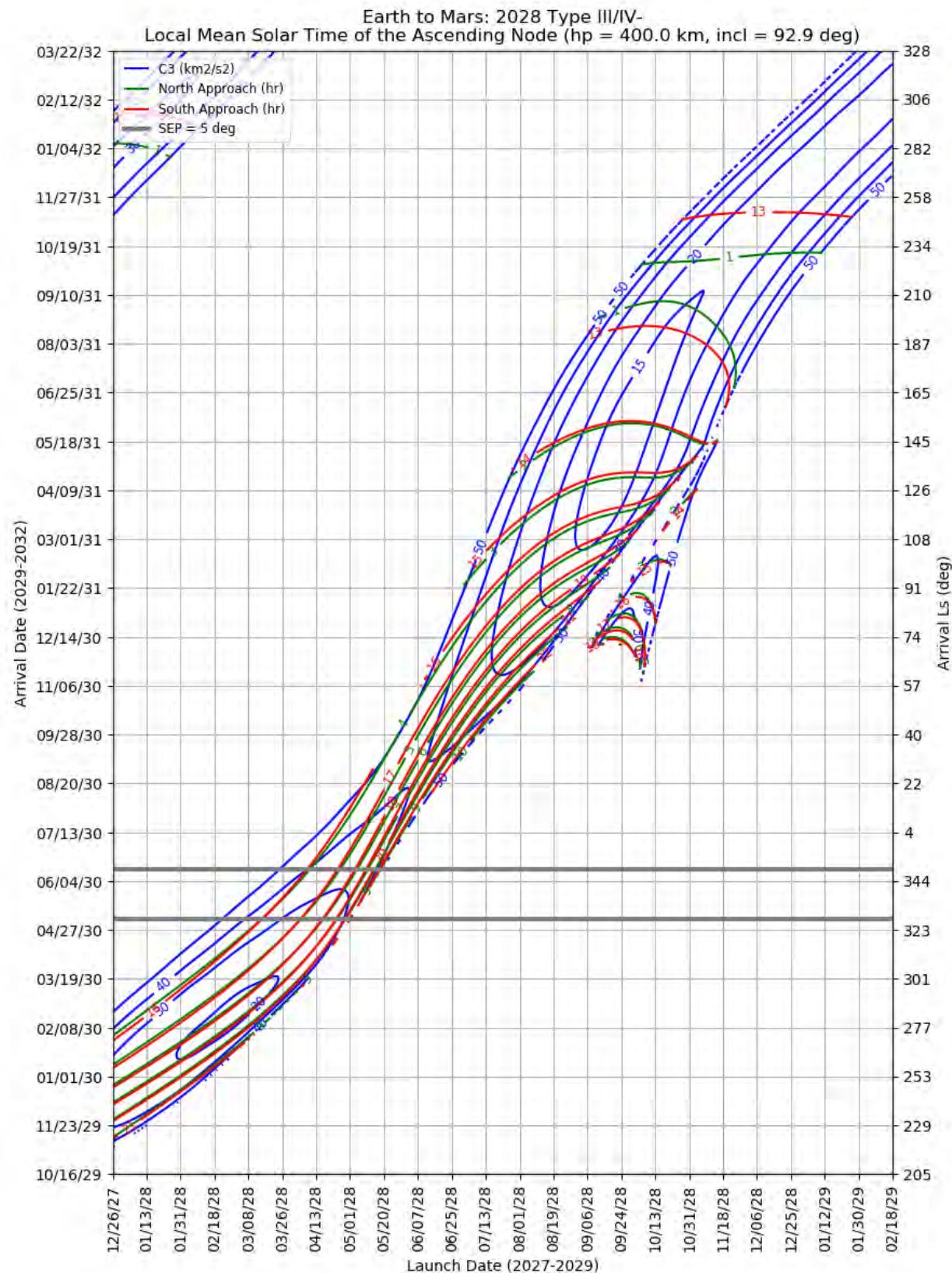


Figure 402: Earth to Mars 2028 Type III/IV- – LMST of the Ascending Node for North and South Approaches

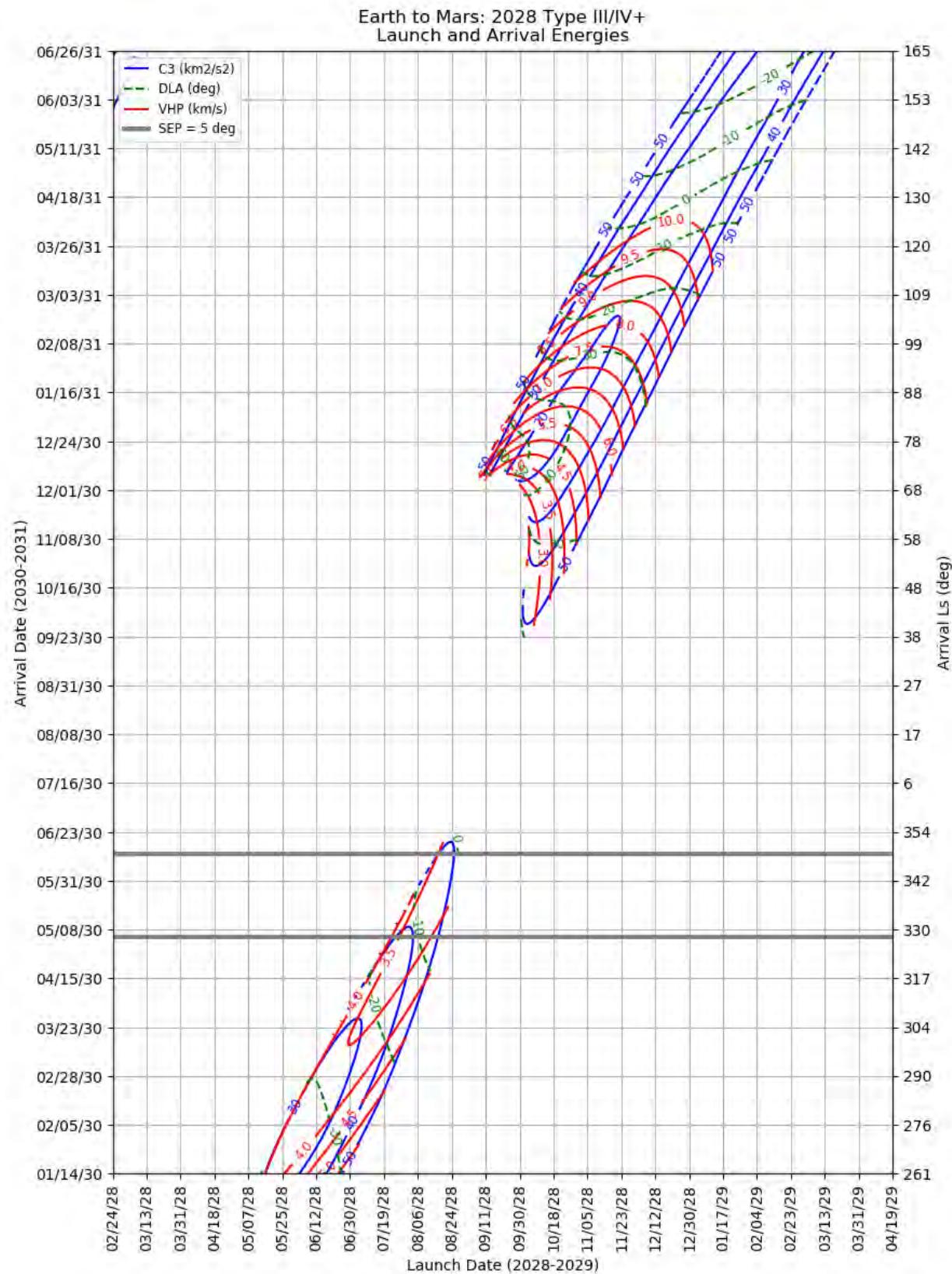
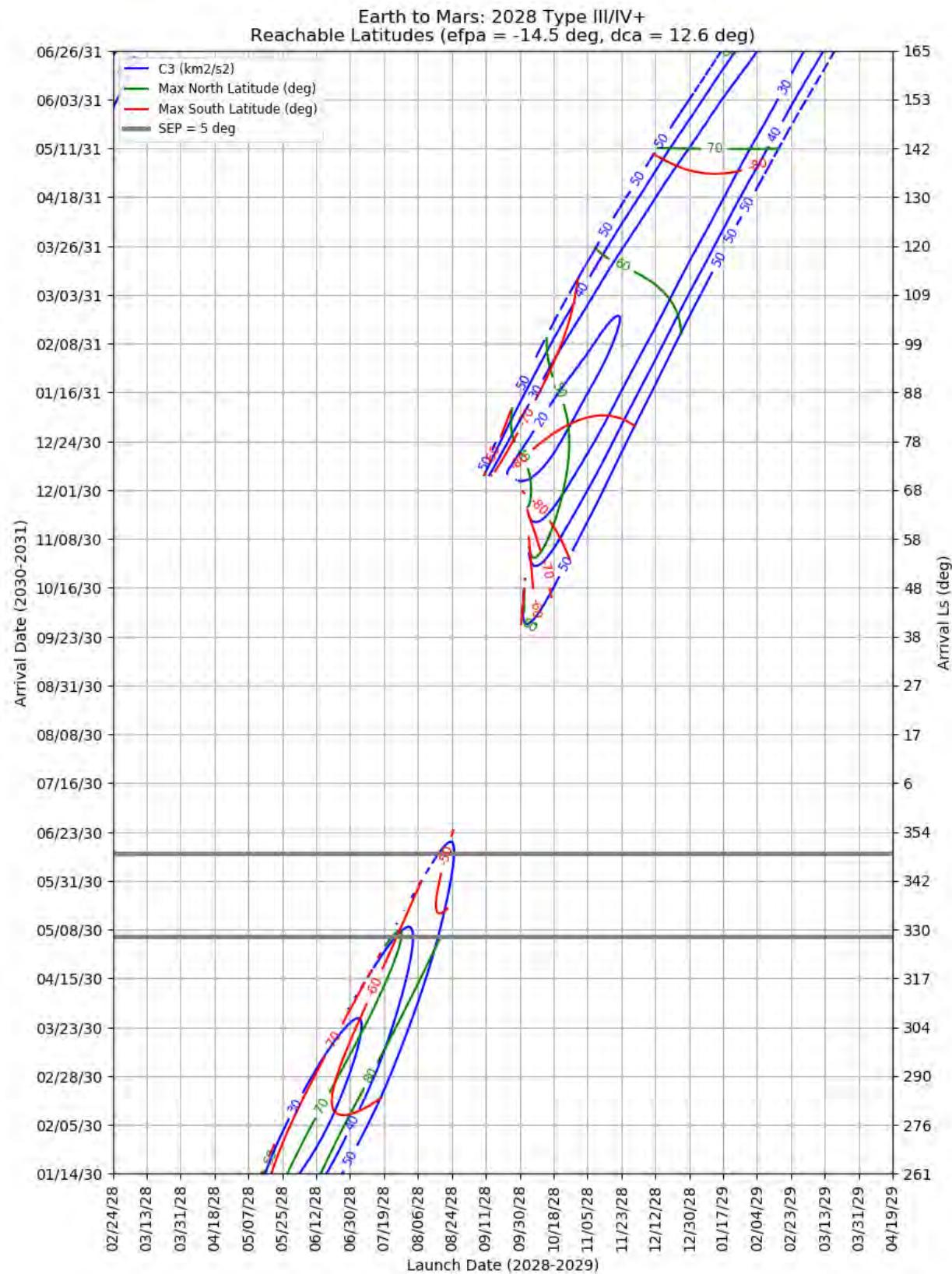
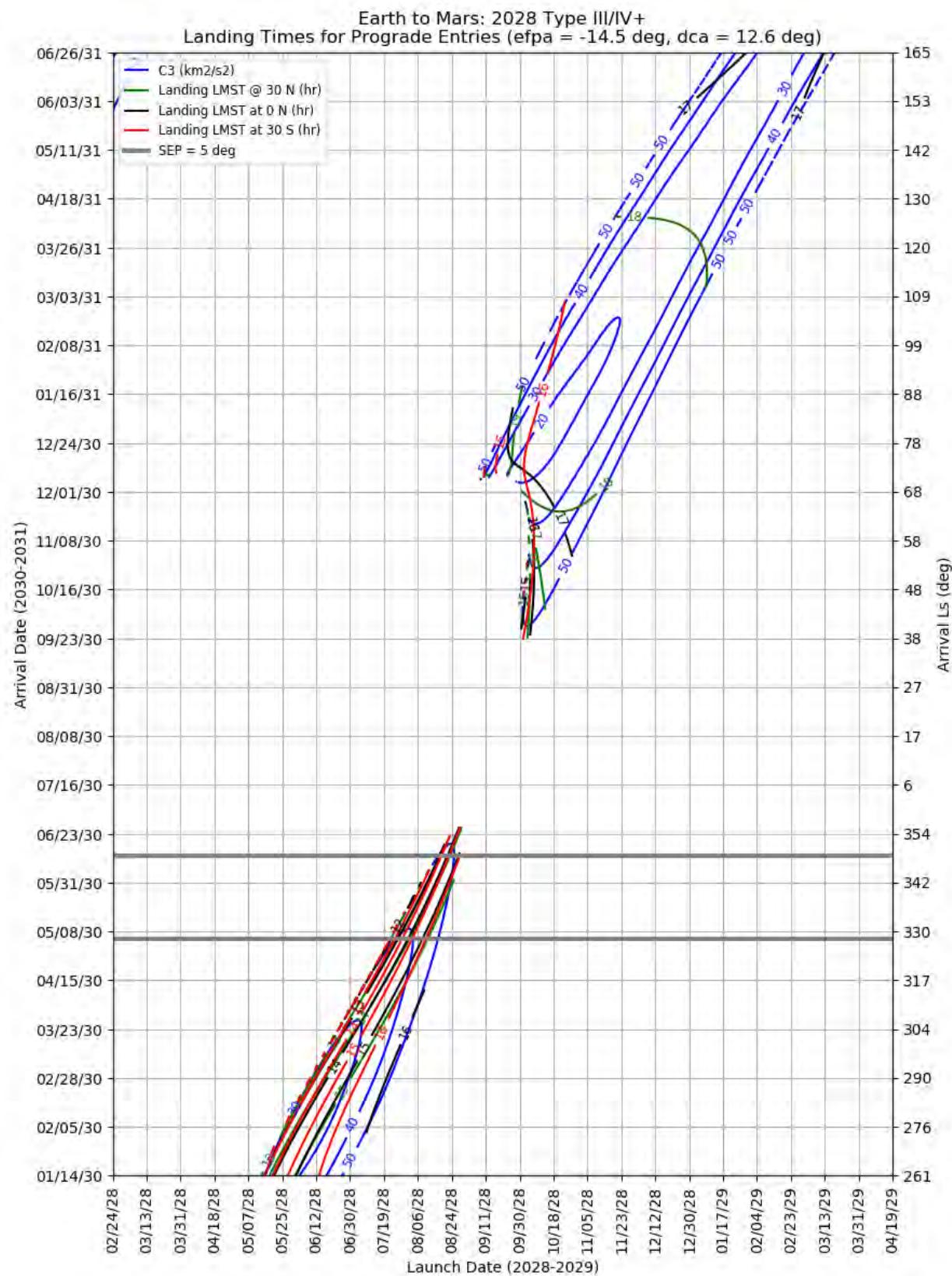


Figure 403: Earth to Mars 2028 Type III/IV+ – Launch and Arrival Energy



**Figure 404: Earth to Mars 2028 Type III/IV+ – Maximum Reachable North and South Latitude**



**Figure 405: Earth to Mars 2028 Type III/IV+ – Landing LMST for Prograde Entries**

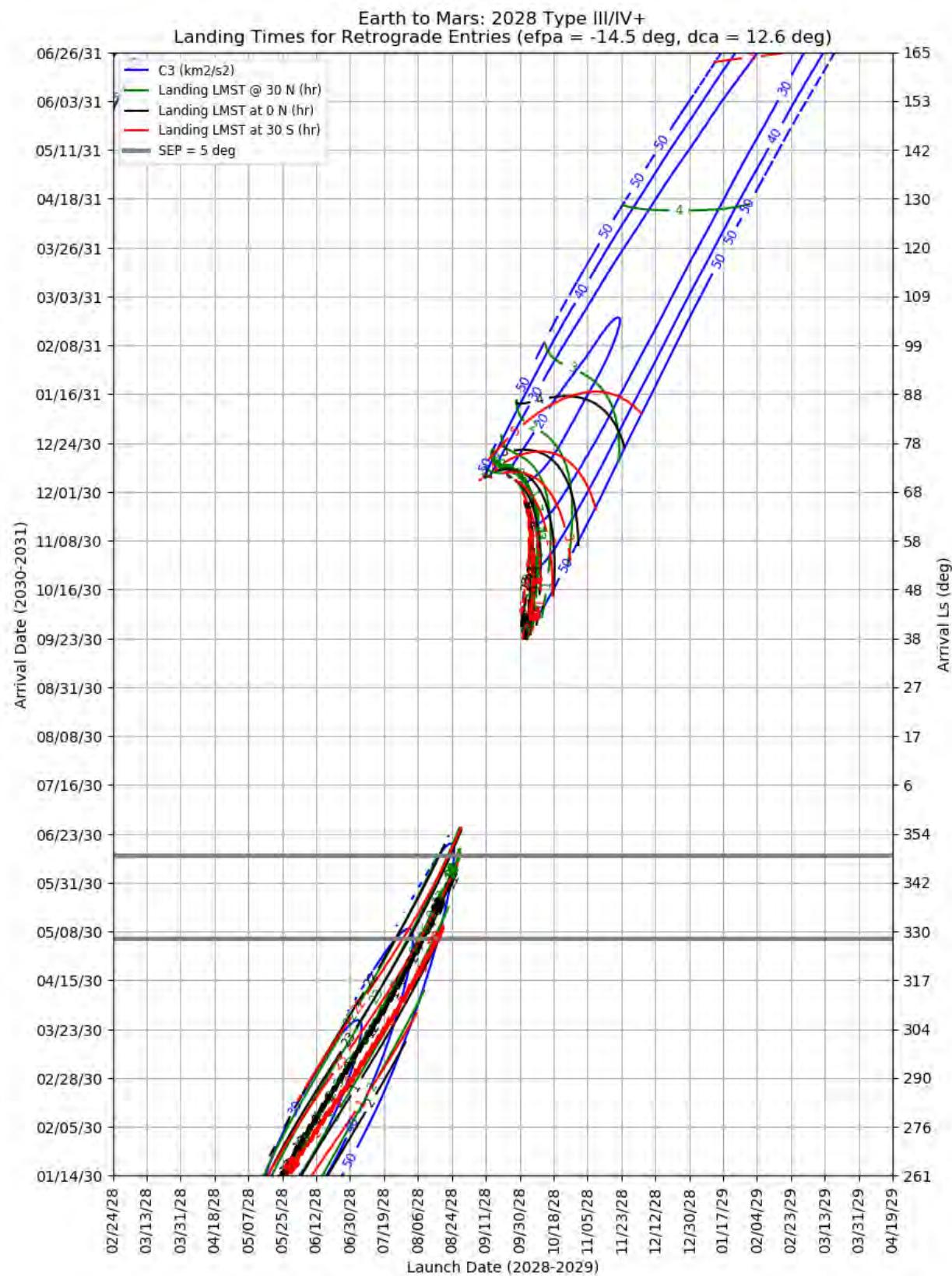


Figure 406: Earth to Mars 2028 Type III/IV+ – Landing LMST for Retrograde Entries

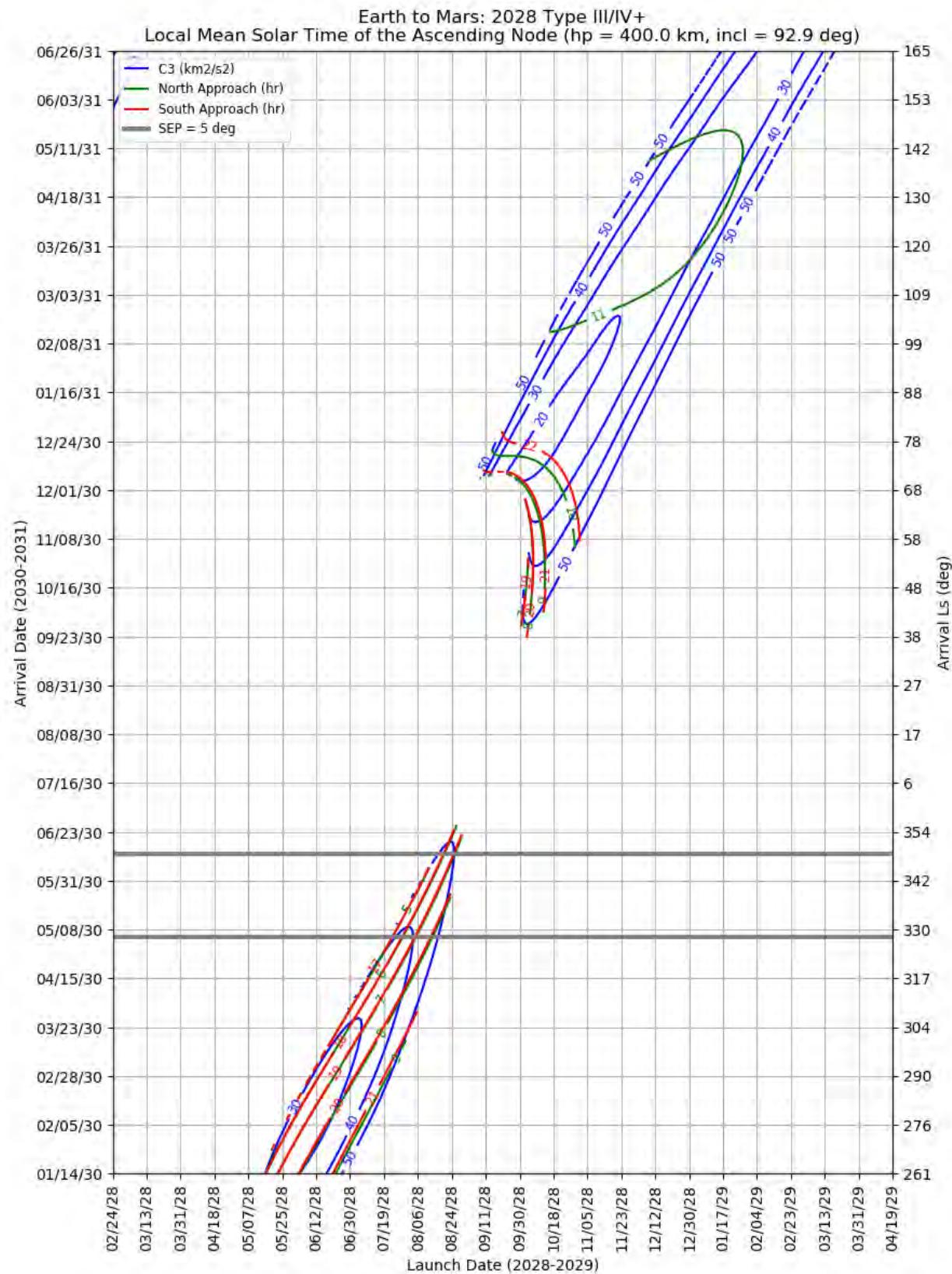


Figure 407: Earth to Mars 2028 Type III/IV+ – LMST of the Ascending Node for North and South Approaches

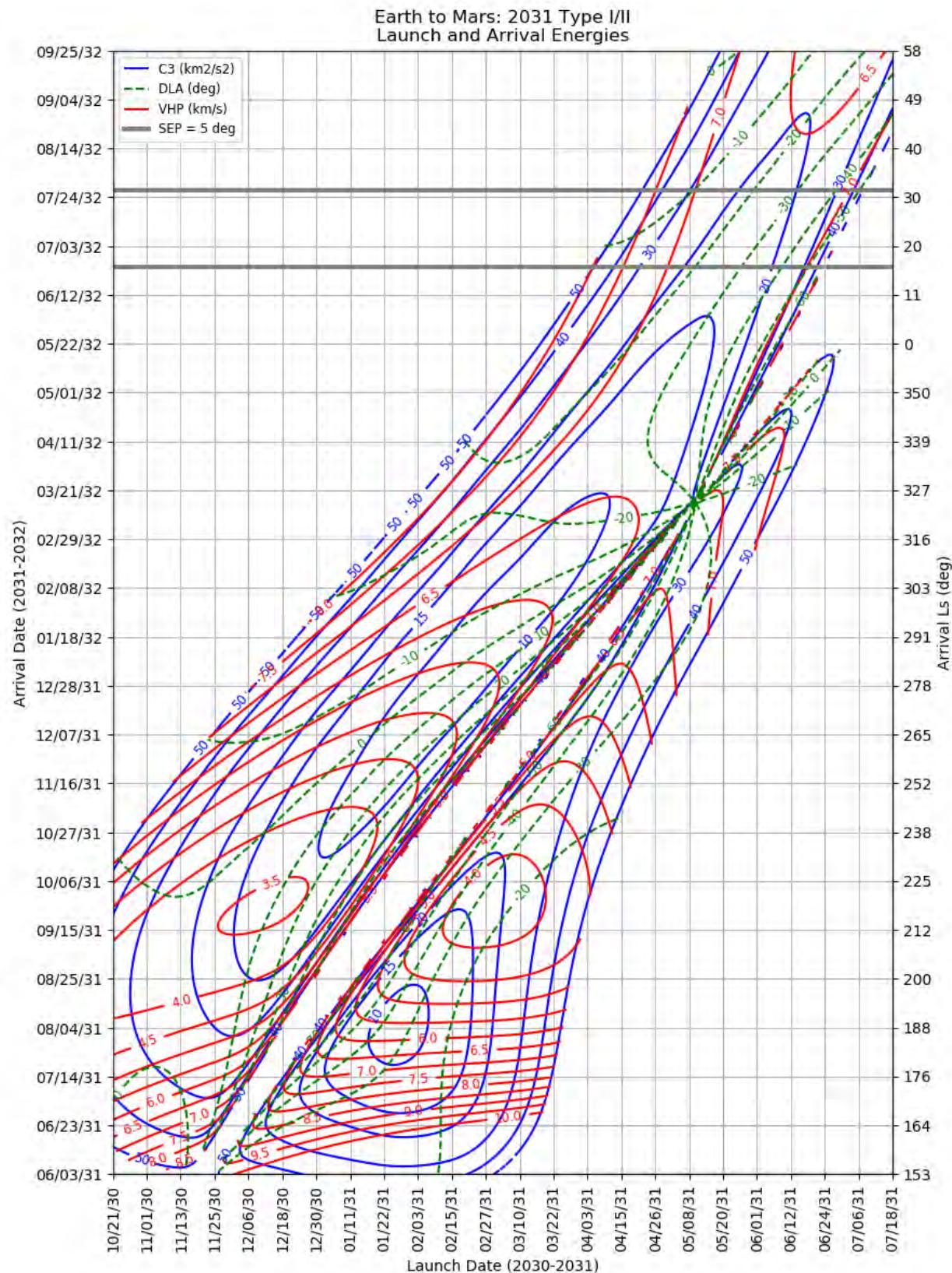
### 10.5.6 Earth to Mars 2031

This section contains porkchop plots for the Earth-to-Mars 2031 opportunities. Table 32 contains the optimal single-day transfers for minimum launch energy (C3) and arrival velocity (VHP) as well as the maximum launch-mass and captured-mass launch periods for each trajectory type within the opportunity. These data should only be used for preliminary analysis and planning purposes.

**Table 32: Earth to Mars 2031 Optimal Launch/Arrival Data**

Optimization Criteria	Trajectory Type	Departure Date (dd-mmm-yyyy)	Arrival Date (dd-mmm-yyyy)	Launch Energy, C3 (km <sup>2</sup> /s <sup>2</sup> )	Declination of the Launch Asymptote, DLA (deg)	Approach V-Infinity, VHP (km/s)
<b>Single-Day Optimization</b>						
Minimum C3	I	27-Jan-2031	05-Aug-2031	9.0	-34.6	5.61
Minimum C3	II	23-Feb-2031	09-Jan-2032	8.2	1.2	5.53
Minimum C3	III-	19-Oct-2030	23-Dec-2032	17.2	52.2	3.77
Minimum C3	IV-	02-Oct-2030	22-Mar-2033	11.4	19.9	2.58
Minimum C3	III+	29-Oct-2030	28-Dec-2032	15.9	42.2	5.12
Minimum C3	IV+	27-Aug-2030	20-Nov-2032	60.0	-9.7	6.36
Minimum VHP	I	01-Mar-2031	26-Sep-2031	17.9	-24.7	3.78
Minimum VHP	II	14-Dec-2030	26-Sep-2031	12.4	8.9	3.45
Minimum VHP	III-	28-Oct-2030	16-Jan-2033	28.4	41.0	2.37
Minimum VHP	IV-	08-Sep-2030	08-Feb-2033	15.5	11.7	2.40
Minimum VHP	III+	06-Nov-2030	25-Nov-2032	48.1	30.5	2.84
Minimum VHP	IV+	13-Apr-2030	28-Mar-2032	101.6	4.7	5.62
<b>Launch Period Optimization</b>						
Maximum Launch Mass	I	21-Jan-2031	29-Jul-2031	9.5	-36.3	6.07
		10-Feb-2031		10.9	-22.1	6.16
Maximum Launch Mass	II	22-Feb-2031	23-Jan-2032	9.0	-8.7	5.86
		14-Mar-2031		9.2	2.2	5.85
Maximum Launch Mass	III-	10-Oct-2030	24-Dec-2032	22.3	66.6	3.87
		30-Oct-2030		30.3	36.6	2.55
Maximum Launch Mass	IV-	25-Sep-2030	02-Apr-2033	12.4	21.9	2.74
		15-Oct-2030		12.6	23.2	2.73
Maximum Launch Mass	III+	06-Nov-2030	14-Jan-2033	17.9	28.7	6.75
		26-Nov-2030		18.3	28.7	6.73
Maximum Launch Mass	IV+	Not Possible				
Maximum Captured Mass	I	02-Feb-2031	02-Sep-2031	11.8	-43.6	4.39
		22-Feb-2031		14.7	-21.1	4.17
Maximum Captured Mass	II	21-Dec-2030	13-Oct-2031	11.3	8.3	3.57

Optimization Criteria	Trajectory Type	Departure Date (dd-mmm-yyyy)	Arrival Date (dd-mmm-yyyy)	Launch Energy, C3 (km <sup>2</sup> /s <sup>2</sup> )	Declination of the Launch Asymptote, DLA (deg)	Approach V-Infinity, VHP (km/s)	
		10-Jan-2031		11.4	29.1	3.72	
Maximum Captured Mass	III-	10-Oct-2030	26-Dec-2032	23.3	68.9	3.65	
		30-Oct-2030		30.6	36.6	2.51	
Maximum Captured Mass	IV-	21-Sep-2030	11-Mar-2033	12.6	17.4	2.51	
		11-Oct-2030		12.8	14.2	2.57	
Maximum Captured Mass	III+	20-Oct-2030	23-Dec-2032	16.7	50.9	4.08	
		09-Nov-2030		19.6	37.7	4.93	
Maximum Captured Mass	IV+			Not Possible			



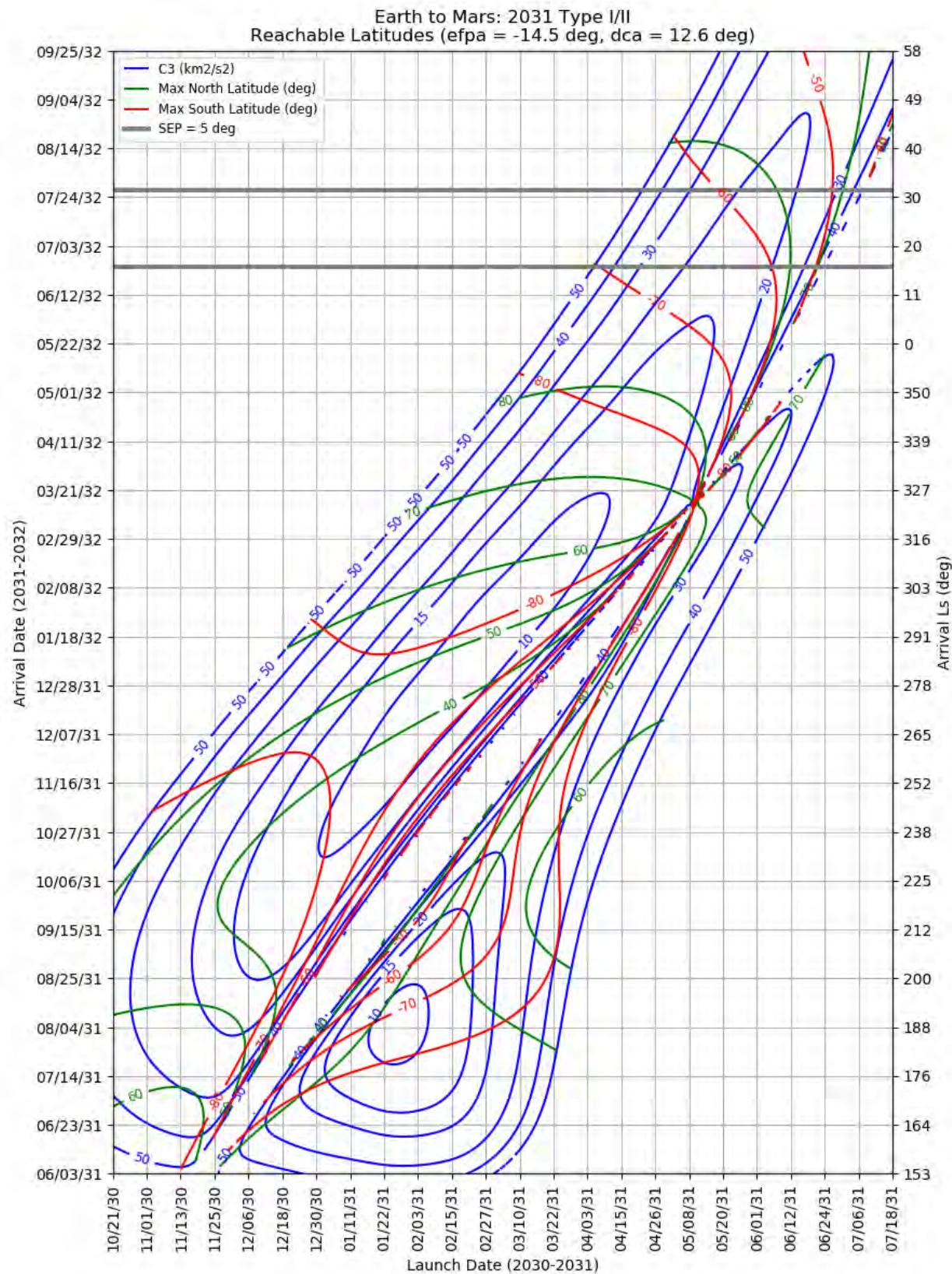


**Figure 409: Earth to Mars 2031 Type I/II – Maximum Reachable North and South Latitude**

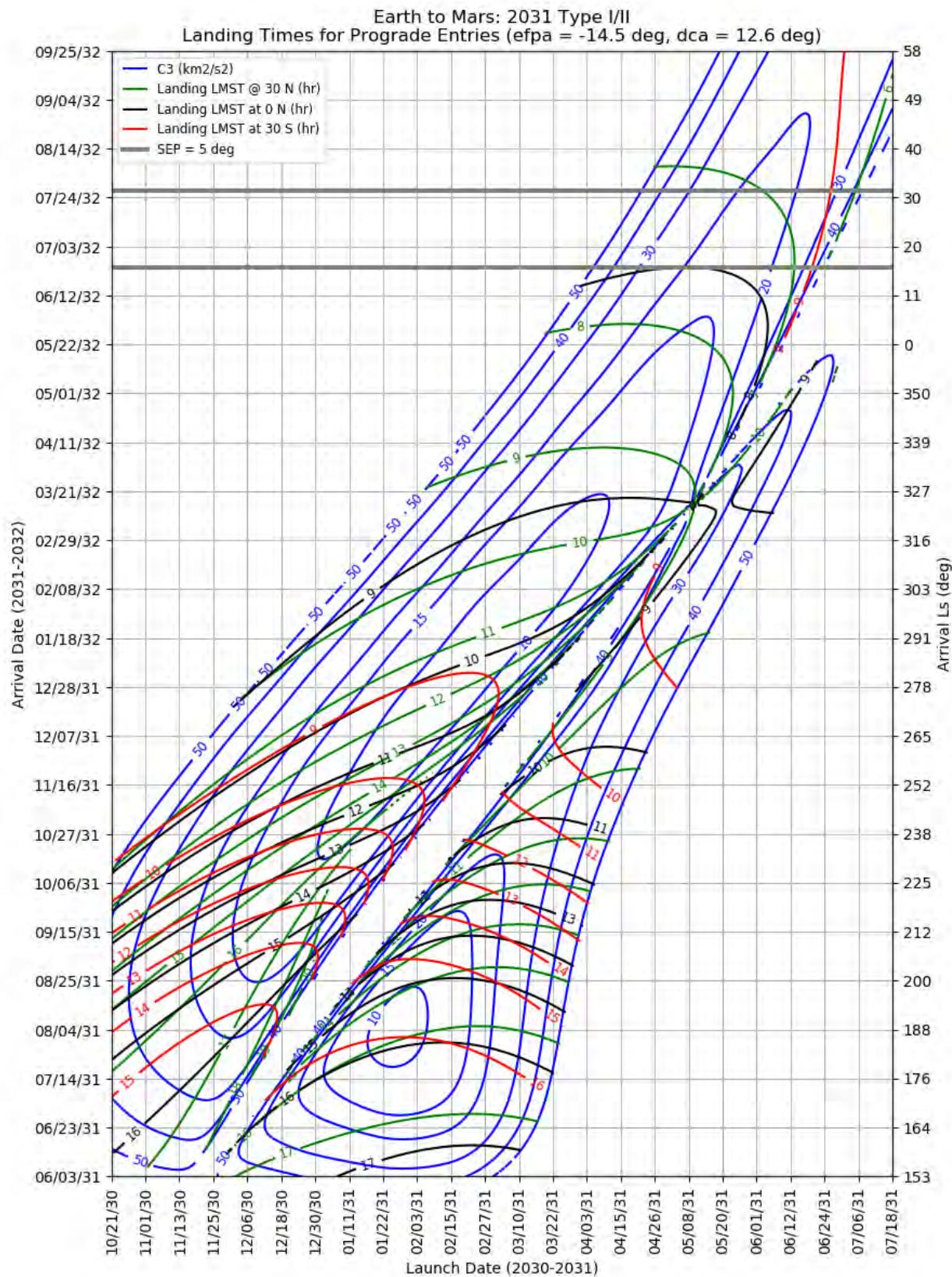


**Figure 410: Earth to Mars 2031 Type I/II – Landing LMST for Prograde Entries**

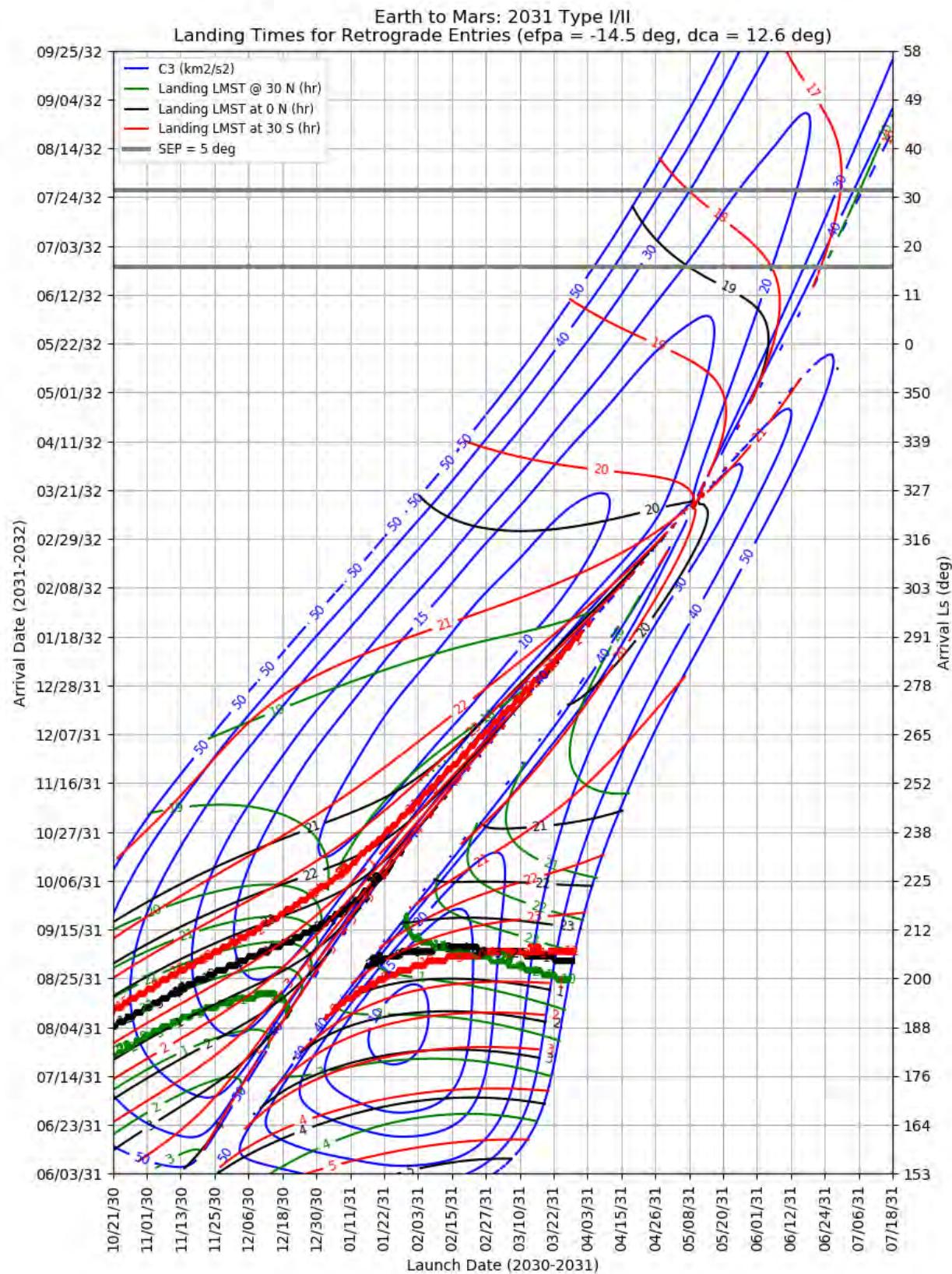


**Figure 411: Earth to Mars 2031 Type I/II – Landing LMST for Retrograde Entries**

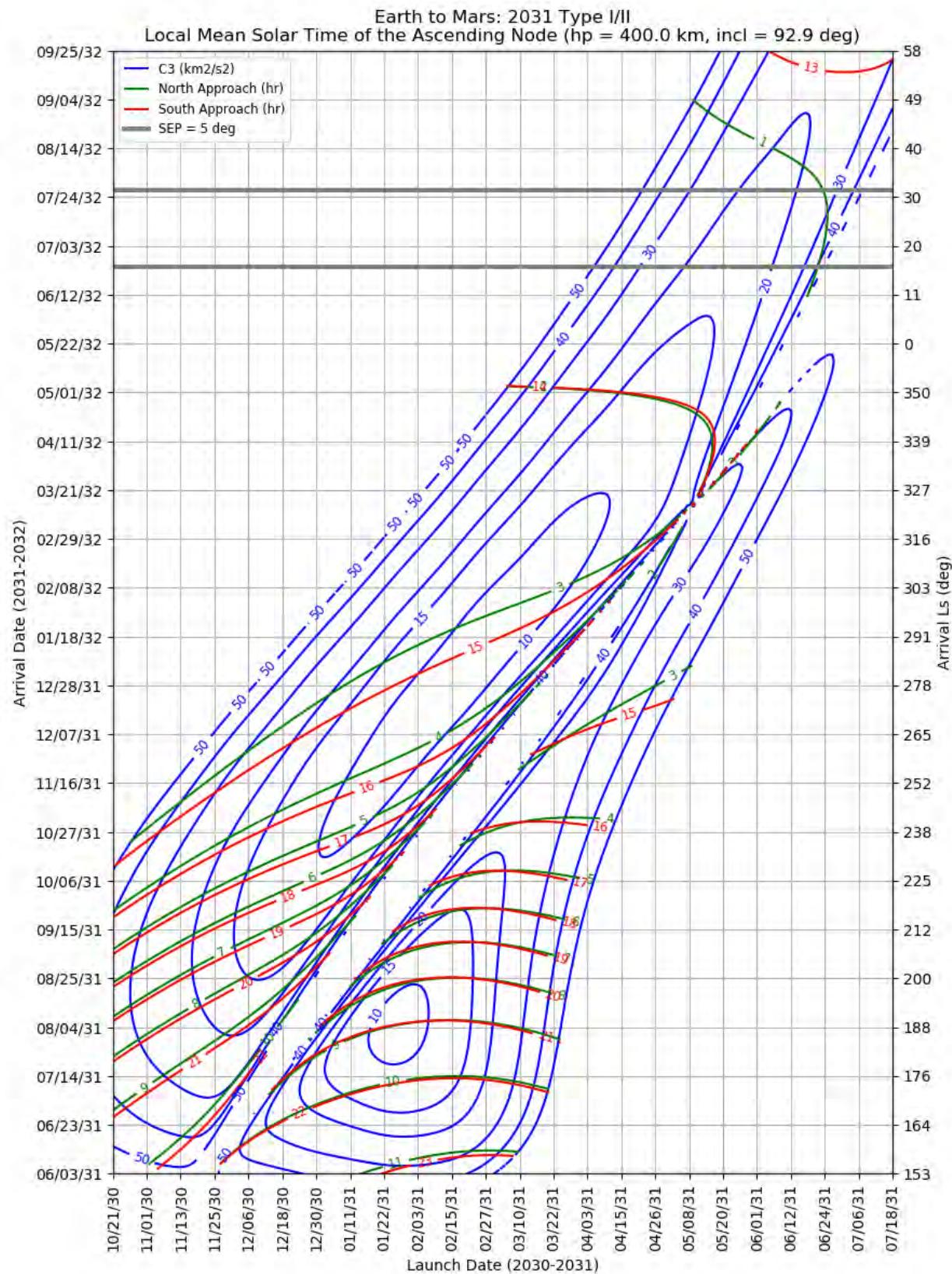


**Figure 412: Earth to Mars 2031 Type I/II – LMST of the Ascending Node for North and South Approaches**

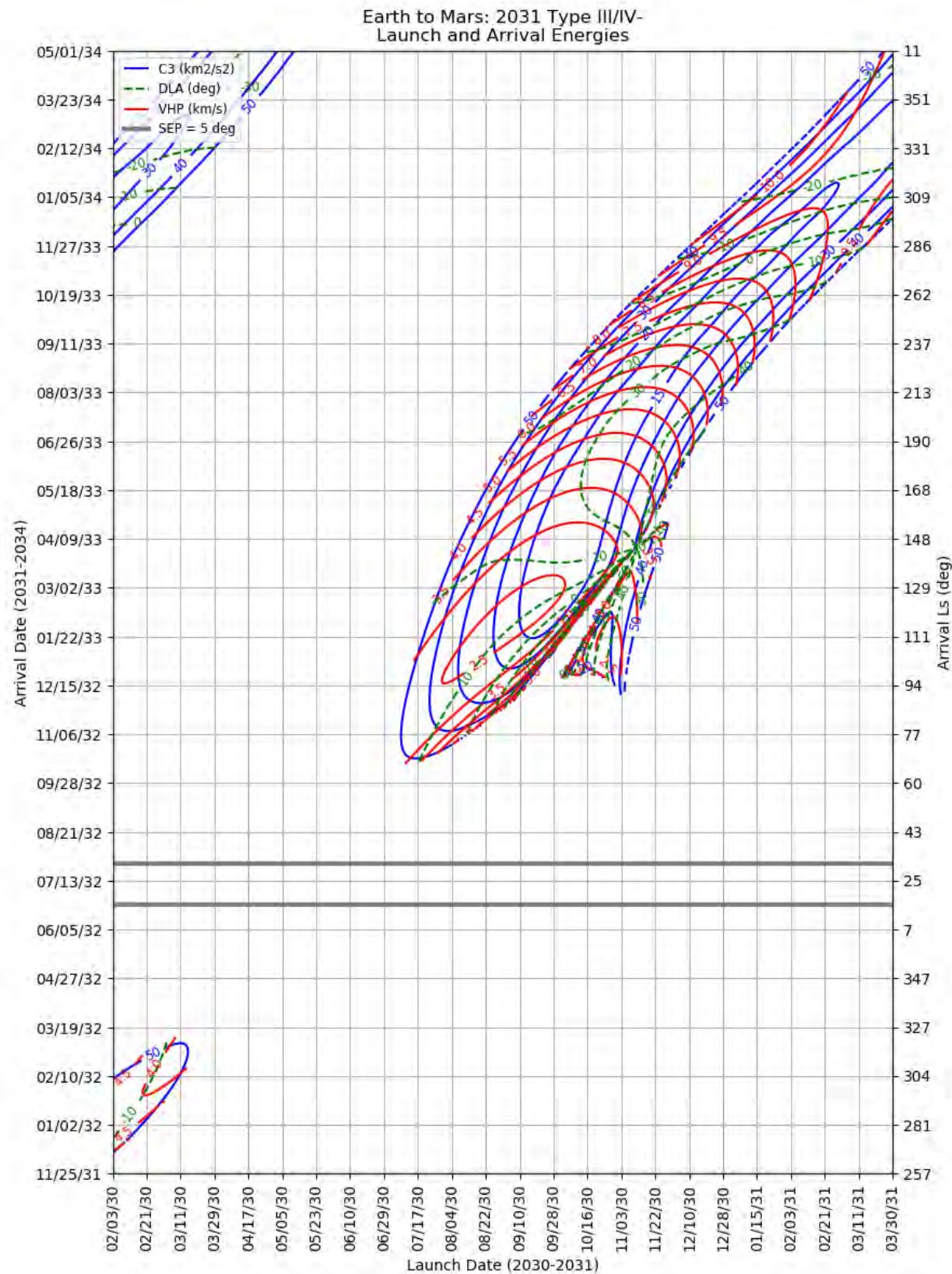
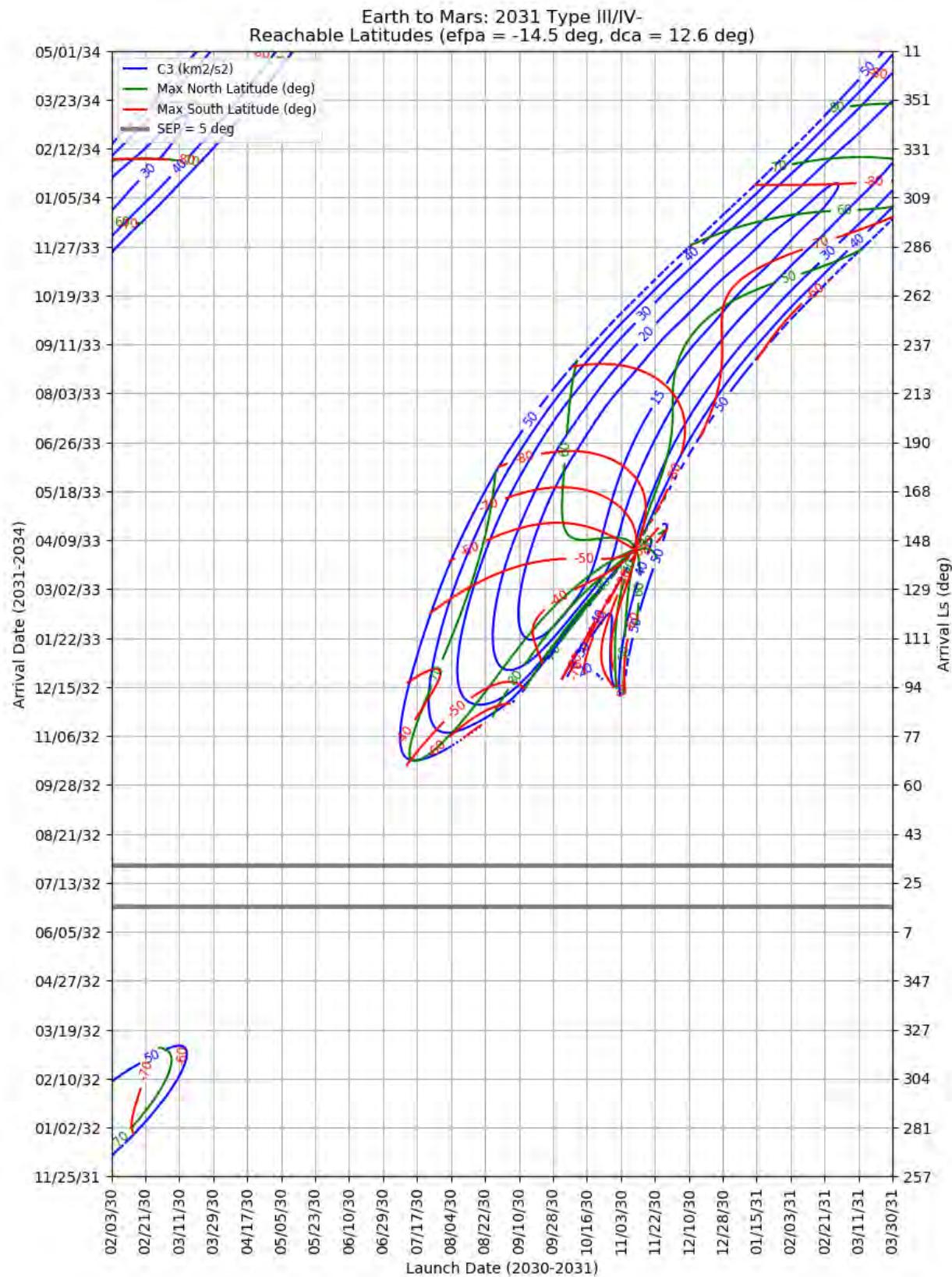
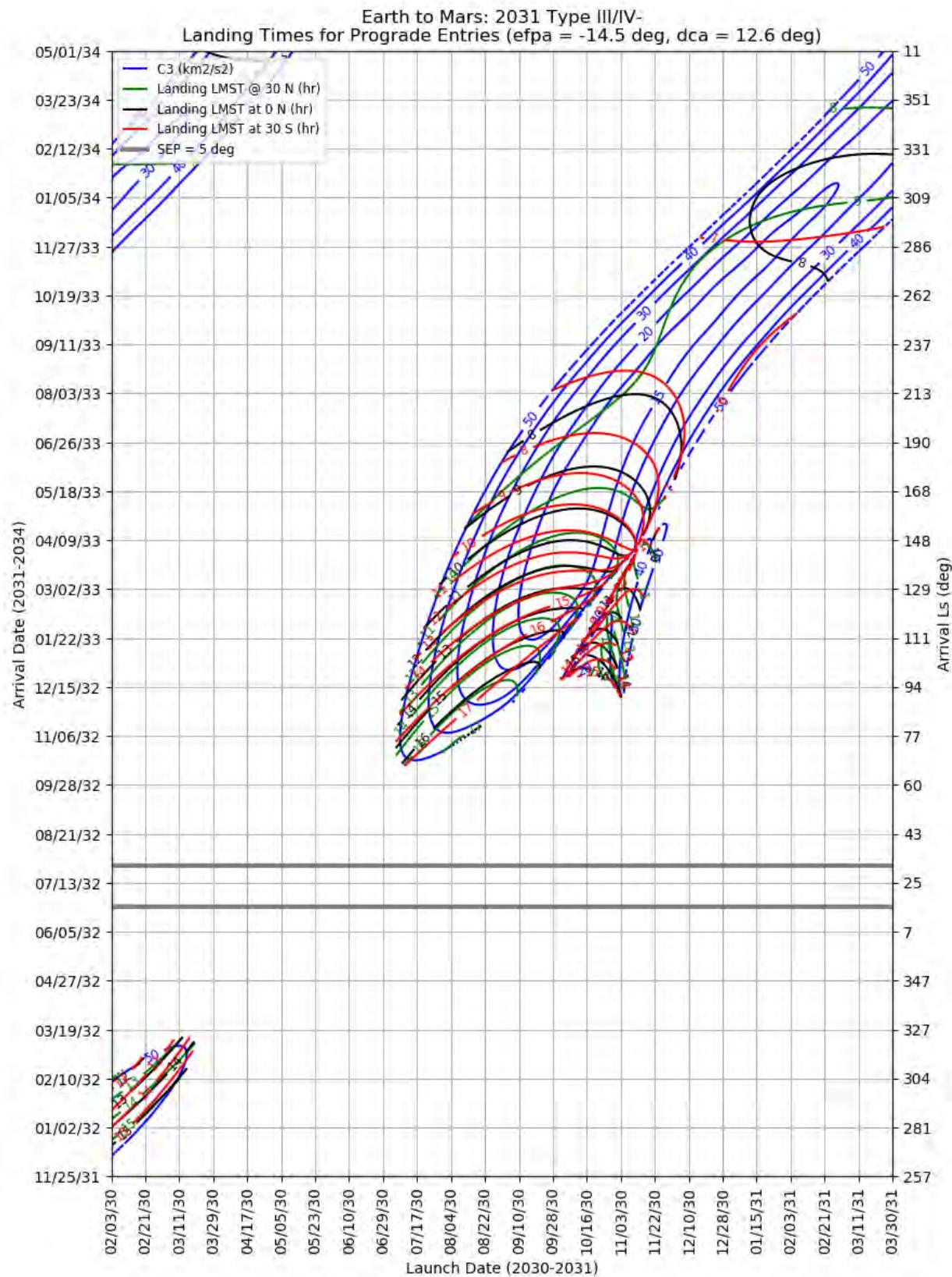


Figure 413: Earth to Mars 2031 Type III/IV- – Launch and Arrival Energy



**Figure 414: Earth to Mars 20312 Type III/IV- – Maximum Reachable North and South Latitude**



**Figure 415: Earth to Mars 2031 Type III/IV- – Landing LMST for Prograde Entries**

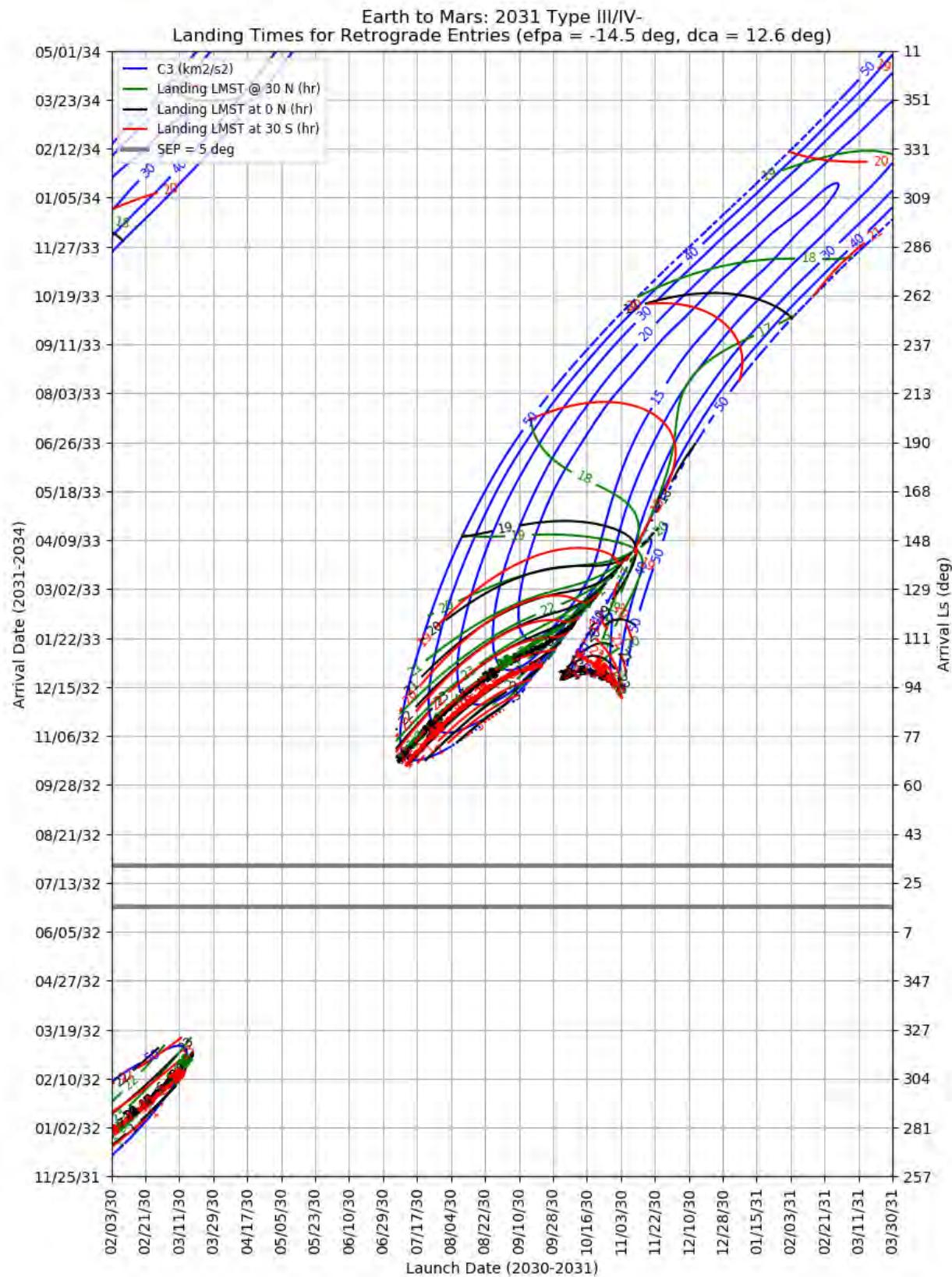


**Figure 416: Earth to Mars 2031 Type III/IV- – Landing LMST for Retrograde Entries**

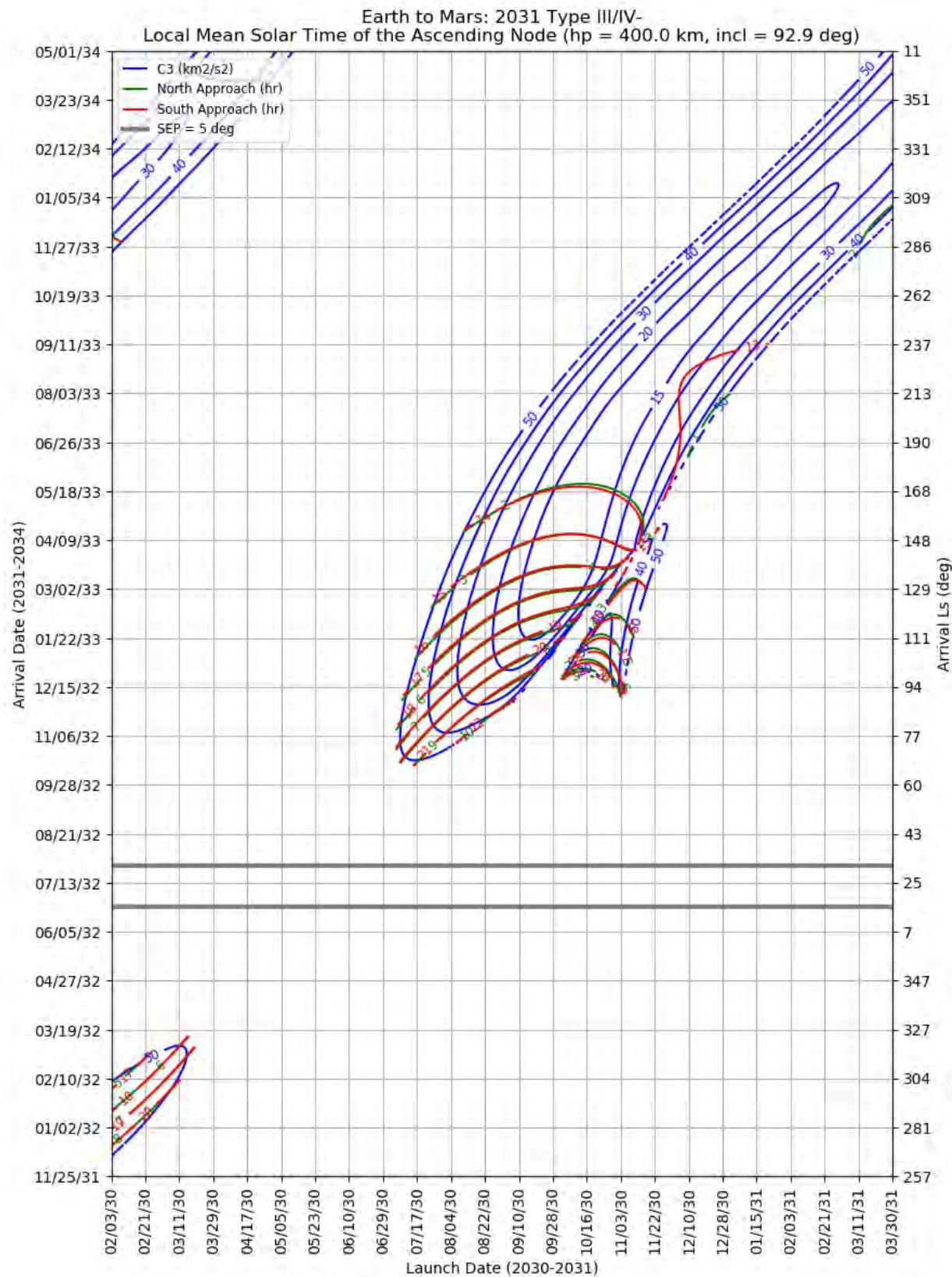
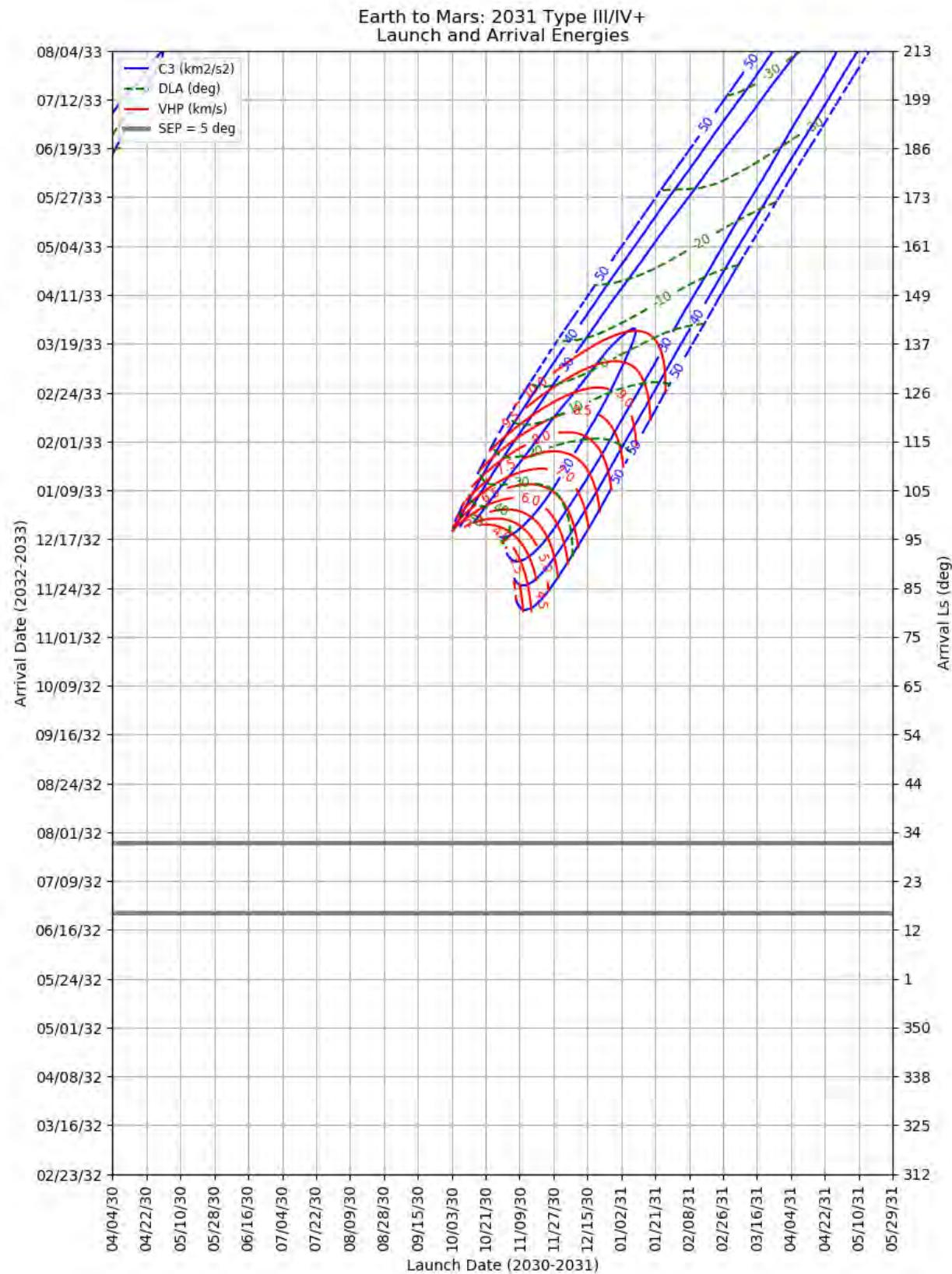
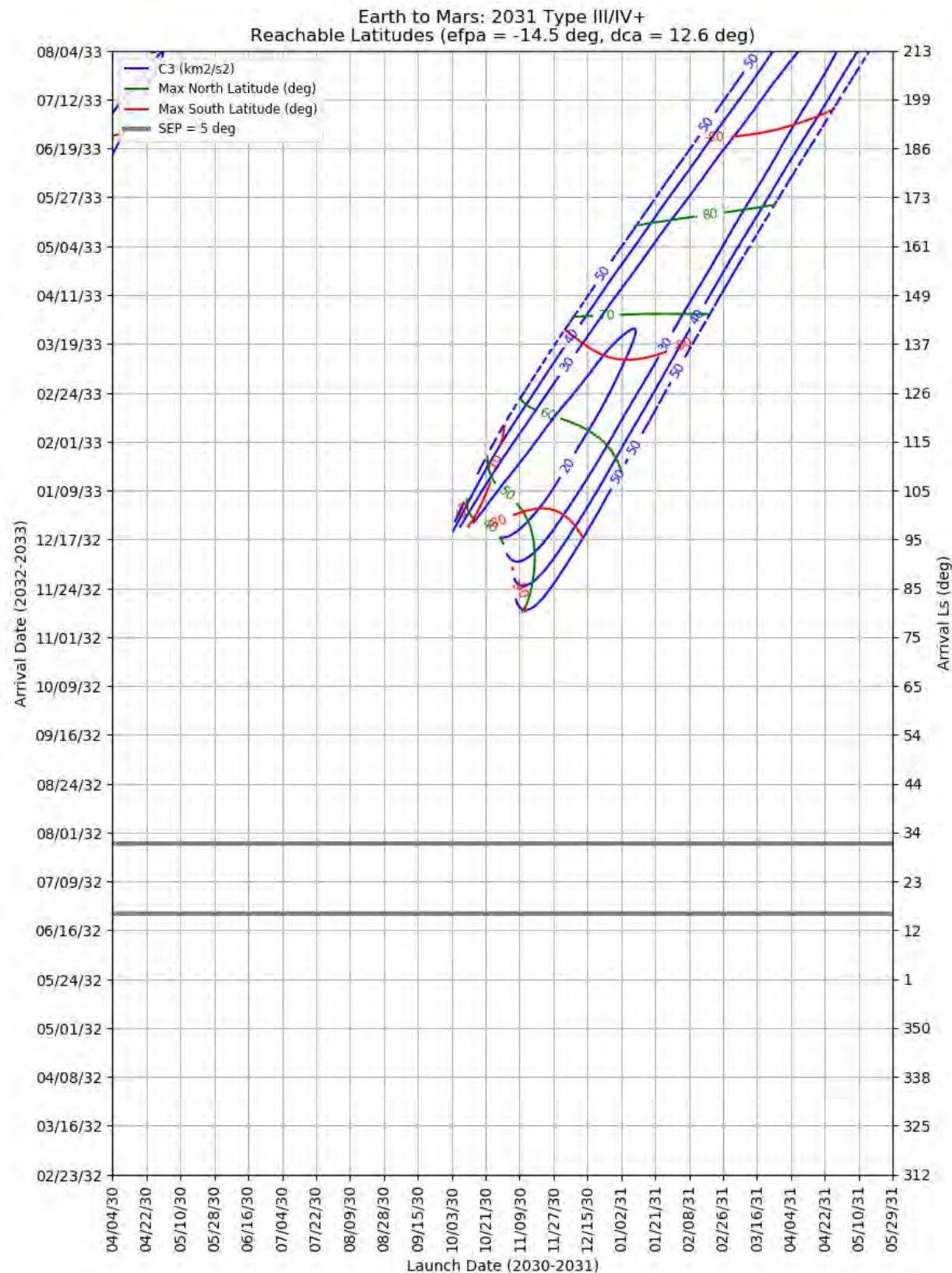


Figure 417: Earth to Mars 2031 Type III/IV- – LMST of the Ascending Node for North and South Approaches



**Figure 418: Earth to Mars 2031 Type III/IV+ – Launch and Arrival Energy**



**Figure 419: Earth to Mars 2031 Type III/IV+ – Maximum Reachable North and South Latitude**

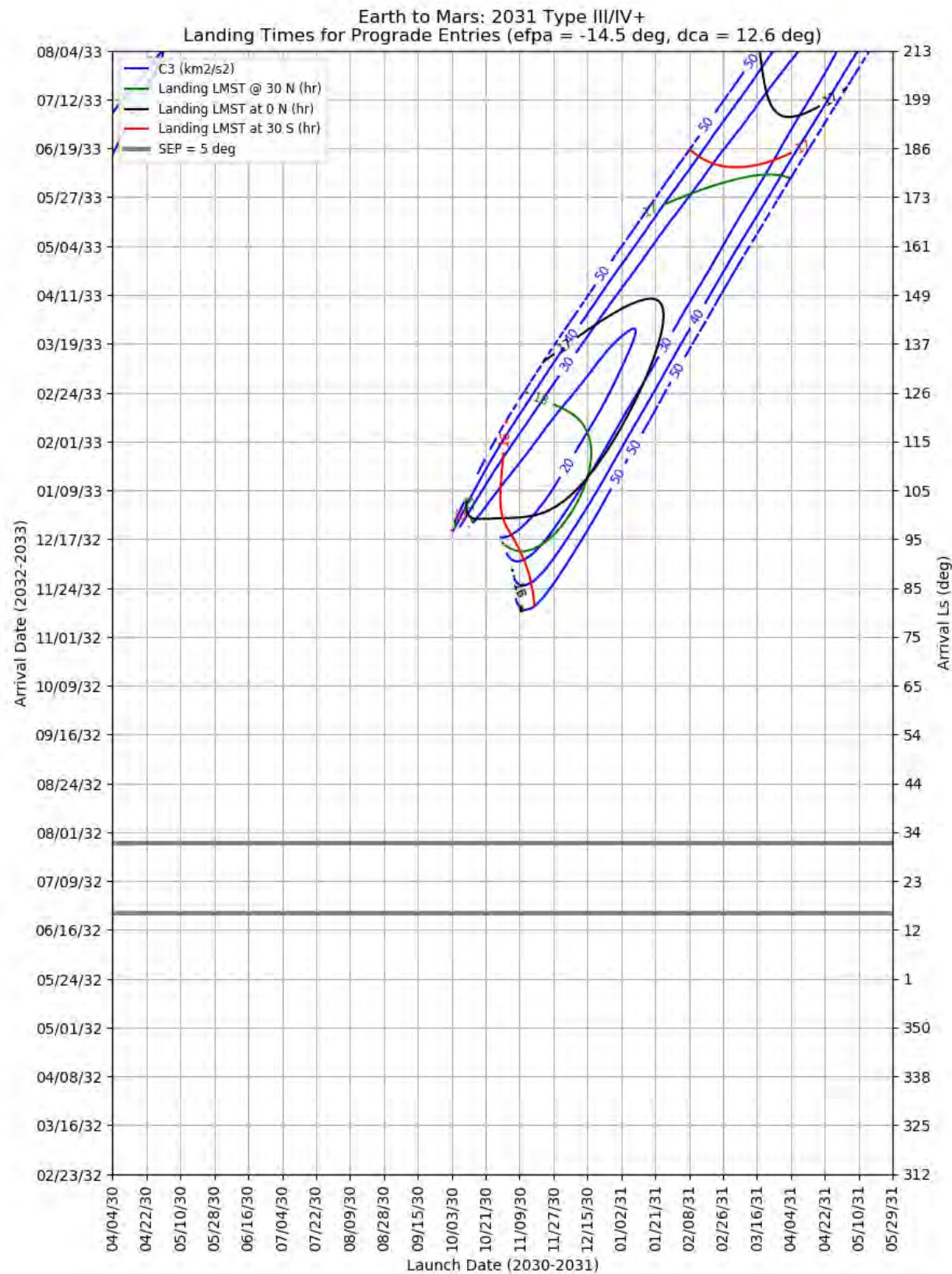


**Figure 420: Earth to Mars 2031 Type III/IV+ – Landing LMST for Prograde Entries**

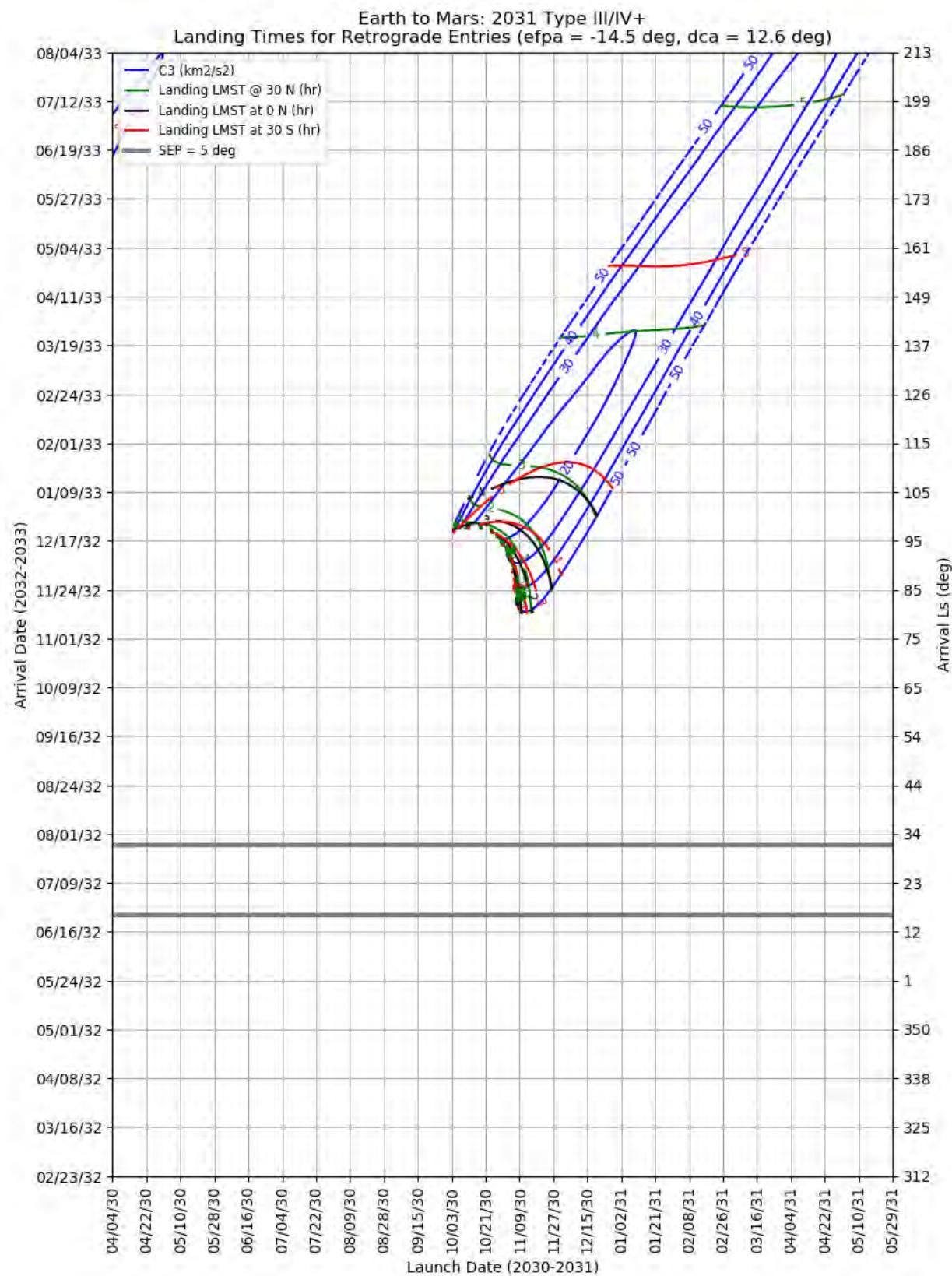


**Figure 421: Earth to Mars 2031 Type III/IV+ – Landing LMST for Retrograde Entries**

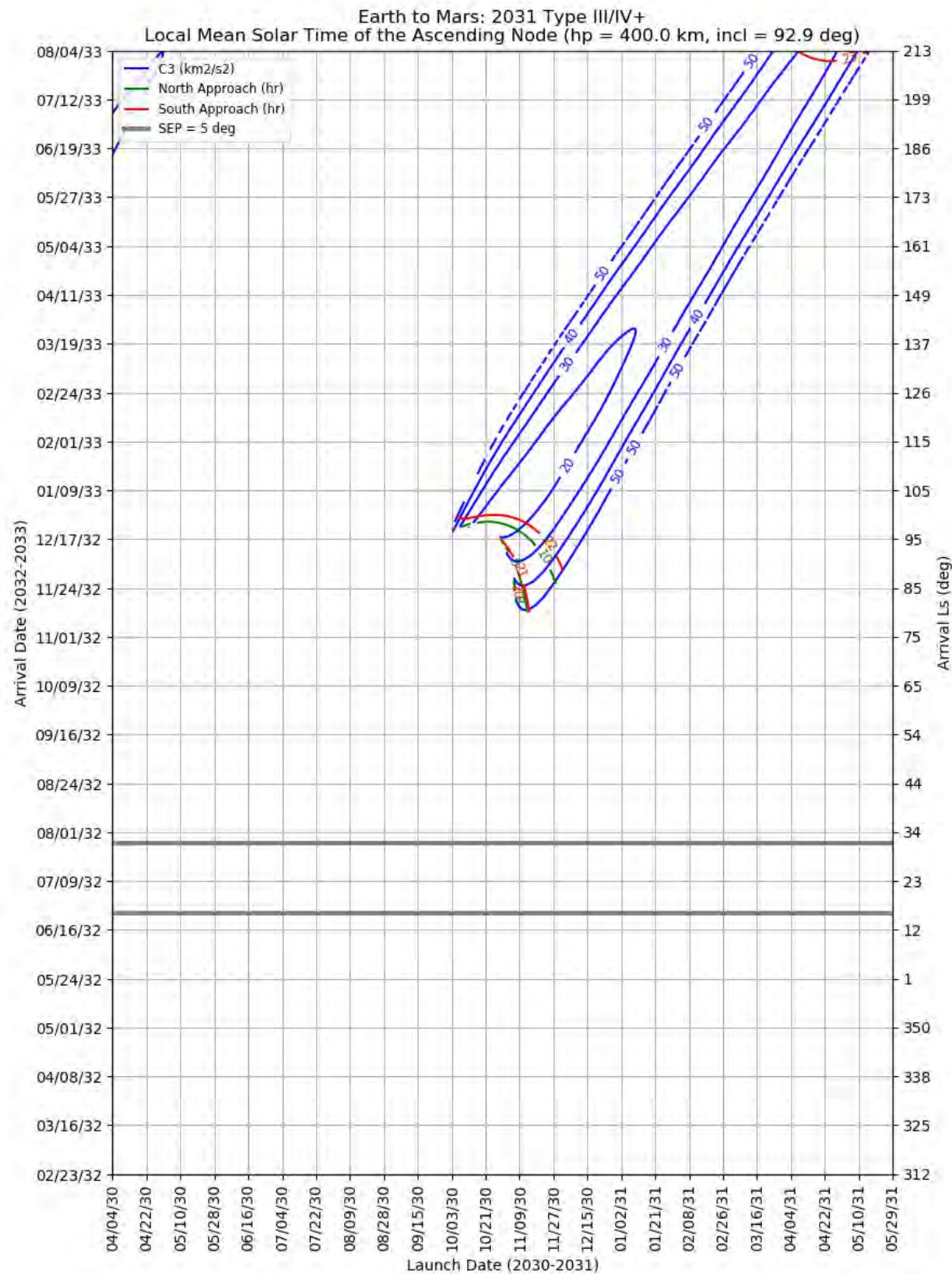


**Figure 422: Earth to Mars 2031 Type III/IV+ – LMST of the Ascending Node for North and South Approaches**

### 10.5.7 Earth to Mars 2033

This section contains porkchop plots for the Earth-to-Mars 2033 opportunities. Table 33 contains the optimal single-day transfers for minimum launch energy (C3) and arrival velocity (VHP) as well as the maximum launch-mass and captured-mass launch periods for each trajectory type within the opportunity. These data should only be used for preliminary analysis and planning purposes.

**Table 33: Earth to Mars 2033 Optimal Launch/Arrival Data**

Optimization Criteria	Trajectory Type	Departure Date (dd-mmm-yyyy)	Arrival Date (dd-mmm-yyyy)	Launch Energy, C3 (km <sup>2</sup> /s <sup>2</sup> )	Declination of the Launch Asymptote, DLA (deg)	Approach V-Infinity, VHP (km/s)
<b>Single-Day Optimization</b>						
Minimum C3	I	04-Apr-2033	29-Sep-2033	8.4	-55.7	4.04
Minimum C3	II	29-Apr-2033	28-Jan-2034	7.7	-12.5	4.38
Minimum C3	III-	04-Nov-2032	26-Dec-2034	13.5	40.7	4.64
Minimum C3	IV-	16-Oct-2032	19-Feb-2035	10.1	21.4	2.47
Minimum C3	III+	11-Nov-2032	27-Dec-2034	13.2	33.7	5.11
Minimum C3	IV+	28-Sep-2032	07-Dec-2034	50.9	-20.0	7.21
Minimum VHP	I	20-Apr-2033	06-Nov-2033	9.3	-53.3	3.31
Minimum VHP	II	28-Jan-2033	18-Oct-2033	17.4	-1.7	3.83
Minimum VHP	III-	11-Nov-2032	05-Feb-2035	19.4	39.0	2.46
Minimum VHP	IV-	17-Oct-2032	20-Feb-2035	10.1	21.9	2.47
Minimum VHP	III+	01-Dec-2032	19-Nov-2034	68.1	28.7	3.26
Minimum VHP	IV+	20-Sep-2032	30-Nov-2034	51.8	-9.5	7.02
<b>Launch Period Optimization</b>						
Maximum Launch Mass	I	10-May-2033	31-Jan-2034	10.3	-45.7	4.29
		30-May-2033		13.6	-21.9	4.47
Maximum Launch Mass	II	22-Apr-2033	01-Feb-2034	8.5	-15.6	4.45
		12-May-2033		8.6	-18.3	4.37
Maximum Launch Mass	III-	28-Oct-2032	27-Dec-2034	16.4	53.9	4.16
		17-Nov-2032		22.4	34.3	3.16
Maximum Launch Mass	IV-	07-Oct-2032	20-Feb-2035	10.8	20.3	2.48
		27-Oct-2032		11.0	23.4	2.49
Maximum Launch Mass	III+	09-Nov-2032	30-Dec-2034	14.7	28.0	5.92
		29-Nov-2032		14.9	26.4	5.86
Maximum Launch Mass	IV+	Not Possible				
Maximum Captured Mass	I	16-Apr-2033	25-Oct-2033	9.0	-53.7	3.37
		06-May-2033		14.3	-39.2	3.50
Maximum Captured Mass	II	30-Apr-2033	01-Feb-2034	7.8	-17.3	4.39

Optimization Criteria	Trajectory Type	Departure Date (dd-mmm-yyyy)	Arrival Date (dd-mmm-yyyy)	Launch Energy, C3 (km <sup>2</sup> /s <sup>2</sup> )	Declination of the Launch Asymptote, DLA (deg)	Approach V-Infinity, VHP (km/s)	
		20-May-2033		10.1	-20.4	4.39	
Maximum Captured Mass	III-	29-Oct-2032	04-Jan-2035	18.0	61.5	3.42	
		18-Nov-2032		26.0	32.9	2.77	
Maximum Captured Mass	IV-	07-Oct-2032	20-Feb-2035	10.8	20.3	2.48	
		27-Oct-2032		11.0	23.4	2.49	
Maximum Captured Mass	III+	05-Nov-2032	27-Dec-2034	14.3	34.6	5.36	
		25-Nov-2032		15.0	29.1	5.44	
Maximum Captured Mass	IV+			Not Possible			

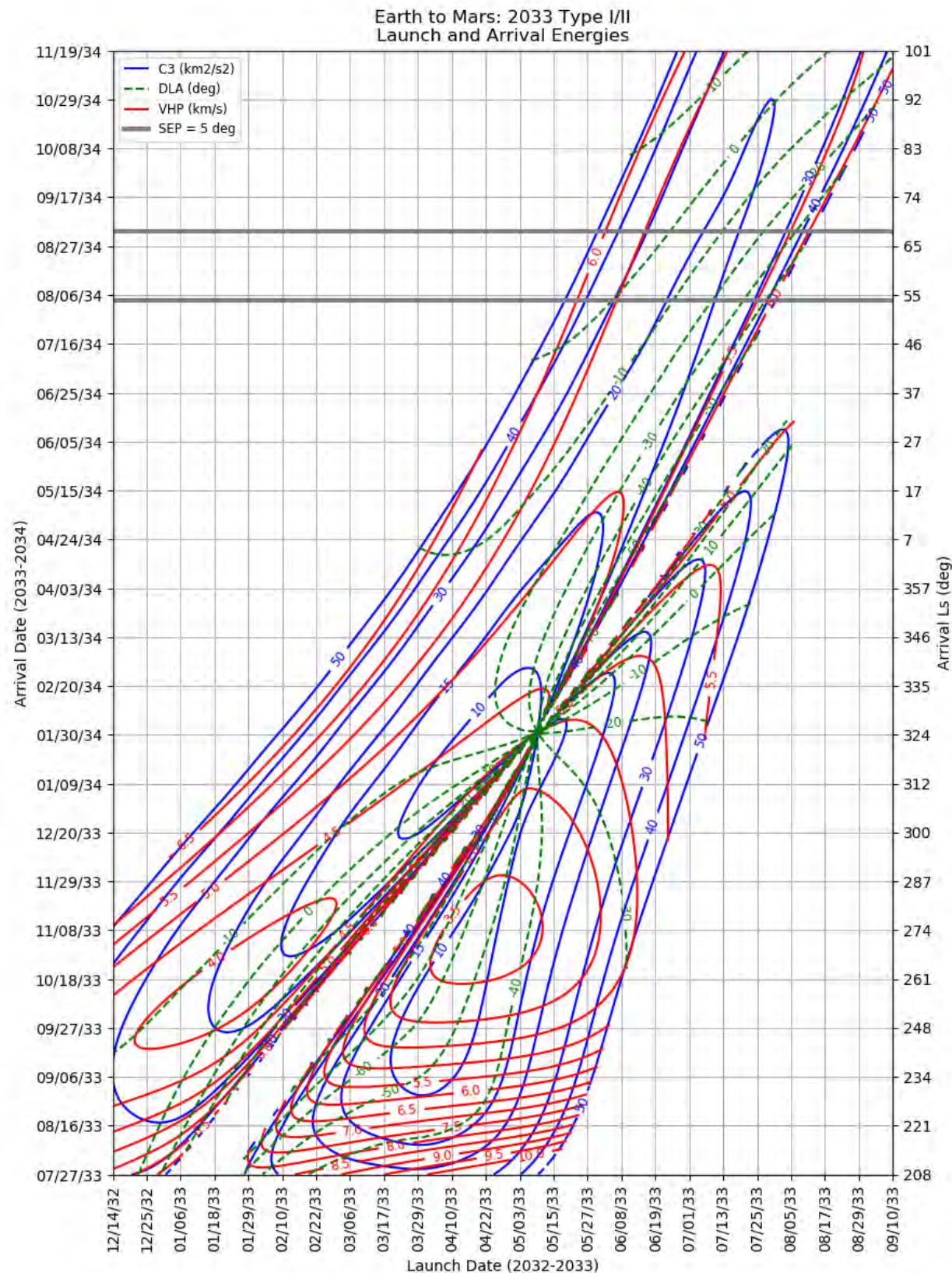


**Figure 423: Earth to Mars 2033 Type I/II - Launch and Arrival Energy**

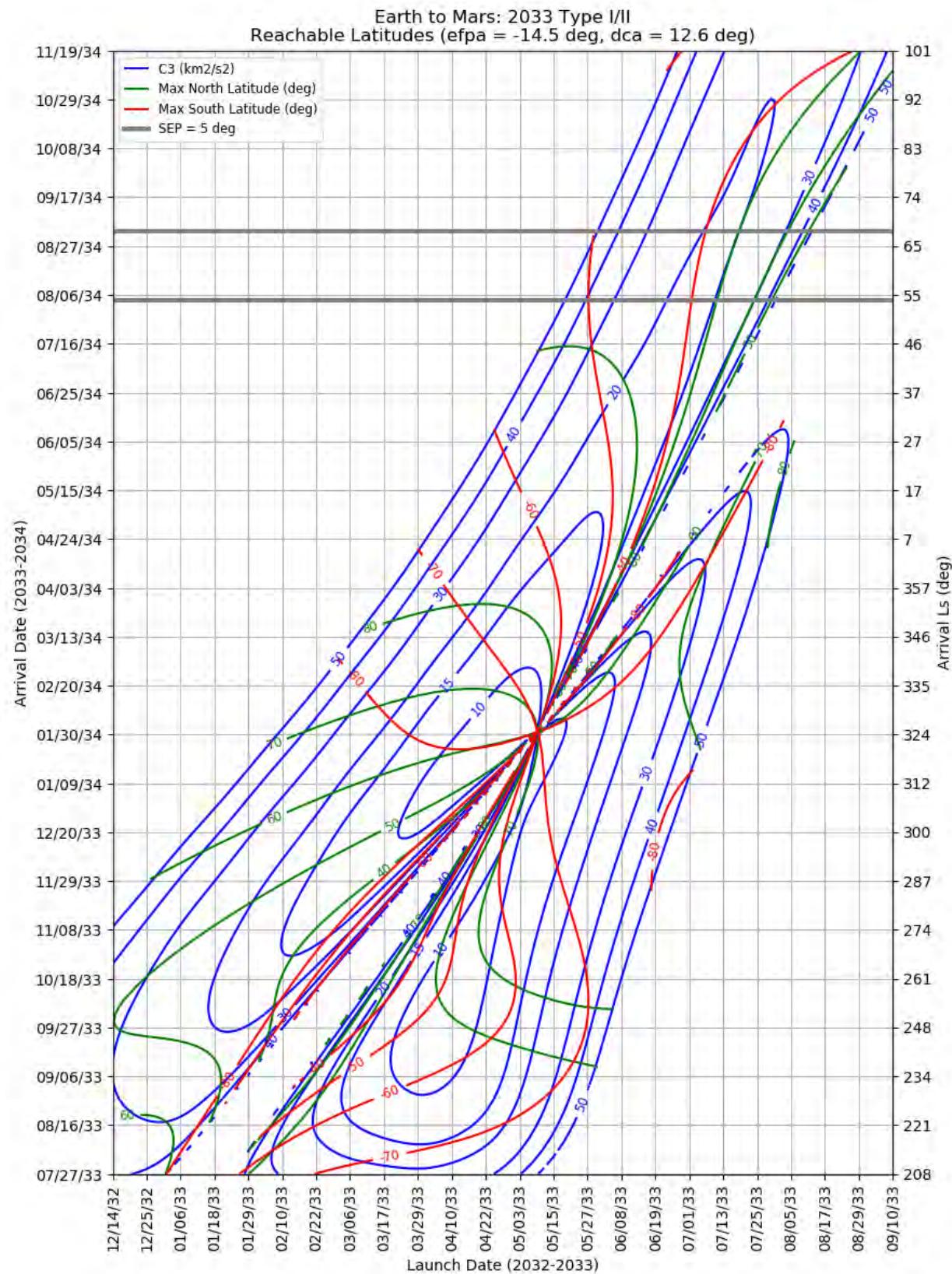


**Figure 424: Earth to Mars 2033 Type I/II – Maximum Reachable North and South Latitude**

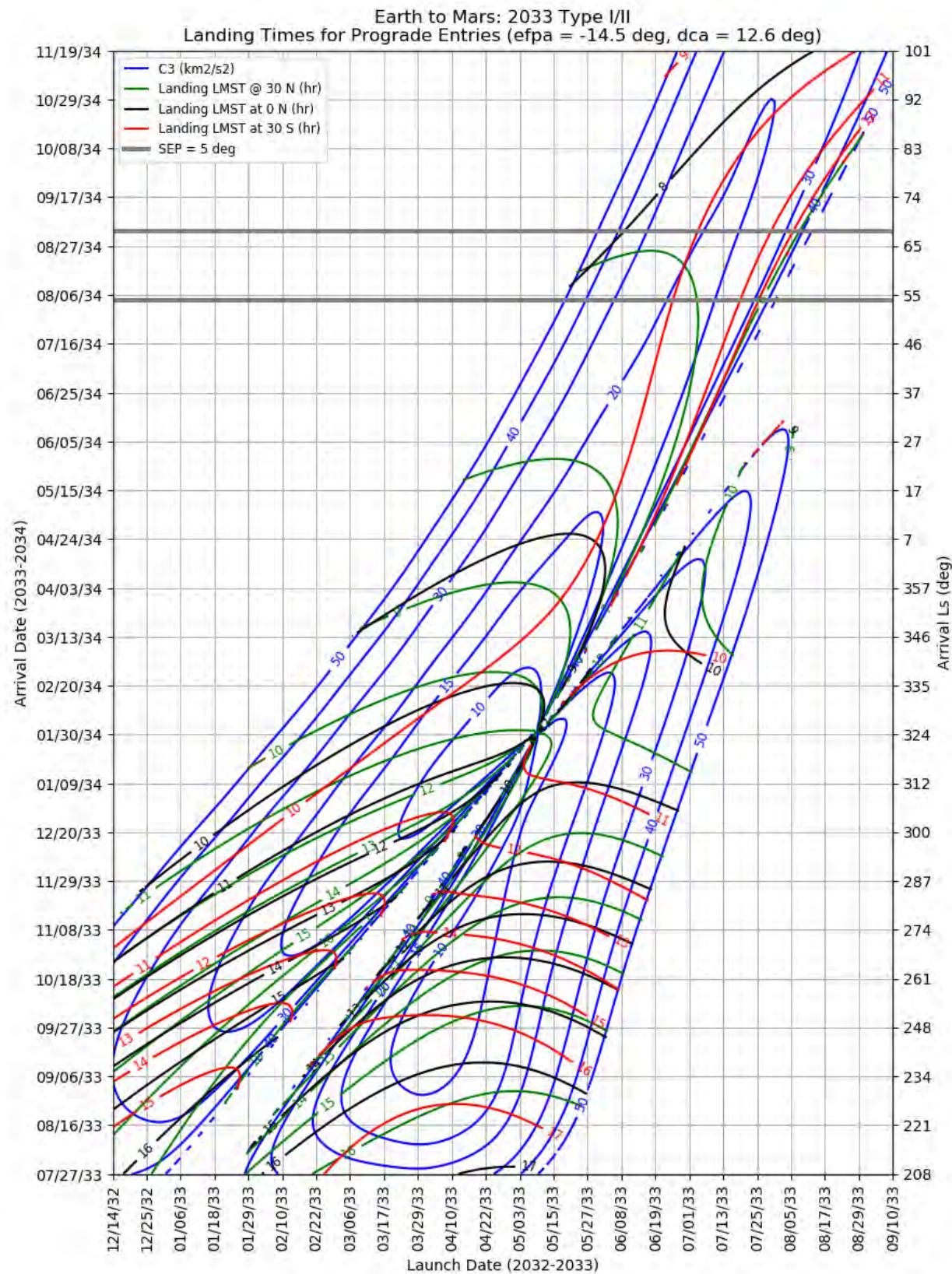
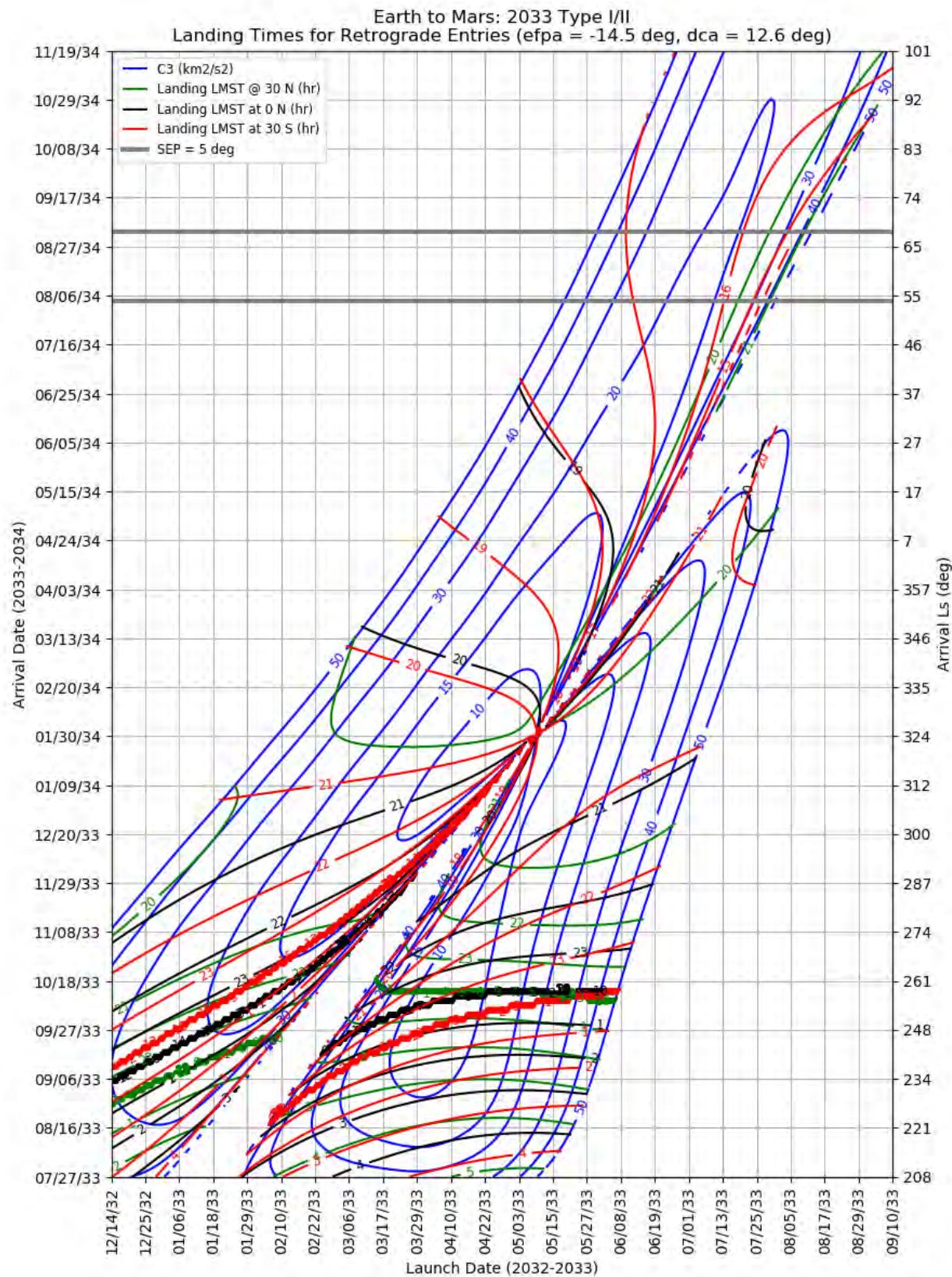
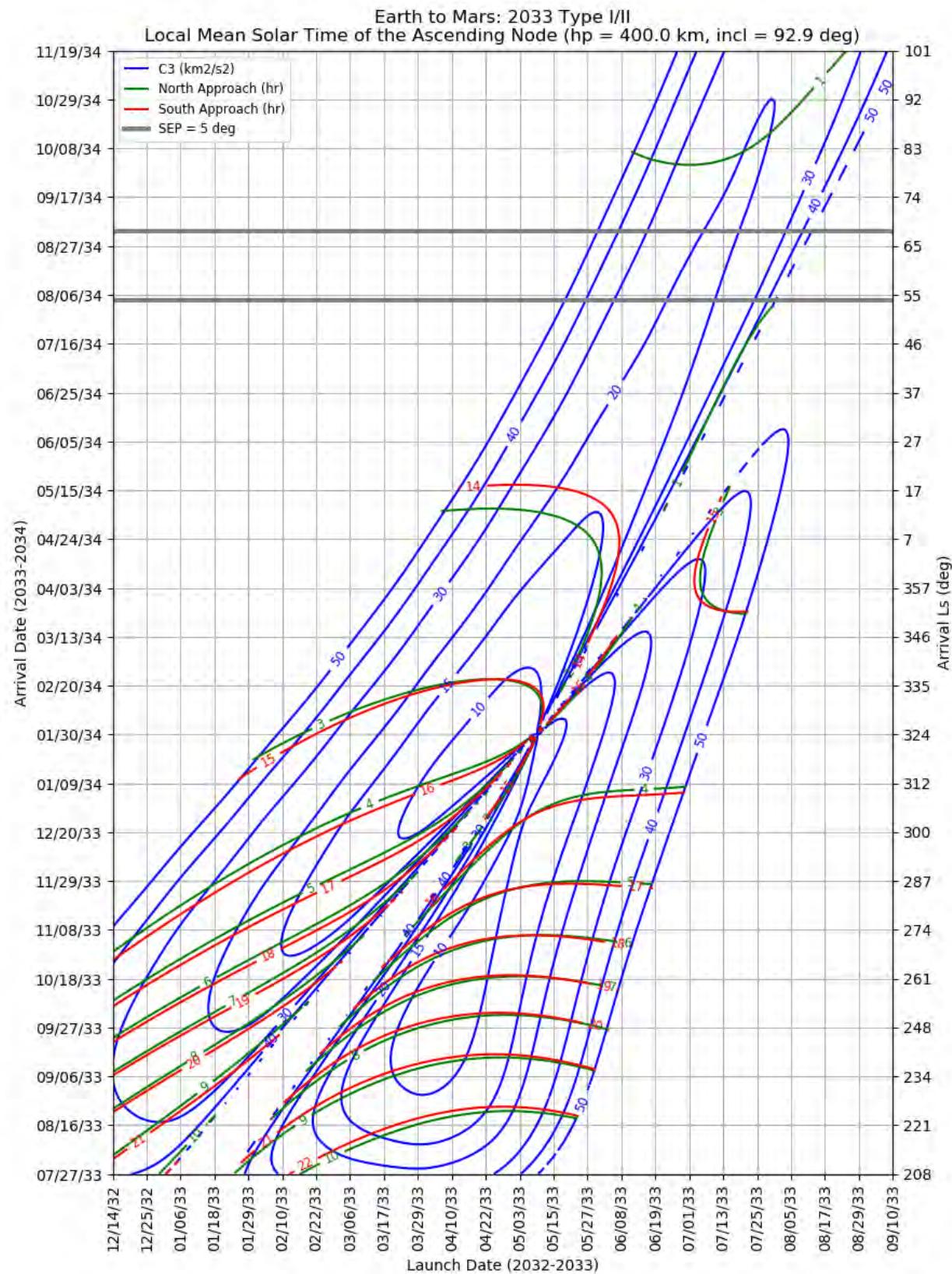


Figure 425: Earth to Mars 2033 Type I/II – Landing LMST for Prograde Entries



**Figure 426: Earth to Mars 2033 Type I/II – Landing LMST for Retrograde Entries**



**Figure 427: Earth to Mars 2033 Type I/II – LMST of the Ascending Node for North and South Approaches**

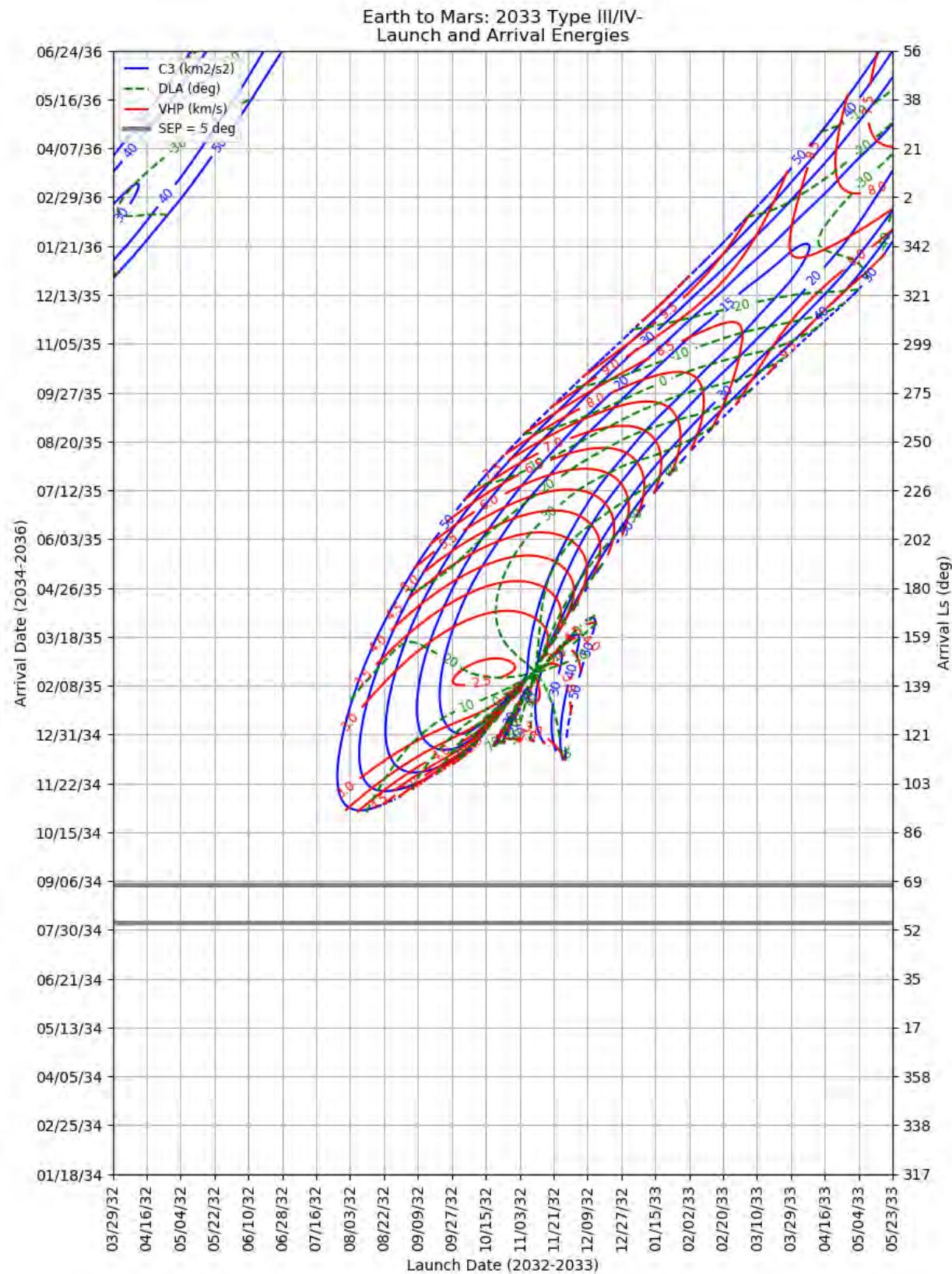
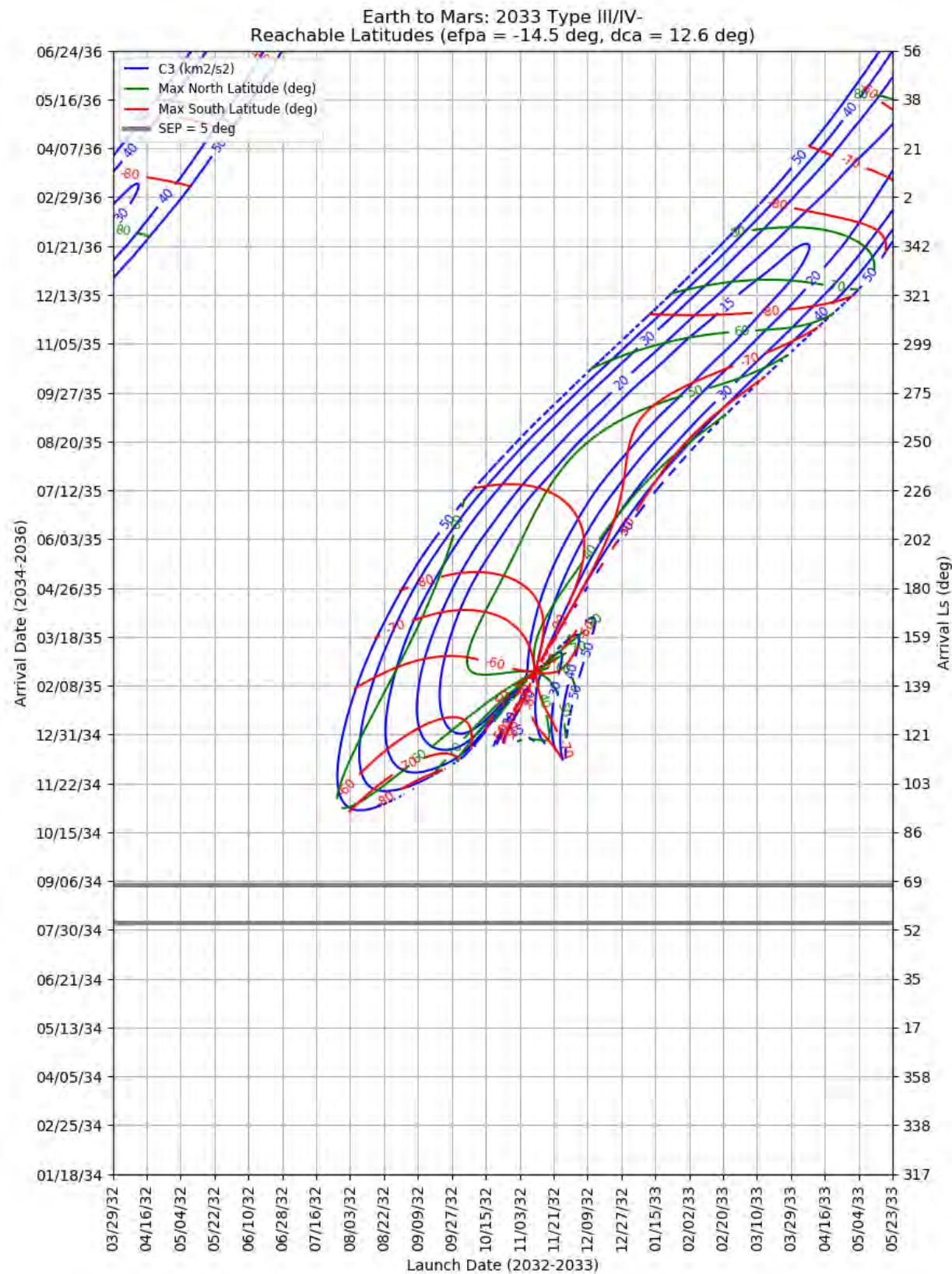


Figure 428: Earth to Mars 2033 Type III/IV- – Launch and Arrival Energy



**Figure 429: Earth to Mars 20332 Type III/IV- – Maximum Reachable North and South Latitude**

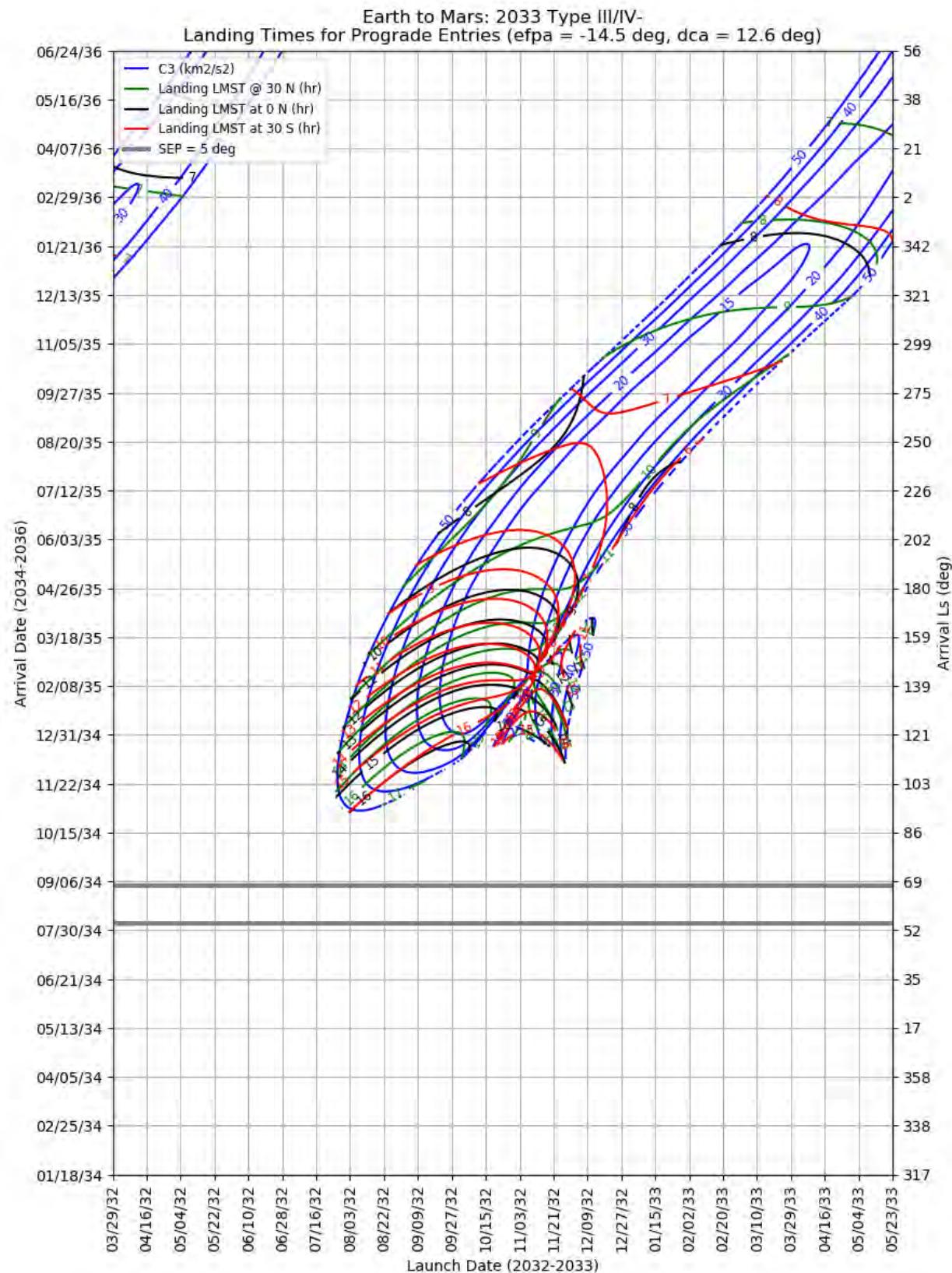


Figure 430: Earth to Mars 2033 Type III/IV- – Landing LMST for Prograde Entries

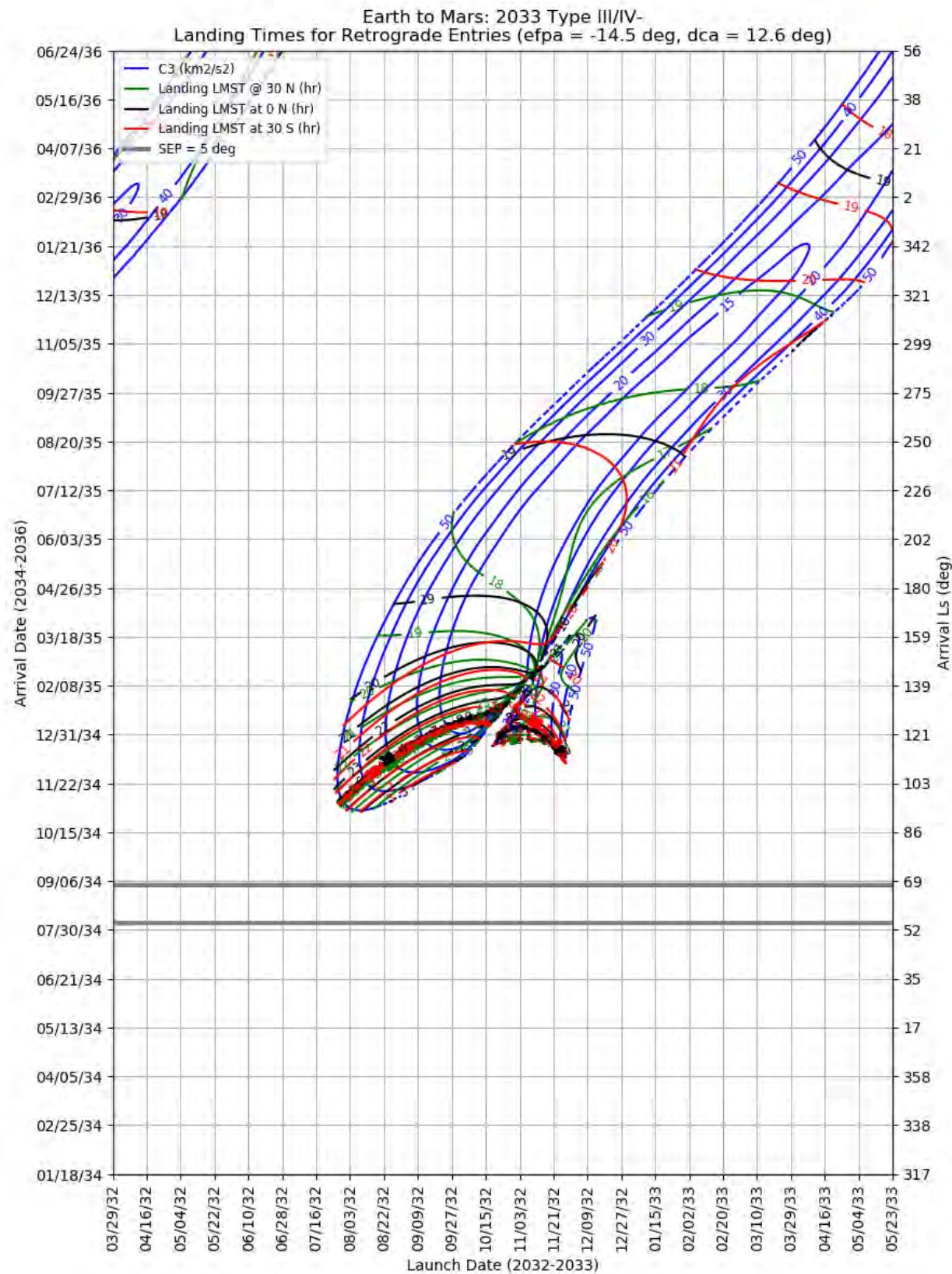
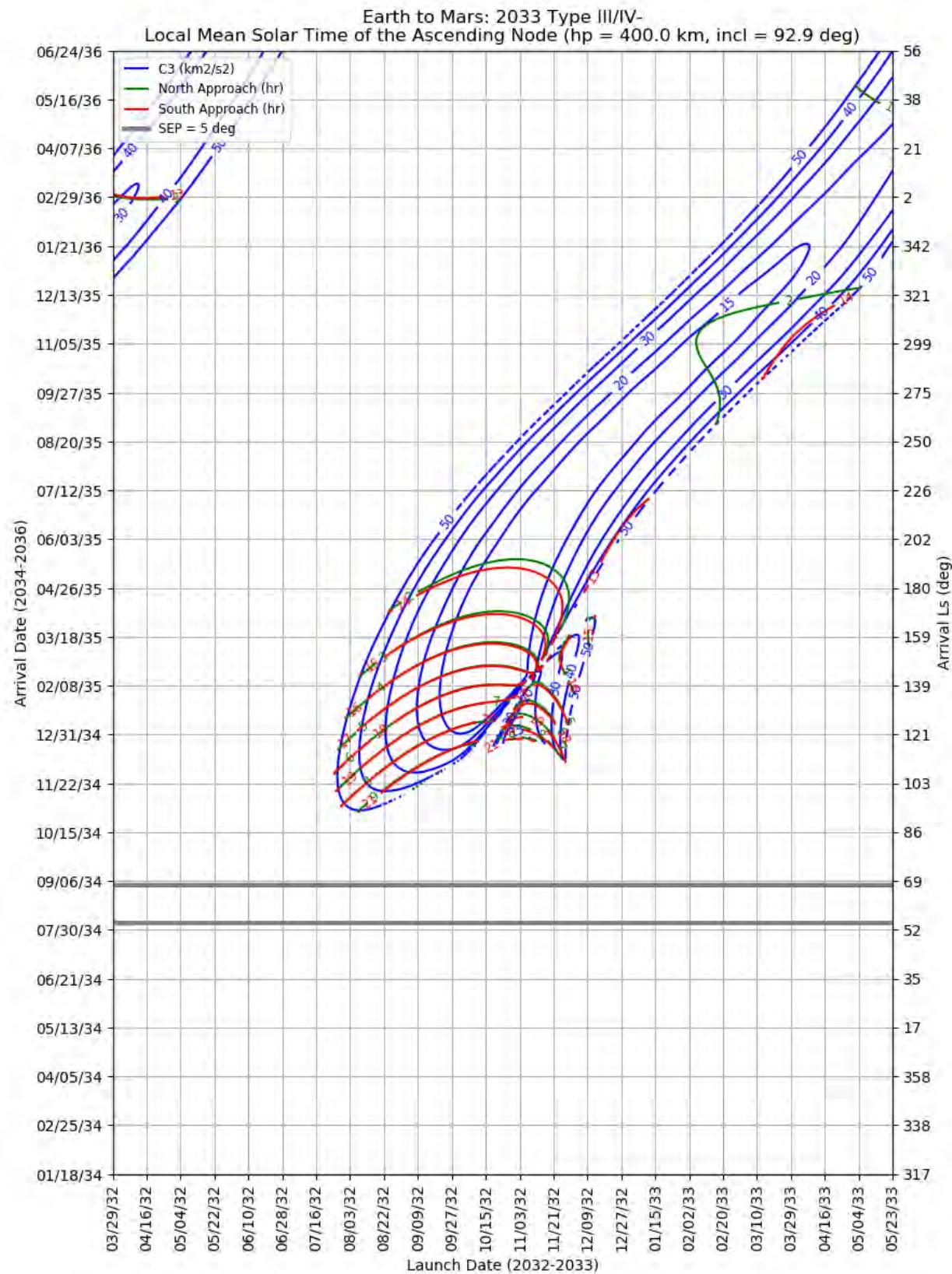
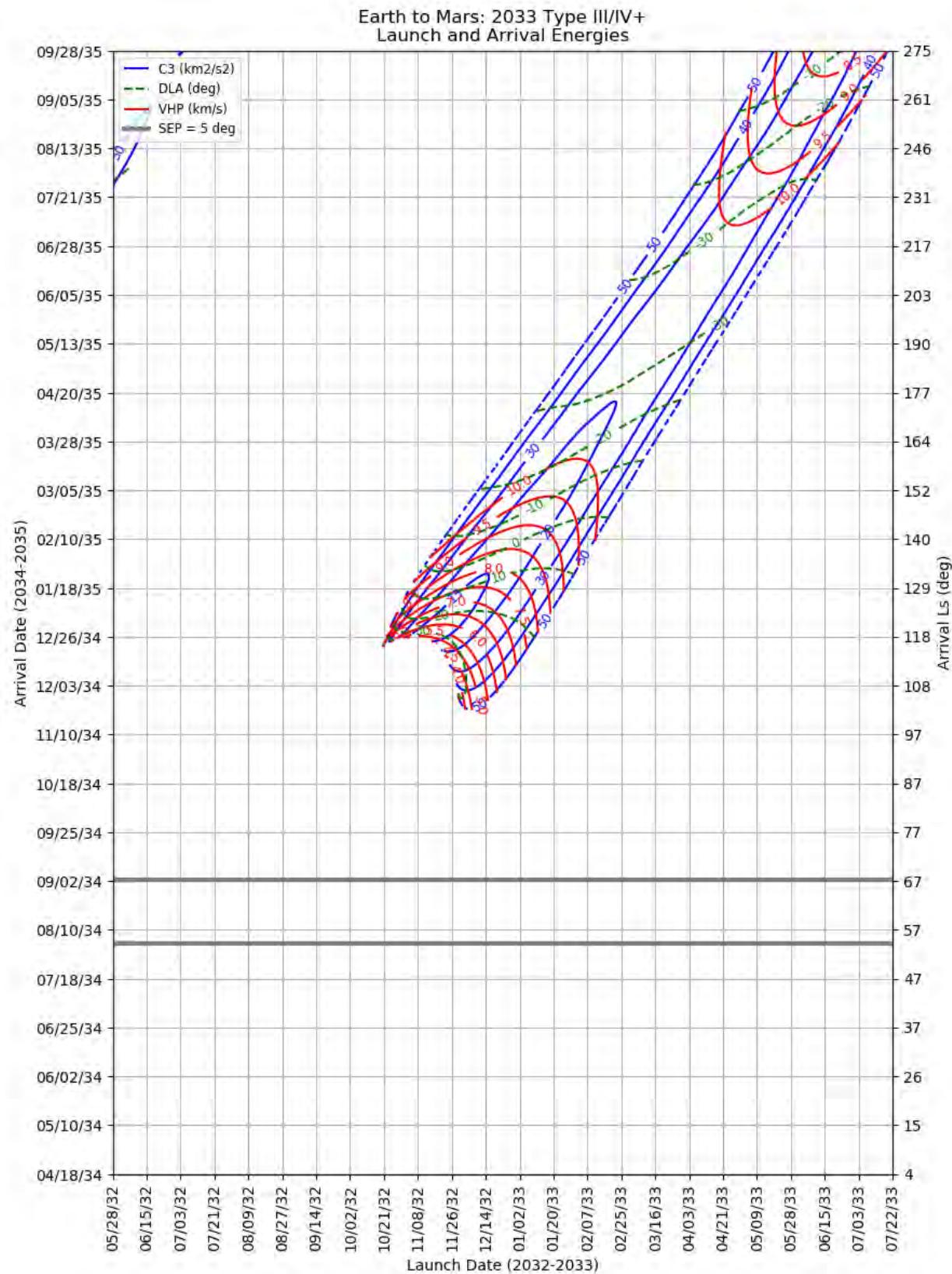
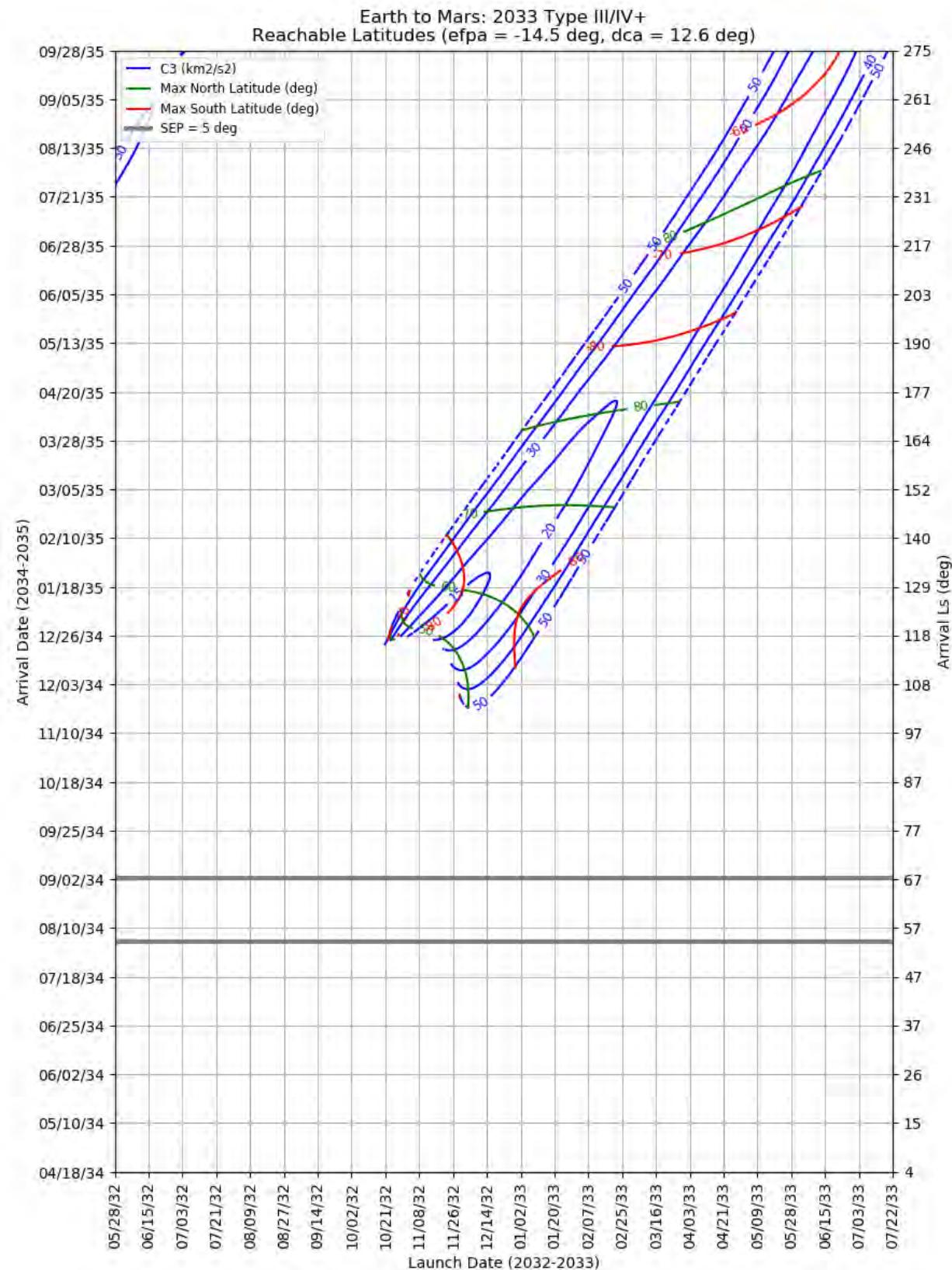


Figure 431: Earth to Mars 2033 Type III/IV- – Landing LMST for Retrograde Entries



**Figure 432: Earth to Mars 2033 Type III/IV- – LMST of the Ascending Node for North and South Approaches**





**Figure 434: Earth to Mars 2033 Type III/IV+ – Maximum Reachable North and South Latitude**

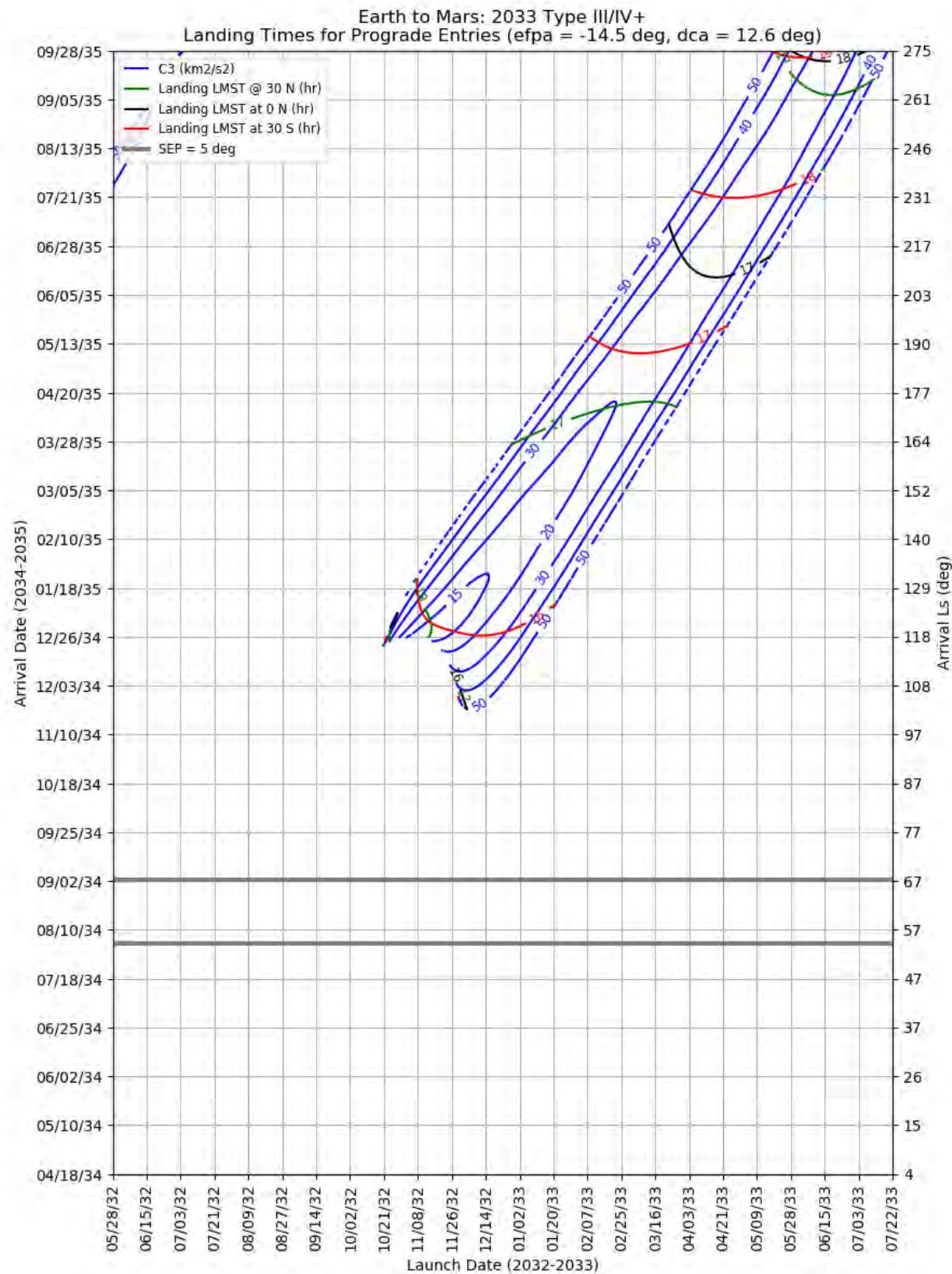
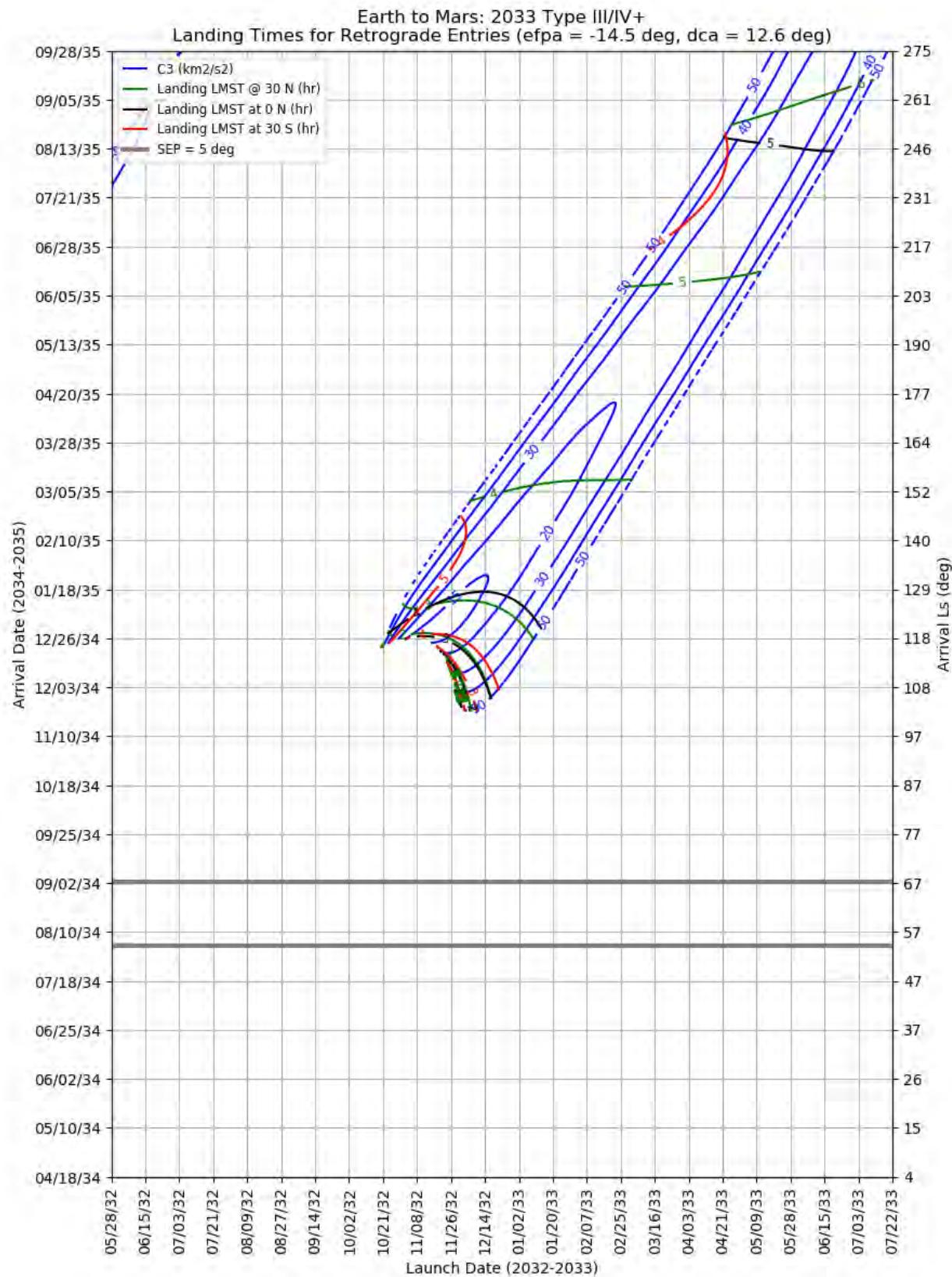


Figure 435: Earth to Mars 2033 Type III/IV+ – Landing LMST for Prograde Entries



**Figure 436: Earth to Mars 2033 Type III/IV+ – Landing LMST for Retrograde Entries**

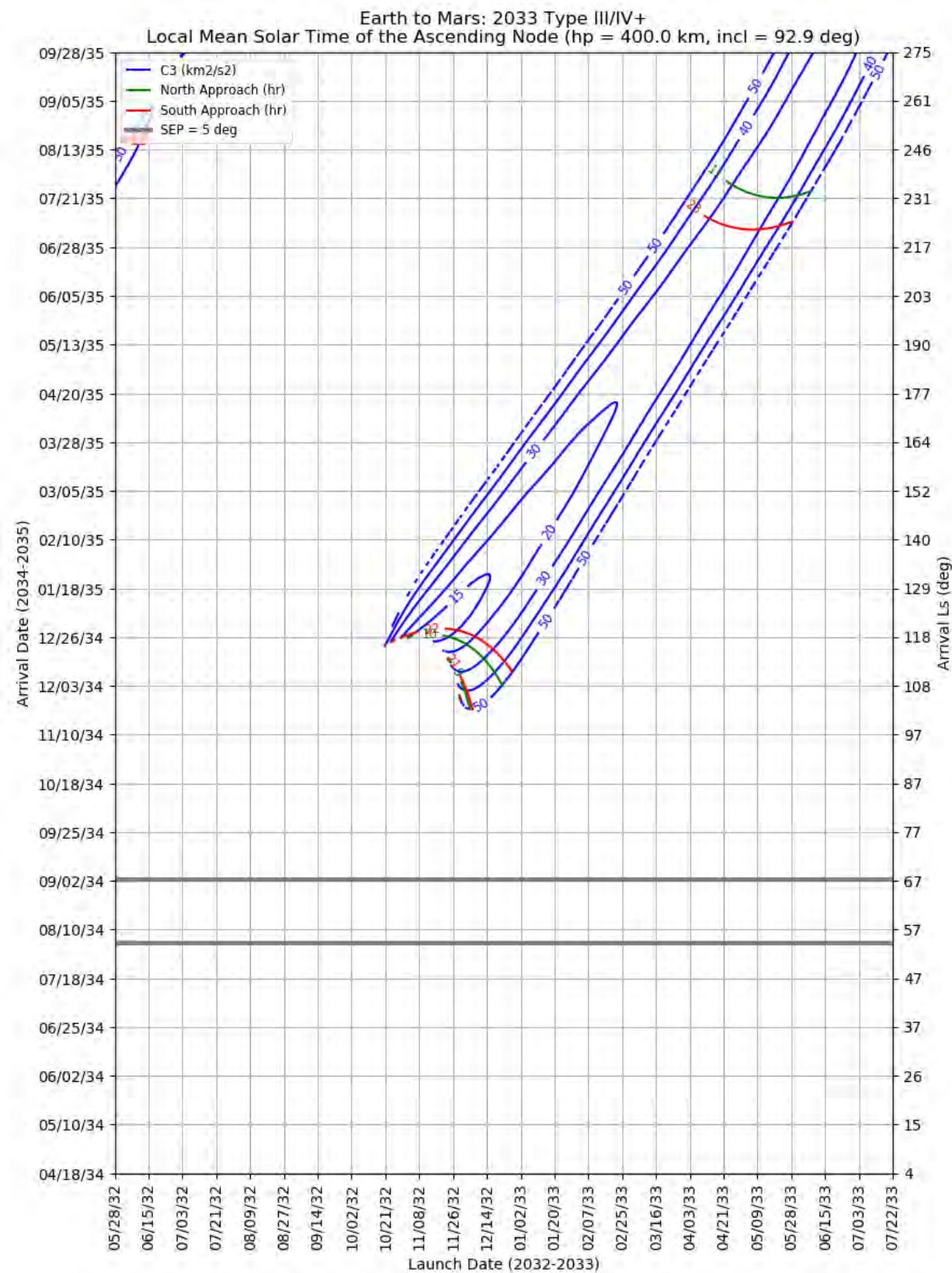


Figure 437: Earth to Mars 2033 Type III/IV+ – LMST of the Ascending Node for North and South Approaches

### 10.5.8 Earth to Mars 2035

This section contains porkchop plots for the Earth-to-Mars 2035 opportunities. Table 34 contains the optimal single-day transfers for minimum launch energy (C3) and arrival velocity (VHP) as well as the maximum launch-mass and captured-mass launch periods for each trajectory type within the opportunity. These data should only be used for preliminary analysis and planning purposes.

**Table 34: Earth to Mars 2035 Optimal Launch/Arrival Data**

Optimization Criteria	Trajectory Type	Departure Date (dd-mmm-yyyy)	Arrival Date (dd-mmm-yyyy)	Launch Energy, C3 (km <sup>2</sup> /s <sup>2</sup> )	Declination of the Launch Asymptote, DLA (deg)	Approach V-Infinity, VHP (km/s)
<b>Single-Day Optimization</b>						
Minimum C3	I	24-Jun-2035	05-Jan-2036	10.3	5.6	2.69
Minimum C3	II	10-May-2035	20-Dec-2035	17.5	1.1	2.86
Minimum C3	III-	13-Nov-2034	05-Jan-2037	9.2	20.9	3.37
Minimum C3	IV-	07-Nov-2034	08-Jan-2037	8.9	20.4	3.22
Minimum C3	III+	24-Nov-2034	23-Dec-2036	10.6	15.7	5.27
Minimum C3	IV+	25-Oct-2034	10-Dec-2036	37.5	-23.0	7.40
Minimum VHP	I	10-Jul-2035	25-Jan-2036	12.0	6.1	2.60
Minimum VHP	II	14-May-2035	09-Jan-2036	19.2	-13.8	2.70
Minimum VHP	III-	07-Dec-2034	17-Jan-2037	22.1	18.2	2.96
Minimum VHP	IV-	09-Nov-2034	10-Feb-2037	9.5	34.8	2.61
Minimum VHP	III+	22-Dec-2034	26-Nov-2036	55.6	25.7	3.67
Minimum VHP	IV+	25-Oct-2034	10-Dec-2036	37.5	-23.0	7.40
<b>Launch Period Optimization</b>						
Maximum Launch Mass	I	13-Jun-2035	02-Jan-2036	10.7	8.0	2.73
		03-Jul-2035		10.8	1.2	2.75
Maximum Launch Mass	II	10-May-2035	20-Dec-2035	17.5	1.1	2.86
		30-May-2035		12.8	4.0	2.86
Maximum Launch Mass	III-	11-Nov-2034	24-Dec-2036	11.4	33.3	4.32
		01-Dec-2034		12.3	22.4	4.20
Maximum Launch Mass	IV-	22-Oct-2034	18-Jan-2037	10.2	18.8	2.84
		11-Nov-2034		9.7	34.7	2.85
Maximum Launch Mass	III+	24-Nov-2034	24-Dec-2036	12.2	9.7	5.97
		14-Dec-2034		12.3	14.9	5.75
Maximum Launch Mass	IV+	Not Possible				
Maximum Captured Mass	I	14-Jun-2035	07-Jan-2036	10.7	10.4	2.71
		04-Jul-2035		10.9	2.4	2.69
Maximum Captured Mass	II	10-May-2035	20-Dec-2035	17.5	1.1	2.86

Optimization Criteria	Trajectory Type	Departure Date (dd-mmm-yyyy)	Arrival Date (dd-mmm-yyyy)	Launch Energy, C3 (km <sup>2</sup> /s <sup>2</sup> )	Declination of the Launch Asymptote, DLA (deg)	Approach V-Infinity, VHP (km/s)	
		30-May-2035		12.8	4.0	2.86	
Maximum Captured Mass	III-	12-Nov-2034	04-Jan-2037	10.7	40.1	3.38	
		02-Dec-2034		16.4	21.9	3.20	
Maximum Captured Mass	IV-	21-Oct-2034	04-Feb-2037	10.3	22.2	2.65	
		10-Nov-2034		9.6	35.5	2.62	
Maximum Captured Mass	III+	26-Nov-2034	24-Dec-2036	11.3	11.3	5.77	
		16-Dec-2034		12.8	14.9	5.82	
Maximum Captured Mass	IV+			Not Possible			

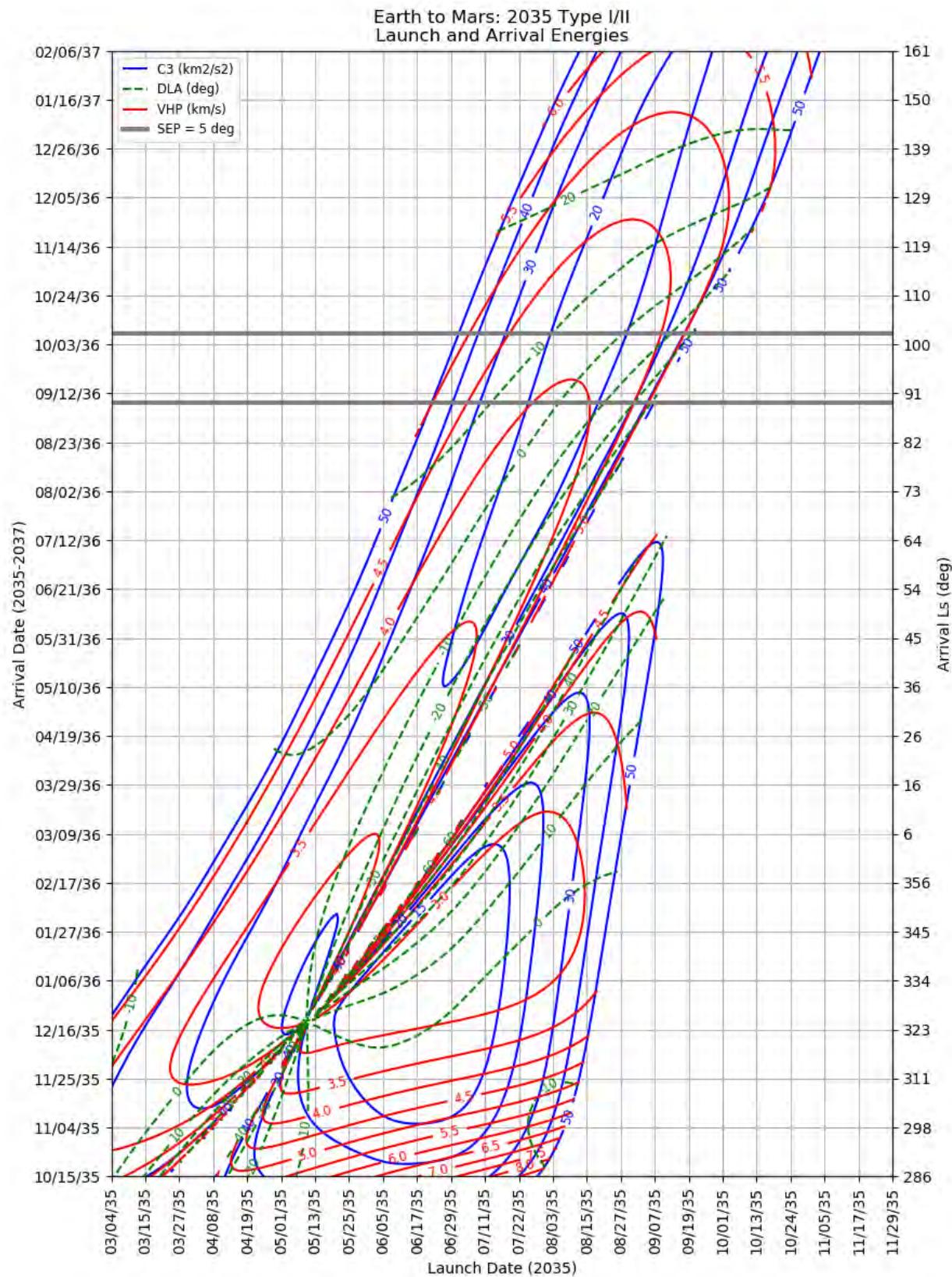
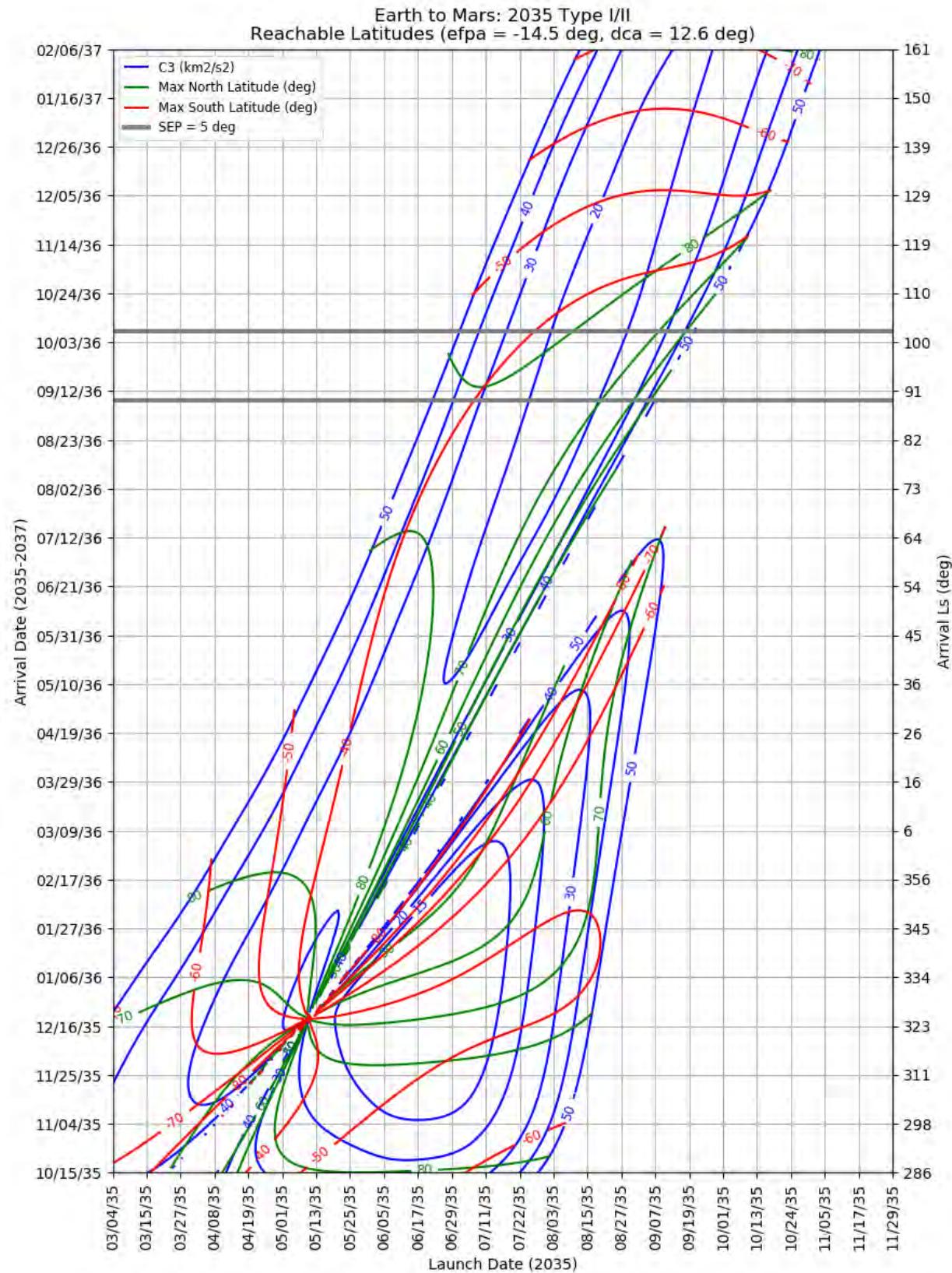
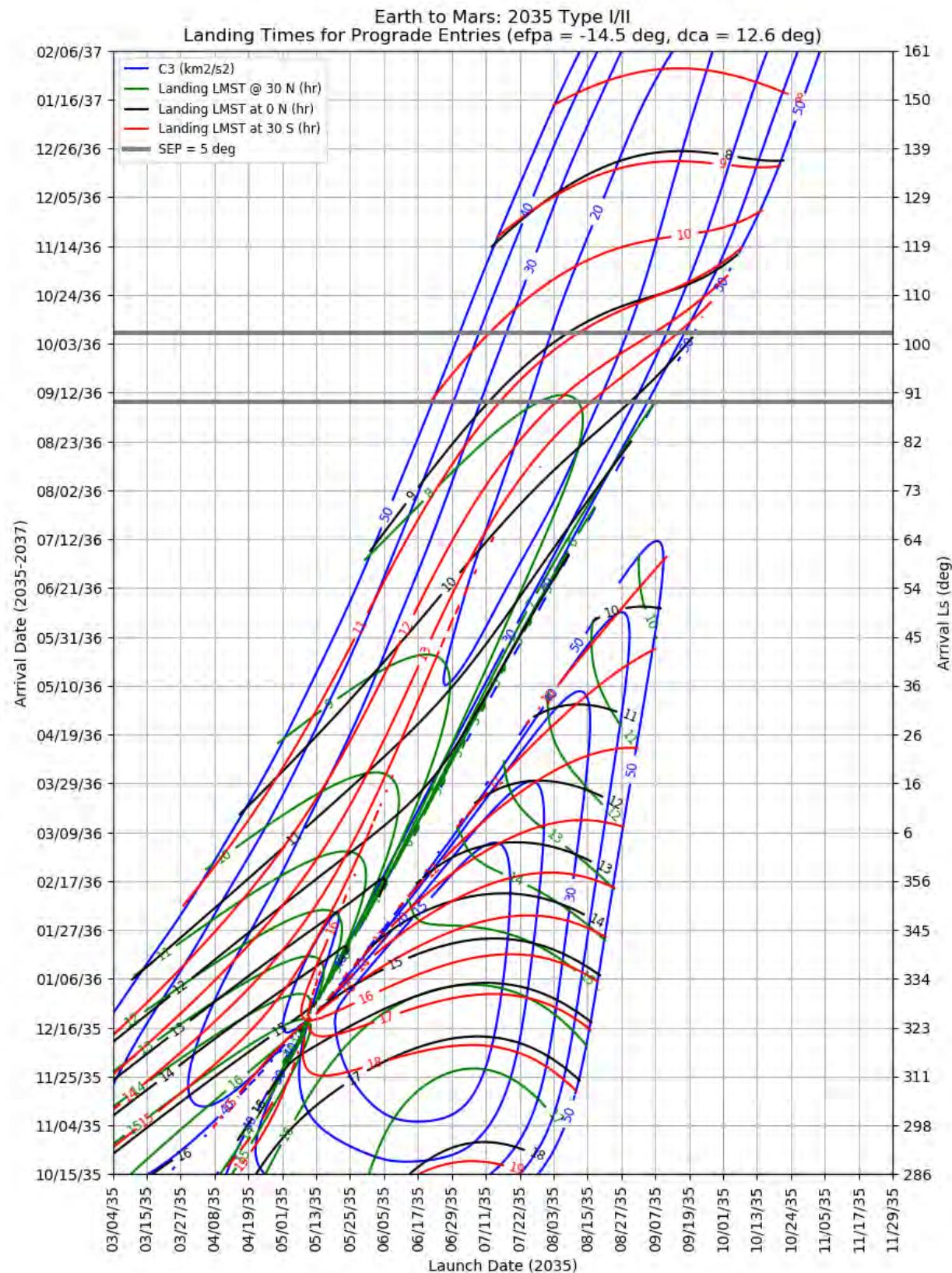


Figure 438: Earth to Mars 2035 Type I/II - Launch and Arrival Energy



**Figure 439: Earth to Mars 2035 Type I/II – Maximum Reachable North and South Latitude**



**Figure 440: Earth to Mars 2035 Type I/II – Landing LMST for Prograde Entries**

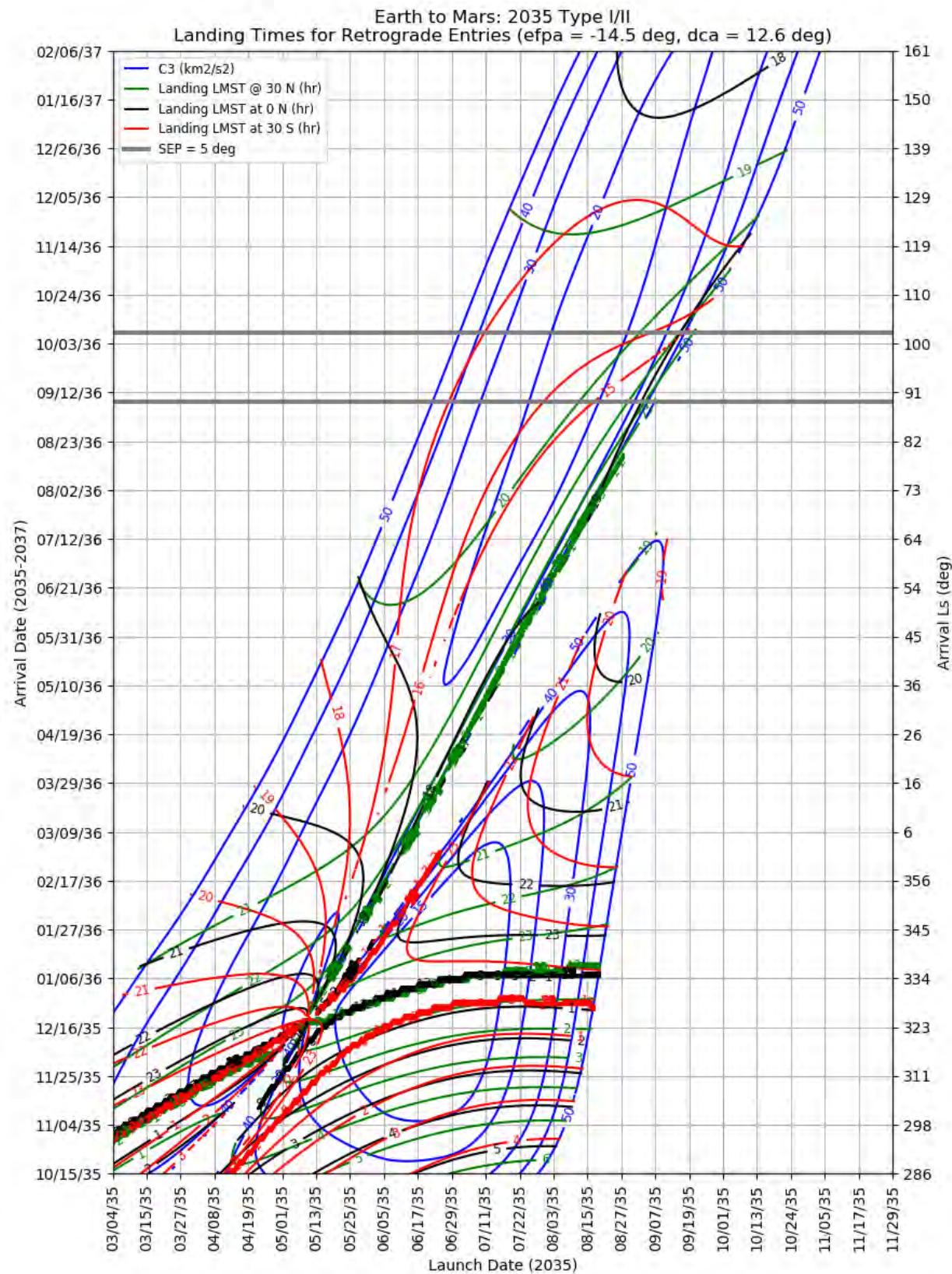


**Figure 441: Earth to Mars 2035 Type I/II – Landing LMST for Retrograde Entries**

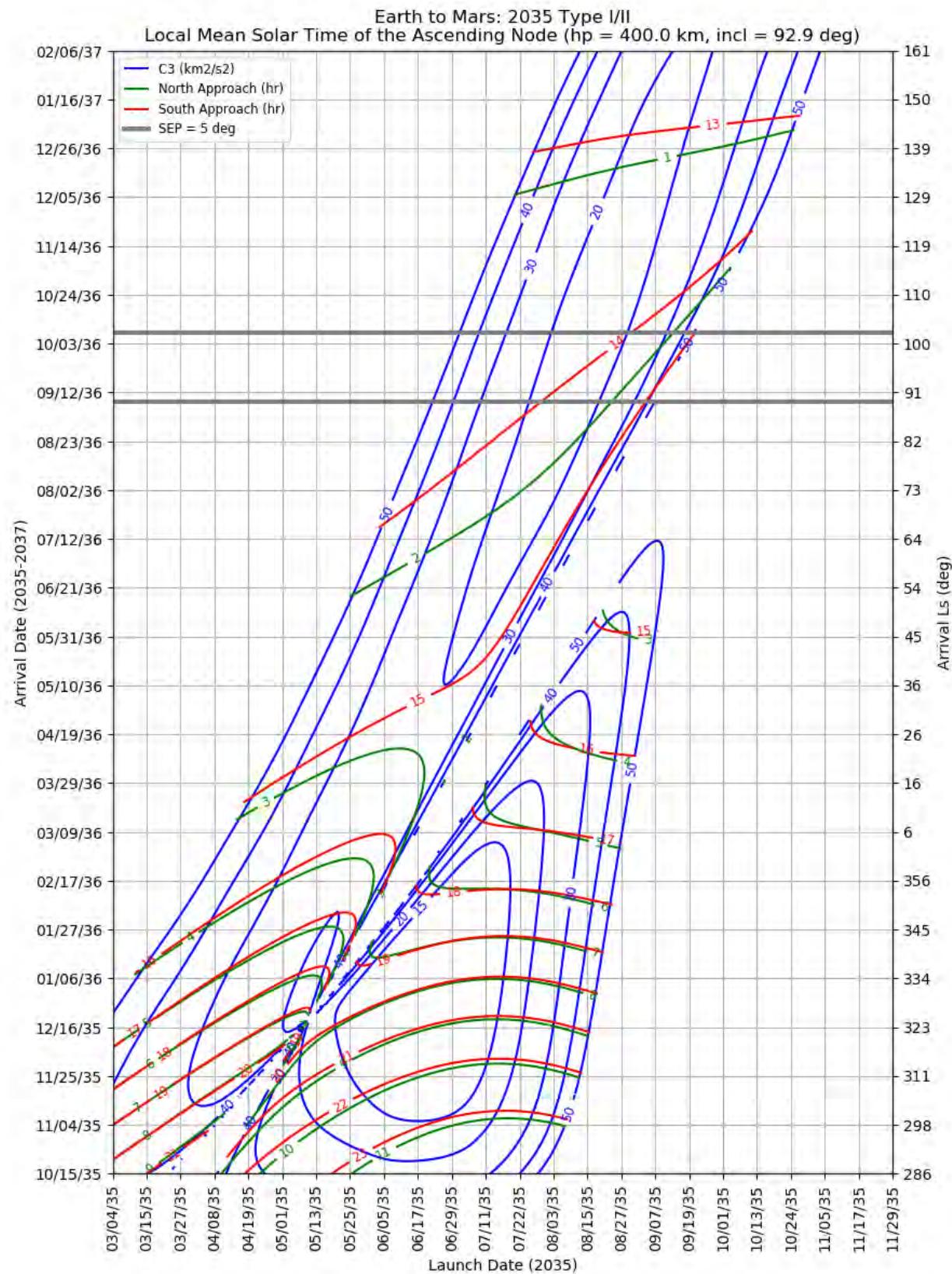


**Figure 442: Earth to Mars 2035 Type I/II – LMST of the Ascending Node for North and South Approaches**

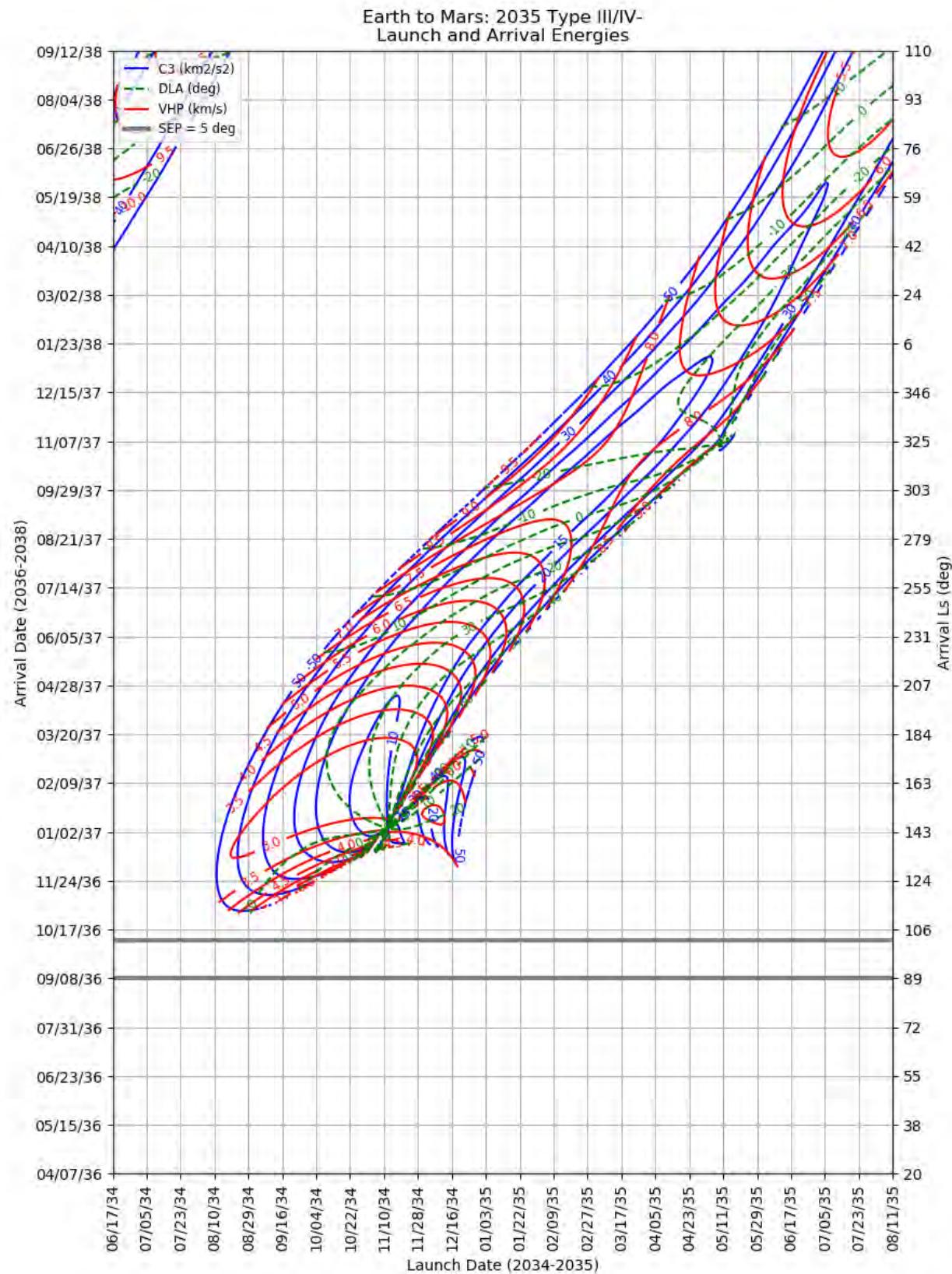


**Figure 443: Earth to Mars 2035 Type III/IV- – Launch and Arrival Energy**

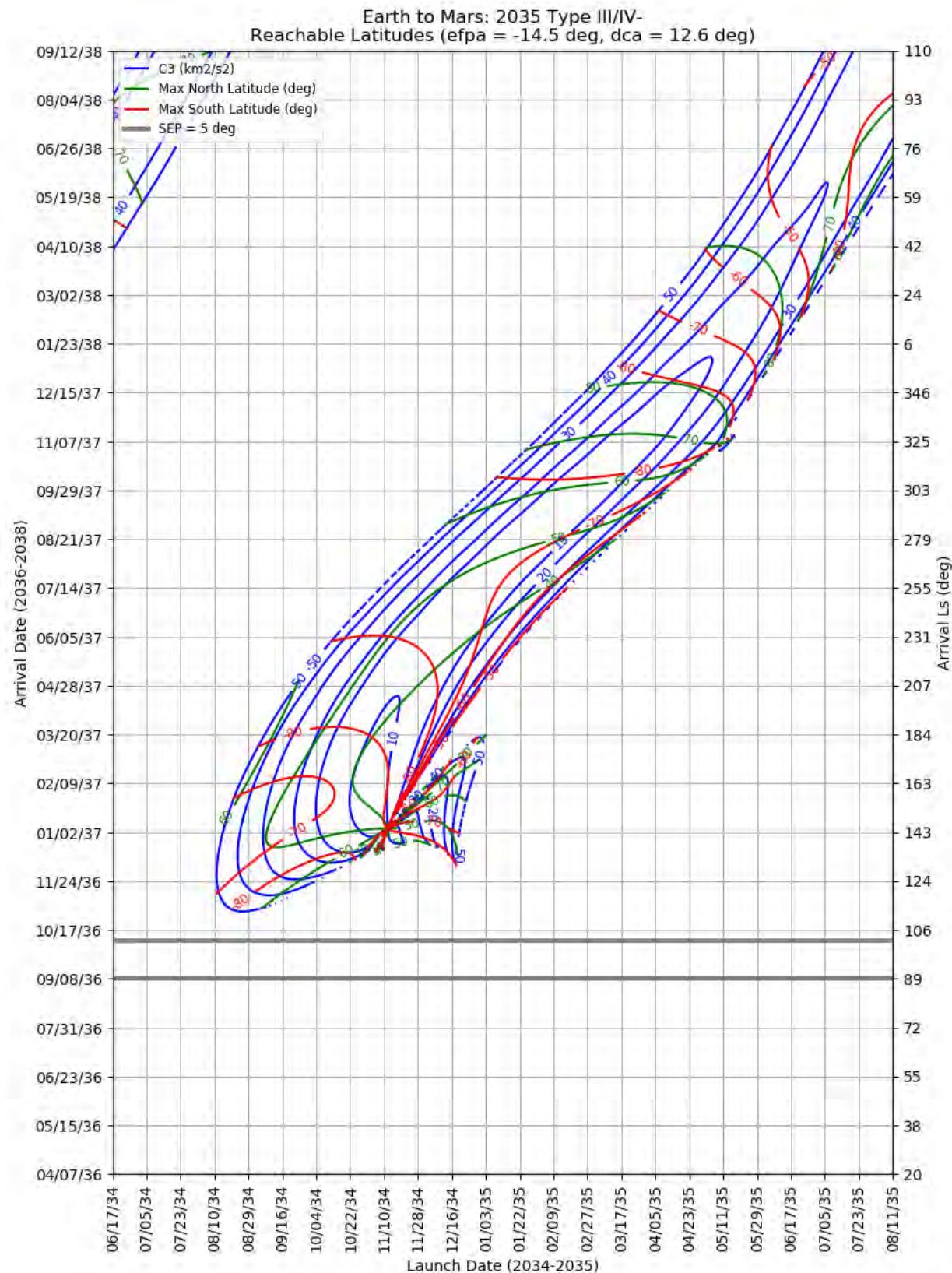


**Figure 444: Earth to Mars 20352 Type III/IV- – Maximum Reachable North and South Latitude**

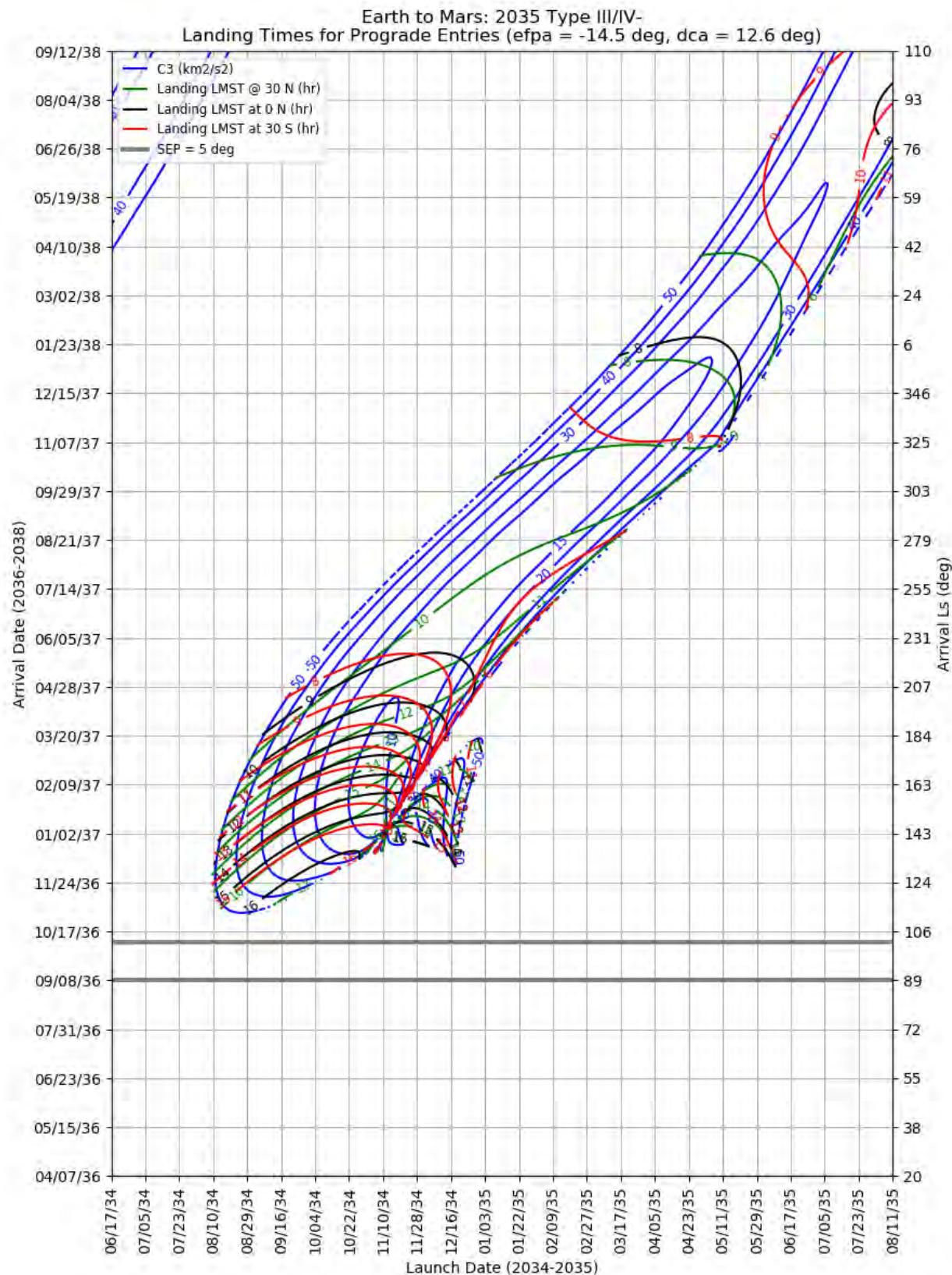


**Figure 445: Earth to Mars 2035 Type III/IV- – Landing LMST for Prograde Entries**

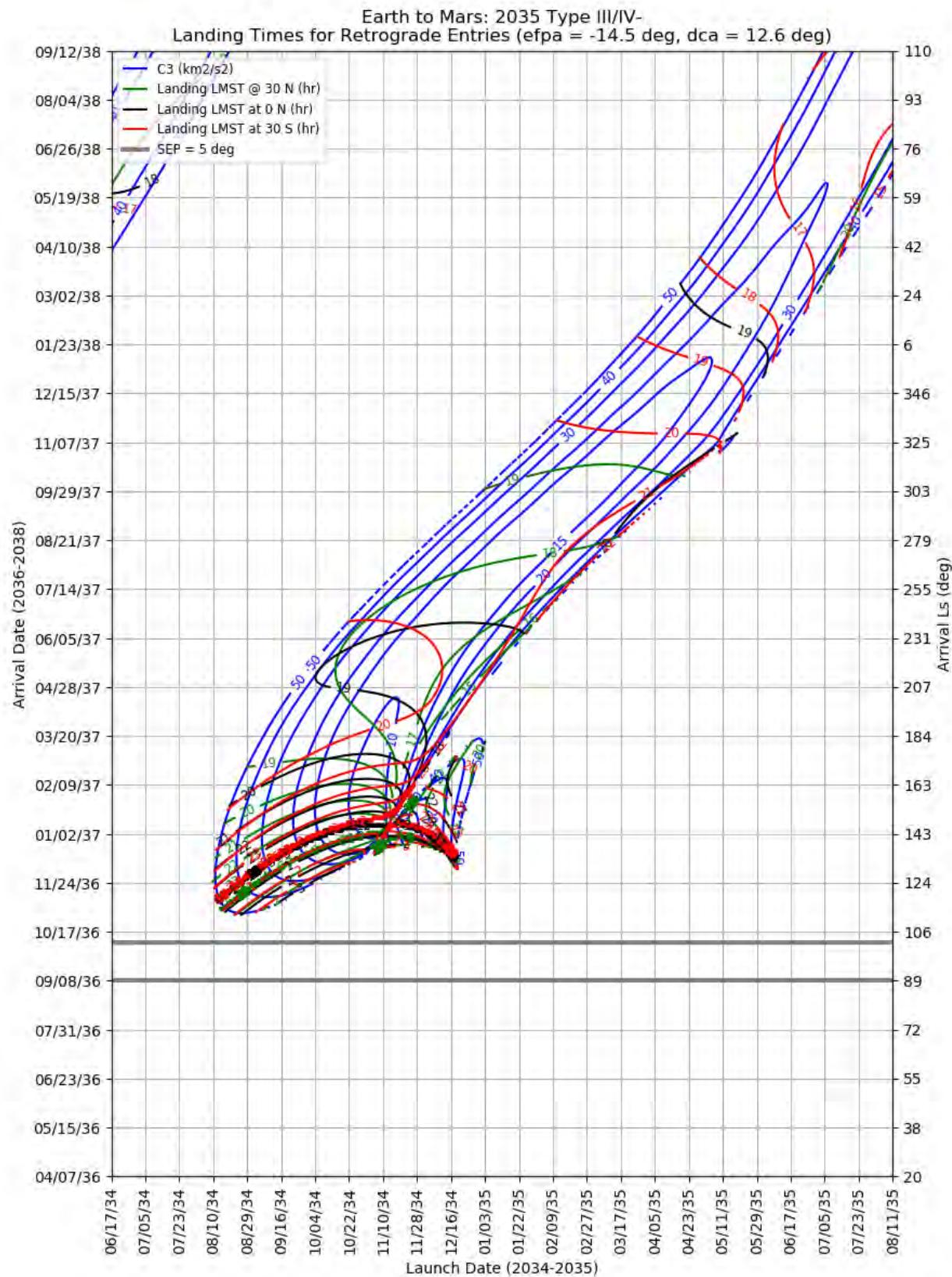
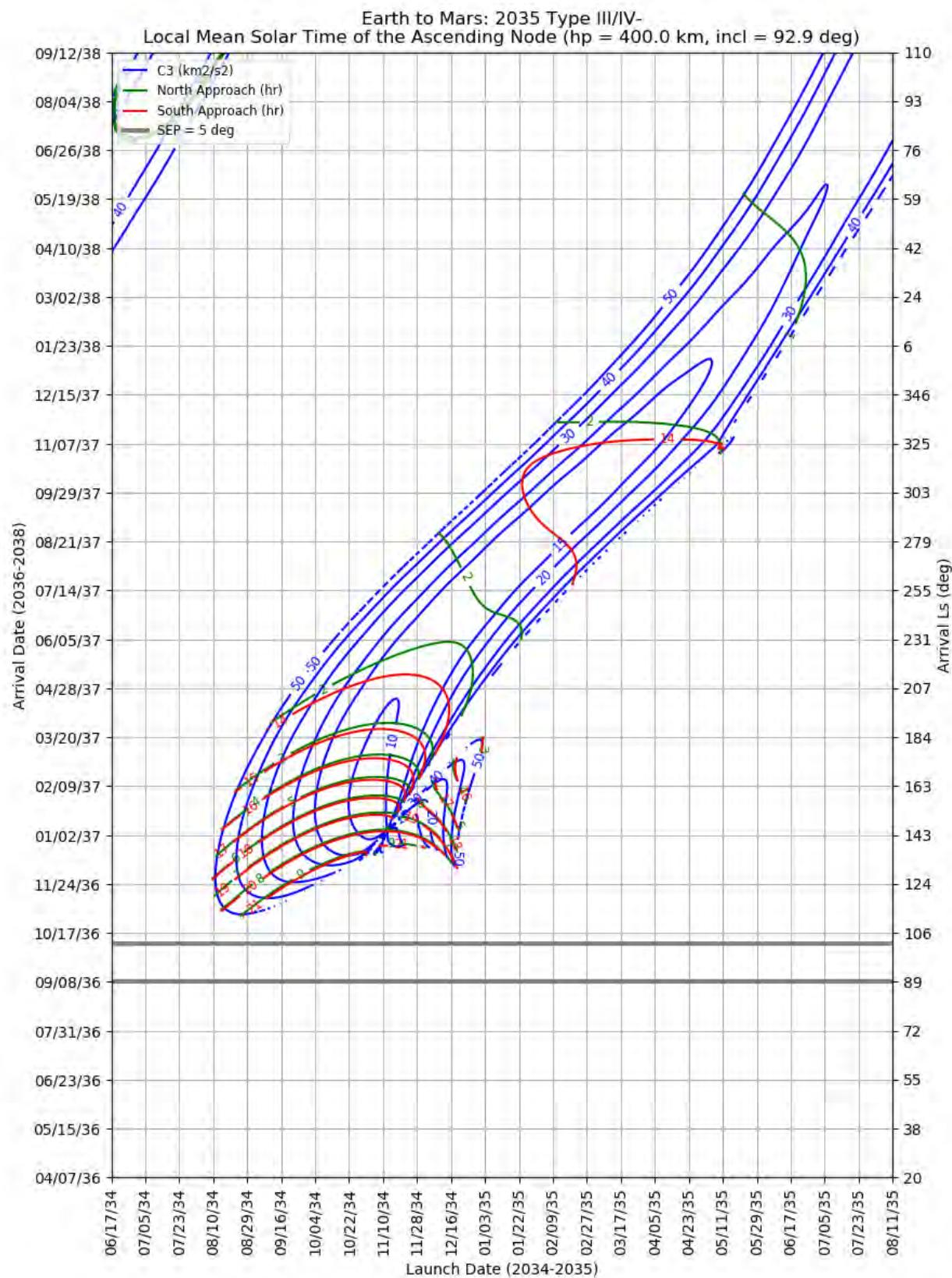


Figure 446: Earth to Mars 2035 Type III/IV- – Landing LMST for Retrograde Entries



**Figure 447: Earth to Mars 2035 Type III/IV- – LMST of the Ascending Node for North and South Approaches**

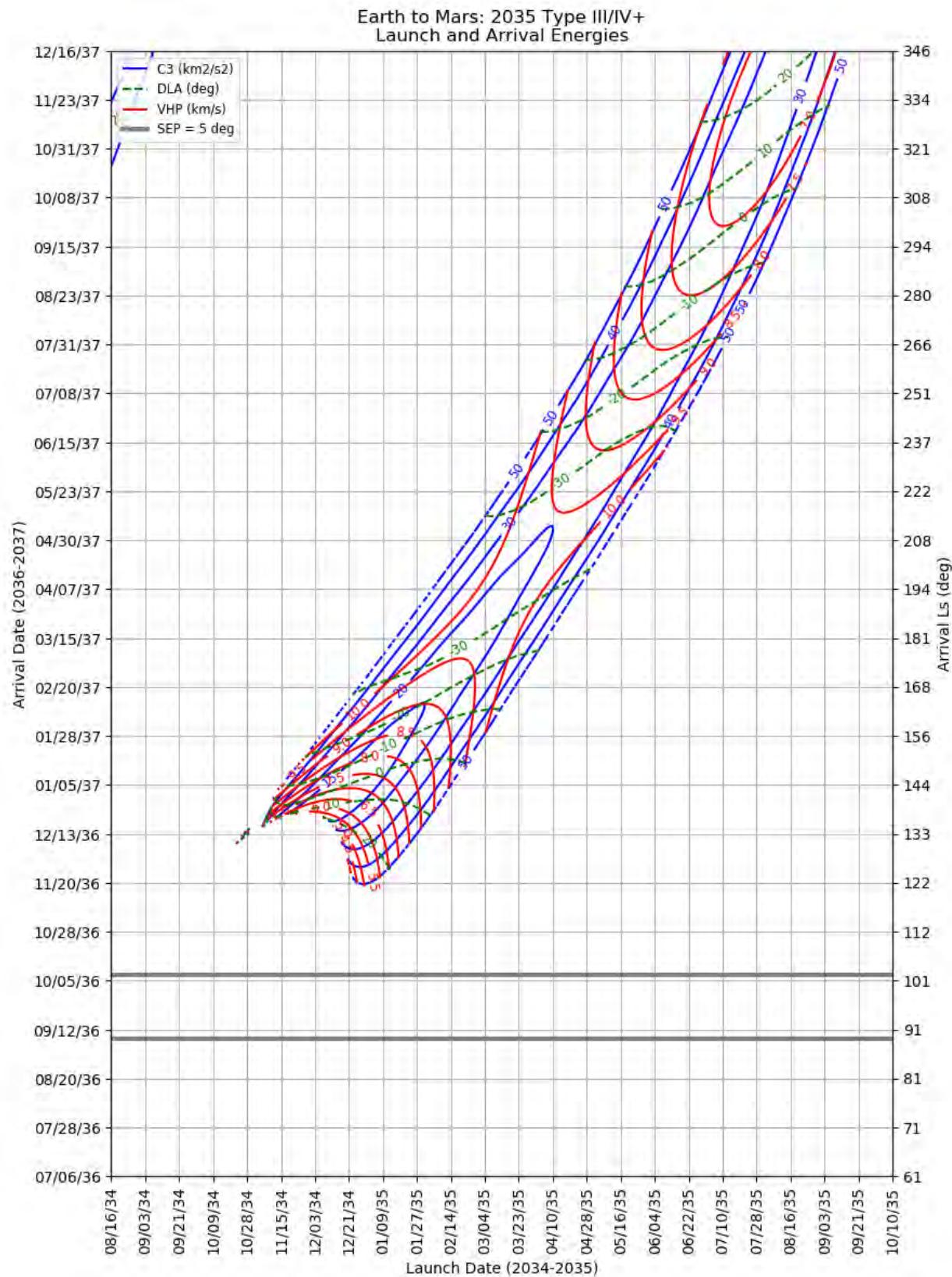
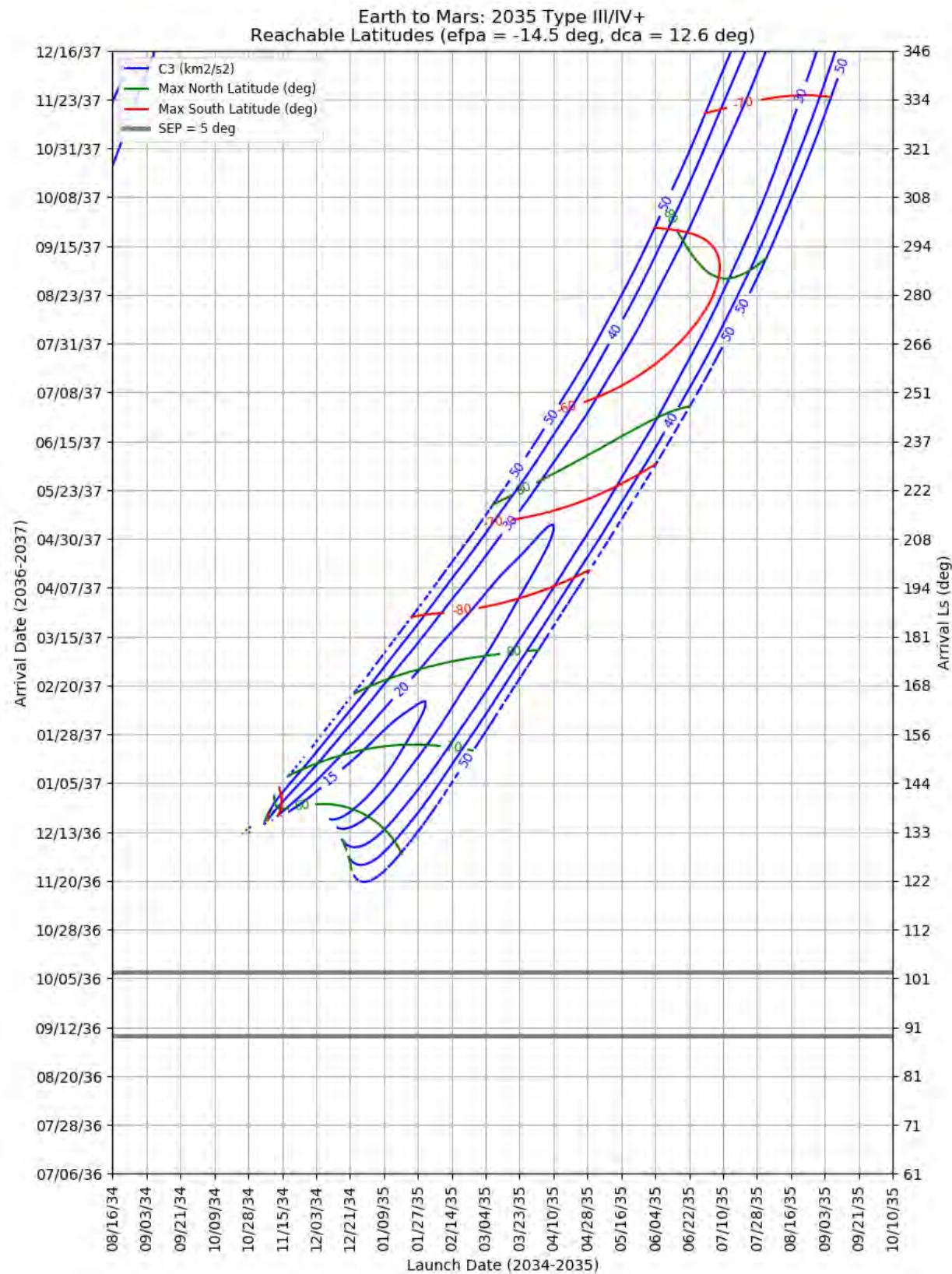
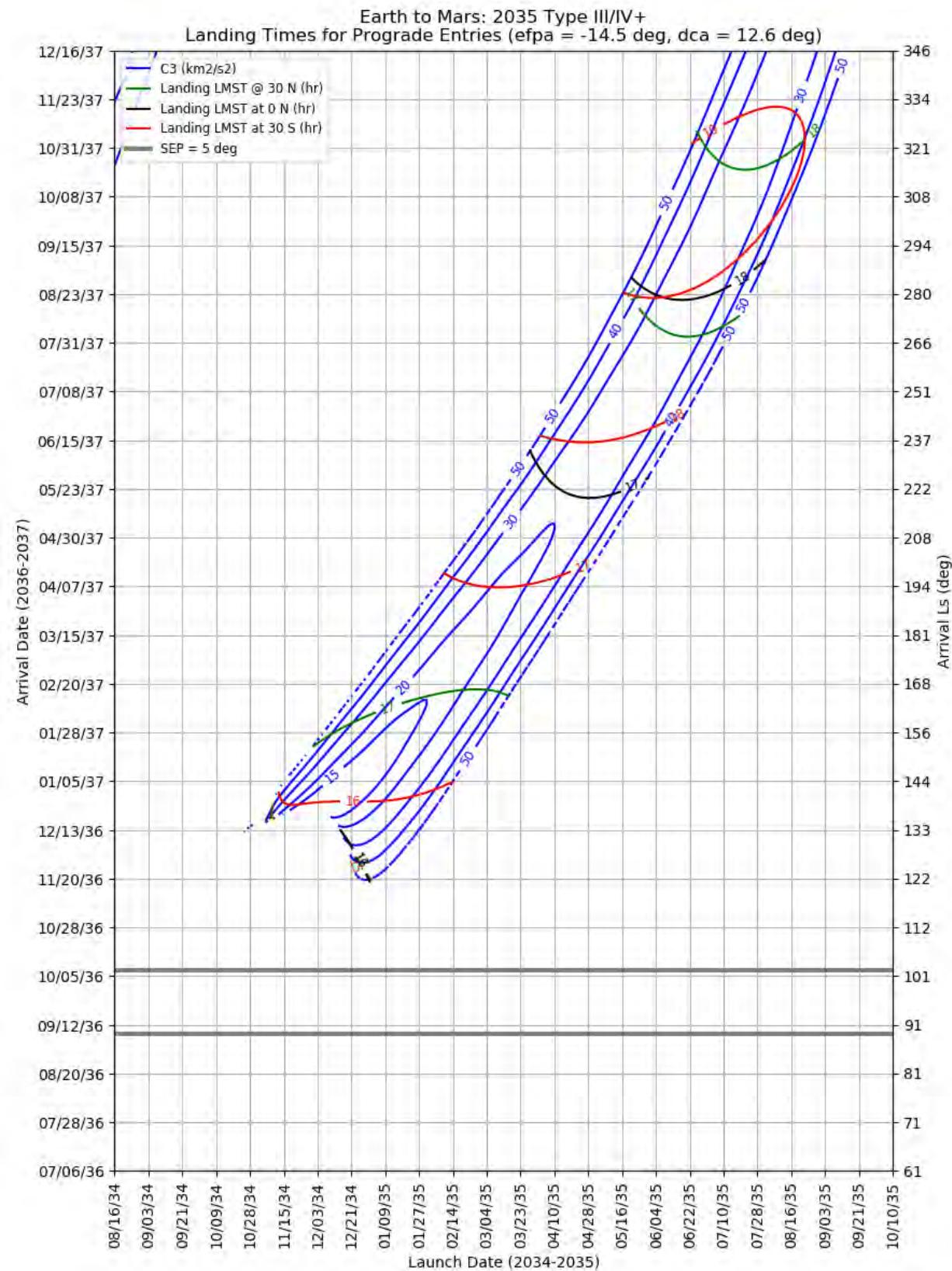
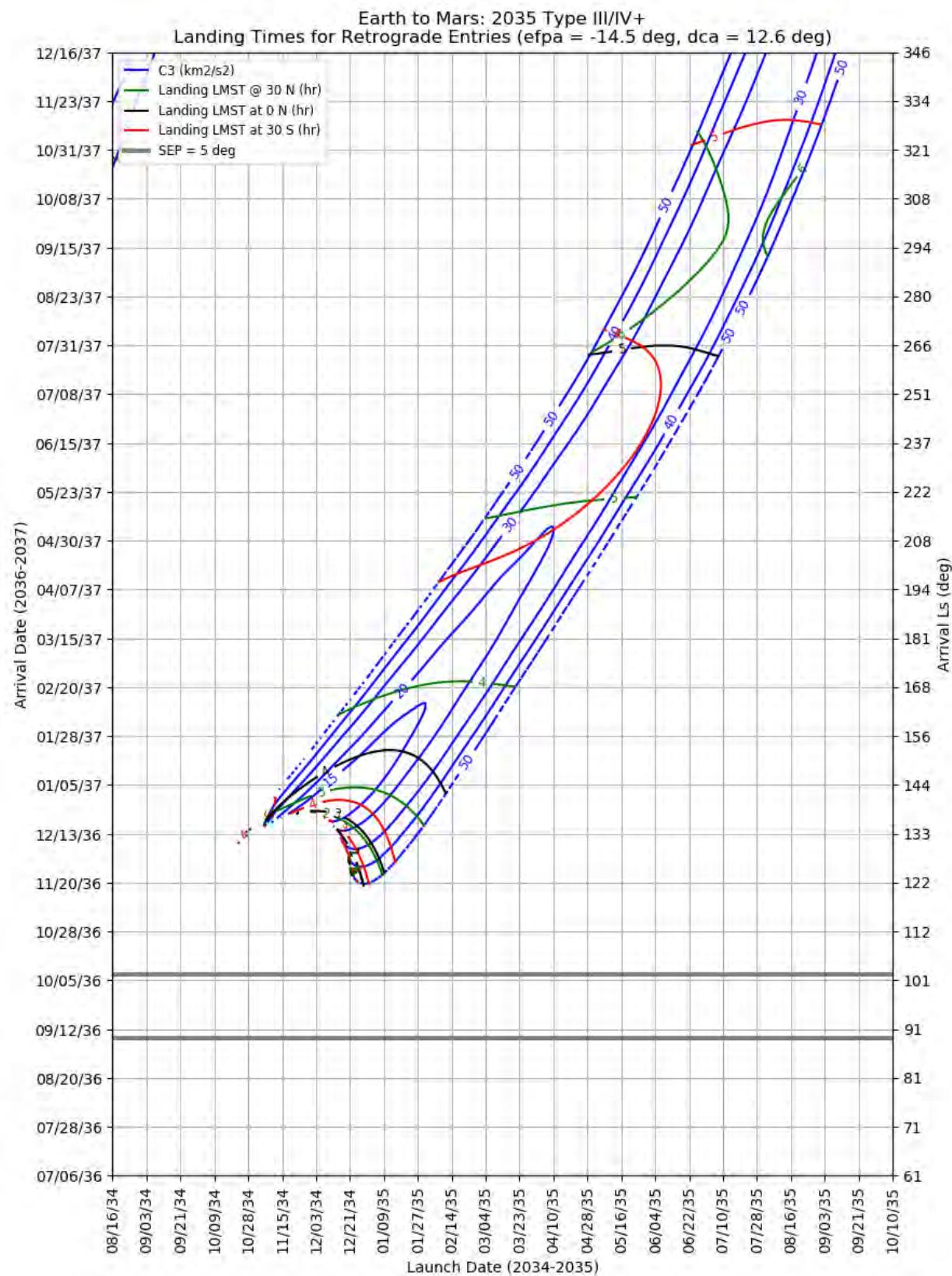


Figure 448: Earth to Mars 2035 Type III/IV+ – Launch and Arrival Energy



**Figure 449: Earth to Mars 2035 Type III/IV+ – Maximum Reachable North and South Latitude**





**Figure 451: Earth to Mars 2035 Type III/IV+ – Landing LMST for Retrograde Entries**

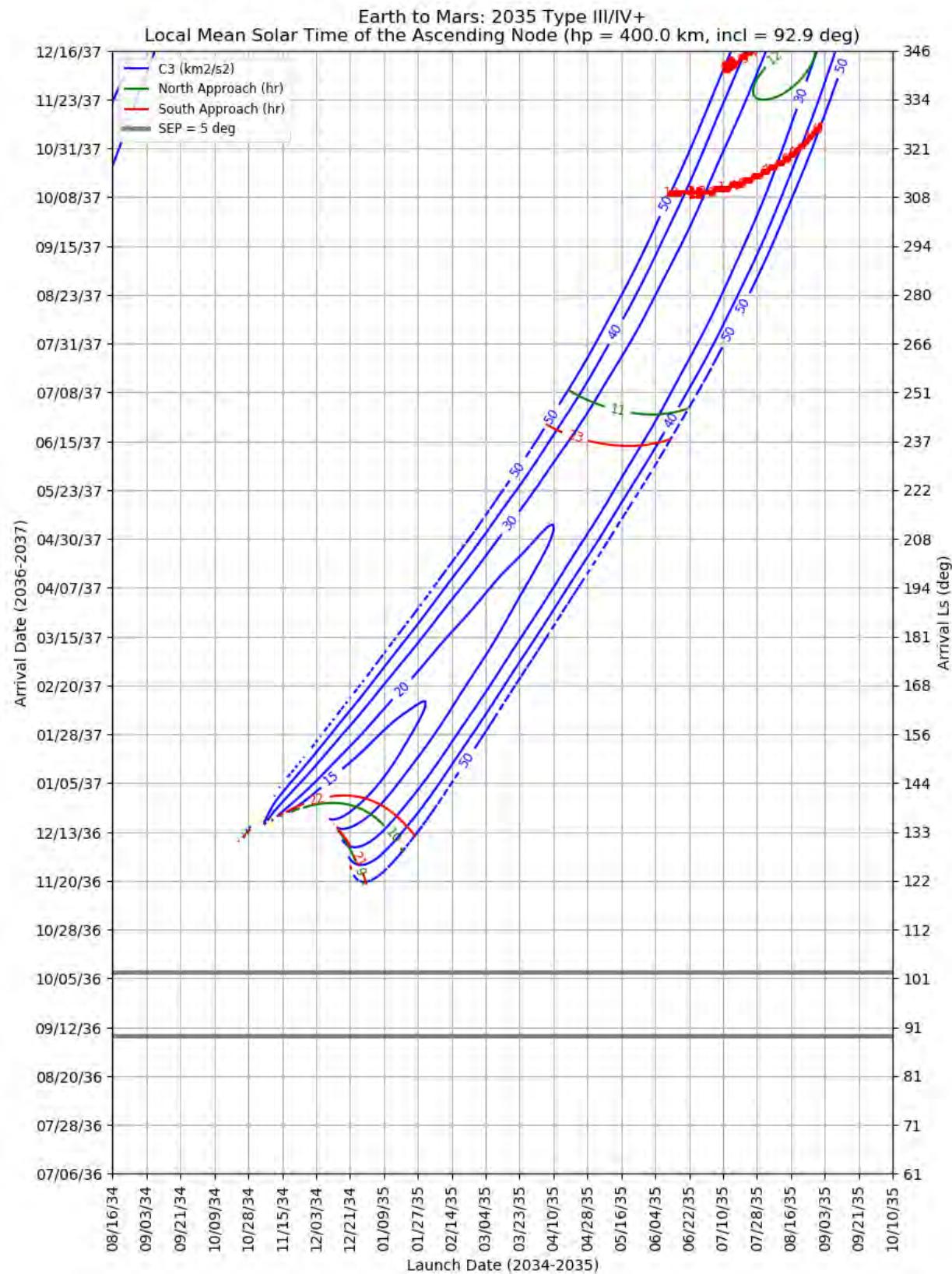


Figure 452: Earth to Mars 2035 Type III/IV+ – LMST of the Ascending Node for North and South Approaches

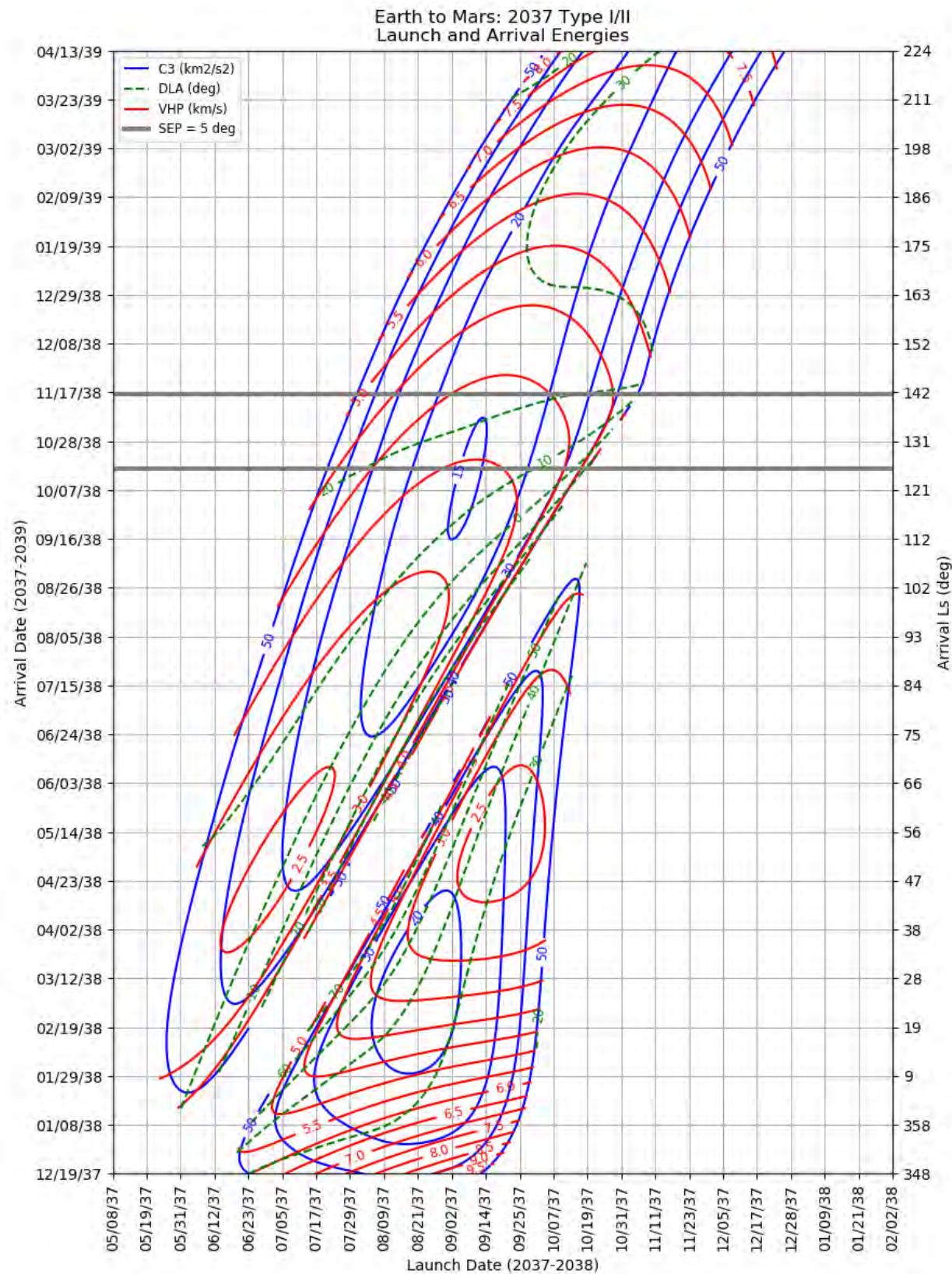
### 10.5.9 Earth to Mars 2037

This section contains porkchop plots for the Earth-to-Mars 2037 opportunities. Table 35 contains the optimal single-day transfers for minimum launch energy (C3) and arrival velocity (VHP) as well as the maximum launch-mass and captured-mass launch periods for each trajectory type within the opportunity. These data should only be used for preliminary analysis and planning purposes.

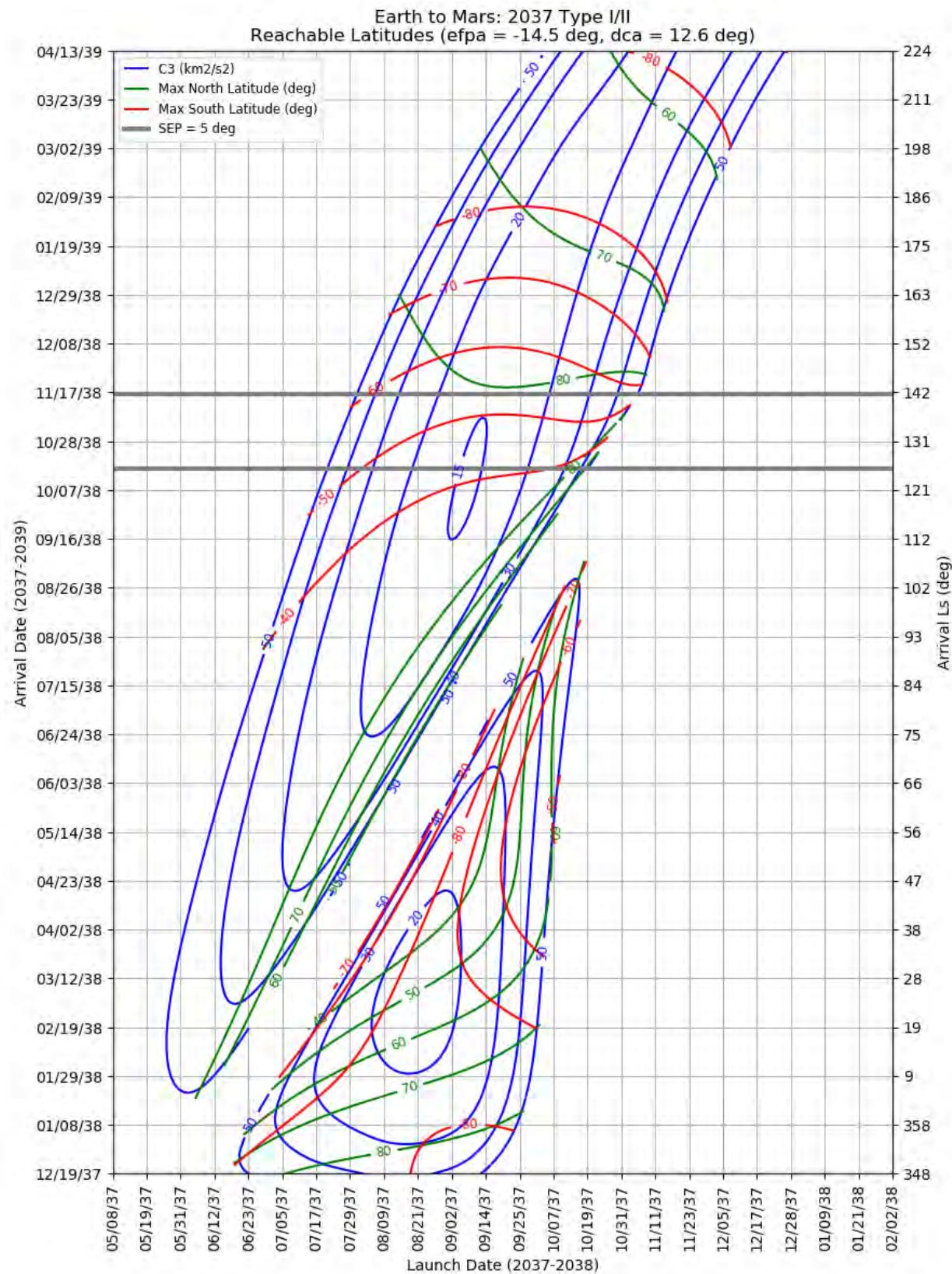
**Table 35: Earth to Mars 2037 Optimal Launch/Arrival Data**

Optimization Criteria	Trajectory Type	Departure Date (dd-mmm-yyyy)	Arrival Date (dd-mmm-yyyy)	Launch Energy, C3 (km <sup>2</sup> /s <sup>2</sup> )	Declination of the Launch Asymptote, DLA (deg)	Approach V-Infinity, VHP (km/s)
<b>Single-Day Optimization</b>						
Minimum C3	I	21-Aug-2037	07-Mar-2038	17.1	39.9	3.37
Minimum C3	II	08-Sep-2037	11-Oct-2038	14.8	14.2	3.39
Minimum C3	III-	14-Dec-2036	21-Dec-2038	9.0	-8.1	4.85
Minimum C3	IV-	20-Nov-2036	12-Feb-2039	8.9	31.4	2.91
Minimum C3	III+	22-Dec-2036	21-Dec-2038	9.3	-9.3	5.74
Minimum C3	IV+	14-Nov-2036	07-Dec-2038	33.0	6.7	7.42
Minimum VHP	I	20-Sep-2037	11-May-2038	29.2	31.3	2.34
Minimum VHP	II	04-Jul-2037	30-Apr-2038	30.8	1.5	2.42
Minimum VHP	III-	01-Jan-2037	06-Jan-2039	26.1	9.2	3.36
Minimum VHP	IV-	16-Nov-2036	01-Feb-2039	9.0	29.2	2.86
Minimum VHP	III+	11-Jan-2037	27-Nov-2038	44.1	18.2	4.10
Minimum VHP	IV+	07-Nov-2036	02-Dec-2038	34.7	-2.1	7.41
<b>Launch Period Optimization</b>						
Maximum Launch Mass	I	14-Aug-2037	26-Feb-2038	17.7	41.5	3.65
		03-Sep-2037		19.6	30.6	3.77
Maximum Launch Mass	II	28-Aug-2037	06-Oct-2038	16.0	15.3	3.37
		17-Sep-2037		16.3	9.9	3.39
Maximum Launch Mass	III-	04-Dec-2036	21-Dec-2038	11.3	-25.1	4.95
		24-Dec-2036		12.5	5.5	4.28
Maximum Launch Mass	IV-	22-Dec-2036	22-May-2039	10.3	10.9	5.41
		11-Jan-2037		10.4	23.3	5.41
Maximum Launch Mass	III+	16-Dec-2036	21-Dec-2038	10.5	-16.5	6.12
		05-Jan-2037		10.9	-2.6	5.94
Maximum Launch Mass	IV+	Not Possible				
Maximum Captured Mass	I	19-Aug-2037	24-Mar-2038	18.1	48.0	3.02
		08-Sep-2037		21.1	31.1	2.90
Maximum Captured Mass	II	18-Aug-2037	30-Aug-2038	16.6	8.7	2.99

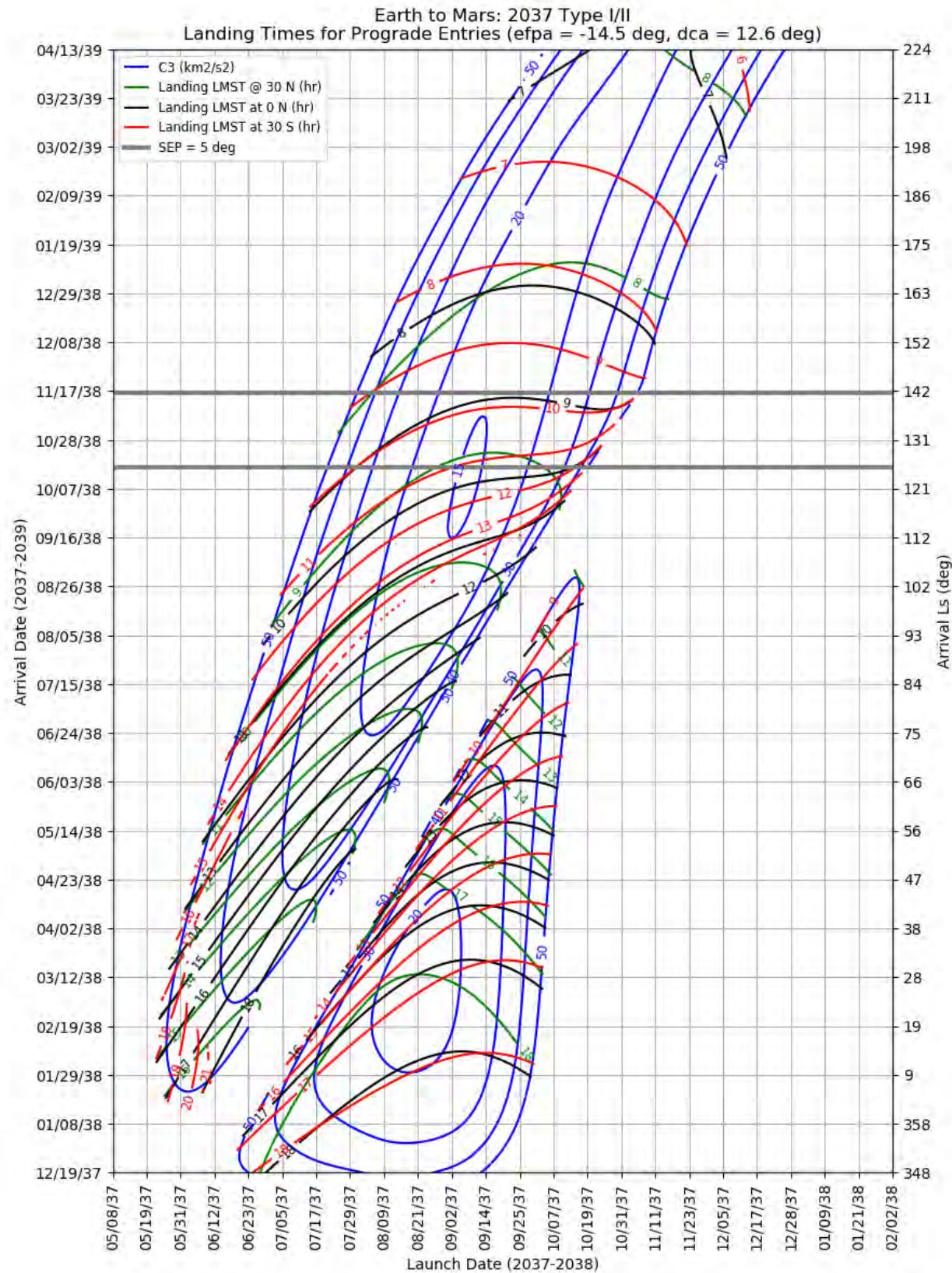
Optimization Criteria	Trajectory Type	Departure Date (dd-mmm-yyyy)	Arrival Date (dd-mmm-yyyy)	Launch Energy, C3 (km <sup>2</sup> /s <sup>2</sup> )	Declination of the Launch Asymptote, DLA (deg)	Approach V-Infinity, VHP (km/s)	
		07-Sep-2037		16.8	-3.0	3.11	
Maximum Captured Mass	III-	04-Dec-2036	22-Dec-2038	11.8	-26.8	4.87	
		24-Dec-2036		13.2	6.1	4.13	
Maximum Captured Mass	IV-	04-Nov-2036	31-Jan-2039	10.7	20.7	2.88	
		24-Nov-2036		9.4	38.1	2.88	
Maximum Captured Mass	III+	18-Dec-2036	21-Dec-2038	9.8	-13.8	5.93	
		07-Jan-2037		11.3	-2.1	6.00	
Maximum Captured Mass	IV+			Not Possible			



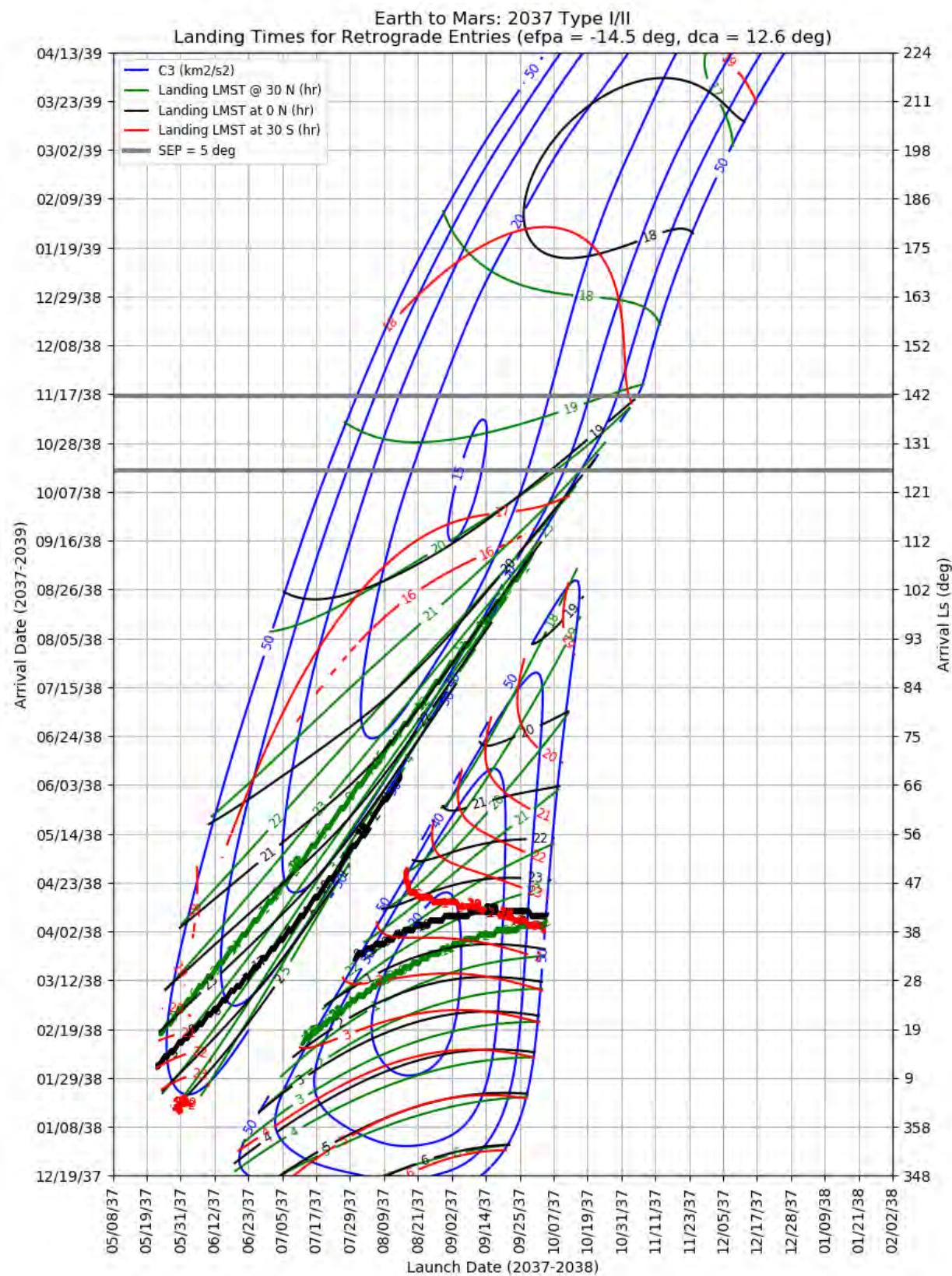
**Figure 453: Earth to Mars 2037 Type I/II - Launch and Arrival Energy**



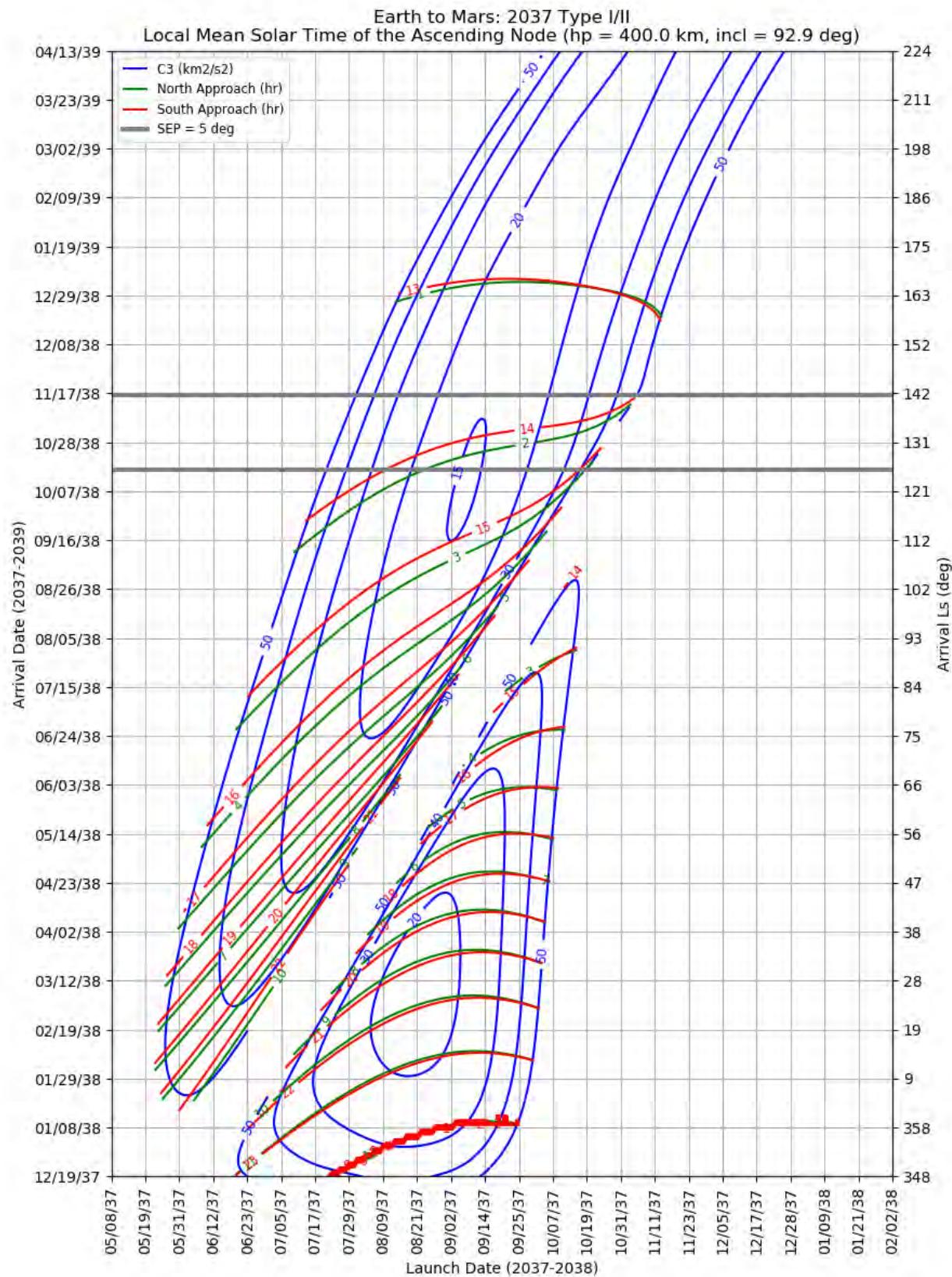
**Figure 454: Earth to Mars 2037 Type I/II – Maximum Reachable North and South Latitude**



**Figure 455: Earth to Mars 2037 Type I/II – Landing LMST for Prograde Entries**



**Figure 456: Earth to Mars 2037 Type I/II – Landing LMST for Retrograde Entries**



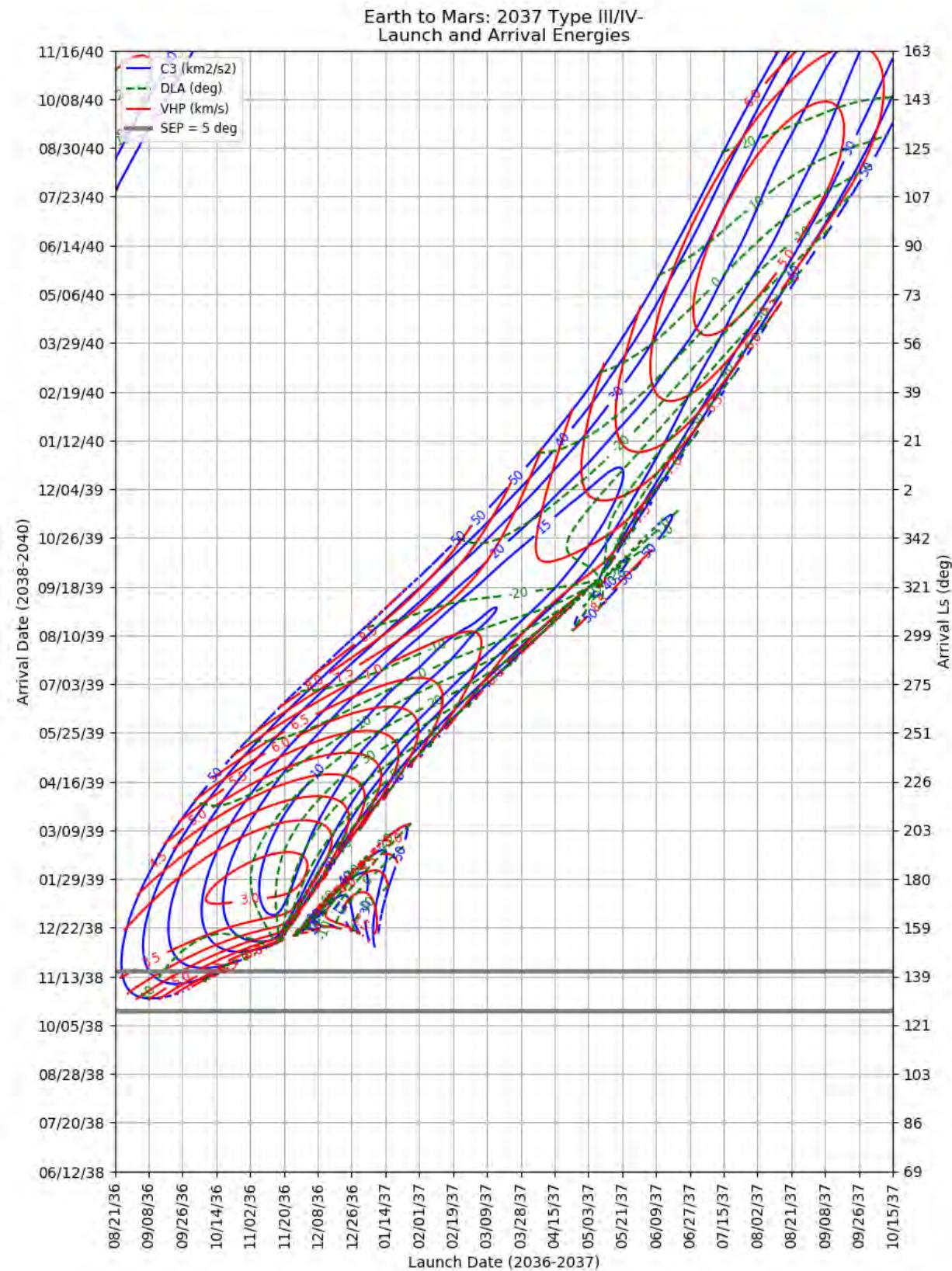
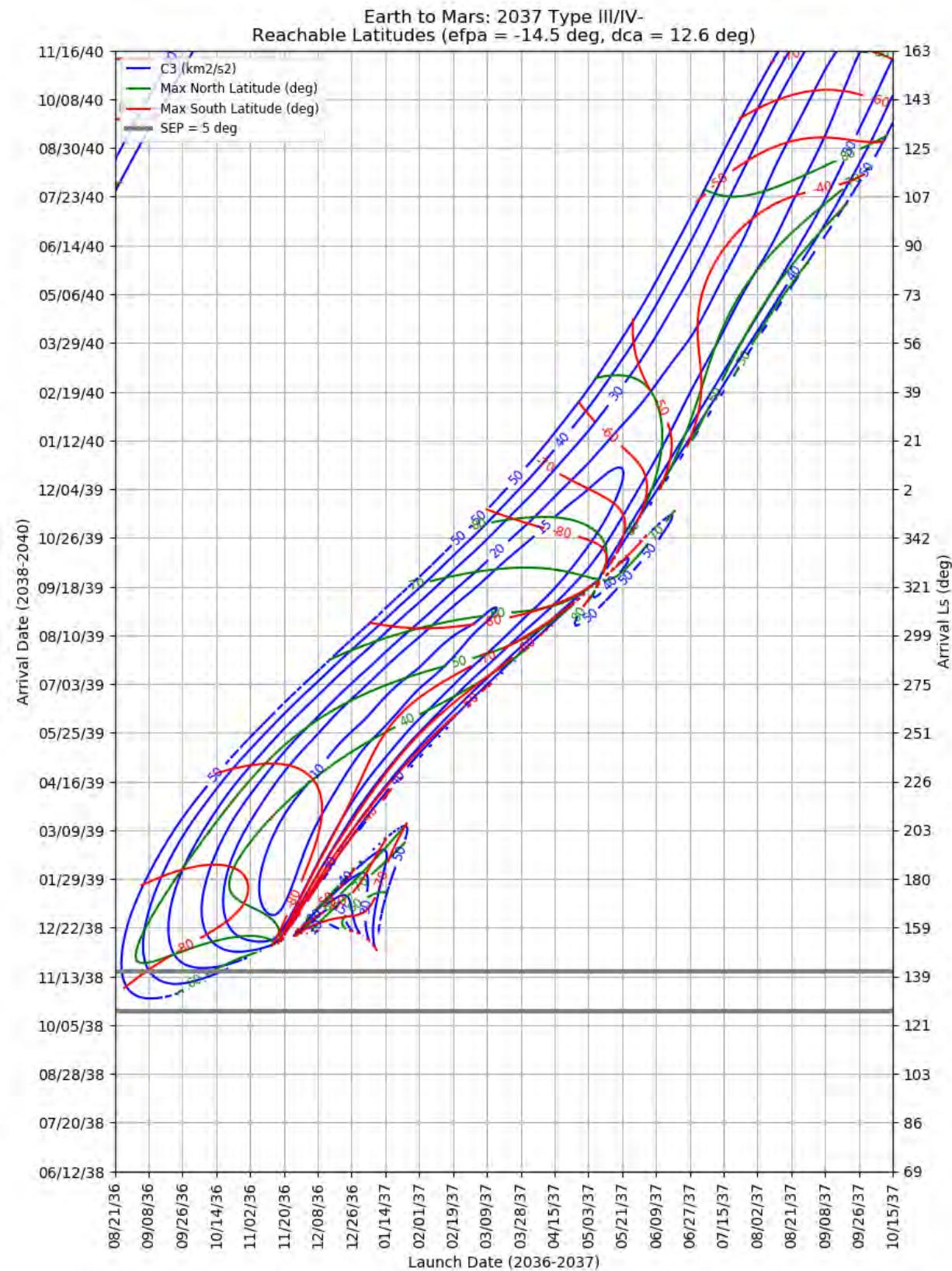
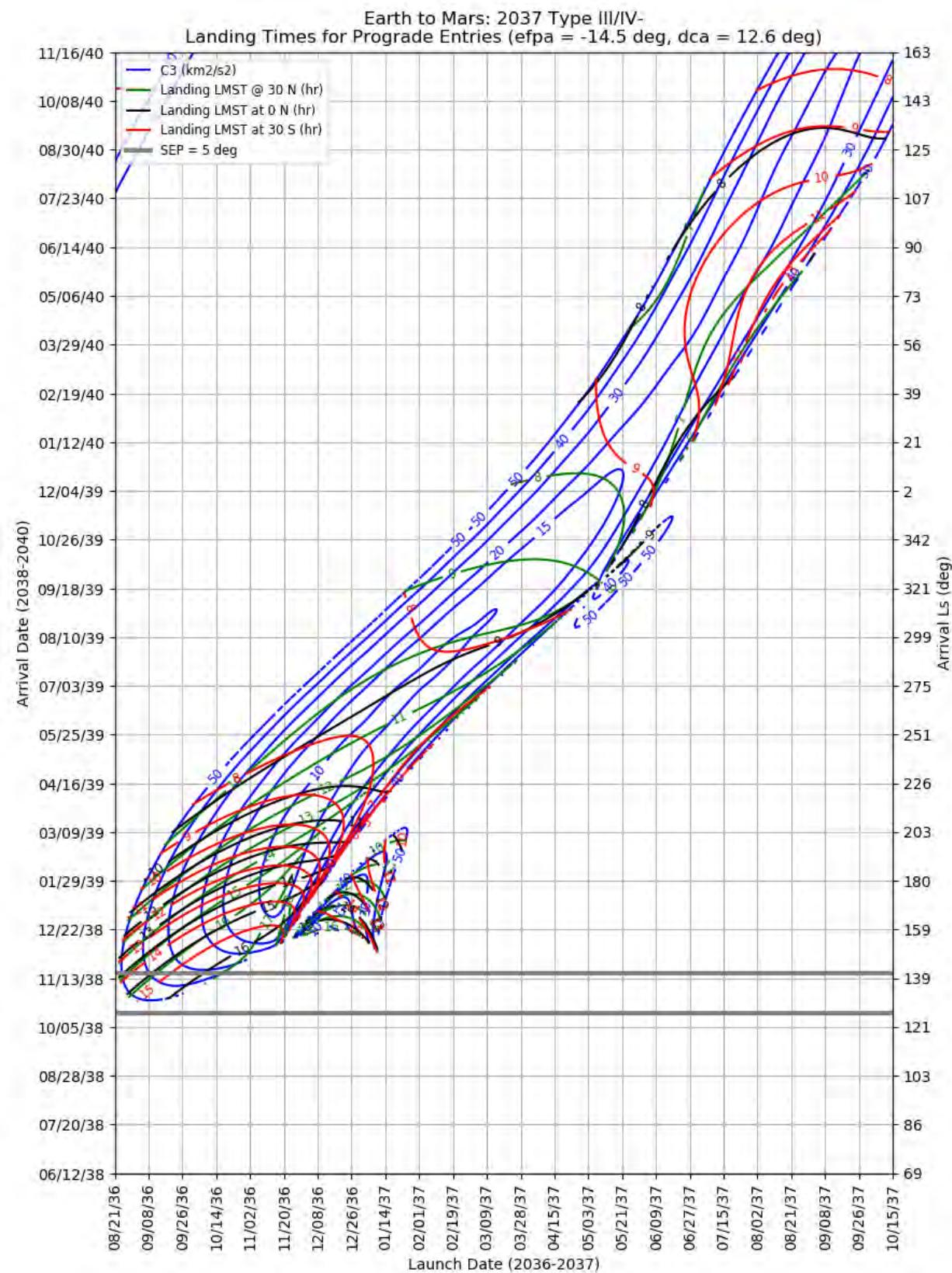


Figure 458: Earth to Mars 2037 Type III/IV- – Launch and Arrival Energy



**Figure 459: Earth to Mars 20372 Type III/IV- – Maximum Reachable North and South Latitude**



**Figure 460: Earth to Mars 2037 Type III/IV- – Landing LMST for Prograde Entries**

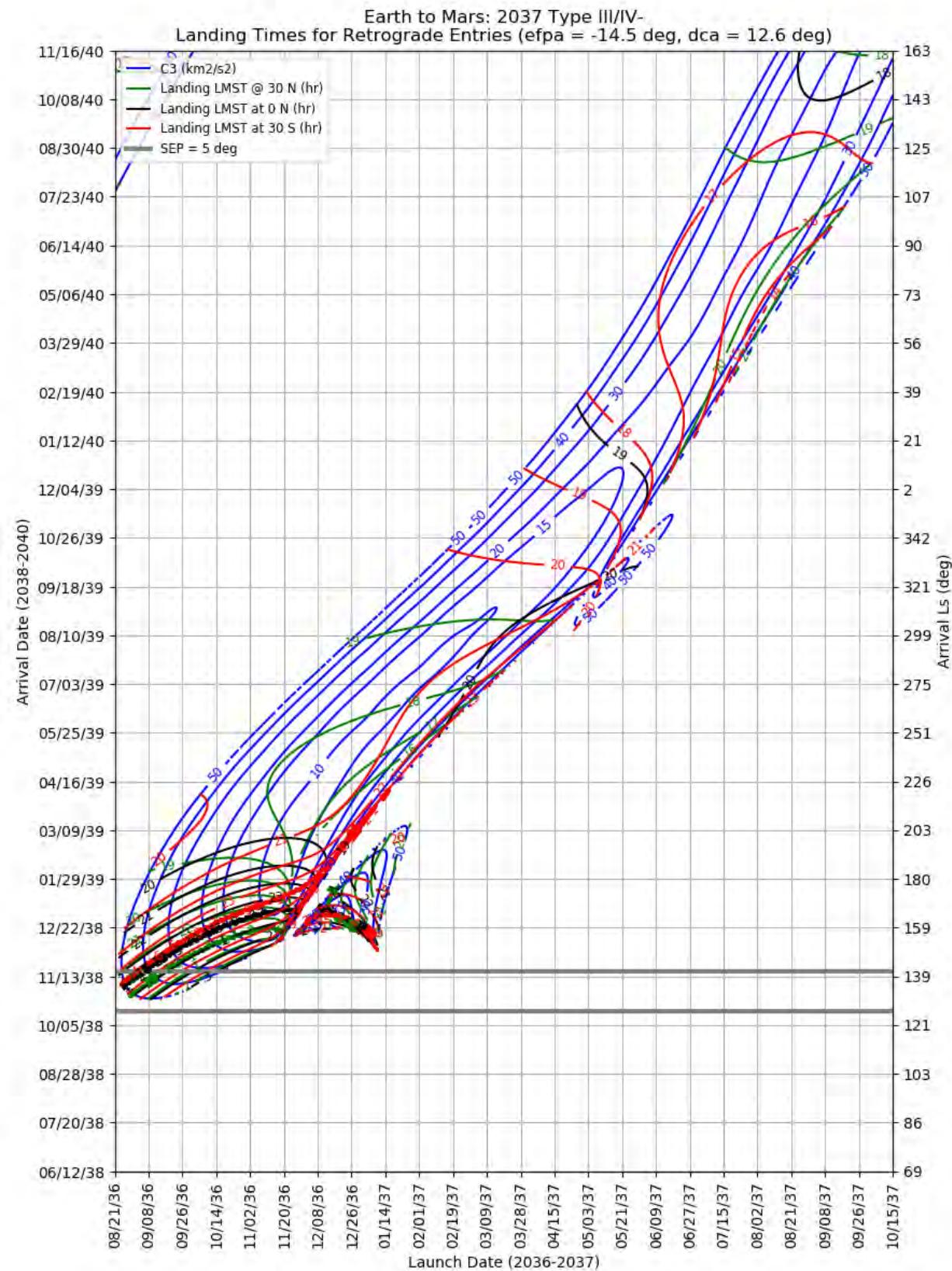
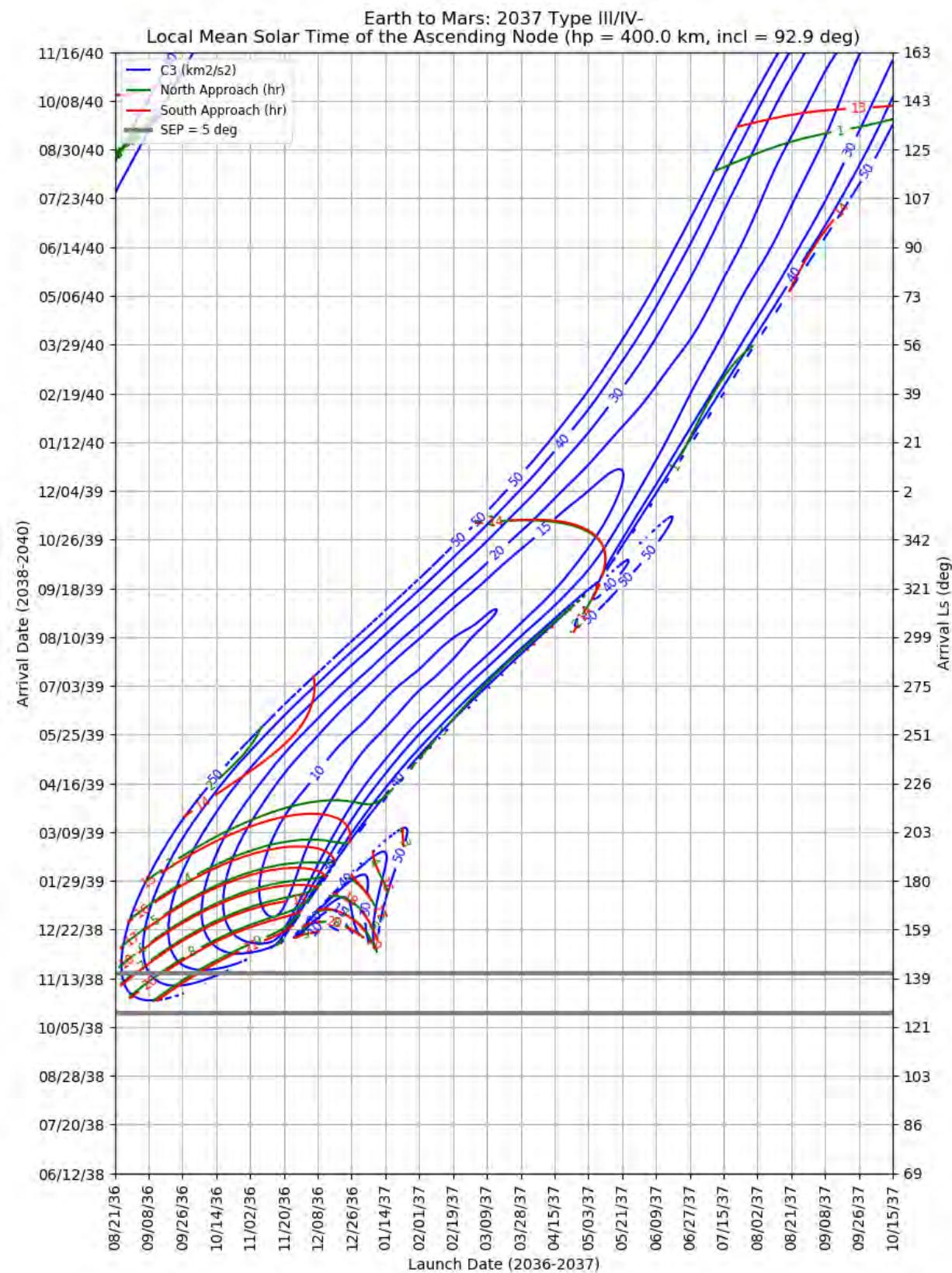
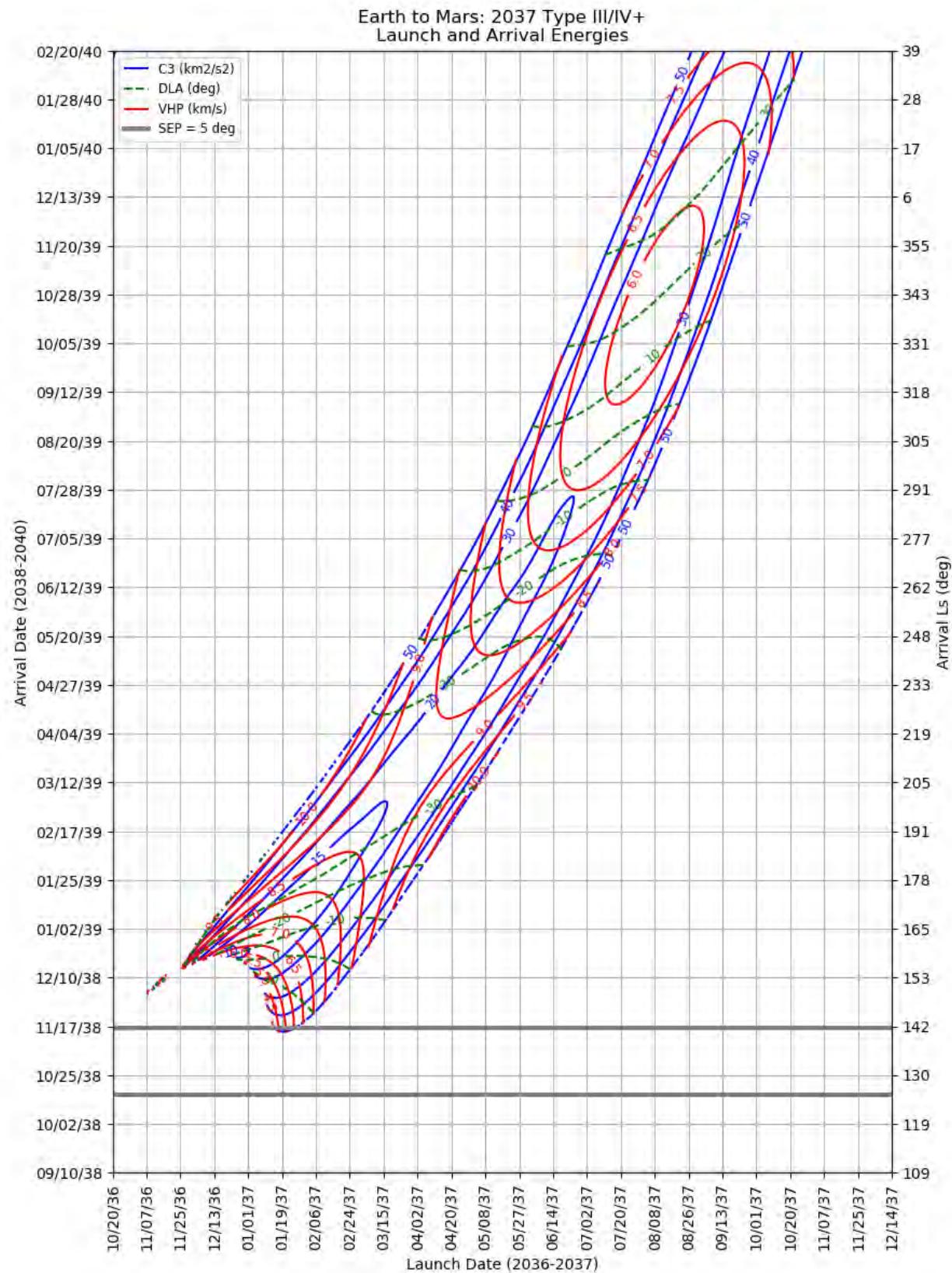


Figure 461: Earth to Mars 2037 Type III/IV- – Landing LMST for Retrograde Entries



**Figure 462: Earth to Mars 2037 Type III/IV- – LMST of the Ascending Node for North and South Approaches**



**Figure 463: Earth to Mars 2037 Type III/IV+ – Launch and Arrival Energy**

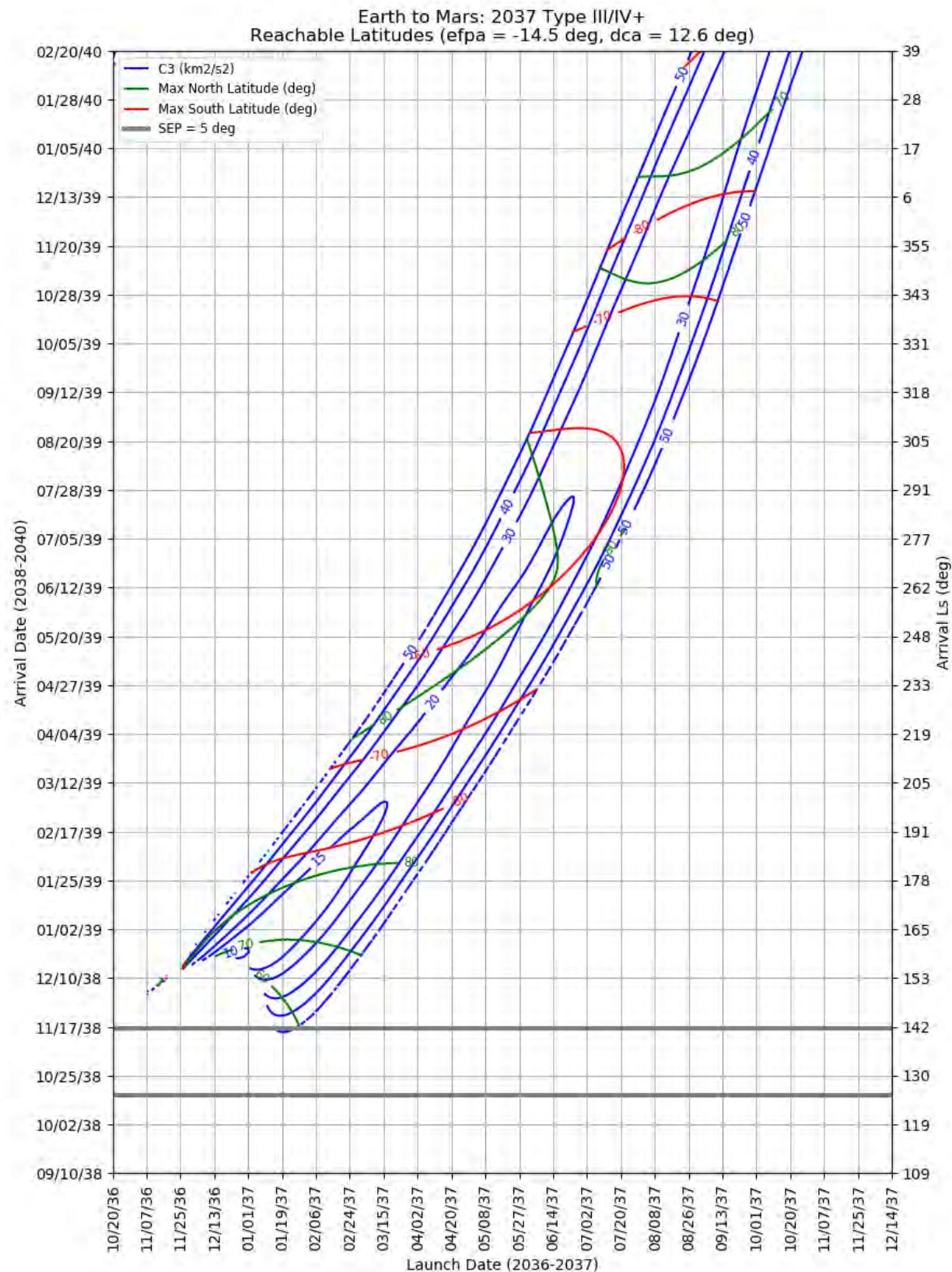


**Figure 464: Earth to Mars 2037 Type III/IV+ – Maximum Reachable North and South Latitude**

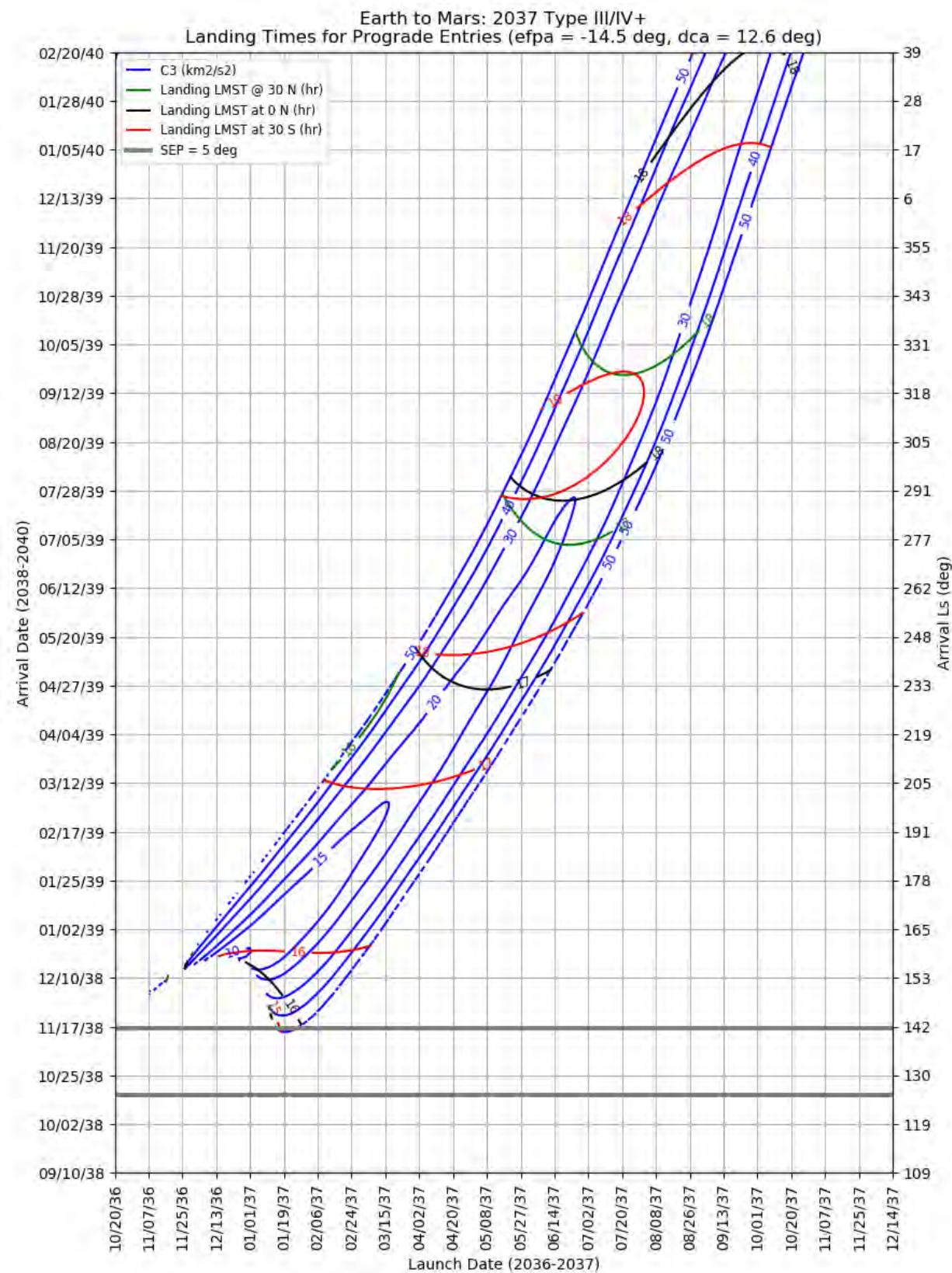
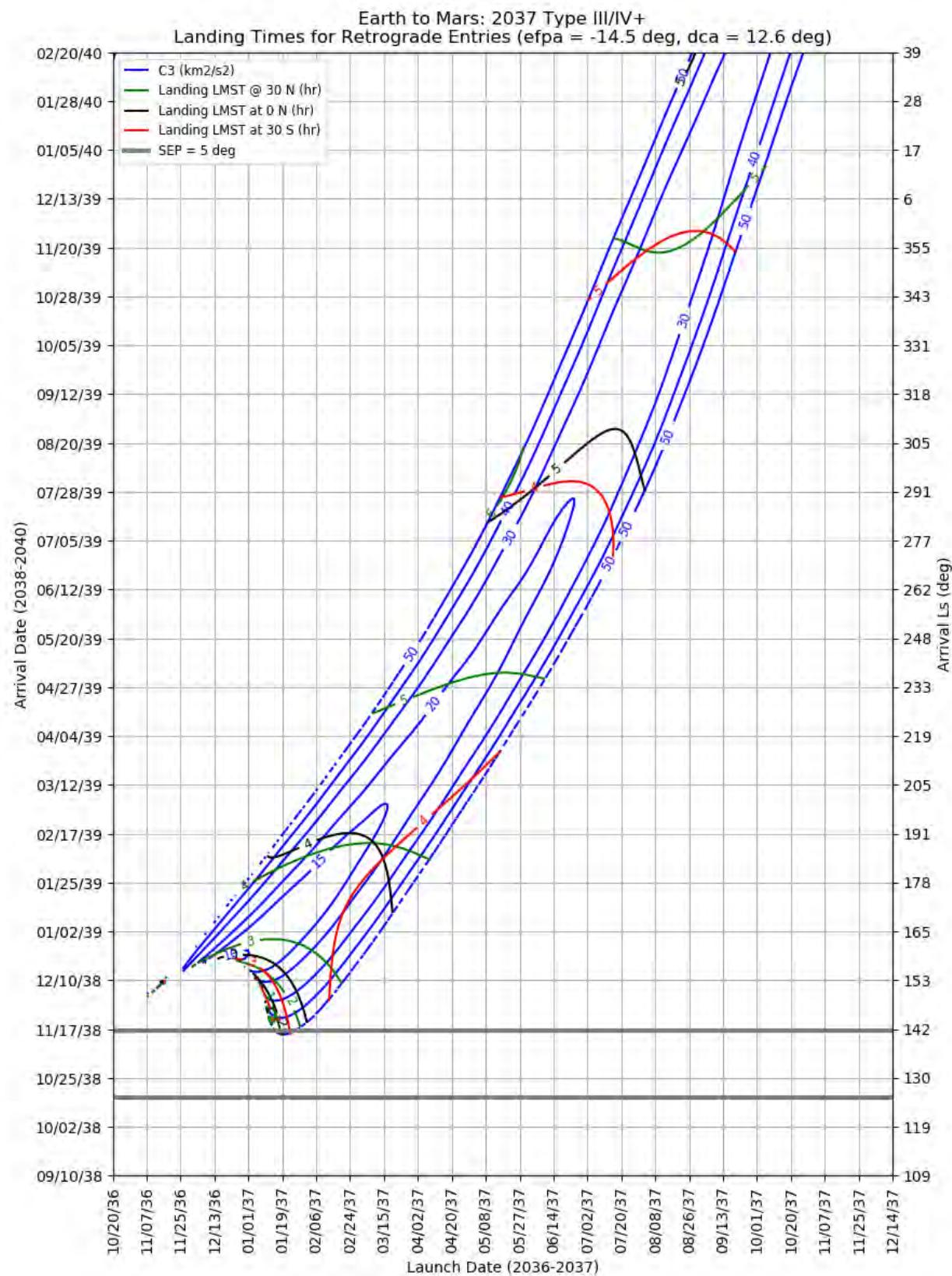


Figure 465: Earth to Mars 2037 Type III/IV+ – Landing LMST for Prograde Entries



**Figure 466: Earth to Mars 2037 Type III/IV+ – Landing LMST for Retrograde Entries**

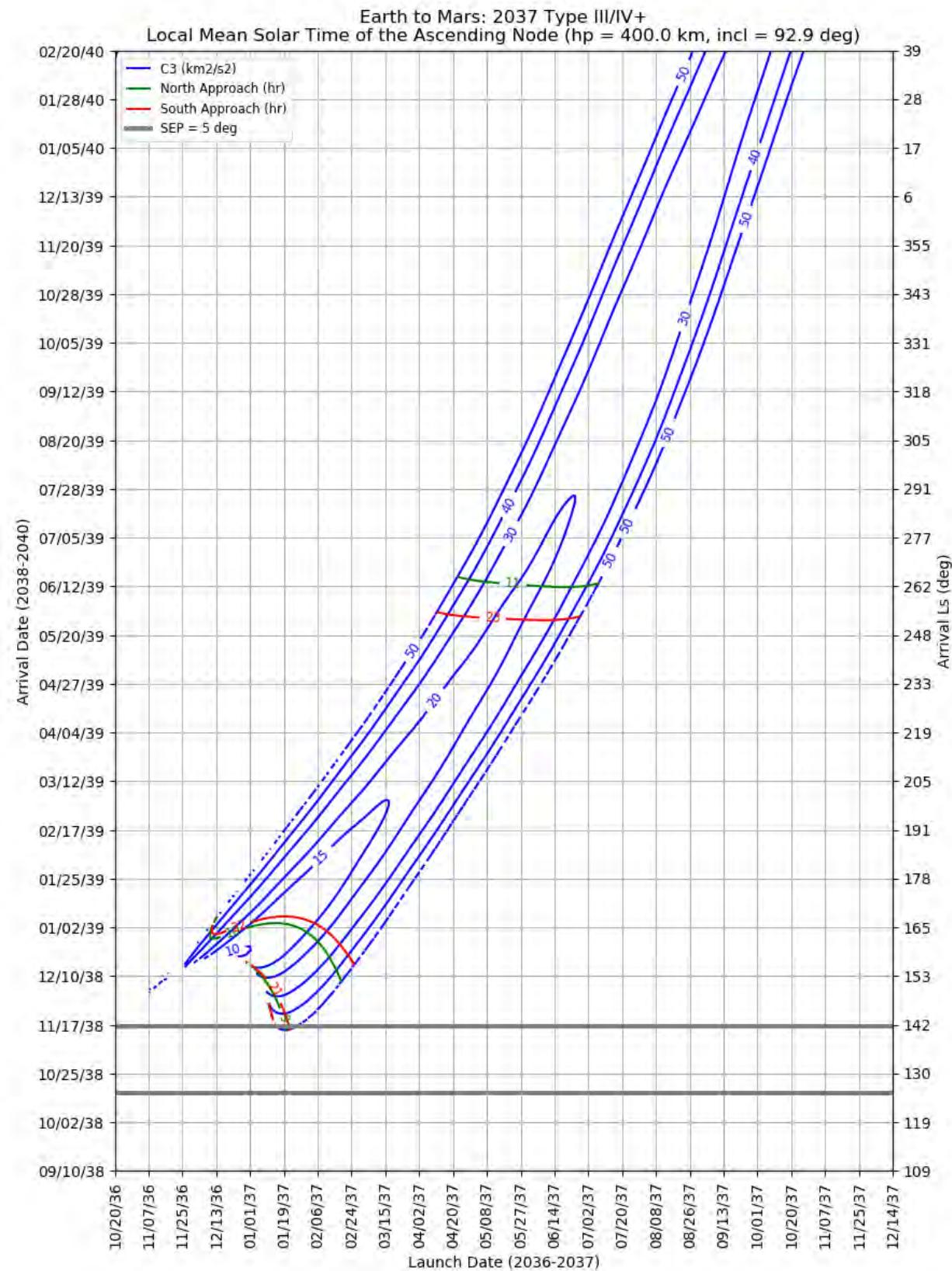


Figure 467: Earth to Mars 2037 Type III/IV+ – LMST of the Ascending Node for North and South Approaches

### 10.5.10 Earth to Mars 2039

This section contains porkchop plots for the Earth-to-Mars 2039 opportunities. Table 36 contains the optimal single-day transfers for minimum launch energy (C3) and arrival velocity (VHP) as well as the maximum launch-mass and captured-mass launch periods for each trajectory type within the opportunity. These data should only be used for preliminary analysis and planning purposes.

**Table 36: Earth to Mars 2039 Optimal Launch/Arrival Data**

Optimization Criteria	Trajectory Type	Departure Date (dd-mmm-yyyy)	Arrival Date (dd-mmm-yyyy)	Launch Energy, C3 (km <sup>2</sup> /s <sup>2</sup> )	Declination of the Launch Asymptote, DLA (deg)	Approach V-Infinity, VHP (km/s)
<b>Single-Day Optimization</b>						
Minimum C3	I	01-Oct-2039	01-May-2040	18.7	50.2	4.03
Minimum C3	II	26-Sep-2039	18-Sep-2040	12.2	17.7	2.66
Minimum C3	III-	12-Jan-2039	19-Dec-2040	9.7	-27.7	4.85
Minimum C3	IV-	23-Feb-2039	10-Jun-2041	8.4	-1.9	5.92
Minimum C3	III+	22-Jan-2039	20-Dec-2040	9.0	-29.6	5.75
Minimum C3	IV+	03-Dec-2038	01-Dec-2040	51.1	20.7	7.99
Minimum VHP	I	25-Oct-2039	17-Jul-2040	28.5	41.6	2.36
Minimum VHP	II	27-Aug-2039	26-Jul-2040	18.4	9.9	2.38
Minimum VHP	III-	27-Jan-2039	29-Dec-2040	25.5	-1.9	3.66
Minimum VHP	IV-	27-Nov-2038	19-Jan-2041	10.2	18.5	3.15
Minimum VHP	III+	03-Feb-2039	26-Nov-2040	38.4	7.5	4.24
Minimum VHP	IV+	03-Dec-2038	01-Dec-2040	51.1	20.7	7.99
<b>Launch Period Optimization</b>						
Maximum Launch Mass	I	23-Sep-2039	12-Apr-2040	20.2	49.7	4.86
		13-Oct-2039		22.1	40.1	5.03
Maximum Launch Mass	II	19-Sep-2039	29-Sep-2040	13.1	20.6	2.83
		09-Oct-2039		13.3	20.0	2.82
Maximum Launch Mass	III-	02-Jan-2039	19-Dec-2040	13.0	-45.4	5.18
		22-Jan-2039		16.0	-6.1	4.02
Maximum Launch Mass	IV-	26-Feb-2039	27-Jun-2041	9.2	-11.2	6.13
		18-Mar-2039		9.4	-2.6	6.13
Maximum Launch Mass	III+	14-Jan-2039	19-Dec-2040	9.5	-35.0	5.65
		03-Feb-2039		10.6	-19.8	5.84
Maximum Launch Mass	IV+	Not Possible				
Maximum Captured Mass	I	02-Oct-2039	28-May-2040	20.4	58.2	3.21
		22-Oct-2039		26.6	37.9	3.07
Maximum Captured Mass	II	15-Sep-2039	08-Sep-2040	13.2	16.2	2.57

Optimization Criteria	Trajectory Type	Departure Date (dd-mmm-yyyy)	Arrival Date (dd-mmm-yyyy)	Launch Energy, C3 (km <sup>2</sup> /s <sup>2</sup> )	Declination of the Launch Asymptote, DLA (deg)	Approach V-Infinity, VHP (km/s)
		05-Oct-2039		13.5	11.3	2.64
Maximum Captured Mass	III-	03-Jan-2039	22-Dec-2040	14.0	-43.6	4.88
		23-Jan-2039		18.6	-4.4	3.82
Maximum Captured Mass	IV-	26-Nov-2038	30-Jan-2041	10.6	15.8	3.22
		16-Dec-2038		10.0	34.2	3.27
Maximum Captured Mass	III+	14-Jan-2039	19-Dec-2040	9.5	-35.0	5.65
		03-Feb-2039		10.6	-19.8	5.84
Maximum Captured Mass	IV+			Not Possible		

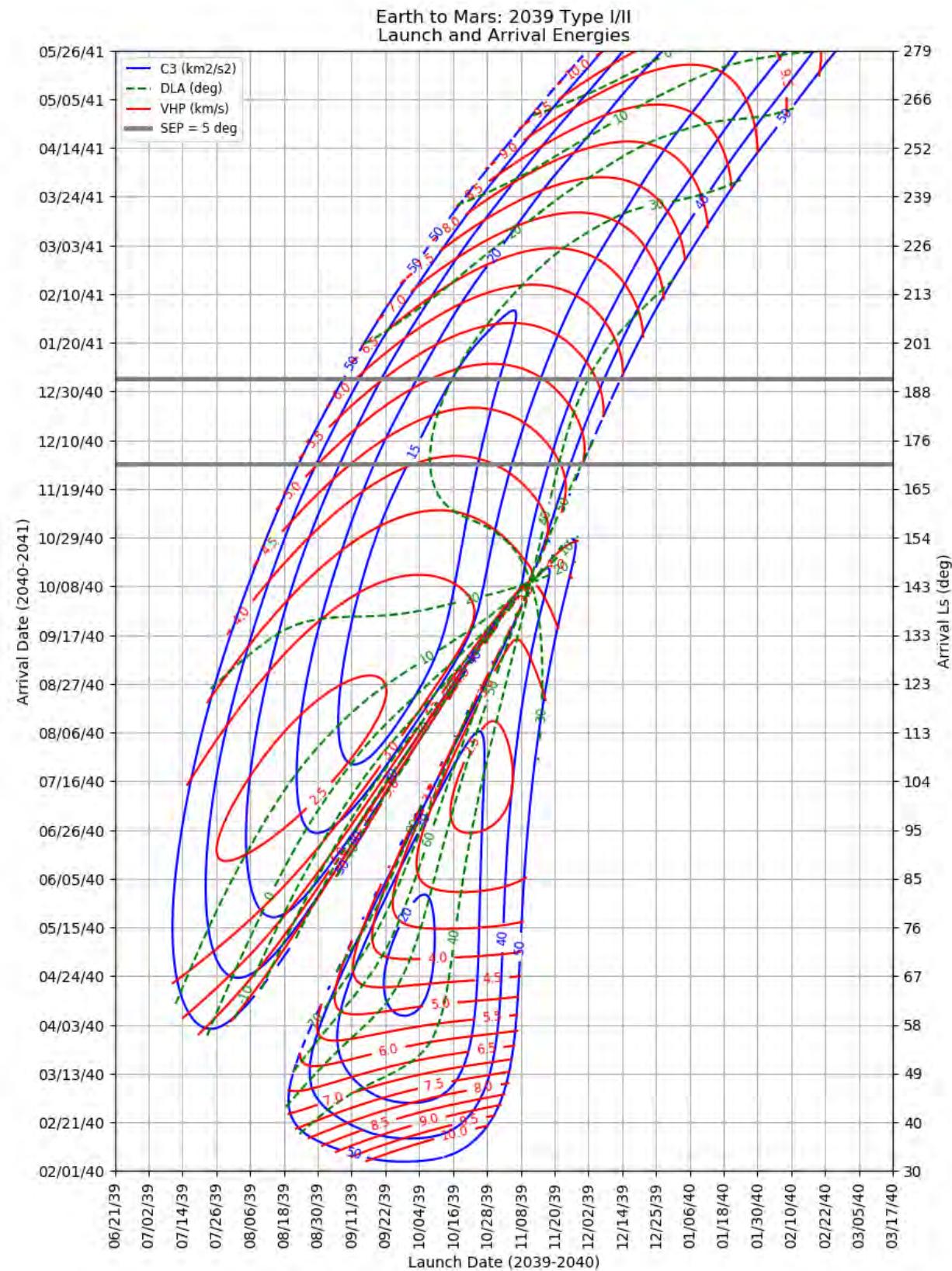


**Figure 468: Earth to Mars 2039 Type I/II - Launch and Arrival Energy**

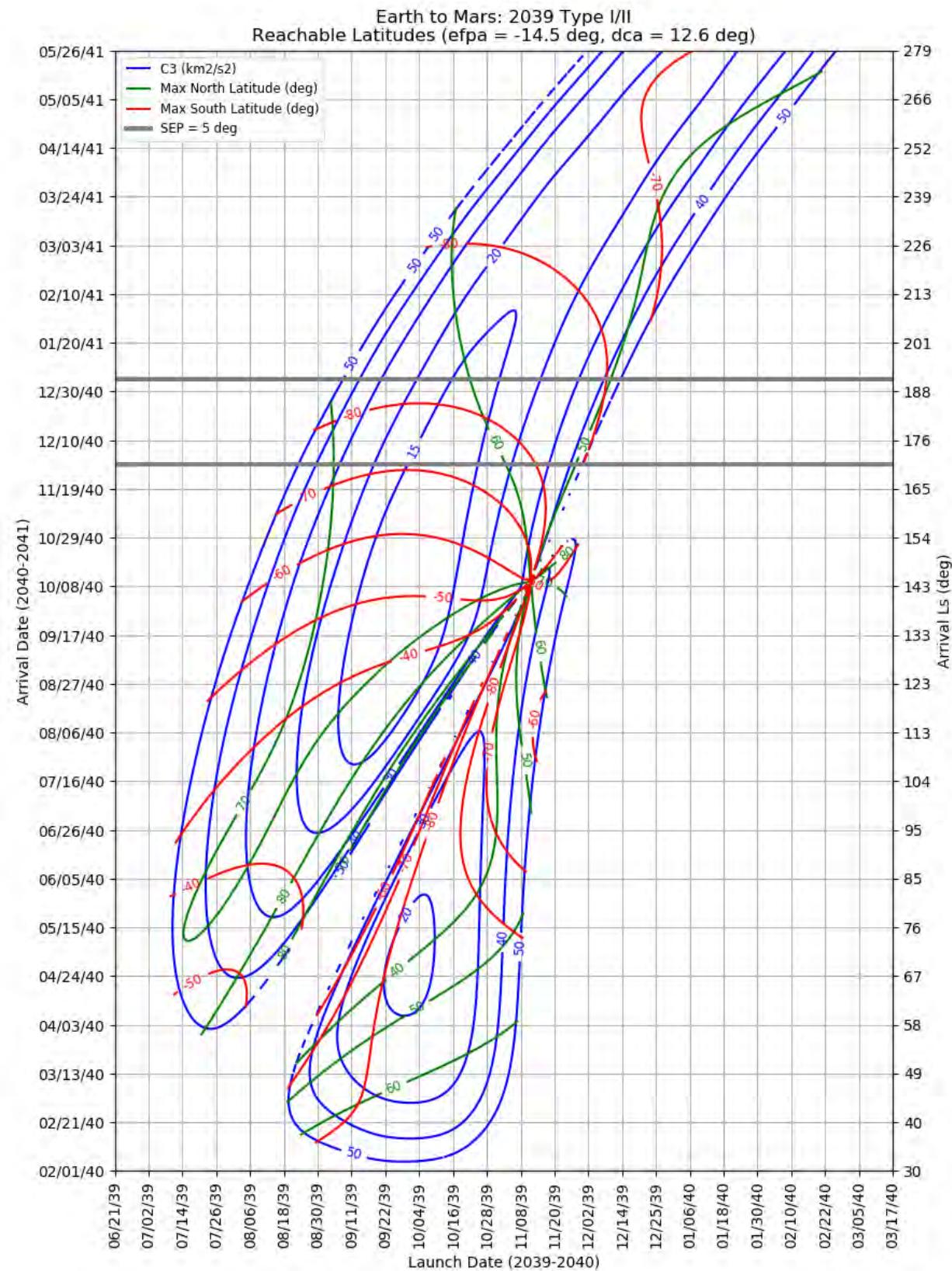


**Figure 469: Earth to Mars 2039 Type I/II – Maximum Reachable North and South Latitude**

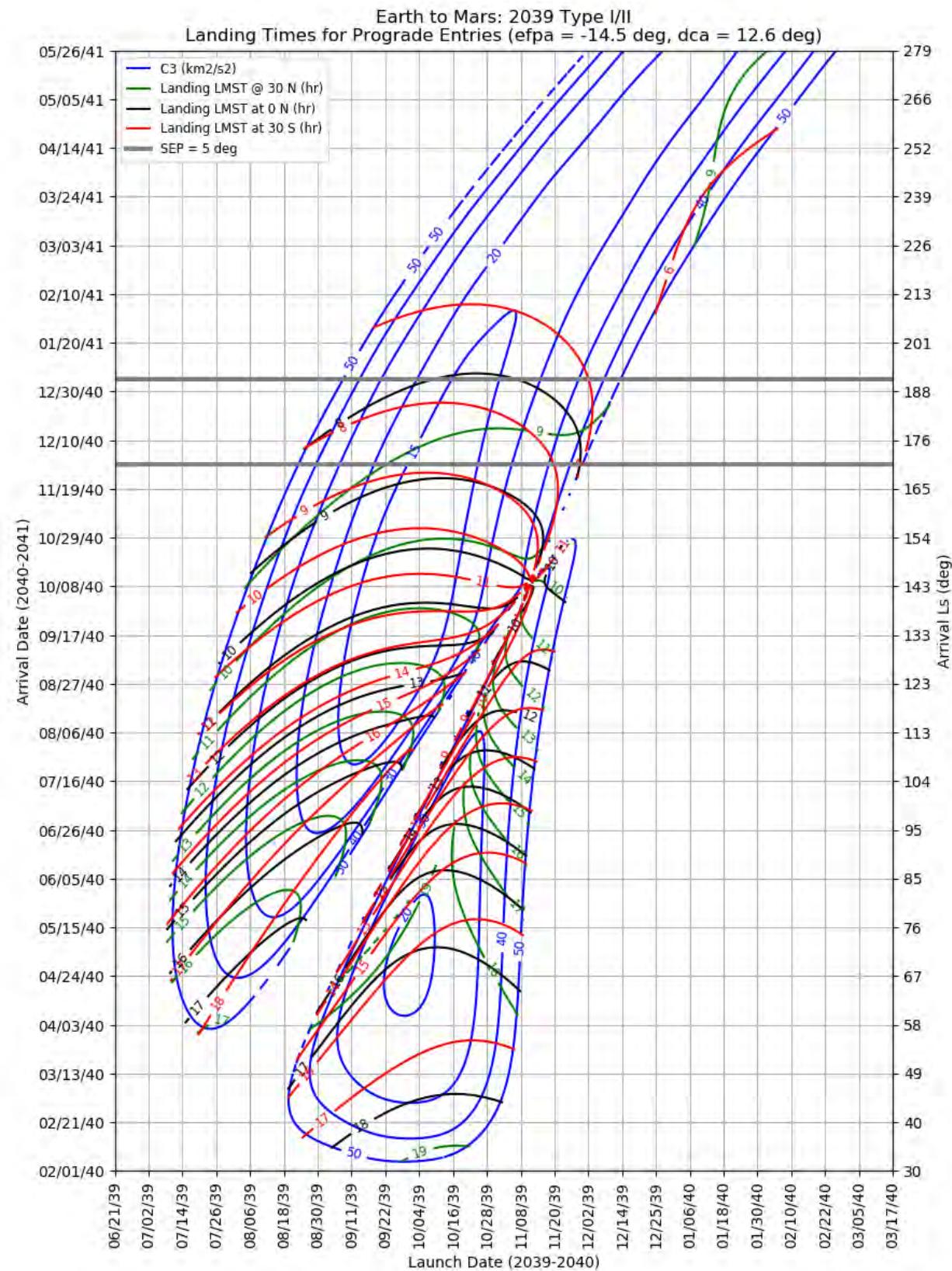


**Figure 470: Earth to Mars 2039 Type I/II – Landing LMST for Prograde Entries**

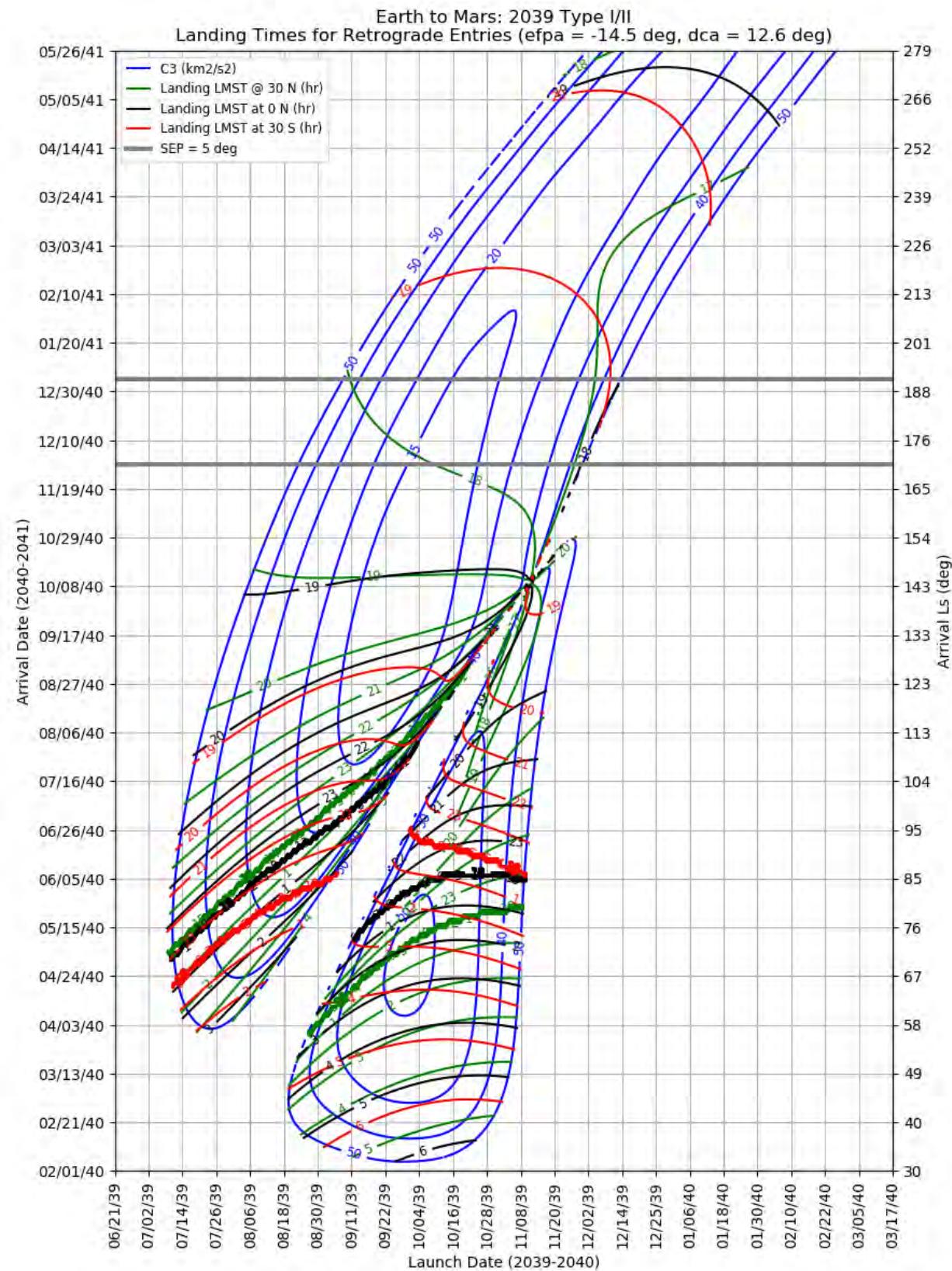


**Figure 471: Earth to Mars 2039 Type I/II – Landing LMST for Retrograde Entries**

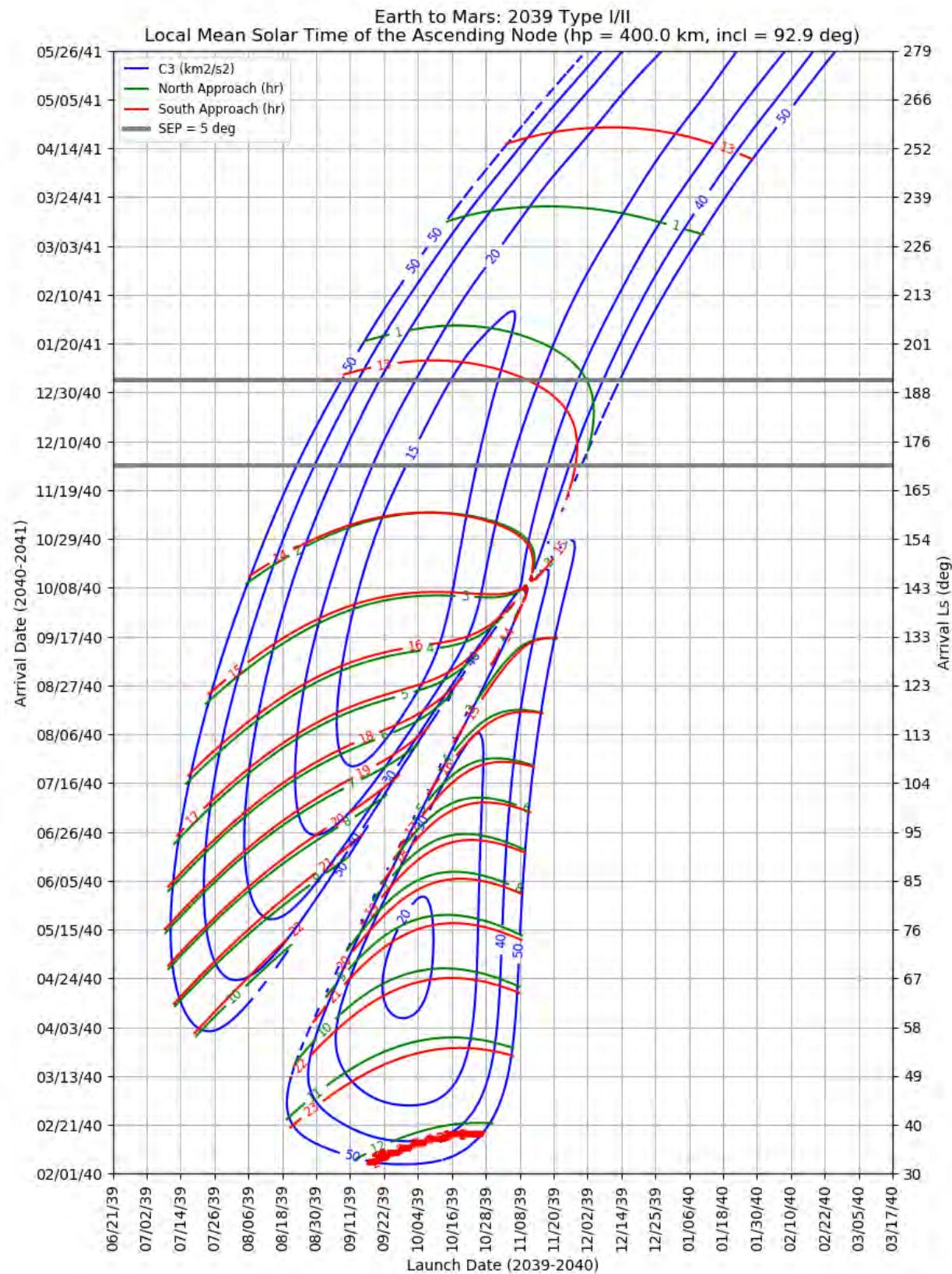


**Figure 472: Earth to Mars 2039 Type I/II – LMST of the Ascending Node for North and South Approaches**

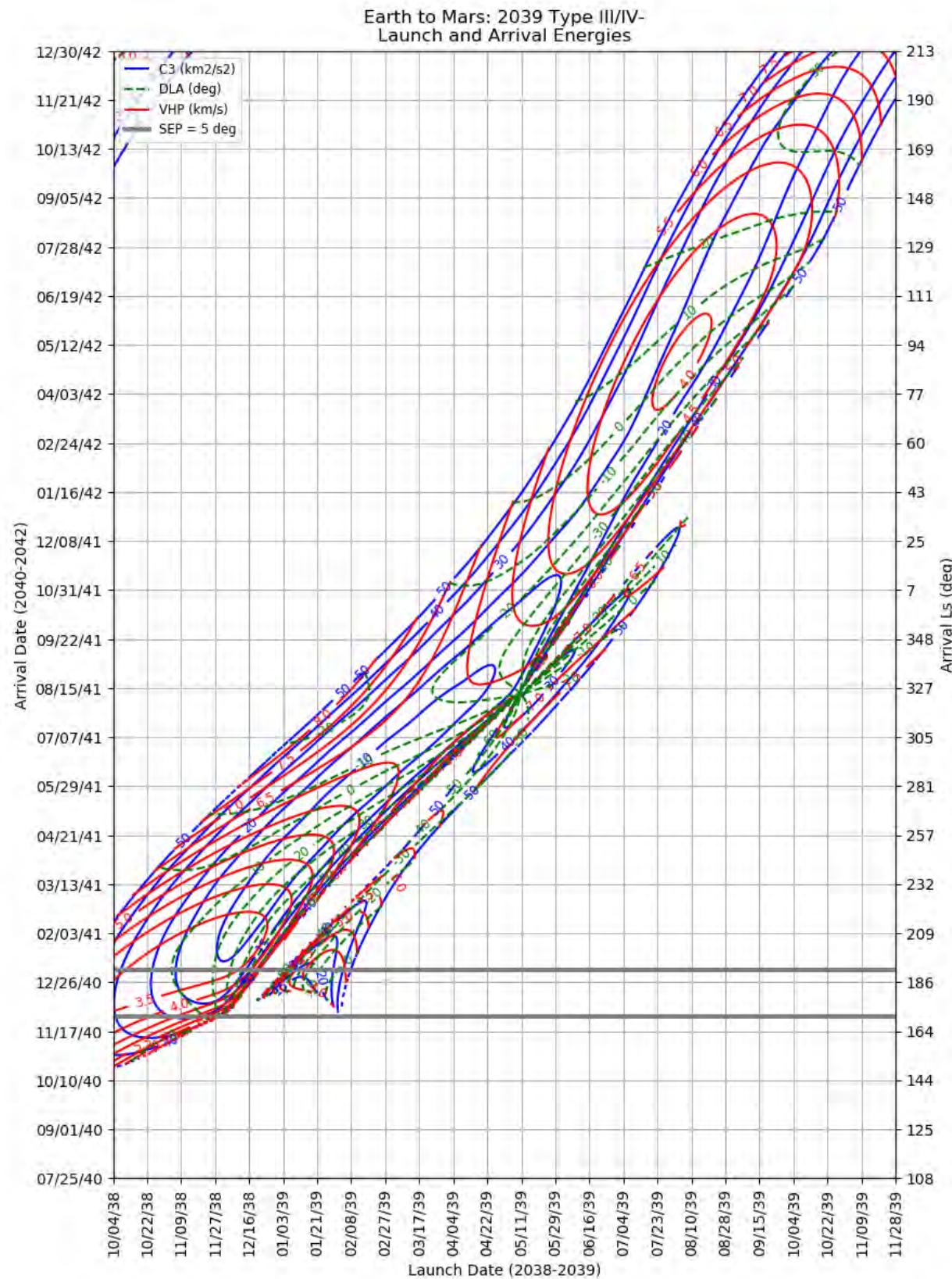
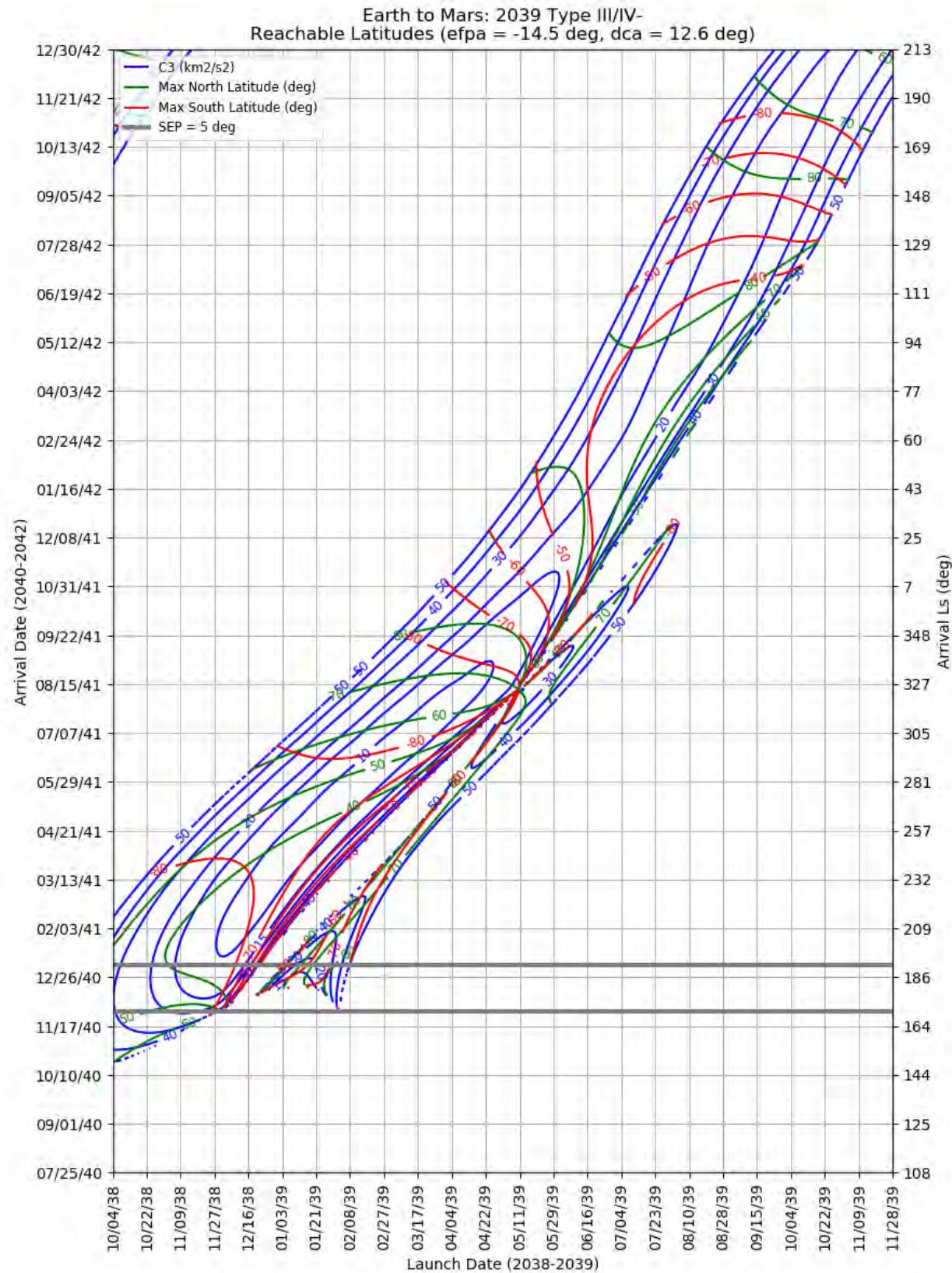
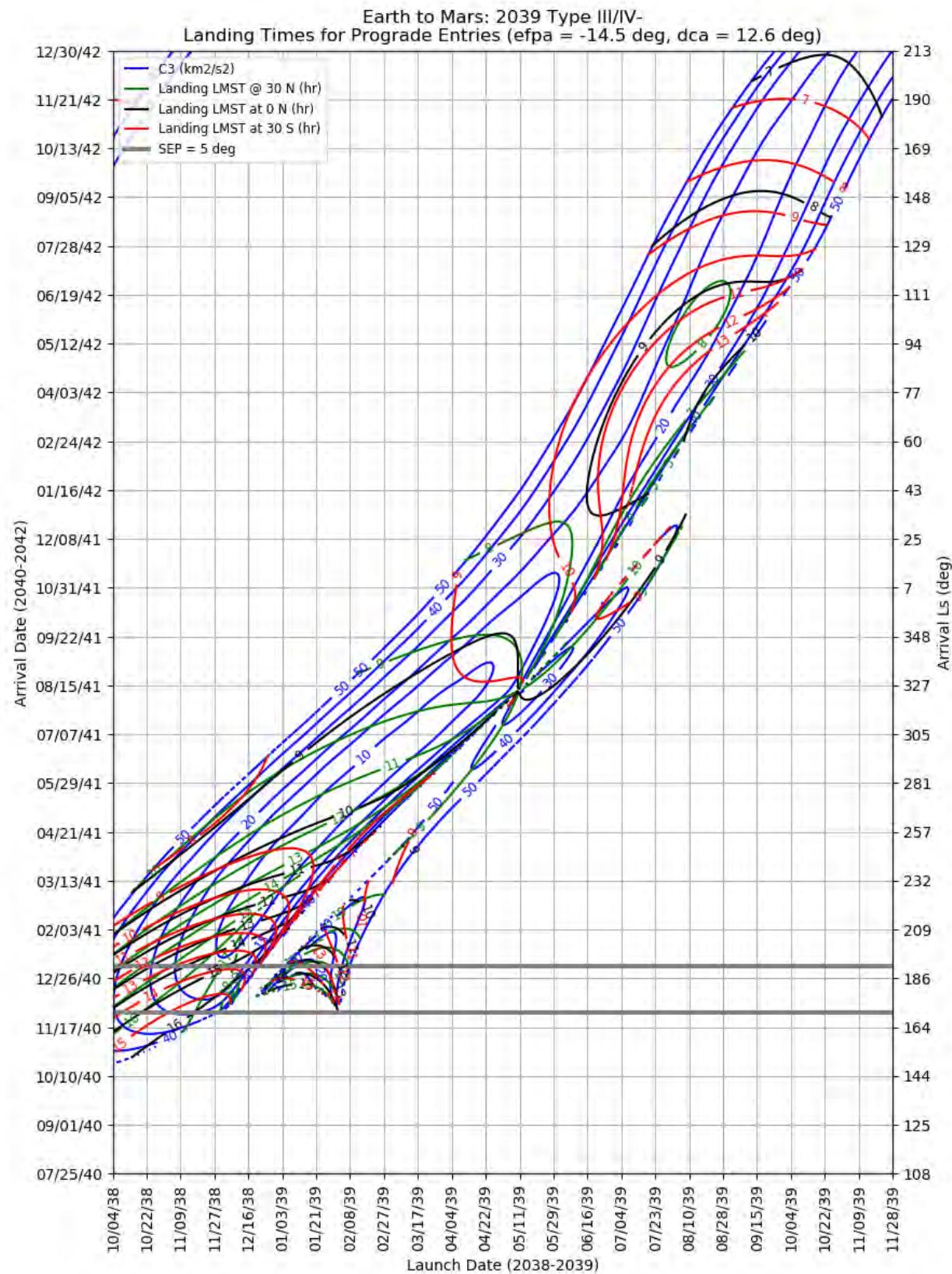


Figure 473: Earth to Mars 2039 Type III/IV- – Launch and Arrival Energy



**Figure 474: Earth to Mars 20392 Type III/IV- – Maximum Reachable North and South Latitude**



**Figure 475: Earth to Mars 2039 Type III/IV- – Landing LMST for Prograde Entries**

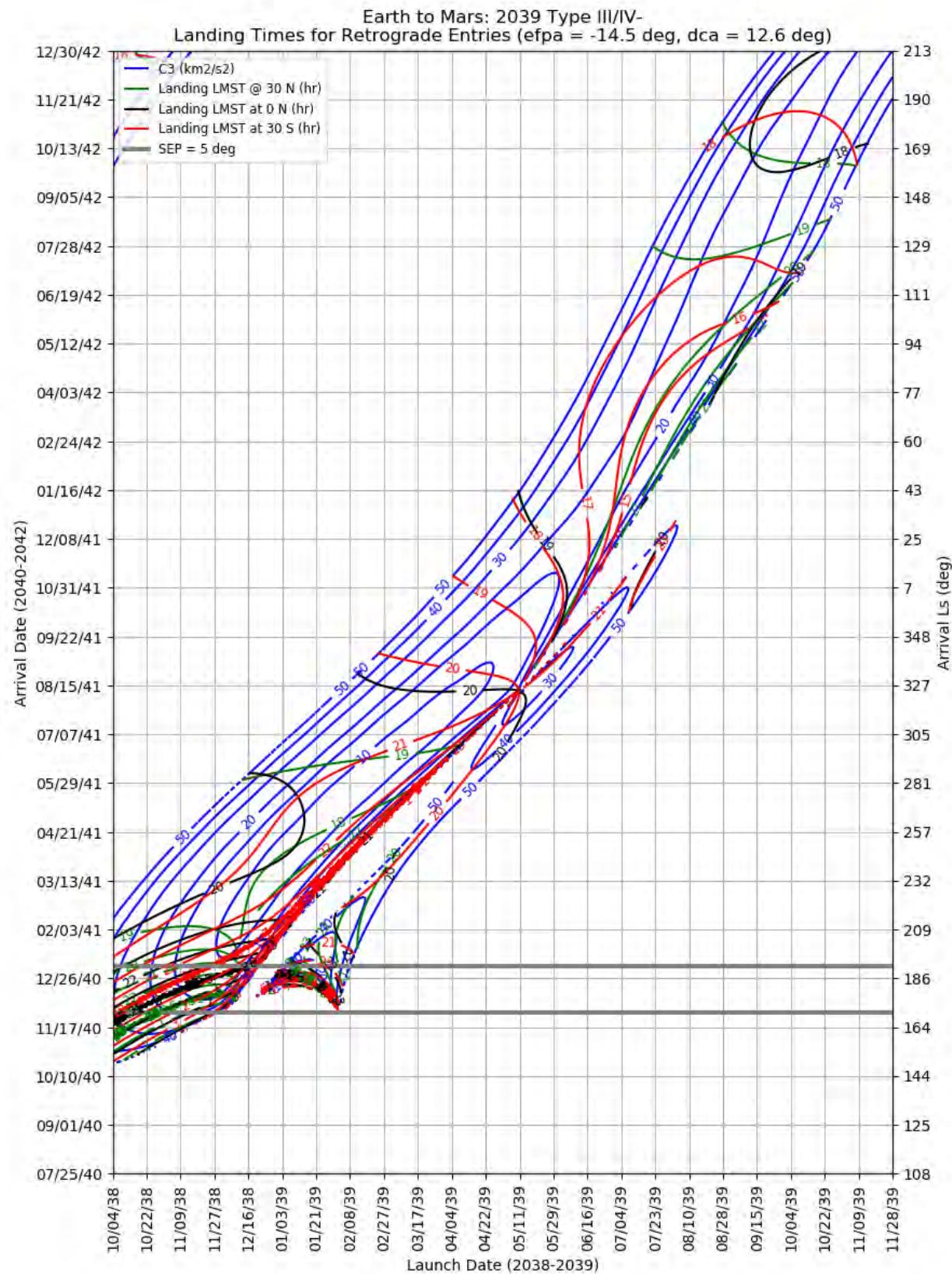


Figure 476: Earth to Mars 2039 Type III/IV- – Landing LMST for Retrograde Entries

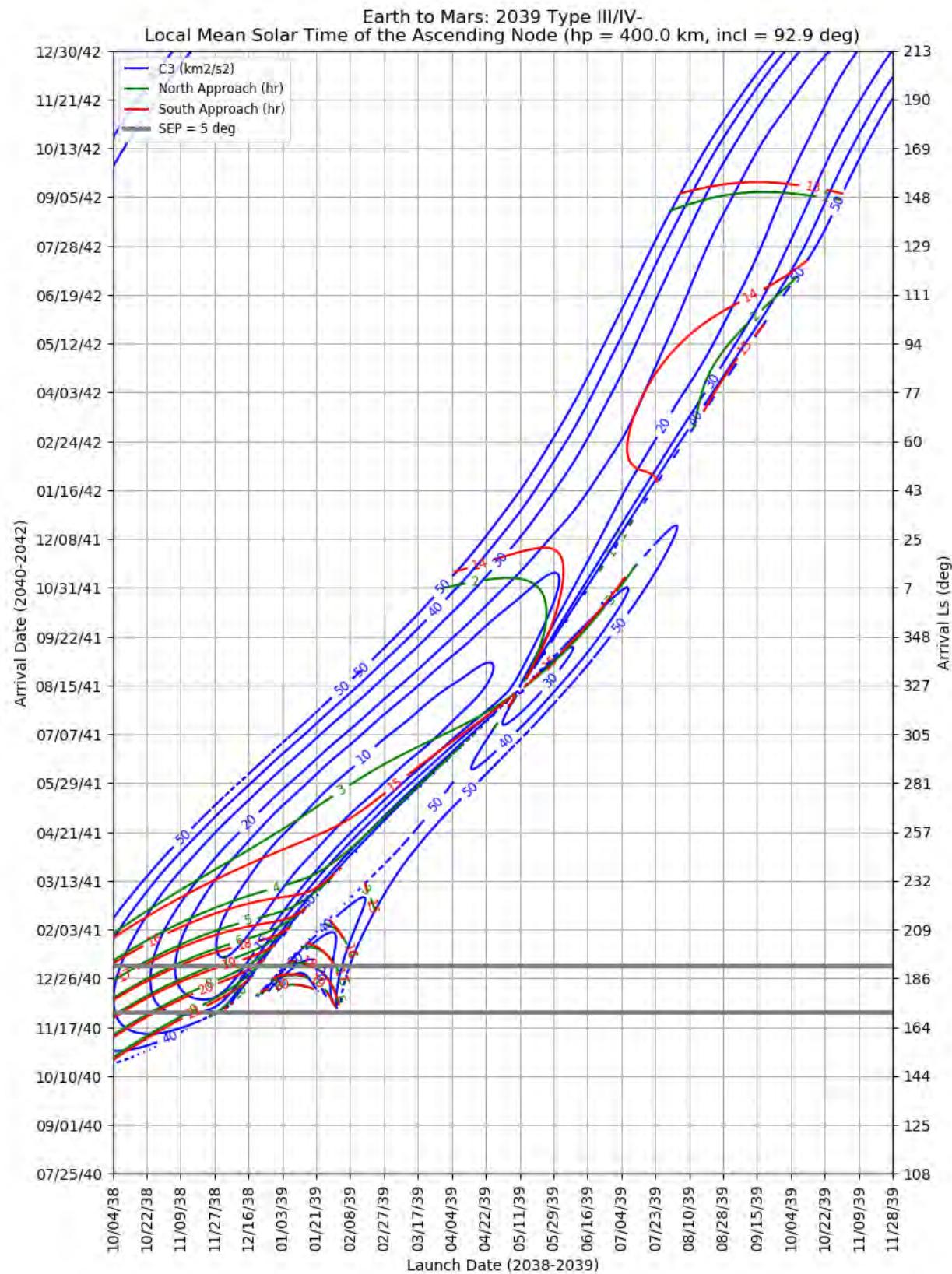
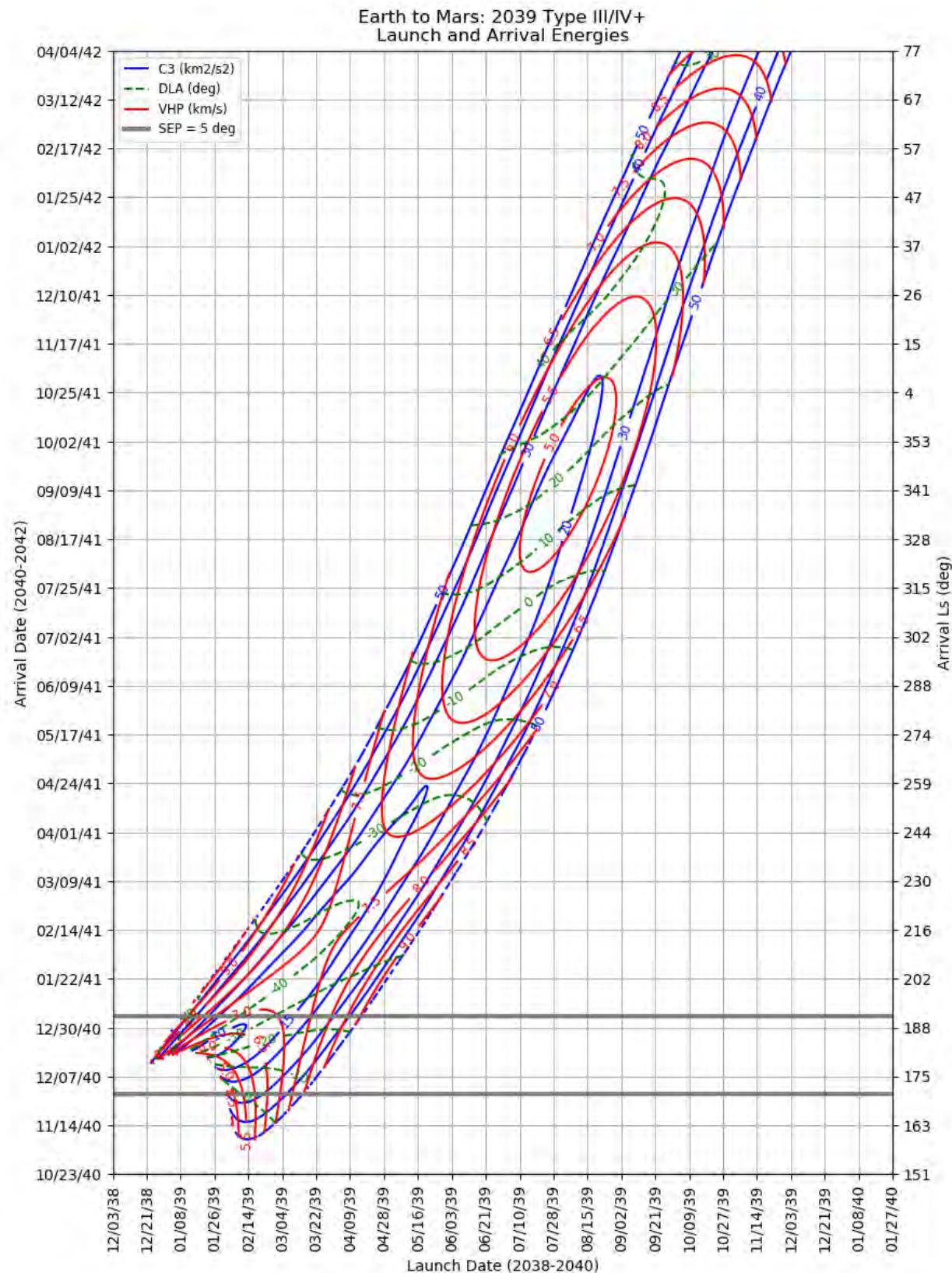
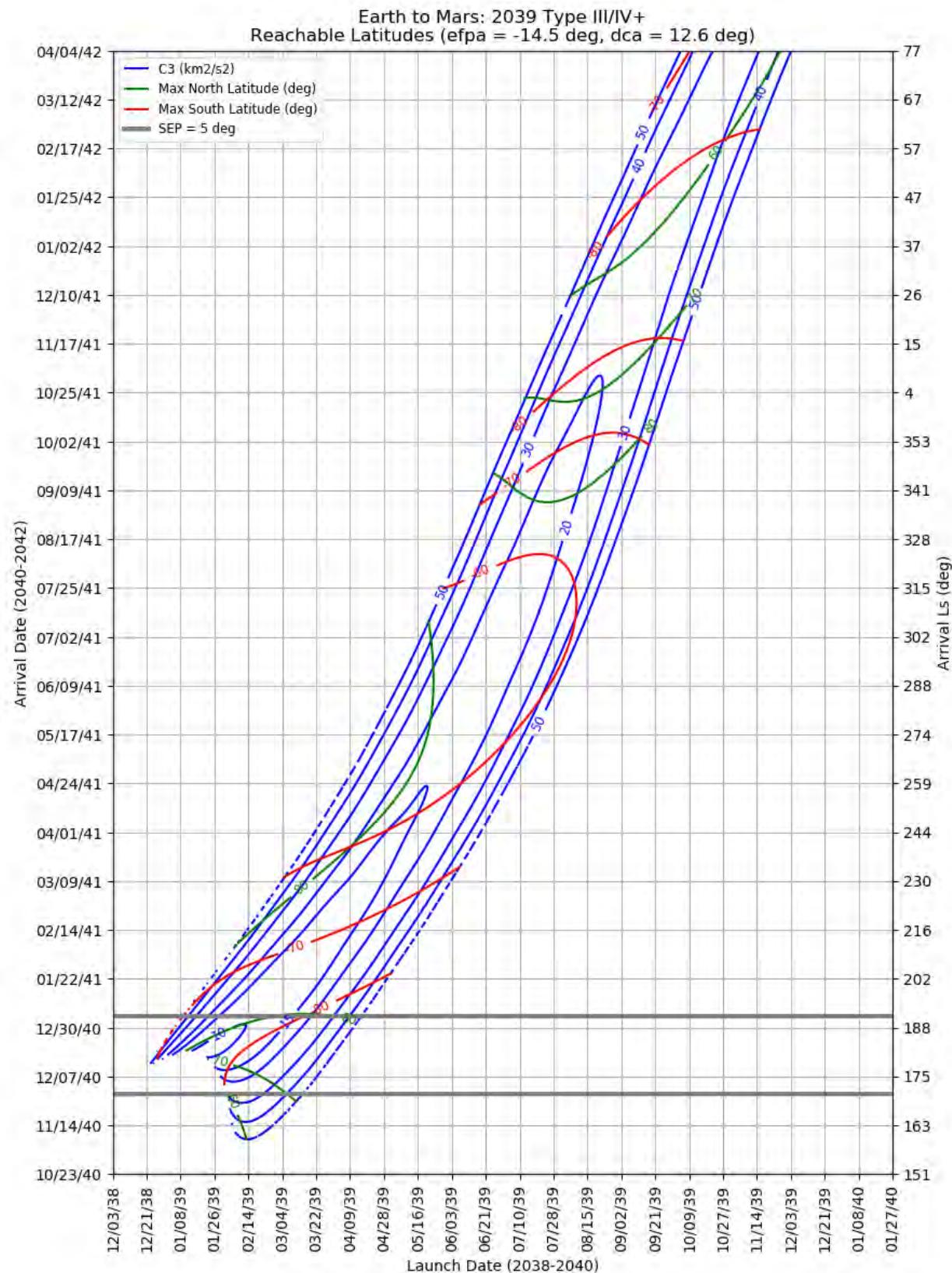


Figure 477: Earth to Mars 2039 Type III/IV- – LMST of the Ascending Node for North and South Approaches



**Figure 478: Earth to Mars 2039 Type III/IV+ – Launch and Arrival Energy**



**Figure 479: Earth to Mars 2039 Type III/IV+ – Maximum Reachable North and South Latitude**

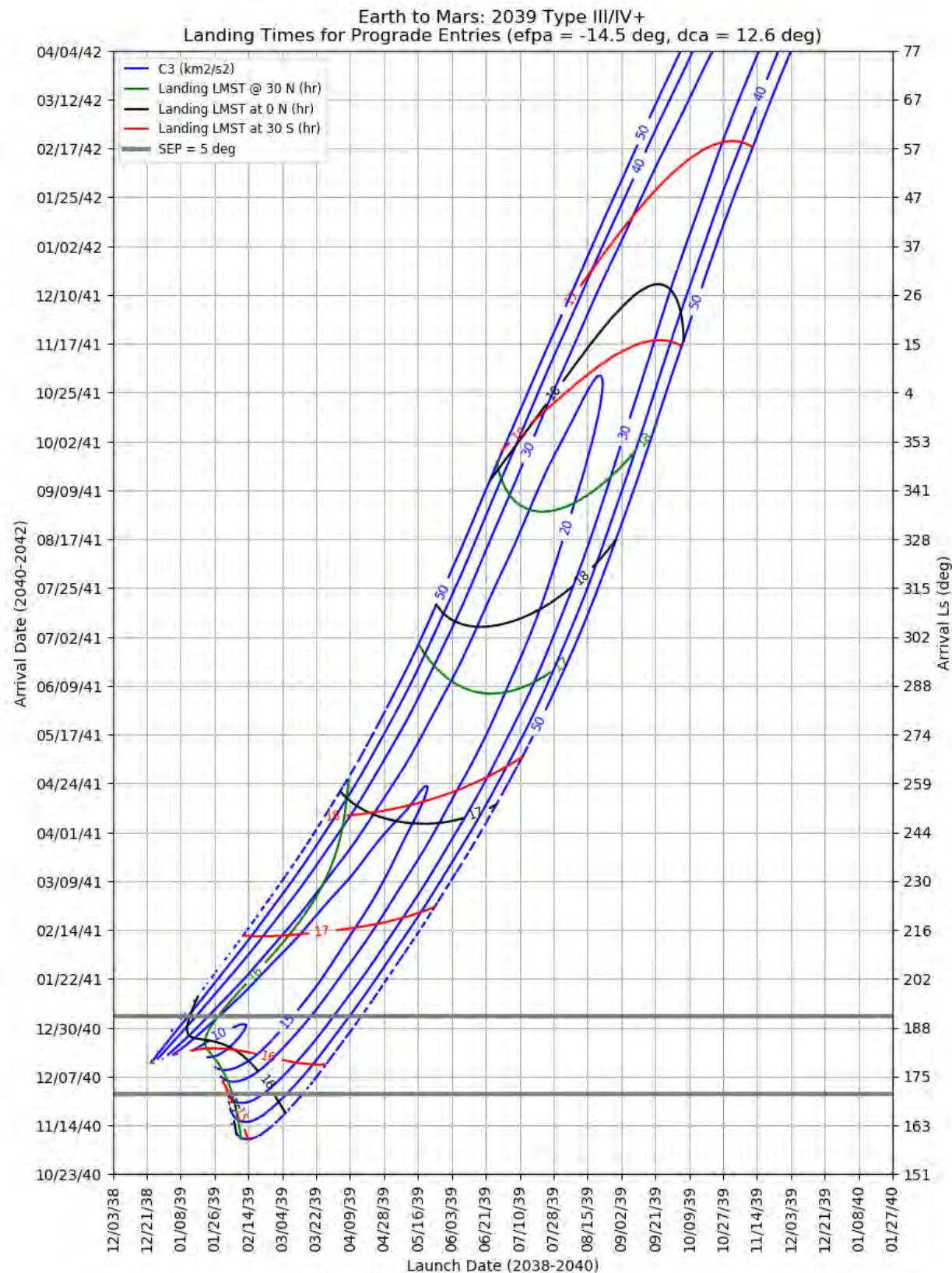
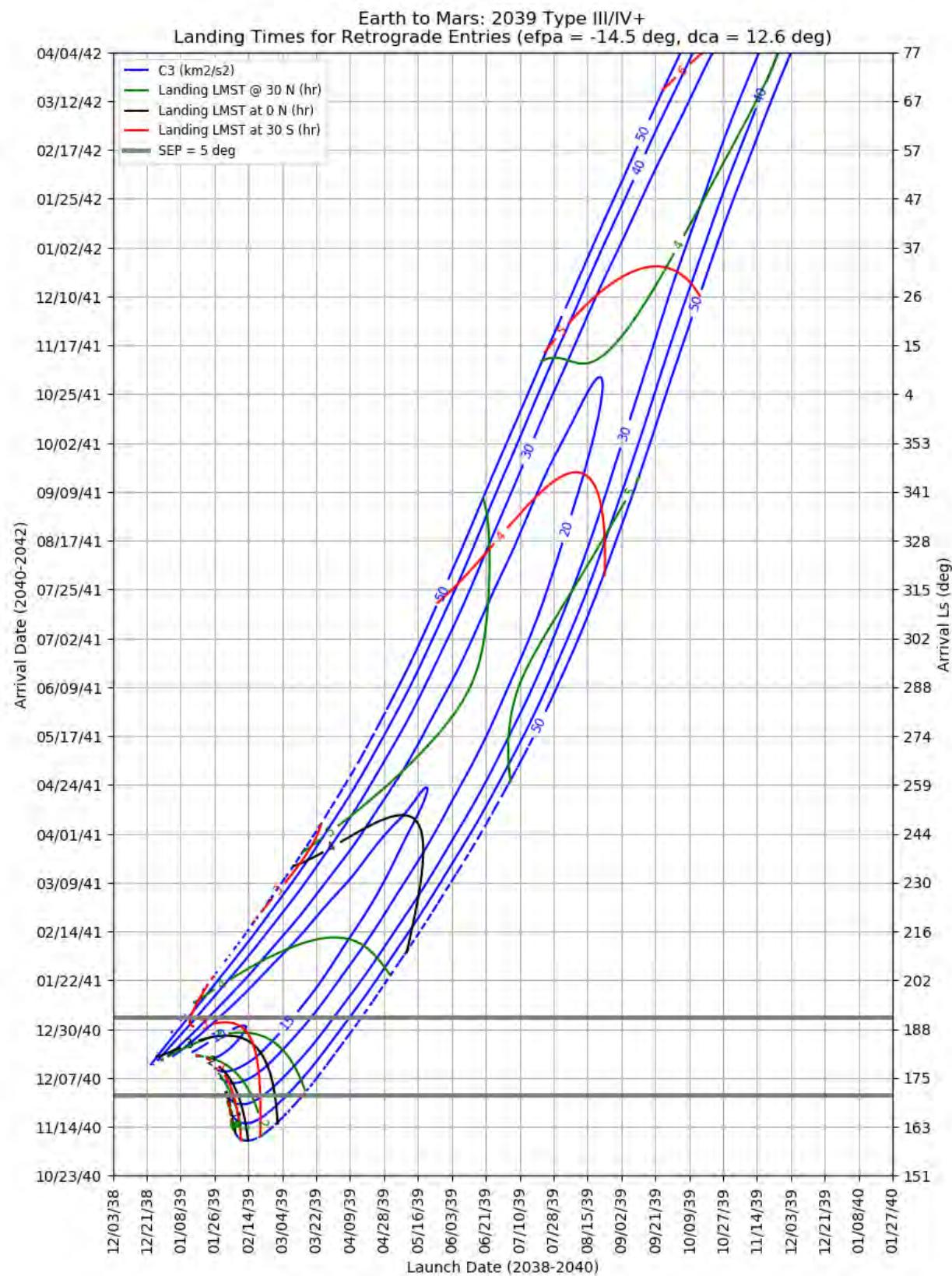


Figure 480: Earth to Mars 2039 Type III/IV+ – Landing LMST for Prograde Entries



**Figure 481: Earth to Mars 2039 Type III/IV+ – Landing LMST for Retrograde Entries**

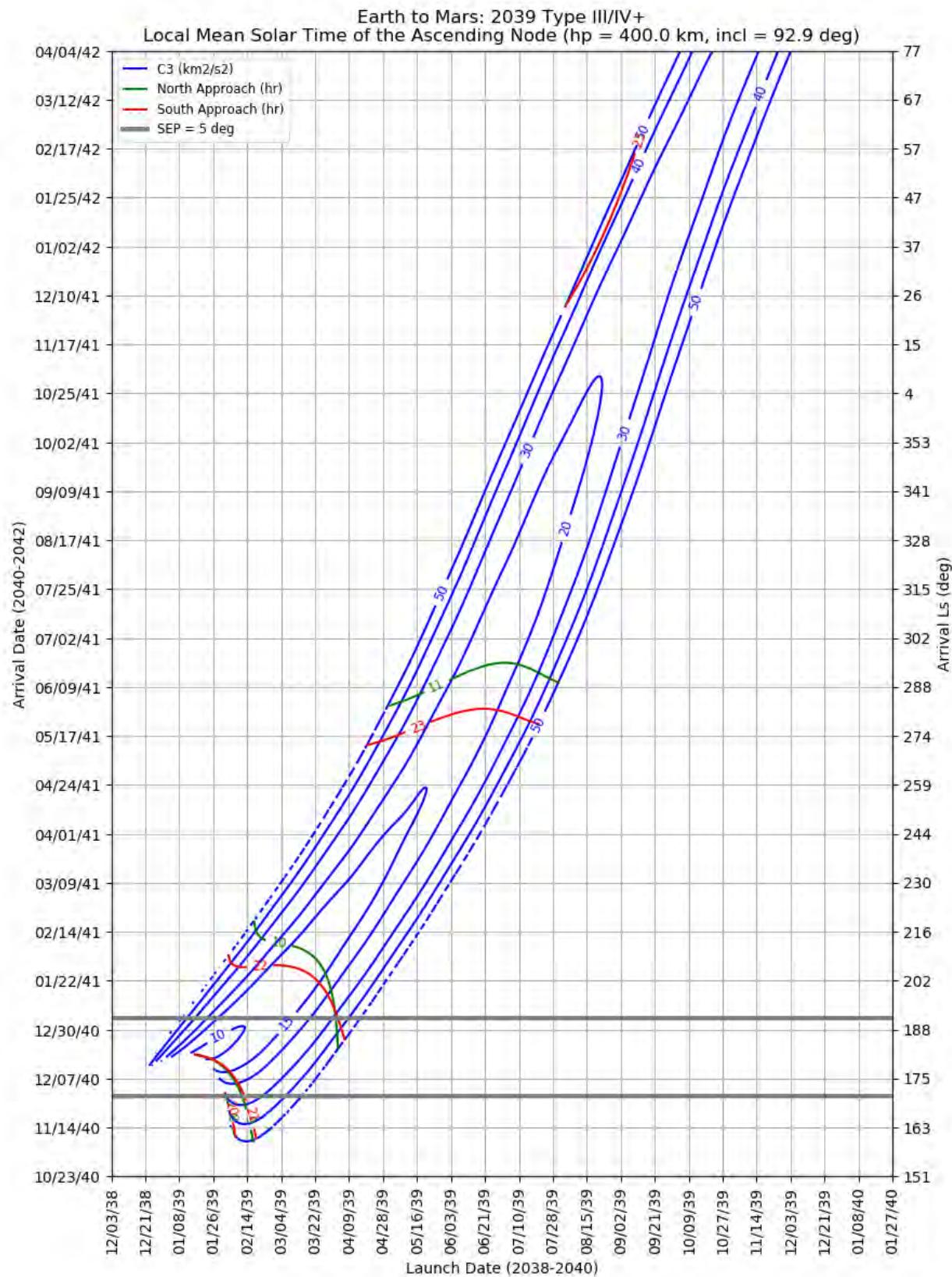


Figure 482: Earth to Mars 2039 Type III/IV+ – LMST of the Ascending Node for North and South Approaches

# 11 Mars to Earth Ballistic Transfer Data: 2024-2041

## 11.1 Overview

Not all Mars-to-Earth ballistic opportunities are created equal. That Mars is in a noticeably elliptical orbit means that more or less energy is required to drop perihelion down to Earth's orbit, and the spacecraft arrives at Earth with more or less energy as a result. The inclination of Mars with respect to the Earth orbital plane, combined with the obliquity of both Mars and Earth mean that the spacecraft approaches Earth from variable directions. These energies and geometries thus vary from one opportunity to the next. Some opportunities require more (or less) energy, have higher (or lower) declinations, etc.

This chapter contains porkchop plots for the 10 Earth-to-Mars ballistic opportunities in the 2024-2041 timeframe, as well as summary information about the opportunities themselves and "optimal" launch periods.

## 11.2 Summary of Opportunities

There are many ways of comparing one ballistic opportunity to another. Within each opportunity and type (e.g. 2022 Type II, 2030 Type IV-), there is a single launch/arrival date pair that minimizes the launch energy (C3) and another pair that minimizes the hyperbolic approach velocity (VHP). There may be large gradients about these minima, however, so it is useful to consider the effect of a launch period on these minima. A 7-day launch period is considered for Mars to Earth transfers, in contrast to a 20-day launch period for Earth to Mars.

Figures 483 through 485 illustrate the C3 and VHP for two trajectory types (I and II, III- and IV-, III+ and IV+, respectively) for each Mars-to-Earth opportunity when the C3 is minimized. Figures 486 through 488 do the same for minimized VHP. All of these plots have the C3 axis capped at  $35 \text{ km}^2/\text{s}^2$  and the VHP axis capped at 7 km/s. The Type III+ and IV+ trajectories frequently exceed one or both of these limits, but they are held constant at those levels to aid in comparison.

The Pareto front is the set of C3/VHP pairs where one cannot reduce the C3 without increasing VHP and vice versa and are illustrated for Mars to Earth opportunities in Figures 489 to 491. The globally minimum C3 is the left most-point on these curves, while the globally minimum VHP is the bottom-most point. A short curve indicates that the C3 and VHP minima are well aligned. That is, the minimizing launch/arrival date pairs are near each other in the porkchop.

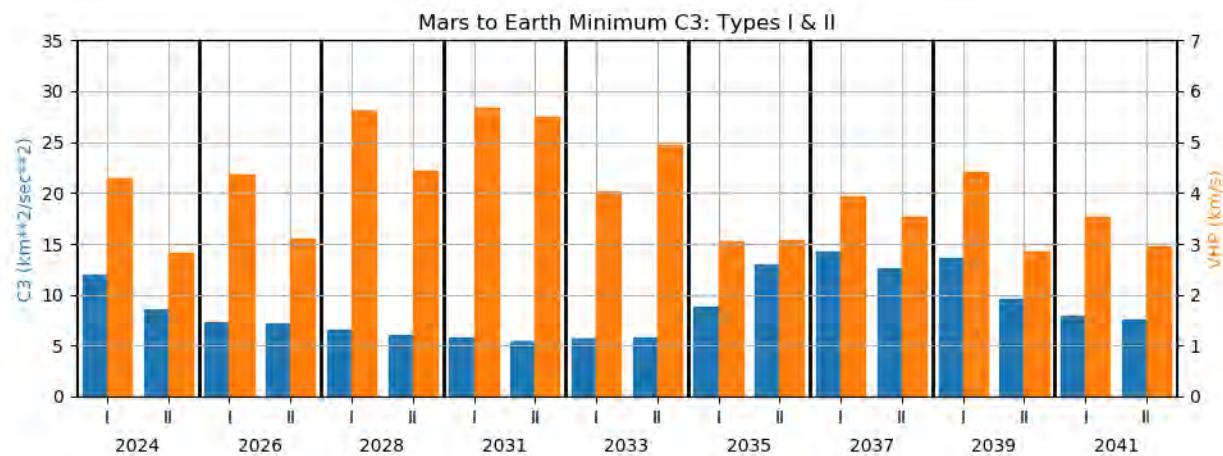


Figure 483: Minimum C3 and Associated VHP for Mars to Earth Type I and II Trajectories, 2022-2041

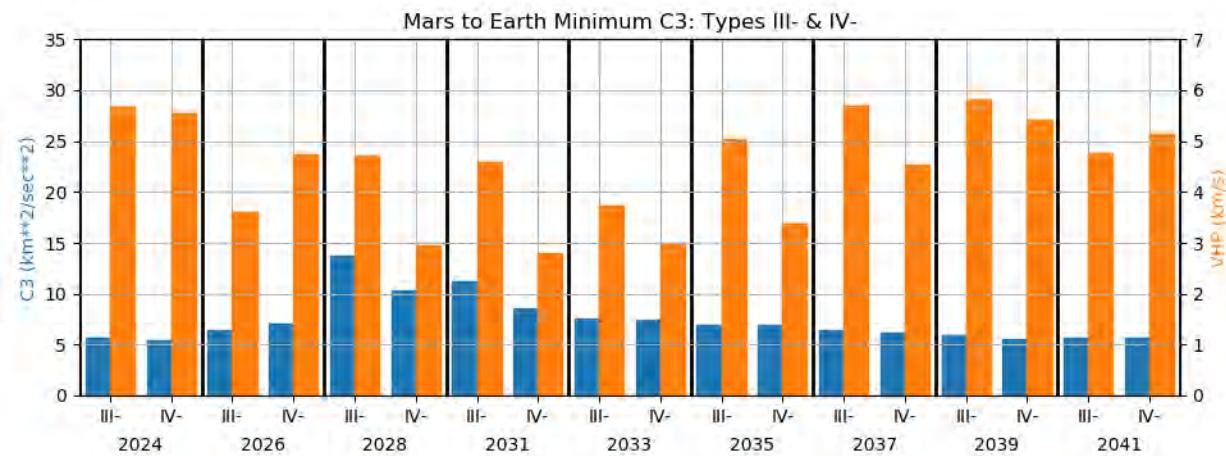


Figure 484: Minimum C3 and Associated VHP for Mars to Earth Type III- and IV- Trajectories, 2022-2041

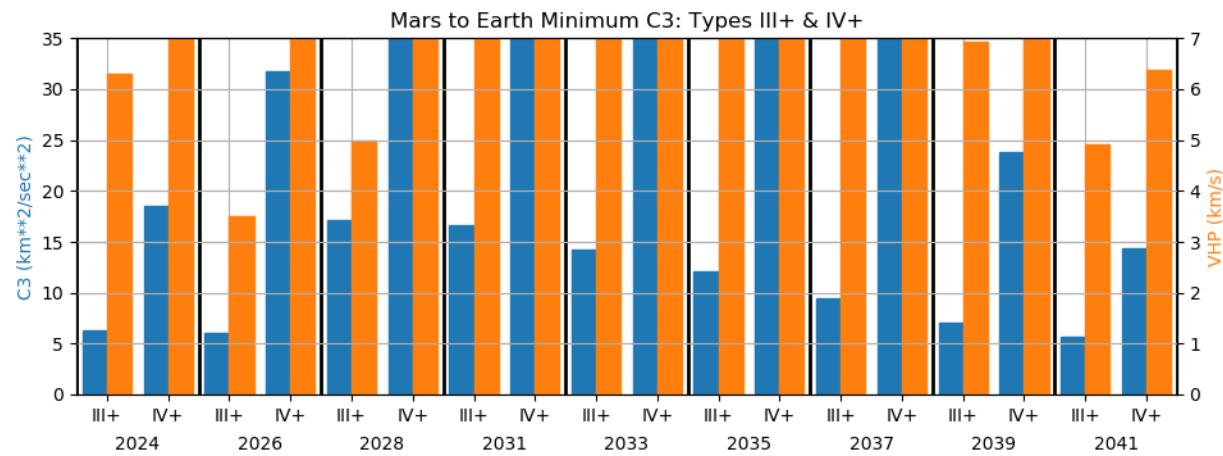


Figure 485: Minimum C3 and Associated VHP for Mars to Earth Type III+ and IV+ Trajectories, 2022-2041

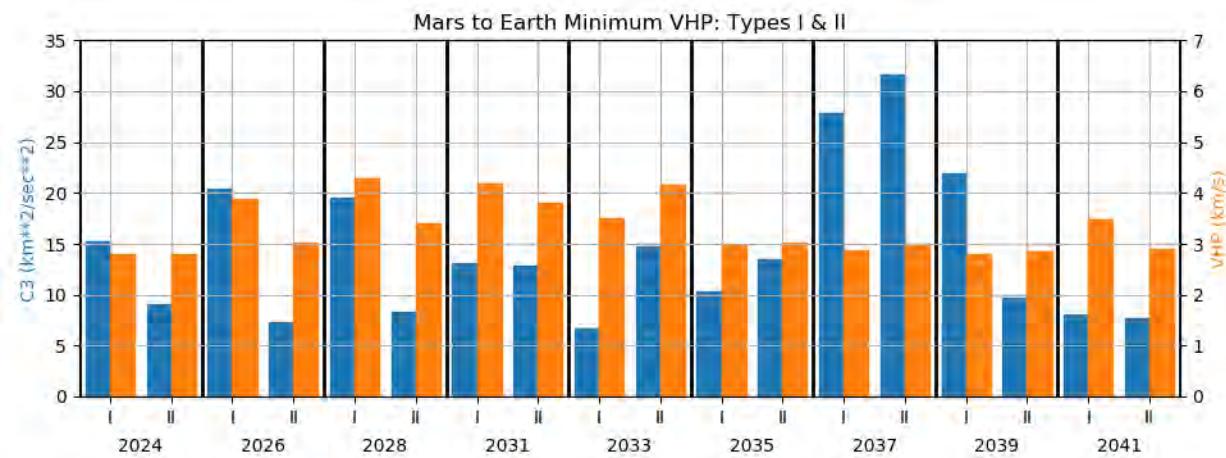


Figure 486: Minimum VHP and Associated C3 for Mars to Earth Type I and II Trajectories, 2022-2041

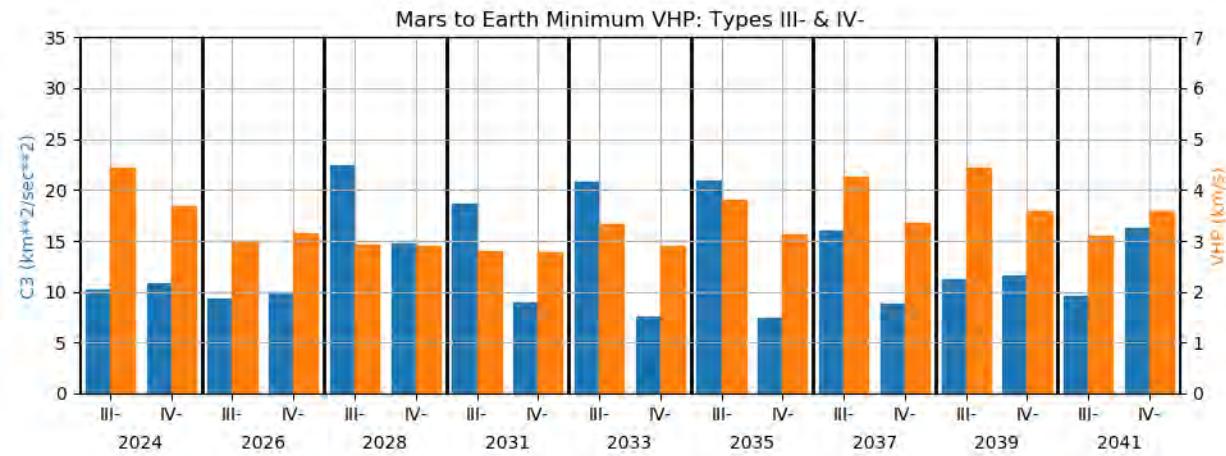


Figure 487: Minimum VHP and Associated C3 for Mars to Earth Type III- and IV- Trajectories, 2022-2041

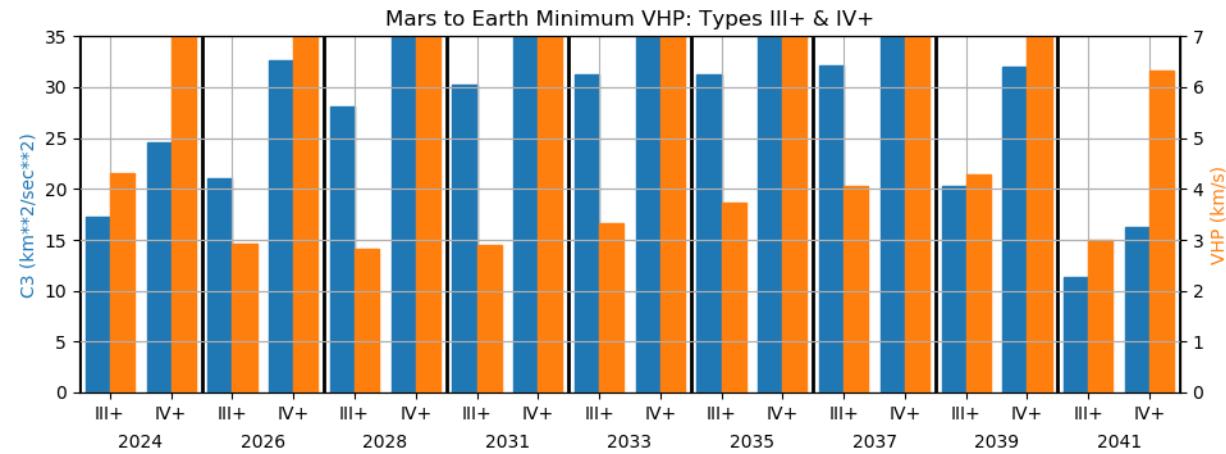


Figure 488: Minimum VHP and Associated C3 for Mars to Earth Type III+ and IV+ Trajectories, 2022-2041

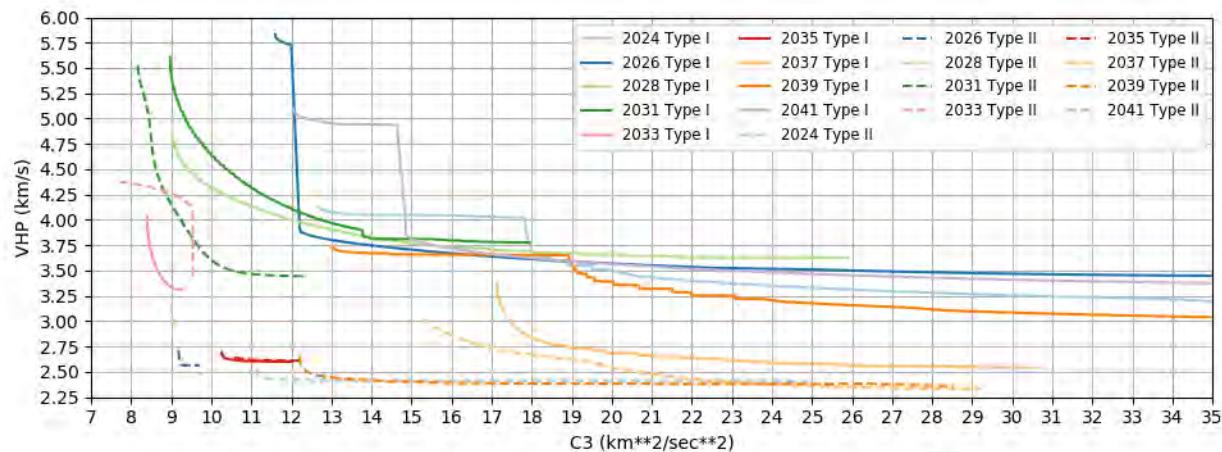


Figure 489: C3/VHP Pareto Fronts for Mars to Earth Type I and II Trajectories

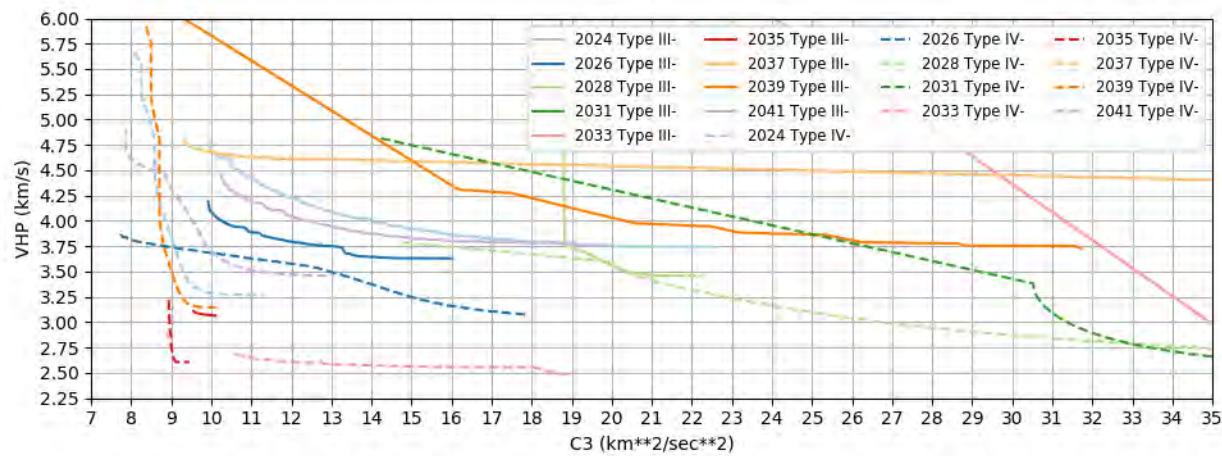


Figure 490: C3/VHP Pareto Fronts for Mars to Earth Type III- and IV- Trajectories

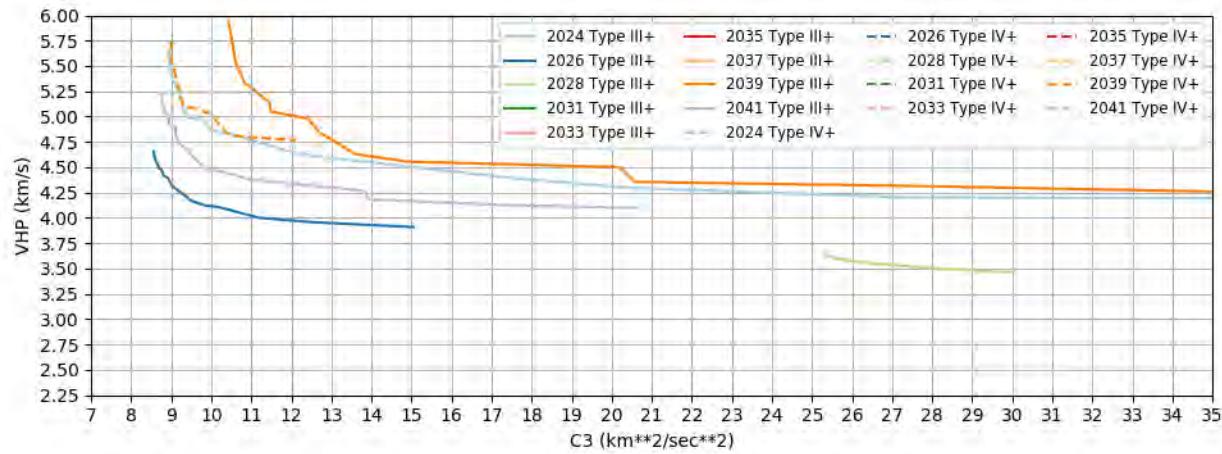


Figure 491: C3/VHP Pareto Fronts for Mars to Earth Type III+ and IV+ Trajectories

## 11.3 Launch Periods

For the purposes of this Handbook, we consider only the problem of direct Earth return; that is, a spacecraft entering Earth's atmosphere directly from a hyperbolic approach like Stardust did in January 2006. The Utah Test and Training Range (UTTR) has been the preferred landing site for robotic sample return missions (Stardust in 2006, Genesis in 2004), although other options such as White Sands Missile Range are possible. For the purposes of this handbook, UTTR is used as the baseline landing site and so the launch period data presented here considers 7-day launch periods with a constant Earth arrival date that minimize the Mars departure C3 for a given fixed arrival date. There may be operational considerations for a landing at UTTR (such as landing in the morning to maximize the time for the recovery team prior to sunset, or aiming for a particular season) that justify carrying the additional propellant to Mars for the Earth return maneuver(s).

With this in mind, Figures 492 through 532 plot the local true solar time (LTST) of landing at UTTR following a prograde or retrograde entry as a function of the offset in the minimum Mars departure C3 arrival date. An entry flight path angle of -25 deg and a descent central angle of 1.95 deg are assumed. These values are consistent with the MSR campaign's design assumptions as of the summer of 2020. Each point on these curves is a separate 7 day launch period with the departure date re-optimized for the minimum C3. The arrival dates are shifted earlier and later from the optimal until the C3 increased above  $30 \text{ km}^2/\text{s}^2$  or the VHP exceeded 7 km/s. As a result, the spread of viable arrival dates varies significantly from opportunity to opportunity. Each pair of LTST lines represents the minimum and maximum value across the 7-day launch period. They generally don't vary much, so the pair is often hard to distinguish from a single line. Finally, the LTST lines may have gaps; these are arrival dates where the approach declinations are incompatible with a landing at UTTR with the assumed EDL system.

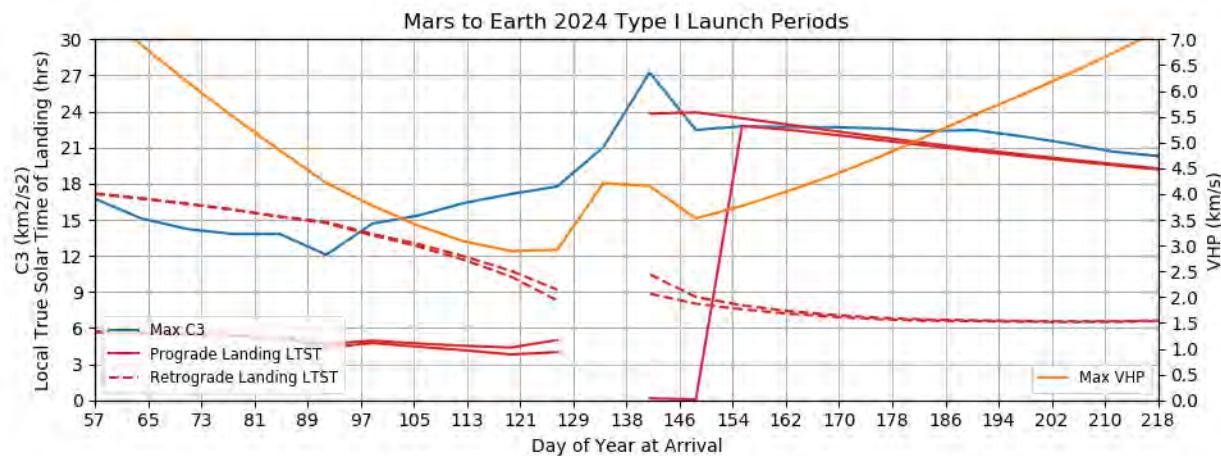


Figure 492: Mars to Earth 2024 Type I Launch Periods

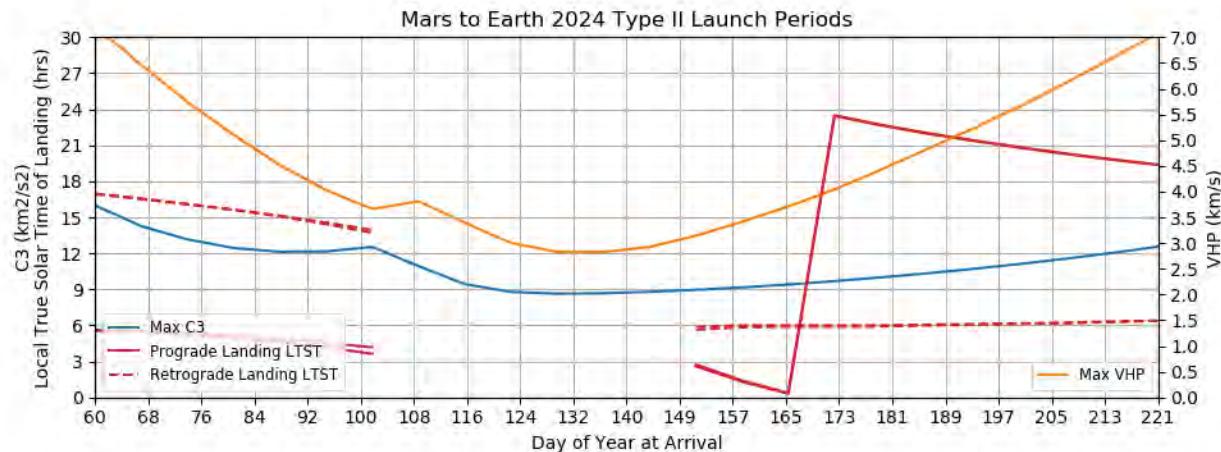


Figure 493: Mars to Earth 2024 Type II Launch Periods

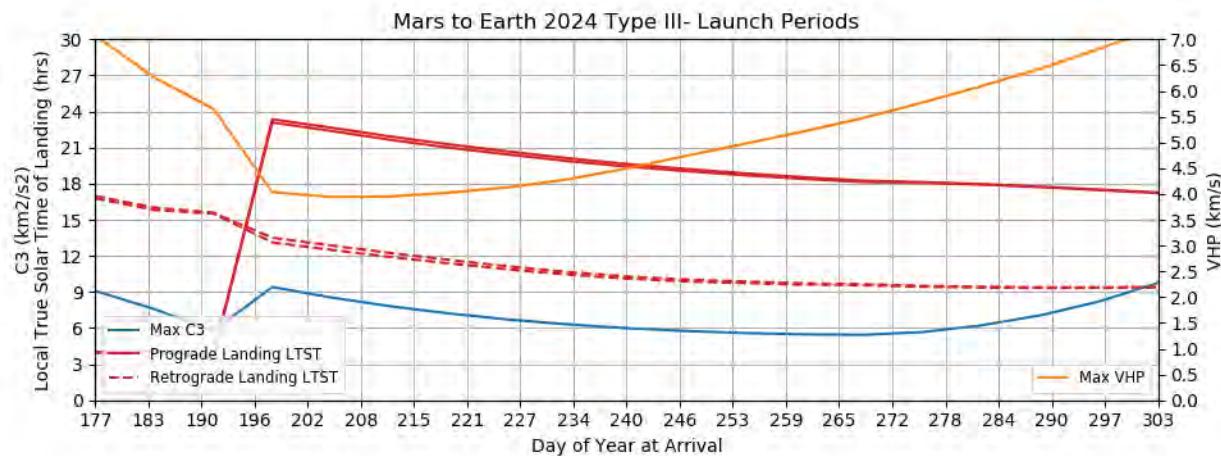


Figure 494: Mars to Earth 2024 Type III- Launch Periods

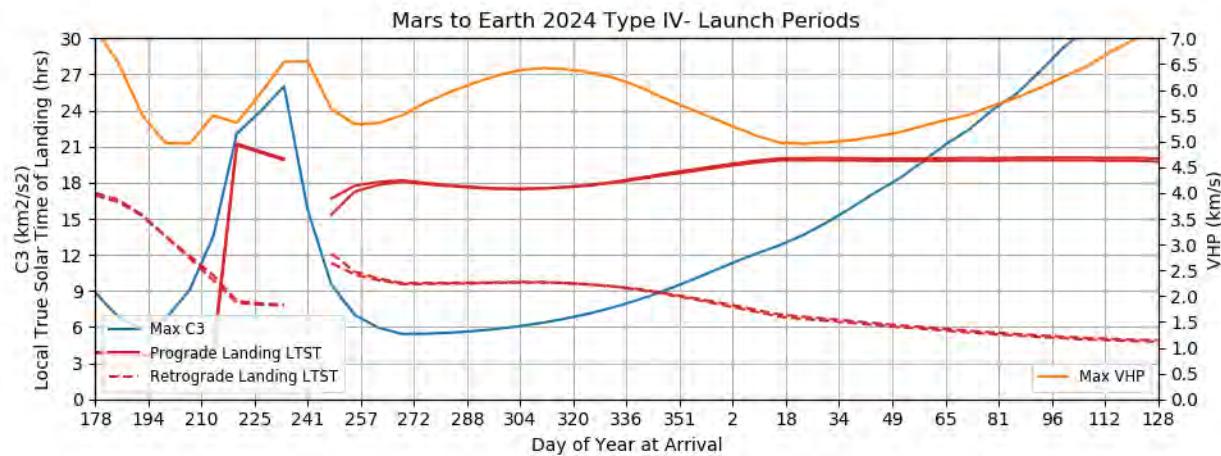


Figure 495: Mars to Earth 2024 Type IV- Launch Periods

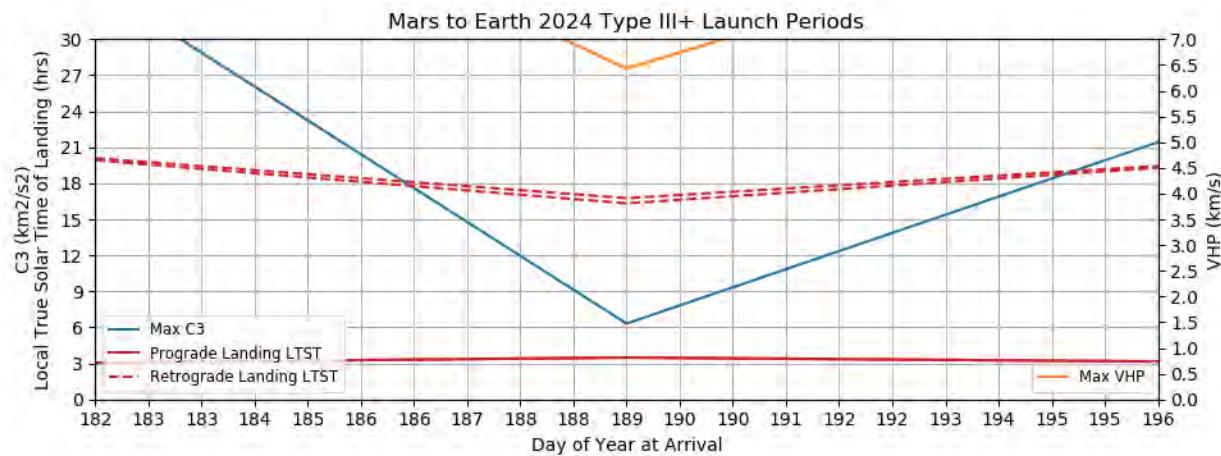


Figure 496: Mars to Earth 2024 Type III+ Launch Periods

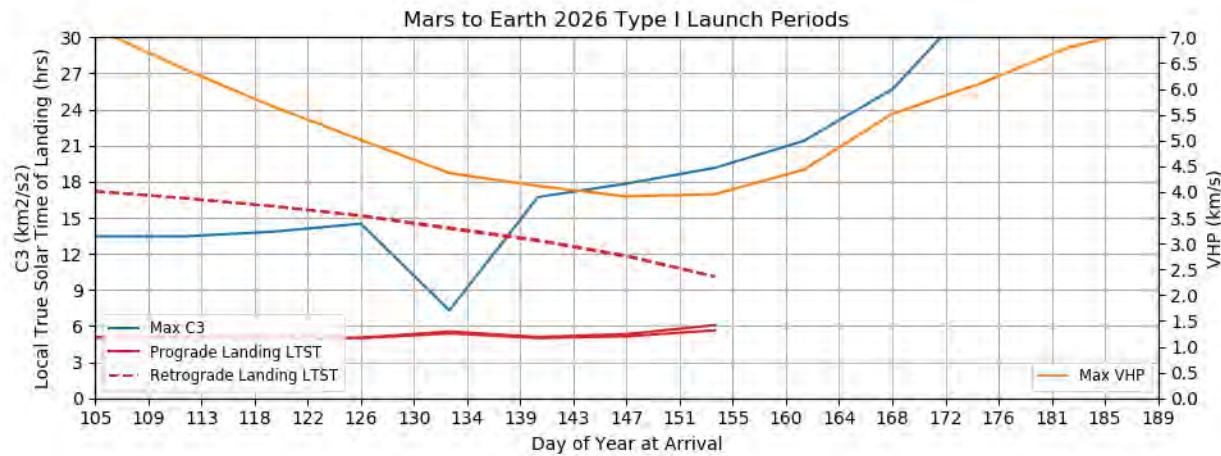


Figure 497: Mars to Earth 2026 Type I Launch Periods

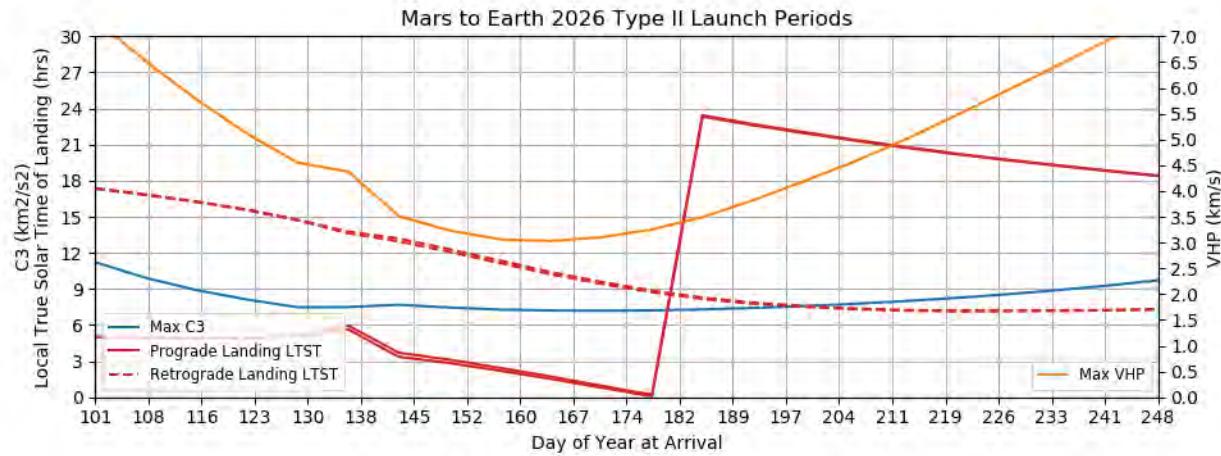


Figure 498: Mars to Earth 2026 Type II Launch Periods

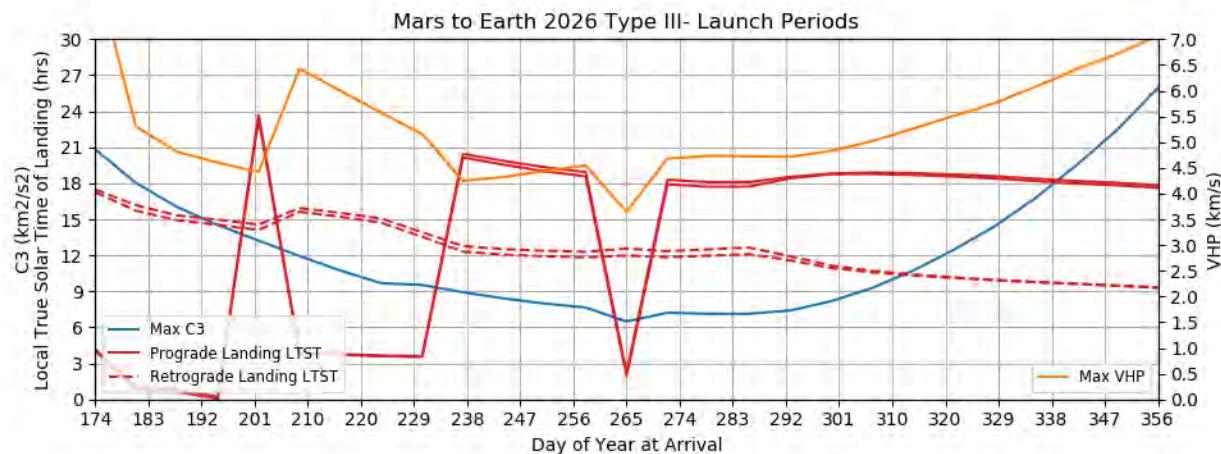


Figure 499: Mars to Earth 2026 Type III- Launch Periods

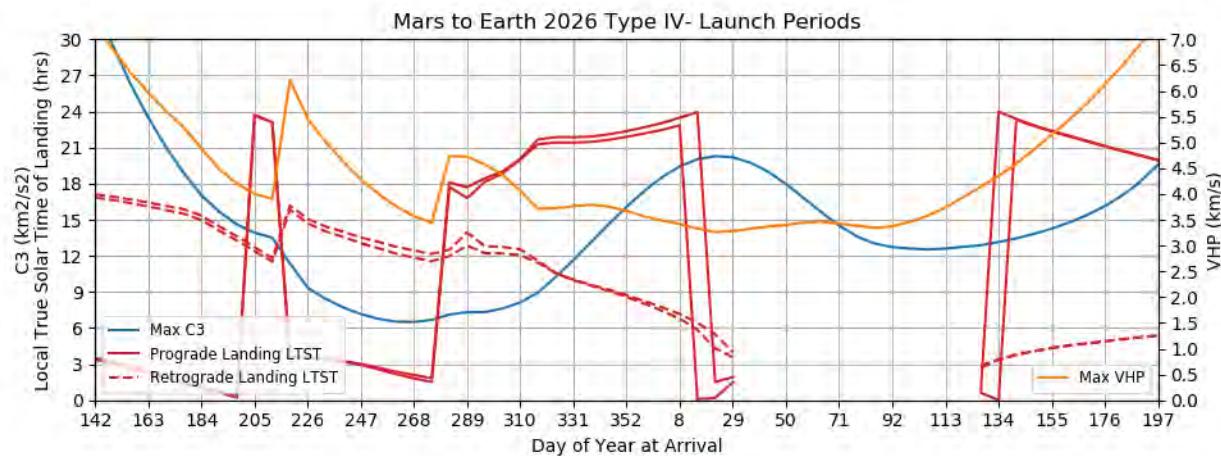


Figure 500: Mars to Earth 2026 Type IV- Launch Periods

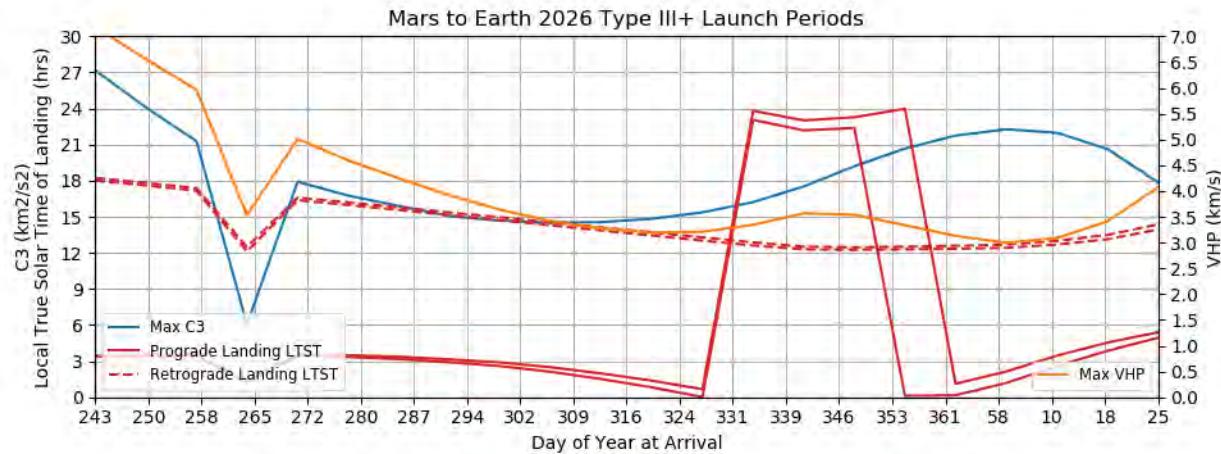
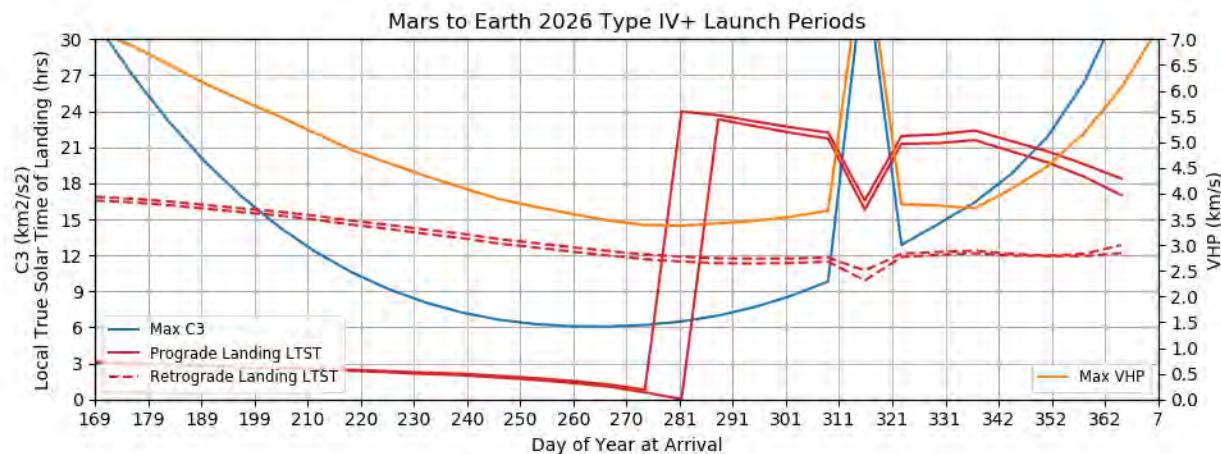
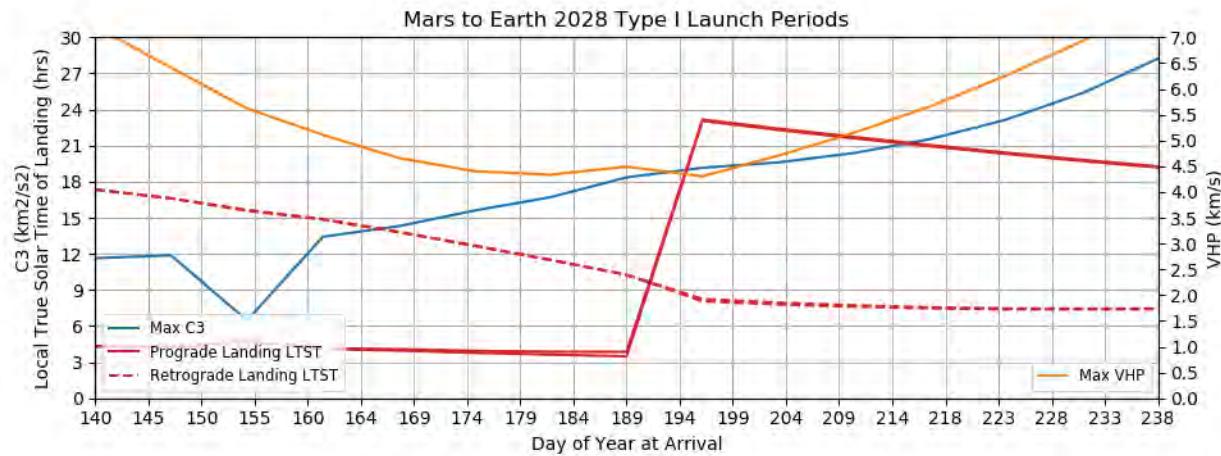


Figure 501: Mars to Earth 2026 Type III+ Launch Periods



**Figure 502: Mars to Earth 2026 Type IV+ Launch Periods**



**Figure 503: Mars to Earth 2028 Type I Launch Periods**

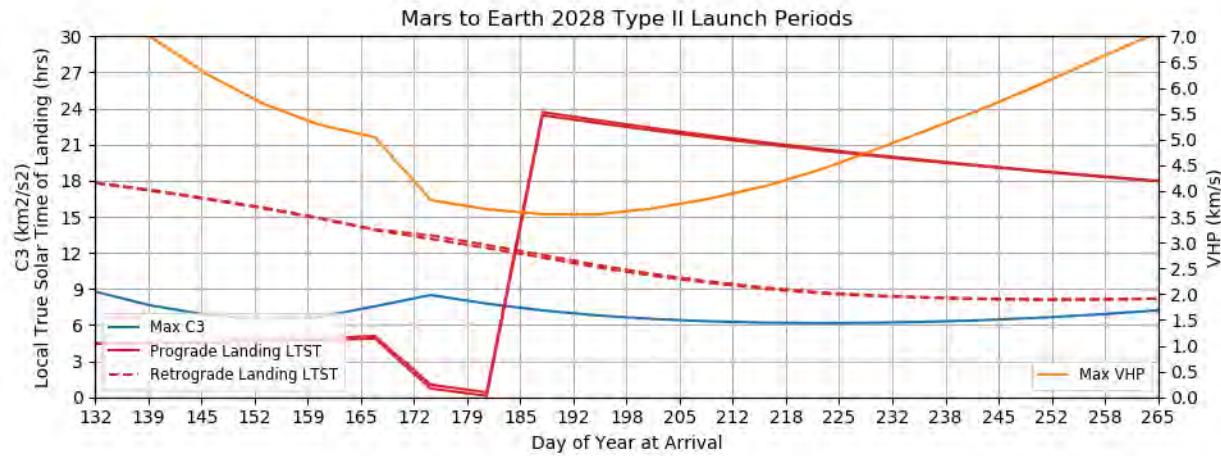


**Figure 504: Mars to Earth 2028 Type II Launch Periods**

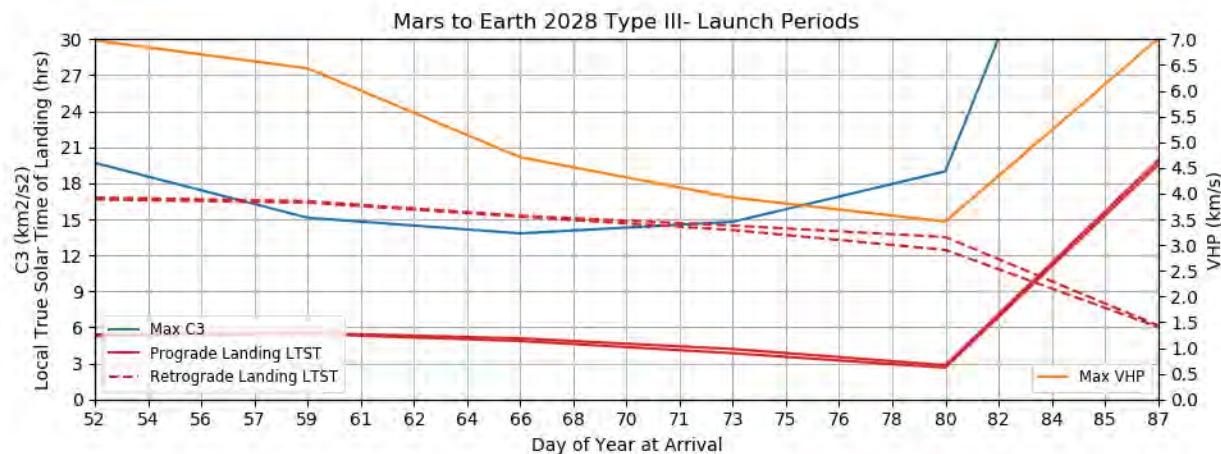


**Figure 505: Mars to Earth 2028 Type III- Launch Periods**

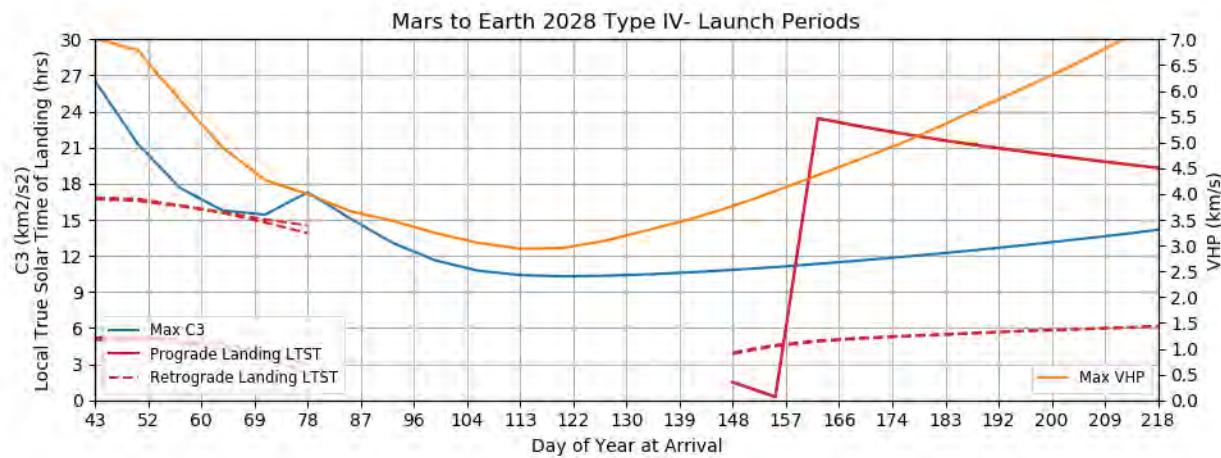


**Figure 506: Mars to Earth 2028 Type IV- Launch Periods**

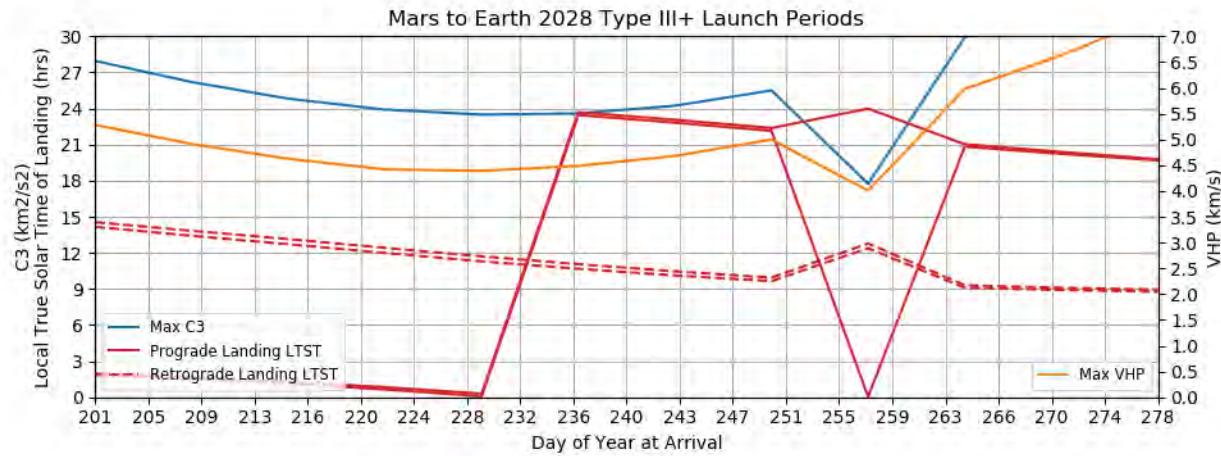


**Figure 507: Mars to Earth 2028 Type III+ Launch Periods**

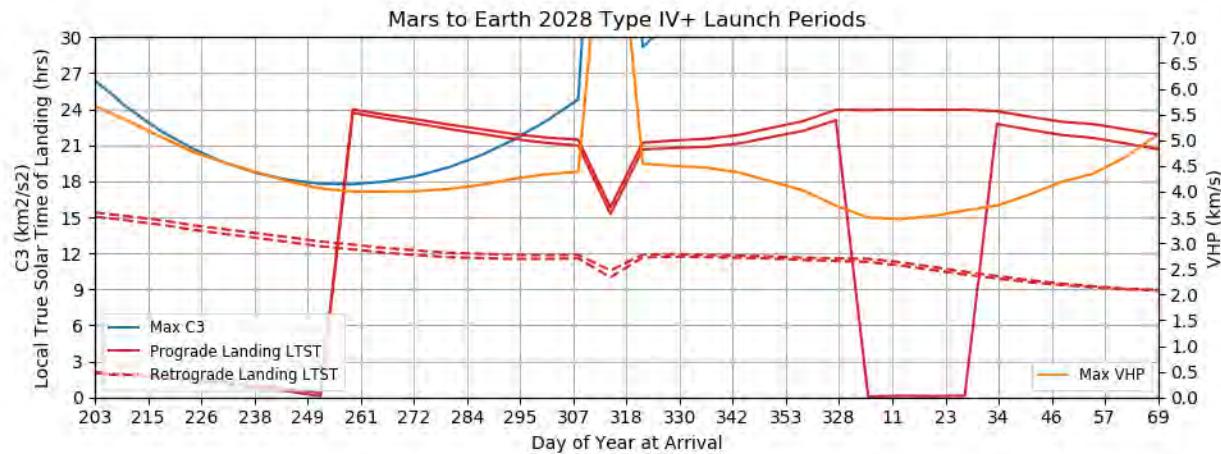


**Figure 508: Mars to Earth 2028 Type IV+ Launch Periods**

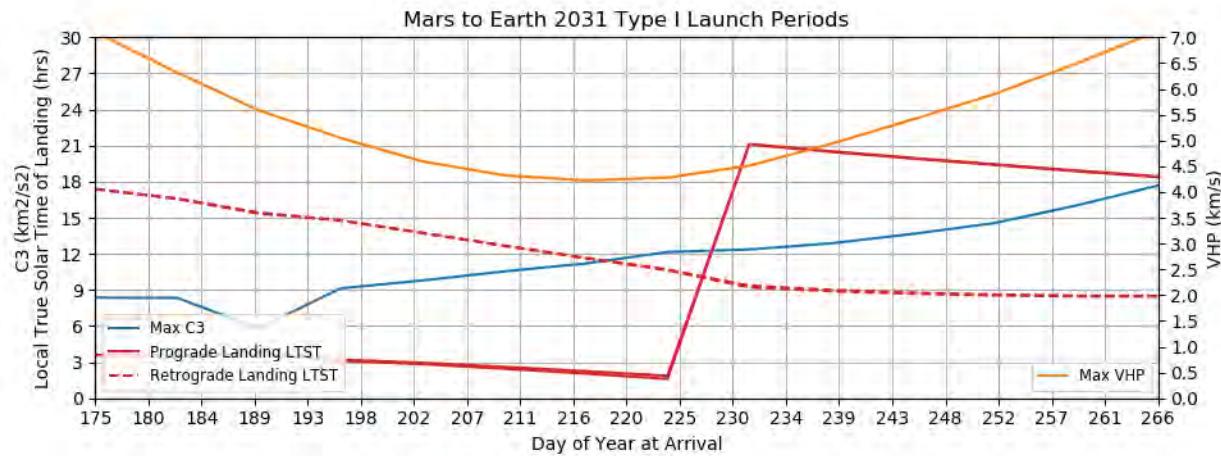


**Figure 509: Mars to Earth 2031 Type I Launch Periods**

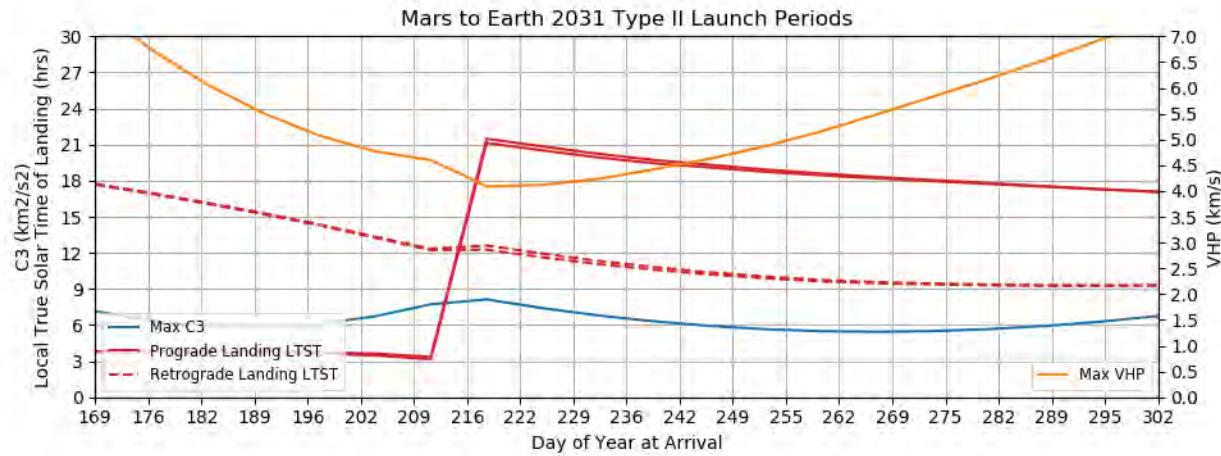


**Figure 510: Mars to Earth 2031 Type II Launch Periods**

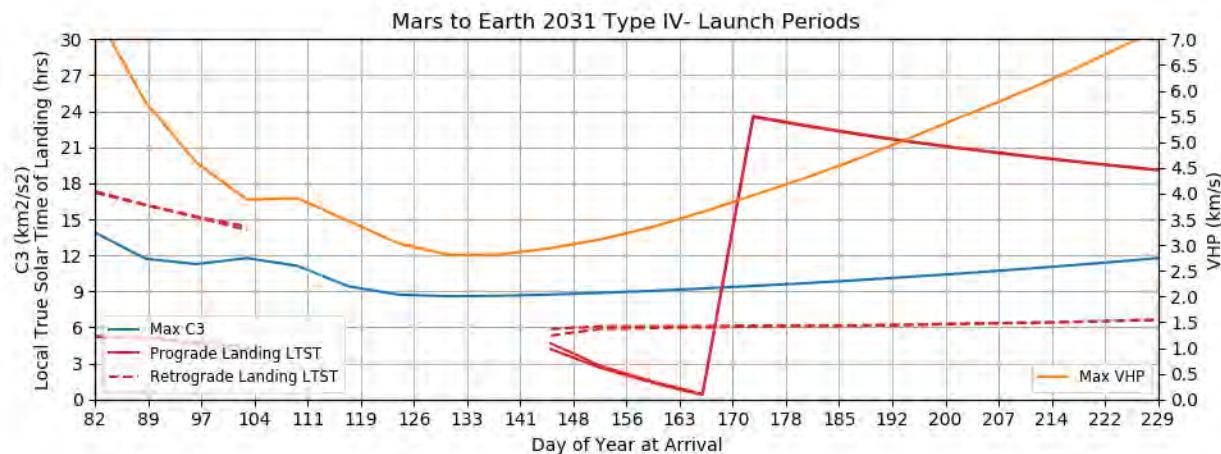


**Figure 511: Mars to Earth 2031 Type IV- Launch Periods**

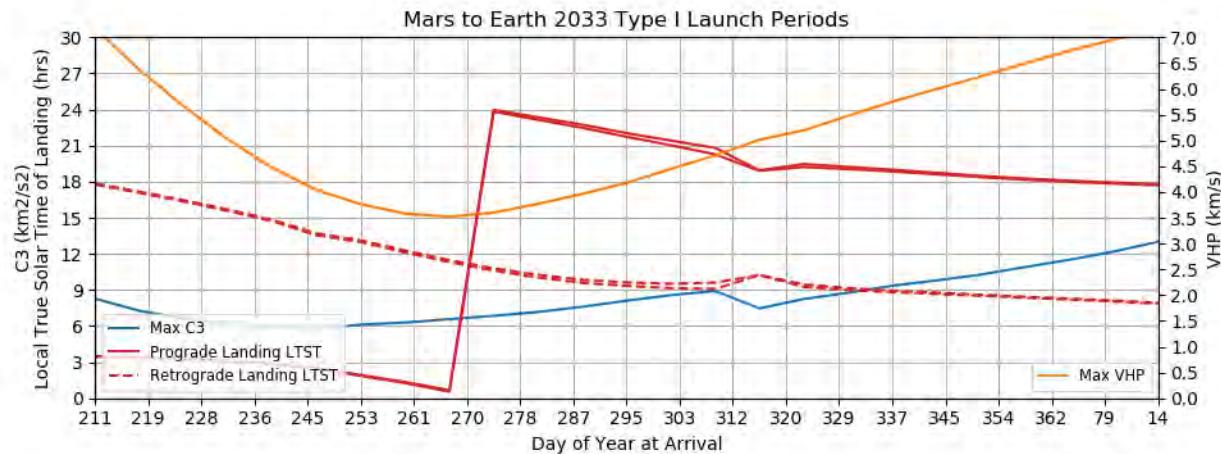


**Figure 512: Mars to Earth 2033 Type I Launch Periods**

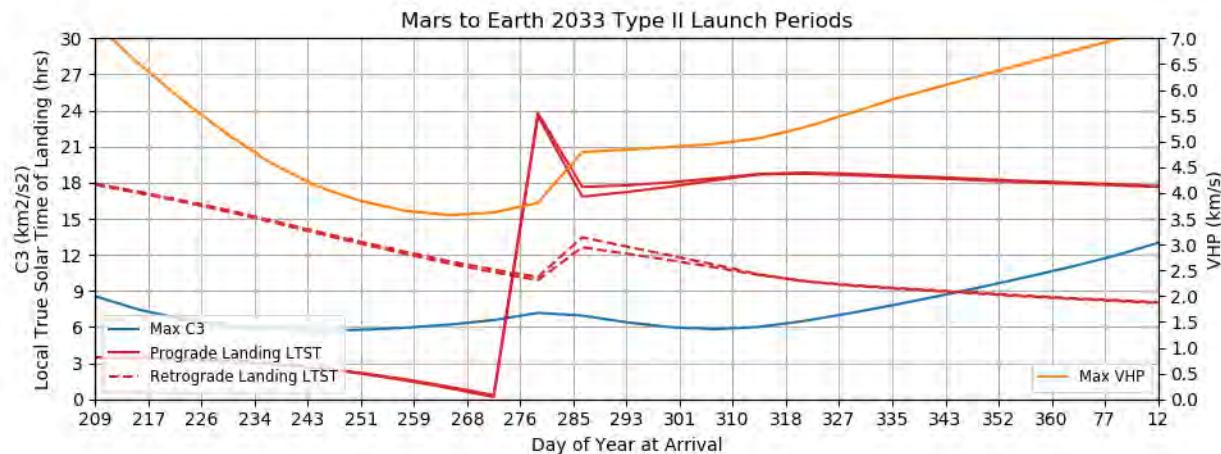


**Figure 513: Mars to Earth 2033 Type II Launch Periods**

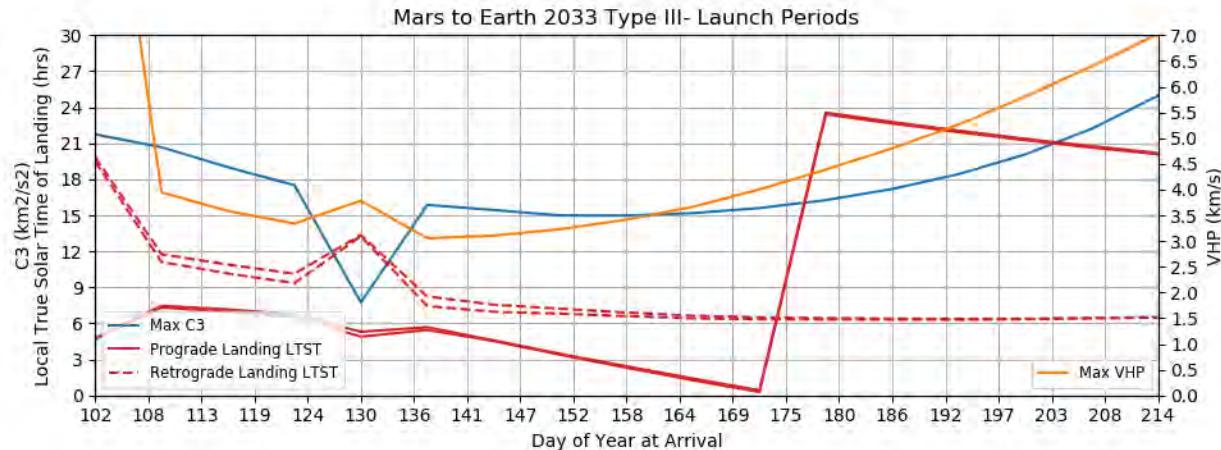


**Figure 514: Mars to Earth 2033 Type III- Launch Periods**

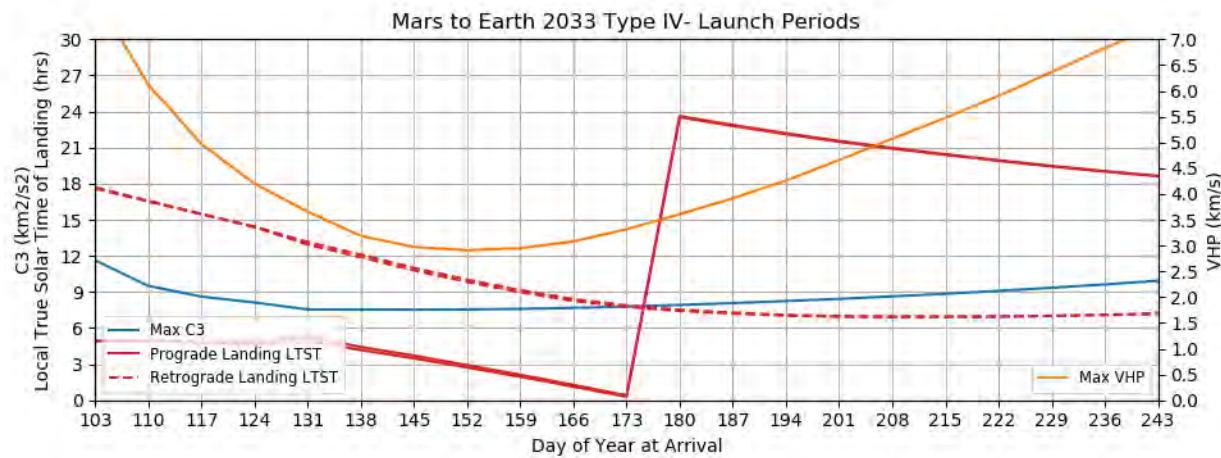


**Figure 515: Mars to Earth 2033 Type IV- Launch Periods**

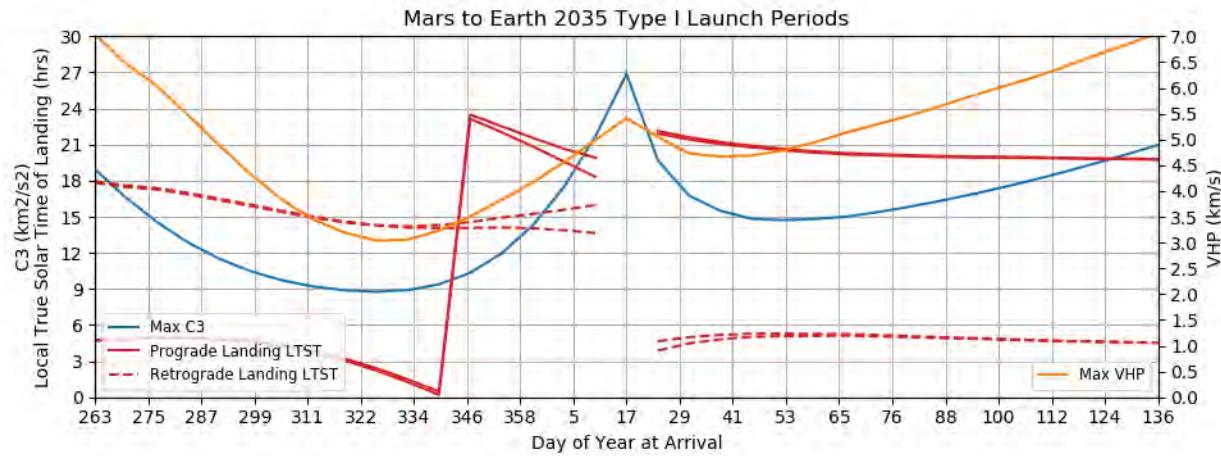


**Figure 516: Mars to Earth 2035 Type I Launch Periods**

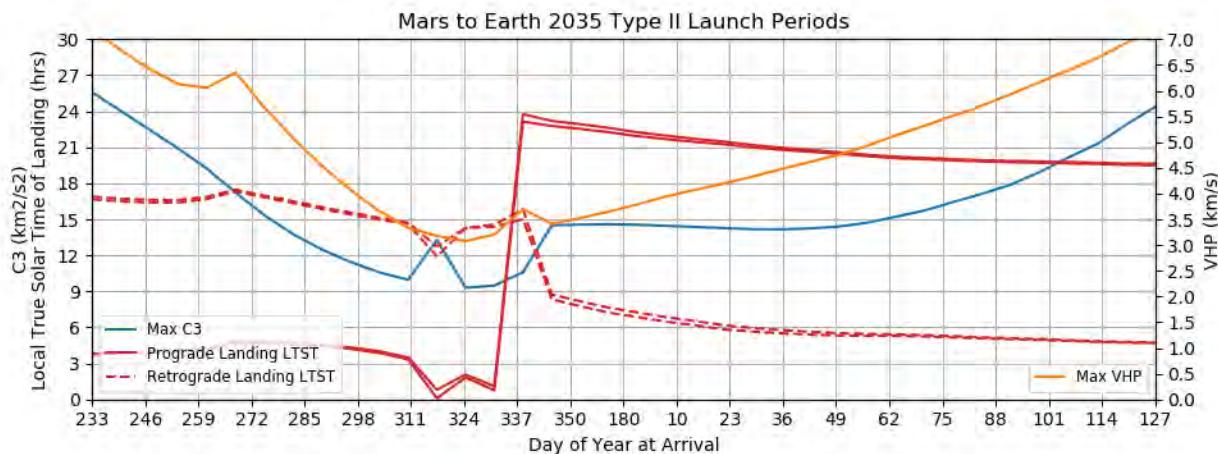


**Figure 517: Mars to Earth 2035 Type II Launch Periods**

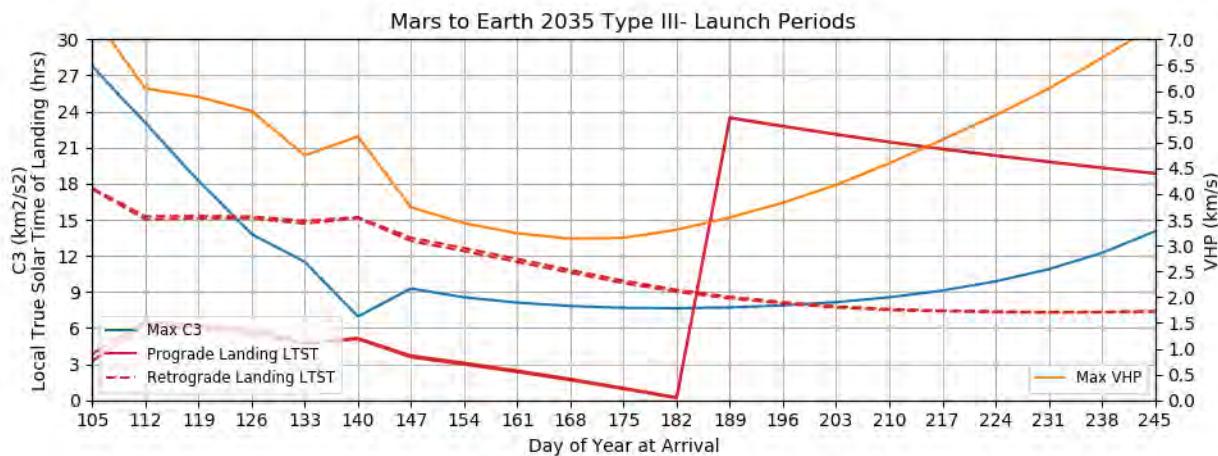


**Figure 518: Mars to Earth 2035 Type III- Launch Periods**

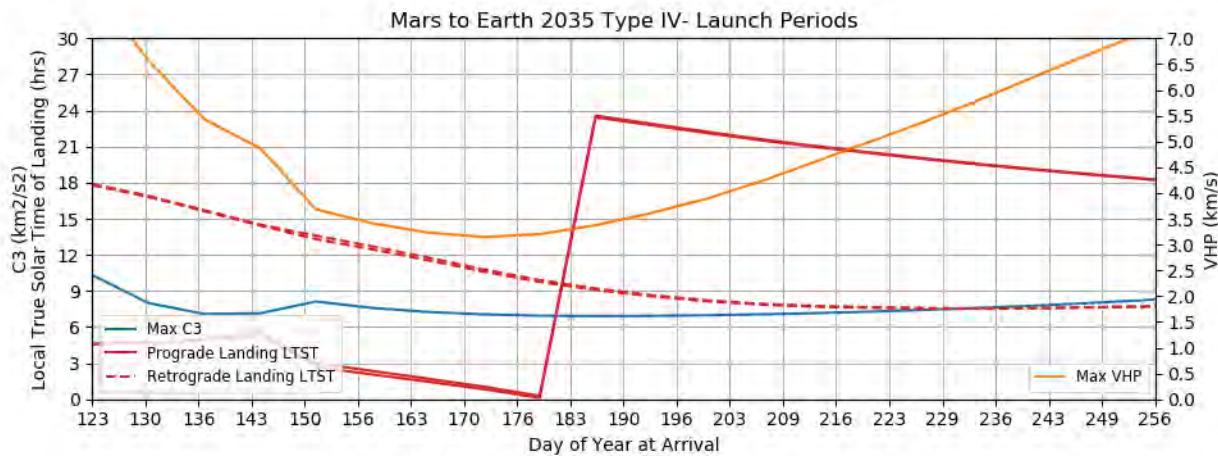


**Figure 519: Mars to Earth 2035 Type IV- Launch Periods**

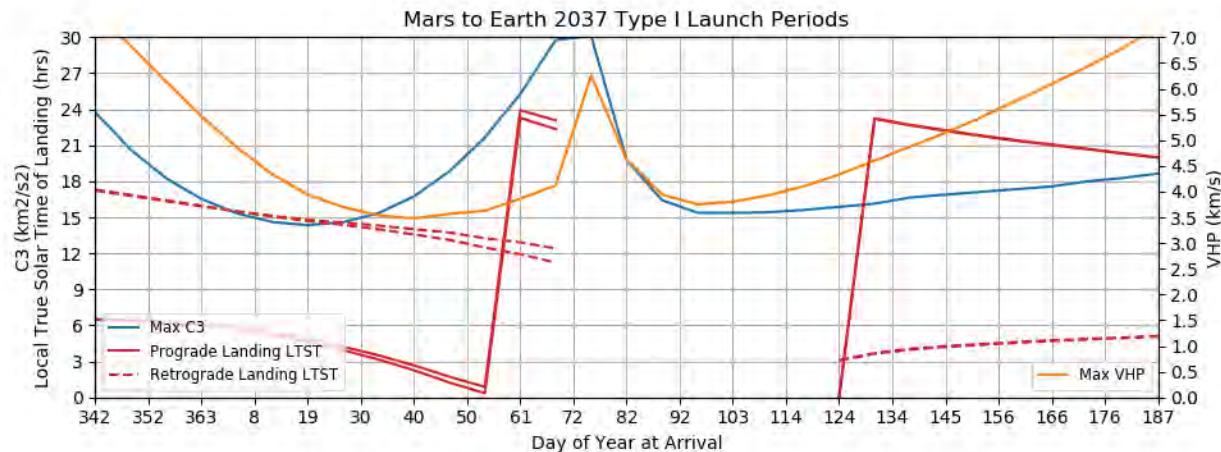


Figure 520: Mars to Earth 2037 Type I Launch Periods

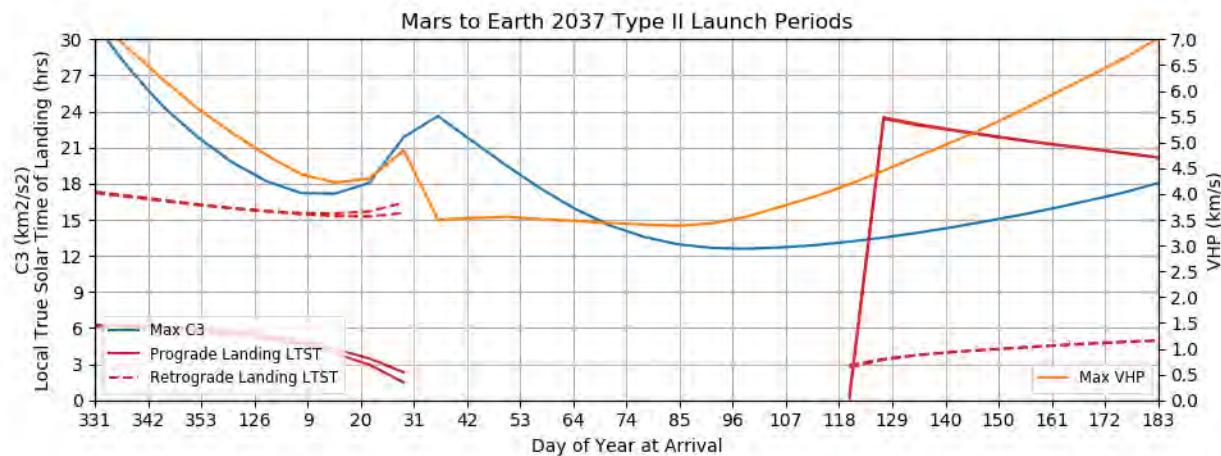


Figure 521: Mars to Earth 2037 Type II Launch Periods

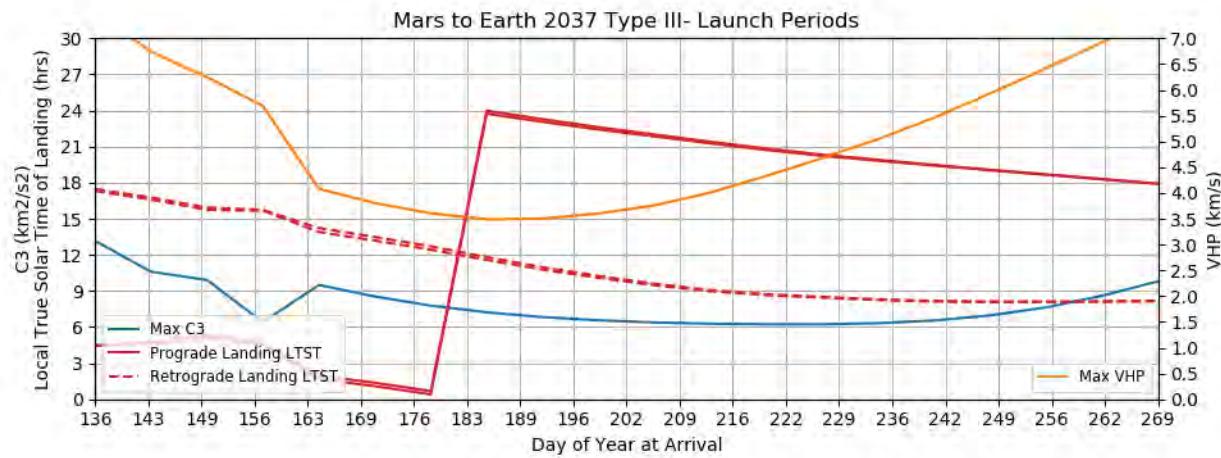
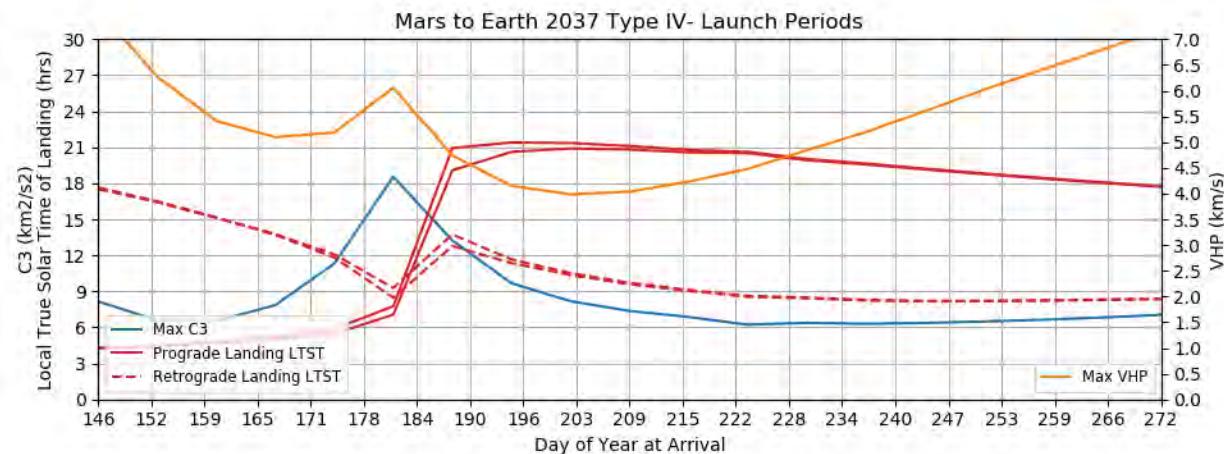
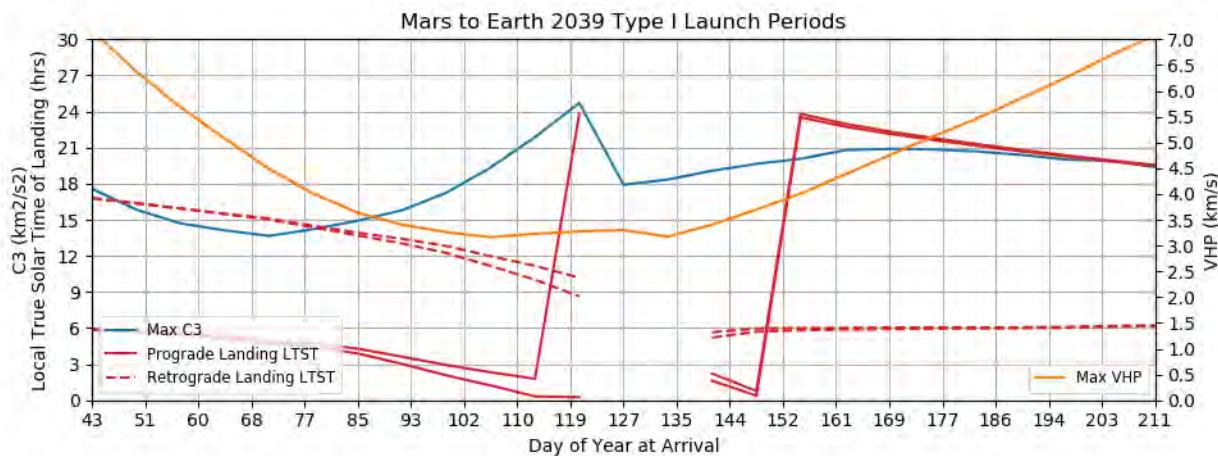


Figure 522: Mars to Earth 2037 Type III- Launch Periods



**Figure 523: Mars to Earth 2037 Type IV- Launch Periods**



**Figure 524: Mars to Earth 2039 Type I Launch Periods**

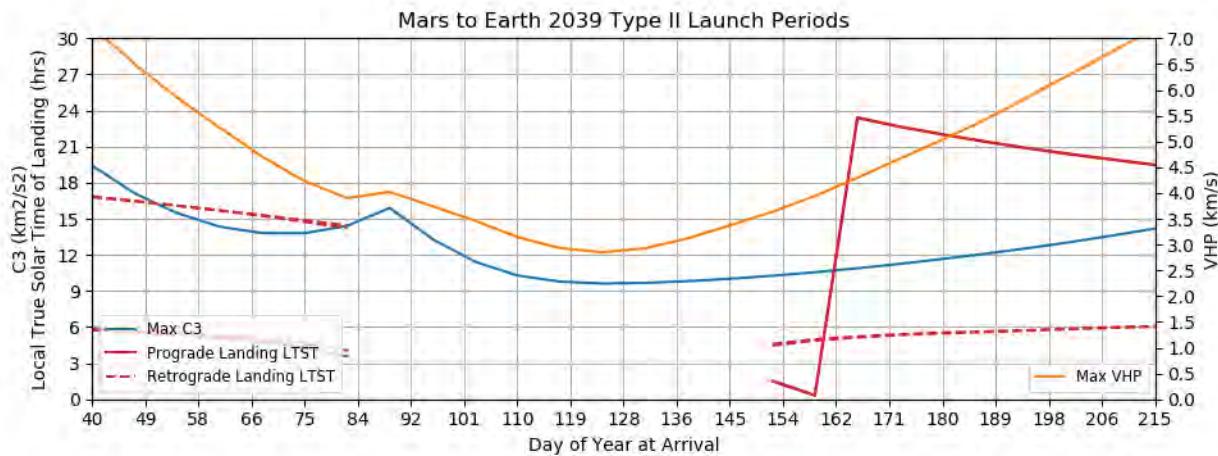


**Figure 525: Mars to Earth 2039 Type II Launch Periods**

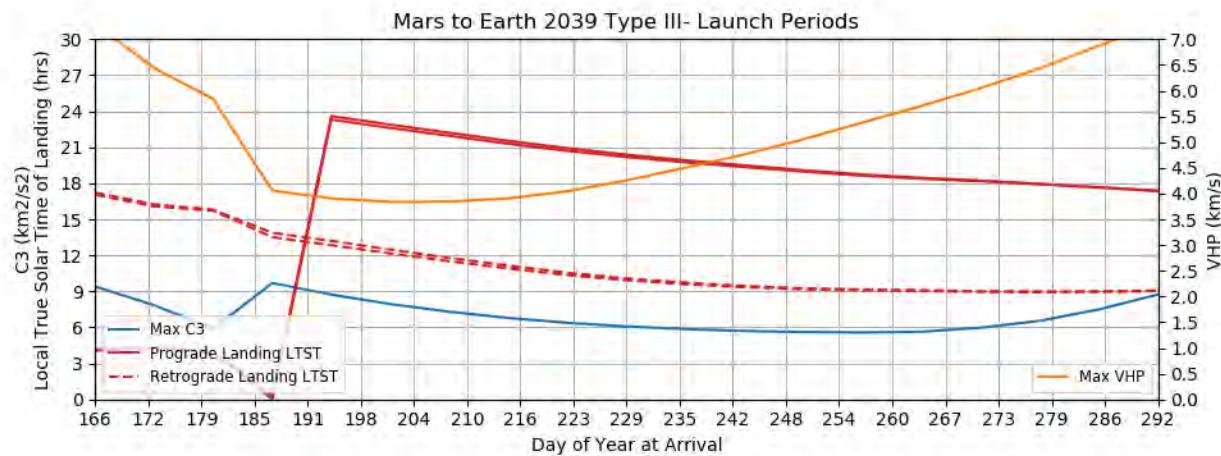


Figure 526: Mars to Earth 2039 Type III- Launch Periods

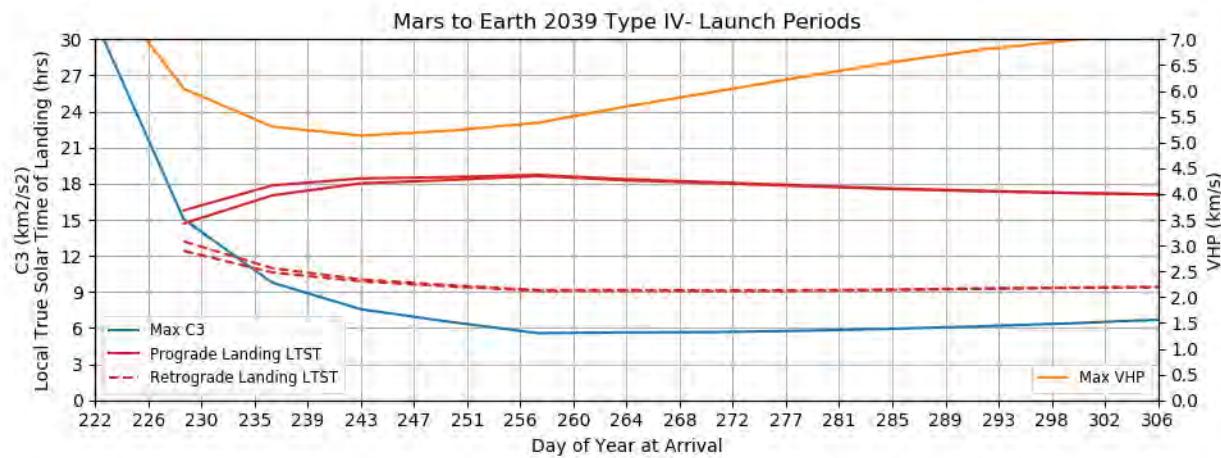


Figure 527: Mars to Earth 2039 Type IV- Launch Periods

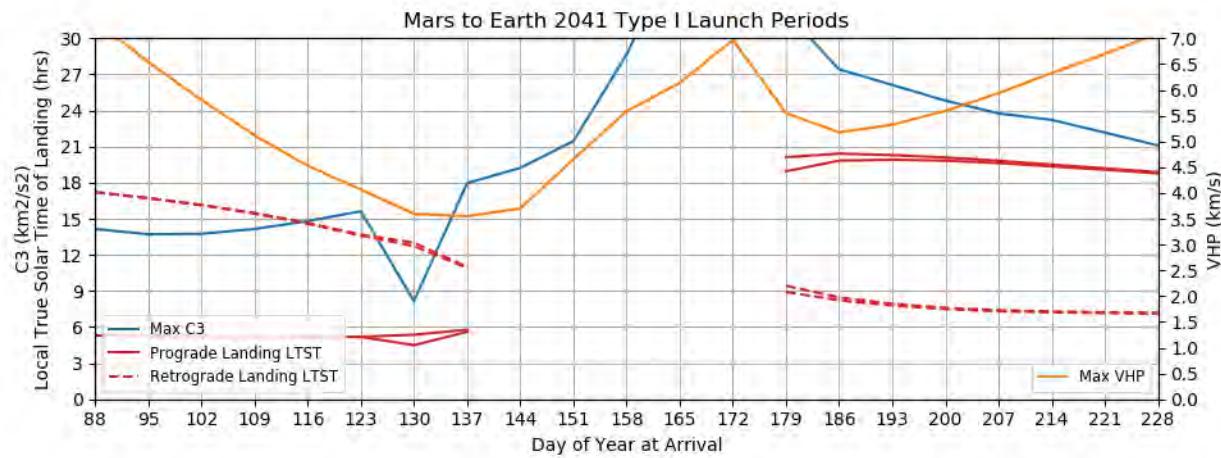
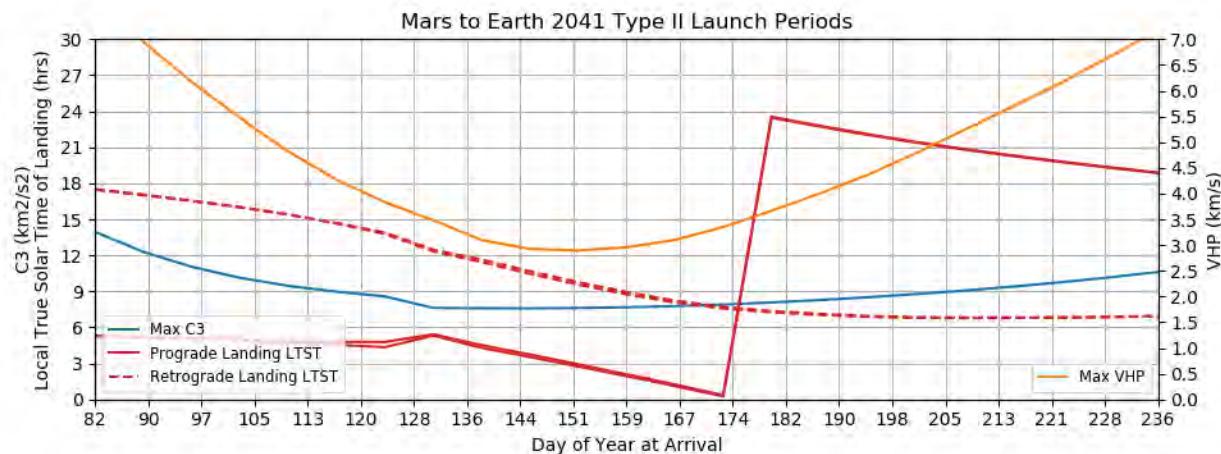
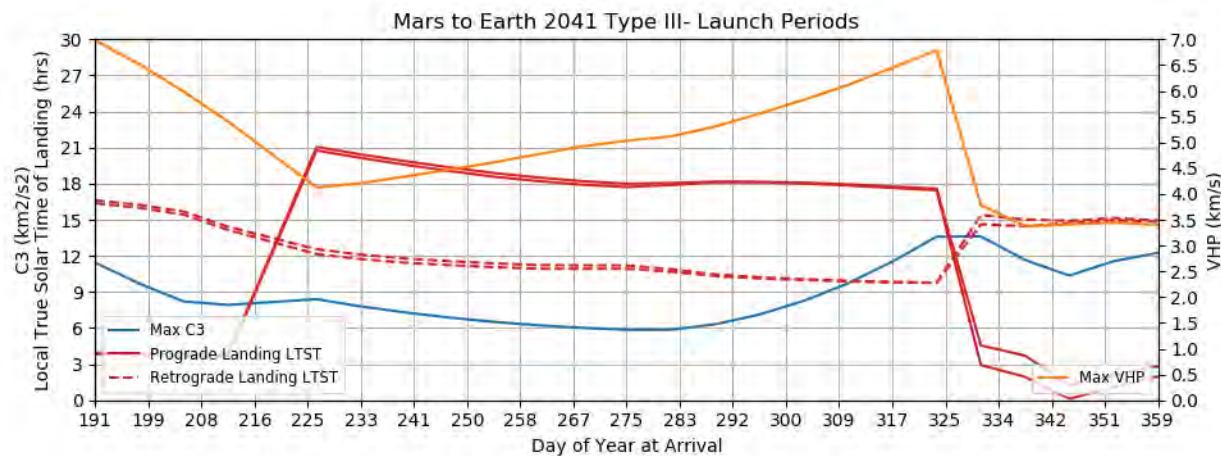


Figure 528: Mars to Earth 2041 Type I Launch Periods



**Figure 529: Mars to Earth 2041 Type II Launch Periods**



**Figure 530: Mars to Earth 2041 Type III- Launch Periods**

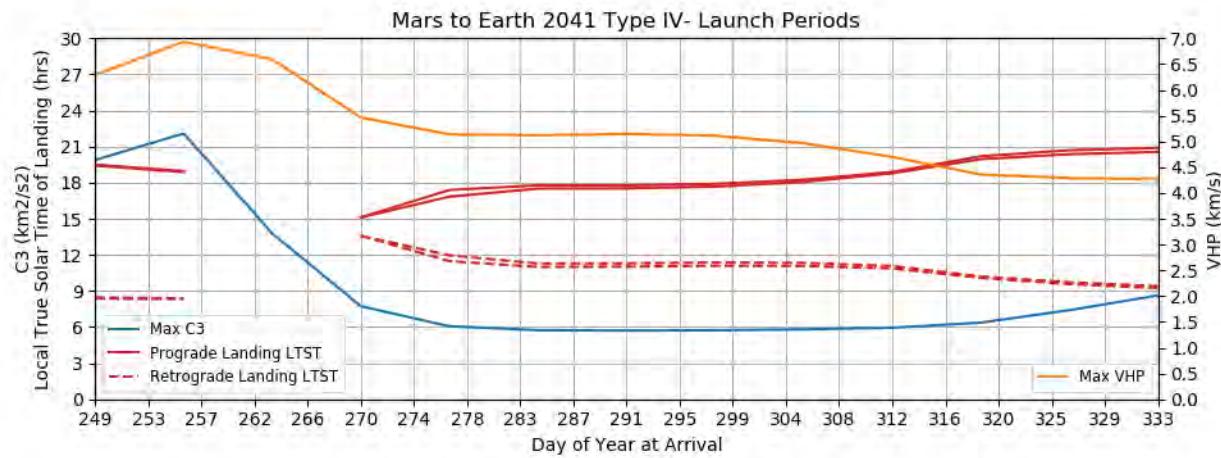


**Figure 531: Mars to Earth 2041 Type IV- Launch Periods**

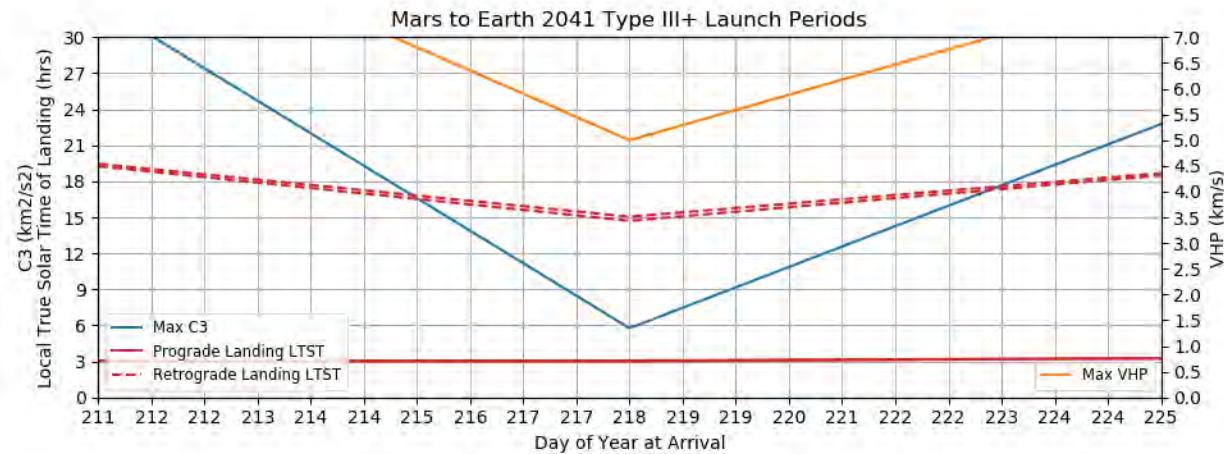


Figure 532: Mars to Earth 2041 Type III+ Launch Periods

## 11.4 Porkchop Plots

### 11.4.1 Introduction

This selection of porkchop plots are a representative set. For readability, each plot only contains a few contours, and for brevity, only a few sets of contours are included. The local solar time of landing at the Utah Test and Training Range (UTTR) is dependent on the entry flight path angle and the descent central angle. These plots assume an entry flight path angle of -25 deg and a descent central angle of 1.95 deg.

### 11.4.2 Mars to Earth 2024

This section contains porkchop plots for the Mars-to-Earth 2024 opportunities. Table 37 contains the optimal single-day transfers for minimum launch energy (C3) and arrival velocity (VHP) as well as the maximum launch-mass and captured-mass launch periods for each trajectory type within the opportunity. These data should only be used for preliminary analysis and planning purposes.

**Table 37: Mars to Earth 2024 Optimal Launch/Arrival Data**

Optimization Criteria	Trajectory Type	Departure Date (dd-mmm-yyyy)	Arrival Date (dd-mmm-yyyy)	Launch Energy, C3 (km <sup>2</sup> /s <sup>2</sup> )	Declination of the Launch Asymptote, DLA (deg)	Approach V-Infinity, VHP (km/s)
<b>Single-Day Optimization</b>						
Minimum C3	I	10-Aug-2024	01-Apr-2025	12.0	-7.9	4.28
Minimum C3	II	25-Jul-2024	11-May-2025	8.6	10.7	2.82
Minimum C3	III-	06-May-2023	10-Jul-2025	5.7	34.9	5.66
Minimum C3	IV-	13-May-2023	27-Sep-2025	5.4	-9.2	5.54
Minimum C3	III+	04-Jun-2023	08-Jul-2025	6.3	27.0	6.30
Minimum C3	IV+	09-Nov-2023	30-Nov-2025	18.5	5.1	7.74
Minimum VHP	I	06-Sep-2024	08-May-2025	15.3	-5.6	2.79
Minimum VHP	II	07-Aug-2024	15-May-2025	9.1	6.1	2.80
Minimum VHP	III-	06-May-2023	22-Jul-2025	10.2	50.0	4.43
Minimum VHP	IV-	29-Nov-2022	20-Jul-2025	10.9	4.8	3.69
Minimum VHP	III+	02-May-2023	12-Jul-2025	17.3	39.2	4.31
Minimum VHP	IV+	10-Jan-2024	28-Dec-2025	24.6	8.8	7.17
<b>Launch Period Optimization</b>						
Minimum C3	I	07-Aug-2024	02-Apr-2025	12.1	-9.5	4.22
		14-Aug-2024		12.1	-7.2	4.21
Minimum C3	II	22-Jul-2024	10-May-2025	8.6	11.7	2.82
		29-Jul-2024		8.7	10.4	2.83
Minimum C3	III-	03-May-2023	10-Jul-2025	5.8	35.2	5.65
		10-May-2023		5.8	34.7	5.65
Minimum C3	IV-	08-May-2023	26-Sep-2025	5.4	-9.0	5.51
		15-May-2023		5.4	-9.6	5.51
Minimum C3	III+	01-Jun-2023	08-Jul-2025	6.3	29.8	6.08
		01-Jun-2023		6.3	25.2	6.46
Minimum C3	IV+	Not Possible				

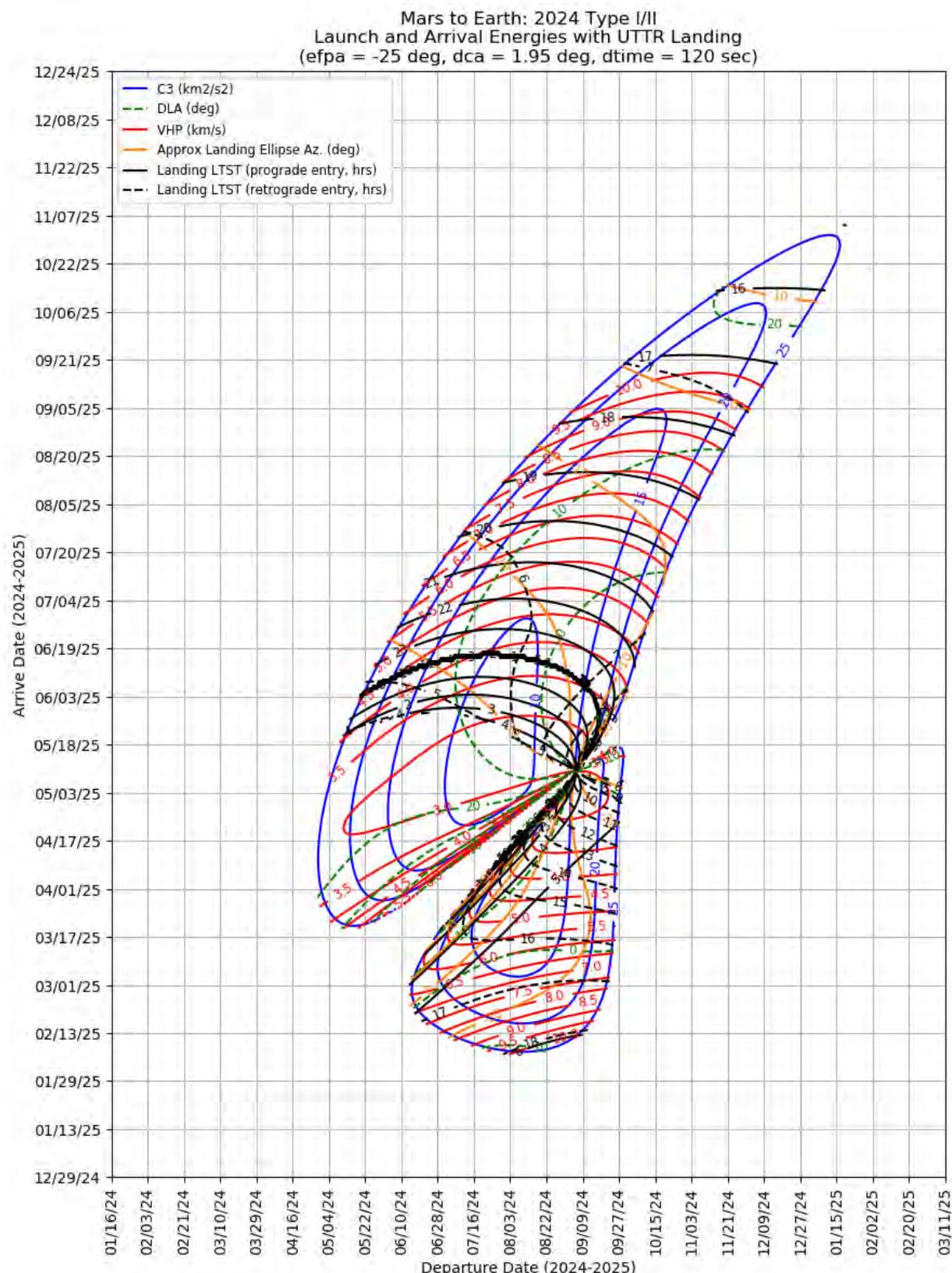


**Figure 533: Mars to Earth 2024 Type I/II – Launch/Arrival Energy and UTTR Landing Times**

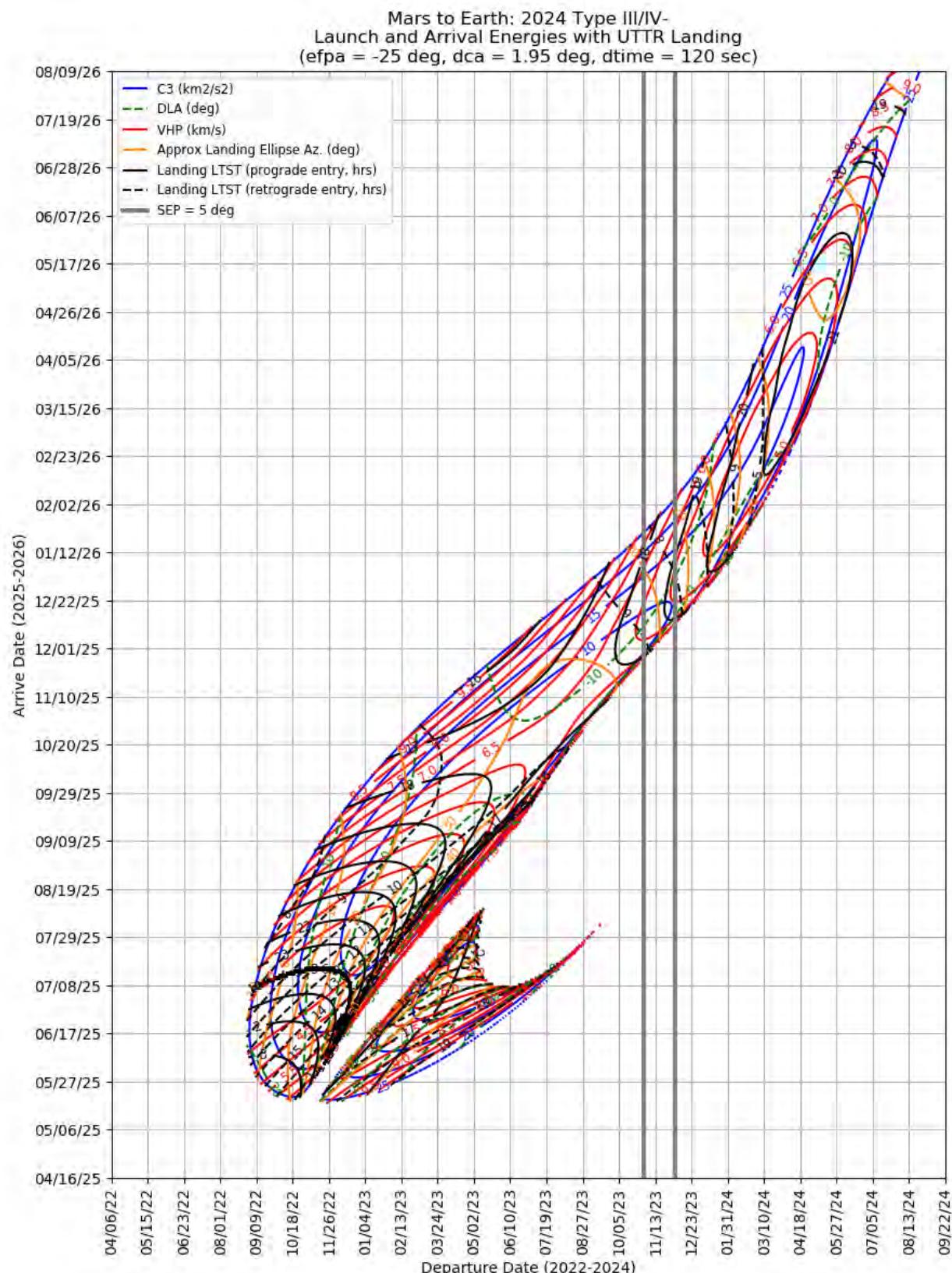


**Figure 534: Mars to Earth 2024 Type III/IV- – Launch/Arrival Energy and UTTR Landing Times**

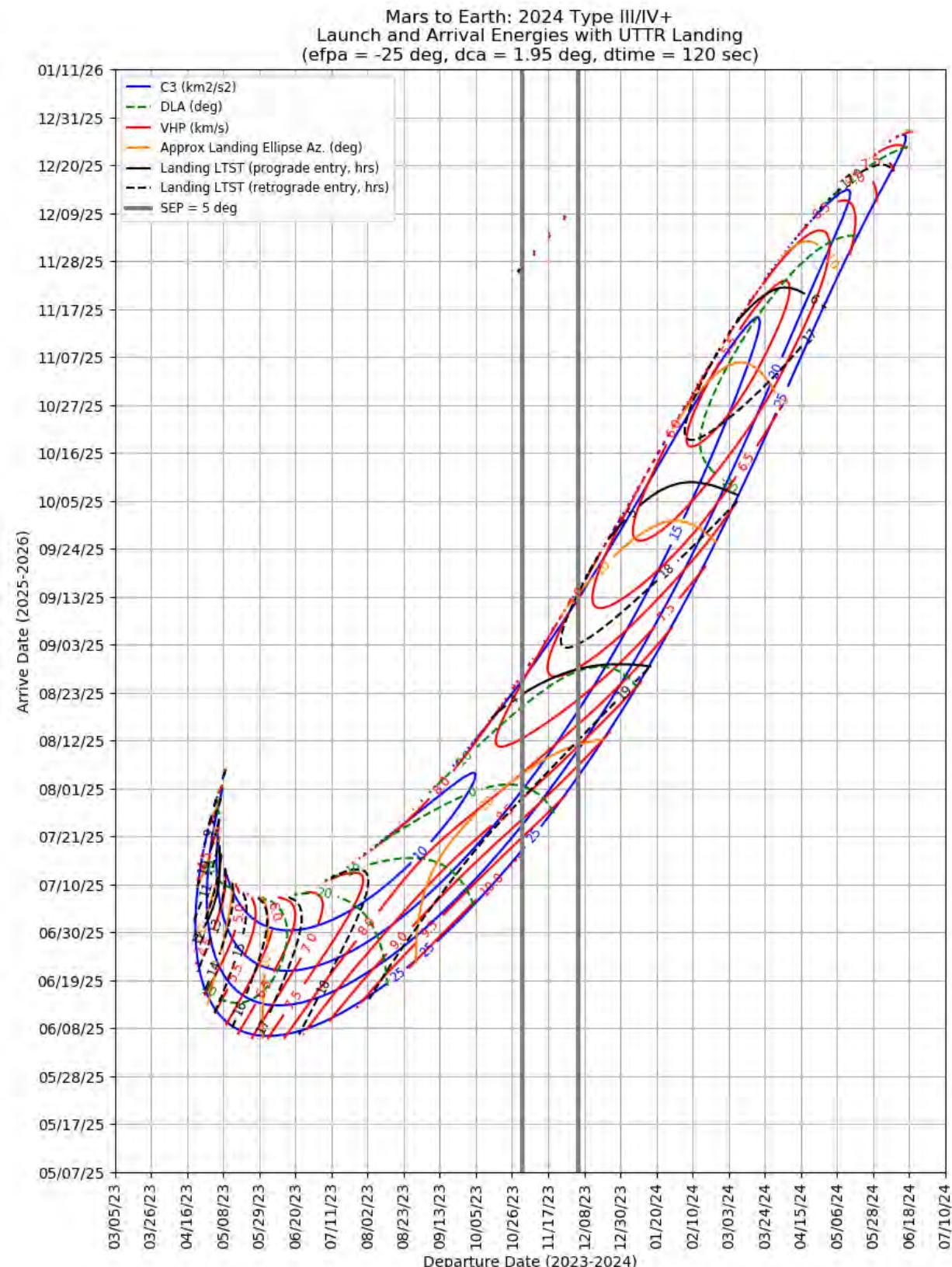


**Figure 535: Mars to Earth 2024 Type III/IV+ – Launch/Arrival Energy and UTTR Landing Times**

### 11.4.3 Mars to Earth 2026

This section contains porkchop plots for the Mars-to-Earth 2024 opportunities. Table 38 contains the optimal single-day transfers for minimum launch energy (C3) and arrival velocity (VHP) as well as the maximum launch-mass and captured-mass launch periods for each trajectory type within the opportunity. These data should only be used for preliminary analysis and planning purposes.

**Table 38: Mars to Earth 2026 Optimal Launch/Arrival Data**

Optimization Criteria	Trajectory Type	Departure Date (dd-mmm-yyyy)	Arrival Date (dd-mmm-yyyy)	Launch Energy, C3 (km <sup>2</sup> /s <sup>2</sup> )	Declination of the Launch Asymptote, DLA (deg)	Approach V-Infinity, VHP (km/s)
<b>Single-Day Optimization</b>						
Minimum C3	I	11-Aug-2026	13-May-2027	7.3	26.2	4.36
Minimum C3	II	03-Aug-2026	19-Jun-2027	7.2	4.7	3.09
Minimum C3	III-	04-Aug-2025	23-Sep-2027	6.4	10.2	3.61
Minimum C3	IV-	23-May-2025	09-Oct-2027	7.1	-31.2	4.73
Minimum C3	III+	20-Aug-2025	22-Sep-2027	6.1	12.3	3.51
Minimum C3	IV+	22-Sep-2025	12-Nov-2027	31.8	-2.2	8.44
Minimum VHP	I	19-Oct-2026	31-May-2027	20.4	21.6	3.87
Minimum VHP	II	23-Jul-2026	10-Jun-2027	7.3	7.9	3.02
Minimum VHP	III-	01-Oct-2025	04-Nov-2027	9.3	-16.2	2.99
Minimum VHP	IV-	24-Sep-2025	14-Nov-2027	10.0	-11.0	3.15
Minimum VHP	III+	02-Apr-2026	22-Jan-2028	21.0	-34.9	2.93
Minimum VHP	IV+	24-Sep-2025	13-Nov-2027	32.6	13.0	8.21
<b>Launch Period Optimization</b>						
Minimum C3	I	09-Aug-2026	13-May-2027	7.3	27.3	4.37
		16-Aug-2026		7.3	24.4	4.37
Minimum C3	II	31-Jul-2026	20-Jun-2027	7.2	5.7	3.10
		07-Aug-2026		7.2	3.5	3.10
Minimum C3	III-	30-Jul-2025	22-Sep-2027	6.5	13.1	3.64
		06-Aug-2025		6.5	7.4	3.65
Minimum C3	IV-	19-May-2025	09-Oct-2027	7.1	-29.6	4.73
		26-May-2025		7.1	-32.5	4.74
Minimum C3	III+	16-Aug-2025	21-Sep-2027	6.1	14.0	3.53
		23-Aug-2025		6.1	11.0	3.53
Minimum C3	IV+	16-Sep-2025	12-Nov-2027	36.3	5.4	8.92
		23-Sep-2025		38.4	26.1	8.61

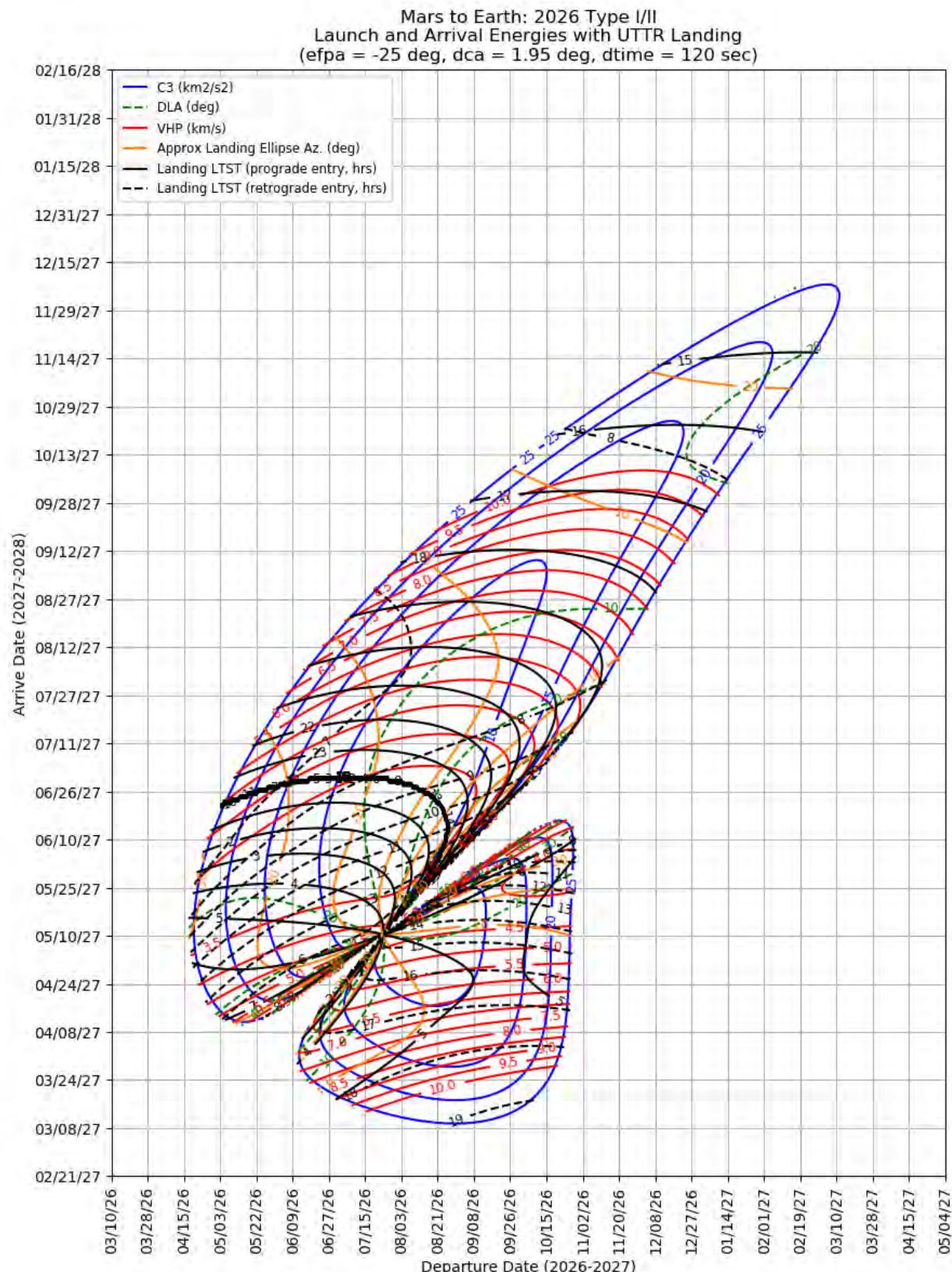


**Figure 536: Mars to Earth 2026 Type I/II – Launch/Arrival Energy and UTTR Landing Times**

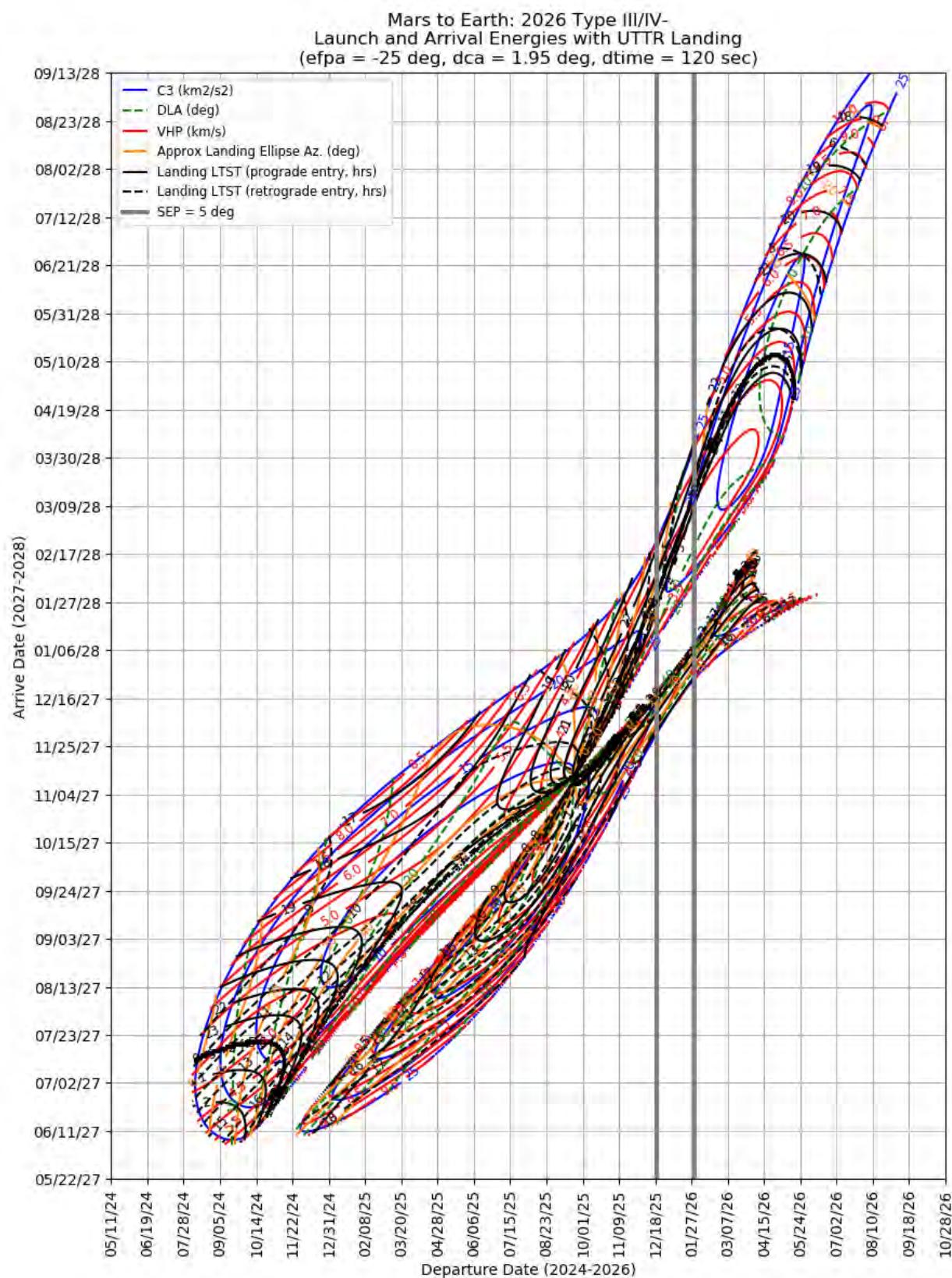


**Figure 537: Mars to Earth 2026 Type III/IV- – Launch/Arrival Energy and UTTR Landing Times**

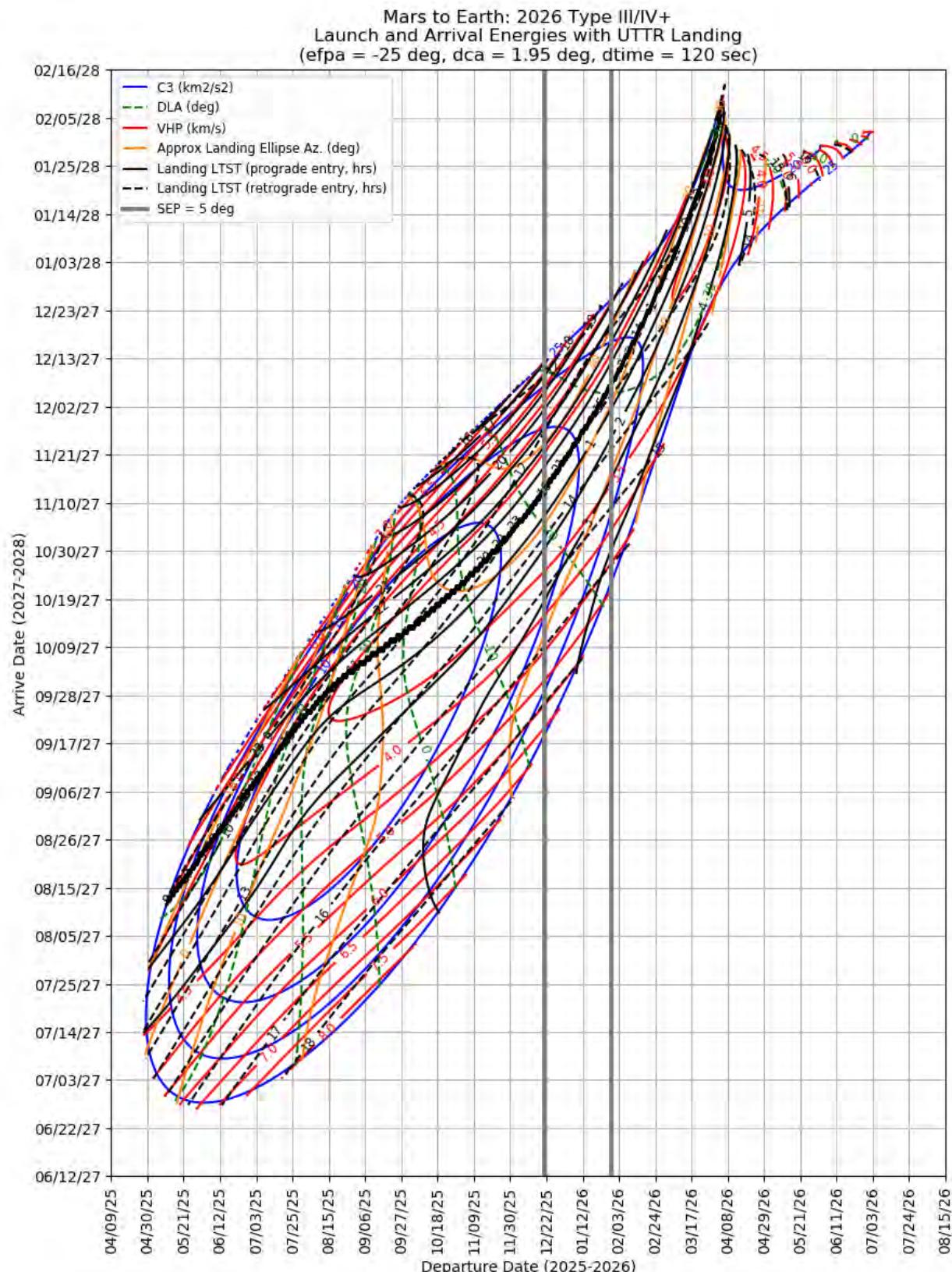


**Figure 538: Mars to Earth 2026 Type III/IV+ – Launch/Arrival Energy and UTTR Landing Times**

#### 11.4.4 Mars to Earth 2028

This section contains porkchop plots for the Mars-to-Earth 2024 opportunities. Table 39 contains the optimal single-day transfers for minimum launch energy (C3) and arrival velocity (VHP) as well as the maximum launch-mass and captured-mass launch periods for each trajectory type within the opportunity. These data should only be used for preliminary analysis and planning purposes.

**Table 39: Mars to Earth 2028 Optimal Launch/Arrival Data**

Optimization Criteria	Trajectory Type	Departure Date (dd-mmm-yyyy)	Arrival Date (dd-mmm-yyyy)	Launch Energy, C3 (km <sup>2</sup> /s <sup>2</sup> )	Declination of the Launch Asymptote, DLA (deg)	Approach V-Infinity, VHP (km/s)
<b>Single-Day Optimization</b>						
Minimum C3	I	11-Sep-2028	03-Jun-2029	6.5	39.2	5.62
Minimum C3	II	06-Sep-2028	11-Aug-2029	6.1	1.4	4.43
Minimum C3	III-	19-Apr-2028	07-Mar-2030	13.8	-11.4	4.71
Minimum C3	IV-	28-Mar-2028	01-May-2030	10.3	6.9	2.96
Minimum C3	III+	10-May-2028	03-Mar-2030	17.2	-9.6	5.00
Minimum C3	IV+	11-Aug-2027	12-Nov-2029	61.3	8.5	10.49
Minimum VHP	I	27-Nov-2028	02-Jul-2029	19.5	36.2	4.28
Minimum VHP	II	08-Jul-2028	07-Jul-2029	8.3	6.3	3.41
Minimum VHP	III-	25-Apr-2028	22-Mar-2030	22.4	-25.2	2.92
Minimum VHP	IV-	13-Feb-2028	07-Apr-2030	14.8	14.8	2.89
Minimum VHP	III+	25-Apr-2028	14-Mar-2030	28.1	-23.9	2.83
Minimum VHP	IV+	11-Aug-2027	12-Nov-2029	61.3	8.5	10.49
<b>Launch Period Optimization</b>						
Minimum C3	I	08-Sep-2028	03-Jun-2029	6.5	39.9	5.62
		15-Sep-2028		6.5	38.2	5.62
Minimum C3	II	03-Sep-2028	11-Aug-2029	6.2	1.9	4.43
		10-Sep-2028		6.2	0.8	4.43
Minimum C3	III-	15-Apr-2028	07-Mar-2030	13.8	-12.0	4.70
		22-Apr-2028		13.8	-11.2	4.70
Minimum C3	IV-	25-Mar-2028	30-Apr-2030	10.3	7.7	2.95
		01-Apr-2028		10.3	6.5	2.96
Minimum C3	III+	11-Aug-2027	14-Sep-2029	17.7	13.0	4.01
		18-Aug-2027		17.8	11.0	4.01
Minimum C3	IV+	03-Aug-2027	11-Nov-2029	66.7	7.9	11.09
		10-Aug-2027		87.4	34.1	12.16

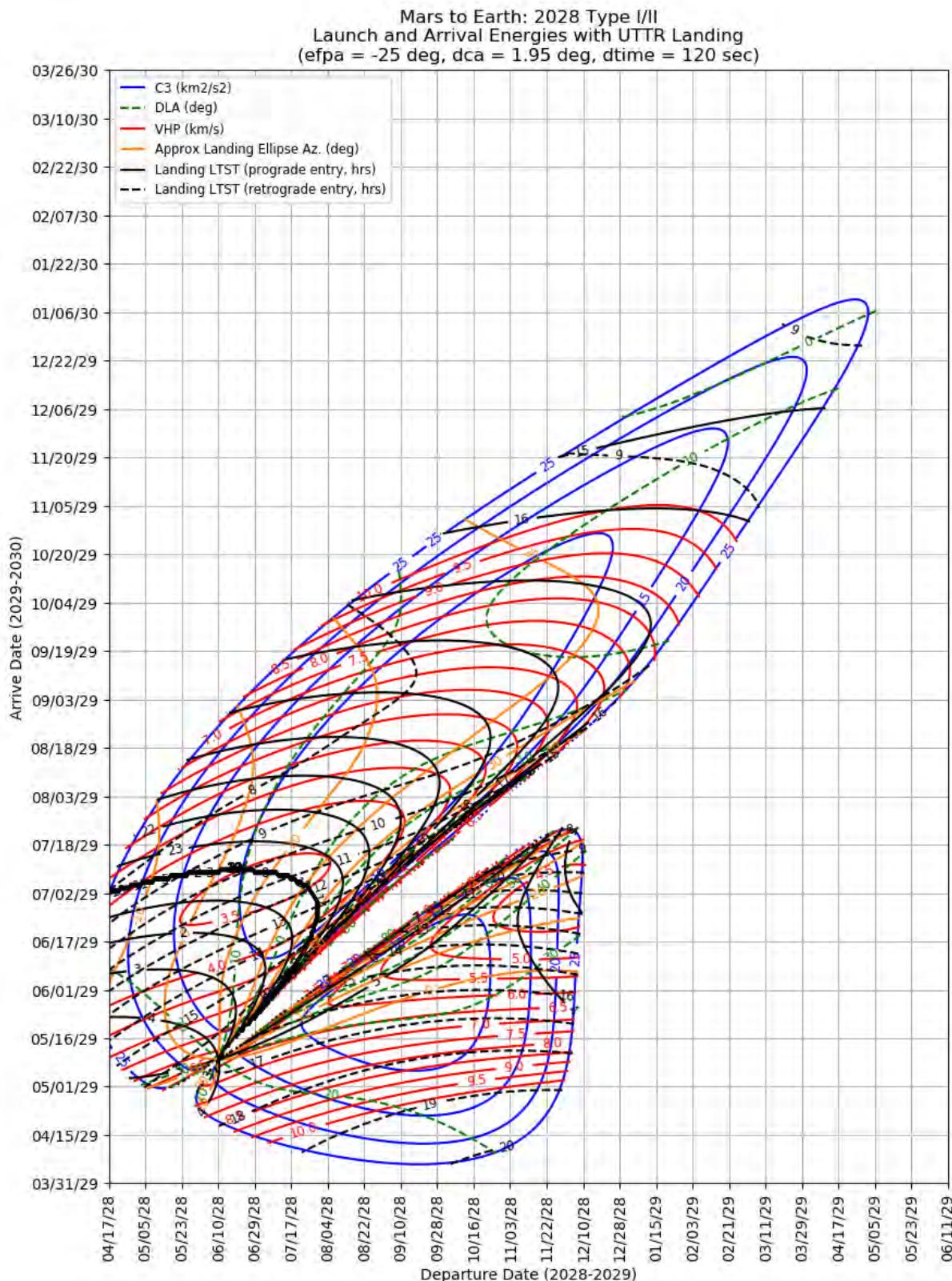


**Figure 539: Mars to Earth 2028 Type I/II – Launch/Arrival Energy and UTTR Landing Times**

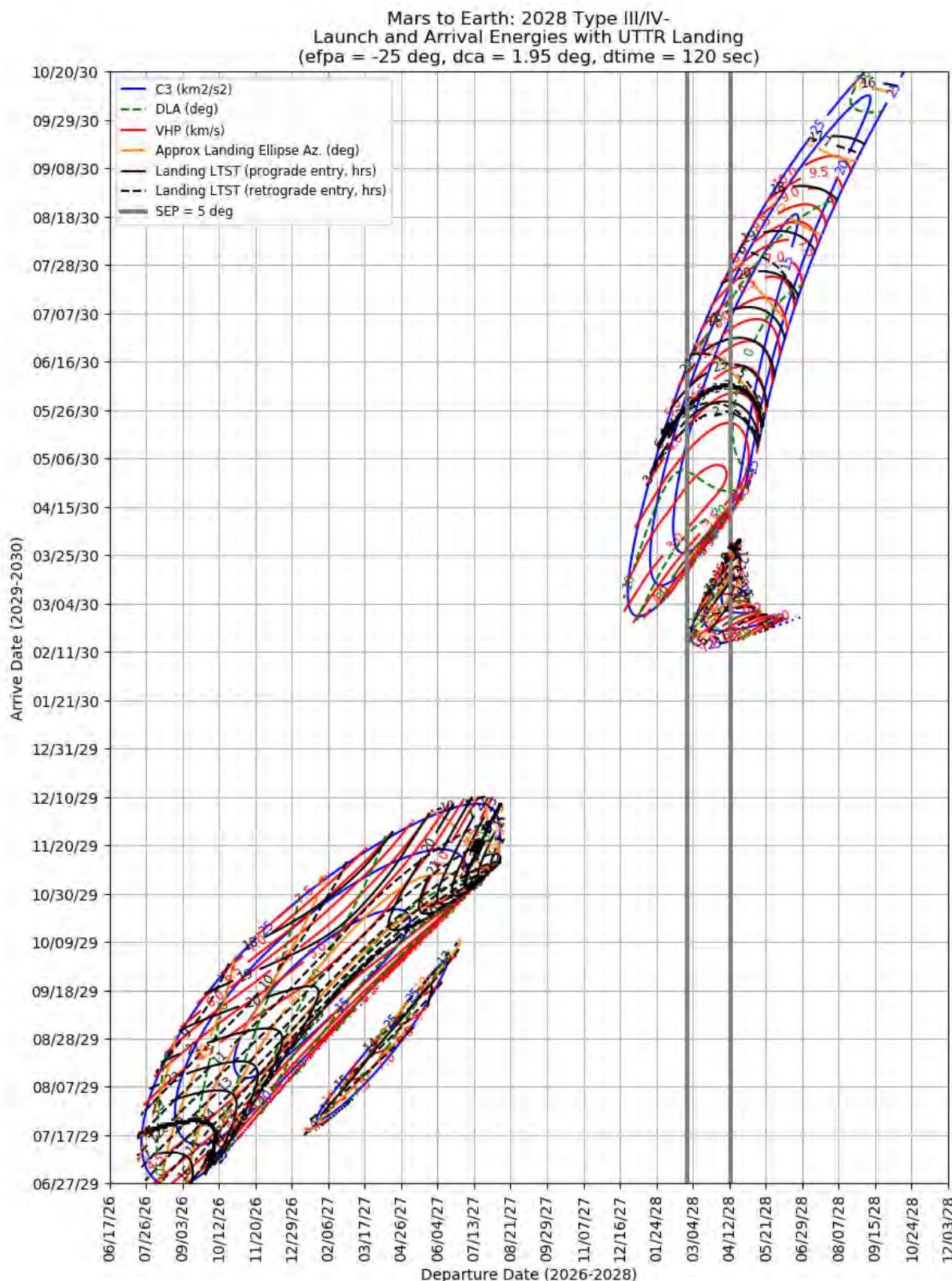


**Figure 540: Mars to Earth 2028 Type III/IV- – Launch/Arrival Energy and UTTR Landing Times**

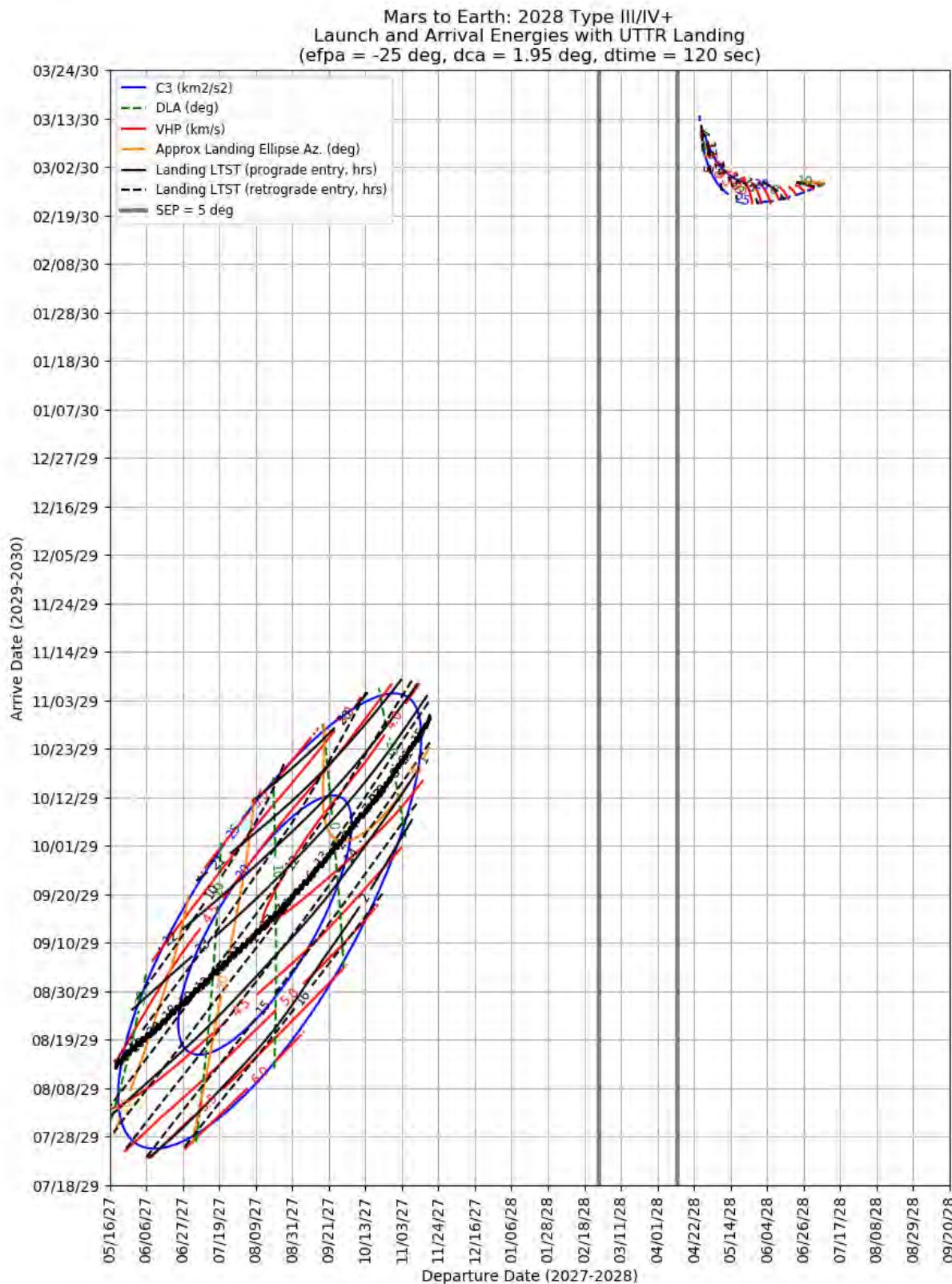


**Figure 541: Mars to Earth 2028 Type III/IV+ – Launch/Arrival Energy and UTTR Landing Times**

#### 11.4.5 Mars to Earth 2031

This section contains porkchop plots for the Mars-to-Earth 2024 opportunities. Table 40 contains the optimal single-day transfers for minimum launch energy (C3) and arrival velocity (VHP) as well as the maximum launch-mass and captured-mass launch periods for each trajectory type within the opportunity. These data should only be used for preliminary analysis and planning purposes.

**Table 40: Mars to Earth 2031 Optimal Launch/Arrival Data**

Optimization Criteria	Trajectory Type	Departure Date (dd-mmm-yyyy)	Arrival Date (dd-mmm-yyyy)	Launch Energy, C3 (km <sup>2</sup> /s <sup>2</sup> )	Declination of the Launch Asymptote, DLA (deg)	Approach V-Infinity, VHP (km/s)	
<b>Single-Day Optimization</b>							
Minimum C3	I	01-Nov-2030	07-Jul-2031	5.8	37.2	5.66	
Minimum C3	II	10-Nov-2030	24-Sep-2031	5.4	-8.2	5.49	
Minimum C3	III-	10-Apr-2030	05-Apr-2032	11.2	-3.2	4.60	
Minimum C3	IV-	18-Mar-2030	11-May-2032	8.6	10.8	2.80	
Minimum C3	III+	26-May-2030	23-Mar-2032	16.6	7.6	7.20	
Minimum C3	IV+	27-Jun-2029	12-Nov-2031	86.2	3.8	12.09	
Minimum VHP	I	09-Jan-2031	08-Aug-2031	13.1	40.1	4.18	
Minimum VHP	II	10-Jun-2030	23-Jul-2031	12.8	4.3	3.80	
Minimum VHP	III-	24-Apr-2030	29-Apr-2032	18.6	-10.5	2.80	
Minimum VHP	IV-	28-Mar-2030	14-May-2032	8.9	7	2.78	
Minimum VHP	III+	27-Apr-2030	13-Apr-2032	30.3	-10.2	2.91	
Minimum VHP	IV+	14-Apr-2030	04-May-2032	114.5	-4.1	8.87	
<b>Launch Period Optimization</b>							
Minimum C3	I	30-Oct-2030	08-Jul-2031	5.8	38.4	5.58	
		06-Nov-2030		5.8	37.5	5.58	
Minimum C3	II	07-Nov-2030	24-Sep-2031	5.4	-7.9	5.50	
		14-Nov-2030		5.4	-8.5	5.50	
Minimum C3	III-	07-Apr-2030	05-Apr-2032	11.3	-4.0	4.60	
		14-Apr-2030		11.3	-2.5	4.59	
Minimum C3	IV-	15-Mar-2030	10-May-2032	8.6	11.9	2.81	
		22-Mar-2030		8.6	10.5	2.81	
Minimum C3	III+	Not Possible					
Minimum C3	IV+	Not Possible					

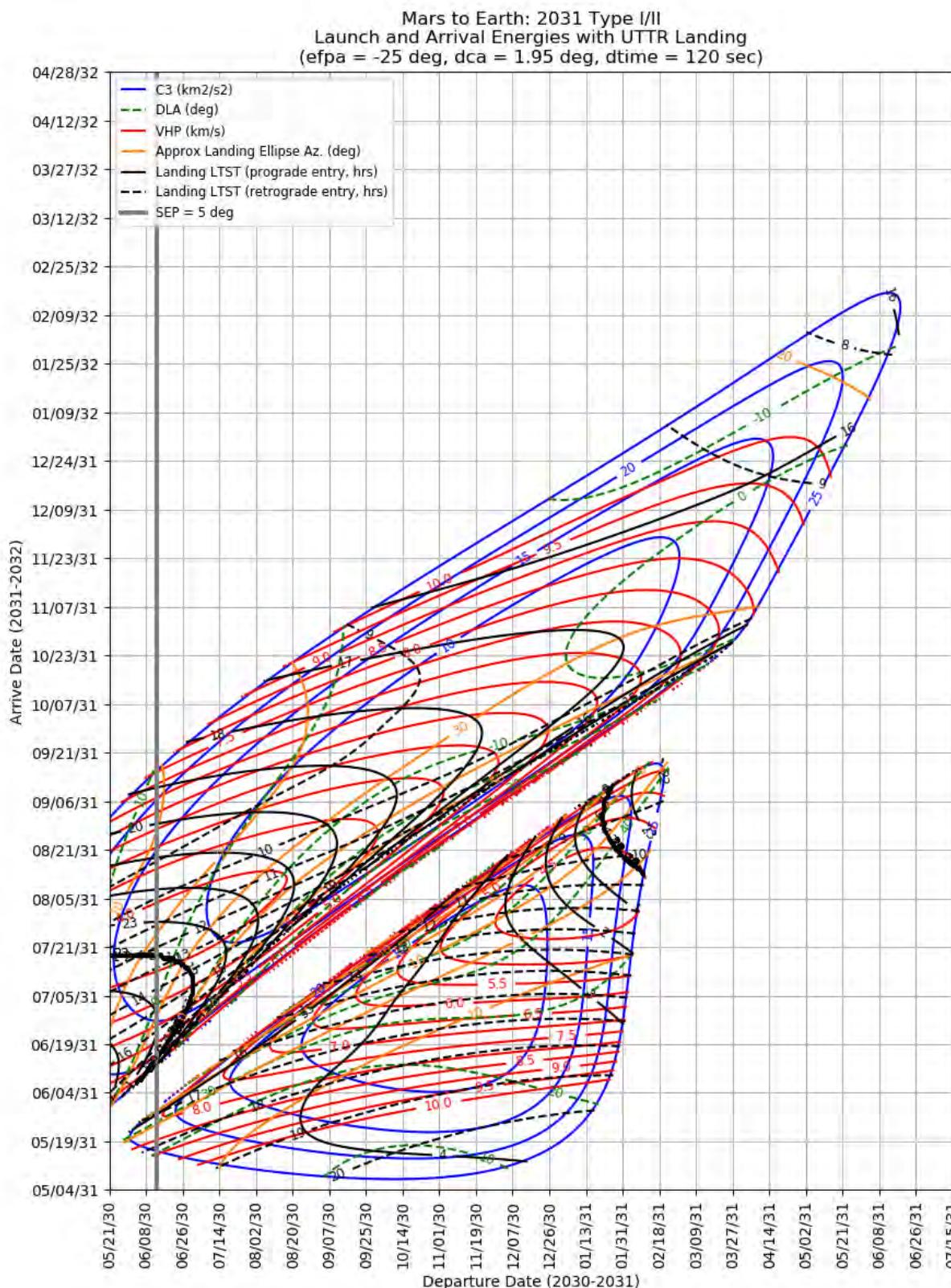


**Figure 542: Mars to Earth 2031 Type I/II – Launch/Arrival Energy and UTTR Landing Times**

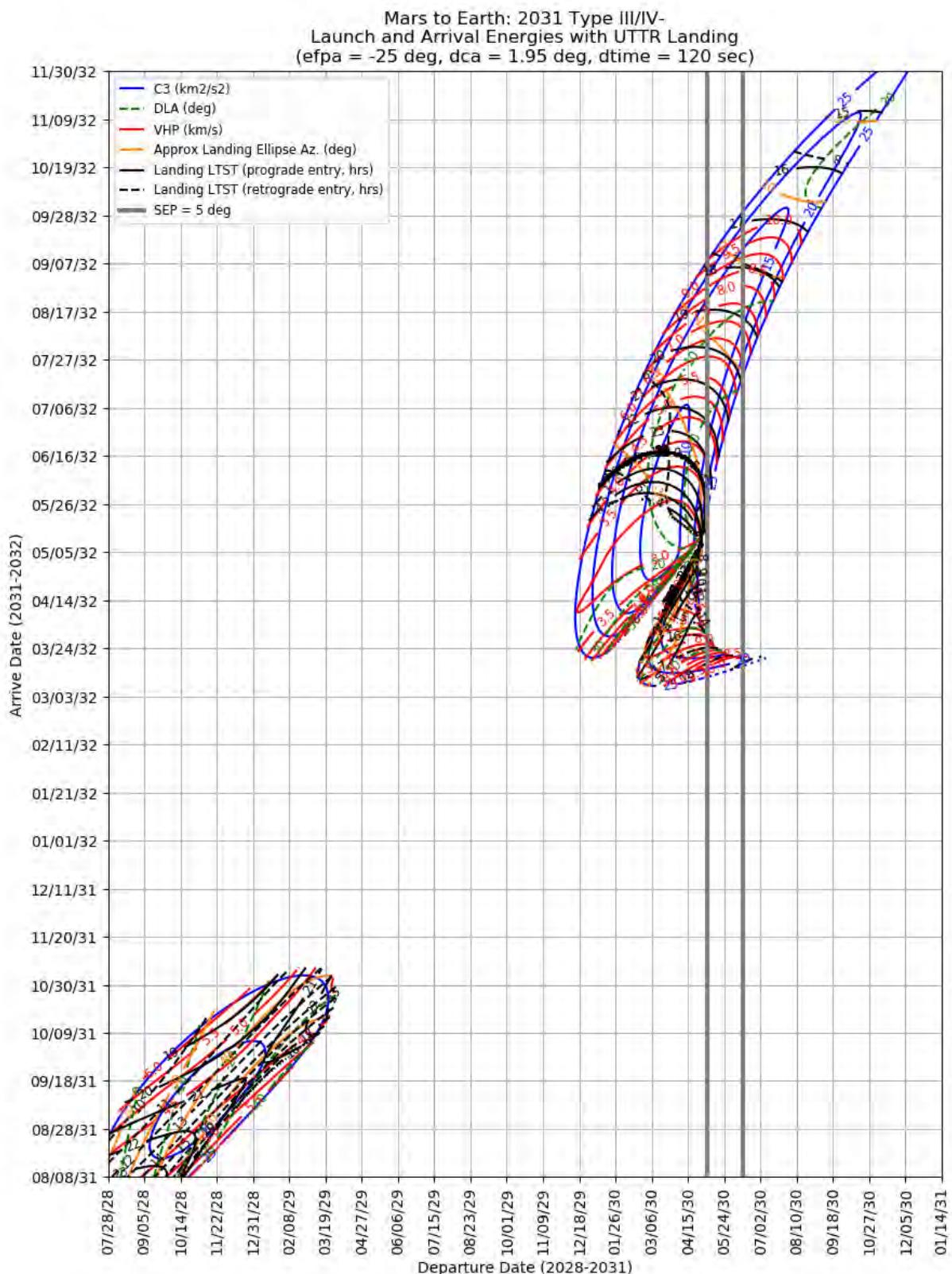


**Figure 543: Mars to Earth 2031 Type III/IV- – Launch/Arrival Energy and UTTR Landing Times**

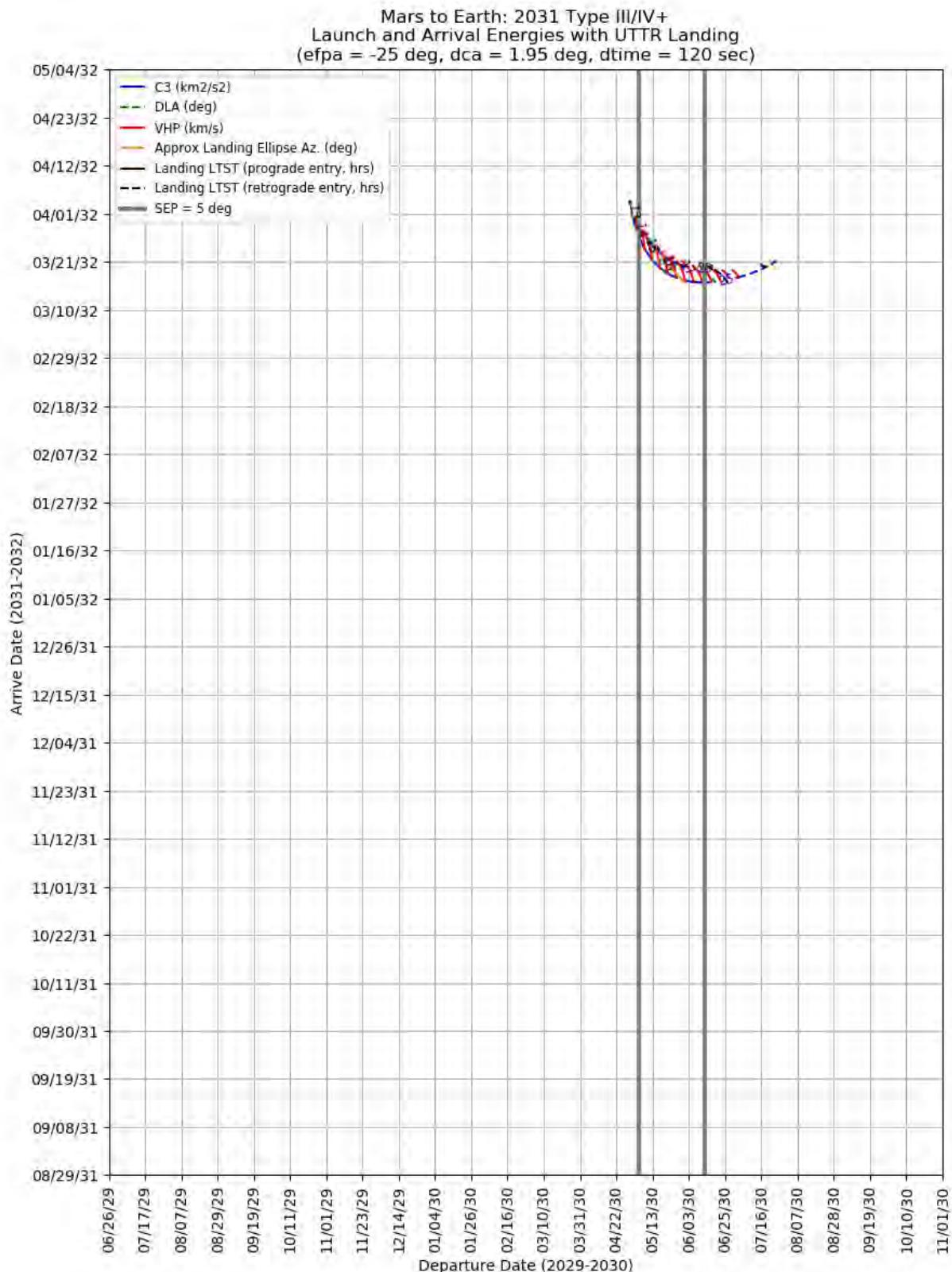


**Figure 544: Mars to Earth 2024 Type III/IV+ – Launch/Arrival Energy and UTTR Landing Times**

#### 11.4.6 Mars to Earth 2033

This section contains porkchop plots for the Mars-to-Earth 2024 opportunities. Table 41 contains the optimal single-day transfers for minimum launch energy (C3) and arrival velocity (VHP) as well as the maximum launch-mass and captured-mass launch periods for each trajectory type within the opportunity. These data should only be used for preliminary analysis and planning purposes.

**Table 41: Mars to Earth 2033 Optimal Launch/Arrival Data**

Optimization Criteria	Trajectory Type	Departure Date (dd-mmm-yyyy)	Arrival Date (dd-mmm-yyyy)	Launch Energy, C3 (km <sup>2</sup> /s <sup>2</sup> )	Declination of the Launch Asymptote, DLA (deg)	Approach V-Infinity, VHP (km/s)	
<b>Single-Day Optimization</b>							
Minimum C3	I	28-Jan-2033	03-Sep-2033	5.7	15.1	4.03	
Minimum C3	II	13-Feb-2033	03-Nov-2033	5.8	-24	4.95	
Minimum C3	III-	18-Mar-2032	10-May-2034	7.6	14.9	3.74	
Minimum C3	IV-	05-Mar-2032	25-May-2034	7.5	8.5	2.97	
Minimum C3	III+	18-May-2032	15-Apr-2034	14.2	15.1	7.08	
Minimum C3	IV+	19-May-2032	28-Jun-2034	63.1	-7.1	7.22	
Minimum VHP	I	28-Feb-2033	24-Sep-2033	6.7	15.4	3.51	
Minimum VHP	II	27-Jun-2032	20-Aug-2033	14.8	-8.6	4.16	
Minimum VHP	III-	23-Apr-2032	13-May-2034	20.8	8.5	3.32	
Minimum VHP	IV-	12-Mar-2032	02-Jun-2034	7.6	4.6	2.9	
Minimum VHP	III+	23-Apr-2032	04-May-2034	31.3	2.7	3.32	
Minimum VHP	IV+	15-May-2032	23-Jun-2034	63.6	-10.4	7.09	
<b>Launch Period Optimization</b>							
Minimum C3	I	25-Jan-2033	03-Sep-2033	5.7	15.5	4.03	
		01-Feb-2033		5.7	14.7	4.03	
Minimum C3	II	10-Feb-2033	03-Nov-2033	5.8	-23.5	4.95	
		17-Feb-2033		5.8	-24.8	4.96	
Minimum C3	III-	17-Mar-2032	10-May-2034	7.6	13.0	3.71	
		22-Mar-2030		7.8	16.4	3.79	
Minimum C3	IV-	02-Mar-2032	25-May-2034	7.5	9.7	2.97	
		09-Mar-2032		7.5	6.8	2.97	
Minimum C3	III+	Not Possible					
Minimum C3	IV+	Not Possible					

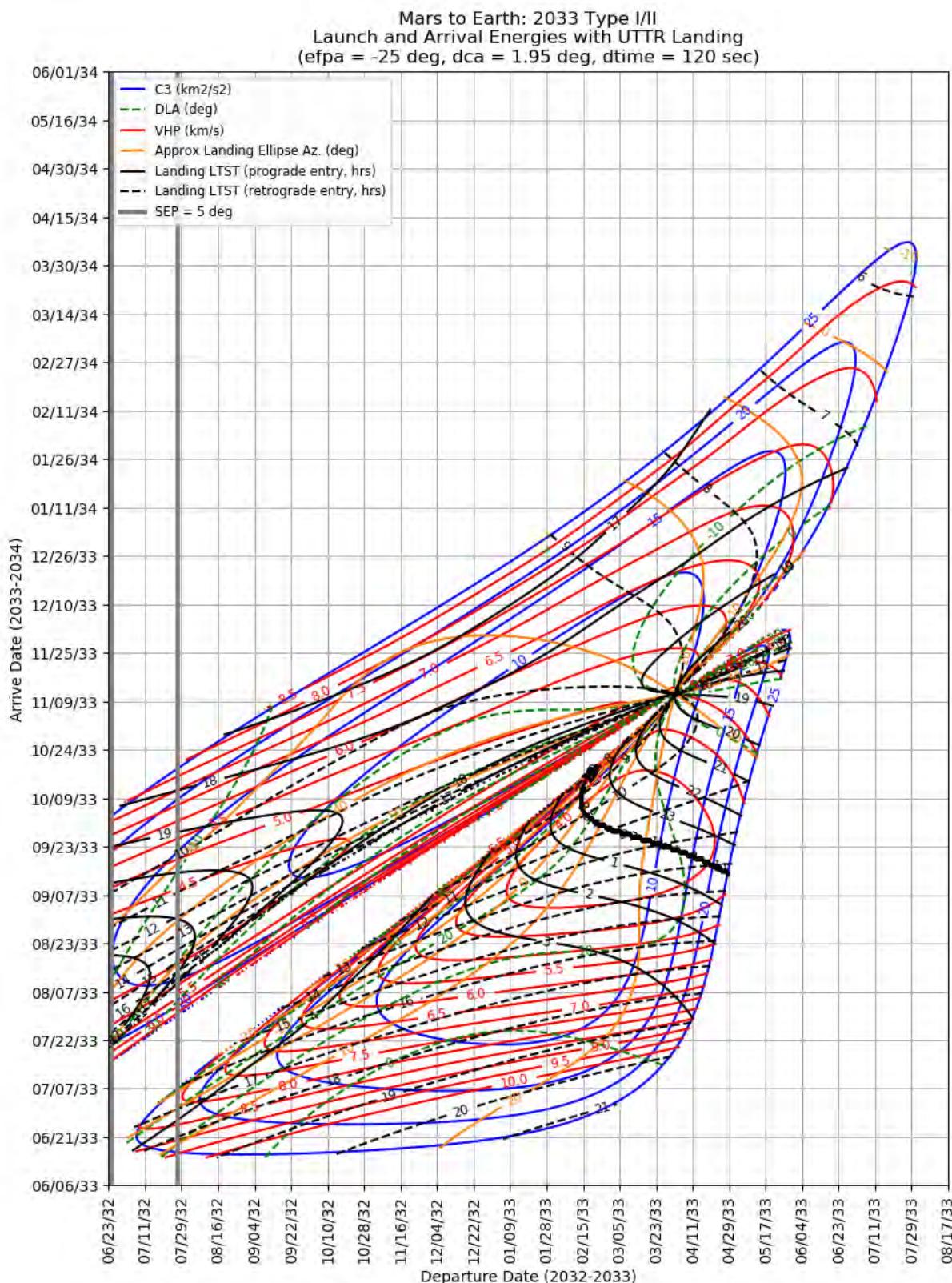


**Figure 545: Mars to Earth 2033 Type I/II – Launch/Arrival Energy and UTTR Landing Times**

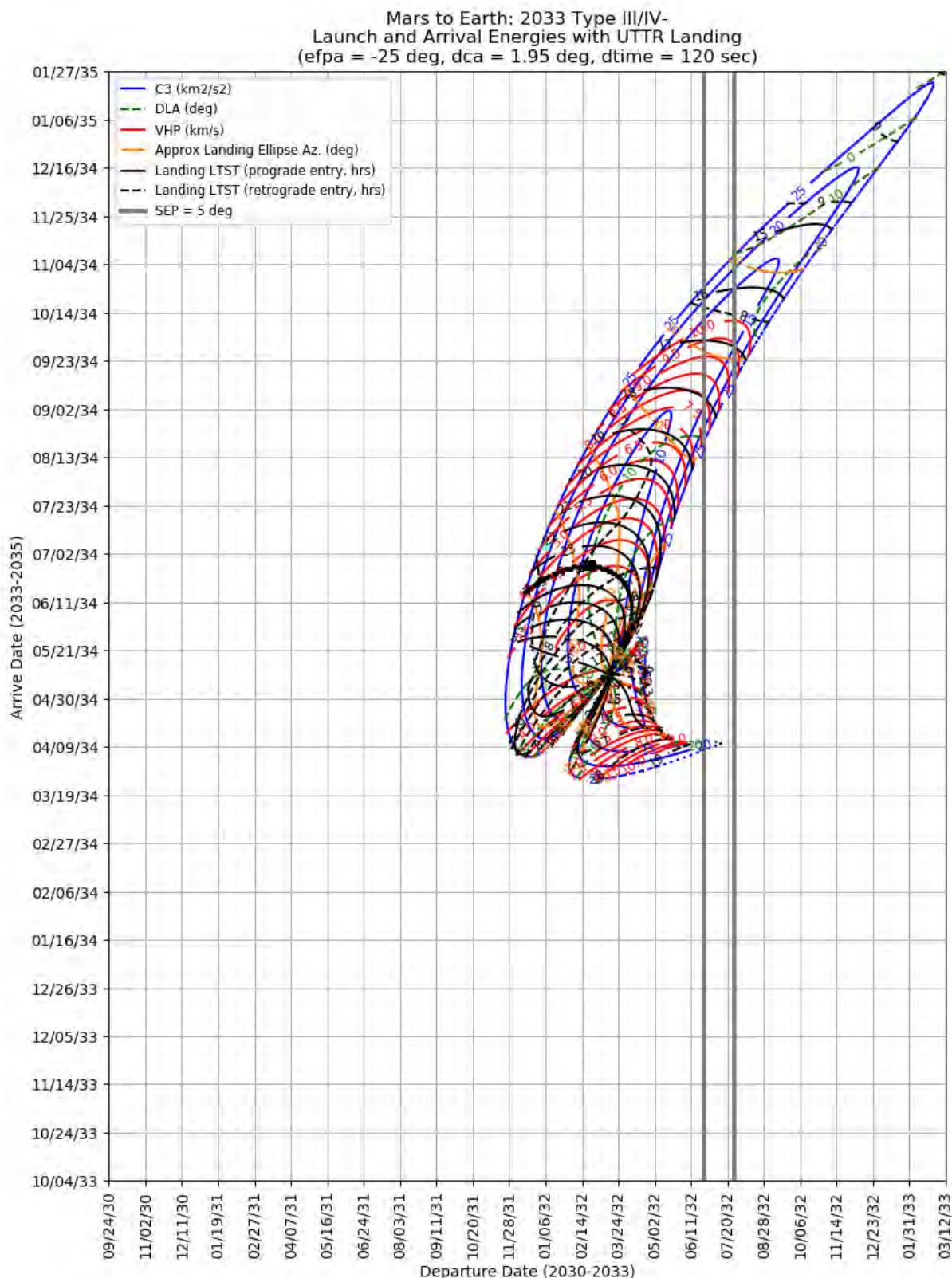


**Figure 546: Mars to Earth 2033 Type III/IV- – Launch/Arrival Energy and UTTR Landing Times**

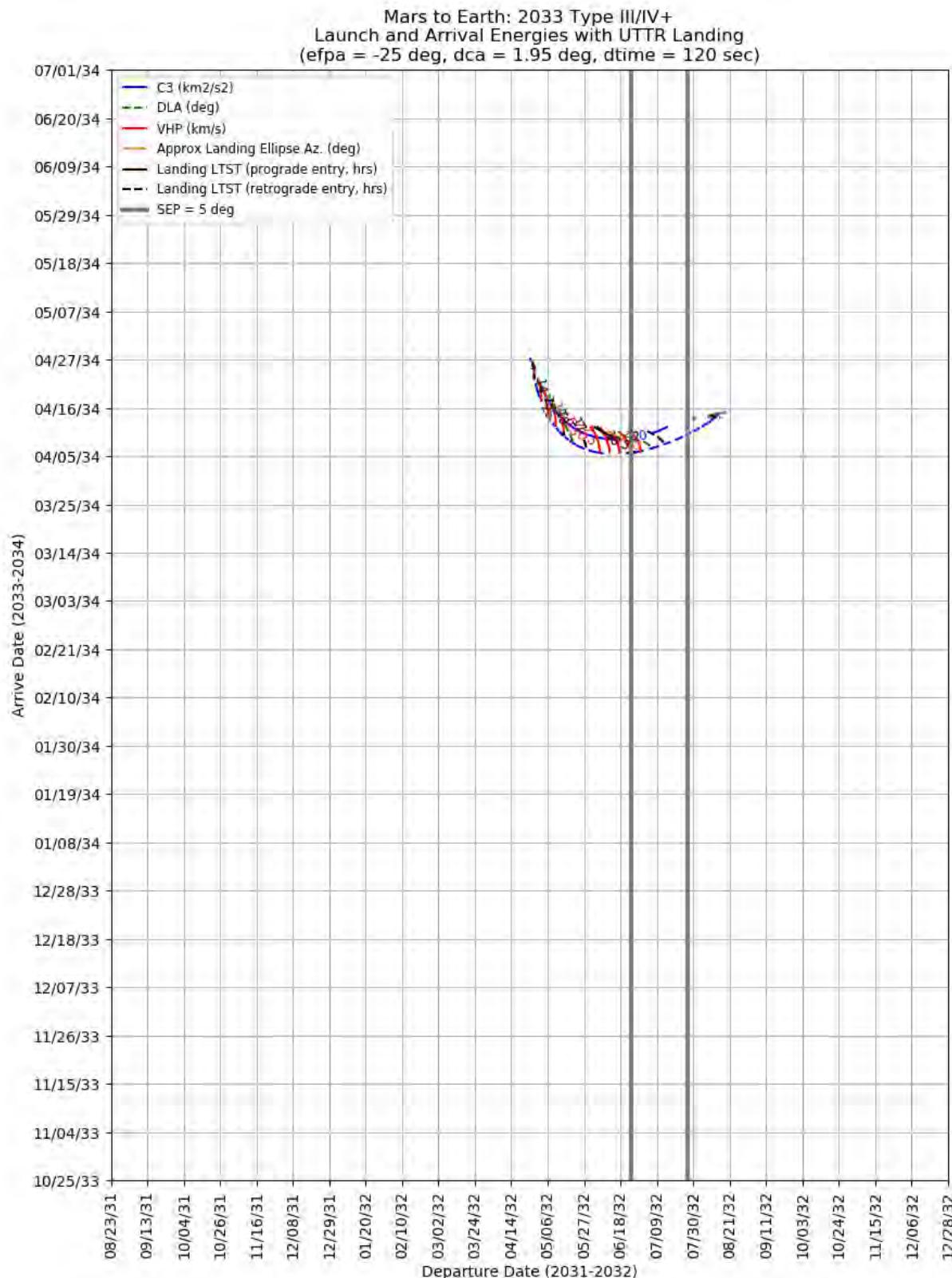


**Figure 547: Mars to Earth 2033 Type III/IV+ – Launch/Arrival Energy and UTTR Landing Times**

### 11.4.7 Mars to Earth 2035

This section contains porkchop plots for the Mars-to-Earth 2024 opportunities. Table 42 contains the optimal single-day transfers for minimum launch energy (C3) and arrival velocity (VHP) as well as the maximum launch-mass and captured-mass launch periods for each trajectory type within the opportunity. These data should only be used for preliminary analysis and planning purposes.

**Table 42: Mars to Earth 2035 Optimal Launch/Arrival Data**

Optimization Criteria	Trajectory Type	Departure Date (dd-mmm-yyyy)	Arrival Date (dd-mmm-yyyy)	Launch Energy, C3 (km <sup>2</sup> /s <sup>2</sup> )	Declination of the Launch Asymptote, DLA (deg)	Approach V-Infinity, VHP (km/s)	
<b>Single-Day Optimization</b>							
Minimum C3	I	08-May-2035	22-Nov-2035	8.8	-28.9	3.04	
Minimum C3	II	17-Feb-2035	13-Nov-2035	13	-19.8	3.07	
Minimum C3	III-	20-Mar-2034	20-May-2036	6.9	33.5	5.03	
Minimum C3	IV-	28-Feb-2034	04-Jul-2036	6.9	3.6	3.37	
Minimum C3	III+	05-Jun-2034	03-May-2036	12.1	23.8	9.02	
Minimum C3	IV+	14-Jun-2034	14-Aug-2036	60.8	8.8	9.28	
Minimum VHP	I	04-Jun-2035	01-Dec-2035	10.3	-31.9	2.98	
Minimum VHP	II	19-Feb-2035	15-Nov-2035	13.5	-12.7	3.02	
Minimum VHP	III-	21-Apr-2034	29-May-2036	20.9	20.5	3.8	
Minimum VHP	IV-	07-Feb-2034	19-Jun-2036	7.4	7.8	3.12	
Minimum VHP	III+	19-Apr-2034	21-May-2036	31.3	13.6	3.72	
Minimum VHP	IV+	16-May-2034	16-Jul-2036	61.9	-7	8.05	
<b>Launch Period Optimization</b>							
Minimum C3	I	05-May-2035	22-Nov-2035	8.8	-29.1	3.04	
		12-May-2035		8.8	-28.8	3.04	
Minimum C3	II	12-Feb-2035	13-Nov-2035	13.3	-23.2	3.18	
		19-Feb-2035		15	-3.6	3.2	
Minimum C3	III-	17-Mar-2034	19-May-2036	7.0	33.2	5.11	
		22-Mar-2030		7.0	31.2	5.12	
Minimum C3	IV-	25-Feb-2034	04-Jul-2036	6.9	4.5	3.37	
		04-Mar-2034		6.9	2.5	3.38	
Minimum C3	III+	Not Possible					
Minimum C3	IV+	Not Possible					

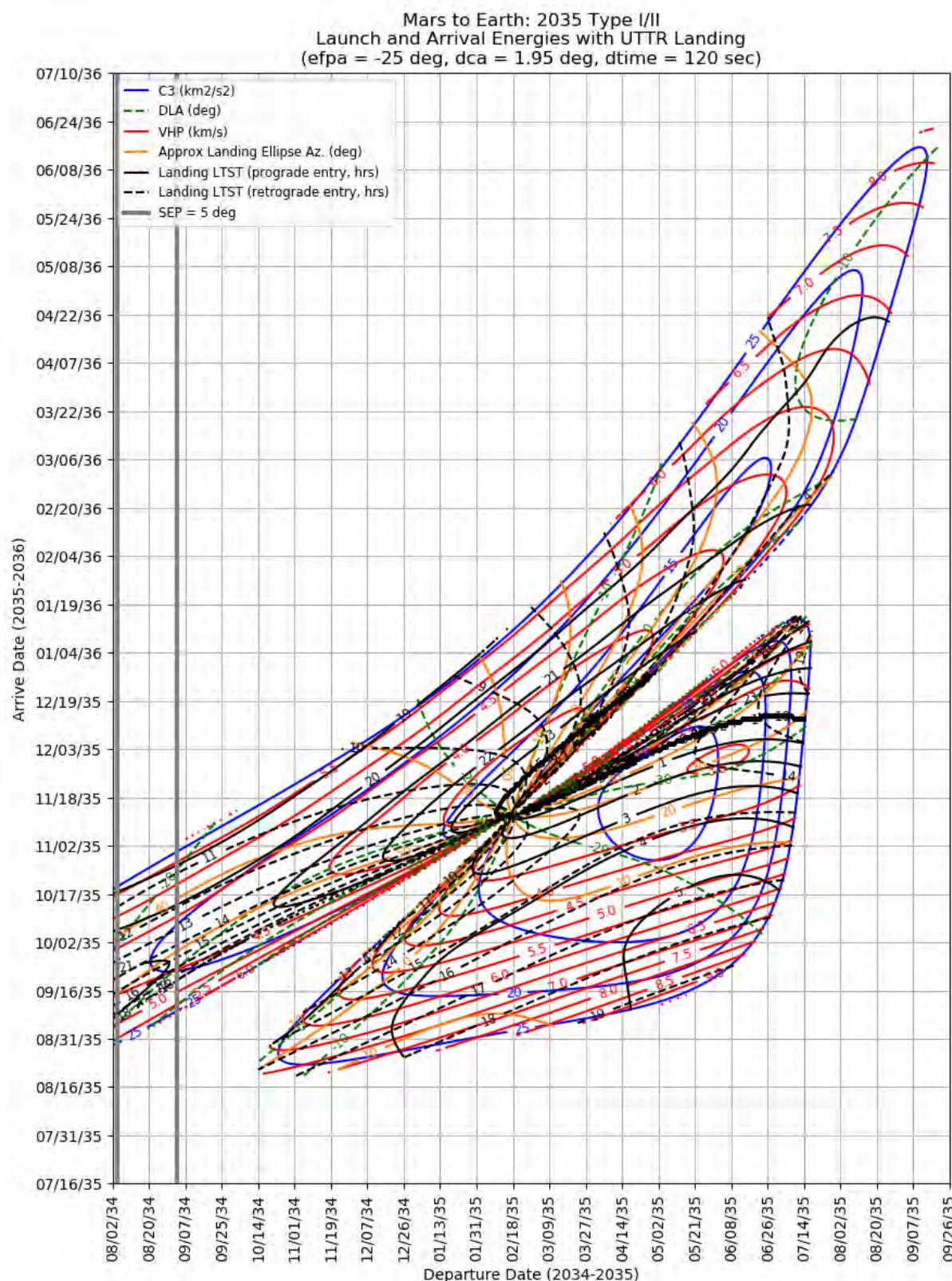


**Figure 548: Mars to Earth 2035 Type I/II – Launch/Arrival Energy and UTTR Landing Times**

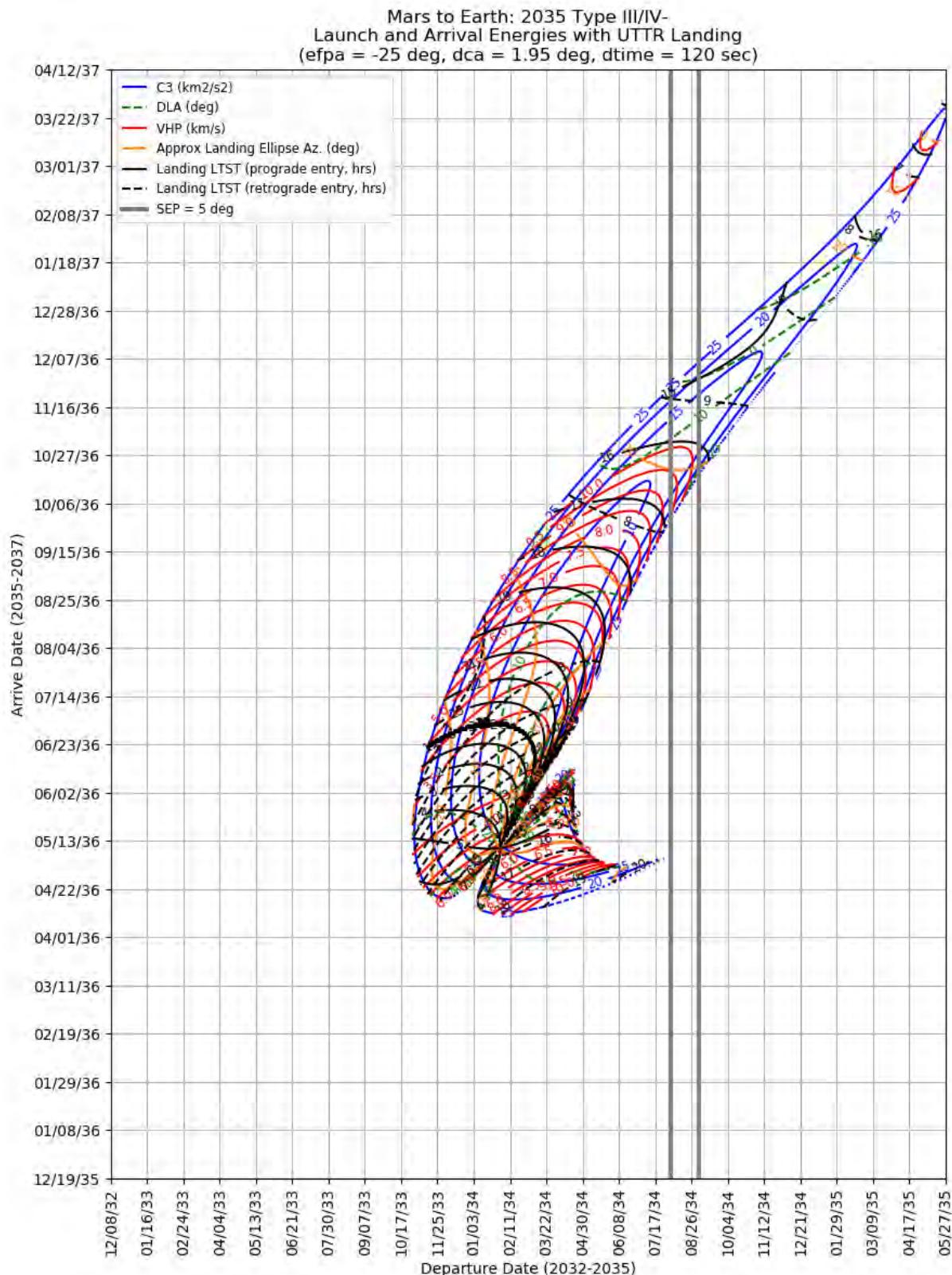


**Figure 549: Mars to Earth 2035 Type III/IV- – Launch/Arrival Energy and UTTR Landing Times**

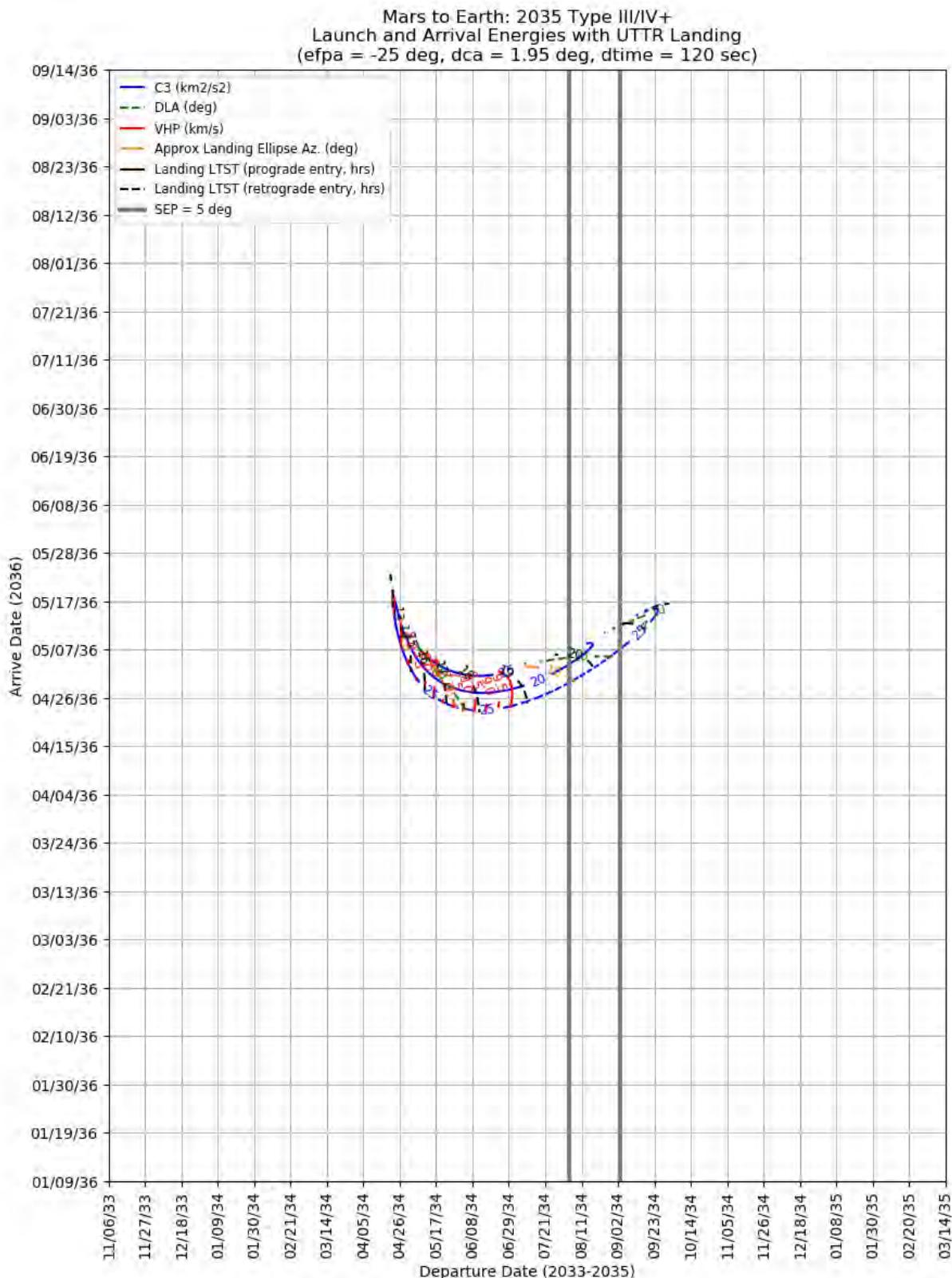


**Figure 550: Mars to Earth 2035 Type III/IV+ – Launch/Arrival Energy and UTTR Landing Times**

#### 11.4.8 Mars to Earth 2037

This section contains porkchop plots for the Mars-to-Earth 2024 opportunities. Table 43 contains the optimal single-day transfers for minimum launch energy (C3) and arrival velocity (VHP) as well as the maximum launch-mass and captured-mass launch periods for each trajectory type within the opportunity. These data should only be used for preliminary analysis and planning purposes.

**Table 43: Mars to Earth 2037 Optimal Launch/Arrival Data**

Optimization Criteria	Trajectory Type	Departure Date (dd-mmm-yyyy)	Arrival Date (dd-mmm-yyyy)	Launch Energy, C3 (km <sup>2</sup> /s <sup>2</sup> )	Declination of the Launch Asymptote, DLA (deg)	Approach V-Infinity, VHP (km/s)
<b>Single-Day Optimization</b>						
Minimum C3	I	08-Jul-2037	19-Jan-2038	14.3	-25.3	3.94
Minimum C3	II	12-Jul-2037	08-Apr-2038	12.6	2.4	3.53
Minimum C3	III-	30-Mar-2036	06-Jun-2038	6.4	39.4	5.69
Minimum C3	IV-	14-Mar-2036	12-Aug-2038	6.2	2.3	4.53
Minimum C3	III+	20-May-2036	28-May-2038	9.5	28.9	7.26
Minimum C3	IV+	12-Sep-2036	29-Oct-2038	42.4	19.6	11.59
Minimum VHP	I	24-Aug-2037	19-Feb-2038	27.9	-29.5	2.88
Minimum VHP	II	01-Mar-2037	08-Jan-2038	31.6	-3	3
Minimum VHP	III-	20-Apr-2036	19-Jun-2038	16	35.3	4.25
Minimum VHP	IV-	04-Jan-2036	02-Jul-2038	8.8	8.7	3.35
Minimum VHP	III+	14-Apr-2036	04-Jun-2038	32.2	21.3	4.05
Minimum VHP	IV+	24-May-2036	12-Aug-2038	48.8	-2.8	8.44
<b>Launch Period Optimization</b>						
Minimum C3	I	05-Jul-2037	19-Jan-2038	14.4	-25.6	3.94
		12-Jul-2037		14.4	-25.1	3.94
Minimum C3	II	10-Jul-2037	09-Apr-2038	12.6	2.3	3.56
		17-Jul-2037		12.6	1.7	3.56
Minimum C3	III-	27-Mar-2036	06-Jun-2038	6.4	40.1	5.69
		03-Apr-2036		6.4	38.6	5.69
Minimum C3	IV-	10-Mar-2036	11-Aug-2038	6.2	2.6	4.48
		17-Mar-2036		6.2	1.5	4.48
Minimum C3	III+	31-May-2036	27-May-2038	9.6	27.2	8.06
		07-Jun-2036		9.6	25.1	8.63
Minimum C3	IV+	Not Possible				

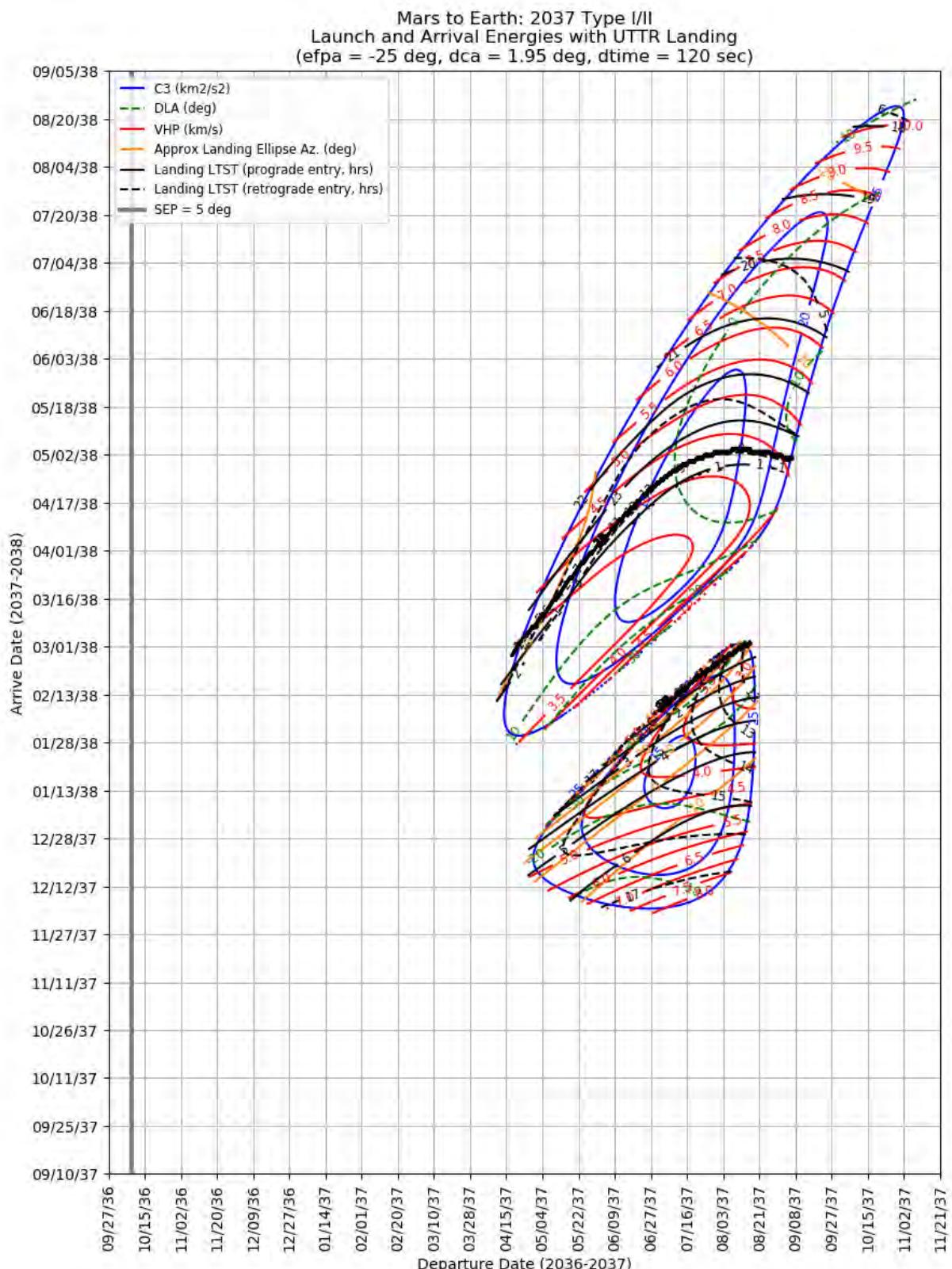


**Figure 551: Mars to Earth 2037 Type I/II – Launch/Arrival Energy and UTTR Landing Times**

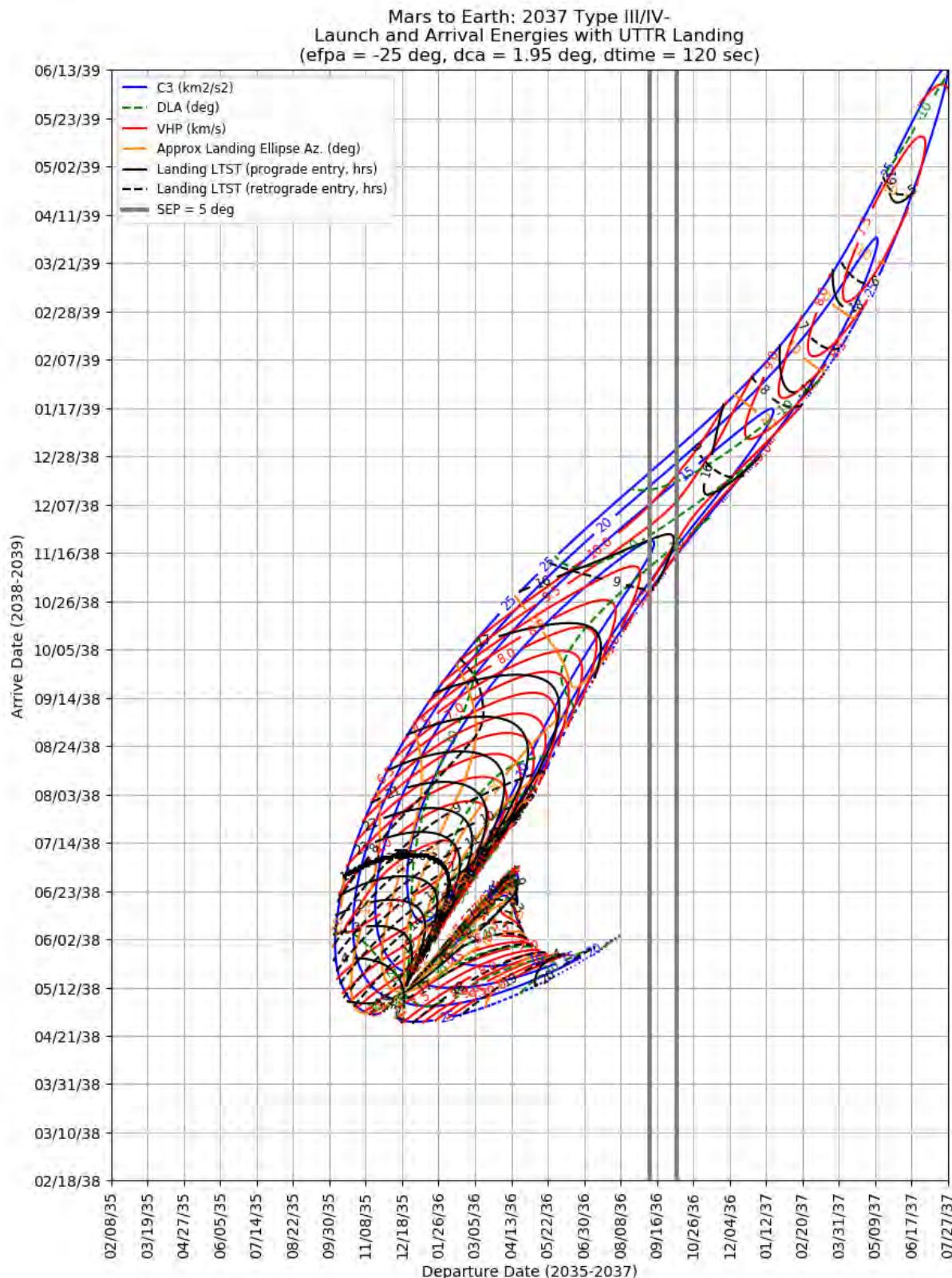


**Figure 552: Mars to Earth 2037 Type III/IV- – Launch/Arrival Energy and UTTR Landing Times**

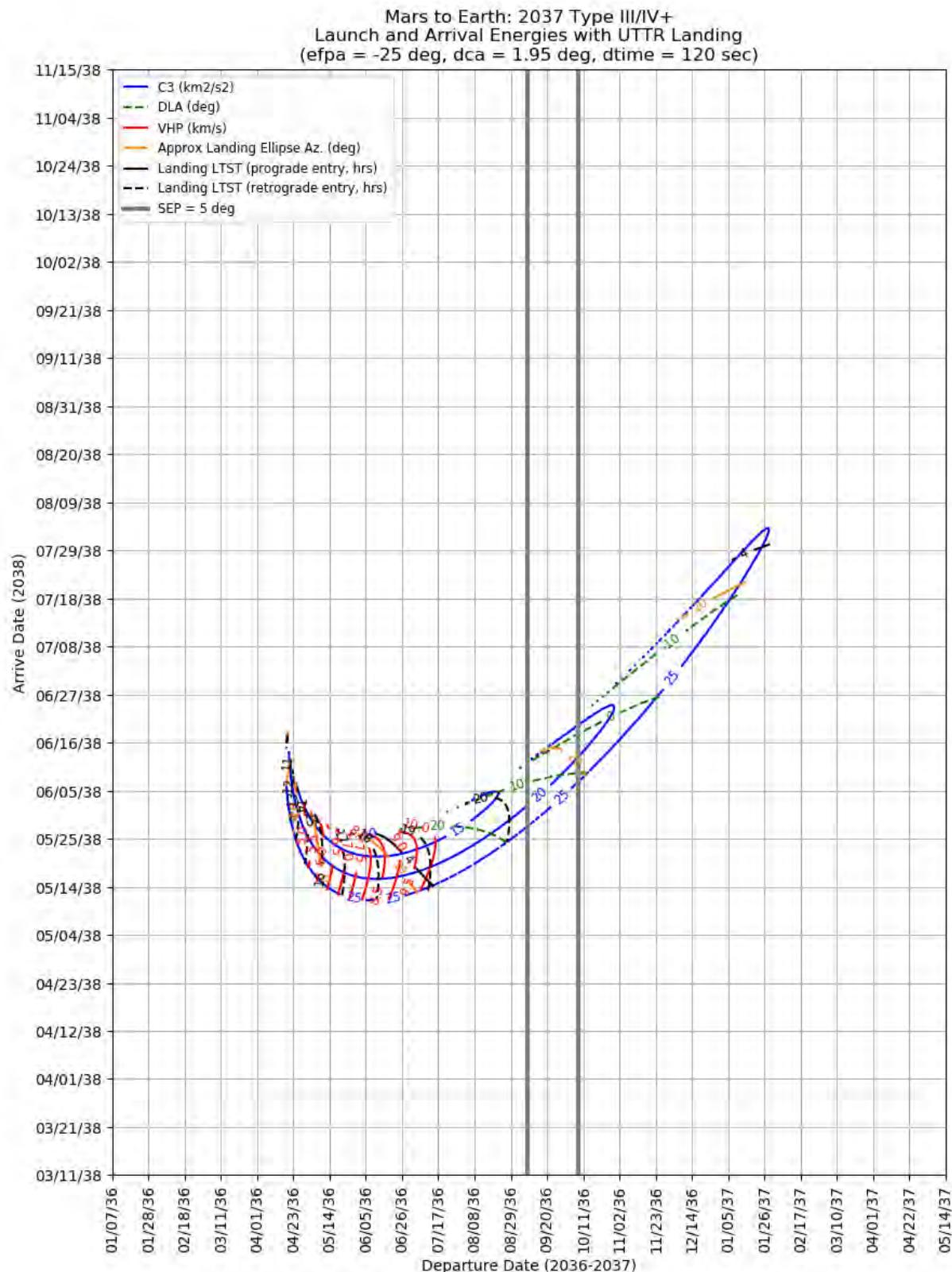


**Figure 553: Mars to Earth 2037 Type III/IV+ – Launch/Arrival Energy and UTTR Landing Times**

### 11.4.9 Mars to Earth 2039

This section contains porkchop plots for the Mars-to-Earth 2024 opportunities. Table 44 contains the optimal single-day transfers for minimum launch energy (C3) and arrival velocity (VHP) as well as the maximum launch-mass and captured-mass launch periods for each trajectory type within the opportunity. These data should only be used for preliminary analysis and planning purposes.

**Table 44: Mars to Earth 2039 Optimal Launch/Arrival Data**

Optimization Criteria	Trajectory Type	Departure Date (dd-mmm-yyyy)	Arrival Date (dd-mmm-yyyy)	Launch Energy, C3 (km <sup>2</sup> /s <sup>2</sup> )	Declination of the Launch Asymptote, DLA (deg)	Approach V-Infinity, VHP (km/s)
<b>Single-Day Optimization</b>						
Minimum C3	I	04-Aug-2039	12-Mar-2040	13.6	-13.2	4.4
Minimum C3	II	23-Jul-2039	04-May-2040	9.6	8.8	2.85
Minimum C3	III-	21-Apr-2038	28-Jun-2040	5.9	38.1	5.83
Minimum C3	IV-	20-Apr-2038	14-Sep-2040	5.6	-3.6	5.43
Minimum C3	III+	01-Jun-2038	24-Jun-2040	7	27.9	6.93
Minimum C3	IV+	01-Dec-2038	11-Dec-2040	23.8	3.9	8.91
Minimum VHP	I	11-Sep-2039	17-Apr-2040	21.9	-13.7	2.79
Minimum VHP	II	16-Jul-2039	01-May-2040	9.7	11	2.85
Minimum VHP	III-	29-Apr-2038	08-Jul-2040	11.2	44.8	4.43
Minimum VHP	IV-	25-Nov-2037	10-Jul-2040	11.6	8.9	3.58
Minimum VHP	III+	25-Apr-2038	02-Jul-2040	20.3	35.8	4.28
Minimum VHP	IV+	21-Jun-2038	14-Sep-2040	32	0.3	8.45
<b>Launch Period Optimization</b>						
Minimum C3	I	01-Aug-2039	11-Mar-2040	13.7	-13.3	4.48
		08-Aug-2039		13.7	-12	4.48
Minimum C3	II	20-Jul-2039	03-May-2040	9.6	9.7	2.85
		27-Jul-2039		9.7	8.6	2.85
Minimum C3	III-	18-Apr-2038	28-Jun-2040	5.9	38.4	5.83
		25-Apr-2038		5.9	37.7	5.83
Minimum C3	IV-	15-Apr-2038	13-Sep-2040	5.6	-3.5	5.38
		22-Apr-2038		5.6	-4.0	5.38
Minimum C3	III+	30-May-2038	24-Jun-2040	7.1	29.2	6.77
		06-Jun-2038		7.1	25.6	7.19
Minimum C3	IV+	Not Possible				

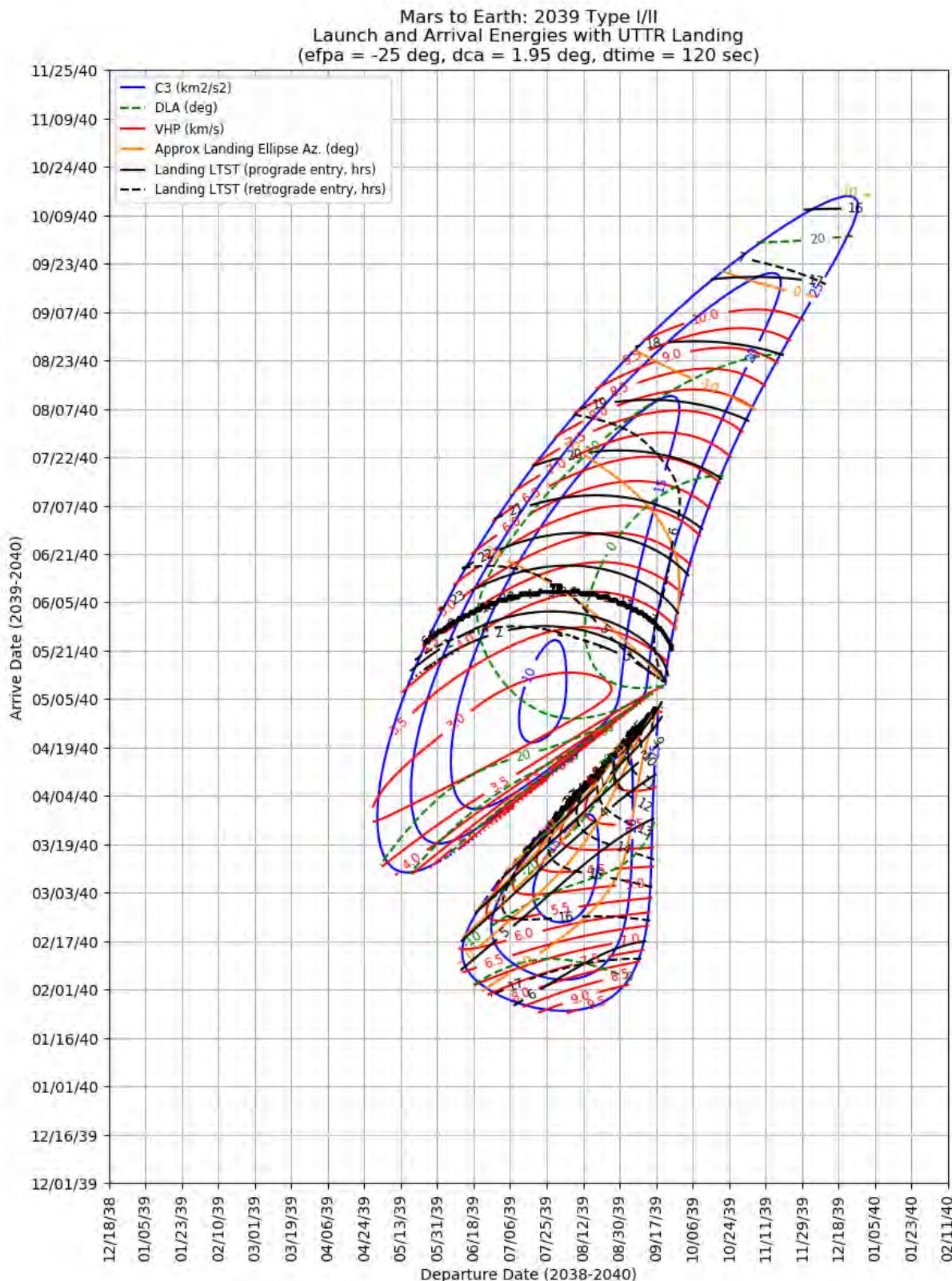


**Figure 554: Mars to Earth 2039 Type I/II – Launch/Arrival Energy and UTTR Landing Times**

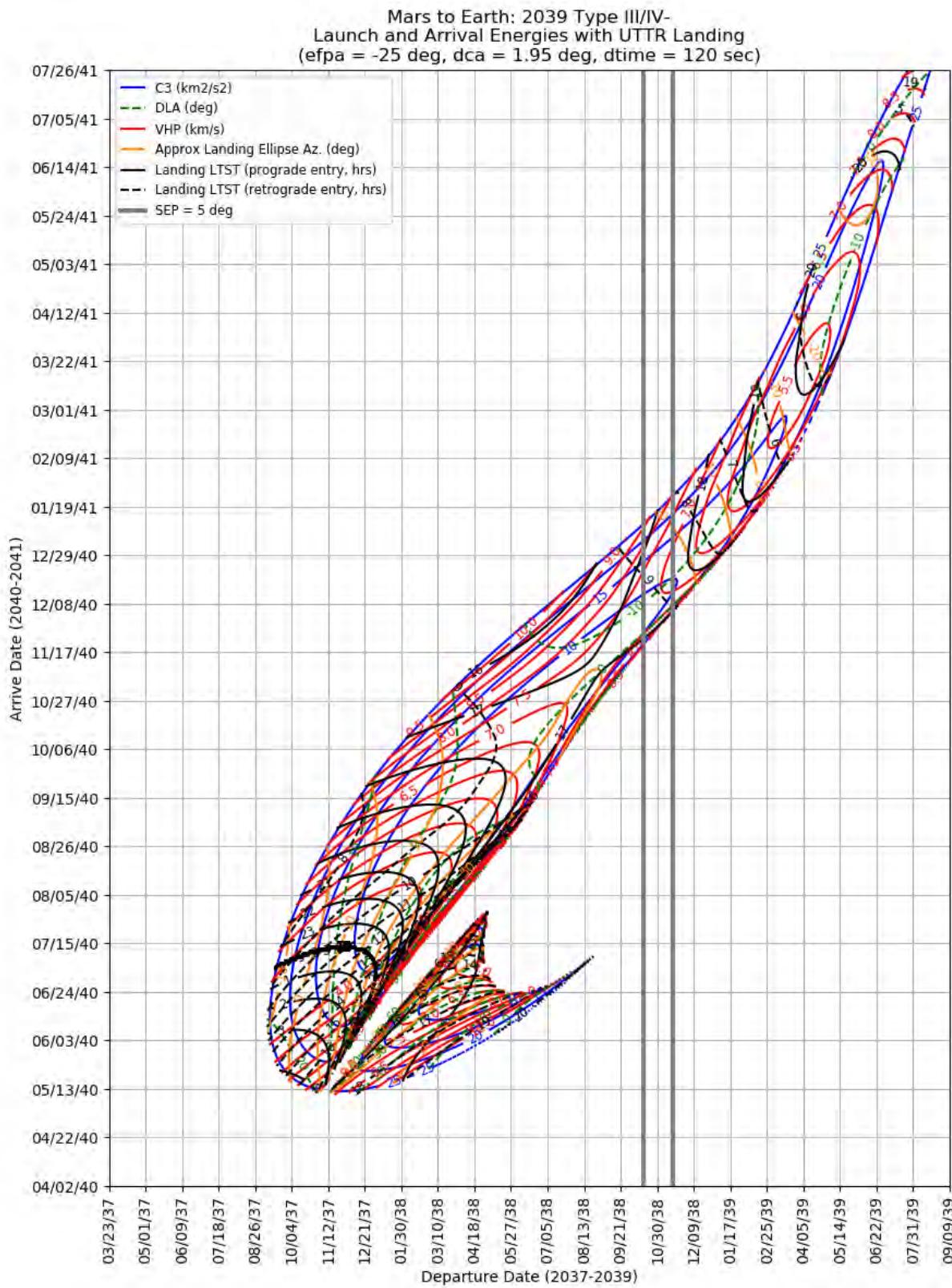


**Figure 555: Mars to Earth 2039 Type III/IV- – Launch/Arrival Energy and UTTR Landing Times**

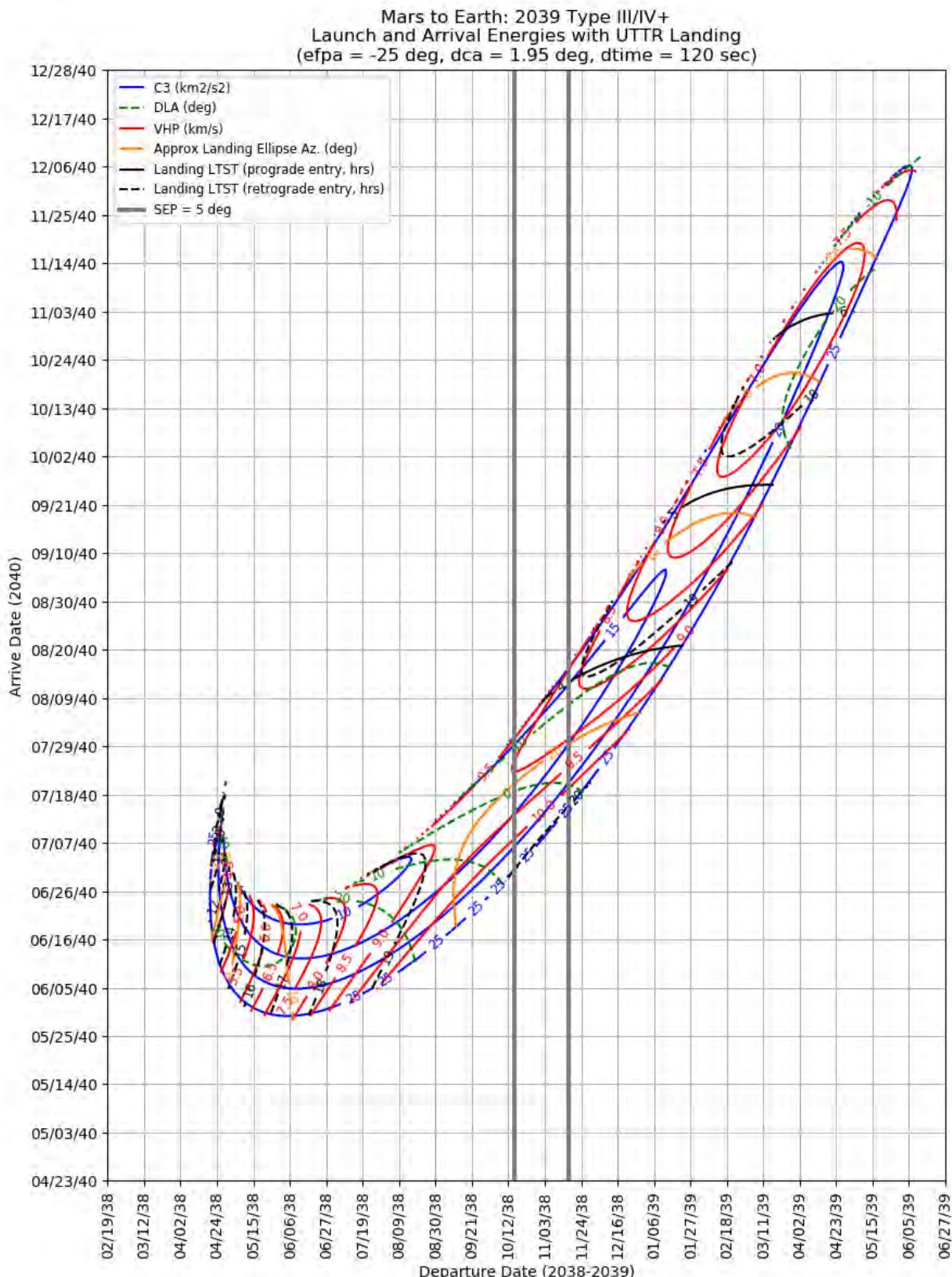


**Figure 556: Mars to Earth 2039 Type III/IV+ – Launch/Arrival Energy and UTTR Landing Times**

#### 11.4.10 Mars to Earth 2041

This section contains porkchop plots for the Mars-to-Earth 2024 opportunities. Table 45 contains the optimal single-day transfers for minimum launch energy (C3) and arrival velocity (VHP) as well as the maximum launch-mass and captured-mass launch periods for each trajectory type within the opportunity. These data should only be used for preliminary analysis and planning purposes.

**Table 45: Mars to Earth 2041 Optimal Launch/Arrival Data**

Optimization Criteria	Trajectory Type	Departure Date (dd-mmm-yyyy)	Arrival Date (dd-mmm-yyyy)	Launch Energy, C3 (km <sup>2</sup> /s <sup>2</sup> )	Declination of the Launch Asymptote, DLA (deg)	Approach V-Infinity, VHP (km/s)
<b>Single-Day Optimization</b>						
Minimum C3	I	12-Aug-2041	10-May-2042	7.9	11.8	3.52
Minimum C3	II	29-Jul-2041	23-May-2042	7.6	9	2.96
Minimum C3	III-	07-Jun-2040	07-Aug-2042	5.7	29.6	4.77
Minimum C3	IV-	02-Jul-2040	18-Oct-2042	5.7	-25	5.14
Minimum C3	III+	20-Jun-2040	06-Aug-2042	5.7	26.1	4.91
Minimum C3	IV+	09-Oct-2040	12-Nov-2042	14.4	-5.2	6.37
Minimum VHP	I	11-Aug-2041	10-May-2042	8.1	7.3	3.47
Minimum VHP	II	05-Aug-2041	31-May-2042	7.7	4.9	2.89
Minimum VHP	III-	10-Jan-2041	04-Dec-2042	9.6	-34.2	3.1
Minimum VHP	IV-	31-Jan-2041	11-Feb-2043	16.2	5.3	3.58
Minimum VHP	III+	10-Feb-2041	12-Dec-2042	11.3	-34.7	2.99
Minimum VHP	IV+	11-Oct-2040	13-Nov-2042	16.3	13.5	6.32
<b>Launch Period Optimization</b>						
Minimum C3	I	11-Aug-2041	10-May-2042	8.1	7.3	3.47
		18-Aug-2041		8.2	14.5	3.60
Minimum C3	II	26-Jul-2041	25-May-2042	7.6	9.5	2.92
		02-Aug-2041		7.6	6.9	2.92
Minimum C3	III-	Not Possible				
Minimum C3	IV-	29-Jun-2040	18-Oct-2042	5.7	-24.3	5.15
		06-Jul-2040		5.7	-26.2	5.15
Minimum C3	III+	18-Jun-2040	06-Aug-2042	5.8	27.4	4.86
		25-Jun-2040		5.8	24.0	5.02
Minimum C3	IV+	Not Possible				

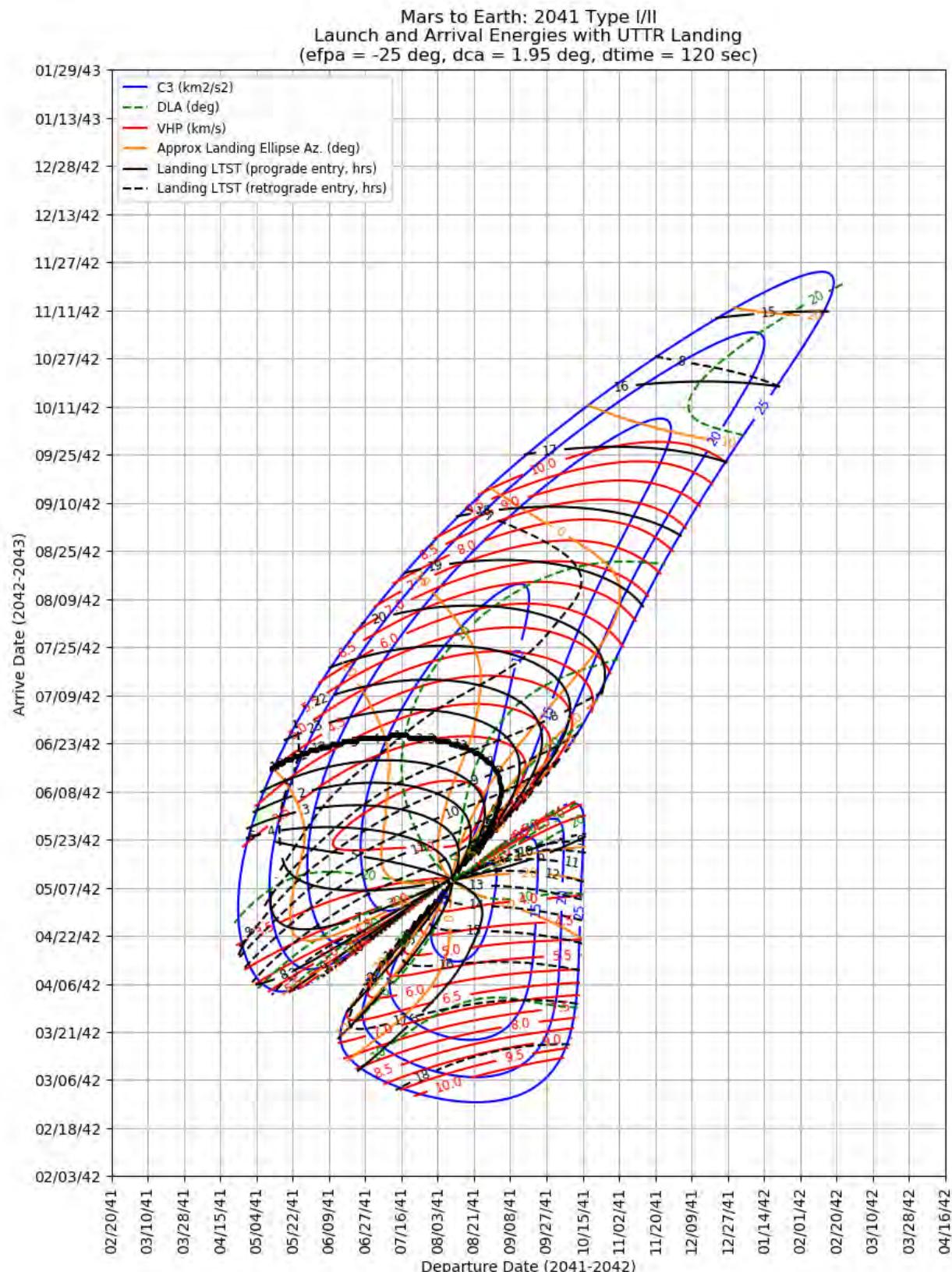


**Figure 557: Mars to Earth 2041 Type I/II – Launch/Arrival Energy and UTTR Landing Times**

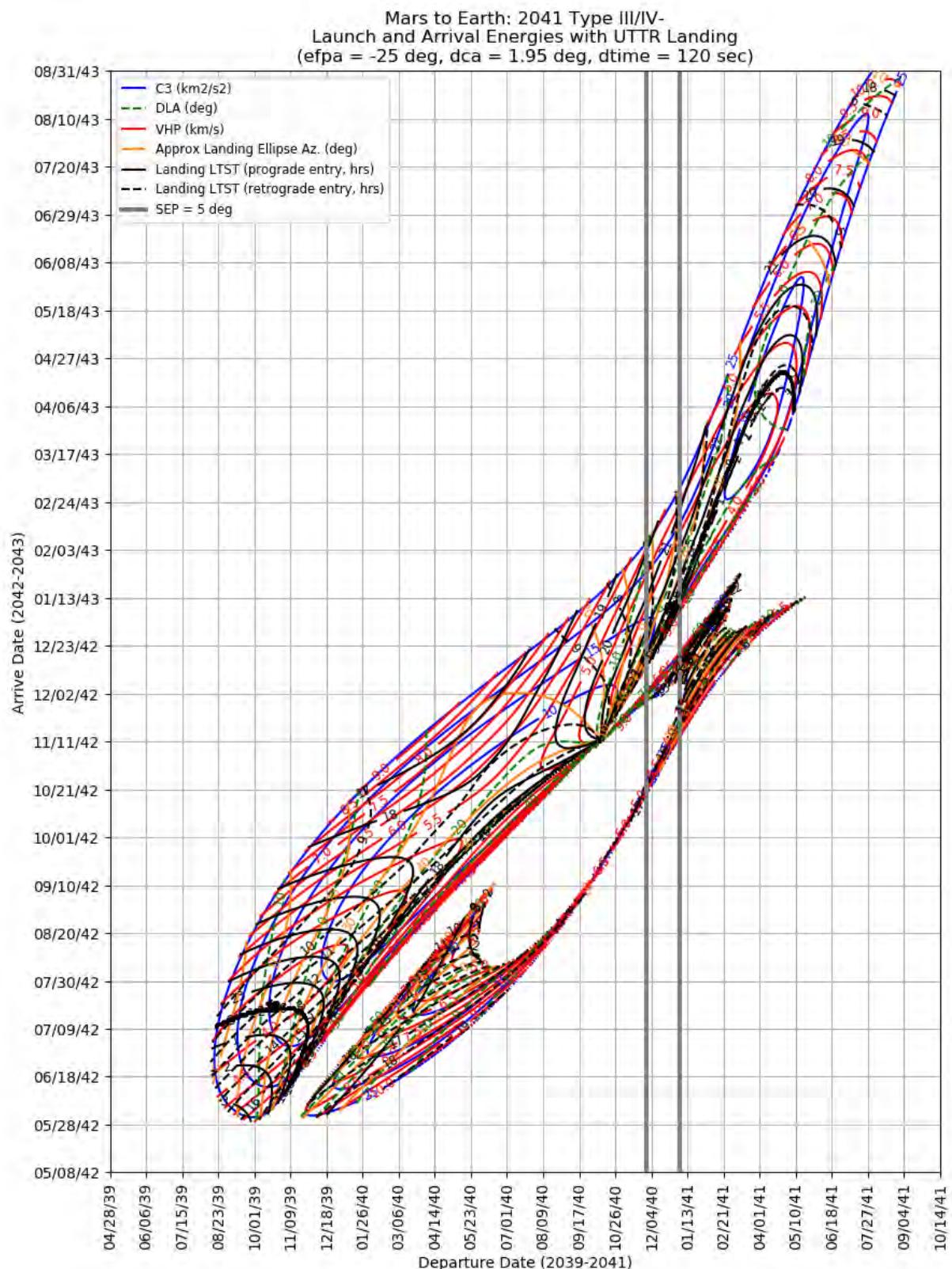


**Figure 558: Mars to Earth 2041 Type III/IV- – Launch/Arrival Energy and UTTR Landing Times**

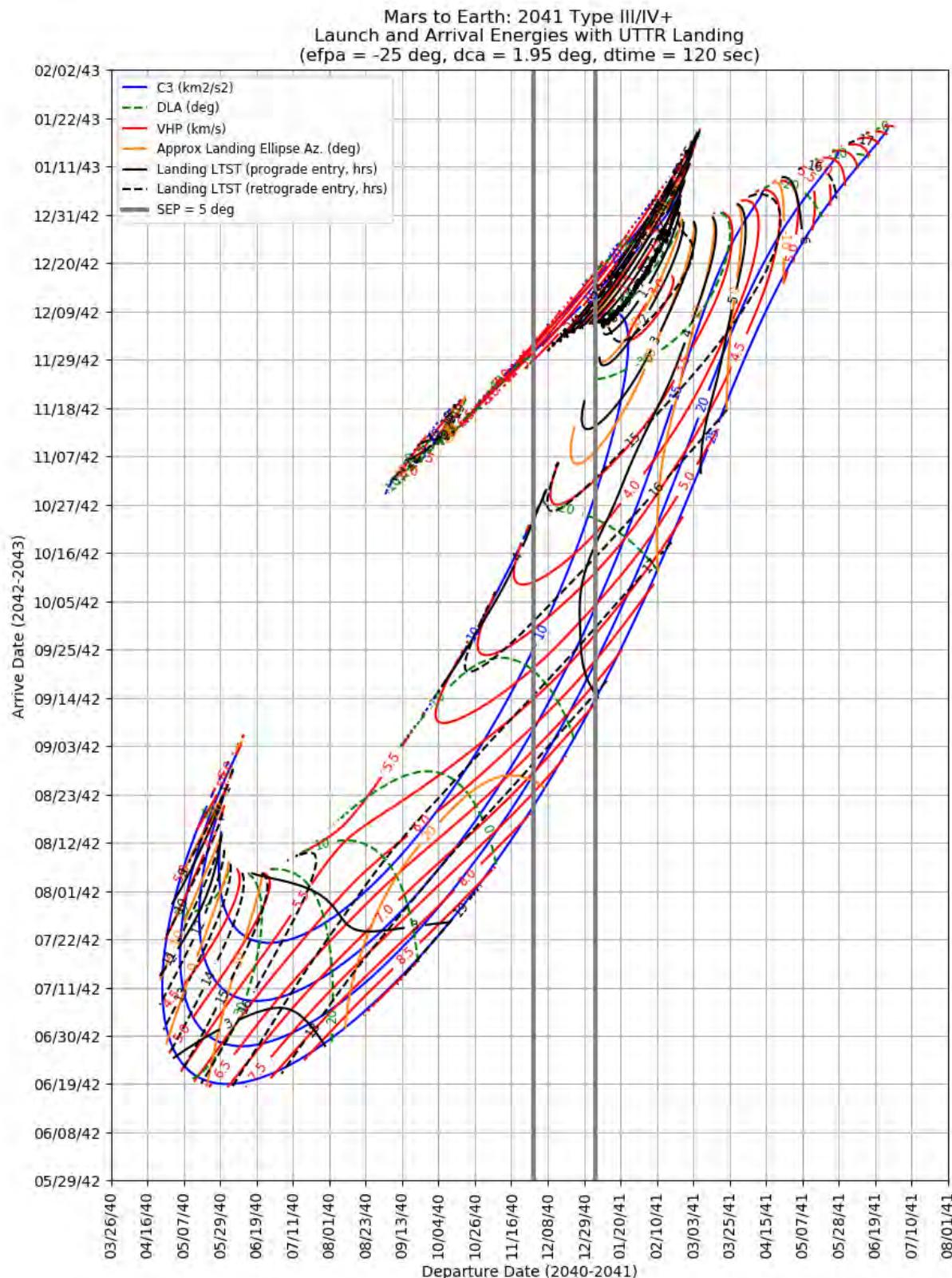


**Figure 559: Mars to Earth 2041 Type III/IV+ – Launch/Arrival Energy and UTTR Landing Times**

## 12 Roundtrip Mission Transfer Data: 2022-2041

### 12.1 Overview

Roundtrip mission designs are, by necessity, very complex. The interplay of requirements is extensive, and adding a Venus flyby into the mix increases the degrees of freedom and constraints dramatically. This chapter takes an exceptionally narrow view of the problem. Rather than consider the combinatorics of looking at every Earth-to-Mars opportunity and every Mars-to-Earth opportunity, with or without a Venus flyby on either leg that follows at the same level of detail as in the prior chapters, this chapter only looks at the various “optimal” designs.

The first design is the conjunction-class mission that maximizes the return mass. That is, a Type I/II launch period followed by the next Type I/II and III/IV $\pm$  launch period, and vice versa (e.g. a Type III/IV $\pm$  followed by a Type I/II or III/IV $\pm$ ). The Earth-to-Mars launch periods are the “Orbiter” launch periods described by Chapter 10, while the Mars-to-Earth launch periods are the minimum C3 periods, as described by Chapter 11. Within an opportunity, only the highest-performing trajectory within the types is used. For example, the 2033 Type II “Orbiter” launch period delivers slightly more mass to Mars than the 2033 Type I does, and the 2033 Type IV- delivers far more mass than the 2033 Type III- or III+. Designs launching using the 2033 opportunities thus include only the 2033 Type II and Type IV- designs. These designs do not constrain the timeline. In the case where an optimal departure time is prior to the optimal arrival time, the stay times are noted as negative, but not eliminated from consideration. Optimizing for mass is not necessarily the best design approach. In these cases, a potentially small mass penalty may permit a desirable design. The intent of these data are not to provide a definitive trajectory set, but to offer a guide to the quality of the various opportunities over the next two decades.

The second design is the opposition-class mission that maximizes the return mass while minimizing the mission timeline using a Venus flyby. For each of the minimum-VHP Earth-Venus-Mars trajectories, the next minimum C3 Mars to Earth Type I or II trajectory is selected. Likewise, for each of the minimum C3 Mars-Venus-Earth trajectories, the Earth to Mars Type I or II “Orbiter Launch Period” with the greatest delivered mass that arrives prior to the Mars departure is selected..

For both designs, the mass metric considered uses the same initial mass, capture orbit, and propulsion system assumptions as the Earth to Mars Orbiter Launch Periods (see Sections 1.4, 10.2, and 0). That is, a Falcon Heavy Recoverable launch performance, a 300-second specific impulse propulsion system, and a 36-hour capture orbit. In addition, the departure burn is assumed to take place from a 36-hour orbit after the spacecraft expends 1500 m/s at Mars. This is a large enough budget to aerobrake down to a low circular orbit and then increase the orbit period to 36 hours again prior to the departure burn. It is also sufficient to achieve a high circular orbit (e.g. to rendezvous with Phobos or Deimos), including plane changes for moderate incoming and outgoing declinations.

## 12.2 Venus-Enabled Trajectories

The Earth-Venus-Mars (Table 46) and Mars-Venus-Earth (Table 47) trajectories shown below are the minimum departure C3 and minimum approach v-infinity (VHP) single-day trajectories. The Venus flyby altitude was constrained to be no less than 200 km in all cases, but the trajectories were not otherwise constrained.

**Table 46: Earth-Venus-Mars Trajectories departing Earth 2020-2040**

Optimization Criteria	Earth Departure Date (dd-mmm-yyyy)	Venus Flyby Date (dd-mmm-yyyy)	Mars Arrival Date (dd-mmm-yyyy)	Launch Energy, C3 (km <sup>2</sup> /s <sup>2</sup> )	Approach V-Infinity, VHP (km/s)
Minimum C3	27-Oct-2021	25-Mar-2022	31-Aug-2022	14.6	5.710
Minimum C3	30-Aug-2023	09-Feb-2024	08-May-2024	22.5	12.171
Minimum C3	24-Mar-2026	21-Oct-2026	30-Apr-2027	47.0	6.173
Minimum C3	26-Mar-2028	24-Aug-2028	25-Feb-2029	27.0	6.136
Minimum C3	25-Jan-2030	09-Jul-2030	03-Dec-2030	24.4	7.874
Minimum C3	26-Jul-2032	04-Mar-2033	23-Aug-2033	54.2	6.300
Minimum C3	28-Jul-2034	10-Dec-2034	13-Jul-2035	14.0	5.574
Minimum C3	01-Jun-2036	15-Nov-2036	01-Mar-2037	22.1	13.335
Minimum C3	24-Feb-2039	04-Aug-2039	14-Mar-2040	46.4	5.016
Minimum VHP	30-Aug-2021	05-Apr-2022	25-Sep-2022	29.6	5.288
Minimum VHP	12-Sep-2023	19-Feb-2024	12-Jul-2024	25.8	6.328
Minimum VHP	28-Mar-2026	22-Oct-2026	16-May-2027	48.1	5.509
Minimum VHP	30-Mar-2028	05-Aug-2028	22-Apr-2029	46.4	4.519
Minimum VHP	01-Feb-2030	13-Jul-2030	13-Feb-2031	25.6	4.736
Minimum VHP	07-Aug-2032	09-Mar-2033	09-Sep-2033	55.0	5.978
Minimum VHP	14-Aug-2034	17-Dec-2034	20-Jul-2035	16.7	5.565
Minimum VHP	14-Jun-2036	24-Nov-2036	15-May-2037	24.7	6.369
Minimum VHP	02-Feb-2039	19-Aug-2039	16-Mar-2040	54.2	4.497

**Table 47: Mars-Venus-Earth Trajectories Departing Mars 2022-2041**

Optimization Criteria	Mars Departure Date (dd-mmm-yyyy)	Venus Flyby Date (dd-mmm-yyyy)	Earth Arrival Date (dd-mmm-yyyy)	Launch Energy, C3 (km <sup>2</sup> /s <sup>2</sup> )	Approach V-Infinity, VHP (km/s)
Minimum C3	04-Nov-2022	09-Jul-2023	14-Dec-2023	23.8	5.893
Minimum C3	02-Jun-2027	06-Dec-2027	16-May-2028	22.7	4.935
Minimum C3	24-Mar-2029	17-Oct-2029	13-Mar-2030	18.9	6.315
Minimum C3	23-Jan-2031	25-Aug-2031	21-Mar-2032	20.6	8.225
Minimum C3	13-Jan-2033	14-Jul-2033	09-Apr-2034	56.6	12.726
Minimum C3	22-Nov-2033	06-Jul-2034	22-Jan-2035	32.3	4.590
Minimum C3	29-Sep-2035	08-May-2036	06-Feb-2037	33.3	8.297
Minimum C3	01-Aug-2037	07-Mar-2038	17-Nov-2038	34.4	8.969
Minimum C3	14-May-2038	12-Nov-2038	27-Mar-2039	36.3	8.447
Minimum C3	27-Feb-2040	04-Oct-2040	14-Mar-2041	20.1	4.352
Minimum C3	19-Dec-2041	18-Aug-2042	16-Apr-2043	17.8	6.822
Minimum VHP	17-Aug-2022	07-Jul-2023	12-Dec-2023	59.8	5.868
Minimum VHP	06-Apr-2027	29-Dec-2027	16-Jun-2028	34.5	4.338
Minimum VHP	06-Sep-2028	03-Oct-2029	25-Feb-2030	53.4	4.847
Minimum VHP	15-Feb-2031	28-Aug-2031	28-Mar-2032	22.8	8.121
Minimum VHP	17-Jan-2033	15-Jul-2033	11-Apr-2034	58.6	12.650
Minimum VHP	21-Oct-2033	26-Jun-2034	18-Dec-2034	39.7	3.674
Minimum VHP	30-Jul-2035	15-Apr-2036	22-Aug-2036	52.3	4.420
Minimum VHP	17-May-2037	04-Feb-2038	11-Oct-2038	59.0	7.552
Minimum VHP	06-Jul-2038	17-Nov-2038	04-Apr-2039	59.5	8.154
Minimum VHP	04-Feb-2040	17-Oct-2040	31-Mar-2041	23.0	4.100
Minimum VHP	04-Aug-2041	29-Jul-2042	06-Dec-2042	59.6	4.196

## 12.3 Conjunction-Class Designs

Conjunction-class designs are here organized by the type of outbound (Earth to Mars) and inbound (Mars to Earth) trajectory used. The “Classical” missions (Table 48) use Type I/II trajectories for both. These missions have stay times in around 15 months, with a total mission duration of about three years. The “Slow Outbound” missions (Table 49) use a Type III/IV outbound and a Type I/II inbound, while “Slow Inbound” missions (Table 50) reverse this, using a Type I/II to Mars and a Type III/IV for the Earth Return. These both have flight times slightly longer than the Classical designs – about 40 months. However, the stay times for these trajectories are exceptionally short, with some optimal departure dates being several months before the optimal arrival dates. The “Long Conjunction” missions (Table 51) have stay times comparable to the Classical conjunction missions, but because they use Type III or IV transfers on both legs, the flight times are exceptionally long: over 70 months.

**Table 48: Classical Conjunction-Class Missions**

Trajectory	Departure At Open (mm-dd-yyyy)	Arrival (mm-dd-yyyy)	Launch Energy, C3 (km <sup>2</sup> /s <sup>2</sup> )	Launch Declination (deg)	Approach V-Infinity, VHP (km/s)	Total Flight Time (mo.)	Stay Time (mo.)	Returned Mass Fraction (%)
Earth to Mars 2022 Type II	29-Aug-2022	4-Sep-2023	15.5	11.7	2.89	32.4	10.6	31
Mars to Earth 2024 Type II	22-Jul-2024	10-May-2025	8.7	11.7	2.83			
Earth to Mars 2024 Type II	24-Sep-2024	6-Sep-2025	12.4	18	2.53	32.8	10.8	34
Mars to Earth 2026 Type II	31-Jul-2026	20-Jun-2027	7.2	5.7	3.1			
Earth to Mars 2026 Type II	19-Oct-2026	26-Aug-2027	10.1	32.2	2.64	33.7	12.3	35
Mars to Earth 2028 Type II	3-Sep-2028	11-Aug-2029	6.2	1.9	4.43			
Earth to Mars 2028 Type II	12-Nov-2028	23-Sep-2029	10.6	37.2	3.02	34.4	13.5	33
Mars to Earth 2031 Type II	7-Nov-2030	24-Sep-2031	5.4	-8.5	5.5			
Earth to Mars 2031 Type II	21-Dec-2030	13-Oct-2031	11.4	29.1	3.72	32.4	15.4	29
Mars to Earth 2033 Type I	25-Jan-2033	3-Sep-2033	5.7	15.5	4.03			
Earth to Mars 2033 Type II	30-Apr-2033	1-Feb-2034	10.1	-20.4	4.39	30.8	15.0	23
Mars to Earth 2035 Type I	5-May-2035	22-Nov-2035	8.8	-29.1	3.04			
Earth to Mars 2035 Type I	14-Jun-2035	7-Jan-2036	10.9	10.4	2.71	33.8	18.1	28
Mars to Earth 2037 Type II	10-Jul-2037	9-Apr-2038	12.6	2.3	3.56			
Earth to Mars 2037 Type II	18-Aug-2037	30-Aug-2038	16.8	8.7	3.11	32.5	10.6	29
Mars to Earth 2039 Type II	20-Jul-2039	3-May-2040	9.7	9.7	2.85			
Earth to Mars 2039 Type II	15-Sep-2039	8-Sep-2040	13.5	16.2	2.64	32.3	10.5	33
Mars to Earth 2041 Type II	26-Jul-2041	25-May-2042	7.6	9.5	2.92			

**Table 49: Slow-Outbound Conjunction-Class Missions**

Trajectory	Departure At Open (mm-dd-yyyy)	Arrival (mm-dd-yyyy)	Launch Energy, C3 (km <sup>2</sup> /s <sup>2</sup> )	Launch Declination (deg)	Approach V-Infinity, VHP (km/s)	Total Flight Time (mo.)	Stay Time (mo.)	Returned Mass Fraction (%)
Earth to Mars 2022 Type IV-	12-Nov-2021	1-Feb-2024	10.6	37.0	3.02	41.9	5.7	30
Mars to Earth 2024 Type II	22-Jul-2024	10-May-2025	8.7	11.7	2.83			
Earth to Mars 2024 Type IV-	6-Dec-2023	28-Jan-2026	10.8	32.4	3.45	42.4	6.0	29
Mars to Earth 2026 Type II	31-Jul-2026	20-Jun-2027	7.2	5.7	3.1			
Earth to Mars 2026 Type III+	26-Jun-2026	3-Jul-2028	12.8	14.0	3.01	37.5	2.0	33
Mars to Earth 2028 Type II	3-Sep-2028	11-Aug-2029	6.2	1.9	4.43			
Earth to Mars 2028 Type IV-	4-Sep-2028	26-Mar-2031	14.8	13.5	2.81	36.6	<span style="color:red">-4.6</span>	35
Mars to Earth 2031 Type II	7-Nov-2030	24-Sep-2031	5.4	-8.5	5.5			
Earth to Mars 2031 Type IV-	21-Sep-2030	11-Mar-2033	12.8	17.4	2.57	35.4	<span style="color:red">-1.5</span>	36
Mars to Earth 2033 Type I	25-Jan-2033	3-Sep-2033	5.7	15.5	4.03			
Earth to Mars 2033 Type IV-	7-Oct-2032	20-Feb-2035	11.0	23.4	2.49	37.5	2.4	33
Mars to Earth 2035 Type I	5-May-2035	22-Nov-2035	8.8	-29.1	3.04			
Earth to Mars 2035 Type IV-	21-Oct-2034	4-Feb-2037	10.3	35.5	2.65	41.6	5.1	29
Mars to Earth 2037 Type II	10-Jul-2037	9-Apr-2038	12.6	2.3	3.56			
Earth to Mars 2037 Type IV-	4-Nov-2036	31-Jan-2039	10.7	38.1	2.88	41.9	5.6	30
Mars to Earth 2039 Type II	20-Jul-2039	3-May-2040	9.7	9.7	2.85			
Earth to Mars 2039 Type IV-	26-Nov-2038	30-Jan-2041	10.6	34.2	3.27	41.9	5.8	30
Mars to Earth 2041 Type II	26-Jul-2041	25-May-2042	7.6	9.5	2.92			

**Table 50: Slow-Inbound Conjunction-Class Missions**

Trajectory	Departure At Open (mm-dd-yyyy)	Arrival (mm-dd-yyyy)	Launch Energy, C3 (km <sup>2</sup> /s <sup>2</sup> )	Launch Declination (deg)	Approach V-Infinity, VHP (km/s)	Total Flight Time (mo.)	Stay Time (mo.)	Returned Mass Fraction (%)
Earth to Mars 2022 Type II	29-Aug-2022	04-Sep-2023	15.5	11.7	2.89	36.9	<span style="color:red">-3.9</span>	34
Mars to Earth 2024 Type IV-	08-May-2023	26-Sep-2025	5.4	-9.6	5.51			
Earth to Mars 2024 Type II	24-Sep-2024	6-Sep-2025	12.4	18	2.53	35.9	<span style="color:red">-0.7</span>	35
Mars to Earth 2026 Type III+	16-Aug-2025	21-Sep-2027	6.1	14	3.53			
Earth to Mars 2026 Type II	19-Oct-2026	26-Aug-2027	10.1	32.2	2.64	42.3	7.0	31
Mars to Earth 2028 Type IV-	25-Mar-2028	30-Apr-2030	10.3	7.7	2.96			
Earth to Mars 2028 Type II	12-Nov-2028	23-Sep-2029	10.6	37.2	3.02	41.9	5.7	30
Mars to Earth 2031 Type IV-	15-Mar-2030	10-May-2032	8.6	11.9	2.81			
Earth to Mars 2031 Type II	21-Dec-2030	13-Oct-2031	11.4	29.1	3.72	41.1	4.6	27
Mars to Earth 2033 Type IV-	02-Mar-2032	25-May-2034	7.5	9.7	2.97			
Earth to Mars 2033 Type II	30-Apr-2033	1-Feb-2034	10.1	-20.4	4.39	38.1	0.8	24
Mars to Earth 2035 Type IV-	25-Feb-2034	4-Jul-2036	6.9	4.5	3.38			
Earth to Mars 2035 Type I	14-Jun-2035	7-Jan-2036	10.9	10.4	2.71	37.9	2.1	34
Mars to Earth 2037 Type IV-	10-Mar-2036	11-Aug-2038	6.2	2.6	4.48			
Earth to Mars 2037 Type II	18-Aug-2037	30-Aug-2038	16.8	8.7	3.11	36.9	<span style="color:red">-4.5</span>	33
Mars to Earth 2039 Type IV-	15-Apr-2038	13-Sep-2040	5.6	-4	5.38			
Earth to Mars 2039 Type II	15-Sep-2039	08-Sep-2040	13.5	16.2	2.64	37.1	<span style="color:red">-2.3</span>	35
Mars to Earth 2041 Type IV-	29-Jun-2040	18-Oct-2042	5.7	-26.2	5.15			

**Table 51: Long Conjunction-Class Missions**

Trajectory	Departure At Open (mm-dd-yyyy)	Arrival (mm-dd-yyyy)	Launch Energy, C3 (km <sup>2</sup> /s <sup>2</sup> )	Launch Declination (deg)	Approach V-Infinity, VHP (km/s)	Total Flight Time (mo.)	Stay Time (mo.)	Returned Mass Fraction (%)
Earth to Mars 2022 Type IV-	12-Nov-2021	1-Feb-2024	10.6	37	3.02	70.3	18.5	33
Mars to Earth 2026 Type III+	16-Aug-2025	21-Sep-2027	6.1	14	3.53			
Earth to Mars 2024 Type IV-	06-Dec-2023	28-Jan-2026	10.8	32.4	3.45	76.8	25.9	27
Mars to Earth 2028 Type IV-	25-Mar-2028	30-Apr-2030	10.3	7.7	2.96			
Earth to Mars 2026 Type III+	26-Jun-2026	03-Jul-2028	12.8	14	3.01	70.5	20.4	30
Mars to Earth 2031 Type IV-	15-Mar-2030	10-May-2032	8.6	11.9	2.81			
Earth to Mars 2028 Type IV-	04-Sep-2028	26-Mar-2031	14.8	13.5	2.81	68.6	11.2	33
Mars to Earth 2033 Type IV-	02-Mar-2032	25-May-2034	7.5	9.7	2.97			
Earth to Mars 2031 Type IV-	21-Sep-2030	11-Mar-2033	12.8	17.4	2.57	69.4	11.5	34
Mars to Earth 2035 Type IV-	25-Feb-2034	04-Jul-2036	6.9	4.5	3.38			
Earth to Mars 2033 Type IV-	7-Oct-2032	20-Feb-2035	11	23.4	2.49	70.1	12.6	36
Mars to Earth 2037 Type IV-	10-Mar-2036	11-Aug-2038	6.2	2.6	4.48			
Earth to Mars 2035 Type IV-	21-Oct-2034	4-Feb-2037	10.3	35.5	2.65	70.8	14.3	35
Mars to Earth 2039 Type IV-	15-Apr-2038	13-Sep-2040	5.6	-4	5.38			
Earth to Mars 2037 Type IV-	4-Nov-2036	31-Jan-2039	10.7	38.1	2.88	71.4	16.9	34
Mars to Earth 2041 Type IV-	29-Jun-2040	18-Oct-2042	5.7	-26.2	5.15			
Earth to Mars 2039 Type IV-	26-Nov-2038	30-Jan-2041	10.6	34.2	3.27	70	13.3	27
Mars to Earth 2043 Type IV-	10-Mar-2042	25-Sep-2044	10.4	-29.4	4.42			

## 12.4 Opposition-Class Designs

The Opposition-Class missions detailed here are organized by when the Venus flyby occurs. Outbound flyby missions perform the Venus flyby on the way to Mars, while inbound flyby mission do so on their way back to Earth. These are also referred to as EVM and MVE trajectories. The outbound flyby missions use the minimum Mars-arriving VHP Earth-Venus-Mars trajectory and the lowest-C3 Mars to Earth Type I or II launch period to depart Mars after that trajectory arrives. If the Type I departs before the arrival, for example, the Type II will be used, even if it has a higher C3. If there is not a return trajectory with a short stay time, that outbound opportunity is skipped. For example, the Earth-Venus-Mars 2021 trajectory arrives in late September 2022. The next Earth return opportunity is in July 2024, resulting in a stay time and mission duration longer than most conjunction class missions (22 and 44 months, respectively). This obviates the primary purpose of a Venus flyby – to enable short total mission durations. An exception is made for cases where the stay optimal stay time is slightly negative and no short-stay-time options exist.

Similarly, the inbound Venus-flyby trajectories are paired with the Earth to Mars maximum-captured-mass launch period that arrives prior to its departure. The same basic rules apply: the higher performing option is selected, unless it arrives more than six months before the MVE departs, and long missions are skipped.

**Table 52: Earth-Venus-Mars Opposition-Class Missions**

Trajectory	Departure (dd-mmm-yyyy)	Flyby (dd-mmm-yyyy)	Arrival (dd-mmm-yyyy)	Launch Energy, C3 (km <sup>2</sup> /s <sup>2</sup> )	Approach V-Infinity, VHP (km/s)	Stay Time (mo)	Flight Time (mo)	Returned Mass Fraction
Earth-Venus-Mars 2023	12-Sep-2023	19-Feb-2024	12-Jul-2024	25.8	6.328	0.3	19.9	14
Mars to Earth 2024 Type II	22-Jul-2024	N/A	10-May-2025	8.7	2.830			
Earth-Venus-Mars 2034	14-Aug-2034	17-Dec-2034	20-Jul-2035	16.7	5.565	<span style="color:red">-2.5</span>	15.3	17
Mars to Earth 2035 Type I	05-May-2035	N/A	22-Nov-2035	8.8	3.040			
Earth-Venus-Mars 2036	14-Jun-2036	24-Nov-2036	15-May-2037	24.7	6.369	1.8	21.8	12
Earth to Mars 2037 Type II	10-Jul-2037	N/A	09-Apr-2038	12.6	3.560			

**Table 53: Mars-Venus-Earth Opposition-Class Missions**

Trajectory	Departure (dd-mmm-yyyy)	Flyby (dd-mmm-yyyy)	Arrival (dd-mmm-yyyy)	Launch Energy, C3 (km <sup>2</sup> /s <sup>2</sup> )	Approach V-Infinity, VHP (km/s)	Stay Time (mo)	Flight Time (mo)	Returned Mass Fraction
Earth to Mars 2026 Type I	11-Nov-2026	N/A	06-Aug-2027	18.3	3.08	-2.1	18.1	20
Mars-Venus-Earth 2027	02-Jun-2027	06-Dec-2027	16-May-2028	22.7	4.935			
Earth to Mars 2033 Type II	16-Apr-2033	N/A	25-Oct-2033	14.3	3.5	0.9	21.2	15
Mars-Venus-Earth 2033	22-Nov-2033	06-Jul-2034	22-Jan-2035	32.3	4.59			
Earth to Mars 2037 Type II	19-Aug-2037	N/A	24-Mar-2038	21.1	3.02	1.7	19.2	15
Mars-Venus-Earth 2038	14-May-2038	12-Nov-2038	27-Mar-2039	36.3	8.447			
Earth to Mars 2039 Type I	02-Oct-2039	N/A	28-May-2040	26.6	3.21	-3.0	17.4	21
Mars-Venus-Earth 2040	27-Feb-2040	04-Oct-2040	14-Mar-2041	20.1	4.352			

## 13 Appendices

### 13.1 Gravity Coefficients

#### 13.1.1 MRO120D

The normalized spherical harmonic coefficients for the MRO120D Mars gravity field is summarized in Table 54.

**Table 54: Mars Gravity Parameters (Normalized)**

Parameter	Value	Parameter	Value
<b>Bulk Body</b>			
GM (from MAR097)	42828.37362069909 km <sup>3</sup> /s <sup>2</sup>	R <sub>ref</sub>	3396.0 km
<b>Zonal Coefficients</b>			
J( 1)	0	J( 5)	1.7267702404260E-06
J( 2)	8.7502209245370E-04	J( 6)	-1.3463714866160E-06
J( 3)	1.1897015037300E-05	J( 7)	-1.0598968092880E-06
J( 4)	-5.1290958301340E-06	J( 8)	-1.4437523554120E-07
<b>Tesseral Coefficients</b>			
C( 2, 1)	4.022333063820E-10	S( 2, 1)	2.3031838535520E-11
C( 2, 2)	-8.4633026559830E-05	S( 2, 2)	4.8939418321670E-05
C( 3, 1)	3.8049981991010E-06	S( 3, 1)	2.5177117707630E-05
C( 3, 2)	-1.5947431923720E-05	S( 3, 2)	8.3623939784670E-06
C( 3, 3)	3.5056298360330E-05	S( 3, 3)	2.5571325457370E-05
C( 4, 1)	4.2163911582170E-06	S( 4, 1)	3.7632643561220E-06
C( 4, 2)	-9.5306695299840E-07	S( 4, 2)	-8.9807968418080E-06
C( 4, 3)	6.4568519841300E-06	S( 4, 3)	-1.9377212284160E-07
C( 4, 4)	3.0824936247700E-07	S( 4, 4)	-1.2873056977380E-05
C( 5, 1)	4.8384215630660E-07	S( 5, 1)	2.1231129753950E-06
C( 5, 2)	-4.2981760456790E-06	S( 5, 2)	-1.1656954440860E-06
C( 5, 3)	3.3126670085550E-06	S( 5, 3)	2.7144097785790E-07
C( 5, 4)	-4.6407608474120E-06	S( 5, 4)	-3.3815536222490E-06
C( 5, 5)	-4.4492645268970E-06	S( 5, 5)	3.7804789409520E-06
C( 6, 1)	1.8023583692130E-06	S( 6, 1)	-1.5185193991260E-06
C( 6, 2)	8.6171342848250E-07	S( 6, 2)	1.4691007371520E-06
C( 6, 3)	9.5567075435960E-07	S( 6, 3)	3.3292558689320E-07
C( 6, 4)	1.0087553624920E-06	S( 6, 4)	2.6386569471530E-06
C( 6, 5)	1.6578866158220E-06	S( 6, 5)	1.6226764849180E-06
C( 6, 6)	2.7622296666680E-06	S( 6, 6)	8.2135333243850E-07
C( 7, 1)	1.3749994266810E-06	S( 7, 1)	-2.2737194866050E-07

Parameter	Value	Parameter	Value
C( 7, 2)	2.8139783170420E-06	S( 7, 2)	-6.2967694381360E-07
C( 7, 3)	8.8048981361710E-07	S( 7, 3)	-3.9698286606070E-07
C( 7, 4)	2.4689899049820E-06	S( 7, 4)	-4.2245529297430E-07
C( 7, 5)	-1.9168169008940E-07	S( 7, 5)	-1.3585219042100E-06
C( 7, 6)	-5.5960104736480E-07	S( 7, 6)	-1.9013643905730E-06
C( 7, 7)	4.4039558349960E-07	S( 7, 7)	-1.7756701426830E-06
C( 8, 1)	-1.3253837279380E-07	S( 8, 1)	7.5052081765850E-07
C( 8, 2)	1.8104244435100E-06	S( 8, 2)	5.0705823024380E-07
C( 8, 3)	-1.2070336086800E-06	S( 8, 3)	-1.3413009168640E-06
C( 8, 4)	1.5882837683240E-06	S( 8, 4)	1.4812074290120E-07
C( 8, 5)	-2.7917524692450E-06	S( 8, 5)	-1.6297926112810E-06
C( 8, 6)	-9.1440928257930E-07	S( 8, 6)	-1.7899324707530E-06
C( 8, 7)	-4.7364667411900E-07	S( 8, 7)	1.6446964596680E-06
C( 8, 8)	-3.1065725923520E-07	S( 8, 8)	-2.5028184874420E-07

### 13.1.2 GGM05C

The normalized spherical harmonic coefficients for the GGM05C Earth gravity field is summarized in Table 55.

Table 55: Earth Gravity Parameters (Normalized)

Parameter	Value	Parameter	Value
Bulk Body			
GM (from DE43)	398600.43543609 km <sup>3</sup> /s <sup>2</sup>	R <sub>ref</sub>	6378.1363 km
Zonal Coefficients			
J( 1)	0.0	J( 5)	-6.8650323458391e-08
J( 2)	0.00048416945732	J( 6)	1.4997605610883e-07
J( 3)	-9.5716475834116e-07	J( 7)	-9.0500819789642e-08
J( 4)	-5.3998153921365e-07	J( 8)	-4.9478326949545e-08
Tesseral Coefficients			
C( 2, 1)	-3.1034310672386e-10	S( 2, 1)	1.4107575094423e-09
C( 2, 2)	2.4393734159398e-06	S( 2, 2)	-1.4002940118364e-06
C( 3, 1)	2.0304466371688e-06	S( 3, 1)	2.4824063468478e-07
C( 3, 2)	9.0476467441002e-07	S( 3, 2)	-6.1900662463325e-07
C( 3, 3)	7.2128525517036e-07	S( 3, 3)	1.4144000651650e-06
C( 4, 1)	-5.3618081337028e-07	S( 4, 1)	-4.7357697696907e-07
C( 4, 2)	3.5049214427031e-07	S( 4, 2)	6.6250516574391e-07
C( 4, 3)	9.9086103111508e-07	S( 4, 3)	-2.0095089980582e-07

Parameter	Value	Parameter	Value
C( 4, 4)	-1.8849242252755e-07	S( 4, 4)	3.0881857855702e-07
C( 5, 1)	-6.2914579409678e-08	S( 5, 1)	-9.4342598600045e-08
C( 5, 2)	6.5205860316915e-07	S( 5, 2)	-3.2334307981429e-07
C( 5, 3)	-4.5183137844644e-07	S( 5, 3)	-2.1494236736021e-07
C( 5, 4)	-2.9532340917041e-07	S( 5, 4)	4.9810578844048e-08
C( 5, 5)	1.7481435046942e-07	S( 5, 5)	-6.6935467701596e-07
C( 6, 1)	-7.5943265879397e-08	S( 6, 1)	2.6525683249700e-08
C( 6, 2)	4.8635603179946e-08	S( 6, 2)	-3.7376947326560e-07
C( 6, 3)	5.7251326495652e-08	S( 6, 3)	8.9731654074799e-09
C( 6, 4)	-8.5996937469007e-08	S( 6, 4)	-4.7142652438675e-07
C( 6, 5)	-2.6716319362048e-07	S( 6, 5)	-5.3649603802896e-07
C( 6, 6)	9.4799107163032e-09	S( 6, 6)	-2.3738360514414e-07
C( 7, 1)	2.8088622262423e-07	S( 7, 1)	9.5159759814302e-08
C( 7, 2)	3.3039550420017e-07	S( 7, 2)	9.3020287728326e-08
C( 7, 3)	2.5046335396041e-07	S( 7, 3)	-2.1709707579017e-07
C( 7, 4)	-2.7498638931989e-07	S( 7, 4)	-1.2405070527179e-07
C( 7, 5)	1.6469638664557e-09	S( 7, 5)	1.7930957773652e-08
C( 7, 6)	-3.5879864059130e-07	S( 7, 6)	1.5179288962731e-07
C( 7, 7)	1.5230586682001e-09	S( 7, 7)	2.4103042687242e-08
C( 8, 1)	2.3140759375679e-08	S( 8, 1)	5.8905000941228e-08
C( 8, 2)	8.0020451775005e-08	S( 8, 2)	6.5300088951785e-08
C( 8, 3)	-1.9359078476200e-08	S( 8, 3)	-8.5941592936614e-08
C( 8, 4)	-2.4434458705958e-07	S( 8, 4)	6.9812156090700e-08
C( 8, 5)	-2.5701616796151e-08	S( 8, 5)	8.9205635687968e-08
C( 8, 6)	-6.5971100477032e-08	S( 8, 6)	3.0894511043496e-07
C( 8, 7)	6.7256526485194e-08	S( 8, 7)	7.4864353638378e-08
C( 8, 8)	-1.2403256812475e-07	S( 8, 8)	1.2054023904735e-07

### 13.1.3 Converting Between Normalized and Un-Normalized Gravity Coefficients

The relationships between normalized ( $\bar{S}_{lm}$ ,  $\bar{C}_{lm}$ , and  $\bar{J}_{lm}$ ) and un-normalized ( $S_{lm}$ ,  $C_{lm}$ , and  $J_{lm}$ ) gravity coefficients are the following:

$$\bar{S}_{lm} = \Pi_{lm} S_{lm} \quad (32)$$

$$\bar{C}_{lm} = \Pi_{lm} C_{lm} \quad (33)$$

$$\bar{J}_{lm} = \Pi_{lm} J_{lm} \quad (34)$$

where the conversion factor is given by:

$$\Pi_{lm} = \sqrt{\frac{(l+m)!}{k(l-m)!(2l+1)}} \begin{cases} k = 1 \text{ if } m = 0 \\ k = 2 \text{ if } m \neq 0 \end{cases} \quad (35)$$

## 13.2 References

- [1] J. E. Prussing and B. E. Conway, Orbital Mechanics, New York: Oxford University Press, 1993.
- [2] J. A. Sims and S. N. Flanagan, "Preliminary Design of Low-Thrust Interplanetary Missions," in *AAS/AIAA Astrodynamics Specialists Conference*, AAS 99-338, Girdwood, AK, August 16-19, 1999.
- [3] Jet Propulsion Laboratory Office of the Chief Engineer, "JPL Design Principles, Rev 7 (D-43913)".
- [4] National Space and Aeronautics Administraion, "Discovery 2019 Annoucement of Opportunity (AO) Launch Services Information Summary," 2019.
- [5] M. S. Wallace, "InSight Planetary Constants and Models Document, Revision C," JPL D-75286, 2017.
- [6] A. S. Konopliv, R. S. Park and W. M. Folkner, "An improved JPL Mars gravity field and orientation from Mars orbiter and lander tracking data," *Icarus*, vol. 274, pp. 253-260, 2016.
- [7] R. Jacobson and V. Lainey, "Martian satellite orbits and ephemeris," *Planetary and Space Science*, vol. 102, pp. 35-44, 1 November 2014.
- [8] P. K. Seidelmann, V. K. Abalakin, M. Bursa, D. M. E., C. de Bergh, J. H. Lieske, O. J., J. L. Simon, E. M. Standish, S. P. and P. C. Thomas, "Report of the IAU/IAG Working Group on Cartographic Coordinates and Rotational Elements of the Planets and Satellites: 2000," *Celestial Mechanics and Dynamical Astronomy*, vol. 82, no. 1, pp. 83-111, 2002.
- [9] D. E. Smith, M. T. Zuber, S. C. Solomon, R. J. Phillips, J. W. Head, J. B. Garvin, W. B. Banerdt, D. O. Muhleman, G. H. Pettengill, G. A. Neumann, F. G. Lemoine, J. B. Abshire, O. Aharonson and C. Da, "The Global Topography of Mars and Implications for Surface Evolution," *Science*, vol. 284, no. 5419, pp. 1495-1503, 1999.
- [10] R. Vaughan, "Mars Pathfinder Planetary Constants and Models," JPL D-12947, 1995.
- [11] W. M. Folkner, C. F. Yoder, D. N. Yuan, E. M. Standish and R. A. Preston, "Interior Structure and Seasonal Mass Redistribution of Mars from Radio Tracking of Mars Pathfinder," *Science*, vol. 278, no. 5344, pp. 1749-1752, 1997.
- [12] Roncoli, Ralph, B. Strauss and D. Highsmith, "Mars Exploration Rover Project Planetary Constants and Models - Version 2," JPL IOM 312.F-02-003, 2002.
- [13] M. Allison and M. McEwen, "A Post-Pathfinder Evaluation of Aerocentric Solar Coordanates with Improved Iming Recipes for Mars Seasonal/Diurnal Climate Studies," *Planetary and Space Science*, vol. 48, pp. 215-235, 1999.
- [14] M. Lisano and M. Grover, "Riders on the Storm: NASA InSight Lander and the 2018 Mars Global Dust Storm," in *IEEE Aerospace Conference*, Big Sky, MT, 2019.
- [15] S. Wagner and P. Menon, "Mars Reconnaissance Orbiter Maneuver Plan for Mars 2020

Entry, Descent, and Landing Support and Beyond (AAS 19-233)," in *AAS/AIAA Space Flight Mechanics Meeting*, Maui, HI, 2019.

- [16] C. M. McCullough, "High Fidelity Earth Background Models based on GRACE/GRACE-FO Release 06 (RL06)," JPL IOM 392R-19-003, 2019.
- [17] D. D. (. McCarthy and G. (. Petit, "International Earth Rotation and Reference Systems Service (IERS) Conventions (2003), IERS Technical Note No. 32," Verlag des Bundesamts für Kartographie und Geodäsie, rankfurt am Main, 2004.
- [18] T. D. Moyer, Formulation for Observed and Computed Values of Deep Space Network Data Types for Navigation; JPL Publication 00-7, Mongraph 2, Deep Space Communications and Navigation Systems Center of Excellence, Jet Propulsion Laboratory, 2000.
- [19] P. J. Mohr and B. N. Taylor, "CODATA Recommended Values of the Fundamental Physical Constants: 1998," National Institute of Standards and Technology, Gaithersburg, MD, 1998.
- [20] W. M. Folkner, G. Williams and D. H. Boggs, "Planetary ephemeris DE438 for InSight," JPL IOM 392R-18-011, 2018.
- [21] "Space Environment (Natural and Artificial) - Process for Determining Solar Irrandiances," ISO/WD 21348, ISO 1999.
- [22] M. S. Wallace, D. Litton, T. Martin-Mur and S. Wagner, "Orbiters, Cubsats, and Radio Telescopes, Oh My; Entry Descent, and Landing Communications for the 2018 InSight Mars Lander Mission," in *29th AAS/AIAA Space Flight Mechanics Meeting*, Ka'anapali, Maui, Hawaii, 2019.
- [23] W. G. Melbourne and C. G. Sauer, "Performance Computations with Pieced Solutions of Planetocentric and Helio-centric Trajectories for Low-Thrust Missions," *Space Programs Summary*, vol. IV, no. 37-36, pp. 14-19, 31 December 1965.
- [24] A. Nicholas, R. Woolley, D. A., F. Laipert, Z. Olikara, R. Webb and R. Lock, "Simultaneous Optimization of Spacecraft and Trajectory Design for Interplanetary Mission Utilizing Solar Electric Propulsion (AAS 19-456)," in *AAS/AIAA Spaceflight Mechanics Meeting*, Maui, HI, 2019.
- [25] R. Woolley and Z. Olikara, "Optimized Low-Thrust Missions from GTO to Mars," in *IEEE Aerospace Conference*, Big Sky, MT, 2019.
- [26] R. Woolley and A. Nicholas, "SEP Mission Design Space for Mars Orbiters (AAS 15-632)," in *AIAA/AAS Astrodynamics Specialist Conference*, Vail, CO, Aug 2015.
- [27] R. Woolley, F. Laipert, N. A.K. and Z. Olikara, "Low-Thrust Trajectory Bacon Plots for Mars Mission Design (AAS 19-326)," in *AAS/AIAA Spaceflight Mechanics Meeting*, Maui, HI, Jan 2019.
- [28] R. Potter, R. Woolley, N. A.K. and L. J., "Features and Characteristics of Earth-Mars Bacon Plots," in *AIAA/AAS Astrodynamics Specialist Conference*, Stevenson, WA, Aug 2017.
- [29] P. Patel and D. Scheeres, "Maximizing Payload Mass Fractions of Spacecraft for Interplanetary Electric Propulsion Missions," *Journal of Spacecraft and Rockets*, vol. 43, no. 4, 2006.
- [30] National Aeronautics and Space Administration, "Announcement of Opportunity: Discovery 2014 (NNH14ZDA014O)," 16 January 2015. [Online]. [Accessed 17 January 2020].
- [31] National Aeronautics and Space Administration, "NASA Selects Two Missions to Explore

- the Earth Solar System," 4 January 2017. [Online]. [Accessed 17 January 2020].
- [32] National Aeronautics and Space Administration, "Final Minutes of Curiosity's Arrival at Mars," 19 July 2010. [Online]. Available: [https://www.nasa.gov/mission\\_pages/msl/multimedia/gallery/pia13282.html](https://www.nasa.gov/mission_pages/msl/multimedia/gallery/pia13282.html). [Accessed 7 February 2020].
- [33] Jet Propulsion Laboratory, "Mission Overview," [Online]. Available: [https://www.jpl.nasa.gov/news/press\\_kits/insight/landing/mission/](https://www.jpl.nasa.gov/news/press_kits/insight/landing/mission/). [Accessed 7 February 2020].
- [34] W. Hurd, P. Estabrook, C. Racho and E. Satorius, "Critical Spacecraft-to-Earth Communications for Mars Exploration Rover (MER) Entry, Descent, and Landing," *IEEE Aerospace Conference Proceedings*, vol. 3, pp. 1283-1292, 2002.
- [35] R. Kornfield, M. Garcia, L. Craig, S. Butman and G. Sinori, "Entry, Descent, and Landing Communications for the 2007 Mars Phoenix Lander," *Journal of Spacecraft and Rockets*, vol. 45, no. May-June, pp. 534-547, 2008.
- [36] F. Abilleira and J. Shinder, "Entry, Descent, and Landing Communications for the 2011 Mars Science Laboratory," in *AIAA Guidance, Navigation, and Control Conference and Co-located Conferences*, Minneapolis, Minnesota, 2012.
- [37] M. Wallace and M. Jesick, "Argos," 16 April 2019. [Online]. Available: <https://github.jpl.nasa.gov/mswallac/Argos>. [Accessed 25 February 2020].
- [38] M. Wallace, J. Parker, N. Strange and D. Grebow, "Orbital Operations for Phobos and Deimos Exploration," in *AIAA/AAS Astrodynamics Specialist Conference (AIAA 2012-5067)*, Minneapolis, MN, 2012.
- [39] National Aeronautics and Space Administration, "NASA Procedural Requirements (NPR) 8020.12D, Chapter 5," 20 April 2011. [Online]. [Accessed 5 March 2020].
- [40] M. A. Vincent, "Explanation and History of the New Solar Cycle/Atmospheric Model used in Mars Planetary Protection Analysis (JPL D-21422)," December 19, 2003.
- [41] S. Wong, T. You and e. al, "Navigating Through the Venus Atmosphere (AAS 94-116)," in *AAS/AIAA Spaceflight Mechanics Meeting*, Cocoa Beach, FL, 1994.
- [42] J. Giorgini, S. Wong and e. al, "MAgellan Aerobrake Navigation," *British Interplanetary Society Journal*, vol. 48, no. 3, pp. 111-122, March 1995.
- [43] M. Johnston and e. al, "Mars Global Surveyor Aerobraking at Mars (AAS 98-112)," in *AIAA Spaceflight Mechanics Meeting*, Monterery, CA, 1998.
- [44] M. Denis, P. Schmitz and e. al, "Thousand Times through the Atmosphere of Mars: Aerobraking the ExoMars Trace Gas Orbiter," in *AIAA, SpaceOps Conferences*, Marseille, France, 2018.
- [45] T. You, A. Halsell and e. al, "Navigating Mars Reconnaissance Orbiter: Launch Through Primary Science Orbit (AIAA 2007-6093)," in *AIAA SPACE 2007 Conference and Exposition*, Long Beach, CA, 2007.

